THÈSE POUR OBTENIR LE GRADE DE DOCTEUR DE L'UNIVERSITÉ DE MONTPELLIER

En Paléobiologie

École doctorale GAIA

Institut des Sciences de l'Évolution de Montpellier

Systématique et dynamique évolutive des Metatheria (marsupiaux et fossiles apparentés) en Europe durant les réchauffements climatiques intenses de l'Éocène inférieur

Présentée par Killian GERNELLE

Le 12 décembre 2024

Sous la direction de Rodolphe TABUCE (Directeur)
et de Sandrine LADEVÈZE (Co-encadrante)

Devant le jury composé de

M. Robin Michael Davenport BECK, Maître de conférences, University of Salford (EN)	Rapporteur
M. Thierry SMITH, Chef d'unité de recherche, Royal Belgian Institute of Natural Sciences, Bruxelles (BE)	Rapporteur
Mme. Mélanie DEBIAIS-THIBAUD, Professeure, Université de Montpellier (FR)	Examinatrice
M. Stéphane DUCROCQ, Directeur de recherche CNRS, Université de Poitiers (FR)	Examinateur
M. Grégoire MÉTAIS, Chargé de recherche CNRS, Muséum National d'Histoire Naturelle, Paris (FR)	Examinateur
Mme. Maëva ORLIAC, Directrice de recherche CNRS, Université de Montpellier (FR)	Examinatrice, Présidente du jury

UNIVERSITÉ DE MONTPELLIER

Remerciements

Mes premiers remerciements vont aux membres de mon jury de thèse pour avoir accepté d'évaluer ce travail. Aux rapporteurs Thierry Smith et Robin M. D. Beck, avec qui j'ai eu le plaisir d'échanger scientifiquement à plusieurs reprises en amont, ainsi qu'aux examinateurs, Mélanie Debiaid-Thibaud, Stéphane Ducrocq, Grégoire Métais et Maëva Orliac, à qui j'exprime toute ma gratitude.

Mes seconds remerciements sont destinés à mon directeur, Rodolphe Tabuce, et ma co-encadrante, Sandrine Ladevèze, pour leur disponibilité, leurs encouragements appuyés et leurs conseils pendant ces trois années de thèse, ainsi que pour m'avoir laissé toute latitude pour traiter ce sujet comme je l'entendais. Merci Rodolphe d'avoir su me transmettre ta passion pour la paléo(micro)mammalogie et de m'avoir, avec Fabrice Lihoreau, embarqué dans l'étude des faunes de l'Éocène inférieur lors de ma licence, il y a maintenant plus de cinq ans. J'espère avoir été à la hauteur de la confiance que vous avez placée en moi depuis ! Votre entrain quotidien, et toutes les discussions que l'on a pu avoir m'ont été très profitables, d'un point de vue professionnel et personnel.

Je remercie les personnes qui ont fait partie de mon comité de suivi de thèse, Carole Smadja, Anne-Laure Decombeix et Guillaume Billet, pour leur écoute et leurs conseils lors de nos réunions. Ton aide, Guillaume, a été précieuse pour organiser l'emprunt d'une quantité considérable de matériel au MNHN, et vous avez assuré avec Vincent Pernègre la numérotation de spécimens au fil de l'eau. Tu m'as encouragé à aller au bout de mes idées pour quantifier mes observations et déceler des biais potentiels dans mes analyses, à la fois dans le cadre de notre collaboration sur Palette et durant les comités de suivi, je t'en suis très reconnaissant. Je joins à ces remerciements Emmanuel Gheerbrant, Grégoire Métais, ainsi que Marc Godinot, pour m'avoir confié plusieurs spécimens lors de mes venues au MNHN, et par la suite pour votre aide répétée, même à distance !

À Thierry Smith, ainsi qu'à Annelise Folie, merci beaucoup pour votre accueil à Bruxelles, et pour avoir organisé au mieux mes visites de collections à l'IRSNB à deux reprises. Une partie conséquente des réflexions développées dans cette thèse en est tributaire. Du côté de Montpellier, cette thèse doit aussi beaucoup à Renaud Lebrun, Anne-Lise Charruault, et Hélène Bourget pour leur contribution technique. Merci à Renaud de m'avoir accompagné dans l'apprentissage des méthodes d'imagerie et pour sa patience, à Anne-Lise pour avoir réussi à sauver par sa minutie certains des spécimens qui illustrent ces pages, et à Hélène pour m'avoir formé au traitement des sédiments, pour les coups de pouce pendant mes deux premières années de thèse, et avoir assuré la découverte de nouveautés au tri !

Merci à l'ensemble des paléontologues de l'ISEM de m'avoir offert un cadre de travail humain et chaleureux. Je remercie particulièrement Lionel Hautier pour sa direction de l'équipe pendant la majeure partie de ma thèse, et Rodolphe pour avoir repris le flambeau sur la fin. Merci à Laurent Marivaux pour tout ce que nos conversations m'ont inspiré**,** et pour ton soutien indéfectible**.** L'ambiance du couloir du

rez-de-chaussé, du côté de la route de Mende, doit beaucoup à la sympathie de Maëva, Romain, PierreO (merci pour ton encadrement en master, entre autres !), Rodolphe, Laurent, Narla (équipe Metatheria !), Monique, Fabrice, Catherine, et Renaud. Merci à vous pour votre gentillesse ! Et pour toutes les pauses déjeuner partagées, y compris avec ceux que je n'ai pas cité ici.

Je remercie chaleureusement Dominique Vidalenc pour son accueil dans sa collection privée. Merci à vous ainsi qu'à Dominique Téodori pour votre générosité, qui a permis de faire avancer cette thèse. Merci à Xavier Valentin, Géraldine Garcia et Olivier Jansen de l'Université de Poitiers pour leur collaboration lors des fouilles au Théron. Merci à Thomas Lehmann pour les discussions que nous avons pu avoir à propos du matériel de Messel.

Merci à Bernard Marandat pour nos nombreux échanges lors de tes visites, et l'engouement constant que tu as manifesté pour l'avancement de mes recherches. Ta connaissance poussée des faunes de l'Éocène et tes encouragements ont sensiblement contribué à ce travail ! Mes sincères remerciements à Sylvie Agret pour être régulièrement venue prendre de mes nouvelles, toujours avec le sourire, même en dehors de mes longues sessions de mesures. Merci à Pierre-Henri Fabre pour m'avoir initié au monitorat en début de thèse. Merci à Augustin pour son travail durant son stage de licence.

J'ai eu la chance d'être colocataire de bureau un temps avec Jacob Maugoust, dont le franc-parler et la propension pour les petites provocations ne s'oublient pas. Merci d'avoir été là durant mes premiers mois de thèse. Merci ensuite à Moritz Dirnberger d'avoir été quelqu'un de si agréable et de m'avoir supporté (dans les deux sens du terme) ces dernières années au bureau. J'ai une pensée particulière pour Léa Da Cunha et Félix Nesme, car nous avons commencé nos thèses la même année. Merci à vous deux et à Romain Weppe pour les longues mais pertinentes discussions scientifiques (et moins scientifiques !) que nous avons pu avoir. Un grand merci à Alexandre, Céline, Alexis, Mehdi, Arthur, Narla, Alba, Abdessamad, plus récemment Lorenzo et Hugo, plus anciennement Manon et Quentin, pour l'esprit de camaraderie que vous avez fait et continuez de faire vivre. Sans oublier les collègues de Baillarguet, c'est-à-dire Alicia, Kenji, Bryan, Alexandre, Charlotte et Maxime pour m'avoir permis de changer d'air de temps en temps !

Au-delà de cette thèse, je remercie toute ma famille, y compris ceux qui s'y sont greffés au fil du temps (je pense notamment à Viviane, Georges et Claudio), pour leur soutien. En particulier, merci à mes parents d'avoir toujours donné le meilleur d'eux-mêmes et de m'avoir constamment soutenu, ainsi qu'à Orane pour tout ce que nous partageons. C'est grâce à vous trois que j'en suis là.

Mes derniers mots de remerciement sont dédiés à ma compagne, Natasha. Ils ne seront sans doute que peu de choses, comparés à tout ce que tu m'as apporté personnellement et à combien tu m'as fait grandir au cours des huit dernières années. Merci pour ton épaulement inconditionnel et quotidien. Et surtout, merci pour tout ton amour.

Sommaire

Introduction générale 1

1. Généralités sur l'histoire évolutive des Metatheria 1
2. Les métathériens européens du Cénozoïque 3
3. Particularités des molaires des métathériens : impacts sur la compréhension de l'évolution du groupe 6
4. Contexte : les changements climatiques de l'Éocène inférieur 9
5. Objectifs et plan de thèse 11
1. Objectifs 11
2. Plan 14

Matériel et méthodes 17

1. Matériel 17
2. Biochronologie mammalienne et datations 18
3. Localités fossilifères étudiées 19

Partie 1. Reconstruction des relations inter- et intraclades des Peradectidae, une famille clé dans l'histoire évolutive des Metatheria : apport de la caractérisation morphologique des taxons européens **..... 22**

Chapitre 1. Taxonomie et histoire évolutive des Peradectidae : nouvelles données de l'Éocène inférieur de la France **..... 23**

Taxonomy and evolutionary history of peradectids (Metatheria): New data from the early Eocene of France (Manuscrit 1) 24
Introduction 24
Materials and methods 25
Provenance of the specimens 25
Ages of the localities 26
Dental nomenclature 28
Orientation of molariform teeth for descriptions and measurements 29
Evaluation of the heights of stylar cusps 30
High-resolution x-ray microtomography 31
Intrafamilial phylogenetic analysis 31
Abbreviations 32
Systematic paleontology 32
Peradectes crocheti sp. nov. 33
Peradectes louisi Crochet, 1979. 46
Peradectes cf. *louisi* 52
Peradectes russelli Crochet, 1979 52
Results 55
Quantitative comparisons 55
Intrafamilial phylogenetic analysis 58
Discussion 60
Characters and spatiotemporal distribution of the earliest European peradectid species, *Peradectes crocheti* sp. nov. 60

Phylogenetic relationships between late Paleocene – middle Eocene peradectids 64
Diagnostic characters and taxonomic status of the middle early Eocene European peradectids, *Peradectes louisi* and *Peradectes russelli* 66
Revision of putative occurrences of typical MP8 + 9 and ~MP8 + 9 peradectids in MP10 and ~MP10 69
Conclusion 70
References 71
Online Resources 77

3D models related to the publication: Taxonomy and evolutionary history of peradectids (Metatheria): new data from the early Eocene of France. 96
Introduction 96
Methods 96
Acknowledgements 97
Bibliography 97

Chapitre 2. Taxonomie des nouveaux péradectidés européens de la fin de l'Éocène inférieur **..... 101**

Chapter 2. Taxonomy of new European peradectids from the late early Eocene **..... 101**
Peradectes sp. nov. 1 101
Peradectes sp. nov. 2 105
Peradectes sp. nov. 3 107
Peradectes sp. indet. 111
Semilandmark-based geometric morphometric analysis 113
Conclusion 115
References 115

Chapitre 3. Une histoire évolutive complète des Peradectidae (Metatheria) révélée par un nouveau cadre phylogénétique basé sur la morphologie dentaire **..... 118**

A comprehensive evolutionary history of Peradectidae (Metatheria) revealed by a new phylogenetic framework based on dental evidence (Manuscrit 2) 120
Introduction 121
Materials and methods 123
Taxa and characters of the initial set of phylogenetic analyses 123
Preliminary identification of correlations between dental characters 125
Phylogenetic reconstruction procedures 127
Subsequent phylogenetic analyses 129
Results of phylogenetic analyses 131
Branching sequence of Mesozoic marsupialiforms – "Boreometatheria" 131
Cenozoic marsupialiform clade - Notometatheria 133
Peradectidae, Peradectinae, and Peradectini 134
"Herpetotheriidae" and Marsupialia clade 136
Discussion 138
The rise of Notometatheria after the K-Pg mass extinction 138

Fewer marsupialiform lineages than expected crossed the K-Pg boundary: macroevolutionary implications 138
A phylogenetic definition of Notometatheria, the Cenozoic marsupialiform clade 139
A comprehensive evolutionary history of unequivocal peradectids 142
Position and origin of Peradectidae 142
Phylogenetic definition of Peradectidae: implication for their taxonomic content and morphological characteristation 143
Early stages of peradectid evolution during the Paleocene 145
Reassessement of "*Peradectes*" based on a phylogenetic systematics context 146
Diversity dynamics and dispersal in unequivocal peradectids 147
Taxonomic status of Gondwanan and Asian putative peradectids: were there peradectids or close relatives outside North America and Europe? Palaeobiogeographic implications 148
Paleocene-Eocene presumed peradectids from South America: peradectid synapomorphies matter 148
New insights on the disputed nature and affinities of the African taxon *Kasserinotherium* 152
Upper molars of Oligo-Miocene Asian "peradectids" 153
Anatoliadelphyidae: affinities with peradectids or Gondwanan metatherians ? A third hypothesis 154
Conclusion 155
References 156
Supplemental materials 170

Partie 2. Nouvelles données sur les premiers Herpetotheriidae européens **..... 221**

Chapitre 4. Le premier métathérien du Paléocène d'Europe et plus ancien herpétothériidé avéré **..... 222**

The first metatherian mammal from the Paleocene of Europe and oldest unequivocal herpetotheriid (Manuscrit 3) 223
Introduction 224
Materials and methods 225
Systematic palaeontology 226
gen. and sp. nov. 227
Discussion 233
References 235

Chapitre 5. Réflexions sur l'évolution de la morphologie dentaire chez les premiers Peratheriinae, à travers le cas des espèces de relativement grande taille **..... 240**

Dental morphology evolution in early peratheriines, including a new morphologically cryptic species and findings on the largest early Eocene European metatherian (Manuscrit 4) 242
Introduction 242
Institutional and locality abbreviations / Other abbreviations 244
Ages of the localities 244
Materials and methods 244
Provenance of the specimens 244

High-resolution x-ray microtomography 244
Dental anatomy and measurements 245
Quantitative analysis based on isolated lower molars 246
Systematic palaeontology 247
Peratherium musivum sp. nov. 247
Peratherium cf. *musivum* sp. nov. 252
Peratherium maximum (Crochet, 1979) comb. nov. 254
Results 257
Comparisons of upper molar length and width measurement ratios between selected early peratheriine species 257
Quantitative analysis based on isolated lower molars of *Peratherium maximum* comb. nov. 257
Discussion 258
Reappraisal of the specific status of MP7-MP8 + 9 interval 'larger' peratheriines: phylogenetic, biochronologic, and palaeobiogeographic implications 258
Investigating significant dental characters: is *Amphiperatherium* likely to be represented in the earliest phases of Peratheriinae evolution? 260
Conclusions 263
References 264
Supplemental materials 267
Addendum 272
3D models related to the publication..... 273

Chapitre 6. Révision systématique des Peratheriinae de l'Éocène inférieur **..... 277**

1. Taxonomie des Peratheriinae de l'Éocène inférieur précoce (MP7) à moyen (MP8+9) 277
A. *Peratherium constans* vs *Peratherium matronense* : évolution des premiers petits pérathériinés de l'Éocène inférieur 277
Paléontologie systématique 277
Peratherium constans Teilhard de Chardin, 1927 278
Peratherium matronense Crochet, 1979 289
Comparaisons de la taille des spécimens 302
Analyse de forme des contours des molaires supérieures par morphométrie géométrique 305
B. Complément à l'étude des pérathériinés de grande taille de l'Éocène inférieur 309
Peratherium maximum (Crochet, 1979) 309
aff. *Peratherium maximum* 315
2. Taxonomie des Peratheriinae de l'Éocène inférieur tardif (MP10 à MP10-11) 318
A. Le métathérien des localités ~MP10 du Sud de la France 318
Peratherium monspeliense Crochet, 1979 318
cf. *Peratherium monspeliense* 322
B. Les taxons cryptiques de grande taille de l'EECO 324
Peratherium sp. nov. 1 324
cf. *Peratherium* sp. nov. 1 328
cf. *Peratherium maximum* 328
C. Une nouvelle espèce de pérathériiné abondante de Prémontré (~MP10) 330
Peratherium sp. nov. 2 330
D. La dernière espèce de pérathériiné connue de l'Éocène inférieur (MP10-11) 336
Peratherium sp. nov. 3 337

Conclusion générale et perspectives 342

1. Absence d'espèces panchroniques lors de l'Éocène inférieur 342
2. Corrélations entre les réchauffements climatiques de l'Éocène inférieur et les évènements de l'histoire évolutive des métathériens européens 342
3. Dynamiques évolutives liées aux tailles des métathériens européens 345
4. Relations phylogénétiques intrafamiliales et tendances évolutives 346
5. Des familles endémiques à l'hémisphère Nord 348
6. Perspectives – Les métathériens de la transition Yprésien – Lutétien de Messel 349

Références bibliographiques 350

Annexes 359

A revision of the late early Eocene mammal faunas from Mas de Gimel and Naples (Montpellier, Southern France) and the description of a new theridomorph rodent 376

Résumé / Abstract..... 412

Introduction générale

1. Généralités sur l'histoire évolutive des Metatheria

Les métathériens comprennent l'ensemble des mammifères plus apparentés aux marsupiaux qu'aux placentaires. Les usages des termes « métathérien(s) » et « marsupial/marsupiaux » sont réservés, respectivement, aux Metatheria et aux Marsupialia tout au long de ce travail. Les marsupiaux actuels sont typiquement distingués des monotrèmes et des placentaires par leur stratégie de reproduction, impliquant le développement post-natal des juvéniles à l'état larvaire au sein du marsupium (la poche marsupiale) (Edwards et Deakin 2012). Les marsupiaux (groupe couronne) sont moins diversifiés que les placentaires et sont quasi-exclusivement restreints à l'Amérique du Sud, et à l'Australasie (Sánchez-Villagra et al. 2013), l'unique exception étant l'opossum de Virginie en Amérique du Nord. La formule dentaire des Metatheria leur est propre, elle comporte notamment trois prémolaires supérieures et inférieures, et quatre molaires supérieures et inférieures, à l'inverse des Eutheria (Figure 1A). La première dent de la série de dents molariformes définitives des Metatheria (classiquement M1/m1) a été identifiée comme homologue à la dP5/dp5 des euthériens (Figure 1B ; O'Leary et al. 2013), mais cette hypothèse n'est pas appliquée ici.

Les premiers métathériens avérés et les plus basaux appartiennent aux Deltatheroida (Figure 2B) et proviennent de l'Albien (Crétacé inférieur) d'Amérique du Nord (~110 Ma ; Davis et al. 2008), contrairement aux mammifères euthériens, qui sont d'abord apparus en Asie (Figure 2A). Le taxon asiatique *Sinodelphys* Luo et al., 2003, considéré depuis sa publication comme le plus ancien métathérien, a récemment été réinterprété comme un euthérien (Bi et al. 2018 ; Figure 2A). Vullo et al. (2009) ont proposé le nom Marsupialiformes pour le clade regroupant les métathériens non-deltathéroïdiens (Figure 2A), correspondant traditionnellement à la définition inclusive de « Marsupialia » (e.g., Kielan-Jaworowska et al. 2004), un clade soutenu par de nombreuses analyses phylogénétiques (e.g. Ni et al. 2016, voir aussi Beck 2023). La classification des marsupialiformes fossiles crétacés à éocènes est complexe : aucun taxon de haut rang (i.e., suprafamilial) ne regroupe formellement des familles de l'hémisphère Nord (= Laurasie) (Eldridge et al. 2019 : tab. 1).

Les métathériens n'apparaissent dans le registre fossile de l'hémisphère sud qu'à partir du Paléocène précoce, juste après la limite Crétacé-Paléogène (Goin et al. 2006). Contrairement à l'actuel, l'essentiel de la diversité taxonomique des Metatheria était localisée en Amérique du Nord au Crétacé (Williamson et al. 2014 ; voir aussi Figure 2A). Plusieurs représentants, dont certains appartenaient à des familles bien documentées sur ce continent, avaient déjà atteint (probablement secondairement et à plusieurs reprises) l'Europe (Martin et al. 2005 ; Vullo et al. 2009, 2020) et l'Asie (e.g., Kielan-Jaworowska 1975 ; Szalay et Trofimov 1996 ; Averianov et al. 2010 ; Gao et al. 2024). À la fin du Crétacé, la richesse taxonomique

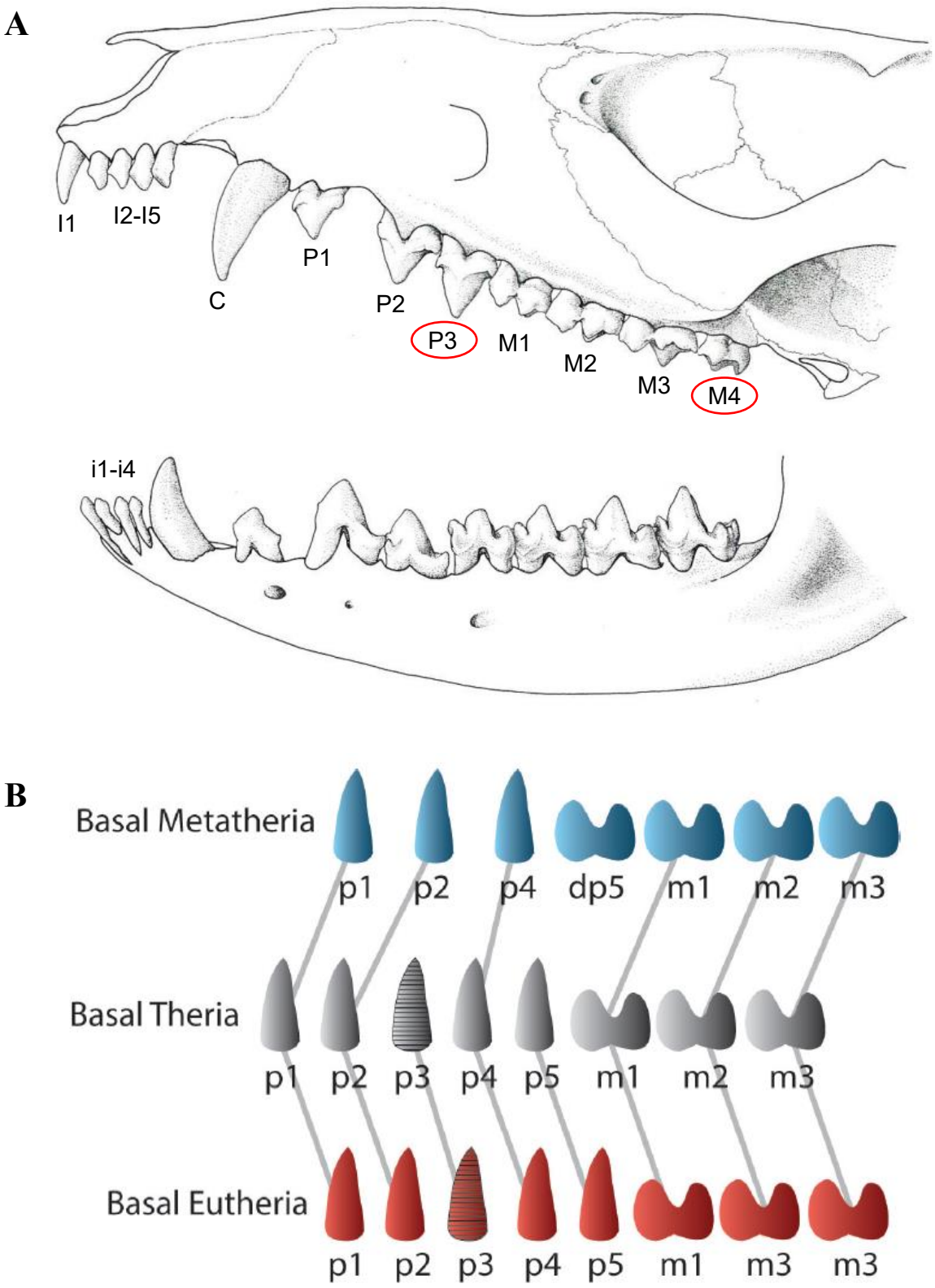

Figure 1. **A**. Noms des loci dentaires classiquement privilégiés chez les métathériens, sur une représentation d'un crâne de l'espèce actuelle *Philander opossum* (Didelphidae). Les trois dents prémolariformes définitives sont nommées P1-P3 / p1-p3, les quatre dents molariformes définitives sont nommées M1-M4 / m1-m4. Dessin modifié d'après Hershkovitz (1997). **B**. Hypothèse d'homologies entre les dents jugales des métathériens, thériens et euthériens basaux, proposée par O'Leary et al. (2013). Illustration de Williamson et al. (2014).

des métathériens en Amérique du Nord équivalait au moins celle des euthériens (Wilson 2014), et la diversité de leurs régimes alimentaires était plus importante que chez ces derniers (Brannick et al. 2023). Cependant, ils ont été profondément affectés sur ces deux plans par la crise Crétacé – Paléogène (Wilson 2014 ; Beck 2023). Seuls des taxons de petite taille et à la denture peu spécialisée (e.g., Ni et al. 2016) sont ensuite connus en Laurasie. La paléobiogéographie des métathériens s'est complexifiée à partir de l'Éocène inférieur : dans les deux hémisphères, des évènements de dispersion vers l'est ont eu lieu, de l'Amérique du Sud à l'Australie en passant par l'Antarctique d'une part (Beck 2012), et de l'Amérique du Nord à l'Europe d'autre part (Hooker 2015). Dans le dernier cas de figure, les deux familles impliquées sont les Herpetotheriidae et Peradectidae, étudiés ci-après.

2. Les métathériens européens du Cénozoïque

Le premier « marsupial » européen connu, *Peratherium cuvieri* (Fisher, 1829), d'abord rapproché des sarigues américaines, a été décrit par Cuvier (1804) dans le but d'illustrer la « loi de corrélation des organes » : une denture « didelphidienne » (Figure 3A) avec notamment quatre molaires supérieures et inférieures (Figure 3B) contre trois chez les mammifères placentaires implique la présence d'os épipubiens ayant pu porter la poche marsupiale (Figure 3A). Aymard (1850) a créé le genre *Peratherium* pour différencier tous les nouveaux fossiles européens décrits du genre américain actuel *Didelphis*. Un second genre, *Amphiperatherium*, a été reconnu par Filhol (1879), et regroupe selon lui les espèces dont les molaires inférieures sont de taille similaire de la première à la quatrième. Cependant, jusqu'à la fin du XXe siècle, ce point de vue n'a globalement pas été suivi (e.g. Depéret et Douxami 1902 ; von Koenigswald 1970). En parallèle en Amérique du Nord, un certain nombre d'espèces éocènes ont d'abord également été rapprochées de *Peratherium* (e.g., Simpson 1928), mais ont été finalement attribuées à *Herpetotherium* (e.g., Fox 1983 ; Korth 2008 ; Figure 4B), un genre absent en Europe.

La multiplication du nombre d'espèces de *Peratherium* en Europe au fil des travaux (e.g. Lavocat 1951) a conduit Crochet (1969) à entamer une révision du genre, focalisée sur les taxons des phosporites du Quercy dans un premier temps. Ce travail a ensuite été étendu à l'ensemble des « marsupiaux » européens du Cénozoïque (Crochet 1977, 1979, 1980). Parmi les principales contributions de cette première révision systématique, sont à retenir (i) la réhabilitation et redéfinition complète d'*Amphiperatherium*, formant avec *Peratherium* les Peratheriinae (sensu Ladevèze et al. 2020 ; Figure 4B) et avec le précédent et *Herpetotherium* les Herpetotheriidae (e.g., Case et al. 2005 ; = « Didelphini » sensu Crochet 1980) et (ii) la reconnaissance d'un troisième genre et d'une deuxième famille, *Peradectes* Matthew & Granger, 1921, parmi les Peradectidae (= « Peradectini » sensu Crochet 1980) dans l'Éocène inférieur d'Europe (jusqu'alors restreint à l'Amérique du Nord à la même période). Par addition des résultats d'études postérieures aux travaux de J.Y. Crochet (Kurz 2007 ; Ladevèze et al. 2012 ; Smith et Smith 2013), deux familles, quatre genres, et 26 espèces de métathériens cénozoïques européens, dont seulement 10

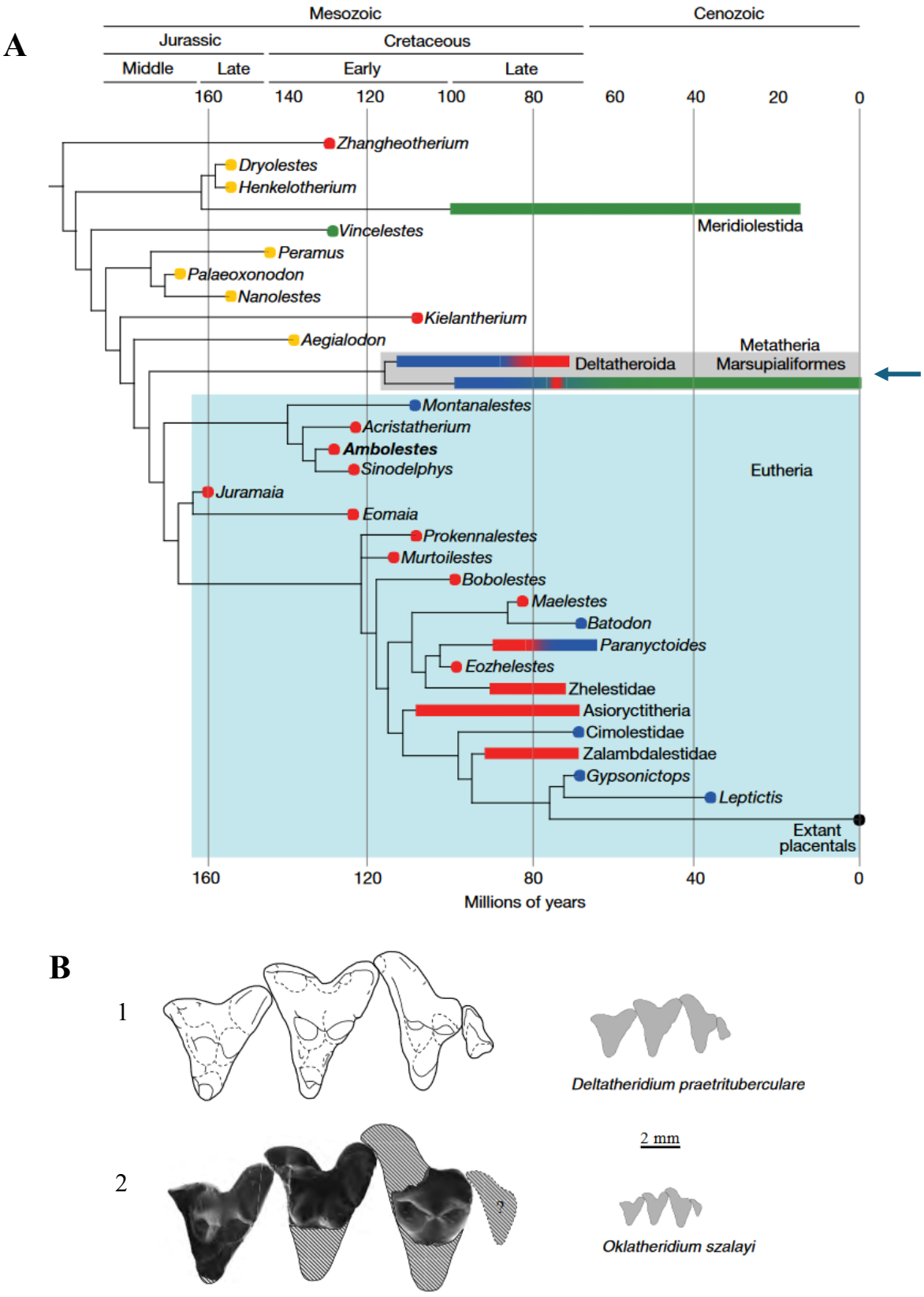

Figure 2. Position phylogénétique des Metatheria (Deltatheroida + Marsupialiformes) au sein des Trechnotheria. bleu, Amérique du Nord ; jaune, Europe ; rouge, Asie ; vert, Amérique du Sud. Modifié d'après Bi et al. (2018). **B**. Exemple d'espèces appartenant aux métathériens les plus basaux : les Deltatheroida. Parmi eux, *Oklatheridium* (B.2) est l'un des deux plus anciens métathériens avérés connus. Modifié d'après Davis et al. (2008).

retrouvées dans l'Éocène inférieur, étaient valides en l'état des connaissances précédent le présent travail de thèse (Tableau 1).

Plusieurs espèces de Peratheriinae semblent panchroniques (Crochet 1980), comme chez les Herpetotheriidae d'Amérique du Nord (= Herpetotheriinae sensu Ladevèze et al. 2020) depuis leur dernière révision systématique (Krishtalka et Stucky 1983). Le genre *Peradectes* apparaît limité à l'Éocène inférieur en Europe (mais voir Morlo et al. 2004). En revanche, les extensions temporelles de *Peratherium* et *Amphiperatherium* s'étendent de l'Éocène inférieur à l'Oligocène supérieur et au Miocène inférieur, respectivement (Crochet 1980). L'espèce-type de *Peratherium* est oligocène et celle d'*Amphiperatherium* est miocène (Tableau 1). A priori, les deux familles sont aussi caractérisées par une distribution paléobiogéographique large : les Peradectidae/Herpetotheriidae auraient été présents sur tous les continents, excepté en Australasie et aux pôles (e.g., Crochet et al. 2007 : fig. 4 ; Muizon et Ladevèze 2020 ; Crespo et Goin 2021 ; Carneiro et al. 2024). Des squelettes complets de Messel (Allemagne, début de l'Éocène moyen) attribués à des péradectidés putatifs et à des herpétothériidés montrent à partir d'arguments postcrâniens (la morphologie de la queue et de l'astragale notamment) que les premiers étaient sûrement plus arboricoles que les seconds (Figure 4A ; Kurz 2005 ; Rose 2012).

De nombreuses données relatives aux histoires évolutives des métathériens cénozoïques de Laurasie doivent être étayées. Ainsi, ceux-ci ne forment peut-être pas des groupes naturels (Williamson et al. 2012, 2014 ; Ladevèze et al. 2020). Les hypothèses d'origines nord-américaines et d'arrivées asynchrones en Europe des deux familles au début de l'Éocène inférieur (Hooker 1998, 2015), n'ont jamais été testées formellement. Les origines profondes des Peradectidae/Herpetotheriidae, possiblement au Crétacé (Fox 1983 ; Case et al. 2005 ; Williamson et al. 2012), sont aussi mal comprises. Les Peradectidae pourraient être des métathériens souches, et les herpétothériidés des marsupiaux souches (Sánchez-Villagra et al. 2007 ; Ladevèze et al. 2020). Des analyses phylogénétiques menées à partir des caractères dentaires et de représentants nord-américains ont montré une faible résolution des relations obtenues, probablement due à un faible nombre de caractères disponibles et à un excès d'homoplasies (Williamson et al. 2012, 2014). Aucune analyse phylogénétique n'a intégré de taxons européens cénozoïques connus seulement par des dents (Ladevèze et al. 2020). Ainsi, les premiers représentants des Peradectidae/Herpetotheriidae en Europe n'ont jamais été étudiés dans un cadre phylogénétique, ce qui serait pourtant crucial pour en comprendre les premières cladogenèses (e.g., Marivaux et al. 2004 pour les rongeurs). Enfin, les travaux récents ayant décrit ou rapporté des spécimens de métathériens européens de l'Éocène inférieur sont rares (Hooker 2010, 2020 ; Smith et al. 2011 ; Marandat et al. 2012 ; Ladevèze et al. 2012 ; Smith et Smith 2013), et il s'agit surtout de molaires isolées.

A

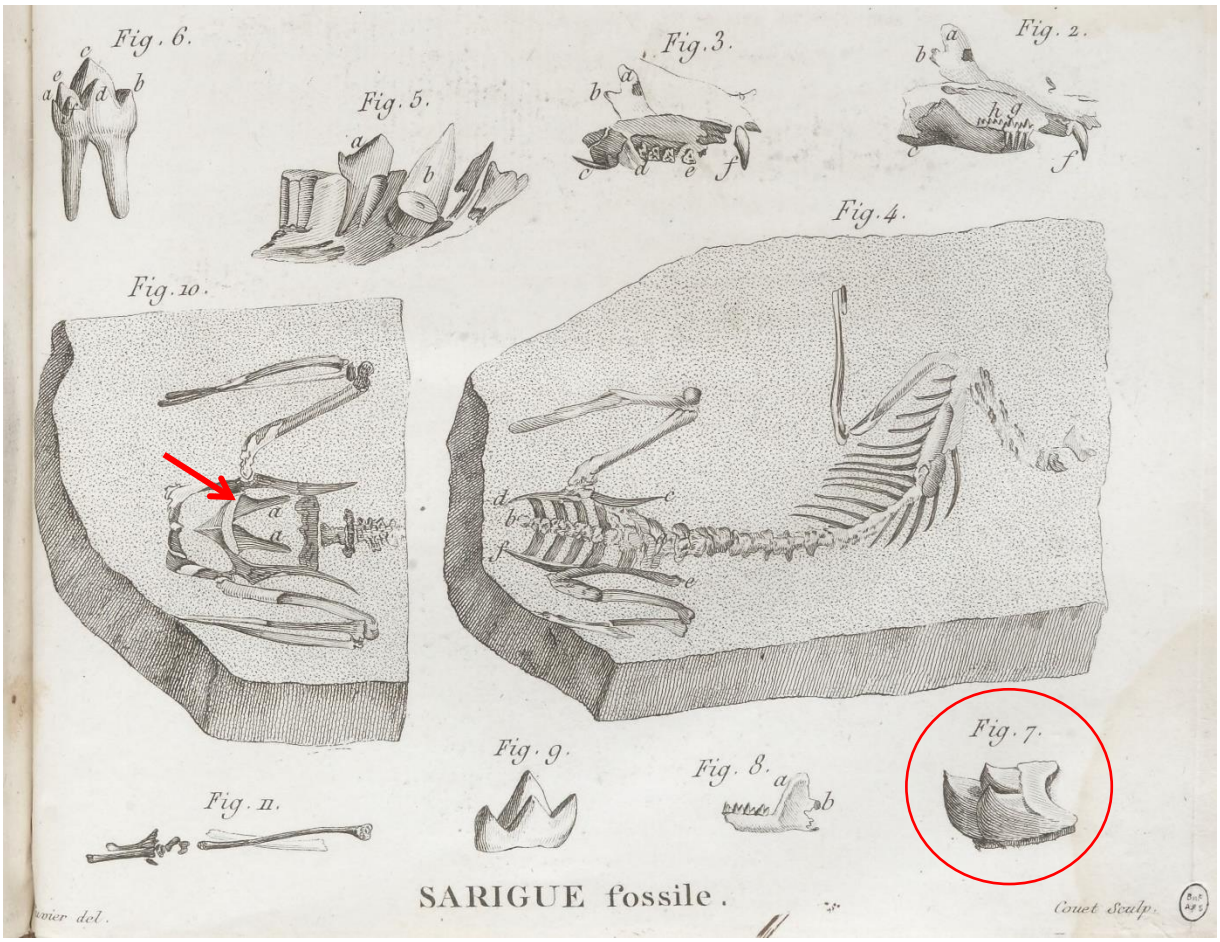

B

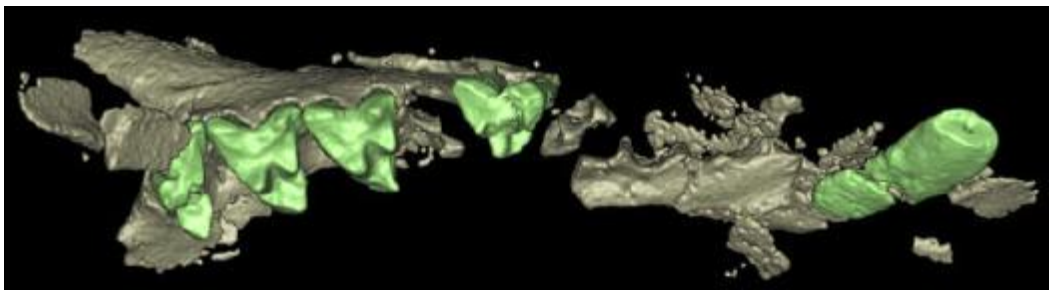

Figure 3. La « sarigue » des gypses de Montmartre (Éocène supérieur, Bassin de Paris) étudiée par G. Cuvier. **A**. Dessin du bloc de gypse renfermant le squelette postcrânien de *Peratherium cuvieri* (Fisher, 1829) dégagée par G. Cuvier. La morphologie de la molaire supérieure aussi figurée est entourée, et l'un des os épipubiens est indiqué par une flèche. Modifié d'après Cuvier (1804). **B**. Modèle 3D (non à l'échelle) de la denture supérieure du spécimen de *Peratherium cuvieri* préservant M1-M4, étudié par G. Cuvier (GY679b). Modifié d'après Selva et Ladevèze (2017).

3. Particularités des molaires des métathériens : impacts sur la compréhension de l'évolution du groupe

Seule la dernière prémolaire déciduale (dP3/dp3) des métathériens est remplacée. Certains taxons diffèrent quant à leur séquence d'éruption dentaire (Forasiepi et Sánchez-Villagra 2014), mais la diversité des patrons d'éruption dentaire chez les marsupiaux actuels ne semble pas être reflétée dans les patrons adultes des dents minéralisées éruptées (McKay et al. 2023). Un dimorphisme sexuel, le plus souvent

caractérisé par la plus grande taille des individus mâles, est connu chez les espèces de marsupiaux actuels, dont un peu plus de la moitié des espèces de Didelphidae (e.g., Astúa 2010), avec possiblement des exceptions (e.g., Parés-Casanova 2024). Au cours de l'histoire évolutive des marsupialiformes, un dimorphisme sexuel associé à un mode de vie grégaire (différant des marsupiaux actuels sur ce dernier point) est apparus au moins une fois au début du Paléocène, chez *Pucadelphys* (Ladevèze et al. 2011). Les mâles et femelles d'une espèce de marsupialiforme donnée, fossile ou actuelle, ne diffèrent vraisemblablement pas par la taille de leurs molaires (Ladevèze et al. 2011 : données supplémentaires ; Chemisquy et al. 2015 ; Engelman et Croft 2016 : fig. 3 vs fig. 7). Magnus et Cáceres (2017) ont mis en évidence un dimorphisme sexuel à partir d'un échantillon important de m1s de didelphidés (130 spécimens femelles et 131 mâles), mais il n'a pas été évalué au sein d'une espèce donnée (ces 261 spécimens appartiennent à 37 espèces et 14 genres ; Magnus et Cáceres 2017 : tableau 1). En conséquence, même si un dimorphisme sexuel était présent chez les espèces de péradectidés et herpétothériidés, cela n'empêcherait probablement pas la possibilité de discrimination interspécifique à partir des dents molariformes. Chez les Didelphidae, les variations interspécifiques de la morphologie dentaire semblent mieux expliquées par l'héritage phylogénétique que par la taille et le régime alimentaire ou l'habitat (Chemisquy et al. 2015 ; Magnus et Cáceres 2017).

Les métathériens possèdent des cuspides stylaires sur le flanc labial des dents molariformes supérieures (Figures 5-6). Les critères permettant la reconnaissance de cuspides stylaires homologues entre les métathériens par l'intermédiaire de leurs positions relatives ont été formalisés par Clemens (1966) à partir de fossiles de divers taxons du Crétacé supérieur du Wyoming (USA). La ligne stylaire du plateau stylaire longeant le bord labial des molaires supérieures n'entrant pas en occlusion avec les molaires inférieures lors des cycles de mastications (Crompton et Hiimae 1970 ; Figure 6A), leur rôle pourrait consister à rediriger la nourriture vers les surfaces en occlusion ou assurer des perforations apicales (Crompton 1971 ; Davis 2011). Les cuspides stylaires des métathériens, et le plateau stylaire dans son ensemble seraient concernés par des variations morphologiques intraspécifiques prépondérantes y compris chez les taxons européens (Ladevèze et al. 2012 ; Wessels et al. 2024). Des études de développement dentaire montrent que les cuspides de petite taille des molaires peuvent évoluer rapidement, mais ont tendance à être plus homoplastiques que les autres (e.g., Jernvall et Jung 2000). Ainsi, même si des études se sont presque exclusivement focalisées sur l'utilisation des cuspides stylaires en plus de la taille et des proportions des spécimens pour résoudre des problèmes de taxonomie chez les métathériens cénozoïques d'Amérique du Nord (e.g., Korth 2015, 2018), peu de travaux sur les métathériens ont analysé les variations des tailles relatives des cuspides stylaires, en particulier chez les marsupiaux actuels (Figure 6C ; Hershkovitz 1997). De plus, aucune méthodologie standardisée n'a été définie pour évaluer les paramètres relatifs aux cuspides stylaires, les méthodes d'étude changeant parfois entre les auteurs (e.g., les orientations choisies du plateau stylaire diffèrent entre la Figure 6B et la Figure 6C).

Tableau 1. Liste et classification des espèces de métathériens présentes en Europe de l'Ouest durant le Cénozoïque. Les espèces connues dans l'Éocène inférieur sont signalées en gras. Les espèces types des genres sont signalées en rouge. Liste établie d'après Crochet (1980), Kurz (2007), Ladevèze et al. (2012, 2020), et Smith et Smith (2013).

Peradectidae
Peradectes Matthew & Granger, 1921
***Peradectes louisi* Crochet, 1979**
***Peradectes russelli* Crochet, 1979**
***Peradectes mutigniensis* Crochet, 1979**
Armintodelphys Krishtalka & Stucky, 1983
***Armintodelphys dufraingi* Smith & Smith, 2013**
Herpetotheriidae
Peratheriinae
Amphiperatherium Filhol, 1879
Amphiperatherium ambiguum (Filhol, 1877)
Amphiperatherium bastbergense Crochet, 1979
***Amphiperatherium bourdellense* Crochet, 1979**
Amphiperatherium exile (Gervais, 1848-52)
Amphiperatherium fontense Crochet, 1979
Amphiperatherium frequens (von Meyer, 1846)
***Amphiperatherium goethei* Crochet, 1979**
Amphiperatherium lamandini (Filhol, 1876)
***Amphiperatherium maximum* Crochet, 1979**
Amphiperatherium minutum (Aymard, 1846)
P*eratherium* Aymard, 1850
Peratherium antiquum (Blainville, 1840)
Peratherium bretouense Crochet, 1979
Peratherium cayluxi (Filhol, 1873)
***Peratherium constans* Teilhard de Chardin, 1927**
Peratherium cuvieri (Fisher, 1829)
Peratherium elegans (Aymard, 1846)
?*Peratherium giselense* Heller, 1936
Peratherium lavergnense Crochet, 1979
***Peratherium matronense* Crochet, 1979**
***Peratherium monspeliense* Crochet, 1979**
Peratherium perrierense Crochet, 1979
Peratherium sudrei Crochet, 1979

La morphologie des molaires chez la plupart des métathériens est relativement homogène, même entre taxons peu apparentés et/ou d'âges différents (Szalay 1993 ; Figure 5). Les dentures des taxons « généralistes » (= ressemblant superficiellement aux opossums) s'écartent peu du plan tribosphénique, c'est-à-dire que les acquisitions et/ou pertes de crêtes et cuspides, et les changements profonds de formes au sein des Metatheria sont rares (Figure 5), excepté chez les taxons plus spécialisés (e.g., Goin et al.

2003 ; Maga et Beck 2017 ; Métais et al. 2018). L'impossibilité de différencier plusieurs espèces d'herpétothériidés en se basant sur la morphologie de leurs molaires a été soulignée (Selva et Ladevèze 2017), en particulier pour ce qui est des premiers représentants (Hooker et al. 2008). Des modifications morphologiques graduelles entre séries de molaires semblent en effet exister (e.g., Crochet 1980 ; Korth 2015). A fortiori, la difficulté de résolution des relations phylogénétiques des métathériens à denture généraliste exclusivement à partir des dents est bien établie dans la littérature (e.g., Szalay 1993 ; Williamson et al. 2012). Ces constats soulignent la nécessité de mener des travaux étudiant l'évolution des caractères dentaires des métathériens dans des cadres chronologiques restreints, pour pouvoir comprendre les transitions subtiles possibles d'états de caractères.

4. Contexte : les changements climatiques de l'Éocène inférieur

L'Éocène inférieur (Yprésien) est une période d'environ 8 Ma (~56-48 Ma) jalonnée de réchauffements climatiques majeurs. Le Maximum Thermique du Paléocène-Éocène (PETM), qui définit la base de l'Éocène, est associé à une forte excursion négative du $\delta^{13}C$ (Figure 7A). C'est un évènement mondial relativement bref (~ 250 000 ans) correspondant à une hausse des températures globales d'environ 4-5°C en milieu continental (Wing et al. 2005), et ayant profondément affecté les faunes de mammifères (e.g., Hooker 2000). En effet, le PETM coïncide avec de nombreux cas de nanisme (e.g., Rankin et al. 2015 ; D'Ambrosia et al. 2017 ; Gingerich et al. 2023), et surtout avec l'apparition brutale et la dispersion rapide dans tout l'hémisphère nord des ordres de mammifères « modernes » (Mammalian Dispersal Event, MDE ; e.g., Hooker 2015) : les primates, artiodactyles et périssodactyles (e.g., Smith et al. 2006 ; Boivin et al. 2018 ; Bronnert et al. 2018). Les voies de passages possibles entre continents aux hautes latitudes étaient alors sous un climat chaud et tropical (e.g., Eberle et Greenwood 2012). Pour parvenir en Europe, les métathériens ont probablement emprunté le pont transcontinental Groenland-Atlantique Nord (e.g., Hooker 2015), dit « route thuléenne », connectant l'Amérique du Nord et l'Europe au début de l'Éocène (Brikiatis 2014). Le PETM est suivi de deux réchauffements climatiques de moindre intensité, les ETMs (Maxima thermiques de l'Éocène) 2 et 3 (le PETM correspond à l'ETM1). Ces trois ETMs sont de bons équivalents au réchauffement climatique actuel par leur rapidité et leur état transitoire (e.g., Zachos et al. 2008). D'autres ETMs, de plus faible amplitude, sont connus dans la seconde partie de l'Yprésien. Ils se surimposent à l'Optimum Climatique de l'Éocène inférieur (EECO ; ~53-49 Ma ; Figure 7A ; Westerhold et al. 2018), qui est corrélé à la diversification des faunes de mammifères en Amérique du Nord (Woodburne et al. 2009). Les impacts potentiels de l'EECO sur les faunes de mammifères européennes sont peu connus à cause du manque de sections stratigraphiques fossilifères suffisamment continues et synchrones avec cet évènement.

Durant l'Éocène inférieur précoce (les premiers ETMs), les compositions fauniques au niveau générique apparaissent plus proches entre l'Amérique du Nord et l'Europe du Nord qu'entre l'Europe du Nord et

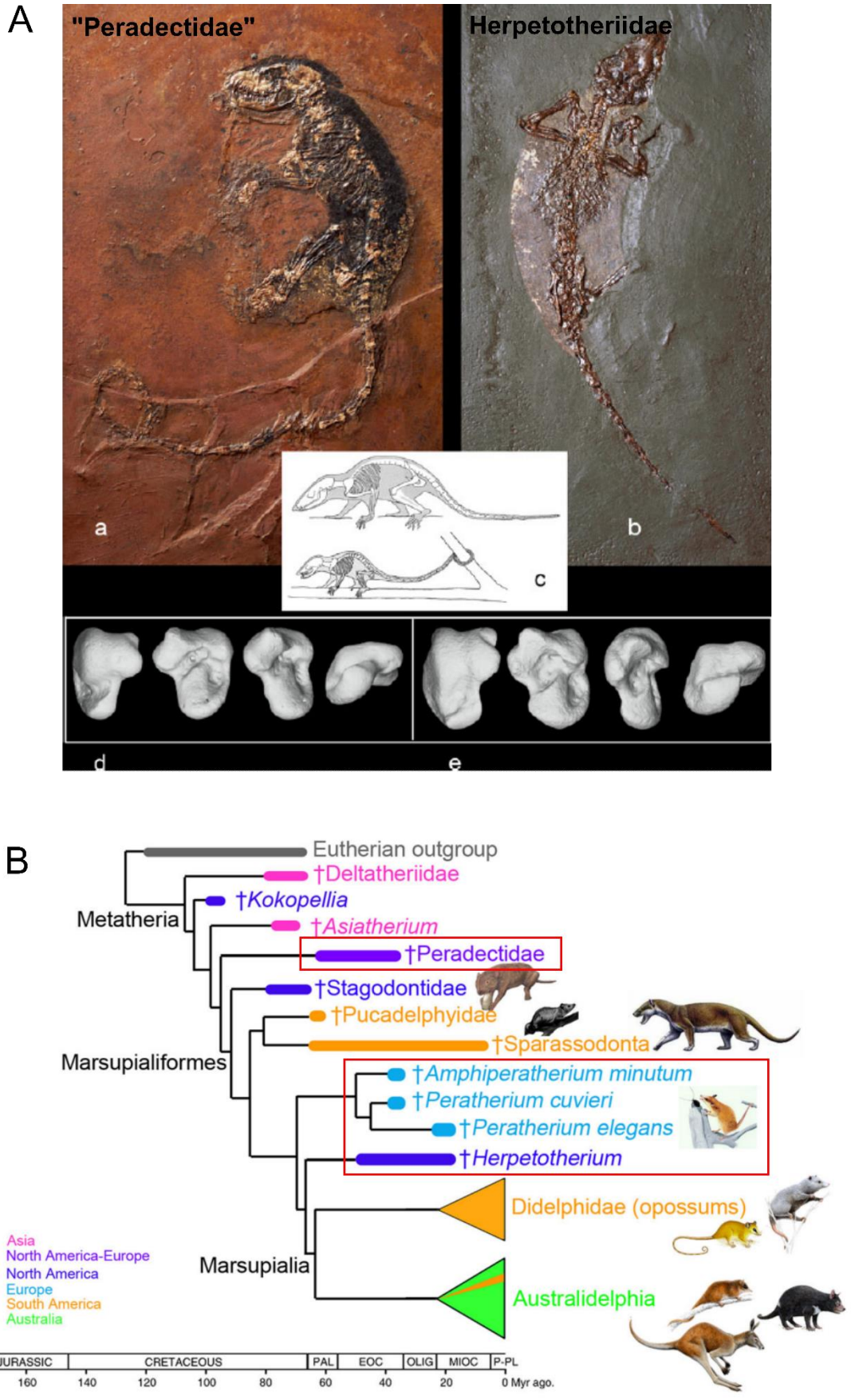

Figure 4. Peradectidae vs Herpetotheriidae. **A**. Comparaison de squelettes complets d'un « péradectidé » (sensu Morlo et al. 2004) et d'un herpétothériidé de Messel (Allemagne, Lutetien inférieur) et d'astragales du Wyoming (USA) attribués à ces deux familles. Modifié d'après Rose (2012). **B**. Positions phylogénétiques des Peradectidae et des Herpetotheriidae (*Amphiperatherium*, *Peratherium*, *Herpetotherium*) au sein des Metatheria d'après Ladevèze et al. (2020).

l'Europe du Sud (e.g., Marandat 1997 ; Smith 2000 ; Marandat et al. 2012). Des indices environnementaux discutés par Marandat et al. (2012) soutiennent aussi un clivage entre deux bioprovinces Nord/Sud en Europe à cette période, séparées par une barrière climatique plutôt que physique : la province mésogéenne serait la plus chaude et la moins humide des deux. Il est possible que cette barrière s'atténue légèrement après l'ETM2 (Noiret et al. 2016). Les faunes de mammifères semblent complètement s'homogénéiser vers l'Éocène inférieur moyen (e.g., Figure 7B). Les métathériens font a priori exception à ce schéma : la première espèce de pérathériiné, *Peratherium constans* (Ladevèze et al. 2012), semble connue à la fois au Nord et au Sud de l'Europe de l'Ouest contrairement à presque tous les autres mammifères (e.g., Marandat 1997 ; Boivin et al. 2018), alors que plusieurs espèces apparaissant plus tardivement sont restreintes au Nord (trois espèces de péradectidés appartenant à deux genres, et le pérathériiné *Amphiperatherium maximum*) ou au Sud (*Peratherium monspeliense*) notamment d'après Crochet (1980). Des subdivisions en deux provinces biogéographiques lors de l'Éocène inférieur ont aussi été proposées, au sein de l'Amérique du Nord au Wasatchien NALMA (début de l'Éocène inférieur ; Beard et Dawson 2009) et à plus large échelle au sein de l'Amérique du Sud dès l'Éocène inférieur (« royaume » holotropical vs austral ; e.g., Goin et al. 2016 : fig. 4.2 ; Beck 2017, 2023).

5. Objectifs et plan de thèse

1. Objectifs

Ce travail de thèse consiste en premier lieu en une révision exhaustive de la taxonomie des métathériens européens, par considération des faunes yprésiennes les mieux documentées. Depuis la révision fondatrice de Crochet (1979, 1980), prenant en compte l'ensemble du Cénozoïque, de nombreuses nouvelles localités fossilifères cruciales de l'Éocène inférieur ont été découvertes en France et ont livré une quantité importante de spécimens dont la plupart doivent être étudiés formellement (e.g., Godinot et al. 1987 ; Marandat 1986, 1991 ; Dégremont et al. 1985), l'âge de certaines localités s'est affiné notamment à partir de méthodes bio/chémostratigraphiques (e.g., Yans et al. 2014 ; Noiret et al. 2016 ; Steurbaut et al. 2016), et les variabilités morphologiques intra- et interspécifiques chez les métathériens ont été précisées grâce à de nouveaux fossiles (e.g., Ladevèze et al. 2011, 2012). En prenant pour exemple les taxons européens, il s'agit de tester si, comme le suggère l'état actuel des connaissances pour l'ensemble de leur registre fossile européen et nord-américain au niveau spécifique (Crochet 1980; Krishtalka et Stucky 1983), les herpétothériidés et péradectidés sont effectivement :

(i) majoritairement ubiquistes (dans les limites du continent propre à chaque espèce) et panchroniques, et

(ii) caractérisés par une faible diversité spécifique superposée à leur faible disparité morphologique potentielle (cas d'absence de diversité cryptique).

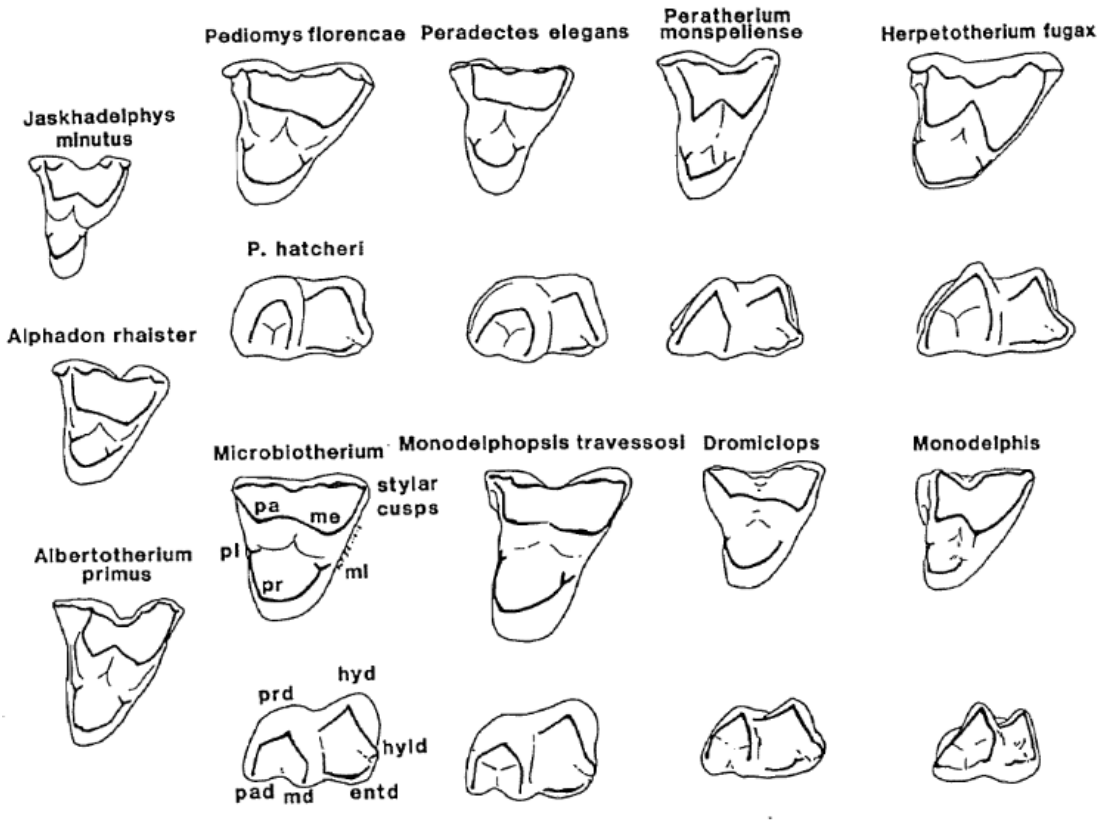

Figure 5. Représentations schématiques des morphologies de molaires supérieures et inférieures de taxons marsupialiformes sélectionnés. D'après Szalay (1993).

La résolution de ces points m'amènera à discuter :

a) l'existence ou non de dynamiques évolutives entre les faunes métathériennes du Nord et du Sud de l'Europe de l'Ouest, et

b) l'intérêt biochronologique potentiel de la caractérisation morphologique des métathériens européens.

Ce travail a largement bénéficié de l'imagerie 3D (par micro-tomographie à rayons X) pour l'illustration des spécimens, souvent des molaires isolées. Grâce à cela, l'une des bases de données les plus conséquentes à ce jour d'illustrations de la variation intra- et interspécifique dentaire chez des métathériens a sans doute été constituée. En effet, vu l'échantillonnage hétérogène caractérisant cette étude, c'est-à-dire un nombre conséquent de spécimens complets par locus dentaire et par espèce issus de certaines localités, contre un nombre extrêmement restreint de dents isolées souvent fragmentaires dans d'autres, la clarification de la variabilité intra-spécifique est primordiale et doit être mentionnée dans la plupart des descriptions. Il s'agit en effet de rechercher les caractères dentaires diagnostiques parmi les caractères variant le moins entre spécimens (e.g., Murphey et al. 2018 : 19). La distinction réalisée des différentes espèces passe donc par un effort soutenu de comparaisons morphologiques. La recherche d'un soutien à posteriori de certains des caractères dentaires identifiés comme diagnostiques

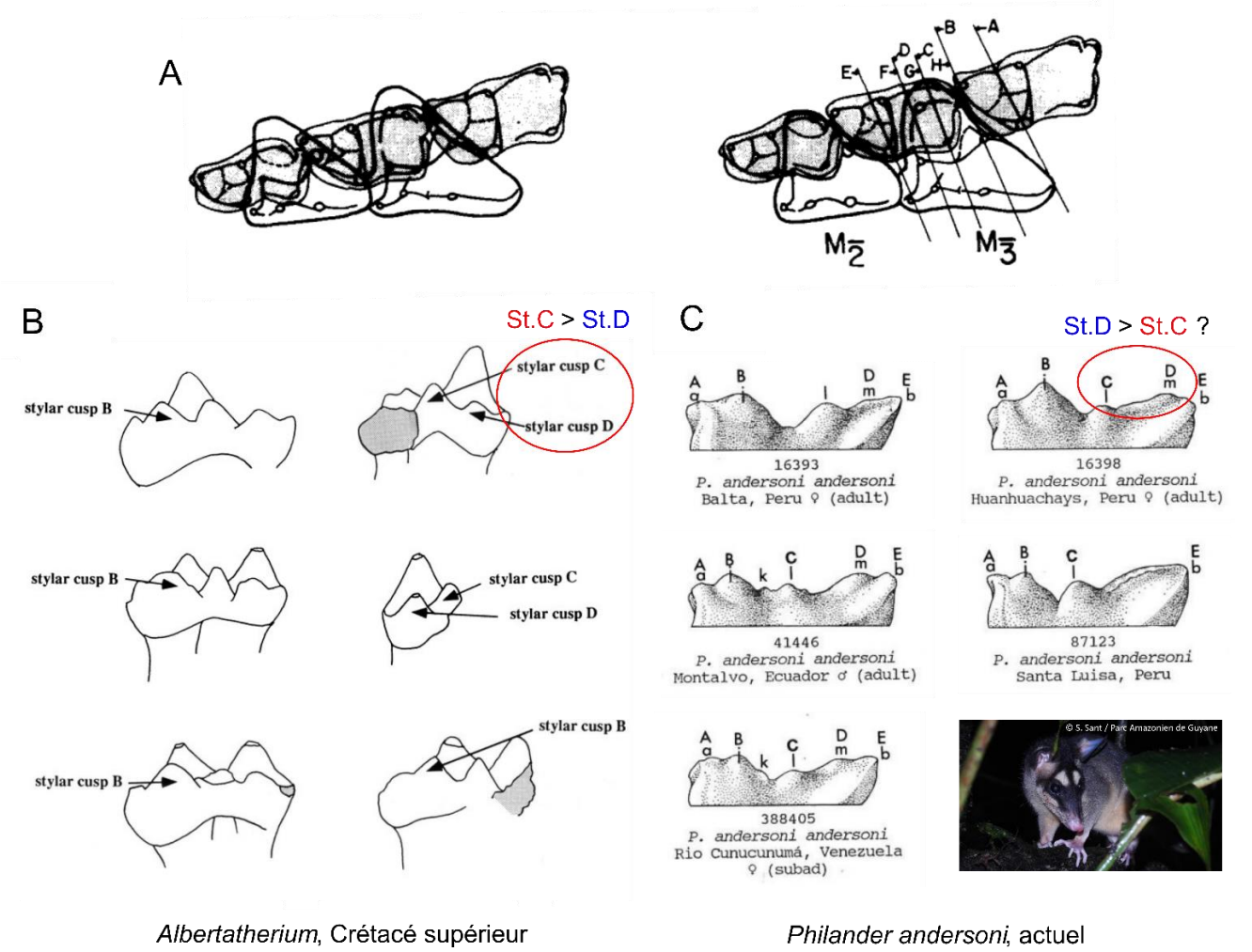

Figure 6. Illustration des cuspides stylaires des Metatheria durant les cycles de mastication (A) et exemple de variation intraspécifiques en taille et en forme dans différentes vues (B et C). **A**. Position des molaires supérieures par rapport aux molaires inférieures durant les cycles de mastication chez *Didelphis*, au début du contact entre dents (gauche) et lors de la phase de puissance (droite). Noter la position latérale des cuspides stylaires lors des cycles masticatoires. Schéma modifié d'après Crompton et Hiimae (1970). **B**. Molaires supérieures d'*Albertatherium primus* Fox, 1971 (Crétacé supérieur) en vue labiale. Modifié d'après Johanson (1994). **C**. Molaires supérieures de *Philander andersoni* (Osgood, 1913) en vue linguale. Modifié d'après Hershkovitz (1997).

et portant potentiellement un signal phylogénétique est menée via des approches quantitatives. Une telle démarche n'a jamais été employée jusqu'alors pour caractériser les métathériens cénozoïques de l'hémisphère nord. L'évolution au cours du temps de certains traits, de la richesse spécifique des faunes métathériennes, et les extensions temporelles nouvellement définies pour les espèces permettront d'envisager d'éventuelles corrélations de ces paramètres avec les importants changements climatiques (ponctuels ou longs) du début de l'Éocène.

La présence des deux genres de pérathériinés *Amphiperatherium* et *Peratherium* tout au long de l'Éocène inférieur telle qu'établie par Crochet (1977, 1979, 1980) doit être réévaluée (Ladevèze et al. 2012) dans un contexte de systématique phylogénétique. À cet égard, une compréhension poussée des premiers

stades de l'évolution des pérathériinés, en termes de caractères morphologiques dentaires, est visée, et sera étayée par un matériel abondant. Il en va de même pour le début de l'histoire évolutive floue des Peradectidae en Europe et l'existence de deux genres (*Peradectes* et *Armintodelphys*) au lieu d'un (*Peradectes*) sur ce continent, proposée par Smith et Smith (2013). L'identité au niveau générique des métathériens européens est donc à questionner au regard de données inédites.

Le nouveau contexte phylogénétique établi permettra également :

(i) de retracer les scénarios des arrivées des deux familles en Europe pour la première fois, et

(ii) ultimement, d'établir leurs positions phylogénétiques au sein des Marsupialiformes et leurs relations intra- et interfamiliales, en prenant en compte les limites des reconstructions phylogénétiques basées en grande partie sur les molaires isolées (Williamson et al. 2012).

2. Plan

Ce travail s'organise en deux parties principales. J'ai choisi de répondre aux objectifs ci-dessus d'abord en organisant le premier axe de recherche (Partie 1) autour de l'évolution des péradectidés. En effet, selon des analyses phylogénétiques récentes, les Peradectidae sont possiblement ancestraux par rapport aux Herpetotheriidae parmi les Metatheria (e.g., Figure 4 ; Engelman et al. 2020 ; Beck et al. 2022 ; Muizon et Ladevèze 2022). De plus, l'échantillonnage conduit pendant ma première année de thèse a permis de découvrir des fossiles relativement complets de péradectidés anciens (par rapport aux herpétothériidés du même âge) qui ont motivé le choix de cette famille pour débuter la révision des métathériens cénozoïques d'Europe.

La première sous-section (Chapitre 1 / Manuscrit 1) traite donc de l'histoire évolutive (dont l'origine) des péradectidés d'Europe à partir de matériel inédit et publié. Des points généraux concernant cette thèse, comme des mises à jour de la nomenclature dentaire, des méthodes de mesures, de l'utilisation des cuspides stylaires en systématique, et des différences de caractères dentaires Peradectidae/Herpetotheriidae, sont également développés. Le Chapitre 2 permet la description de plusieurs nouvelles espèces de péradectidés européens de l'EECO, et vient compléter le Chapitre 1 en achevant la révision systématique des péradectidés européens. Enfin, les connaissances accumulées sur la morphologie dentaire des péradectidés m'amènent à fonder un cadre phylogénétique spatiotemporellement large dans lequel leur histoire évolutive complète et leurs relations inter-familiales peuvent être discutées (Chapitre 3 / Manuscrit 2). Dans cette sous-section, la position phylogénétique des herpétothériidés au sein des Metatheria, notamment par rapport aux péradectidés et aux possibles herpétothériidés souches, est également explicitée.

Cela permet d'aborder le second axe de recherche (Partie 2) consacré aux représentants européens de cette dernière famille. La première sous-section (Chapitre 4 / Manuscrit 3) porte sur la découverte du

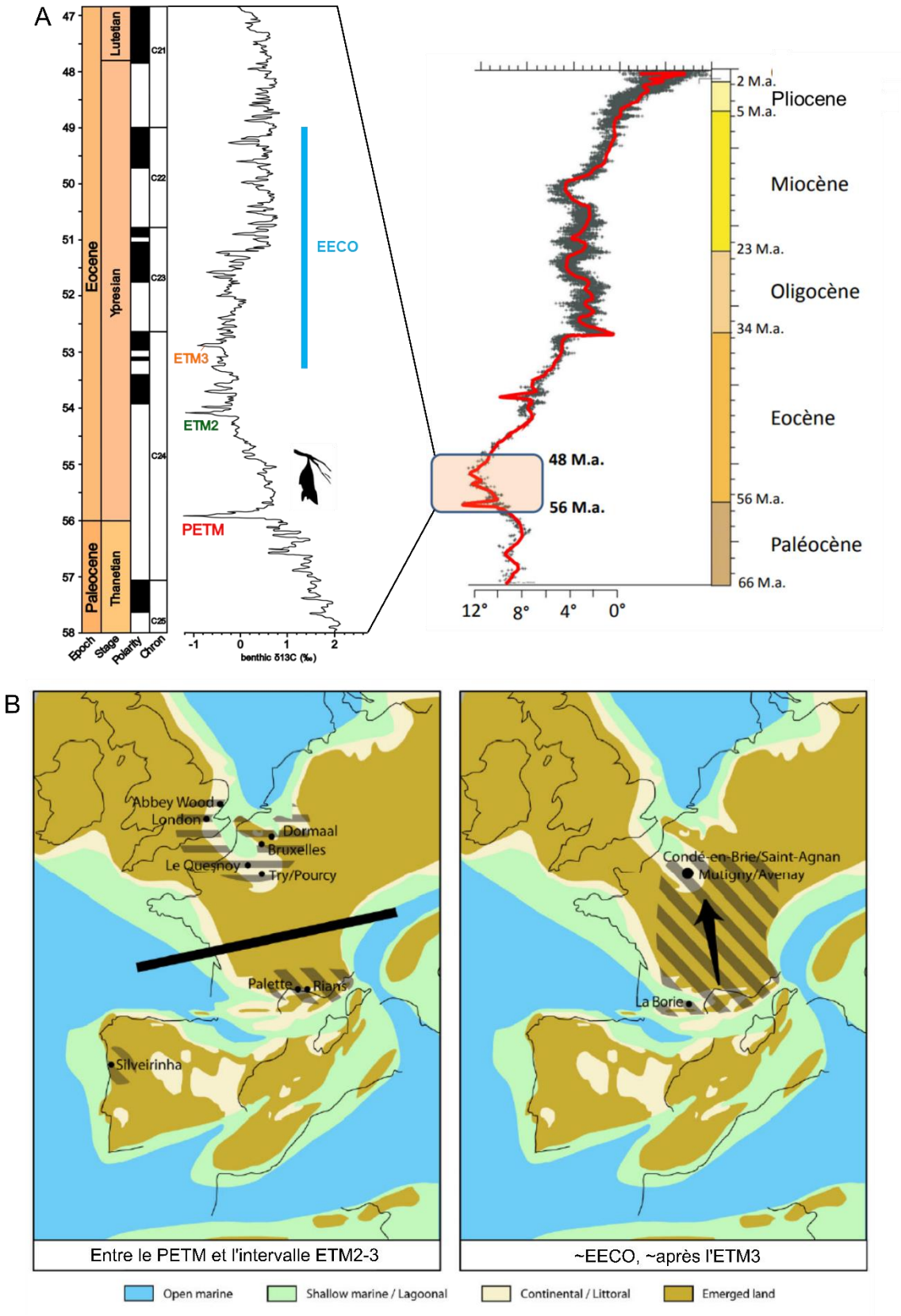

Figure 7. Les réchauffements climatiques intenses de l'Éocène inférieur. **A**. Courbe isotopique du carbone de la fin du Paléocène au début de l'Éocène moyen, corrélée aux évènements climatiques majeurs de l'Éocène inférieur. Adapté de Westerhold et al. (2018). L'intervalle de temps d'intérêt est positionné au sein d'une courbe des variations de température estimées lors du Cénozoïque. Adapté de Zachos et al. (2001). **B**. Représentation schématique de la barrière climatique entre les bioprovinces Nord/Sud au début de l'Éocène inférieur en Europe de l'Ouest (gauche). Les faunes de mammifères s'homogénéisent suite aux ETMs (droite). Modifié d'après Solé et al. (2014).

premier métathérien paléocène d'Europe et plus ancien herpétothériidé avéré. La révision exhaustive des herpétothériidés européens de l'Éocène inférieur est présentée dans les Chapitres 5 et 6. Dans le Chapitre 5 (Manuscrit 4) des réflexions sur l'évolution de la morphologie dentaire des premiers pérathériinés sont conduites à travers le cas des espèces de relativement grande taille apparaissant dans la première moitié de l'Éocène inférieur. Enfin, la caractérisation de toutes les espèces de pérathériinés de cette période est poursuivie dans le Chapitre 6. Ce découpage permet de dresser une image globale du début de l'évolution des métathériens cénozoïques d'Europe.

Références

Les références citées dans les parties Introduction, Matériel et méthodes, Chapitre 6, et Conclusion générale sont détaillées à la fin du manuscrit de thèse.

Matériel et méthodes

Des sections Matériel et méthodes sont présentées dans chacun des articles ou projets de manuscrits composant les chapitres de la thèse. La nomenclature dentaire mise à jour, les protocoles de mesures inédits, les analyses quantitatives, et les méthodes et paramètres des analyses phylogénétiques y sont notamment détaillés. Les cuspides stylaires des dents molariformes supérieures ont été identifiées à partir des définitions topologiques (positions relatives sur le plateau stylaire, notamment par rapport aux cuspides principales) proposées par Clemens (1966). Des points généraux concernant le matériel d'étude et les sites fossilifères sont abordés ci-dessous.

1. Matériel

La majorité du matériel décrit et illustré dans ce travail (surtout du matériel dentaire) provient des collections de l'Université de Montpellier (UM), pour les localités du sud de la France, et des collections du Muséum National d'Histoire Naturelle (MNHN), surtout pour les localités du Bassin de Paris. Les spécimens provençaux de Palette sont déposés au sein des collections du Museum d'Histoire Naturelle d'Aix-en-Provence. Certains de ces derniers proviennent de fouilles récentes menées à Palette (2017-2018, collaboration MNHN / ISEM / MHH Aix-en-Provence). J'ai pu traiter chimiquement une partie des sédiments issus de ces fouilles (~150 kg) durant ma première année de thèse. Cela a notamment permis de découvrir des fossiles clés pour comprendre l'histoire évolutive des métathérien européens, étudiés dans le Chapitre 1. Le matériel du Théron (commune de Siran, Hérault, Minervois), conservé à l'Université de Poitiers, a été découvert au cours de cette thèse à la suite de fouilles organisées par des membres de l'ISEM et du laboratoire Paléontologie, Évolution, Paléoécosystèmes et Paléoprimatologie de l'Université de Poitiers, auxquelles j'ai pu participer en 2022 et 2023. Un spécimen de la localité de La Borie provient initialement de la collection privée de D. Téodori qui a généreusement autorisé le dépôt de ce fossile dans les collections de l'UM au cours de la thèse.

Les spécimens provenant du MNHN sont pour la plupart encore en cours de catalogage à la fin de cette thèse. Ainsi, les spécimens publiés résultant de mon travail ont déjà reçu un numéro d'inventaire définitif, ce qui n'est pas nécessairement le cas pour tous les autres, souvent mentionnés ici par l'ancien numéro (cela concerne par exemple les numéros de spécimens se terminant par les initiales d'une collection privée [e.g., BN, collection Braillon ; L, collection Louis]). Des spécimens inédits des localités de Fordones, Le Clot, Avenay, La Borie, Mas de Gimel, Naples, Le Lien, Azillanet, et Cos ont été ajoutés aux collections de l'UM durant la thèse.

Les comparaisons et le codage (dans les analyses phylogénétiques) des spécimens extra-européens ont bénéficié de la collection de moulages de l'UM et de la consultation des spécimens originaux et moulages de l'Institut Royal des Sciences Naturelles de Belgique (IRSNB). Les fossiles provenant des localités des phosphorites du Quercy (souvent d'âge post-Yprésien), étudiés par Crochet (1980), ont été utilisés à de nombreuses reprises à titre de comparaison. Toutes les illustrations du matériel présentées dans les chapitres de ce travail sont inédites. Les spécimens ont été imagés par CT-scan avec une résolution inférieure ou égale à 10 µm, à partir d'une station EasyTom 150 / Rx Solutions (Montpellier RIO Imaging, ISE-M, Montpellier, France). Des illustrations de modèles surfaciques 3D sont présentées. Les procédures ayant permis de générer ces modèles 3D (via le logiciel Avizo® 9.3), autres qu'une segmentation semi-automatique via l'outil « threshold » de Avizo® 9.3, sont détaillées dans les Chapitres 1 et 5.

2. Biochronologie mammalienne et datations

Les niveaux-repères mammaliens du Paléogène (MP1 à MP30) ont été fondés sur la base du degré évolutif des faunes mammaliennes et la présence / absence de certains taxons. Ils ont été formalisés lors du congrès de Mayence (Schmidt-Kittler et al. 1987), puis mis à jour lors du congrès BiochroM'97 (1997). Chaque niveau-repère de l'échelle biochronologique MP possède une faune de référence choisie parmi les plus riches taxonomiquement. Dans cette thèse, une faune rapprochée d'une faune de référence donnée est désignée par l'abréviation de niveau-repère « ~MP ». Seuls trois niveaux-repères sont connus dans l'Éocène inférieur : MP7 (Dormaal, en Belgique ; Éocène inférieur précoce), MP8+9 (Avenay, Bassin de Paris ; Éocène inférieur moyen), et MP10 (Grauves, Bassin de Paris ; Éocène inférieur supérieur). L'absence de distinction entre des niveau-repères « MP8 » et « MP9 » (mais voir par exemple Legendre et Hartenberger [1992]) est due au fait que peu de taxons diffèrent entre Avenay et la localité supposée plus ancienne de Mutigny (Godinot, dans Schmidt-Kittler et al. 1987). Il faut souligner ici que les différences fauniques les plus importantes au moment de la définition des MP (à la suite du travail de Crochet [1980]) concernaient les pérathériinés (Godinot, dans Schmidt-Kittler et al. 1987) : les représentants des « lignées évolutives » *Peratherium constans* / *Peratherium matronense*, et *Amphiperatherium brabantense* (depuis synonyme junior de *Pt. constans*, cf. Ladevèze et al. 2012) / *Amphiperatherium* sp. 1 dans Crochet (1980), ne seraient pas les mêmes à Mutigny et Avenay. Il faut noter que peu de caractères morphologiques distinguent les espèces de ces lignées (Smith et Smith 2004 ; Ladevèze et al. 2012). D'après Crochet (1980), la faune métathérienne de Mutigny est donc plus proche de celle de Dormaal que celle d'Avenay. Depuis, de nombreuses localités d'âge intermédiaire entre Dormaal et Mutigny ont livré des restes de métathériens (Tableau 2). Ici, ces localités sont considérées dans l'intervalle de temps relativement long entre MP7 et MP8+9 (cf. Chapitre 1), c'est-à-dire qu'elles sont plus récentes que les localités MP7 / ~MP7 (Dormaal, Le Quesnoy, Silveirinha) et plus anciennes

que les localités MP8+9 / ~MP8+9 (e.g., Mutigny, Avenay, Condé-en-Brie, Sables de Brasles, Sézanne-Broyes) (Tableau 2).

Un découpage en biozones (PE I à PE V) de l'Éocène inférieur précoce à moyen a été établi par Hooker (1996a). Les taxons utilisés pour définir ces biozones sont uniquement ceux de sites de la province Nord d'Europe de l'Ouest, ce qui complexifie leur application aux localités du Sud de l'Europe de l'Ouest. Néanmoins, Marandat et al. (2012 : tableau 3) ont proposé des corrélations hypothétiques entre les successions de faunes du Nord et du Sud d'Europe de l'Ouest, et par conséquent entre les biozones PE et certaines faunes du Sud. Ces biozones sont donc ponctuellement utilisées et commentées de façon complémentaire aux niveaux-repères MP ici (Tableau 2).

Enfin, l'âge d'un nombre relativement réduit de localités (Palette, Sotteville-sur-Mer, Le Clot, Fournes, Azillanet) a été précisé par des méthodes de chémostratigraphie (Cojan et al. 2000 ; Smith et al. 2011 ; Yans et al. 2014 ; Noiret et al. 2016).

3. Localités fossilifères étudiées

Une première présentation des principaux gisements de l'Éocène inférieur de la France étudiés ici (MP7 à MP10-11) a été réalisée par Escarguel (1999). Toutes les attributions de taxons métathériens de cet intervalle de temps réalisées avant la thèse sont résumées dans le Tableau 2. La position chronologique relative des gisements de l'Éocène inférieur moyen de l'Est du Bassin de Paris (du plus ancien au plus récent : Pourcy, Mutigny, Avenay, Condé-en-Brie, Sables de Brasles, Sézanne-Broyes, Saint-Agnan) suit ici Louis et Laurain (1983) (voir Tableau 2). Une discussion plus précise sur les âges d'une partie des localités étudiées est présentée dans la section Matériel et méthodes du Chapitre 1 : Fordones, Fournes, Palette, Rians, dans le Sud de la France ; Sotteville-sur-Mer, Meudon, Soissons, Mutigny, Avenay, Condé-en-Brie, Sables de Brasles, Sézanne-Broyes, Saint-Agnan, dans le Nord de la France ; et Abbey Wood et Croydon, en Angleterre. Les âges de Le Clot, Pourcy et La Borie sont ensuite discutés dans le Chapitre 5.

En plus des localités dont les taxons métathériens sont détaillés dans le Tableau 2, des localités du Sud de la France ayant livré des spécimens inédits ont été ajoutées à l'échantillonnage. Il s'agit d'Albas, Naples, Le Théron, et Le Lien. Albas (Corbières) est une localité inédite de la fin du Paléocène supérieur (voir Chapitre 4). Naples (NAP, Montpellier) est géographiquement et temporellement proche de Mas de Gimel (~MP10) et a fait l'objet d'une étude détaillée s'inscrivant dans ce travail (Vianey-Liaud et al. 2024, voir Annexes). Le Théron (SRT ; commune de Siran, Minervois), inclus dans la formation des « Calcaires d'Agel » à l'instar d'Azillanet, est rapproché du niveau-repère ~MP10. Le Lien (LLN ; nord de Montpellier), est aussi une localité inédite, sous-jacente aux calcaires lacustres ?lutétiens de Montpellier ; elle est également rapprochée du niveau-repère ~MP10. Enfin, quelques dents jugales

isolées de métathériens sont connues dans des localités probablement d'âge post-Yprésien (e.g., Crochet et al. 1988, 1997). Les attributions de celles-ci ne sont pas réétudiées en détail ici. Des comparaisons sont notamment effectuées avec le matériel appartenant aux taxons définis à partir des gisements de Bouxwiller (~MP13, Éocène moyen ; *Amphiperatherium bastbergense* Crochet, 1979 ; *A. goethei* Crochet, 1979 ; Tableau 2), et de Le Bretou ou d'âge équivalent (~MP16 ; *Amphiperatherium bourdellense* Crochet, 1979).

Abréviations institutionnelles pour les spécimens originaux (pour les sections autres que les Chapitres 1 et 5, correspondant aux articles publiés).

IRSNB, Institut Royal des Sciences Naturelles de Belgique, Bruxelles

MHN.AIX, Muséum d'Histoire Naturelle d'Aix-en-Provence

MNHN, Muséum National d'Histoire Naturelle, Paris

NHMUK, Natural History Museum, Londres

NMB, Naturhistorisches Museum Basel

UM-, Université de Montpellier

Tableau 2 (page suivante). Synthèse de toutes les mentions de taxons Peradectidae et Herpetotheriidae de l'Éocène inférieur avant cette révision systématique, dans un cadre chronologique (niveaux-repères MP, biozones PE, et datations biochémostratigraphiques). Les croix rouges indiquent les localités-types. Les localités surlignées en bleu sont celles du Sud de la France, les autres sont celles des bassins parisien, belge et anglais. Les mentions en vert sont celles de localités probablement à la limite Ypresien-Lutétien ou plus jeunes, et ne seront pas réévaluées ici. Abréviations des localités (dans leur ordre d'apparition) : DO, Dormaal ; QNY, Le Quesnoy ; SI, Silveirinha ; STV, Sotteville-sur-Mer, PAT, Palette ; FDN, Fordones ; CLO, Le Clot ; MEU, Meudon ; SN, Soissons ; CR, Croydon ; AW, Abbey-Wood ; RI, Rians ; FNR, Fournes ; GAS, La Gasque ; POU, Pourcy ; MU, Mutigny ; AV, Avenay ; CB, Condé-en-Brie ; GLD, Sables de Brasles ; SZ, Sézanne-Broyes ; BRI, La Borie ; EG, Egem ; SA, Saint-Agnan ; MGL, Mas de Gimel ; CLR, Coulondres ; SRD, La Soucarède ; AZI, Azillanet ; GR, Grauves ; PRE, Prémontré ; VIE, Vielase ; AUM, Aumelas ; POT, Le Pont, GST+ME, Geiseltal + Messel ; SMF, Saint-Martin-de-Londres ; BOUX, Bouxwiller. Attributions d'après Crochet (1980) ; Godinot (1981) ; Louis et Laurain (1983) ; Dégremont et al. (1985) ; Marandat (1986) ; Godinot et al. (1987) ; Crochet et al. (1988, 1997) ; Russell et al. (1988) ; Storch et Haubold (1989) ; Marandat (1991) ; Legendre et al. (1992) ; Louis (1996) ; Nel et al. (1999) ; Estravís (2000) ; Kurz (2007) ; Hooker (2010, 2020) ; Smith et al. (2011) ; Ladevèze et al. (2012) ; Marandat et al. (2012) ; Smith et Smith (2013). Cadre chronologique déduit d'après Louis et Laurain (1983) ; Legendre et al. (1992) ; Hooker (1996a) ; BiochroM'97 (1997) ; Escarguel (1999) ; Cojan et al. (2000) ; Laurent et al. (2010) ; Smith et al. (2011) ; Marandat et al. (2012) ; Smith et Smith (2013) ; Yans et al. (2014) ; Noiret et al. (2016) ; Steurbaut et al. (2016) ; Hooker (2020). *, les mentions de *A.* « *brabantense* » concernent les localités dont les spécimens n'ont pas été réatribués suite à la synonymisation de *A.* « *brabantense* » avec *Pt. constans* (Ladevèze et al. 2012).

	MP7				~55 Ma			?			~54 Ma					MP8+9						MP8+9-10	~MP10		~51-50 Ma	MP10	50.4-3 Ma	MP10-11			~MP11-12 > 47.6 Ma		~MP13
	PE I			PE II							PE III				PE IV	PE V																	
	DO	QNY	SI	STV	PAT	FDN	CLO	MEU	SN	CR	AW	RI	FNR	GAS	POU	MU	AV	CB	GLD	SZ	BRI	EG	SA	MGL	CLR	AZI	GR	PRE	VIE	AUM	POT	GST+ME	SMF	BOUX
Peradectidae																																		
Peradectes																																		
Peradectes louisi	-	-	-	-	-	-	-	-	X	X	-	X	-	-	-	X	X	X	X	X	-	-	-	-	-	-	X	-	-	-	-	-	-	-
Peradectes russelli	-	-	-	-	-	-	-	-	-	-	-	-	-	-	-	-	X	X	X	-	-	-	-	-	-	-	-	-	-	-	-	-	-	-
Peradectes mutigniensis	-	-	-	-	-	-	-	-	-	-	-	-	-	-	-	X	X	X	X	-	-	-	X	-	-	-	-	-	?	-	-	-	-	-
Peradectes sp. in Crochet 1980	-	-	-	-	-	cf.	-	-	-	-	-	-	-	-	-	X	X	X	-	-	-	-	-	-	X	-	-	-	-	-	-	-	-	-
Peradectes sp. in Marandat 1986	-	-	-	-	-	-	-	-	-	-	-	-	-	-	-	-	-	-	-	-	-	-	-	-	-	X	-	-	-	-	-	-	-	-
Peradectes sp. in Russell et al. 1988	-	-	-	-	-	-	-	X	-	-	-	-	-	-	-	-	-	-	-	-	-	-	-	-	-	-	-	-	-	-	-	-	-	-
Peradectes sp. in Hooker 2010	-	-	-	-	-	-	-	-	-	-	X	-	-	-	-	-	-	-	-	-	-	-	-	-	-	-	-	-	-	-	-	-	-	-
Peradectes sp. 1 in Smith et al. 2011	-	-	-	X	-	-	-	-	-	-	-	-	-	-	-	-	-	-	-	-	-	-	-	-	-	-	-	-	-	-	-	-	-	-
Peradectes sp. 2 in Smith et al. 2011	-	-	-	X	-	-	-	-	-	-	-	-	-	-	-	-	-	-	-	-	-	-	-	-	-	-	-	-	-	-	-	-	-	-
"*Peradectes*" (Peradectidae ?)	-	-	-	-	-	-	-	-	-	-	-	-	-	-	-	-	-	-	-	-	-	-	-	-	-	-	-	-	-	-	-	X	-	-
Armintodelphys																																		
Armintodelphys dufraingi	-	-	-	-	-	-	-	-	-	-	-	-	-	-	-	-	-	-	-	-	-	X	-	-	-	-	-	-	-	-	-	-	-	-
Herpetotheriidae																																		
Peratherium sp. or *A.* sp. in Nel et al. 1999	-	X	-	-	-	-	-	-	-	-	-	-	-	-	-	-	-	-	-	-	-	-	-	-	-	-	-	-	-	-	-	-	-	-
Peratherium sp. or *A.* sp. in Kurz 2007	-	-	-	-	-	-	-	-	-	-	-	-	-	-	-	-	-	-	-	-	-	-	-	-	-	-	-	-	-	-	-	X	-	-
Peratherium																																		
Peratherium constans	X	-	cf.	-	X	X	X	-	-	-	-	-	-	-	-	X	-	-	-	-	-	-	-	-	-	-	-	-	-	-	-	-	-	-
Peratherium matronense	-	-	-	-	-	-	-	cf.	-	-	-	X	cf.	-	-	-	X	X	X	X	-	-	-	X	X	-	-	-	X	-	-	-	-	-
Peratherium monspeliense	-	-	-	-	-	-	-	-	-	-	-	-	cf.	cf.	-	-	-	-	-	-	-	-	-	X	X	X	-	-	-	-	-	aff.	-	-
?*Peratherium giselense*	-	-	-	-	-	-	-	-	-	-	-	-	-	-	-	-	-	-	-	-	-	-	-	-	-	-	-	-	-	-	-	X	X	-
Peratherium sp. 1 in Crochet 1980	-	-	-	-	-	-	-	-	X	-	-	-	-	-	-	-	-	-	-	-	-	-	-	-	-	cf.	-	-	aff.	-	-	-	-	X
Peratherium sp. in Kurz 2007	-	-	-	-	-	-	-	-	-	-	-	-	-	-	-	-	-	-	-	-	-	-	-	-	-	-	-	-	-	-	-	X	-	-
Amphiperatherium																																		
Amphiperatherium "brabantense" *	-	-	-	-	-	cf.	-	-	-	-	-	aff.	-	-	-	X	-	-	-	-	-	-	-	-	-	-	-	-	-	-	-	-	-	-
Amphiperatherium maximum	-	-	-	-	-	-	-	X	cf.	-	-	cf.	cf.	-	X	X	X	X	X	X	-	-	X	-	-	-	X	-	-	-	-	aff.	-	-
Amphiperatherium goethei	-	-	-	-	-	-	-	-	-	-	-	X	-	-	-	-	X	X	-	X	-	-	-	-	-	-	X	X	X	X	-	X	X	X
Amphiperatherium bourdellense	-	-	-	-	-	-	-	-	-	-	-	-	-	-	-	-	X	X	X	X	X	-	-	X	-	-	-	X	-	-	-	-	-	-
Amphiperatherium bastbergense	-	-	-	-	-	-	-	-	-	-	-	-	-	-	-	-	-	-	-	-	-	-	-	-	-	-	-	-	-	X	X	-	-	X
Amphiperatherium sp. 1 in Crochet 1980	-	-	-	-	-	-	-	-	-	-	-	-	-	-	-	-	X	X	X	X	-	-	-	-	-	-	X	-	-	-	-	-	-	-
Amphiperatherium sp. 2 in Crochet 1980	-	-	-	-	-	-	-	-	-	-	-	-	-	-	-	X	X	X	-	-	-	-	-	-	-	-	-	-	-	-	-	-	-	-
Amphiperatherium sp. 1 in Hooker 2010	-	-	-	-	-	-	-	-	-	-	X	-	-	-	-	-	-	-	-	-	-	-	-	-	-	-	-	-	-	-	-	-	-	-
Amphiperatherium sp. 2 in Hooker 2010	-	-	-	-	-	-	-	-	-	-	X	-	-	-	-	-	-	-	-	-	-	-	-	-	-	-	-	-	-	-	-	-	-	-
Amphiperatherium sp. in Marandat 1986	-	-	-	-	-	-	-	-	-	-	-	-	-	-	-	-	-	-	-	-	-	-	-	-	-	X	-	-	-	-	-	-	-	-
Amphiperatherium sp. in Legendre et al. 1992	-	-	-	-	-	-	-	-	-	-	-	-	-	-	-	-	-	-	-	-	-	-	-	-	-	-	-	-	X	-	-	-	-	-

Partie 1. Reconstruction des relations inter- et intraclades des Peradectidae, une famille clé dans l'histoire évolutive des Metatheria : apport de la caractérisation morphologique des taxons européens

Cette première partie se décline en deux temps. À partir de matériel quasi exclusivement dentaire, à la fois inédit ou publié par ailleurs, une révision systématique exhaustive des péradectidés européens de l'Éocène inférieur est conduite, en tentant de démêler la variation intraspécifique prépondérante du signal phylogénétique porté par les dents jugales de ces métathériens (Chapitre 1). Cette étude est suivie par la description de nouvelles espèces de péradectidés intra- et possiblement post-EECO, les plus jeunes formellement décrites en Europe (Chapitre 2). Cela a constitué une base de travail afin (i) d'élucider les étapes de l'histoire évolutive du groupe, à travers la séquence d'apparition des caractères dentaires, et finalement, (ii) dans un contexte spatiotemporel large, de clarifier les étapes de l'évolution des faunes de métathériens durant les premiers temps du Cénozoïque, dans lesquelles les péradectidés et herpétothériidés s'inscrivent (Chapitre 3).

Chapitre 1. Taxonomie et histoire évolutive des Peradectidae : nouvelles données de l'Éocène inférieur de la France.

Cette section correspond à l'article suivant : Gernelle K, Billet G, Gheerbrant E, Godinot M, Marandat B, Ladevèze S, Tabuce R. 2024. Taxonomy and evolutionary history of peradectids (Metatheria): new data from the early Eocene of France. Journal of Mammalian Evolution 31(3):31.

Résumé. Les Peradectidae sont des métathériens souches paléogènes, majoritairement restreints à l'hémisphère nord, qui ressemblent superficiellement aux opossums, et dont l'histoire évolutive est peu claire. À partir de nouveaux restes (principalement dentaires) découverts dans plusieurs localités fossilifères françaises, la révision systématique complète de tous les péradectidés de l'Éocène inférieur d'Europe est menée (du niveau-repère ~MP7 à l'intervalle MP10-11). Nous décrivons des spécimens particulièrement bien conservés de Palette (Sud de la France, intervalle MP7-MP8+9), documentant la plus ancienne espèce de péradectidé européen, *Peradectes crocheti* nov. sp. Cette nouvelle espèce présente une intéressante mosaïque de caractères, incluant des traits plésiomorphes présents chez l'espèce-type nord-américaine du genre, *Peradectes elegans* Matthew et Granger, 1921. Des molaires attribuées à *Peradectes crocheti* sp. nov., une espèce étonnamment ubiquiste, ont été par ailleurs trouvées dans huit localités supplémentaires du nord et du sud de l'Europe de l'Ouest, toutes restreintes à l'intervalle de temps entre MP7 et MP8+9. En outre, l'étude de matériel inédit des péradectidés MP8+9 / ~MP8+9 nous permet de reconnaître deux espèces contemporaines, plus jeunes que *Peradectes crocheti* sp. nov. (*Peradectes louisi* Crochet, 1979 et *Peradectes russelli* Crochet, 1979). Nos conclusions taxonomiques sont soutenues a posteriori par la première évaluation quantitative de la variation de la hauteur des cuspides stylaires chez les métathériens. L'holotype de *Peradectes louisi* est réinterprété, et *Peradectes* « *mutigniensis* » Crochet, 1979, apparaît être un synonyme de *Peradectes russelli*. En plus de la taille, *Peradectes louisi* et *Peradectes russelli*, autrement similaires, peuvent être distinguées à partir de différences subtiles mais constantes, telle que celle concernant les proportions des molaires inférieures. Des analyses phylogénétiques s'appuyant sur une nouvelle matrice de caractères dentaires clarifient les relations au sein des péradectidés éocènes, confirmant la paraphylie de *Peradectes* par rapport à *Armintodelphys* et *Mimoperadectes*. Nos résultats suggèrent qu'une seule dispersion de l'Amérique du Nord vers l'Europe a eu lieu au cours de l'histoire évolutive des péradectidés, très probablement immédiatement après le PETM. *Peradectes crocheti* sp. nov. apparait comme l'espèce la plus basale au sein du clade européen. De rares molaires inférieures provenant de localités MP10 / ~MP10, analysées dans ce cadre phylogénétique contraint temporellement, révèlent une tendance au rétrécissement de l'entoconide au sein de la lignée européenne, tout au long de l'Éocène inférieur.

Journal of Mammalian Evolution (2024) 31:31
https://doi.org/10.1007/s10914-024-09724-5

RESEARCH

Taxonomy and evolutionary history of peradectids (Metatheria): New data from the early Eocene of France

Killian Gernelle[1] · Guillaume Billet[2] · Emmanuel Gheerbrant[2] · Marc Godinot[3] · Bernard Marandat[1] · Sandrine Ladevèze[2] · Rodolphe Tabuce[1]

Accepted: 21 May 2024
© The Author(s), under exclusive licence to Springer Science+Business Media, LLC, part of Springer Nature 2024

Abstract

Peradectidae are Paleogene 'opossum-like' stem-metatherians, largely Laurasian, whose evolutionary history remains unclear. Based on new remains (mainly dental) discovered in several French localities, we carry out a comprehensive systematic revision of all early Eocene peradectids from Europe (~MP7 reference level to MP10-11 interval). We describe well-preserved specimens from Palette (Southern France, MP7-MP8 + 9 interval) documenting the earliest European peradectid, *Peradectes crocheti* sp. nov. This new species exhibits an interesting mosaic of characters, including plesiomorphic traits found in the North American type species, *Peradectes elegans* Matthew and Granger, 1921. Molars allocated to the strikingly ubiquitous *Peradectes crocheti* sp. nov. are found in eight additional localities from northwestern and southwestern Europe, all limited to the time interval MP7-MP8 + 9. Moreover, the study of unpublished material of the MP8 + 9 and ~MP8 + 9 peradectids allows us to recognize two younger coeval species (*Peradectes louisi* Crochet, 1979, and *Peradectes russelli* Crochet, 1979). Our taxonomic conclusions are supported a posteriori by the first quantitative assessment of the variation in height of metatherian stylar cusps. The holotype of *Peradectes louisi* is reinterpreted, and *Peradectes 'mutigniensis'* Crochet, 1979 appears to be a junior synonym of *Peradectes russelli*. In addition to size, the otherwise similar *Peradectes louisi* and *Peradectes russelli* can be distinguished based on subtle yet consistent differences, such as lower molar proportions. Phylogenetic analyses using a novel matrix of dental characters shed new light on the relationships among Eocene peradectids, confirming the paraphyly of *Peradectes* with respect to *Armintodelphys* and *Mimoperadectes*. Our results suggest a single dispersal from North America to Europe in the evolutionary history of peradectids, which likely occurred immediately after the Paleocene-Eocene Thermal Maximum, *Peradectes crocheti* sp. nov. being recovered as the earliest offshoot of the European clade. Scarce lower molars from the MP10 reference locality and ~MP10 localities analyzed within this constrained phylogenetic framework reveal a trend towards shrinking of the entoconid in the European lineage throughout the early Eocene.

Keywords Dentition · Europe · Paleobiogeography · Paleogene · Peradectidae · Systematics

Introduction

Peradectidae are an assemblage of extinct and small Cenozoic stem-metatherians with a superficially 'opossum-like' unspecialized tribosphenic dentition (e.g., Ladevèze et al. 2020). They have long been distinguished based on plesiomorphic dental features within Metatheria (but see Williamson et al. 2012, 2014), and were likely arboreally adapted (e.g., Szalay 1994; Kurz 2005; Rose 2012; Rose et al. 2012). Most of their occurrences are from North America (earliest Paleocene to early Oligocene; e.g., Korth 2008, 2018) and Europe (early to possibly earliest middle Eocene; Crochet 1979, 1980b; Kurz 2007). Putative peradectid isolated molars have also been identified in South America (early Paleocene to early Eocene;

Sandrine Ladevèze and Rodolphe Tabuce are co-senior authors.

This article is registered in ZooBank under urn: lsid: zoobank.org: pub: CCD67F33-98A5-40DC-B1C1-C1D1F549FA96.

✉ Killian Gernelle
killian.gernelle@umontpellier.fr

[1] Institut des Sciences de l'Évolution de Montpellier (ISEM, UMR 5554), Univ Montpellier, CNRS, IRD, cc64, Place Eugène Bataillon, Montpellier Cedex 05 F-34095, France

[2] Centre de Recherche en Paléontologie - Paris (CR2P, UMR 7207), Sorbonne Université, Muséum National d'Histoire Naturelle, CNRS, 8 rue Buffon, Paris F-75005, France

[3] Ecole Pratique des Hautes Etudes, PSL, UMR 7207, CR2P, 8 rue Buffon, F75005, Paris, France

Published online: 27 July 2024

Sigé 1971, 1972; Marshall and Muizon 1988; Muizon 1991; Tejedor et al. 2009), Asia (early Oligocene to Early Miocene; Ducrocq et al. 1992; Mein and Ginsburg 1997; Storch and Qiu 2002; Ni et al. 2007) and Africa (early Eocene; Crochet 1986; Crespo and Goin 2021; but see Hooker 1998: p. 443; Gunnell 2010). Although Peradectidae is a key metatherian taxon for paleobiogeographic reconstructions, controversies remain about its monophyly and phylogenetic affinities (e.g., Horovitz et al. 2009; Williamson et al. 2012; Maga and Beck 2017; Ladevèze et al. 2020; Beck 2023). This is particularly true due to the apparent uniformity of their dental morphology, and because early Eocene European peradectids, last studied in detail by Crochet (1977a, b, 1979, 1980a, b), have not been revised in light of new material nor included in phylogenetic analyses.

Two genera first defined in North America are hitherto recognized in Europe, namely *Peradectes*, with at least three species, mostly known from French localities (Crochet 1980b), and possibly *Armintodelphys*, with one species from Belgium (Smith and Smith 2013). *Peradectes* is a genus of uncertain monophyly spanning the whole of the Paleocene and Eocene epochs (e.g.Krishtalka and Stucky 1983b; Williamson et al. 2012). The earliest reports of European *Peradectes* were made by Crochet (1977a, 1979, 1980b), who recognized up to four species from early to late early Eocene localities of France, mainly represented by isolated molars. Crochet (1979) also coined the tribe Peradectini, later elevated to a familial rank (Reig et al. 1985, 1987). Contrary to the fossil record of North America, peradectids and metatherians as a whole are absent from the Paleocene of Europe (Gheerbrant 1991). Peradectids first appeared in Europe in various localities following the Paleocene-Eocene Thermal Maximum (PETM), which are somewhat younger than the reference level MP7 (earliest Eocene; BiochroM'97 1997) but older than MP8 + 9 and ~MP8 + 9 (i.e., MP7–MP8 + 9 interval) (Crochet 1980b; Godinot 1981; Russell et al. 1988; Marandat 1991; Louis 1996; Hooker 2010, 2020; Smith et al. 2011). Consequently, the dispersal of peradectids from North America to Europe after the PETM was formally proposed by Hooker (1998: p. 434, 2015: fig. 8), but is still blurred by the lack of identified morphological intermediate(s) between representatives of the two continents.

In this study, we report fossils of a new early European peradectid species, *Peradectes crocheti*, collected after recent excavations (2017–2019) in Palette (Provence, southern France), a locality within the MP7-MP8 + 9 interval (Cojan et al. 2000; Marandat et al. 2012; Yans et al. 2014), although initially considered close to MP7 (Godinot et al. 1987). These new specimens represent the most comprehensive assemblage attributed to *Peradectes* since the definition of its type species (Matthew and Granger 1921; Simpson 1928, 1935). We identified *Peradectes crocheti* sp. nov. in all MP7-MP8 + 9 interval localities that have yielded rare peradectid specimens (e.g., Fordones and Meudon). Moreover, the characterization of the morphology of the earliest European peradectids allowed us to carry out a revision of the species from the middle early Eocene (MP8 + 9 and ~MP8 + 9) of the Paris Basin, first described by Crochet (1979). This includes the referral of numerous unpublished dental specimens from the MP8 + 9 reference locality (Avenay) and various ~MP8 + 9 localities (Mutigny, Condé-en-Brie, Sables de Brasles, Sézanne-Broyes and Saint-Agnan). The greater abundance of remains of these later occurring species enabled us to account for intraspecific variation, and to refine their diagnostic characters and taxonomic status. In order to provide a more complete revised picture for the early Eocene, we also discuss the taxonomic status of the rare MP10 and ~MP10 peradectids. The phylogenetic position of the European taxa within Peradectidae was finally assessed via a phylogenetic analysis including most late Paleocene – middle Eocene Peradectidae sensu stricto, to provide formal insights on the origin of its European representatives, and on the Laurasian evolution of peradectids.

Materials and methods

Provenance of the specimens

Most of the material from the fossiliferous locality of Palette (MHN.AIX.PV.), including the dental rows assigned to *Peradectes crocheti* sp. nov., was found after the field expeditions conducted between 2017 and 2019 by some of us (GB, EG and RT). The material was isolated after processing the sampled sediment by careful acid etching, use of screen-washing, and sorting methods. This is the first occurrence of a peradectid metatherian in the Palette fauna, which adds to the 16 previously listed mammalian species in this locality (Table 1), most of which correspond to eutherian taxa that have been extensively studied (Godinot 1984, 1992; Godinot et al. 1987; Russell and Godinot 1988; Marandat 1991: 110; Ramdarshan et al. 2015; Solé et al. 2015, 2018, 2023; Boivin et al. 2018; Orliac et al. 2018; Vautrin et al. 2020; Vianey-Liaud and Marivaux 2021). *Peradectes crocheti* sp. nov. represents the first addition to the alpha diversity of the mammalian fauna of Palette (excepting an unidentified rodent species; Marandat et al. 2012: p. 427) since the establishment of the first and single faunal list of Godinot et al. (1987) for mammals, althought the taxonomic status or classification of some taxa have changed (Table 1).

The new peradectid specimens from Palette are permanently stored at the Muséum d'Histoire Naturelle of Aix-en-Provence (France). Other studied specimens are also the result of past or recent long and fruitful field research. The specimens from Meudon, Rians, Soissons, Avenay, Condé-en-Brie, Mutigny, Sables de Brasles, Sézanne-Broyes, Saint-Agnan,

Table 1 Updated list of mammals from Palette (Provence; MP7-MP8 + 9 interval, ~55 Ma). Attributions up to family rank are from Godinot et al. (1987), Russell and Godinot (1988), Marandat (1991), Rose et al. (1994), López-Martínez et al. (2006), Hooker and Russell (2012), Marandat et al. (2012), Hand and Sigé (2017), Boivin et al. (2018), Solé et al. (2018, 2023), Vautrin et al. (2020), Vianey-Liaud and Marivaux (2021), and this study

Metatheria
Peradectidae
Peradectes crocheti sp. nov.
Herpetotheriidae
Peratherium constans
Eulipotyphla
Nyctitheriidae
Saturninia sp. or *Leptacodon* sp.
Order incertae sedis
Adapisoricidae
gen. and sp. indet.
Chiroptera
?Archaeonycteridae
gen. and sp. indet.
Pantolesta
Paroxyclaenidae
Merialus martinae
Plesiadapiformes
Paromomyidae
Arcius rougieri
Primates
Notharctidae
Donrussellia magna
Rodentia
Ischyromyiformes, family incertae sedis
Corbarimys cezannei
gen. and sp. indet.
'Condylarthra'
Hyopsodontidae
Lessnessina praecipuus
Louisinidae
Paschatherium plaziati
Mesonychia
Mesonychidae
Hyaenodictis rougierae
Hyaenodonta
Hyaenodontidae
Parvagula palulae
Artiodactyla
Diacodexeidae
Diacodexis cf. *gigasei*
Perissodactyla
Lophiodontidae
Lophiaspis maurettei
Equoidea, family incertae sedis
Cymbalophus hookeri

Cuis and Grauves (MNHN.F.) are housed in the paleontological collections of the Muséum National d'Histoire Naturelle (Paris, France). Specimens from Fordones, Fournes, one specimen from Palette, one specimen from Coulondres, two specimens from Mas de Gimel, and one specimen from Vielase, are housed at the University of Montpellier (France). The two specimens from Sotteville-sur-Mer are housed at the Royal Belgian Institute of Natural Sciences (Brussels, Belgium). The single specimens from Croydon and Abbey Wood are housed at the Natural History Museum, London (England), and were studied via photographs available in the literature. Casts of North American peradectids (AMNH, UCMP, UM, USNM) were used for comparisons with European peradectids. We accounted for intraspecific variation in the descriptions of dental material based on comparisons with the variation ranges of morphological characters known in other marsupialiforms, such as *Pucadelphys* (Ladevèze et al. 2011) and *Peratherium* (Ladevèze et al. 2012).

Ages of the localities

The nine studied fossil-bearing localities of the MP7-MP8 + 9 interval are younger than the PETM (MP7). Four of them are located in southern France (Palette and Rians, in Provence; Fordones, in Corbières; Fournes, in Minervois), the five others being in northern France (Meudon, Île-de-France; Soissons, Aisne; Sotteville-sur-Mer, Normandie) and England (Abbey Wood and Croydon, London) (Fig. 1a). Palette and Fordones, correlated in age with Le Clot locality (Corbières) based on evolutionary stages of mammalian lineages (Marandat et al. 2012), are considered by chemostratigraphic analysis approximately 1 myr younger than the MP7 reference locality of Dormaal (Belgium; ~56 Ma), and hence close to 55 Ma (Yans et al. 2014). Fournes (Minervois) is positioned by marine correlation and chemostratigraphic analysis just after the ETM2 (~ 54 Ma), closer to the MP8 + 9 than to the MP7 reference level (Noiret et al. 2016: fig. 2), and is probably coeval with the Wasatchian Wa-5 mammal fauna (Noiret et al. 2016: p. 477). Rians (Provence) is a locality possibly similar in age to Fournes, based on mammalian biostratigraphy (Marandat et. 2012; Noiret et al. 2016; Philip et al. 2017: p. 328). Fournes and Rians are the youngest faunas of the MP7-MP8 + 9 interval here studied. The age retained for Abbey Wood (London; biozone PE III of Hooker 1996) is 55.12 Ma (Hooker 2010), and therefore older than Fournes and Rians. Sotteville-sur-Mer is probably the oldest of all the MP7-MP8 + 9 localities studied. It is probably older than Soissons and Meudon (both in biozone PE II; Hooker 1996) according to Smith et al. (2011), and was thus assigned to biozone PE II (Hooker 2015). These two northern localities are considered penecontemporaneous with the southern localities of Palette and Fordones (Marandat et al. 2012). Altogether, except Fournes

and Rians, the MP7-MP8 + 9 interval localities are bracketed between the PETM and the Eocene Thermal Maximum 2 (ETM2), and are closer to MP7 than to MP8 + 9 given the approximate age of Mutigny, the oldest ~MP8 + 9 locality (see below).

Five localities MP8 + 9 or ~MP8 + 9 in age from the Paris Basin (northwestern Europe) are here studied, namely Mutigny (Marne), Avenay (MP8 + 9 reference level, Marne), Condé-en-Brie (Aisne), Sables de Brasles (='Gland', Aisne) and Sézanne-Broyes (Marne) (Fig. 1a). Mutigny (biozone PE IV) is the oldest ~MP8 + 9 locality considered (slightly older than MP8 + 9), with an approximate age of 54 to 52 Ma (Neal 1996; Duprat 1997). Avenay, Condé-en-Brie and Sables de Brasles (biozone PE V) must be slightly younger than Mutigny according to the study of metatherian and rodent lineages (Schmidt-Kittler et al. 1987; Escarguel 1999), and slightly older than Sézanne-Broyes (also in PE V; Hooker 1996) (Louis 1970; Louis and Laurain 1983). Saint-Agnan (Aisne), of which the attribution of the single peradectid specimen is here revised, has been alternatively placed in the MP8 + 9 and MP10 reference level, depending on authors (e.g., Bronnert and Métais 2023 vs BiochroM'97 1997: table 1). The Saint-Agnan fauna is probably younger than MP8 + 9, and might be positioned in the MP8 + 9-MP10 interval according to most authors (Louis and Laurain 1983; Lecomte 1994; Escarguel 1999; Solé et al. 2018). Finally, rare localities from the late early Eocene have yielded peradectids (see Discussion), notably Grauves and Cuis (MP10, Paris Basin, BiochroM'97 1997), Mas de Gimel (~MP10; Vianey-Liaud et al. 2024) and Vielase (?MP10-11, Quercy, Legendre et al. 1992). The localities of Grauves and Cuis have long been considered distinct (Stehlin 1940: p. 293; Rat 1965: p. 251), but the two names may designate the same locality (e.g., Escarguel 1999).

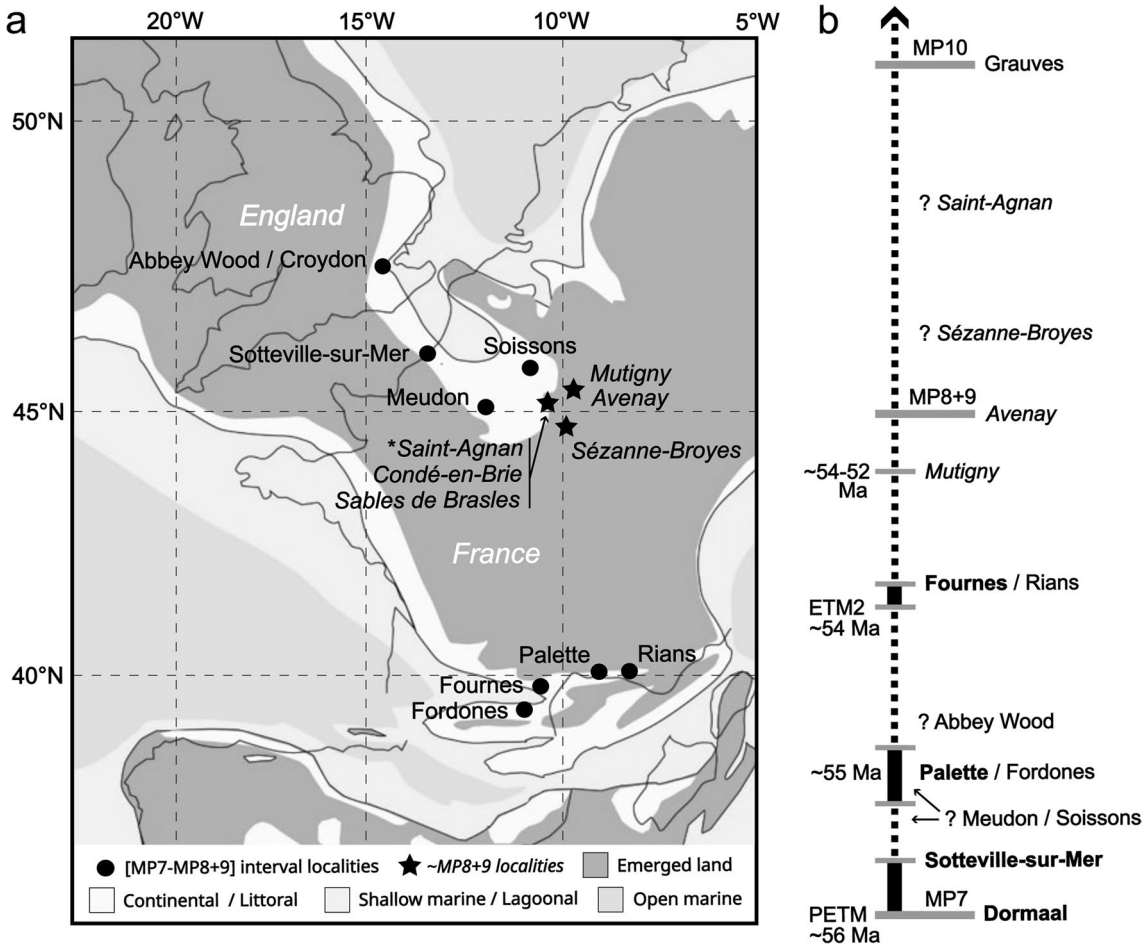

Fig. 1 Geographical and temporal positions of the studied MP7-MP8 + 9 interval and ~MP8 + 9 faunas (including that of Avenay, the MP8 + 9 reference locality) that yielded peradectid remains. **a**. paleogeographic map of France and England during the early Eocene. (modified from Marandat et al. 2012) with the position of studied localities. *, the Saint-Agnan locality is more likely in the MP8 + 9-MP10 interval rather than MP8 + 9 or MP10. **b**. schematic relative temporal positionning of MP7-MP10 reference levels, PETM and ETM2, and selected MP7-MP10 localities mentioned in the main text. The dashed parts of the temporal extension indicate uncertain temporal gaps. The age of localites in bold have been discussed via chemostratigraphic data (Cojan et al. 2000; Steurbaut et al. 2003; Noiret et al. 2016)

Dental nomenclature

For upper molars, the nomenclatures and homologies of Williamson et al. (2014: fig. 3), Goin et al. (2016: fig. 1.2) and Muizon and Ladevèze (2022: fig. 1) are mostly followed. Following these studies, the internal edge of all teeth (upper and lower), including premolars and canines, is designated as lingual, and the external edge as labial. The anterior and the posterior edges are designated as mesial and distal, respectively (Fig. 2b and c). An updated nomenclature for upper molars (Fig. 2b) includes the following structures. The paraconular cristae are termed pre- and postparaconular crista and the metaconular cristae are termed pre- and postmetaconular crista, as in Muizon and Ladevèze (2022). The postparaconular and the premetaconular cristae are the internal conular cristae. The term 'talon' designates the part of the crown which is lingual to the bases of the paracone and metacone (e.g., Marshall and Muizon 1995: fig. 5; Oliveira and Goin 2011: fig. 2); it includes the protocone, paraconule, metaconule, the conular cristae, the trigon basin (= protofossa of Crochet 1980b: fig. 2, or Gheerbrant 1992: fig. 1B), and the lingual part of the paracingulum. In occlusal view, a concave distal margin between the talon and stylar shelf is called a 'distal emargination' of the molariform tooth outline. The 'stylar cusp E' (not figured) corresponds to the labial termination of the postmetacrista, which is similar to a stylar cusp in labial view. The metastylar wing (e.g., Rothecker and Storer 1996; = 'metastylar lobe', e.g., Williamson and Taylor 2011; and 'metastylar area', e.g., Muizon and Ladevèze 2022) is the distolabial corner of the stylar shelf of molariform teeth, distal to the ectoflexus. It encompasses the stylar cusp D and the postmetacrista. The parastylar wing is the mesiolabial corner of the stylar shelf, mesial to the ectoflexus. It encompasses the stylar cusp A and the labial part of the paracingulum.

We propose a terminology of lower molars accounting for the dental peculiarities of European peradectids (Fig. 2c). We use the term 'protocristid' (= protolophid) as in Muizon and Ladevèze (2022), which encompasses the distolingual cristid of the protoconid (= postprotocristid) and the labial cristid of the metaconid; the latter was often considered as a 'postmetacristid' in metatherians (e.g., Goin et al. 2016). The metaconid of peradectids and other marsupialiforms, such as *Glasbius* (Williamson et al. 2014: fig. 3) and herpetotheriids (Wessels et al. 2024: fig. 1), also bears a sharp distal cristid in addition to this 'postmetacristid' (Fig. 2c). In the dental terminology of Williamson et al. (2014: fig. 3), the 'postmetacristid' of Goin et al. (2016) has thus been interpreted as the premetacristid and the distal cristid of the metaconid as the postmetacristid. However, some deltatheroidans (such as *Oklatheridium*) and early marsupialiforms (such as *Arcantiodelphys*) can have a mesial cristid of the metaconid (Averianov 2015: fig. 5), termed the 'premetacristid' (Vullo et al. 2009: p. 19912, fig. 2A). Thus, the cristids described as the premetacristid and postmetacristid in Vullo et al. (2009) and Williamson et al. (2014) are not homologous. In order to avoid confusion and to maintain structural homology among therians, the labial cristid of the metaconid is here named the 'protocristid lingual segment', a term derived from the terminology of primitive tribosphenic molars (e.g., Van Valen 1966: fig. 1; Crochet 1980b; Gheerbrant 1992). The distal cristid of the metaconid is named the 'postmetacristid' due to its position (a cristid which is itself possibly not homologous with the 'distal metacristid' of some stem therians, see Martin et al. 2023). In the same way, the paracristid is subdivided into the preprotocristid, on the mesiolingual edge of the protoconid, and the 'paracristid lingual segment' on the labial edge of the paraconid. The 'paracristid lingual segment' is not a widely-used name in studies of metatherian molars. The labial cristid of the paraconid has been alternatively named the 'postparacristid' (e.g., Abello 2013: fig. 2D; Goin et al. 2016), or the 'preparacristid' (e.g., Ladevèze et al. 2012: p. 259; Muizon et al. 2018), by various authors. As before, in some deltatheroidans and stem marsupialiforms, a distal cristid of the paraconid (= postparacristid) lingually closes the trigonid basin, together with the premetacristid (Vullo et al. 2009: p. 19912, fig. 2A; Averianov 2015: fig. 5). Moreover, some peradectid molars studied here have a small cristid on the paraconid keel, mesial to the paraconid, which is the preparacristid. In lingual view, the lingual opening of the trigonid basin (= prefossid in Crochet 1980b; Gheerbrant 1992) refers to the opening between the paraconid and metaconid, and the lingual opening of the talonid basin (= postfossid) refers to the opening between the metaconid and the entoconid. The lingual opening between the entoconid and the hypoconulid is referred to as the entoconid – hypoconulid notch. The entocristid of Crochet (1980b), Gheerbrant (1992), and Muizon and Ladevèze (2022) is named the pre-entocristid, as in Goin et al. (2016), because a small postentocristid often occurs in the entoconid – hypoconulid notch of peradectids (Fig. 2c). When present, the postentocristid is a true cristid; it differs from the 'hypoconulid-entoconid talonid fold' present in some herpetotheriid and didelphid species (Hooker et al. 2008: p. 644, pl. 1, figs. 1-2) in being observable even on unworn lower molars. The distolingual cristid of the hypoconid is designated as the postcristid following Crochet (1980b); Gheerbrant (1992), instead of the posthypocristid, because it generally implicitly includes the posthypocristid and also the unnamed labial cristid of the hypoconulid, which occurs in some peradectid specimens (Fig. 2c). In occlusal view, a concave labial margin between trigonid and talonid is called a labial emargination of the molar outline (not illustrated in Fig. 2c).

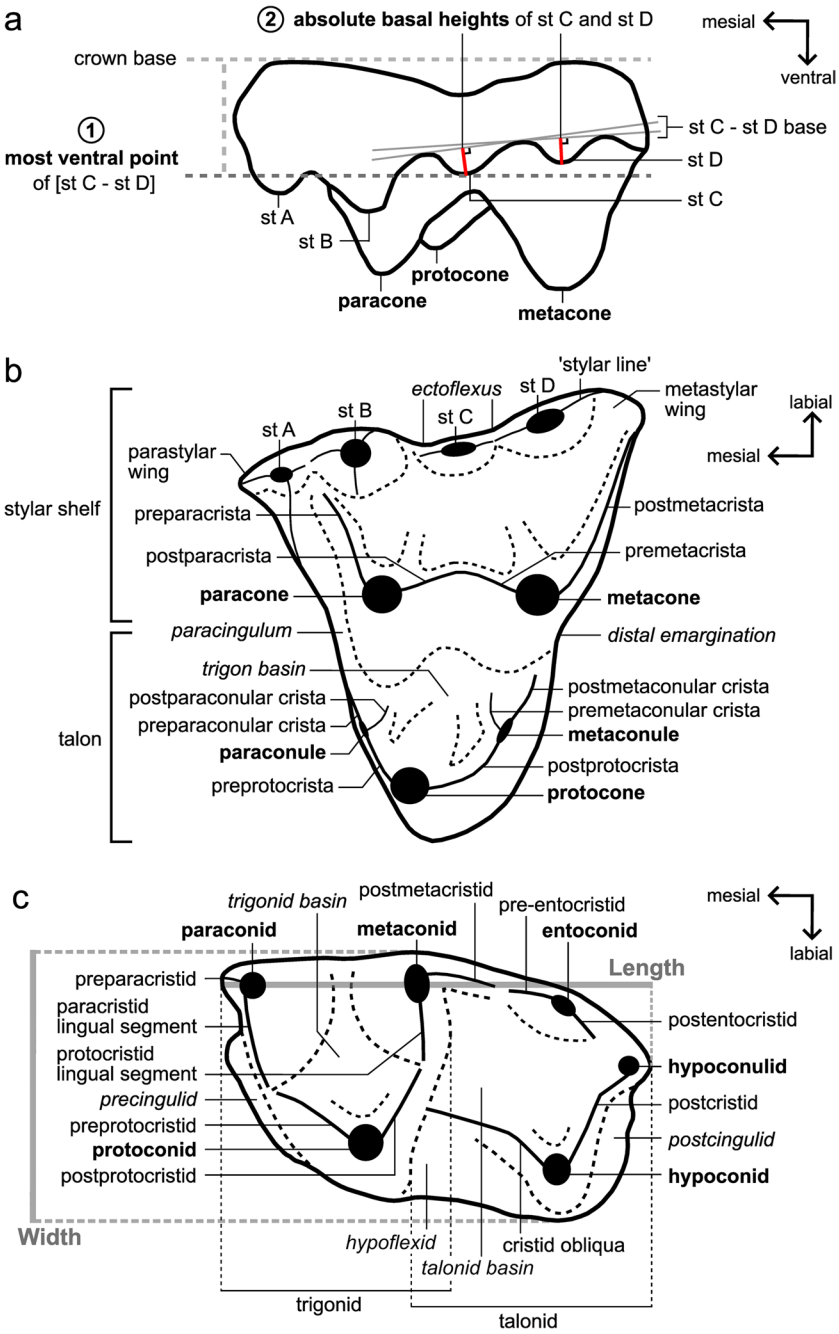

Fig. 2 Molar nomenclature and measurement methods used in this study, based on schematic drawings of peradectid molars. **a**. upper molar in labial view, with the two methods employed for estimations of the heights of stylar cusps C and D: (1) position of the most ventral point of the [stylar cusp C – stylar cusp D] mesiodistal extension parallel to the crown base, and (2) absolute basal height of stylar cusps C and D, with a ratio calculated from the two values. **b**. upper molar in occlusal view. **c**. lower molar in occlusal view. The measurement methods for length and width of lower molars are illustrated in grey. The dashed lines concern depressions on the occlusal surface (**b** and **c**). Cusps (except stylar cusps) / cuspids and conules are indicated in bold text, crests / cristids are in full text, and cingula / cingulids, emarginations of the crown and basins are in italics. The molar nomenclature is mainly derived from Crochet (1980b); Gheerbrant (1992); Williamson et al. (2014); Goin et al. (2016); Muizon and Ladevèze (2022). Abbreviations: **st A**, stylar cusp A; **st B**, stylar cusp B; **st C**, stylar cusp C; **st D**, stylar cusp D. Schematic drawings are not to scale

Orientation of molariform teeth for descriptions and measurements

Clemens (1966: p. 4) was the first author to stress the need for an orientation method of metatherian molariform teeth ensuring consistent descriptions and measurements. The repeatability of measurements and descriptions of the upper molars and deciduous premolar has been achieved using the paracone – metacone axis for orientation. This method was efficiently used by several authors working on upper molars of metatherians since the work of Clemens (1966) (see Rose 2010: p. 561).

Regarding metatherian lower molars, the orientation used for descriptions and/or measurements differ between authors and was often unspecified. The methodology of Crochet (1980b); Korth (1994) to measure lower molars is not detailed, although their drawings (e.g., Crochet 1980b: figs. 3, 10; Korth 1994: fig. 1) suggest the chosen orientation of lower molars allowed their maximum length to be measured. This protocol has been used by other workers for measurements of small mammal teeth in general, and is still employed for metatherian lower molars in recent studies (e.g., Muizon and Ladevèze 2022). However, it does not

allow to locate structures properly on the occlusal surface of lower molars and to define characters consisting in precise relative position of structures, because the chosen orientation may vary between specimens and dental loci. Lower molars have tentatively been precisely oriented using the paraconid - entoconid apices axis (Clemens 1966: p. 4) or the metaconid – entoconid apices axis (Lillegraven 1969: p. 16, fig. 5; Gheerbrant 1992: p. 80). On the lower molars of most metatherians, including herpetotheriids and the earliest *Peradectes* species *Peradectes minor* Clemens, 2006 (see also Williamson et al. 2012), and *Peradectes coprexeches* Williamson & Taylor, 2011, the paraconid, the metaconid, and the entoconid are aligned. As a consequence, the orientation of the lower molars for most Cenozoic metatherians varies little, no matter which lingual cuspid axis is chosen as reference. We noted that the relative configuration between the trigonid and talonid cuspids is different in most peradectids, such as the type species *Peradectes elegans* Matthew & Granger, 1921 (Gazin 1956: pl. 2, fig. 6; Krishtalka and Stucky 1983b: fig. 3), *Peradectes protinnominatus* McKenna, 1960 (see also Bown 1979: fig. 40b, Rose 1981: fig. 8A, Gingerich and Smith 2006: fig. 26b), all European peradectid species (this study), and the genus *Armintodelphys* (Krishtalka and Stucky 1983a: fig. 5; Krishtalka and Stucky 1984: fig. 4A), where the entoconid, pre-entocristid and postentocristid are oblique with respect the the mesiodistal axis. Such a 'curved talonid lingual edge' was first noted in a description of some peradectid lower molars by Smith and Smith (2013: p. 305), but it is not exclusive to the species included in *Armintodelphys* by these authors. A curved talonid implies that the paraconid, metaconid and entoconid are often not aligned on the lower molars of the concerned taxa. The entoconid apex is either more labial than the paraconid and metaconid apices if these two trigonid cuspids are chosen to form the reference axis for orientation, or the metaconid apex is lingually deflected if the paraconid and entoconid apices are chosen as reference. The entoconid has been highlighted as one of the most variable structures of lower molars of extant and extinct metatherians, especially for the last lower molar (e.g., Martin 2005: fig. 4; Ladevèze et al. 2012: p. 256). We consequently regard the use of the paraconid-metaconid apices axis as a reference as the best way to produce reliable measurements (Fig. 2c) and dental descriptions (including the coding of dental characters) of tribosphenic metatherian material, and we thus use it in this study for both purposes.

Maximum values were retained for the mesiodistal length, parallel to the paraconid – metaconid apices axis, and the labiolingual width, perpendicular to the paraconid - metaconid apices axis. All measurements are given with an accuracy of 0.01 millimetres. Measurement values for molars are presented in Online Resource 1: Tables S1-S3. Unbiased coefficients of variation (CV) were calculated to compare variability between dental measurements. Statistical treatment of the data was carried out using the R software environment (R Core Team 2020; v.4.0.2). In order to statistically compare mean molar proportions between *Peradectes louisi* Crochet, 1979, and *Peradectes russelli* Crochet, 1979 (at a 5% alpha risk), Welch's unequal variances *t*-test were performed (as recommended in Ruxton 2006). The measurement method for premolars is the one of Clemens (1966: p. 4). Mandibular heights were taken on the lingual aspect of the mandible, from its ventral edge to the adjacent dorsal molar alveolus. All measurements were made on screenshots of volume rendering or surface models of the scanned specimens (see below), using Avizo® 9.3 (Thermo Fisher Scientific-FEI) measurement tools, and/or via photographs of specimens taken with an optical stereomicroscope (Leica M 205 C) connected to a camera (Leica DFC 420 C), using tools of the Leica Application Suite v. 4.13. Body mass estimates were calculated using the predictive equation for M3 length (the most accurate predictor, as indicated by R^2 values) from the 'pooled Didelphidae and Dasyuridae' (i.e., dentally conservative marsupials) dataset of Gordon (2003: fig. 7).

Evaluation of the heights of stylar cusps

In studies directly addressing stylar shelf intraspecific variation among extant and extinct metatherian taxa, no clear pattern of variation of the relative sizes of the stylar cusps C and D for a given molar locus of a given species was noted, although the stylar cusps C and D are known to vary in absolute size (confounded with height by most authors), morphology, and position within a comprehensive series of metatherian teeth (e.g., Storer 1991: table 6; Johanson 1994: fig. 2; Eberle and Storer 1995: p. 791; Hershkovitz 1997: fig. 19; Flores and Abdala 2001: p. 105; Hayes 2005: fig. 4; Korth 2018; but see Kihm and Schumaker 2015: p. 105). Few authors formally used the sizes of stylar cusps to distinguish metatherian species or genera (e.g., Crochet 1979, 1980b; Marshall et al. 1990: tables 1-2; Korth 1994: table 2; Muizon and Lange-Badré 1997: table 1), and in particular peradectid species (Williamson and Taylor 2011). Although the vast majority of the fossil record of metatherians is composed of molars, there has not been a procedure to objectively decide which one of two given stylar cusps on one specimen is higher, nor an attempt to quantify the size of these stylar cusps.

For this purpose, we here propose two methods to evaluate the relative height of the stylar cusps, examplified by the stylar cusps C and D, based on labial views of the upper molars (Fig. 2a). One can first find the most ventral point of the [st. C – st. D] mesiodistal extension parallel to the base of the crown (Fig. 2a [1]). In previous works, the relative height of the stylar cusps was probably implicitly estimated in this way. This method is used in the "Systematic

Paleontology" section of this study (in differencial diagnoses of species and comparative descriptions).

Second, the absolute basal height of a stylar cusp corresponds to a measurement performed (in mm, also in labial view) perpendicular to a baseline drawn between the most mesial and distal points of this stylar cusp, that are the most dorsal (i.e. the closest to the crown base). The measurement is taken between the baseline of the stylar cusp and its most ventral point (i.e., the stylar cusp tip) (Fig. 2a [2]). The measurements of the absolute basal heights of the stylar cusps C and D were here conducted on stylar shelves with limited and homogeneous wear, of upper molars of the three European peradectids *Peradectes crocheti* sp. nov., *Peradectes louisi* and *Peradectes russelli*. For each available specimen, a ratio of the absolute basal height of the stylar cusp C to the absolute basal height of the sylar cusp D was calculated for comparative purposes, because one out of the three species studied (*Peradectes russelli*) is larger than the others. This second method allows to precisely quantify the variation in height of the stylar cusps. It is used in the "Results" section of this study, a posteriori of taxonomic attributions. Measurements of stylar cusp heights and ratio values are available in Online Resource 1: Table S4. Non-parametric Wilcoxon-Mann-Whitney tests were performed with the R software environment on species pairs (the normality assumption was not met for the st. C / st. D heights ratio values of *Peradectes crocheti* sp. nov. [Shapiro-Wilk normality test; $W = 0.892$, $P = 0.042$]), in order to define between which species the sum rank of the ratio values of the absolute basal height of st. C / st. D differ significantly (at a 5% alpha risk). Parametric Welch's *t*-test were alternatively performed on the same species pairs. The R package *ggplot2* (Wickham 2016) was employed to produce boxplots of absolute basal stylar cusp heights ratio values, as well as bivariate diagrams of length x width of molars.

High-resolution x-ray microtomography

Illustrated specimens were scanned using a µ-CT-scanning station EasyTom 150 / Rx Solutions (Montpellier RIO Imaging, ISE-M, Montpellier, France). Images of these specimens were achieved using the 'snapshot' tool of Avizo® 9.3. The segmentation of the cheek teeth and dentary of MHN.AIX.PV.2017.6.8 (scanned with a resolution of 6.5 µm) was performed with the Avizo® 9.3 'blow' tool, in order to clarify the morphology and positioning of peradectid premolars on the dentary. The segmentation of the holotype of *Peradectes crocheti* sp. nov., MHN.AIX.PV.2018.26.14 (scanned with a resolution of 5.3 µm), required the 'threshold' tool. An attempt was made to position the segmented fragments of the maxilla MHN.AIX.PV.2018.26.14 in anatomical position, using the MorphoDig® software (Lebrun 2018), with comparison to the complete maxilla of '*Peradectes*' from Messel (Kurz and Habersetzer 2004: figs. 2-3) and accounting for the typical crushing of fossil bones from Palette, which may have suffered from synsedimentary compression (e.g., Vautrin et al. 2020: figs. 3-4). The 'threshold' tool was also used for segmenting the isolated M3 MHN.AIX.PV.2017.6.7 and MNHN.F.SN18, as a way to numerically assemble the lingual and labial halves of the former, and extract sediment from the trigon basin of the latter.

Intrafamilial phylogenetic analysis

The aim of the phylogenetic analysis was to unravel relationships within part of Peradectidae sensu stricto, with a focus on European representatives. Fourteen metatherian taxa were coded for this purpose. The outgroup is composed of two stem-metatherian species, the deltatheroidan (= non-marsupialiform metatherian) *Deltatheridium pretituberculare* Gregory & Simpson, 1928, and the stem-marsupialiform *Asiatherium reshetovi* Trofimov & Szalay, 1994 (taxon data used for coding are in Online Resource 2). Among marsupialiforms, *As. reshetovi* is usually found to be more basal than Peradectidae (e.g., Williamson et al. 2014; Ladevèze et al. 2020; Muizon and Ladevèze 2022; but see Maga and Beck 2017: fig. 38 vs. fig. 39). All late Paleocene – middle Eocene species of Laurasian Peradectidae sensu stricto were included in the ingroup (12 taxa), with the exception of *Mimoperadectes houde*i Horovitz, Martin, Bloch, Ladevèze, Kurz & Sánchez-Villagra, 2009, and *M. sowasheensis* Beard & Dawson, 2009, because we mainly aimed to resolve phylogenetic relationships of *Peradectes* and *Armintodelphys* species (both genera having been recognized in Europe and North America before this study), and because *M. sowasheensis* is known by a single isolated upper molar (Beard and Dawson 2009). *Mimoperadectes* is thus only represented in this analysis by its type species, *Mimoperadectes labrus* Bown & Rose, 1979. The 11 remaining taxa of the ingroup belong to *Peradectes* and *Armintodelphys*. *Peradectes pauli* Gazin, 1956, was here not considered as a valid species, following Kurz (2007: p. 44) and Williamson et al. (2012); it is probably a junior synonym of the type species *Peradectes elegans* (Williamson et al. 2012: p. 631). Consequently, dental material previously ascribed to *Peradectes pauli* (Gazin 1956; Krishtalka and Stucky 1983b) was used here for the coding of *Peradectes elegans*, following Williamson et al. (2012: supplemental material, appendix 1). The ingroup taxa, along with their precise temporal extension (all occurring in the Eocene) and the nature of data used for their coding, are listed in Online Resource 2.

The fossil record of peradectids comprising predominantly isolated cheek teeth and incomplete dental rows, our dataset is composed of 37 characters which concern only the postcanine dentition. Among them, three are related to the morphology of lower premolars (characters 1 to 3), 18

to lower molars (characters 4 to 21) and 16 to upper molars (characters 22 to 37). The characters of these three subpartitions relate to the occlusal, lingual and labial morphology of cheek teeth. Approximately half of the characters (18) were either directly taken (8), or modified in their spelling or character states (10), from characters of the data matrices of Williamson et al. (2014) and Muizon and Ladevèze (2022). The others (19 characters) are here newly defined to reflect substantial differences observed among the dentition of peradectid taxa. The only two multistate characters (3 and 34) were unordered because we did not hypothesize a hierarchical transformation for them (i.e., getting from state 0 to state 2, or vice versa, does not necessarily involve an intermediate state 1). All characters were unweighted. Ranges of measurements were coded onto four new discrete characters (4, 5, 14 and 22) by gap coding. The characters implying comparisons of length and/or width between molar loci (4, 6, 22) were coded using available means of dental measurements if these loci are known only by isolated molars for the concerned taxon. Frequencies of observation of character states in our sample were employed in four new characters (11, 31, 36 and 37). We paid attention to avoid cases of similar characters being repeatedly scored at successive molar loci since these may highly covary (serial homologs, see Billet and Bardin 2019). Thus, although 32 out of 37 characters are restricted in their application to given molar loci because of their spelling, only two characters (10 and 11) may represent serial homologs at successive molar loci (however, their coding differs greatly). The illustration of most of the new characters is available in Online Resource 3: Figs. S1-S12. The numbers in superscript used after a character number in the main text and figures denote the character state.

The new character-taxon matrix (Online Resource 4) was edited with Mesquite v. 3.61 (Maddison and Maddison 2019). The parsimony analysis was performed with PAUP* v. 4.0a169 (Swofford 2002), through the Heuristic search method, with a random step-wise addition (1000 replications with randomized input order of taxa) and tree-bisection-reconnection (TBR) branch swapping options. Intraspecific variation was accounted as polymorphic states in PAUP* (noted 'x&y' in Mesquite and '(xy)' in PAUP*). Non-applicable states have been coded '-' in Mesquite. The robustness of each clade was evaluated with Bremer indices (BI, Bremer 1994), going up to five additional steps. A second analysis, with the same parameters, was run with a new scoring of characters requiring frequencies of observation to be scored (characters 11, 31 and 36). The frequencies were replaced by polymorphism when needed. Character 37 was additionally scored as such in a third analysis. The changes in the spelling of characters and scoring, and the result of the second and third analysis are presented in Online Resource 5. A fourth analysis with the same scoring as the previous one (i.e., polymorphism included in the scoring of the characters 11, 31, 36 and 37) was performed, but with implied weighting instead of unweighted characters, with the Goloboff constant (k) value = 3 (as recommended by Goloboff 1993) in order to downweight homoplasic characters. Finally, the multistate characters (3 and 34) were ordered in a fifth analysis, which is otherwise identical to the first one.

Abbreviations

Institutions and localities: AMNH, American Museum of Natural History, New York; **MHN.AIX.PV.,** Muséum d'Histoire Naturelle d'Aix en Provence, collection from Palette; **MNHN.F.,** Muséum National d'Histoire Naturelle, Paris, fossil collections; **MNHN.F.Av,** Avenay; **MNHN.F.CB,** Condé-en-Brie; **MNHN.F.GL** Sables de Brasles (= 'Gland'); **MNHN.F.Gr,** Grauves; **MNHN.F.Me,** Meudon; **MNHN.F.Mu,** Mutigny; **MNHN.F.Ri,** Rians; **MNHN.F.SN,** Soissons; **MNHN.F.STA,** Saint-Agnan; **MNHN.F.SZ,** Sézanne-Broyes; **NHMUK.PV.M,** Natural History Museum, London, UK, palaeontological vertebrate collections; **UCMP,** University of California Museum of Paleontology, Berkeley; **UM,** University of Michigan Museum of Paleontology; **UM-AV-SK,** Avenay, Université de Montpellier (France), Schmidt-Kittler collection; **UM-BRT,** Le Bretou, Université de Montpellier; **UM-CLR,** Coulondres, Université de Montpellier; **UM-FDN,** Fordones, Université de Montpellier; **UM-FNR2,** Fournes 2, Université de Montpellier; **UM-MGL,** Mas de Gimel, Université de Montpellier; **UM-PAT,** Palette, Université de Montpellier; **UM-VIE,** Vielase, Université de Montpellier; **USNM,** United States National Museum.

Other abbreviations: L, maximal mesiodistal length; **st.,** stylar cusp; **W,** maximal labiolingual width.

Reference levels and biozones: MP, Mammal Paleogene reference level (BiochroM'97 1997); ~MP is used when the designated locality/localities is/are similar in age to the reference locality (i.e., possibly slightly older or younger); **PE,** *Paleocene-Eocene* biozone (Hooker 1996).

Dental loci: C, upper canine; **c,** lower canine; **dPX,** upper deciduous premolar; **dpX,** lower deciduous premolar; **MX,** Xth upper molar; **mX,** Xth lower molar; **PX,** Xth upper premolar; **pX,** Xth lower premolar.

Systematic paleontology

Mammalia Linnaeus, 1758
Metatheria Huxley, 1880
Marsupialiformes Vullo, Gheerbrant, Muizon & Néraudeau, 2009
Peradectidae Crochet, 1979

Peradectes Matthew & Granger, 1921

Type species: *Peradectes elegans* (see Krishtalka and Stucky 1983b; Fox 1983), early Tiffanian (middle Paleocene) to early Wasatchian (early Eocene).

Peradectes crocheti sp. nov.
LSID urn:lsid:zoobank.org:act:DDB4D655-E26D-46AA-96BA-192DB23B61D4
Figures 3, 4, 5, 6, 7 and 8

1980b *Peradectes louisi* Crochet; Crochet: p. 39–42 (in part).
1981 *Peradectes louisi* Crochet; Godinot: p. 51–52, pl. 1, fig. 1 (no fig. 4a; pl. 1, fig. 2) (in part).
1987 *Peratherium constans* Teilhard de Chardin; Godinot et al.: p. 283 (in part).
1988 *Peradectes* sp.; Russell et al.: p. 431.
1991 *Peradectes* sp. indet. (cf. *Peradectes* sp. indet. in Crochet 1980); Marandat: p. 66–68, pl. 1, figs. 1-2, 18 (in part).
1991 *Peratherium constans* Teilhard de Chardin; Marandat: p. 68–69 (in part).
1991 *Amphiperatherium* cf. *brabantense* Crochet; Marandat: p. 71–72 (no pl. 1, fig. 4) (in part).
1996 *Peradectes louisi* Crochet; Louis: p. 94, pl. 2, fig. 7.
2010 *Peradectes* sp.; Hooker: p. 17, fig. 8a-b.
2011 *Peradectes* sp. 2; Smith et al.: p. 18, fig. 5.18.
2020 *Peradectes louisi* Crochet; Hooker: p. 461, fig. 3F-G.

Holotype: MHN.AIX.PV.2018.26.14 (Fig. 3a-c), fragmentary left maxilla with C-P1, anterior root of P2, and M1-M3, housed at the Natural History Museum of Aix-en-Provence. A 3D surface model of this specimen is available on MorphoMuseuM (Lebrun and Orliac 2016).

Etymology: Dedicated to Jean-Yves Crochet, who was the first to describe peradectids from Europe (Crochet 1977a), and who erected the tribe Peradectini (Crochet 1979), later elevated to familial rank (Reig et al. 1985, 1987).

Nomenclatural remark: This new species must be referred to as *Peradectes crocheti* Gernelle, 2024, following the article 50.1 and the recommendation 50 A concerning multiple authors of the International Code of Zoological Nomenclature (ICZN 1999: p. 52).

Remark on abbreviations: We use the abbreviation '*Pd.*' for the genus *Peradectes* in order to avoid confusion with species of the genus *Peratherium*, which is abbreviated '*Pt.*'. In fact, the type species of these genera, mentioned for comparative purposes in this study, have the same species name: *Peradectes elegans* and *Peratherium elegans* (Aymard, 1846).

Type locality: Palette, in Provence, France; early Eocene, MP7-MP8 + 9 interval, ~ 55 Ma.

Other localities: Fordones, Fournes and Rians in southern France; Meudon, Soissons and Sotteville-sur-Mer in northern France; Abbey Wood and Croydon in England.

Age: Early Ypresian, known from localities younger than the reference level MP7 and older than MP8 + 9 (~ mammalian biozones PE II and PE III).

Material: Additional material from Palette: left P2 (MHN.AIX.PV.2017.6.6), mesiolabial fragment of left M1 (MHN.AIX.PV.2017.6.11), right M1 (MHN.AIX.PV.2018.26.20), left M3 (MHN.AIX.PV.2017.6.7), talon of left M3 (MHN.AIX.PV.2017.6.13), lingual fragment of left M4 (MHN.AIX.PV.2017.6.12), fragment of right dentary with alveoli of p1, and p2–m3 (MHN.AIX.PV.2017.6.8), left m1–m4 with fragments of dentary (MHN.AIX.PV.2017.6.9), left worn m3 lacking enamel (MHN.AIX.PV.2017.6.10), right worn m3 (UM-PAT-103), right astragalus (MHN.AIX.PV.2017.6.14). 3D surface models of the specimens MHN.AIX.PV.2017.6.6, MHN.AIX.PV.2017.6.7, MHN.AIX.PV.2017.6.8, MHN.AIX.PV.2017.6.9 and MHN.AIX.PV.2017.6.14 are available on MorphoMuseuM.

Material from Fordones: right M1 (UM-FDN-1, Marandat 1991: pl. 1, fig. 1), fragmentary right M1 (UM-FDN-2), right partial maxillary with fragmentary M2-M3 (UM-FDN-21), labial fragment of right M2 (UM-FDN-285), distal fragment of right M2 (UM-FDN-287), worn fragment of left M2 (UM-FDN-288), labial fragment of right M3 (UM-FDN-23, Marandat 1991: pl. 1, fig. 2), labial fragment of right M4 (UM-FDN-286), worn fragment of left M4 (UM-FDN-289).

Material from Soissons: left M1 (MNHN.F.SN76), left M3 (MNHN.F.SN18), fragment of left M3 (MNHN.F.SN78), right m1 (MNHN.F.SN121), right m3 (MNHN.F.SN2508; Louis 1996: pl. 2, fig. 7).

Material from Meudon: right worn M1 (MNHN.F.Me16079), labial fragment of right M2 (MNHN.F.Me15975), left M4 (MNHN.F.Me16084), left m2 (MNHN.F.Me16101), left trigonid (MNHN.F.Me16167).

Material from Sotteville-sur-Mer: right M3 (Smith et al. 2011: fig. 5.18).

Material from Croydon: right M2 (NHMUK.PV.M66046; Hooker 2020: fig. 3F-G).

Material from Abbey Wood: labial fragment of left M2 (NHMUK.PV.M44991; Hooker 2010: fig. 8a-b).

Material from Fournes: left M1 (UM-FNR2-1), fragment of left M2 (UM-FNR2-2). The acronym FNR2 is relative to a recent sampling of the fossiliferous level, lateral to the classic FNR locality (Marandat 1991).

Material from Rians: right m1 (MNHN.F.Ri516), left m2 (MNHN.F.Ri221; Godinot 1981: pl. 1, fig. 1).

Differential diagnosis: Differs from all other European peradectids (*Pd. russelli*, *Pd. louisi* and '*Armintodelphys*'

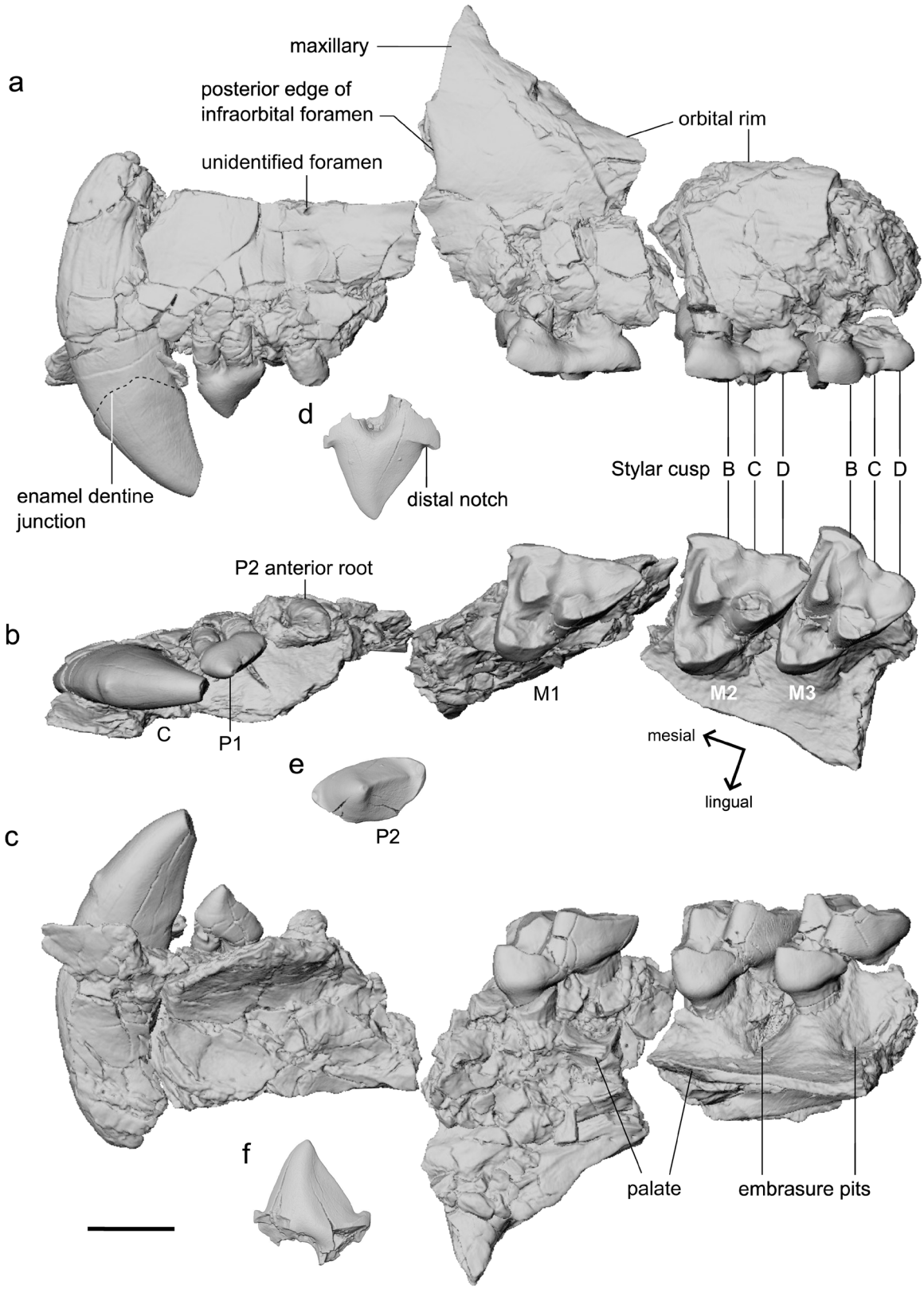

Fig. 3 Composite upper dental row of *Peradectes crocheti* sp. nov. from Palette (Provence; MP7-MP8 + 9 interval). **a-c**. MHN.AIX. PV.2018.26.14, holotype, fragmentary left maxilla with C-P1, anterior root of P2, and M1-M3 (surface model); **a**. labial (lateral) view; **b**. occlusal (ventral) view; **c**. lingual (medial) view. **d-f**. MHN.AIX. PV.2017.6.6, left P2; **d**. labial view; **e**. occlusal view; **f**. lingual view. The arrows indicating mesial and lingual directions apply to the occlusal view of M1 and M2 (**b**). Scale bar equals 1 mm

dufraingi Smith & Smith, 2013) in having lower molars with: (i) a weaker, sometimes absent, labial emargination of the crown; (ii) trigonid as labiolingually wide as talonid on m3; (iii) relatively higher entoconid and hypoconulid separated by a deeper notch; and (iv) distinct postcingulid on m4. Further differs from *Pd. louisi* and *Pd. russelli* in having stylar cusp C apex as or more ventral than stylar cusp D apex on M3 (upper molars of '*Arm.*' *dufraingi* are unknown). Further differs from *Pd. louisi* and '*Arm.*' *dufraingi* in: (i) its relatively wider lower molars; and (ii) always curved instead of at least most often rectilinear postcristid. Further differs from *Pd. louisi* in having: (i) stylar cusp D labial instead of distolabial to metacone apex on M3; and (ii) stylar cusp C apex as or more ventral than stylar cusp D apex also on M1 and M2. Further differs from *Pd. russelli* in its smaller size. Further differs from '*Arm.*' *dufraingi* notably by: (i) entoconid higher than hypoconulid on m2 and as high as hypoconulid on m3; and (ii) larger postcingulid on m2 and m3.

Peradectes crocheti sp. nov. differs from the North American species *Pd. elegans* (type species) and *Pd. protinnominatus* (Fig. 4) in having: (i) p3 higher than m1; (ii) stylar cusp D distolabial instead of labial to metacone apex on M1; (iii) stylar cusp B labial instead of mesiolabial to paracone apex on M3; (iv) asymmetric ectoflexus on M3; and (v) less disparity between length to width ratio of M2 and M3. Further differs from *Pd. elegans* in having: (i) m1 slightly shorter than m2; (ii) m4 shorter than m3; (iii) postcingulid that attenuates labially to the hypoconulid; (iv) stylar cusp B much larger than stylar cusp A on M3; (v) postmetaconular crista that ends lingually to the base of the metacone; (vi) less mesiodistally long talon on upper molars; and (vii) protocone strictly lingual to the paracone apex on M1 and M2.

Comparative description

Remarks: Due to its status as the oldest known European peradectid, and the relative completeness of allocated fossils, *Peradectes crocheti* sp. nov. is compared to Paleocene – Eocene North American peradectids (e.g., Fig. 4), in addition to other European species.

Maxillary region: The holotype MHN.AIX.PV.2018.26.14 is composed of three fragments of maxillary. The fragment bearing the canine, P1, the anterior root of P2 and part of the palate is crushed transversally (Fig. 3a-c). On the fragment bearing M1, the wide distal opening of the infraorbital foramen, with a vertical and straight distal edge, was positioned dorsally to P3 (Fig. 3a). This is congruent with the position of the infraorbital foramen in the other few peradectids in which the maxillary is known, namely *Pd. gulottai* Rose, 2010, M. *houdei* (Horovitz et al. 2009: fig. 2B), and a possible unnamed peradectid from Messel (Kurz and Habersetzer 2004: fig. 2). A small foramen is present dorsally to the anterior root of P2. Compared to the position that would be expected for an incisivomaxillary foramen (just mesial to the infraorbital foramen; e.g., Rose 2010), it is more ventral and probably more mesially positioned. The fragment bearing the M1 extends more dorsally than the two others. It potentially preserved the most external part of the lacrimal on its dorsoposterior crushed region. The maxillary-jugal suture is not visible, as in *Pt. cuvieri* (Fisher, 1829) (Selva and Ladevèze 2017: p. 5). However, the rostrum fragment with the M2 and the M3 probably includes part of the jugal in addition to the maxillary, because the orbital rim is preserved on the most dorsal points between M1 and M3 (Fig. 3a). The most ventral point of the orbital rim is distal to the infraorbital foramen. The orbital rim ascends dorsally on the maxillary distally to the infraorbital foramen, and dorsally to the posterior root of the M1. These observations are also congruent with the position and morphology of the orbital rim in other peradectids. The palate region of the maxillary is preserved without apparent deformation distolingually to M1, and lingually and around M2 and M3 (Fig. 3b-c). M1-M4 alveoli are separated by deep embrasure pits (Fig. 3c).

Upper canine: MHN.AIX.PV.2018.26.14 documents the most complete upper canine of *Peradectes*. Only the apex of the crown is not preserved. The whole tooth is sharp and distally curved. The base of the crown is transversally compressed, less than twice as long as wide (Table 2). The crown is relatively low compared to the root, the latter being dorsoventrally longer (Fig. 3a). The crown is also less than twice as high as the one of P2. In *Mimoperadectes*, the crown of the upper canine is on the contrary much higher than its root and more than twice as high as P2 (Horovitz et al. 2009: fig. 2B). Compared to the upper premolars, the upper canine has an oval-shaped cross-section with equally convex lingual and labial edges. This tooth is particularly short in cross-section, being mesiodistally longer than P1 (MHN.AIX.PV.2018.26.14), but shorter than P2 (MHN.AIX.PV.2017.6.6). Such a mesiodistally relatively short upper canine is known in *Pd. elegans*, for which the section of a partial right canine is documented (Simpson 1935: fig. 3), but not in *Mimoperadectes*, in which the single specimen preserving this tooth has a upper canine longer than the P2 (Horovitz et al. 2009: fig. 2B). The relative height and length of the upper canine of MHN.AIX.PV.2018.26.14 are similar to those of specimens interpreted as females of *Pucadelphys* by Ladevèze et al. (2011) (Muizon and Ladevèze 2022: p. 616–617), and to some herpetotheriids (Crochet 1980b: figs. 165, 166 and 167; Sánchez-Villagra et al. 2007: fig. 1c). The crescentiform distal edge of the crown is labiolingually pinched, unlike the convex mesial edge. Mesial and distal edges are both flanked by a small bulge positioned at the base of the crown. The upper canine is separated from the premolars by a small space, which could be the result of fragmentation (see the lingual view, Fig. 3c). Furthermore,

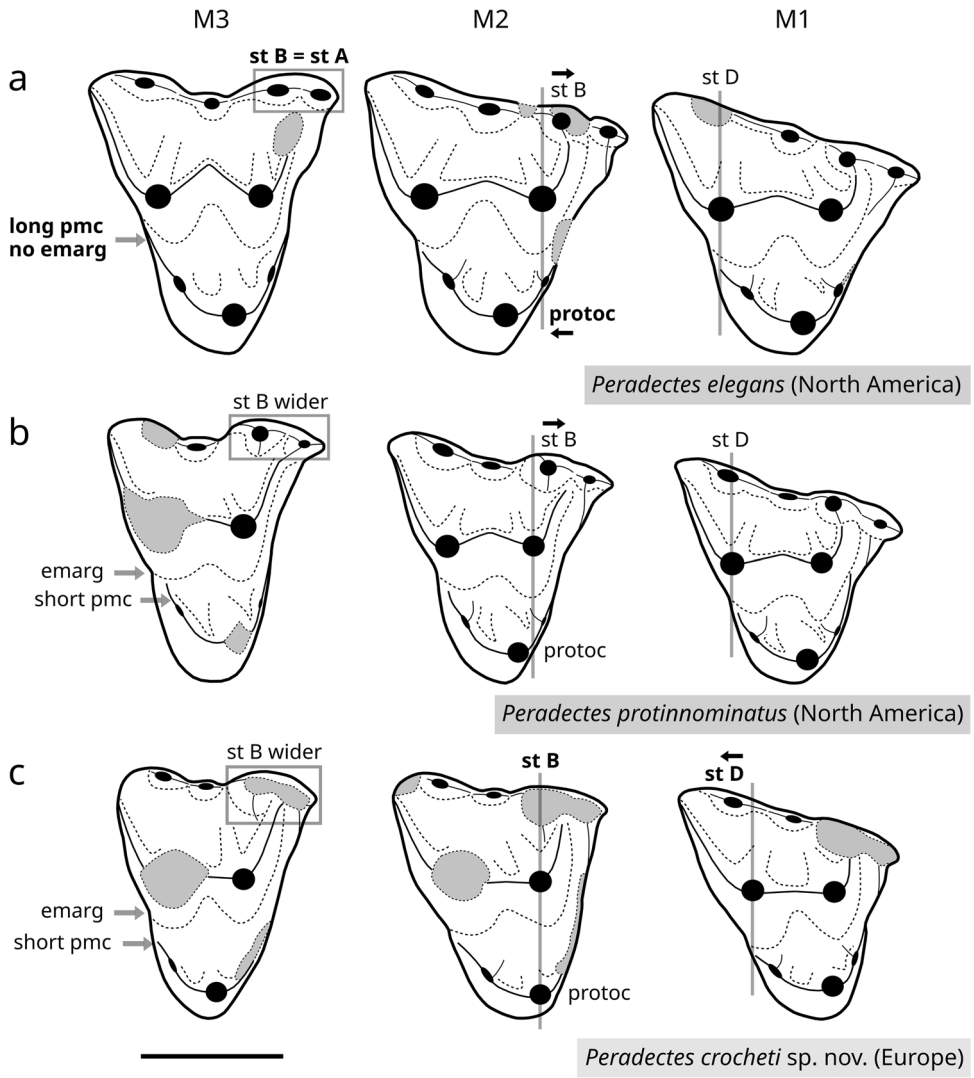

Fig. 4 Interpretative drawings of the occlusal morphology of upper molar rows (M1-M3) of *Peradectes elegans*, *Pd. protinnominatus* and *Pd. crocheti* sp. nov. **a**. *Peradectes elegans*, based on a cast of AMNH 17383 (attribution from Simpson 1935). Grey coloured areas are either broken or lacking on the available cast. **b**. *Peradectes protinnominatus*, based on casts of the holotype, UCMP 44077. The metacone is broken (here in grey coloured area) on the M3 of the original specimen (McKenna 1960). **c**. *Peradectes crocheti* sp. nov., based on the original specimen MHN.AIX.PV.2018.26.14 (reversed view). Note the progressive loss of metastylar wing preservation from M1 to M3 on this specimen. The grey coloured areas are either broken (metacone) or worn (stylar cusps A and B, and mesial edge of the talon). The dashed lines concern depressions on the occlusal surface on all drawings. Main morphological differences between the three dental rows are figured on drawings. Abbreviations: **emarg**, distal emargination; **pmc**, postmetaconular crista; **protoc**, protocone; **st A**, stylar cusp A; **st B**, stylar cusp B; **st D**, stylar cusp D. Black arrows indicate the offset position of a cusp or stylar cusp compared to the axis perpendicular to the paracone – metacone axis. Scale bar equals 1 mm

no diastema is present between the upper canine and the P1 of *Pd. elegans* (Simpson 1935: fig. 3), *Mimoperadectes houdei* (Horovitz et al. 2009: figs. 1A, 2B), or the most complete possible peradectid specimen from Messel (Kurz and Habersetzer 2004: fig. 3B).

Upper premolars: The upper premolars are two-rooted. The mesial root of P2 has a much larger diameter and is higher than the roots of P1 (MHN AIX.PV.2018.26.14, Fig. 3a-b); thus, P2 was considerably larger than P1. The mesial root of P2 is aligned with the roots of P1. The crown of P1 is asymmetric, with the apex of the main cusp mesially placed, ventral to the posterior margin of its anterior root. The convex anterior edge of the crown is slightly triangular in shape in lateral view. The most mesial point of the crown is closer to the base than to the apex of the crown. The lingual and labial edges of P1 are equally convex. The main cusp of P1 bears a relatively long and worn distal crista. In lateral view, this distal crista is not strictly rectilinear, but more vertically inclined near the apex. There are no basal accessory cusps nor cingula on P1. P1 and P2

Table 2 Measurements (in mm) of selected teeth of *Peradectes crocheti* sp. nov. from Palette (MHN.AIX.PV.)

Locus	Length (mm) x Width (mm) [Length / Width]			
	MHN.AIX. PV.2018.26.14 (upper)	2017.6.6 (upper)	2017.6.8 (lower)	2017.6.9 (lower)
C	1.23×0.69 [1.78]	-	-	-
P1	0.93×0.44 [2.11]	-	-	-
P2 or p2	-	1.35×0.64 [2.11]	? x 0.71	-
p3	-	-	1.20×0.68 [1.76]	-
M1 or m1	1.55×1.59 [0.97]	-	-	1.57×0.93 [1.69]
M2 or m2	1.50×1.70 [0.88]	-	1.65×1.04 [1.59]	1.64×1.03 [1.59]
M3 or m3	1.40×1.77 [0.79][a]	-	1.66×1.04 [1.60]	1.68×1.06 [1.58]
m4	-	-	-	1.55×0.92 [1.68]

[a] Metastylar wing worn; length value possibly slightly underestimated

are separated by a small diastema, slightly longer than the space between C and P1. P1 and P2 are also separated by a diastema in *Mimoperadectes houdei* and in the most complete peradectid-like specimen from Messel, but not in *Pd. elegans*. No crown of P2 or P3 is preserved on the holotype, but an isolated premolar crown from Palette is interpreted as a left P2 (MHN.AIX.PV.2017.6.6, Fig. 3d-f), based on its similarity with that premolar locus in other peradectids, as detailed below. It is longer and wider than the crown of P1, and approximately twice as high as P1, as for *Pd. elegans* (Simpson 1935: fig. 3), whereas it is much higher in *Mimoperadectes* (Horovitz et al. 2009). P1 and P2 of *Pd. crocheti* sp. nov. have the same value for their length to width ratio (Table 2). Similarly to *Pd. elegans* and *Mimoperadectes*, the P2 MHN.AIX.PV.2017.6.6 is relatively less mesiodistally elongated than that of *Pd. gulottai*. P2 is less asymmetric than P1, the apex of the former being positioned more distally relatively to the ventral inter-alveolar septum. In occlusal view, the labial edge of the crown is almost rectilinear, whereas the lingual edge is convex. The main cusp is surrounded by one mesial and one distal basal accessory cusp. The mesial accessory cusp is placed slightly labially to the mesiodistal axis of P2. Each accessory cusp is connected to a lingual and a labial cingulum. Both accessory cusps of P2 are the same height, but the distal one is longer, wider, and has stronger cingula. In *Pd. elegans* and *Pd. gulottai*, for which both P2 and P3 are documented, the mesial accessory cusp of P3 has more distally extended cingula than the one of P2 in occlusal and lingual views. The whole labial edge of P3 in *Pd. elegans* is evenly surrounded by a cingulum. The mesial accessory cusp of MHN.AIX.PV.2017.6.6 has cingula relatively weakly developed, like the P2 of other peradectid species (Fig. 3d-e). In lateral view, the mesial edge of the main cusp is convex and the crested distal edge is slightly concave near the apex (Fig. 3d, f). In the same view, there is a notch between the distal crista of the main cusp and the distal accessory cusp, as on all P2 and P3 known for *Peradectes*, namely *Pd. elegans* (AMNH 17383, pers. obs.), *Pd. gulottai* (Rose 2010: fig. 1) and *Peradectes californicus* (Stock, 1936) (Lillegraven 1976: fig. 6). By contrast, the distal crest and accessory cusp are highly connected in *Mimoperadectes* and in most herpetotheriids, so that this notch is absent in, for example, *Herpetotherium* (e.g., Lillegraven 1976: pl. 5, figs. 1-2; Sánchez-Villagra et al. 2007: fig. 1c; Korth 2018: figs. 1c-9a), *Peratherium* (e.g., Crochet 1980b: fig. 205) and the type species of *Amphiperatherium* (Koenigswald 1970: fig. 16). In occlusal and distal views, the distal crista of the main cusp is slightly curved lingually, so that it distally terminates mesiolingually to the distal accessory cusp.

Upper molars: Upper molars are three-rooted. M1 are triangular in shape, almost as long as wide. M2 are shorter and wider than M1 (Table 2). In turn M3 are shorter and wider than M2, so that the length to width (L/W) ratio decreases from M1 to M3 on the holotype (Table 2). The low disparity of length to width ratio between M2 and M3 (= L/W M2 - L/W M3 < 0.10, Table 2) evidences a low discrepancy of proportions between upper molars of MHN.AIX.PV.2018.26.14. The protocone is strictly lingual to the paracone on M1 and M2, like *Pd. protinnominatus*, but unlike *Pd. elegans*, in which the protocone is distolingual to the paracone on these upper molar loci (Fig. 4), and is slightly distolingual to the paracone on M3 and M4 (Figs. 4c and 5t). The protocone may be more mesial on other M3 (e.g., UM-FDN-21, Fig. 5d; MNHN.F.SN18, Fig. 5q) or almost lingual to the centrocrista midpoint on the M3 of the holotype (Fig. 4c). The talon is more mesiodistally expanded on M1 and M2 than on M3. Among M3, the talon is distinctly mesiodistally narrow only on MNHN.F.SN78. A sharp ridge is present on the lingual edge of the acute protocone of the M3 of UM-FDN-21 (Fig. 5d). Such a sharp protocone ridge occurs at least in some other peradectid species (e.g., McGrew 1937: fig. 3). The protocone is always procumbent and lower than the paracone, on all upper molar loci (e.g., Fig. 5n, s). Both conules are relatively small. The metaconule is larger than

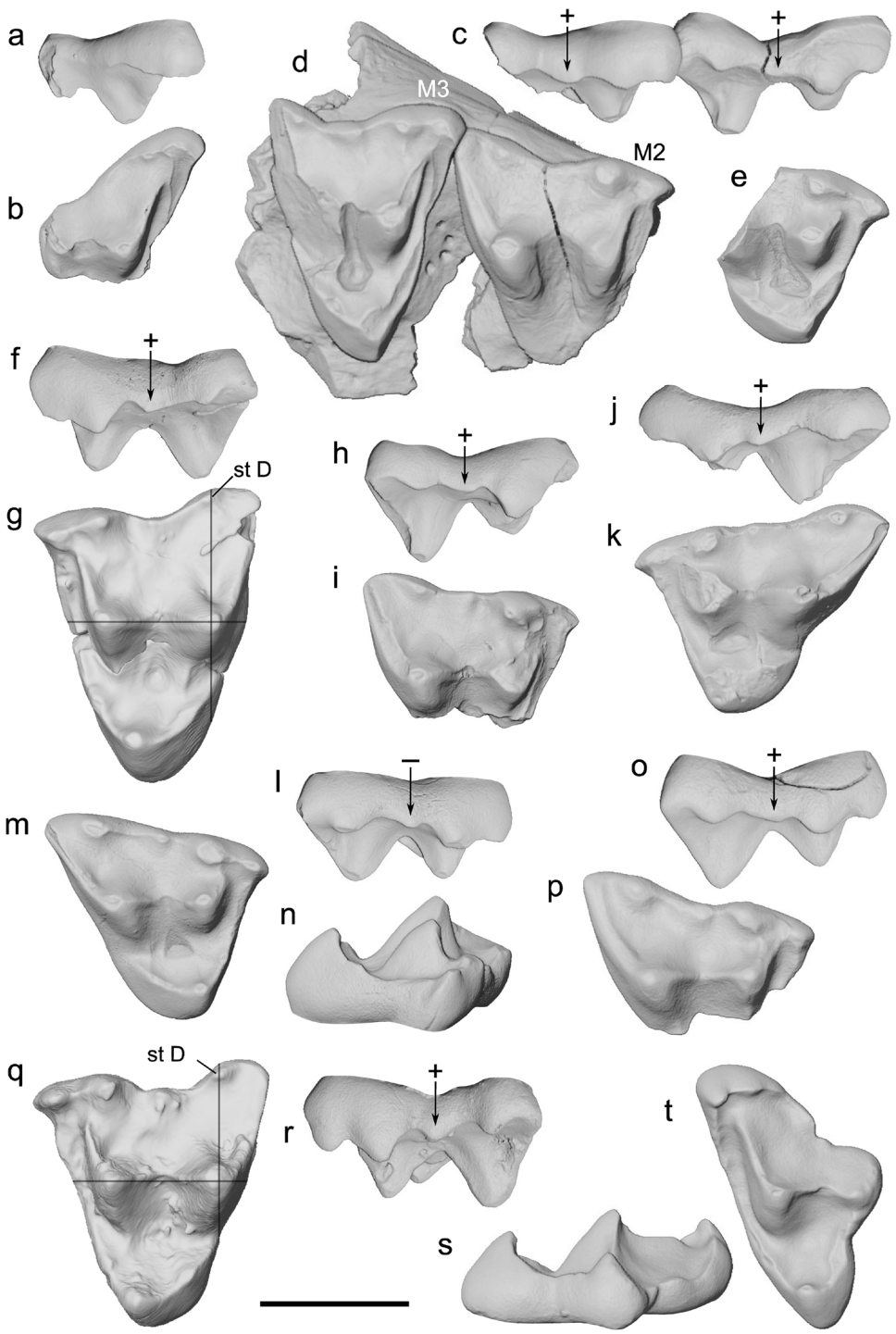

Fig. 5 Upper molars of *Peradectes crocheti* sp. nov. from Fordones, Fournes, Meudon, Palette and Soissons (France; MP7-MP8 + 9 interval). **a-b.** UM-FDN-286, labial fragment of right M4; **a**. labial view; **b**. occlusal view. **c-d.** UM-FDN-21, right partial maxillary with fragmentary M2-M3; **c**. labial view; **d**. occlusal view. **e**. UM-FDN-2, fragmentary right M1 in occlusal view. **f-g.** MHN.AIX.PV.2017.6.7, left M3 (surface model); **f**. labial view; **g**. occlusal view. **h-i.** UM-FDN-285, labial fragment of right M2; **h**. labial view; **i**. occlusal view. **j-k.** UM-FNR2-1, left M1; **j**. labial view; **k**. occlusal view. **l-n.** MHN.AIX.PV.2018.26.20, right M1; **l**. labial view; **m**. occlusal view; **n**. mesial view. **o-p.** MNHN.F.Me15975, labial fragment of right M2; **o**. labial view; **p**. occlusal view. **q-r.** MNHN.F.SN18, left M3 (surface model); **q**. occlusal view; **r**. labial view. **s-t**. MNHN.F.Me16084, left M4; **s**. distal view; **t**. occlusal view. The arrows denoting the stylar cusp C on labial views are followed by '+' if the most ventral point on the st. C – st. D mesiodistal extension is reached on the st. C, and by '-' if this most ventral point is reached on the st. D. The segments on the occlusal views of MHN.AIX.PV.2017.6.7 and MNHN.F.SN18 (**g** and **q**) are positioned on the paracone – metacone axis and its perpendicular line. Abbreviation: **st D**, stylar cusp D. Scale bar equals 1 mm

the paraconule (e.g., Fig. 5n), although still low in distolingual view (Fig. 3c). The paraconule is positioned slightly more labially than the metaconule. The preparaconular crista extends labially to form the mesial edge of the paracingulum, and the postmetaconular crista ends lingually to the base of the metacone. Faint internal conular cristae often connect the conules to the base of the paracone or metacone, mostly on M1 (e.g., Figs. 4c and 5e and k). Such serial variation for the presence of the internal conular cristae is noted in the dental rows of *Pd. elegans* and *Pd. protinnominatus*, with their M3 lacking the internal conular cristae (Fig. 4b-c). Only one M3 of *Pd. crocheti* sp. nov. has an internal conular crista, on the metaconule (Smith et al. 2011: fig. 5.18B). A deep basin is present on

the talon distolabially to the paraconule and mesiolabially to the metaconule of all upper molars.

The distal edge of M1-M3 is often emarginated between the talon and stylar shelf. This emargination is deep (e.g., UM-FNR2-1, Fig. 5k) to occasionally absent on Palette specimens (MHN.AIX.PV.2017.6.7 and MHN.AIX.PV.2018.26.20, Fig. 5g, m). The distal emargination is present on M3 of *Pd. protinnominatus*, but not on M3 of *Pd. elegans*, for which the postmetaconular crista extends distolabially to the lingual extremity of the metacone base (Fig. 4a; Krishtalka and Stucky 1983b: fig. 3) unlike the M3 of both *Pd. crocheti* sp. nov. and *Pd. protinnominatus*. The paracingulum is straight and mesiodistally long on most specimens, whereas the mesial edge is slightly emarginated mesially to the paracone on the M1 of the holotype (Fig. 3b), the M2 from Croydon (Hooker 2020: fig. 3G), and more strongly emarginated on the M1, M3 and one M4 from Fordones (UM-FDN-286, Fig. 5b; UM-FDN-21; Fig. 5d; UM-FDN-23; Marandat 1991: pl. 1, fig. 2). The height of the paracone and metacone varies for a given molar locus, but the paracone is always lower on M1-M3. For example, on the unworn M1 the paracone and metacone can be subequal in height, the paracone being slightly lower (e.g., MHN.AIX.PV.2017.6.11, MHN.AIX.PV.2018.26.20; Fig. 5l), or the paracone can be much lower than the metacone (e.g., MNHN.F.SN76). It is worth mentioning that a paracone and metacone that are subequal in height have also been documented in *Pt. constans* (e.g., Ladevèze et al. 2012: fig. 5Ga). The paracone is also less mesiodistally long than the metacone. The paracone and metacone are conical, with a convex labial edge contrary to herpetotheriids, where these main cusps are triangular. The labial edge of these cusps is narrower labiolingually than their lingual edge. The centrocrista is straight, unlike the V-shaped centrocrista of most herpetotheriids. Some upper molars have a less straight centrocrista than M1-M3 of the holotype, such as UM-FDN-1 for M1 (Fig. 5e), UM-FDN-21 for M2 (Fig. 5d), MNHN.F.SN18 for M3 (Fig. 5q) and MNHN.F.Me16084 for M4 (Fig. 5t). The same variation is established for *Pd. elegans* specimens, with the centrocrista of AMNH 17383 upper molars being more V-shaped (especially on the M3 and M4, Fig. 4a) with respect to the strictly straight centrocrista of the upper molars of the paratype AMNH 17369 (Krishtalka and Stucky 1983b: fig. 3). The postmetacrista is generally low, and it does not define a distal wall on the less worn stylar shelf (e.g., MHN.AIX.PV.2017.6.7, Fig. 5g; MNHN.F.Me15975, Fig. 5p), except on two upper molars, namely the M1 MHN.AIX.PV.2018.26.20 (Fig. 5n) and the fragmentary M3 MNHN.F.SN78. Distal to the metacone, the distal margin of the tooth is mesiodistally long instead of being strictly vertical on one M3 and two M1 from Palette (MHN.AIX.PV.2017.6.7, Fig. 5g; MHN.AIX.PV.2017.6.11 and MHN.AIX.PV.2018.26.20, Fig. 5m). The same variation is seemingly also present in the herpetotheriid *Peratherium constans* Teilhard de Chardin, 1927 (Ladevèze et al. 2012: fig. 5Gb vs. fig. 5Hb). The stylar shelf labiolingually widens relative to the talon from M1 to M4. It is approximately slightly narrower than the talon on M3, and subequal in width with the talon on the M4 MNHN.F.Me16084 (Fig. 5t).

The stylar line bears four stylar cusps, from stylar cusp A to stylar cusp D, in most specimens. However, there is a distinct stylar cusp E on a single specimen of the sample, MNHN.F.SN78, where it is as high as stylar cusps C and D, but less mesiodistally long. Stylar cusp B is dominant in size over the other stylar cusps in *Pd. crocheti* sp. nov. and *Pd. protinnominatus*, whereas it is subequal in length and width to stylar cusp A in *Pd. elegans* (Fig. 4b-c vs. Fig. 4a). It is worth noting that stylar cusps A and B are of the same labiolingual width on the M3 of UM-FDN-21 (Fig. 5d). On M1-M3 of *Pd. crocheti* sp. nov., stylar cusp A is higher than stylar cusps C and D. The spur-like stylar cusp A can be mesiolabial or labial to the paracingulum on M1 (Figs. 3b and 5k vs. Fig. 5m), M2 (Fig. 5d and UM-FNR2-2 vs. Figs. 3b and 5i and p) and M3 (Fig. 5g, q vs. Figs. 3b and 5d). Stylar cusp A bears a sharp mesial crest. Stylar cusp A is most frequently placed mesiolingually to stylar cusp B on M2 and M3, as in the European *Pd. louisi* and *Pd. russelli*, or *Peradectes chesteri* Gazin, 1952 (e.g., Murphey et al. 2018: fig. 13.3), and *Pd. californicus* (e.g., Lillegraven 1976: pl. 7, fig. 1c), wheareas the two stylar cusps are most often aligned in *Pd. elegans* and *Pd. protinnominatus* (e.g., Fig. 4; see also comparison in Online Resource 3: Fig. S10). An exception for *Pd. crocheti* sp. nov. is the M3 of UM-FDN-21 on which stylar cusp A is strictly mesial to stylar cusp B. From M1 to M4, the preparacrista elongates, stylar cusps A and B are increasingly close, and the relative height of stylar cusp A gradually increases, so that stylar cusp A is higher than stylar cusp B on the unworn M4 (Fig. 5s). All these tendencies are evidenced on the composite upper molar series from Fordones (Fig. 5a-e). On the holotype MHN.AIX.PV.2018.26.14, the preparacrista labially connects stylar cusp B on the M1 and M2, and stylar cusp A on the M3 (Fig. 4c). In the whole sample, the connection of the labial end of the preparacrista is as such in 6 out of 8 of the M1 (e.g., Fig. 5m), 4 out of 6 of the M2 with available preparacrista and stylar cusps A and B (e.g., Fig. 5i), and 4 out of 6 of the M3 (e.g., Fig. 5d, g). M1 to M3 specimens with a different labial connection of this crest have a preparacrista that labially ends in an intermediate position between stylar cusps A and B, namely UM-FDN-2 and UM-FNR2-1 for M1 (Fig. 5e, k), MNHN.F.Me15975 for M2 (Fig. 5p) and MNHN.F.SN18 and the upper molar from Sotteville-sur-Mer for M3 (Fig. 5q; Smith et al. 2011: fig. 5.18B). The M2 of the holotype of *Pd. protinnominatus* also has a preparacrista that labially ends in an intermediate position between the anterior stylar cusps (Fig. 4b). One M2 of *Pd. crocheti*

sp. nov. (UM-FDN-21) has a preparacrista that connects to stylar cusp A (Fig. 5d). The preparacrista of most M1 and M2 connects to stylar cusp B through a thin crest situated on the lingual edge of stylar cusp B. Even without connection between these structures on M3, such a crest may be present (e.g., UM-FDN-21, Fig. 5d). On M1-M3, stylar cusp B is conical, lower than the paracone (labial views of Fig. 5) and generally positioned strictly labially to the paracone apex. Stylar cusp B is relatively slightly more mesial on the M3 of the holotype (Fig. 4c), on UM-FDN-23 and maybe on the M3 of UM-FDN-21 (Fig. 5d), but the broken metacone of the latter prevents unequivocal observation. Stylar cusp B is mesiolabial to the paracone apex on M1-M3 of Paleocene - Eocene North American peradectids, such as *Pd. elegans* (Fig. 4a; Krishtalka and Stucky 1983b: fig; 3), *Pd. protinnominatus* (Fig. 4b; McKenna 1960: fig. 18b; Bown 1979: fig. 40a right), and *Pd. chesteri* (e.g., West 1973: pl. 1, figs. c-d). We should mention that stylar cusp B is also strictly labial to the paracone apex on upper molars of *Pd. protinnominatus* from the Clarkforkian-3 (late Paleocene) and Wasatchian-M (early Eocene) localities of the northern Bighorn Basin (pers. obs.; Gingerich and Smith 2006: fig. 26E), and of cf. *Pd. protinnominatus* from the Wasatchian-0 of the southern Bighorn Basin (Rose et al. 2012: fig. 14A-C).

Stylar cusps C and D are more labiolingually pinched than stylar cusp B. Stylar cusp C is labial to the midpoint of the centrocrista. The single upper molar with a double stylar cusp C is the M2 from Abbey Wood (Hooker 2010: fig. 8a-b), on which the distal stylar cusp C is larger than the mesial one. The doubling of stylar cusp C is as rare as in *Pd. louisi* (see below); it is more frequent in herpetotheriids such as *Pt. constans* (Ladevèze et al. 2012) and *Amphiperatherium maximum* Crochet, 1979 (Crochet 1980b: p. 98–100), and seemingly in *Mimoperadectes* (M2 in Bown and Rose 1979: fig. 2; Gingerich and Smith 2006: fig. 15C; Beard and Dawson 2009: fig. 4A; M1 in Horovitz et al. 2009: fig. S1C). Stylar cusp C has an intermediate position between stylar cusps B and D, with the exception of two M1 where stylar cusps B and C are more closely appressed together (MNHN.F.SN76 and UM-FNR2-1; Fig. 5j-k). On a given molar locus, stylar cusps C and D can be highly connected or separated by a fossa (e.g., for M3, Fig. 5f vs. Fig. 5r). In occlusal view, the area occupied by stylar cusp C is less important than the area of stylar cusp D on M1 and M2 (especially on M1, Figs. 4c and 5i, k, m and p). Stylar cusps C and D are subequal in width on M3. In labial view, the apex of stylar cusp C is as ventral or more ventral than the apex of stylar cusp D on all M1-M3, with the exception of the M1 MHN.AIX.PV.2018.26.20 (Figs. 5l, 1 out of 18 available specimens). Altogether, the relative heights of the stylar cusps of M1 to M3 of *Pd. crocheti* sp. nov. are mostly as follows: st. B > A ≥ C ≥ D (Table 3). Among ascertained peradectids, the apex of stylar cusp C is also at least as ventral as the apex of stylar cusp D only in the oldest *Peradectes* species, namely *Pd. minor*, *Pd. coprexeches*, *Pd. elegans*, *Pd. protinnominatus*, and in *Mimoperadectes labrus* and *M. sowasheensis* (Table 3). Stylar cusp C is also relatively prominent (equal in size to stylar cusp B) on the only upper molar attributed to *Armintodelphys* (Table 3). In labial view, the distal crest of stylar cusp C is always mesiodistally longer than its mesial crest on M1-M3. Stylar cusp D is distolabial to the metacone on M1 (labial to the metacone on M1 of *Pd. elegans* and *Pd. protinnominatus*; Fig. 4) and strictly labial to the metacone on M3. Stylar cusp D of M2 can be strictly labial or distolabial to the metacone (e.g., Fig. 5i vs. Figs. 4c and 5p). This variation may occur also in *Pd. protinnominatus* because unillustrated M2 attributed to this species by Gingerich and Smith (2006: p. 254) (UM 113378 and UM 113391, pers. obs. of corresponding casts) have a stylar cusp D distolabial to the metacone contrary to the holotype of *Pd. protinnominatus* (Fig. 4b). The relatively lowest stylar cusp D of the sample is on the M3 UM-FDN-23 (Marandat 1991: pl. 1, fig. 2). The ectoflexus is absent on all M1, which have a straight labial margin unlike M1 in *Pd. protinnominatus* (e.g., Fig. 4b vs. Fig. 4c). M2 have shallower asymmetric ectoflexus than M3. The ectoflexus is always long and asymmetric on M3, with a metastylar wing more labially extended than the parastylar wing. Variations in the depth and degree of asymmetry of the ectoflexus of M3 exist, both in Palette (MHN.AIX.PV.2018.26.14, Fig. 4c vs. MHN.AIX.PV.2017.6.7, Fig. 5g) and Fordones (UM-FDN-21, Fig. 5d vs. UM-FDN-23, Marandat 1991: pl. 1, fig. 2). The metastylar wing is worn on the M2 and M3 of MHN.AIX.PV.2018.26.14, especially on the M3 (Fig. 4c), resulting in the weak asymmetry of the ectoflexus mentioned. The metastylar wing is acute on unworn M1-M3.

Additional description of the M4 can be made. This locus is documented by four specimens, of which only the left M4 from Meudon (MNHN.F.Me16084, Fig. 5s-t) is complete. The straight centrocrista of M4 is shorter than on more anterior molars, and this upper molar is mesiodistally shorter than others. On MNHN.F.Me16084, the protocone is lower than the paracone but higher than the metacone (Fig. 5s). On MHN.AIX.PV.2017.6.12, the protocone is higher than the metacone, and relatively more mesial than on MNHN.F.Me16084, so that it is strictly lingual to the paracone. A protocone higher than the metacone on M4 is known in other peradectids such as *Mimoperadectes labrus* (pers. obs., UM 66144) and *Pd. russelli*. The crescentiform paraconule is indistinct in lateral view on MHN.AIX.PV.2017.6.12, but present on MNHN.F.Me16084 (Fig. 5s). Both specimens have a tiny metaconule close to the lingual edge of the metacone. The conules lack internal cristae. The distal edge of the talon of both MNHN.F.Me16084 and UM-FDN-289 is deeply emarginated (Fig. 5t), whereas it is straight on MHN.AIX.

Table 3 Height relationships of stylar cusps (A to D) of all ascertained peradectid species for which M2 and/or M3 are known. See method [1] for estimating stylar cusp heights in Fig. 2a. Species positioned above the median horizontal line of the table have stylar cusp C apex at least as ventral as stylar cusp D apex; species positioned below the median horizontal line have stylar cusp C apex less ventral than stylar cusp D apex, at least on one locus, or have vestigial stylar cusp C. Height relationships of stylar cusps are partially in bold when stylar cusp B is not dominant over other stylar cusps. *, more than one specimen of the species (including illustrated specimens) has been observed in labial view in this study

Species	Stylar height relationships	References
Armintodelphys dawsoni	M2: **B = C**	Krishtalka and Stucky (1984: p. 40)
*Mimoperadectes labrus**	M2: B > C ≥ D ≥ A M3: B > A > C > D[a]	Gingerich and Smith (2006: fig. 15C); Rose et al. (2012: fig. 12E)
Mimoperadectes sowasheensis	M2: B > A > C > D	Beard and Dawson (2009: fig. 4A)
Peradectes coprexeches	M3: **C ≥ B** > D	Williamson and Taylor (2011: fig. 6.7)
Peradectes crocheti sp. nov.*	M2-M3: B > A ≥ C ≥ D	this study; e.g., Smith et al. (2011: fig. 5.18A); Hooker (2020: fig. 3F)
Peradectes elegans	M2: **B = C** > A = D M3: B > A > C ≥ D	cast of AMNH 17383 (in Simpson 1935: fig. 3)
Peradectes minor	M2-M3: B = A > C > D	Clemens (2006: fig. 2C, E)
*Peradectes protinnominatus**	M2-M3: B > A = C = D	cast of UCMP 44077 (holotype); Gingerich and Smith (2006: fig. 26D)
Didelphidectes cf. *pumilis*	M3: B > D > > C (vestigial or absent)	Kihm and Schumaker (2015: fig. 13N-O)
Mimoperadectes houdei	M2: B > D > > A = C M3: B = A > D > > C	Horovitz et al. (2009: fig. S1C)
Nanodelphys hunti	M2-M3: B > D > > C (vestigial or absent)	McGrew (1939: 394, fig. 114); Korth (1994: 390, fig. 7.1-2)
Peradectes californicus	M3: B = A > D > > C	Lillegraven (1976: pl. 7, fig. 1a)
Peradectes chesteri	M2-M3: B > > C, D (vestigial or absent)	Krishtalka and Stucky (1983b, 1984); Murphey et al. (2018)
Peradectes gulottai	M2: B > A > D > > C M3: B = A > D > > C	Rose (2010: fig. 1.1)
*Peradectes louisi**	M2: B > A > D > C[b] M3: B > A > > D > C	this study
*Peradectes russelli**	M2: B > A = C = D M3: B > A > D > C	this study

[a]the relative height of stylar cusp A of M3 differs from the one reported by Bown and Rose (1979: p. 90) for the holotype

[b]in one M2 specimen (MNHN.F.CB3228; Fig. 10i), stylar cusp C is lower than stylar cusp D

PV.2017.6.12. On all specimens, the paracone is much higher, longer and wider than the metacone. The labial edge of the paracone of UM-FDN-286 is almost as convex as the lingual edge, whereas MNHN.F.Me16084 has a more triangular paracone (Fig. 5s). The preparacrista is directed towards stylar cusp A but it ends distolingually to it. Stylar cusps A and B are placed mesiolabially to the paracone on both UM-FDN-286 and MNHN.F.Me16084. Stylar cusps A and B are separated by a shallow notch on MNHN.F.Me16084 (this area is worn on UM-FDN-286). On the specimen from Meudon, stylar cusp A is reduced in surface compared to stylar cusp B, which is mesiodistally long and doubled (Fig. 5t). The specimen from Fordones being worn in its most mesiolabial part, it is not possible to conclude whether the stylar cusps in the A and B positions are a relatively large stylar cusp B and small stylar cusp A, or a doubled stylar cusp B (Fig. 5b). Stylar cusp C is here the lowest stylar cusp, and there is no stylar cusp D. Stylar cusp C is positioned mesiolabially to the midpoint of the centrocrista in both specimens (Fig. 5b, t), as in *Pd. elegans* (Krishtalka and Stucky 1983b: fig. 3), but unlike, for example, certain European herpetotheriids in which it is strictly labial to the centrocrista (e.g., *Peratherium constan*s, Ladevèze et al. 2012: figs. 4D, 5D; *Pt. elegan*s, Ladevèze et al. 2012: fig. 7a; *Pt. cuvieri*, Selva and Ladevèze 2017: fig. 5Ab). Interestingly, stylar cusp C is also mesiolabial to the midpoint of the centrocrista in some herpetotheriid species (e.g., Crochet 1980b: figs. 109 and 223). Stylar cusp C is more crescentiform on UM-FDN-286 than on MNHN.F.Me16084. The ectoflexus is well-developed, again as in *Pd. elegans*, which distinguishes the isolated M4 of *Pd. crocheti* sp. nov. from those of the coeval herpetotheriid *Pt. constans* or the type species of herpetotheriids, *Herpetotherium fugax* Cope, 1873 (e.g., Fox 1983: fig. 2a), which lack the ectoflexus.

Mandible and lower premolars: The right dentary MHN.AIX.PV.2017.6.8 is preserved from the canine alveolus to the m3 (Fig. 6). The canine alveolus is labially broken. The dentary bears an anterior mental foramen situated below the posterior root of the p1 (Fig. 6b-c), and a posterior mental foramen situated below the posterior root of the m1 (Fig. 6c). The presence of mental foramina below p1 and m1 (with slight variations) is almost always observed in peradectids and herpetotheriids (e.g., Korth 1994: fig. 8; Ladevèze et al. 2012: fig. 3A-B; Smith and Smith 2013: fig. 4A; Korth 2018: fig. 14f; but see Korth

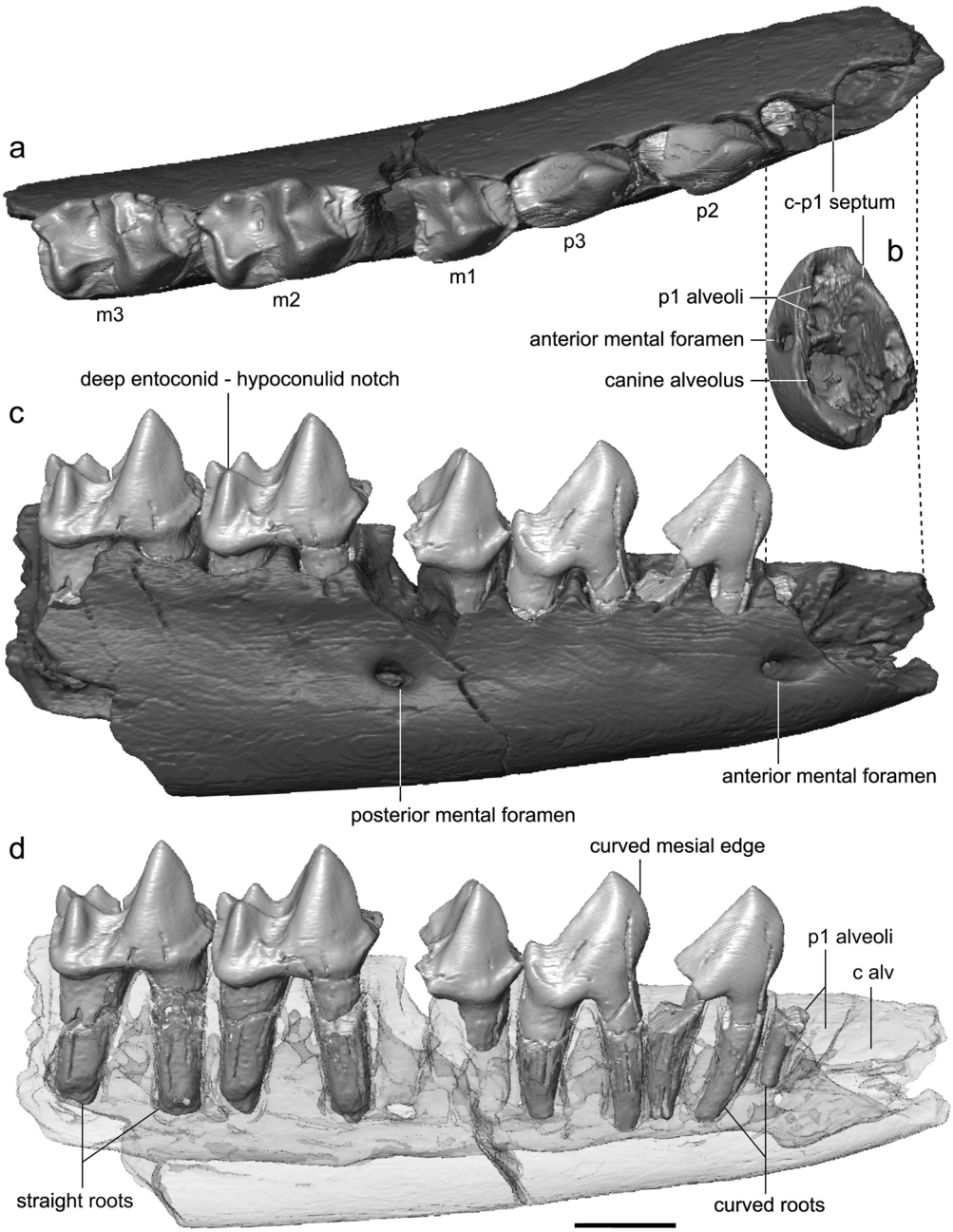

Fig. 6 Surface model of MHN.AIX.PV.2017.6.8, right hemi-mandible fragment with canine alveolus, posterior root of p1, partial p2, p3, partial m1, and m2-m3 of *Peradectes crocheti* sp. nov. from Palette (Provence; MP7-MP8 + 9 interval) in: **a**. occlusal (dorsal) view; **b**. mesiolabial (anterolateral) view with focus on c-p1 alveoli; **c**. labial (lateral) view; **d**. labial (lateral) view with transparent dentary. Abbreviation: **c alv**, canine alveolus. Scale bar equals 1 mm

1994: p. 393, for *Armintodelphys*). The depth of the dentary gradually increases posteriorly to the canine alveolus. The unfused mandibular symphysis extends posteriorly to a point ventral to the posterior alveolus of the p2 (Online Resource 6), as in *Pd. elegans* (Simpson 1935: fig. 2; pers. obs. of a cast of AMNH 17376) and alphadontids (e.g., Clemens 1966: figs. 58a, 61a; Cifelli and Muizon 1998: fig. 2B). The maximum posterior dorsoventral width value of the mandibular symphysis of *Peradectes* is lower than the value of the width between the most posterodorsal point of the symphysis and the posterior alveolus of p2 (Online Resource 6), contrary to figured alphadontid hemi-mandibles with a preserved symphysis (Clemens 1966: figs. 58a, 61a), in which these two width values appear at least subequal (but see the juvenile alphadontid specimen in Cifelli and Muizon 1998:

fig. 2B). The symphyseal angle between the long axis of the symphysis and the horizontal axis of the tooth row measures approximately 20°; this is close to the lowest values obtained from similar measurements performed in several fossil and extant marsupialiforms (Muizon and Ladevèze 2020: table 7). The posterior root of the p1 is preserved within its posterior alveolus. It is much smaller than the posterior root of p2 and p3, and it descends less deeply ventrally, within the dentary (Fig. 6d). The whole p1 was thus much smaller than the p2 and p3. There are no diastemata between the lower premolars. In occlusal view, the position of the anterior alveolus of the p1, mesially or distally to the inter-alveolar septum, is unclear (Fig. 6a). A similar uncertainty applies to the holotype of both *Pd. elegans* (AMNH 17376) and *Pd. californicus* (Stock 1936: pl. 1, fig. 2a), so that the p1 of *Pd. elegans* was first considered to be single rooted (Simpson 1935: p. 10). In occlusal view of MHN.AIX.PV.2017.6.8 (Fig. 6a), alike in *Pd. elegans* (pers. obs. of a cast of AMNH 17376), the alveolus apparently anterior to the posterior root of the p1 is larger than expected for this premolar locus. The p1 is actually two rooted in both *Pd. elegans* (Fox 1983: fig. 3) and *Pd. crocheti* sp. nov. (Fig. 6d), with a smaller anterior than posterior root in cross section, as revealed by computed tomography study of MHN.AIX.PV.2017.6.8 for the European species. In *Pd. crocheti* sp. nov., the anterior root of the p1 is laterally adjacent to the inter-alveolar septum separating the canine alveolus from the p1 roots (Fig. 6b, d). Consequently, there is no diastema between between the p1 and lower canine, these two teeth being close together (Fig. 6b), as in *Pd. elegans* (Fox 1983).

Contrary to the lower molars, all lower premolars have mesiodistally curved roots (Fig. 6d). This character has not been studied so far for both peradectids and herpetotheriids. Interestingly, lower premolars of some Eocene herpetotheriids exhibit straight roots, similar to the lower molars (e.g., holotype of *Amphiperatherium fontense* Crochet, 1979; Crochet 1980b: fig. 123; pers. obs. of UM-BRT-574, *Amphiperatherium bourdellense* Crochet, 1979, Le Bretou, in Quercy). The posterior root of all preserved cheek teeth of MHN.AIX.PV.2017.6.8 is larger than the anterior root in cross section. The roots of all lower cheek teeth decrease in circumference ventrally to the crown. The unworn p2 and p3 of MHN.AIX.PV.2017.6.8 are the first lower premolar crowns allocated to European peradectids. The posterior heel of the p2 is broken. The p2 and p3 are similar in width, the p2 being only slightly wider (Table 2). The p3 is relatively labiolingually wider than in *Pd. elegans* (Krishtalka and Stucky 1983b: table 2). The apex of the p3, situated on the main cuspid, is slightly but distinctly higher than the apex of the p2 and of the m1, which is situated on the protoconid for the latter (Fig. 6c-d; Online Resource 6). On the p2 and p3, the apex overhangs its respective anterior root. The p2 is slightly procumbent, because its apex is positioned dorsomesially to the most ventral point of the anterior root, whereas the apex of the p3 is strictly dorsal to the most ventral point of its anterior root. In lateral view, the main cuspid of the p2 and p3 forms the mesial edge of these teeth, which is projected mesially to the anterior root. It is curved as in other *Peradectes* species (e.g., AMNH 17376, holotype of *Pd. elegans*; UCMP 45950, paratype of *Pd. protinnominatus*), contrary to herpetotheriids in which it is V-shaped (e.g., Korth 1994: fig. 8.1 for *Herpetotherium fugax*). In mesial view, the main cuspid is bent lingually. The distal cristid of the main cuspid is straight in lateral view. The p3 is almost as long as high. The distal heel of the p3 is short and bears two accessory cuspids (Fig. 6a), whereas the described p3 of North American peradectids have only one accessory cuspid on their distal heel. The distal heel is lower in *Mimoperadectes* and *Armintodelphys* (see illustration in Online Resource 3: Fig. S1). Some rare herpetotheriid specimens also have double accessory cuspids on the heels of their lower premolars (e.g., Hooker 2010: fig. 8n-p). These accessory cuspids are positioned on the cingulid that surrounds the distal heel. The larger and higher distal cuspid, on the distal margin of the p3, is connected to the distal cristid of the main cuspid (Fig. 6a). This first accessory cuspid is pointed, dorsal to the ventralmost point reached by the distal cristid of the main cuspid. The second distal cuspid is smaller, and is positioned on the distolingual margin of the p3. The connection between the distal cristid of the main cuspid and the main accessory cuspid divides the heel into unequal lingual and labial parts, the labial surface being both lower and less laterally spread than the lingual surface. Both accessory cuspids of the heel of the p3 are connected by a high cristid formed by the heel cingulid. The lingual cingulid is mesiodistally longer than the labial cingulid. However, as in *Mimoperadectes* (Bown and Rose 1979: fig. 1), the lingual cingulid is much shorter than in *Pd. elegans* and *Pd. protinnominatus*, in which it ascends the distolingual edge of the main cuspid (e.g., Simpson 1935: fig. 2).

Lower molars: The description of the lower molars is primarily based on the two lower tooth rows from Palette (MHN.AIX.PV.2017.6.8, right, and MHN.AIX.PV.2017.6.9, left), possibly representing the same individual. The partial right hemi-mandible MHN.AIX.PV.2017.6.9 (Fig. 7a-c) preserves a complete molar series (m1-m4). The m1 is smaller (in length and width) than the m2, which is in turn as large or slightly smaller than the m3 (Table 2). The m4 is the smallest locus of the lower molar row. The trigonid is narrower labiolingually than the talonid on the m1, the reverse on the m4. m2 have a labiolingually wider talonid than trigonid (e.g., MHN.AIX.PV.2017.6.9, Fig. 7a; MNHN.F.Ri221, Fig. 7g), with the exception of the m2 from Meudon (MNHN.F.Me16101, Fig. 7i), on which the trigonid and talonid are as wide. All m3 have a trigonid

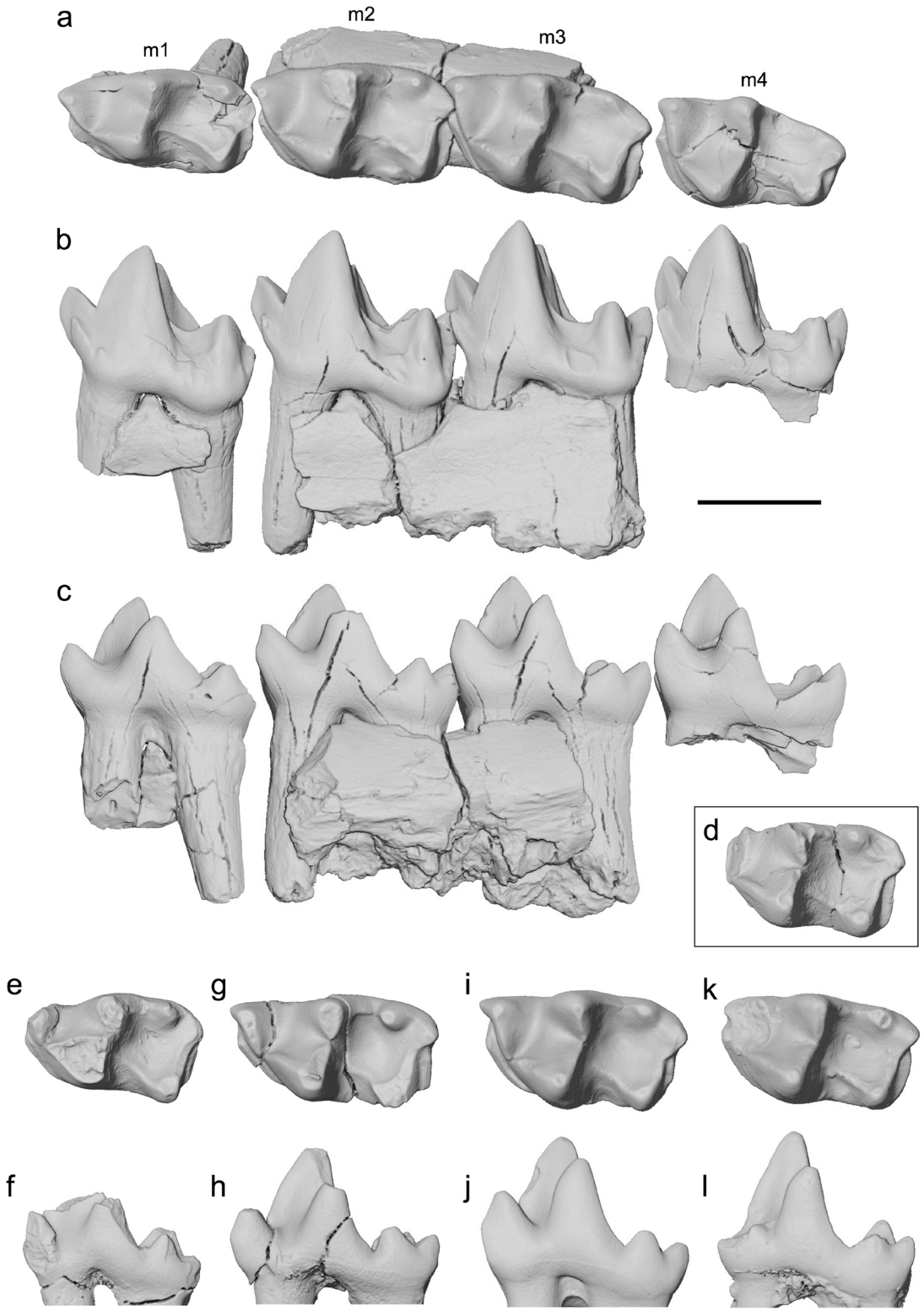

Fig. 7 Lower molars of *Peradectes crocheti* sp. nov. (except **d**) from Palette, Meudon, Rians and Soissons (France; MP7-MP8 + 9 interval). **a-c.** MHN.AIX.PV.2017.6.9, left m1-m4 row with fragments of dentary; **a**. occlusal view; **b**. labial view; **c**. reversed lingual view. **d**. comparison with UM-FDN-18, fragmentary right m2 from Fordones (Corbières) attributed to *Peratherium constans* (Marandat 1991: p. 68), in reversed occlusal view. **e-f.** MNHN.F.Ri516, right m1; **e**. reversed occlusal view; **f**. lingual view. **g-h.** MNHN.F.Ri221, left m2; **g**. occlusal view; **h**. reversed lingual view. **i-j.** MNHN.F.Me16101, left m2; **i**. occlusal view; **j**. reversed lingual view. **k-l** MNHN.F.SN2508, right m3; **k**. reversed occlusal view; **l**. lingual view. Scale bar equals 1 mm

equal in labiolingual width to the talonid (e.g., MHN.AIX.PV.2017.6.9, Fig. 7a; MNHN.F.SN2508, Fig. 7k), as in *Pd. elegans* and contrary to the other European peradectid species. The trigonid is longer than the talonid on all molars. One of the three known m1, MNHN.F.SN121, has a trigonid less labiolingually wide than the m1 from Palette and Rians, with a relatively longer paracristid lingual segment, which is also found in *Pd. louisi* and *Pd. russelli*. On both molar rows from Palette (Figs. 6a and 7a), the m2 and m3 have a trigonid as mesiodistally long as labiolingually wide. Only one isolated m3, also from the type locality (MHN.AIX.PV.2017.6.10), exhibits a trigonid longer than wide.

On MHN.AIX.PV.2017.6.9, a groove on the mesial surface of the paraconid of the m3, lingual to the precingulid, contacts the hypoconulid of the m2. In anatomical position on the dentary, the apex of the hypoconulid of m2 is ventral to the apex of the paraconid of m3. The precingulid labiolingually extends from a point mesial or slightly mesiolabial to the apex of the paraconid, to a point mesial to the apex of the protoconid. In lingual view, the paraconid is less and less mesially projected from m1 to m4 (Fig. 7c), but its mesiolingual edge is always keel-like, as in all metatherians. The preparacristid is longer on the m2 from Meudon (Fig. 7i) than on the m2 of MHN.AIX.PV.2017.6.9. In occlusal view, the paracristid lingual segment elongates from m1 to m4. The postmetacristid shortens from m1 to m4 on occlusal view (Fig. 7a), so that it is almost vertical in lingual view on the m4 (Fig. 7c). On m1 and m2, the metaconid is longer than the paraconid, and longer than the metaconid of m3 and m4. The metaconid of m3 is only slightly longer than the paraconid. Those two cuspids are of equivalent length on m4. The protoconid is the highest cuspid of the trigonid on all lower molars. The metaconid is higher than the paraconid, their height difference being less marked on m4 than on anterior molar loci (Fig. 7c). The metaconid is either well distolingual to the protoconid (e.g., Fig. 7a) or relatively closer to it mesiolabially (e.g., Fig. 7g). The paracristid is always longer than the protocristid. On the mesial edge of the protoconid, the preprotocristid is convex in mesiolabial view (Fig. 6c), except on m4. The labial edge of the protoconid is weakly convex in mesial or distal view.

The protocristid notch opens more ventrally than both the paracristid notch and the lingual opening of the trigonid basin. The latter is always higher than the lingual opening of the talonid basin, unlike in herpetotheriids. The difference in height between those two lingual openings increases gradually from m1 to m4 (Fig. 7c). The talonid basin is a deep, rounded depression. None of the lower molars are labially emarginated. The lingual edge of the talonid is curved, with an entoconid that is obliquely positioned relative to the paraconid – metaconid axis, as in all late Paleocene – Eocene peradectids (e.g., Hough 1961: fig. 2A, for the late Eocene genus *Didelphidectes*). The lingual edge of the talonid is straight and the entoconid is not obliquely oriented in the early peradectids *Pd. minor* (e.g., Williamson et al. 2012: fig. 8A, D) and *Pd. coprexeches* (e.g., Williamson and Taylor 2011: fig. 7A, 7D, 7J), as in herpetotheriids.

The entoconid and hypoconulid are labiolingually pinched. The entoconid is often labial to the paraconid – metaconid axis (e.g., Fig. 7a, k) but the three cuspids are aligned on some m2 specimens (e.g., MNHN.F.Ri221, Fig. 7g; MNHN.F.Me16101, Fig. 7i). The pre-entocristid is always sharp and joins the postmetacristid on the postmetacristid – pre-entocristid notch. The postentocristid is absent on the m2, but present on the m3 of MHN.AIX.PV.2017.6.9. The entoconid is positioned more and more distally to the metaconid from m1 to m4, so that the metaconid – entoconid notch mesiodistally elongates from m1 to m4 (Fig. 7c). In occlusal view, the entoconid of m2 and m3 is in intermediate position between the distal edge of the trigonid and the distal margin of the tooth, whereas the entoconid is closer to the distolingual corner of the tooth on equivalent loci in *Pd. elegans* (e.g., Krishtalka and Stucky 1983b: fig. 4b for occlusal view, Mckenna 1960: fig. 17c [lower] for lateral view). The entoconid of m4 is closer to the distal margin of the tooth than from the distal wall of the trigonid. The entoconid has a symmetrical shape in lingual view, with equally long pre-entocristid and postentocristid. In absolute height, the entoconid of m1 and m2 are subequal (Fig. 7c, f, h), it is lower on m3 (e.g., Fig. 7l) and much lower on m4 (Fig. 7c).

The entoconid - hypoconulid notch is deep, as deep as the entoconid – metaconid notch on m2 (Fig. 6c), as in *Pd. protinnominatus* (e.g., Gingerich and Smith 2006: fig. 26a, c). In comparison, the lowest point of the entoconid – hypoconulid notch of *Pd. elegans* can be higher than the lowest point of the entoconid – metaconid notch (e.g., McKenna 1960: fig. 17c), even on m2 (e.g., pers. obs., AMNH 17376), or as high as the lowest point of the entoconid – metaconid notch (e.g., Fox 1983: fig. 3). The hypoconulid occupies approximately one third of the labiolingual width of the distal margin of the talonid on m2 and m3 and one half of it on m1 and m4 (Fig. 7a). The hypoconulid is lower than the entoconid on m1 and m2 (e.g., Fig. 7f, h, j), as high and as long on m3 (e.g., Fig. 7l), and much higher on m4 (see the increasing height of hypoconulid along the molar series, Fig. 7c). A lingual cristid of the hypoconulid descends on the entoconid – hypoconulid notch only on the m2 from Rians (MNHN.F.Ri221, Fig. 7g).

The hypoconid is mesiodistally pinched, with an angle of approximately 70° between the cristid obliqua and postcristid. This cuspid is mesiolabial to labial to the entoconid apex (e.g., Fig. 6a); distolabial to the protoconid on m1, m2, and m3, and strictly distal to the protoconid on m4. In distal view, the entoconid and hypoconid are subequal in height, unlike in herpetotheriids, in which the entoconid is higher (pers. obs.). The hypoconid of m4 is much lower than the

hypoconid of more anterior lower molar loci. The cristid obliqua is curved on all loci, and its mesial end is positioned labially to the protocristid notch on all lower molar loci. The curvature of this crest is more pronounced on m4 than on more anterior molars (Fig. 7a). The cristid obliqua ascends slightly on the distal wall of the trigonid; it reaches approximately half the dorsoventral height of the distal wall of the trigonid, between the talonid basin and the protocrisid notch. The postingulid is lingually and labially convex; it attenuates labially to the hypoconulid instead of extending lingually towards it (see illustrations in Online Resource 3: Fig. S6). On the specimens from Palette, the hypoflexid is labiolingually wide, so that it is directly connected to the postcingulid. In this case, the hypoconid is totally internalized within the talonid (Figs. 6a and 7a).

Postcranial: The sole postcranial material attributed to *Peradectes crocheti* sp. nov. is a minute, complete right astragalus (MHN.AIX.PV.2017.6.14, Fig. 8) not found in association with dental remains of this species. This specimen has been confidently attributed to *Pd. crocheti* sp. nov. based on the following: (1) compatibility of size (proximodistal length = 1.97 mm; mediolateral width = 1.59 mm); (2) morphological and size similarity with a left astragalus of cf. *Peradectes protinnominatus* from the Wasatchian-0 of the southern Bighorn Basin (Rose et al. 2012: fig. 11E-H) and with Wasatchian peradectid astragali described by Szalay (1994: fig. 6.10D-F); (3) *Pd. crocheti* sp. nov. is the only peradectid recorded in Palette, based on dental remains. In dorsal view (Fig. 8a), the trochlea is smooth and nearly ungrooved, and there is no distal astragalar tubercle. The astragalar neck and head are relatively proximodistally long (Fig. 8a-b). In turn, the astragalar neck and head have the same mediolateral width, the two being well distinguished in ventrolateral view (Fig. 8c). In distal view, the astragalus is relatively flat (Fig. 8d). Its medial tibial facet is only gently sloping, so that there is a rounded angle between the medial and lateral tibial facets (Fig. 8d). The distal end of the lateral tibial facet is located on the astragalar neck.

In contrast to MHN.AIX.PV.2017.6.14, known herpetotheriid astragali are less dorsoventrally flat, and have a more grooved trochlea in addition to an almost vertical medial tibial facet (Rose 2012; Rose et al. 2012), characters which would be expected on astragali of the coeval herpetotheriid *Pt. constans* in Palette (only calcanei of *Pt. constans* are known from its type locality; Coillot et al. 2013). Unlike in cf. *Pd. protinnominatus* and *M. labrus*, the medial border of the astragalar neck of MHN.AIX.PV.2017.6.14, formed by the proximal extension of the large navicular facet, does not reach the trochlea (Fig. 8b-c). The ovoid fossa is thus more open medially than in cf. *Pd. protinnominatus*. The ovoid fossa of the composite drawing of Szalay (1994: fig. 6.10E) for Wasatchian peradectid astragali is also open, but relatively more distally. MHN.AIX.PV.2017.6.14 compares better with the astragalus of cf. *Pd. protinnominatus* than with the one of the larger *Mimoperadectes labrus* (Rose et al. 2012: fig. 11A-D), for example in having an astragalar sulcus (narrower than in *Herpetotherium innominatum* [Simpson, 1928]) and shorter ectal facet with a rounded instead of triangular distlolateral extremity (Fig. 8b).

Peradectes louisi Crochet, 1979
Figures 9, 10 and 11 (except 11 g-h)

1977a *Peradectes* sp. nov. 1; Crochet: p. 359
1979 *Peradectes louisi* Crochet; Crochet: p. 367, fig. 1.
1980b *Peradectes louisi* Crochet; Crochet: p. 39–42, figs. 6-13 (in part).
1980b *Peradectes* sp.; Crochet: p. 49–51, figs. 26-27, 29 (in part).

Holotype: left M3, MNHN.F.GL197, first figured by Crochet (1979: fig. 1, 1980b: fig. 9a, b) and housed in the collections of the Muséum National d'Histoire Naturelle, Paris.

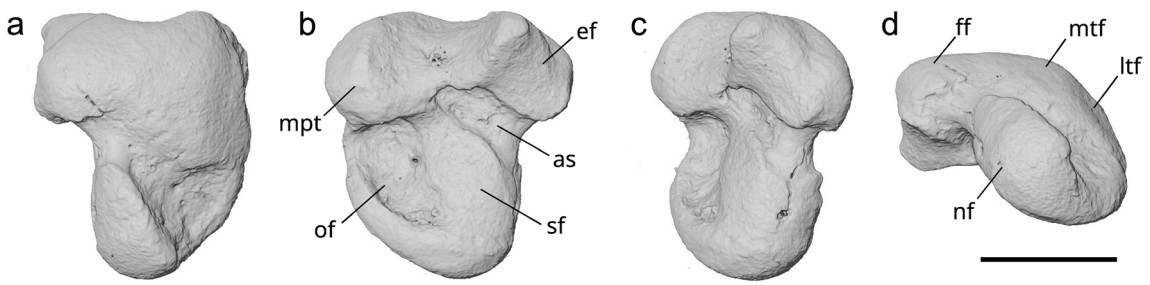

Fig. 8 Right astragalus of *Peradectes crocheti* sp. nov. from Palette (Provence, MP7-MP8 + 9 interval), MHN.AIX.PV.2017.6.14. **a**. dorsal view; **b**. ventral view; **c**. ventrolateral view; **d**. distal view. Abbreviations, terminology following Rose et al. (2012): **as,** astragalar sulcus; **ef,** ectal facet; **ff,** fibular facet; **ltf,** lateral tibial facet; **mpt,** medial plantar tubercle; **mtf,** medial tibial facet; **nf,** navicular facet; **of,** ovoid fossa; **sf,** sustentacular facet. Scale bar equals 1 mm

Localities: Sables de Brasles (type locality), Avenay, Mutigny, Condé-en-Brie and Sézanne-Broyes; all in the eastern Paris Basin.

Age: middle Ypresian (middle early Eocene), MP8 + 9 and ~MP8 + 9 reference level (~mammalian biozones PE IV and PE V).

Remarks: We here propose a revision of *Pd. louisi* based on a re-description of the holotype, and allocate to this species several new upper and lower molar remains from its type locality (Fig. 9), and other MP8 + 9 and ~MP8 + 9 Paris Basin localities in order to study polymorphism and enhance comparisons with other European peradectids.

Translation to English of the original French diagnosis (Crochet 1979): 'European species of small size. On M3, stylar cusp B subequal in height to C and D. Ectoflexus poorly formed and symmetric; conules weak; M3 relatively long. Lingual opening of the prefossid higher than the entocristid notch located between the metaconid and entoconid. Except on m4, base of the hypoconid mesio-distally pinched and cristid obliqua with a concavity before joining the posterior base of the trigonid. m4 smaller than m3.'

New differential diagnosis: Differs from *Pd. crocheti* sp. nov. and *Pd. russelli* in having: (i) relatively mesiodistally longer lower molars; (ii) stylar cusp D distolabial to metacone apex on M3 (upper molars of '*Arm.*' *dufraingi* are unknown); and (iii) stylar cusp C less ventral than stylar cusp D apex on M1 and M2. Further differs from *Pd. crocheti* sp. nov. by: (i) stylar cusp C less ventral than stylar cusp D apex also on M3; (ii) presence of crown labial emargination on all lower molars; (iii) trigonid more labiolingually wide than talonid on m3; (iv) relatively lower entoconid and hypoconulid separated by a shallower notch; and (v) in lacking postcingulid on m4. Further differs from *Pd. russelli* in being noticeably smaller. Differs from '*Armintodelphys*' *dufraingi* in: (i) being larger; in having (ii) talonid mostly labiolingually as wide or wider than trigonid on m2; (iii) entoconid higher than hypoconulid on m2 and as high as hypoconulid on m3; and (iv) larger postcingulid on m2 and m3.

Material: Additional material from Sables de Brasles: left M1 (MNHN.F.GL1, MNHN.F.GL296), worn left M1 (MNHN.F.GL57), worn right M2 (MNHN.F.GL154), labial half of left M2 (MNHN.F.GL272), worn right M3 (MNHN.F.GL265), right m1 (MNHN.F.GL136), left m3 (MNHN.F.GL261, MNHN.F.GL263), right m3 (MNHN.F.GL383), right m4 (MNHN.F.GL301).

Material from Mutigny: right dP3 (MNHN.F.Mu18005; Crochet 1980b: fig. 6), left M1 (MNHN.F.Mu18006; Crochet 1980b: fig. 26), left M2 (MNHN.F.Mu6511; Crochet 1980b: fig. 8), left worn M3 (MNHN.F.Mu18001).

Material from Avenay: left M1 (MNHN.F.Av16023, MNHN.F.Av16036; Crochet 1980b: fig. 7, UM-AV-1-SK, UM-AV-3-SK), right M1 (MNHN.F.Av16057, UM-AV-2-SK), mesial fragment of left M2 (MNHN.F.Av4582), left M2 (MNHN.F.Av18003), right M2 (MNHN.F.Av18004), left m1 (UM-AV-7-SK, UM-AV-12-SK), right m1 (MNHN.F.Av16028; Crochet 1980b: fig. 10, MNHN.F.Av7229), left m2 (MNHN.F.Av16016, MNHN.F.Av16044, MNHN.F.Av18001, MNHN.F.Av6830, UM-AV-10-SK, UM-AV-11-SK), right m2 (MNHN.F.Av16027; Crochet 1980b: fig. 11), left m3 (MNHN.F.Av18000, UM-AV-4-SK, UM-AV-5-SK), right m3 (MNHN.F.Av18002; Crochet 1980b: fig. 12, MNHN.F.Av16149, MNHN.F.Av16158, UM-AV-6-SK, UM-AV-9-SK), fragmentary right m3

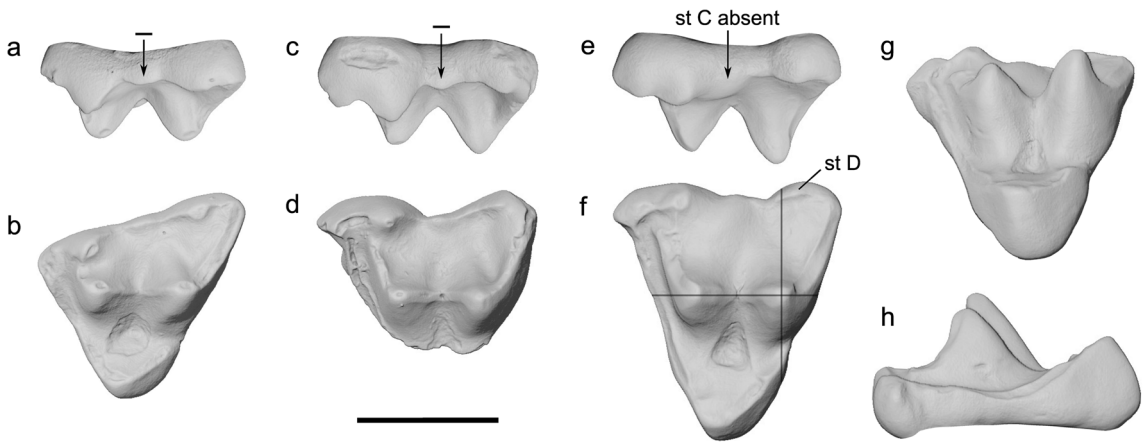

Fig. 9 Upper molars of *Peradectes louisi* from its type locality, Sables de Brasles (Aisne, France; ~MP8+9). **a-b** MNHN.F.GL1, left M1; **a**. labial view; **b**. occlusal view. **c-d.** MNHN.F.GL272, labial half of left M2; **c**. labial view; **d**. occlusal view. **e-h.** MNHN.F.GL197, holotype, left M3; **e**. labial view; **f**. occlusal view, the segments are positioned on the paracone – metacone axis and its perpendicular line; **g**. lingual view; **h**. mesial view. The arrows denoting stylar cusp C on the labial views **a** and **c** are followed by '-', meaning the most ventral point on the [stylar cusp C – stylar cusp D] mesiodistal extension is reached on stylar cusp D. Abbreviations: **st C**, stylar cusp C; **st D**, stylar cusp D. Scale bar equals 1 mm

(UM-AV-8-SK), fragment of left dentary with worn m3 and trigonid of m4 (MNHN.F.Av4642), left m4 (MNHN.F.Av16032, MNHN.F.Av16037; Crochet 1980b: fig. 13).

Material from Condé-en-Brie: left M2 (MNHN.F.CB1486, MNHN.F.CB3707, MNHN.F.CB3637), left worn M2 (MNHN.F.CB835, MNHN.F.CB4183), right M2 (MNHN.F.CB1080; Crochet 1980b: fig. 27, MNHN.F.CB3213, MNHN.F.CB3228), right M3 (MNHN.F.CB4182), left m1 (MNHN.F.CB962, MNHN.F.CB4391), right dentary with fragmentary m2-m4 (MNHN.F.CB226; Crochet 1980b: fig. 29), left m2 (MNHN.F.CB5090, MNHN.F.CB5092, MNHN.F.CB5097, MNHN.F.CB828), right m2 (MNHN.F.CB872, MNHN.F.CB878), left m3 (MNHN.F.CB5104, MNHN.F.CB959), right m3 (MNHN.F.CB4213).

Material from Sézanne-Broyes: right M3 (MNHN.F.SZ18005), worn left M3 (MNHN.F.SZ18000), left M4 (MNHN.F.SZ18004), left m1 (MNHN.F.SZ18003), left m2 (MNHN.F.SZ18001), left m3 (MNHN.F.SZ18006).

Comparative description

Remark: *Peradectes louisi* being similar to *Pd. crocheti* sp. nov., detailed comparisons of *Pd. louisi* with North American peradectids are not proposed, except where necessary (see 'Deciduous upper premolar' below).

Deciduous upper premolar: Only one isolated DP3, from Mutigny, is known for European peradectids (MNHN.F.Mu18005, Fig. 10a-b). This specimen was part of the hypodigm of *Pd. louisi* (Crochet 1979). Although *Pd. louisi* is coeval with *Pd. russelli* in Mutigny, MNHN.F.Mu18005 certainly belongs to *Pd. louisi* instead of *Pd. russelli* due to its small size (L = 1.54 mm; W = 1.26 mm). It is as long and less wide than the M1 of *Pd. louisi*. The dP3 is also identified as such by the long and wide stylar cusp A spur and the deep mesial emargination of the short paracingulum. Compared to dP3 of *Pd. chesteri* (Murphey et al. 2018: fig. 13.1) and *Pd. californicus* (Rothecker and Storer 1996: fig. 1O), the only other described and figured peradectid dP3 with ascertained specific attribution, MNHN.F.Mu18005 is relatively longer. The ratio of the labiolingual width of dP3 to the labiolingual width of M1 is similar in *Pd. louisi* and *Pd. chesteri*. The protocone is strictly lingual to the midpoint of the centrocrista on MNHN.F.Mu18005. The paracone and metacone are identical in mesiodistal length and height, whereas the protocone is much smaller. Contrary to *Pd. chesteri*, the paraconule and the ectoflexus are absent, and the distal emargination of the crown is present. MNHN.F.Mu18005 retains a postparaconular crista reaching the base of the paracone. Stylar cusps C and D are present in this specimen. Stylar cusp C is vestigial compared to stylar cusp D, whereas stylar cusp C is absent in *Pd. chesteri* and *Pd. californicus* (note that the long stylar cusp in the D position in *Pd. chesteri* was interpreted as a stylar cusp C by Murphey et al. 2018). Stylar cusp D is placed slightly distolabially to the metacone apex on MNHN.F.Mu18005. Stylar cusp D is rather mesiolabial to the metacone apex in *Pd. californicus* according to the available illustration.

Upper molars: The protocone is lower than paracone and metacone as in other European peradectids (Fig. 9h). The trigon basin is in intermediate position between the protocone, paracone and metacone on M1 (Fig. 9b). The protocone is positioned more lingually on M3, so that the trigon basin is closer to the paracone and metacone (Fig. 9f). A sharp ridge is present on the lingual edge of the acute protocone of the M3 on which this cusp is mesiodistally pinched (MNHN.F.SZ18005, Fig. 10n-o). The paraconule is faint. The holotype bears a premetaconular crista unlike the other unworn M3, which lack internal conular cristae (the worn MNHN.F.GL265 retains internal conular cristae). Various M1 and M2 have faint internal conular cristae (e.g., Fig. 10d, f, h). The postmetaconular crista elongates from M1 to M3. Similar to *Pd. crocheti* sp. nov., the paracingulum is either of constant mesiodistal length or it is occasionally emarginated mesially to the paracone apex (e.g., MNHN.F.Mu6511, Fig. 10l for M2, MNHN.F.SZ18005, Fig. 10o for M3). The distal emargination of the crown is rarely lacking, the distal margin being straight on the M1 MNHN.F.GL1 (Fig. 9b) and the M3 MNHN.F.CB4182 (Fig. 10p). The preparacrista elongates from M1 to M3 as illustrated on the molar series from the type locality (Fig. 9). This crest is connected to stylar cusp A on M1 and M2 and to stylar cusp B on M3 and M4. The M2 MNHN.F.GL272 has an unworn and salient postmetacrista forming a high distal wall on the stylar shelf (Fig. 9c-d), which is not found in *Pd. crocheti* sp. nov. This distal wall is absent in most specimens (e.g., Fig. 10n).

Stylar cusp A is positioned mesiolingually to stylar cusp B on M2 and M3, except for the M2 MNHN.F.CB3228 having a stylar cusp A strictly mesial to stylar cusp B (Fig. 10j). Stylar cusp B is more conical on the M3 holotype than on the M3 MNHN.F.CB4182 (Fig. 10p) or MNHN.F.SZ18005 (Fig. 10o) for which it is labiolingually pinched. This stylar cusp is labial to the paracone apex on M1 and M2, and mesiolabial to the paracone apex on M3. Stylar cusp B of the holotype (Fig. 9f) and of MNHN.F.SZ18005 has a small crest on its lingual edge directed towards the preparacrista, similar to the one connected to the preparacrista on M1 and M2.

Stylar cusp C is absent on the holotype (Fig. 9e-g) and on the M3 MNHN.F.CB4182. Variation in the positioning of this stylar cusp exists, as in *Pd. crocheti* sp. nov., so that it can be closer to stylar cusp B than to stylar cusp D (e.g., for M2, MNHN.F.CB1486 or MNHN.F.GL272, Fig. 9c vs. MNHN.F.Mu6511, Fig. 10k). The doubling of stylar cusp C occurs only in one specimen (MNHN.F.CB1080,

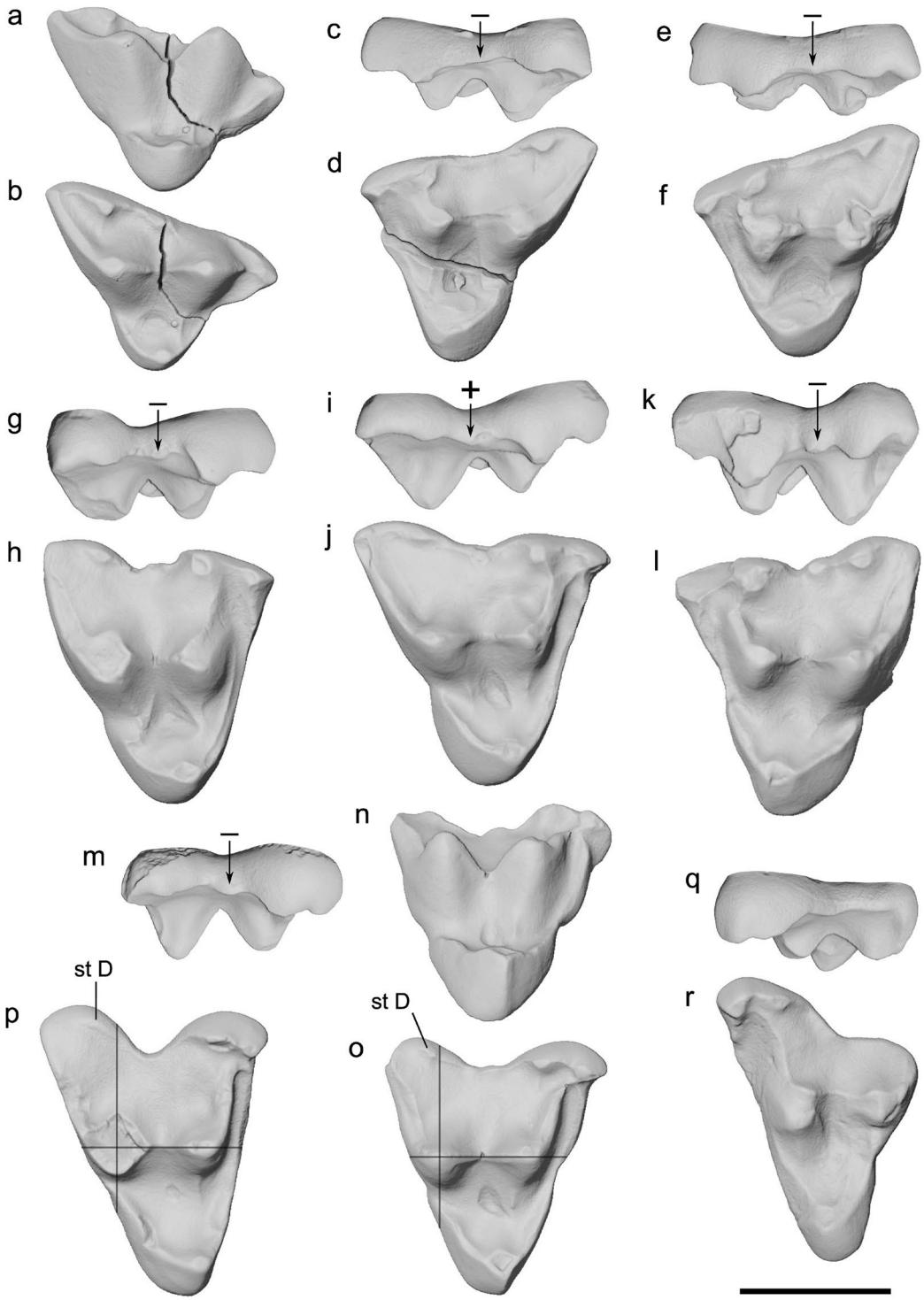

Fig. 10 Upper molars of *Peradectes louisi* from Avenay (MP8 + 9), Condé-en-Brie, Mutigny and Sézanne-Broyes (~MP8 + 9), all in the Paris Basin. **a-b.** MNHN.F.Mu18005, right dP3; **a**. lingual view; **b**. occlusal view. **c-d.** MNHN.F.Mu18006, left M1; **c**. labial view; **d**. occlusal view. **e-f.** UM-AV-1-SK, left M1; **e**. labial view; **f**. occlusal view. **g-h.** MNHN.F.CB3213, right M2; **g**. labial view; **h**. occlusal view. **i-j.** MNHN.F.CB3228, right M2; **i**. labial view; **j**. occlusal view. **k-l.** MNHN.F.Mu6511, left M2; **k**. labial view; **l**. occlusal view. **m-o.** MNHN.F.SZ18005, right M3; **m**. labial view; **n**. lingual view; **o**. occlusal view. **p**. MNHN.F.CB4182, right M3 in occlusal view. **q-r.** MNHN.F.SZ18004, left M4; **q**. labial view; **r**. occlusal view. The arrows denoting stylar cusp C on labial views are followed by '+' if the most ventral point on the [stylar cusp C – stylar cusp D] mesiodistal extension is reached on stylar cusp C, and by '-' if this most ventral point is reached on stylar cusp D. The segments on the occlusal views of MNHN.F.SZ18005 (**o**) and MNHN.F.CB4182 (**p**) are positioned on the paracone – metacone axis and its perpendicular line. Abbreviation: **st D**, stylar cusp D. Scale bar equals 1 mm

Crochet 1980b: fig. 27), as in *Pd. crocheti* sp. nov. Unlike other peradectid species, stylar cusp D is distolabial to the metacone apex on M3, in addition to M1 and M2 (e.g., molar series of Fig. 9). Conversely, M2 specimens from various localities have a stylar cusp D strictly labial instead of distolabial to the metacone apex (MNHN.F.Mu6511, Fig. 10l; MNHN.F.Av18004; MNHN.F.CB3213, Fig. 10h). On M2, stylar cusp D is either conical (e.g., Fig. 10l) or labiolingually pinched (Figs. 9d and 10j). The apex of stylar cusp C is less ventral than the apex of stylar cusp D on all M1 to M3, except on the M2 MNHN.F.CB3228 (Fig. 10i). Altogether, the relative heights of the stylar cusps A to D of M1 to M3 of *Pd. louisi* are mostly as follows: st. B > A > D > C (Table 3). Among ascertained peradectids, the apex of stylar cusp C is also less ventral than the apex of stylar cusp D on M2 and M3 only in *Pd. russelli* (only on M3), *M. houdei* (differs from *M. labrus* and *M. sowasheensis*, pers. obs.), *Pd. gulottai*, *Pd. californicus*, *Nanodelphys hunti* (Cope, 1873) (stylar cusp C is absent on the holotype, preserving M2 and M3 [McGrew 1937: figs. 3-4]) and *Didelphidectes* cf. *pumilis* (stylar cusp C is absent and stylar cusp D is present in the latter) (Table 3). Stylar cusp C is also vestigial in *Pd. chesteri* (Table 3). Stylar cusp E is notably present in UM-AV-1-SK, on which it is as high as stylar cusp D (Fig. 10e), and on UM-AV-2-SK. Stylar cusp E occurs more frequently than in *Pd. crocheti* sp. nov.

M1 lack the ectoflexus (e.g., Figs. 9b and 10f), except UM-AV-2-SK on which it is narrow and MNHN.F.Mu18006 with a longer ectoflexus (Fig. 10d). The ectoflexus is asymmetric on M3 as in other European peradectids (e.g., Fig. 9f), particularly on MNHN.F.SZ18000 with a metastylar wing much more labially extended than the parastylar wing. The asymmetry is less marked on MNHN.F.SZ18005 (Fig. 10o) from the same locality. The ectoflexus of M2 can be deeper than on M3 (e.g., Figs. 9d and 10h vs. Fig. 9f).

We report the first M4 of *Pd. louisi*, from Sézanne-Broyes (MNHN.F.SZ18004, Fig. 10q-r). The ectoflexus is deep as in other peradectids. The talon is relatively labiolingually wider than on M4 of *Pd. crocheti* sp. nov. As in *Pd. russelli* (Crochet 1979: fig. 2) and contrary to *Pd. crocheti* sp. nov., stylar cusp C is greatly reduced (Fig. 10q). Stylar cusp A is the highest. Contrary to the M4 of both *Pd. crocheti* sp. nov. and *Pd. russelli*, the metastylar wing is relatively larger, and the protocone is subequal in height to the metacone instead of being higher. The paracone and metacone are subequal in height, but both cusps are worn.

Lower molars: m2 have a talonid most often as labiolingually wide or wider than the trigonid (e.g., Fig. 11m, o), as in *Pd. crocheti* sp. nov. and almost all m2 of *Pd. russelli*. However, one m2 has a talonid slightly narrower than the trigonid (MNHN.F.SZ18001, Fig. 11k), resembling the condition seen in the m2 of '*Arm.*' *dufraingi*. The m3 MNHN.F.Av16149 has a trigonid relatively longer (L/W trigonid = 1.20) than any other m3 of *Pd. louisi*, for which the trigonid is most often as long as wide (e.g., Fig. 11r, t, v, x). The development of the precingulid varies for a given molar locus (e.g., Fig. 11r vs. 11t). The protoconid is always markedly higher than on m4 of '*Arm.*' *dufraingi*. The metaconid is always distolingual to the protoconid. On m3, the paraconid and metaconid are either equal in mesiodistal length (e.g., Fig. 11s) or the metaconid is longer (e.g., Fig. 11y).

The cristid obliqua is almost straight on some m2 (e.g., MNHN.F.CB878, Fig. 11o; MNHN.F.Av16027, Crochet 1980b: fig. 11), m3 (e.g., MNHN.F.GL261; Fig. 11v) and m4 (MNHN.F.GL301; Fig. 11e), whereas it is curved on most lower molar specimens (Fig. 11). There is notable variation of the positionning of the mesial end of the cristid obliqua for a given molar locus. For example, the cristid obliqua ends mesially labial to the protocristid notch on the m3 MNHN.F.CB4213 (Fig. 11r), but is close to the protocristid notch on the m3 MNHN.F.Av18002 (Fig. 11t). The postcristid is straight instead of curved (i.e., the hypoconulid is weakly distally projected) on all m1 (e.g., Fig. 11a, c), 8 out of 13 m2 specimens (e.g., MNHN.F.CB828, Fig. 11m; MNHN.F.CB878, Fig. 11o), only 6 out of 17 m3 specimens (e.g., MNHN.F.Av4642, Fig. 11i; UM-AV-6-SK), and 2 out of 3 m4 specimens (MNHN.F.GL301, Fig. 11e; MNHN.F.Av16037, Crochet 1980b: fig. 13).

On the partial hemi-mandible MNHN.F.CB226, the only partial molar row known for *Pd. louisi*, the m3 has a much smaller entoconid than the m2, so that the entoconid is minute on the m3 (Fig. 11j). The talonid is slightly labiolingually wider on the m2 than on the m3 on this specimen. The talonid is as labiolingually wide as the trigonid on most of the m2 specimens (see above), whereas the talonid is narrower than the trigonid on the m3 (e.g., Fig. 11k, m, o for m2 vs. Fig. 11r, t, v, x for m3). Among the 46 lower molar specimens, 41 have a strong labial emargination of the crown. The emargination is weaker in five specimens with a relatively wider hypoflexid, namely the m1 MNHN.F.CB4391 and UM-AV-12-SK, the m2 MNHN.F.Av16016 and MNHN.F.CB5092, and the m3 MNHN.F.GL383. Among them, only MNHN.F.Av16016 and MNHN.F.GL383 have a labial emargination as weak as in equivalent molar loci in *Pd. crocheti* sp. nov.

The entoconid and hypoconulid are small on all molars, so that the entoconid – hypoconulid notch is shallow (Fig. 11l). These two cuspids are sometimes so minute on the m3 that the notch between them is shallower than on m1 and m2 (e.g., MNHN.F.GL261, Fig. 11w) to indistinct (e.g., MNHN.F.GL383, UM-AV-5-SK). The entoconid is asymmetrical in lateral view because the entoconid – metaconid notch is deeper than the entoconid – hypoconulid notch. The postentocristid is sometimes absent on m2 (e.g., MNHN.F.CB878; Fig. 11o vs. Fig. 11j, m) and m3 (e.g., MNHN.F.CB4213; Fig. 11r vs. Fig. 11j, t, v), so that the

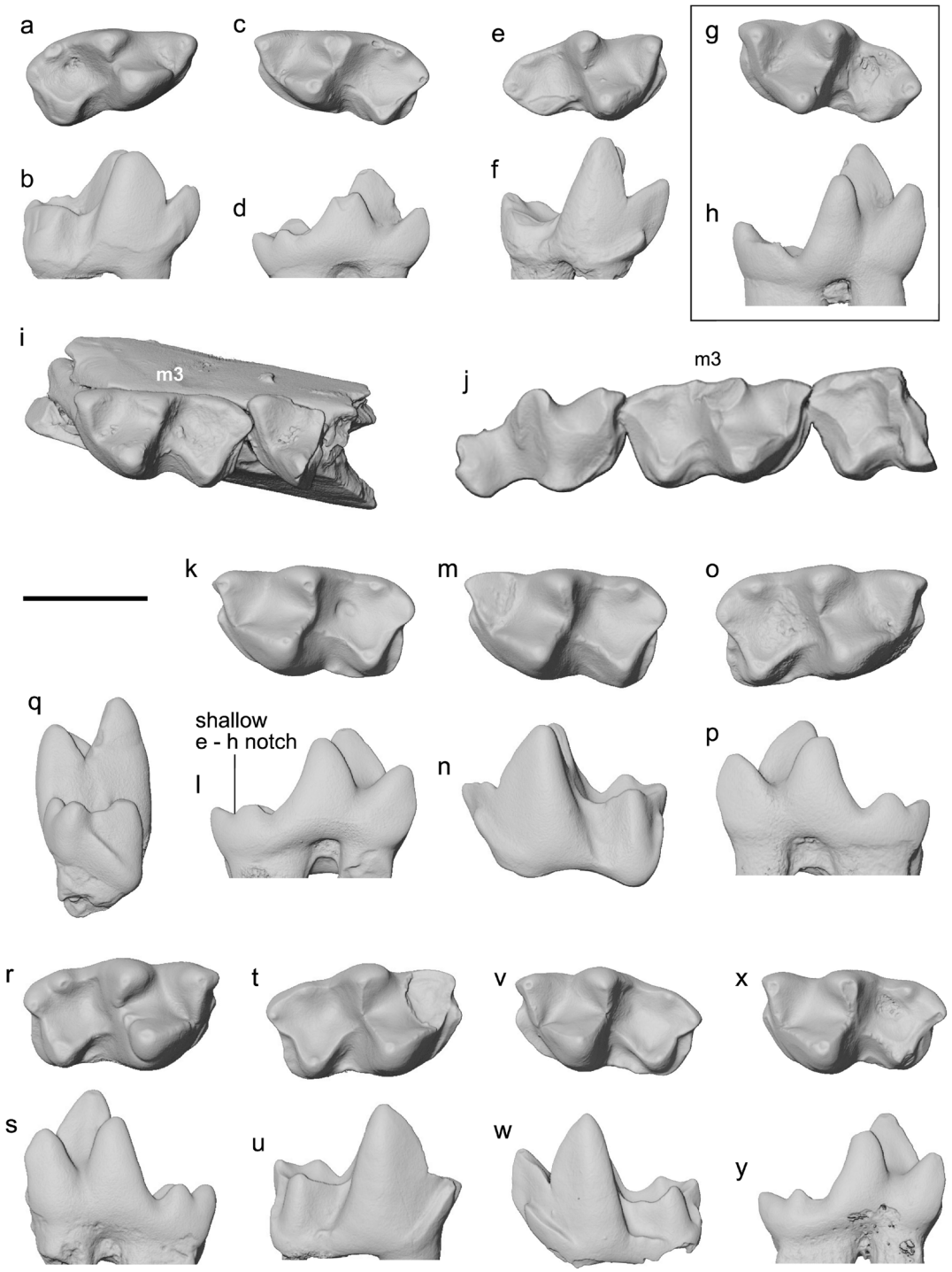

Fig. 11 Lower molars of *Peradectes louisi* (except **g-h**) from Avenay (MP8 + 9), Condé-en-Brie, Sables de Brasles, Sézanne-Broyes (~MP8 + 9) and of *Peradectes* cf. *louisi* from Saint-Agnan (MP8 + 9-MP10 interval), all localities being in the Paris Basin. **a-b.** MNHN.F.GL136, right m1; **a**. occlusal view; **b**. labial view. **c-d.** MNHN.F.SZ18003, left m1; **c**. occlusal view; **d**. lingual view. **e-f** MNHN.F.GL301, right m4; **e**. occlusal view; **f**. mesiolabial view. **g-h.** comparison with MNHN.F.STA296, left m4 of *Peradectes* cf. *louisi* from Saint-Agnan (Aisne, MP8 + 9-MP10 interval); **g**. occlusal view; **h**. lingual view. **i**. MNHN.F.Av4642, left hemi-mandible fragment with fragmentary trigonid of m2 and worn m3 in occlusal view. **j**. MNHN.F.CB226, m2-m4 from a right hemi-mandible fragment in occlusal view. **k-l.** MNHN.F.SZ18001, left m2; **k**. occlusal view; **l**. lingual view. **m-n.** MNHN.F.CB828, left m2; **m**. occlusal view; **n**. labial view. **o-p.** MNHN.F.CB878, right m2; **o**. occlusal view; **p**. lingual view. **q-s.** MNHN.F.CB4213, right m3; **q**. distal view; **r**. occlusal view; **s**. lingual view. **t-u.** MNHN.F.Av18002, right m3; **t**. occlusal view; **u**. labial view. **v-w.** MNHN.F.GL261, left m3; **v**. occlusal view; **w**. labial view. **x-y**. MNHN.F.GL263, left m3; **x**. occlusal view; **y**. lingual view. Abbreviation: **e – h notch**, entoconid – hypoconulid notch. Scale bar equals 1 mm

entoconid and hypoconulid are not connected by a crest on the concerned specimens. Even on the m2 with a small entoconid (e.g., MNHN.F.SZ18001, Fig. 11l), the entoconid is always at least slightly higher than the hypoconulid. These two cuspids are mostly subequal in height on the m3 (Fig. 11s, u, w, y), but some specimens have a slightly higher entoconid as for the m2 (e.g., UM-AV-4-SK). The relative length of the entoconid of the m3 varies from shorter than the hypoconulid (e.g., MNHN.F.GL263, Fig. 11y) to as long as the hypoconulid (e.g., MNHN.F.CB4213, Fig. 11s). The entoconid is as high as the hypoconid in distal view (Fig. 11q). MNHN.F.Av18002 has a lingually unreduced postcingulid (Fig. 11t). The degree of lingual curvature of the talonid also varies, especially on m3 (e.g., Fig. 11v vs. Fig. 11x).

The lower molar MNHN.F.Av16032 exhibits typical peradectid traits such as a lingually curved talonid and a hypoconid mesiolabial to entoconid, and is similar to other *Pd. louisi* m4 in occlusal view in having a small labiolingually pinched talonid with an almost centered hypoconulid on the distal margin of the talonid, and an absence of a prominent postcingulid reaching the base of the hypoconulid (e.g., MNHN.F.GL301, Fig. 11e). However, although other peradectid m4 have an entoconid much lower than the hypoconulid (Fig. 11f, h), and other *Pd. louisi* m4 (MNHN.F.GL301 and MNHN.F.Av16037) have a straight postcristid, on MNHN.F.Av16032 the entoconid is large, as high as the hypoconulid and higher than the hypoconid, and the postcristid is curved. Because the relative height of the entoconid varies as such in *Pt. constans* m4 (e.g., Ladevèze et al. 2012: fig. 6Hc vs. fig. 6Ic) and because m4 of the closely related *Pd. crocheti* sp. nov. and *Pd.* cf. *louisi* have a curved postcristid (Figs. 7a and 11g), MNHN.F.Av16032 is identified as m4 of *Pd. louisi*. The hypoconid apex is placed slightly distolabially to the protoconid apex on MNHN.F.Av16032, this character being observed also in ascertained peradectid m4 (e.g., fig. 11g). The preprotocristid is not convex in labial view on two m4 specimens (MNHN.F.Av16037, Crochet 1980b: fig. 13a; MNHN.F.GL301, Fig. 11f) contrary to other molar loci (e.g., Fig. 11b vs. Fig. 11f) and to the m4 MNHN.F.Av16032.

Peradectes cf. *louisi*.
Figure 11g

?1983 *Peradectes mutigniensis* Crochet; Louis and Laurain: p. 8.

Material: MNHN.F.STA296, left m4.

Locality and age: Saint-Agnan, Aisne, eastern Paris Basin; MP8 + 9 – MP10 interval (see Louis and Laurain 1983; Lecomte 1994; Escarguel 1999; Solé et al. 2018).

Description and comment: The only peradectid specimen from Saint-Agnan is the m4 MNHN.F.STA296. It is much smaller than the m4 of *Pd. russelli*, and larger and with a higher crown than the m4 of '*Arm.*' *dufraingi*. MNHN.F.STA296 does not differ in size and morphology from the m4 of *Pd. louisi* MNHN.F.GL301 and MNHN.F.Av16037 (e.g., Fig. 11e-f vs. Fig. 11g-h; Online Resource 1: Table S2). However, peradectid m4 are rare and bear less diagnostic characters than m2 and m3. For example, the relative height of the entoconid and hypoconulid in addition to the morphology of the notch between them allow to distinguish the European species *Pd. crocheti* sp. nov., *Pd. lousi* / *Pd. russelli* and '*Arm.*' *dufraingi* based on m2 and m3. On m4, the configuration of these cuspids is the same for the four valid species and MNHN.F.STA296, with the entoconid much lower than the hypoconulid (Fig. 11h; except MNHN.F.Av16032). Because of this, and the lack of other molar loci from Saint-Agnan, MNHN.F.STA296 can only be tentatively ascribed to *Peradectes* cf. *louisi*. Furthermore, it is worth mentioning that undescribed peradectid species, also equivalent in size to *Pd. louisi*, probably occur in localities younger than MP8 + 9 (see Discussion, 'Revision of putative occurrences of typical MP8 + 9 and ~MP8 + 9 peradectids in MP10 and ~MP10 faunas').

Peradectes russelli Crochet, 1979
Figure 12

1977a *Peradectes* sp. nov. 2; Crochet: p. 359, pl. 1, fig. C.
1979 *Peradectes russelli* Crochet; Crochet: p. 367–368, fig. 2 (in part).
1979 *Peradectes mutigniensis* Crochet; Crochet: p. 368, fig. 3.
1980b *Peradectes louisi* Crochet; Crochet: fig. 4a (in part).
1980b *Peradectes russelli* Crochet; Crochet: p. 43–46, figs. 14-17 (no fig. 18) (in part).
1980b *Peradectes mutigniensis* Crochet; Crochet: p. 46–49, figs. 19-25.
1980b *Peradectes* sp.; Crochet: p. 51 (in part).

Remark: *Peradectes 'mutigniensis'* Crochet, 1979, is considered a junior synonym of *Pd. russelli* (see Discussion).

Holotype: MNHN.F.CB924, fragment of right maxilla with M3-M4, housed at the Muséum National d'Histoire Naturelle (Paris), and figured by Crochet (1977a: pl. 1, fig. C_3, 1979: fig. 2, 1980b: fig. 16).

Localities: Condé-en-Brie (type locality), Avenay, Mutigny, Sables de Brasles, Sézanne-Broyes; all in the eastern Paris Basin.

Age: middle Ypresian (middle early Eocene), ~MP8 + 9 reference level (~ mammalian biozones PE IV and PE V).

Material: Additional material from Condé-en-Brie: left M1 (MNHN.F.CB2501; Crochet 1977a: pl. 1, fig. C_1, 1980b: fig. 14, MNHN.F.CB3275), right M1 (MNHN.F.CB3007),

left M2 (MNHN.F.CB5103; Crochet 1977a: pl. 1, fig. C_2, 1980b: fig. 15, MNHN.F.CB840, MNHN.F.CB850), right M2 (MNHN.F.CB3644), labial half of right M2 (MNHN.F.CB2753), left M3 (MNHN.F.CB742), right M3 (MNHN.F.CB2502), right m1 (MNHN.F.CB3021), right m2 (MNHN.F.CB5098, MNHN.F.CB5100, MNHN.F.CB928), fragment of right dentary with worn m2 (MNHN.F.CB925).

Material from Avenay: left M1 (UM-AV-13-SK), right M1 (MNHN.F.Av16024; Crochet 1980b: fig. 19), right M3 (MNHN.F.Av4813; Crochet 1980b: fig. 4a, MNHN.F.Av6837), left m2 (MNHN.F.Av7235; Crochet 1980b: fig. 17, UM-AV-14-SK), right m2 (UM-AV-15-SK).

Material from Mutigny: left M1 (MNHN.F.Mu18004; Crochet 1980b: fig. 20), right M1 (MNHN.F.Mu5532), left M2 (MNHN.F.Mu18002; Crochet 1980b: fig. 21), right M3 (MNHN.F.Mu5521; Crochet 1980b: fig. 22), right m2 (MNHN.F.Mu18000; Crochet 1980b: fig. 23), left m3 (MNHN.F.Mu6451; Crochet 1980b: fig. 24), right m4 (MNHN.F.Mu18003).

Material from Sables de Brasles: right m2 (MNHN.F.GL92; Crochet 1980b: fig. 25), right m3 (MNHN.F.GL410).

Material from Sézanne-Broyes: left m1 (MNHN.F.SZ18002).

Translation to English of the original French diagnosis (Crochet 1979): 'European species of median size. On M3, stylar cusp B slightly higher than other stylar cusps. Ectoflexus symmetric, wide and well-developed, stylar cusp C reduced. Paraconule not very pronounced or absent, metaconule weak. In occlusal view, M3 with a rather massive aspect (stylar line relatively long, preprotocrista – postprotocrista angle quite open). On lower molars, lingual opening of the prefossid higher than the lowest point of the entocristid. m4 longer than m3.'

New differential diagnosis: Differs from the other European peradectid species in being significantly larger. Further differs from *Pd. crocheti* sp. nov. in having: (i) stylar cusp C apex less ventral than stylar cusp D apex on M3; (ii) crown labial emargination on m3 and m4, and often m2; (iii) trigonid more labiolingually wide than talonid on m3; and (iv) entoconid and hypoconulid separated by a shallower notch. Differs also from *Pd. louisi* and '*Arm.*' *dufraingi* in having relatively wider lower molars. Further differs from *Pd. louisi* in having: (i) stylar cusp D strictly labial to metacone apex; and (ii) stylar cusp C apex as ventral as stylar cusp D apex on M1 and M2. Further differs from '*Arm.*' *dufraingi* notably by: (i) entoconid higher than hypoconulid on m2 and as high as hypoconulid on m3; and (ii) larger postcingulid on m2 and m3.

Comparative description

Remark: *Peradectes russelli* being similar to *Pd. crocheti* sp. nov. and *Pd. louisi*, detailed comparisons of *Pd. russelli* with North American peradectids are not proposed.

Upper molars: The mesiodistal length of the talon and of the centrocrista varies positively with the mesiodistal length of the specimens (e.g., MNHN.F.CB3007, Fig. 12b vs. MNHN.F.CB3275, Fig. 12d for M1; MNHN.F.Av6837, Fig. 12f vs. MNHN.F.CB2502, Fig. 12h for M3). The protocone of one M1 (MNHN.F.Av16024; Crochet 1980b: fig. 19b) and two M2 (MNHN.F.Mu18002, Crochet 1980b: fig. 21; MNHN.F.CB850, Fig. 12j) is relatively more distally positioned than for other specimens (still mesiolingual to the midpoint of the centrocrista). The tiny paraconule preserved on molars of the holotype (Crochet 1979: fig. 2; pers. obs.) is indistinct on most other upper molars (Fig. 12b, d, f, h, j), as in *Pd. louisi*. M1 and M2 have a faint premetaconular crista in addition to the postmetaconular crista (e.g., Fig. 12b, d, j), the former being more marked on some specimens (e.g., MNHN.F.CB2501). The M3 MNHN.F.CB2502 has a doubled stylar cusp A (Fig. 12g-h). One of the two small cusps in the stylar cusp A position is directly mesial to stylar cusp B, and is connected to it by a crest; the second small A cusp is placed mesiolingually to stylar cusp B, as on other M3. Stylar cusp B is strictly labial to the paracone on the M3 of the holotype (MNHN.F.CB924; Crochet 1979: fig. 2) and mesiolabial to the paracone on the M3 MNHN.F.Mu5521, former holotype of *Pd. 'mutigniensis'* (Crochet 1979: fig. 3). Apart from MNHN.F.CB924, only the M3 MNHN.F.Av4813 (Crochet 1980b: fig. 4a) has a stylar cusp B strictly labial to the paracone (2 out of 6 M3 specimens). This character state is present on all M1 and M2 as in *Pd. crocheti* sp. nov. and *Pd. louisi*. In occlusal view, stylar cusp C is closer to stylar cusp B than to stylar cusp D on 4 out of 7 M1 (MNHN.F.CB2501; MNHN.F.CB3275, fig. 12c; MNHN.F.Mu18004; MNHN.F.Mu5532) and 2 out of 5 M2 (MNHN.F.CB5103; MNHN.F.CB850, Fig. 12i). The apices of stylar cusps C and D are equally ventral on both M1 and M2 contrary to *Pd. louisi*, except for the M1 MNHN.F.CB3007 on which stylar cusp D is more ventral than the vestigial stylar cusp C (1 out of 12 M1 to M2 specimens, Fig. 12a). The height relationships of stylar cusps of *Pd. russelli* are as follows: st. B > A = C = D for M2, and st. B > A > D > C for M3 (e.g., Fig. 12e) (Table 3). On 5 out of 18 isolated M1-M3 (MNHN.F.Mu18004 and MNHN.F.CB3275 for M1, MNHN.F.CB850 for M2, MNHN.F.CB742 and MNHN.F.CB924 for M3), stylar cusp D has a lingual crest of variable labiolingual length (e.g., Fig. 12d, j), which is unseen in *Pd. crocheti* sp. nov. and *Pd. louisi*. The ectoflexus is relatively deep on 4 out of 7 M1 (e.g., MNHN.F.CB3007, Fig. 12b), especially on UM-AV-13-SK. The M4 (MNHN.F.CB924, Crochet 1979: fig. 2) lacks stylar cusp C unlike *Pd. crocheti* sp. nov. and *Pd. louisi*, and has minute stylar cusps A and B. The M4 lacks internal conular cristae. As in *Pd. crocheti* sp. nov. and *Pd. louisi*, stylar cusp A of M4 is higher than stylar cusp B and there is a deep ectoflexus.

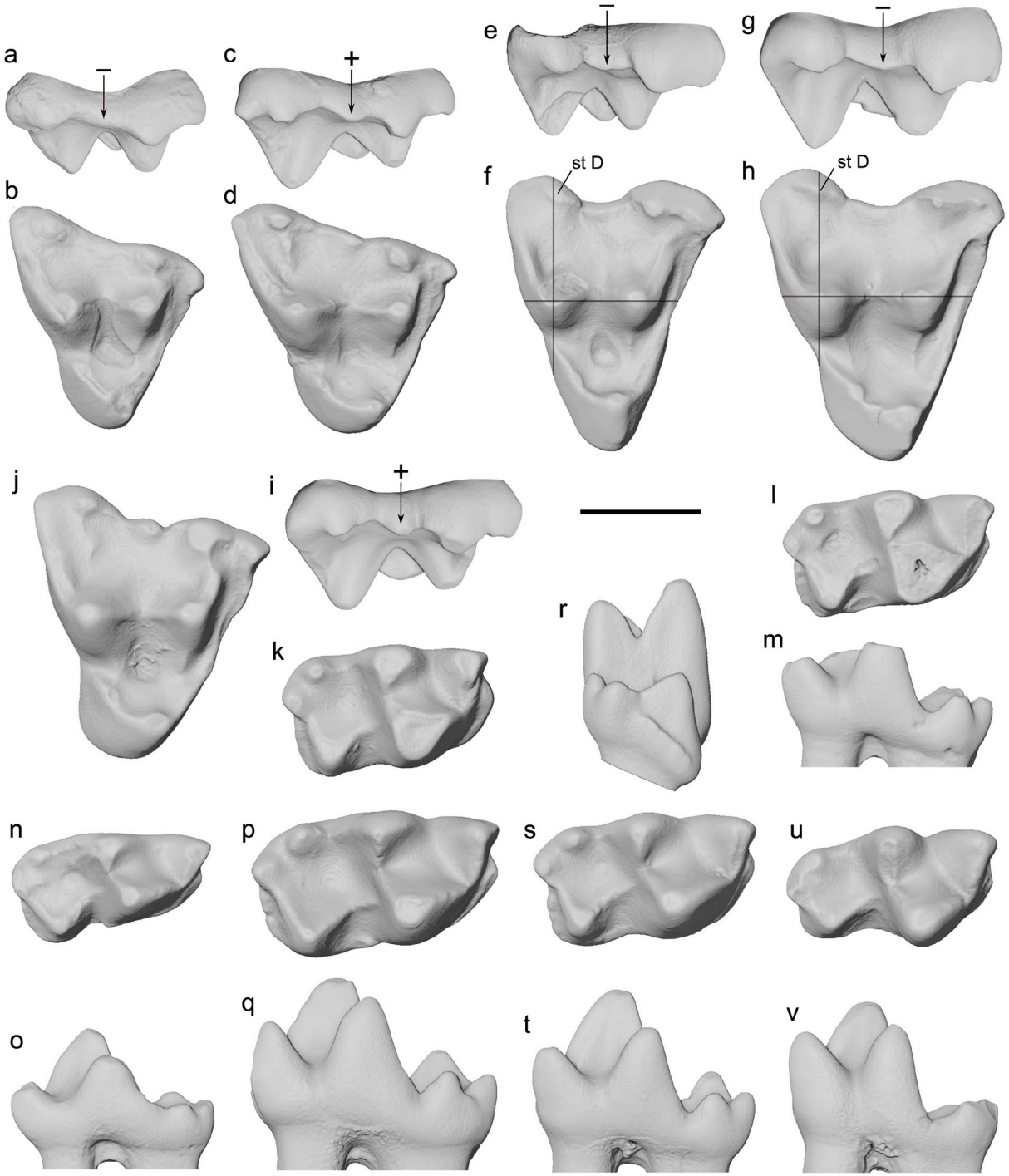

Fig. 12 Upper and lower molars of *Peradectes russelli* from Avenay (MP8 + 9), Condé-en-Brie, Mutigny, Sables de Brasles and Sézanne-Broyes (~MP8 + 9), all in the Paris Basin. **a-b.** MNHN.F.CB3007, right M1; **a**. labial view; **b**. occlusal view. **c-d.** MNHN.F.CB3275, left M1; **c**. reversed labial view; **d**. reversed occlusal view. **e-f.** MNHN.F.Av6837, right M3; **e**. labial view; **f**. occlusal view. **g-h.** MNHN.F.CB2502, right M3; **g**. labial view; **h**. occlusal view. **i-j** MNHN.F.CB850, left M2; **i**. reversed labial view; **j**. reversed occlusal view. **k**. UM-AV-14-SK, left m2 in reversed occlusal view. **l-m.** MNHN.F.Mu18000, right m2; **l**. occlusal view; **m**. lingual view. **n-o.** MNHN.F.SZ18002, left m1; **n**. reversed occlusal view; **o**. reversed lingual view. **p-q.** MNHN.F.CB928, right m2; **p**. occlusal view; **q**. lingual view. **r-t**. MNHN.F.GL410, right m3; **r**. distal view; **s**. occlusal view; **t**. lingual view. **u-v.** MNHN.F.Mu18003, right m4; **u**. occlusal view; **v**. lingual view. The arrows denoting the stylar cusp C on labial views are followed by '+' if the most ventral point on the st. C – st. D mesiodistal extension is reached on the st. C, and by '-' if this most ventral point is reached on the st. D. The segments on the occlusal views of MNHN.F.Av6837 (**f**) and MNHN.F.CB2502 (**h**) are positioned on the paracone – metacone axis and its perpendicular line. Abbreviation: **st D**, stylar cusp D. Scale bar equals 1 mm

Lower molars: The m1 and m4 described here are the first reported for this species. The m1 has a relatively long paracristid and a metaconid much higher than the paraconid. The m1 from Sézanne-Broyes (MNHN.F.SZ18002, Fig. 12n-o) is significantly larger than the m1 of *Pd. louisi* from the same locality (MNHN.F.SZ18003, Fig. 11c-d). As in *Pd. louisi*, m2 differs from m3 in having as labiolingually wide trigonid and talonid instead of a narrower talonid, and entoconid higher than the hypoconulid instead of equal in height (e.g., Fig. 12l-m, p-q vs. Fig. 12s-t). The talonid is as labiolingually wide or wider than the trigonid on m2, except for MNHN.F.GL92, for which the talonid is slightly narrower than the trigonid (Crochet 1980b: fig. 25). The metaconid is longer than the paraconid on m1 and m2 (Fig. 12o, q), these two cuspids are subequal in length on m3 (Fig. 12t), and the paraconid is longer than the metaconid on the single available m4 (Fig. 12v). The labial emargination of the crown is present in one out of the two m1 (MNHN.F.SZ18002, Fig. 12n), slightly on 4/9 m2 (e.g., UM-AV-14-SK, Fig. 12k vs. MNHN.F.Mu18000, Fig. 12l) and all m3-m4 (Fig. 12s, u). The entoconid and hypoconid are of the same height in distal view (e.g., Fig. 12r), with the exception of the m2 MNHN.F.CB928, with a hypoconid higher than the entoconid. The hypoconid is unambiguously mesiolabial instead of labial to the entoconid on some lower molars (e.g., Fig. 12k, l, n, u), as in *Pd. louisi*. On m2, the entoconid can be positioned either close to the distolingual corner of the molar (e.g., UM-AV-14-SK, Fig. 12k or MNHN.F.Mu18000, Fig. 12l) or intermediate between the distal edge of the trigonid and the distal margin of the molar (e.g., MNHN.F.CB928, Fig. 12p). The entoconid – hypoconulid notch is slightly higher than the metaconid – entoconid notch on m2 (e.g., MNHN.F.CB928, Fig. 12q) and much higher on m3 (e.g., MNHN.F.GL410, Fig. 12t). m1 and m4 have a straight postcristid, whereas it is curved on m2 and m3. The m4 has a relatively long paracristid lingual segment, a relatively high paraconid and a labiolingually narrow talonid (Fig. 12u), as in *Pd. crocheti* sp. nov. and *Pd. louisi*. The mesial end of the cristid obliqua of m4 is slightly labial to the protocristid notch on the trigonid wall. There is no distinct postcingulid on m4, as in *Pd. louisi*.

Results

Quantitative comparisons

Size and proportions of molars Univariate statistics based on molar measurements for the three studied peradectid species are presented in Table 4. The two complete and unworn upper molars from Palette are the M1 MHN.AIX.PV.2018.26.20, which is smaller than the M1 of the holotype, and the M3 MHN.AIX.PV.2017.6.7, which is larger than the M3 of the holotype (Online Resource 1: Table S1). In particular, the length and width of MHN.AIX.PV.2018.26.20 represent the minimum of the observed range values for M1, and the width of MHN.AIX.PV.2017.6.7 is the maximum of the observed range values for M3 (material from all localities included). Thus, most of the size variation of *Pd. crocheti* sp. nov. is represented in its type locality. The disparity of length to width ratio between the M2 and M3 (=L/W M2 - L/W M3) is weak based on mean values (i.e., < 0.10) for *Pd. louisi* and *Pd. russelli* (isolated molars only). Because of the low number of specimens with calculated L/W ratios for M2 of *Pd. crocheti* sp. nov. (two specimens, including the holotype), only the disparity of M2-M3 from the type specimen is retained for comparisons of this character between *Pd. crocheti* sp. nov. and other peradectids (Table 2). The m1 of *Pd. crocheti* sp. nov. and *Pd. louisi* are a mean of 9% mesiodistally shorter than the m2, whereas this value is 12.5% for *Pd. russelli* (Table 4).

The standard deviation and coefficient of variation values for the length of the M2 of *Pd. crocheti* sp. nov. are relatively higher than for the other molar loci, probably because the M2 from Croydon (Hooker 2020) is much larger than other M2 specimens ascribed to this species. However, the normal distribution for the length of the M2 of *Pd. crocheti* sp. nov. is not rejected. The low standard deviation value for the length of the m2 of *Pd. crocheti* sp. nov. is most likely because two out of the four specimens included probably represent the same individual (MHN.AIX.PV.2017.6.8 and MHN.AIX.PV.2017.6.9). The normal distribution is rejected for the width of M1 of *Pd. crocheti* sp. nov. (Table 4). This is most likely because no size continuum is recorded between the six M1 forming two clusters for *Pd. crocheti* sp. nov. (Online Resource 1: Table S1). For all other molar measurements, the normal distribution is not rejected (see Table 4).

The observed ranges for dental measurements of *Pd. crocheti* sp. nov. and *Pd. louisi* are alike, except for the labiolingual width values of the lower molars, which are lower in the latter (Table 4). There is a statistically significant difference between the L/W ratios of lower molars of the coeval *Pd. louisi* and *Pd. russelli*, either when m1 to m4, m2 to m3 or only m2 are taken into account (Table 5). However, the mean L/W ratio for lower molars of *Pd. russelli* and *Pd. crocheti* sp. nov. do not differ significantly (Table 5). Similarly to *Pd. crocheti* sp. nov., the lower molars of *Pd. russelli* are relatively labiolingually wider than those of *Pd. louisi*, except for m1 (Table 4). For the three species studied, the m2 are larger than the m3 in mean (Table 4; Fig. 13). The m2 to m4 of *Pd. louisi* are larger than equivalent loci in '*Arm.*' *dufraingi* (Table 4 vs. Smith and Smith 2013: p. 304).

Taking into account all molar loci, the size distributions of *Pd. louisi* and *Pd. russelli* show almost

Table 4 Univariate statistics associated with measurements (in mm) of upper and lower molars of *Peradectes crocheti* sp. nov., *Pd. louisi* and *Pd. russelli*. Abbreviations: **N** number of specimens measured; **OR** observed range, **SD** standard deviation, **CV** unbiased coefficient of variation (%), **W** Shapiro–Wilk normality test (**ns**, normal distribution cannot be rejected, **s** normal distribution is rejected; $P < 0.05$)

Peradectes crocheti sp. nov.								*Peradectes louisi*								*Peradectes russelli*							
Locus		*N*	OR	Mean	SD	CV	W	Locus		*N*	OR	Mean	SD	CV	W	Locus		*N*	OR	Mean	SD	CV	W
M1	L	5	1.51–1.71	1.60	0.079	4.91	ns	M1	L	9	1.47–1.65	1.56	0.060	3.86	ns	M1	L	7	1.62–1.97	1.81	0.117	6.45	ns
	W	6	1.40–1.59	1.49	0.093	6.27	s		W	9	1.45–1.66	1.55	0.070	4.50	ns		W	7	1.78–2.09	1.89	0.099	5.25	ns
	L/W	5	0.97–1.21	1.06	0.092	8.67	ns		L/W	9	0.94–1.07	1.01	0.042	4.19	ns		L/W	7	0.88–1.03	0.96	0.048	5.01	ns
M2	L	7	1.45–1.81	1.57	0.117	7.46	ns	M2	L	6	1.52–1.71	1.61	0.068	4.23	ns	M2	L	5	1.82–2.11	1.97	0.110	5.58	ns
	W	3	1.66–1.85	1.74					W	9	1.69–1.87	1.77	0.067	3.79	ns		W	4	2.07–2.27	2.19	0.097	4.43	ns
	L/W	2	0.88–0.98	0.93					L/W	4	0.86–0.98	0.91	0.056	6.15	ns		L/W	4	0.85–0.92	0.88	0.030	3.38	ns
M3	L	5	1.40–1.60	1.53	0.078	5.10	ns	M3	L	4	1.41–1.63	1.51	0.093	6.17	ns	M3	L	6	1.78–2.02	1.92	0.096	5.01	ns
	W	6	1.77–1.98	1.85	0.083	4.49	ns		W	4	1.72–1.92	1.83	0.083	4.53	ns		W	6	2.27–2.52	2.36	0.103	4.36	ns
	L/W	4	0.77–0.87	0.82	0.044	5.44	ns		L/W	4	0.77–0.88	0.82	0.051	6.23	ns		L/W	6	0.78–0.86	0.81	0.030	3.74	ns
M4	L	2	1.12–1.26	1.19				M4	L	1	1.33					M4	L	1	1.35				
	W	1	1.79						W	1	1.88						W	1	2.36				
	L/W	1	0.70						L/W	1	0.71						L/W	1	0.57				
m1	L	2	1.47–1.57	1,52				m1	L	8	1.40–1.56	1.50	0.063	4.19	ns	m1	L	2	1.65–1.71	1.68			
	W	3	0.86–0.94	0.91					W	8	0.76–0.85	0.81	0.038	4.73	ns		W	2	0.89–0.92	0.91			
	L/W	2	1.69–1.71	1.70					L/W	8	1.75–2.03	1.85	0.087	4.69	ns		L/W	2	1.79–1.92	1.86			
m2	L	4	1.64–1.69	1.67	0.026	1.58	ns	m2	L	13	1.54–1.73	1.65	0.060	3.66	ns	m2	L	9	1.75–2.05	1.92	0.114	5.94	ns
	W	3	0.99–1.04	1.02					W	14	0.87-1.00	0.94	0.044	4.62	ns		W	9	1.04–1.25	1.14	0.074	6.49	ns
	L/W	3	1.59–1.71	1.63					L/W	13	1.61–1.83	1.74	0.060	3.45	ns		L/W	9	1.62–1.79	1.69	0.053	3.14	ns
m3	L	5	1.53–1.66	1.60	0.068	4.24	ns	m3	L	18	1.47–1.66	1.57	0.050	3.20	ns	m3	L	2	1.74–1.85	1.80			
	W	5	0.87–1.06	0.97	0.078	8.02	ns		W	16	0.84–0.95	0.89	0.036	4.02	ns		W	2	1.05–1.11	1.08			
	L/W	5	1.58–1.77	1.65	0.077	4,66	ns		L/W	16	1.62–1.87	1.77	0.063	3.58	ns		L/W	2	1.66–1.67				
m4	L	1	1.55					m4	L	3	1.44–1.53	1.48				m4	L	1	1.75				
	W	1	0.92						W	3	0.78–0.85	0.83					W	1	1.00				
	L/W	1	1.68						L/W	3	1.74–1.85	1.80					L/W	1	1.75				

Table 5 Results of Welch's *t*-test for comparisons of mean length to width ratio values between lower molars of *Peradectes louisi* and *Peradectes russelli*. The equality of mean L/W ratios is rejected for the three subsamples (which differ in the molar loci included) comparing lower molars of *Pd. louisi* and *Pd. russelli*, but not for the sample comparing lower molars of *Pd. crocheti* sp. nov. and *Pd. russelli*. Abbreviations: **d.f.** degree of freedom, **L** length, **N** number of lower molars, **P** p-value, **ns** mean values not significantly different, **s** mean values significantly different, $P < 0.05$, **t** Welch Two Sample t-test value, **W** width

Compared samples for L / W ratio	Result of Welch's t-test
m1-4 *Pd. louisi* ($N = 40$) vs. *Pd. russelli* ($N = 14$)	s ($t = 2.58$, d.f. = 21.79, $P = 0.017$)
m2-3 *Pd. louisi* ($N = 29$) vs. *Pd. russelli* ($N = 11$)	s ($t = 3.79$, d.f. = 23.32, $P = 0.001$)
m2 *Pd. louisi* ($N = 13$) vs. *Pd. russelli* ($N = 9$)	s ($t = 2.11$, d.f. = 18.68, $P = 0.049$)
m1-4 *Pd. crocheti* sp. nov. ($N = 11$) vs. *Pd. russelli* ($N = 14$)	ns ($t = 1.88$, d.f. = 22.99, $P = 0.073$)

no overlap (Fig. 13a-b). Only one M1 of *Pd. russelli* (MNHN.F.CB3007) is similar in size to M2 and M3 of the smaller *Pd. louisi* (Online Resource 1: Table S3). In the same way, the two m1 of *Pd. russelli* (MNHN.F.CB3021 and MNHN.F.SZ18002) are closer in size to both m2 and the largest m3 of *Pd. louisi* (Fig. 13b). However, M1 and m1 of *Pd. louisi* and *Pd. russelli* form two distinct size clusters. MNHN.F.SZ18004, the single M4 of *Pd. louisi*, is attributed to this species in part because it is closer in width to the M3 of *Pd. louisi* than to the M3 of *Pd. russelli* (Fig. 13a).

MNHN.F.Mu5521, former holotype of *Pd. 'mutignien-sis'*, is the M3 of *Pd. russelli* with the lowest length and width, whereas the M3 of the holotype of *Pd. russelli* (MNHN.F.CB924) has the highest width value of the sample (Fig. 13a). *Peradectes russelli* occupies a larger length x width space than *Pd. louisi* (Fig. 13a-b), probably due to its larger size. In particular, the M3 and M4 of the holotype MNHN.F.CB924 differ greatly in length, more than what would be expected for the same molar loci in *Pd. louisi* based on available M3 and M4 specimens (Fig. 13a). The M2 and M3 overlap more in width in *Pd. louisi* than in *Pd. russelli*. Conversely, the M2 and M3 overlap more in length in *Pd. russelli* than in *Pd. louisi*.

Absolute basal heights of stylar cusps C and D In the whole sample, the values of the absolute basal height of stylar cusp C to the absolute basal height of stylar cusp D are comprised in a range from 0.215 (i.e., the absolute basal height value of stylar cusp C is more than four times lower than for stylar cusp D; M1 MNHN.F.CB3007 of *Pd. russelli*) to 1,939 (i.e., the absolute basal height value of stylar cusp C is almost two times higher than for stylar cusp D; M3 UM-FDN-23 of *Pd. crocheti* sp. nov.) (Fig. 14; Online Resource 1: Table S4). The values equal or lower than the first quartile are only those of some M1 or M2 for *Pd. crocheti* sp. nov., whereas it concerns also some M3 specimens for the distributions of the values of *Pd. louisi* (MNHN.F.Mu18001) and *Pd. russelli* (MNHN.F.Av6837; MNHN.F.CB742). Conversely, the values equal or higher than the third quartile concern only M3 (five specimens) for *Pd. crocheti* sp. nov.; M1 (one specimen), M2 (three specimens) and M3 (one specimen) for *Pd. louisi*, with only M2 specimens as outlier values; and M1 (one specimen) and mostly M2 (four specimens) for *Pd. russelli* (Fig. 14). It is worth noting that fewer M3 specimens are known for *Pd. louisi* (five specimens) than for the two other species. Among these specimens, two lack stylar cusp C (MNHN.F.GL197 and MNHN.F.CB4182), one is damaged in the stylar cusp C area, and only two have measurable absolute basal heights for stylar cusps C and D (MNHN.F.Mu18001 and MNHN.F.SZ18005; Online Resource 1: Table S4). *Peradectes russelli* differs from *Pd. crocheti* sp. nov. and *Pd. louisi* in having a lower value for the interquartile range, almost equal mean and median values, and the lowest ratio values of the whole sample (the M1 MNHN.F.CB2501 and MNHN.F.CB3007, and the M3 MNHN.F.CB742; Online Resource 1: Table S4).

There is a statistically significant difference between the rank sum of the absolute basal height of stylar cusp C to the absolute basal height of stylar cusp D of *Pd. crocheti* sp. nov. and *Pd. louisi* (Fig. 14; Wilcoxon-Mann-Whitney test; $W = 226$, $P = 0.043$), and *Pd. crocheti* sp. nov. and *Pd. russelli* (Wilcoxon-Mann-Whitney test; $W = 256$, $P = 0.0004$). We should mention that without including the *Pd. crocheti* sp. nov. M3 UM-FDN-23, which has a high value for the calculated ratio (Online Resource 1: Table S4), there is no statistically significant difference between *Pd. crocheti* sp. nov. and *Pd. louisi* for this character (Wilcoxon-Mann-Whitney test; $W = 208$, $P = 0.072$), and the statistical difference still occurs between *Pd. crocheti* sp. nov. and *Pd. russelli* (Wilcoxon-Mann-Whitney test; $W = 239$, $P = 0.0007$). There is no statistically significant difference between the rank sum of the calculated ratios of *Pd. louisi* and *Pd. russelli* (Wilcoxon-Mann-Whitney test; $W = 204$, $P = 0.096$). Noteworthy, a statistically significant difference is recovered between *Pd. louisi* and *Pd. russelli* using a parametric instead of a non-parametric test (Welch's *t*-test; $t = 2.11$, d.f. = 28.49, $P = 0.044$). Finally, the range of variation for the absolute basal height of the stylar cusp C for *Pd. russelli* (0.033 –0.123 mm) is included in the one of *Pd. crocheti* sp. nov. (0.030 –0.131 mm) (Online Resource 1: Table S4), although the former species is larger than the latter.

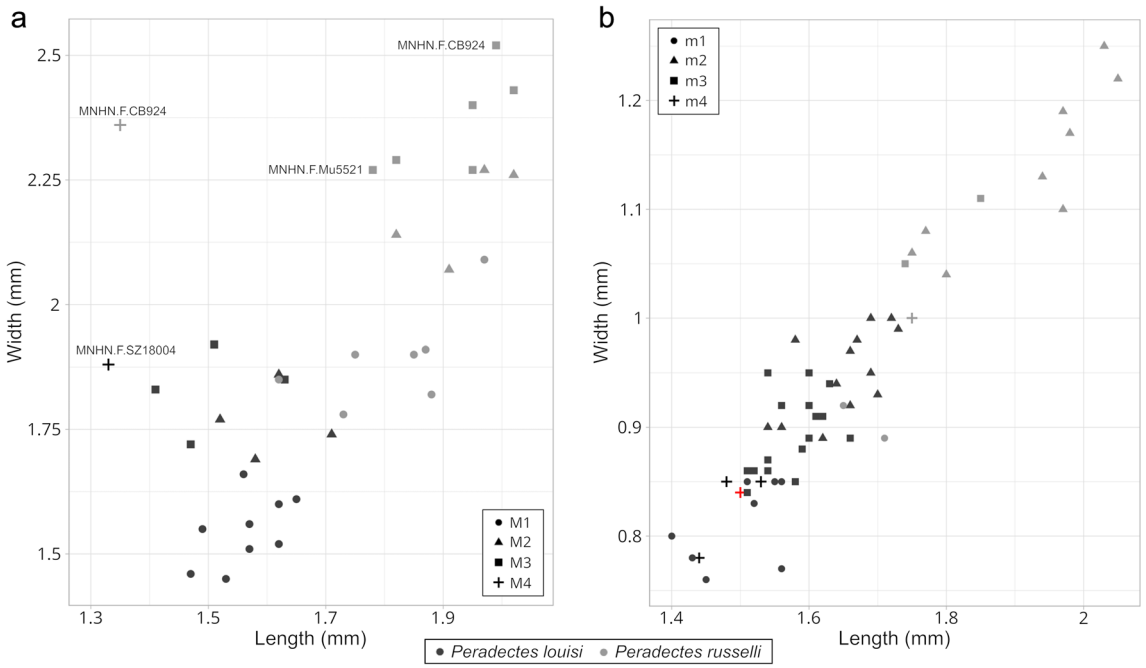

Fig. 13 Bivariate graphs (length x width) of upper molars (**a**) and lower molars (**b**) of the two species of *Peradectes* (*Pd. louisi* and *Pd. russelli*) from MP8 + 9, ~MP8 + 9 and MP8 + 9-MP10 interval localities of the Paris Basin. For upper molars (**a**), specimen numbers indicate the holotype of *Pd. russelli* (MNHN.F.CB924), the former holotype of *Pd. 'mutigniensis'* chosen by Crochet (1979) (MNHN.F.Mu5521) and the M4 of *Pd. louisi* (MNHN.F.SZ18004). For lower molars (**b**) the m4 specimen representing *Peradectes* cf. *louisi* is plotted in red. All measurements are from isolated molars with the exception of MNHN.F.CB924

Height of the dentary The dentary of MNHN.F.CB226 (*Pd. louisi*) is relatively higher below m2-m3 than those of MHN.AIX.PV.2017.6.8 (*Pd. crocheti* sp. nov.) and MNHN.F.CB925 (*Pd. russelli*) (Online Resource 1: Table S5). In turn, the dentary of *Pd. crocheti* sp. nov. is relatively lower than the one of *Pd. russelli*. No conclusion can be made out of these height data, because of the small number of specimens, and because the height of the dentary and its elongation in opossum and 'opossum-like' metatherians may vary depending on the age and sex of the individuals (e.g., Hough 1961; Crochet 1980b: p. 35, fig. 5).

Intrafamilial phylogenetic analysis

Main cladistic analysis The heuristic search yielded a single most-parsimonious tree (MPT) of 103 steps (Fig. 15), with a consistency index (CI) of 0.563 and a retention index (RI) of 0.526, which are indicative of high level of homoplasy in the dental characters used. A value of RI just above 0.5 indeed indicates that almost half of the similarities coded in the data matrix correspond to homoplasy (Farris 1989a, b). The single MPT supports the monophyly of the ingroup, the Peradectidae, with a Bremer value of 4. 7 out of 37 (= 19%) characters are not parsimony informative for resolving relationships between the ingroup taxa. Within the ingroup (late Paleocene – middle Eocene peradectids), *Pd. elegans* is the earliest diverging offshoot of the branching sequence formed with *Pd. protinnominatus* and its sister-clade, which includes strictly Eocene *Peradectes* species as well as *Armintodelphys* and *Mimoperadectes* (hereafter designated as the 'Eocene' peradectid clade; Fig. 15). All late Paleocene – middle Eocene species distinct from *Pd. elegans* form a clade (Bremer index [BI] = 2, relatively to the mean Bremer value of 2.1) and share the following non-ambiguous synapomorphies: m1 slightly shorter (< 10%) than the m2 (4^1), postcingulids that attenuate labially to the hypoconulid (16^1), and stylar cusp A distinctly smaller than stylar cusp B on M3 (32^1).

The 'Eocene' clade is supported (BI = 2) by three non-ambiguous synapomorphies: p3 higher than m1 (3^0), the low disparity between the L/W ratios of M2 and M3 (22^1), and stylar cusp D placed distolabially to the metacone apex on M1 (35^1); two of these are non-homoplasic (3^0, 35^1). The four European species (*Pd. crocheti* sp. nov., *Pd. russelli*, *Pd. louisi* and '*Armintodelphys*' *dufraingi*) are clustered in a clade that is unambiguously supported (BI = 2) by four synapomorphies: the entoconid has an intermediate position, between the distal edge of the trigonid and the distal margin of m2 and m3 (21^1, non-homoplasic), stylar cusp A most frequently positioned mesiolingually to stylar cusp B on M2 or M3 (31^1, convergent), stylar cusp B positioned strictly labially to the apex of the paracone, at least on M1 and M2 (33^1, non-homoplasic), and the ectoflexus of

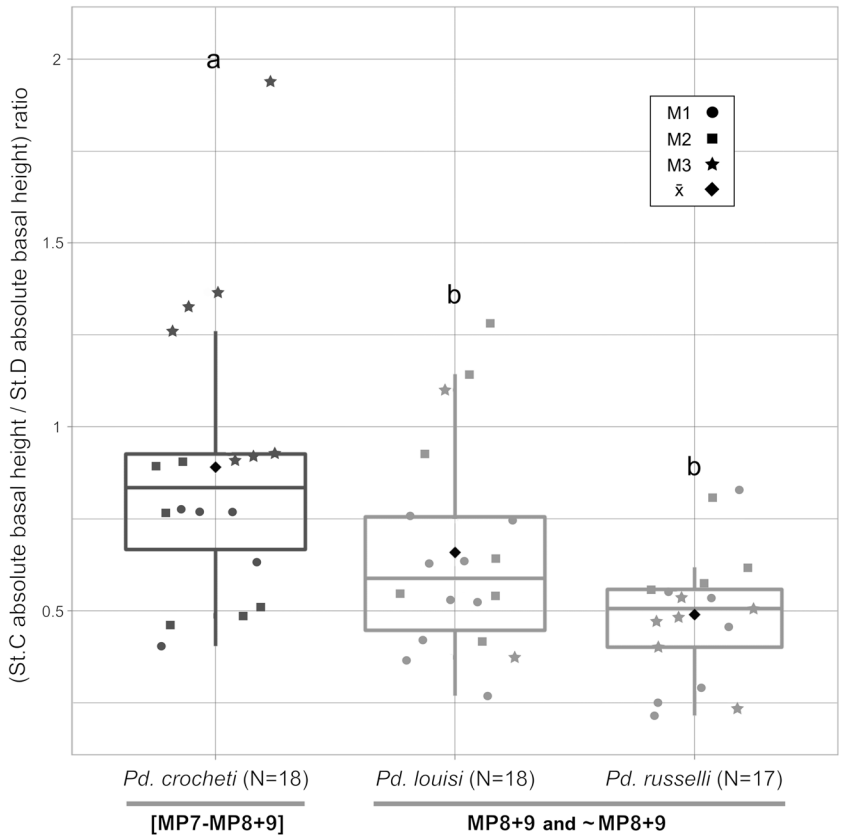

Fig. 14 Boxplots showing the distribution of the ratio values of the absolute basal height of stylar cusp C to the absolute basal height of stylar cusp D for *Peradectes crocheti* sp. nov. (MP7-MP8 + 9 interval), *Pd. louisi* and *Pd. russelli* (MP8 + 9 and ~MP8 + 9). M1 to M3 loci are considered. The value of the calculated ratio for each specimen is displayed for each box. The rank sum of ratio values of *Pd. crocheti* sp. nov. statistically significantly differs (letter 'a' above the box) from those of *Pd. louisi* and *Pd. russelli* (letter 'b') (non-parametric Wilcoxon-Mann-Whitney tests, $P < 0.05$; see main text). Abbreviation: [**MP7-MP8+9**], time interval between MP7 and MP8+9 reference levels

their M3 is asymmetric (37^1, convergent). The relationships within the European clade are well-resolved despite the high amount of missing data for '*Arm.*' *dufraingi* (17 out of 37 [=46%] scored characters). Within this clade, *Pd. crocheti* sp. nov. is the earliest diverging species. The clade comprising *Pd. russelli*, *Pd. louisi*, and '*Arm.*' *dufraingi* is supported (BI = 2) by two non-ambiguous synapomorphies: the presence of a straight postcristid at least on one m2-m4 locus (15^0, convergent) and the relatively small stylar cusp C compared to stylar cusps B and D (34^1, convergent). The less inclusive clade *Pd. louisi* + '*Arm.*' *dufraingi* is also supported (BI = 2) by two non-ambiguous synapomorphies: relatively long m2 or m3 with a L/W ratio equal to or higher than 1.75 (5^1, convergent) and the mesial end of the cristid obliqua sometimes ventral to the protocristid notch on m4 (11^1, convergent).

The sister group of the European peradectids is formed by a clade that includes the strictly Eocene North American peradectids (*Mimoperadectes labrus*, *Armintodelphys blacki* Krishtalka and Stucky, 1983a, *Armintodelphys dawsoni* Krishtalka and Stucky, 1983a, *Pd. chesteri*, *Pd. gulottai* and *Pd. californicus*). This clade is supported (BI = 2) by the following non-ambiguous synapomorphies: small distal heel on lower premolars (1^1, non-homoplasic), hypoconulid higher than the entoconid on m3 and m4 (19^1, convergent with '*Arm.*' *dufraingi*), and postmetacrista subequal in length or shorther than the preparacrista on M2 or M3 (29^0, with intraclade reversion). North American *Armintodelphys* species are more closely related to the strictly Eocene North American *Peradectes* species than to *Mimoperadectes labrus* based on the absence of internal cristae on the conules (26^0, with intraclade reversion). The p3 lower than the m1 (3^2) is an ambiguous non-homoplasic character which supports the latter clade with the accelerated transformation (Acctran) optimization, or only the Eocene North American *Peradectes* clade with the delayed transformation (Deltran) optimization. The genus *Armintodelphys* is recovered as monophyletic based on two non-ambiguous synapomorphies not observed in '*Arm.*' *dufraingi*, namely a trigonid as wide as the talonid on m3 (7^1) and a talonid as long as the trigonid on m4 (8^1, non-homoplasic within the ingroup). In this topology, the genus *Peradectes* is not monophyletic, because a subclade of three *Peradectes* species is well nested (BI = 2) within the 'Eocene' North American clade that also includes *Mimoperadectes* and *Armintodelphys*. One of the most strongly supported clades of the ingroup is *Pd. gulottai* + *Pd. californicus* (BI = 3), although *Pd. gulottai* is the taxon with the least complete scoring (15 out of 37 [~41%] scored characters).

Subsequent cladistic analyses dealing with more characters concerned by polymorphic coding, implied weighting or ordered characters A single MPT with the same topology is recovered from the second analysis (111

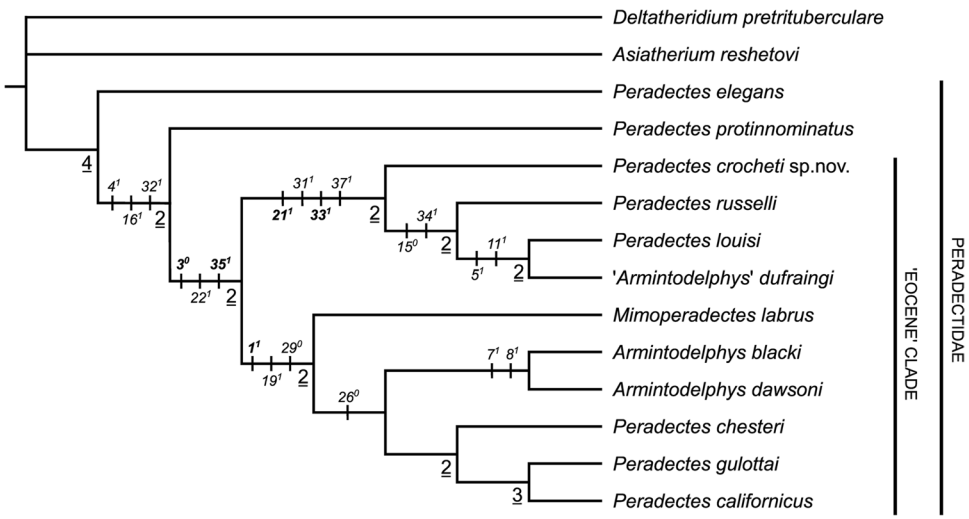

Fig. 15 Single most-parsimonious tree of 103 steps (CI = 0.563, RI = 0.526) from the first cladistics analysis (non-polymorphic characters 11, 31, 36 and 37; all characters unweighted and unordered). Underlined values under the branches at nodes are Bremer indices (BI) when > 1. The non-ambiguous synapomorphies are figured at the nodes of interest in this work, within the ingroup. The character states in superscript are summarized in Online Resource 3. The non-ambiguous and non-homoplasic synapomorphies (CI = RI = 1) are in bold

steps, CI = 0.604, RI = 0.517), for which the frequencies of observation were replaced by polymorphisms in the scoring of the characters 11, 31 and 36 (Online Resource 5: Fig. S1 and text). The differences with the first analysis concern notably (but not exclusively) two non-ambiguous synapomorphies of the first analysis that become ambiguous synapomorphies at their respective node with the accelerated transformation optimization, which are: stylar cusp A positioned mesiolingually to the stylar cusp B on the M2 or M3 (31^1) for the European peradectid clade, and the presence of a mesial end of the cristid obliqua ventral to the protocristid notch on the m4 (11^1) for the clade *Pd. louisi* + '*Arm.*' *dufraingi*. Numerous clades have a value of Bremer index decreasing from BI = 2 to BI = 1, namely the European clade, the *Pd. russelli* + *Pd. louisi* + '*Arm.*' *dufraingi* clade, the *Pd. louisi* + '*Arm.*' *dufraingi* clade, the strictly Eocene North American peradectid clade and the strictly Eocene North American *Peradectes* clade. The value of the Bremer index of the clade *Pd. gulottai* + *Pd. californicus* also decreases from 3 to 2.

As for the third analysis (addition of a polymorphic scoring for the character 37 to changes of the second analysis; see Online Resource 5), two different MPTs of 112 steps each (CI = 0.607, RI = 0.511) are obtained, and the strict consensus tree is weakly resolved, with no Bremer index values higher than BI = 1 within the ingroup (Online Resource 5: Fig. S2), and a large polytomy at the base of the 'Eocene' clade. *Peradectes crocheti* sp. nov. branches at this polytomy with other strictly Eocene peradectids, and thus does not form a clade with the other European species. *Peradectes louisi*, *Pd. russelli* and '*Arm.*' *dufraingi* still form a clade on the strict consensus tree, but its internal topology is also unresolved. A monophyletic North American *Armintodelphys* is retained. One of the two MPTs has the same topology as the single MPT found in the previous analyses.

The fourth analysis of identical parameters and scoring as the previous one (which has the highest frequency of polymorphisms in its scoring), but with downweighted homoplasic characters instead of unweighted characters, resulted in a single MPT. The topology obtained is the same as in the main and second analyses (Fig. 15), and is that of one of the two trees of the third analysis; it is here favored for this reason. The same tree length, CI and RI scores as those of the third analysis are recovered. Finally, the fifth analysis with characters 3 and 34 ordered recovered a single MPT (105 steps, CI = 0.552, RI = 0.505), again with the favored topology. The only differences with the first analysis are as follows: (i) the p3 higher than m1 (3^0) becomes homoplasic, and an ambiguous instead of non-ambiguous synapomorphy (Acctran optimization) supporting the 'Eocene' clade (for which BI = 1 instead of BI = 2); (ii) the Bremer value of the 'Eocene' North American clade decreases from BI = 2 to BI = 1; (iii) the acquisitions of a well-developed stylar cusp C (34^2) in the ingroup (still non-ambiguous) and of a p3 lower than m1 (3^2) in the *Armintodelphys* + 'Eocene' North American *Peradectes* clade (still ambiguous with Acctran optimization) take two steps instead of one each.

Discussion

Characters and spatiotemporal distribution of the earliest European peradectid species, *Peradectes crocheti* sp. nov.

The earliest occurrence of Peradectidae in Europe Two *Peradectes* species were recognized in the Sotteville-sur-Mer fauna from the Mortemer Formation (~ MP7, Normandie, Paris Basin; Smith et al. 2011), each represented by a single specimen. The Sotteville-sur-Mer

locality being considered as intermediate in age between Dormaal and both Soissons and Meudon (Smith et al. 2011; Marandat et al. 2012; Hooker 2015), both of these *Peradectes* species were proposed as the first European peradectids. *Peradectes* sp. 1 was identified after a fragment of a small left dentary, preserving a complete worn molar and a worn talonid (Smith et al. 2011: fig. 5.17), and would be the smallest peradectid recorded so far in Europe (Smith et al. 2011). On the molar designated as m3, the trigonid is mesiodistally narrow, much shorter than the talonid, the small protoconid is almost strictly labial to the metaconid, and the preprotocristid is rectilinear in mesiolabial view. On the putative m3 and better-preserved talonid of m2, the hypoconid is distolabial to the entoconid on the anteroposterior axis of the molar. The hypoconulid, though worn, is much lower than the entoconid, and these cuspids are not connected. Here, we rule out the attribution of this specimen to *Peradectes* because of the absence of the aforementioned characters in peradectids (Table 6). Furthermore, the low and mesiodistally pinched paraconid lacks the mesiolingual paraconid keel, a distinctive feature of metatherian mammals and of some basal therians and eutherians (Averianov et al. 2013; Averianov 2015: p. 175). The metaconid is subequal in height to the protoconid, but to our knowledge, no Laurasian metatherian with a metaconid subequal to or higher than the protoconid on lower molars exists. This feature occurs in, for example, some Paleocene South American metatherians from Tiupampa (e.g., Goin et al. 2003: p. 873; Muizon and Ladevèze 2022: p. 631–632), and is a synapomorphy of Eutheria (O'Leary et al. 2013). Finally, the entoconid and hypoconulid are not as twinned as in metatherians on the most anterior molar, and the postcingulid is absent, as seen in earliest marsupialiforms (e.g., Vullo et al. 2009) and eutherians, which also indicate the eutherian nature of this material.

Regarding the upper molar with a rectilinear centrocrista referred to as *Peradectes* sp. 2 (Smith et al. 2011: fig. 5.18), the depth of the ectoflexus and the relative length of the preparacrista indicate it is a M3 rather than a M2. According to the authors, this molar is comparable in size and morphology to both *Pd.* '*mutigniensis*' (= *Pd. russelli*; MP8 + 9 and ~MP8 + 9 localities of the Paris Basin) and *Pd. protinnominatus* (Clarkforkian and early Wasatchian of the Bighorn Basin). However, among European peradectids, *Peradectes* sp. 2 from Sotteville-sur-Mer (L = 1.58 mm, W = 1.91 mm) is smaller than M2 and M3 of *Pd.* '*mutigniensis*', and closer in size to the holotype of *Pd. louisi*, as stated by Hooker (2020), and to the M3 of *Pd. crocheti* sp. nov. As in *Pd. crocheti* sp. nov. and *Pd. protinnominatus*, and contrary to *Pd. louisi*, stylar cusp D is labial instead of distolabial to the metacone apex, and stylar cusp C is much higher instead of subequal or lower than stylar cusp D. Although *Peradectes* sp. 2 and *Pd. protinnominatus* are almost the same size, *Peradectes* sp. 2 has a stylar cusp B positioned labially to the apex of the paracone on the stylar shelf, and the ectoflexus is asymmetric, as seen on M3 of *Pd. crocheti* sp. nov. from Palette. On the holotype of *Pd. protinnominatus* (UCMP 44077; McKenna 1960: fig. 17a) and on M3 from the Bighorn Basin (Bown 1979: fig. 40a right) attributed to *Pd. protinnominatus* in the last comprehensive revision of the species (Krishtalka and Stucky 1983b: p. 246–247), stylar cusp B is located mesiolabially to the paracone, and the ectoflexus has a symmetric shape (Fig. 4). It is worth mentioning that Gingerich and Smith (2006) did not report ascertained M3 of *Pd. protinnominatus* from the Bighorn Basin localities they studied. Considering its size and morphology, *Peradectes* sp. 2 is consequently better assigned to *Pd. crocheti* sp. nov., and it represents the earliest occurrence of this species. Therefore, *Pd. crocheti* sp. nov. is definitely the oldest European peradectid currently known (see Smith et al. 2011).

Recognition of other synonyms of *Peradectes crocheti* sp. nov. All other here proven peradectid dental material of MP7-MP8 + 9 interval localities attributed to *Peradectes* sp. (Russell et al. 1988; Marandat 1991; Hooker 2010) and *Pd. louisi* (Godinot 1981; Hooker 2020) have been allocated to *Pd. crocheti* sp. nov. in this study. These specimens conform to the size range and morphological variation observed in *Pd. crocheti* sp. nov. from Palette. In Hooker's view, the labial fragment of upper molar from Abbey Wood (London, Blackheath Formation) he considered as *Peradectes* sp. (Hooker 2010: p. 17, fig. 8a-b) differs from all upper molars of the French *Peradectes* species in its much weaker stylar cusps and its more gracile metacone. The relative heights of the stylar cusps have been used here instead of the absolute height of the stylar line as diagnosic features of European peradectid species. Although both stylar cusps C and D are low on the M2 from Abbey Wood (e.g., compared to stylar cusp B), as on most upper molars of *Pd. crocheti* sp. nov. and *Pd. louisi* (Figs. 5, 9 and 10), the most ventral point of the stylar cusp C – D mesiodistal extension in labial view is on stylar cusp C, which is consequently higher than stylar cusp D, as in almost all specimens of *Pd. crocheti* sp. nov. (Fig. 5) and unlike *Pd. louisi* (Figs. 9 and 10). It is worth noting that Hooker (2020: p. 461) made the same observation for the relative heights of the stylar cusps of the M2 from Croydon (here re-referred as *Pd. crocheti* sp. nov.), which was however attributed to *Pd. louisi*. Furthermore, the metacone of the specimen from Abbey Wood is not significantly more gracile when compared with other unworn M2 of *Pd. crocheti* sp. nov. (e.g., MNHN.F.Me15975, Fig. 5o-p); thus, the shape of this cusp on the specimen from Abbey Wood is not exclusively shared with *Pd. protinnominatus* (*contra* Hooker

Table 6 Summary of the main morphological differences between cheek teeth of ascertained late Paleocene – middle Eocene Peradectidae and Eocene Herpetotheriidae (and *Herpetotherium fugax*), deduced from comparisons of peradectid material described in this study. The character states in bold are documented absent in one or more species of the concerned group. Comparative data for *Herpetotherium fugax*: Korth (1994: fig. 8.1) for lower premolars, cast of AMNH 5254 (holotype) and Korth (2018: fig. 6b) for lower molars, Sánchez-Villagra et al. (2007: fig. 1c; *Herpetotherium* cf. *fugax*) for upper premolars, e.g., Green and Martin (1976: fig. 2), Fox (1983) and Korth (2018: fig. 6a) for upper molars

	late Paleocene – middle Eocene Peradectidae	Eocene Herpetotheriidae + *Herpetotherium fugax*
Lower premolars		
Shape of mesial edge in labial or lingual view	curved	V-shaped, at least on one locus
Shape of roots	curved	straight
Upper premolars (P2-P3)		
Distal crista and accessory cusp configuration	**separated by a notch**	highly connected
Lower molars		
Preprotocristid shape on m1-3	fully convex	almost vertical
Metaconid most frequent position	**distolingual to protoconid**	almost strictly lingual to protoconid
Lingual opening of trigonid basin on m2	higher than metaconid-entoconid notch	as high as metaconid-entoconid notch
Entoconid vs. hypoconid height in distal view	subequal	entoconid higher
Hypoconid position compared to entoconid on m2 or m3	mesiolabial to labial	labial to distolabial
Lingual edge of talonid on m2 or m3	curved, with oblique entoconid	straight, without oblique entoconid
Postcingulid lingual shape on m1-3	**attenuates labially to the hypoconulid**	**extends lingually towards hypoconulid tip**
Upper molars		
Protocone relative height on M1-M3	lower than paracone	subequal to higher than paracone
Conules relative size and structure	small, with rare internal cristae	larger, with frequent internal cristae
Paracone and metacone shape	conical, convex labial edge	triangular, flat labial edge
Centrocrista	rectilinear	strongly ‘v’-shaped
Doubling of stylar cusp C or D	**rare**	**frequent**
Stylar cusp D position on M1	**distolabial to metacone**	labial or mesiolabial to metacone
Ectoflexus on M4	present and deep	absent or weak

2010). Peradectid upper molars from Fordones (UM-FDN-1 and UM-FDN-23) were first found to be more similar to *Peradectes* sp. from MP8 + 9 and ~MP8 + 9 localities of the Paris Basin (= *Pd. louisi* in part, see below) than to any other peradectids then known, because, as on the M1 from Mutigny (MNHN.F.Mu18006; Fig. 10d), they are mesiodistally pinched at the base of the main cusps (Marandat 1991: p. 67, pl. 1, figs. 1-2), i.e., the distal edge of these upper molars is emarginated. The shape of the distal edge or mesiodistal constriction of the upper molars is here regarded as variable within the European *Peradectes* species. For example, the M1 UM-FDN-2 (Fig. 5e) of *Pd. crocheti* sp. nov., first assigned to a herpetotheriid by Marandat (1991: p. 71), shows a relatively long talon and a weak distal emargination, which is the opposite condition to UM-FDN-1. Since this character varies substantially in the European peradectid species, its use to diagnose peradectid species (e.g., Horovitz et al. 2009) may be doubtful.

The two lower molars from Fordones would also be similar to the MP8 + 9 and ~MP8 + 9 *Peradectes* sp. due to the lingual position of the hypoconulid (Marandat 1991: p. 67, pl. 1, fig. 18). However, in addition to this character, the distolingual orientation of the hypoconulid, the entoconid higher than the hypoconid in distal view, the hypoconid positioned distolabially to the entoconid, and the pronounced labial emargination of the crown are more evocative of a herpetotheriid species. The presence of subequally-sized entoconid and hypoconulid as seen on these specimens is known to be not exclusive to Peradectidae (it also occurs in e.g., Herpetotheriidae [Crochet 1980b: p. 149, fig. 162] and 'Alphadontidae' [Johanson 1996: p. 1028]), and thus does not prevent the attribution of the lower molars from Fordones to herpetotheriids (*contra* Marandat 1991). Fragmentary lower molars of peradectids and herpetotheriids may be particularly difficult to distinguish in occlusal view. For example, a fragmentary lower molar from Fordones, lacking the paraconid and ascribed to the herpetotheriid *Pt. constans* (UM-FDN-18, Fig. 7d; Marandat 1991: p. 68) exhibits a curved lingual edge of the talonid with a relatively labiolingually wide hypoconulid, which may be superficially evocative of peradectids. If the metaconid and entoconid apex are considered aligned as on, for example, MNHN.F.Me16101 (Fig. 7i), the lingual edge of the talonid appears straight between the entoconid and metaconid (i.e., not fully curved) on UM-FDN-18, and its hypoconid is distolabial instead of labial or mesiolabial to its entoconid. In labial and lingual views, the entoconid is relatively higher and the entoconid – hypoconulid notch is deeper than in m2 of *Pd. crocheti* sp. nov. (Figs. 6 and 7) and some m2 of *Pd. protinnominatus* (Gingerich and Smith 2006: fig. 26A-C). The postcingulid is also less convex than on figured peradectid m2 on which this cingulid is entirely preserved. These subtle differences probably led to confusion with herpetotheriids. As a matter of fact, the difficulty in differentiating early peradectids from early herpetotheriids, based on lower molars with subtle differences, has often been pointed out (Johanson 1996: p. 1030; Williamson and Lofgren 2014; but see Rose et al. [2012: p. 17] for an opposing view). In an attempt to overcome this issue, we summarize here (Table 6) the morphological differences between the cheek teeth of European Peradectidae and Herpetotheriidae, deduced from our comparisons of the peradectid material here described. Among the late Paleocene – Eocene peradectids, *Pd. crocheti* sp. nov. displays a combination of both derived features, mainly on upper molars, and primitive features, mostly but not exclusively on lower molars.

Intra-European paleobiogeographic and biostratigraphic implications A biotic provincialism between northwestern European (Anglo-Belgian and Paris Basins) and southwestern European (south of France and Iberian Peninsula) mammal faunas was proposed based on occurrences of most of the eutherian taxa around the reference level ~ MP7 (Marandat 1997; Smith 2000; Solé et al. 2011, 2013, 2018; Marandat et al. 2012). Exceptions are limited to two cases when considering only recent taxonomic revisions. The teeth of the artiodactyl *Diacodexis* from Dormaal (Belgium) and Palette (Provence) show strong similarities (Boivin et al. 2018), and the three plesiadapiform species *Arcius fuscus* Russell, Louis & Savage, 1967, *Arcius lapparenti* Russell, Louis & Savage, 1967, and *Arcius zbyszewskii* Estravís, 2000, have been documented in several deposits in northwestern and southwestern Europe (e.g., López-Torres and Silcox 2018). As for metatherians, *Peradectes crocheti* is newly recorded from localities closer in age to MP7 than to MP8 + 9, which are located in both northwestern Europe (Abbey Wood, Croydon, Meudon, Soissons and Sotteville-sur-Mer) and southwestern Europe (Fordones and Palette) (Fig. 1a). The herpetotheriid *Peratherium constans* also probably did not follow this dispersal pattern if both earliest Eocene (MP7) and MP7-MP8 + 9 interval occurrences are considered (Godinot et al. 1987; Marandat 1991; Estravís 2000; Ladevèze et al. 2012). *Amphiperatherium* cf. *maximum*, smaller than the typical MP8 + 9 and ~MP8 + 9 species *A. maximum* (Crochet 1979, 1980b), is also found in the MP7-MP8 + 9 interval localities of Soissons in the northwestern European province (Louis 1996) and Fournes and Rians in the southwestern European province (Godinot 1981; Marandat 1991). Whether the northern form from Soissons represents the same species as the southern form from Fournes and Rians has yet to be thoroughly tested. Note that *Amphiperatherium* cf. *maximum* represents one of the earliest occurrences of *Amphiperatherium* since *A. brabantense* Crochet, 1979 (Dormaal), was synonymized with *Pt. constans* (Ladevèze et al. 2012). Altogether, the definition of *Pd. crocheti* sp. nov. reveals that none of the earliest

species of the three metatherian genera present in Europe from the MP7 reference level to slightly after (*Peradectes crocheti* sp. nov. in Peradectidae, *Peratherium constans*, and *Amphiperatherium* cf. *maximum*, if indeed a single species, in Herpetotheriidae) seems to be affected by biotic provincialism, a conclusion challenging the bioprovinces scheme of Marandat et al. (2012), at least for metatherian mammals. Three herpetotheriid species have recently been demonstrated to be widespread between western and south-eastern European assemblages, as early as the latest Eocene based on the occurrences of *Amphiperatherium exile* (Gervais, 1848–1852), contrary to coeval rodents which are mainly represented by distinct species from these two parts of Europe (Wessels et al. 2024). This reinforces the originality of the dispersal patterns of Laurasian metatherians compared to most coeval eutherians, as supported here.

Peradectes crocheti sp. nov. is the only peradectid documented in the MP7-MP8 + 9 localities where the family is present. It is unrecorded from younger localities from the Paris Basin (MP8 + 9 and ~MP8 + 9) that yielded exclusively *Pd. louisi* and *Pd. russelli*, the last occurrences of *Pd. crocheti* sp. nov. being from Fournes and Rians, after the ETM2 (see Material and methods). This documents the first well-supported species turnover for an early European metatherian lineage during the early Ypresian, as it is known at the same period for some eutherian groups, but at the generic level (e.g., Solé 2014: fig. 3; Solé et al. 2018: table 10; Bronnert and Métais 2023: table 1). This peradectid species turnover is characterized, among other morphological characters, by a clear decrease of the mean absolute basal height of stylar cusp C relative to the mean absolute basal height of stylar cusp D during the early to middle early Eocene (MP7-MP8 + 9 interval to ~MP8 + 9) (Fig. 14).

Phylogenetic relationships between late Paleocene – middle Eocene peradectids

Origin and endemism of European peradectids An apparent lack of support for the monophyly of European peradectids has been a consequence of previous studies regarding their taxonomic status (Crochet 1980b; Smith and Smith 2013). Crochet (1980b: p. 54, fig. 33), based on the morphology of upper molars only, suggested stronger affinities between *Peradectes elegans*, *Pd. louisi* and *Pd. russelli* on the one hand, and between *Pd. protinnominatus* and *Pd. 'mutigniensis'* on the other hand. The conclusions of Crochet (1980b) hence involved at least two independent peradectid dispersals of unspecified direction between North America and Europe. Smith and Smith (2013) described a new peradectid species from Egem (Belgium, ~MP8 + 9, 51–52 Ma, during the Early Eocene Climatic Optimum [EECO]) attributed to the North American genus *Armintodelphys* ('*Arm.*' *dufraingi*), and thus argued for an *Armintodelphys* dispersal from North America to Europe around the Early Eocene Climatic Optimum. However, most of our phylogenetic analyses have recovered the four European species *Pd. crocheti* sp. nov., *Pd. louisi*, *Pd. russelli* and '*Arm.*' *dufraingi* forming a clade nested within other late Paleocene to middle Eocene peradectids, with *Pd. crocheti* sp. nov. as the earliest diverging species (Fig. 16). Even in the less resolved third analysis, '*Arm.*' *dufraingi* forms a clade with *Pd. louisi* and *Pd. russelli*, rather than being included in the North American *Armintodelphys* clade. These results suggest that *Armintodelphys* did not disperse between North America and Europe (*contra* Smith and Smith 2013), and that late Paleocene to Eocene peradectids have experienced a unique dispersal from North America to Europe during their evolutionary history (*contra* Crochet 1980b; Smith and Smith 2013). These conclusions imply that European peradectids certainly evolved as an endemic group until their extinction on this continent (the putative South American record of *Armintodelphys* compared with *'Arm.' dufraingi* [see Carneiro and Oliveira 2023: p. 37-38, fig. 15] has been reinterpreted as a putative herpetotheriid taxon; Carneiro et al. 2024), as European herpetotheriids probably also did (Ladevèze et al. 2012, 2020), at least until the middle early Eocene (MP8 + 9 or close in age, to MP8 + 9-MP10 interval). New dental material of late early Eocene (MP10 to MP11 reference levels) peradectids is further needed to definitely verify this hypothesis, because paleobiogeographic analyses of nyctitheriids show that dispersal events of small mammals from North America to Europe may have occurred multiple times and later than the middle early Eocene (Manz and Bloch 2015: p. 27–28, fig. 7).

The dispersal of peradectids perhaps occurred later than the arrival of herpetotheriid metatherians in Europe from North America, so far envisioned during the Paleocene-Eocene Thermal Maximum (PETM) for the latter, because peradectids are still unknown in the MP7 localities of Erquelinnes (Missiaen et al. 2013), Dormaal (Ladevèze et al. 2012), Le Quesnoy (Nel et al. 1999; pers. obs.) and Silveirinha (Estravis 2000), the last three having yielded the earliest herpetotheriid metatherians of Europe to date. According to the known fossil record, a putative dispersal event including peradectids by the Thulean route (a land bridge connecting North America and Europe via Greenland; Brikiatis 2014), probably followed (and was triggered by) the PETM, and took place between the PETM and ETM2, as has been established so far for paromomyid plesiadapiforms and the mesonychid *Pachyaena* (Fig. 16; Smith et al. 2011; Hooker 2015; Solé et al. 2018: p. 31). The finding of a peradectid astragalus in Palette (Fig. 8), with a nearly ungrooved trochlea (Fig. 8b) and a sloping medial tibial facet (Fig. 8d) suggesting tibioastragalar mobility (Rose 2012), shows that the first European peradectids were probably already arboreally adapted, like their small (the body mass of

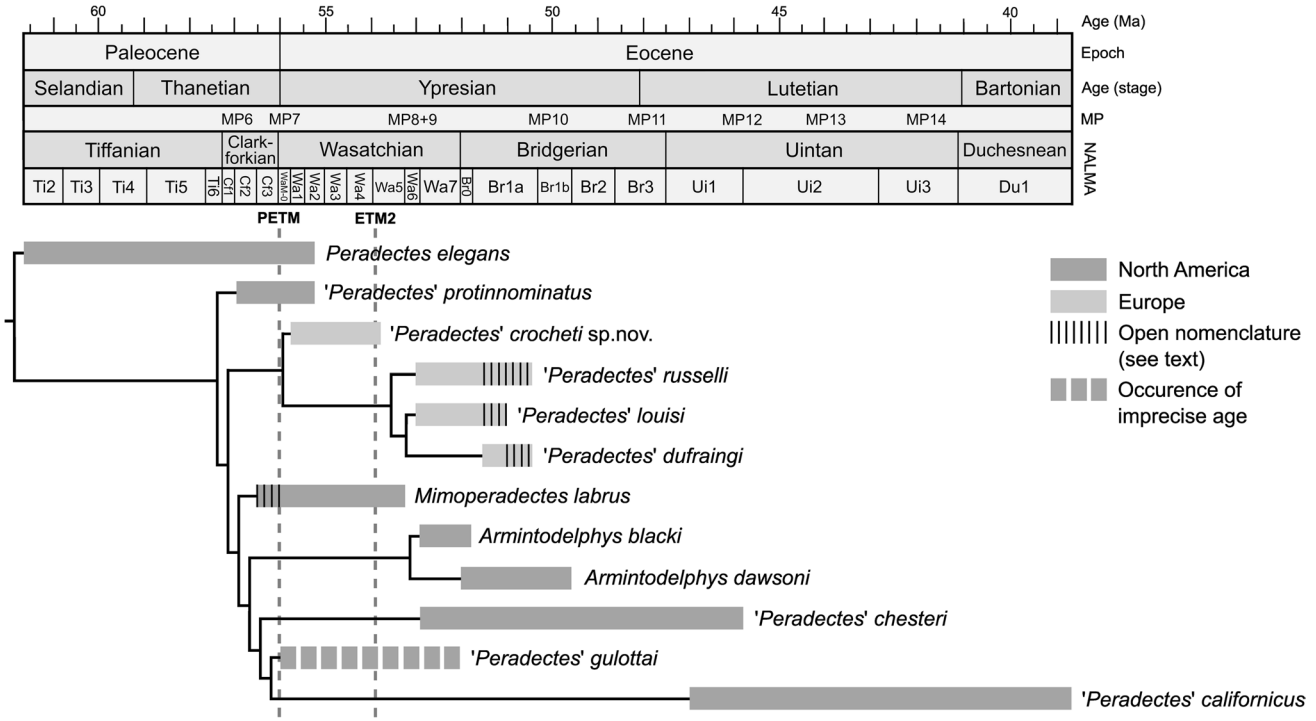

Fig. 16 Favored topology of the peradectid ingroup, recovered from four out of the five analyses, mapped on the Paleogene time scale (Speijer et al. 2020) and with the geographic distribution of species and selected thermal maxima of the early Eocene (PETM and ETM2). The European peradectid clade probably differentiated immediately after the PETM. *Peradectes* appears paraphyletic with the generic attributions here retained. Temporal extensions of taxa are detailed in Online Resource 2

Pd. crocheti is estimated between approximately 26–30 g, using the lengths of the four available unworn M3 [Online Resource 1: Table S1] in the appropriate predictive equation of Gordon 2003: fig. 7), similarly sized, contemporaneous North American counterparts during the late Paleocene – early Eocene (Szalay 1994; Rose 2012), and like possible peradectid specimens from Messel (Kurz 2005). The Palette astragalus is very similar to astragali of small earliest Eocene North American peradectids (Rose et al. 2012), which provide further support to the close phylogenetic affinities between North American and European peradectids. A dispersal of peradectids from North America to Europe during the PETM or slightly later is also congruent with our phylogenetic framework, since the earliest offshoots of the European and strictly Eocene North American peradectid clades, namely *Pd. crocheti* sp. nov. and *M. labrus* respectively, together with the more basal *Pd. protinnominatus*, are recovered from early Eocene localities of similar age (Fig. 16). In particular, *Pd. crocheti* sp. nov. and *M. labrus* are not formally documented earlier than the early Eocene (Fig. 16; but see Rose 1981: p. 36), which supports the occurrence of a global cladogenesis event during or immediately after, and thus potentially driven by, the PETM in the evolutionary history of peradectids.

Definitions of *Peradectes, Armintodelphys*, and Peradectidae The intrafamilial phylogenetic analysis highlighted disentangles relationships between all late Paleocene – middle Eocene peradectids. First, we concur with Williamson et al. (2012, 2014) in evidencing a lack of support for the monophyly of the genus *Peradectes*. It was recovered as polyphyletic in their phylogenetic analyses, including all valid North American *Peradectes* species, whereas it is paraphyletic in the analysis here performed, which does not include the earliest North American *Peradectes* species (early Paleocene, Danian), *Pd. minor* and *Pd. coprexeches* (Clemens 2006; Williamson and Taylor 2011; Williamson et al. 2012). The paraphyletic status of *Peradectes*, the genus being here valid if monospecific (i.e., restricted to *Pd. elegans*) or alternatively if it includes the species of the genera *Mimoperadectes* and *Armintodelphys* (and potentially *Didelphidectes* and *Nanodelphys*, which have not been included in our analyses), has long been suggested by an early diagram of the probable relationships between peradectid species (Krishtalka and Stucky 1983b: fig. 6), in the same way as in the topology obtained from most of our analyses. Second, Williamson et al. (2012: p. 629) proposed a phylogenetic definition of Peradectidae, as 'the most inclusive clade containing *Peradectes elegans*, but not *Herpetotherium fugax*, *Pediomys elegans* or *Didelphis virginiana*'. Contrary to the phylogenetic analyses of

Williamson et al. (2012, 2014), our topology recovering only relationships among peradectids is fully resolved, and *Peradectes elegans* and *Pd. californicus* (which form the clade Peradectidae in Williamson et al. [2012, 2014], according to the definition of Williamson et al. [2012]) are not found as sister taxa. This implies that a Peradectidae clade as originally conceived (e.g.Krishtalka and Stucky 1983b: fig. 6) or similar to that recovered in this study (Fig. 16), more inclusive than *Pd. elegans* + *Pd. californicus* as found by Williamson et al. (2012, 2014), could effectively exist, as Williamson et al. (2012: p. 632) suggested themselves. For these reasons, a broader phylogenetic analysis encompassing all *Peradectes* species nested in the whole Metatheria will be needed, but it is beyond the scope of this paper. Pending further study, we take a conservative and convenient approach in maintaining the use of the genus name *Peradectes*, even for European species. This encompasses '*Arm.*' *dufraingi*, here rereferred to *Peradectes* (*Pd. dufraingi*; see below).

Armintodelphys appears polyphyletic if the species *dufraingi* is included, but is monophyletic when this European species is not considered (as in Williamson et al. [2012, 2014]), or not included in the genus (this study). The lower molars of *Pd. dufraingi* and *Pd. louisi* are relatively more elongated than any late Paleocene to middle Eocene peradectid, *Armintodelphys* included (L/W of m3 > 1.75, see Table 4 for *Pd. louisi*), and the two European species share a labial emargination of lower molars that is absent in m3 of *Arm. blacki* and *Arm. dawsoni* (pers. obs., *contra* Krishtalka and Stucky 1983a). A relatively minute entoconid, lower than the hypoconulid on molar loci more anterior than m4, that has been proposed as a diagnostic character of *Armintodelphys* (Krishtalka and Stucky 1983a), is not only present in the *Armintodelphys* species and *Pd. dufraingi*, but also in other Eocene peradectids such as *Mimoperadectes labrus* (Bown and Rose 1979: fig. 1B; Rose et al. 2012: fig. 12H), *Pd. californicus* (Lillegraven 1976: pl. 9, fig. 2b) and *Didelphidectes* (Korth 1994). In turn, the characters here supporting the monophyly of North American *Armintodelphys* were not mentioned in the diagnosis of the genus by Krishtalka and Stucky (1983a). The morphological similarities pointed out between *Pd. louisi* and *Pd. dufraingi*, in addition to the subtle differences of their lower molars (see diagnosis of *Pd. louisi*), do not justify assigning the species *Pd. dufraingi* to a genus other than that of the species *Pd. louisi* (hence *Peradectes*).

Limits of phylogenetics analyses A caveat is in order on the phylogenetic analyses of peradectids, which are only based on dental characters due to the current lack of cranial and postcranial material for the group. Past research has shown that the dominance of dental characters in matrices may lead to inaccurate phylogenies, potentially due to higher levels of homoplasy in this anatomical partition (Sansom et al. 2017; Brocklehurst and Benevento 2020). The high homoplasy levels detected in our analyses (RI ~ 0.5) do not contradict these cautionary statements. In addition, small cusps were mentioned to be possibly poorly reliable for reconstructing phylogenies due to their late occurrence in the patterning cascade of cusp development (Jernvall and Jung 2000). Whether this can apply to the stylar cusps present on upper molars of peradectids remains to be investigated, but our observations in the present study are suggestive of the presence of some phylogenetic signal in the subtle variation of these structures, for their relative position (representing 3 out of 37 characters used in the phylogenetic analyses), length and width (1 out of 37 characters), and height (1 out of 37 characters). In particular, the two methods employed to evaluate the relative height of the stylar cusps C and D produced an identical main result (the relative shrinking of the stylar cusp C between the MP7-MP8 + 9 interval and ~MP8 + 9). Meanwhile, the difficulty of accurately scoring complex dental variation (e.g., Billet and Bardin 2019) and the presence of high levels of homoplasy urge caution when interpreting current phylogenetic results on peradectids. The discovery of more complete fossils (like the material from Palette), and the use of geometric morphometric methods to characterize dental variation within peradectids, would allow to propose more robust characters in further studies.

Diagnostic characters and taxonomic status of the middle early Eocene European peradectids, *Peradectes louisi* and *Peradectes russelli*

Systematics of *Peradectes louisi* Crochet (1979) chose the left M3 MNHN.F.GL197 as the holotype of *Pd. louisi*, which was then the sole available M3 for this species (Crochet 1980b). An isolated M3 from Avenay (MNHN.F.Av4813) was referred to *Pd. louisi* earlier in his work (Crochet 1980b: Fig. 4a) but was not included in the material referred to this species (Crochet 1980b: table 3). MNHN.F.Av4813 is of the size of the larger *Pd. russelli*, and is here allocated to this species. The original diagnostic characters of the upper molars of *Pd. louisi* were thus explicitly based on MNHN.F.GL197 alone (Crochet 1979, 1980b: p. 39). We have proposed a new description and figuration of the holotype (Fig. 9f). On a drawing of MNHN.F.GL197 in labial view from Crochet (1980b: fig. 9a), the stylar cusps B, C and D are subequal in height. Contrary to the original diagnosis and figure of Crochet (1980b), and although the stylar shelf of this M3 is worn, its stylar cusp B is clearly dominant in height over stylar cusp D, and stylar cusp C is absent or entirely worn (Fig. 9e-g). The slightly elevated surface interpreted as the summit of stylar cusp C of MNHN.F.GL197 by Crochet (1980b) is actually lingual to the stylar line. Moreover, the M3 of *Pd. louisi* MNHN.F.CB4182 also lacks stylar cusp C (Fig. 10p). The relative heights of the stylar cusps of MNHN.F.GL197 are similar on all the upper molars here attributed to *Pd. louisi* (Fig. 10), stylar cusp B being the

highest, and stylar cusp C being most often lower than stylar cusp D or absent. As mentioned by Crochet (1979) in the diagnosis, the ectoflexus of MNHN.F.GL197 is weakly developed, but the newly reported M3 of *Pd. louisi* from Condé-en-Brie (MNHN.F.CB4182, Fig. 10p) and Sézanne-Broyes (MNHN.F.SZ18000, MNHN.F.SZ18005, Fig. 10o) have deeper ectoflexi. A similar variation of this trait is here noted on the M3 of *Pd. crocheti* sp. nov. from Palette and Fordones. The ectoflexus was also considered symmetric on M3 of *Pd. louisi* (Crochet 1979, 1980b). Here again, the new description of the holotype and a more comprehensive sampling of M3, all properly oriented, show that the ectoflexus of this dental locus is asymmetric in *Pd. louisi* (Figs. 9f and 10p and o), although this asymmetry is, on average, less pronounced than in *Pd. crocheti* sp. nov. The relative weakness of the conules of the upper molars described by Crochet (1979, 1980b) was interpreted as a synapomorphy of peradectids by various authors (e.g.Krishtalka and Stucky 1983b; Korth 2008), rather than a diagnostic character at the species level. Finally, the M3 is not relatively longer than other upper molar loci of *Pd. louisi*, or M3 of other European *Peradectes* species (Table 4) (*contra* Crochet 1979, 1980b). As for lower molars, a lingual opening of the trigonid basin higher than the lingual opening of the talonid basin was also proposed as a specific feature of *Pd. louisi* (Crochet 1979, 1980b). However, this character is also present in *Pd. crocheti* sp. nov. and *Pd. russelli*, and consequently the relative heights of the lingual opening of the trigonid versus talonid basin cannot be used to discriminate between European *Peradectes* species. Moreover, since only (at least) some ascertained herpetotheriids (i.e., from the earliest Eocene; Ladevèze et al. 2012), such as *Peratherium* and *Herpetotherium*, exhibit the reverse condition of this character (the trigonid and talonid basin open lingually at the same level), the character state of *Pd. louisi* is rather interpreted as a symplesiomorphy for the whole of Metatheria. According to Crochet (1979, 1980b), the hypoconid is mesiodistally pinched and the cristid obliqua is curved on the lower molars of *Pd. louisi*, except on m4. Nonetheless, we did not make the same observation based on the two m4 from the original hypodigm we consulted (MNHN.F.Av16032 and MNHN.F.Av16037). In particular, on MNHN.F.Av16037 the cristid obliqua is curved near the distal edge of the trigonid contrary to the drawing of Crochet (1980b: fig. 13). Characters of the talonid of m4 of *Pd. louisi* are probably highly impacted by polymorphism, as for m4 of other metatherians (e.g., Martin 2005: fig. 4). Moreover, the shape of the cristid obliqua varies among the m3 of *Pd. louisi*. Finally, as noted by Crochet (1979, 1980b), the m4 of *Pd. louisi* are smaller than the m3, but the new report of m4 of *Pd. crocheti* sp. nov. and *Pd. russelli* in the present study shows that it is the same for these species. Altogether, none of the characters proposed by Crochet (1979, 1980b) are diagnostic of *Pd. louisi*; they are either actually not observed on the material, or are plesiomorphies. However, *Peradectes louisi* is definitely distinct from all other peradectid species in combining a stylar cusp D located distolabially to the metacone on the stylar shelf of M3, a stylar cusp C relatively lower than the stylar cusp D on M1-M3, and relatively long m3 with subequal entoconid and hypoconulid.

With the exception of the peradectid M2 from Coulondres (Southern France, ~MP10; UM-CLR-1; Crochet 1980b: fig. 28), the m1 MNHN.F.CB3021 here referred to *Pd. russelli* (interpreted as a dp3 by Crochet 1980b), and one possible m4 not found in collections (see Crochet 1980b: p. 49, bottom), all molars attributed to *Peradectes* sp. (Crochet 1980b: p. 49–51, figs. 26, 27 and 29) are here better allocated to *Pd. louisi*. According to Crochet (1980b: p. 49), two worn and fragmentary lower molar rows (MNHN.F.Av4642 and MNHN.F.CB226, Fig. 11i-j) differ from *Pd. louisi* in having a talonid with a rectilinear lingual edge and a hypoconulid more lingually positioned, hence characters for which a lingual axis of reference is needed to relatively locate structures. However, on both specimens the metaconid is totally worn (MNHN.F.Av4642, Fig. 11i) or incomplete (MNHN.F.CB226, Fig. 11j) on m3, the best preserved molar of each row, which probably prevented Crochet (1980b: fig. 29b) from describing them with an accurate orientation. With a corrected orientation, these specimens resemble *Pd. louisi*, with a subequal entoconid and hypoconulid on a relatively long m3. The differences in shape of the entoconid and cristid obliqua pointed out by Crochet (1980b) have been shown here to be typical variable traits of *Pd. louisi* (Fig. 11). All differences noted by Crochet (1980b) between upper molars of *Peradectes* sp. and *Pd. louisi*, such as the doubling of stylar cusp C on one specimen (Crochet 1980b: fig. 27), or the small size of stylar cusp D (Fig. 10i-j) are here interpreted as variable features of *Pd. louisi*. In fact, the doubling of stylar cusp C is known to be as rare in other *Peradectes* species with various upper molars described, namely *Pd. coprexeches* (Williamson and Taylor 2011: p. 13, fig. 6.2) and *Pd. crocheti* sp. nov. (a single specimen concerned; this study). Note that the doubling of stylar cusp C is probably more frequent in *Mimoperadectes* (see Comparative description of *Pd. crocheti* sp. nov.), and in the oldest *Peradectes* species, *Pd. minor* (Clemens 2006: p. 28), than in other peradectid species.

Larger European peradectids, *Peradectes russelli* versus *Peradectes 'mutigniensis'* Based on their original diagnoses (Crochet 1979) and comparisons (Crochet 1980b: p. 52), *Pd. russelli* and *Pd. 'mutigniensis'* would appear to differ in possessing (i) M3 relatively wider for *Pd. 'mutigniensis'* (i.e., with a mesiodistally shorter centrocrista and ectoflexus), (ii) M3 with a symmetric versus asymmetric ectoflexus, (iii) a lingual opening of the trigonid basin

higher versus not higher than the lingual opening of the talonid basin (metaconid-entoconid notch) on lower molars and (iv) a less curved cristid obliqua on m2 and m3 of *Pd. 'mutigniensis'*. We disagree with these four arguments. First, the length to width ratio here calculated for M3 reported by Crochet (1980b) to both species are similar (Online Resource 1: Table S3). In particular this ratio is almost identical for the M3 of the holotype of *Pd. russelli* (MNHN.F.CB924, L/W = 0.79) and the 'holotype' of *Pd. 'mutigniensis'* (MNHN.F.Mu5521, L/W = 0.78). Second, the ectoflexus of the M3 of the holotype of *Pd. russelli* and all specimens originally attributed to this species is asymmetric, with a metastylar wing more labially expanded, when the paracone and metacone are aligned (e.g., MNHN.F.CB2502, fig. 12h). Third, as in all peradectids, the trigonid basin of lower molars of *Pd. 'mutigniensis'* actually opens higher lingually than the talonid basin (e.g., MNHN.F.Mu18000, Fig. 12m). Fourth, although the single m3 of *Pd. 'mutigniensis'* has effectively a weakly curved cristid obliqua (MNHN.F.Mu6451; Crochet 1980b: fig. 24), a variation in the curvature of this cristid has been noted in the coeval *Pd. louisi*. It is worth mentioning that molars originally attributed to *Pd. russelli* are slightly larger or subequal in size to those of *Pd. 'mutigniensis'* (Online Resource 1: Table S3), with one exception (the M3 MNHN.F.CB742 of *Pd. 'mutigniensis'* is larger than the M3 MNHN.F.Av4813 of *Pd. russelli sensu* Crochet [1980b]). Altogether, all characters proposed by Crochet (1979, 1980b) to distinguish *Pd. russelli* from *Pd. 'mutigniensis'* either are not observed on the concerned specimens or represent intraspecific morphological variation. The species name *Peradectes russelli* has page priority and is thus valid over its junior synonym *Pd. 'mutigniensis'* (see Crochet 1979: p. 367–368). Morphological variation found in molars of *Pd. russelli* are here documented, as for other European *Peradectes* species. Notably, some M1 to M3 of *Pd. russelli* have a transverse accessory crista on their stylar shelf, lingual to stylar cusp D (see Comparative description of *Pd. russelli*). This reminds the recent observation of transverse cristae variably present between the metacone and stylar cusp D in various herpetotheriid species (Wessels et al. 2024: p. 15, figs. 3h-j and 6a).

Crochet (1980b: p. 52, tables 4-5) argued that m4 of *Pd. russelli* and *Pd. 'mutigniensis'* are larger than m3. Among the collections of the MNHN, two specimens interpreted as m4 of *Pd. russelli* by Crochet (1980b: table 4) were found, namely MNHN.F.CB5114 from Condé-en-Brie and MNHN.F.Av9019 from Avenay. However, the lingual edge of their talonid is straight, and their talonid is relatively mesiodistally longer than in ascertained European metatherian m4. MNHN.F.CB5114 also exhibits as high protoconid and metaconid. MNHN.F.CB5114 and MNHN.F.Av9019 are most likely respectively m2 and m3 of an eutherian mammal taxon that lacks the paraconid keel of metatherians. We did not find the figured m4 specimen of *Pd. russelli* (Crochet 1980b: fig. 18) in the collections, but it is more similar to a herpetotheriid than to a peradectid metatherian considering characters such as the lingual alignment of the paraconid, metaconid and entoconid with a straight distolingual edge of the talonid, the transversally aligned protoconid and metaconid, and the mesiodistally long entoconid (Table 6). The two specimens reported as m4 of *Pd. 'mutigniensis'* by Crochet (1980b: table 5, fig. 25), MNHN.F.CB5100 and MNHN.F.GL92, lack the relative labiolingual reduction of the talonid compared to the other lower molar loci, which is a characteristic of m4 of most marsupialiforms. MNHN.F.CB5100 and MNHN.F.GL92 are here better interpreted as m2 of *Pd. russelli*, given the relative width of their trigonid and talonid. The single true isolated m4 of *Pd. russelli* is the newly reported MNHN.F.Mu18003 (Fig. 12u-v), which is subequal in length and shorter, respectively, than the two ascertained m3 of *Pd. russelli*.

Paleoecological and biostratigraphic implications *Peradectes louisi* and *Pd. russelli* are coeval and are the only two peradectid species in MP8 + 9 and ~MP8 + 9 localities from the Paris Basin (Avenay, Condé-en-Brie, Mutigny, Sables de Brasles and Sézanne-Broyes), while Crochet (1980b) recognized up to four *Peradectes* species (*Pd. louisi*, *Pd. russelli*, *Pd. 'mutigniensis'* and *Peradectes* sp.) in Avenay and Condé-en-Brie. *Peradectes louisi* and *Pd. russelli* represent two distinct species that differ in a few morphological characters in addition to size difference, namely in the proportions of their lower molars (Table 5), and in two discrete features, namely the relative positioning of stylar cusp D on M3, and the relative ventral extension of stylar cusps C and D on M1 and M2 (Fig. 10 vs. Fig. 12). Because the area of stylar cusps C and D is known to have minor functional importance during molar occlusion (e.g., Crompton and Hiiemae 1970: fig. 5A; Crochet 1980a: fig. 2a; Davis 2011: fig. 1B; Wessels et al. 2024: p. 15, fig. 8b) and because *Pd. louisi* and *Pd. russelli* group into two distinct size clusters (Fig. 13), these two species could probably partition their ecological niches (hypothetical arboreal and insectivorous to frugivorous small mammals, as partly deduced from the peradectid-like taxon from Messel; Kurz 2005) mostly based on size (body masses estimated to 22.9–31.4 g for *Pd. louisi*, and 41.2–60.6 g for *Pd. russelli*, using lengths of the unworn M3 [Online Resource 1: Tables S2-S3] in the appropriate predictive equation of Gordon 2003: fig. 7). Similar cases of sympatry in the MP8 + 9 and ~MP8 + 9 mammal faunas studied, between two morphologically similar species that differ in size, concern other taxa, such as (among recent revisions) the plesiadapiform *Arcius*, because *Arc. fuscus* and the larger *Arc. lapparenti* co-occur

in Mutigny, Avenay, Condé-en-Brie, Sables de Brasles, and Sézanne-Broyes (López-Torres and Silcox 2018), and the theridomorph rodent *Euromys*, because *E. thaleri* (Michaux, 1964) and the larger *E. woodi* (Michaux, 1964) co-occur in Mutigny, Avenay and Condé-en-Brie (Escarguel 1999; Vianey-Liaud and Marivaux 2021). The coexistence of two peradectid species differing in size apparently continues during the EECO (~MP10; Vianey-Liaud et al. 2024).

European peradectid species larger than the small *Pd. crocheti* sp. nov. first occur in Mutigny (~MP8 + 9, PE IV), with *Pd. russelli*. The mammalian faunas of Mutigny and Avenay are considered to exhibit major differences based on two herpetotheriid lineages, still unrevised, following the conclusions of Crochet (1980b) (Schmidt-Kittler et al. 1987: p. 21), and also on the absence of *Pd. russelli sensu* Crochet (1980b) in Mutigny (Crochet 1980b: fig. 30). This diffence in faunal composition is here reduced because *Pd. russelli* is recorded in both localities, and molars of this species from Mutigny, such as M1, do not significantly differ in size from *Pd. russelli* of other MP8 + 9 and ~MP8 + 9 localities (Online Resource 1: Table S3).

Revision of putative occurrences of typical MP8 + 9 and ~MP8 + 9 peradectids in MP10 and ~MP10

Peradectes louisi was recorded in Grauves (MP10) by two isolated lower molars which were not described (Crochet 1980b: table 3). The right m1 MNHN.F.Gr10010 is completely worn. This specimen effectively displays a peradectid-like outline shape for a m1, with a trigonid much longer than the talonid, the hypoconid mesiolabial to the entoconid, the convex distolingual margin of the talonid, and the lingual opening of the trigonid basin higher than the talonid one (see Table 6). MNHN.F.Gr10010 (L = 1.56 mm, W = 0.79 mm) is similar in size to m1 of *Pd. louisi*. However, this is not sufficient to propose a specific allocation, in part because the m1 of the slightly smaller *Pd. dufraingi* are so far undocumented.

MNHN.F.GR10013 (Fig. 17b-c; L = 1.56 mm, W = 0.85 mm) was listed as a left m4 (Crochet 1980b). It is less worn than MNHN.F.GR10010, especially on the talonid. MNHN.F.GR10013 is more likely a m3, rather than a m2 or m4, given that its talonid is relatively not as wide as on m2 of peradectids and also unreduced compared to m4 of peradectids (Fig. 17b). The lingual margin of the talonid is less worn than the rest of the molar, and preserves a minute entoconid smaller than the hypoconulid (Fig. 17c). Contrary to all m3 of *Pd. louisi*, the entoconid is lower than the hypoconulid. This character is exclusively shared with *Pd. dufraingi*, from the Egem locality (Smith and Smith 2013: fig. 4B-G). Because MNHN.F.GR10013 differs from m3 of *Pd. dufraingi* only in being larger (but is as long and wide as m3 of *Pd. louisi*), and in its stronger postcingulid (also similar to *Pd. louisi* in this respect), we here tentatively attribute this peradectid m3 from Grauves to *Peradectes* aff. *dufraingi*. Regarding the exhibited features of this material, *Pd. louisi* is hence clearly absent from Grauves. If the attribution we propose is correct, and following the conclusion of Smith and Smith (2013: p. 308–309) on the age of the Egem locality, MNHN.F.GR10013 would represent a species close to *Pd. dufraingi*, occurring in the MP10 reference level (instead of ~MP8 + 9 for *Pd. dufraingi*), and a second peradectid species with a minute entoconid recorded around the EECO.

Peradectes louisi was also recorded in Cuis (~MP10; = Grauves?, see Material and methods) by Crochet (1980b: table 3), by an unlabeled right upper molar (Fig. 17a;

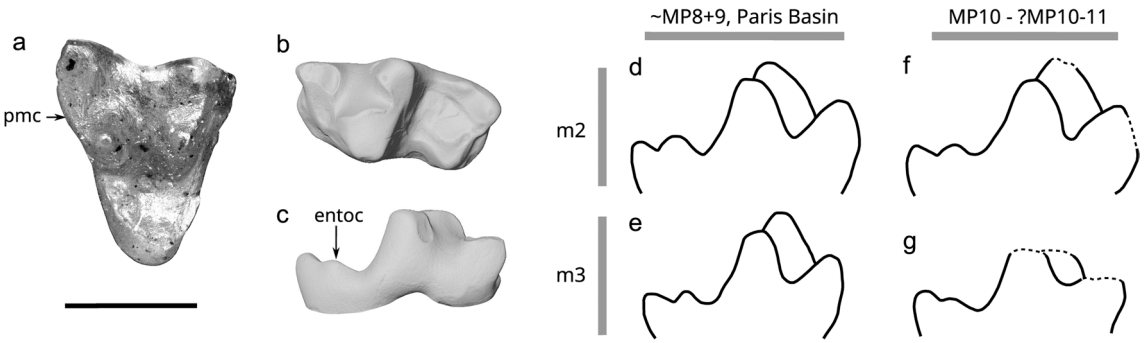

Fig. 17 Revision and comparisons of peradectid molars from MP10 and ?MP10-11 faunas. **a-c.** molars from the MP10 faunas of Cuis and Grauves (Paris Basin) attributed to *Peradectes louisi* by Crochet (1980b). **a**. cast of an unlabelled right M2 from Cuis in occlusal view. **b-c.** MNHN.F.GR10013, left m3 here attributed to *Peradectes* aff. *dufraingi*; **b**. occlusal view; **c** lingual view. The arrows (**a** and **c**) denote character states discussed in the main text. **d-g.** comparisons of outline of lingual views of m2 and m3 from the MP10 and ?MP10-11 faunas to those of typical m2 and m3 from MP8 + 9 and ~MP8 + 9 faunas of the Paris Basin. Note differences in the relative height and length of the entoconid; **d**. right m2 (reversed) MNHN.F.CB878 (*Pd. louisi*); **e**. left m3 MNHN.F.CB4213 (*Pd. louisi*); **f**. left m2 UM-VIE-106 (?*Pd. mutigniensis* in Legendre et al. 1992); **g**. left m3 MNHN.F.GR10013. Abbreviations: **pmc**, postmetacrista; **entoc**, entoconid. All outlines are to scale. Scale bar equals 1 mm

L > 1.37 mm, W = 1.73 mm), the sole metatherian tooth from this locality, for which only a cast is available in the fossil collections of the MNHN. The specimen is completely worn on its main cusps, stylar cusps, and conules. The most distolabial part of the metastylar wing and stylar cusp A are broken. Given the depth and asymmetry of the ectoflexus of this specimen, and the length of the preparacrista, it is most likely a M2 as listed by Crochet (1980b). It is similar in size to both upper molars of *Pd. louisi* and *Peradectes* sp. from Azillanet (Minervois, southern France, ~MP10), the latter being limited to one M3 (Marandat 1986: pl. 1, fig. 2). The unworn M3 from Azillanet differs from all upper molars of *Pd. louisi* in having a slightly V-shaped centrocrista (distinct from the V-shaped centrocrista of herpetotheriids), as in *Peradectes* specimens in open nomenclature from the ~MP10 southern France localities of Coulondres and Mas de Gimel (UM-CLR-1 and UM-MGL-716; Crochet 1980b: fig. 28; Vianey-Liaud et al. 2024: fig. 2C), and in its more curved and distally projected postmetacrista relatively to the paracone – metacone axis. On the M2 from Cuis, the centrocrista is completely worn and cannot be described, but the postmetacrista is curved and distally projected (Fig. 17a), in the same way as for the M3 from Azillanet. The M2 from Cuis sharing this character with the unnamed species from Azillanet and being highly worn on all cusps, the presence of *Pd. louisi* in Cuis is here no longer supported with confidence. Altogether, the revision of peradectids from Grauves and Cuis shows that *Pd. louisi* is most likely absent from the MP10 and ~MP10 localities where it was reported to date. The MP8 + 9-MP10 interval locality of Saint-Agnan yielded a possible *Pd. louisi* specimen here described as *Peradectes* cf. *louisi*. The occurrences of *Pd. louisi* are hence formally limited to MP8 + 9 and ~MP8 + 9 localities of the Paris Basin (Mutigny, Avenay, Condé-en-Brie, Sables-de-Brasles, and Sézanne-Broyes).

A fragment of a peradectid m4 from Mas de Gimel (~MP10; Montpellier, France) was attributed to *Peradectes* cf. *mutigniensis* (UM-MGL-320; Vianey-Liaud et al. 2024: fig. 2D). Based on the morphology of the mesiolingual part of the trigonid (the only well-preserved part of the molar) and the apparently labiolingually pinched talonid, UM-MGL-320 is similar in size and morphology, only to the m4 of *Pd. russelli* (MNHN.F.Mu18003, Fig. 12u), and is thus tentatively re-attributed to *Peradectes* cf. *russelli*. A lower molar belonging to a peradectid was reported from the Vielase fauna (?MP10-11, Quercy) as ?*Peradectes mutigniensis* (Legendre et al. 1992). This specimen (UM-VIE-106; L = 1.73 mm, W = 0.99 mm) is a m2, given the relative width of the talonid. It is comparable in size to the largest m2 of *Pd. louisi* (e.g., MNHN.F.CB5092; Online Resource 1: Table S2) rather than the m2 of *Pd. russelli* (= *Pd. 'mutigniensis'*), which are larger. The entoconid and hypoconulid of UM-VIE-106 are small, identical in height and mesiodistal length (Fig. 17f), whereas the entoconid is most often higher and always mesiodistally longer than the hypoconulid on all m2 of the MP8 + 9 and ~MP8 + 9 European peradectids (e.g., Fig. 17d). The m2 from Vielase thus might belong to a different unnamed peradectid species. The comparison with *Peradectes* aff. *dufraingi* from Grauves is difficult because the cuspids of the talonid are described only for the m3 of this taxon.

Altogether, the peradectid m2 from Vielase and m3 from Grauves here revised, both of which are late Ypresian in age, exhibit a configuration of the entoconid and hypoconulid that differs from any peradectid molar of equivalent locus from the MP8 + 9 reference locality and ~MP8 + 9 localities of the Paris Basin, with a relatively less high entoconid (Fig. 17d-g). This may highlight a second species turnover among European peradectids, between middle early Eocene (MP8 + 9 or close in age) and late early Eocene (MP10 or close in age), although more dental material from MP10 and ~MP10 localities would be needed to update their tentative taxonomic status and confidently assess this hypothesis. To date, such low entoconids have been documented for *Peradectes dufraingi* (absent from the MP8 + 9 or localities close in age of the Paris Basin) from the Egem fauna, which would correlate with MP8 + 9 and the Early Eocene Climatic Optimum according to Smith and Smith (2013).

Peradectids are represented in southern France only in the MP7-MP8 + 9 interval localities that yielded *Pd. crocheti* sp. nov. and in MP10, ~MP10 and younger localities (Crochet 1977a, 1980b; Marandat 1986; Legendre et al. 1992). They are still unrecorded from southern France localities close in age to the MP8 + 9 of the Paris Basin, namely La Borie (= Saint-Papoul; Laurent et al. 2010) and Sainte-Eulalie (Danilo et al. 2013) probably due to the scarcity of small mammals in such localities. So far, only the ~MP8 + 9 locality of La Borie yielded an isolated lower molar of metatherian, belonging to a herpetotheriid (Crochet 1980b: p. 69).

Conclusion

European peradectids long remained less well documented than both the coeval North American peradectids and the also superficially 'opossum-like' Herpetotheriidae, in terms of spatial distribution and completeness of available fossil material. The fossils described here for the early peradectid *Peradectes crocheti* sp. nov., widespread in Western Europe and being represented by dental rows, enhance our knowledge of the ancestral morphotype of European peradectids, through accurate comparisons with the later occurring species *Pd. louisi* and *Pd. russelli*, and the tentative characterization of morphological intraspecific variation. We encourage further quantification of characters based on isolated molars, because it may enable to decipher cryptic diagnostic

features between coeval metatherian species (e.g., Table 5) or to support evidenced species turnover (e.g., Fig. 14) for a given lineage (e.g., Fig. 15). In the same way, the study of the relative heights of the stylar cusps of metatherian upper molars also appears meaningful to resolve systematics, at least for peradectids (Fig. 5 vs. Fig. 10 vs. Fig. 12).

Altogether, the evolution of peradectids in Europe appears simpler than suggested by previous studies. In fact, the newly recorded species turnovers between the early (MP7-MP8 + 9 interval), middle (MP8 + 9 and ~MP8 + 9) and late (MP10 and ~MP10) early Eocene (Figs. 14 and 17) must have resulted from the endemic evolution of a European lineage, originating from an unique dispersal from North America to Europe possibly triggered by the PETM, which is consistent with the monophyly of European peradectids (Fig. 16), rather than from a more complicated evolutionary history punctuated by multiple dispersals. In turn and although the precise relationships between the late Paleocene – middle Eocene peradectids are here established, their complex taxonomy at the generic level is to be addressed. These conclusions regarding the evolutionary history of peradectids are derived from the definition of multiple relevant dental characters for the first time, which provide support for many peradectid clades. Such effort will be crucial for understanding the origin and phylogenetic affinities of peradectids in the whole of Marsupialiformes.

To date, the last putative European peradectids are known by three complete specimens from Messel (~MP11, ~47.2 to ~47.6 Ma for the Middle Messel Formation; Kaboth-Bahr et al. 2024) preserving the skeleton, skull and teeth rows, but still of unclear taxonomic status (Kurz and Habersetzer 2004; Kurz 2007; Beck et al. 2022: p. 315). Furthermore, peradectids are known by only eight isolated teeth regarding MP10 and ~MP10, and ?MP10-11 localities (Crochet 1980b; Marandat 1986; Legendre et al. 1992), which represent the youngest ascertained record of this family in Europe so far. For these reasons, the last steps of the evolution of peradectids in Europe until their extinction, possibly after the MP11, remain blurry, awaiting for more fossil material to be described. This work is a prelude of the complete systematic revision of metatherians from the early Eocene of Europe.

Supplementary information The online version contains supplementary material available at https://doi.org/10.1007/s10914-024-09724-5.

Acknowledgements This article is dedicated to the memory of Jean-Yves Crochet, who passed away on 21 October 2023. As a long time colleague of the Institut des Sciences de l'Evolution – Montpellier (ISEM) and friend, he greatly improved our knowledge of metatherian and insectivorous mammals. We are indebted to the Rougier family, owner of the Palette site, who kindly provided access, help and support for paleontological research on this locality. We acknowledge Y. Dutour and N. Vialle (Muséum d'Histoire Naturelle of Aix-en-Provence), Q. Vautrin (Parc Naturel Régional UNESCO Global Geopark Causses du Quercy), C. Bronnert and R. Vacant (MNHN), and E. Turini and L. Mohring for their precious help during these excavations. R. Vacant also carefully treated the sediments from Palette collected in 2018, that yielded the holotype of *Peradectes crocheti* sp. nov. We warmly thank A.-L. Charruault (ISEM), who performed the µ-CT-scanning and segmentation of this holotype specimen. V.N. Pernègre (MNHN) managed the allocation of various new MNHN specimen numbers. G. Escarguel (LENHA, Lyon) sampled the locality of Fournes 2. We are grateful to T. Smith and A. Folie (Royal Belgian Institute of Natural Sciences, Brussels) for access to comparative material and casts of the two specimens from Sotteville-sur-Mer here revised. We thank V.D. Crespo and an anonymous reviewer, as well as the editors R.M.D. Beck and D.A Croft, for their constructive remarks on an early version of the manuscript. This is ISEM publication n° 2024-118.

Author contributions KG and RT designed the study. KG prepared the figures and wrote the manuscript, which was completed by comments and feedbacks from GB, EG, MG, BM, SL and RT. Field expeditions in the Palette locality were conducted by GB, EG and RT. The peradectid specimens labelled MHN.AIX.PV.2017- were isolated by KG after processing sediments. Data acquisition (including CT-scans) and analyses were performed by KG. All authors read and approved the final manuscript.

Funding This research was financially supported by a PhD thesis funding from the French Ministry of Higher Education, Research, and Innovation, and also in part by the ANR project EDENs (ANR-20-CE02-0007). Recent excavations at Palette were funded thanks to the Actions Transversales du Muséum (ATM Palette, MNHN funding). Three-dimensional data acquisition was performed using the micro-computed tomography (µ-CT) facilities of the MRI platform member of the national infrastructure France-BioImaging supported by the French National Research Agency (ANR-10-INBS-04, 'Investments for the future'), the labex CEMEB (ANR-10-LABX-0004) and NUMEV (ANR-10-LABX-0020). The Leica optical and digital station used to take photographs was acquired as part of the ANR-ERC PALASIAFRICA (ANR-08-JCJC-0017). A CC-BY public copyright license has been applied by the authors to the present document and will be applied to all subsequent versions up to the Author Accepted Manuscript arising from this submission, in accordance with the grant's open access conditions.

Data availability The 3D surface models of the most complete or informative specimens of *Peradectes crocheti* sp. nov. from Palette, namely the holotype (maxillary MHN.AIX.PV.2018.26.14), the P2 (MHN.AIX.PV.2017.6.6), a M3 (MHN.AIX.PV.2017.6.7), the two lower dental rows (MHN.AIX.PV.2017.6.8 and MHN.AIX.PV.2017.6.9), and the astragalus (MHN.AIX.PV.2017.6.14), are available on MorphoMuseuM. The other 3D surfaces and data are available upon request to the corresponding author. The character – taxon matrix used in the first phylogenetic analysis is available in MorphoBank (project 5399).

Declarations

Competing interests The authors declare no competing interests.

References

Abello MA (2013) Analysis of dental homologies and phylogeny of Paucituberculata (Mammalia: Marsupialia). Biol J Linn Soc 109:441–465. https://doi.org/10.1111/bij.12048

Averianov AO (2015) Taxonomic revision of tribosphenic mammals from the Lower Cretaceous Antlers Formation of Texas and

Oklahoma, USA. Proc Zool Inst RAS 319:141–181.https://doi.org/10.31610/trudyzin/2015.319.2.141
Averianov AO, Martin T, Lopatin AV, Krasnolutskii SA (2013) Stem therian mammal *Amphibetulimus* from the Middle Jurassic of Siberia. Paläontol Z 89:197–206. https://doi.org/10.1007/s12542-013-0217-x
Beard KC, Dawson MR (2009) Early Wasatchian mammals of the Red Hot local fauna, uppermost Tuscahoma Formation, Lauderdale County, Mississippi. Ann Carnegie Mus 78:193–243. https://doi.org/10.2992/007.078.0301
Beck RMD (2023) Diversity and phylogeny of marsupials and their stem relatives (Metatheria). In: Cáceres NC, Dickman CR (eds) American and Australasian Marsupials. Springer, Cham, Switzerland, pp 23–88. https://doi.org/10.1007/978-3-031-08419-5_35
Beck RMD, Voss RS, Jansa SA (2022) Craniodental morphology and phylogeny of marsupials. Bull Am Mus Nat Hist 457:1–350. https://doi.org/10.1206/0003-0090.457.1.1
Billet G, Bardin J (2019) Serial homology and correlated characters in morphological phylogenetics: modeling the evolution of dental crests in placentals. Syst Biol 68:267–280. https://doi.org/10.1093/sysbio/syy071
BiochroM'97 (1997) Synthèse et tableaux de corrélation. In: Aguilar JP, Legendre S, Michaux J (eds) Actes du Congrès BiochroM'97, Mémoires et travaux de l'EPHE 21. Montpellier: Ecole Pratique des Hautes Etudes, Institut de Montpellier, pp 769–805.
Boivin M, Orliac MJ, Telles Antunes M, Godinot M, Laurent Y, Marandat B, Vidalenc D, Tabuce R (2018) New material of *Diacodexis* (Mammalia, Artiodactyla) from the early Eocene of Southern Europe. Geobios 51:285–306. https://doi.org/10.1016/j.geobios.2018.06.003
Bown TM (1979) Geology and mammalian paleontology of the Sand Creek Facies, lower Willwood Formation (lower Eocene), Washakie County, Wyoming. Geol Surv Wyo Mem 2:1–151.
Bown TM, Rose KD (1979) *Mimoperadectes*, a new marsupial, and *Worlandia*, a new dermopteran, from the lower part of the Willwood Formation (early Eocene), Bighorn Basin, Wyoming. Contr Mus Paleontol Univ Mich 25:89–104.
Bremer K (1994) Branch support and tree stability. Cladistics 10:295–304. https://doi.org/10.1111/j.1096-0031.1994.tb00179.x
Brikiatis L (2014) The De Geer, Thulean and Beringia routes: key concepts for understanding early Cenozoic biogeography. J Biogeogr 41:1036–1054. https://doi.org/10.1111/jbi.12310
Brocklehurst N, Benevento GL (2020) Dental characters used in phylogenetic analyses of mammals show higher rates of evolution, but not reduced independence. PeerJ 8:e8744. https://doi.org/10.7717/peerj.8744
Bronnert C, Métais G (2023) Early Eocene hippomorph perissodactyls (Mammalia) from the Paris Basin. Geodiversitas 45:277–326. https://doi.org/10.5252/geodiversitas2023v45a9
Carneiro LM, Oliveira ÉV (2023) Paleogene metatherians from the Itaboraí Basin: diversity and affinities. In: Cáceres NC, Dickman CR (eds) American and Australasian Marsupials. Springer, Cham, Switzerland, pp 269–324.https://doi.org/10.1007/978-3-030-88800-8_5-1
Carneiro LM, Goin FJ, Bampi H, Silva RC, Rangel CC, Guimarães BMG, Arêas MR (2024) A tiny-sized Herpetotheriidae (Mammalia, Metatheria) from the Itaboraí basin (early Eocene), Brazil: Paleobiogeographic and systematic implications for Herpetotheriidae. J South Am Earth Sci 144. https://doi.org/10.1016/j.jsames.2024.105016
Cifelli RL, Muizon C de (1998) Marsupial mammal from the Upper Cretaceous North Horn Formation, central Utah. J Paleontol 72:532–537. https://doi.org/10.1017/S0022336000024306
Clemens WA (1966) Fossil mammals of the type Lance Formation, Wyoming. Part II, Marsupialia. Univ Calif Publ Geol Sci 62:1–122.
Clemens WA (2006) Early Paleocene (Puercan) peradectid marsupials from northeastern Montana, North American Western Interior. Palaeontogr Abt A 277:19–31. https://doi.org/10.1127/pala/277/2006/19
Coillot T, Smith R, Gigase P, Smith T (2013) Tarsal diversity in the earliest Eocene mammal fauna of Dormaal, Belgium. Geol Belg 16:274–283.
Cojan I, Moreau MG, Stott LE (2000) Stable carbon isotope stratigraphy of the Paleogene pedogenic series of southern France as a basis for continental-marine correlation. Geology 28:259–262.
Crespo VD, Goin FJ (2021) Taxonomy and affinities of African cenozoic metatherians. Span J Palaeontol 36:133–148. https://doi.org/10.7203/sjp.36.2.20974
Crochet JY (1980a) L'occlusion dentaire chez *Peradectes*, *Amphiperatherium* et *Peratherium*, marsupiaux du Tertiaire d'Europe. Palaeovertebrata 9:79–89.
Crochet JY (1977a) Les Didelphidae (Marsupicarnivora, Marsupialia) holarctiques tertiaires. C R Acad Sci Paris 284:357–360.
Crochet JY (1977b) Les didelphidés paléogènes holarctiques: historique et tendances évolutives. Geobios Mem Spec 1:127–134
Crochet JY (1979) Diversité systématique des Didelphidae (Marsupialia) européens tertiaires. Geobios 12:365–378.
Crochet JY (1980b) Les marsupiaux du Tertiaire d'Europe. Edtions Foundation Singer-Polignac, Paris.
Crochet JY (1986) *Kasserinotherium tunisiense* nov. gen., nov. sp., troisième marsupial découvert en Afrique (Eocène inférieur de Tunisie). C R Acad Sci Paris 302:923–926.
Crompton AW, Hiiemae K (1970) Molar occlusion and mandibular movements during occlusion in the American opossum, *Didelphis marsupialis* L. Zool J Linn Soc 49:21–47. https://doi.org/10.1111/j.1096-3642.1970.tb00728.x
Danilo L, Remy J, Vianey-Liaud M, Marandat B, Sudre J, Lihoreau F (2013) A new Eocene locality in southern France sheds light on the basal radiation of Palaeotheriidae (Mammalia, Perissodactyla, Equoidea). J Vertebr Paleontol 33:195–215. https://doi.org/10.1080/02724634.2012.711404
Davis BM (2011) Evolution of the tribosphenic molar pattern in early mammals, with comments on the "dual-origin" hypothesis. J Mamm Evol 18:227–244. https://doi.org/10.1007/s10914-011-9168-8
Ducrocq S, Buffetaut E, Buffetaut-Tong H, Jaeger JJ, Jongkanjanasoontorn Y, Suteethorn V (1992) First fossil marsupial from South Asia. J Vertebr Paleontol 12:395–399.
Duprat M (1997) Les faciès à mammifères (MP 6 à MP 16) dans le Nord-Est du Bassin de Paris (France): argumentation du modèle tectono-sédimentaire des dépôts paléogènes. In: Aguilar JP, Legendre S, Michaux J (eds) Actes du Congrès BiochroM'97, Mémoires et travaux de l'EPHE 21. Ecole Pratique des Hautes Etudes, Institut de Montpellier, Montpellier, pp 315–336.
Eberle J, Storer JE (1995) *Herpetotherium valens* (Lambe), a didelphid marsupial from the Calf Creek Local Fauna (Chadronian), Saskatchewan. J Vertebr Paleontol 15:785–794.
Escarguel G (1999) Les rongeurs de l'Eocène inférieur et moyen d'Europe occidentale. Systématique, phylogénie, biochronologie et paléobiogéographie des niveaux repères MP 7 à MP 14. Palaeovertebrata 28:89–351.
Estravís C (2000) Nuevos mamíferos del Eoceno Inferior de Silveirinha (Baixo Mondego, Portugal). Coloquios Paleontol 51:281–311.
Farris JS (1989b) The retention index and the rescaled consistency index. Cladistics 5:417–419. https://doi.org/10.1111/j.1096-0031.1989.tb00573.x
Farris JS (1989a) The retention index and homoplasy excess. Syst Biol 38:406–407. https://doi.org/10.2307/2992406
Flores DA, Abdala F (2001) Diferencias morfológicas de cráneo y dentición en *Didelphis albiventris* y *D. marsupialis*

(Didelphimorphia: Didelphidae) de Argentina y Bolivia. Comun Mus Ciênc Tecnol PUCRS, Sér Zool 14:101–110.
Fox RC (1983) Notes on the North American Tertiary marsupials *Herpetotherium* and *Peradectes*. Can J Earth Sci 20:1565–1578.
Gazin CL (1956) Paleocene mammalian faunas of the Bison Basin in South-Central Wyoming. Smithson Misc Collect 131:1–57.
Gheerbrant E (1991) *Bustylus* (Eutheria, Adapisoriculidae) and the absence of ascertained marsupials in the Palaeocene of Europe. Terra Nov 3:586–592.
Gheerbrant E (1992) Les mammifères paléocènes du bassin d'Ouarzazate (Maroc). I. Introduction générale et Palaeoryctidae. Palaeontogr Abt A 224:67–132.
Gingerich PD, Smith T (2006) Paleocene-Eocene land mammals from three new latest Clarkforkian and earliest Wasatchian Wash sites at Polecat Bench in the Northern Bighorn Basin. Contrib Mus Paleontol Univ Mich 31:245–303.
Godinot M (1981) Les mammifères de Rians (Eocène inférieur, Provence). Palaeovertebrata 10:43–126.
Godinot M (1984) Un noveau genre de Paromomyidae (Primates) de l'Eocène Inférieur d'Europe [A new genus of Paromomyidae (Primates) from the early Eocene of Europe]. Folia Primatol 43:84–96.
Godinot M (1992) Apport à la systématique de quatre genres d'Adapiformes (Primates, Eocène). C R Acad Sci Paris 314:237–242.
Godinot M, Crochet JY, Hartenberger JL, Lange-Badré B, Russell DE, Sigé B (1987) Nouvelles données sur les mammifères de Palette (Eocène inférieur, Provence). Münch Geowiss Abh (A) 10:273–288.
Goin FJ, Candela AM, Muizon C de (2003) The affinities of *Roberthoffstetteria nationalgeographica* (Marsupialia) and the origin of the polydolopine molar pattern. J Vertebr Paleontol 23:869–876. https://doi.org/10.1671/2383-11
Goin FJ, Woodburne MO, Zimicz AN, Martin GM, Chornogubsky L (2016) A Brief History of South American Metatherians: Evolutionary Contexts and Intercontinental Dispersals. Springer, Dordrecht, Netherlands.
Goloboff PA (1993) Estimating character weights during tree search. Cladistics 9:83–91.
Gordon CL (2003) A first look at estimating body size in dentally conservative marsupials. J Mamm Evol 10:1–21. https://doi.org/10.1023/A:1025545023221
Green M, Martin JE (1976) *Peratherium* (Marsupialia: Didelphidae) from the Oligocene and Miocene of South Dakota. In: Churcher CS (ed) Athlon: Essays on Palaeontology in Honour of Loris Shano Russell. Roy Ontario Mus Misc Publ, Toronto, pp 155–168.
Gunnell GF (2010) Marsupialia. In: Werdelin L, Sanders WJ (eds) Cenozoic Mammals of Africa. University of California Press, Berkeley, pp 77–79.
Hand SJ, Sigé B (2017) A new archaic bat (Chiroptera: Archaeonycteridae) from an Early Eocene forest in the Paris Basin. Hist Biol 30:227–236. https://doi.org/10.1080/08912963.2017.1297435
Hayes FG (2005) Arikareean (Oligocene-Miocene) *Herpetotherium* (Marsupialia, Didelphidae) from Nebraska and Florida. Bull Fla Mus Nat Hist 45:335–353.
Hershkovitz P (1997) Composition of the family Didelphidae Gray, 1821 (Didelphoidea: Marsupialia), with a review of the morphology and behavior of the included four-eyed pouched opossums of the genus *Philander* Tiedemann, 1808. Fieldiana Zool 86:1–103.
Hooker JJ (1996) Mammalian biostratigraphy across the Paleocene-Eocene boundary in the Paris, London and Belgian basins. In: Knox RWOB, Corfield RM, Dunay RE (eds) Correlation of the Early Paleogene in Northwest Europe. Geol Soc Lond, Spec Publ 101, pp 205–218. https://doi.org/10.1144/gsl.sp.1996.101.01.13
Hooker JJ (1998) Mammalian faunal change across the Paleocene-Eocene transition in Europe. In: Aubry MP, Berggren WA, Lucas SG (eds) Late Paleocene-Early Eocene Climatic and Biotic Events in the Marine and Terrestrial Records. Columbia University Press, New York, pp 419–441.
Hooker JJ (2010) The mammal fauna of the early Eocene Blackheath formation of Abbey Wood, London. Monogr Palaeontogr Soc 164:1–153. https://doi.org/10.1080/25761900.2022.12131814
Hooker JJ (2015) A two-phase mammalian dispersal event across the Paleocene–Eocene transition. Newsl Stratigr 48:201–220 https://doi.org/10.1127/nos/2015/0060
Hooker JJ (2020) A mammal fauna from the Paleocene-Eocene Thermal Maximum of Croydon, London, UK. Proc Geol Assoc 131:458–473. https://doi.org/10.1016/j.pgeola.2018.01.001
Hooker JJ, Russell DE (2012) Early Palaeogene Louisinidae (Macroscelidea, Mammalia), their relationships and north European diversity. Zool J Linn Soc 164:856–936. https://doi.org/10.1111/j.1096-3642.2011.00787.x
Hooker JJ, Sánchez-Villagra MR, Goin FJ, Simons EL, Attia Y, Seiffert ER (2008) The origin of Afro-Arabian 'didelphimorph' marsupials. Palaeontology 51:635–648. https://doi.org/10.1111/j.1475-4983.2008.00779.x
Horovitz I, Martin T, Bloch J, Ladevèze S, Kurz C, Sánchez-Villagra MR (2009) Cranial anatomy of the earliest marsupials and the origin of opossums. PLoS One 4:1–9. https://doi.org/10.1371/journal.pone.0008278
Hough JR (1961) Review of Oligocene didelphid marsupials. J Paleontol 35:218–228.
International Commission of Zoological Nomenclature (ICZN) (1999) International Code of Zoological Nomenclature. The International Trust for Zoological Nomenclature, London. http://www.nhm.ac.uk/hosted-sites/iczn/code/
Jernvall J, Jung HS (2000) Genotype, phenotype, and developmental biology of molar tooth characters. Am J Phys Anthropol 113:171–190.
Johanson Z (1994) New information concerning the Late Cretaceous marsupial *Albertatherium* Fox, 1971. J Vertebr Paleontol 14:595–602.
Johanson Z (1996) New marsupial from the Fort Union Formation, Swain Quarry, Wyoming. J Paleontol 70:1023–1031.
Kaboth-Bahr S, Schmitt C, Bauersachs T, Zeeden C, Wonik T, Schandl J, Lenz O, Wedmann S, Vasiliev I, Mulch A, Lourens L, Pross J, Bahr A (2024) Improved chronostratigraphy for the Messel Formation (Hesse, Germany) provides insight into early to middle Eocene climate variability. Newsletters on Stratigraphy. https://doi.org/10.1127/nos/2024/0799
Kihm AJ, Schumaker KK (2015) Marsupials from the Chadronian (latest Eocene) Medicine Pole Hills local fauna, North Dakota. Paludicola 10: 93–112.
Koenigswald W von (1970) *Peratherium* (Marsupialia) im Ober-Oligozän und Miozän von Europa. Bayer Akad Wiss Math-Natur Kl Abh (NF) 144:1–79.
Korth WW (1994) Middle Tertiary marsupials (Mammalia) from North America. J Paleontol 68:376–397.
Korth WW (2008) Marsupialia. In: Janis CM, Gunnell GF, Uhen MD (eds) Evolution of Tertiary Mammals of North America: Volume 2, Small Mammals, Xenarthrans, and Marine Mammals. Cambridge University Press, Cambridge, pp 39–47.
Korth WW (2018) Review of the marsupials (Mammalia: Metatheria) from the late Paleogene (Chadronian–Arikareean: late Eocene–late Oligocene) of North America. PalZ 92:499–523. https://doi.org/10.1007/s12542-017-0396-y
Krishtalka L, Stucky RK (1983b) Paleocene and Eocene marsupials of North America. Ann Carnegie Mus 52:229–263.
Krishtalka L, Stucky RK (1983a) Revision of the Wind River faunas, early Eocene of Central Wyoming. Part 3. Marsupialia. Ann Carnegie Mus 52:205–227.
Krishtalka L, Stucky RK (1984) Middle Eocene marsupials (Mammalia) from northeastern Utah and the mammalian fauna from Powder Wash. Ann Carnegie Mus 53:31–45.

Kurz C (2005) Ecomorphology of opossum-like marsupials from the Tertiary of Europe and a comparison with selected taxa. Kaupia 14:21–26.
Kurz C (2007) The opossum-like marsupials (Didelphimorphia and Peradectia, Marsupialia, Mammalia) from the Eocene of Messel and Geiseltal – Ecomorphology, diversity and palaeogeography. Kaupia 15:3–65.
Kurz C, Habersetzer J (2004) Untersuchungen der zahnmorphologie von beutelratten aus Messel mit der mikroröntgenmethode CORR. Cour Forsch-Inst Senckenberg 252:13–21.
Ladevèze S, Muizon C de, Beck RMD, Germain D, Cespedes-Paz R (2011) Earliest evidence of mammalian social behaviour in the basal Tertiary of Bolivia. Nature 474:83–86. https://doi.org/10.1038/nature09987
Ladevèze S, Selva C, Muizon C de (2020) What are "opossum-like" fossils? The phylogeny of herpetotheriid and peradectid metatherians, based on new features from the petrosal anatomy. J Syst Palaeontol 18:1463–1479. https://doi.org/10.1080/14772019.2020.1772387
Ladevèze S, Smith R, Smith T (2012) Reassessment of the morphology and taxonomic status of the earliest herpetotheriid marsupials of Europe. J Mamm Evol 19:249–261. https://doi.org/10.1007/s10914-012-9195-0
Laurent Y, Adnet S, Bourdon E, Corbalan D, Danilo L, Duffaud S, Fleury G, Garcia G, Godinot M, Le Roux G, Maisonnave C, Métais G, Mourer-Chauviré C, Presseq B, Sigé B, Solé F (2010) La Borie (Saint-Papoul, Aude): un gisement exceptionnel dans l'Éocène basal du Sud de la France. Bull Soc Hist Nat Toulouse 146:89–103.
Lebrun R (2018) MorphoDig, an open-source 3D freeware dedicated to biology. 5th International Paleontological Congress (IPC5) – *The Fossil Week*, July 9–13th, 2018 (Paris, France).
Lebrun R, Orliac MJ (2016) MorphoMuseuM: an online platform for publication and storage of virtual specimens. Paleontol Soc Pap 22:183–195. https://doi.org/10.1017/scs.2017.14
Lecomte G (1994) Étude paléontologique et sédimentologique de l'Yprésien de l'est du bassin de Paris. Dissertation, University Paris VI, France.
Legendre S, Marandat B, Sigé B, Crochet JY, Godinot M, Hartenberger JL, Sudre J, Vianey-Liaud M, Muratet B, Astruc JG (1992) La faune de mammifères de Vielase (phosphorites du Quercy, Sud de la France): Preuve paléontologique d'une karstification du Quercy dès l'Eocène inférieur. Neues Jahrb Geol Paläontol 7:414–428.
Lillegraven J (1969) Latest Cretaceous mammals from the upper part of the Edmonton Formation of Alberta, Canada, and review of marsupial placental dichotomy in mammalian evolution. Univ Kans Paleontol Contrib 50:1–122.
Lillegraven J (1976) Didelphids (Marsupialia) and *Uintasorex* (?Primates) from later Eocene sediments of San Diego County, California. Trans San Diego Soc Nat Hist 18:85–112.
López-Martínez N, Smith R, Peláez-Campomanes P, Smith T (2006). The acme of the micromammal *Paschatherium* across the Paleocene-Eocene boundary in continental Europe. Micropaleontology 52:267–280.
López-Torres S, Silcox MT (2018) The European Paromomyidae (Primates, Mammalia): Taxonomy, phylogeny, and biogeographic implications. J Paleontol 92:920–937. https://doi.org/10.1017/jpa.2018.10
Louis P (1970) Note préliminaire sur un gisement de mammifères de l'Eocène inférieur situé Route de Broyes à Sézanne (Marne). Ann Univ A.R.E.R.S. Reims 8:48–62.
Louis P (1996) Recherches de mammifères paléogènes dans les départements de l'Aisne et de la Marne pendant la deuxième moitié du vingtième siècle. Palaeovertebrata 25:83–113.
Louis P, Laurain M (1983) Nouveau gisement de vertébrés dans le Cuisien supérieur de Saint-Agnan (Aisne). Ses relations stratigraphiques avec les autres gisements yprésiens du Bassin parisien. Bull Inf Géol Bass Paris 20:3–20.
Maddison WP, Maddison DR (2019) Mesquite, a modular system for evolutionary analysis. Version 3.61. http://mesquiteproject.org
Maga AM, Beck RMD (2017) Skeleton of an unusual, cat-sized marsupial relative (Metatheria: Marsupialiformes) from the middle Eocene (Lutetian: 44 – 43 million years ago) of Turkey. PLoS One 12:e0181712. https://doi.org/10.1371/journal.pone.0181712
Manz CL, Bloch JI (2015) Systematics and phylogeny of Paleocene-Eocene Nyctitheriidae (Mammalia, Eulipotyphla?) with description of a new species from the late Paleocene of the Clarks Fork Basin, Wyoming, USA. J Mamm Evol 22:307–342. https://doi.org/10.1007/s10914-014-9284-3
Marandat B (1986) Decouverte d'une faune de micromammiferes d'âge cuisien superieur dans les marno-calcaires d'Agel à Azillanet (Minervois, Hérault). Geol Fr 2:197–204.
Marandat B (1991) Mammifères de l'Ilerdien Moyen (Eocène Inférieur) des Corbières et du Minervois. Palaeovertebrata 20:55–144.
Marandat B (1997) La disparité des faunes mammaliennes du niveau MP 7 (Eocène inférieur) des domaines péri-mésogéens et nordiques. Investigation d'un provincialisme intra-européen. Newsl Stratigr 35:63–82.
Marandat B, Adnet S, Marivaux L, Martinez A, Vianey-Liaud M, Tabuce R (2012) A new mammalian fauna from the earliest Eocene (Ilerdian) of the Corbières (Southern France): Palaeobiogeographical implications. Swiss J Geosci 105:417–434. https://doi.org/10.1007/s00015-012-0113-5
Marshall LG, Case JA, Woodburne MO (1990) Phylogenetic relationships of the families of marsupials. In: Genoways HH (ed) Current Mammalogy, Volume 2. Plenum Press, New York, pp 433–505.
Marshall LG, Muizon C de (1995) Part II: The skull. In: Muizon C de (ed) *Pucadelphys andinus* (Marsupialia, Mammalia) from the early Paleocene of Bolivia. Mém Mus Hist Nat 195:21–90.
Marshall LG, Muizon C de (1988) The dawn of the age of mammals in South America. Natl Geogr Res 4:23–55.
Martin GM (2005) Intraspecific variation in *Lestodelphys halli* (Marsupialia: Didelphimorphia). J Mammal 86:793–802. https://doi.org/10.1644/1545-1542(2005)086[0793:IVILHM]2.0.CO;2
Martin T, Averianov AO, Schultz JA, Schwermann AH (2023) A stem therian mammal from the Lower Cretaceous of Germany. J Vertebr Paleontol 42:e2224848. https://doi.org/10.1080/02724634.2023.2224848
Matthew W, Granger W (1921) New genera of Paleocene mammals. Am Mus Novit 13:1–7.
McGrew PO (1937) New marsupials from the Tertiary of Nebraska. J Geol 45:448–455.
McGrew PO (1939) *Nanodelphys*, an Oligocene didelphine. Field Mus Nat Hist Geol Ser 6:393–400. https://doi.org/10.5962/bhl.title.5208
McKenna M (1960) Fossil Mammalia from the early Wasatchian Four Mile fauna, Eocene of northwest Colorado. Univ Calif Publ Geol Sci 37:1–130.
Mein P, Ginsburg L (1997) Les mammifères du gisement miocène inférieur de Li Mae Long, Thaïlande: systématique, biostratigraphie et paléoenvironnement. Geodiversitas 19:783–844.
Missiaen P, Quesnel F, Dupuis C, Storme JY, Smith T (2013) The earliest Eocene mammal fauna of the Erquelinnes Sand Member near the French-Belgian border. Geol Belg 16:262–273.
Muizon C de (1991) La fauna de mamíferos de Tiupampa (Paleoceno Inferior, Formacion Santa Lucia), Bolivia. In: Suarez-Soruco R (ed) Fósiles y Facies de Bolivia, Vol. 1. Vertebrados. Yacimientos Petrolíferos Fiscales Bolivianos, Santa Cruz, Bolivia, pp 575–624.
Muizon C, Lange-Badré B (1997) Carnivorous dental adaptations in tribosphenic mammals and phylogenetic reconstruction. Lethaia 30:353–366. https://doi.org/10.1111/j.1502-3931.1997.tb00481.x

Muizon C de, Ladevèze S (2020) Cranial anatomy of *Andinodelphys cochabambensis*, a stem metatherian from the early Paleocene of Bolivia. Geodiversitas 42:597–739. https://doi.org/10.5252/geodiversitas2020v42a30

Muizon C de, Ladevèze S (2022) New material of *Incadelphys antiquus* (Pucadelphyda, Metatheria, Mammalia) from the early Palaeocene of Bolivia reveals phylogenetic affinities with enigmatic North and South American metatherians. Geodiversitas 44:609–643. https://doi.org/10.5252/geodiversitas2022v44a22

Muizon C de, Ladevèze S, Selva C, Vignaud R., Goussard F. (2018) *Allqokirus australis* (Sparassodonta, Metatheria) from the early Palaeocene of Tiupampa (Bolivia) and the rise of the metatherian carnivorous radiation in South America. Geodiversitas 40:363–459. https://doi.org/10.5252/geodiversitas2018v40a16

Murphey PC, Kelly TS, Chamberlain KR, Tsukui K, Clyde WC (2018) Mammals from the earliest Uintan (middle Eocene) Turtle Bluff Member, Bridger Formation, southwestern Wyoming, USA, Part 3: Marsupialia and a reevaluation of the Bridgerian-Uintan North American Land Mammal Age transition. Palaeontol Electron 21(2):25A:1–52. https://doi.org/10.26879/804

Neal JE (1996) Summary of Paleogene sequence stratigraphy in northwest European and the North Sea. In: Knox RWOB, Corfield RM, Dunay RE (eds) Correlation of the Early Paleogene in Northwest Europe. Geol Soc London Spec Publ 101, pp 15–42. https://doi.org/10.1144/GSL.SP.1996.101.01.02

Nel A, de Plöeg G, Dejax J, Dutheil D, de Franceschi D, Gheerbrant E, Godinot M, Hervet S, Menier JJ, Augé M, Bignot G, Cavagnetto C, Duffaud S, Gaudant J, Stéphane H, Jossang A, de Lapparent de Broin F, Pozzi JP, Paicheler JC, Beuchet F, Rage JC (1999) Un gisement sparnacien exceptionnel à plantes, arthropodes et vertébrés (Eocène basal, MP7): Le Quesnoy (Oise, France). C R Acad Sci Paris 329:65–72. https://doi.org/10.1016/S1251-8050(99)80229-8

Ni X, Meng J, Wu W, Ye J (2007) A new Early Oligocene peradectine marsupial (Mammalia) from the Burqin region of Xinjiang, China. Naturwissenschaften 94:237–241. https://doi.org/10.1007/s00114-006-0182-2

Noiret C, Steurbaut E, Tabuce R, Marandat B, Schnyder J, Storme JY, Yans J (2016) New bio-chemostratigraphic dating of a unique early sequence from southern results in precise mammalian biochronological tie-points. Newsl Stratigr 49:469–480. https://doi.org/10.1127/nos/2016/0336

O'Leary MA, Bloch JI, Flynn JJ, Gaudin TJ, Giallombardo A, Giannini NP, Goldberg SL, Kraatz BP, Luo ZX, Meng J, Ni X, Novacek MJ, Perini FA, Randall ZS, Rougier GW, Sargis EJ, Silcox MT, Simmons NB, Spaulding M, Velazco PM, Weksler M, Wible JR, Cirranello AL (2013) The placental mammal ancestor and the Post-K-Pg radiation of placentals. Science 339:662–667. https://doi.org/10.1126/science.1229237

Oliveira ÉV, Goin FJ (2011) A reassessment of bunodont metatherians from the Paleogene of Itaboraí (Brazil): systematics and age of the Itaboraian SALMA. Rev Bras Paleontol 14:105–136. https://doi.org/10.4072/rbp.2011.2.01

Orliac MJ, Boivin M, Tabuce R (2018) A mandible of Diacodexis cf. gigasei (Artiodactyla, Diacodexeidae) from the Early Eocene locality of Palette (Bouches-du-Rhône, France). MorphoMuseuM 4:1–4. https://doi.org/10.18563/journal.m3.60.

Philip J, Vianey-Liaud M, Martin-Closas C, Tabuce R, Léonide P, Margerel JP, Noël J (2017) Stratigraphy of the Haut Var Paleogene continental series (Northeastern Provence, France): New insight on the age of the 'Sables bleutés du Haut Var' Formation. Geobios 50:319–339. https://doi.org/10.1016/j.geobios.2017.06.002

R Core Team (2020) R: A language and environment for statistical computing. R Foundation for Statistical Computing, Vienna, Austria. https://www.R-project.org

Ramdarshan A, Godinot M, Bédécarrats S, Tabuce R (2015) Holotype specimen of *Donrussellia magna*, an adapiform primate from the early Eocene (MP7) of Southern France. MorphoMuseuM 1:1–3. https://doi.org/10.18563/m3.1.2.e2

Rat P (1965). La succession stratigraphique des Mammifères dans l'Eocène du bassin de Paris. Bull Soc Géol Fr 7:248–256.

Reig OA, Kirsch JAW, Marshall LG (1985) New conclusions on the relationships of the opossum-like marsupials, whith an annotated classifícation of the Didelphimorphia. Ameghiniana 21:335–343.

Reig OA, Kirsch JAW, Marshall LG (1987) Systematic relationships of the living and Neocenozoic American "opossum-like" marsupials (suborder Didelphimorphia), with comments on the classification of these and the Cretaceous and Paleogene New World and European metatherians. In: Archer M (ed) Possums and Opossums: Studies in Evolution. Surrey Bea, Sydney, pp 1–89.

Rose KD (1981) The Clarkforkian Land-Mammal Age and mammalian faunal composition across the Paleocene-Eocene boundary. Univ Mich Pap Paleontol 26:1–197.

Rose KD (2010) New marsupial from the Early Eocene of Virginia. J Paleontol 84:561–565. https://doi.org/10.1666/09-140.1

Rose KD (2012) The importance of Messel for interpreting Eocene Holarctic mammalian faunas. Palaeobiodivers Palaeoenviron 92:631–647. https://doi.org/10.1007/s12549-012-0090-8

Rose KD, Chew AE, Dunn RH, Kraus MJ, Fricke HC, Zack SP (2012) Earliest Eocene mammalian fauna from the Paleocene-Eocene Thermal Maximum at Sand Creek Divide, Southern Bighorn Basin, Wyoming. Univ Mich Pap Paleontol 36:1–122.

Rose KD, Godinot M, Bown TM (1994) The early radiation of euprimates and the initial diversification of Omomyidae. In: Fleagle J, Kay R (eds) Anthropoid Origins. Plenum Press, New York, pp 1–28.

Rothecker J, Storer JE (1996) The marsupials of the Lac Pelletier Lower Fauna, Middle Eocene (Duchesnean) of Saskatchewan. J Vertebr Paleontol 16:770–774.

Russell DE, Galoyer A, Louis P, Gingerich PD (1988) Nouveaux vertébrés sparnaciens du Conglomérat de Meudon à Meudon, France. C R Acad Sci Paris 307:429–433.

Russell DE, Godinot M (1988) The Paroxyclaenidae (Mammalia) and a new form from the Early Eocene of Palette, France. Paläontol Z 62:319–331.

Ruxton GD (2006) The unequal variance *t*-test is an underused alternative to Student's *t*-test and the Mann–Whitney U test. Behav Ecol 17:688–690. https://doi.org/10.1093/beheco/ark016

Sánchez-Villagra M, Ladevèze S, Horovitz I, Argot C, Hooker JJ, Macrini TE, Martin T, Moore-Fay S, Muizon C de, Schmelzle T, Asher RJ (2007) Exceptionally preserved North American Paleogene metatherians: Adaptations and discovery of a major gap in the opossum fossil record. Biol Lett 3:318–322. https://doi.org/10.1098/rsbl.2007.0090

Sansom RS, Wills MA, Williams T (2017) Dental data perform relatively poorly in reconstructing mammal phylogenies: Morphological partitions evaluated with molecular benchmarks. Syst Biol 66:813–822. https://doi.org/10.1093/sysbio/syw116

Schmidt-Kittler N, Godinot M, Franzen JL, Hooker JJ, Legendre S, Brunet M, Vianey-Liaud M (1987) European reference levels and correlation tables. Münch Geowiss Abh (A) 10:13–31.

Selva C, Ladevèze S (2017) Computed microtomography investigation of the skull of Cuvier's famous 'opossum' (Marsupialiformes, Herpetotheriidae) from the Eocene of Montmartre. Zool J Linn Soc 180:672–693. https://doi.org/10.1111/zoj.12495

Sigé B (1971) Les Didelphoidea de Laguna Umayo (formation Vilquechico, Crétacé supérieur, Pérou), et le peuplement marsupial d'Amérique du Sud. C R Acad Sci Paris 273:2479–2481.

Sigé B (1972) La faunule de mammifères du Crétacé supérieur de Laguna Umayo (Andes péruviennes). Bull Mus Natl Hist Nat 99:375–405.

Simpson GG (1928) American Eocene didelphids. Am Mus Novit 307:1–7.

Simpson GG (1935) The Tiffany Fauna, upper Paleocene: I. Multituberculata, Marsupialia, Insectivora, and ?Chiroptera. Am Mus Novit 795:1–20.
Smith T (2000) Mammals from the Paleocene-Eocene transition in Belgium (Tienen formation, MP7): palaeobiogeographical and biostratigraphical implications. GFF 122:148–149.
Smith T, Dupuis C, Folie A, Quesnel F, Storme JY, Iacumin P, Riveline J, Missiaen P, Ladevèze S, Yans J (2011) Un nouveau site à vertébrés terrestres juste après la limite Paléocène-Eocène, dans la Formation de Mortemer en Haute-Normandie, France. C R Palevol 10:11–20. https://doi.org/10.1016/j.crpv.2010.11.004
Smith T, Smith R (2013) A land micro-mammal fauna from the Early Eocene marine Egem deposits (NP12, Belgium) and the first occurrence of the peradectid marsupial *Armintodelphys* outside North America. Geol Belgica 16:302–310.
Solé F (2014) New carnivoraforms from the early Eocene of Europe and their bearing on the evolution of the Carnivoraformes. Palaeontology 57:963–978. https://doi.org/10.1111/pala.12097
Solé F, Fournier M, Ladevèze S, Le Verger K, Godinot M, Laurent Y, Smith T (2023) New postcranial elements of mesonychid mammals from the Ypresian of France: New hypotheses for the radiation and evolution of the mesonychids in Europe. J Mamm Evol 30:371–401. https://doi.org/10.1007/s10914-023-09651-x
Solé F, Gheerbrant E, Godinot M (2011) New data on the Oxyaenidae from the Early Eocene of Europe; biostratigraphic, paleobiogeographic and paleoecologic implications. Palaeontol Electron 14(2):13A:1–41. https://palaeo-electronica.org/2011_2/258/index.html
Solé F, Gheerbrant E, Godinot M (2013) Sinopaninae and Arfianinae (Hyaenodontida, Mammalia) from the Early Eocene of Europe and Asia; evidence for dispersal in Laurasia around the Paleocene/Eocene boundary and for an unnoticed faunal turnover in Europe. Geobios 46:313–327. https://doi.org/10.1016/j.geobios.2013.02.003
Solé F, Godinot M, Laurent Y, Galoyer A, Smith T (2018) The European mesonychid mammals: Phylogeny, ecology, biogeography, and biochronology. J Mamm Evol 25:339–379. https://doi.org/10.1007/s10914-016-9371-8
Solé F, Smith T, Tabuce R, Marandat B (2015) New dental elements of the oldest proviverrine mammal from the early Eocene of Southern France support possible African origin of the subfamily. Acta Palaeontol Pol 60:527–538. https://doi.org/10.4202/app.00146.2014
Speijer RP, Pälike H, Hollis CJ, Hooker JJ, Ogg JG (2020) The Paleogene Period. In: Gradstein FM, Ogg JG, Schmitz MD, Ogg GM (eds) Geologic Time Scale 2020. Elsevier, Amsterdam, pp 1087–1140. https://doi.org/10.1016/B978-0-12-824360-2.00028-0
Stehlin HG (1940) Über die säugetierfauna der teredinasande von Epernay und umgebung. Eclogae Geol Helv 33:291–298.
Steurbaut E, Magioncalda R, Dupuis C, Van Simaeys S, Roche E, Roche M (2003) Palynology, paleoenvironments, and organic carbon isotope evolution in lagoonal Paleocene-Eocene boundary settings in North Belgium. Spec Pap Geol Soc Am 369:291–317. https://doi.org/10.1130/0-8137-2369-8.291
Stock C (1936) Sespe Eocene didelphids. Proc Natl Acad Sci USA 22:122–124.
Storch G, Qiu Z (2002) First Neogene marsupial from China. J Vertebr Paleontol 22:179–181. https://doi.org/10.1671/0272-4634(2002)022[0179:FNMFC]2.0.CO;2
Storer JE (1991) The mammals of the Gryde local fauna, Frenchman Formation (Maastrichtian: Lancian), Saskatchewan. J Vertebr Paleontol 11:350–369.
Swofford DL (2002) PAUP* Phylogenetic analysis using parsimony (* and other methods). Version 4. Sinauer Associates, Sunderland.
Szalay FS (1994) Evolutionary History of the Marsupials and an Analysis of Osteological Characters. Cambridge University Press, Cambridge.
Tejedor MF, Goin FJ, Gelfo JN, López G, Bond M, Carlini AA, Scillato-Yane GJ, Woodburne MO, Chornogubsky L, Aragón E, Reguero MA, Czaplewski NJ, Vincon S, Martin GM, Ciancio MR (2009) New early Eocene mammalian fauna from western Patagonia, Argentina. Am Mus Novit 3638:1–43. https://doi.org/10.1206/577.1
Van Valen L (1966) Deltatheridia, a new order of mammals. Bull Am Mus Nat H 132:1–126.
Vautrin Q, Tabuce R, Lihoreau F, Bronnert C, Gheerbrant E, Godinot M, Metais G, Yans J, Dutour Y, Vialle N, Philip J, Billet G (2020) New remains of *Lophiaspis maurettei* (Mammalia, Perissodactyla) from the early Eocene of France and the implications for the origin of the Lophiodontidae. J Vertebr Paleontol 40:1–20. https://doi.org/10.1080/02724634.2020.1878200
Vianey-Liaud M, Lihoreau F, Solé F, Gernelle K, Vautrin Q, Bronnert C, Bourget H, Vidalenc D, Tabuce R (2024). A revision of the late early Eocene mammal faunas from Mas de Gimel and Naples (Montpellier, Southern France) and the description of a new theridomorph rodent. Geodiversitas 46:387–422. https://doi.org/10.5252/geodiversitas2024v46a10
Vianey-Liaud M, Marivaux L (2021) The beginning of the adaptive radiation of Theridomorpha (Rodentia) in Western Europe: morphological and phylogenetic analyses of early and middle Eocene taxa; implications for systematics. Palaeovertebrata 44:1–105. https://doi.org/10.18563/pv.44.2.e2
Vullo R, Gheerbrant E, Muizon C de, Néraudeau D (2009) The oldest modern therian mammal from Europe and its bearing on stem marsupial paleobiogeography. Proc Natl Acad Sci USA 106:19910–19915. https://doi.org/10.1073/pnas.0902940106
Wessels W, van de Weerd AA, Marković Z (2024) Marsupials (herpetotheriids) from the late Palaeogene of south-east Serbia. Palaeobio Palaeoenv. https://doi.org/10.1007/s12549-024-00600-x
West RM (1973) Geology and mammalian paleontology of the New Fork-Big Sandy area, Sublette County, Wyoming. Fieldiana Zool 29:1–193.
Wickham H (2016) ggplot2: Elegant graphics for data analysis. Use R!, Springer. doi: 10.1007/978-3-319-24277-4.
Williamson TE, Brusatte SL, Carr TD, Weil A, Standhardt BR (2012) The phylogeny and evolution of Cretaceous-Palaeogene metatherians: Cladistic analysis and description of new early Palaeocene specimens from the Nacimiento Formation, New Mexico. J Syst Palaeontol 10:625–651. https://doi.org/10.1080/14772019.2011.631592
Williamson TE, Brusatte SL, Wilson GP (2014) The origin and early evolution of metatherian mammals: The Cretaceous record. Zookeys 465:1–76. https://doi.org/10.3897/zookeys.465.8178
Williamson TE, Lofgren DL (2014) Late Paleocene (Tiffanian) metatherians from the Goler Formation, California. J Vertebr Paleontol 34:477–482. https://doi.org/10.1080/02724634.2013.804413
Williamson TE, Taylor LH (2011) New species of *Peradectes* and *Swaindelphys* (Mammalia: Metatheria) from the Early Paleocene (Torrejonian) Nacimiento Formation, San Juan Basin, New Mexico, USA. Palaeontol Electron 14(3):23A:1–16. https://palaeo-electronica.org/2011_3/21_williamson/index.html
Yans J, Marandat B, Masure E, Serra-Kiel J, Schnyder J, Storme JY, Marivaux L, Adnet S, Vianey-Liaud M, Tabuce R (2014) Refined bio-(benthic foraminifera, dinoflagellate cysts) and hemostratigraphy (δ13Corg) of the earliest Eocene at Albas-Le Clot (Corbières, France): Implications for mammalian biochronology in Southern Europe. Newsl Stratigr 47:331–353. https://doi.org/10.1127/nos/2014/0050

Publisher's Note Springer Nature remains neutral with regard to jurisdictional claims in published maps and institutional affiliations.

Springer Nature or its licensor (e.g. a society or other partner) holds exclusive rights to this article under a publishing agreement with the author(s) or other rightsholder(s); author self-archiving of the accepted manuscript version of this article is solely governed by the terms of such publishing agreement and applicable law.

Online Resource 1 Additional tables

Table S1. Measurements of molars of *Peradectes crocheti* sp. nov. Abbreviations: L, length (mm); W, width (mm); L/W, length to width ratio.

Specimen	Locality	Locus	L (mm)	W (mm)	L/W
MHN.AIX.PV.2018.26.14	Palette	M1	1,55	1,59	0,97
MHN.AIX.PV.2018.26.20	Palette	M1	1,51	1,4	1,08
UM-FDN-1	Fordones	M1	1,64	1,57	1,04
UM-FNR2-1	Fournes	M1	1,71	1,41	1,21
MNHN.F.Me16079	Meudon	M1		1,41	
MNHN.F.SN76	Soissons	M1	1,58	1,57	1,01
MHN.AIX.PV.2018.26.14	Palette	M2	1,5	1,7	0,88
NHMUK.PV.M44991	Abbey Wood	M2	1,57		
NHMUK.PV.M66046	Croydon	M2	1,81	1,85	0,98
UM-FDN-21	Fordones	M2	1,5		
UM-FDN-285	Fordones	M2	1,45		
UM-FDN-287	Fordones	M2		1,66	
UM-FNR2-2	Fournes	M2	1,58		
MNHN.F.Me15975	Meudon	M2	1,56		
MHN.AIX.PV.2017.6.7	Palette	M3	1,53	1,98	0,77
MHN.AIX.PV.2018.26.14	Palette	M3	1,4	1,77	0,79
UM-FDN-21	Fordones	M3		1,79	
UM-FDN-23	Fordones	M3	1,53		
MNHN.F.SN18	Soissons	M3	1,6	1,83	0,87
MNHN.F.SN78	Soissons	M3		1,79	
Fig. 5.18 Smith et al. 2011	Sotteville-sur-Mer	M3	1,58	1,91	0,83
UM-FDN-286	Fordones	M4	1,12		
MNHN.F.Me16084	Meudon	M4	1,26	1,79	0,70
MHN.AIX.PV.2017.6.9	Palette	m1	1,57	0,93	1,69
MNHN.F.Ri516	Rians	m1		0,94	
MNHN.F.SN121	Soissons	m1	1,47	0,86	1,71
MHN.AIX.PV.2017.6.8	Palette	m2	1,65	1,04	1,59
MHN.AIX.PV.2017.6.9	Palette	m2	1,64	1,03	1,59
MNHN.F.Me16101	Meudon	m2	1,69	0,99	1,71
MNHN.F.Ri221	Rians	m2	1,69		
MHN.AIX.PV.2017.6.8	Palette	m3	1,66	1,04	1,60
MHN.AIX.PV.2017.6.9	Palette	m3	1,68	1,06	1,58
MHN.AIX.PV.2017.6.10	Palette	m3	1,54	0,87	1,77
UM-PAT-103	Palette	m3	1,53	0,94	1,63
MNHN.F.SN2508	Soissons	m3	1,61	0,95	1,69
MHN.AIX.PV.2017.6.9	Palette	m4	1,55	0,92	1,68

Table S2. Detailed measurements of molars of *Peradectes louisi*. Abbreviations: L, length (mm); W, width (mm); L/W, length to width ratio; *, *Peradectes* cf. *louisi*.

Specimen	Locality	Locus	L (mm)	W (mm)	L/W
MNHN.F.Mu18005	Mutigny	dP3/	1,54	1,26	1,22
MNHN.F.Mu18006	Mutigny	M1	1,57	1,56	1,01
MNHN.F.Av16023	Avenay	M1	1,56	1,66	0,94
MNHN.F.Av16036	Avenay	M1	1,57	1,51	1,04
MNHN.F.Av16057	Avenay	M1	1,65	1,61	1,02
UM-AV-1-SK	Avenay	M1	1,49	1,55	0,96
UM-AV-2-SK	Avenay	M1	1,62	1,52	1,07
UM-AV-3-SK	Avenay	M1	1,62	1,6	1,01
MNHN.F.GL1	Sables de Brasles	M1	1,47	1,46	1,01
MNHN.F.GL296	Sables de Brasles	M1	1,53	1,45	1,06
MNHN.F.Mu6511	Mutigny	M2	1,62	1,86	0,87
MNHN.F.Av18003	Avenay	M2		1,78	
MNHN.F.Av18004	Avenay	M2		1,87	
MNHN.F.GL154	Sables de Brasles	M2		1,71	
MNHN.F.GL272	Sables de Brasles	M2	1,56		
MNHN.F.CB1486	Condé-en-Brie	M2		1,71	
MNHN.F.CB3213	Condé-en-Brie	M2	1,52	1,77	0,86
MNHN.F.CB3228	Condé-en-Brie	M2	1,71	1,74	0,98
MNHN.F.CB3637	Condé-en-Brie	M2	1,65		
MNHN.F.CB3707	Condé-en-Brie	M2	1,58	1,69	0,93
MNHN.F.CB4183	Condé-en-Brie	M2		1,83	
MNHN.F.CB4182	Condé-en-Brie	M3	1,51	1,92	0,79
MNHN.F.GL197	Sables de Brasles	M3	1,63	1,85	0,88
MNHN.F.SZ18000	Sézanne-Broyes	M3	1,41	1,83	0,77
MNHN.F.SZ18005	Sézanne-Broyes	M3	1,47	1,72	0,85
MNHN.F.SZ18004	Sézanne-Broyes	M4	1,33	1,88	0,71
MNHN.F.Av16028	Avenay	m1	1,56	0,77	2,03
MNHN.F.Av7229	Avenay	m1	1,51	0,85	1,78
UM-AV-7-SK	Avenay	m1	1,45	0,76	1,91
UM-AV-12-SK	Avenay	m1	1,55	0,85	1,82
MNHN.F.CB962	Condé-en-Brie	m1	1,56	0,85	1,84
MNHN.F.CB4391	Condé-en-Brie	m1	1,52	0,83	1,83
MNHN.F.GL136	Sables de Brasles	m1	1,4	0,8	1,75
MNHN.F.SZ18003	Sézanne-Broyes	m1	1,43	0,78	1,83
MNHN.F.Av16016	Avenay	m2	1,54	0,9	1,71
MNHN.F.Av16027	Avenay	m2	1,64	0,94	1,74

MNHN.F.Av16044	Avenay	m2	1,62	0,89	1,82
MNHN.F.Av18001	Avenay	m2	1,58	0,98	1,61
MNHN.F.Av6830	Avenay	m2	1,69	1	1,69
UM-AV-10-SK	Avenay	m2		0,87	
UM-AV-11-SK	Avenay	m2	1,56	0,9	1,73
MNHN.F.CB5090	Condé-en-Brie	m2	1,7	0,93	1,83
MNHN.F.CB5092	Condé-en-Brie	m2	1,73	0,99	1,75
MNHN.F.CB5097	Condé-en-Brie	m2	1,67	0,98	1,70
MNHN.F.CB828	Condé-en-Brie	m2	1,66	0,97	1,71
MNHN.F.CB872	Condé-en-Brie	m2	1,69	0,95	1,78
MNHN.F.CB878	Condé-en-Brie	m2	1,72	1	1,72
MNHN.F.SZ18001	Sézanne-Broyes	m2	1,66	0,92	1,80
MNHN.F.Av18000	Avenay	m3	1,63	0,94	1,73
MNHN.F.Av18002	Avenay	m3	1,6	0,95	1,68
MNHN.F.Av4642	Avenay	m3	1,47		
MNHN.F.AV16149	Avenay	m3	1,58	0,85	1,86
MNHN.F.AV16158	Avenay	m3	1,61	0,91	1,77
UM-AV-4-SK	Avenay	m3	1,51	0,86	1,76
UM-AV-5-SK	Avenay	m3	1,51	0,84	1,80
UM-AV-6-SK	Avenay	m3	1,54	0,95	1,62
UM-AV-8-SK	Avenay	m3	1,56	0,92	1,70
UM-AV-9-SK	Avenay	m3	1,59	0,88	1,81
MNHN.F.CB226	Condé-en-Brie	m3	1,61		
MNHN.F.CB5104	Condé-en-Brie	m3	1,6	0,89	1,80
MNHN.F.CB959	Condé-en-Brie	m3	1,62	0,91	1,78
MNHN.F.CB4213	Condé-en-Brie	m3	1,6	0,92	1,74
MNHN.F.GL261	Sables de Brasles	m3	1,54	0,86	1,79
MNHN.F.GL263	Sables de Brasles	m3	1,52	0,86	1,77
MNHN.F.GL383	Sables de Brasles	m3	1,66	0,89	1,87
MNHN.F.SZ18006	Sézanne-Broyes	m3	1,54	0,87	1,77
MNHN.F.Av16032	Avenay	m4	1,53	0,85	1,80
MNHN.F.Av16037	Avenay	m4	1,48	0,85	1,74
MNHN.F.GL301	Sables de Brasles	m4	1,44	0,78	1,85
*MNHN.F.STA296	Saint-Agnan	m4	1,5	0,84	1,79

Table S3. Detailed measurements of molars of *Peradectes russelli*, with the original attribution of the specimens in Crochet (1980). Dash denote unpublished specimens. Abbreviations: L, length (mm); W, width (mm); L/W, length to width ratio.

Specimen	Original attribution	Locality	Locus	L (mm)	W (mm)	L/W
MNHN.F.Mu18004	*Peradectes mutigniensis*	Mutigny	M1	1,88	1,82	1,03
MNHN.F.Mu5532	-	Mutigny	M1	1,85	1,9	0,97
MNHN.F.Av16024	*Peradectes mutigniensis*	Avenay	M1	1,75	1,9	0,92
UM-AV-13-SK	-	Avenay	M1	1,73	1,78	0,97
MNHN.F.CB2501	*Peradectes russelli*	Condé-en-Brie	M1	1,97	2,09	0,94
MNHN.F.CB3007	*Peradectes mutigniensis*	Condé-en-Brie	M1	1,62	1,85	0,88
MNHN.F.CB3275	*Peradectes russelli*	Condé-en-Brie	M1	1,87	1,91	0,98
MNHN.F.Mu18002	*Peradectes mutigniensis*	Mutigny	M2	1,82	2,14	0,85
MNHN.F.CB5103	*Peradectes russelli*	Condé-en-Brie	M2	1,91	2,07	0,92
MNHN.F.CB840	-	Condé-en-Brie	M2	2,02	2,26	0,89
MNHN.F.CB850	-	Condé-en-Brie	M2	1,97	2,27	0,87
MNHN.F.CB2753	*Peradectes russelli*	Condé-en-Brie	M2	2,11		
MNHN.F.Mu5521	*Peradectes mutigniensis*	Mutigny	M3	1,78	2,27	0,78
MNHN.F.Av4813	*Peradectes russelli*	Avenay	M3	1,95	2,27	0,86
MNHN.F.Av6837	*Peradectes mutigniensis*	Avenay	M3	1,82	2,29	0,79
MNHN.F.CB742	*Peradectes mutigniensis*	Condé-en-Brie	M3	1,95	2,4	0,81
MNHN.F.CB924	*Peradectes russelli*	Condé-en-Brie	M3	1,99	2,52	0,79
MNHN.F.CB2502	*Peradectes russelli*	Condé-en-Brie	M3	2,02	2,43	0,83
MNHN.F.CB924	*Peradectes russelli*	Condé-en-Brie	M4	1,35	2,36	0,57
MNHN.F.CB3021	*Peradectes* sp.	Condé-en-Brie	m1	1,71	0,89	1,92
MNHN.F.SZ18002	-	Sézanne-Broyes	m1	1,65	0,92	1,79
MNHN.F.Mu18000	*Peradectes mutigniensis*	Mutigny	m2	1,75	1,06	1,65
MNHN.F.Av7235	*Peradectes russelli*	Avenay	m2	1,98	1,17	1,69
UM-AV-14-SK	-	Avenay	m2	1,77	1,08	1,64
UM-AV-15-SK	-	Avenay	m2	1,97	1,19	1,66
MNHN.F.CB5098	*Peradectes mutigniensis*	Condé-en-Brie	m2	1,8	1,04	1,73
MNHN.F.CB5100	*Peradectes mutigniensis*	Condé-en-Brie	m2	1,94	1,13	1,72
MNHN.F.CB925	*Peradectes russelli*	Condé-en-Brie	m2	2,03	1,25	1,62
MNHN.F.CB928	-	Condé-en-Brie	m2	2,05	1,22	1,68
MNHN.F.GL92	*Peradectes mutigniensis*	Sables de Brasles	m2	1,97	1,1	1,79
MNHN.F.Mu6451	*Peradectes mutigniensis*	Mutigny	m3	1,74	1,05	1,66
MNHN.F.GL410	-	Sables de Brasles	m3	1,85	1,11	1,67
MNHN.F.Mu18003	-	Mutigny	m4	1,75	1	1,75

Table S4. Absolute basal heights of stylar cusps C and D in *Peradectes crocheti* sp. nov., *Pd. louisi* and *Pd. russelli* (attributions from this study). Abbreviations: HC, absolute basal height of stylar cusp C (mm); HD, absolute basal height of stylar cusp D (mm); HC/HD, absolute basal height of stylar cusp C to absolute basal height of stylar cusp D ratio.

Specimen	Species	Locality	Locus	HC (mm)	HD (mm)	HC/HD
MHN.AIX.PV.2018.26.14	*Peradectes crocheti*	Palette	M1	0,03	0,039	0,769
MHN.AIX.PV.2018.26.20	*Peradectes crocheti*	Palette	M1	0,047	0,061	0,77
UM-FDN-1	*Peradectes crocheti*	Fordones	M1	0,083	0,107	0,776
UM-FNR2-1	*Peradectes crocheti*	Fournes	M1	0,057	0,09	0,633
MNHN.F.SN76	*Peradectes crocheti*	Soissons	M1	0,059	0,146	0,404
MHN.AIX.PV.2018.26.14	*Peradectes crocheti*	Palette	M2	0,036	0,074	0,486
NHMUK.PV.M44991	*Peradectes crocheti*	Abbey Wood	M2	0,058	0,064	0,906
NHMUK.PV.M66046	*Peradectes crocheti*	Croydon	M2	0,109	0,122	0,893
MNHN.F.Me15975	*Peradectes crocheti*	Meudon	M2	0,049	0,096	0,51
UM-FDN-285	*Peradectes crocheti*	Fordones	M2	0,046	0,06	0,767
UM-FDN-21	*Peradectes crocheti*	Fordones	M2	0,03	0,065	0,462
MHN.AIX.PV.2017.6.7	*Peradectes crocheti*	Palette	M3	0,086	0,063	1,365
MHN.AIX.PV.2018.26.14	*Peradectes crocheti*	Palette	M3	0,05	0,055	0,909
UM-FDN-21	*Peradectes crocheti*	Fordones	M3	0,073	0,055	1,327
UM-FDN-23	*Peradectes crocheti*	Fordones	M3	0,095	0,049	1,939
MNHN.F.SN18	*Peradectes crocheti*	Soissons	M3	0,103	0,111	0,928
MNHN.F.SN78	*Peradectes crocheti*	Soissons	M3	0,069	0,075	0,92
Fig. 5.18 Smith et al. 2011	*Peradectes crocheti*	Sotteville-sur-Mer	M3	0,131	0,104	1,26
MNHN.F.Mu18006	*Peradectes louisi*	Mutigny	M1	0,018	0,067	0,269
UM-AV-1-SK	*Peradectes louisi*	Avenay	M1	0,024	0,057	0,421
UM-AV-2-SK	*Peradectes louisi*	Avenay	M1	0,068	0,107	0,636
UM-AV-3-SK	*Peradectes louisi*	Avenay	M1	0,062	0,083	0,747
MNHN.F.Av16023	*Peradectes louisi*	Avenay	M1	0,033	0,063	0,524
MNHN.F.Av16036	*Peradectes louisi*	Avenay	M1	0,047	0,062	0,758
MNHN.F.Av16057	*Peradectes louisi*	Avenay	M1	0,03	0,082	0,366
MNHN.F.GL1	*Peradectes louisi*	Sables de Brasles	M1	0,039	0,062	0,629
MNHN.F.GL296	*Peradectes louisi*	Sables de Brasles	M1	0,053	0,1	0,53
MNHN.F.Mu6511	*Peradectes louisi*	Mutigny	M2	0,053	0,127	0,417
MNHN.F.Av18003	*Peradectes louisi*	Avenay	M2	0,04	0,074	0,541
MNHN.F.Av18004	*Peradectes louisi*	Avenay	M2	0,029	0,053	0,547
MNHN.F.CB3213	*Peradectes louisi*	Condé-en-Brie	M2	0,038	0,041	0,927
MNHN.F.CB3228	*Peradectes louisi*	Condé-en-Brie	M2	0,048	0,042	1,143

MNHN.F.GL154	*Peradectes louisi*	Sables de Brasles	M2	0,045	0,07	0,643
MNHN.F.GL272	*Peradectes louisi*	Sables de Brasles	M2	0,041	0,032	1,281
MNHN.F.Mu18001	*Peradectes louisi*	Mutigny	M3	0,019	0,051	0,373
MNHN.F.SZ18005	*Peradectes louisi*	Sézanne-Broyes	M3	0,044	0,04	1,1
MNHN.F.Mu18004	*Peradectes russelli*	Mutigny	M1	0,037	0,127	0,291
MNHN.F.Mu5532	*Peradectes russelli*	Mutigny	M1	0,061	0,114	0,535
MNHN.F.Av16024	*Peradectes russelli*	Avenay	M1	0,068	0,082	0,829
UM-AV-13-SK	*Peradectes russelli*	Avenay	M1	0,069	0,125	0,552
MNHN.F.CB2501	*Peradectes russelli*	Condé-en-Brie	M1	0,047	0,187	0,251
MNHN.F.CB3007	*Peradectes russelli*	Condé-en-Brie	M1	0,023	0,107	0,215
MNHN.F.CB3275	*Peradectes russelli*	Condé-en-Brie	M1	0,064	0,14	0,457
MNHN.F.Mu18002	*Peradectes russelli*	Mutigny	M2	0,097	0,12	0,808
MNHN.F.CB5103	*Peradectes russelli*	Condé-en-Brie	M2	0,067	0,12	0,558
MNHN.F.CB850	*Peradectes russelli*	Condé-en-Brie	M2	0,096	0,167	0,575
MNHN.F.CB2753	*Peradectes russelli*	Condé-en-Brie	M2	0,123	0,199	0,618
MNHN.F.Mu5521	*Peradectes russelli*	Mutigny	M3	0,044	0,087	0,506
MNHN.F.Av4813	*Peradectes russelli*	Avenay	M3	0,057	0,121	0,471
MNHN.F.Av6837	*Peradectes russelli*	Avenay	M3	0,073	0,182	0,401
MNHN.F.CB924	*Peradectes russelli*	Condé-en-Brie	M3	0,069	0,143	0,483
MNHN.F.CB2502	*Peradectes russelli*	Condé-en-Brie	M3	0,075	0,14	0,536
MNHN.F.CB742	*Peradectes russelli*	Condé-en-Brie	M3	0,033	0,141	0,234

Table S5. Measurements (in mm) of dentary height under m2 or m3 and results of dentary height to molar length ratios for *Peradectes crocheti* sp. nov., *Pd. louisi* and *Pd. russelli*. Abbreviations: Hm2, mandibular height below m2; Hm3, mandibular height below m3; Lm2, length of m2; Lm3, length of m3.

Specimen	Species	Hm2 (mm)	Hm3 (mm)	Hm2/Lm2	Hm3/Lm3
MHN.AIX.PV.2017.6.8	*Peradectes crocheti*	2.71	2.73	1.64	1.64
MNHN.F.CB226	*Peradectes louisi*	2.99	3.01	-	1.87
MNHN.F.CB925	*Peradectes russelli*	3.53	-	1.74	-

Supplementary reference for Table S3.

Crochet JY (1980) Les marsupiaux du Tertiare d'Europe. Editions Foundation Singer-Polinac, Paris, France.

Online Resource 2 List of taxa included in the phylogenetic analyses (with authorship and year), their systematic position, the specimens used for coding and references, and the stratigraphic extension of the species.

Deltatheridiidae Gregory and Simpson 1926

Deltatheridium pretrituberculare Gregory and Simpson 1926. Casts of ZPAL MGM-I/91 and ZPAL MGM-I/102 (University of Montpellier, France). Descriptions and illustrations from Kielan-Jaworowska (1975).

Marsupialiformes Vullo et al. 2009; family *incertae sedis*

Asiatherium reshetovi Trofimov and Szalay 1994. Descriptions and illustrations from Szalay and Trofimov (1996).

Peradectidae Crochet 1979

Armintodelphys blacki Krishtalka and Stucky, 1983a. Cast of CM 41159 (holotype) consulted (Royal Belgian Institute of Natural Sciences [RBINS], Brussels). Descriptions and illustrations from Krishtalka & Stucky (1983a, 1983b) and Smith and Smith (2013). From latest Wasatchian (Wa-7) to earliest Bridgerian (Br-0) (Krishtalka and Stucky 1983a; Korth 2008).

Armintodelphys dawsoni Krishtalka and Stucky, 1983a. Cast of CM 55569 (holotype) consulted (Royal Belgian Institute of Natural Sciences [RBINS], Brussels). Descriptions and illustrations from Krishtalka & Stucky (1983a, 1983b, 1984) and Smith and Smith (2013). Early Bridgerian (Br-0-Br-1) (Krishtalka and Stucky 1983a; Korth 2008).

Armintodelphys dufraingi Smith and Smith, 2013. Original specimens IRSNB M2152 (holotype) and IRSNB M2153 consulted (Royal Belgian Institute of Natural Sciences [RBINS], Brussels). Descriptions and illustrations from Smith and Smith (2013). Known from ~51-52 Ma (Egemkapel Clay Member; Smith and Smith 2013) to possibly MP10 reference level (this study).

Mimoperadectes labrus Bown and Rose 1979. Casts of UM 66144 (holotype, dental rows illustrated in pl. 1 and pl. 2, fig. 1 in Bown and Rose [1979]) and UM 113418 consulted (RBINS). Descriptions and illustrations from Bown and Rose (1979), Gingerich (1989), Strait (2001), Gingerich and Smith (2006) and Rose et al. (2012). Definitive *M. labrus* specimens are recorded in Wa-M and Wa-0 faunas (Bown and Rose 1979; Strait 2001; Gingerich and Smith 2006; Rose et al. 2012). The species maybe extends back to the latest Paleocene (Rose 1981: 36) and further into the early-middle Wasatchian, *Cantius trigonodus* zone (biochrons Wa-4-Wa-5) (Bown and Rose 1979: 96; Korth 2008: 716; Rose et al. 2012: 22).

Peradectes californicus (Stock 1936). Descriptions and illustrations from Stock (1936), Setoguchi (1975), Lillegraven (1976), Rothecker and Storer (1996) (fig. 1P interpreted as M2

instead of M3) and Murphey et al. (2018). From early Uintan (biochron Ui-1a, ~47 Ma) to late Duchesnean (biochron Du) (Murphey et al. 2018).

Peradectes chesteri (Gazin, 1952). Descriptions and illustrations from Gazin (1952), West (1973), Krishtalka and Stucky (1983a, 1983b, 1984) and Murphey et al. (2018). From late Wasatchian (biochron Wa-7) to early Uintan (biochron Ui-1b) (Murphey et al. 2018).

Peradectes crocheti sp. nov. All original material included in this study. Cast of the M3 from Sotteville-sur-Mer. Additional illustrations from Hooker (2010, 2020) for each Abbey Wood and Croydon specimen. Restricted to the [MP7-MP8+9 reference level] interval, with first occurrence just after the PETM (Smith et al. 2011) and last occurrences after the Eocene Thermal Maximum 2 (~biochron Wa5; Noiret et al. 2016).

Peradectes elegans Matthew and Granger, 1921. Casts of AMNH 17376 (holotype), 17383 and USNM 20879 (University of Montpellier, France). Descriptions and illustrations from Simpson (1928, 1935), Gazin (1956), Mckenna (1960), Fox (1983) and Krishtalka and Stucky (1983b). We followed Williamson et al. (2012) in considering *Pd. pauli* as a junior synonym of *Pd. elegans*. Thus, specimens allocated to *Pd. pauli* (Krishtalka and Stucky 1983b), including USNM 20879, have been used for the coding of *Pd. elegans*. From early Tiffanian (biochron Ti-2 according to Korth 2008, biochron Ti-3 according to Secord 2008) to early Wasatchian (between biochrons Wa1-Wa3; McKenna 1960; Korth 2008).

Peradectes gulottai Rose 2010. Descriptions and illustrations from Rose (2010). Wasatchian in age (Rose 2010).

Peradectes louisi Crochet 1979. All original material included in the revision of *Pd. louisi* (this study). From (~)MP8+9 reference level (Mutigny; ~52-54 Ma; Neal 1996; Duprat 1997), to possibly [MP8+9-MP10] interval (this study).

Peradectes protinnominatus McKenna 1960. Casts of UCMP 44077 (holotype) and UCMP 45950 (University of Montpellier, France). Casts of UM 71663, UM 113305, UM 113391 and UM 113378 consulted at the Royal Belgian Institute of Natural Sciences (Brussels, Belgium). Descriptions and illustrations from McKenna (1960), Bown (1979), Rose (1981), Krishtalka and Stucky (1983b) and Gingerich and Smith (2006). Isolated molars of *Pd. protinnominatus* described by Strait (2001) are not included, because the only available illustration for this species is a herpetotheriid M3 (with a V-shaped centrocrista). From Clarkforkian (biochron Cf-2; Rose 1981) to early Wasatchian (biochron Wa-M to between biochrons Wa-1-Wa-3) (McKenna 1960; Gingerich and Smith 2006; Korth 2008).

Peradectes russelli Crochet 1979. All original material included in the revision of *Pd. russelli* (this study). From (~)MP8+9 reference level (Mutigny; ~52-54 Ma; Neal 1996; Duprat 1997), to possibly ~MP10 reference level (this study).

Supplementary references for Online Resource 2

Bown TM (1979) Geology and mammalian paleontology of the Sand Creek Facies, lower Willwood Formation (lower Eocene), Washakie County, Wyoming. Geological Survey of Wyoming Memoir 2: 1–151.

Bown TM, Rose KD (1979) *Mimoperadectes*, a new marsupial, and *Worlandia*, a new dermopteran, from the lower part of the Willwood Formation (early Eocene), Bighorn Basin, Wyoming. Contributions from the Museum of Paleontology, The University of Michigan 25: 89–104.

Crochet JY (1979) Diversité systématique des Didelphidae (Marsupialia) européens tertiaires. Géobios 12: 365–378.

Duprat M (1997) Les faciès à mammifères (MP 6 à MP 16) dans le Nord-Est du Bassin de Paris (France): argumentation du modèle tectono-sédimentaire des dépôts paléogènes. In: Aguilar JP, Legendre S, Michaux J (eds) Actes du Congrès BiochroM'97, Mémoires et travaux de l'EPHE 21. Ecole Pratique des Hautes Etudes, Institut de Montpellier, Montpellier, pp 315–336.

Gazin CL (1952) The lower Eocene knight formation of western Wyoming and its mammalian faunas. Smithsonian Miscellaneous Collections 117: 1–82.

Gazin CL (1956) Paleocene mammalian faunas of the Bison Basin in south-central Wyoming. Smithsonian Miscellaneous Collections 131: 1-57.

Gingerich PD (1989) New earliest Wasatchian mammalian fauna from the Eocene of northwestern Wyoming: composition and diversity in a rarely sampled high-floodplain assemblage. University of Michigan Papers on Paleontology 28: 1–97.

Gingerich PD, Smith T (2006) Paleocene-Eocene land mammals from three new latest Clarkforkian and earliest Wasatchian wash sites at Polecat Bench in the northern Bighorn Basin, Wyoming. Contributions from the Museum of Paleontology, University of Michigan 31: 245–303.

Gregory WK, Simpson GG (1926) Cretaceous Mammal Skulls from Mongolia. Nature 118: 698–699.

Hooker JJ (2010) The mammal fauna of the early Eocene Blackheath formation of Abbey Wood, London. Monographs of the Palaeontographical Society 164: 1–153.

Hooker JJ (2020) A mammal fauna from the Paleocene-Eocene Thermal Maximum of Croydon, London, UK. Proceedings of the Geologists' Association 131: 458–473.

Kielan-Jaworowska Z (1975) Evolution of the therian mammals in the Late Cretaceous of Asia. Part I. Deltatheridiidae. Palaeontologia Polonica 33: 103–132.

Korth WW (2008) Marsupialia. In: Janis CM, Gunnell GF, Uhen MD (eds) Evolution of Tertiary Mammals of North America: Volume 2, Small Mammals, Xenarthrans, and Marine Mammals. Cambridge University Press, Cambridge, pp 39–47.

Krishtalka L, Stucky RK (1983a) Revision of the Wind River faunas, early Eocene of Central Wyoming. Part 3. Marsupialia. Annals of Carnegie Museum 52: 205–227.

Krishtalka L, Stucky RK (1983b) Paleocene and Eocene marsupials of North America. Annals of Carnegie Museum 52: 229–263.

Krishtalka L, Stucky RK (1984) Middle Eocene marsupials (Mammalia) from northeastern Utah and the mammalian fauna from Powder Wash. Annals of Carnegie Museum 53: 31–45.

Lillegraven JA (1976) Didelphids (Marsupialia) and *Uintasorex* (?Primates) from later Eocene sediments of San Diego County, California. Transactions of the San Diego Society of Natural History 18: 85–112.

McKenna MC (1960) Fossil Mammalia from the early Wasatchian Four Mile fauna, Eocene of northwest Colorado. University of California Publications in Geological Sciences 37: 1–130.

Murphey P, Kelly T, Chamberlain K, Tsukui K, Clyde W (2018) Mammals from the earliest Uintan (middle Eocene) Turtle Bluff Member, Bridger Formation, southwestern Wyoming, USA, Part 3: Marsupialia and a reevaluation of the Bridgerian-Uintan North American Land Mammal Age transition. Palaeontologia Electronica 21(2):25A: 1–52.

Neal JE (1996) Summary of Paleogene sequence stratigraphy in northwest European and the North Sea. In: Knox RWOB, Corfield RM, Dunay RE (eds) Correlation of the Early Paleogene in Northwest Europe. Geol Soc London Spec Publ 101, pp 15–42.

Noiret C, Steurbaut E, Tabuce R, Marandat B, Schnyder J, Storme JY, Yans J (2016) New bio-chemostratigraphic dating of a unique early Eocene sequence from southern Europe results in precise mammalian biochronological tie-points. Newsletters on Stratigraphy 49: 469-480.

Rose KD (1981) The Clarkforkian Land-Mammal Age and mammalian faunal composition across the Paleocene-Eocene boundary. University of Michigan Papers on Paleontology 26: 1–197.

Rose KD (2010) New marsupial from the early Eocene of Virginia. Journal of Paleontology 84: 561–565.

Rose KD, Chew AE, Dunn RH, Kraus MJ, Fricke HC, Zack SP (2012) Earliest Eocene mammalian fauna from the Paleocene-Eocene Thermal Maximum at Sand Creek Divide, Southern Bighorn Basin, Wyoming. University of Michigan Papers on Paleontology 36: 1–122.

Rothecker J, Storer JE (1996) The marsupials of the Lac Pelletier lower fauna, Middle Eocene (Duchesnean) of Saskatchewan. Journal of Vertebrate Paleontology 16: 770–774.

Secord R (2008) The Tiffanian Land-Mammal Age (Middle and Late Paleocene) in the Northern Bighorn Basin, Wyoming. University of Michigan Papers on Paleontology 35: 1–192.

Setoguchi T (1975) Paleontology and geology of the Badwater Creek area, central Wyoming. Part 11. Late Eocene marsupials. Annals of Carnegie Museum 45: 263-275.

Simpson GG (1928) American Eocene didelphids. American Museum Novitates 307: 1–7.

Simpson GG (1935) The Tiffany fauna, Upper Paleocene. I.-Multituberculata, Marsupialia, Insectivora, and ?Chiroptera. American Museum Novitates 795: 1–19.

Smith T, Dupuis C, Folie A, Quesnel F, Storme J-Y, Iacumin P, Riveline J, Missiaen P, Ladevèze S, Yans J (2011) A new terrestrial vertebrate site just after the Paleocene–Eocene boundary in the Mortemer Formation of Upper Normandy, France. Comptes Rendus Palevol 10: 11–20.

Smith T, Smith R (2013) A land micro-mammal fauna from the Early Eocene marine Egem deposits (NP12, Belgium) and the first occurrence of the peradectid marsupial *Armintodelphys* outside North America. Geologica Belgica 16: 302–310.

Stock C (1936) Sespe Eocene Didelphids. Proceedings of the National Academy of Sciences 22: 122–124.

Strait SG (2001) New Wa-0 mammalian fauna from Castle Gardens in the southeastern Bighorn Basin. In: Gingerich, PD (ed) Paleocene-Eocene stratigraphy and biotic change in the Bighorn and Clarks Fork basins, Wyoming. University of Michigan Papers on Paleontology 33, pp. 127–143.

Szalay FS, Trofimov BA (1996) The Mongolian Late Cretaceous *Asiatherium* , and the early phylogeny and paleobiogeography of Metatheria. Journal of Vertebrate Paleontology 16: 474–509.

Trofimov BA, Szalay FS (1994) New Cretaceous marsupial from Mongolia and the early radiation of Metatheria. Proceedings of the National Academy of Sciences 91: 12569–12573.

Vullo R, Gheerbrant E, Muizon C de, Néraudeau D (2009) The oldest modern therian mammal from Europe and its bearing on stem marsupial paleobiogeography. Proceedings of the National Academy of Sciences 106: 19910–19915.

West RM (1973) Geology and mammalian paleontology of the New Fork-Big Sandy area, Sublette County, Wyoming. Fieldiana 29: 1–193.

Williamson TE, Brusatte SL, Carr TD, Weil A, Standhardt BR (2012) The phylogeny and evolution of Cretaceous–Palaeogene metatherians: cladistic analysis and description of new early Palaeocene specimens from the Nacimiento Formation, New Mexico. Journal of Systematic Palaeontology 10: 625–651.

Online Resource 3 List of characters included in the cladistic analyses. It is mentioned if a dental character is taken or modified (change in the spelling and / or character states) from Williamson et al. (2014) or Muizon and Ladevèze (2022), or if it is 'new' [i.e. not mentioned in Williamson et al. (2014) or Muizon and Ladevèze (2022)]. For characters taking biometrics into account, the mean of the observed value for a given taxa was used to select the appropriate character state. States of characters newly introduced and informative for resolving relationships of peradectid species are illustrated (not to scale) when needed.

1. Distal heel on lower premolars [new]: at least one cuspid well-developed (0), small to undistinct (1).

Figure S1. States 0 and 1 for the character 1, illustrated on right p3 of *Peradectes crocheti* sp. nov. (0) and *Mimoperadectes labrus* (1). Drawing of *M. labrus* (reversed view) from Bown and Rose (1979).

2. Diastema posterior to p1 [character 17 in Muizon and Ladevèze 2022]: present (0), absent (1).

3. Relative height of p3 [new]: higher than m1 (0), as high as m1 (1), lower than m1 (2).

4. m1 slightly shorter (< 10% shorter) than m2 [new]: absent (0), present (1).

5. Proportions of m2 or m3 [new]: length / width ratio < 1.75 (0), length / width ratio >= 1.75 (1).

6. m4 relative length [new]: shorter than m3 (0), as long as or longer than m3 (1).

7. Trigonid vs talonid width on m3 [modified from character 60 in Williamson et al. 2014; character 56 in Muizon and Ladevèze 2022]: trigonid wider than talonid (0), trigonid as wide as talonid (1).

8. Talonid length on m4 [new]: shorter than trigonid (0), as long as or longer than trigonid (1).

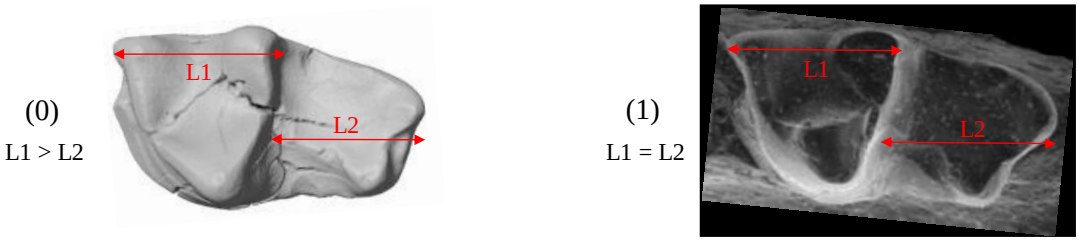

Figure S2. States 0 and 1 for the character 8, illustrated on left m4 of *Peradectes crocheti* sp. nov. (0) and *Armintodelphys blacki* (1). Picture of *Arm. blacki* modified from Smith and Smith (2013).

9. Metaconid position on the anteroposterior axis of m2 or m3 [new]: metaconid almost directly lingual to protoconid (0), metaconid well distolingual to protoconid (1).

(0) 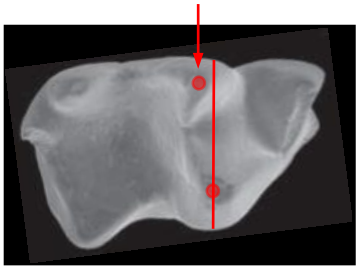 (1) 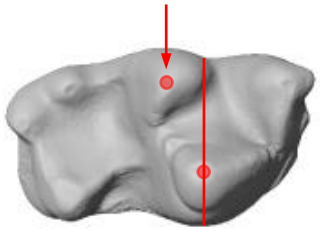

Figure S3. States 0 and 1 for the character 9, illustrated on right m2 and right m3, respectively, of *Peradectes protinnominatus* (0) and *Peradectes louisi* (1). Picture of *Pd. protinnominatus* modified from Gingerich & Smith (2006).

10. Mesial end of cristid obliqua position on m2 or m3 [modified from character 80 in Williamson *et al.*, 2014; character 69 in Muizon & Ladevèze 2022]: ventral or lingual to protocristid notch (0), labial to protocristid notch (1).

11. Mesial end of cristid obliqua on m4 ventral to protocristid notch [modified from character 81 in Williamson et al. 2014]: absent (0), sometimes present (1).

12. Hypoflexid width [character 78 in Muizon & Ladevèze 2022]: deep (ca. 40-50% of talonid width) (0), shallow (less than 40% of talonid width) (1).

13. Emargination of the labial margin of m3 [new]: present (0), absent (1).

(0) 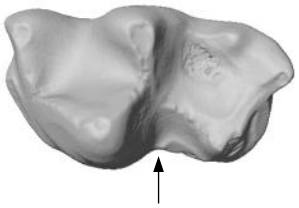 (1) 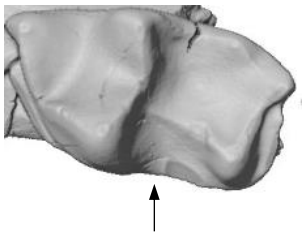

Figure S4. States 0 and 1 for the character 13, illustrated on left m3 of *Peradectes louisi* (0) and *Peradectes crocheti* sp. nov. (1).

14. Angle (in degree of arc) between cristid obliqua and postcristid on m2 or m3 [new]: ca. 70° or more (0), ca. 65° or less (1).

15. Postcristid morphology on m2-m4 [new]: straight at least on one molar locus (0), curved (1).

(0) 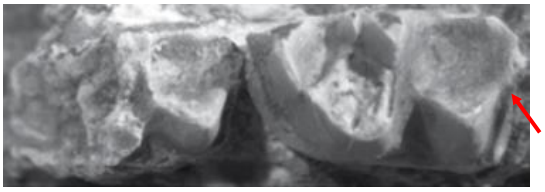 (1) 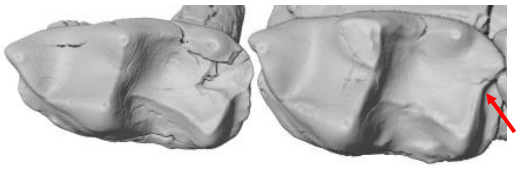

Figure S5. States 0 and 1 for the character 15, illustrated on left m2 of *Mimoperadectes labrus* (0) and *Peradectes crocheti* sp. nov. (1). Picture of *M. labrus* modified from Rose et al. (2012).

16. Postcingulid morphology on m1-m3 [new]: extends lingually towards the hypoconulid tip (0), attenuates labially to the hypoconulid (1).

(0) (1)

Figure S6. States 0 and 1 for the character 16, illustrated on left m3 and m2, respectively, of *Armintodelphys dawsoni* (0) and *Peradectes louisi* (1). Picture of *Arm. dawsoni* modified from Krishtalka and Stucky (1984).

17. Postcingulid on m4 [character 74 in Williamson et al. 2014; character 79 in Muizon and Ladevèze 2022]: present (0), absent (1).

18. Notch between entoconid and hypoconulid on m3 [new]: shallower than the metaconid – entoconid notch (0), almost as deep as the metaconid – entoconid notch (1).

(0) 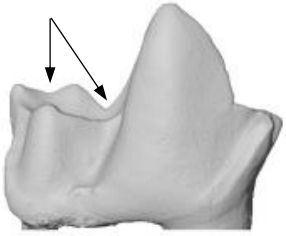 (1) 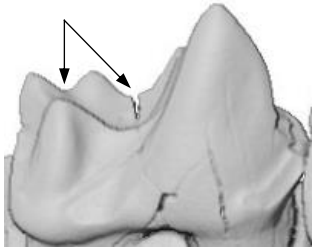

Figure S7. States 0 and 1 for the character 18, illustrated on right m3 of *Peradectes louisi* (0) and *Peradectes crocheti* sp. nov. (1).

19. Relative height of entoconid and hypoconulid [new]: hypoconulid lower than or equal in height to entoconid on all molars, or higher than entoconid only on m4 (0), hypoconulid higher than entoconid on m3 and m4 (1).

(0) 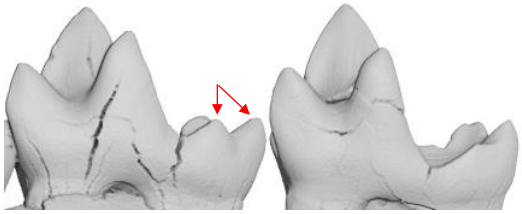 (1) 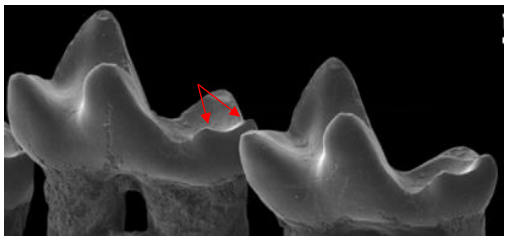

Figure S8. States 0 and 1 for the character 19, illustrated on left (reversed view) and right, respectively, m3 and m4 of *Peradectes crocheti* sp. nov. (0) and '*Armintodelphys*' *dufraingi* (1). Picture of '*Arm.*' *dufraingi* modified from Smith and Smith (2013).

20. Pre-entocristid morphology [character 76 in Muizon and Ladevèze 2022]: absent or weakly developed (0), well-developed and sharp (1).

21. Entoconid apex position relative to trigonid on m2 and m3 [character 75 in Muizon and Ladevèze 2022]: closer to the distolingual corner of the tooth (posterior) (0), intermediate between distal edge of trigonid and distal margin of the tooth (anterior) (1).

22. Disparity of length (L) / width (W) ratio between M2 and M3 [new]: (M2 L/W – M3 L/W) > 0.10 (0), (M2 L/W – M3 L/W) <= 0.10 (1).

23. Talon size [modified from character 46 in Muizon and Ladevèze 2022]: mesiodistally narrow (0), mesiodistally expanded (1).

24. Protocone position [modified from character 51 in Williamson et al. 2014]: lingual to paracone (0), distolingual to paracone (1).

25. Protocone relative height on M1-M3 [modified from character 50 in Williamson et al. 2014]: lower than paracone and metacone (0), subequal or higher than paracone or metacone (1).

26. Conules wing-like (internal and external) cristae on M1-M3 [character 45 in Muizon and Ladevèze 2022]: absent (0), present (1).

27. Largest conule on M1-M3 [new]: paraconule larger or conules subequal in size (0), metaconule larger (1).

28. Relative height of paracone vs metacone on M1-M3 [modified from character 41 in Williamson et al. 2014; character 37 in Muizon and Ladevèze 2022]: sligthly taller (0), sligthly smaller (1).

29. Postmetacrista length on M2 or M3 [character 29 in Muizon and Ladevèze 2022]: subequal to or shorter than preparacrista (0), longer than preparacrista (1).

30. Distal margin morphology on M1-M3 [new]: rectilinear at least on one molar locus, or with a postmetaconular crista extending distolabially to the lingual extremity of the metacone base (0), emarginated between talon and stylar shelf (1).

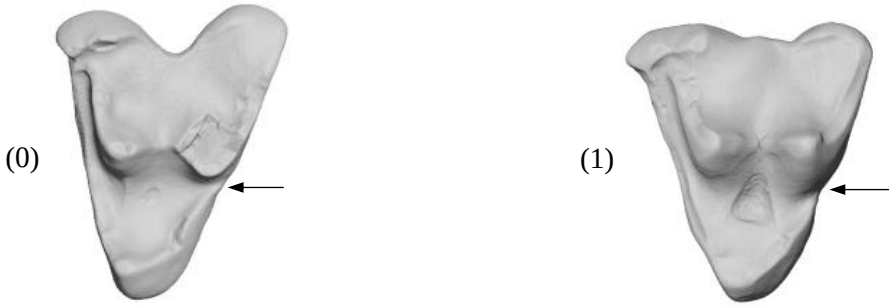

Figure S9. States 0 and 1 for the character 30, illustrated on M3 (reversed view for state 0) of *Peradectes louisi*. The arrow points the distal emargination.

31. Stylar cusp A most frequent position on M2 or M3 [new]: mesial to stylar cusp B (0), mesiolingual to stylar cusp B (1).

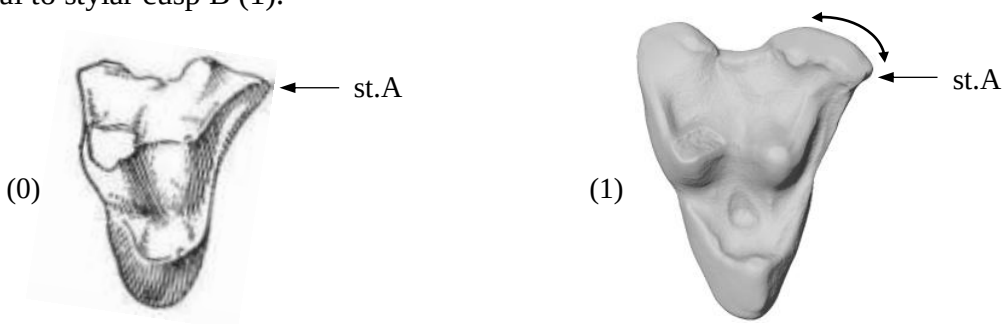

Figure S10. States 0 and 1 for the character 31, illustrated on right M3 of *Peradectes protinnominatus* (0) and *Peradectes russelli* (1). Picture of *Pd. protinnominatus* modified from McKenna (1960).

32. Stylar cusp A relative size (length and width) on M3 [character 22 in Williamson et al. 2014]: subequal to or larger than stylar cusp B (0), distinctly smaller than stylar cusp B (1).

33. Stylar cusp B position on M1-M3 [modified from character 24 in Williamson et al. 2014]: mesiolabial to paracone apex (0), strictly labial to paracone apex at least on M1 and M2 (1).

34. Stylar cusp C on M2-M3 [modified from character 25 in Williamson et al. 2014; character 33 in Muizon and Ladevèze 2022]: absent (0), small (lower than st. B and st. D at least on one molar locus) (1), well-developed (as high as or higher than st. B or st. D) (2).

35. Stylar cusp D position on M1 [modified from character 32 in Williamson et al. 2014]: mesiolabial or strictly labial to metacone apex (0), distolabial to metacone apex (1).

36. M1 ectoflexus [new]: sometimes present (0), absent (1).

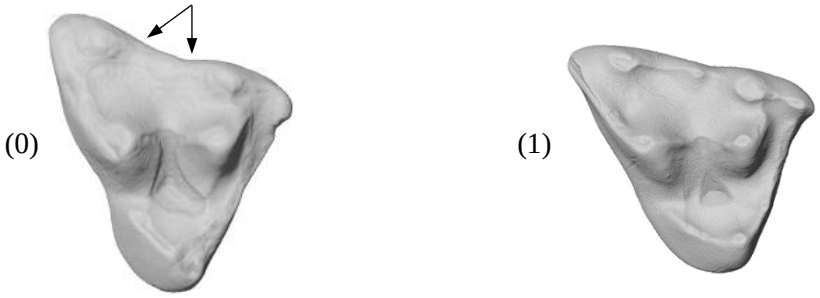

Figure S11. States 0 and 1 for the character 36, illustrated on right M1 of *Peradectes russelli* (0) and *Peradectes crocheti* sp. nov. (1).

37. Ectoflexus symmetry [new]: present on M2 or M3, at least on one specimen (0), absent (1).

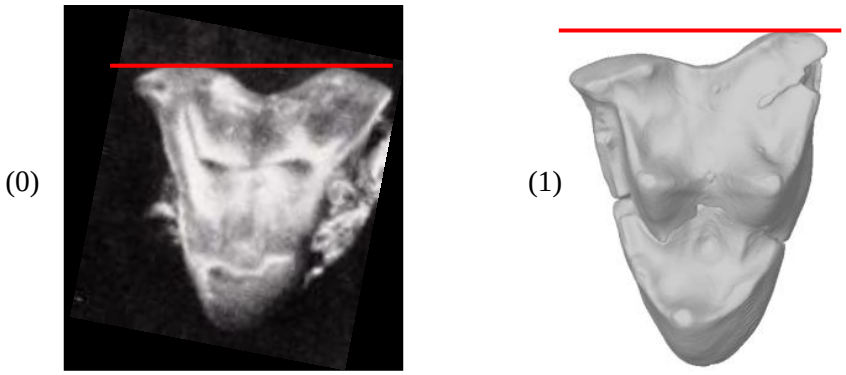

Figure S12. States 0 and 1 for the character 37, illustrated on right M2 of *Peradectes chesteri* (0) and left M3 of *Peradectes crocheti* sp. nov. (1). Picture of *Pd. chesteri* (reversed view) modified from Krishtalka & Stucky (1984).

Supplementary references (not present in Online Resource 2) for Online Resource 3

Muizon C de, Ladevèze S (2022) New material of *Incadelphys antiquus* (Pucadelphyda, Metatheria, Mammalia) from the early Palaeocene of Bolivia reveals phylogenetic affinities with enigmatic North and South American metatherians. Geodiversitas 44:609-643.

Williamson TE, Brusatte SL, Wilson GP (2014) The origin and early evolution of metatherian mammals: the Cretaceous record. ZooKeys 465:1–76.

Online Resource 4 Taxon-character matrix (14 taxa, 37 characters) of the first phylogenetic analysis. A dash denotes inapplicability. Brackets denote morphological polymorphism.

Deltatheridium pretrituberculare	001000001000000-10-000000000010000-00
Asiatherium reshetovi	00100101101001100000011111001010000001
Peradectes elegans	0(01)1001100101(01)0100(01)0100110111100002010
Peradectes protinnominatus	011100000101(01)0110101(01)00001111101(01)2000
Peradectes crocheti sp. nov.	01010010(01)10110110101110(01)01111(01)1112111
Peradectes russelli	???00100110100011001(01)10001111(01)1111101
Peradectes louisi	???11000111100(01)11001110001111(01)1111101
Armintodelphys dufraingi	????1100111100011011??????????????????
Mimoperadectes labrus	11010100111(01)1001(01)01101(01)(01)1111000102100
Armintodelphys blacki	11??011111011011011???????????????
Armintodelphys dawsoni	????011101011000?0110?0000?1000?02??0
Peradectes chesteri	??21(01)000(01)101111100?000000011011101100
Peradectes gulottai	??????????????????????100101111100 1??1
Peradectes californicus	11211100010111111010010011111111001101

Online Resource 5 Modified spelling of characters or character states (modified parts are in bold), subsequent amendments in the scoring and results of the second and third phylogenetic analysis, replacing frequencies of observations by morphological polymorphism.

Changes in the spelling and scoring, and result for the second phylogenetic analysis:

11. Mesial end of cristid obliqua on m4 ventral to protocristid notch [modified from character 81 in Williamson et al. 2014]: absent (0), **present** (1).

31. **Stylar cusp A position** on M2 or M3 [new]: mesial to stylar cusp B (0), mesiolingual to stylar cusp B (1).

36. M1 ectoflexus [new]: **present** (0), absent (1).

Changes in the scoring of character **11**. *Peradectes louisi*, *Mimoperadectes labrus*: 1 -> 0&1

Changes in the scoring of character **31**. *Peradectes protinnominatus*; 0 -> 0&1; *Peradectes crocheti* sp. nov., *Peradectes louisi*, *Peradectes chesteri*, *Peradectes californicus*: 1 -> 0&1

Changes in the scoring of character **36**. *Peradectes louisi*, *Peradectes russelli*: 0 -> 0&1

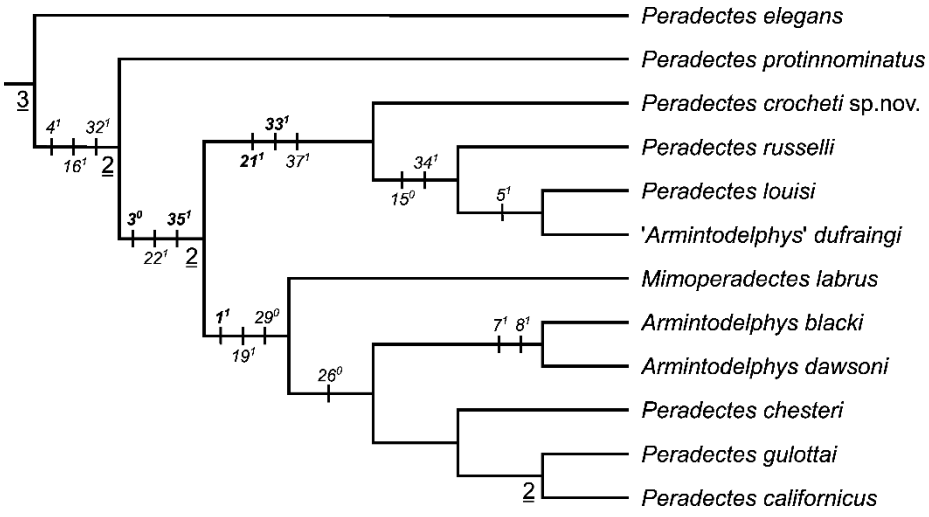

Figure S1 Ingroup from the single most-parsimonious tree obtained in the second analysis (111 steps, same topology as the first analysis; CI = 0.604, RI = 0.517; see main text for described changes in Bremer indices and non-ambiguous synapomorphies).

Additional changes (characters 11, 31 and 36 modified as in the second analysis) in the spelling and scoring, and result for the third phylogenetic analysis:

37. Ectoflexus symmetry [new]: **present on M2 or M3** (0), absent (1).
'present on M2 or M3, **at least on one specimen**' (analysis 1 and 2) > 'present on M2 or M3' (analysis 3).

Change in the scoring of character **37**. *Peradectes chesteri*: 0 -> 0&1

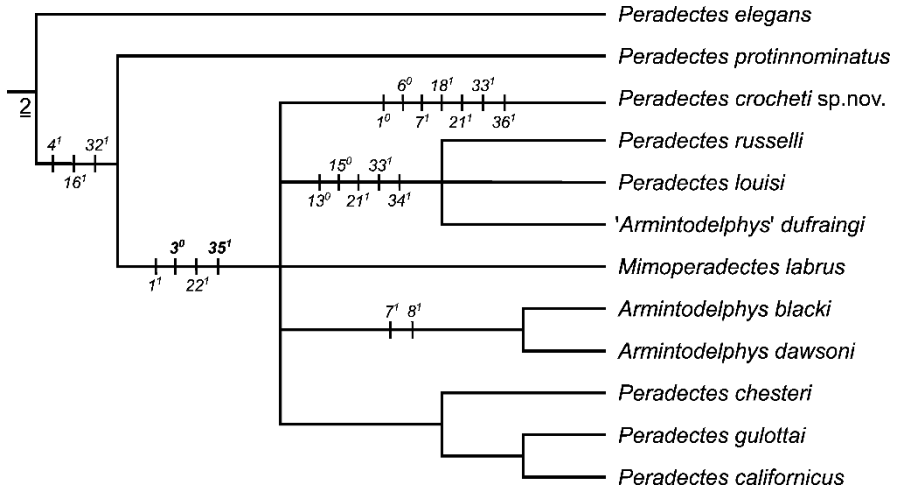

Figure S2 Ingroup from the two most-parsimonious tree obtained in the third analysis, of 112 steps each (CI = 0.607, RI = 0.511). The non-ambiguous synapomorphies for taxa of main interest are figured at node or branch.

Online resource 6 Lingual (medial) view of the surface model of the right hemi-mandible fragment MHN.AIX.PV.2017.6.8, *Peradectes crocheti* sp. nov. from Palette (Provence; MP7-MP8+9 interval).

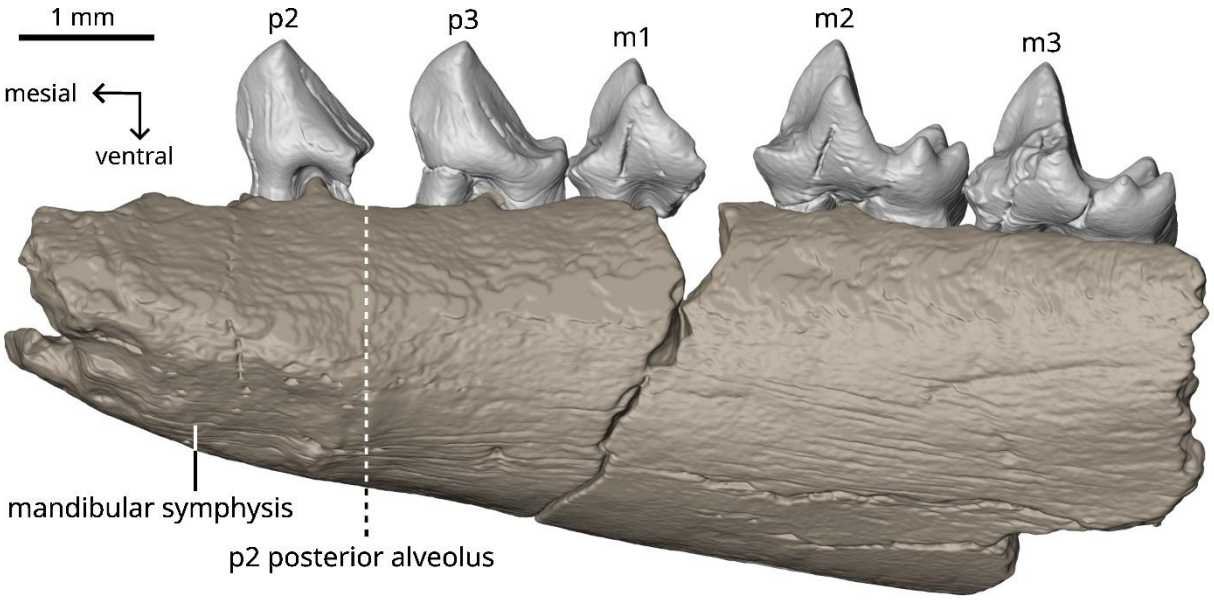

The 3D models related to this publication are also presented as Supplemental material for this section, in the following MorphoMuseuM data paper

Dataset

3D models related to the publication: Taxonomy and evolutionary history of peradectids (Metatheria): new data from the early Eocene of France.

Killian Gernelle[1*], Guillaume Billet[2], Emmanuel Gheerbrant[2], Marc Godinot[3], Bernard Marandat[1], Sandrine Ladevèze[2†], Rodolphe Tabuce[1†]

[1] *Institut des Sciences de l'Évolution de Montpellier (ISEM, UMR 5554), Univ Montpellier, CNRS, IRD, c.c. 064, Place Eugène Bataillon, F-34095 Montpellier Cedex 05, France*
[2] *CR2P–MNHN, CNRS, UPMC-Paris 6 (Sorbonne Universités) – Museum National d'Histoire Naturelle, CP 38, 8 rue Buffon, 75005 Paris, France.*
[3] *Ecole Pratique des Hautes Etudes, PSL, UMR 7207, CR2P, 8 rue Buffon, F75005, Paris, France*
***Corresponding author**: killian.gernelle@umontpellier.fr; †Co-senior authors

Abstract
This contribution contains the three-dimensional models of the most complete and/or informative fossil materials attributed to *Peradectes crocheti* Gernelle, 2024, the earliest peradectid metatherian species of Europe, from its type locality (Palette, Provence, ∼55 Ma). These specimens were analyzed and discussed in: Gernelle et al. (2024), Taxonomy and evolutionary history of peradectids (Metatheria): new data from the early Eocene of France. https://doi.org/10.1007/s10914-024-09724-5

Keywords: dentition, Eocene, Europe, Peradectidae, systematics

Submitted: 01/07/2024, published online: 05/08/2024. https://doi.org/10.18563/journal.m3.239

INTRODUCTION

Peradectidae are an assemblage of extinct and small Cenozoic stem-metatherians, likely arboreally adapted, with a superficially "opossum-like" unspecialized tribosphenic dentition (e.g., Rose, 2012; Ladevèze et al., 2020). A set of phylogenetic analyses supports a single dispersal of peradectids from North America to Europe, during or immediately after the Paleocene-Eocene Thermal Maximum (PETM; at or just after ∼56 Ma) (Gernelle et al., 2024). The early Eocene fossiliferous locality of Palette (Provence; ∼MP7, ∼55 Ma) yielded a mammalian fauna composed of 17 species (Godinot et al., 1987; updated in Gernelle et al., 2024: table 1), of which the eutherians have been extensively studied, notably through works focused on three-dimensional (3D) digital models of iconic specimens from this locality (i.e., of the adapiform primate *Donrussellia magna* and the artiodactyl *Diacodexis* cf. *gigasei*; Ramdarshan et al., 2015; Orliac et al., 2018). Palette is the type locality of the earliest-diverging European peradectid metatherian, *Peradectes crocheti* Gernelle, 2024, a species which was widespread in Western Europe during the MP7-MP8+9 interval (Gernelle et al., 2024). We present here the 3D digital models of the most complete and/or informative specimens of *Peradectes crocheti* from Palette (Table 1). The fossils figured here were found after the field expeditions conducted between 2017 and 2019 by some of us (GB, EG and RT) in Palette. The specimens labelled "MHN.AIX.PV.2017" were isolated by one of us (KG) after processing the sampled sediment by careful acid etching, use of screen-washing, and sorting methods. The height relationships of stylar cusps (which are small cusps pointing ventrally along the labial margin of upper molars) are informative regarding the systematics of peradectids (Gernelle et al. 2024). Such a height relationship can be observed on the labial view of the well-preserved MHN.AIX.PV.2017.6.7 M3 (Fig. 1F), in addition to M2 and M3 of the maxilla holotype (Fig. 1A). The new fossils revealed the ancestral morphology of European peradectids, and their differences with Herpetotheriidae, the other Paleogene Laurasian "opossum-like" family. For example, the present left and right mandibles of *Pd. crocheti* (MHN.AIX.PV.2017.6.8 and MHN.AIX.PV.2017.6.9; Fig. 2), possibly representing a single individual, have curved lower premolar roots, differing from the roots of their molars and the roots of lower premolars in herpetotheriids, which are straight (Gernelle et al., 2024: table 6). The astragalus MHN.AIX.PV.2017.6.14 (Fig. 3), by its nearly ungrooved trochlea and strong similarity with Wyoming peradectid astragali (see Rose, 2012), suggests that *Pd. crocheti* was arboreally adapted, like its close relatives from North America (Gernelle et al., 2024). The peradectid specimens from Palette are permanently housed in the collections of the Muséum d'Histoire Naturelle of Aix-en-Provence (France).

METHODS

The six peradectid specimens were scanned using a µ-CT-scanning station EasyTom 150/Rx Solutions (Montpellier RIO Imaging [MRI], ISEM, Montpellier, France). All specimens were scanned with a resolution between ∼5 and 7 µm. The segmentation of the cheek teeth and dentary of MHN.AIX.PV.2017.6.8 (Fig. 2C-E) was performed with the Avizo 9.3 blow selection tool, in order to clarify the morphology and positioning of the peradectid premolars on the dentary, with transparency applied in the figuration of the latter (Fig. 2E; see also Gernelle et al., 2024: fig. 6b). The segmentation of the holotype of *Peradectes crocheti*, MHN.AIX.PV.2018.26.14 (Fig. 1A-B), required the

Inv nr.	Description
MHN.AIX.PV.2018.26.14	fragmentary left maxilla with C-P1, anterior root of P2, and M1-M3
MHN.AIX.PV.2017.6.6	left P2
MHN.AIX.PV.2017.6.7	left M3
MHN.AIX.PV.2017.6.8	right hemi-mandible fragment with canine alveolus, posterior root of p1, partial p2, p3, partial m1, and m2-m3
MHN.AIX.PV.2017.6.9	left m1-m4 row with fragments of dentary
MHN.AIX.PV.2017.6.14	right astragalus

Table 1. List of 3D models of *Peradectes crocheti* specimens from Palette (Provence). Collection: Muséum d'Histoire Naturelle of Aix-en-Provence, Southern France.

threshold selection tool. An attempt was made to position the segmented fragments of the maxilla MHN.AIX.PV.2018.26.14 in anatomical position, using the MorphoDig open-source 3D freeware (Lebrun, 2018; https://morphomuseum.com/morphodig), with comparison to the complete maxilla of the peradectid-like "*Peradectes*" from Messel (Kurz and Habersetzer, 2004: figs. 2-3) and accounting for the typical crushing of fossil bones from Palette, which may have suffered from synsedimentary compression (e.g., Vautrin et al., 2020). The threshold selection tool was also used for (i) segmenting the isolated M3 MHN.AIX.PV.2017.6.7 (Fig. 1E-F), as a way to numerically assemble its lingual and labial halves, and (ii) extracting semi-automatically the 3D surfaces of the isolated P2 MHN.AIX.PV.2017.6.6 (Fig. 1C-D), the lower molar row MHN.AIX.PV.2017.6.9 (Fig. 2A-B) and the astragalus MHN.AIX.PV.2017.6.14 (Fig. 3). The 3D surface models are provided in .ply format, and can therefore be opened with a wide range of software programs (e.g., MorphoDig).

ACKNOWLEDGEMENTS

We are indebted to the Rougier family, owner of the Palette site, who kindly provided access, help and support for paleontological research on this locality. We acknowledge Y. Dutour and N. Vialle (Muséum d'Histoire Naturelle of Aix-en-Provence), Q. Vautrin (Parc Naturel Régional UNESCO Global Geopark Causses du Quercy), C. Bronnert and R. Vacant (MNHN), and E. Turini and L. Mohring for their precious help during these excavations. R. Vacant also carefully treated the sediments from Palette collected in 2018, that yielded the holotype of *Peradectes crocheti* (MHN.AIX.PV.2018.26.14). We warmly thank A.-L. Charruault (ISEM), who performed the µ-CT-scanning and segmentation of this holotype specimen. Recent excavations at Palette were funded thanks to the Actions Transversales du Muséum (ATM Palette, MNHN funding). Three-dimensional data acquisition was performed using the micro-computed tomography (µ-CT) facilities of the MRI platform member of the national infrastructure France-BioImaging supported by the French National Research Agency (ANR-10-INBS-04, 'Investments for the future'), the labex CEMEB (ANR-10-LABX-0004) and NUMEV (ANR-10-LABX-0020). This research was financially supported by a PhD thesis funding from the French Ministry of Higher Education, Research, and Innovation, and also in part by the ANR project EDENs (ANR-20-CE02-0007). This is ISEM publication n° 2024-157

BIBLIOGRAPHY

Gernelle, K., Billet, G., Gheerbrant, E., Godinot, M., Marandat, B., Ladevèze, S., Tabuce, R. 2024. Taxonomy and evolutionary history of peradectids (Metatheria): new data from the early Eocene of France. Journal of Mammalian Evolution. https://doi.org/10.1007/s10914-024-09724-5

Godinot, M., Crochet, J. Y., Hartenberger, J. L., Lange-Badré, B., Russell, D. E., Sigé, B. 1987. Nouvelles données sur les mammifères de Palette (Eocène inférieur, Provence). Münchner Geowissenschaftliche Abhandlungen (A) 10, 273-288.

Kurz, C., Habersetzer, J. 2004. Untersuchungen der zahnmorphologie von beutelratten aus Messel mit der mikroröntgenmethode CORR. Courier Forschungsinstitut Senckenberg 252, 13–21.

Ladevèze, S., Selva, C., Muizon, C. de. 2020. What are "opossum-like" fossils? The phylogeny of herpetotheriid and peradectid metatherians, based on new features from the petrosal anatomy. Journal of Systematic Palaeontology 18, 1463–1479. https://doi.org/10.1080/14772019.2020.1772387

Lebrun, R. 2018. MorphoDig, an open-source 3D freeware dedicated to biology. 5th International Paleontological Congress (IPC5). Available at https://morphomuseum.com/downloadMorphodig

Orliac, M. J., Boivin, M., Tabuce, R. 2018. A mandible of *Diacodexis* cf. *gigasei* (Artiodactyla, Diacodexeidae) from the Early Eocene locality of Palette (Bouches-du-Rhône, France). MorphoMuseuM 4, 1–4. https://doi.org/10.18563/journal.m3.60

Ramdarshan, A., Godinot, M., Bédécarrats, S., Tabuce, R. 2015. Holotype specimen of *Donrussellia magna*, an adapiform primate from the early Eocene (MP7) of Southern France. MorphoMuseuM 1, 1–3. https://doi.org/10.18563/m3.1.2.e2

Rose, K. D. 2012. The importance of Messel for interpreting Eocene Holarctic mammalian faunas. Palaeobiodiversity and Palaeoenvironments 92, 631–647. https://doi.org/10.1007/s12549-012-0090-8

Vautrin, Q., Tabuce, R., Lihoreau, F., Bronnert, C., Gheerbrant, E., Godinot, M., Metais, G., Yans, J., Dutour, Y., Vialle, N., Philip, J., Billet, G. 2020. New remains of *Lophiaspis maurettei* (Mammalia, Perissodactyla) from the early Eocene of France and the implications for the origin of the Lophiodontidae. Journal of Vertebrate Paleontology 40, 1–20. https://doi.org/10.1080/02724634.2020.1878200

ISSN: 2274-0422

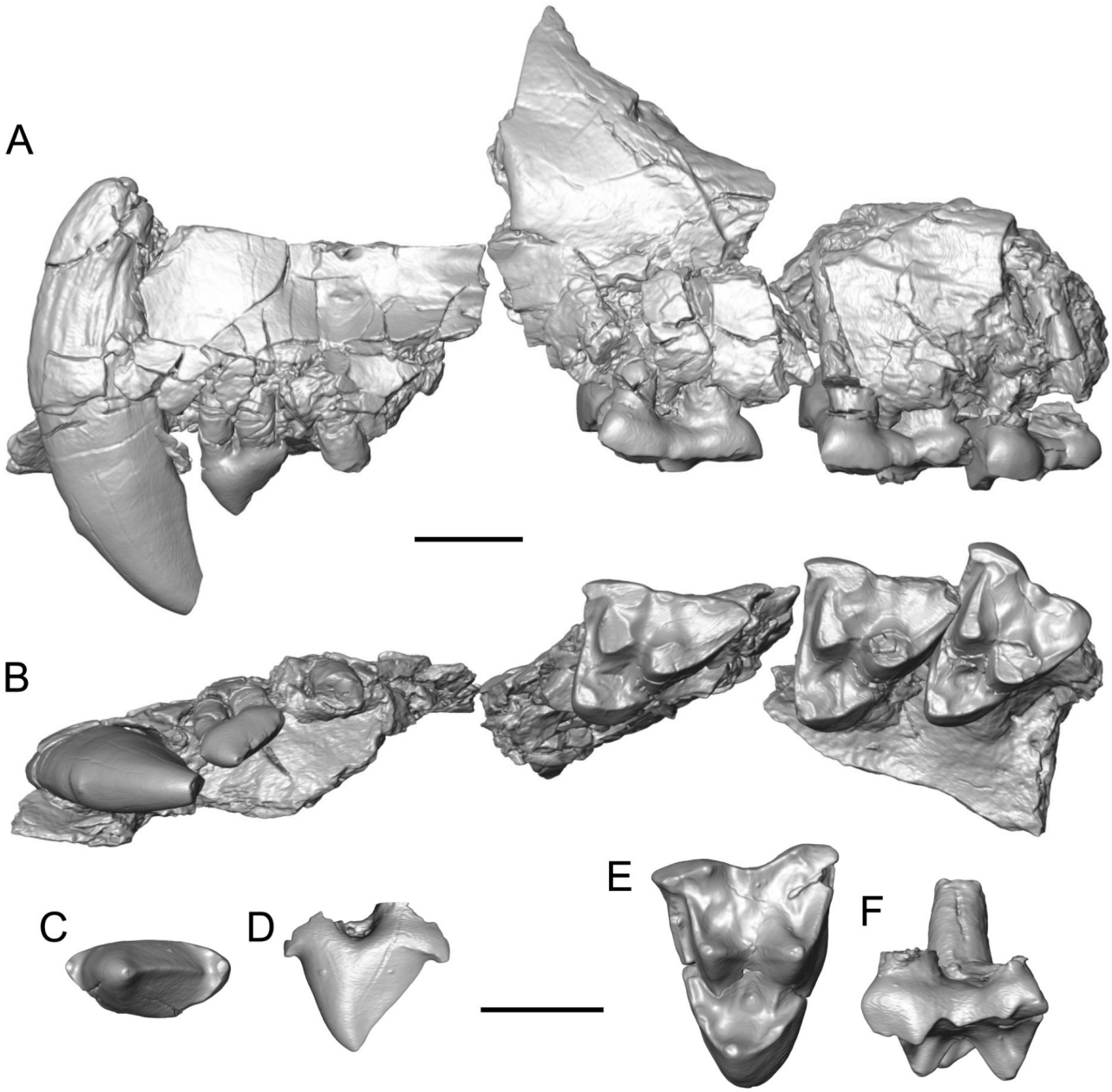

Figure 1. Three-dimensional models of maxilla and upper cheek teeth of *Peradectes crocheti* from Palette (Provence, ~55 Ma). A-B, MHN.AIX.PV.2018.26.14, holotype, fragmentary left maxilla with C-P1, anterior root of P2, and M1-M3, in lateral (labial) (A) and ventral (occlusal) (B) views. C-D, MHN.AIX.PV.2017.6.6, left P2, in occlusal (C) and labial (D) views. E-F, MHN.AIX.PV.2017.6.7, left M3, in occlusal (E) and labial (F) views. Scale bars (A-B, C-F) equal 1 mm.

ISSN: 2274-0422

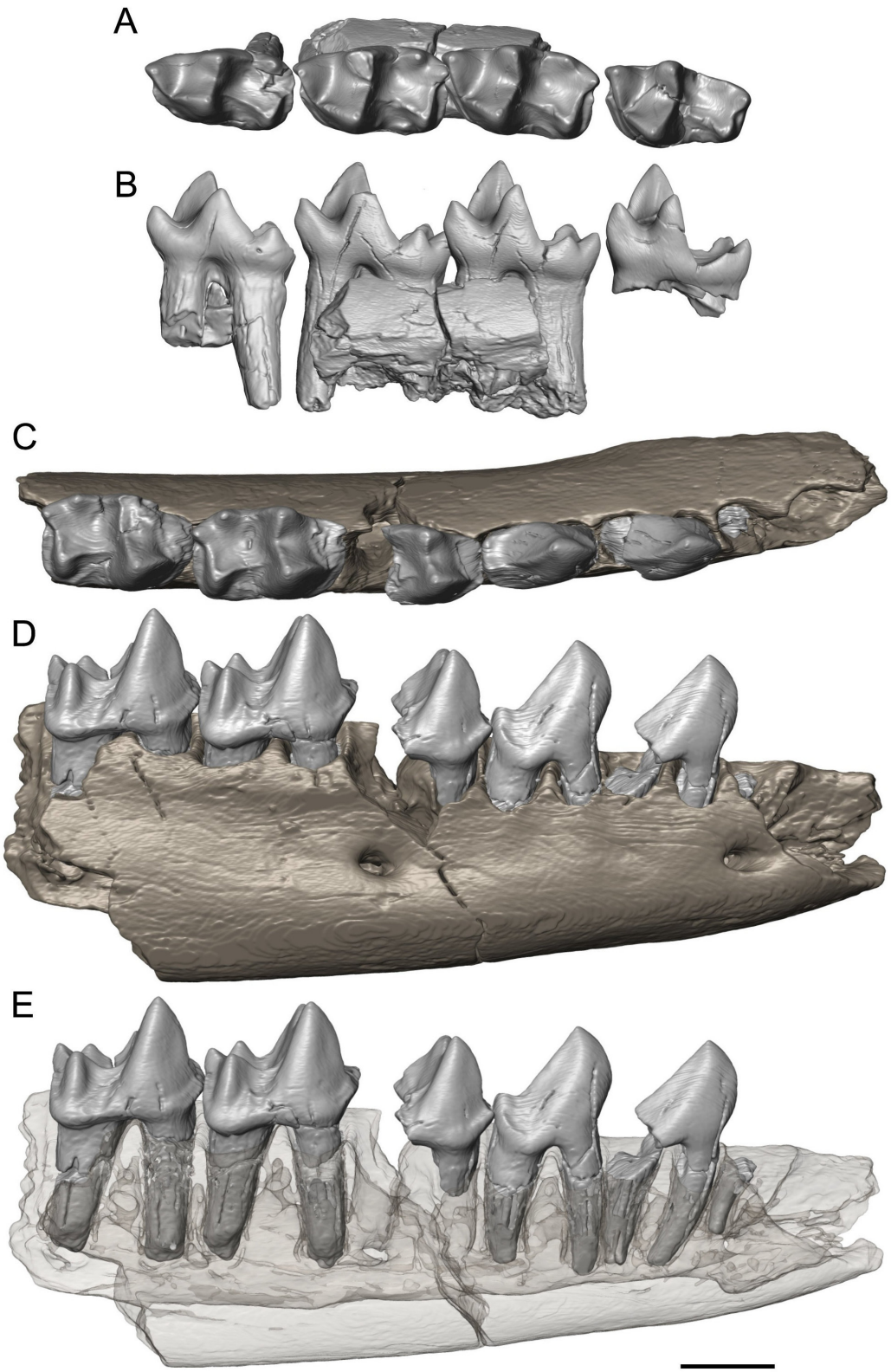

Figure 2. Three-dimensional models of hemi-mandibles and lower cheek teeth of *Peradectes crocheti* from Palette (Provence, ~55 Ma). A-B, MHN.AIX.PV.2017.6.9, left m1-m4 row with fragments of dentary, in occlusal (A) and reversed lingual (B) views. C-E, MHN.AIX.PV.2017.6.8, right hemi-mandible fragment with canine alveolus, posterior root of p1, partial p2, p3, partial m1, and m2-m3 in dorsal (occlusal) (C), lateral (labial) (D) and lateral with transparent dentary (E) views. Scale bar equals 1 mm.

ISSN: 2274-0422

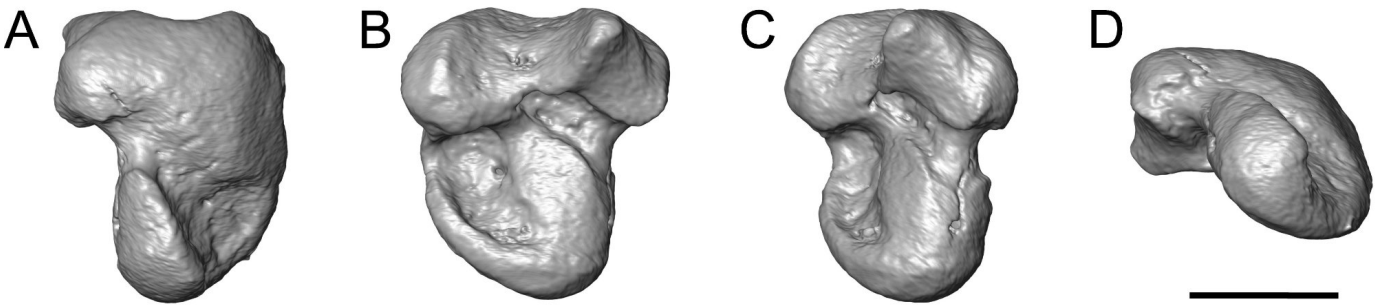

Figure 3. Three-dimensional model of right astragalus of *Peradectes crocheti* from Palette (Provence, ~55 Ma), MHN.AIX.PV.2017.6.14, in dorsal (A), ventral (B), ventrolateral (C) and distal (D) views. Scale bar equals 1 mm.

ISSN: 2274-0422

Chapitre 2. Taxonomie de nouveaux péradectidés européens de la fin de l'Éocène inférieur.

Remarques : L'ensemble de cette section est en anglais. La numérotation des spécimens de Prémontré (PRE) présentant l'abréviation « SLP » (Société laonnoise de Paléontologie) est provisoire.

Chapter 2. Taxonomy of new European peradectids from the late early Eocene.

The peradectid material from the late early Eocene of France studied in the discussion by Gernelle et al. (2024a) was composed of only eight isolated and mostly fragmentary molars, of which some have been newly described in the frame of this thesis (Vianey-Liaud et al. 2024; see Appendix). Here, a few more complete unpublished specimens from the localities of Prémontré (in Aisne; Dégremont et al. 1985) and Cos (in Quercy; Godinot et al. 2021) allow the erection of three new peradectid species, which are the latest known in Europe prior to the Ypresian/Lutetian boundary. Unlike metatherians, many eutherians from the rich mammal fauna of Prémontré have been formally described, namely pantolestids (Smith 2001), paroxyclaenids (Solé et al. 2019), paromomyids (López-Torres and Silcox 2018), primates (Godinot et al. 1992), rodents (Escarguel 1999; Vianey-Liaud and Marivaux 2021), hyaenodonts (Solé et al. 2021), chiropterans (Hand et al. 2016; Hand and Sigé 2018), perissodactyls (Bronnert and Métais 2023) and artiodactyls (Sudre and Erfurt 1996). The Cos mammal fauna is still under study (Vianey-Liaud et al. 2022). Some puzzling metatherian upper molars from southwestern France are also described here. Finally, an attempt is made to discriminate a posteriori some peradectid species based on the outline shape of their upper molars.

Remark: As in Gernelle et al. (2024a), the attribution of the new peradectid species to *Peradectes* in this section are only tentative. A resolution of the generic classification of all peradectid species is fully discussed in Chapter 3, with respect to the phylogenetic context there established.

Marsupialiformes Vullo et al., 2009

Peradectidae (Crochet, 1979)

Peradectes sp. nov. 1

Figures 1, 2A-G

Holotype: MNHN.F.SLP29-PR-2745, fragment of right maxilla with M3-M4 from Prémontré (Figure 1D-E).

Localities and age: Prémontré, in Paris Basin (Aisne), ~MP10, early late Ypresian, ~50.3-50.4 Ma (Steurbaut et al. 2016); and probably Grauves (GR), in Paris Basin (Marne), MP10 reference level.

Other material: left M2 (MNHN.F.SLP29-PR-3039), worn right M2 (MNHN.F.SLP29-PE-1587), labial fragment of left M4 (MNHN.F.PRE509), right m1 (MNHN.F.GR10010, MNHN.F.PRE694), left m2 (MNHN.F.SLP29-PR-2962), left m3 (MNHN.F.GR10013; Gernelle et al. 2024a: fig. 17b-c), worn left m4 (MNHN.F.SLP29-PR-2321).

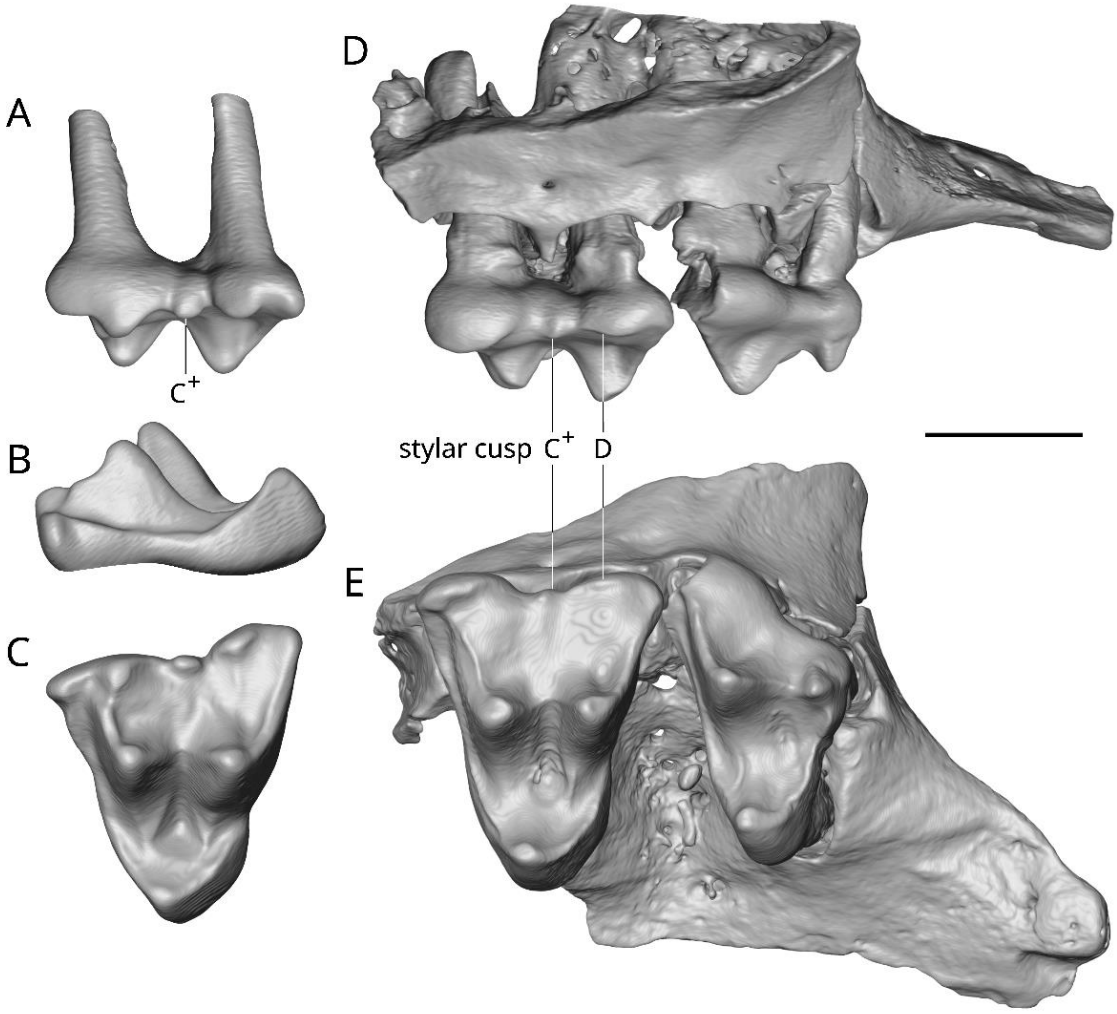

Figure 1. Upper molars of *Peradectes* sp. nov. 1, from Prémontré (Paris Basin; ~MP10, ~50.3-50.4 Ma), based on 3D surface models. **A-C**. MNHN.F.SLP29-PR-3039, left M2 in labial (A), mesial (B) and occlusal (C) views. **D-E**. MNHN.F.SLP29-PR-2745, fragment of right maxilla with M3-M4 in lateral (labial) (D) and ventral (occlusal) (E) views. Abbreviation: C^+, stylar cusp C tip as or more ventral than stylar cusp D tip. Scale bar equals 1 mm.

Differential diagnosis: Similar in size to *Pd. crocheti*, *Pd. louisi*, and *Peradectes* sp. nov. 3, but some upper molar specimens are slightly labiolingually wider. Differs from *Pd. crocheti*, *Pd. louisi*, and *Pd. russelli* in the entoconid lower than the hypoconulid on m3, and in the equally labial parastylar and metastylar wings on M3. Further differs from *Pd. crocheti* and *Pd. russelli* in having relatively longer

lower molars. Further differs from *Pd. louisi*, *Pd. russelli*, and *Peradectes* sp. nov. 3 in having stylar cusp C apex more ventral than stylar cusp D apex on M3 (upper molars of *Pd. dufraingi* are unknown). Further differs from *Pd. louisi* in having stylar cusp D directly labial to the metacone apex on M3. Further differs from *Peradectes* sp. nov. 3 in the relatively longer entoconid of m1 and m2. Differs from *Pd. dufraingi* in having larger lower molars with a developed postcingulid, and a m2 with a relatively wider talonid.

Description: The M2 MNHN.F.SLP29-PR-3039 and the M3 of MNHN.F.SLP29-PR-2745 have L/W values corresponding to the lower limit known in equivalent loci in other European peradectid species, and these two specimens are slightly wider than those of other subequally sized European peradectid species (Table 1 vs Table 4 and Gernelle et al. 2024a: table 4). Similarly to other European peradectids, in mesial view of M2-M3 the conules are almost indistinct, and the protocone is the lowest principal cusp (e.g., Figure 1B); the M4 is close to the M3 in term of labiolingual width value (Table 1), and an ectoflexus is present on the former (Figure 1E). The crown of the M2 has a deep distal emargination. The two upper molars with preserved stylar cusps, the M2 MNHN.F.SLP29-PR-3039 and the M3 of the maxilla fragment MNHN.F.SLP29-PR-2745, have stylar cusp C apex more ventral than stylar cusp D apex (Figure 1A, D), unlike in M1s-M3s of *Pd. louisi* and M3s of *Pd. russelli*. Stylar cusp D is directly labial to the metacone apex on both M2 and M3. The single known M3 has equally labial parastylar and metastylar wings, but the ectoflexus is slightly deeper close to the parastylar wing. The postparaconular crista is preserved on M4. The metacone of M4, although much smaller than the paracone (Figure 1D), is as high as the protocone in distal view, as on the M4 of *Pd. louisi*. The mesiolabial termination of the parastylar wing is not preserved on M4. Thus, stylar cusps A and B of M4 cannot be described. Stylar cusp C is absent, as in *Pd. louisi* and *Pd. russelli*.

Table 1. Measurements of upper molars of *Peradectes* sp. nov. 1 from Prémontré (Paris Basin; ~50.3-50.4 Ma). Italic values are estimated for the M4 MNHN.F.SLP29-PR-2745, and indicate that the whole labial margin of MNHN.F.SLP29-PE-1587 is worn.

Specimen	Locus	L (mm)	W (mm)	L/W
MNHN.F.SLP29-PE-1587	M2	1.67	*1.83*	*0.91*
MNHN.F.SLP29-PR-3039	M2	1.64	1.92	0.85
MNHN.F.SLP29-PR-2745	M3	1.58	2.04	0.77
	M4	*1.25*	*1.96*	*0.64*
MNHN.F.PRE509	M4	1.33	-	-

All lower molars are smaller than those of *Peradectes* sp. nov. 2. The m2 is the largest lower molar locus (Table 2) as identified in *Pd. crocheti*, *Pd. louisi* and *Pd. russelli*, based on mean values yielded from various specimens (Gernelle et al. 2024a: table 4), and *Peradectes* sp. nov. 2 (Table 2). All lower molars have a length to width value > 1.75, and m1 and m4 are relatively longer than m2 and m3, with two specimens in which the length is almost twice the width (Table 2). As in all other peradectids, the trigonid

is longer than the talonid (this character has not been mentioned in Gernelle et al. 2024a: table 6). The entoconid is as high as and longer than the hypoconulid on m2 and is lower than the hypoconulid on m3, similarly to *Pd. dufraingi*. The ectocingulid is absent on m2 and m3 as in *Pd. dufraingi* (contrary to *Peradectes* sp. nov. 2 [Figure 2C, E vs Figure 2J, L], *Pd. louisi* and *Pd. russelli*), but a postcingulid is developed.

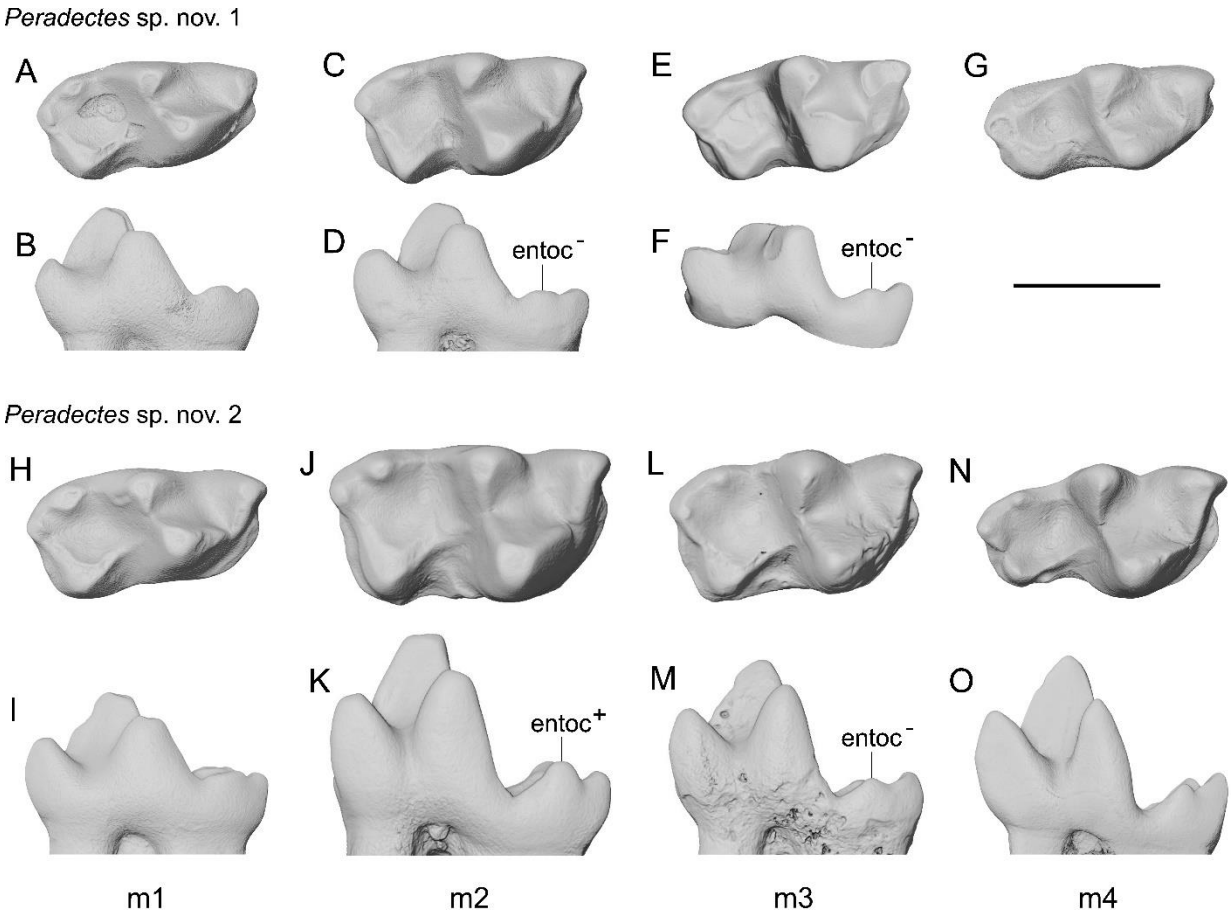

Figure 2. Lower molars of *Peradectes* sp. nov. 1, from Prémontré (Paris Basin; ~MP10, ~50.3-50.4 Ma) and Grauves (MP10) (A-G) and *Peradectes* sp. nov. 2 (H-O) from Prémontré. **A-B**. MNHN.F.PRE694, right m1 in occlusal (A) and lingual (B) views. **C-D**. MNHN.F.SLP29-PR-2962, left m2 in occlusal (C) and lingual (D) reversed views. **E-F**. MNHN.F.GR10013, left m3 in occlusal (E) and lingual (F) reversed views. **G**. MNHN.F.SLP29-PR-2321, worn left m4 in occlusal reversed view. **H-I**. MNHN.F.PRE272, right m1 in occlusal (H) and lingual (I) views. **J-K**. MNHN.F.PRE643, left m2 in occlusal (J) and lingual (K) reversed views. **L-M**. MNHN.F.PRE26, right m3 in occlusal (L) and lingual (M) views. **N-O**. MNHN.F.SLP29-PR-2934, left m4 in occlusal (N) and lingual (O) reversed views. Scale bar equals 1 mm. Abbreviations: entoc^{+}, entoconid higher than the hypoconulid; entoc^{-}, entoconid as high as or lower than the hypoconulid.

Discussion: The differences between *Peradectes* sp. nov. 1 and *Peradectes dufraingi* are subtle, and, as specified above and partly in Gernelle et al. (2024a), concern lower molar size (upper molars of *Pd. dufraingi* are unknown), the development of the postcingulid, and the relative width of the talonid of m2, which are somewhat subject to intraspecific variation in better-documented European species. As such,

these two species occurring during the EECO are possible synonyms. However, although the comparison between *Pd. dufraingi* and *Peradectes* sp. indet. from Mas de Gimel and Azillanet (~MP10, see below) is difficult, pending the discovery of lower molars of the latter, a synonymy between these two EECO taxa cannot be ruled out either (see discussion below). The m3 from Grauves with a tiny entoconid (Figure 2F; MNHN.F.GR10013, as well as the worn m1 MNHN.F.GR10010) is tentatively attributed to *Peradectes* sp. nov. 1 because it is larger and has a much more developed postcingulid (Figure 2E) than *Pd. dufraingi* m3s (see Smith and Smith 2013: fig. 4C, F). Among the selected peradectid species of the Table 3, *Peradectes* sp. nov. 1 and *Pd. dufraingi*, as well as two out of 16 m3 specimens of *Pd. louisi* (for the latter species, see detail in Gernelle et al. 2024a: Online Material 1: table S2), have relatively longer m3 than any other species sampled.

Peradectes sp. nov. 2

Figure 2H-O

Holotype: MNHN.F.PRE26, right m3 (Figure 2L-M).

Locality and age: Prémontré, in Paris Basin (Aisne); ~MP10, early late Ypresian, ~50.3-50.4 Ma (Steurbaut et al. 2016).

Other material: right m1 (MNHN.F.PRE272, MNHN.F.PRE1226), left m2 (MNHN.F.PRE643), left m4 (MNHN.F.SLP29-PR-2934), right m4 (MNHN.F.SLP29-PE-906).

Differential diagnosis: Differs from all European peradectids, except *Pd. russelli*, in being markedly larger (similar in size to *Pd. russelli*). Differs from *Pd. russelli* in the entoconid – hypoconulid notch much higher than the metaconid – entoconid notch on m2, and in the entoconid distinctly lower than the hypoconulid on m3. Differs from all European peradectids, including *Pd. russelli*, in having a notched postcristid on m4.

Description: Only lower molars are known. As in *Pd. russelli*, m1s are much shorter than m2 (~15% shorter; 12.5% shorter on average in *Pd. russelli*, see Gernelle et al. 2024a: 32). As in *Pd. louisi* and *Pd. russelli*, the m2 (MNHN.F.PRE643) is the largest lower molar locus (Table 2). The m3 is not as relatively long as other loci and all *Peradectes* sp. nov. 1 lower molars (i.e., L/W < 1.75; Table 2). The two m4s are respectively as long as and longer than the single known m3 (Table 2). The lingual emargination at the level of the lingual opening of the trigonid becomes deeper from m1 to m4 in occlusal view (Figure 2H, J, L, N; absent on m1, moderate on m2 and m3, and deep on m4). This character was not studied in Gernelle et al. (2024a) but is also displayed by the composite lower molar serie of *Pd. russelli* (Gernelle et al. 2024a: fig. 12n, p, s, u). The distolingual margin of the m2 is straight between the metaconid and the entoconid (Figure 3J), instead of being typically curved in most peradectids. Interestingly, this character varies in *Pd. russelli*. For example, the *Pd. russelli* m2 MNHN.F.CB5098 shows a straight

Table 2. Measurements of lower molars of *Peradectes* sp. nov. 1 and *Peradectes* sp. nov. 2 from Prémontré (MNHN.F.PRE/SLP29; Paris Basin; ~50.3-50.4 Ma) and Grauves (MNHN.F.GR; Paris Basin; MP10).

Species	Specimen	Locus	L (mm)	W (mm)	L/W
Peradectes sp. nov. 1	MNHN.F.PRE694	m1	1.50	0.81	1.85
	MNHN.F.GR10010	m1	1.56	0.79	1.97
	MNHN.F.SLP29-PR-2962	m2	1.59	0.90	1.77
	MNHN.F.GR10013	m3	1.56	0.85	1.84
	MNHN.F.SLP29-PR-2321	m4	1.57	0.80	1.96
Peradectes sp. nov. 2	MNHN.F.PRE272	m1	1.64	0.89	1.84
	MNHN.F.PRE1226	m1	1.63	0.92	1.77
	MNHN.F.PRE643	m2	1.92	1.10	1.75
	MNHN.F.PRE26	m3	1.73	1.04	1.66
	MNHN.F.SLP29-PR-2934	m4	1.71	0.92	1.86
	MNHN.F.SLP29-PE-906	m4	1.84	1.02	1.80

margin between these cuspids, as on MNHN.F.PRE643 (and these specimens exhibit traits found in peradectids such as a relatively long trigonid, lingual opening of the trigonid basin higher than that of the talonid basin, and hypoconid and entoconid subequal in height). The entoconid is much longer than the hypoconulid on m1-m3. For example, see the relative length of the m1 entoconid base (Figure 2I; this is also true for the m1 MNHN.F.PRE1226) compared to that of the m1 entoconid of *Peradectes* sp. nov. 3. The entoconid – hypoconulid notch is much higher than the metaconid – entoconid notch on m2 (Figure 2K), unlike other European peradectids. The entoconid is higher than the hypoconulid on the m2. The hypoconulid becomes relatively labiolingually wider from m1 to m4, so that it occupies half of the distal margin of the talonid on m3 (Figure 2L), and more than half of it on m4 (Figure 2N). The two m4s have a deep notch on the postcristid, unseen in other European species, between the posthypocristid and the labial cristid of the hypoconulid (e.g., Figure 2N). An ectocingulid is present (Figure 2J, L). The cristid obliqua is straight in all loci, except the m4 MNHN.F.SLP29-PE-906. A postcingulid is present on the m4 MNHN.F.SLP29-PR-2934 but is absent on the m4 MNHN.F.SLP29-PE-906. The angle between the cristid obliqua and the postcristid is more open (i.e., ~ 90°) on m4 than on other loci (e.g. Figure 2N). A similar angle of ~90° is recovered between these cristids on the m4s of *Pd. louisi*, *Pd. russelli*, *Pd. dufraingi*, and most likely *Peradectes* sp. nov. 1 (this character has not been mentioned in Gernelle et al. 2024a).

Discussion: Peradectids were unknown in the Prémontré fauna before this work (see Dégremont et al. 1985). Although the metatherians of Prémontré are well-sampled, peradectids represent only 13 out of more than 220 available specimens, the rest belonging to herpetotheriid metatherians (see Chapter 5). The relatively large fragmentary peradectid m4 from Mas de Gimel previously attributed to *Peradectes* cf. *russelli* (UM-MGL-320; Gernelle et al. 2024a; Vianey-Liaud et al. 2024) could rather belong to

Peradectes sp. nov. 2, because only size permits the attribution of the specimen (unfortunately, the m4 postcristid allowing the differentiation of *Peradectes* sp. nov. 2 from *Pd. russelli* is not preserved on UM-MGL-320). *Peradectes louisi* and *Pd. russelli* are markedly distinct in size, a conclusion that have been drawn based on various specimens (Gernelle et al. 2024a: fig. 13, table 4). Here, the confident distinction between two differently-sized peradectid lower molar groups in Prémontré, namely *Peradectes* sp. nov. 1 and *Peradectes* nov. 2 (see Gernelle et al. [2024a: 45-46] for a discussion regarding the co-occurrence of two morphologically similar species), is made possible by the size identity between *Pd. louisi* and *Peradectes* sp. nov. 1 on the one hand, and *Pd. russelli* and *Peradectes* sp. nov. 2 on the other hand.

Table 3. Comparison of length to width ratios (L/W) of m3s of selected peradectid species. The measurements of *Peradectes crocheti*, *Pd. russelli* and *Pd. louisi* are provided by Gernelle et al. (2024a: table 4), those of *Pd. dufraingi* m3s by Smith and Smith (2013). L/W values for *Armintodelphys* m3s have been obtained based on illustrations of Smith and Smith (2013) for type specimens, and also Krishtalka and Stucky (1984). The m3 from Grauves tentatively attributed to *Peradectes* sp. nov. 1 here represents this species. *, calculated ratio of the type specimen.

Species	N	OR L/W	Mean
Peradectes crocheti	5	1.58 - 1.77	1.65
Peradectes russelli	2	1.66 - 1.67	-
Peradectes louisi	16	1.62 - 1.87	1.77
Peradectes dufraingi	2	1.88* - 1.90	1.89
Peradectes sp. nov. 1	1	1.84	-
Peradectes sp. nov. 2	1	1.66*	-
Armintodelphys blacki	1	1.69*	-
Armintodelphys dawsoni	2	1.62*-1.82	1.72

Peradectes sp. nov. 3

Figures 3-4

1992 – ?*Peradectes mutigniensis* Crochet in Legendre et al. p. 418, table 1.

? 2024a – “Unnamed peradectid species” in Gernelle et al. p. 47., fig. 17f.

Holotype: UM-COS-327, fragment of right maxilla with M2-M3 from Cos (Figure 3).

Localities and age: Cos and possibly Vielase, in Quercy (southern France); MP10-MP11 interval, close to the Ypresian-Lutetian transition (Legendre et al. 1992; Godinot et al. 2021; Vianey-Liaud et al. 2022).

Other material: Additional material from Cos: fragment of left hemi-mandible with p2, erupting p3, and m1 (UM-COS-50). The two specimens from Cos were excavated and prepared by D. Vidalenc. Material from Vielase tentatively attributed: left m2 (UM-VIE-106; Gernelle et al. 2024a: fig. 17f).

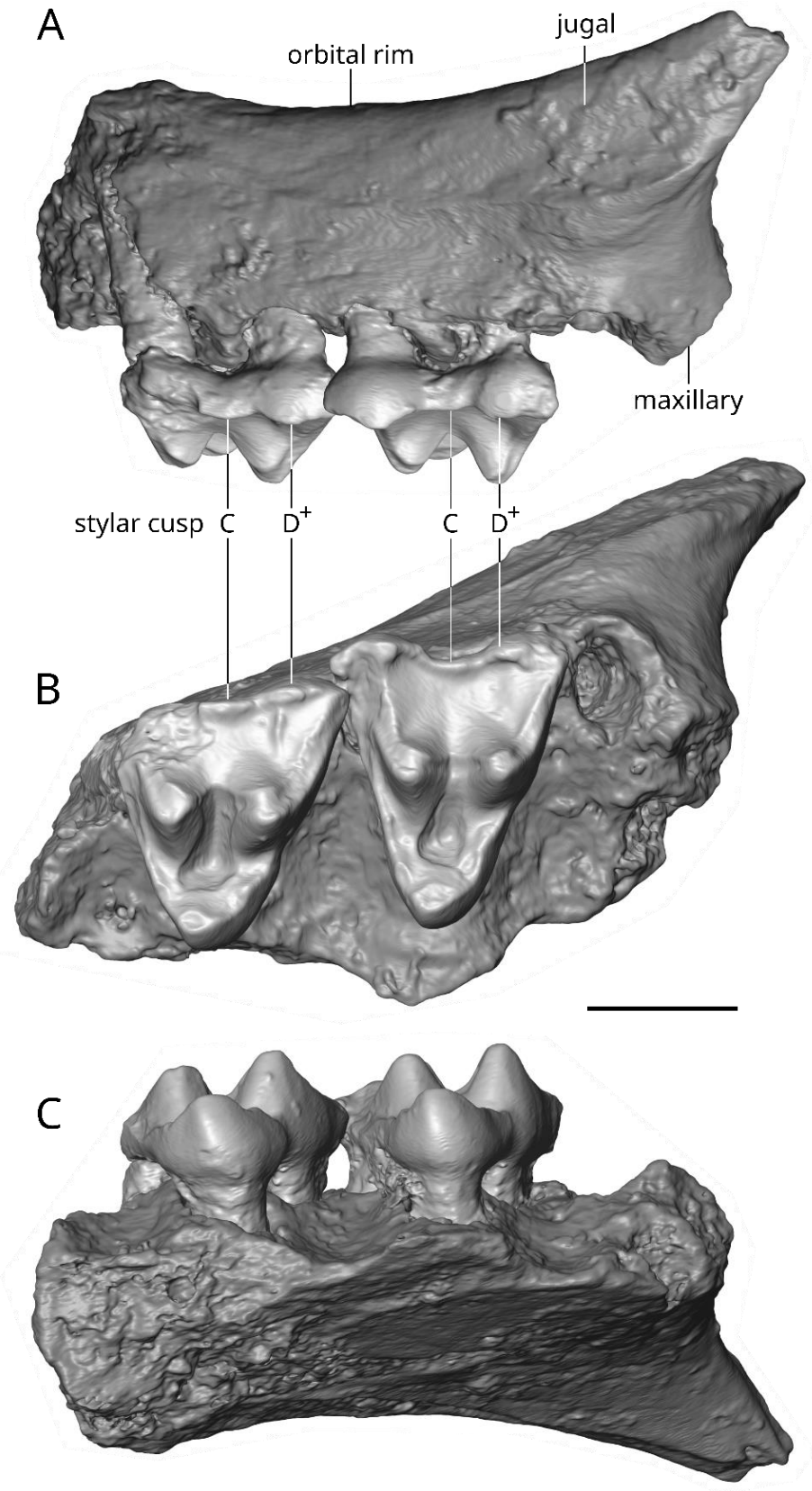

Figure 3. 3D surface model of UM-COS-327, fragment of right maxilla of *Peradectes* sp. nov. 3 from Cos (Quercy; MP10-11 interval), preserving M2-M3, in labial (A), occlusal (B), and lingual (C) reversed views. Abbreviation: D+, stylar cusp D tip more ventral than stylar cusp C tip. Scale bar equals 1 mm.

Differential diagnosis: Peradectid similar in size to the small *Pd. crocheti*, *Pd. louisi*, and *Peradectes* sp. nov. 1. Based on molar features: differs from all other European peradectids in having a relatively mesiodistally shorter entoconid, with a relatively short pre-entocristid. Further differs from *Pd. crocheti* and *Pd. louisi* in the equally labial parastylar and metastylar wings on M3, and possibly in the entoconid as high as the hypoconulid on m2. Further differs from *Pd. crocheti* and *Peradectes* sp. nov. 1 in having stylar cusp C apex much less ventral than stylar cusp D apex on M2 and M3. Further differs from *Pd. louisi* in having stylar cusp D directly labial to the metacone apex on M3.

Description: The maxilla fragment from Cos (UM-COS-327; Figure 3) is well preserved. The lower margin of the orbit is distinct above the upper molars (Figure 3A). In lateral view, above the M3 crown, the maxillary and the jugal are approximately equally wide. The width of the maxillary + jugal between above the M2-M3 roots and the orbital rim is of approximately 1.50 mm (that of *Pd. crocheti* from Palette is only slightly wider). Based on the positions of the preserved M4 roots, the M3 and the M4 were probably subequal in width (Figure 3B), like in other peradectids. The M2 lacks its parastylar wing, including stylar cusps A and B. The mesial side of the parastylar and the distal side of the metastylar wings of the M3 are also partly damaged, including the labial ends of the paracingulum and of the preparacrista, as well as stylar cusp A, for the parstylar wing. Similarly to *Peradectes* sp. nov. 1, the exact length of the postmetacrista cannot be appreciated. The paracone is slightly lower than the metacone, and both of them are higher than the protocone (Figure 3C) and conical (Figure 3B). These features related to the principal cusps, as well as the faint conules, are known in all European peradectids. Contrary to *Peradectes* sp. nov. 1 and similarly to *Pd. louisi*, the stylar cusp C apex is much less ventral than the stylar cusp D apex on M2 and M3 (Figure 3A). However, stylar cusp C is particularly mesiodistally long. Stylar cusp D is distolabial to the metacone on M2, and, contrary to *Pd. louisi*, this stylar cusp is directly labial to the metacone on M3 (Figure 3B). Finally, the parastylar and metastylar wings are equally labial on M3, alike in *Peradectes* sp. nov. 1.

Table 4. Measurements of cheek teeth of *Peradectes* sp. nov. 3 from Cos (UM-COS) and of its possible representative lower molar from Vielase (UM-VIE).

Specimen	Locus	L (mm)	W (mm)	L/W
UM-COS-327	M2	-	1,82	-
	M3	1,6	1,97	0,81
UM-COS-50	p2	1,23	0,59	2,09
	p3	1,36	0,65	2,09
	m1	1,56	0,84	1,86
UM-VIE-106	m2	1,72	0,98	1,76

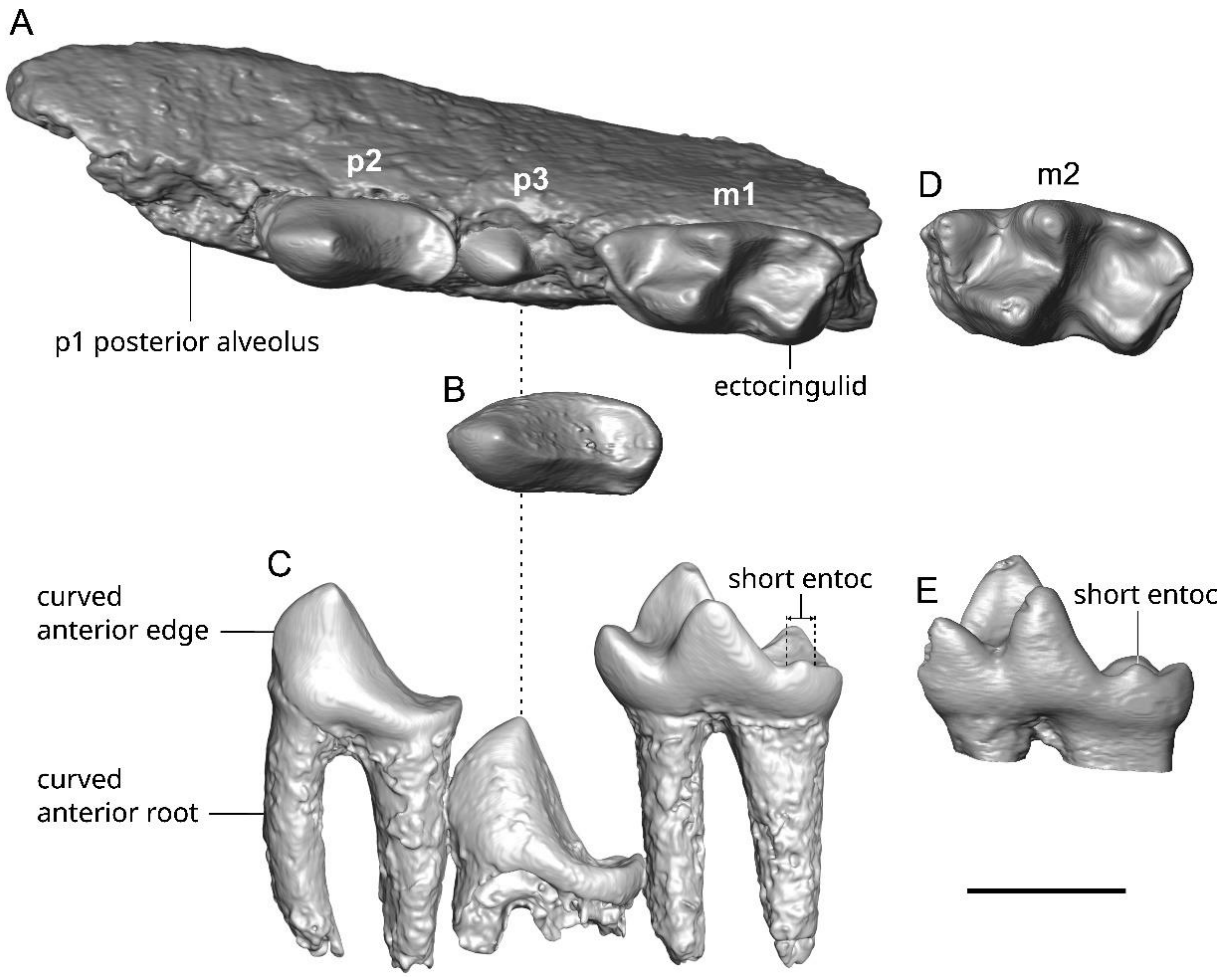

Figure 4. Lower cheek teeth of *Peradectes* sp. nov. 3 from Cos and ?Vielase (Quercy; MP10-11 interval). **A-C**. UM-COS-50, fragment of left hemi-mandible with p1 posterior alveolus and p2-m1, from Cos, in occlusal view (A), occlusal view focused on occlusal view of the p3 numerically isolated from the dentary (B), and in lingual view of p2-m1 numerically isolated from the dentary (C). **D-E**. UM-VIE-106, left m2 from Vielase in occlusal (D) and lingual (E) views. Abbreviation: entoc, entoconid. Scale bar equals 1 mm.

There are no diastemata between the lower premolars of UM-COS-50 (Figure 4A). The posterior root of the p1 is relatively long, more so than in *Pd. crocheti* (Gernelle et al. 2024a: fig. 6a), which is the single other European peradectid with documented dentary and lower premolars. The p3 is erupting (Figure 4A, C). The p3 crown is higher than both the p2 and the m1 crowns (Figure 4C), as in *Pd. crocheti*. The p2 and the p3 are more than two times longer than wide (Table 4), whereas the p3 of *Pd. crocheti* is less than two times longer than wide (Gernelle et al. 2024a: table 2). However, the lower premolars are not blade-like *sensu* Muizon and Ladevèze (2022). As seen in *Pd. crocheti*, the anterior root of (at least) the p2 is curved, whereas the molar roots are straight, and the mesial edge of the lower premolars is curved (Figure 4C; these characters distinguish peradectids from herpetotheriids according to Gernelle et al. 2024a: table 6). The UM-COS-50 p3 has two small distal heel cuspids, of which one is located at the contact between the distal end of the main crisitd and the distal margin of the tooth, in the distolabial corner (Figure 4B-C). The second accessory cuspid is smaller and positioned on the distolingual corner, again alike *Pd.*

crocheti. Similarly to the premolars, the m1 of UM-COS-50 presents an elongated aspect (Figure 4A); as such its L/W ratio value is subequal to the average L/W value for the relatively long *Pd. louisi* m1s (Gernelle et al. 2024a: table 4). The m1 talonid has an ectocingulid (Figure 4A), and the m2 talonid is broken along the lingual flank of the hypoconid. The entoconid of both m1 and m2 is mesiodistally short compared to the hypoconulid (Figure 4C-E), and as such it is relatively shorter than in, for example, *Peradectes* sp. nov. 1 and *Peradectes* sp. nov. 2. The entoconid of the m2 from Vielase (UM-VIE-106) lacks a postentocristid, its short pre-entocristid is not sharp (Figure 4D), and it is as high as the hypoconulid (Figure 4E).

Discussion: Compared to both *Peradectes crocheti* and *Pd. russelli*, the three species *Pd. louisi*, *Pd. dufraingi*, and *Peradectes* sp. nov. 1 unequivocally show a slight relative elongation of lower molars (Gernelle et al. 2024a: table 5; this chapter). This relative elongation seems to be present also in *Peradectes* sp. nov. 3 and, interestingly, it likely also concerns the lower premolars, based on a comparison of p3 proportions between *Peradectes* sp. nov. 3 and *Pd. crocheti* (Table 4 vs Gernelle et al. 2024a: table 2). The tentative grouping of the m2 from Vielase with p2-m1 from Cos, is possible based on the shared relatively short entoconid, unknown in older European peradectid lower molars. The combination of a relatively low and short entoconid represents the most extreme condition so far for the entoconid shrinking trend discussed in Gernelle et al. (2024a). According to Archer (1981: 208), dasyurid (Australidelphia) species occupying arid inland areas have smaller entoconids (often absent) than species occupying areas of higher rainfall. *Peradectes* sp. nov. 3 becomes the oldest European peradectid species formally described. The taxon considered (pending further characterisation) as peradectid-like from Messel (Germany, ~MP11) in various studies (e.g., Morlo et al. 2004; Beck et al. 2022; Gernelle et al. 2024a) is, with little doubt, the last representative of Peradectidae in Europe. In fact, based on available photographs (Kurz and Habersetzer 2004: fig. 5), the p2 anterior root is curved, so is the mesial edge in lower premolar crowns, the lingual opening of the trigonid basin is higher than the lingual opening of the talonid basin in lingual view of lower molars, the entoconid is relatively small (if not totally reduced), and the centrocrista of the upper molars is straight, with conical paracone and metacone. The detailed study of the complete available teeth rows will be needed to precise the systematic status of this taxon and document unpublished dental loci for peradectids as a whole, and must provide insights regarding the controversial dietary type of this family (Peradectidae may not have been frugivorous, contrary to what Kurz [2005] proposed; see discussion in Gernelle et al. 2024b; Chapter 5).

Peradectes sp. indet.

Figure 5

? 1977 – "Une dent de Coulondres (Hérault)" in Crochet p. 132.

? 1980 – *Peradectes* sp. indet in Crochet p. 49, fig. 28.

1986 – *Peradectes* sp. in Marandat p. 199, pl. 1, fig. 2.

2024 – cf. *Peradectes* sp. in Marandat, 1986, in Vianey-Liaud et al. p. 391, fig. 2C.

Localities and age: Southern France localities: Mas de Gimel and possibly Coulondres, both in the Montpellieran area; and Azillanet, in Minervois. ~MP10 reference level. A refined age for the Azillanet mammalian site is approximately between the late Biochron NP12 and the early Biochron NP13 (Noiret et al. 2016; ~50-51 Ma).

Material and measurements: fragment of right M2 from Mas de Gimel (UM-MGL-716; L = 1.48 mm; Vianey-Liaud et al. 2024: fig. 2C), possibly a left M2 from Coulondres (UM-CLR-1; L = 1.74 mm, W = 1.77 mm; Crochet 1980: fig. 28), fragmentary right M3 from Azillanet (UM-AZI6-7; W = 1.79 mm; Marandat 1986: pl. 1, fig. 2).

Remark: The attribution of UM-CLR-1 to this taxon, and even to peradectids, is doubtful (see discussion).

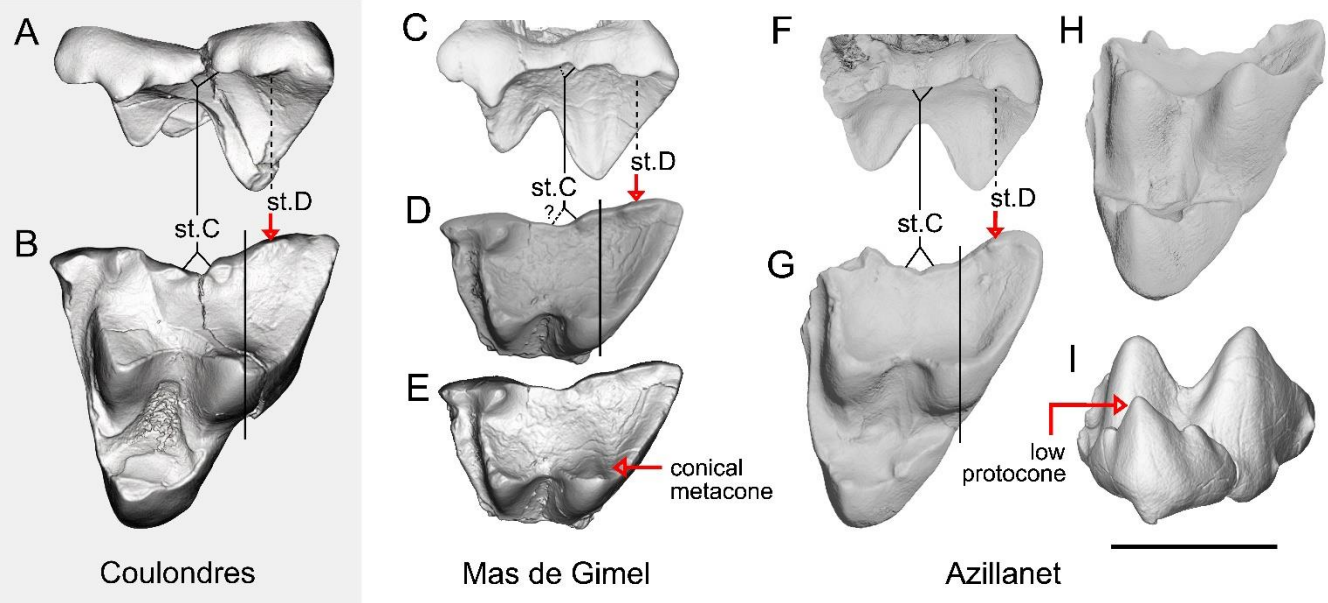

Figure 5. Upper molars of *Peradectes* sp. indet. from ~MP10 localities of southwestern France. **A-B**. UM-CLR-1, left M2 from Coulondres (Montpellieran area) in labial (A) and occlusal (B) views. **C-E**. UM-MGL-716, stylar shelf of right M2 from Mas de Gimel (Montpellier) in labial (C), and occlusal (D-E) reversed views. **F-I**. UM-AZI6-7, right M3 (with fragmented parastylar wing) from Azillanet (Minervois) in labial (F), occlusal (G), occluso-lingual (H), and lingual (I) reversed views. Scale bar equals 1 mm.

Description: Only the M2 specimen from Coulondres is complete (Figure 5A-B). It is almost as long as wide, whereas all better documented European peradectid M2s are relatively more transverse (Figure 1C, Table 1; Gernelle et al. 2024a: table 4). The metaconule is well-developed, with a long postmetaconular

crista, on the M3 (Figure 5G). The protocone is lower than both the paracone and the metacone, especially on the M3 from Azillanet (Figure 5H-I), and is relatively short (Figure 5B, G). The paracone and the metacone are closer in height on UM-AZI6-7 than on the two M2s (Figure 5A, C, F). In particular, although worn, the paracone of the M2 from Coulondres is much smaller than its metacone (Figure 5A). The centrocrista is only slightly labially curved: it is not straight contrary to other peradectids, and not strongly V-shaped contrary to herpetotheriids. This is particularly true for the specimens from Mas de Gimel and Azillanet, but here again, the space between the approximate position of the centrocrista tip and stylar cusp(s) in C position is (are) lower on the Coulondres M2. The paracone and the metacone are mostly triangular in the weakly worn specimens (UM-MGL-716 and UM-AZI6-7; Figure 5D-E, G), but the labial flank of the metacone is slightly curved (Figure 5E). There are two centred stylar cusps in C position at the level of the deepest points of the ectoflexus (Figure 5B, G). While these distinctly represent a doubled stylar cusp C on the M3 from Azillanet, this is less clear for UM-CLR-1, because the distal centred cusp is more closely connected to stylar cusp D via the stylar line (Figure 5B). Stylar cusp D is positioned almost at the labial extremity of the metastylar wing in the three specimens (Figure 5B, D, G). Stylar cusp D distolabial to the metacone apex on M3 (Figure 5G) is otherwise only known in *Pd. louisi* (see Gernelle et al. 2024a: fig. 9f, 10p-o).

Discussion: This peradectid species from the late early Eocene of southwestern France, somewhat defies traditional classifications, in that it represents a slight shift from typical peradectid and herpetotheriid morphologies of the centrocrista. Williamson and Lofgren (2014) argued for possibilities of drastic changes of configuration of the centrocrista in herpetotheriids and peradectids (but see Discussion in Chapter 3). To our knowledge, an intermediate condition for the centrocrista and the paracone and metacone shape (the two characters being probably correlated; see Material and methods in Chapter 3) such as that of the only slightly worn UM-MGL-716 and UM-AZI6-7 has not been documented before for Cenozoic Laurasian marsupialiforms. The discovery of lower molars for this taxon will be crucial to precise its taxonomic status. Despite recent sampling effort (e.g., in Azillanet), no more peradectid specimens from the Minervois and Montpellieran localities have been found so far. Pending further discoveries, it should be noted that the M2 from Mas de Gimel is the shortest known for a peradectid (L = 1.48 mm), and that the smallest peradectid lower molars are those of *Pd. dufraingi* (Smith and Smith 2013), for which no upper molar is reported to date.

Semilandmark-based geometric morphometric analysis

Quantitative analyses of outline shapes of metatherian upper molars allowed the characterisation of subtle dental variation in recent studies. For instance, isolated upper molar loci can be accurately distinguished by employing geometric morphometric methods, even in metatherian taxa in which M1, M2, and M3 are less distinct from each other than in Cenozoic Laurasian marsupialiforms (Sparassodonts in Engelman

and Croft 2022). Here, geometric morphometrics are used in an attempt to explore morphological shape variation of a small sample of isolated molars (17 M3s), each already allocated to a peradectid species, as proposed in Gernelle et al. (2024a: 43). Two-dimensional semilandmark (*sensu* Bookstein 1991) curves of 49 points approximating the complete outline of each peradectid isolated upper molar were digitised on the basis of comparable occlusal images, using the softwares tpsDig 2.31 and tpsUtil 1.83 (Rohlf 2017, 2018). Pictures of right molars were mirrored to facilitate comparison with left molars. Landmark points have not been put on crests, cusps, and conules, because the degree of wear impacting these structures varies a lot between specimens (i.e., there are different wear stages). Semilandmarks were placed using the "draw background curves" tools in tpsDig, and the "resample" function to automatically place equally spaced points. The obtained semilandmark curves have been converted into landmarks in tpsUtil. Procrustes superimposition was performed in MorphoJ (Klingenberg 2011). Finally, also in MorphoJ, the coordinates of each specimen were used to perform principal components analyses (PCA), and shape changes were visualised using wireframe diagrams (Figure 6).

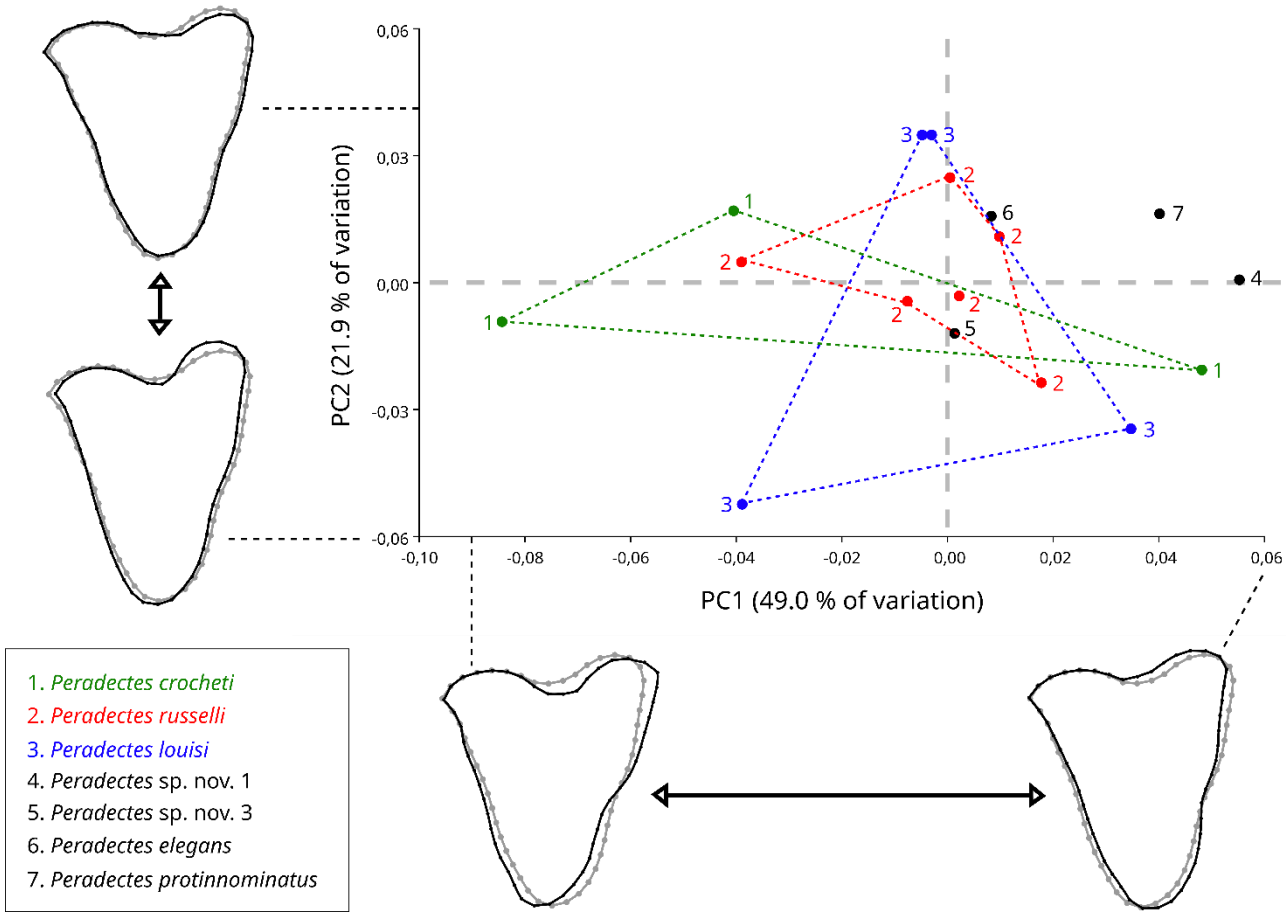

Figure 6. Plot of the first two principal components (PCs) of variation of the peradectid (M3) landmark dataset after Procrustes transformation, along with wireframe diagrams representing the extreme changes in shape on each axis (black outline) relative to the mean shape of the entire sample (grey dotted outline). M3 specimens are plotted by species. Species with more than one M3 specimen included are plotted in colour.

The first two PCs summarise 70.9 % of the total variation (PC1 = 49.0 %, PC2 = 21.9 %). The plot of the first two PCs shows an overlap among the morphospaces of the three species *Pd. crocheti*, *Pd. russelli* and *Pd. louisi* (Figure 6). Positive values on PC1 are correlated with, compared to mean shape and negative PC1 values: (i) a metastylar wing less distally projected relative to the talon, (ii) a distally shallower ectoflexus, and (iii) a talon positioned relatively more distally. Positive values on PC2 are correlated with, compared to mean shape and negative PC2 values: (i) a slightly mesiodistally longer stylar shelf, and (ii) a less labially projected metastylar wing, resulting in a shallower ectoflexus. The three species with a few M3s known show little clustering. The specimens with the most negative values and one of the specimens with the more positive value on PC1 are the *Peradectes crocheti* M3s. The specimens exhibiting the most extreme positive and negative values on PC2 are the *Peradectes louisi* M3s. The *Peradectes russelli* M3s plot in between. There is no correlation between any of the first two PCs and the centroid size. More specimens appear to be needed to propely assess the upper molar outline variation of peradectids. In the current state, it is not possible to conclude if the subtle differences of morphospace occupation observed between species reflect only a part of their intraspecific variation or else consistent differences.

Conclusion

The fossil record of the late early Eocene peradectids is patchy, each of the four species described here being known from no more than two localities, which are either only from the Northern or the Southern French bioprovince. Nevertheless, the late early Eocene is probably the time range of the Ypresian with the most important specific diversity of peradectids (at least four species). Altogether, seven European peradectid species are formally documented during the Ypresian (i.e., not accounting for species in open nomenclature). With the possible exception of the two specimens form Southern France ascribed to *Peradectes* sp. indet., the dental morphology of European peradectids is otherwise extremely conservative throughout the Ypresian. The next chapter will include all peradectid taxa known to date into a broad phylogenetic context (Metatheria).

References

Archer M. 1981. Results of the Archbold Expeditions. No. 104. Systematic revision of the marsupial dasyurid genus *Sminthopsis* Thomas. Bull Am Mus Nat Hist. 168(2):61–224.

Beck RMD, Voss RS, Jansa SA. 2022. Craniodental morphology and phylogeny of marsupials. Bull Am Mus Nat Hist. 457:1–350.

Bookstein FL. 1991. Morphometric Tools for Landmark Data: Geometry and Biology. 1st Edition. Cambridge: Cambridge University Press.

Bronnert C, Metais G. 2023. Early Eocene hippomorph perissodactyls (Mammalia) from the Paris Basin. Geodiversitas. 45(9):277‑326.

Crochet JY. 1977b. Les didelphidés paléogènes holarctiques : historique et tendances évolutives. Geobios Mem spec. 1:127–134.

Crochet JY. 1980. Les marsupiaux du Tertiaire d'Europe. Paris: Edtions Foundation Singer-Polignac.

Dégremont E, Duchaussois F, Hautefeuille F, Laurain M, Louis P, Tétu R. 1985. Paléontologie: découverte d'un gisement du Cuisien tardif à Prémontré (Aisne). Bull Inf Géol Bass Paris. 22(2): 11-18.

Engelman R, Croft D. 2022. Identifying tooth position of isolated teeth of sparassodonts (Mammalia: Metatheria) using geometric morphometrics. Palaeontol Electron. 25(1): a8.

Erfurt J, Sudre J. 1996. Eurodexeinae, eine neue unterfamilie der Artiodactyla (Mammalia) aus dem unter-und mitteleozän Europas. Palaeovertebrata. 25(2-4):371-390.

Escarguel G. 1999. Les rongeurs de l' Eocene inferieur et moyen d'Europe occidentale. Systematique, phylogenie, biochronologie et paleobiogeographie des niveaux reperes MP 7 a MP 14. Palaeovertebrata 28:89‑351.

Gernelle K, Billet G, Gheerbrant E, Godinot M, Marandat B, Ladevèze S, Tabuce R. 2024a. Taxonomy and evolutionary history of peradectids (Metatheria): new data from the early Eocene of France. J Mamm Evol. 31(3):31.

Gernelle K, Godinot M, Marandat B, Téodori D, Ladevèze S, Tabuce R. 2024b [early view online]. Dental morphology evolution in early peratheriines, including a new morphologically cryptic species and findings on the largest early Eocene European metatherian. Hist Biol. https://doi.org/10.1080/08912963.2024.2403602.

Godinot M, Blondel C, Escarguel G, Lézin C, Pélissié T, Tabuce R, Vidalenc D. 2021. Primates and Plesiadapiformes from Cos (Eocene; Quercy, France). Geobios. 66:153-176.

Godinot M, Russell DE, Louis P. 1992. Oldest known nannopithex (primates, omomyiformes) from the early eocene of france. Folia Primatol. 58(1):32-40.

Hand SJ, Sigé B. 2018. A new archaic bat (Chiroptera: Archaeonycteridae) from an Early Eocene forest in the Paris Basin. Hist Biol. 30(1-2):227-236.

Hand SJ, Sigé B, Archer M, Black KH. 2016. An evening bat (Chiroptera: Vespertilionidae) from the late Early Eocene of France, with comments on the antiquity of modern bats. Palaeovertebrata. 40(2):e2.

Klingenberg CP. 2011. MorphoJ: an integrated software package for geometric morphometrics. Molecular Ecology Resources. 11:353-357.

Krishtalka L, Stucky RK. 1984. Middle Eocene marsupials (Mammalia) from northeastern Utah and the mammalian fauna from Powder Wash. Ann Carnegie Mus. 53:31–45.

Kurz C. 2005. Ecomorphology of opossum-like marsupials from the Tertiary of Europe and a comparison with selected taxa. Kaupia. 14:21–26.

Kurz C, Habersetzer J. 2004. Untersuchungen der zahnmorphologie von beutelratten aus Messel mit der mikroröntgenmethode CORR. Cour Forsch-Inst Senckenberg. 252:13–21.

Legendre S, Marandat B, Sigé B, Crochet JY, Godinot M, Hartenberger JL, Sudre J, Vianey-Liaud M, Muratet B, Astruc JG. 1992. La faune de mammifères de Vielase (phosphorites du Quercy, Sud de la France): Preuve paléontologique d'une karstification du Quercy dès l'Eocène inférieur. Neues Jahrb Geol Paläontol. 7:414–428.

Lopez-Torres S, Silcox MT. 2018. The European Paromomyidae (Primates, Mammalia): Taxonomy, phylogeny, and biogeographic implications. J Paleontol 92:920‑937.

Marandat B. 1986. Decouverte d'une faune de micromammiferes d'âge cuisien superieur dans les marno-calcaires d'Agel à Azillanet (Minervois, Hérault). Geol Fr. 2:197–204.

Morlo M, Schaal S, Mayr G, Seiffert C. 2004. An annotated taxonomic list of the Middle Eocene (MP 11) Vertebrata of Messel. Cour Forsch-Inst Senckenberg. 252:95-108.

Muizon C de, Ladevèze S. 2022. New material of *Incadelphys antiquus* (Pucadelphyda, Metatheria, Mammalia) from the early Palaeocene of Bolivia reveals phylogenetic affinities with enigmatic North and South American metatherians. Geodiversitas. 44(22):609–643.

Noiret C, Steurbaut E, Tabuce R, Marandat B, Schnyder J, Storme JY, Yans J. 2016. New bio-chemostratigraphic dating of a unique early sequence from southern Europe results in precise mammalian biochronological tie-points. Newsl Stratigr. 49(3):469–480.

Rohlf FJ. 2017. tpsDig. Stony Brook: Department of Ecology and Evolution, State University of New York at Stony Brook.

Rohlf FJ. 2018. tpsUtil. Stony Brook: Department of Ecology and Evolution, State University of New York at Stony Brook.

Smith R. 2001. Les pantolestides (Mammalia, Pantolesta) de l'Éocene inférieur de Prémontré (Aisne, France). Palaeovertebrata. 30(1-2):11-35.

Smith T, Smith R. 2013. A land micro-mammal fauna from the Early Eocene marine Egem deposits (NP12, Belgium) and the first occurrence of the peradectid marsupial *Armintodelphys* outside North America. Geol Belgica. 16:302–310.

Solé F, Morlo M, Schaal T, Lehmann T. 2021. New hyaenodonts (Mammalia) from the late Ypresian locality of Prémontré (France) support a radiation of the hyaenodonts in Europe already at the end of the early Eocene. Geobios. 66-67(7):119-141.

Solé F, Plateau O, Le Verger K, Phélizon A. 2019. New paroxyclaenid mammals from the early Eocene of the Paris Basin (France) shed light on the origin and evolution of these endemic European cimolestans. J Syst Palaeontol. 17(20):1711-1743.

Steurbaut E, Coninck J de, Van Simaeys S. 2016. Micropalaeontological dating of the Prémontré mammal fauna (MP10, Prémontré Sands, Eeco, early late Ypresian, Paris Basin). Geol Belgica. 19(3-4):273-280.

Vianey-Liaud M, Lihoreau F, Solé F, Gernelle K, Vautrin Q, Bronnert C, Bourget H, Vidalenc D, Tabuce R. 2024. A revision of the late early Eocene mammal faunas from Mas de Gimel and Naples (Montpellier, Southern France) and the description of a new theridomorph rodent. Geodiversitas. 46(10):387-422.

Vianey-Liaud M, Marivaux L. 2021. The beginning of the adaptive radiation of Theridomorpha (Rodentia) in Western Europe: morphological and phylogenetic analyses of early and middle Eocene taxa; implications for systematics. Palaeovertebrata. 44(2):e2.

Vianey-Liaud M, Vidalenc D, Orliac MJ, Maugoust J, Lézin C, Pélissié T. 2022. Rongeurs de la localité éocène de Cos (Tarn-et-Garonne, Quercy, France). Comparaison avec les rongeurs de localités de la transition Éocène inférieur/Éocène moyen. Geodiversitas. 44(26):753-800.

Williamson TE, Lofgren DL. 2014. Late Paleocene (Tiffanian) metatherians from the Goler Formation, California. J Vertebr Paleontol. 34:477‑482.

Chapitre 3. Une histoire évolutive complète des Peradectidae (Metatheria) révélée par un nouveau cadre phylogénétique basé sur la morphologie dentaire

Clearly, the difficulty of separating ancestral from derived patterns has reached a particular zenith in mammal studies with the dentition of the "opossum-like" marsupials

F. S. Szalay 1993: 220

Cette section correspond au manuscrit suivant: **Gernelle K, Ladevèze S, Tabuce R. A comprehensive evolutionary history of Peradectidae (Metatheria) revealed by a new phylogenetic framework based on dental evidence.**

Remarque. Il s'agit d'un projet d'article qui devra être complété. La description des deux nouvelles espèces de péradectidés de Prémontré (Chapitre 2) sera ajoutée à ce manuscrit afin d'illustrer le genre européen à créer, annoncé ici (Chapitre 3). La partie de résultats / discussion portant sur les affinités des Anatolidadelphyidae est ici préliminaire.

Résumé. Les marsupialiformes cénozoïques de l'hémisphère nord évoquant superficiellement les opossums (les Peradectidae et les Herpetotheriidae) sont surtout connus via des molaires tribosphéniques isolées. Leurs histoires évolutives respectives sont floues, ponctuées par plusieurs transformations de caractères subtiles et souvent homoplastiques. Cependant, démêler leurs affinités est essentiel afin de documenter une histoire évolutive complète des Metatheria. Nous introduisons ici une nouvelle matrice de caractères dentaires, avec un échantillonnage sélectif de taxons encadrant la limite Crétacé / Paléogène, pour tenter d'élucider les positions phylogénétiques des péradectidés et des herpetotheriidés dans l'ensemble des métathériens, ainsi que les relations intrafamiliales des péradectidés. Les analyses phylogénétiques ainsi obtenues révèlent que tous les marsupialiformes cénozoïques étudiés se regroupent au sein de leur propre clade, nouvellement identifié comme les Notometatheria, confirmant ainsi que les métathériens ont été sévèrement impactés par l'extinction de masse K-Pg. Deux genres énigmatiques du Paléocène inférieur, *Thylacodon* et *Swaindelphys*, ont des positions cruciales parmi les premiers notométathériens, ce qui nous permet de préciser la divergence rapide des péradectidés et des herpétothériidés en Amérique du Nord. Pour la première fois, un clade Peradectidae inclusif et résolu est retrouvé, et ce dans un cadre spatiotemporel et taxonomique large. Il contient en effet les 22 espèces nords-américaines et européennes attribuées à cette famille à ce jour. La reconstruction de la séquence

d’apparition des caractères dentaires au sein des péradectidés nous conduit à caractériser chaque phase de leur évolution morphologique et à émender leur systématique complexe. À la lumière du cadre phylogénétique nouvellement établi, la révision de tous les spécimens précedemment attribués aux péradectidés provenant d’Amérique du Sud, d’Afrique, et d’Asie, notamment sous le prisme des synapomorphies des péradectidés avérés, démontre que cette famille était très vraisemblablement endémique à l’Amérique du Nord et à l’Europe tout au long de son histoire évolutive. Le rôle clé de l’anatomie dentaire comparée dans la compréhension de l’évolution et ultimement de la paléobiogéographie des métathériens est souligné à travers cette étude, par-dessus tout pour les taxons ayant une morphologie apparamment conservatrice.

A comprehensive evolutionary history of Peradectidae (Metatheria) revealed by a new phylogenetic framework based on dental evidence

Killian Gernelle[1], Sandrine Ladevèze[2], Rodolphe Tabuce[1]

[1] Institut des Sciences de l'Évolution de Montpellier (ISEM, UMR 5554), Univ Montpellier, CNRS, IRD, cc64, Place Eugène Bataillon, F-34095 Montpellier Cedex 05, France

[2] Centre de Recherche en Paléontologie - Paris (CR2P, UMR 7207), Sorbonne Université, Muséum National d'Histoire Naturelle, CNRS, 8 rue Buffon, F-75005, Paris, France

Abstract. Cenozoic Laurasian 'opossum-like' marsupialiforms (Peradectidae and Herpetotheriidae) are mostly known by isolated tribosphenic molars. Their blurred evolutionary histories are marked by several subtle and often homoplastic morphological character transformations. However, disentangling their affinities is essential for documenting a substantial evolutionary history of the Metatheria. Here, we introduce a novel matrix of dental characters, with a selective sampling of taxa focused on after and just before the Cretaceous/Palaeogene boundary, in an attempt to unravel the phylogenetic positions of both the peradectids and herpetotheriids within Metatheria, and the intrafamilial relationships of peradectids. Phylogenetic analyses thus obtained reveal that all Cenozoic marsupialiforms studied assemble into a clade of their own, newly identified as the Notometatheria, thereby confirming that metatherians were severely impacted by the K-Pg mass extinction. The two enigmatic early Paleocene genera *Thylacodon* and *Swaindelphys* have crucial positions among early notometatherians, allowing us to identify the rapid Paleocene North American divergence of peradectids and herpetotheriids. For the first time, an inclusive and resolved monophyletic Peradectidae with the 22 North American and European species allocated to this family to date is found, in a broad spatiotemporal and taxonomic context. The reconstruction of the sequence of appearance of dental features within peradectids leads us to characterize each phase of their morphological evolution and to refine their complex systematics. In light of the new phylogenetic framework established, the revision of all specimens previously ascribed to Peradectidae from South America, Africa, and Asia, notably based on the synapomorphies of unequivocal peradectids, demonstrates that this family was most likely endemic to North America and Europe along its whole evolutionary history. The pivotal role of compared dental anatomy in understanding the evolution and ultimately the palaeobiogeography of metatherians is emphasized throughout this study, above all for taxa with an apparent conservative morphology.

Keywords: Cenozoic, Laurasia, opossum-like, Palaeobiogeography, phylogeny, tribosphenic teeth

Introduction

Paleogene Laurasian 'opossum-like' metatherians have traditionally been allocated by a few molar traits to two dentally-conservative families, namely the Peradectidae and Herpetotheriidae. A limited number of studies formally aimed to position these groups in a phylogeny of metatherians (Horovitz et al., 2009; Ladevèze et al., 2020; Sánchez-Villagra et al., 2007; Williamson et al., 2012). In particular, only Williamson et al. (2012, 2014) intended to assess the question of their affinities with a reasonable number of species in their exhaustive sampling of Cretaceous to Eocene North American metatherians, but the tree topologies recovered were largely unresolved. Their analyses were based only on cheek teeth, that make up the majority, if not the entirety for some taxa, of the metatherian fossil record (e.g., Williamson et al., 2012, 2014). Although somewhat concerning results indicate that morphological matrices, and especially dental characters, may perform poorly in accurately resolving relationships between extant mammal groups (Phillips et al., 2023; Sansom et al., 2017), it is also clear that metatherian dental characters convey an important phylogenetic signal (see Muizon & Ladevèze, 2020: fig. 50).

Numerous difficulties in establishing the polarity of dental characters of Peradectidae and Herpetotheriidae have long been stressed (Szalay, 1993: 220). They are likely due to predominant dental polymorphism, recurrent homoplasies, and the low disparity of marsupialiform tribosphenic molars (e.g., Szalay, 1993: fig. 15.2; Williamson et al., 2014: fig. 5). These factors, coupled with only subtle morphological changes between taxa, imply a scarcity of synapomorphies, complicating efforts to distinguish a sufficient number of independent characters for use in intrafamilial and especially broader scale phylogenetic reconstructions (e.g., Beck, 2023; Gernelle et al., 2024a, 2024b). Consequently, neither the modalities of emergence of the Peradectidae and Herpetotheriidae, nor their intrafamilial relationships and their existence as natural groups in the whole Metatheria have been confidently assessed so far. Even the positioning of peradectids, often scored as a single terminal taxon, produced conflicting results (e.g., Fig. 1; see, for the more recent tree topologies by distinct authors: Beck et al., 2022: fig. 33; Carneiro et al., 2024a; Engelman et al., 2020; Muizon & Ladevèze, 2022; Wilson et al., 2016).

The starting point of this work has been the recent exhaustive taxonomic revision of European peradectids, followed by a tentative resolution of intrafamilial relationships of all late Paleocene to middle Eocene European peradectids (Gernelle et al., 2024a). In this study, we intended to build a phylogenetic framework for the purpose of a reappraisal of the evolution of the 'opossum-like' marsupialiforms through the best defined and less redundant of all available dental features. We thus chose to score a wide array of peradectid/herpetotheriid taxa including all unequivocal peradecids, together with some of their unconsensual earliest representatives (e.g., the Paleocene genera *Thylacodon* Matthew and Granger, 1921, and *Swaindelphys* Johanson, 1996), Cretaceous marsupialiforms, and Marsupialia species. To our knowledge, no such sampling has ever been conducted before. It leads us to address key questions regarding the evolutionary history of early Cenozoic marsupialiforms and

especially Peradectidae. In fact, the last aim has been to infer a morphological characterisation of Peradectidae, allowing to discuss the spatio-temporally diverse putative occurrences of the family through comparative anatomy in a phylogenetic context.

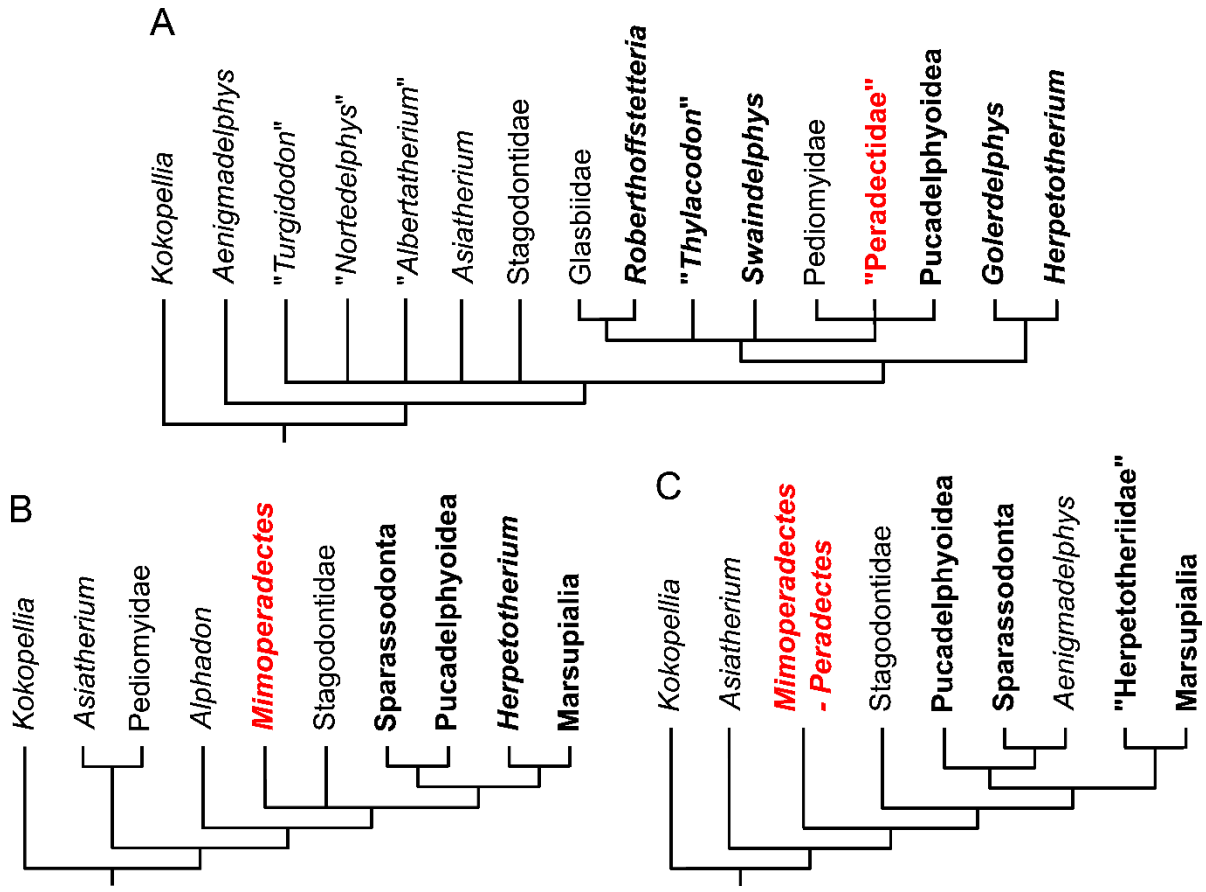

Figure 1. Simplified strict consensus tree topologies yielded by the equally weighted maximum parsimony analyses of Williamson et al. (2014) (A), Engelman et al. (2020) (B), and Muizon and Ladevèze (2022) (C). Only taxa also sampled in this study are considered. Cenozoic taxa are in bold text. Peradectid representatives in the analyses are highlighted in bold red text. Quotation marks indicate that a given taxon has not been recovered as monophyletic by the analysis.

Institutional and locality abbreviations

IRSNB-M, mammal collection of the Royal Belgium Institute of Natural Sciences; **IVPP**, Institute of Vertebrate Paleontology and Paleoanthropology, Chinese Academy of Sciences; **LU**, Laguna Umayo; **MHN.AIX.PV.**, Muséum d'Histoire Naturelle d'Aix en Provence, France, collection from Palette; **MNHN.F.,** fossil collection of the Muséum National d'Histoire Naturelle, Paris, France; **MNHN.F.GL**, Sables de Brasles; **MNHN.F.MU**, Mutigny; **NMMNH**, New Mexico Museum of Natural History and Science, Albuquerque, USA; **OMNH**, Oklahoma Museum of Natural History, Norman, USA; **TF**, Department of Mineral Resources, Bangkok; **UM-**, Université de Montpellier, France; **UM-AV-SK**, Avenay, Schmidt-Kittler collection; **UM-EY**, Cartographic Service, National Mining Bureau, Tunisia;

UM-FNR2, Fournes 2; **YPFB Pal**, paleontology collection of the Yacimientos Petroleros y Fiscales de Bolivia.

Other abbreviations

APU-M/apu-m, antepenultimate molar; **BI**, Bremer index; **BPP**, Bayesian posterior probabilities; **CI**, consistency index; **EECO**, Early Eocene Climatic Optimum; **ETM**, Eocene Thermal Maximum; **K-Pg**, Cretaceous-Paleogene; **L**, length; **MP**, Mammal Palaeogene reference level (BiochroM'97, 1997); **MPT**, most parsimonious tree; **MX**, Xth upper molar; **mX**, Xth lower molar; **NALMA**, North American land mammal ages; **PETM**, Paleocene-Eocene Thermal Maximum; **PU-M/pu-m**, penultimate molar; **PX**, Xth upper premolar; **pX**, Xth lower premolar; **RI**, retention index; **SALMA**, South American land mammal ages; **U-M/u-m**, ultimate molar; **US**, unambiguous synapomorphy; **W**, width.

Material and methods

Taxa and characters of the initial set of phylogenetic analyses

The cladistic analyses of Williamson et al. (2012, 2014), including the largest sample of Cretaceous and Paleogene metatherian taxa, and necessarily based on dental features only, exhibits more taxa than dental characters (95 taxa and 83 characters in Williamson et al., 2014). Here, we intended to always keep a number of characters at least twice the number of taxa, in order to achieve better tree topology resolution (e.g., Bremer et al., 1999). The character-taxon matrix on which the initial analyses (see Table 1) were conducted hence contains 42 taxa and 98 dental characters. Because 26 of the taxa included are documented only by teeth, characters relative to other anatomical partitions were not scored, in order to avoid a large number of missing scores, and thereby potential inaccurate results (e.g., Wiens, 2006). We also did not score taxa known by a single molar specimen, although some of them may be of important palaeobiogeographic significance (e.g., *Maastrichtidelphys* Martin et al., 2005). Characters were polarized with the outgroup comparison method (Watrous & Wheeler, 1981), using the two Cretaceous eutherian species, *Prokennalestes minor* Kielan-Jaworowska and Dashzeveg, 1989, and *Maelestes gobiensis* Wible et al., 2007 (taxon data used for coding are indicated in Supplemental material 1). *Deltatheridium pretrituberculare* Gregory and Simpson, 1926, represents the non-marsupialiform metatherians (Deltatheroida) in our analyses. Because "North America was a centre of metatherian origins and diversification during the Cretaceous, and it was the ancestral area for Palaeocene lineages" (Williamson et al., 2012: 647) we composed a branching group (sensu Antoine, 2002: 32) of Late Cretaceous, predominantly North American, stem-marsupialiforms, and sampled taxa that occurred around the K-Pg mass extinction. This branching group is composed of nine Cretaceous species: *Kokopellia juddi* Cifelli, 1993; *Asiatherium reshetovi* Trofimov and Szalay, 1994; *Aenigmadelphys*

archeri Cifelli and Johanson, 1994; *Albertatherium* Fox, 1971; *Turgidodon rhaister* (Clemens, 1966); *Nortedelphys jasoni* (Storer, 1991); *Didelphodon vorax* Marsh, 1889; *Pediomys elegans* Marsh, 1889; and *Glasbius intricatus* Clemens, 1966. Given the assertion of Williamson and collaborators above, among the early Paleocene taxa scored are the enigmatic *Thylacodon*, *Swaindelphys* (represented by *S. encinensis* Williamson and Taylor, 2011), which are of uncertain affinities (e.g., Johanson, 1996; Williamson et al., 2012), and the putative herpetotheriid *Golerdelphys* Williamson and Lofgren, 2014. Although *Albertatherium* and *Thylacodon* were not recovered as monophyletic by Williamson et al. (2012, 2014) (see Fig. 1A), they have been scored as such here, following Johanson (1994) and Williamson et al. (2012: 634-635). The 12 peradectid taxa of the matrix from Gernelle et al. (2024a) are included, with *Mimoperadectes labrus* Bown and Rose, 1979, replaced by *Mimoperadectes* spp. (the monophyly of *Mimoperadectes* has been confirmed by the analyses of Williamson et al. [2012, 2014]). Furthermore, *Peradectes minor* Clemens, 2006, and *Peradectes coprexeches* Williamson and Taylor, 2011, have also been added to complete the sampling of Paleocene peradectids. Unequivocal herpetotheriids are represented by the earliest known peratheriine (= earliest European herpetotheriid sensu Ladevèze et al., 2020), *Peratherium constans* Teilhard de Chardin, 1927, and the two herpetotheriines (= North American herpetotheriids sensu Ladevèze et al., 2020) *Herpetotherium edwardi* (Gazin, 1952) and *Herpetotherium fugax* Cope, 1873 (the type species of herpetotheriids). Finally, a total of ten Southern Hemisphere species were scored. Four of them are from the Paleocene Tiupampa fauna (*Pucadelphys andinus* Marshall and Muizon, 1988; *Incadelphys antiquus* Marshall and Muizon, 1988; *Mayulestes ferox* Muizon, 1998; and *Roberthoffstetteria nationalgeographica* Marshall et al., 1983), one is from the early Eocene Itaborai fauna (*Derorhynchus singularis* Paula Couto, 1952), and five are extant marsupials (two australidelphians and three didelphids, see Supplemental material 1). The definitions of the high-rank taxa which are used in the results section (e.g., Notometatheria, Peradectidae, Peradectinae, and Peradectini) are provided in the discussion section.

The updated therian dental nomenclature of Gernelle et al. (2024a: fig. 2) has been employed. Compared with the characters used by Williamson et al. (2014), Muizon and Ladevèze (2022), and Gernelle et al. (2024a), 27 new characters have been defined, among which eight concern premolars, eleven concern lower molars, and eight concern upper molars. They are listed, and illustrated when needed, in Supplemental material 2, along with other selected dental characters, and sometimes modified, from the three studies cited above. Altogether, among the 98 dental characters, two concern the canines, 15 concern the premolars, 39 concern specifically the lower molars, and 41 concern specifically the upper molars. No changes have been made to the content of the cells already present in the character-taxon matrix of Gernelle et al. (2024a), except for the characters which have had a slightly modified definition (see indications in Supplemental material 2). Dental loci (except M1/m1) are indicated by their position relative to the ultimate molar (i.e., antepenultimate, penultimate, or ultimate molar) because the outgroup

eutherian taxa have a dental formula assumed distinct from that of metatherians (but see O'Leary et al., 2013: fig. 3A). Here, upper/lower premolars are labelled as P1/p1 to P3/p3 and upper/lower molars as M1/m1 to M4/m4. The numbers in superscript used after character numbers in the main text and figures denote the character states. The characters with a retention index (RI) value ≥ 0.75 are indicated in bold text.

Table 1. Summary of all additional phylogenetic analyses conducted, with detailed changes related to the characters and taxa scored. Abbreviations: Bay., Bayesian; cons., consensus; MP, maximum parsimony; MPT, most parsimonious tree; M-R, majority-rule.

Analyses sets	Changes compared with the initial analysis	Trees figured (yielded by parsimony analysis when not precised)
Initial	42 taxa, 98 characters (4 ordered)	Fig. 3, strict cons., MP analysis; Fig. 4, M-R (50%), Bay. analysis
1	All characters unordered	Fig. S1, **A**. strict cons., **B**. majority-rule (50%)
2	Characters 19, 20, 26, 45, 46, 57, 59 (with threshold discretization or gap coding) deleted	Fig. S2, **A**. strict cons., **B**. majority-rule (50%)
3	Late early Eocene European peradectids (*Peradectes* sp. nov. 1/2/3) added	Fig. S3, strict cons., **A**. *Pd*. sp. nov. 2 added, **B**. *Pd*. sp. nov. 1/2/3 added, **C**. *Pd*. sp. nov. 1/2/3 added + characters 19, 20, 26, 45, 46, 57, 59 deleted
4	*Didelphidectes* and *Nanodelphys* added	Supplemental material 5 — Fig. S4, **A.** strict cons., **B.** majority-rule (50%), **C**. majority-rule (50%) + characters 19, 20, 26, 45, 46, 57, 59 deleted
5	*Djarthia murgonensis* added	Fig. S5, **A**. strict cons., **B**. majority-rule (50%)
6	*Orhaniyeia nauta* added	Fig. S6, **A**. strict cons., **B**. downweighted homoplastic characters (k=12), single MPT
7	*Peradectes* sp. nov. 1/2, *Djarthia*, *Didelphidectes* and *Nanodelphys* added, characters 19, 20, 26, 45, 46, 57, 59 deleted	Fig. S7, Bayesian analysis

Preliminary identification of correlations between dental characters

A recent study has shown that marsupials are among the extant mammals (with primates) with the least independent dental characters (Brocklehurst & Benevento, 2020). Cases of full character redundancy (i.e., non-independent characters) have been circumvented here by selecting characters that convey different morphological information (i.e., their codings are not identical) prior to the analyses (note that Herrera and Davalos [2016] presented a script to identify characters that show identical scorings, which is particularly useful for large datasets but has not been used here). This procedure has been employed in other phylogenetic studies focused on the dentition of mammals, primarily to prevent potential full redundancy between the characters of the upper and lower molars, which are functionally dependent across much of their occlusal surface (e.g., Marivaux et al., 2004; see discussion in Gernelle et al., 2024b).

Such strong trait correlations may not only occur between these two anatomical subpartitions, but also between structures of a given molar. Two examples based on metatherian molars are presented hereafter (Fig. 2). For the lower molars, the position of the mesial end of the cristid obliqua and the relative width of the hypoflexid were regarded as independent characters in Muizon and Ladevèze (2022, their characters 69 and 78, respectively). In numerous Cretaceous stem-marsupialiforms such as *Aenigmadelphys*, the mesial end of the cristid obliqua lies beneath or lingual to the carnassial notch of the protocristid (close to the midpoint of the trigonid's labiolingual width or lingually to it in all metatherians), and the hypoflexid, spanning the portion of the molar between the cristid obliqua and the labialmost margin of the tooth, is relatively wide (Fig. 2A). In marsupialiform taxa, such as peradectids, in which the cristid obliqua is labial to the carnassial notch of the protocristid, the hypoflexid is expected to be necessarily narrower (Fig. 2A-B). A fortiori, (i) the scoring of Muizon and Ladevèze (2022: supplementary data) for these characters provides almost no different morphological information, and our attempt to score them independently led to strictly identical information, (ii) even for extant marsupials: for instance, *Perameles* Geoffroy, 1804, is distinct from *Dromiciops* Thomas, 1894, and didelphids by exhibiting both a cristid obliqua beneath or lingual to the protocristid notch and a wide hypoflexid on m2-m3 (Travouillon, 2016: fig. 8A, C, E). Given our assumption that morphological characters need to be equally weighted and as independent as possible, we define a composite character (n°37 in our character-taxon matrix) termed 'Position of mesial end of cristid obliqua on apu-m and pu-m + hypoflexid relative width', with the character states illustrated in Fig. 2A-B (see full description in Supplemental material 2). As for the upper molars, the shape of the paracone and metacone, as well as the morphology of the centrocrista, were considered independent (characters 38 and 41, respectively, in Muizon and Ladevèze, 2022). However, (i) the morphology of the centrocrista could affect a whole character complex in the upper molar morphology (Goin, 2003: 35), and (ii) we have remarked that in M1s to M3s with a strictly straight centrocrista, such as those of peradectids, the paracone and the metacone are conical, their labial edge being almost as convex as their lingual edge (Fig. 2C), whereas M1s to M3s with a V-shaped centrocrista (typically those of the herpetotheriids among Laurasian marsupialiforms) have triangular paracone and metacone, with no convex labial edge (Fig. 2D). Although the correlation between these two characters is less obvious than in the previous case, their scoring by Muizon and Ladevèze (2022: supplementary data) again carries almost no distinct information. According to these authors, only the australidelphian *Dromiciops* (among the selected taxa) differs from this pattern, in combining a straight centrocrista and triangular paracone and metacone. However, *Dromiciops* actually has conical paracone and metacone (pers. obs. KG, including one specimen also scored in Muizon and Ladevèze [2022], see Supplemental material 1). For these reasons, we propose the composite upper molar character (n°80 in our character-taxon matrix) 'Centrocrista morphology + shape of paracone and metacone', of which the character states are illustrated in Fig. 2C-D (see full description in Supplemental material 2), in order to prevent repetitive scoring.

We paid attention to avoid cases of similar characters being repeatedly scored at successive molar loci since these may highly covary (serial homologs, see Billet and Bardin, 2019). Only four pairs of characters from our dataset possibly represent serial homologs: the relative length of the trigonid, compared with that of the talonid, on m2/m3 (character 24) and m4 (character 25; Gernelle et al., 2024a: Online Resource 3, fig. S2); the position of the mesial end of the cristid obliqua on m2/m3 (character 37) and m4 (character 38), already signaled in Gernelle et al. (2024a: 9); the angle value between the cristid obliqua and the postcristid, on m1/m2/m3 (character 45) and m4 (character 46; Supplemental material 2: Fig. S16); and the presence/absence of ectoflexus on M1 (character 95; Gernelle et al., 2024a: Online Resource 3, fig. S11) and M4 (character 96; Supplemental material 2: Fig. S26). However, they were retained in the analyses because their scorings differ greatly (see Marivaux et al., 2004).

There are also several examples, in our matrix, of correlated characters that may convey similar information. The most obvious cases of information redundancy are listed hereafter, although they are preserved as independent characters because, again, their scoring partly differ. Three sets of upper and/or lower molar characters with some degree of correlations must be signaled. (i) The protocone length (character 61) and the width of the talonid relative to the trigonid (character 23) may both depend on the relative size of the protocone/talonid functional complex, as depicted by Gernelle et al. (2024b). (ii) The small size of the last upper and lower molars of several taxa, such as *Glasbius* (Archibald, 1982: fig. 45), *Deltatheridium* (e.g., Rougier et al., 1998), and *Dromiciops*, are necessarily (at least partly) correlated and may constrain the scorings of the characters 21 (relative length of m4), 60 (relative width of M4), and 76 (relative length of the preparacrista on M4). For this reason, the latter has been scored as inapplicable in *Deltatheridium* and *Dromiciops*. Finally, and perhaps not exclusively, (iii) the height of the metaconid has been estimated relative to the heights of the paraconid (character 31), protoconid (character 33), and entoconid (character 57).

Phylogenetic reconstruction procedures

The new character-taxon matrix (Supplemental material 3) was edited with Mesquite v. 3.61 (Maddison & Maddison, 2019). Cladistic analyses, using the maximum parsimony criterion, were performed with PAUP* v. 4.0a169 (Swofford, 2002), through the Heuristic search method, with a random step-wise addition (1000 replications with randomized input order of taxa) and tree-bisection-reconnection (TBR) branch swapping options. Intraspecific variation was accounted as polymorphic states in PAUP* (noted ‘x&y’ in Mesquite and ‘(xy)’ in PAUP*). Polymorphic states were treated distinctly from uncertain states (noted ‘x/y’ in Mesquite and ‘{xy}’ in PAUP*) by PAUP* (‘msTaxa=polymorph’), a setting which may affect tree length but not tree topology (Serra Silva, 2024: 7). Non-applicable character states have been coded ‘-’ in Mesquite. The robustness of each clade was mostly evaluated with Bremer indices (BI, Bremer, 1994), going up to five additional steps, in addition to Bootstrap percentages obtained by 1000

replicates in the initial cladistic analysis. The dental synapomorphies of each taxon as optimized by parsimony (with AccTran optimisation) on the strict consensus issued from the initial cladistic analysis are listed in Supplemental material 4, together with a table of consistency index (CI) and retention index (RI) values of each character.

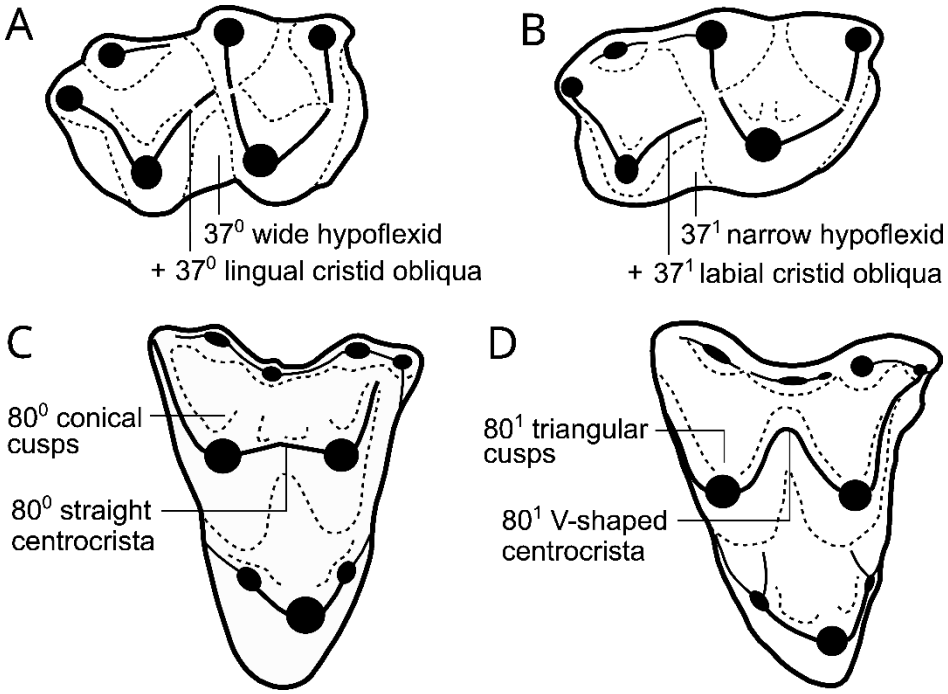

Figure 2. Composite molar characters defined in this study, illustrated on interpretative drawings (in occlusal view) of sampled marsupialiform taxa. **A-B.** States of the character 37, concerning m2 and m3. **A.** State 0, wide hypoflexid + cristid obliqua beneath or lingual to the protocristid notch, illustrated on the m3 of *Aenigmadelphys* Cifelli and Johanson, 1994 (OMNH 20531; based on Muizon & Ladevèze, 2022: fig. 12B). **B.** State 1, narrow hypoflexid + cristid obliqua labial to the protocristid notch, illustrated on an m3 of *Peradectes russelli* Crochet, 1979 (MNHN.F.GL410). **C-D.** States of the character 80, concerning upper molars. **C.** State 0, straight centrocrista + conical paracone and metacone, illustrated on an M3 of *Peradectes minor* Clemens, 2006 (NMMNH P-47293; based on Williamson et al., 2012: fig. 7D). **D.** State 1, V-shaped centrocrista + triangular paracone and metacone, illustrated on an M3 of *Peratherium constans* Teilhard de Chardin, 1927 (IRSNB-M-2030; after Gernelle et al., 2024b).

A Bayesian analysis (the second analysis of the initial set; Table 1) using a standard, undated Bayesian approach was conducted using MrBayes v. 3.2.7a (Ronquist et al., 2012) and the implemented 'Mkv' model for discrete morphological characters (Lewis, 2001). Note that all cases of polymorphism and uncertainty may be treated as missing data (i.e., '?') in MrBayes (v. 3.2.7a), which would represent an important loss of dental scores (Beck et al., 2023: 3, 13; Marivaux et al., 2023: Supporting Information Appendix, Text S2), although polymorphism is treated as uncertainty (and not missing data) according to the most recent version of the MrBayes manual (https://github.com/NBISweden/MrBayes/blob/develop/doc/manual/Manual_MrBayes_v3.2.pdf; see also Serra Silva, 2024: 7). A gamma distribution was selected to model rate variation across characters

('lset rates=gamma'). Parsimony-informative characters, but not constant characters and autapomorphies, were scored ('lset coding=informative'). The latter correction, informing that the matrix is restricted to parsimony-informative characters, is likely implemented in MrBayes assuming only binary characters (Matzke & Irmis, 2018). Multistate characters representing possible morphoclines (see above) have been ordered ('ctype ordered: 23 24 37 82'). Two independent runs were performed simultaneously with four Markov Chain Monte Carlo (MCMC) chains for 10 million generations, sampled every 1000 generations, and removing the first 25% of the samples as burn-in. At the end of the analyses, the deviation of split frequencies was below 0.01 and the potential scale reduction factor (PSRF) value was of 1.0. A 50 % majority rule consensus was computed at the end of the analyses. The Bayesian posterior probabilities (BPP) > 50% are given as support values for each node.

The temporal extension of each taxon (converted when needed to absolute ages using data from Speijer et al. [2020] for Cenozoic occurrences; see detail and procedure for Cretaceous occurrences in Supplemental material 1) were used to temporally calibrate phylogenetic trees yielded by the initial set of two analyses (see Table 1) by constraining the age of each branch, following the 'strict' approach of Loewen et al. (2013: 12), in which a minimal length (here ~0.2 Ma) is assigned to unconstrained branches. This procedure may result in series of divergences concentrated in short time intervals (e.g., Loewen et al., 2013: fig. 8). Estimated ages of the first divergence within Theria (> 120 Ma) and Marsupialia have been accounted for (see summary in Beck, 2023: table 2). The intraclade divergence age retained here for Marsupialia corresponds to the minimum bound of 54.7 Ma found by Beck et al. (2022), and to the K-Ar date for the Tingamarra Local Fauna (Australia, ~54.6 Ma; Godthelp et al., 1992) that yielded one of the oldest probable crown-clade marsupials currently known, *Djarthia murgonensis* Godthelp et al., 1999 (Beck, 2017b; Eldridge et al., 2019).

Subsequent phylogenetic analyses

A reasonable assumption regarding the treatment of multistate morphological characters must be to consider them as ordered (= additive) only when the states form an hypothesized morphocline (e.g., Grand et al., 2013). As for eutherian mammals, character ordering affected the placement of various taxa in phylogenetic analyses performed without molecular scaffold (Brady et al., 2024). Thus, four characters that have been identified as representing morphoclines by Muizon and Ladevèze (2022: 611, and references therein) have been set as ordered, namely: 23 (trigonid vs talonid width on pu-m), 24 (trigonid vs talonid length on apu-m or pu-m), 37 (composite character; on apu-m and pu-m, relative position of cristid obliqua mesial end + relative width of hypoflexid), and 82 (relative height of paracone vs metacone on APU-M and PU-M). Alternatively, these characters have been set as unordered in the subsequent analysis n°1 (see Table 1). Seven molar characters introduced in this study or in Gernelle et al. (2024a) have their two to three states defined based on a threshold discretization (for binary characters)

or gap coding procedure (for three state characters). These methods employ comparisons of taxon-dependent ranges of qualitatively described features (length, length/width ratios, height, and angle values in our dataset), which are necessarily subjective and imply a loss of information (e.g., Swiderski et al., 1998; Darlu et al., 2019: 148, and references therein). For this reason, some of the subsequent analyses have been run without these characters (in the analyses sets n°2-4, 7; see Table 1), which mainly concern lower molars, namely: 19 (m1 relative length), 20 (pu-m proportions), 26 (protoconid relative height on pu-m; Supplemental material 2: Fig. S8), 45 (angle cristid obliqua/postcristid, except on u-m), 46 (angle cristid obliqua/postcristid on u-m; Supplemental material 2: Fig. S16) (note that characters 45 and 46 also probably represent serial homologs; see above), 57 (relative height of entoconid compared with metaconid on pu-m), and 59 (disparity of length/width ratios between APU-M and PU-M).

We aimed to score all undisputed Peradectidae (i.e., early Paleocene to early Oligocene North American and European taxa). In order to test the effects of the inclusion of the latest European and North American peradectids to the initial dataset (with their addition to the initial matrix, all unequivocal peradectid taxa known so far are represented), these have been added only in some subsequent analyses (Table 1). The late early Eocene *Peradectes* sp. nov. 1, *Peradectes* sp. nov. 2, and *Peradectes* sp. nov. 3 from Western Europe (see Chapter 2) have been added in the third set of analyses (Table 1). The monotypic late Eocene *Didelphidectes* Hough, 1961, and the early Oligocene *Nanodelphys* McGrew, 1937, have been added in the fourth set of analyses (Table 1). The australidelphian *Djarthia murgonensis*, has been included in the fifth analysis set (Table 1) to determine whether the monophyly of Marsupialia—and the probable australidelphian status of *Djarthia* (e.g., Beck, 2012)—can be recovered on the basis of dental evidence when early Eocene dentally conservative crown-group marsupials are added. In the sixth set of phylogenetic analyses, the anatoliadelphyid *Orhaniyeia nauta* Métais et al., 2018, has been scored to test the disputed phylogenetic position of Anatoliadelphyidae (e.g., Beard et al., 2023; Beck, 2023; Maga & Beck, 2017; Métais et al., 2018), particularly because they have been suspected to emerge from a "peradectid"-like ancestor (Beck, 2023; Maga & Beck, 2017). Phylogenetic analyses yielded different results regarding the affinities of anatoliadelphyids likely because the taxon and character sampling differs between studies (Beck, 2023). Here, we add a new different sampling context, with an unpublished combination of characters, numerous 'opossum-like' metatherians, and a few bunodont taxa. *Orhaniyeia nauta* has been chosen to represent this family over the single other known anatoliadelphyid (*Anatoliadelphys maasae* Maga & Beck, 2017), because its molar morphology has been assumed more primitive (i.e., less autapomorphic) than that of *Anatoliadelphys* (Beard et al., 2023). Finally, a Bayesian analysis (seventh set of analyses) differs from the one of the initial set of phylogenetic analyses in including *Peradectes* sp. nov. 1, *Peradectes* sp. nov. 2, *Didelphidectes*, and *Nanodelphys*, and in deleting the seven characters implying threshold discretisation or gap coding (Table 1).

Results of phylogenetic analyses

The results related to the strict consensus tree yielded by the initial maximum parsimony analysis (Fig. 3) and the 50% majority-rule consensus tree from the initial Bayesian analysis (Fig. 4) are mainly detailed here. We refer when needed to the results of the supernumerary phylogenetic analyses (Table 1). The heuristic search of the maximum parsimony analysis yielded six most-parsimonious trees (MPTs) of 593 steps each, with a consistency index (CI) of 0.368 and a retention index (RI) of 0.584, which are indicative of high level of homoplasy in the dental characters used. Whilst the CI value is negatively correlated to the number of taxa (Archie, 1989), a RI value slightly above 0.5 indicates that slightly more than half of the similarities coded in the data matrix do not correspond to homoplasy (e.g., Farris, 1989). Consensus trees from the initial analyses are well resolved. Only two characters are not parsimony-informative for resolving relationships between the taxa of the strongly supported (Bremer index [BI] > 5) ingroup (Metatheria), namely the number of fully molariform definitive dental loci (character 18) and the presence/absence of a mesiolingual paraconid keel (character 30). *Deltatheridium* (Deltatheroida) is the earliest diverging metatherian of the sample, and *Kokopellia* represents the earliest offshoot of the Marsupialiformes. Only 4 out of the 98 characters are non-homoplastic (CI = RI = 1; characters 18, 30, 51, and 72). Among them, only two contribute to resolving the relationships between the metatherian taxa: the hypoconulid shifted lingually, close to the entoconid (**51^{1}**) and the paraconule more labial than the metaconule (**72^{1}**) support the Marsupialiformes excluding *Kokopellia* clade which includes *Asiatherium* (Fig. 3; see below). Note that some of the unambiguous synapomorphies described below are non-homoplastic within Metatheria (but not within the outgroup + ingroup).

Branching sequence of Mesozoic marsupialiforms – "Boreometatheria"

All Mesozoic marsupialiforms included appear successively in a stem-marsupialiform branching sequence (or 'branching group' sensu Antoine, 2002) in the strict consensus tree (Fig. 3). The basalmost taxa in each clade of this sequence are, from the earliest to the latest diverging, with the number of unambiguous synapomorphies (US) at the corresponding internal nodes (Supplemental material 4): *Kokopellia* (seven US), *Asiatherium* (six US), *Aenigmadelphys* (five US), the Alphadontidae sensu Eaton (1993) (*Albertatherium*, *Turgidodon*, and *Nortedelphys*) (three US), and a clade comprising *Didelphodon* and *Pediomys* + *Glasbius* (six US), which is the sister taxon of Notometatheria (the latter corresponding to the clade of South American and Australasian marsupialiforms [Kirsch et al., 1997], which here comprises all Cenozoic marsupialiforms sampled). The same topology is recovered in the Bayesian 50% majority-rule consensus tree, except that *Albertatherium* diverges earlier than other 'alphadontids' in the branching sequence (Fig. 4). All the corresponding subclades lack support in the initial parsimony analysis (BI = 1, relatively to the mean BI value of 1.9). When the four initially ordered characters are specified as unordered (i.e., all characters are unordered; Supplemental material 5: Fig. S1), the branching

sequence is weakened: it is recovered only by the 50% majority rule consensus tree (Supplemental material 5: Fig. S1B). Conversely, in parsimony analyses with characters based on threshold/gap coding deleted (Supplemental material 5: Figs. S2A, S3C), the most inclusive clades of the MPTs (i.e., the successive clades of the Mesozoic taxa branching sequence) are more supported than when these characters are included (for all of them, BI ≥ 2), but the relationships within Peradectini appear less resolved. As for the Bayesian analysis, both the most inclusive marsupialiform clades and most of the relationships within Peradectini receive moderate support (Fig. 4).

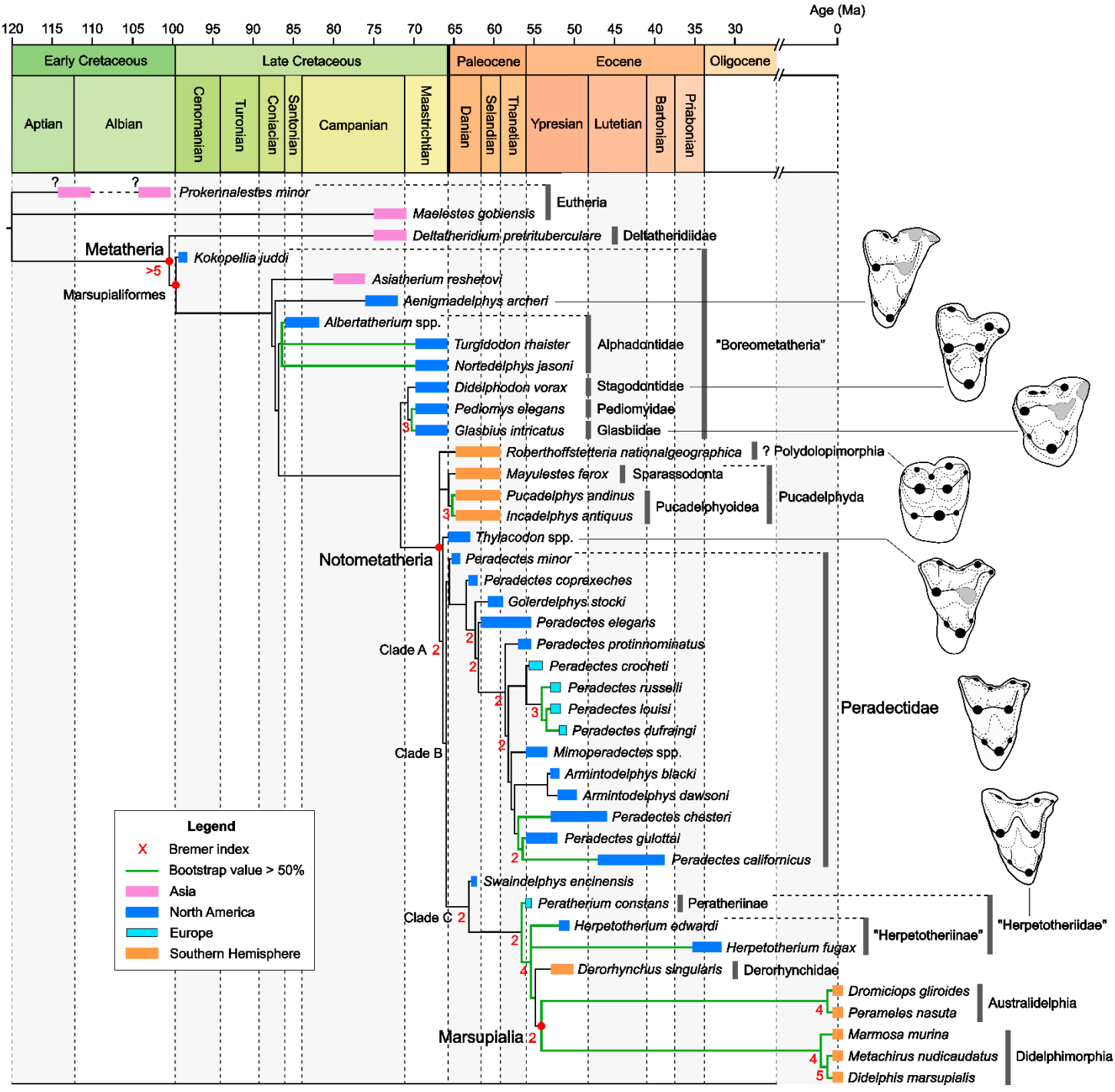

Figure 3. Strict consensus tree (CI = 0.376; RI = 0.573) of the six-most parsimonious trees of 593 steps each, resulting from the initial phylogenetic analysis set (42 taxa, 98 unweighted characters of which four are ordered), with the geographical and temporal extensions of the taxa mapped (see Supplemental

material 1) using a strict temporal calibration. The geologic time scale is adapted from Speijer et al. (2020). Bremer index values > 1 are plotted at nodes. Branches of the nodes supported by bootstrap values > 50% are highlighted in green. Interpretative drawings of M3s of selected taxa (not to scale) with right tooth orientation have been made using the illustrations of Cifelli and Johanson (1994: fig. 1E), Davis et al. (2007: fig. 23A$_1$), Gernelle et al. (2024b: fig. 4N), Goin et al. (2003: fig. 1A), Williamson et al. (2012: fig. 7D), Wilson (2013: fig. 5) and Wilson et al. (2016: fig. 1E).

Only the non-ambiguous synapomorphies at part of the nodes and some of the clade support need to be specified in detail here for the branching sequence of the Mesozoic taxa. *Aenigmadelphys* is the sister taxon of all other marsupialiforms minus *Kokopellia* and *Asiatherium*, notably (but not exclusively) on the basis of the presence of a notch on the cristid obliqua (39^1; Fig. 2A, Supplemental material 2: Fig. S12), which is lost in Notometatheria and *Glasbius* (see below), and the procumbency of the protocone (64^1), which is non-homoplastic within Metatheria. The alphadontids, such as *Nortedelphys*, with a bootstrap support value > 50%, unambiguously share an m3 with moderate L/W ratio values (1.55 ≤ L/W ≤ 1.75; 20^1; convergent with many notometatherians), trigonid and talonid subequal in width on m3 (23^1), the protocone lower than both the paracone and the metacone (62^1, convergent with Peradectinae; Fig. 5A, G), and stylar cusp C occasionally lingual to the labial edge of the stylar shelf of M1-M3 (90^1). The clade *Pediomys* + *Glasbius* is quite well supported (BI = 3 in parsimony analysis; and moderate support in Bayesian analysis). These taxa are united with *Didelphodon* by their postcingulid that attenuates labially to the hypoconulid (**48^1**, Gernelle et al., 2024a: Online Resource 3: fig. S6), the paraconule closer to the paracone than to the protocone (71^1; e.g., Fig. 3 for M3s of *Didelphodon* and *Glasbius*), which is non-homoplastic within Metatheria, and the paracone distinctly lower than the metacone (82^2). None of these three traits are found in *Roberthoffstetteria*. Finally, the sister taxon relationship of the *Didelphodon* + (*Pediomys* + *Glasbius*) clade with Notometatheria is notably recovered on the basis of the combination of the mesial end of the cristid obliqua labial to the carnassial notch of the protocristid and the narrow hypoflexid on m2/m3 (**37^2**, RI = 0.8), among six US.

Cenozoic marsupialiform clade - Notometatheria

The Notometatheria clade is relatively weakly supported (BI = 1; and low support in the Bayesian analysis, see Fig. 4) by five non-ambiguous synapomorphies: P1 is strongly asymmetrical (12^0); P2 is much larger than P1 (15^1, Supplemental material 2: Fig. S5) (an intraclade reversal concerns the Australidelphia for these two characters); the trigonid is not shorter than the talonid (**24$^{1/2}$**, trigonid and talonid subequal in length or trigonid longer), with no intraclade reversal but intraclade transformations from the state **24^1** (at this node) to the state **24^2**; there is no notch on the cristid obliqua (39^0, notably convergent with *Glasbius* and *Nortedelphys*; Supplemental material 2: Fig. S12); and, when the conules are present, the metaconule is larger than the paraconule (**70^1**, convergent only with *Glasbius*), without intraclade reversal (RI = 0.9; this is one of the less homoplastic characters of the datastet, see

Supplemental material 4). Within Notometatheria, a polytomy between *Roberthoffstetteria*, Pucadelphyda, and the clade A is yielded by the parsimony analysis (Fig. 3). It is resolved either as a sister taxon relationship between (i) *Roberthoffstetteria* and pucadelphydans (i.e., a "Tiupampan" clade, sister group of the "clade A") in two out six MPTs, or (ii) between *Roberthoffstetteria* and all other notometatherians (i.e., Pucadelphyda + clade A) in the four remaining MPTs. The second hypothesis is favoured by the Bayesian analysis, but with a polytomy between *Mayulestes*, Pucadelphyoidea, and the clade A. The longest terminal branches of the 50% majority-rule consensus tree from the Bayesian analyses are those of *Roberthoffstetteria*, *Mayulestes*, and *Deltatheridium* (Supplemental material 5: Fig. S7).

The clade A which includes *Thylacodon* and the clade B, sharing notably a metaconid almost directly lingual to the protoconid on m2/m3 (34^0), and an entoconid in intermediate position between the distal edge of the trigonid and the distal edge of m2/m3 (56^1; there are four other US, with lower RI values, see Supplemental material 4), has a moderate support based on BI value (= 2, relatively to the mean BI value of 1.9). The clade A yielded by the Bayesian analysis, moderately supported, is a polytomy between *Thylacodon*, *Peradectes minor*, the Peradectidae (= Peradectidae of the parsimony analysis less *Pd. minor*) and the clade C (Fig. 4; the clade B is not recovered). Among the five US of the clade B, in which a monophyletic Peradectidae and the clade C are sister taxa, those less subject to intraclade transformations are the trigonid as wide as long or longer than wide on m3 (22^1), and the paracristid longer than the protocristid on m2 and m3 (**35^2**). The inclusion of the anatoliadelphyid *Orhaniyeia* to the initial matrix causes a largely more unresolved strict consensus tree topology, with only the ingroup and the clade A preserved among the most inclusive clades (Supplemental material 5: Fig. S6A). *Orhaniyeia* is in polytomy with several taxa within the clade A. It thus does not appear closely related to the bunodont *Glasbius* and *Roberthoffstetteria*, which diverge earlier. *Orhaniyeia* is also neither closely related to nor included in the Peradectidae in the seven MPTs. Three of these MPTs, as well as the single MPT from the analysis with downweighted characters (k = 12) have *Orhaniyeia* nested within the clade C with "herpetotheriids" (Supplemental material 5: Fig. S6; the non-ambiguous synapomorphies of the clade C and of its subclades are depicted in this figure). In the single MPT of the analysis with downweighted characters, *Orhaniyeia* is the most autapomorphic terminal, with 12 non-ambiguous autapomorphies.

Peradectidae, Peradectinae, and Peradectini

The support for an exhaustive monophyletic Peradectidae (i.e., including all *Peradectes* species) is quite weak (BI = 1; Fig. 3), but the few synapomorphies have high RI values. In fact, all peradectids share a trigonid longer than the talonid on m2 and m3 (**24^2**, without intraclade reversal; Fig. 5B) and stylar cusp D directly labial to the metacone apex (**94^1**; Fig. 5E), that becomes distolabial to the metacone apex (**94^2**; Fig. 5F) in the Peradectini (Fig. 5A; see below). A monophyletic Peradectidae is always found (but the

clade found in Bayesian analyses is slightly less inclusive; Fig. 4; Supplemental material 5: Fig. S7). On the basis of low BI and Bayesian posterior probabilities (BPP) values, the support for the clade having *Pd. coprexeches* as earliest offshoot (i.e., the Peradectidae in the Bayesian analysis) is weak (Figs. 3-4). These taxa have a convex preprotocristid in mesiolabial view (36^{1}, without intraclade reversal; Supplemental material 2: Fig. S11), and a curved cristid obliqua (40^{1}, Fig. 5B; with intraclade reversal, notably within European peradectids). *Golerdelphys stocki* is recovered as a peradectid in all analyses. It diverges latter than *Pd. minor* and *Pd. coprexeches*, and earlier than the Peradectinae (Fig. 5A). The clade encompassing *Golerdelphys* and the Peradectinae is the most inclusive peradectid subclade with support close to the average in both initial analyses (Figs. 3-4; e.g., BI = 2, compared with the mean BI value of 1.9). Among the three non-ambiguous synapomorphies at the corresponding node, the talonid lingual edge mostly curved along the whole talonid length on m1-m3 (**50^{1}**, Fig. 5C; Supplemental material 2: Fig. S18), which is one of the less homoplastic characters of the dataset (RI = 0.9), and the small conules of the upper molars (**68^{1}**, Fig. 5F), are fewly (**50^{1}**) or not (**68^{1}**) homoplastic within the clade. The Peradectinae correspond to the clade with *Peradectes elegans* Matthew and Granger, 1921, as the outermost taxon (BI = 2). Most peradectines unambiguously share the presence of a distinct talonid ectocingulid (i.e., the hypoconid is internal to the talonid; 47^{1}, Fig. 5D) and a protocone lower than both the paracone and the metacone on M1-M3 (62^{1}, Fig. 5G). Within Peradectinae, *Pd. protinnominatus* McKenna, 1960, is the sister taxon of the Peradectini (the latter is the 'Eocene' peradectid clade in Gernelle et al., 2024a: fig. 15), again with moderate support (BI = 2), on the basis of six US (Fig. 5A): the m1 shorter than the m2 (19^{1}), the trigonid distinctly wider than the talonid on m3 (23^{0}, Fig. 5C; with reversal in, for example, the *Armintodelphys* species), the postcingulid that attenuates labially to the hypoconulid (**48^{1}**, Gernelle et al., 2024a: Online Resource 3: fig. S6), the mesiodistally narrow protocone (**61^{0}**) which is almost directly labial to the protocone (63^{1}, Fig. 5F), and the M1 ectoflexus sometimes present (95^{0}, Gernelle et al., 2024a: Online Resource 3: fig. S11). The Peradectini (BI = 2) are characterized by two US: on m3 the paraconid and metaconid are subequal in length or the paraconid is longer (32^{1}, Fig. 5C), and stylar cusp D is distolabial to the metacone apex, at least on M1 (**94^{2}**, Fig. 5F).

Within Peradectini, the monophyletic European peradectids represent the sister taxon of the clade formed by *Mimoperadectes* and all strictly Eocene North American peradectids (Figs. 3-4). The US of the European clade (BI = 1; the Europen subclade excluding *Pd. crocheti* Gernelle, 2024, is more supported, with BI value = 3) are: a low entoconid compared with the metaconid on m3 (≤ 30% of metaconid height, 57^{0}), the stylar shelf occupying 50% or more of the transverse width of M2 and M3 (73^{0}), stylar cusp A most often mesiolingual to stylar cusp B on M2 or M3 (84^{0}, Gernelle et al., 2024a: Online Resource 3: fig. S10), stylar cusp B directly labial to the paracone apex, at least on M1 or M2 (87^{1}), and the absence of ectoflexus symmetry (97^{1}, Gernelle et al., 2024a: Online Resource 3, fig. S12). A detail of the US of the other Peradectini subclades is not provided, because this group has been extensively studied in

Gernelle et al. (2024a) (e.g., the US supporting the least inclusive clade comprising *Mimoperadectes* are the same as those found in Gernelle et al., 2024a: fig. 15). More crucial here is the positioning of newly added peradectid species from Europe (the late early Eocene *Peradectes* sp. nov. 1, 2, and 3) and North America (*Didelphidectes* and *Nanodelphys*) in the subsequent phylogenetic analyses. In all maximum parsimony analyses of the third set (Supplemental material 5: Fig. S3A-C), *Peradectes dufraingi* (Smith & Smith, 2013) has a close relationship with at least one of the late early Eocene European peradectid species. When only *Peradectes* sp. nov. 2 is added, *Pd. louisi* Crochet, 1979, diverges earlier than *Pd. russelli* Crochet, 1979 (Supplemental material 5: Fig. S3A). The inclusion of the three new *Peradectes* species at the same time causes a major polytomy within the Peradectini (Supplemental material 5: Fig. S3B), probably due to the low completion of their scoring (especially for *Peradectes* sp. nov. 2 and 3). The resolution within Peradectini with the addition of these species is enhanced when the characters dealing with threshold discretization or gap coding are deleted (Supplemental material 5: Fig. S3C). In this case, *Pd. dufraingi* and *Peradectes* sp. nov. 1, 2, and 3, form a clade only on the basis of the straight cristid obliqua on m1-m3 (40^0) as unique US. Thus, based on the resolved nodes of the parsimony analyses, a possible hypothesis of relationships is that this clade is in polytomy with *Pd. russelli* and *Pd. louisi* (Fig. 5A). An alternative, yielded by a Bayesian analysis, is that *Peradectes* sp. nov. 2 is closer to *Pd. russelli*, and *Peradectes* sp. nov. 1 is closer to *Pd. louisi* and *Pd. dufraingi* (Supplemental material 5: Fig. S7). The youngest peradectids, *Didelphidectes* and *Nanodelphys*, are always united with *Pd. chesteri* (Gazin, 1952), *Pd. californicus* (Stock, 1936), and *Pd. gulottai* Rose, 2010 (e.g., Fig. 5A, and the strict consensus tree, when these genera are added; Supplemental material 5: Fig. S4A). The clade *Didelphidectes* + *Nanodelphys* is possibly the sister taxon of the clade *Pd. gulottai* + *Pd. californicus* (Supplemental material 5: Fig. S4C), an hypothesis supported by the supernumerary Bayesian analysis (Supplemental material 5: Fig. S7). It is worth adding that an European clade is found within Peradectini even when *Peradectes* sp. nov. 1, *Peradectes* sp. nov. 2, *Didelphidectes*, and *Nanodelphys* are added simultaneously (Supplemental material 5: Fig. S7).

'Herpetotheriidae' and Marsupialia clade

The clade C, including the stem-herpetotheriid *Swaindelphys* (BI = 2), is defined by four US: a talonid subequal in length or longer than the trigonid on m4 (25^1, Gernelle et al., 2024a: Online Resource 3, fig. S2), a cristid obliqua at least sometimes ventral to the protocristid notch on m4 (38^0), a protocone almost lingual to the paracone (63^1, Fig. 5F; with almost no intraclade reversal), and a V-shaped centrocrista combined with triangular paracone and metacone (80^1, Fig. 2D; with intraclade reversal only in *Dromiciops*). The 'Herpetotheriidae' and *Derorhynchus* together with the Marsupialia form a clade (BI = 2; BPP ≥ 0.95 obtained by Bayesian inference, Fig. 4) supported by the lingual opening of the trigonid basin as high as the lingual opening of the talonid basin on m2 (28^1, Supplemental material 2: Fig. S9; with reversal in the [*Derorhynchus* + Marsupialia] clade), the hypoconid distolabial or labial to the

entoconid (**42**[1], Supplemental material 2: Fig. S14; with reversal only in *Dromiciops*), the conical entoconid (54[0]), and stylar cusp B directly labial to the paracone apex, at least on M1 or M2 (87[1], with reversal only in *Derorhynchus*, due to morphological polymorphism). Based on the three herpetotheriid species scored (the peratheriine *Peratherium constans*, and the herpetotheriines *Herpetotherium edwardi* and *H. fugax*), herpetotheriids are paraphyletic with respect to *Derorhynchus* and the Marsupialia. The clade *Herpetotherium* + (*Derorhynchus* + Marsupialia) is one of the strongly

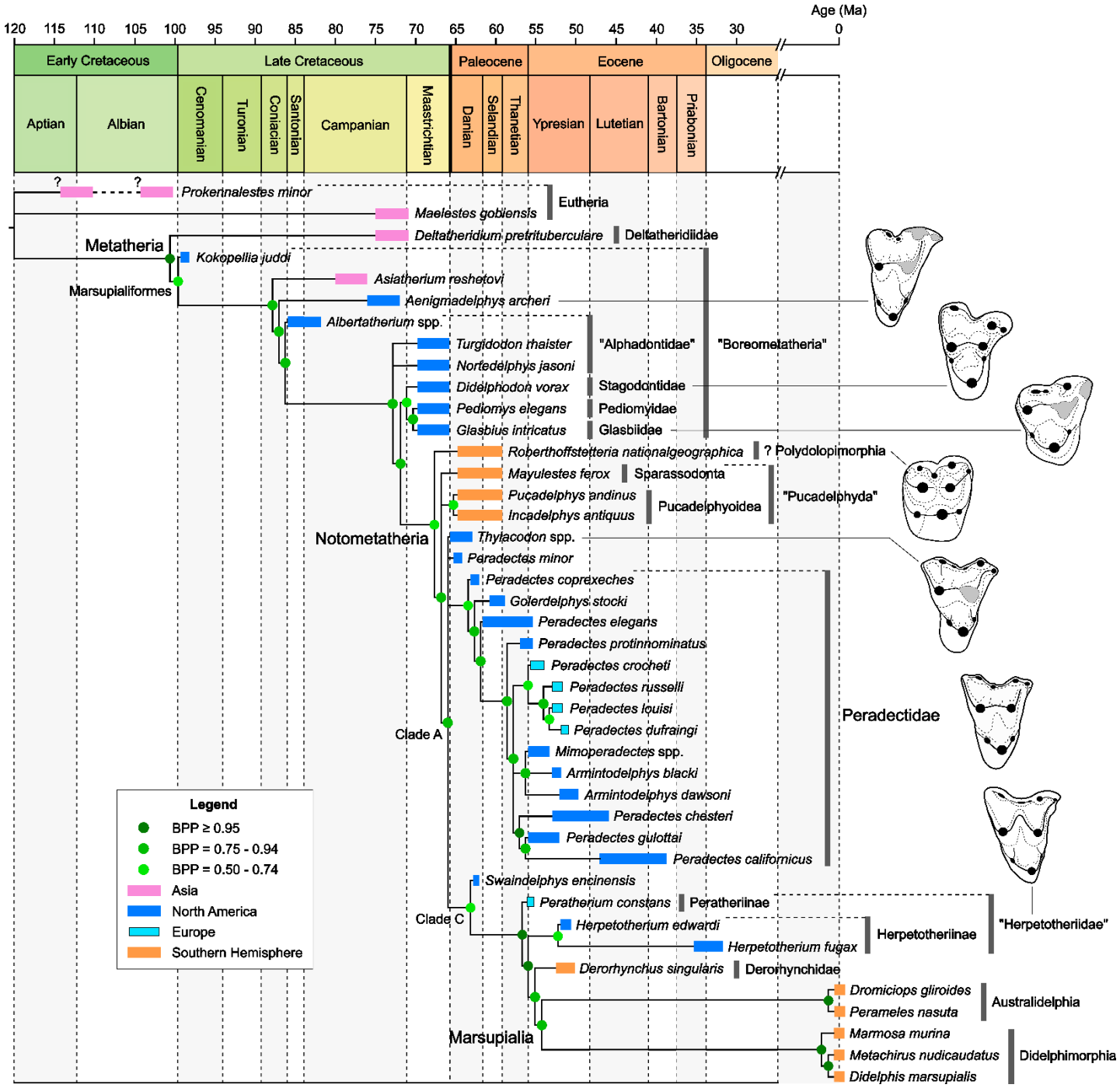

Figure 4. 50% majority-rule consensus tree of post-burn-in trees (7.50×10^6 generations), based on Bayesian analysis resulting from the initial phylogenetic analysis set (42 taxa, 98 unweighted characters of which four are ordered). Bayesian posterior probabilities (BPP) are represented at nodes. Branch lengths are not proportional to the estimated number of character state changes, but are strictly constrained by the stratigraphic ranges of the sampled taxa (see Fig. 3 and Supplemental material 1).

supported in both maximum parsimony (BI = 4), by eight US (among which the absence of a high and short crest connecting vertical stylar cusps A and B on M3 [**88^0**, RI = 0.82; Supplemental material 2: Fig. S23]), and Bayesian analyses (BPP ≥ 0.95). MPTs differ in the resolution of the relationships between *Herpetotherium* species. *Herpetotherium* is monophyletic in three MPTs, whilst *H. edwardi* diverges earlier than *H. fugax* in the three remaining MPTs. The former alternative is found by Bayesian analyses. The *Derorhynchus* + Marsupialia clade is characterized by only 3 US, it is better supported in the Bayesian analyses. When *Djarthia* is added (Supplemental material 5: Fig. S5) it is in polytomy with *Derorhynchus*, the Australidelphia and the Didelphimorphia in the strict consensus tree (Supplemental material 5: Fig. S5A). In the 50% majority-rule tree of the maximum parsimony analysis, *Djarthia* is in Australidelphia, within a monophyletic Marsupialia (Supplemental material 5: Fig. S5B). The Marsupialia (BI = 2) have three US, relative to lower molars: the postcristid is straight, at least on one m2 to m4 locus (44^0, Gernelle et al., 2024a: Online Resource 3: fig. S5; reversal in *Didelphis* Linnaeus, 1758), the postcingulid is absent (**48^0**), and the entoconid apex is positioned closer to the distolingual corner of the molar than to the distal edge of the trigonid (56^0). In all analyses, among the most supported clades of the ingroup are the Australidelphia and the Didelphimorphia (BI = 4, BPP ≥ 0.95, in the initial analyses) and the subclade *Metachirus* Burmeister, 1854 + *Didelphis* (BI = 5, BPP ≥ 0.95, in the initial analyses) (Figs. 3-4).

Discussion

The rise of Notometatheria after the K-Pg mass extinction

Fewer marsupialiform lineages than expected crossed the K-Pg boundary: macroevolutionary implications

Some Cretaceous North American marsupialiforms have been suspected to be related to given Paleogene taxa, and would thus be multiple examples of lineages surviving the K-Pg mass extinction (note that a single, convincing, similar example exist in non-marsupialifom metatherians; Ni et al., 2016). However, all these affinities, except the presence of shortly surviving pediomyids and alphadontids in the earliest Paleocene (Puercan North American land mammal age [NALMA], biozone Pu-1; Claytor et al., 2023; Smith et al., 2018), are currently controversial (see a summary of these in Beck, 2023: 40-42). The present analyses focused on dental remains yield new conclusions regarding three of these putative lineages. (i) *Aenigmadelphys* from the Campanian of North America has been claimed as a pucadelphyoid (Muizon & Ladevèze, 2022), whilst it is nested in the branching sequence with all stem-marsupialiforms in our phylogenetic analyses, and Pucadelphyoidea form a stem-notometatherian clade of their own (Figs. 3-4; contra Muizon & Ladevèze, 2022, see Fig. 1C). This position of *Aenigmadelphys* is roughly consistent

with those found by Williamson et al. (2012, 2014) (e.g., Fig. 1A). (ii) In the same way, the late Maastrichtian North American *Nortedelphys*, first described as a herpetotheriid (Case et al., 2005) and considered a possible stem-representative of these in numerous studies (e.g., Hooker et al., 2008; Ladevèze et al., 2020; Martin et al., 2005; Wilson et al., 2016), is here also found in the branching sequence of stem-marsupialiforms (see also Williamson et al., 2012, 2014; Fig. 1A), in a clade with alphadontids (at least in most of our parsimony analyses) instead of as a stem-"herpetotheriid" (see also Johanson, 1996: 1028, and Carneiro & Oliveira, 2017, in which *Nortedelphys* is considered an alphadontid). The early-herpetotheriid status of *Nortedelphys* is thus discarded here (contra Case et al., 2005). (iii) The bunodont Glasbiidae, of which *Glasbius* is also from the late Maastrichtian of North America, have been considered included in the otherwise South American Polydolopimorphia or sister taxon to the earliest putative polydolopimorphian, *Roberthoffstetteria* (e.g., Beard et al., 2023; Eberle et al., 2019, 2024; Goin et al., 2003, 2016; Williamson et al., 2012, 2014), which has a more advanced bunodont condition. Here again, *Glasbius* and *Roberthoffstetteria*, are never recovered related in our analyses, *Glasbius* being in the stem-marsupialiform branching sequence in a clade with *Didelphodon* and especially *Pediomys* (a close relationship of *Glasbius* with the latter, forming the Pediomyoidea sensu Cohen et al. [2020], is consistent with various phylogenetic analyses, namely those of: Cohen et al., 2020; Davis, 2007: fig. 24; Eberle et al., 2019, 2024; Wilson et al., 2016), whereas *Roberthoffstetteria* appears as an early-diverging taxon among Notometatheria (see below). This position of *Roberthoffstetteria* is roughly consistent with that found for the younger early polydolopimorphian *Epidolops* Paula Couto, 1952, when it is scored using both cranial and postcranial material (Beck, 2017b: fig. 14b). We thus concur with Beck (2023: 41) that the superficial similarities between *Glasbius* and *Roberthoffstetteria*, including the bunodont features, are probably better explained by convergence (e.g., contra Beard et al., 2023; Eberle et al., 2019, 2024; Goin et al., 2003, 2016; Williamson et al. 2012, 2014, see Fig. 1A). Furthermore, the recovery of *Thylacodon*, *Swaindelphys*, and all peradectid and 'herpetotheriid' species in a single clade exclusively composed of Cenozoic marsupialiforms suggests that there has probably not been several lineages comprising the aforementioned Cenozoic Laurasian 'opossum-like' taxa that crossed the K-Pg boundary (contra Williamson et al., 2012: 645-646). In conclusion, because none of the Cretaceous Laurasian marsupialiforms included in this study presents an exclusive, or even close relationship, with a given Cenozoic marsupialiform taxon (in other words, Cenozoic marsupialiforms possibly emerged from a unique lineage), our phylogenetic framework provides further evidence that metatherians were severely affected, even taxonomically speaking, by the K-Pg mass extinction (e.g., Wilson, 2014).

A phylogenetic definition of Notometatheria, the Cenozoic marsupialiform clade

Kirsch et al. (1997) classified all marsupialiforms (= 'Marsupialia' sensu Kirsch et al., 1997) from South America and Australasia within Notometatheria Kirsch et al., 1997 (see also Rougier et al., 1998), the

phylogenetic status of which has been considered ambiguous (Ladevèze & Muizon, 2007). Carneiro et al. (2018: 128), Rangel et al. (2019: 279), and more recent studies by Carneiro and collaborators (e.g., Carneiro & Oliveira, 2023: table 1) consider that notometatherians are restricted to the Herpetotheriidae, Derorhynchidae, Sternbergiidae, and Marsupialia, following the definition of Kirsch et al. (1997). However, in their classification of the notometatherian taxa, Kirsch et al. (1997: table 5) include the mainly Laurasian herpetotheriids (contra Ladevèze & Muizon, 2007: 1133) as well as all Southern Hemisphere metatherians, for instance members of the Pucadelphyda sensu Muizon et al. (2018), such as sparassodonts. The equivalent of Notometatheria sensu Kirsch et al. (1997) in Carneiro and collaborators' classification is in fact their Sudameridelphia, a name originally coined by Szalay (1994) for a group including only some taxa from South America. Herpetotheriids have been quite convincingly confirmed as notometatherians based on analyses including a reasonable sampling of Laurasian and Gondwanan marsupialiforms (e.g., Engelman et al., 2020; Ladevèze et al., 2020; see Fig. 1B-C). Peradectids were classified within Boreometatheria Kirsch et al., 1997, a group otherwise composed of Mesozoic-only Laurasian marsupialiforms (see Rougier et al., 1998; and further works in which updated versions of the original matrix of these authors are used; e.g., Ni et al., 2016). Peradectidae have been recovered as the sister taxon of Notometatheria sensu Kirsch et al. (1997) only in the implied weighting maximum parsimony analysis of Muizon et al. (2018: fig. 29B; through the composite taxon *Mimoperadectes* – *Peradectes*), and in the maximum parsimony analysis of Carneiro et al. (2024b; through *Mimoperadectes*), among those in which some Mesozoic 'boreometatherian' taxa have also been included (i.e., the Stagodontidae in Muizon et al., 2018). Here, 'Boreometatheria', composing our branching group, are found paraphyletic with respect to Notometatheria sensu Kirsch et al. (1997) (Figs. 3-4), which encompass Peradectidae for the first time to be monophyletic. We here favour the name Notometatheria over Sudameridelphia because it has a broader palaeobiogeographic significance: Notometatheria, in opposition to "Boreometatheria", denotes the appearance of metatherians in the Southern Hemisphere, as early as the earliest Cenozoic (see below).

No high-level clade intermediate to Marsupialiformes and the crown-group Marsupialia has received a formal phylogenetic definition in past studies (Table 2). According to several authors, dental evidence alone must be insufficient for establishing higher-category groupings within metatherians (e.g., Kirsh et al., 1997; Szalay, 1994), although teeth make up most of the metatherian fossil record. As a consequence, two remarks are in order of the phylogenetic analyses and new definitions of clades. First, to our knowledge, the analyses here conducted are the first recovering, based on dental evidence alone, a monophyletic Marsupialia which only emcompasses unequivocal members of the crown group, with monophyletic Australidelphia and Didelphimorphia also found (but based on a few extant species). The two latter are among the best supported clades in all our analyses (with strong support in the initial Bayesian analysis; Fig. 4). Noteworthy, the australidelphian nature of the plesiomorphic *Djarthia*

Table 2. Phylogenetic definitions of the clade Metatheria and its high-level subclades, including Notometatheria, as well as of the clade Peradectidae and its subclades.

Clade	Phylogenetic definition	Reference
Metatheria Huxley, 1880	"The most inclusive clade containing *Didelphis marsupialis* but not *Mus musculus*"	Sereno (2006: table 10.1)
Marsupialiformes Vullo et al., 2009	"The most inclusive clade containing *Didelphis marsupialis* but not *Deltatheridium pretrituberculare*"	Beck (2017a: table 13.1)
Notometatheria Kirsch et al., 1997	The most inclusive clade containing *Didelphis* but not *Didelphodon* or *Pediomys*	This study
Marsupialia Illiger, 1811	"The least inclusive clade containing *Didelphis marsupialis*, *Caenolestes fuliginosus* and *Phalanger orientalis*"	Beck et al. (2014: 131)
Peradectidae (Crochet, 1979)	"The most inclusive clade containing *Peradectes elegans* but not *Herpetotherium fugax*, *Pediomys elegans*, or *Didelphis virginiana*"	Williamson et al. (2012: 629)
Peradectinae (Crochet, 1979)	The least inclusive clade containing *Peradectes elegans*	This study
Peradectini Crochet, 1979	The least inclusive clade containing *Peradectes crocheti* and *Mimoperadectes*	This study

murgonensis (e.g., Beck, 2012; Beck et al., 2008) is at least verified by the 50% majority-rule consensus tree of the maximum parsimony analysis, even if only dental specimens of this species are scored (Supplemental material 5: Fig. S5; contra Carneiro et al., 2024a; Crespo & Goin, in press). Altogether, these data warrant the use of dental characters, as (at least some) consensual relationships within Metatheria can be found using them. Second, based on our results, we propose a phylogenetic definition of Notometatheria as the most inclusive clade containing *Didelphis* but not *Didelphodon* or *Pediomys* (Table 2). A definition invoking these three taxa will allow future studies dealing with cranial (notably from the ear region) and/or postcranial characters to reassess the monophyly and content of Notometatheria, of which the support is here relatively weak. Noteworthy, given this phylogenetic definition, several studies actually do not recover a Notometatheria clade comprising all Southern Hemisphere metatherians scored in these (e.g., Maga and Beck, 2017, in which pucadelphydans are excluded; Wilson et al., 2016). The earliest probable metatherian from the Southern Hemisphere, *Cocatherium lefipanum* Goin et al., 2006, known by a single and worn bunodont lower molar, possibly also belongs to Notometatheria, given that it has been recovered in a clade with *Roberthoffstetteria* in the phylogenetic analysis based on a revised version of Goin et al. (2006)'s matrix (Beck, in press). Interestingly, the Notometatheria also correspond here to the clade including all Cenozoic marsupialiforms, even *Thylacodon* and peradectids, which are early notometatherians (Figs. 3-4). The assumption of such close phylogenetic relationship between all Cenozoic marsupialiforms is implicit in the phylogenetic definition provided for Notometatheria (Table 2).

The comprehensive evolutionary history of unequivocal peradectids

Phylogenetic position and origin of Peradectidae

We recovered the "bloom" taxon *Thylacodon*, the single Cenozoic-only metatherian known from the earliest Puercan (biozone Pu-1) (Claytor et al., 2023: table 2; Smith et al., 2018; Wilson, 2014: table 1), as the earliest diverging Cenozoic Laurasian marsupialiform in the maximum parsimony analyses, basal to the Peradectidae and the stem-herpetotheriid *Swaindelphys*, the latter two being in distinct sister groups (Fig. 5A). Consequently, we concur (i) with Krishtalka and Stucky (1983) and Williamson et al. (2012) that *Thylacodon* is probably not a peradectid (contra Clemens, 2006; Dahlberg et al., 2016; Korth, 2008: 43; Wilson, 2013), and (ii) with Williamson and Taylor (2011) that *Swaindelphys* is morphologically distinct from *Thylacodon*, even based on lower molars (contra Johanson, 1996); and establish that (iii) peradectids, and 'herpetotheriids' (considering *Swaindelphys* as a stem-'herpetotheriid'; contra Goin, 2003: 37), emerged from a newly evidenced rapid North American cladogenetic event post K-Pg crisis, in early Puercan (early Danian) times. Following the results of the Bayesian analyses, it is possible that this cladogenesis occurred slightly earlier and comprised *Thylacodon* as well as the clade including most

peradectids and the clade including the 'herpetotheriid' lineage (Fig. 4). In all cases, and without considering the puzzling unique upper molar of *Maastrichtidelphys* (see Martin et al., 2005), of which the initial familial attribution to herpetotheriids has not been adequately established (Williamson et al., 2012: 626), this implies that the latest common ancestor of peradectids and "herpetotheriids" is probably younger than the Late Cretaceous (e.g., contra Fox, 1983; Horovitz et al., 2009: fig. 5B; Williamson et al., 2012: 646). Occurrences of putative Cretaceous indeterminate peradectids concern specimens that either (i) do not exhibit the US of the Peradectidae such as stylar cusp D labial or distolabial to the metacone apex (see below), alike typical Cretaceous "boreometatherians" (e.g., Cifelli, 1994: fig. 8; pers. obs. [KG] of casts of these upper molars; contra Carneiro & Oliveira, 2023: 285), or (ii) are too fragmentary to be distinguished from the latter taxa (e.g., see Eberle & Lillegraven, 1998: 37), or (iii) are alphadondids (Cifelli, 1994; Williamson & Weil, 2008: 813, fig. 8), the representatives of which have occasionally been considered peradectids (e.g., the Alphadontinae [Cretaceous] in Peradectidae together with Peradectinae [Paleogene], in Marshall et al., 1990). The position of peradectids relative to Tiupampan taxa is consistent with both the total evidence analysis of Beck et al. (2016: fig. 8) and the choice of Pucadelphyda as outgroup terminals when peradectids are also included (see Beck et al., 2022). We confirm that a close relationship between peradectids and Marsupialia is unlikely (e.g., Beck, 2012; Beck et al., 2022; Engelman et al., 2020: fig. 16; Ladevèze et al., 2020) given their respective positioning in all of our tree topologies (contra Engelman et al., 2020: fig. 17; Horovitz et al., 2009; O'Leary et al., 2013: table 1; Williamson et al., 2012, 2014; Wilson et al., 2016).

Phylogenetic definition of Peradectidae: implication for their taxonomic content and morphological characterisation

Williamson et al. (2012: 629) proposed a stem-based definition of the Peradectidae, as "the most inclusive clade containing *Peradectes elegans* but not *Herpetotherium fugax*, *Pediomys elegans* or *Didelphis virginiana*" (Table 2). Due to this definition and their results, the Peradectidae clade recovered by Williamson et al. (2012, 2014) comprised only *Pd. elegans* and *Pd. californicus*, but the authors mentioned that "future studies may likely recover a more inclusive phylogenetically-defined Peradectidae" (Williamson et al., 2012: 632). Intrafamilial relationships of late Paleocene to middle Eocene peradectids have been first resolved by Gernelle et al. (2024a), but this result has not been obtained in a broad phylogenetic context (i.e., with an ingroup larger than Peradectidae). Here, the stem-based definition of Peradectidae from Williamson et al. (2012) is followed, and the taxa used in this definition (*Pd. elegans*, *H. fugax*, *Pe. elegans*, and a species of *Didelphis*) have been included in our analyses. As predicted by Williamson et al. (2012), a monophyletic Peradectidae encompassing all 22 Northern Hemisphere peradectid species described so far (in *Armintodelphys*, *Didelphidectes*, *Golerdelphys* [see familial reallocation of this genus below], *Mimoperadectes*, *Nanodelphys*, and *Peradectes* [*Peradectes pauli* Gazin, 1956, is not included following Williamson et al., 2012]) must be

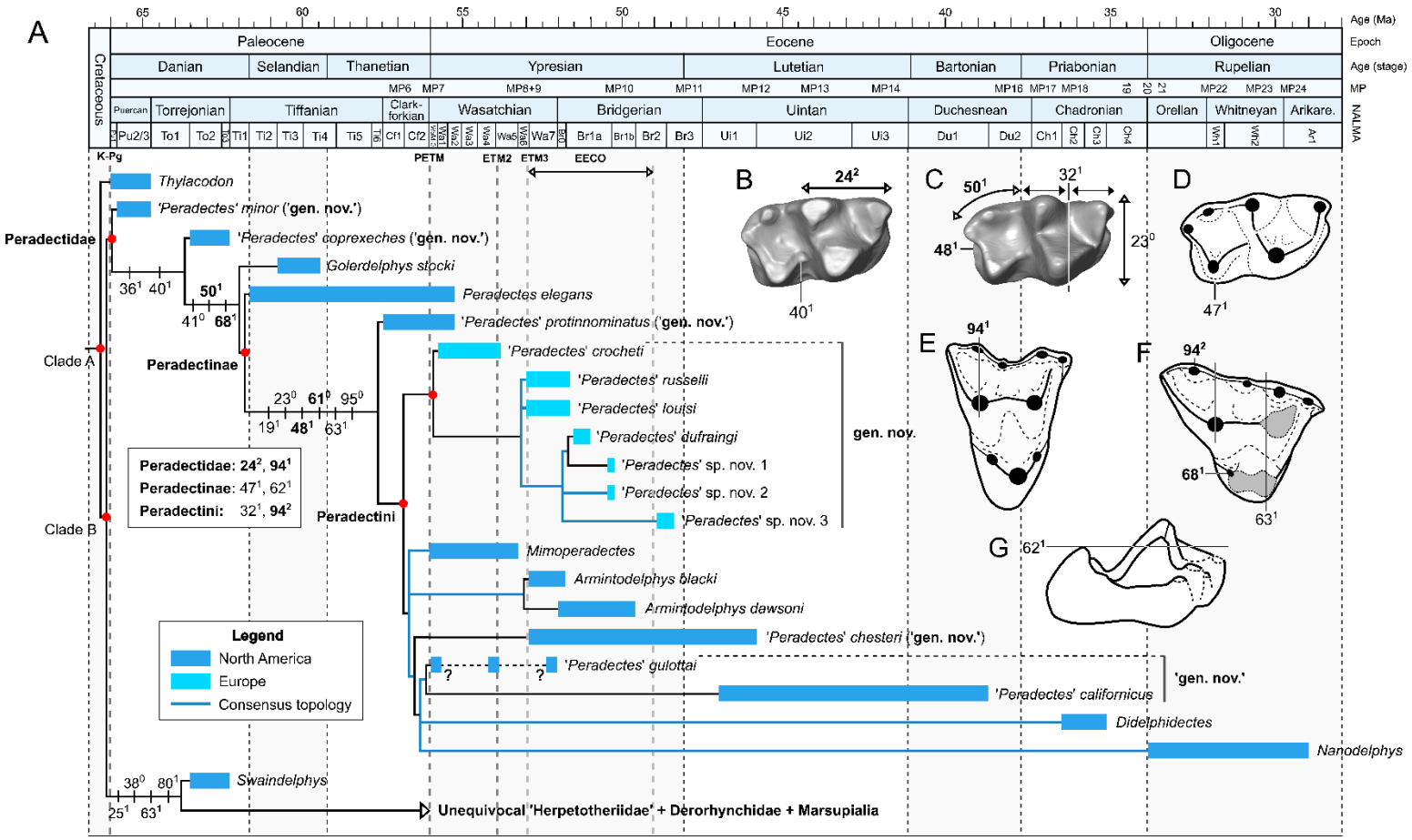

Figure 5. **A**. Phylogenetic relationships within the clade A yielded by parsimony analyses, with a focus on Peradectidae. The non-ambiguous synapomorphies recovered from the initial maximum parsimony analysis supporting the Peradectidae, Peradectinae, Peradectini and intermediate subclades are specified, either at nodes or in the synapomorphy box. The most informative of them are illustrated on molars (not to scale) of *Peradectes russelli* (**B**. m2 UM-AV-15-SK. **C**. m3 MNHN.F.MU6451. **D**. m3 MNHN.F.GL410), *Pd. minor* (**E**. M3 NMMNH P-47293; interpretative drawing based on Williamson et al., 2012: fig. 7D), and *Pd. crocheti* (**F**. M1 UM-FNR2-1. **G**. M1 MHN.AIX.PV.2018.26.20). Non-ambiguous synapomorphies with RI ≥ 0.5 are in bold. Each tentative unresolved node results from a compromise from the resolved relationships recovered by the initial phylogenetic analysis and the third and fourth sets of additional parsimony analyses (Supplemental material 5: Figs. S3-4). Tentative generic attributions are figured. Open nomenclature occurrences are not considered in the ranges of taxa. The positions of the ETMs/EECO follow Westerhold et al. (2018), the biozonation of the Clarkforkian follows Anemone et al. (2024), and the geologic time scale is adapted from Speijer et al. (2020).

valid (Fig. 5A). In maximum parsimony analyses, its earliest diverging taxon is the oldest *Peradectes* species, the Puercan NALMA (Danian; Pu-2/3) *Peradectes minor*, which is coeval with the Pu-2/3 representatives of *Thylacodon* ("*Peradectes* cf. *P. pusillus*" in Wilson, 2014). Alternatively, the tree topologies yielded by the Bayesian anlayses show *Pd. coprexeches*, which is coeval with the stem-herpetotheriid *Swaindelphys* (Fig. 4), or *Golerdelphys stocki* (Supplemental material 5: Fig. S7) as the oldest and earliest diverging peradectids (following the phylogenetic definition of Peradectidae). In all tree topologies, the order in which peradectid taxa diverge within the peradectid clade is quite congruent with their order of appearance in the fossil record (e.g., Fig. 5A; the exceptions being *Golerdelphys* and possibly *Pd. gulottai*).

All peradectids have a trigonid longer than the talonid on m2 and m3 (**24**$^{\mathbf{2}}$, Fig. 5B), and stylar cusp D labial or distolabial to the metacone apex (**94**$^{\mathbf{1/2}}$, Fig. 5E-F). Because no reversal from this condition is known so far within Peradectidae (Supplemental material 4), the presence of both character states (provided that lower and upper molars are known) can be confidently considered necessary to support the attribution of any marsupialiform molar to Peradectidae. Interestingly, the short talonids of m1-m3 were first considered a diagnostic character of *Peradectes* by Krishtalka and Stucky (1983). In a phylogenetic context, the dental features generally advocated to distinguish peradectids from herpetotheriids (e.g., see Gernelle et al., 2024a: table 6; Korth, 2008: 40) are either symplesiomorphies of peradectids and "boreometatherians" (for instance the straight centrocrista of upper molars [80^{0}] and the relatively high lingual opening of the trigonid of lower molars [28^{0}]) or have been acquired during the evolutionary history of peradectids and thus do not concern all species of the family (e.g., the small conules [**68**$^{\mathbf{1}}$, Fig. 5F; see below], as envisioned by Korth [2008: 43]). Alike the Puercan *Pd. minor* and the Torrejonian *Pd. coprexeches*, peradectids and similar unidentified metatherians from Puercan and Torrejonian localities, such as *Peradectes* sp. from the Dawson Creek area (To-2; Leslie et al., 2018: fig. 8B), and a lower molar from the Dragon Canyon area (Tomida & Butler, 1980: pl. 1, fig. 3A) notably differ from younger peradectids in retaining a straight talonid lingual edge along the whole talonid length on available m1-m3 specimens (**50**$^{\mathbf{0}}$; pers. obs. KG).

Early stages of peradectid evolution during the Paleocene

Golerdelphys was first described as a herpetotheriid possessing a mixture of herpetotheriid and peradectid characters (e.g., small conules and straight centrocrista on upper molars, contrary to herpetotheriids sensu Korth, 2008) that defies traditional classifications (Williamson & Lofgren, 2014: 480). In phylogenetic analyses by Williamson and collaborators (Williamson et al., 2012; Williamson & Lofgren, 2014), *Golerdelphys* only shares stylar cusp A positioned lower than stylar cusp B with *Ectocentrocristus* and unequivocal herpetotheriids. However, we note that stylar cusp A becomes relatively higher compared with stylar cusp B from M1 to M3 in Cenozoic Laurasian metatherian species

(e.g., Archibald, 1982: fig. 42; for *Thylacodon*), so that the former stylar cusp can be as high as the latter on M3 in both peradectids and herpetotheriids (e.g., Gernelle et al., 2024a: fig. 10; Ladevèze et al., 2012: fig. 5; Rose et al., 2012: fig. 12E). However, the M2 of *Golerdelphys* is the single upper molar of this taxon preserving stylar cusps A and B, and the definition of the concerned character by Williamson et al. (2012) does not specify a upper molar locus (our similar character 85 is scored only based on M3), which weakens the inclusive 'herpetotheriid' clade found by Williamson and collaborators. Here, *Golerdelphys* is nested in the branching sequence of early diverging peradectids (as sister taxon to the subfamily Peradectinae; see US in the Results section and in Fig. 5). It has been stated that the morphology of the centrocrista (whether straight or V-shaped) is a highly homoplastic character (Williamson et al., 2012: 634), as illustrated by the straight centrocrista of *Golerdelphys*, which was previously considered a herpetotheriid—a family traditionally characterized by a V-shaped centrocrista (Williamson & Lofgren, 2014). Although we agree with Williamson and collaborators that the V-shaped centrocrista is a homoplastic character (e.g., acquired independently in *Nortedelphys*, Pucadelphyoidea and the clade containing herpetotheriids; Supplemental material 4), the statement regarding its possible lability within peradectids and herpetotheriids needs to be somewhat tempered. In fact, (i) our composite character 80 concerning the morphology of the centrocrista has a moderately high RI value (RI = 0.73; although we did not score *Maastrichtidelphys*, with a V-shaped centrocrista; see Martin et al., 2005), partly because *Swaindelphys* (with a V-shaped centrocrista) is not found in a polytomy, contrary to the tree topologies of Williamson et al. (2012, 2014), and (ii) the only unequivocal inferred transformation of the morphology of the centrocrista documented to date in these families is not drastic (i.e., not from a straight to a fully V-shaped centrocrista; see Vianey-Liaud et al., 2024: fig. 2C). Based on the branching sequence of early peradectids, we define the Peradectinae, denoting the appearance of the type species of peradectids, as the least inclusive clade containing *Peradectes elegans*, and the Peradectini, denoting the Eocene cladogenesis event and the arrival of peradectids in Europe, as the least inclusive clade containing *Peradectes crocheti* and *Mimoperadectes* (Fig. 5A; Table 2).

Reassessement of '**Peradectes**' *based on a phylogenetic systematics context*

Peradectes is a paraphyletic genus with respect to *Armintodelphys*, *Didelphidectes*, *Golerdelphys*, *Mimoperadectes*, and *Nanodelphys* (Fig. 5A). Thus, it is not closer to *Nanodelphys* than to any other unequivocal peradectids (contra Korth, 2008: 43). Following the two alternatives proposed by Gernelle et al. (2024a: 42), a first hypothetical solution to avoid this paraphyly (i.e., in a phylogenetic systematics context) should be to include all peradectids into *Peradectes*. Although a broader *Peradectes* genus could be possible, based on the conservative dental morphology and the recurrence of a *Peradectes* – *Mimoperadectes* terminal in the literature (e.g., Horovitz et al., 2009; Muizon & Ladevèze, 2020, 2022), it should be noted, however, that (i) other small mammal genera generally have longevity values much lower than ~35 myr (e.g., mostly < 10 myr for eulipotyphlans and glires; see Hoek Ostende et al., 2023:

fig. 8.4), which is the approximate longevity value for a broad monophyletic *Peradectes*, and that (ii) available astragali of *Mimoperadectes* (Rose et al., 2012: fig. 11A-D) show marked morphological differences with those known for the unequivocal North American and European peradectids grouped in *Peradectes* so far (Gernelle et al., 2024a: 23). A second solution to circumvent the paraphyly of *Peradectes* is to erect (at least) six genera, of which four are necessarily monospecific ('*Peradectes*' species *minor*, *coprexeches*, *protinnominatus*, and *chesteri*), so that *Peradectes* becomes monospecific, with the type species *Pd. elegans* only (Fig. 5A). This alternative seems the most correct, although (i) it does not reflect the conservative aspect of the dental morphology of peradectids, and (ii) the North American species with a relatively long apparent time range (at least *Pd. elegans*, '*Pd.*' *chesteri*, and '*Pd.*' *californicus*, for which the last revision to date is that of Krishtalka and Stucky [1983]) should be thoroughly revised. For the time being, a new convincingly monophyletic group with multiple species (apart *Mimoperadectes* and *Armintodelphys*) is the European lineage, composed so far of seven species restricted to the Ypresian (< 8 myr duration), for which a new genus is to be created.

Diversity dynamics and dispersal in unequivocal peradectids

Marsupialiform faunas from the earliest Cenozoic are depauperate (Wilson, 2014), with no contemporaneous (i.e., sharing a given time range) peradectid species until the end of the Danian age (Fig. 5A; Williamson and Taylor, 2011). Occurences in open nomenclature are not taken into account below, except when indicated. The concomitance of two peradectid species occurs during the rest of the Paleocene. This amount of coeval species becomes at least of three through a modest radiation just after the Paleocene Eocene Thermal Maximum (PETM), with the appearance of *Mimoperadectes* species (at least *M. labrus*, and *M. houdei* Horovitz et al., 2009, the latter appearing later than *M. labrus*, after the extinction of *Pd. elegans* and *Pd. protinnominatus*; see Horovitz et al. [2009] and Fig. 5A) and the first European species, *Pd. crocheti*. Four or more species must have been coeval at some point of the Early Eocene Climatic Optimum (EECO) sensu Westerhold et al. (2018), beginning with the Eocene Thermal Maximum 3 (ETM3) (Fig. 5A). More than a third of the specific diversity of peradectids is represented during the EECO (~49-53 Ma; Fig. 5A), which is known as a phase of mammal diversification compared with the previous and next phases, at least in North America (Woodburne et al., 2009). After the Ypresian/Lutetian boundary, the diversity of coeval peradectid species decreases, due to the disappearance of peradectids in Europe (Gernelle et al., 2024a). This event coincides with the North American major faunal diversity loss known as the 'Bridgerian Crash' (Woodburne et al., 2009). The family Peradectidae is still represented by two species in North American mammal faunas until the late Eocene, when open nomenclature occurences are accounted (Kihm & Schumaker, 2015). Finally, there was only one early Oligocene peradectid species (Korth, 2018: fig. 16).

Comparing the results of our phylogenetic analyses results with those of Gernelle et al. (2024a), and given the inclusion of early peradectids, as well as the latest North American (*Didelphidectes* and *Nanodelphys*) and European peradectids (the late early Eocene *Peradectes* sp. nov. 1/2/3) in our dataset, we confidently confirm that peradectids likely dispersed only once from North America to Europe (contra Crochet, 1980; Smith & Smith, 2013), seemingly just after the PETM. *Peradectes gulottai* appears more related to some peradectid species from North America than to those from Europe, as hypothesized by Rose (2010). Marsupialiform dispersals between these two landmasses probably occured several times during the Late Cretaceous (Vullo et al., 2020), but never after the respective, probably unique, dispersals of herpetotheriids (see Ladevèze et al., 2012: 260) and peradectids. Putative dispersals of peradectids outside North America and Europe are adressed in the following section.

Taxonomic status of Gondwanan and Asian putative peradectids: were there peradectids or close relatives outside North America and Europe? Palaeobiogeographic implications

Paleocene-Eocene presumed peradectids from South America: *peradectid synapomorphies matter*

A few (less than 10) molars from South American Paleocene-Eocene localities were allocated to Peradectidae. The taxonomic reassessment of these rare putative peradectid fossils, in the light of the new phylogenetic framework presented here, is critical to propose accurate palaeobiogeographic scenarios, in particular because the suspected relationships of these taxa with the unequivocal Laurasian representatives of the Peradectidae (e.g., Crochet, 1977, 1980: fig. 33) have not been formally demonstrated so far (Beck et al., 2022: 309-310).

An isolated M3 from Tiupampa (Bolivia, early/middle Paleocene; see Beck et al., 2022: 309-310 for the age of Tiupampa) with a straight centrocrista was referred to as *Peradectes* cf. *austrinum* (YPFB Pal 6132; Marshall & Muizon, 1988: fig. 12). It probably represents a different species from *Peradectes austrinum* (Sigé, 1971) (= cf. *Peradectes austrinum* or ?*Peradectes austrinum* sensu Kielan-Jaworowska et al. [2004]) from Laguna Umayo (Muizon, 1991; Sigé et al., 2004). According to Muizon and Ladevèze (2020: 607), *Peradectes* cf. *austrinum* presents more similarities with the type species of the Peradectidae, *Pd. elegans*, than with any other South American metatherians except *Pd. austrinum* from Laguna Umayo. The diagnostic features proposed to attribute the Tiupampan specimen to *Peradectes*, namely the straight centrocrista and the subequal volume and height of the paracone and the metacone (Marshall & Muizon, 1988; Muizon, 1991), are here regarded as symplesiomorphies among stem-marsupialiforms. The *Peradectes* cf. *austrinum* M3 (Muizon, 1991: fig. 1g-i) bears a stylar cusp D mesiolabial to the metacone (Fig. 6A; see also Zimicz, 2012: fig. 12.11), as well as a strong metaconule, and a relatively high protocone, distolingual to the paracone. These characters are known, not exclusively, in M3s of the earliest peradectids, with the notable exception of the mesiolabially positioned

stylar cusp D compared with the metacone (e.g., see the early Danian *Pd. minor*; Fig. 6; Clemens, 2006: fig. 2E; Williamson et al., 2012: fig. 7D). Interestingly, among the Tiupampa fauna, this latter character occurs in most pucadelphydans (e.g., *Andinodelphys* Marshall and Muizon, 1988, *Incadelphys*, *Mayulestes*, *Mizquedelphys* Marshall and Muizon, 1988, *Pucadelphys*, *Szalinia* Muizon and Cifelli, 2001; see illustrations in Muizon [1991], Muizon and Cifelli [2001], and Muizon and Ladevèze [2020]), whereas it is absent in the 19 unequivocal peradectid species with documented upper molars (see species list in Gernelle et al., 2024a: table 3; in addition to *Golerdelphys stocki* and *Peradectes* sp. nov. 1 and 3 [this work]). Based on our results, the presence of stylar cusp D labial (**94[1]**) or distolabial to the metacone (**94[2]**) is interpreted, within Metatheria, as a synapomorphy of Peradectidae (convergent with, for example, Peratheriinae; the reverse condition in the early diverging notometatherian pucadelphydans, *Thylacodon* and *Swaindelphys* is here a synplesiomorphy shared with the Cretaceous marsupialiforms; e.g., Fig. 3 for the M3 of *Thylacodon*). For these reasons, '*Peradectes*' cf. *austrinum* is here not regarded as a peradectid (contra Muizon & Ladevèze, 2020). A more parsimonious hypothesis is that this taxon possibly represents an offshoot of the early South American radiation represented by the Pucadelphyda (sensu Beck et al., 2022: 341; Muizon et al., 2018). Beck et al. (2022: 309) pointed out that the close affinity of the Tiupampan (SALMA) and Puercan (NALMA) faunas recovered in Gelfo et al. (2009) and more recently supported in Muizon and Ladevèze (2020), which is largely due to the shared presence of *Peradectes*, is problematic for at least four reasons related to *Peradectes*. Thus, the absence of peradectids in Tiupampa strengthens the conclusions of Beck et al. (2022) regarding the compromise, approximate age, of the Tiupampa mammal fauna, provisionally considered between ~65 and 59 Ma by these authors (instead of correlated with chron 28r).

Peradectes austrinum was recorded from the Laguna Umayo fossil-bearing red mudstone unit (Peru; most likely latest Paleocene/earliest Eocene in age; Sigé et al., 2004) by three labial fragments of upper molars (Sigé, 1972: pl. 1, figs. 1-3). The peradectid status of *Pd. austrinum* has long been questioned (Agnolín, 2024: 186; Clemens, 1982; Kielan-Jaworowska et al., 2004: table 2.21; Montellano, 1992: 46), yet not on the basis of detailed morphological comparisons. The M3 holotype (LU 5968-10) has a much higher metacone than paracone (contra Muizon & Ladevèze, 2022: 632; note that the M1 or M2 metacone is broken apically, hampering any conclusion regarding this specimen) and, above all, both M1 or M2 (although this is less certain because of the broken metacone) and M3 have stylar cusp D mesiolabial to the metacone (Fig. 6B-C; see also Kielan-Jaworowska et al. [2004: fig. 12.11E$_2$], and Sigé [1972: fig. 3a]). Although a metacone much higher than the paracone occurs in some early *Peradectes* species (e.g., *Peradectes coprexeches*, Williamson & Taylor, 2011: fig. 6.7), stylar cusp D mesiolabial to the metacone is absent in all peradectids, as shown above. Interestingly, this character state occurs even in early Eocene South American 'opossum-like' taxa such as *Derorhynchus* (Carneiro & Oliveira, 2023: fig. 14I) and *Itaboraidelphys* Marshall and Muizon, 1984 (Marshall & Muizon, 1984: fig. e) from the Brasilian

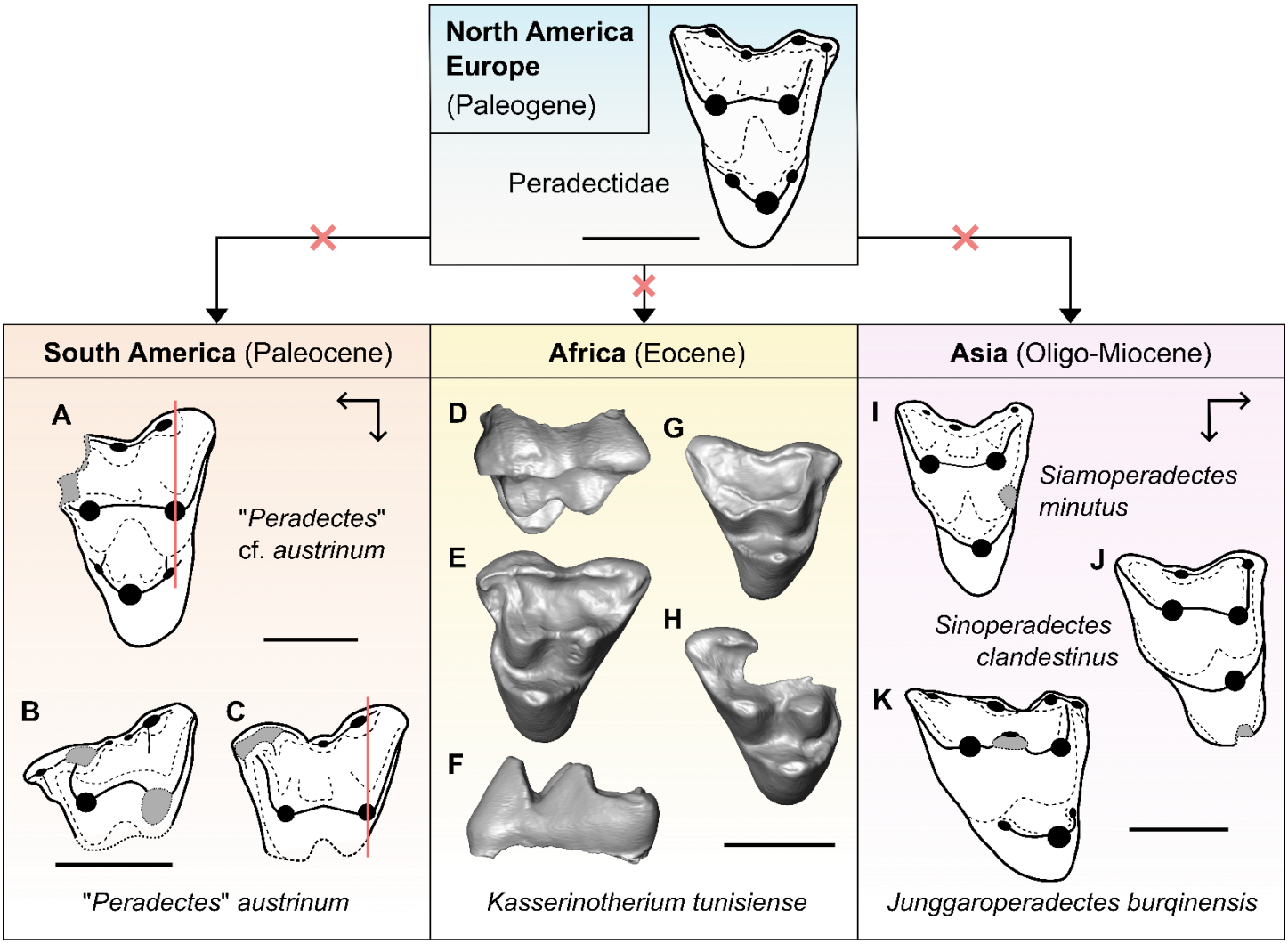

Figure 6. Peradectidae (here illustrated by an M3 of *Peradectes minor*) are endemic to North America and Europe based on all fossil material discovered to date. Illustrations of all taxa from South America, Africa, and Asia, considered peradectids before this study are provided. **A-C**. Interpretative drawings of occlusal views of upper molars from South America (Tiupampa and Laguna Umayo), based on casts. **A**. Left M3 YPFB Pal 6132 of '*Peradectes*' cf. *austrinum* from Tiupampa (Bolivia, early/middle Paleocene). **B-C**. Labial fragments of the left M1 or M2 LU 5968-6 (B) and of the left M3 holotype LU 5968-10 (C) of '*Peradectes*' *austrinum* (Sigé, 1971) from Laguna Umayo (latest Paleocene/earliest Eocene). The axis perpendicular to the paracone-metacone axis is depicted on M3s drawings by the red vertical line passing through the metacone. **D-H**. 3D surface models of the upper molars of *Kasserinotherium tunisiense* Crochet, 1986, from Chambi (Tunisia; late Ypresian/early Lutetian). **D-F**. Left ?M2 UM-EY-10, holotype of *K. tunisiense* in labial (D), occlusal (E), and distal (F) views. **G**. Right ?M1 UM-EY-12 in occlusal view. **H**. Right ?M2 fragment UM-EY-11 in occlusal view. **I-K**. Interpretative drawings of occlusal views of upper molars from Asia (Thailand and China). **I**. Right upper molar holotype of *Siamoperadectes minutus* Ducrocq et al., 1992 (TF 2630), from Mae Long (Thailand; Early Miocene). **J**. Right upper molar holotype of *Sinoperadectes clandestinus* Storch and Qiu, 2002 (IVPP V12564), from Songlinzhuang (eastern China, Early Miocene). **K**. Right M2 holotype of *Junggaroperadectes burqinensis* Ni et al., 2007 (IVPP V14410), from the Keziletuogayi Formation, in the Burqin region (China, early Oligocene). The arrows show the mesiolingual direction for South American and Asian molars. On all drawings, grey coloured areas are broken on the specimen, and dashed lines concern depressions on the occlusal surface. All scale bars equal 1 mm.

Itaboraí fauna. Thus, the attribution of the species from Laguna Umayo to peradectids is here discarded for the same reason as for the Tiupampan species: because of the relative position of the stylar cusp D, they do not share a 'peradectine upper molar pattern' (contra Sigé et al., 2004). The absence of peradectids in both Tiupampa and Laguna Umayo challenges the putative close affinity between these faunas, which has thus far been supported solely by the shared occurrence of *Peradectes* in recent parsimony analyses (contra Bergqvist et al., 2024: figs. 12-13, Online Resource 7).

A new still unnamed peradectid genus and species from the early Eocene Patagonian Laguna Fría fauna has been erected in the preliminary study of Tejedor et al. (2009), based on three lower molars and a figured M2. The metacone of the latter upper molar is completely broken, which prevents the correct orientation of the specimen allowing to describe with precision the relative position of stylar cusp D (Tejedor et al., 2009: fig. 3A; Zimicz, 2012: fig. 12.16). As for lower molars, it is mentioned that 'Trigonids and talonids are subequal in length but talonids are wider' (Tejedor et al., 2009: 7). In contrast to this description, we have shown that trigonids longer than talonids on m2s and m3s is a synapomorphy of Peradectidae within Metatheria (**24**^{2}), and trigonids are always subequal in width to (23^{1}) or wider than talonids (23^{0}) on peradectid m3s. Consequently, peradectids were probably not present in the early Eocene Laguna Fría fauna either (contra Tejedor et al., 2009). Goin (2006: 64) announced the discovery of a 'surprising diversity of peradectids' from the Las Flores and Tufolitas Laguna del Hunco Formations (Patagonia), and justified in this way the provisional allocation of the family Peradectidae in the 'Peradectoidea' (Crochet, 1979) sensu Marshall et al., 1990 (the 'Peradectoidea' sensu Goin [2006] are equivalent to the 'Peradectia' Marshall et al., 1990 sensu Carneiro & Oliveira [2023]) together with the bunodont South American Caroloameghiniidae. Only two of these 'peradectid' materials from the Las Flores Formation have been formally illustrated (Goin 2003: fig. 3C-D) since the claim of Goin (2006). The stylar cusp D mesiolabial to the metacone apex on the M2 (Goin 2003: fig. 3D) once again invalidates the attribution of this unknown taxon to Peradectidae (contra Goin, 2003, 2006). The same applies to the prominent talonid of the lower molar reported as an m2 (Goin 2003: fig. 3C). Furthermore, none of the Las Flores Formation molars attributed to Peradectidae in the unpublished Phd thesis of Zimicz (2012: figs. 12.13-12.15) exhibits the synapomorphies of this clade. Thus, both the 'Peradectoidea' (sensu Goin et al., 2016) and 'Peradectia' (sensu Carneiro & Oliveira, 2023) concepts as currently defined should be regarded with extreme caution, all the more so because of the lack of phylogenetic corroboration for the purported relationship (Agnolín, 2024: 69; Beck, 2023: 43). Finally, one of the smallest specimens from the Itaborai metatherian fauna, a fragment of right dentary with an m4 and a partial m3 first considered a close relative of *Armintodelphys* by Carneiro and Oliveira (2023: fig. 15), has recently been reinterpreted as a herpetotheriid by Carneiro et al. (2024a).

Altogether and based on all current evidence, the occurrence of the Peradectidae or close relatives in South America seems highly unlikely, as recently suggested by Agnolín (2024: 70). The possibility of

an origin of all European peradectids from South America argued by Crespo and Goin (2021) is thus not supported.

New insights on the disputed nature and affinities of the African taxon Kasserinotherium

Three upper molars from the late Ypresian or early Lutetian of the Chambi massif (Tunisia; see Ravel et al., 2016), each with a straight centrocrista, were described as *Kasserinotherium tunisiense* Crochet, 1986 (Fig. 6D-H), a taxon first interpreted as a peradectid (Crochet, 1986). The metatherian nature of *Kasserinotherium* has been challenged by various authors (Gunnell, 2010; Hooker, 1998; McKenna & Bell, 1997; Van Couvering & Delson, 2020). According to Goin and Candela (2004) and Beck (2015), *Kasserinotherium* shares numerous dental features with the metatherians *Wirunodon* Goin and Candela, 2004, from the Santa Rosa fauna (Peruvian Amazonia; possibly middle/late Eocene), or with both *Wirunodon* and *Archaeonothos* Beck, 2015 (Tingamarra Local Fauna, Australia; early Eocene), respectively. More recently, in a revision of the taxonomy of African metatherians, Crespo and Goin (2021: 139) argued that *Kasserinotherium*, *Wirunodon*, and *Archaeonothos* are probably part of a dubious 'early peradectoid offshoot' (see 'Peradectoidea' above) restricted to the three Gondwanan continents (Africa, South America and Oceania). *Kasserinotherium* has thus been considered an example of metatherian colonization of Africa from South America (Beard et al., 2023; Crespo & Goin, 2021), or alternatively from Europe given its first putative affinities with Peradectidae sensu stricto (Tabuce et al., 2005). For these reasons, a correct morphological characterisation of *Kasserinotherium* is crucial for establishing palaeobiogeographical scenarios.

Here, a new comparative description of *Kasserinotherium* is proposed based on the study of the original specimens (upper molars only), here illustrated through pictures of the 3D surface models. The holotype is complete and is the best preserved specimen (Fig. 6D-F). *Kasserinotherium* has an unexpected combination of upper molar features for a marsupialiform, namely: (i-a) the majority of the talon surface is occupied by the protocone (see its labiolingual width), so that (i-b) a longitudinal fossa instead of a trigon basin is present on the three specimens (Fig. 6E, G-H); (ii) the protocone is not procumbent on the holotype; (iii) an emargination close to the distal margin of the protocone base is present, instead of a distal emargination of the crown between the talon and the stylar shelf (Fig. 6E, G); (iv) the protocone is higher than both the paracone and the metacone (Fig. 6F), and especially, the paracone is slightly higher than the metacone (Fig. 6D); (v) there are no conules, even as trace in mesial and distal views; (vi) the paracingulum of the holotype is interrupted at the level of the connection preparacrista/protocone by a deep mesial emargination; (vii) the paracone and the metacone are adjoined at base (Fig. 6D); (viii) the parastylar wing is (viii-a) more developed labially than the metastylar wing on the holotype (the putative M3), instead of the opposite or equally labially projecting wings in most marsupialiform M3s, and (viii-b) as developed labially as the metastylar wing on the putative M1 UM-EY-12 (Fig. 6G), instead of less

labial than the metastylar wing in most marsupialiform M1s; and (ix) although there is a stylar line, no metatherian stylar cusp pattern is present; in particular, no stylar cusps A and B are clearly delimited (Fig. 6D).

As a matter of fact, none of the characters cited above are present in *Wirunodon*, *Archaeonothos*, and Cenozoic Laurasian marsupialiforms. However, most of these traits can be occasionally observed in at least some small Paleocene-Eocene African eutherians (e.g., the adapisoriculid *Afrodon* Gheerbrant, 1988; see in particular *Afrodon tagourtensis* Gheerbrant, 1993, of which the holotype has three features cited above [iii, viii, ix] out of the seven assessable; pers. obs. KG), as first mentioned by Hooker (1998: 443). *Kasserinotherium* is thus here regarded as a eutherian rather than a metatherian (contra Beck, 2015; Crespo & Goin 2021; Crespo et al., 2022; Crochet, 1986; Goin & Candela, 2004). As in many other small insectivorous eutherians, possible morphological similarities with metatherians are only superficial (e.g., see Gheerbrant, 1991). As a consequence of this reallocation, UM-EY-10 (holotype) and UM-EY-11 are interpreted as M2s rather than M3s (Fig. 6D-F, H), and UM-EY-12 is probably an M1 (Fig. 6G). The 'stylar cusps' of *Kasserinotherium* are interpreted as a parastyle, a mesostyle, and a metastyle. The only metatherians known from Africa become the peratheriine *Peratherium africanum* Simons and Bown, 1984, and, putatively, the ?herpetotheriid *Morotodon* Crespo et al., 2022 (see Crespo & Goin, 2021).

Upper molars of Oligo-Miocene Asian 'peradectids'

The three genera *Siamoperadectes* Ducrocq et al., 1992, from Mae Long, in Thailand (Early Miocene; see Mein & Ginsburg, 1997), *Sinoperadectes* Storch and Qiu, 2002 (Early Miocene), and *Junggaroperadectes* Ni et al., 2007 (early Oligocene) from China (Fig. 6I-K), have been described as peradectids based on a few upper molars (two for *Siamoperadectes* and one each for *Sinoperadectes* and *Junggaroperadectes*; see Ducrocq et al., 1992; Mein & Ginsburg, 1997; Ni et al., 2007; Storch & Qiu, 2002). The Neogene *Siamoperadectes* and *Sinoperadectes* (Fig. 6I-J), both assumed to be from the MN4 biozone, share an unusual morphology compared with unequivocal Cenozoic Laurasian marsupialiforms, with a distal cingulum extending along the distal edge of the metacone, and the absence of any stylar cusp A spur (contra Ducrocq et al., 1992, for the latter character). Contrary to the description of Mein and Ginsburg (1997: 785), the second illustrated and described specimen of *Siamoperadectes* seems to present a faint distal cingulum. Likewise, the protocone of *Sinoperadectes* (Fig. 6J) also bears mesial and distal cingula (Storch & Qiu, 2002: fig. 2C-D). The additional cingula were already regarded as unusual features for Cenozoic Laurasian marsupialiforms by both Ducrocq et al. (1992) and Storch and Qiu (2002), which led these authors to consider the additional cingula as diagnostic features (compared with unequivocal peradectids) of the genera they defined. Because stylar cusp A is lacking, the two distinct but low stylar cusps evoke by their position a parastyle/mesostyle pattern rather than the metatherian stylar cusps B and C. These observations shed serious doubts on the metatherian status of

Siamoperadectes and *Sinoperadectes*, here reinterpreted as indeterminate eutherian taxa (contra Ducrocq et al., 1992; Storch & Qiu, 2002).

The affinity of *Junggaroperadectes* (Fig. 6K) with Cenozoic marsupialiforms from the Northern Hemisphere is less questionable: it presents four distinct stylar cusps in A to D positions (stylar cusp D is small but present; contra Ni et al., 2007), as well as a single cingulum (paracingulum). Ni et al. (2007) stated that *Junggaroperadectes* represents a morphological 'intermediate' between Paleogene Euro-American peradectids and the Neogene *Siamoperadectes* and *Sinoperadectes*, and discarded possible affinities with the almost coeval herpetotheriid *Asiadidelphis* Gabunia et al., 1990, which shows 'significant morphological differences' according to the authors (i] a V-shaped centrocrista; ii] a relatively labiolingually narrower stylar shelf; and iii] a dominant central stylar cusp). A clear clue of the presence of a V-shaped centocrista similar to that of herpetotheriids, including *Asiadidelphis zaissanense* Gabunia et al., 1990 (type species of *Asiadidelphis*), is often the presence of a labial tip of the centrocrista (sometimes cusp-like: 'central cusp' in Godthelp et al., 1999; 'central cuspule/ridge' in Carneiro & Oliveira, 2023; 'centrocrista tip' in Gernelle et al., 2024b: fig. 4K) marked labially to the paracone/metacone level, approximately midway between the paracone/metacone and stylar cusp C (e.g., see Ziegler et al., 2007: fig. 3.4-5, for *Asiadidelphis zaissanense*). Such a structure seems to occur in *Junggaroperadectes* (i) (see labial view; Ni et al., 2007: fig. 2b), but is absent in peradectids and, more generally, in taxa with a straight centrocrista (e.g., *Siamoperadectes*). Noteworthy, in *Junggaroperadectes* the paracone and the much larger metacone are triangular (correlated with a V-shaped centrocrista, see Material and methods section above). Some *Asiadidelphis* specimens have as relatively wide stylar shelf as in *Junggaroperadectes* (ii) on comparable locus (M2; Ziegler et al., 2007: fig. 3.5), and stylar cusp C or central stylar cusp is dominant in height (iii) in the latter as in at least some *Asiadidelphis* species (Emry et al., 1995). Thus, the molar features of *Junggaroperadectes* are more in keeping with unequivocal herpetotheriids like *Asiadidelphis* than with peradectids (contra Ni et al., 2007).

Altogether, following the reassessment of all putative peradectids from South America, Africa, and Asia, Peradectidae appear strictly restricted so far to North America, from early Paleocene to early Oligocene, and to Europe, during the early Eocene (Figs. 5-6).

Anatoliadelphyidae: affinities with peradectids or Gondwanan metatherians ? A third hypothesis

The clade *Anatoliadelphys* + Peradectidae recovered by the dated Bayesian analysis of Maga and Beck (2017: fig. 39) has not been supported by unambiguous synapomorphies in their study (Maga & Beck, 2017: table 6), but overall resemblance between the calcanei of *Anatoliadelphys* and probable peradectids have been proposed (Beck, 2023: 46; Maga & Beck, 2017). Given that our maximum parsimony analysis with unweighted characters comprising most peradectids, including the large *Mimoperadectes*, and the

dentally plesiomorphic anatoliadelphyid *Orhaniyeia*, does not yield a close relationship between them (Supplemental material 5: Fig. S6A), we concur with Beard et al. (2023) that the use of dental morphology fails in supporting any affinity of anatoliadelphyids with peradectids (contra Beck, 2023; Maga & Beck, 2017). In turn, Beard et al. (2023), strengthening the conclusions of Métais et al. (2018) through new dental specimens of *Orhaniyeia* and a phylogenetic analysis based on an updated matrix, recovered the Anatoliadelphyidae as part of the bunodont, predominantly South American Polydolopimorphia. The 'Polydolopimorphia' clade of Beard et al. (2023) includes *Glasbius* (of which the polydolopimorphian status has been questioned; see Beck, 2023, as well as this study) and *Roberthoffstetteria*. However, our analysis recovers *Orhaniyeia* nested within a clade with notometatherians except those from Tiupampa (Supplemental material 5: Fig. S6A), hence neither close to *Glasbius* nor *Roberthoffstetteria* (contra Beard et al., 2023; Métais et al., 2018). Anatoliadelphyidae have also been found as protodidelphids (e.g., Carneiro et al., 2018) but this hypothesis is not tested here. Given the result of a parsimony analysis equivalent to the previous one, but with downweighted homoplastic characters (Supplemental material 5: Fig. S6B), a third, still to be explored hypothesis, is that anatoliadelphyids emerged from a Laurasian 'herpetotheriid' stock, with which they share, among other characters, a V-shaped centrocrista (80^1), a relatively long talonid on m4 (25^1), and a hypoconid positioned distalabially to the entoconid (**42^1**). However, this result must be interpreted with care. In fact, the use of implied weighting in phylogenetics has been criticized (e.g., Congreve & Lamsdell, 2016; but see Goloboff et al., 2018). Second, at least another polydolopimorphian considered closer to anatoliadelphyids than to *Roberthoffstetteria* by Beard et al. (2023), such as *Chulpasia*, should be included. In order to test the alternative of an 'herpetotheriid' origin for anatoliadelphyids, a possible promising approach should be to study the relatively large herpetotheriids from the latest early to earliest middle Eocene (close to the Ypresian/Lutetian boundary, ~MP11) Messel Pit locality (*Amphiperatherium* aff. *maximum* in Kurz, 2007; named *Amphiperatherium* sp. in Kurz & Habersetzer, 2018; Smith et al., 2024) and the early middle Eocene (early Lutetian, MP12) Geiseltal Untere Mittelkohle locality (*Amphiperatherium* aff. *maximum* in Storch & Haubold, 1989) (note that the anatoliadelphyids are also Lutetian in age), which preserve postcranials, cranial bones, and teeth. For instance, Anatoliadelphyidae present relatively large M4s/m4s (e.g., the m4 is much longer than the more anterior molars). This character is unknown in herpetotheriids, except in the specimens from Messel and Geiseltal (see Gernelle et al., 2024b; and illustrations in Supplemental material 6: Figs. S1-2).

Conclusion

The well resolved tree topologies resulting from new phylogenetic inferences led us to hypothesize that all Cenozoic marsupialiforms form a natural group, the Notometatheria, that first moderately but rapidly diversified just after the K-Pg mass extinction (Figures 3-4), notably through the emergences of the

Laurasian peradectids and ‘herpetotheriids’, never characterized in a phylogenetic context beforehand. Although we advocate that the dental morphology of metatherians convey a fundamental phylogenetic signal (see also Goin, 2003: 40), especially when an attempt to control their redundancy is performed (Figure 2), the previous hypothesis will need to be reassessed through the consideration of other sources of morphological characters. Because the concept of Notometatheria is of broad palaeobiogeographic significance, a more balanced sampling in favour of Southern Hemisphere taxa should be conducted. Based on the phylogenetic framework newly established, quite congruent with the appearance order of taxa in the fossil record, the intrafamilial systematics of the convincingly monophyletic Peradectidae turns out to be complex (with for instance the necessary allocation of European ‘*Peradectes*’ to a new genus; Figure 5), whereas their comprehensive palaeobiogeographic history is much simpler than expected, with most likely a single dispersal from North America to Europe just after the Paleocene-Eocene Thermal Maximum (Figure 5), and apparently no dispersals outside these continents (Figure 6). The evolutionary history inferred for Laurasian notometatherians thus appears less puzzling than the complex biogeography of the more diversified Southern Hemisphere notometatherians as understood based on fossil evidence (Sigé et al. 2009; Beck 2012) from the ‘Austral Kingdom’, within which the early evolution of Marsupialia probably occurred (Beck, 2017b). Future research should focus on the resolution of the intrafamilial relationships of the Herpetotheriidae, initiated by Gernelle et al. (2024b) for the European representatives, the Peratheriinae. This will draw a complete revised picture of the evolutionary history of Cenozoic Laurasian marsupialiforms in a global spatiotemporal context.

References

Agnolín, F. L. (2024). *History of Cenozoic Mammals from South America: A New Model*. Springer. https://doi.org/10.1007/978-3-031-56266-2

Anemone, R. L., Jones, M. F., Van Regenmorter, J., & **Beard, K. C.** (2024). A latest Paleocene mammal fauna from the Great Divide Basin in southern Wyoming and a revised biozonation of the Clarkforkian land mammal age. *Journal of Vertebrate Paleontology*, *e2424139*. https://doi.org/10.1080/02724634.2024.2424139

Antoine, P.-O. (2002). Phylogénie et évolution des Elasmotheriina (Mammalia, Rhinocerotidae). *Mémoires du Muséum National d’Histoire Naturelle, 188*, 1–358.

Archibald, J. D. (1982). A study of Mammalia and geology across the Cretaceous-Tertiary boundary in Garfield County, Montana. *University of California Publications in Geological Sciences, 122*, 1-286.

Archie, J. W. (1989). Homoplasy excess ratios: new indices for measuring levels of homoplasy in phylogenetic systematics and a critique of the consistency index. *Systematic Zoology*, *38*(3), 253-269. https://doi.org/10.2307/2992286

Beard, K. C., Coster, P. M., Ocakoğlu, F., Licht, A., & **Métais, G.** (2023). Dental anatomy, phylogenetic relationships and paleoecology of *Orhaniyeia nauta* (Metatheria, Anatoliadelphyidae), a Gondwanan

component of the insular Eocene mammal fauna of Balkanatolia (north-central Turkey). *Journal of Mammalian Evolution, 30*(4), 859-872. https://doi.org/10.1007/s10914-023-09680-6

Beck, R. M. D. (2012). An 'ameridelphian'marsupial from the early Eocene of Australia supports a complex model of Southern Hemisphere marsupial biogeography. *Naturwissenschaften, 99*(9), 715-729. https://doi.org/10.1007/s00114-012-0953-x

Beck, R. M. D. (2015). A peculiar faunivorous metatherian from the early Eocene of Australia. *Acta Palaeontologica Polonica, 60*(1), 123-129. http://dx.doi.org/10.4202/app.2013.0011

Beck, R. M. D. (2017a). The biogeographical history of non-marine mammaliaforms in the Sahul region. In M. C. Ebach (Ed.), Handbook of Australasian Biogeography (pp. 329-366). CRC Press, Boca Raton.

Beck, R. M. D. (2017b). The skull of *Epidolops ameghinoi* from the early Eocene Itaboraí fauna, southeastern Brazil, and the affinities of the extinct marsupialiform order Polydolopimorphia. *Journal of Mammalian Evolution, 24*(4), 373-414. https://doi.org/10.1007/s10914-016-9357-6

Beck, R. M. D. (2023). Diversity and phylogeny of marsupials and their stem relatives (Metatheria). In N. C. Cáceres, & C. R. Dickman (Eds.), *American and Australasian Marsupials* (pp. 23-88). Springer. https://doi.org/10.1007/978-3-030-88800-8_35-1

Beck, R. M. D. (in press). Current understanding of the phylogeny of Metatheria: a review. In F. J. Goin, & A. M. Forasiepi (Eds.), *New World marsupials and their extinct relatives: 100 million years of evolution*. Springer.

Beck, R. M. D., Godthelp, H., Weisbecker, V., Archer, M., & **Hand, S. J.** (2008). Australia's oldest marsupial fossils and their biogeographical implications. *PLoS ONE, 3*(3), e1858. https://doi.org/10.1371/journal.pone.0001858

Beck, R. M. D., Travouillon, K. J., Aplin, K. P., Godthelp, H., & **Archer, M.** (2014). The osteology and systematics of the enigmatic Australian oligo-Miocene metatherian *Yalkaparidon* (Yalkaparidontidae; Yalkaparidontia;? Australidelphia; Marsupialia). *Journal of Mammalian Evolution, 21*, 127-172. https://doi.org/10.1007/s10914-013-9236-3

Beck, R. M. D., Voss, R. S., & **Jansa, S. A.** (2022). Craniodental morphology and phylogeny of marsupials. *Bulletin of the American Museum of Natural History, 457*, 1-350. https://doi.org/10.1206/0003-0090.457.1.1

Beck, R. M. D., Vries, D. de, Janiak, M. C., Goodhead, I. B., & **Boubli, J. P.** (2023). Total evidence phylogeny of platyrrhine primates and a comparison of undated and tip-dating approaches. *Journal of Human Evolution, 174*, 103293. https://doi.org/10.1016/j.jhevol.2022.103293

Beck, R. M. D., Warburton, N. M., Archer, M., Hand, S. J., & **Aplin, K. P.** (2016). Going underground: postcranial morphology of the early Miocene marsupial mole *Naraboryctes philcreaseri* and the evolution of fossoriality in notoryctemorphians. *Memoirs of Museum Victoria, 74*, 151-171. http://doi.org/10.24199/j.mmv.2016.74.14

Bergqvist, L. P., Carneiro, L. M., Zanesco, T., Castro, L. O. R., & **Oliveira, J. A. de** (2024). Revisiting old data to unveil the history and age of the Itaboraí Basin fossil mammals. *Journal of Mammalian Evolution, 31*, 42. https://doi.org/10.1007/s10914-024-09738-z

Billet, G., & **Bardin, J.** (2019). Serial homology and correlated characters in morphological phylogenetics: modeling the evolution of dental crests in placentals. *Systematic Biology, 68*(2), 267–280. https://doi.org/10.1093/sysbio/syy071

BiochroM'97. (1997). Synthèse et tableaux de corrélation. In J. Aguilar, S. Legendre, & J. Michaux (Eds.), *Actes du Congrès BiochroM'97 Vol. 21* (pp. 769-805). Mémoire et Travaux de l'E.P.H.E., Institut de Montpellier.

Bown, T. M., & **Rose, K. D.** (1979). *Mimoperadectes*, a new marsupial, and *Worlandia*, a new dermopteran, from the lower part of the Willwood Formation (early Eocene), Bighorn Basin, Wyoming. *Contributions from the Museum of Paleontology, The University of Michigan, 25*(4), 89–104.

Brady, P. L., Castrellon Arteaga, A., López-Torres, S., & **Springer, M. S.** (2024). The effects of ordered multistate morphological characters on phylogenetic analyses of eutherian mammals. *Journal of Mammalian Evolution, 31*(3), 28. https://doi.org/10.1007/s10914-024-09727-2

Bremer, B., Jansen, R. K., Oxelman, B., Backlund, M., Lantz, H., & **Kim, K. J.** (1999). More characters or more taxa for a robust phylogeny—case study from the coffee family (Rubiaceae). *Systematic Biology, 48*(3), 413-435. https://doi.org/10.1080/106351599260085

Bremer, K. (1994). Branch support and tree stability. *Cladistics, 10*, 295–304. https://doi.org/10.1111/j.1096-0031.1994.tb00179.x

Brocklehurst, N., & **Benevento, G. L.** (2020). Dental characters used in phylogenetic analyses of mammals show higher rates of evolution, but not reduced independence. *PeerJ, 8*, e8744. https://doi.org/10.7717/peerj.8744

Burmeister, H. (1854). *Systematische Übersicht der Thiere Brasiliens, welche während einer Reise durch die Provinzen von Rio de Janeiro und Minas Geraës gesammelt oder beobachtet*. G. Reimer, Berlin.

Carneiro, L. M., Goin, F. J., Bampi, H., Silva, R. C., Rangel, C. C., Guimarães, B. M. G., & **Arêas, M. R.** (2024a). A tiny-sized Herpetotheriidae (Mammalia, Metatheria) from the Itaboraí basin (early Eocene), Brazil: Paleobiogeographic and systematic implications for Herpetotheriidae. *Journal of South American Earth Sciences, 144*, 105016. https://doi.org/10.1016/j.jsames.2024.105016

Carneiro, L. M., & **Oliveira, É. V.** (2017). The Eocene South American metatherian *Zeusdelphys complicatus* is not a protodidelphid but a hatcheriform: Paleobiogeographic implications. *Acta Palaeontologica Polonica, 62*(3), 497-507. https://doi.org/10.4202/app.00351.2017

Carneiro, L. M., & **Oliveira, É. V.** (2023). Paleogene metatherians from the Itaboraí Basin: diversity and affinities. In N. C. Cáceres, & C. R. Dickman (Eds.), *American and Australasian Marsupials* (pp. 269-324). Springer. https://doi.org/10.1007/978-3-030-88800-8_5-1

Carneiro, L. M., Oliveira, É. V., & **Goin, F. J.** (2018). *Austropediomys marshalli* gen. et sp. nov., a new Pediomyoidea (Mammalia, Metatheria) from the Paleogene of Brazil: Paleobiogeographic implications. *Revista Brasileira de Paleontologia, 21*(2), 120-131. https://doi.org/10.4072/rbp.2018.2.03

Carneiro, L. M., Oliveira, É. V., Silva, R. C., Bampi, H. & **Arêas, M. R.** (2024b). Systematic and trophic diversity of protodidelphines (Mammalia, Marsupialia, Protodidelphidae): Evidence of a short time diversification during the onset of the Eocene. *Journal of South American Earth Sciences, 148*, 105104. https://doi.org/10.1016/j.jsames.2024.105104

Case, J. A., Goin, F. J. & **Woodburne, M. O.** (2005). "South American" marsupials from the Late Cretaceous of North America and the origin of marsupial cohorts. *Journal of Mammalian Evolution, 12*(3-4), 461-494. https://doi.org/10.1007/s10914-005-7329-3

Cifelli, R. L. (1993). Early Cretaceous mammal from North America and the evolution of marsupial dental characters. *Proceedings of the National Academy of Sciences, 90*(20), 9413-9416. https://doi.org/10.1073/pnas.90.20.9413

Cifelli, R. L. (1994). Therian mammals of the Terlingua local fauna (Judithian), Aguja Formation, Big Bend of the Río Grande, Texas. *Rocky Mountain Geology*, *30*(2), 117-136.

Cifelli, R. L., & **Johanson, Z.** (1994). New marsupial from the Upper Cretaceous of Utah. *Journal of Vertebrate Paleontology*, *14*(2), 292-295. https://doi.org/10.1080/02724634.1994.10011558

Claytor, J. R., Weaver, L. N., Tobin, T. S., & **Wilson, G. P.** (2023). New mammalian local faunas from the first ca. 80 ka of the Paleocene in northeastern Montana and a revised model of biotic recovery from the Cretaceous–Paleogene mass extinction. *Journal of Vertebrate Paleontology*, *42*(6), e2222777. https://doi.org/10.1080/02724634.2023.2222777

Clemens, W. A. (1966). Fossil mammals of the type Lance Formation, Wyoming. Part II, Marsupialia. *University of California Publications in Geological Sciences*, *62*, 1–122.

Clemens, W. A. (1982). Review of J.-Y. Crochet, Les Marsupiaux du Tertiaire d'Europe (Éditions de la Fondation Singé-Polignac). *Journal of Mammalogy*, *63*(4), 724-725. https://doi.org/10.2307/1380299

Clemens, W. A. (2006). Early Paleocene (Puercan) peradectid marsupials from northeastern Montana, North American Western Interior. *Palaeontographica Abteilung A*, *277*(1-6), 19–31. https://doi.org/10.1127/pala/277/2006/19

Cohen, J. E., Davis, B. M., & **Cifelli, R. L.** (2020). Geologically oldest Pediomyoidea (Mammalia, Marsupialiformes) from the Late Cretaceous of North America, with implications for taxonomy and diet of earliest Late Cretaceous mammals. *Journal of Vertebrate Paleontology*, *40*(5), e1835935. https://doi.org/10.1080/02724634.2020.1835935

Congreve, C. R., & **Lamsdell, J. C.** (2016). Implied weighting and its utility in palaeontological datasets: a study using modelled phylogenetic matrices. *Palaeontology*, *59*(3), 447–462. https://doi.org/10.1111/pala.12236

Cope, E. D. (1873). Third notice of the extinct Vertebrata from the Tertiary of the Plains. *Paleontological Bulletin*, *16*, 1–8.

Crespo, V. D., & **Goin, F. J.** (2021). Taxonomy and affinities of African cenozoic metatherians. *Spanish Journal of Palaeontology*, *36*(2), 133–148. https://doi.org/10.7203/sjp.36.2.20974

Crespo, V. D., & **Goin, F. J.** (in press). The Weddell Line, an early Cenozoic biogeographical barrier among Southern Hemisphere terrestrial mammals. *Ameghiniana*. https://doi.org/10.5710/AMGH.10.10.2024.3613

Crespo, V. D., Goin, F. J., & **Pickford, M.** (2022). The last African metatherian. *Fossil Record*, *25*(1), 173–186. https://doi.org/10.3897/fr.25.80706.

Crochet, J.-Y. (1977). Les didelphidés paléogènes holarctiques : historique et tendances évolutives. *Geobios, Mémoire spécial*, *1*, 127–134. https://doi.org/10.1016/S0016-6995(77)80012-0

Crochet, J.-Y. (1979). Diversité systématique des Didelphidae (Marsupialia) européens tertiaires. *Geobios*, *12*(3), 365‑378. https://doi.org/10.1016/S0016-6995(79)80117-5

Crochet, J.-Y. (1980). *Les Marsupiaux du Tertiaire d'Europe*. Edtions Foundation Singer-Polignac, Paris. https://doi.org/10.1163/9789004630802

Crochet, J.-Y. (1986). *Kasserinotherium tunisiense* nov. gen., nov. sp., troisième marsupial découvert en Afrique (Eocène inférieur de Tunisie). *Comptes Rendus de l'Académie des Sciences*, *302*(14), 923-926.

Dahlberg, E. L., Eberle, J. J., Sertich, J. J. W., & **Miller, I. M.** (2016). A new earliest Paleocene (Puercan) mammalian fauna from Colorado's Denver Basin, U.S.A. *Rocky Mountain Geology*, *51*(1), 1-22. https://doi.org/10.2113/gsrocky.51.1.1

Davis, B. M. (2007). A revision of "pediomyid" marsupials from the Late Cretaceous of North America. *Acta Palaeontologica Polonica*, *52*(2), 217-256.

Darlu, P., Tassy, P., Haese, C. d', & **Zaragüeta-Bagils, R.** (2019). *La Reconstruction phylogénétique: Concepts et Méthodes*. Editions matériologiques.

Ducrocq, S., Buffetaut, E., Buffetaut-Tong, H., Jaeger, J. J., Jongkanjanasoontorn, Y., & **Suteethorn, V.** (1992). First fossil marsupial from South Asia. *Journal of Vertebrate Paleontology*, *12*(3), 395–399. https://doi.org/10.1080/02724634.1992.10011468

Eaton, J. G. (1993). Therian mammals from the Cenomanian (Upper Cretaceous) Dakota Formation, southwestern Utah. *Journal of Vertebrate Paleontology*, *13*(1), 105-124. https://doi.org/10.1080/02724634.1993.10011491

Eberle, J. J., Clemens, W. A., McCarthy, P. J., Fiorillo, A. R., Erickson, G. M., & **Druckenmiller, P. S.** (2019). Northernmost record of the Metatheria: a new Late Cretaceous pediomyid from the North Slope of Alaska. *Journal of Systematic Palaeontology*, *17*(21), 1805-1824. https://doi.org/10.1080/14772019.2018.1560369

Eberle, J. J., Cohen, J., Foster, J., Hunt-Foster, R., & **Heckert, A.** (2024). A new Late Cretaceous metatherian from the Williams Fork Formation, Colorado. *PLoS ONE*, *19*(10), e0310948. https://doi.org/10.1371/journal.pone.0310948

Eberle, J. J., & **Lillegraven, J. A.** (1998). A new important record of earliest Cenozoic mammalian history: Geologic setting, Multituberculata, and Peradectia. *Rocky Mountain Geology*, *33*(1), 3-47. https://doi.org/10.2113/33.1.3

Eldridge, M. D. B., Beck, R. M. D., Croft, D. A., Travouillon, K. J., & **Fox, B. J.** (2019). An emerging consensus in the evolution, phylogeny, and systematics of marsupials and their fossil relatives (Metatheria). *Journal of Mammalogy*, *100*(3), 802-837. https://doi.org/10.1093/jmammal/gyz018

Emry, R. J., Lucas, S. G., Szalay, F. S., & **Tleuberdina, P. A.** (1995). A new herpetotheriine didelphid (Marsupialia) from the Oligocene of Central Asia. *Journal of Vertebrate Paleontology*, *15*(4), 850-854. https://doi.org/10.1080/02724634.1995.10011268

Engelman, R. K., Flynn, J. J., Wyss, A. R., & **Croft, D. A.** (2020). *Eomakhaira molossus*, a new saber-toothed sparassodont (Metatheria: Thylacosmilinae) from the early Oligocene (? Tinguiririan) Cachapoal locality, Andean Main Range, Chile. *American Museum Novitates*, *3957*, 1-75. https://doi.org/10.1206/3957.1

Farris, J. S. (1989). The retention index and the rescaled consistency index. *Cladistics*, *5*(4), 417-419. https://doi.org/10.1111/j.1096-0031.1989.tb00573.x

Fox, R. C. (1971). Marsupial mammals from the early Campanian Milk River Formation, Alberta, Canada. In D. M. Kermack, & K. A. Kermack (Eds.), *Early Mammals* (pp. 145-164). Zoological Journal of the Linnean Society.

Fox, R. C. (1983). Notes on the North American Tertiary marsupials *Herpetotherium* and *Peradectes*. *Canadian Journal of Earth Sciences*, *20*(10), 1565–1578. https://doi.org/10.1139/e83-146

Gabunia, L. R., Shevyreva, N. S., & **Gabunia, V. D.** (1990). A new oposssum (Didelphidae, Marsupialia, Metatheria, Mammalia) from the lowermost Oligocene in the Zaysan Basin (Eastern Kazakhstan) [in Russian]. *Paleontological Journal*, 101–109.

Gazin, C. L. (1952). The lower Eocene knight formation of western Wyoming and its mammalian faunas. *Smithsonian Miscellaneous Collections*, *117*(18), 1–82.

Gazin, C. L. (1956). Paleocene mammalian faunas of the Bison Basin in south-central Wyoming. *Smithsonian Miscellaneous Collections*, *131*(6), 1-57.

Gelfo, J. N., Goin, F. J., Woodburne, M. O., & **Muizon, C. de** (2009). Biochronological relationships of the earliest South American Paleogene mammalian faunas. *Palaeontology*, *52*(1), 251-269. https://doi.org/10.1111/j.1475-4983.2008.00835.x

Geoffroy, E. (1804) Mémoire sur un nouveau genre de mammifères à bourse, nommé *Péraméles*. *Annales du Muséum d'Histoire Naturelle, Paris*, *4*, 56–64.

Gernelle, K., Billet, G., Gheerbrant, E., Godinot, M., Marandat, B., Ladevèze, S., & **Tabuce, R.** (2024a). Taxonomy and evolutionary history of peradectids (Metatheria): new data from the early Eocene of France. *Journal of Mammalian Evolution*, *31*(3), 31. https://doi.org/10.1007/s10914-024-09724-5

Gernelle, K., Godinot, M., Marandat, B., Téodori, D., Ladevèze, S., & **Tabuce, R.** (2024b). Dental morphology evolution in early peratheriines, including a new morphologically cryptic species and findings on the largest early Eocene European metatherian. *Historical Biology*. https://doi.org/10.1080/08912963.2024.2403602

Gheerbrant, E. (1988). *Afrodon chleuhi* nov. gen., nov. sp., "insectivore" (Mammalia, Eutheria) lipotyphlé (?) du Paléocène marocain: données préliminaires. *Comptes Rendus de l'Académie des Sciences*, *307*(5), 1303-1309.

Gheerbrant, E. (1991). *Bustylus* (Eutheria, Adapisoriculidae) and the absence of ascertained marsupials in the Palaeocene of Europe. *Terra Nova*, *3*, 586–592. https://doi.org/10.1111/j.1365-3121.1991.tb00200.x

Gheerbrant, E. (1993). Premières données sur les mammifères insectivores de l'Yprésien du Bassin d'Ouarzazate (Maroc: site de N'Tagourt 2). *Neues Jahrbuch für Geologie und Paläontologie, Abhandlungen*, *187*(2), 225-242.

Godthelp, H., Archer, M., Cifelli, R., Hand, S. J., & **Gilkeson, C. F.** (1992). Earliest known Australian Tertiary mammal fauna. *Nature*, *356*, 514-516. https://doi.org/10.1038/356514a0

Godthelp, H., Wroe, S., & **Archer, M.** (1999). A new marsupial from the early Eocene Tingamarra Local Fauna of Murgon, southeastern Queensland: a prototypical Australian marsupial? *Journal of Mammalian Evolution*, *6*(3), 289-313. https://doi.org/10.1023/A:1020517808869

Goin, F. J. (2003). Early marsupial radiations in South America. In M. Jones, C. Dickman, & M. Archer (Eds.), *Predators with Pouches: the Biology of Carnivorous Marsupials* (pp. 30-42). CSIRO, Collingwood, Australia.

Goin, F. J. (2006). A review of the Caroloameghiniidae, Paleogene South America "primate-like" marsupials (?Didelphimorphia, Peradectoidea). In D. Kalthoff, T. Martin, & T. Möors (Eds.), *Festband für Herrn Professor Wighart v. Koenigswald anlässlich seines 65 Geburtstages. Palaeontographica Abteilung A*, *278*(1-6), 57–67. https://doi.org/10.1127/pala/278/2006/57

Goin, F. J., & **Candela, A. M.** (2004). New Paleogene marsupials from the Amazon Basin of eastern Perú. *Natural History Museum of Los Angeles County, Science Series*, *40*, 15–60.

Goin, F. J., Candela, A. M., & **Muizon, C. de** (2003). The affinities of *Roberthoffstetteria nationalgeographica* (Marsupialia) and the origin of the polydolopine molar pattern. *Journal of Vertebrate Paleontology*, *23*(4), 869-876. https://doi.org/10.1671/2383-11

Goin, F. J., Pascual, R., Tejedor, M. F., Gelfo, J. N., Woodburne, M. O., Case, J. A., Reguero, M. A., Bond, M., López, G. M., Cione, A. L., Sauthier, D. U., Balarino, L., Scasso, R. A., Medina, F. A., & **Ubaldón, M. C.** (2006). The earliest Tertiary therian mammal from South America. *Journal of Vertebrate Paleontology*, *26*(2), 505-510. https://doi.org/10.1671/0272-4634(2006)26[505:TETTMF]2.0.CO;2

Goin, F. J., Woodburne, M. O., Zimicz, A. N., Martin, G. M., & **Chornogubsky, L.** (2016). *A Brief History of South American Metatherians: Evolutionary Contexts and Intercontinental Dispersals*. Springer.

https://doi.org/10.1007/978-94-017-7420-8

Goloboff, P. A., Torres, A., & **Arias, J. S.** (2018). Weighted parsimony outperforms other methods of phylogenetic inference under models appropriate for morphology. *Cladistics*, *34*(4), 407-437. https://doi.org/10.1111/cla.12205

Grand, A., Corvez, A., Duque Velez, L. M., & **Laurin, M.** (2013). Phylogenetic inference using discrete characters: performance of ordered and unordered parsimony and of three-item statements. *Biological Journal of the Linnean Society*, *110*(4), 914-930. https://doi.org/10.1111/bij.12159

Gregory, W. K., & **Simpson, G. G.** (1926). Cretaceous Mammal Skulls from Mongolia. *Nature*, *118*, 698–699. https://doi.org/10.1038/118698a0

Gunnell, G. F. (2010). Marsupialia. In L. Werdelin, & W. J. Sanders (Eds.), *Cenozoic Mammals of Africa* (pp. 77-79). University California Press.

Herrera, J. P., & **Dávalos, L. M.** (2016). Phylogeny and divergence times of lemurs inferred with recent and ancient fossils in the tree. *Systematic Biology*, *65*(5), 772-791. https://doi.org/10.1093/sysbio/syw035

Hoek Ostende, L. W. van de, Bilgin, M., Braumuller, Y., Cailleux, F., & **Skandalos, P.** (2023). Live long and prosper? Assessing longevity of small mammal taxa using the NOW database. In I. Casanovas-Vilar, L. W. van de Hoek Ostende, C. M. Janis, & J. Saarinen (Eds.), *Evolution of Cenozoic Land Mammal Faunas and Ecosystems: 25 Years of the NOW Database of Fossil Mammals, Vertebrate Paleobiology and Paleoanthropology* (pp. 111–129). Springer. https://doi.org/10.1007/978-3-031-17491-9_8

Hooker, J. J. (1998). Mammalian faunal change across the Paleocene-Eocene transition in Europe. In M. P. Aubry, W. A. Berggren, & S. G. Lucas (Eds.), *Late Paleocene-Early Eocene Climatic and Biotic Events in the Marine and Terrestrial Records* (pp. 419–441). Columbia University Press.

Hooker, J. J., Sanchez-Villagra, M. R., Goin, F. J., Simons, E. L., Attia, Y., & **Seiffert, E. R.** (2008). The origin of Afro-Arabian 'didelphimorph' marsupials. *Palaeontology*, *51*(3), 635–648. https://doi.org/10.1111/j.1475-4983.2008.00779.x

Horovitz, I., Martin, T., Bloch, J., Ladevèze, S., Kurz, C., & **Sánchez-Villagra, M. R.** (2009). Cranial anatomy of the earliest marsupials and the origin of opossums. *PLoS One*, *4*(12), e8278. https://doi.org/10.1371/journal.pone.0008278

Hough, J. R. (1961). Review of Oligocene didelphid marsupials. *Journal of Paleontology*, *35*(1), 218–228.

Huxley, T. H. (1880). On the application of the laws of evolution to the arrangement of the Vertebrata and more particularly of the Mammalia. *Proceedings of the Zoological Society of London*, *43*, 649–662.

Illiger, C. (1811). *Prodromus Systematis Mammalium et Avium, Additis Terminis Zoographicis Utriusque Classis, Eorumque Versione Germanica*. C. Salfeld, Berlin.

Johanson, Z. (1994). New information concerning the late Cretaceous marsupial *Albertatherium* Fox, 1971. *Journal of Vertebrate Paleontology*, *14*(4), 595-602. https://doi.org/10.1080/02724634.1995.10011581

Johanson, Z. (1996). New marsupial from the Fort Union Formation, Swain Quarry, Wyoming. *Journal of Paleontology*, *70*(6), 1023–1031. https://doi.org/10.1017/S0022336000038725

Kielan-Jaworowska, Z., Cifelli R. L., & **Luo, Z.-X.** (2004). *Mammals from the Age of Dinosaurs: Origins, Evolution, and Structure*. Columbia University Press. https://doi.org/10.7312/kiel11918

Kielan-Jaworowska, Z., & **Dashzeveg, D.** (1989). Eutherian mammals from the Early Cretaceous of Mongolia. *Zoologica Scripta*, *18*(2), 347-355. https://doi.org/10.1111/j.1463-6409.1989.tb00460.x

Kihm, A. J., & **Schumaker, K. K.** (2015). Marsupials from the Chadronian (latest Eocene) Medicine Pole Hills local fauna, North Dakota. *Paludicola, 10*(2), 93-112.

Kirsch, J. A., Springer, M. S., & **Lapointe, F. J.** (1997). DNA-hybridisation studies of marsupials and their implications for metatherian classification. *Australian Journal of Zoology, 45*(3), 211-280. https://doi.org/10.1071/ZO96030

Korth, W. W. (2008). Marsupialia. In C. M. Janis, G. F. Gunnell, & M. D. Uhen (Eds.), *Evolution of Tertiary Mammals of North America: Volume 2, Small Mammals, Xenarthrans, and Marine Mammals* (pp 39–47). Cambridge University Press. https://doi.org/10.1017/CBO9780511541438

Korth, W. W. (2018). Review of the marsupials (Mammalia: Metatheria) from the late Paleogene (Chadronian–Arikareean: late Eocene–late Oligocene) of North America. *PalZ, 92*(3), 499-523. https://doi.org/10.1007/s12542-017-0396-y

Krishtalka, L., & **Stucky, R. K.** (1983). Paleocene and Eocene marsupials of North America. *Annals of Carnegie Museum, 52*(10), 229–263. https://doi.org/10.5962/p.330761

Kurz, C. (2007). The opossum-like marsupials (Didelphimorphia and Peradectia, Marsupialia, Mammalia) from the Eocene of Messel and Geiseltal – Ecomorphology, diversity and palaeogeography. *Kaupia, 15*, 3–65.

Kurz, C., & **Habersetzer, J.** (2018). Marsupials – a Surprise in Messel. In K. T. Smith, S. F. K. Schall, & J. Habersetzer (Eds.), *Messel – An Ancient Greenhouse Ecosystem* (pp. 217-221). Schweizerbart.

Ladevèze, S., & **Muizon, C. de** (2007). The auditory region of early Paleocene Pucadelphydae (Mammalia, Metatheria) from Tiupampa, Bolivia, with phylogenetic implications. *Palaeontology, 50*(5), 1123-1153. https://doi.org/10.1111/j.1475-4983.2007.00703.x

Ladevèze, S., Selva, C., & **Muizon, C. de** (2020). What are "opossum-like" fossils? The phylogeny of herpetotheriid and peradectid metatherians, based on new features from the petrosal anatomy. *Journal of Systematic Palaeontology, 18*(17), 1463–1479. https://doi.org/10.1080/14772019.2020.1772387

Ladevèze, S., Smith, R., & **Smith, T.** (2012). Reassessment of the morphology and taxonomic status of the earliest herpetotheriid marsupials of Europe. *Journal of Mammalian Evolution, 19*, 249–261. https://doi.org/10.1007/s10914-012-9195-0

Leslie, C. E., Peppe, D. J., Williamson, T. E., Heizler, M., Jackson, M., Atchley, S. C., Nordt, L., & **Standhardt, B.** (2018). Revised age constraints for Late Cretaceous to early Paleocene terrestrial strata from the Dawson Creek section, Big Bend National Park, west Texas. *Geological Society of America Bulletin, 130*(7-8), 1143-1163. https://doi.org/10.1130/B31785.1

Lewis, P. O. (2001). A likelihood approach to estimating phylogeny from discrete morphological character data. *Systematic Biology, 50*(6), 913-925. https://doi.org/10.1080/106351501753462876

Linnaeus, C. (1758). *Systema naturae per regna tria naturae, secundum classes, ordines, genera, species, cum characteribus, differentiis, synonymis, locis. Volume 1.* 10th Edition. Laurentii Salvii, Stockholm, 824 pp.

Loewen, M. A., Irmis, R. B., Sertich, J. J., Currie, P. J., & **Sampson, S. D.** (2013). Tyrant dinosaur evolution tracks the rise and fall of Late Cretaceous oceans. *PloS one, 8*(11), e79420. https://doi.org/10.1371/journal.pone.0079420

Maddison, W. P., & **Maddison, D. R.** (2019). Mesquite, a modular system for evolutionary analysis. Version 3.61.

Maga, A. M., & **Beck, R. M.** (2017). Skeleton of an unusual, cat-sized marsupial relative (Metatheria: Marsupialiformes) from the middle Eocene (Lutetian: 44-43 million years ago) of Turkey. *PLoS One, 12*(8), e0181712. https://doi.org/10.1371/journal.pone.0181712

Marivaux, L., Negri, F. R., Antoine, P.-O., Stutz, N. S., Condamine, F. L., Kerber, L., Pujos, F., Santos, R. V., Alvim, A. M. V., Hsiou, A. S., Bissaro, M. C. Jr., Adami-Rodrigues, K., & **Ribeiro, A. M.** (2023). An eosimiid primate of South Asian affinities in the Paleogene of Western Amazonia and the origin of New World monkeys. *Proceedings of the National Academy of Sciences*, *120*(28), e2301338120. https://doi.org/10.1073/pnas.2301338120

Marivaux, L., Vianey-Liaud, M., & **Jaeger, J.-J.** (2004). High-level phylogeny of early Tertiary rodents: dental evidence. *Zoological Journal of the Linnean Society*, *142*(1), 105-134. https://doi.org/10.1111/j.1096-3642.2004.00131.x

Marsh, O. C. (1889). Discovery of Cretaceous Mammalia. *American Journal of Science*, *3*(38), 81–92. https://doi.org/10.2475/ajs.s3-38.223.81

Marshall, L. G., Case, J. A., & **Woodburne, M. O.** (1990). Phylogenetic relationships of the families of marsupials. In H. H. Genoways (Ed.), *Current Mammalogy, Volume 2* (pp. 433-505). Plenum Press.

Marshall, L. G., & **Muizon, C. de** (1984). Un nouveau Marsupial didelphidé (*Itaboraidelphys camposi* nov. gen. nov. sp.) du Paléocène moyen (Itaboraïen) de Sao José de Itaboraí (Brésil). *Comptes Rendus de l'Académie des Sciences*, *299*(18), 1297-1300.

Marshall, L. G., & **Muizon, C. de** (1988). The dawn of the age of mammals in South America. *National Geographic Research*, *4*(1), 23–55.

Marshall, L. G., Muizon, C. de, & **Sigé, B.** (1983). Late Cretaceous mammals (Marsupialia) from Bolivia. *Geobios*, *16*(6), 739-745. https://doi.org/10.1016/S0016-6995(83)80090-4

Martin, J. E., Case, J. A., Jagt, J. W., Schulp, A. S., & **Mulder, E. W.** (2005). A new European marsupial indicates a Late Cretaceous high-latitude transatlantic dispersal route. *Journal of Mammalian Evolution*, *12*(3-4), 495-511. https://doi.org/10.1007/s10914-005-7330-x

Matthew, W. D., & **Granger, W.** (1921). New genera of Paleocene mammals. *American Museum Novitates*, *13*, 1–7.

Matzke, N. J., & **Irmis, R. B.** (2018). Including autapomorphies is important for paleontological tip-dating with clocklike data, but not with non-clock data. *PeerJ*, *6*, e4553. https://doi.org/10.7717/peerj.4553

McGrew, P. O. (1937). New marsupials from the Tertiary of Nebraska. *The Journal of Geology*, *45*(4), 448-455. https://doi.org/10.1086/624552

McKenna, M. C. (1960). Fossil Mammalia from the early Wasatchian Four Mile fauna, Eocene of northwest Colorado. *University of California Publications in Geological Sciences*, *37*(1), 1–130.

McKenna, M. C., & **Bell, S. K.** (1997). *Classification of Mammals: Above the Species Level*. Columbia University Press.

Mein, P., & **Ginsburg, L.** (1997). Les mammifères du gisement miocène inférieur de Li Mae Long, Thaïlande: systématique, biostratigraphie et paléoenvironnement. *Geodiversitas*, *19*(4), 783-844.

Métais, G., Coster, P. M., Kappelman, J. R., Licht, A., Ocakoğlu, F., Taylor, M. H., & **Beard, K. C.** (2018). Eocene metatherians from Anatolia illuminate the assembly of an island fauna during Deep Time. *PloS One*, *13*(11), e0206181. https://doi.org/10.1371/journal.pone.0206181

Montellano, M. (1992). Mammalian fauna of the Judith River Formation (Late Cretaceous, Judithian), northcentral Montana. *University of California Publications in Geological Sciences*, *136*, 1–115.

Muizon, C. de (1991). La fauna de mamíferos de Tiupampa (Paleoceno Inferior, Formacion Santa Lucia), Bolivia. In R. Suarez Soruco (Ed.), *Fósiles y Facies de Bolivia, Vol. 1. Vertebrados* (pp. 575-624). Revista Técnica de Yacimientos Petrolíferos Fiscales Bolivianos, 12(3-4).

Muizon, C. de (1998). *Mayulestes ferox*, a borhyaenoid (Metatheria, Mammalia) from the early Palaeocene of Bolivia. Phylogenetic and paleobiologic implications. *Geodiversitas, 20*(1), 19-142.

Muizon, C. de, & **Cifelli, R. L.** (2001). A new basal "didelphoid" (Marsupialia, Mammalia) from the early Paleocene of Tiupampa (Bolivia). *Journal of Vertebrate Paleontology*, *21*(1), 87-97. https://doi.org/10.1671/0272-4634(2001)021[0087:ANBDMM]2.0.CO;2

Muizon, C. de, & **Ladevèze, S.** (2020). Cranial anatomy of *Andinodelphys cochabambensis*, a stem metatherian from the early Paleocene of Bolivia. *Geodiversitas, 42*(30), 597-739. https://doi.org/10.5252/geodiversitas2020v42a30

Muizon, C. de, & **Ladevèze, S.** (2022). New material of *Incadelphys antiquus* (Pucadelphyda, Metatheria, Mammalia) from the early Palaeocene of Bolivia reveals phylogenetic affinities with enigmatic North and South American metatherians. *Geodiversitas, 44*(22), 609–643. https://doi.org/10.5252/geodiversitas2022v44a22

Muizon, C. de, Ladevèze, S., Selva, C., Vignaud, R., & **Goussard, F.** (2018). *Allqokirus australis* (Sparassodonta, Metatheria) from the early Palaeocene of Tiupampa (Bolivia) and the rise of the metatherian carnivorous radiation in South America. *Geodiversitas, 40*(16), 363-459. https://doi.org/10.5252/geodiversitas2018v40a16

Ni, X., Li, Q., Stidham, T. A., Li, L., Lu, X., & **Meng, J.** (2016). A late Paleocene probable metatherian (? deltatheroidan) survivor of the Cretaceous mass extinction. *Scientific Reports, 6*, 38547. https://doi.org/10.1038/srep38547

Ni, X., Meng, J., Wu, W., & **Ye, J.** (2007). A new Early Oligocene peradectine marsupial (Mammalia) from the Burqin region of Xinjiang, China. *Naturwissenschaften, 94*, 237–241. https://doi.org/10.1007/s00114-006-0182-2

O'Leary, M. A., Bloch, J. I., Flynn, J. J., Gaudin, T. J., Giallombardo, A., Giannini, N. P., Goldberg, S. L., Kraatz, B. P., Luo, Z. X., Meng, J., Ni, X., Novacek, M. J., Perini, F. A., Randall, Z. S., Rougier, Z. W., Sargis, E. J., Silcox, M. T., Simmons, N. B., Spaulding, M., … **Cirranello, A. L.** (2013). The placental mammal ancestor and the Post-K-Pg radiation of placentals. *Science, 339*, 662–667. https://doi.org/10.1126/science.1229237

Paula Couto, C. D. (1952). Fossil mammals from the beginning of the Cenozoic in Brazil. Marsupialia: Didelphidae. *American Museum Novitates, 1567*, 1-26.

Phillips, M. J., Celik, M. A., & **Beck, R. M. D.** (2023). The evolutionary relationships of Diprotodontia and improving the accuracy of phylogenetic inference from morphological data. *Alcheringa: An Australasian Journal of Palaeontology, 47*(4), 686-698. https://doi.org/10.1080/03115518.2023.2184492

Rangel, C. C., Carneiro, L. M., Bergqvist, L. P., Oliveira, É. V., Goin, F. J., & **Babot, M. J.** (2019). Diversity, affinities and adaptations of the basal sparassodont *Patene* (Mammalia, Metatheria). *Ameghiniana, 56*(4), 263-289. https://doi.org/10.5710/AMGH.06.05.2019.3222

Ravel, A., Adaci, M., Bensalah, M., Charruault, A.-L., Essid, E. M., Ammar, H. K., Marzougui, W., Mahboubi, M., Mebrouk, F., Merzeraud, G., Vianey-Liaud, M., Tabuce, R., & **Marivaux, L.** (2016). Origine et radiation initiale des chauves-souris modernes: nouvelles découvertes dans l'Éocène d'Afrique du Nord. *Geodiversitas, 38*(3), 355-434. https://doi.org/10.5252/g2016n3a3

Ronquist, F., Teslenko, M., Van Der Mark, P., Ayres, D. L., Darling, A., Höhna, S., Larget, B., Liu, L., Suchard, M. A., & **Huelsenbeck, J. P.** (2012). MrBayes 3.2: efficient Bayesian phylogenetic inference and model choice across a large model space. *Systematic Biology, 61*(3), 539-542. https://doi.org/10.1093/sysbio/sys029

Rose, K. D. (2010). New marsupial from the Early Eocene of Virginia. *Journal of Paleontology*, *84*(3), 561–565. https://doi.org/10.1666/09-140.1

Rose, K. D., Chew, A. E., Dunn, R. H., Kraus, M. J., Fricke, H. C., & **Zack, S. P.** (2012). Earliest Eocene mammalian fauna from the Paleocene-Eocene Thermal Maximum at Sand Creek Divide, Southern Bighorn Basin, Wyoming. *University of Michigan Papers on Paleontology*, *36*, 1–122.

Rougier, G. W., Wible, J. R., & **Novacek, M. J.** (1998). Implications of *Deltatheridium* specimens for early marsupial history. *Nature*, *396*, 459-463. https://doi.org/10.1038/24856

Sánchez-Villagra, M., Ladevèze, S., Horovitz, I., Argot, C., Hooker, J. J., Macrini, T. E., Martin, T., Moore-Fay, S., Muizon, C. de, Schmelzle, T., & **Asher, R. J.** (2007). Exceptionally preserved North American Paleogene metatherians: Adaptations and discovery of a major gap in the opossum fossil record. *Biology Letters*, *3*(3), 318–322. https://doi.org/10.1098/rsbl.2007.0090

Sansom, R. S., Wills, M. A., & **Williams, T.** (2017). Dental data perform relatively poorly in reconstructing mammal phylogenies: Morphological partitions evaluated with molecular benchmarks. *Systematic Biology*, *66*(5), 813–822. https://doi.org/10.1093/sysbio/syw116

Sereno, P. C. (2006). Shoulder girdle and forelimb in multituberculates: evolution of parasagittal forelimb posture in mammals. In M. T. Carrano, T. J. Gaudin, R. W. Blob, & J. R. Wible (Eds.), *Amniote Paleobiology: Perspectives on the Evolution of Mammals, Birds, and Reptiles* (pp. 315-316). University of Chicago Press.

Serra Silva, A. (2024). Extended Lissamphibia: a tale of character non-independence, analytical parameters and islands of trees. *Journal of Systematic Palaeontology*, *22*(1), 2321620. https://doi.org/10.1080/14772019.2024.2321620

Sigé, B. (1971). Les Didelphoidea de Laguna Umayo (formation Vilquechico, Crétacé supérieur, Pérou), et le peuplement marsupial d'Amérique du Sud. *Comptes Rendus de l'Académie des Sciences*, *273*(3), 2479–2481.

Sigé, B. (1972). La faunule de mammifères du Crétacé supérieur de Laguna Umayo (Andes péruviennes). *Bulletin du Museum National d'Histoire Naturelle*, *99*(3), 375–405.

Sigé, B., Archer, M., Crochet, J.-Y., Godthelp, H., Hand, S., & **Beck, R.** (2009). *Chulpasia* and *Thylacotinga*, late Paleocene-earliest Eocene trans-Antarctic Gondwanan bunodont marsupials: New data from Australia. *Geobios*, *42*(6), 813-823. https://doi.org/10.1016/j.geobios.2009.08.001

Sigé, B., Sempere, T., Butler, R. F., Marshall, L. G., & **Crochet, J.-Y.** (2004). Age and stratigraphic reassessment of the fossil-bearing Laguna Umayo red mudstone unit, SE Peru, from regional stratigraphy, fossil record, and paleomagnetism. *Geobios*, *37*(6), 771-794. https://doi.org/10.1016/j.geobios.2003.06.006

Simons, E. L., & **Bown, T. M.** (1984). A new species of *Peratherium* (Didelphidae; Polyprotodonta): the first African marsupial. *Journal of Mammalogy*, *65*(4), 539–548. https://doi.org/10.2307/1380836

Smith, K. T., Collinson, M., Folie, A., Habersetzer, J., Hennicke, F., Kothe, E., Lehmann, T., Lenz, O. K., Mayr, G., Micklich, N., Rabenstein, R., Racicot, R., Schaal, S. F. K., Smith, T., Tosal, A., Uhl, D.,Wappler, T., Wedmann, S., & **Wuttke, M.** (2024). The biodiversity of the Eocene Messel Pit. *Palaeobiodiversity and Palaeoenvironments*, *104*, 859-940. https://doi.org/10.1007/s12549-024-00633-2

Smith, S. M., Sprain, C. J., Clemens, W. A., Lofgren, D. L., Renne, P. R., & **Wilson, G. P.** (2018). Early mammalian recovery after the end-Cretaceous mass extinction: A high-resolution view from McGuire Creek area, Montana, USA. *GSA Bulletin*, *130*(11-12), 2000-2014. https://doi.org/10.1130/B31926.1

Smith, T., & **Smith, R.** (2013). A land micro-mammal fauna from the Early Eocene marine Egem deposits (NP12, Belgium) and the first occurrence of the peradectid marsupial *Armintodelphys* outside North America. *Geologica Belgica*, *16*(4), 302-310.

Speijer, R. P., Pälike, H., Hollis, C. J., Hooker, J. J., & **Ogg, J. G.** (2020). The Paleogene Period. In F. M. Gradstein, J. G. Ogg, M. D. Schmitz, & G. M. Ogg (Eds.), *Geologic Time Scale 2020* (pp. 1087– 1140). Elsevier, Amsterdam. https://doi.org/10.1016/B978-0-12-824360-2.00028-0

Stock, C. (1936) Sespe Eocene Didelphids. *Proceedings of the National Academy of Sciences*, *22*(2), 122–124. https://doi.org/10.1073/pnas.22.2.122

Storch, G., & **Qiu, Z.** (2002). First Neogene marsupial from China. *Journal of Vertebrate Paleontology*, *22*(1), 179–181. https://doi.org/10.1671/0272-4634(2002)022[0179:FNMFC]2.0.CO;2

Storer, J. E. (1991). The mammals of the Gryde Local Fauna, Frenchman Formation (Maastrichtian: Lancian), Saskatchewan. *Journal of Vertebrate Paleontology*, *11*(3), 350-369. https://doi.org/10.1080/02724634.1991.10011403

Swiderski, D. L., Zelditch, M. L., & **Fink, W. L.** (1998). Why morphometrics is not special: coding quantitative data for phylogenetic analysis. *Systematic Biology*, *47*(3), 508-519.

Swofford, D. L. (2002). PAUP* Phylogenetic analysis using parsimony (* and other methods). Version 4. Sinauer Associates, Sunderland.

Szalay, F. S. (1993). Metatherian taxon phylogeny: Evidence and interpretation from the cranioskeletal system. In F. S. Szalay, M. J. Novacek, M. C. McKenna (Eds.), *Mammal Phylogeny, Vol. 1. Mesozoic Differentiation, Multituberculates, Monotremes, Early Therians, and Marsupials* (pp. 216-242). Springer. https://doi.org/10.1007/978-1-4613-9249-1_15

Szalay, F. S. (1994) *Evolutionary History of the Marsupials and an Analysis of Osteological Characters*. Cambridge University Press. https://doi.org/10.1017/CBO9780511565571

Tabuce, R., Adnet, S., Cappetta, H., Noubhani, A., & **Quillevéré, F.** (2005). Aznag (bassin d'Ouarzazate, Maroc), nouvelle localité à sélaciens et mammifères de l'Eocène moyen (Lutétien) d'Afrique. Bulletin de la Société Géologique de France, 176(4), 381-400. https://doi.org/10.2113/176.4.381

Teilhard de Chardin, P. (1927). Les mammifères de l'Éocène inférieur de la Belgique. *Mémoires du Musée Royal d'Histoire Naturelle de Belgique*, *36*, 1–33.

Tejedor, M. F., Goin F. J., Gelfo, J. N., López, G., Bond, M., Carlini, A. A., Scillato-Yane, G. J., Woodburne, M. O., Chornogubsky, L., Aragón, E., Reguero, M. A., Czaplewski, N. J., Vincon, S., Martin, G. M., & **Ciancio, M. R.** (2009). New early Eocene mammalian fauna from western Patagonia, Argentina. *American Museum Novitates*, *3638*, 1–43. https://doi.org/10.5167/uzh-20519

Thomas, O. (1894). On *Micoureus griseus*, Desm., with the description of a new genus and species of Didelphyidæ. *Annals and Magazine of Natural History*, *14*(81), 184–188. https://doi.org/10.1080/00222939408677788

Tomida, Y., & **Butler, R. F.** (1980). Dragonian mammals and Paleocene magnetic polarity stratigraphy, North Horn Formation, central Utah. *American Journal of Science*, *280*(8), 787-811. https://doi.org/10.2475/ajs.280.8.787

Travouillon, K. J. (2016). Investigating dental variation in *Perameles nasuta* Geoffroy, 1804, with morphological evidence to raise *P. nasuta pallescens* Thomas, 1923 to species rank. *Zootaxa*, *4114*(4), 351-392. https://doi.org/10.11646/zootaxa.4114.4.1

Trofimov, B. A., & **Szalay, F. S.** (1994). New Cretaceous marsupial from Mongolia and the early radiation of Metatheria. *Proceedings of the National Academy of Sciences*, *91*(26), 12569–12573. https://doi.org/10.1073/pnas.91.26.12569

Van Couvering, J. A., & **Delson, E.** (2020). African land mammal ages. *Journal of Vertebrate Paleontology*, *40*(5), e1803340. https://doi.org/10.1080/02724634.2020.1803340

Vianey-Liaud, M., Lihoreau, F., Solé, F., Gernelle, K., Vautrin, Q., Bronnert, C., Bourget, H., Vidalenc, D., & **Tabuce, R.** (2024). A revision of the late early Eocene mammal faunas from Mas de Gimel and Naples (Montpellier, Southern France) and the description of a new theridomorph rodent. *Geodiversitas*, *46*(10), 387-422. https://doi.org/10.5252/geodiversitas2024v46a10

Vullo, R., Gheerbrant, E., Beurel, S., Swajda, M., & **Néraudeau, D.** (2020). A stagodontid mammal from the mid-Cretaceous of France confirms the Euramerican distribution of early marsupialiforms. *Palaeogeography, Palaeoclimatology, Palaeoecology*, *560*, 110034. https://doi.org/10.1016/j.palaeo.2020.110034

Vullo, R., Gheerbrant, E., Muizon, C. de, & **Neraudeau, D.** (2009). The oldest modern therian mammal from Europe and its bearing on stem marsupial paleobiogeography. *Proceedings of the National Academy of Sciences*, *106*(47), 19910-19915. https://doi.org/10.1073/pnas.0902940106

Watrous, L. E., & **Wheeler, Q. D.** (1981). The out-group comparison method of character analysis. Systematic Biology 30(1): 1-11. https://doi.org/10.1093/sysbio/30.1.1

Westerhold, T., Röhl, U., Donner, B., & **Zachos, J. C.** (2018). Global extent of early Eocene hyperthermal events: A new Pacific benthic foraminiferal isotope record from Shatsky Rise (ODP Site 1209). *Paleoceanography and Paleoclimatology*, *33*(6), 626-642. https://doi.org/10.1029/2017PA003306

Wible, J. R., Rougier, G. W., Novacek, M. J., & **Asher, R. J.** (2007). Cretaceous eutherians and Laurasian origin for placental mammals near the K/T boundary. *Nature*, *447*, 1003-1006. https://doi.org/10.1038/nature05854

Wiens, J. J. (2006). Missing data and the design of phylogenetic analyses. *Journal of Biomedical Informatics*, *39*(1), 34-42. https://doi.org/10.1016/j.jbi.2005.04.001

Williamson, T. E., Brusatte, S. L., Carr, T. D., Weil, A., & **Standhardt, B. R.** (2012). The phylogeny and evolution of Cretaceous-Palaeogene metatherians: Cladistic analysis and description of new early Palaeocene specimens from the Nacimiento Formation, New Mexico. *Journal of Systematic Palaeontology*, *10*(4), 625–651. https://doi.org/10.1080/14772019.2011.631592

Williamson, T. E., Brusatte, S. L., & **Wilson, G. P.** (2014). The origin and early evolution of metatherian mammals: The Cretaceous record. *Zookeys*, *465*, 1–76. https://doi.org/10.3897/zookeys.465.8178

Williamson, T. E., & **Lofgren, D. L.** (2014). Late Paleocene (Tiffanian) metatherians from the Goler Formation, California. *Journal of Vertebrate Paleontology*, *34*(2), 477–482. https://doi.org/10.1080/02724634.2013.804413

Williamson, T. E., & **Taylor, L. H.** (2011). New species of *Peradectes* and *Swaindelphys* (Mammalia: Metatheria) from the Early Paleocene (Torrejonian) Nacimiento Formation, San Juan Basin, New Mexico, USA. *Palaeontologia Electronica*, *14*, 23A.

Williamson, T. E., & **Weil, A.** (2008). Metatherian mammals from the Naashoibito Member, Kirtland Formation, San Juan Basin, New Mexico and their biochronologic and paleobiogeographic significance. *Journal of Vertebrate Paleontology*, *28*(3), 803-815. https://doi.org/10.1671/0272-4634(2008)28[803:MMFTNM]2.0.CO;2

Wilson, G. P. (2013). Mammals across the K/Pg boundary in northeastern Montana, U.S.A.: dental morphology and body-size patterns reveal extinction selectivity and immigrant-fueled ecospace filling. *Paleobiology*, *39*(3), 429-469. https://doi.org/10.1666/12041

Wilson, G. P. (2014). Mammalian extinction, survival, and recovery dynamics across the Cretaceous-Paleogene boundary in northeastern Montana, USA. In G. P. Wilson, W. A. Clemens, J. R. Horner, & J. H. Hartman (Eds.), *Through the End of the Cretaceous in the Type Locality of the Hell Creek Formation in Montana and Adjacent Areas* (pp. 365-392). The Geological Society of America, Special Papers, 503. https://doi.org/10.1130/2014.2503(15)

Wilson, G. P., Ekdale, E. G., Hoganson, J. W., Calede, J. J., & **Vander Linden, A.** (2016). A large carnivorous mammal from the Late Cretaceous and the North American origin of marsupials. *Nature Communications*, *7*, 13734. https://doi.org/10.1038/ncomms13734

Woodburne, M. O., Gunnell, G. F., & **Stucky, R. K.** (2009). Climate directly influences Eocene mammal faunal dynamics in North America. *Proceedings of the National Academy of Sciences*, *106*(32), 13399-13403. https://doi.org/10.1073/pnas.0906802106

Ziegler, R., Dahlmann, T., & **Storch, G.** (2007). 4. Marsupialia, Erinaceomorpha and Soricomorpha (Mammalia). In G. Daxner-Höck (Ed.), *Oligocene-Miocene Vertebrates from the Valley of Lakes (Central Mongolia): Morphology, phylogenetic and stratigraphic implications* (pp. 53-164). Annalen des Naturhistorischen Museums in Wien, 108 A.

Zimicz, A. N. (2012). Ecomorfología de los marsupiales paleógenos de América del Sur. Unpublished PhD thesis, Universidad Nacional de La Plata, 452 pp.

Supplemental material 1. List of taxa included in the phylogenetic analyses (with authorship and year), their systematic position, the specimens used for coding and references, and the stratigraphic extension of the species. Taxa in light blue text are only included in supernumerary phylogenetic analyses (see Supplemental material 5).

Outgroup (eutherians)

Maelestes gobiensis Wible, Rougier, Novacek & Asher, 2007. Descriptions and illustrations from Wible et al. (2009). From Ukhaa Tolgod, Djadokhta Formation (Late Cretaceous, ~75-71 Ma; see Wible et al. 2007 and references therein).

Prokennalestes minor Kielan-Jaworowska & Dashzeveg, 1989. Descriptions and illustrations from Kielan-Jaworowska and Dashzeveg (1989) and Lopatin and Averianov (2017). Late Albian or late Aptian – Albian in age (Lopatin and Averianov 2017).

Deltatheridiidae Gregory & Simpson, 1926

Deltatheridium pretrituberculare Gregory & Simpson, 1926. Casts of ZPAL MGM-I/91 and ZPAL MGM-I/102. Descriptions and illustrations from Kielan-Jaworowska (1975) and Rougier et al. (1998). From Ukhaa Tolgod, Djadokhta Formation (~75-71 Ma; see above).

Marsupialiformes Vullo, Gheerbrant, Muizon & Néraudeau, 2009; order and family *incertae sedis*

Aenigmadelphys archeri Cifelli & Johanson, 1994. Descriptions and illustrations from Cifelli (1990), Cifelli and Johanson (1994) and Muizon and Ladevèze (2022). Probably from the Upper Campanian (Cifelli and Johanson 1994; ~76-72 Ma).

Asiatherium reshetovi Trofimov & Szalay, 1994. Descriptions and illustrations from Szalay and Trofimov (1996). Approximately equivalent to middle Campanian in age (~80-76 Ma; Szalay and Trofimov 1996).

Kokopellia juddi Cifelli, 1993. Descriptions and illustrations from Cifelli and Muizon (1997). Radiometric datings indicate an age of ~98.4 Ma, close to the Albian-Cenomanian (Early – Late Cretaceous) boundary (Cifelli and Muizon 1997).

Alphadontidae Marshall, Case & Woodburne, 1990

Albertatherium spp. Fox, 1971. *Albertatherium primus* Fox, 1971 and *A. secundus* Johanson, 1994, and *Albertatherium* sp. in Davis et al. (2016) are included. Descriptions and illustrations from Fox (1971), Johanson (1994) and Davis et al. (2016). The lower molar of *A. primus* illustrated by Fox (1971: pl. 3,

figs. B-C) and of *Albertatherium* sp. illustrated by Davis et al. (2016: fig. 5E) are considered as m3. Santonian in age (Davis et al. 2016). From Santonian (Davis et al. 2016) to early Campanian (Aquilian NALMA; Johanson 1994) (= from ~86 to ~82 Ma).

Nortedelphys jasoni (Storer, 1991). Cast of UCMP 47464 and 51385. Combination from Williamson et al. (2012). Descriptions and illustrations from Lillegraven (1969), Storer (1991), Johanson (1996) and Case et al. (2005). Lancian NALMA (La-1 and La-2) in age (Wilson 2014).

Turgidodon rhaister (Clemens, 1966). Casts of UCMP 48221 (m2), 50292 (holotype), 52346 (m3), 52413 (M4), 52461 (m4) and 52483 (m1). Descriptions and illustrations from Clemens (1966), Lillegraven (1969), Archibald (1982), Johanson (1996), and Muizon and Ladevèze (2020: fig. 46D). UCMP 52346 (Clemens 1966: fig. 64), included in Muizon and Ladevèze (2020: p. 737), is interpreted as an m3 rather than an m4. Lancian NALMA (La-1 and La-2) in age (Wilson 2014).

Stagodontidae Marsh, 1889b

Didelphodon vorax Marsh, 1889a. Casts of UCMP 46962, 47517, 48189, 48208, 48581, 52289, 52290, 52326, and 52342. Descriptions and illustrations from Clemens (1966) and Wilson et al. (2016). Lancian NALMA (La-1 and La-2) in age (Wilson 2014).

Pediomyidae Simpson, 1927

Pediomys elegans Marsh, 1889a. Casts of UCMP 47035, 47049, 47478, 47527, 50243, 50293, 51406, 52719. Descriptions and illustrations from Clemens (1966), Lillegraven (1969) and Davis (2007). One specimen referred to as *Pediomys* ?*elegans* (Clemens 1966: fig. 66b) is here included. Unequivocal specimens are Lancian NALMA (La-1 and La-2) in age (Davis 2007; Wilson 2014).

Glasbiidae Clemens, 1966

Glasbius intricatus Clemens, 1966. Casts of UCMP 46414, 48047 (holotype), 52045. Descriptions and illustrations from Clemens (1966) and Davis (2007). Lancian (NALMA) in age (Davis 2007).

Pucadelphyda Muizon, Ladevèze, Selva, Vignaud & Goussard, 2018

Pucadelphys andinus Marshall & Muizon, 1988. Casts of YPFB Pal 6105 (holotype), 6107, 6470 and 6472. Descriptions and illustrations from Marshall and Muizon (1995) and Ladevèze et al. (2011). We follow Beck et al. (2022: 309-310) in attributing to Tiupampan terminals a compromise age between the maximum age of the chron 28r and the minimum age of the chron 26r (~65-59 Ma in age) in age.

Incadelphys antiquus Marshall & Muizon, 1988. Cast of YPFB Pal 6251 (holotype). Descriptions and illustrations from Muizon and Ladevèze (2022). Tiupampan SALMA; ~65-59 Ma in age, as for *Pucadelphys andinus*.

Mayulestes ferox Muizon, 1998. Descriptions and illustrations from Muizon (1998) and Muizon and Ladevèze (2020: figs. 46-48, 53-58). Tiupampan SALMA; ~65-59 Ma in age, as for *Pucadelphys andinus*.

? **Polydolopimorphia** Archer, 1984

Roberthoffstetteria nationalgeographica Marshall, Muizon & Sigé, 1983. Casts of MNHN.F.Vil101, 102, MNHC 8351, and an unlabelled cast unambiguously representing p2-m4 of *R. nationalgeographica* (= MNHC 8365 in Goin et al. 2003: p. 870 ? The morphology of the p3, with a "posterior root […] much larger than the anterior one" corresponds to the description of MNHC 8365). Descriptions and illustrations from Marshall et al. (1983) and Goin et al. (2003). "Stylar cusp D" of the M4 of MNHC 8351 (Goin et al. 2003) is interpreted as stylar cusp C. Tiupampan SALMA; ~65-59 Ma in age, as for *Pucadelphys andinus*.

Notometatheria Kirsch, Springer & Lapointe, 1997; family *incertae sedis*

Thylacodon spp. *Thylacodon pusillus* Matthew & Granger, 1921 and *T. montanensis* Williamson, Brusatte, Carr, Weil & Standhardt, 2012, are included. Descriptions and illustrations from Matthew (1937), Archibald (1982), Dewar (2003), Clemens (2006), Williamson et al. (2012), Wilson (2013), Dahlberg et al. (2016) and Claytor et al. (2023: Supplementary data). Because the familial attribution of *Thylacodon* has not been resolved by Williamson et al. (2012, 2014), we here retain this genus in Marsupialiformes family *incertae sedis*. Early Paleocene, Puercan NALMA (Pu-1 to Pu-2/3, ~66-63 Ma) in age (Williamson et al. 2012; Wilson 2014).

Swaindelphys encinensis Williamson & Taylor, 2011. Descriptions and illustrations from Williamson and Taylor (2011). The lower molar (m2 or m3) NMMNH P-1972 (Williamson and Taylor 2011: fig. 5.1-3) is interpreted as an m3. The familial attribution of *Swaindelphys* to Herpetotheriidae has not been confirmed by previous phylogenetic analyses (Williamson et al. 2012; Carneiro et al. 2018; this study). *Mixodectes pungens* biozone in age (in late Danian, late Torrejonian NALMA, biochron To-3; Williamson and Taylor 2011).

Peradectidae Crochet, 1979

Armintodelphys blacki Krishtalka and Stucky, 1983a. Cast of CM 41159 (holotype) consulted (Royal Belgian Institute of Natural Sciences [RBINS], Brussels). Descriptions and illustrations from Krishtalka & Stucky (1983a, 1983b) and Smith and Smith (2013). From latest Wasatchian (Wa-7) to earliest Bridgerian (Br-0) (Krishtalka and Stucky 1983a; Korth 2008).

Armintodelphys dawsoni Krishtalka and Stucky, 1983a. Cast of CM 55569 (holotype) consulted (Royal Belgian Institute of Natural Sciences [RBINS], Brussels). Descriptions and illustrations from Krishtalka & Stucky (1983a, 1983b, 1984) and Smith and Smith (2013). Early Bridgerian (Br-0-Br-1) (Krishtalka and Stucky 1983a; Korth 2008).

Didelphidectes spp. *Didelphidectes pumilis* Hough, 1961, and *Didelphidectes* cf. *pumilis* in Kihm and Schumaker (2015), are included. Descriptions and illustrations from Hough (1961), Korth (1994), and Kihm and Schumaker (2015). Late Eocene, early to middle Chadronian NALMA (Ch-2 to Ch-3; ~35-36.5 Ma) according to Korth (2018).

Golerdelphys stocki Williamson & Lofgren, 2014. Descriptions and illustrations from Williamson and Lofgren (2014). First included in Herpetotheriidae, *Golerdelphys* was not recovered as such in phylogenetic analyses by Williamson and collaborators (Williamson et al. 2012, 2014; Williamson and Lofgren 2014) and is most likely a peradectid (this study, see Discussion; see also Carneiro et al. 2018: fig. 5). The only complete available m2 or m3 has been scored as an m3. From the Goler Formation, middle Tiffanian NALMA (probably Ti-3/Ti-4a) in age (Selandian; Lofgren et al. 2014).

Mimoperadectes spp. *Mimoperadectes labrus* Bown & Rose, 1979, *M. houdei* Horovitz, Martin, Bloch, Ladevèze, Kurz & Sánchez-Villagra, 2009, and *M. sowasheensis* Beard & Dawson, 2009, are included. Casts of UM 66144 (holotype, dental rows illustrated in pl. 1 and pl. 2, fig. 1 in Bown and Rose [1979]) and UM 113418 consulted (RBINS). Descriptions and illustrations from Bown and Rose (1979), Gingerich (1989), Strait (2001), Gingerich and Smith (2006), Beard and Dawson (2009), Horovitz et al. (2009), Rose et al. (2012) and Vitek et al. (2017). The lower molar UF 251318 (Vitek et al. 2017: fig. 1a; 3D model available on MorphoSource) is a m3 (trigonid wider than talonid). The 3D models of several other lower molar specimens studied in Vitek et al. (2017) are available on MorphoSource. Definitive *M. labrus* specimens are recorded in Wa-M and Wa-0 faunas (Bown and Rose 1979; Strait 2001; Gingerich and Smith 2006; Rose et al. 2012). The species maybe extends back to the latest Paleocene (Rose 1981: 36) and further into the early-middle Wasatchian, *Cantius trigonodus* zone (biochrons Wa-4-Wa-5) (Bown and Rose 1979: 96; Korth 2008: 716; Rose et al. 2012: 22). *Mimoperadectes houdei* is from the *Arfia shoshoniensis* zone (54.4 - 54.7 Ma ; Horovitz et al. 2009)

Nanodelphys hunti (Cope, 1873). Descriptions and illustrations from McGrew (1937), Korth (1994, 2018), and Korth et al. (2021). From Orellan NALMA to early Arikareean NALMA (Or-1 to Ar-1; ~29-34 Ma) according to Korth (2018).

Peradectes californicus (Stock, 1936). Descriptions and illustrations from Stock (1936), Setoguchi (1975), Lillegraven (1976), Rothecker and Storer (1996) (fig. 1P interpreted as M2 instead of M3) and Murphey et al. (2018). From early Uintan (biochron Ui-1a, ~47 Ma) to late Duchesnean (biochron Du) (Murphey et al. 2018).

Peradectes chesteri (Gazin, 1952). Descriptions and illustrations from Gazin (1952), West (1973), Krishtalka and Stucky (1983a, 1983b, 1984) and Murphey et al. (2018). From late Wasatchian (biochron Wa-7) to early Uintan (biochron Ui-1b) (Murphey et al. 2018).

Peradectes coprexeches Williamson & Taylor, 2011. Descriptions and illustrations from Williamson and Taylor (2011). From *Pantolambda cavirictum – Mixodectes pungens* biozone (biochron To-2) to *Mixodectes pungens* biozone (biochron To-3) (late Danian; Williamson and Taylor 2011).

Peradectes crocheti Gernelle, 2024. Descriptions, illustrations and all original material from Gernelle et al. (2024). Cast of the M3 from Sotteville-sur-Mer (see Smith et al. 2011). Additional illustrations from Hooker (2010, 2020) for each Abbey Wood and Croydon specimen. Restricted to the [MP7-MP8+9

reference level] interval, with first occurrence just after the PETM (Smith et al. 2011) and last occurrences after the Eocene Thermal Maximum 2 (~biochron Wa5; Noiret et al. 2016).

Peradectes dufraingi Smith and Smith, 2013. Original specimens IRSNB M2152 (holotype) and IRSNB M2153 consulted (Royal Belgian Institute of Natural Sciences [RBINS], Brussels). Descriptions and illustrations from Smith and Smith (2013). Known from ~51-52 Ma (Egemkapel Clay Member; Smith and Smith 2013) to possibly MP10 reference level (*Peradectes* aff. *dufraingi* in Gernelle et al. 2024).

Peradectes elegans Matthew and Granger, 1921. Casts of AMNH 17376 (holotype), 17383 and USNM 20879 (University of Montpellier, France). Descriptions and illustrations from Simpson (1928, 1935), Gazin (1956), Mckenna (1960), Fox (1983) and Krishtalka and Stucky (1983b). We followed Williamson et al. (2012) in considering *Pd. pauli* as a junior synonym of *Pd. elegans*. Thus, specimens allocated to *Pd. pauli* (Krishtalka and Stucky 1983b), including USNM 20879, have been used for the coding of *Pd. elegans*. From early Tiffanian (biochron Ti-2 according to Korth 2008, biochron Ti-3 according to Secord 2008) to early Wasatchian (between biochrons Wa1-Wa3; McKenna 1960; Korth 2008).

Peradectes gulottai Rose, 2010. Descriptions and illustrations from Rose (2010). Wasatchian in age (Rose 2010).

Peradectes louisi Crochet, 1979. Descriptions, illustrations, and all original material included in the revision of *Pd. louisi* (Gernelle et al. 2024). From (~)MP8+9 reference level (Mutigny; ~52-54 Ma; Neal 1996; Duprat 1997), to possibly MP8+9-MP10 interval.

Peradectes minor Clemens, 2006. Descriptions and illustrations from Clemens (2006) and Williamson et al. (2012). Middle to late Puercan NALMA (Pu-2/3) in age (Williamson et al. 2012).

Peradectes protinnominatus McKenna 1960. Casts of UCMP 44077 (holotype) and UCMP 45950 (University of Montpellier, France). Casts of UM 71663, UM 113305, UM 113391 and UM 113378 consulted at the Royal Belgian Institute of Natural Sciences (Brussels, Belgium). Descriptions and illustrations from McKenna (1960), Bown (1979), Rose (1981), Krishtalka and Stucky (1983b), Gingerich and Smith (2006), Vitek et al. (2017) and Anemone et al. (2024). The middle Wasatchian m4 specimen (not illustrated) allocated to this species by Davidson (1987) is not included because the diagnostic value of this locus is low. Isolated molars of *Pd. protinnominatus* described by Strait (2001) are not included, because the only available illustration for this species is a herpetotheriid M3 (with a V-shaped centrocrista). The lower molar UM 113307 (Gingerich and Smith 2006: fig. 26A-B) is interpreted as m2 rather than m3. The lower molar UF 326912 (Vitek et al. 2017: fig. 1b; 3D model available on MorphoSource at https://www.morphosource.org/concern/media/000013983?locale=en) is a m3 (trigonid wider than talonid). The 3D models of several other lower molar specimens studied in Vitek et al. (2017) are available on MorphoSource. Known from early Clarkforkian (biochron Cf-1) to early Wasatchian (biochron Wa-M to between biochrons Wa-1-Wa-3) (McKenna 1960; Gingerich and Smith 2006; Korth 2008; Anemone et al. 2024). Numerous metatherian dental remains form the early Clarkforkian Big Multi Quarry fauna (Cf-1, following the biozonation scheme of Anemone et al. 2024) have been attributed to *Pd. protinnominatus* (Wilf et al. 1998; Anemone et al. 2024), whitout available description and illustration so far. *Peradectes protinnominatus* is possibly also known from older, middle Tiffanian localities, biochron Ti-3/Ti-4 to Ti-4 (Krishtalka 1973; Krishtalka et al. 1975; Korth 2008), although these occurrences have not been discussed in the revision of the species by Krishtalka and Stucky (1983b) or later. Furthermore, the report of Tiffanian specimens of *Pd. protinnominatus* by Krishtalka et al. (1975) has recently been considered unreliable (Anemone et al. 2024).

Peradectes russelli Crochet 1979. Descriptions, illustrations, and all original material included in the revision of *Pd. russelli* (Gernelle et al. 2024). (~)MP8+9 reference level (Mutigny; ~52-54 Ma; Neal 1996; Duprat 1997) in age.

Peradectes sp. nov. 1. All original material included in the description of the species (this study). MP10 reference level (Grauves locality) and ~ 50.3-50.4 Ma (~MP10) in age (Steurbaut et al. 2016).

Peradectes sp. nov. 2. All original material included in the description of the species (this study). From Prémontré: ~ 50.3-50.4 Ma (~MP10) in age (Steurbaut et al. 2016).

Peradectes sp. nov. 3. All original material included in the description of the species (this study). Time interval between MP10-MP11 in age (e.g., see Vianey-Liaud et al. 2022).

Peratheriinae Ladevèze, Selva & Muizon, 2020

Peratherium constans Teilhard de Chardin, 1927. Casts of IRSNB-M-2, 1328, 1331, 1332, 1333 and NBM Om.1, 3, 158, 159, all from the type locality. Descriptions and illustrations from Ladevèze et al. (2012). The specimens of *Pt. constans* from Palette (Provence) studied by Godinot et al. (1987) have also been scored. MP7 (~56 Ma) in age based on the type locality.

Herpetotheriinae (Trouessart, 1879)

Herpetotherium edwardi (Gazin, 1952). Casts of USNM 19200 (holotype) and 19206. Descriptions and illustrations from Gazin (1952) and Krishtalka & Stucky (1983b). Late Wasatchian (Wa-7) in age (Korth 2008).

Herpetotherium fugax Cope, 1873. Cast of AMNH 5254 (holotype). Descriptions and illustrations from Green and Martin (1976), Fox (1983), Korth (1994, 2018), Hayes (2005), Lofgren et al. (2020) and Korth et al. (2021). *Herpetotherium* cf. *fugax* described by Sánchez-Villagra et al. (2007) is not included. From Orellan NALMA (early Oligocene; Or-1) to Arikareean NALMA (late Oligocene; Ar-2) (Korth 2018; ~34-28 Ma).

Anatoliadelphyidae Métais, Coster, Kappelman, Licht, Ocakoğlu, Taylor & Beard, 2018

Orhaniyeia nauta Métais, Coster, Kappelman, Licht, Ocakoğlu, Taylor & Beard, 2018. Descriptions et illustrations from Maas et al. (1998), Métais et al. (2018) and Beard et al. (2023). The specimen figured by Maas et al. (1998) is interpreted as a M2. Late middle Eocene (Lutetian) in age (Métais et al. 2018).

Derorhynchidae (Marshall, 1987)

Derorhynchys singularis Paula Couto, 1952. Cast of MNRJ 1348-V (holotype), AMNH 49826 and DGM 803-M. Descriptions and illustrations from Paula Couto (1952), Oliveira et al. (2021) and Carneiro and Oliveira (2023). Itaboraian SALMA in age (EECO, ~53-50 Ma; Woodburne et al. 2014).

Australidelphia Szalay, 1982

Djarthia murgonensis Godthelp, Wroe & Archer, 1999. Descriptions and illustrations from Godthelp et al. (1999). Early Eocene, minimum age of 54.6 Ma (Godthelp et al. 1999).

Dromiciops gliroides Thomas, 1894. Original specimen IEEUACG 2167. CT data of UMMZ 156354 (available on MorphoSource at https://www.morphosource.org/concern/media/000420565?locale=en).

Perameles nasuta Geoffroy, 1804. CT data of AMNH 257605 (available on MorphoSource at https://www.morphosource.org/concern/media/000095519?locale=en). Descriptions and illustrations from Travouillon (2016).

Didelphidae Gray, 1821

Didelphis marsupialis Linnaeus, 1758. Original specimens MNHN-ZM-MO-1932-3003 and MNHN-ZM-2007-8.

Marmosa murina (Linnaeus, 1758). Original specimens MNHN-ZM-MO-2001-1966 and 2001-1967.

Metachirus nudicaudatus (Geoffroy, 1803). Original specimens MNHN-ZM-2004-316 and MNHN-ZM-MO-2001-1422.

References for Supplemental material 1:

Anemone RL, Jones MF, Van Regenmorter J, Beard KC (2024) A latest Paleocene mammal fauna from the Great Divide Basin in southern Wyoming and a revised biozonation of the Clarkforkian land mammal age. Journal of Vertebrate Paleontology: e2424139.

Archibald JD (1982) A study of Mammalia and geology across the Cretaceous-Tertiary boundary in Garfield County, Montana. University of California Publications in Geological Sciences 122: 1-126.

Beard KC, Dawson MR (2009) Early Wasatchian mammals of the red hot local fauna, uppermost Tuscahoma formation, Lauderdale County, Mississippi. Annals of Carnegie Museum 78: 193-243.

Beard KC, Coster PM, Ocakoğlu F, Licht A, Métais G (2023) Dental anatomy, phylogenetic relationships and paleoecology of *Orhaniyeia nauta* (Metatheria, Anatoliadelphyidae), a Gondwanan component of the insular Eocene mammal fauna of Balkanatolia (north-central Turkey). Journal of Mammalian Evolution 30: 859-872.

Beck RMD, Voss RS, Jansa SA (2022) Craniodental morphology and phylogeny of marsupials. Bulletin of the American Museum of Natural History 457: 1-350.

Bown TM (1979) Geology and mammalian paleontology of the Sand Creek Facies, lower Willwood Formation (lower Eocene), Washakie County, Wyoming. Geological Survey of Wyoming Memoir 2: 1–151.

Bown TM, Rose KD (1979) *Mimoperadectes*, a new marsupial, and *Worlandia*, a new dermopteran, from the lower part of the Willwood Formation (early Eocene), Bighorn Basin, Wyoming. Contributions from the Museum of Paleontology, The University of Michigan 25: 89–104.

Carneiro LM, Oliveira ÉV (2023) Paleogene metatherians from the Itaboraí Basin: diversity and affinities. In: Cáceres NC, Dickman CR (eds) American and Australasian Marsupials. Springer, Cham, Switzerland, pp 269–324.

Carneiro LM, Oliveira ÉV, Goin FJ (2018) *Austropediomys marshalli* gen. et sp. nov., a new Pediomyoidea (Mammalia, Metatheria) from the Paleogene of Brazil: Paleobiogeographic implications. Revista Brasileira de Paleontologia 21: 120-131.

Case JA, Goin FJ, Woodburne MO (2005) "South American" marsupials from the Late Cretaceous of North America and the origin of marsupial cohorts. Journal of Mammalian Evolution 12: 461-494.

Cifelli RL (1990) Cretaceous mammals of southern Utah. I. Marsupials from the Kaiparowits Formation (Judithian). Journal of Vertebrate Paleontology 10: 295-319.

Cifelli RL, Johanson Z (1994) New marsupial from the Upper Cretaceous of Utah. Journal of Vertebrate Paleontology 14: 292-295.

Cifelli RL, Muizon C (1997) Dentition and jaw of *Kokopellia juddi*, a primitive marsupial or near-marsupial from the medial Cretaceous of Utah. Journal of Mammalian Evolution 4: 241-258.

Claytor JR, Weaver LN, Tobin TS, Wilson GP (2023) New mammalian local faunas from the first ca. 80 ka of the Paleocene in northeastern Montana and a revised model of biotic recovery from the Cretaceous–Paleogene mass extinction. Journal of Vertebrate Paleontology 42: e2222777.

Clemens WA (1966) Fossil mammals of the type Lance Formation, Wyoming. Part II, Marsupialia. University of California Publications in Geological Sciences 62: 1–122.

Clemens WA (2006) Early Paleocene (Puercan) peradectid marsupials from northeastern Montana, North American Western Interior. Palaeontographica Abteilung A 277: 19–31.

Crochet JY (1979) Diversité systématique des Didelphidae (Marsupialia) européens tertiaires. Géobios 12: 365–378.

Dahlberg EL, Eberle JJ, Sertich JJW, Miller IM (2016) A new earliest Paleocene (Puercan) mammalian fauna from Colorado's Denver Basin, U.S.A. Rocky Mountain Geology 51: 1-22.

Davidson JR (1987) Geology and mammalian paleontology of the Wind River Formation, Laramie basin, southeastern Wyoming. Contributions to Geology, University of Wyoming 25: 103–32

Davis BM (2007). A revision of "pediomyid" marsupials from the Late Cretaceous of North America. Acta Palaeontologica Polonica 52: 217-256.

Davis BM, Cifelli RL, Cohen JE (2016) First fossil mammals from the Upper Cretaceous Eagle Formation (Santonian, northern Montana, USA), and mammal diversity during the Aquilan North American land mammal age. Palaeontologia Polonica 67: 101-126.

Dewar EW (2003) Functional diversity within the Littleton fauna (early Paleocene), Colorado: evidence from body mass, tooth structure, and tooth wear. PaleoBios 23: 1-19.

Duprat M (1997) Les faciès à mammifères (MP 6 à MP 16) dans le Nord-Est du Bassin de Paris (France): argumentation du modèle tectono-sédimentaire des dépôts paléogènes. In: Aguilar JP, Legendre S, Michaux J (eds) Actes du Congrès BiochroM'97, Mémoires et travaux de l'EPHE 21. Ecole Pratique des Hautes Etudes, Institut de Montpellier, Montpellier, pp 315–336.

Fox RC (1971) Marsupial mammals from the early Campanian Milk River Formation, Alberta, Canada. In: Kermack DM, Kermack KA (eds) Early Mammals, Zoological Journal of the Linnean Society 50: Supplement 1, pp 145-164.

Fox RC (1983) Notes on the North American Tertiary marsupials *Herpetotherium* and *Peradectes*. Canadian Journal of Earth Sciences 20: 1565–1578.

Gazin CL (1952) The lower Eocene knight formation of western Wyoming and its mammalian faunas. Smithsonian Miscellaneous Collections 117: 1–82.

Gazin CL (1956) Paleocene mammalian faunas of the Bison Basin in south-central Wyoming. Smithsonian Miscellaneous Collections 131: 1-57.

Gernelle K, Billet G, Gheerbrant E, Godinot M, Marandat B, Ladevèze S, Tabuce R (2024) Taxonomy and evolutionary history of peradectids (Metatheria): new data from the early Eocene of France. Journal of Mammalian Evolution 31(3): 31.

Gingerich PD (1989) New earliest Wasatchian mammalian fauna from the Eocene of northwestern Wyoming: composition and diversity in a rarely sampled high-floodplain assemblage. University of Michigan Papers on Paleontology 28: 1–97.

Gingerich PD, Smith T (2006) Paleocene-Eocene land mammals from three new latest Clarkforkian and earliest Wasatchian wash sites at Polecat Bench in the northern Bighorn Basin, Wyoming. Contributions from the Museum of Paleontology, University of Michigan 31: 245–303.

Godinot M, Crochet JY, Hartenberger JL, Lange-Badré B, Russell DE, Sigé B (1987) Nouvelles données sur les mammifères de Palette (Eocène inférieur, Provence). Münchner Geowissenschaftliche Abhandlungen (A) 10: 273-288.

Godthelp H, Wroe S, Archer M (1999) A new marsupial from the early Eocene Tingamarra Local Fauna of Murgon, southeastern Queensland: a prototypical Australian marsupial? Journal of Mammalian Evolution 6: 289-313.

Goin FJ, Candela AM, Muizon C de (2003) The affinities of *Roberthoffstetteria nationalgeographica* (Marsupialia) and the origin of the polydolopine molar pattern. Journal of Vertebrate Paleontology, 23: 869-876.

Green M, Martin JE (1976) *Peratherium* (Marsupialia: Didelphidae) from the Oligocene and Miocene of South Dakota. In: Churcher CS (ed) Athlon: Essays on Palaeontology in Honour of Loris Shano Russell. Roy Ontario Museum Miscellaneous Publications, Toronto, pp 155–168.

Gregory WK, Simpson GG (1926) Cretaceous Mammal Skulls from Mongolia. Nature 118: 698–699.

Hayes FG (2005) Arikareean (Oligocene-Miocene) *Herpetotherium* (Marsupialia, Didelphidae) from Nebraska and Florida. Bulletin of the Florida Museum of Natural History 45: 335-353.

Hooker JJ (2010) The mammal fauna of the early Eocene Blackheath formation of Abbey Wood, London. Monographs of the Palaeontographical Society 164: 1–153.

Hooker JJ (2020) A mammal fauna from the Paleocene-Eocene Thermal Maximum of Croydon, London, UK. Proceedings of the Geologists' Association 131: 458–473.

Horovitz I, Martin T, Bloch J, Ladevèze S, Kurz C, Sánchez-Villagra MR (2009) Cranial anatomy of the earliest marsupials and the origin of opossums. PLoS One 4: 1–9.

Hough JR (1961) Review of Oligocene didelphid marsupials. Journal of Paleontology 35: 218–228.

Johanson Z (1994) New information concerning the late Cretaceous marsupial *Albertatherium* Fox, 1971. Journal of Vertebrate Paleontology 14: 595-602.

Johanson Z (1996) Revision of the Late Cretaceous North American marsupial genus *Alphadon*. Palaeontographica Abteilung A 242: 127-184.

Kielan-Jaworowska Z (1975) Evolution of the therian mammals in the Late Cretaceous of Asia. Part I. Deltatheridiidae. Palaeontologia Polonica 33: 103–132.

Kielan-Jaworowska Z, Dashzeveg D (1989) Eutherian mammals from the Early Cretaceous of Mongolia. Zoologica Scripta 18: 347-355.

Kihm AJ, Schumaker KK (2015) Marsupials from the Chadronian (latest Eocene) Medicine Pole Hills local fauna, North Dakota. Paludicola 10: 93-112.

Korth WW (1994) Middle Tertiary marsupials (Mammalia) from North America. Journal of Paleontology 68: 376-397.

Korth WW (2008) Marsupialia. In: Janis CM, Gunnell GF, Uhen MD (eds) Evolution of Tertiary Mammals of North America: Volume 2, Small Mammals, Xenarthrans, and Marine Mammals. Cambridge University Press, Cambridge, pp 39–47.

Korth WW (2018) Review of the marsupials (Mammalia: Metatheria) from the late Paleogene (Chadronian–Arikareean: late Eocene–late Oligocene) of North America. PalZ 92: 499-523.

Korth WW, Boyd CA, Emry RJ, Person JJ (2021) Marsupials (Mammalia, Metatheria) from the Brule Formation (Whitneyan, Oligocene) North Dakota. Journal of Paleontology 95: 193-204.

Krishtalka L (1973) Late Paleocene mammals from the Cypress Hills, Alberta. Special Publications of the Museum of Texas Technical University 2: 1–77.

Krishtalka L, Stucky RK (1983a) Revision of the Wind River faunas, early Eocene of Central Wyoming. Part 3. Marsupialia. Annals of Carnegie Museum 52: 205–227.

Krishtalka L, Stucky RK (1983b) Paleocene and Eocene marsupials of North America. Annals of Carnegie Museum 52: 229–263.

Krishtalka L, Stucky RK (1984) Middle Eocene marsupials (Mammalia) from northeastern Utah and the mammalian fauna from Powder Wash. Annals of Carnegie Museum 53: 31–45.

Krishtalka L, Black CC, Riedel DW (1975) Paleontology and geology of the Badwater Creek area, central Wyoming. Part 10. A late Paleocene mammal fauna from the Shotgun Member of the Fort Union Formation. Annals of the Carnegie Museum 45: 179-212.

Ladevèze S, Muizon C de, Beck RMD, Germain D, Cespedes-Paz R (2011) Earliest evidence of mammalian social behaviour in the basal Tertiary of Bolivia. Nature 474: 83–86.

Ladevèze S, Smith R, Smith T (2012) Reassessment of the morphology and taxonomic status of the earliest herpetotheriid marsupials of Europe. Journal of Mammalian Evolution 19: 249–261.

Lillegraven JA (1976) Didelphids (Marsupialia) and *Uintasorex* (?Primates) from later Eocene sediments of San Diego County, California. Transactions of the San Diego Society of Natural History 18: 85–112.

Lillegraven JA (1969) Latest Cretaceous mammals of upper part of Edmonton Formation of Alberta, Canada, and review of marsupial-placental dichotomy in mammalian evolution. The University of Kansas Paleontological Contributions 50: 1-122.

Lofgren D, Hanneman D, Bibbens J, Gerken L, Hu F, Runkel A, Kong I, Tarakji A, Helgeson A, Gerard I, Li R, Li S, Ji Z (2020) Eocene and Oligocene mammals from the Gravelly Range of Southwest Montana. Paludicola 12: 263-297.

Lofgren D, McKenna M, Honey J, Nydam R, Wheaton C, Yokote B, Henn L, Hanlon W, Manning S, Mcgee C (2014) New records of eutherian mammals from the Goler Formation (Tiffanian, Paleocene) of California and their biostratigraphic and paleobiogeographic implications. American Museum Novitates 3797: 1-57.

Lopatin AV, Averianov AO (2017) The stem placental mammal *Prokennalestes* from the Early Cretaceous of Mongolia. Paleontological Journal 51: 1293-1374.

Maas MC, Thewissen JGM, Kappelman J (1998) *Hypsamasia seni* (Mammalia: Embrithopoda) and other mammals from the Eocene Kartal Formation of Turkey. Bulletin of Carnegie Museum of Natural History 34: 286-297.

Marshall LG, Muizon C de (1995) Part II: The skull. In: Muizon C de (ed) *Pucadelphys andinus* (Marsupialia, Mammalia) from the early Paleocene of Bolivia. Mémoires du Muséum national d'Histoire naturelle 195: 21-90.

Marshall LG, Muizon C de, Sigé B (1983) Late Cretaceous mammals (Marsupialia) from Bolivia. Geobios 16: 739-745.

Matthew WD (1937) Paleocene faunas of the San Juan Basin, New Mexico. Transactions of the American Philosophical Society 30: 1–510.

McGrew PO (1937) New marsupials from the Tertiary of Nebraska. The Journal of Geology 45: 448-455.

McKenna MC (1960) Fossil Mammalia from the early Wasatchian Four Mile fauna, Eocene of northwest Colorado. University of California Publications in Geological Sciences 37: 1–130.

Métais G, Coster PM, Kappelman JR, Licht A, Ocakoğlu F, Taylor MH, Beard KC (2018) Eocene metatherians from Anatolia illuminate the assembly of an island fauna during Deep Time. PloS one 13: e0206181.

Muizon C de (1998) *Mayulestes ferox*, a borhyaenoid (Metatheria, Mammalia) from the early Palaeocene of Bolivia. Phylogenetic and paleobiologic implications. Geodiversitas 20: 19-142.

Muizon C de, Ladevèze S (2020) Cranial anatomy of *Andinodelphys cochabambensis*, a stem metatherian from the early Paleocene of Bolivia. Geodiversitas 42: 597-739.

Muizon C de, Ladevèze S (2022) New material of *Incadelphys antiquus* (Pucadelphyda, Metatheria, Mammalia) from the early Palaeocene of Bolivia reveals phylogenetic affinities with enigmatic North and South American metatherians. Geodiversitas 44: 609–643.

Murphey P, Kelly T, Chamberlain K, Tsukui K, Clyde W (2018) Mammals from the earliest Uintan (middle Eocene) Turtle Bluff Member, Bridger Formation, southwestern Wyoming, USA, Part 3: Marsupialia and a reevaluation of the Bridgerian-Uintan North American Land Mammal Age transition. Palaeontologia Electronica 21:25A: 1–52.

Neal JE (1996) Summary of Paleogene sequence stratigraphy in northwest European and the North Sea. In: Knox RWOB, Corfield RM, Dunay RE (eds) Correlation of the Early Paleogene in Northwest Europe. Geol Soc London Spec Publ 101, pp 15–42.

Noiret C, Steurbaut E, Tabuce R, Marandat B, Schnyder J, Storme JY, Yans J (2016) New bio-chemostratigraphic dating of a unique early Eocene sequence from southern Europe results in precise mammalian biochronological tie-points. Newsletters on Stratigraphy 49: 469-480.

Oliveira ÉV, Carneiro LM, Goin FJ (2021) A new derorhynchid (Mammalia, Metatheria) from the early Eocene Itaboraí fauna of Brazil with comments on its affinities. Anais da Academia Brasileira de Ciências 93: e20201554.

Paula Couto CD (1952) Fossil mammals from the beginning of the Cenozoic in Brazil. Marsupialia: Didelphidae. American Museum Novitates 1567: 1-26.

Rose KD (1981) The Clarkforkian Land-Mammal Age and mammalian faunal composition across the Paleocene-Eocene boundary. University of Michigan Papers on Paleontology 26: 1–197.

Rose KD (2010) New marsupial from the early Eocene of Virginia. Journal of Paleontology 84: 561–565.

Rose KD, Chew AE, Dunn RH, Kraus MJ, Fricke HC, Zack SP (2012) Earliest Eocene mammalian fauna from the Paleocene-Eocene Thermal Maximum at Sand Creek Divide, Southern Bighorn Basin, Wyoming. University of Michigan Papers on Paleontology 36: 1–122.

Rothecker J, Storer JE (1996) The marsupials of the Lac Pelletier lower fauna, Middle Eocene (Duchesnean) of Saskatchewan. Journal of Vertebrate Paleontology 16: 770–774.

Rougier GW, Wible JR, Novacek MJ (1998) Implications of *Deltatheridium* specimens for early marsupial history. Nature 396: 459-463.

Sánchez-Villagra M, Ladevèze S, Horovitz I, Argot C, Hooker JJ, Macrini TE, Martin T, Moore-Fay S, Muizon C de, Schmelzle T, Asher RJ (2007) Exceptionally preserved North American Paleogene metatherians: Adaptations and discovery of a major gap in the opossum fossil record. Biology Letters 3: 318–322.

Secord R (2008) The Tiffanian Land-Mammal Age (Middle and Late Paleocene) in the Northern Bighorn Basin, Wyoming. University of Michigan Papers on Paleontology 35: 1–192.

Setoguchi T (1975) Paleontology and geology of the Badwater Creek area, central Wyoming. Part 11. Late Eocene marsupials. Annals of Carnegie Museum 45: 263-275.

Simpson GG (1928) American Eocene didelphids. American Museum Novitates 307: 1–7.

Simpson GG (1935) The Tiffany fauna, Upper Paleocene. I.-Multituberculata, Marsupialia, Insectivora, and ?Chiroptera. American Museum Novitates 795: 1–19.

Smith T, Dupuis C, Folie A, Quesnel F, Storme J-Y, Iacumin P, Riveline J, Missiaen P, Ladevèze S, Yans J (2011) A new terrestrial vertebrate site just after the Paleocene–Eocene boundary in the Mortemer Formation of Upper Normandy, France. Comptes Rendus Palevol 10: 11–20.

Smith T, Smith R (2013) A land micro-mammal fauna from the Early Eocene marine Egem deposits (NP12, Belgium) and the first occurrence of the peradectid marsupial *Armintodelphys* outside North America. Geologica Belgica 16: 302–310.

Steurbaut E, Coninck J de, van Simaeys S (2016). Micropalaeontological dating of the Prémontré mammal fauna (MP10, Prémontré Sands, EECO, early late Ypresian, Paris Basin). Geologica Belgica 19: 273-280.

Stock C (1936) Sespe Eocene Didelphids. Proceedings of the National Academy of Sciences 22: 122–124.

Storer JE (1991) The mammals of the Gryde Local Fauna, Frenchman Formation (Maastrichtian: Lancian), Saskatchewan. Journal of Vertebrate Paleontology 11: 350-369.

Strait SG (2001) New Wa-0 mammalian fauna from Castle Gardens in the southeastern Bighorn Basin. In: Gingerich, PD (ed) Paleocene-Eocene stratigraphy and biotic change in the Bighorn and Clarks Fork basins, Wyoming. University of Michigan Papers on Paleontology 33, pp. 127–143.

Szalay FS, Trofimov BA (1996) The Mongolian Late Cretaceous *Asiatherium*, and the early phylogeny and paleobiogeography of Metatheria. Journal of Vertebrate Paleontology 16: 474–509.

Travouillon KJ (2016) Investigating dental variation in *Perameles nasuta* Geoffroy, 1804, with morphological evidence to raise *P. nasuta pallescens* Thomas, 1923 to species rank. Zootaxa 4114: 351-392.

Vianey-Liaud M, Vidalenc D, Orliac MJ, Maugoust J, Lézin C, Pélissié T (2022) Rongeurs de la localité éocène de Cos (Tarn-et-Garonne, Quercy, France). Comparaison avec les rongeurs de localités de la transition Éocène inférieur/Éocène moyen. Geodiversitas 44: 753-800.

Vitek NS, Manz CL, Gao T, Bloch JI, Strait SG, Boyer DM (2017) Semi-supervised determination of pseudocryptic morphotypes using observer-free characterizations of anatomical alignment and shape. Ecology and Evolution 7: 5041-5055.

Vullo R, Gheerbrant E, Muizon C de, Néraudeau D (2009) The oldest modern therian mammal from Europe and its bearing on stem marsupial paleobiogeography. Proceedings of the National Academy of Sciences 106: 19910–19915.

West RM (1973) Geology and mammalian paleontology of the New Fork-Big Sandy area, Sublette County, Wyoming. Fieldiana 29: 1–193.

Wible JR, Rougier GW, Novacek MJ, Asher RJ (2007) Cretaceous eutherians and Laurasian origin for placental mammals near the K/T boundary. Nature 447: 1003-1006.

Wible JR, Rougier GW, Novacek MJ, Asher RJ (2009) The eutherian mammal *Maelestes gobiensis* from the Late Cretaceous of Mongolia and the phylogeny of Cretaceous Eutheria. Bulletin of the American Museum of Natural History 327: 1-123.

Wilf P, Beard KC, Davies-Vollum KS, Norejko JW (1998) Portrait of a late Paleocene (early Clarkforkian) terrestrial ecosystem; Big Multi Quarry and associated strata, Washakie Basin, southwestern Wyoming. Palaios 13(6): 514-532.

Williamson TE, Lofgren DL (2014) Late Paleocene (Tiffanian) metatherians from the Goler Formation, California. Journal of Vertebrate Paleontology 34: 477–482.

Williamson TE, Taylor LH (2011) New species of *Peradectes* and *Swaindelphys* (Mammalia: Metatheria) from the Early Paleocene (Torrejonian) Nacimiento Formation, San Juan Basin, New Mexico, USA. Palaeontologia Electronica 14(3):23A: 1–16.

Williamson TE, Brusatte SL, Carr TD, Weil A, Standhardt BR (2012) The phylogeny and evolution of Cretaceous–Palaeogene metatherians: cladistic analysis and description of new early Palaeocene specimens from the Nacimiento Formation, New Mexico. Journal of Systematic Palaeontology 10: 625–651.

Williamson TE, Brusatte SL, Wilson GP (2014) The origin and early evolution of metatherian mammals: The Cretaceous record. Zookeys 465: 1–76.

Wilson GP (2013) Mammals across the K/Pg boundary in northeastern Montana, U.S.A.: dental morphology and body-size patterns reveal extinction selectivity and immigrant-fueled ecospace filling. Paleobiology 39: 429-469.

Wilson GP (2014) Mammalian extinction, survival, and recovery dynamics across the Cretaceous-Paleogene boundary in northeastern Montana, USA. In: Wilson GP, Clemens WA, Horner JR, Hartman JH (eds.) Through the end of the Cretaceous in the type locality of the Hell Creek Formation in Montana and adjacent areas. Geological Society of America Special Paper 503, Boulder, Colorado, pp 365-392.

Wilson GP, Ekdale EG, Hoganson JW, Calede JJ, Vander Linden A (2016) A large carnivorous mammal from the Late Cretaceous and the North American origin of marsupials. Nature Communications 7: 13734.

Woodburne MO, Goin FJ, Raigemborn MS, Heizler M, Gelfo JN, Oliveira EV (2014) Revised timing of the South American early Paleogene land mammal ages. Journal of South American Earth Sciences 54: 109-119.

Supplementary material 2. List of characters included in the cladistic analyses of the **Chapter 1.3**. It is mentioned if a dental character is taken or modified (change in the spelling and / or character states) from Williamson et al. (2014), Muizon and Ladevèze (2022) or Gernelle et al. (2024a) or if it is newly defined. The scoring of characters and taxa in common with Williamson et al. (2014) and Muizon and Ladevèze (2022) have sometimes changed due to new observations. For characters taking biometrics into account, the mean of the observed value for a given taxa has been used to select the appropriate character state. States of characters newly introduced and informative for resolving relationships of metatherian species are illustrated (not to scale) when needed. The composite characters made from characters showing only redundant morphological information are highlighted in red text. Abbreviations: apu/APU, antepenultimate; pu/PU, penultimate; u/U, ultimate; p/P, lower/upper premolar; m/M, lower/upper molar.

1. Lower canine procumbent [character 9 in Muizon and Ladevèze 2022]: absent (0), present (1).

2. Relative size of upper canine [**new**]: small: subequal in or shorter than longest upper premolar (0), large: longer than longest upper premolar (1). **Remarks:** the upper canine of *Roberthoffstetteria nationalgeographica* has not been illustrated, but Goin et al. (2003: p. 869) described it as "large" based on the proportions of the available alveolus. The scoring for *Pucadelphys andinus* includes male and female specimens illustrated in Ladevèze et al. (2011).

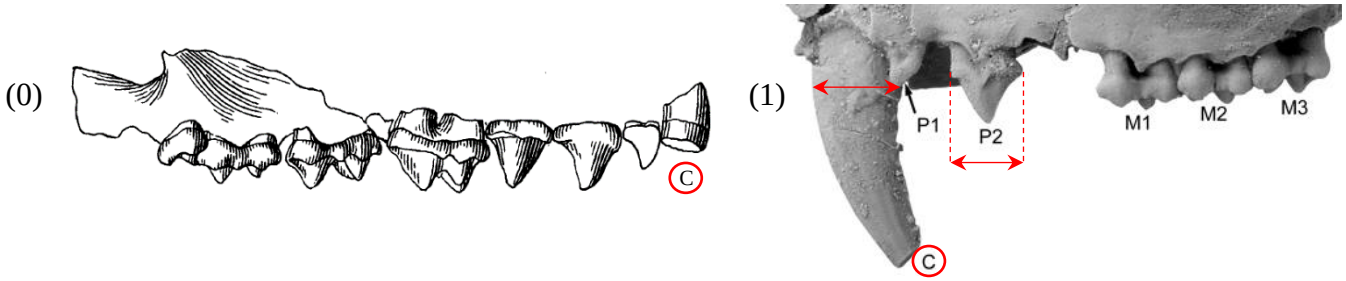

Figure S1. States 0 and 1 for the character 2, illustrated on maxillae of *Peradectes elegans* (0) and *Mimoperadectes houdei* (1). Upper canines are highlighted for comparisons with upper premolars. Drawing of *Pd. elegans* modified from Simpson (1935). Picture of *M. houdei* modified from Horovitz et al. (2009).

3. Distal heel on lower premolars [character 1 in Gernelle et al. 2024a]: at least one cuspid well developed (0), small to indistinct (1).

4. Blade-like pu-p [modified from character 18 in Muizon and Ladevèze 2022]: absent : W >= 40% of L (0), present: W < 40% of L (1).

5. Highest posterior lower premolar [**new**]: pu-p (0) , u-p, or pu-p as high as u-p (1).

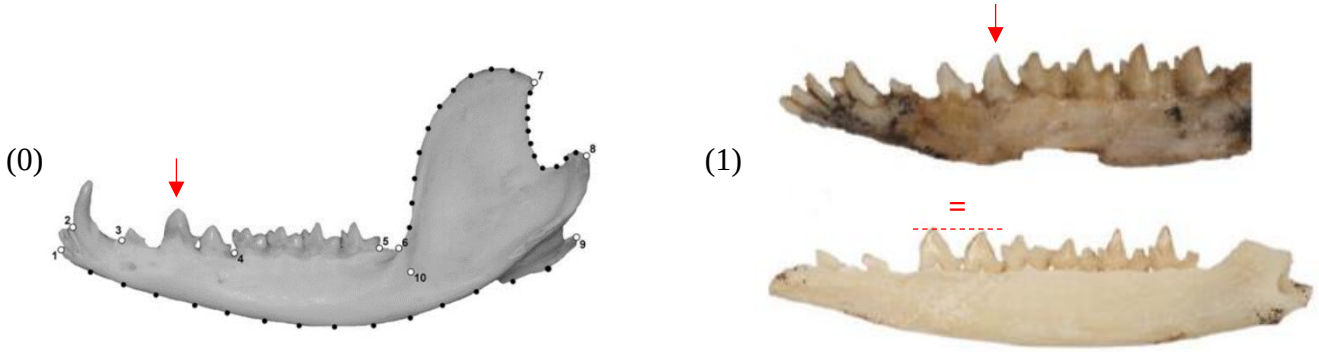

Figure S2. States 0 and 1 for the character 5, illustrated on hemi-mandibles of *Didelphis marsupialis* (0) and *Herpetotherium fugax* (1). The highest lower premolars are highlighted in red. Intraspecific variation is depicted for *H. fugax*. Picture of *D. marsupialis* modified from Brum et al. (2023). Picture of *H. fugax* modified from Lofgren et al. (2020).

6. Shape of anterior edge of u-p main cuspid in lingual or labial view [**new**]: rectilinear or convex (0), triangular (1).

(0) or (1)

M. ferox *Pd. crocheti* *Pu. andinus*

Figure S3. States 0 and 1 for the character 6, illustrated on p3s of *Mayulestes ferox* and *Peradectes crocheti* (0) and *Pucadelphys andinus* (1) in labial view. Pictures of *M. ferox* and *Pd. crocheti* from Muizon and Ladevèze (2020) and Gernelle et al. (2024a), respectively. Picture of *Pu. andinus* from Marshall and Muizon (1995).

7. Relative height of u-p [character 3 in Gernelle et al. 2024a]: higher than m1 (0), as high as m1 (1), lower than m1 (2). **Remark:** the "height" refers here to the crown height.

8. Diastema posterior to p1 [character 17 in Muizon and Ladevèze 2022]: absent (0), present (1).

9. Diastema posterior to pu-p [**new**]: present (0), absent (1).

10. Diastema anterior to P1 [character 15 in Muizon and Ladevèze 2022]: absent (0), present (1).

11. Diastema posterior to P1 [character 16 in Muizon and Ladevèze 2022]: absent (0), present (1).

12. P1 morphology in lateral view [modified from character 14 in Muizon and Ladevèze 2022]: strongly asymmetrical (0), roughly symmetrical (1).

13. P1 basal accessory cusp or cingulum [**new**]: present (0), absent (1).

(0) 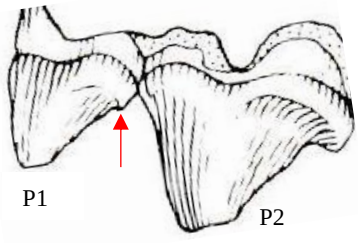

(1)

Figure S4. States 0 and 1 for the character 13, illustrated on P1s of *Roberthoffstetteria nationalgeographica* (0) and *Peradectes crocheti* (1) in labial view. Drawing of *R. nationalgeographica* modified from Marshall et al. (1983). Picture of *Pd. crocheti* from Gernelle et al. (2024a).

14. Orientation of P1 or P2 relative to tooth row [modified from character 13 in Muizon and Ladevèze 2022]: parallel to subparallel (0), at least sometimes oblique (1).

15. Relative size of PU-P [**new**]: subequal to slightly larger than APU-P (0), much larger than APU-P (1).

(0) 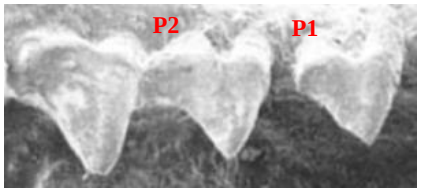

(1) 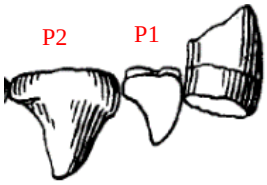

Figure S5. States 0 and 1 for the character 15, illustrated on upper premolars of *Asiatherium reshetovi* (0) and *Peradectes elegans* (1) in labial view. Picture of *A. reshetovi* modified from Szalay and Trofimov (1996). Drawing of *Pd. elegans* modified from Simpson (1935).

16. Notch between PU-P or U-P distal crista of the main cusp and distalmost cusp [**new**]: present (0), absent (1).

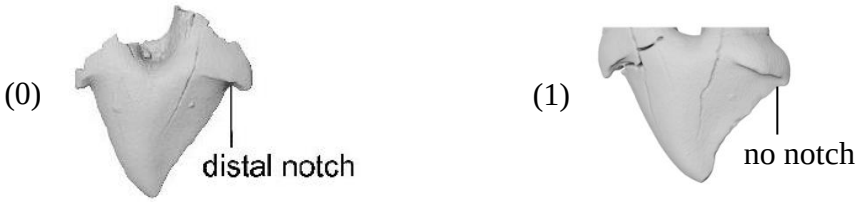

Figure S6. States 0 and 1 for the character 16, illustrated on upper premolars of *Peradectes crocheti* (0) and *Peratherium constans* (1) in labial view. Picture of *Pd. crocheti* from Gernelle et al. (2024a). Picture of *Pt. constans* from this work.

17. Relative heigh of U-P crown in labial view [**new**]: subequal or lower than PU-P or APU-P crown (0), higher than PU-P and APU-P crown (1).

Figure S7. States 0 and 1 for the character 17, illustrated on upper molars of *Perameles nasuta* (0) and *Peradectes gulottai* (1). Picture of *Pe. nasuta* modified from Travouillon (2016). Picture of *Pd. gulottai* modified from Rose (2010).

18. Number of fully molariform definitive dental loci [modified from character 15 in Williamson et al. 2012]: three (0), four (1).

Remark: the length measurements used below (characters 19 to 21) have been taken parallel to the paraconid – metaconid axis (see Gernelle et al. 2024a).

19. m1 relative length [modified from character 4 in Gernelle et al. 2024a]: as long as m2 or longer (0), slightly shorter (< 10% shorter) than m2 (1), much shorter (>= 10% shorter) than m2 (2).

20. Proportions of pu-m in occlusal view [modified from character 5 in Gernelle et al. 2024a]: L/W < 1.55 (0), 1.55 <= L/W <= 1.75 (1), L/W > 1.75 (2).

21. u-m relative length [character 6 in Gernelle et al. 2024a]: distinctively shorter than pu-m (0), as long as or longer than pu-m (1).

Remark: the cingulids (precingulid, ectocingulid, postcingulid) have been considered in comparisons of trigonid and talonid proportions below (characters 22 to 25).

22. Trigonid proportions on pu-m [modified from character 54 in Muizon and Ladevèze 2022]: wider than long (0), as wide as long or longer than wide (1).

23. Trigonid vs talonid width on pu-m [modifed from: character 60 in Williamson et al. 2014; character 56 in Muizon and Ladevèze 2022, character 7 in Gernelle et al. 2024a]: distinctly wider than talonid (0), subequal in width to talonid (1), at least sometimes narrower than talonid (2). **Ordered.**

24. Trigonid vs talonid lenght on apu-m or pu-m [modified from character 57 in Muizon and Ladevèze 2022]: shorter than talonid (0), subequal in length to talonid (1), longer than talonid (2). **Ordered**.

25. Talonid length on u-m [character 8 in Gernelle et al. 2024a]: shorter than trigonid (0), subequal in length or longer than trigonid (1).

26. Protoconid height of pu-m in labial view [**new**]: 50% higher than hypoconid or less (0), more than 50% higher than hypoconid (1). **Remark:** some taxa have not been scored for this character (*Armintodelphys*, *Peradectes* sp. nov. 1) because the protoconid of available specimens is worn (e.g. see Smith and Smith 2013).

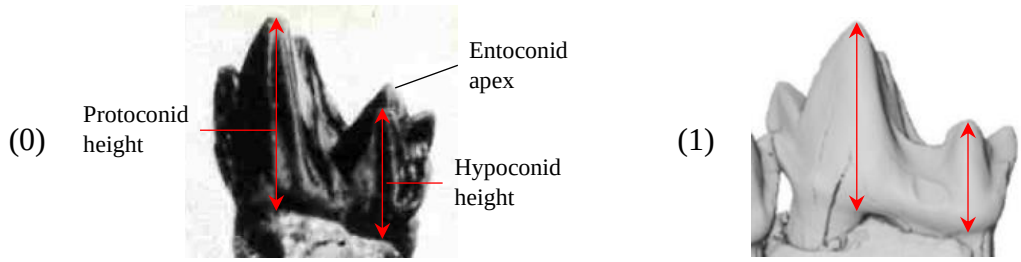

Figure S8. States 0 and 1 for the character 26, illustrated on m3s of *Albertatherium primus* (0) and *Peradectes crocheti* (1). Picture of *Al. primus* modified from Fox (1971). Picture of *Peradectes crocheti* modified from Gernelle et al. (2024a).

27. Relative size and shape of talonid of u-m vs pu-m [character 58 in Muizon and Ladevèze 2022]: talonid of u-m similar to that of pu-m (0), talonid of u-m much reduced and relatively narrower than on pu-m (1).

28. Lingual opening of the trigonid basin vs lingual opening of the talonid basin, except on u-m [**new**]: higher (0), subequal in height (1).

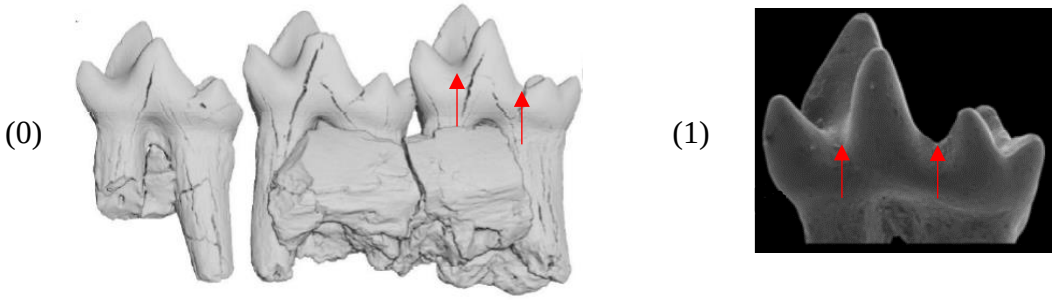

Figure S9. States 0 and 1 for the character 28, illustrated on lower molars of *Peradectes crocheti* (m1-m3) (0) and *Peratherium constans* (1). Picture of *Pd. crocheti* modified from Gernelle et al. (2024a). Picture of *Pt. constans* modified from Ladevèze et al. (2012).

29. Precingulid length on apu-m and pu-m [**new**]: absent or mesiodistally narrow (0), mesiodistally expanded (1).

Figure S10. States 0 and 1 for the character 29, illustrated on m2s and m3s of *Peradectes crocheti* (0) and *Perameles nasuta* (1). Picture of *Pd. crocheti* modified from Gernelle et al. (2024a). Picture of *Pm. nasuta* modified from Travouillon (2016).

30. Anterior keel at mesiolingual angle of paraconid [modified from character 64 in Williamson et al. 2014; character 61 in Muizon and Ladevèze 2022]: absent (0), present (1).

31. Height of metaconid vs paraconid [modified from: character 66 in Muizon and Ladevèze 2022; and character 63 in Williamson et al. 2014]: subequal or lower (0), higher (1).

32. Relative lengths of paraconid and metaconid on pu-m [modified from character 62 in Williamson et al. 2014]: metaconid longer than paraconid (0), paraconid and metaconid subequal in length, or paraconid longer (1).

33. Height of metaconid vs protoconid [**new**]: lower (0), subequal or higher (1). **Remark:** for state 1, see for example Muizon and Ladevèze (2022: fig. 7D).

34. Metaconid most frequent position on the anteroposterior axis of apu-m and pu-m [character 9 in Gernelle et al. 2024a]: metaconid almost directly lingual to protoconid (0), metaconid distolingual to protoconid (1).

35. Relative lengths of para- and protocristid on apu-m and pu-m [modified from character 68 in Muizon and Ladevèze 2022]: protocristid > paracristid (0), subequal, at least on pu-m (1), paracristid > protocristid (2).

36. Preprotocristid shape in labial/mesiolabial view, except on u-m [**new**]: rectilinear (0), convex (1).

(0) (1) 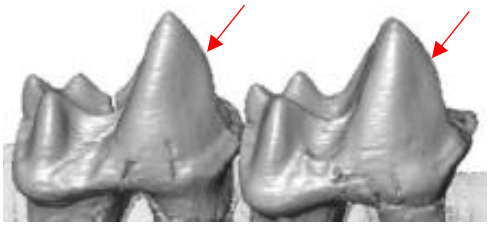

Figure S11. States 0 and 1 for the character 36, illustrated on m3 of *Peratherium constans* (0) and m2 and m3 of *Peradectes crocheti* (1) in labial view. Picture of *Pt. constans* modified from Ladevèze et al. (2012). Picture of *Pd. crocheti* modified from Gernelle et al. (2024a).

37. Position of mesial end of cristid obliqua on apu-m and pu-m [modified from: character 80 in Williamson et al. 2014, and character 69 in Muizon and Ladevèze 2022. Character 10 in Gernelle et al. 2024a] + hypoflexid relative width [character 78 in Muizon and Ladevèze 2022; character 12 in Gernelle et al. 2024a]: cristid obliqua lingual to carnassial notch of protocristid + wide hypoflexid (ca. 40-50% of talonid width) (0), crisitd obliqua beneath carnassial notch of protocristid + wide hypoflexid (ca. 40-50% of talonid width) (1), crisitd obliqua labial to carnassial notch of protocristid + narrow hypoflexid (less than 40% of talonid width) (2). **Ordered**. **Remark:** given their scoring, the merging of the characters 10 and 12 from Gernelle et al. (2024a) does not impact the relationships within the ingroup in their analyses (mentioned as characters “not parsimony informative for resolving relationships between the ingroup taxa”, p. 31).

38. Position of mesial end of cristid obliqua on u-m [modified from: character 81 in Williamson et al. 2014; and character 11 in Gernelle et al. 2024a]: at least sometimes ventral or lingual to the protocristid notch (0), labial to the protocristid notch (1).

39. Notch on cristid obliqua near trigonid wall [**new**]: absent (0), present (1).

(0)

(1) 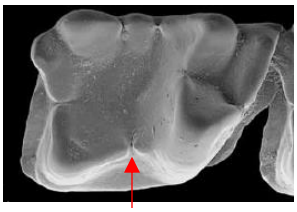

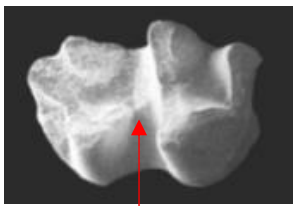

Pd. louisi *Pediomys elegans* *Aenigmadelphys archeri*

Figure S12. States 0 and 1 for the character 39, illustrated on m3s of *Peradectes louisi* (0) and *Pediomys elegans* and *Aenigmadelphys archeri* (1) in occlusal view. Picture of *Pd. lousi* from Gernelle et al. (2024a). Pictures of *Pediomys elegans* and *Ae. archeri* modified from Davis (2007) and Cifelli (1990).

40. Cristid obliqua shape, except on u-m [**new**]: straight (0), curved near hypoconid apex (1).

(0) 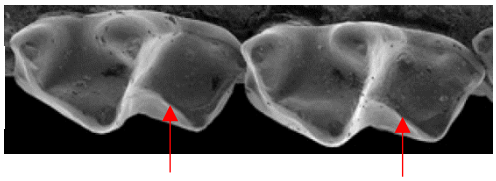

(1)

Figure S13. States 0 and 1 for the character 40, illustrated on lower molars of *Peradectes dufraingi* (0) and *Peradectes coprexeches* (1) in occlusal view. Picture of *Pd. dufraingi* modified from Smith and Smith (2013). Picture of *Pd. coprexeches* modified from Williamson and Taylor (2011).

41. Emargination of the labial margin of pu-m [character 13 in Gernelle et al. 2024a]: absent (0), present (1).

42. Hypoconid position compared with entoconid position, except on u-m [**new**]: mesiolabial to entoconid (0), distolabial or labial to entoconid (1).

(0) 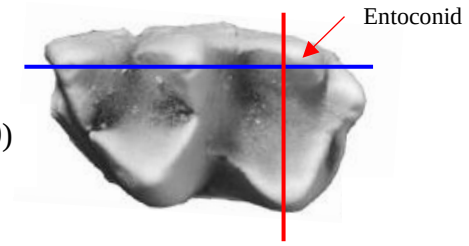

(1) 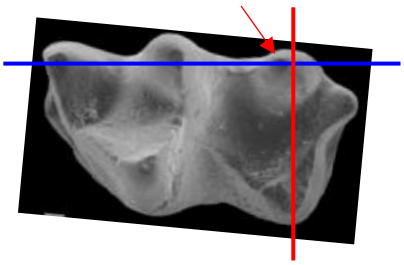

Figure S14. States 0 and 1 for the character 42, illustrated on lower molars of *Golerdelphys stocki* (0) and *Peratherium constans* (1) in occlusal view. Picture of *G. stocki* modified from Williamson and Lofgren (2014). Picture of *Pt. constans* modified from Ladevèze et al. (2012).

43. Hypoconid position compared with protoconid position on u-m [**new**]: distal to protoconid (0), distolingual to protoconid (1).

(0) 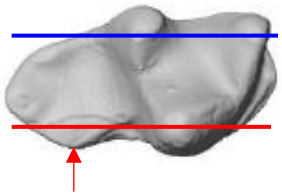

(1) 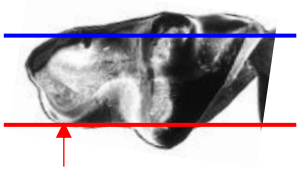

Figure S15. States 0 and 1 for the character 43, illustrated on m4s of *Peradectes louisi* (0) and *Derorhynchus singularis* (1) in occlusal view. Picture of *Pd. louisi* modified from Gernelle et al. (2024a). Picture of *D. singularis* modified from Oliveira et al. (2021).

44. Postcristid morphology on apu-m to u-m [character 15 in Gernelle et al. 2024a]: straight at least on one molar locus (0), curved (1).

45. Angle (in degree of arc) between cristid obliqua and postcristid, except on u-m [modified from character 14 in Gernelle et al. 2024a]: equal or less than 65° (0), between 70 and 85° (1), equal or more than 90° (2). **Remark:** when the postcristid is notched, only the labial segment of the postcristid has been used.

46. Angle (in degree of arc) between cristid obliqua and postcristid on u-m [**new**]: less than 90° (0), subequal to or more than 90° (1).

(0) 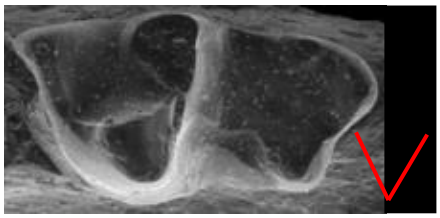 (1) 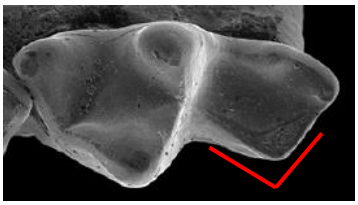

Figure S16. States 0 and 1 for the character 46, illustrated on m4s of *Armintodelphys blacki* (0) and *Peradectes dufraingi* (1) in occlusal view. Pictures of *Arm. blacki* and *Pd. dufraingi* modified from Smith and Smith (2013). The red segments represent the configurations of the adjacent cristid obliqua and postcristid.

47. Talonid ectocingulid, connected to postcingulid when the latter is present (i.e. internal hypoconid) [character 77 in Williamson et al. 2014]: absent (0), present (1).

48. Postcingulid morphology, except on u-m [modified from character 16 in Gernelle et al. 2024a]: absent (0), attenuates labially to the hypoconulid (1), extends lingually towards the hypoconulid tip (2).

49. Postcingulid on u-m [modified from: character 74 in Williamson et al. 2014; and character 79 in Muizon and Ladevèze 2022; character 17 in Gernelle et al. 2024a]: present (0), absent at least on one u-m (1). **Remark:** contrary to Muizon and Ladevèze (2022), the postcingulid of u-m of *Pucadelphys andinus* is regarded as "Present" and variation for this character exists in *Mayulestes ferox* (see below).

(0) and

Figure S17. State 0 for the character 49, illustrated on m4s of *Mayulestes ferox* in occlusal view. On the same specimen, the left m4 shows a postcingulid, but not the right m4. Pictures modified from Muizon and Ladevèze (2020).

50. Talonid lingual edge, except on u-m [**new**]: straight between metaconid and entoconid (parallel to paraconid-metaconid axis) (0), mostly curved along the whole talonid length (1).

(0) 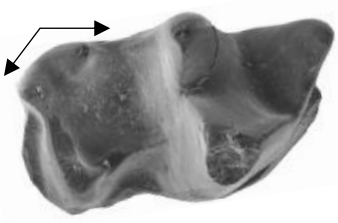 (1) 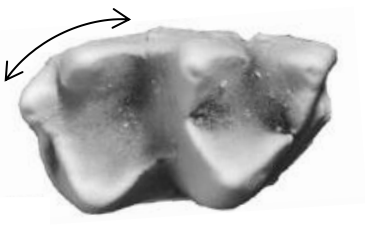

Figure S18. States 0 and 1 for the character 50, illustrated on lower molars of *Peradectes coprexeches* (0) and *Golerdelphys stocki* (1) in occlusal view. Picture of *Pd. coprexeches* modified from Williamson and Taylor (2011). Picture of *G. stocki* from Williamson and Lofgren (2014).

51. Hypoconulid position on the distal margin of molars [character 70 in Muizon and Ladevèze 2022]: in median position (0), shifted lingually, close to entoconid (1).

52. Notch between entoconid and hypoconulid on pu-m [modified from character 18 in Gernelle et al. 2024a]: much shallower than the metaconid - entoconid notch (vestigial notch) (0), almost as deep as the metaconid - entoconid notch (shallow notch) (1), as deep as the metaconid - entoconid notch (deep notch) (2). **Remark:** because the two available talonids of "m2 or m3" of *Golerdelphys stocki* show different configurations, it has been scored as "?" for this taxon.

(2)

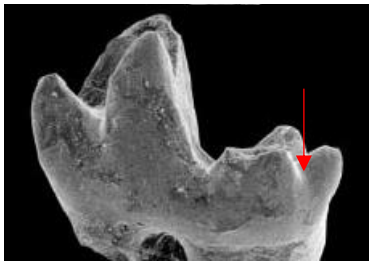

Figure S19. State 2 for the character 52, illustrated on a lower molar (considered as m3) of *Thylacodon pusillus* in lingual view. Picture modified from Williamson et al. (2012). The states 0 and 1 of this character have been illustrated in Gernelle et al. (2024a: Online material 3, fig. S7).

53. Relative height of entoconid and hypoconulid [modified from character 19 in Gernelle et al. 2024a]: hypoconulid lower than or equal in height to entoconid on all molars (0), hypoconulid higher than entoconid only on u-m (1), hypoconulid higher than entoconid on pu-m and u-m (2).

54. Entoconid shape at base, except on u-m (modified from: character 71 in Williamson et al. 2014; and character 73 in Muizon and Ladevèze 2022]: conical (0), relatively transversely compressed (1).

55. Pre-entocristid morphology [character 76 in Muizon and Ladevèze 2022; character 20 in Gernelle et al. 2024a]: absent or weakly developed (0), well-developed and sharp (1).

56. Entoconid apex position relative to trigonid on apu-m and pu-m [modified from character 75 in Muizon and Ladevèze 2022; character 21 in Gernelle et al. 2024a]: closer to the distolingual corner of the tooth (posterior) (0), intermediate between distal edge of trigonid and distal margin of the tooth (anterior) (1).

57. Height of entoconid relative to metaconid on pu-m [modified from character 70 in Williamson et al. 2014]: <= 30% of metaconid height (0), between 35 and approximately 50% of metaconid height (1), >= 60% of metaconid height (2).

Upper molars

58. M1 relative lenght (L) [**new**]: M1 L < M2 L (0), M1 L = M2 L or M1 L > M2 L (1). **Remark:** measurements available based on dental raws, or isolated molars when dental raws are unknown.

59. Disparity of length (L) / width (W) ratio between APU-M and PU-M [modified from character 22 in Gernelle et al. 2024a]: (APU-M L/W - PU-M L/W) > 0.10 (0), (APU-M L/W - PU-M L/W) <= 0.10 (1). **Remark:** such L/W ratios for M2 and M3 were first calculated by Korth (1994) and Rose (2010) to differentiate *Peradectes* species.

60. Width of U-M relative to PU-M or APU-M [character 25 in Muizon and Ladevèze 2022]: U-M subequal in width or wider than PU-M (0), U-M narrower than PU-M (1).

61. Protocone length [modified from: character 46 in Muizon and Ladevèze 2022; and character 23 in Gernelle et al. 2024a]: mesiodistally narrow (0), mesiodistally expanded (1). **Remarks:** compared with Gernelle et al. (2024a), the character is restricted in its spelling to the protocone rather than the talon. This does change the scoring for *Asiatherium reshetovi* (mesiodistally narrow protone but expanded talon), but the scoring for peradectids remains the same as in Gernelle et al. (2024a).

62. Protocone relative height, except on U-M [modified from character 50 in Williamson et al. 2014; character 25 in Gernelle et al. 2024a]: subequal or higher than paracone and/or metacone (0), lower than paracone and metacone (1).

63. Protocone position [modified from character 51 in Williamson et al. 2014; character 24 in Gernelle et al. 2024a]: distolingual to paracone (0), almost lingual to paracone (1). **Remark**: comparison between taxa has been made using identical loci when possible.

64. Protocone procumbency [character 52 in Williamson et al. 2014]: absent (0), present (1). **Remark:** this character can be observed in lingual view.

65. Precingulum on protocone [modified from character 54 in Williamson et al. 2014]: absent (0), present (1).

66. Distal margin morphology, except on U-M [modified from character 30 in Gernelle et al. 2024a]: rectilinear (0), emarginated between talon and stylar shelf (1). **Remark:** the presence/absence of distal emargination shows important intraspecific variation in European peradectids (Gernelle et al. 2024a). However, this character seems phylogenetically significant in some peratheriine species (Gernelle et al. 2024b).

67. Postmetaconular crista or postprotocrista extending distolabially to metacone apex [**new**]: present (0), absent (1).

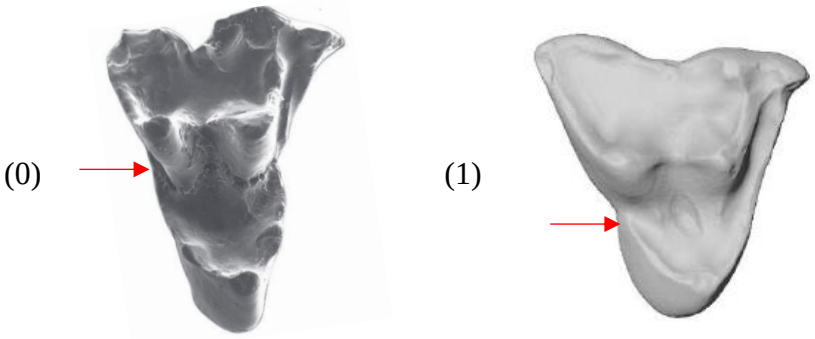

Figure S20. States 0 and 1 for the character 67, illustrated on upper molars of *Aenigmadelphys archeri* (0) and *Peradectes louisi* (1) in occlusal view. Picture of *A. archeri* modified from Muizon and Ladevèze (2022). Picture of *Pd. louisi* modified from Gernelle et al. (2024a).

68. Conules relative size [modified from character 47 in Williamson et al. 2014]: large (0), relatively small or indistinct (1). **Remark:** Williamson and Taylor (2011) highlighted differences in the size of the conules between *Peradectes coprexeches* and the younger *Peradectes elegans*.

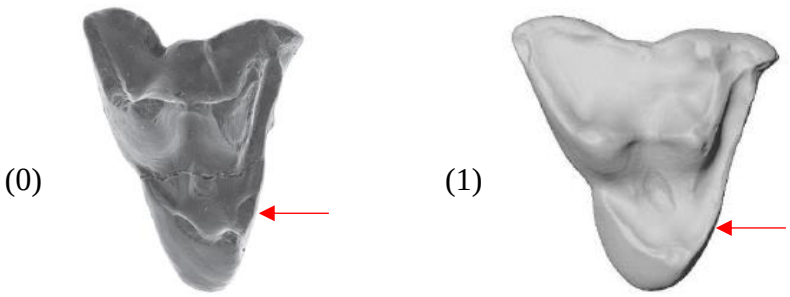

Figure S21. States 0 and 1 for the character 68, illustrated on upper molars of *Peradectes coprexeches* (0) and *Peradectes louisi* (1) in occlusal view. Picture of *Pd. coprexeches* modified from Williamson and Taylor (2011). Picture of *Pd. louisi* modified from Gernelle et al. (2024a).

69. Conules wing-like (internal and external) cristae [modified from: character 49 in Williamson et al. 2014; character 45 in Muizon and Ladevèze 2022; and character 26 in Gernelle et al. 2024a]: present, at least on one conule (0), absent (1).

70. Largest conule, except on U-M [modified from character 27 in Gernelle et al. 2024a]: paraconule larger or conules subequal in size (0), metaconule larger (1).

71. Position of paraconule relative to protocone and paracone [character 48 in Williamson et al. 2014]: closer to protocone or midway between protocone and paracone (0), closer to paracone (1).

72. Labialmost conule [**new**]: metaconule, or conules equally labial (0), paraconule (1).

73. Stylar shelf vs tooth width on APU-M and PU-M [modified from character 27 in Muizon and Ladevèze 2022]: 50% of transverse width or more (0), less than 50% of transverse width (1).

74. Paracingulum [character 49 in Muizon and Ladevèze 2022]: continuous between stylar line and talon (0), interrupted between stylar line and talon (1).

75. Preparacrista orientation on PU-M [character 36 in Williamson et al. 2014]: directed towards the apex of stylar cusp B (0), directed towards a position mesial to the apex of stylar cusp B (1).

76. Preparacrista relative lenght on U-M [modified from character 42 in Muizon and Ladevèze 2022]: shorter or subequal in length to PU-M preparacrista (0), longer than PU-M preparacrista (1). **Remark:** this character has been scored as inapplicable (-) in *Deltatheridium pretrituberculare* and *Dromiciops gliroides*, because their preparacrista much shorter on M4 than M3 is probably highly correlated to their M4 reduced in size, compared with other taxa (see Material and methods section) (also scored "-" in *Glasbius intricatus*, because the m4, and thus the M4, is much smaller).

77. Carnassial notch along preparacrista [character 37 in Williamson et al. 2014]: absent (0), present (1).

78. Carnassial notch in postmetacrista at posterolabial base of metacone [character 38 in Williamson et al. 2014; character 30 in Muizon and Ladevèze 2022]: absent (0), present (1).

79. Postmetacrista length on APU-M or PU-M [character 29 in Muizon and Ladevèze 2022; character 29 in Gernelle et al. 2024a]: subequal to or shorter than preparacrista (0), longer than preparacrista (1). **Remark:** the metastylar wing needs to be unworn for this character to be evaluated, see for example for *Aenigmadelphys archeri*, in Cifelli and Muizon (1994), the M3 of fig. 1E (worn metastylar wing) vs fig. 1F (unworn metastylar wing).

80. Centrocrista morphology [modified from character 46 in Williamson et al. 2014; character 41 in Muizon and Ladevèze 2022] + shape of paracone and metacone [modified from character 43 in Williamson et al. 2014; character 38 in Muizon and Ladevèze 2022]: straight centrocrista + conical paracone and metacone, with labial edge almost as convex as lingual edge (0), V-shaped centrocrista + triangular paracone and metacone (flat labial faces) (1).

81. Paracone and metacone contact [character 45 in Williamson et al. 2014; character 39 in Muizon and Ladevèze 2022]: adjoined at base (0), separated (1).

82. Relative height of paracone vs metacone on APU-M and PU-M [modified from: character 41 in Williamson et al. 2014; character 37 in Muizon and Ladevèze 2022; and character 28 in Gernelle et al.

2024a]: subequal or slightly higher (0), slightly lower (1), distinctly lower (ca. 30% lower or more) (2). **Ordered**.

83. Metacone on last molar [modified from character 40 in Muizon and Ladevèze 2022]: present and distinct (0), extremely reduced (1). **Remark:** this character has been scored as inapplicable (-) in *Deltatheridium pretrituberculare*, because the M4 is weakly developed (see Rougier et al. 1998).

84. Stylar cusp A most frequent position on APU-M or PU-M [modified from character 31 in Gernelle et al. 2024a]: mesiolingual to stylar cusp B (0), mesial to stylar cusp B (1), mesiolabial to stylar cusp B (2).

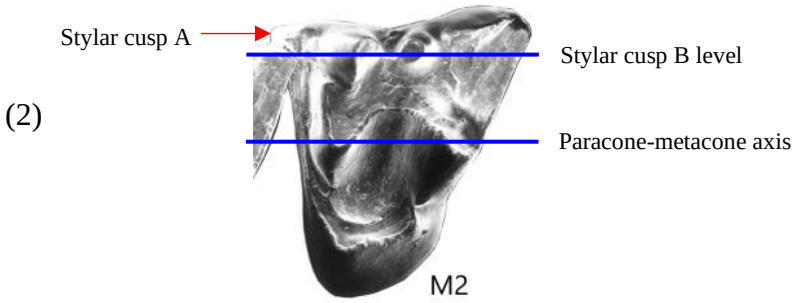

Figure S22. State 2 for the character 84, illustrated on M2 of *Derorhynchus singularis* in occlusal view. Picture modified from Oliveira et al. (2021). The states 0 and 1 of this character have been illustrated in Gernelle et al. (2024a: Online material 3, fig. S10).

85. Stylar cusp A relative size (length and width) on PU-M [modified from character 22 in Williamson et al. 2014; character 32 in Gernelle et al. 2024a]: distinctly smaller than stylar cusp B (0), equal to or larger than stylar cusp B (1).

86. Stylar cusp B relative height, except on U-M [modified from: character 23 in Williamson et al. 2014; and character 32 in Muizon and Ladevèze 2022]: absent or smaller than paracone (0), subequal in height to paracone, at least on one locus (1).

87. Stylar cusp B position, except on U-M [modified from: character 24 in Williamson et al. 2014; and character 33 in Gernelle et al. 2024]: mesiolabial to the paracone apex (0), labial to the paracone apex, at least on M1 or M2 (1).

88. High and short crest connecting vertical stylar cusps A and B on PU-M [**new**]: absent (0), present (1).

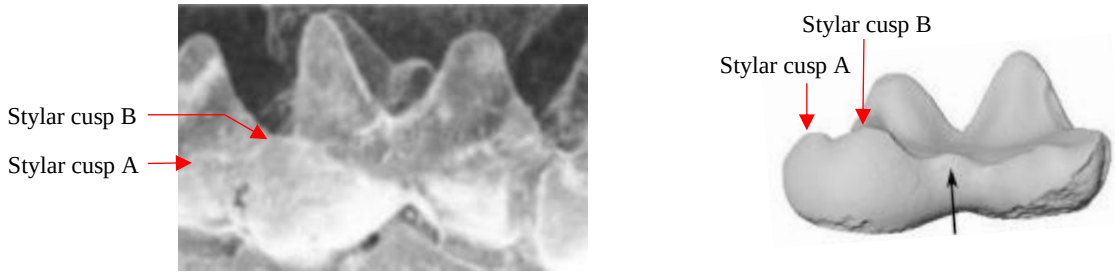

Figure S23. States 0 and 1 for the character 88, illustrated on M3s of *Asiatherium reshetovi* (0) and *Peradectes louisi* (1) in labial view. Picture of *A. reshetovi* modified from Szalay and Trofimov (1996). Picture of *Pd. louisi* modified from Gernelle et al. (2024a).

89. Stylar cusp C on most APU-M and PU-M [modified from: character 25 in Williamson et al. 2014; and character 33 in Muizon and Ladevèze 2022]: absent (0), relatively small (smaller than st.B and st.D) (1), well developed (at least subequal to st.D in height) (2).

90. Stylar cusp C occasionally lingual to the labial edge of the stylar shelf, except on U-M [modified from character 28 in Williamson et al. 2014]: absent (0), present (1).

91. Stylar cusp in C position on U-M [**new**]: absent or labial to centrocrista midline (0), mesiolabial to centrocrista midline (1).

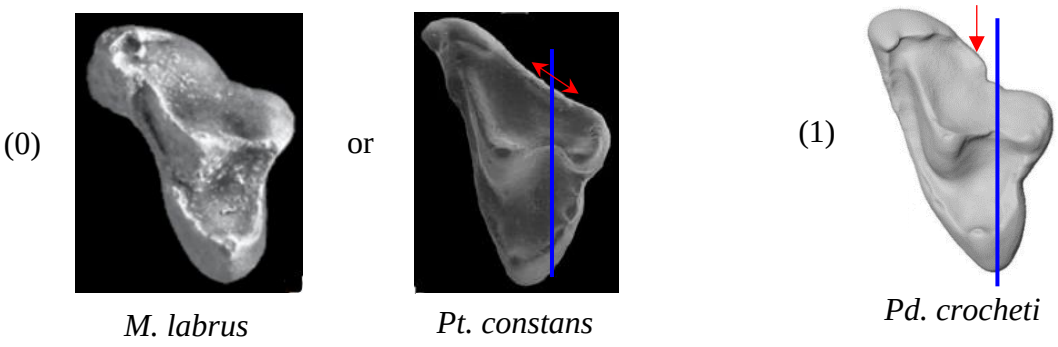

Figure S24. States 0 and 1 for the character 91, illustrated on M4s of *Mimoperadectes labrus* and *Peratherium constans* (0) and of *Peradectes crocheti* (1) in occlusal view. The red arrows indicate stylar cusp C. Picture of *M. labrus* and *Pt. constans* modified from Rose et al. (2012) and Ladevèze et al. (2012), respectively. Picture of *Pd. crocheti* modified from Gernelle et al. (2024a).

92. Stylar cusp D on U-M [**new**]: absent (0), present (1).

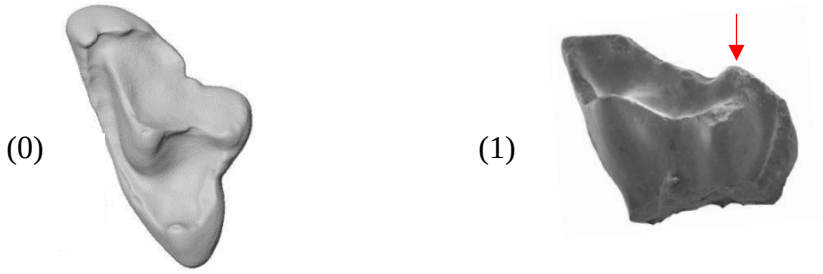

Figure S25. States 0 and 1 for the character 92, illustrated on M4s of *Peradectes crocheti* (0) and *Peradectes coprexeches* (1) in occlusal view. Picture of *Pd. crocheti* from Gernelle et al. (2024a). Picture of *Pd. coprexeches* modified from Williamson and Taylor (2011).

93. Stylar cusp D shape at base on APU-M and PU-M [modified from character 33 in Williamson et al. 2014]: absent (0), relatively mesiodistally long (1), conical (2).

94. Stylar cusp D position [modified from: character 32 in Williamson et al. 2014; and character 35 in Gernelle et al. 2024a]: mesiolabial to metacone apex, on several loci or at least on PU-M (0), strictly labial to metacone apex (1), distolabial to metacone apex, at least on M1 (2).

95. M1 ectoflexus [character 36 in Gernelle et al. 2024a]: sometimes present (0), absent (1).

96. U-M ectoflexus [**new**]: present (0), absent (1).

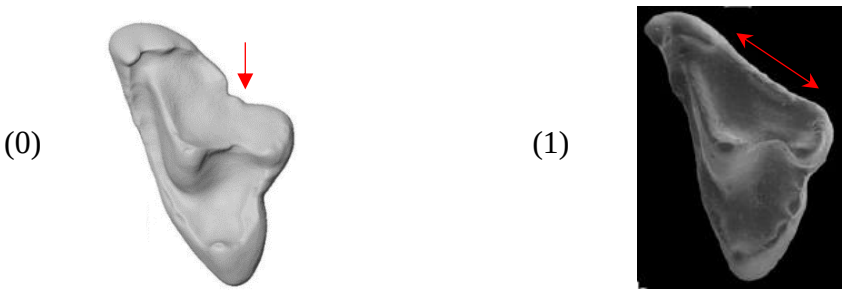

Figure S26. States 0 and 1 for the character 96, illustrated on M4s of *Peradectes crocheti* (0) and *Peratherium*

constans (1) in occlusal view. Picture of *Pd. crocheti* modified from Gernelle et al. (2024a). Picture of *Pt. constans* modified from Ladevèze et al. (2012).

97. Ectoflexus symmetry [character 37 in Gernelle et al. 2024a]: present on M2 or M3, at least on one specimen (0), absent (1). **Remark:** the ectoflexus is considered symmetric when the parastylar and metastylar wings are equally labial (see Gernelle et al. 2024a: Online material 3, fig. S12).

98. Ectoflexus length on APU-M and PU-M [**new**]: mesiodistally narrow (0), long (1).

(0) (1) 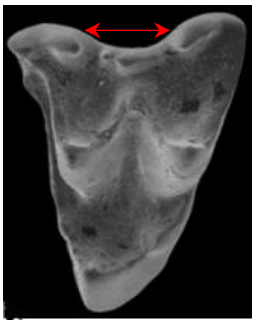

Figure S27. States 0 and 1 for the character 98, illustrated on M3s of *Nortedelphys jasoni* (0) and *Peratherium constans* (1) in occlusal view. Picture of *N. jasoni* modified from Case et al. (2005). Picture of *Pt. constans* modified from Ladevèze et al. (2012).

Additional reference for Appendix S2 (not present in Appendix S1)

Brum MN, Cáceres NC, Bubadué JM (2023) Evolutionary rates, disparity, and ecomorphology of the mandible in American marsupials. Journal of Mammalian Evolution 30: 33-46.

Supplemental material 3. Taxon-character matrix (47 taxa, 98 characters) used in this study. A dash denotes inapplicability. Brackets denote morphological polymorphism. Taxa in blue are only included in additional phylogenetic analyses (analyses sets 3 to 6; see Supplemental material 5).

Prokennalestes minor
?00000200112?0100000100011100010010000001001111010002000211000(01)0(0
1)000100010000000000100010000110000
Maelestes gobiensis
1100000101111011000010001110001011000(01)000100100100000211021000011111
0100101110000000011001000000-0001
Deltatheridium pretrituberculare
0100101111110001011210102011001010120000010-02-001000-
10000010110011(01)100(01)000-110000-1100100000-0?01
Kokopellia juddi
0?0010010????????122110011000101010010000001(12)1020000211021??0100010
00000000?110010?0100000??10??10
Asiatherium reshetovi
?000101111110000112010001000011101101000100100120011000020100000110000
0011011-010100010000000100010
Aenigmadelphys archeri
??0010??????????????1?0100001100110011010101011000200110010201100(01)100
0000011000101010001000100100(01)10
Albertatherium spp.
??????????????????1?1?010?0?00110011011?1010?10?02?011{01}1102110010100
00000110(0 1)?10101000000021001000 10
Turgidodon rhaister
??????????????????12110100110011001101010100 1(01)0(01)2001101102010110
11(01)000001100110101100010021001000 10
Nortedelphys jasoni
??0010011??10?0111(12)1101000100110011010001 0(01)1000200110110211011 0
1000000011 00?101111000100110?100010
Didelphodon vorax
?1101000100100011120100000 10(01)1010110211010002101001001102010100100
10001?101111101200010010002000 10
Pediomys elegans
??0?11?01??????1?120002010100110012121100001(12)0(01)1001201102111100
1110000111011101012001000 2000200110
Glasbius intricatus
??0001201????????1100020001001100010210010011011101201102111 10(01)11(
01)000111101-101012?(12)011011??200?10
Thylacodon spp.
??0??00??????????10100(01)(01)0110011000102100(01)0011002001201112110
1001001001011010001011000001200110100(01)
Peradectes minor
??????????????????101011201100110002021001001100200121(01)11111?100100
10010110 1?001011?1000120??111?01
Peradectes coprexeches
??????????????????10101020110011000212101101111 0(12)00110(01)11111?0?(
01)100100101(01)0100010120110012001111011
Golerdelphys stocki
??????????????????1?1?112?1?00110002?210(01)00?01?02?11?{01}1111??? 100
100110101?0???01012?1?0??20??1????1

Peradectes elegans
000?101(01)10000010{01}10111120110011000212101(01)0011012011(01)11101
10011010011010110110010110110012010111001
Peradectes protinnominatus
??0??0101????????111010201100110002121O1(01)00110110111111(01)110?011
10111010110 1?001011?100(01)120??110?01
Peradectes crocheti
?000100011101010?11101120110011101212101000110110111111011001(01)10(
01)11010100110010110000112010121011
Peradectes russelli
????????????????????12111020 1?001110121210110001111111011 1(01)011001110(
01)110101(01)011001011000011100012001 1
Peradectes louisi
????????????????????11201020110011101212 00(01)100(01)111111011110110011
10(01)11010100110010110000111000120011
Peradectes dufraingi
????????????????????1?211020110011101212000100011011110211 0????????????
??????????????????????????????
Peradectes sp. nov. 1
????????????????????11211020?100111012120001000110111102111??1001(01)101
11010100 1?00101100?01120001??001
Peradectes sp. nov. 2
????????????????????12111020110011101212100100011111(01)10211(01)0??????
??????????????????????????????????
Peradectes sp. nov. 3
??0010001????????11????2???0011?01212?00?0?01?11?11??111???01110(01)
11?10100??001011?000??10??12??01
Mimoperadectes spp.
?11???00?0101011?1111020110011101(12)1200100(01)01(01)11101021101110
(01)0(01)100110101(01)011000011010001 2000120001
Armintodelphys blacki
??1????0?????????1?111121?10011101 2?2101000110111102110{01}?????????
??????????????????????????????????
Armintodelphys dawsoni
????????????????????1?111121?100111002121000000 1?12?1102110 1???011100111
?0110??000011?1?00?20??12??01
Peradectes chesteri
??????2???????????11(12)01020?1001100(01)212101000100110110?100{01}10?
011101111101(01)01?000011000001 10??120001
Peradectes californicus
??1??(01)20????????0?112110201100110002121010001 00(01)111102100011000 1
101110101(01)011001011?01001101012001(01)
Peradectes gulottai
????????????????011???1?001101111
101101?001011?0100110??12??11
Didelphidectes spp.
??1000201????????111110201 1?01??012121010001 00120(01)1?2000????0?1?0(
01)110101101?00101??0000?10??120?11
Nanodelphys hunti
??1010201????????1(12)2(01)1020?1?011?0(01)2?2101(01)000(01)0(01)2101
?{12}000?110001?0(01)110101(01)0(01)100101100000 11000120001

Pucadelphys andinus
0100110100(01)011111110100111100110011021000(01)0(01)1(01)(01)02001120
(01)01(01)1(01)10(01)101100101100010111101010120102000 10
Incadelphys antiquus
0101100100101011111010211110011 01(01)102101(01)001000210112(01)(01)01
10010110110010110(01)1(01)011110100011010100 01(01)
Mayulestes ferox
0100100010100110111111020110011101112 10(01)101100(01)210102111000(01)
10110110 0?0100011010021(12)10010000200110
Roberthoffstetteria nationalgeographica
?100?00?1000011 0?1(12)0102100000110111021011000110010110010200010010 0
00110110100010110001 0(12)100200010
Swaindelphys encinensis
????????????????? 1110111101001100120200010001 1{01}2001111111101011 00
10010110110011120100012010(12)00101
Peratherium constans
?????1101??????1?11101111111011000202000110100020012101111 10(01)0110(
01)100101(01)01100111(12)0100112000110101
Orhaniyeia nauta
??00100????????1?110101(01)10110110002021001100210(02)101000112011101
10(01)1011--(01)01100111201001010002011 1(01)
Herpetotherium edwardi
????????????????? 1?10121111101100020210001011002001201112??1101100100
10100110011202 0?10200020?111
Herpetotherium fugax
10001(01)01011?101111110121(01)111011000202000(01)1110002101200112101
10110010010100110011202001020002001 11
Derorhynchus singularis
1??????10????????1110112011001100020200011110002101200(01)12111101100
100101(01)0010011120101(01)02100101011
Djarthia murgonensis
?10?10201?????101111012011001100021210011000002101200 11?1??11110(01)
100101?01100111202011020001 10?11
Dromiciops gliroides
10101121011110011111011101100110002121001010110010120010211111110011-
---101-0000111--0-02000110001
Perameles nasuta
101011210111000101(12)(01)1011001011101(01)20(01)00011100000101200(01
)021111111001011--0-11000112120110200020(01)001
Marmosa murina
10000101011000110111112201100111002120001110100010 11(01)110211(01)101
10011----000100111202001020001 2(01)011
Metachirus nudicaudatus
10110101011000110112112201101111002021001110100010110110211110110011-
---01110011120100102010120011
Didelphis marsupialis
00110101111(01)001111(01)21122011011110020211011(01)11100101111102111
10(01)10011----01110011120101102010120011

Supplemental material 4. List of ambiguous and unambiguous apomorphies for the strict consensus tree yielded by the initial maximum parsimony analysis, followed by a summary of the CI/RI values of all characters. Node numbers are figured on the consensus tree below. -->, ambiguous apomorphy; ==>, unambiguous apomorphy.

Branch	Character	Steps	CI	Change
node_84 <-> *Prokennalestes minor*				
	2	1	0.250	1 <=> 0
	7	1	0.222	0 <=> 2
	8	1	0.400	1 <=> 0
	45	1	0.400	0 <-> 1
	46	1	0.273	0 <-> 1
	49	1	0.091	0 <-> 1
	54	1	0.364	1 <=> 0
	55	1	0.625	1 <-> 0
	59	1	0.111	0 <-> 1
	63	1	0.769	1 <-> (01)
	65	1	0.400	0 <-> (01)
	66	1	0.667	1 <=> 0
	69	1	0.167	0 <-> 1
	85	1	0.143	1 <=> 0
	93	1	0.333	0 <-> 1
	94	1	0.333	0 <-> 1
	98	1	0.714	1 <-> 0
node_84 --> *Maelestes gobiensis*				
	1	1	0.333	0 --> 1
	13	1	0.200	0 --> 1
	16	1	0.167	0 ==> 1
	33	1	0.250	0 ==> 1
	37	1	0.800	0 --> (01)
	64	1	0.500	0 ==> 1
	65	1	0.400	0 --> 1
	68	1	0.400	0 ==> 1
	71	1	0.500	0 ==> 1
	74	1	0.500	0 ==> 1
	75	1	0.375	0 ==> 1
node_84 --> node_83				
	5	1	0.333	0 ==> 1
	9	1	0.200	0 --> 1
	17	1	0.250	0 ==> 1
	18	1	1.000	0 ==> 1
	19	1	0.545	0 ==> 2
	22	1	0.200	0 --> 1
	30	1	1.000	0 ==> 1
	31	1	0.333	1 --> 0
	32	1	0.143	0 ==> 1
	45	1	0.400	0 --> 2
	47	1	0.556	1 ==> 0
	58	1	0.286	1 ==> 0
	62	1	0.143	0 --> 1
	73	1	0.643	1 --> 0
	76	1	0.167	0 --> 1
	77	1	0.500	0 ==> 1
	78	1	0.333	0 --> 1
node_83 --> *Deltatheridium pretrituberculare*				
	7	1	0.222	0 ==> 1
	12	1	0.500	1 ==> 0
	20	1	0.400	0 ==> 1
	21	1	0.100	1 ==> 0
	24	1	0.500	0 ==> 2

	25	1	0.250	1 ==> 0
	35	1	0.600	0 ==> 2
	44	1	0.182	1 ==> 0
	49	1	0.091	0 --> 1
	55	1	0.625	1 --> 0
	57	1	0.286	2 ==> 0
	60	1	0.571	0 ==> 1
	67	1	0.250	0 ==> 1
	68	1	0.400	0 --> (01)
	69	1	0.167	0 --> 1
	72	1	1.000	0 --> (01)
node_83 --> node_82				
	15	1	0.333	1 --> 0
	27	1	0.333	1 --> 0
	37	1	0.800	0 ==> 1
	48	1	0.500	0 ==> 2
	59	1	0.111	0 --> 1
	63	1	0.769	1 ==> 0
	81	1	0.500	0 ==> 1
	84	1	0.364	1 ==> 0
	88	1	0.250	1 ==> 0
	93	1	0.333	0 --> 1
	97	1	0.143	0 ==> 1
	98	1	0.714	1 --> 0
node_82 --> *Kokopellia juddi*				
	9	1	0.200	1 --> 0
	20	1	0.400	0 ==> 2
	41	1	0.636	1 ==> 0
	45	1	0.400	2 --> (12)
	46	1	0.273	0 --> 1
node_82 --> node_81				
	22	1	0.200	1 --> 0
	26	1	0.143	1 --> 0
	31	1	0.333	0 --> 1
	35	1	0.600	0 ==> 1
	45	1	0.400	2 --> 0
	51	1	1.000	0 ==> 1
	52	1	0.273	0 ==> 1
	53	1	0.333	2 ==> 0
	54	1	0.364	1 --> 0
	62	1	0.143	1 --> 0
	72	1	1.000	0 ==> 1
	73	1	0.643	0 --> 1
	78	1	0.333	1 --> 0
	79	1	0.250	0 ==> 1
node_81 --> *Asiatherium reshetovi*				
	2	1	0.250	1 ==> 0
	7	1	0.222	0 ==> 1
	47	1	0.556	0 ==> 1
	55	1	0.625	1 --> 0
	65	1	0.400	0 ==> 1
	75	1	0.375	0 ==> 1
node_81 --> node_80				
	10	1	0.333	1 --> 0
	16	1	0.167	0 --> 1
	25	1	0.250	1 ==> 0
	27	1	0.333	0 --> 1

32	1	0.143	1 ==> 0
39	1	0.200	0 ==> 1
64	1	0.500	0 ==> 1
66	1	0.667	1 ==> 0
89	1	0.300	0 --> 1

node_80 --> *Aenigmadelphys archeri*

26	1	0.143	0 --> 1
43	1	0.556	0 ==> 1
60	1	0.571	0 ==> 1
63	1	0.769	0 --> (01)
76	1	0.167	1 --> 0
96	1	0.400	0 --> (01)

node_80 --> node_79

54	1	0.364	0 --> 1
58	1	0.286	0 --> 1
61	1	0.500	0 ==> 1
82	1	0.333	0 ==> 1
85	1	0.143	1 ==> 0
86	1	0.111	0 --> 1
89	1	0.300	1 --> 2

node_79 --> node_48

20	1	0.400	0 ==> 1
23	1	0.231	0 ==> 1
62	1	0.143	0 ==> 1
90	1	0.250	0 ==> 1

node_48 --> *Albertatherium* spp.

61	1	0.500	1 ==> 0
75	1	0.375	0 --> (01)
82	1	0.333	1 ==> 0
86	1	0.111	1 --> 0

node_48 --> *Turgidodon rhaister*

26	1	0.143	0 --> 1
45	1	0.400	0 --> (01)
47	1	0.556	0 --> (01)
58	1	0.286	1 --> 0
65	1	0.400	0 ==> 1
66	1	0.667	0 --> (01)

node_48 --> *Nortedelphys jasoni*

19	1	0.545	2 --> (12)
39	1	0.200	1 ==> 0
43	1	0.556	0 --> (01)
80	1	0.250	0 ==> 1
89	1	0.300	2 --> 1

node_79 --> node_78

8	1	0.400	1 ==> 0
37	1	0.800	1 ==> 2
38	1	0.143	0 ==> 1
45	1	0.400	0 ==> 1
67	1	0.250	0 --> 1
75	1	0.375	0 ==> 1
93	1	0.333	1 ==> 2

node_78 --> node_50

11	1	0.500	1 --> 0
48	1	0.500	2 ==> 1
52	1	0.273	1 --> 0
71	1	0.500	0 ==> 1

82	1	0.333	1 ==> 2
89	1	0.300	2 --> 1

node_50 --> *Didelphodon vorax*

3	1	0.250	0 ==> 1
29	1	0.667	0 --> (01)
31	1	0.333	1 ==> 0
32	1	0.143	0 ==> 1
44	1	0.182	1 ==> 0
45	1	0.400	1 ==> 2
46	1	0.273	0 ==> 1
58	1	0.286	1 --> 0
78	1	0.333	0 ==> 1

node_50 --> node_49

6	1	0.600	0 ==> 1
7	1	0.222	0 --> 2
21	1	0.100	1 ==> 0
23	1	0.231	0 ==> 2
47	1	0.556	0 --> 1
52	1	0.273	0 --> 2
60	1	0.571	0 ==> 1
65	1	0.400	0 ==> 1
66	1	0.667	0 --> 1
67	1	0.250	1 --> 0
96	1	0.400	0 --> 1

node_49 --> *Pediomys elegans*

25	1	0.250	0 ==> 1
35	1	0.600	1 ==> 2
36	1	0.200	0 ==> 1
41	1	0.636	1 ==> 0
45	1	0.400	1 --> (12)
47	1	0.556	1 --> (01)
85	1	0.143	0 ==> 1
86	1	0.111	1 --> 0
89	1	0.300	1 --> 2

node_49 --> *Glasbius intricatus*

5	1	0.333	1 ==> 0
19	1	0.545	2 ==> 1
34	1	0.444	1 ==> 0
39	1	0.200	1 ==> 0
49	1	0.091	0 ==> 1
63	1	0.769	0 --> (01)
66	1	0.667	1 --> (01)
70	1	0.500	0 ==> 1
84	2	0.364	0 ==> (12)
87	1	0.500	0 ==> 1
90	1	0.250	0 ==> 1

node_78 --> node_77

12	1	0.500	1 ==> 0
14	1	0.333	0 --> 1
15	1	0.333	0 ==> 1
16	1	0.167	1 --> 0
19	1	0.545	2 --> 1
24	1	0.500	0 ==> 1
26	1	0.143	0 --> 1
39	1	0.200	1 ==> 0
49	1	0.091	0 --> 1
59	1	0.111	1 --> 0

	70	1	0.500	0 ==> 1
	77	1	0.500	1 --> 0
	86	1	0.111	1 --> 0
	88	1	0.250	0 --> 1
node_77 --> node_74				
	2	1	0.250	1 --> 0
	14	1	0.333	1 --> 0
	19	1	0.545	1 --> 0
	20	1	0.400	0 ==> 1
	21	1	0.100	1 ==> 0
	23	1	0.231	0 --> 1
	34	1	0.444	1 ==> 0
	49	1	0.091	1 --> 0
	52	1	0.273	1 --> 2
	56	1	0.500	0 ==> 1
	59	1	0.111	0 --> 1
	93	1	0.333	2 ==> 1
	95	1	0.429	0 --> 1
	97	1	0.143	1 ==> 0
	98	1	0.714	0 --> 1
node_74 --> *Thylacodon* spp.				
	23	1	0.231	1 --> (01)
	24	1	0.500	1 --> (01)
	41	1	0.636	1 --> (01)
	76	1	0.167	1 ==> 0
	92	1	0.500	0 ==> 1
	98	1	0.714	1 --> (01)
node_74 --> node_73				
	7	1	0.222	0 --> 1
	22	1	0.200	0 ==> 1
	35	1	0.600	1 ==> 2
	53	1	0.333	0 ==> 1
	57	1	0.286	2 ==> 1
	82	1	0.333	1 --> 2
	84	1	0.364	0 ==> 1
node_73 --> node_64				
	24	1	0.500	1 ==> 2
	94	1	0.333	0 ==> 1
node_64 --> *Peradectes minor*				
	54	1	0.364	1 --> (01)
	82	1	0.333	2 --> 1
node_64 --> node_63				
	36	1	0.200	0 ==> 1
	40	1	0.500	0 ==> 1
	52	1	0.273	2 --> 1
	85	1	0.143	0 --> 1
node_63 --> *Peradectes coprexeches*				
	23	1	0.231	1 ==> 0
	43	1	0.556	0 ==> 1
	46	1	0.273	0 ==> 1
	48	1	0.500	2 --> (12)
	53	1	0.333	1 ==> 0
	54	1	0.364	1 --> (01)
	61	1	0.500	1 ==> 0
	63	1	0.769	0 --> (01)
	73	1	0.643	1 --> (01)
	76	1	0.167	1 ==> 0

	92	1	0.500	0 ==> 1
	97	1	0.143	0 ==> 1
node_63 --> node_62				
	21	1	0.100	0 --> 1
	41	1	0.636	1 ==> 0
	50	1	0.667	0 ==> 1
	59	1	0.111	1 --> 0
	68	1	0.400	0 ==> 1
	91	1	0.167	0 --> 1
node_62 --> *Golerdelphys stocki*				
	40	1	0.500	1 --> (01)
	44	1	0.182	1 ==> 0
node_62 --> node_61				
	47	1	0.556	0 ==> 1
	56	1	0.500	1 --> 0
	62	1	0.143	0 ==> 1
	82	1	0.333	2 --> 1
node_61 --> *Peradectes elegans*				
	8	1	0.400	0 --> (01)
	11	1	0.500	1 ==> 0
	41	1	0.636	0 --> (01)
	52	1	0.273	1 --> (01)
node_61 --> node_60				
	13	1	0.200	0 --> 1
	19	1	0.545	0 ==> 1
	23	1	0.231	1 ==> 0
	48	1	0.500	2 ==> 1
	61	1	0.500	1 ==> 0
	63	1	0.769	0 ==> 1
	85	1	0.143	1 --> 0
	95	1	0.429	1 ==> 0
node_60 --> *Peradectes protinnominatus*				
	21	1	0.100	1 --> 0
	41	1	0.636	0 --> (01)
	56	1	0.500	0 --> (01)
	66	1	0.667	0 ==> 1
	87	1	0.500	0 --> (01)
node_60 --> node_59				
	7	1	0.222	1 --> 0
	32	1	0.143	0 ==> 1
	34	1	0.444	0 --> 1
	49	1	0.091	0 --> 1
	52	1	0.273	1 --> 0
	59	1	0.111	0 --> 1
	94	1	0.333	1 ==> 2
node_59 --> node_53				
	10	1	0.333	0 --> 1
	56	1	0.500	0 --> 1
	57	1	0.286	1 ==> 0
	73	1	0.643	1 ==> 0
	84	1	0.364	1 ==> 0
	87	1	0.500	0 ==> 1
	97	1	0.143	0 ==> 1
node_53 --> *Peradectes crocheti*				
	21	1	0.100	1 --> 0
	23	1	0.231	0 ==> 1
	49	1	0.091	1 --> 0

	52	1	0.273	0 --> 1
	63	1	0.769	1 --> (01)
	66	1	0.667	0 --> (01)
	95	1	0.429	0 ==> 1
node_53 --> node_52				
	41	1	0.636	0 ==> 1
	44	1	0.182	1 ==> 0
	46	1	0.273	0 ==> 1
	89	1	0.300	2 ==> 1
	91	1	0.167	1 --> 0
node_52 --> *Peradectes russelli*				
	19	1	0.545	1 ==> 2
	56	1	0.500	1 --> (01)
	66	1	0.667	0 --> (01)
	73	1	0.643	0 --> (01)
node_52 --> node_51				
	20	1	0.400	1 ==> 2
	38	1	0.143	1 ==> 0
	40	1	0.500	1 --> 0
node_51 --> *Peradectes louisi*				
	21	1	0.100	1 --> 0
	40	1	0.500	0 --> (01)
	44	1	0.182	0 --> (01)
	66	1	0.667	0 --> (01)
node_51 --> *Peradectes dufraingi*				
	47	1	0.556	1 ==> 0
	53	1	0.333	1 ==> 2
node_59 --> node_58				
	2	1	0.250	0 --> 1
	3	1	0.250	0 ==> 1
	53	1	0.333	1 ==> 2
	79	1	0.250	1 ==> 0
node_58 --> *Mimoperadectes* spp.				
	16	1	0.167	0 ==> 1
	35	1	0.600	2 --> (12)
	38	1	0.143	1 ==> 0
	43	1	0.556	0 --> (01)
	44	1	0.182	1 ==> 0
	46	1	0.273	0 --> (01)
	50	1	0.667	1 ==> 0
	61	1	0.500	0 --> (01)
	62	1	0.143	1 ==> 0
	63	1	0.769	1 --> (01)
	73	1	0.643	1 --> (01)
	91	1	0.167	1 --> 0
node_58 --> node_57				
	7	1	0.222	0 --> 2
	34	1	0.444	1 --> 0
	69	1	0.167	0 ==> 1
node_57 --> node_54				
	23	1	0.231	0 ==> 1
	25	1	0.250	0 ==> 1
node_54 --> *Armintodelphys blacki*				
	34	1	0.444	0 --> 1
node_54 --> *Armintodelphys dawsoni*				
	40	1	0.500	1 ==> 0
	44	1	0.182	1 ==> 0

	48	1	0.500	1 ==> 2
node_57 --> node_56				
	20	1	0.400	1 --> 2
	32	1	0.143	1 ==> 0
	45	1	0.400	1 ==> 0
	55	1	0.625	1 ==> 0
	57	1	0.286	1 --> 0
	66	1	0.667	0 ==> 1
	84	1	0.364	1 ==> 0
	89	1	0.300	2 ==> 1
node_56 --> *Peradectes chesteri*				
	20	1	0.400	2 --> (12)
	21	1	0.100	1 ==> 0
	34	1	0.444	0 --> (01)
	49	1	0.091	1 ==> 0
	59	1	0.111	1 ==> 0
	73	1	0.643	1 --> (01)
node_56 --> node_55				
	62	1	0.143	1 ==> 0
	79	1	0.250	0 ==> 1
	85	1	0.143	0 ==> 1
	97	1	0.143	0 ==> 1
node_55 --> *Peradectes californicus*				
	6	1	0.600	0 --> (01)
	47	1	0.556	1 --> (01)
	69	1	0.167	1 ==> 0
	73	1	0.643	1 --> (01)
	98	1	0.714	1 --> (01)
node_73 --> node_72				
	1	1	0.333	0 --> 1
	6	1	0.600	0 --> 1
	10	1	0.333	0 --> 1
	16	1	0.167	0 --> 1
	19	1	0.545	0 --> 1
	25	1	0.250	0 ==> 1
	38	1	0.143	1 ==> 0
	63	1	0.769	0 ==> 1
	80	1	0.250	0 ==> 1
	95	1	0.429	1 --> 0
	96	1	0.400	0 ==> 1
node_72 --> *Swaindelphys encinensis*				
	26	1	0.143	1 ==> 0
	34	1	0.444	0 ==> 1
	44	1	0.182	1 ==> 0
	46	1	0.273	0 ==> 1
	52	1	0.273	2 --> 1
	91	1	0.167	0 ==> 1
	93	1	0.333	1 --> (12)
node_72 --> node_71				
	28	1	0.500	0 ==> 1
	42	1	0.500	0 ==> 1
	45	1	0.400	1 --> 0
	54	1	0.364	1 ==> 0
	73	1	0.643	1 --> 0
	87	1	0.500	0 ==> 1
node_71 --> *Peratherium constans*				
	61	1	0.500	1 --> (01)

66	1	0.667	0 --> (01)
73	1	0.643	0 --> (01)
82	1	0.333	2 --> (12)
94	1	0.333	0 ==> 1

node_71 --> node_70

7	1	0.222	1 --> 0
8	1	0.400	0 ==> 1
9	1	0.200	1 ==> 0
23	1	0.231	1 --> 2
43	1	0.556	0 --> 1
49	1	0.091	0 --> 1
53	1	0.333	1 ==> 0
57	1	0.286	1 ==> 2
60	1	0.571	0 ==> 1
84	1	0.364	1 ==> 2
88	1	0.250	1 ==> 0
93	1	0.333	1 --> 2
97	1	0.143	0 ==> 1

node_70 --> *Herpetotherium edwardi*

38	1	0.143	0 ==> 1
41	1	0.636	1 ==> 0
43	1	0.556	1 --> 0
45	1	0.400	0 --> 1
49	1	0.091	1 --> 0
54	1	0.364	0 ==> 1

node_70 --> *Herpetotherium fugax*

6	1	0.600	1 --> (01)
13	1	0.200	0 ==> 1
25	1	0.250	1 --> (01)
41	1	0.636	1 --> (01)
59	1	0.111	1 ==> 0

node_70 --> node_69

3	1	0.250	0 --> 1
17	1	0.250	1 --> 0
23	1	0.231	2 --> 1
24	1	0.500	1 --> 2
25	1	0.250	1 ==> 0
28	1	0.500	1 ==> 0
93	1	0.333	2 --> 1
96	1	0.400	1 ==> 0

node_69 --> *Derorhynchus singularis*

55	1	0.625	1 --> (01)
73	1	0.643	0 --> (01)
75	1	0.375	1 ==> 0
84	1	0.364	2 ==> 1
86	1	0.111	0 ==> 1
87	1	0.500	1 --> (01)
90	1	0.250	0 ==> 1
95	1	0.429	0 ==> 1

node_69 --> node_68

21	1	0.100	0 --> 1
44	1	0.182	1 ==> 0
45	1	0.400	0 --> 1
48	1	0.500	2 ==> 0
56	1	0.500	1 ==> 0
68	1	0.400	0 --> 1
69	1	0.167	0 --> 1

node_68 --> node_65

7	1	0.222	0 ==> 2
12	1	0.500	0 ==> 1
15	1	0.333	1 ==> 0
24	1	0.500	2 --> 1
62	1	0.143	0 ==> 1
79	1	0.250	1 ==> 0
83	1	0.500	0 ==> 1
97	1	0.143	1 ==> 0

node_65 --> *Dromiciops gliroides*

13	1	0.200	0 ==> 1
17	1	0.250	0 --> 1
21	1	0.100	1 --> 0
36	1	0.200	0 ==> 1
38	1	0.143	0 ==> 1
42	1	0.500	1 ==> 0
46	1	0.273	0 ==> 1
73	1	0.643	0 ==> 1
80	1	0.250	1 ==> 0
82	1	0.333	2 ==> 1
94	1	0.333	0 ==> 1

node_65 --> *Perameles nasuta*

19	1	0.545	1 --> (12)
20	1	0.400	1 --> (01)
22	1	0.200	1 ==> 0
26	1	0.143	1 ==> 0
29	1	0.667	0 ==> 1
33	1	0.250	0 ==> 1
34	1	0.444	0 --> (01)
37	2	0.800	2 ==> (01)
45	1	0.400	1 --> 0
55	1	0.625	1 --> (01)
68	1	0.400	1 --> 0
86	1	0.111	0 ==> 1
93	1	0.333	1 ==> 2
95	1	0.429	0 --> (01)

node_68 --> node_67

5	1	0.333	1 ==> 0
23	1	0.231	1 --> 2
32	1	0.143	0 ==> 1
52	1	0.273	2 ==> 1
54	1	0.364	0 ==> 1
94	1	0.333	0 ==> 2

node_67 --> *Marmosa murina*

3	1	0.250	1 --> 0
36	1	0.200	0 ==> 1
53	1	0.333	0 --> (01)
60	1	0.571	1 --> (01)
75	1	0.375	1 ==> 0
95	1	0.429	0 --> (01)

node_67 --> node_66

4	1	0.500	0 ==> 1
20	1	0.400	1 ==> 2
29	1	0.667	0 ==> 1
38	1	0.143	0 ==> 1
74	1	0.500	0 ==> 1
84	1	0.364	2 ==> 1

91	1	0.167	0 ==> 1

node_66 --> *Didelphis marsupialis*

1	1	0.333	1 ==> 0
9	1	0.200	0 ==> 1
12	1	0.500	0 --> (01)
17	1	0.250	0 --> 1
19	1	0.545	1 --> (01)
39	1	0.200	0 ==> 1
43	1	0.556	1 --> (01)
44	1	0.182	0 ==> 1
46	1	0.273	0 ==> 1
53	1	0.333	0 ==> 1
63	1	0.769	1 --> (01)
86	1	0.111	0 ==> 1

node_77 --> node_76

45	1	0.400	1 ==> 0
53	1	0.333	0 ==> 2
57	1	0.286	2 --> 0
63	1	0.769	0 ==> 1
66	1	0.667	0 ==> 1
75	1	0.375	1 ==> 0
77	1	0.500	0 --> 1
84	1	0.364	0 ==> 1

node_76 --> node_75

8	1	0.400	0 ==> 1
9	1	0.200	1 ==> 0
13	1	0.200	0 ==> 1
16	1	0.167	0 --> 1
25	1	0.250	0 ==> 1
54	1	0.364	1 --> 0
57	1	0.286	0 --> 1
80	1	0.250	0 ==> 1
91	1	0.167	0 ==> 1

node_75 --> *Pucadelphys andinus*

6	1	0.600	0 ==> 1
11	1	0.500	1 --> (01)
41	1	0.636	1 --> (01)
43	1	0.556	0 --> (01)
45	1	0.400	0 --> (01)
46	1	0.273	0 --> (01)
49	1	0.091	1 --> 0
55	1	0.625	1 --> (01)
58	1	0.286	1 --> (01)
59	1	0.111	0 --> 1
60	1	0.571	0 --> (01)
63	1	0.769	1 --> (01)
76	1	0.167	1 ==> 0
86	1	0.111	0 --> 1

node_75 --> *Incadelphys antiquus*

4	1	0.500	0 ==> 1
14	1	0.333	1 --> 0
23	1	0.231	0 ==> 2
33	1	0.250	0 ==> 1
34	1	0.444	1 --> (01)
40	1	0.500	0 ==> 1
41	1	0.636	1 --> (01)
54	1	0.364	0 --> (01)

55	1	0.625	1 --> (01)
75	1	0.375	0 --> (01)
77	1	0.500	1 --> (01)
89	1	0.300	2 --> 1
93	1	0.333	2 ==> 1
98	1	0.714	0 --> (01)

node_76 --> *Mayulestes ferox*

20	1	0.400	0 ==> 1
22	1	0.200	0 ==> 1
24	1	0.500	1 ==> 2
32	1	0.143	0 ==> 1
36	1	0.200	0 ==> 1
40	1	0.500	0 --> (01)
43	1	0.556	0 ==> 1
47	1	0.556	0 --> (01)
52	1	0.273	1 ==> 0
56	1	0.500	0 ==> 1
58	1	0.286	1 --> 0
60	1	0.571	0 --> (01)
73	1	0.643	1 ==> 0
81	1	0.500	1 ==> 0
82	1	0.333	1 ==> 2
83	1	0.500	0 ==> 1
84	1	0.364	1 --> (12)
85	1	0.143	0 ==> 1
89	1	0.300	2 ==> 0
96	1	0.400	0 ==> 1

node_77 --> *Roberthoffstetteria nationalgeographica*

11	1	0.500	1 ==> 0
19	1	0.545	1 --> (12)
23	1	0.231	0 ==> 2
26	1	0.143	1 --> 0
27	1	0.333	1 ==> 0
33	1	0.250	0 ==> 1
40	1	0.500	0 ==> 1
44	1	0.182	1 ==> 0
46	1	0.273	0 ==> 1
48	1	0.500	2 ==> 0
54	1	0.364	1 ==> 0
58	1	0.286	1 --> 0
67	1	0.250	1 --> 0
69	1	0.167	0 ==> 1
76	1	0.167	1 ==> 0
86	1	0.111	0 --> 1
87	1	0.500	0 ==> 1
88	1	0.250	1 --> 0
89	1	0.300	2 --> (12)
90	1	0.250	0 ==> 1

Summary of CI and RI values of all characters (Ch.) in the initial maximum parsimony analysis:

Ch.	CI	RI
1	0,33	0,67
2	0,25	0,57
3	0,25	0,57
4	0,5	0,5
5	0,33	0,6
6	0,6	0,75
7	0,22	0,22
8	0,4	0,7
9	0,2	0,6
10	0,33	0,67
11	0,5	0
12	0,5	0,6
13	0,2	0,33
14	0,33	0
15	0,33	0,5
16	0,17	0,38
17	0,25	0,25
18	1	1
19	0,55	0,55
20	0,4	0,57
21	1	0,4
22	0,2	0,71
23	0,23	0,52
24	0,5	0,79
25	0,25	0,46
26	0,14	0,25
27	0,33	0
28	0,5	0,5
29	0,67	0,5
30	1	1
31	0,33	0
32	0,14	0,57
33	0,25	0
34	0,44	0,69
35	0,6	0,85
36	0,2	0,71
37	0,8	0,88
38	0,14	0,63
39	0,2	0,2
40	0,5	0,6
41	0,64	0,56
42	0,5	0,86
43	0,56	0,5
44	0,18	0,25
45	0,4	0,31
46	0,27	0,2
47	0,56	0,67
48	0,5	0,79
49	0,09	0,44
50	0,67	0,9
51	1	1
52	0,27	0,64
53	0,33	0,67
54	0,36	0,22
55	0,63	0,25
56	0,5	0,67
57	0,29	0,72
58	0,29	0,17
59	0,11	0
60	0,57	0,7
61	0,5	0,8
62	0,14	0,54
63	0,77	0,73
64	0,5	0,67
65	0,4	0,25
66	0,67	0,55
67	0,25	0,7
68	0,4	0,8
69	0,17	0,17
70	0,5	0,9
71	0,5	0,67
72	1	1
73	0,64	0,5
74	0,5	0,5
75	0,38	0,44
76	0,17	0,17
77	0,5	0,8
78	0,33	0
79	0,25	0,63
80	0,25	0,73
81	0,5	0,67
82	0,33	0,68
83	0,5	0,5
84	0,36	0,61
85	0,14	0,4
86	0,11	0
87	0,5	0,73
88	0,25	0,82
89	0,3	0,5
90	0,25	0,4
91	0,17	0,29
92	0,5	0
93	0,33	0,33
94	0,33	0,75
95	0,43	0,2
96	0,4	0,4
97	0,14	0,54
98	0,71	0,83

Supplemental material 5. Consensus trees yielded by the subsequent phylogenetic analyses (analyses sets 1 to 7). Heuristic searches with 1000 repetitions for the maximum parsimony analyses; bremer index values (for strict consensus) and frequencies > 50% (majority-rule consensus) are indicated at nodes. The results of the additional analyses are described in the main text.

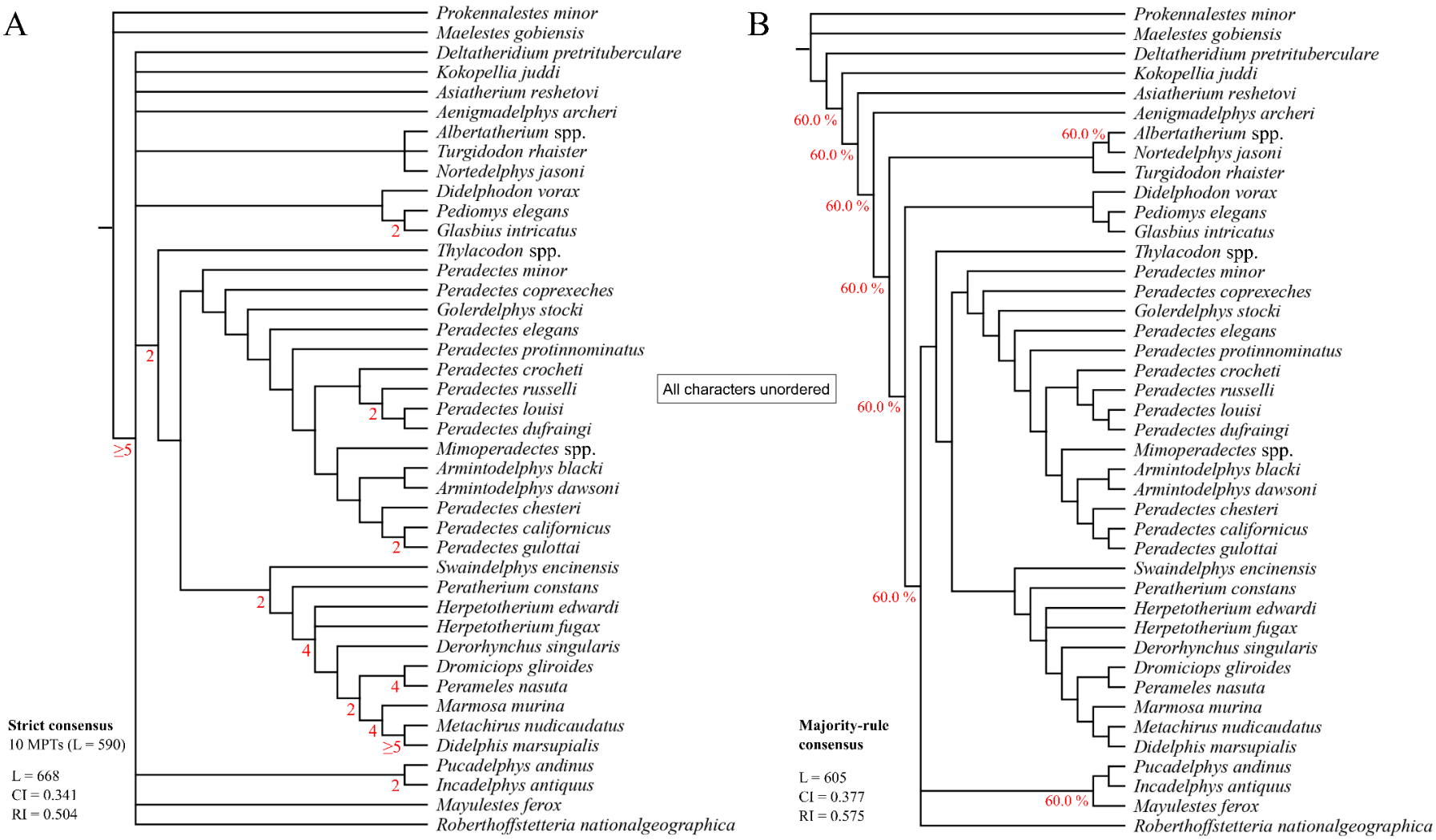

Figure S1. Analysis set 1: all characters are unordered (instead of characters 23, 24, 37, and 82 ordered). **A.** Strict consensus. **B.** 50 % majority-rule consensus.

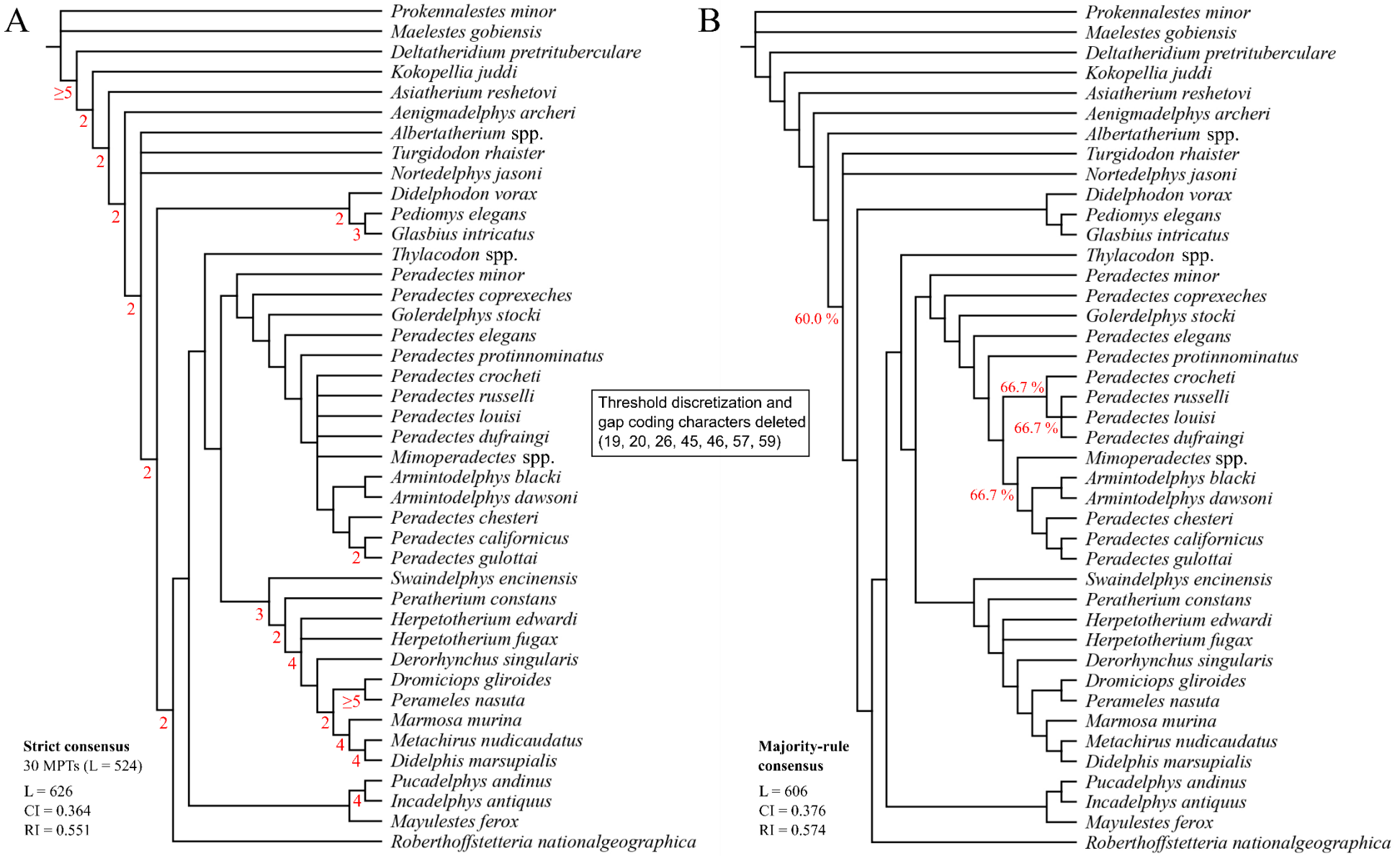

Figure S2. Analysis set 2: characters (introduced in this study or in Gernelle et al. 2024a) employing threshold discretization and gap coding (19, 20, 26, 45, 46, 57, 59) are deleted. **A.** Strict consensus. **B.** 50 % majority-rule consensus.

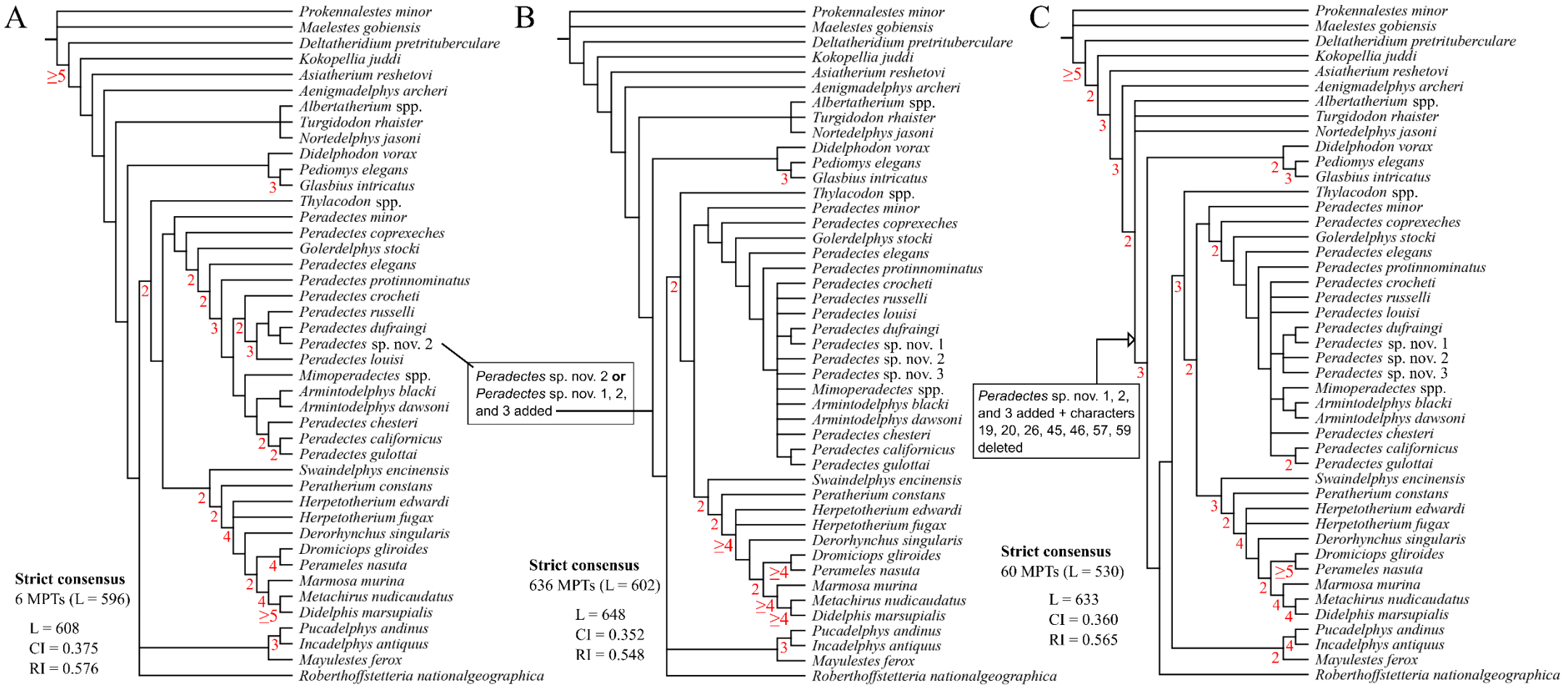

Figure S3. Analysis set 3: new European *Peradectes* species added. **A.** Strict consensus, with only *Peradectes* sp. nov. 2 added. **B.** Strict consensus, with *Peradectes* sp. nov. 1, 2, and 3 added. **C.** Strict consensus, with *Peradectes* sp. nov. 1, 2, and 3 added + characters employing threshold discretization and gap coding (19, 20, 26, 45, 46, 57, 59) deleted.

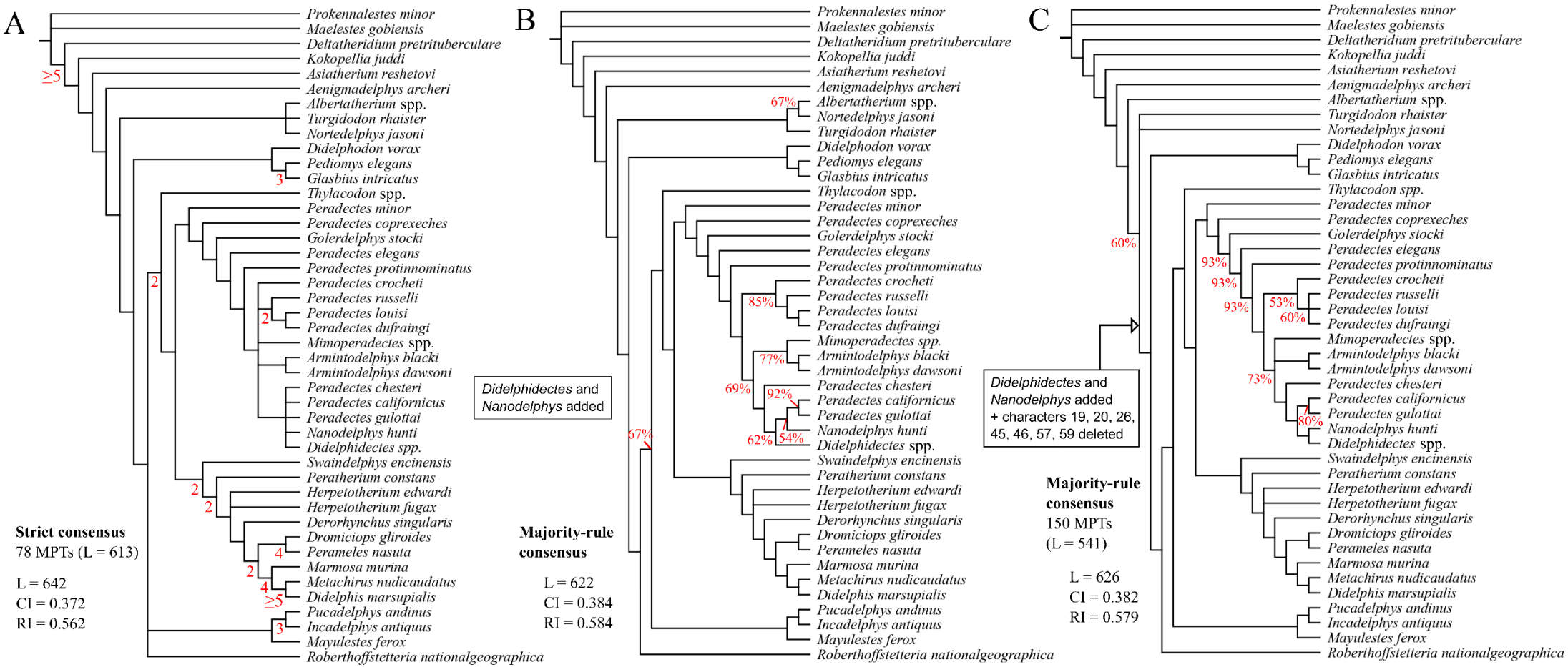

Figure S4. Analysis set 4: *Didelphidectes* and *Nanodelphys* added. **A-B.** Only *Didelphidectes* and *Nanodelphys* are added, see strict consensus (A), and 50 % majority-rule consensus (B). **C.** Majority-rule consensus, with *Didelphidectes* and *Nanodelphys* added + characters employing threshold discretization and gap coding (19, 20, 26, 45, 46, 57, 59) deleted.

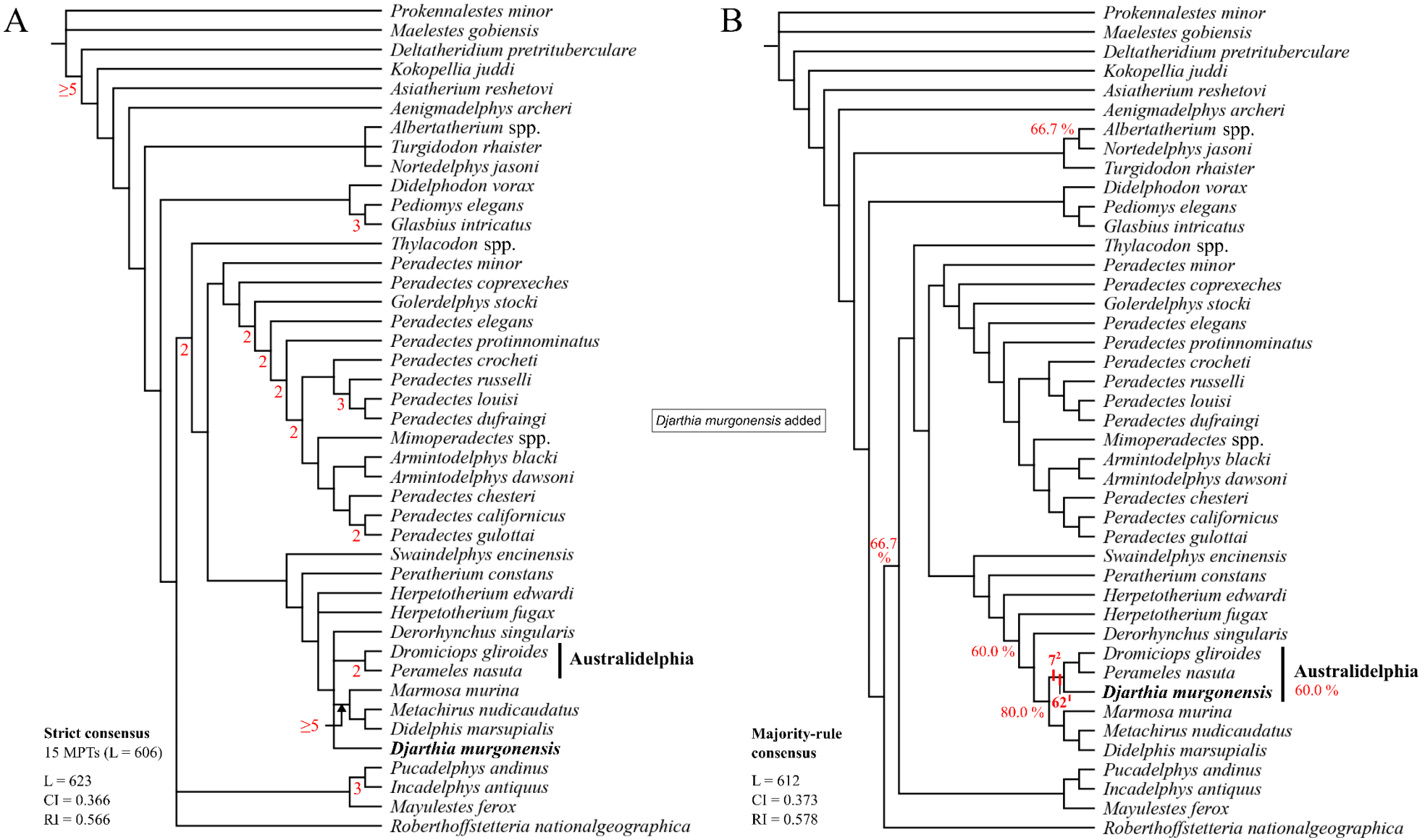

Figure S5. Analysis set 5: *Djarthia murgonensis* added. **A.** Strict consensus. **B.** 50 % majority-rule consensus. Non-ambiguous synapomorphies supporting the clade Australidelphia in the majority-rule consensus are mapped at node.

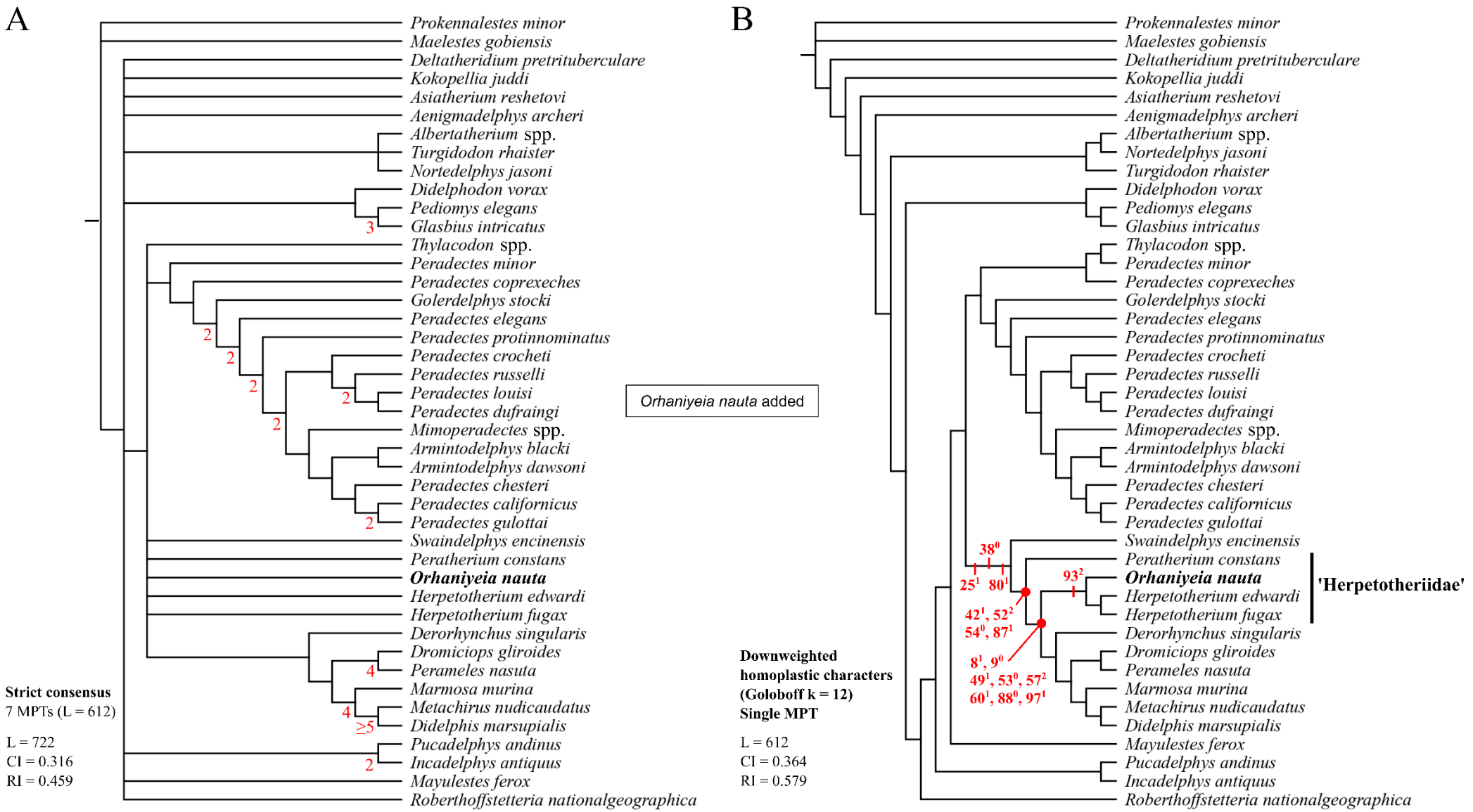

Figure S6. Analysis set 6: *Orhaniyeia nauta* added. **A.** Strict consensus. **B.** Single most parsimonious tree obtained with downweighted homoplasic characters (with Goloboff k = 12). Non-ambiguous synapomorphies supporting the inclusion of *Orhaniyeia* with herpetotheriids are mapped at nodes.

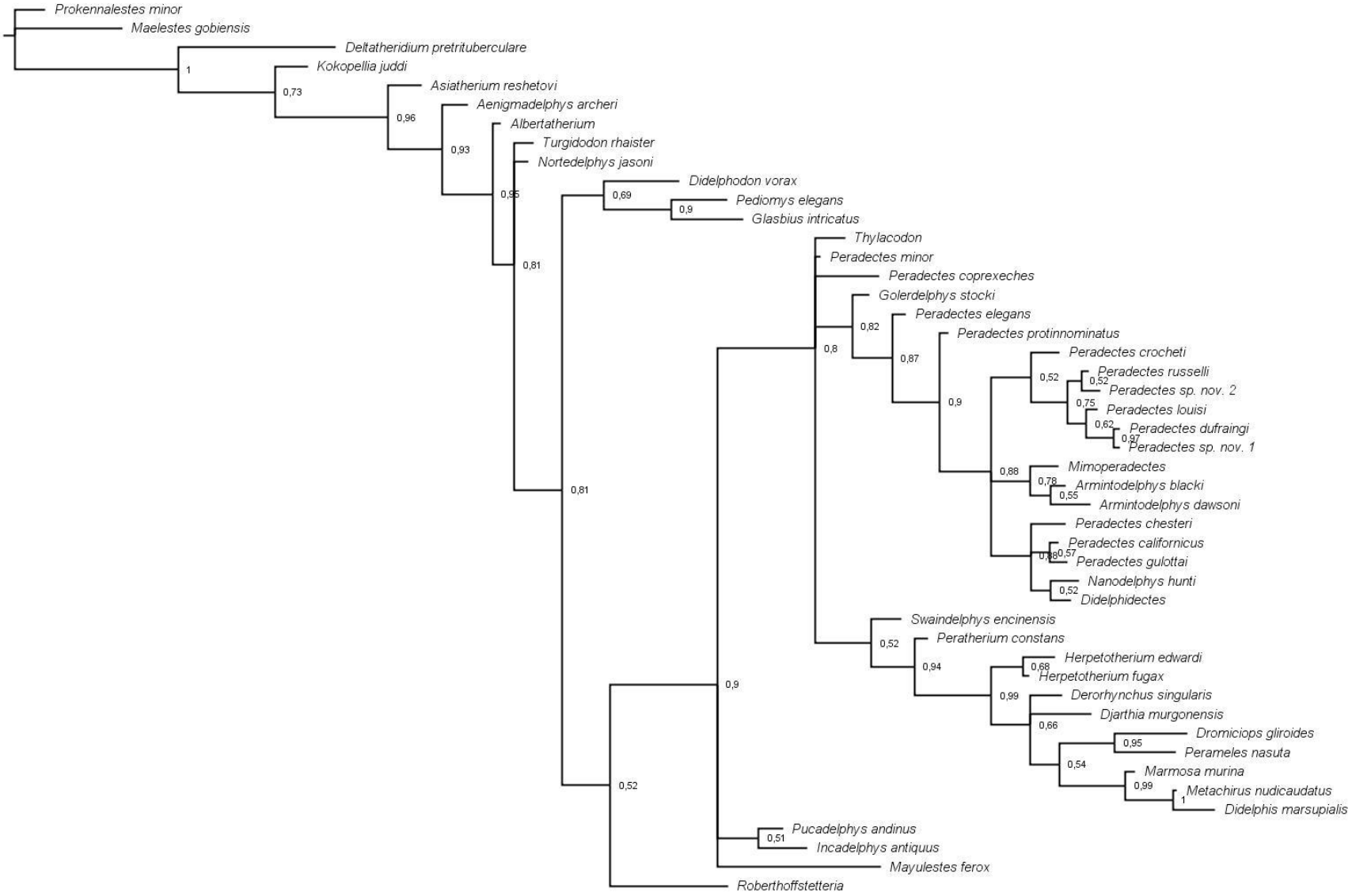

Figure S7. Analysis set 7: 50 % majority-rule consensus tree of post-burn-in trees (7.50×10^6 generations), based on Bayesian analysis with *Peradectes* sp. nov. 1 and 2, *Didelphidectes*, *Nanodelphys* and *Djarthia* added, and characters 19, 20, 26, 45, 46, 57, and 59 deleted. Branch lengths are proportional to the estimated number of character state changes. All characters are included. Bayesian posterior probabilities (BPP) are represented at nodes.

Supplemental material 6. Volume rendering pictures of dental rows of the herpetotheriid SMNK-PAL 983 (‘*Amphiperatherium*’ aff. *maximum* in Kurz 2007 : fig. 25) from Messel (Germany, ~MP11). The m4/M4 are the largest molars. Pictures courtesy of T. Lehmann (Senckenberg Research Institute).

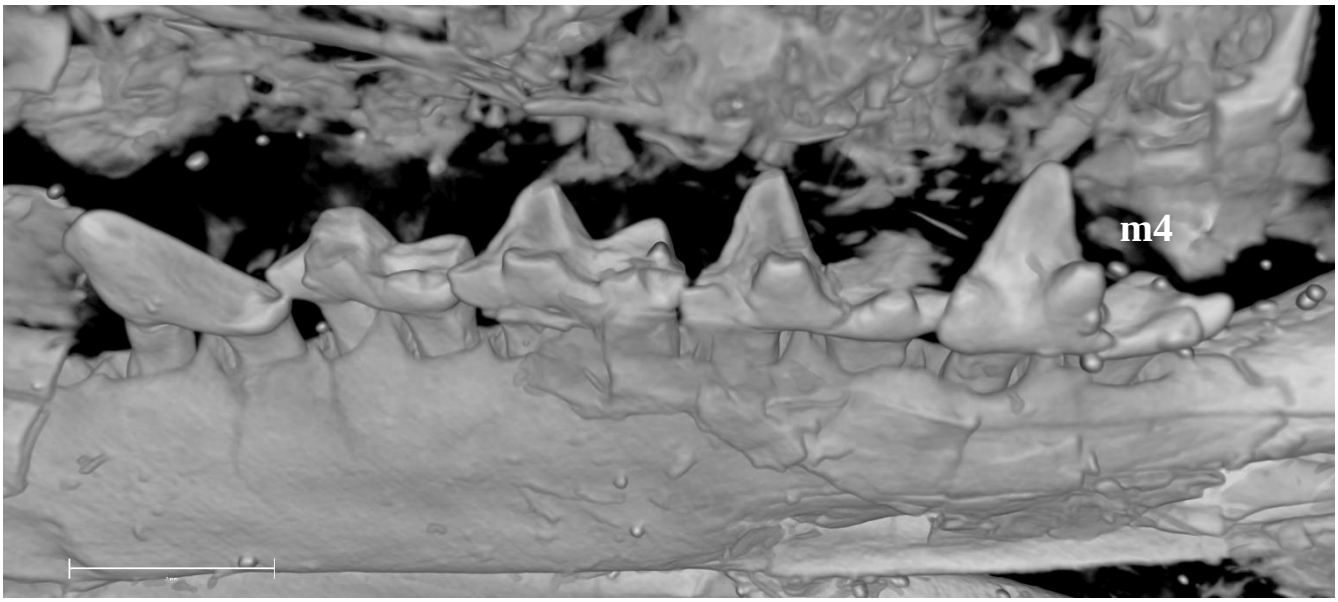

Figure S1. Right p3-m4 of SMNK-PAL 983 in occlusal/lingual view. Scale bar equals 2 mm.

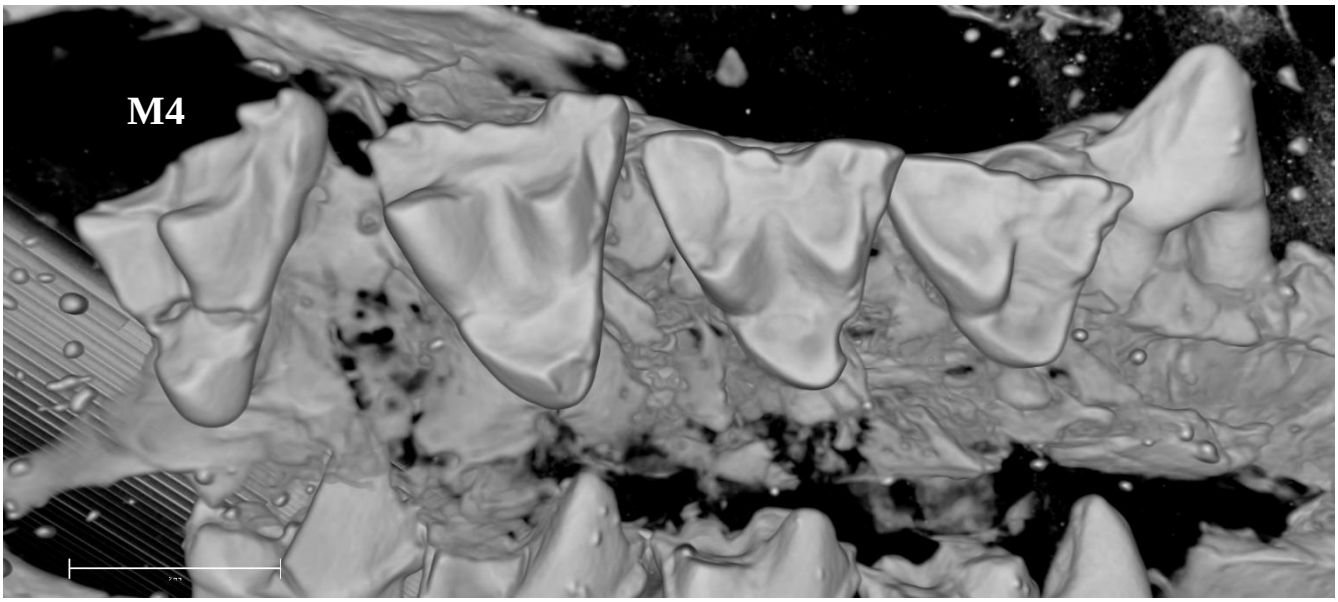

Figure S2. Right P3-M4 of SMNK-PAL 983 in occlusal view. Scale bar equals 2 mm.

Reference for Supplemental material 6.

Kurz C (2007) The opossum-like marsupials (Didelphimorphia and Peradectia, Marsupialia, Mammalia) from the Eocene of Messel and Geiseltal – Ecomorphology, diversity and palaeogeography. Kaupia 15: 3–65.

Partie 2. Nouvelles données sur les premiers Herpetotheriidae européens

La section précédente (Chapitre 3) a permis d'apporter de premiers éléments de réponse formels sur l'origine profonde des « Herpetotheriidae », tout en clarifiant celle des Peradectidae. La présente partie est entièrement consacrée à l'étude des herpétothériidés européens, les Peratheriinae. Ceux-ci persistent en Europe jusqu'au Miocène. Le plus ancien herpétothériidé d'Europe (fin du Paléocène) y est décrit en préambule (Chapitre 4). Il est ensuite proposé d'aborder la révision systématique des pérathériinés yprésiens (Chapitres 5 et 6) en débutant par le cas particulier des premiers pérathériinés de taille relativement grande, à partir duquel sont menées des réflexions sur la façon d'étudier l'évolution des caractères dentaires chez ce groupe à l'histoire évolutive longue mais dont les représentants sont pourtant peu disparate morphologiquement (Chapitre 5). La révision systématique complète des pérathériinés yprésiens est abordée en dernier lieu (Chapitre 6).

Chapitre 4. Le premier métathérien du Paléocène d'Europe et plus ancien herpétothériidé avéré

Cette section correspond au manuscrit suivant: **Gernelle K, Tabuce R. The first metatherian mammal from the Paleocene of Europe and oldest unequivocal herpetotheriid.**

Remarque. Il est fait référence dans ce projet d'article au Chapitre 3, ayant traité des positions phylogénétiques des péradectidés et herpétothériidés, ainsi qu'à un article soumis relatif à Albas, la localité d'intérêt dans cette partie.

Résumé. Éclaircir l'origine des Herpetotheriidae est crucial pour répondre à des questions clés concernant l'histoire évolutive des marsupialiformes du Cénozoique. Des recherches antérieures ont montré que les herpétothériidés avérés apparaissent dans les registres fossiles de l'Éocène inférieur précoce à la fois en Amérique du Nord et en Europe, et que les métathériens étaient apparemment absent durant le Paléocène en Europe. Ici, nous décrivons trois molaires isolées d'un nouveau genre d'herpétothériidé d'Albas (Corbières, Sud de la France), une localité du Paléocène terminal datée juste antérieurement au début du Maximum Thermique du Paléocène-Éocène (PETM). Cela signifie que l'évènement de dispersion généralement admis de l'Amérique du Nord à l'Europe impliquant les herpétothériidés s'est déroulé avant le PETM. Ces spécimens se comparent le mieux aux espèces d'herpétothériidés de l'Éocène inférieur précoce. Cependant, l'holotype diffère de ces derniers et de la plupart des herpétothériidés en présentant une cuspide stylaire B notoirement plus antérieure relativement au sommet du paracône, un caractère que nous interprétons comme une symplésiomorphie au sein des marsupialiformes du Cénozoïque. Cela suggère que les premiers herpétothériidés européens de l'Éocène inférieur précoce sont plus proches des espèces contemporaines d'Amérique du Nord qu'ils ne le sont des spécimens d'Albas. Finalement, nous introduisons de nouvelles méthodes de mesure prenant en compte la nature fragmentaire fréquente des molaires supérieures isolées des métathériens. Cela nous permet de monter que le nouvel herpétothériidé paléocène est le plus petit représentant européen connu de cette famille et documente un possible cas de nanisme mammalien pré-PETM.

Mots-clés. denture, dispersion intercontinentale, Marsupialiformes, paléobiogéographie, PETM, systématique

The first metatherian mammal from the Paleocene of Europe and oldest unequivocal herpetotheriid

Killian Gernelle[1], Rodolphe Tabuce[1]

[1] Institut des Sciences de l'Évolution de Montpellier (ISEM, UMR 5554), Univ Montpellier, CNRS, IRD, cc64, Place Eugène Bataillon, F-34095 Montpellier Cedex 05, France

Abstract. Unravelling the origin of the "opossum-like" Herpetotheriidae through new fossils is critical to address key questions regarding the evolutionary history of Cenozoic marsupialiforms. Past research has shown that undisputed herpetotheriids first appeared in the earliest Eocene fossil records of both North America and Europe, and that metatherians were seemingly absent in the Paleocene of Europe. Here, we describe three isolated molars of a new herpetotheriid genus from Albas (Corbières, Southern France), a latest Paleocene locality dated just anterior to the onset of the Paleocene-Eocene Thermal Maximum (PETM). It means that the generally assumed dispersal event from North America to Europe involving the herpetotheriid lineage most likely occurred prior to the PETM. These specimens compare best with the earliest Eocene herpetotheriid species. However, the holotype differs from the latter ones and most herpetotheriids in displaying a stylar cusp B markedly more anterior relative to the paracone apex, a character we interpret as a symplesiomorphy within Cenozoic marsupialiforms and which suggests that the earliest Eocene European herpetotheriids are more closely related to contemporaneous species from North America than to the Albas specimens. Finally, we introduce new measurement methods taking into account the frequent fragmentary nature of metatherian isolated upper molars. This allows us to show that the new Paleocene herpetotheriid is the smallest European representative of this family known so far, and documents a possible case of mammalian dwarfism prior to the PETM.

Keywords. dentition, intercontinental dispersal, Marsupialiformes, paleobiogeography, PETM, systematics

Introduction

‘Herpetotheriidae’ encompasses small extinct metatherians with a superficially ‘opossum-like’ generalist dentition and likely terrestrial habits (Kurz 2005; Rose 2012). This family is often regarded as a paraphyletic assemblage of stem marsupial taxa since works focused on their cranial anatomy (e.g., Sánchez-Villagra et al. 2007; Horovitz et al. 2008; Selva and Ladevèze 2017; Ladevèze et al. 2020). Although dentally conservative and pending for a comprehensive revision, herpetotheriids experienced a modest diversification in the northern hemisphere during the early Eocene (Crochet 1980; Krishtalka and Stucky 1983b; Korth 2008). Even if it is discussed based solely on dental material, uncovering the origin of unequivocal herpetotheriids represents a milestone in addressing key questions regarding the evolutionary history of Metatheria, notably for palaeobiogeographic and macroevolutionary purposes (e.g., Beck 2023). *Peratherium constans* Teilhard de Chardin, 1927, the only metatherian recognized from the MP7 reference level (earliest Eocene) of Dormaal (Belgium), was reassessed as the first undisputed European herpetotheriid and the oldest Cenozoic metatherian from Northern Europe (Ladevèze et al. 2012) and most likely Southern Europe (Estravis 2000). In fact, metatherians as a whole, present in the Cretaceous fossil record of Europe (Martin et al. 2005; Vullo et al. 2009, 2020), remain unknown in the Paleocene of this continent (Gheerbrant 1991), leaving a profound gap in their early Paleogene evolutionary history.

As for herpetotheriids, the putative oldest representatives proposed are Late Maastrichtian to Paleocene North American taxa, namely *Golerdelphys* (Williamson and Lofgren 2014; Wilson et al. 2016), *Nortedelphys* (Case et al. 2005) and *Swaindelphys* (Johanson 1996; Korth 2008; Williamson and Taylor 2011). Their stem herpetotheriid status has not been confirmed by most phylogenetic analyses (Williamson et al. 2012, 2014; Carneiro and Oliveira 2017; Carneiro et al. 2018). In a recent set of analyses, *Swaindelphys* has been established as a stem-herpetotheriid, contrary to the peradectid *Golderdelphys* and the alphadontid *Nortedelphys* (Chapter 3). Furthermore, the dentary of a putative *Peratherium* from the middle Paleocene listed by Rose (1981: 156) has been transferred in open nomenclature (gen. et sp. indet.) because the material has not been available for study (Secord 2008: 28). Consequently, as it is for Europe, the oldest undisputed herpetotheriids from North America, *Peratherium innominatum* Simpson, 1928 (= *Copedelphys innominata*, see Rothecker and Storer [1996]), and *Peratherium macgrewi* Bown, 1979, are respectively documented from the Wasatchian-M (earliest Eocene) of the Bighorn Basin, in Wyoming (Gingerich and Smith 2006) and the possible Wasatchian-M of the Red Hot local fauna, in Mississippi (Beard and Dawson 2009). At least the Wasatchian-M of the Bighorn Basin is equivalent in age or slightly older than the Dormaal fauna (Smith et al. 2006 ; see also Beard and Dawson 2001: 86-87, for the Red Hot local fauna). It means that, in both continents, the first unequivocal occurrences of ‘Herpetotheriidae’ were so far restricted to deposits coeval with the onset of

the Paleocene-Eocene Thermal Maximum (PETM), which is thought to have triggered the dispersal of many mammal lineages, including herpetotheriids (e.g., Hooker 2015) during the earliest Eocene.

Here we describe one isolated lower molar and two upper molar specimens of the single European Cenozoic metatherian known before the PETM, assigned to a new herpetotheriid genus and species with affinities to early *Peratherium* species. These specimens have been yielded by the unpublished Albas locality, lying at the base of a late Paleocene – early Eocene section in the Corbières (Southern France), which includes mammal-bearing deposits (Marandat et al. 2012). The Albas fauna is part of the upper 'Sparnacien des Corbières' which was suspected to be late Thanetian in age according to one of the two hypotheses of Yans et al. (2014: fig. 2). A recent work (Tabuce et al. submitted) establishes the Albas locality as latest Paleocene in age, bracketed just between the onset of the PETM (earliest Eocene) and a pre-PETM and probably also global hyperthermal event termed the "Pre-Onset Excursion" (POE) of the PETM (Xue et al. 2023). The latest Paleocene age of Albas is also supported by the absence of Primates, Artiodactyla, and Perissodactyla (the so-called 'modern placental orders'), which appeared during the PETM in Europe (e.g., Smith et al. 2006, 2014). The significance of the new latest Paleocene genus in the understanding of the origin and paleobiogeography of herpetotheriids is discussed with respect to current knowledge of this group.

Institutional and locality abbreviations

IRSNB-M, mammal collection of the Royal Belgium Institute of Natural Sciences; MNHN.F., Muséum National d'Histoire Naturelle, Paris, fossil collections; MNHN.F.AV, Avenay; MNHN.F.CB, Condé-en-Brie; MNHN.F.RI, Rians; NMB Om., Dormaal, collection of the Natural History Museum of Basel; UCMP, University of California Museum of Paleontology, Berkeley; UM, University of Michigan Museum of Paleontology; UM-, Université de Montpellier, France; UM-ALB, Albas; UM-FDN, Fordones; UM-PAT, Palette.

Material and methods

The mammal assemblage from Albas including the new herpetotheriid material was collected via bulk-sampling (~500 kilograms), careful acid etching, and screen-washing techniques. The metatherian specimens described are housed in the Palaeontological collections of the Université de Montpellier. They are illustrated by pictures of 3D surface models acquired via X-ray µCT scans, using the scanning station EasyTom 150 / Rx Solutions (Montpellier RIO Imaging, ISEM, Montpellier, France) and the Avizo® 9.3 software (Regional Imaging Platform, Montpellier). All specimens were scanned with a resolution of ~5 µm.

The dental nomenclature, the orientation method of specimens in occlusal view, and the measurement method for the lower molars follow Gernelle et al. (2024). We introduce new measurement methods taking into account the fragmentary nature of the herpetotheriid upper molars from Albas. The paracone-

metacone length (PML) is defined as the greatest length overlaying the paracone-metacone axis. The talon width (TW) is the greatest width lingual and perpendicular to the paracone-metacone axis, taken from the paracone-metacone axis to the lingualmost point of the talon. The stylar shelf width (SSW) is the greatest width labial and perpendicular to the paracone-metacone axis, taken from the paracone-metacone axis to the lingualmost point of the ectoflexus. These dental measurement methods are directly illustrated on the occlusal views of the two upper molars from Albas (Figure 1A[2], B[1]). We used the highest preserved points of the paracone and metacone for orientation and measurements of the specimens. Because of apical wear, the measurements taken on Albas upper molars are necessarily partly approximate. Measurements were made to the nearest 0.01 millimetres (mm). For comparisons with the Albas specimens, PML, TW, and SSW measurements were performed on M2s and M3s of *Peratherium constans* from Dormaal (Costeur and Schneider 2011; Ladevèze et al. 2012), Fordones (Marandat 1991: 68-69), and Palette (Godinot et al. 1987: 283), and of *Peratherium matronense* Crochet, 1979, from Avenay and Condé-en-Brie (Crochet 1980: 147-151), and Rians (Godinot 1981). Dormaal specimens were studied through casts (Université de Montpellier) and available pictures in Ladevèze et al. (2012). Note that both *Pt. constans* in localities other than Dormaal and *Pt. matronense* are pending revision by one of us (KG).

Peratherium and *Amphiperatherium* representatives were ascribed to the subfamily Peratheriinae by Ladevèze et al. (2020). According to these authors, North American herpetotheriid genera such as *Herpetotherium* belong to the subfamily Herpetotheriinae. In the same way, Korth (2008) previously attributed all North American unequivocal herpetotheriids to *Herpetotherium* and *Copedelphys*. However, earliest North American undisputed herpetotheriid species (Wa-M/0 in age), though endemic but hardly distinguishable in morphology and size from earliest European peradectid species (Beard and Dawson 2001; Rose et al. 2012: 19), were referred to as species of *Peratherium* instead of *Herpetotherium* and *Copedelphys* (Gingerich and Smith 2006; Beard and Dawson 2009; but see Rose et al. 2012). Given the complex taxonomy of the earliest unequivocal herpetotheriids, we adopted a conservative approach in maintaining the original attributions for the North American material in our comparisons and discussion (i.e., the Peratheriinae vs Herpetotheriinae dichotomy is not followed).

Systematic palaeontology

Mammalia Linnaeus, 1758

Metatheria Huxley, 1880

Notometatheria Kirsch, Lapointe & Springer, 1997

Herpetotheriidae (Trouessart, 1879)

gen. and sp. nov.

Figure 1, Table 1

Holotype.—UM-ALB-25, labial fragment of left M3 with paracone, metacone and incomplete stylar shelf.

Type locality and age.—Albas, in Corbières (Southern France), latest Paleocene, between the POE and the PETM, and correlated with Clarkforkian 3 zone (NALMA) (Tabuce et al. submitted).

Other material.—UM-ALB-12, left m2 (L = 1.38 mm, W = 0.75 mm); UM-ALB-23, right lingual fragment of ?M2 with talon and partial paracone and metacone.

Diagnosis.—Smaller than all peratheriines. Differs from *Swaindelphys* and the earliest unequivocal herpetotheriids, *Peratherium constans* in Europe and *"Pt." innominatum/"Pt." macgrewi* in North America, in having M3 with (i) minute and labiolingually pinched stylar cusps; (ii) stylar cusp C apex slightly more ventral than stylar cusp B apex, (iii) shallower ectoflexus, and (iv) m2 with a labiolingually pinched entoconid. Further morphologically differs from *Swaindelphys* in having lower molars with (i) a lingual opening of the trigonid basin almost as high as the metaconid – entoconid notch, and (ii) a deeper entoconid – hypoconulid notch. Further differs from the earliest unequivocal herpetotheriids in having stylar cusp B mesiolabial to the paracone.

Description.—The holotype UM-ALB-25 (Figure 1A) is a labial fragment of a left upper molar. The talon is broken, and so are the distal part of the stylar shelf including stylar cusp D and the posterior part of the postmetacrista (Figure 1A^{2}). The metacone is less than twice as high and long as the paracone (Figure 1A^{1}, A^{3}). Given that the enamel is preserved on the paracone apex but not on the metacone apex, it is likely that the metacone was slightly higher than its current condition suggests. Those two major cusps have a triangular shape, with a flat labial face (Figure 1A^{2}, A^{4}). The median valley between the paracone and metacone is deep and narrow. The distal flanks of both the paracone and metacone are particularly vertical (Figure 1A^{3}). The damaged centrocrista is distinctly V-shaped. It occupies most of the labiolingual extension of the stylar shelf, with the labialmost part of the centrocrista positioned near the deepest part of the relatively shallow ectoflexus (Figure 1A^{2}). There are two minute stylar cusps (B and C) preserved without enamel; both are relatively mesiodistally elongate. Stylar cusp C is centered on the ectoflexus, and it is individualised from stylar cusp B, and probably from stylar cusp D. In fact, considering the absence of a stylar cusp D immediately distal to stylar cusp C, it is plausible that stylar cusp D was positioned labially or distolabially to the metacone apex (Figure 1A^{1}). Stylar cusp C is slightly higher, mesiodistally longer and labiolingually narrower than stylar cusp B, and its apex is more acute (Figure 1A^{1}-A^{2}). Stylar cusp B is placed mesiolabially to the paracone and is not strictly vertical but labially inclined (Figure 1A^{2}, A^{4}). Its mesiolabial edge is slightly broken. Stylar cusp A is not

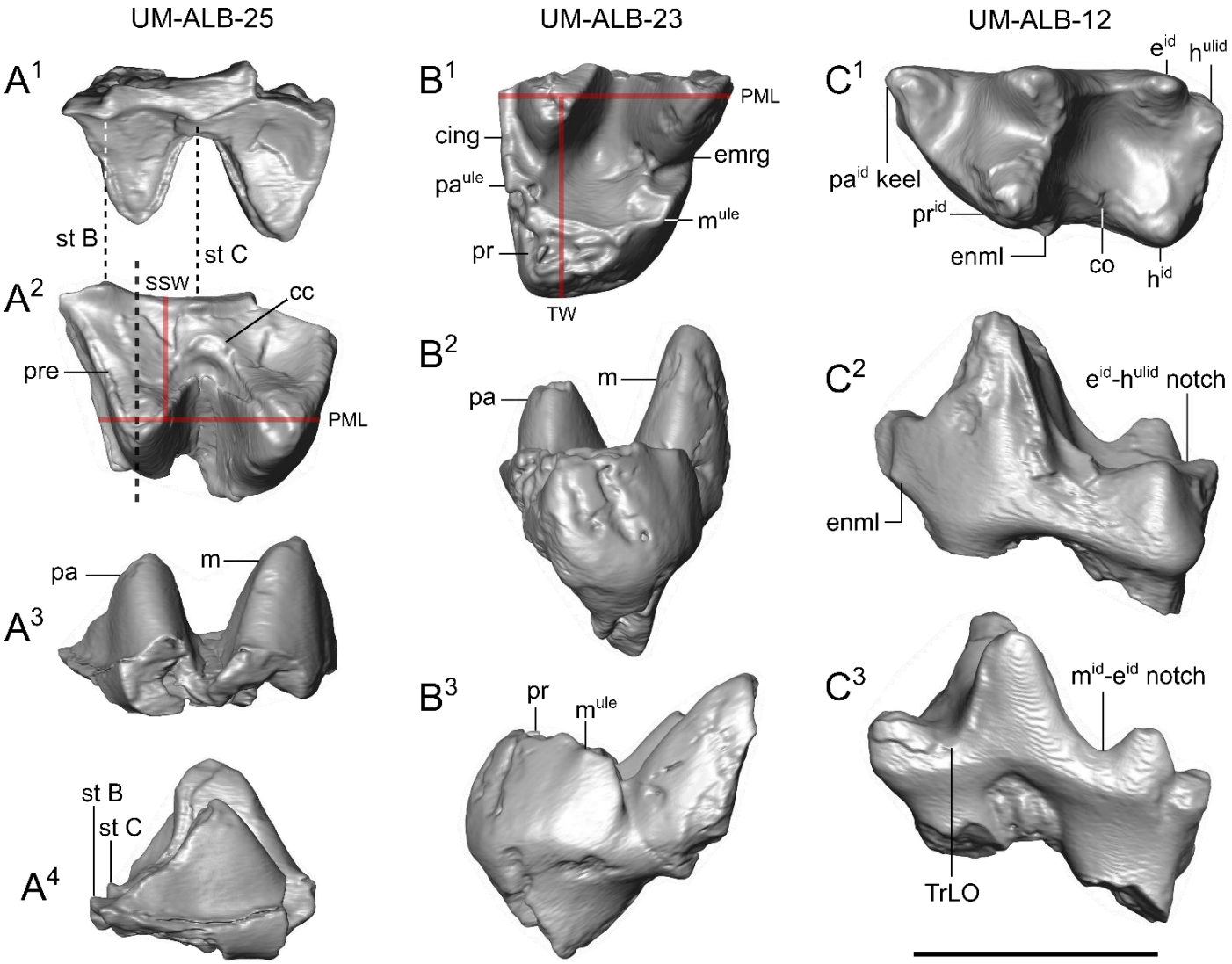

Figure 1. Upper and lower molars of herpetotheriid gen. et sp. nov. from Albas (latest Paleocene, in Corbières). **A**. UM-ALB-25 (holotype), partial stylar shelf of left M3 in labial (A^1), occlusal (A^2), lingual (A^3), and mesial (A^4) views. On the occlusal surface (A^2), the red segments indicate the paracone – metacone length (PML) and the stylar shelf width (SSW), and the dashed line indicates the axis parallel to the PML. **B**. UM-ALB-23, talon of right ?M2 in occlusal (B^1), lingual (B^2), and distal (B^3) reversed views. On the occlusal surface (B^1), the red segments indicate the PML and the talon width (TW) **C**. UM-ALB-12, left m2 in occlusal (C^1), labial (C^2), and lingual reversed views (C^3). Abbreviations: cc, centrocrista; cing, paracingulum; co, cristid obliqua; e^{id}, entoconid; emrg, distal emargination; enml, enamel; h^{id}, hypoconid; h^{ulid}, hypoconulid; m, metacone; m^{id}, metaconid; m^{ule}, metaconule; pa, paracone; pa^{id}, paraconid; pa^{ule}, paraconule; PML, paracone – metacone length; pr, protocone; pre, preparacrista; pr^{id}, protoconid; SSW, stylar shelf width; st, stylar cusp; TrLO, trigonid lingual opening; TW, talon width. Scale bar equals 1 mm.

preserved, but the relatively long preparacrista is directed towards the mesiolabial corner of the molar where stylar cusp A likely lay, rather than towards stylar cusp B (Figure 1A[2]). Given that the preparacrista is as long and mostly mesially inflected towards stylar cusp A on the M3s instead of the M2s of the small early Eocene peratheriine species (e.g., Supplemental material: Table S1), UM-ALB-25 is referred to as M3. The presence of a relatively long ectoflexus also supports the attribution to an M3 (Figure 1A[2]). The

postmetacrista is directed more labially than is the preparacrista. The low and incomplete paracingulum is almost of constant mesiodistal length along all its labiolingual extension (Figure 1A[2]). It is almost straight, from the base of the paracone to the mesiolabial end of the preparacrista. The paracingulum ends mesiolabially, lingual to a point approximately located between stylar cusps A and B. The stylar line is higher mesially to stylar cusp B than distally to it (Figure 1A[1]). The base of stylar cusp A was thus certainly at the same level as the base of stylar cusp B, and the two stylar cusps were probably highly connected. The part of the preparacrista which is mesiolingual to stylar cusp B being close to the labial edge of the molar (Figure 1A[2]), stylar cusp A was necessarily at least as labiolingually pinched as stylar cusps B and C. In occlusal view, the stylar line slightly lingually bends mesially to stylar cusp B. The stylar line is somewhat sharper distally to stylar cusp C than mesially to it and than both sides of stylar cusp B (Figure 1A[1]). The stylar shelf width (SSW) on paracone – metacone length (PML) ratio value of UM-ALB-25 is higher than those of M2s of *Pt. constans* and *Pt. matronense*, but fit in the observed ranges of those of M3s of the two Eocene species (Table 1). This confirms the attribution of the holotype UM-ALB-25 to an M3.

The whole stylar shelf of the right upper molar fragment UM-ALB-23 (Figure 1B) was not preserved labially to the paracone and metacone. The paracone is broken apically, and both the labial edges of the paracone and metacone are broken (Figure 1B[1], B[3]). The metacone is higher than the paracone as in UM-ALB-25, but the difference in height is more important, probably because, contrary to the holotype, the apex of the paracone of UM-ALB-23 lacks enamel, whereas it is fully preserved on the apex of the metacone (Figure 1B[2]). In lingual view, the slender paracone and metacone appear slightly shorter than on the holotype (Figure 1B[2] vs Figure 1A[3]), but here again, this difference is probably because the preparacrista, centrocrista, and postmetacrista are not preserved in UM-ALB-23. The two preserved but worn conules are relatively well-developed, the metaconule being larger and higher than the paraconule (Figure 1B[1]-B[2]). The paraconule is positioned more labially than the metaconule. The internal conular cristae, the postparaconular crista and premetaconular crista, are distinct and reach the base of the paracone and of the metacone, respectively, thereby closing the trigon basin (Figure 1B[1]). The deepest point of the trigon basin lies between the lingual edges of the paracone and metacone. On the talon, the highly worn protocone is asymmetrical, with a longer postprotocrista than preparacrista, and it is mesially shifted in occlusal view and appears somewhat procumbent in lingual view (Figure 1B[3]). The protocone is directly lingual to the paracone (Figure 1B[1]). The relative height of the protocone cannot be estimated because of apical wear. The paracingulum is directed almost strictly labially (Figure 1B[1]). In distal view, there is a deep notch between the lingual slope of the metaconule and the postmetaconular crista (Figure 1B[3]). In occlusal view, a short fossa between the metacone and metaconule is anterior to this notch. This fossa is slanted compared to the paracone-metacone axis (Figure 1B[1]). The angle defined at the base of the protocone between its mesial and distal edges is more acute than on M1s of early Eocene peratheriines

and similar to that of M2s and M3s (e.g., Ladevèze et al. 2012: fig. 5). Between the partial stylar shelf and the talon, there is a deep distal emargination of the crown, distolabial to the postmetaconular crista (Figure 1B[1]). In *Peratherium constans* and Wa-M representatives of *Pt. innominatum*, such a deep distal emargination occurs more often on M2s than on M3s (see figures in Gingerich and Smith 2006; Ladevèze et al. 2012; pers. obs. KG of a cast of the M2 UM 113311). The talon width (TW) on PML ratios of *Pt. constans* and *Pt. matronense* indicate that the talon is relatively longer on M3 than on M2 on average (Table 1). The TW/PML value of UM-ALB-23 is intermediate between the average TW/PML values of M2s ($\bar{x}$ = 0.83) and M3s ($\bar{x}$ = 0.91) of *Pt. constans*, and fits between the upper and lower limits, respectively, of their observed ranges. Thus, the allocation of UM-ALB-23 to an M2 is putative.

The left lower molar UM-ALB-12 (Figure 1C), although damaged, is the single subcomplete specimen attributed to this taxon. The upper part of the mesial and the larger distal roots are preserved (Figure 1C[3]). The crown is composed of a trigonid higher than the talonid (Figure 1C[2]-C[3]). The enamel layer is preserved only on the distal wall of the trigonid, the lingual edge of the paraconid and metaconid, the talonid basin and the entoconid tip. A small enamel spur distolabial to the protoconid apex shows that the trigonid was seemingly labiolingually wider when enclosed by enamel (Figure 1C[1]). The protoconid, fragmentary in lacking part of its mesiolabial edge and of its tip, is nevertheless the largest trigonid cuspid. The paraconid is aligned with the metaconid and the entoconid. The paraconid is relatively labiolingually wide and much shorter than the metaconid. It is mesially projected, forming a mesiolingual paraconid keel (Figure 1C[1]). In lingual view, the metaconid is triangular, taller than the paraconid, and almost symmetrical, with its distal half, extending towards the metaconid – preentocristid notch, slightly longer than the mesial half (Figure 1C[3]). The metaconid apex is located approximately dorsal to the midpoint between the two roots of the molar. The paracristid is longer than the protocristid. In labial view, the damaged preprotocristid appears straight (Figure 1C[2]). The lingual opening of the trigonid is wide, with the bases of the paraconid and metaconid that are fairly spaced. In lingual view, the trigonid basin opens at the same height as opens the talonid basin between the metaconid and entoconid (metaconid – entoconid notch in Figure 1C[2]). On the distolingual border of the talonid, the entoconid and hypoconulid are closely, lingually positioned. The entoconid, positioned relatively distally to the trigonid wall, is much higher than the low hypoconid (less damaged than the protoconid) and hypoconulid (Figure 1C[2]-C[3]). The talonid is markedly wider than the trigonid, and was probably as long as the entoconid when the hypoconulid was complete (Figure 1C[1]). The rectilinear preentocristid is sharp, but the distal edge of the entoconid is not crested. In distal view, the entoconid is slightly lingually inclined, it has a straight lingual flank and a labial flank that is gently sloping. The postcristid seems straight (Figure 1C[1]), but because both this cristid and the hypoconulid (generally distally projected in herpetotheriids) are worn, this observation is doubtful. The cristid obliqua is long, straight, and ends on the trigonid wall labial to the postmetacristid-postprotocristid notch. The angle formed by the postcristid and the cristid obliqua is

wide open (~75-80°), so that the hypoflexid is relatively shallow (Figure 1C[1]). The hypoconid apex is slightly distolabial to the entoconid apex. There are thin traces of pre- and postcingulids.

Comparisons.—UM-ALB-12 presents a relatively large paraconid with a paraconid keel, a protoconid higher than the metaconid, closely appressed distolingual entoconid and hypoconulid, and a postcingulid was probably present. The combination of these features is characteristic of most marsupialiform lower molars (see Gernelle et al. 2024: 31, and references therein). The deep notch between the entoconid and hypoconulid, the prominence in height of the entoconid on the hypoconid and hypoconulid, the lingual alignment between paraconid, metaconid and entoconid, and the relatively low lingual opening of the trigonid basin evoke herpetotheriid marsupialiforms (Gernelle et al. 2024: table 6). Upper molars have a metacone distinctly higher than the metacone (whereas most eutherians such as Eulipotyphla, and some basal marsupialiforms, have a higher paracone; e.g., Smith et al. [2002] for eutherians, Szalay and Trofimov [1996: fig. 9] for marsupialiforms), a wide stylar shelf with distinct stylar cusps, and a procumbent protocone; they are thus confidently ascribed to a marsupialiform. The V-shaped centrocrista is known in all herpetotheriids (see Chapter 3).

Based on PML values, UM-ALB-23 and UM-ALB-25 are shorter than any studied M2 and M3 of *Pt. constans* and *Pt. matronense* (Table 1). They are also shorter than a M3 of *Pt. innominatum* (UM 113434 in Gingerich and Smith 2006; PML = 1.12 mm on the basis of the scalled illustration). Based on SSW values, the M3 UM-ALB-25 is narrower than any studied M3 of *Pt. constans* and *Pt. matronense* (Table 1). The TW value of UM-ALB-23 corresponds to the lowest TW value known for M2 and M3 of *Pt. constans* (Table 1). The m2 UM-ALB-12 (L = 1.38 mm, W = 0.75 mm) is also smaller than lower molars of *Pt. constans* (Marandat 1991: tab. 1), and of the similarly sized *Pt. innominatum* from the Wa-M of the Bighorn Basin (Gingerich and Smith 2006: 269), and *Pt. macgrewi* (Beard and Dawson 2009: 199). Altogether, the Albas taxon appears markedly smaller than one of the smallest peratheriine, *Pt. constans*. It should be noted that a possibly smaller lower molar is documented in the Rians fauna (Provence, MP7-MP8+9 interval), although its paraconid is fragmentary (Godinot 1981: 53-54).

On the M3, stylar cusp B is markedly mesiolabial to the paracone apex instead of being directly labial to it, similar to *Swaindelphys* M3s (Johanson 1996: fig. 1; Williamson and Taylor 2011: figs. 3.3, 4.3) but unlike early Eocene peratheriine M3s known so far, such as early *Peratherium* species (e.g., Crochet 1980; Ladevèze et al. 2012). According to Korth (2008), *Herpetotherium* species have a large central stylar cusp (= stylar cusp C) on upper molars, whereas *Copedelphys* species (including *Copedelphys innominata* = *Herpetotherium innominatum* = *Peratherium innominatum*) have subequal stylar cusps B and C. However, stylar cusp B of the M3 specimen of *Pt. innominatum* illustrated by Gingerich and Smith (2006: fig. 15E-F) is broken, at least a M2 referred to this species by Gingerich and Smith (2006) has a dominant stylar cusp B (pers. obs. KG of a cast of UM 113311), and the M2 and M3 of UCMP

Tableau 1. Paracone – metacone length (PML), talon width (TW), and stylar shelf width (SSW) measurements (in mm), PML/TW and PML/TW ratio values, and labial preparacrista direction (towards stylar cusp [st.] A or stylar cusp B) for the ?M2 and M3 of the herpetotheriid gen. et sp. nov. from Albas (latest Paleocene, in Corbières), compared with those of *Peratherium constans* Teilhard de Chardin, 1927, from Dormaal (specimens published in Costeur and Schneider 2011; Ladevèze et al. 2012), Fordones (Marandat 1991), and Palette (Godinot et al. 1987), and of *Peratherium matronense* Crochet, 1979, from Avenay and Condé-en-Brie (Crochet 1980), and Rians (Godinot 1981).

Taxon	Locus	Locality	Specimen	PML (mm)	TW (mm)	SSW (mm)	TW/ PML	SSW/ PML	pre. dir.
gen et sp. nov.	?M2	Albas	UM-ALB-23	0,95	0,82		0,86		-
	M3		UM-ALB-25	0,90		0,51		0,57	< st. A
Peratherium constans	M2	Dormaal	NMB Om.1	1,10	0,89	0,56	0,81	0,51	st. B >
			IRSNB-M-1	1,19	0,96	0,43	0,81	0,36	st. B >
			IRSNB-M-2	0,99	0,82	0,50	0,83	0,51	st. B >
			IRSNB-M-1324	1,18	0,96	0,51	0,81	0,43	st. B >
			IRSNB-M-2039	1,12	1,02	0,43	0,91	0,38	st. B >
			IRSNB-M-2040	1,08	0,82	0,54	0,76	0,50	< st. A
			NMB Om.158	1,21	1,01	0,48	0,83	0,40	st. B >
			NMB Om.159	1,04	0,86	0,51	0,83	0,49	st. B >
		Fordones	UM-FDN-6	1,15	1,04	0,51	0,90	0,44	st. B >
			UM-FDN-9	1,18	1,02	0,53	0,86	0,45	st. B >
		Palette	UM-PAT-105	1,25	1,01	0,56	0,81	0,45	st. B >
	M3	Dormaal	IRSNB-M-1331	1,10	1,02	0,55	0,93	0,50	< st. A
			IRSNB-M-1333	1,05	0,91	0,57	0,87	0,54	< st. A
			IRSNB-M-1332	1,00	0,85	0,58	0,85	0,58	< st. A
			IRSNB-M-2030	0,97	0,93	0,62	0,96	0,64	< st. A
			IRSNB-M-2041	1,03	0,99	0,54	0,96	0,52	< st. A
			IRSNB-M-2042	1,00	0,91	0,55	0,91	0,55	< st. A
		Fordones	UM-FDN-10	1,16	1,03	0,60	0,89	0,52	st. B >
Peratherium matronense	M2	Avenay	MNHN.F.AV7225	1,26	1,07	0,63	0,85	0,50	st. B >
		CB	MNHN.F.CB159-BN	1,21	0,96	0,59	0,79	0,49	st. B >
			MNHN.F.CB3646	1,27	1,10	0,69	0,87	0,54	-
	M3	Avenay	MNHN.F.AV4707	1,08	1,17	0,64	1,08	0,59	< st. A
			MNHN.F.AV6794	1,17	1,27	0,60	1,09	0,51	< st. A
		CB	MNHN.F.CB155-BN	1,21	1,17	0,62	0,97	0,51	< st. A
			MNHN.F.CB203-BN	1,09	1,11	0,60	1,02	0,55	< st. A
			MNHN.F.CB195-BN	1,11	1,12	0,63	1,01	0,57	< st. A
			MNHN.F.CB1412	1,08	1,10	0,61	1,02	0,56	< st. A
			MNHN.F.CB2845	1,12	1,05	0,57	0,94	0,51	< st. A
		Rians	MNHN.F.RI392	1,08	1,01	0,62	0,94	0,57	-
			MNHN.F.RI378	1,11		0,59		0,53	< st. A

44095, a specimen reallocated to *Pt. innominatum macgrewi* by Krishtalka and Stucky (1983a), also have a stylar cusp B dominant in height (see McKenna 1960: fig. 18a). So is stylar cusp B in *Pt. constans* (Ladevèze et al. 2012). The Albas genus thus differs from the two latter species for this character (Figure 1A[1]). The long and shallow ectoflexus is also found in several *Herpetotherium* species such as *H. knighti* (McGrew, 1959) (McGrew et al. 1959: fig. 3), but not in the earliest unequivocal North American herpetotheriids (Gingerich and Smith 2006: fig. 15F). However, intraspecific variation exists for this character in early peratheriines (Gernelle et al. 2024b: fig. 4I vs 4M). As for the lower molar, a lingual opening of the trigonid as low as that of the Albas taxon is known only in m1s-m3s of unequivocal herpetotheriids among fossil marsupialiforms (e.g., see for earliest representatives Gingerich and Smith 2006: fig. 15I; Beard and Dawson 2009: fig. 4E; Ladevèze et al. 2012: fig. 4Ec, Fc, Gc; Rose et al. 2012: fig. 9G, J, M).

Discussion

The presence of herpetotheriid metatherians in the Paleocene of Europe was unsuspected before the discovery of the Albas specimens (see Gheerbrant 1991; Crespo and Goin 2021), because their dispersal from North America to Europe was thought to have likely been triggered by the PETM (e.g., Hooker 2015), instead of the POE (Tabuce et al. submitted). Conversely, the acquisition of a stylar cusp position pattern in which stylar cusp B becomes directly labial to the paracone was expected from some point of the evolution of the "herpetotheriid" lineage, based on the results of recent phylogenetic analyses focused on the morphology of metatherian molars (Chapter 3), given that this trait differs between *Swaindelphys* and Eocene herpetotheriids. This, in addition to some autapomorphies (e.g., stylar cusps B and C subequal in height, although they are possibly worn) supports the allocation of Albas specimens to a new herpetotheriid genus. Supposing an ancestor-decendant relationship between the Albas genus and *Pt. constans*, the distal displacement of stylar cusp B occurred at least once between the latest Paleocene and the earliest Eocene in European faunas. This shows that morphological characters based on dental evidence alone can be found to distinguish early herpetotheriid taxa from Europe (contra Hooker et al. 2008; Selva and Ladevèze 2017), although few diagnostic characters (if any) are found on lower molars of stem-herpetotheriids (Williamson and Taylor 2011) and first unequivocal herpetotheriids (Rose et al. 2012: 19).

The fact that earliest peratheriines morphologically more closely resemble earliest herpetotheriines (including "*Pt.*" *innominatum* and "*Pt.*" *macgrewi*), both earliest Eocene in age (on this similarity, see also Rose et al. 2012: 19), than the new Paleocene herpetotheriid in terms of stylar cusp position and relative heights is puzzling and hampers for proposing parsimonious palaeobiogeographic scenarios. Interestingly, stylar cusp B also becomes directly labial to the paracone apex in the European peradectid

clade, with respect to most North American peradectid species (Gernelle et al. 2024a: fig. 4; but see Gingerich and Smith 2006: fig. 26E), almost simultaneously to herpetotheriids (again, supposing an ancestor-decendent relationship between the Albas genus and *Pt. constans*) at the beginning of the Eocene. This is interpreted as a convergence between the two European lineages of these families in a phylogenetic context (see Chapter 3). Thus, it is possible that such a transformation occurred also more than once in early herpetotheriids (i.e., not only in European faunas). However, herpetotheriids or stem-herpetotheriids are surprisingly unknown during most of the Paleocene in North America, from Clarkforkian and Tiffanian localities, whereas peradectids are well-sampled in such sites (e.g., Gingerich and Smith 2006; Chapter 3). Based on the probable affinities of the new genus from Albas, we predict that stem-herpetotheriid taxa younger than *Swaindelphys encinensis* and older than the Albas taxon (i.e., Tiffanian or early Clarkforkian NALMA in age; see Williamson and Taylor 2011), were present in North America and are yet to be discovered.

Another critical character to consider for discussing the evolution of herpetotheriids is the relative height of the lingual opening of the trigonid basin. To our knowledge, only unequivocal herpetotheriids present such a low lingual opening of the trigonid basin among Laurasian marsupialiforms (Chapter 3; Gernelle et al. 2024a: table 6). For this reason, in addition to the also low entoconid – hypoconulid notch, the new taxon from Albas is considered as the basalmost known unequivocal herpetotheriid. A synapomorphy of Peratheriinae in the phylogenetic analysis performed by Ladevèze et al. (2020) is the presence of a conical entoconid. Because the Albas genus has a labiolingually pinched entoconid, together with a mosaic of primitive and derived characters with respect to other unequivocal herpetotheriids, it is not regarded as a peratheriine here. It is noteworthy, however, that although the reported intraspecific morphological variation concerning the entoconid is only relative to its size, position and inclination rather than its shape in the earliest peratheriine (Ladevèze et al. 2012), important intraspecific variation of the shape of this cuspid (conical to crescentiform) has been noted based on a comprehensive series of peradectid lower molars (Gernelle et al. 2024a: fig. 11r vs 11t).

This study highlights the possibility of identifying upper molar position of isolated, sometimes fragmentary tribosphenic specimens by studying stylar shelf and talon proportions (Table 1). For this endeavour, another method employing geometric morphometrics has been proposed, based on a different marsupialiform clade, but it requires complete upper molars (Engelman and Croft 2022). Length measurements relative to the talon of upper molars are known to be correlated with full length in several mammal taxa (Cifelli 1994: fig. 2). Based on the new measurement method proposed, we also showed that the new genus from Albas is the smallest European herpetotheriid known so far. Cases of dwarfism have been reported in numerous mammalian lineages, including small mammals, during ancient global warming events such as the PETM (e.g., Rankin et al. 2015; D'Ambrosia et al. 2017; Gingerich et al. 2023). The hypothesis of the latest Paleocene herpetotheriid being a "dwarfed" form applies only when

it is compared with early Eocene herpetotheriids. In fact, the Albas genus is (i) larger than the smallest known early Eocene peradectid species, the Wasatchian *Peradectes gulottai* Rose, 2010 (M3 PML = 0.83 mm, based on the scaled illustration of Rose [2010]), (ii) as large as or larger than several herpetotheriid (e.g., *Copedelphys stevensoni* [Cope, 1873]) and peradectid species (*Nanodelphys hunti* [Cope, 1873]) that inhabited North America during the Oligocene (Korth 2018; Korth et al. 2021), and (iii) much larger than the smallest Northern Hemisphere metatherian, the late Paleocene probable deltatheroidan *Gurbanodelta* (Ni et al., 2016).

According to Crochet (2016), the putative latest Cretaceous herpetotheriid (but see Williamson et al. 2012, 2014) *Maastrichtidelphys meurismeti* from the Maastricht Formation (Europe) may represent a contamination of the Maastrichtian locality by Eocene deposits. In fact, according to him, the single isolated M2 of this taxon would be very similar to those from the upper molar series of *Peratherium sudrei* Crochet, 1979, from Robiac (MP16). However, M1s to M3s of *Pt. sudrei* have a stylar cusp D placed mesiolabially to the metacone apex (Crochet 1980: figs. 171-172; pers. obs. KG), contrary to *Maastrichtidelphys*. An interesting way to test the affinities (and thus the age) of this disputed tooth would be to know the relative position of its stylar cusp B. In fact, among the many marsupialiform taxa known from the Hell Creek Formation, USA (see Wilson 2014: table 1) of which *Maastrichtidelphys* is putatively contemporaneous, only the bunodont *Glasbius* has a stylar cusp B labial to the paracone apex (e.g., Davis 2007: fig. 23A). Thus, the presence in *Maastrichtidelphys* of a stylar cusp B strictly labial to the paracone apex would support an affinity of this taxon with Eocene herpetotheriids. Unfortunately, the position of stylar cusp B, if preserved at all, is unclear in *Maastrichtidelphys*, the discovery of more specimens is critical to conclude.

References

Beard KC, Dawson MR (2001) Early Wasatchian mammals from the Gulf coastal plain of Mississipi : Biostratigraphic and paleobiogeographic implications. In : Gunell GF (ed) Eocene biodiversity : unusual occurrences and rarely sampled habitats. Kluwer Academic/Plenum Publishers, New York, pp 75-94.

Beard KC, Dawson MR (2009) Early Wasatchian mammals of the Red Hot local fauna, uppermost Tuscahoma Formation, Lauderdale County, Mississippi. *Annals of Carnegie Museum* 78(3): 193–243.

Beck RMD (2023) Diversity and phylogeny of marsupials and their stem relatives (Metatheria). In: Cáceres NC, Dickman CR (eds) American and Australasian Marsupials. Springer, Cham, Switzerland, pp 23–88.

Carneiro LM, Oliveira ÉV (2017) The Eocene South American metatherian *Zeusdelphys complicatus* is not a protodidelphid but a hatcheriform: Paleobiogeographic implications. *Acta Palaeontologica Polonica* 62(3): 497-507.

Carneiro LM, Oliveira EV, Goin FJ (2018) *Austropediomys marshalli* gen. et sp. nov., a new Pediomyoidea (Mammalia, Metatheria) from the Paleogene of Brazil: Paleobiogeographic implications. *Revista Brasileira de Paleontologia* 21(2): 120-131.

Case JA, Goin FJ, Woodburne MO (2005) “South American” marsupials from the Late Cretaceous of North America and the origin of marsupial cohorts. *Journal of Mammalian Evolution* 12: 461-494.

Cifelli RL (1994) Therian mammals of the Terlingua local fauna (Judithian), Aguja Formation, Big Bend of the Río Grande, Texas. *Rocky Mountain Geology* 30(2): 117-136.

Costeur L, Schneider M (2011) Catalogue of the Eocene mammal types of the Natural History Museum Basel. *Carnets Geol*.

Crespo VD, Goin FJ (2021) Taxonomy and affinities of african cenozoic metatherians. *Spanish Journal of Palaeontology* 36(2): 1–16.

Crochet JY (1980) Les marsupiaux du Tertiaire d’Europe. Edtions Foundation Singer-Polignac, Paris.

Crochet JY (2016) Valbro: A new site of vertebrates from the early Oligocene (MP 22) of France (Quercy). IV – Marsupialia, Insectivora. *Annales de Paléontologie* 102(1): 7–10.

D’Ambrosia AR, Clyde WC, Fricke HC, Gingerich PD, Abels HA (2017) Repetitive mammalian dwarfing during ancient greenhouse warming events. *Science Advances* 3: e1601430.

Engelman R, Croft D (2022) Identifying tooth position of isolated teeth of sparassodonts (Mammalia: Metatheria) using geometric morphometrics. *Palaeontologia Electronica* 25(1): a8.

Estravís C (2000) Nuevos mamíferos del Eoceno Inferior de Silveirinha (Baixo Mondego, Portugal). *Coloquios de Paleontologia* 51: 281–311.

Gernelle K, Billet G, Gheerbrant E, Godinot M, Marandat B, Ladevèze S, Tabuce R (2024) Taxonomy and evolutionary history of peradectids (Metatheria): new data from the early Eocene of France. *Journal of Mammalian Evolution* 31(3): 31.

Gheerbrant E (1991) *Bustylus* (Eutheria, Adapisoriculidae) and the absence of ascertained marsupials in the Palaeocene of Europe. *Terra Nova* 3: 586–592.

Gingerich PD, Smith T (2006) Paleocene-Eocene land mammals from three new latest Clarkforkian and earliest Wasatchian Wash sites at Polecat Bench in the Northern Bighorn Basin. *Contributions from the Museum of Paleontology, University of Michigan* 31: 245–303.

Gingerich P, Folie A, Smith T (2023) *Didelphodus caloris*, new species (Mammalia, Cimolesta), from the Wasatchian Wa–0 Fauna of the Paleocene-Eocene Thermal Maximum, Clarks Fork Basin, Wyoming. *Contributions from the Museum of Paleontology, University of Michigan* 35(2): 34-45.

Godinot M (1981) Les mammifères de Rians (Eocène inférieur, Provence). *Palaeovertebrata* 10: 43–126.

Godinot M, Crochet JY, Hartenberger JL, Lange-Badré B, Russell DE, Sigé B (1987) Nouvelles données sur les mammifères de Palette (Eocène inférieur, Provence). *Münchner Geowissenschaftliche Abhandlungen (A)* 10: 273-288.

Hooker JJ (2015) A two-phase mammalian dispersal event across the Paleocene–Eocene transition. *Newsletters on Stratigraphy* 48(2): 201–220.

Hooker JJ, Sánchez-Villagra MR, Goin FJ, Simons EL, Attia Y, Seiffert ER (2008) The origin of Afro-Arabian ‘didelphimorph’ marsupials. *Palaeontology* 51(3): 635–648.

Horovitz I, Ladevèze S, Argot C, Hooker JJ, Macrini TE, Martin T, Kurz C, Muizon C de, Sánchez-Villagra MR (2008) The anatomy of *Herpetotherium fugax* Cope, 1873, a metatherian from the Oligocene of North America. *Palaeontographica Abteilung A* 284: 109–141.

Johanson Z (1996) New marsupial from the Fort Union Formation, Swain Quarry, Wyoming. *Journal of Paleontology* 70(6): 1023–1031.

Korth WW (2008) Marsupialia. In: Janis CM, Gunnell GF, Uhen MD (eds) Evolution of Tertiary Mammals of North America: Volume 2, Small Mammals, Xenarthrans, and Marine Mammals. Cambridge University Press, Cambridge, pp 39–47.

Korth WW (2018) Review of the marsupials (Mammalia: Metatheria) from the late Paleogene (Chadronian–Arikareean: late Eocene–late Oligocene) of North America. *PalZ* 92: 499–523.

Korth WW, Boyd CA, Emry RJ, Person JJ (2021) Marsupials (Mammalia, Metatheria) from the Brule Formation (Whitneyan, Oligocene) North Dakota. *Journal of Paleontology* 95(1): 193-204.

Krishtalka L, Stucky RK (1983a) Revision of the Wind River faunas, early Eocene of Central Wyoming. Part 3. Marsupialia. *Annals of Carnegie Museum* 52(9): 205‑227.

Krishtalka L, Stucky RK (1983b) Paleocene and Eocene marsupials of North America. *Annals of Carnegie Museum* 52(10): 229–263.

Kurz C (2005) Ecomorphology of opossum-like marsupials from the Tertiary of Europe and a comparison with selected taxa. *Kaupia* 14: 21–26.

Ladevèze S, Selva C, Muizon C de (2020) What are "opossum-like" fossils? The phylogeny of herpetotheriid and peradectid metatherians, based on new features from the petrosal anatomy. *Journal of Systematic Palaeontology* 18: 1463–1479.

Ladevèze S, Smith R, Smith T (2012) Reassessment of the morphology and taxonomic status of the earliest herpetotheriid marsupials of Europe. *Journal of Mammalian Evolution* 19: 249–261.

Marandat B (1991) Mammifères de l'Ilerdien Moyen (Eocène Inférieur) des Corbières et du Minervois. *Palaeovertebrata* 20: 55–144.

Marandat B, Adnet S, Marivaux L, Martinez A, Vianey-Liaud M, Tabuce R (2012) A new mammalian fauna from the earliest Eocene (Ilerdian) of the Corbières (Southern France): Palaeobiogeographical implications. Swiss Journal of Geosciences 105: 417–434.

Martin JE, Case JA, Jagt JW, Schulp AS, Mulder EW (2005) A new European marsupial indicates a Late Cretaceous high-latitude transatlantic dispersal route. *Journal of Mammalian Evolution* 12(3-4): 495-511.

McKenna M (1960) Fossil Mammalia from the early Wasatchian Four Mile fauna, Eocene of northwest Colorado. University of California Publications Geological Sciences 37: 1‑130.

Ni X, Li Q, Stidham TA, Li L, Lu X, Meng J (2016) A late Paleocene probable metatherian (? deltatheroidan) survivor of the Cretaceous mass extinction. *Scientific Reports* 6: 38547.

Rankin BD, Fox JW, Barrón-Ortiz CR, Chew AE, Holroyd PA, Ludtke JA, Yang X, Theodor JM (2015) The extended Price equation quantifies species selection on mammalian body size across the Palaeocene/Eocene Thermal Maximum. *Proceedings of the Royal Society B: Biological Sciences* 282(1812): 20151097.

Rose KD (1981) The Clarkforkian Land-Mammal Age and mammalian faunal composition across the Paleocene-Eocene boundary. *University of Michigan Papers on Paleontology* 26: 1–197.

Rose KD (2010) New marsupial from the Early Eocene of Virginia. *Journal of Paleontology* 84(3): 561–565.

Rose KD (2012) The importance of Messel for interpreting Eocene Holarctic mammalian faunas. *Palaeobiodiversity and Palaeoenvironments* 92: 631–647.

Rose KD, Chew AE, Dunn RH, Kraus MJ, Fricke HC, Zack SP (2012) Earliest Eocene mammalian fauna from the Paleocene-Eocene Thermal Maximum at Sand Creek Divide, Southern Bighorn Basin, Wyoming. *University of Michigan Papers on Paleontology* 36: 1–122.

Rothecker J, Storer JE (1996) The marsupials of the Lac Pelletier Lower Fauna, Middle Eocene (Duchesnean) of Saskatchewan. *Journal of Vertebrate Paleontology* 16: 770–774.

Sánchez-Villagra M, Ladevèze S, Horovitz I, Argot C, Hooker JJ, Macrini TE, Martin T, Moore-Fay S, Muizon C de, Schmelzle T, Asher RJ (2007) Exceptionally preserved North American Paleogene metatherians: Adaptations and discovery of a major gap in the opossum fossil record. *Biology Letters* 3: 318–322.

Secord R (2008) The Tiffanian Land-Mammal Age (middle and late Paleocene) in the northern Bighorn Basin, Wyoming. *University of Michigan Papers on Paleontology* 35: 1-192.

Selva C, Ladevèze S (2017) Computed microtomography investigation of the skull of Cuvier's famous 'opossum' (Marsupialiformes, Herpetotheriidae) from the Eocene of Montmartre. *Zoological Journal of the Linnean Society* 180(3): 672–693.

Smith T, Quesnel F, De Plöeg G, De Franceschi D, Metais G, De Bast E, Solé F, Folie A, Boura A, Claude J et al. (2014) First Clarkforkian equivalent land mammal age in the latest Paleocene basal Sparnacian facies of Europe: fauna, flora, paleoenvironment and (bio) stratigraphy. *PLoS One* 9(1): e86229.

Smith T, Bloch JI, Strait SG, Gingerich PD (2002) New species of *Macrocranion* (Mammalia, Lipotyphla) from the earliest Eocene of North America and its biogeographic implications. *Contributions from the Museum of Paleontology, the University of Michigan* 30: 373-384.

Smith T, Rose KD, Gingerich PD (2006) Rapid Asia–Europe–North America geographic dispersal of earliest Eocene primate *Teilhardina* during the Paleocene–Eocene thermal maximum. *Proceedings of the National Academy of Sciences USA* 103(30): 11223-11227.

Szalay FS, Trofimov BA (1996) The Mongolian Late Cretaceous Asiatherium, and the early phylogeny and paleobiogeography of Metatheria. *Journal of Vertebrate Paleontology* 16(3): 474-509.

Tabuce R, Marandat B, Adnet S, Gernelle K, Girard F, Marivaux L, Solé F, Steurbaut E, Storme JY, Vianey-Liaud M, Yans J (submitted) European mammal turnover driven by a global rapid warming event preceding the Paleocene-Eocene Thermal Maximum.

Vullo R, Gheerbrant E, Beurel S, Swajda M, Néraudeau, D (2020) A stagodontid mammal from the mid-Cretaceous of France confirms the Euramerican distribution of early marsupialiforms. *Palaeogeography, Palaeoclimatology, Palaeoecology* 560: 110034.

Vullo R, Gheerbrant E, Muizon C de, Néraudeau D (2009) The oldest modern therian mammal from Europe and its bearing on stem marsupial paleobiogeography. *Proceedings of the National Academy of Sciences USA* 106: 19910–19915.

Williamson TE, Lofgren DL (2014) Late Paleocene (Tiffanian) metatherians from the Goler Formation, California. *Journal of Vertebrate Paleontology* 34: 477–482.

Williamson TE, Taylor LH (2011) New species of *Peradectes* and *Swaindelphys* (Mammalia: Metatheria) from the Early Paleocene (Torrejonian) Nacimiento Formation, San Juan Basin, New Mexico, USA. *Palaeontologia Electronica* 14: 23A.

Williamson TE, Brusatte SL, Carr TD, Weil A, Standhardt BR (2012) The phylogeny and evolution of Cretaceous-Palaeogene metatherians: Cladistic analysis and description of new early Palaeocene specimens from the Nacimiento Formation, New Mexico. *Journal of Systematic Palaeontology* 10: 625–651.

Williamson TE, Brusatte SL, Wilson GP (2014) The origin and early evolution of metatherian mammals: The Cretaceous record. *Zookeys* 465: 1–76.

Wilson GP (2014) Mammalian extinction, survival, and recovery dynamics across the Cretaceous-Paleogene boundary in northeastern Montana, USA. In: Wilson GP, Clemens WA, Horner JR, Hartman JH (eds)

Through the end of the Cretaceous in the type locality of the Hell Creek Formation in Montana and adjacent areas. *The Geological Society of America, Special Papers* 503, pp. 365-392.

Wilson GP, Ekdale EG, Hoganson JW, Calede JJ, Vander Linden A (2016) A large carnivorous mammal from the Late Cretaceous and the North American origin of marsupials. *Nature Communications* 7: 13734.

Xue P, Chang L, Thomas E (2023) Abrupt Northwest Atlantic deep-sea oxygenation decline preceded the Palaeocene-Eocene Thermal Maximum. *Earth and Planetary Science Letters* 618: 118304.

Yans J, Marandat B, Masure E, Serra-Kiel J, Schnyder J, Storme JY, Marivaux L, Adnet S, Vianey-Liaud M, Tabuce R (2014) Refined bio-(benthic foraminifera, dinoflagellate cysts) and hemostratigraphy (δ13Corg) of the earliest Eocene at Albas-Le Clot (Corbières, France): Implications for mammalian biochronology in Southern Europe. *Newsletters on Stratigraphy* 47(3): 331–353.

Chapitre 5. Réflexions sur l'évolution de la morphologie dentaire chez les premiers Peratheriinae, à travers le cas des espèces de relativement grande taille

Cette section correspond à l'article suivant : Gernelle K, Godinot M, Marandat B, Téodori D, Ladevèze S, Tabuce R. 2024 (early access online). Dental morphology evolution in early peratheriines, including a new morphologically cryptic species and findings on the largest early Eocene European metatherian. Historical Biology. doi: https://doi.org/10.1080/08912963.2024.2403602

Résumé. Les premiers stades de l'histoire évolutive des pérathériinés, les métathériens herpétothériidés d'Europe, sont en grande partie inconnus, principalement en raison de leur faible disparité morphologique dentaire tout au long du Paléogène, associée à une variation intraspécifique prépondérante. À partir de onze molaires, nous documentons une nouvelle espèce de pérathériiné précoce, ***Peratherium musivum* nov. sp.**, qui est plus grande et morphologiquement similaire au premier pérathériiné, *Peratherium constans* (MP7). Des caractères subtils sont partagés avec le plus grand pérathériiné de l'Éocène inférieur, ***Peratherium maximum* nov. comb.** Nous illustrons l'importance d'étudier les changements possibles dans les proportions cuspides – bassins et les caractères corrélés qui se sont produits au cours de l'évolution des pérathériinés. *Peratherium musivum* nov. sp., qui ne couvre qu'une partie de l'intervalle MP7-MP8+9, et l'espèce ~MP8+9 *Peratherium maximum* nov. comb., étaient probablement répandus en Europe occidentale. La description d'une mandibule bien conservée de ce dernier, provenant de La Borie (~MP8+9), révèle des caractères originaux concernant la taille et la forme relative des alvéoles dentaires, partiellement corroborés à l'aide de molaires isolées. Ces caractères sont absents chez les espèces les plus jeunes et les plus représentatives des deux genres de pérathériinés, *Peratherium* et *Amphiperatherium*. Sur la base des données susmentionnées et d'un examen critique, il est démontré que les genres de pérathériinés manquent de définitions cohérentes, de sorte que la dichotomie *Peratherium* / *Amphiperatherium* est vraisemblablement inapplicable aux représentants de l'Éocène inférieur.

Historical Biology
An International Journal of Paleobiology

Taylor & Francis
Taylor & Francis Group

ISSN: (Print) (Online) Journal homepage: www.tandfonline.com/journals/ghbi20

Dental morphology evolution in early peratheriines, including a new morphologically cryptic species and findings on the largest early Eocene European metatherian

Killian Gernelle, Marc Godinot, Bernard Marandat, Dominique Téodori, Sandrine Ladevèze & Rodolphe Tabuce

To cite this article: Killian Gernelle, Marc Godinot, Bernard Marandat, Dominique Téodori, Sandrine Ladevèze & Rodolphe Tabuce (07 Oct 2024): Dental morphology evolution in early peratheriines, including a new morphologically cryptic species and findings on the largest early Eocene European metatherian, Historical Biology, DOI: 10.1080/08912963.2024.2403602

To link to this article: https://doi.org/10.1080/08912963.2024.2403602

View supplementary material

Published online: 07 Oct 2024.

Submit your article to this journal

View related articles

View Crossmark data

Full Terms & Conditions of access and use can be found at
https://www.tandfonline.com/action/journalInformation?journalCode=ghbi20

HISTORICAL BIOLOGY
https://doi.org/10.1080/08912963.2024.2403602

Taylor & Francis
Taylor & Francis Group

Check for updates

Dental morphology evolution in early peratheriines, including a new morphologically cryptic species and findings on the largest early Eocene European metatherian

Killian Gernelle[a], Marc Godinot[b], Bernard Marandat[a], Dominique Téodori[c], Sandrine Ladevèze[d*] and Rodolphe Tabuce[a*]

[a]Institut des Sciences de l'Évolution de Montpellier (ISEM, UMR 5554), Univ Montpellier, CNRS, IRD, cc64, Place Eugène Bataillon, Montpellier, Cedex, France; [b]Ecole Pratique des Hautes Etudes, PSL, Buffon, France; [c]Haute-Garonne, 8 impasse de San Marino, Pechbonnieu, France; [d]Centre de Recherche en Paléontologie - Paris (CR2P, UMR 7207), Sorbonne Université, Muséum National d'Histoire Naturelle, CNRS, 8 rue Buffon, Paris, France

ABSTRACT

The initial stages of the evolutionary history of peratheriines, the European herpetotheriid metatherians, are largely unknown, primarily due to their limited morphological dental disparity throughout the Palaeogene, coupled with significant intraspecific variation. Based on eleven molars, we document a new early peratheriine species, ***Peratherium musivum* sp. nov**. which is larger than and morphologically similar to the earliest peratheriine, *Peratherium constans* (MP7). Subtle molar characters are shared with the largest early Eocene peratheriine, ***Peratherium maximum* comb. nov**. We illustrate the importance of studying possible changes in molar cusp – basin proportions and correlated characters that occured during peratheriine evolution. *Peratherium musivum* sp. nov. which spanned only part of the MP7-MP8 + 9 time interval, and the ~MP8 + 9 *Peratherium maximum* comb. nov. were probably widespread in Western Europe. The description of a well-preserved mandible of the latter, from La Borie (~MP8 + 9), reveals original features concerning relative size and shape of dental alveoli, partly corroborated using isolated molars. These traits are absent in the younger, most representative species of both peratheriine genera, *Peratherium* and *Amphiperatherium*. Based on the aforementioned data and a critical review, it is demonstrated that peratheriine genera lack consistent definitions, so that the *Peratherium*/*Amphiperatherium* dichotomy is plausibly inapplicable to early Eocene representatives.

This article is registered in ZooBank under urn:lsid:zoobank.org:pub:A2B4DE58-855C-4CB8-BC1D-C9677E6DF97D

ARTICLE HISTORY
Received 18 June 2024
Accepted 28 August 2024

KEYWORDS
France; Herpetotheriidae; Marsupialiformes; molars; systematics; Ypresian

Introduction

Herpetotheriidae are a possibly paraphyletic (with respect to crown-marsupials) assemblage of extinct and small (much less than 500 g) Cenozoic stem-marsupials, with a superficially 'opossum-like' unspecialised tribosphenic dentition (e.g. Sánchez-Villagra et al. 2007; Ladevèze et al. 2020; Beck 2023). The subfamily Peratheriinae, almost restricted to Europe, with one species documented in Africa (Simons and Bown 1984; Hooker et al. 2008; Crespo and Goin 2021), includes the genera *Peratherium* Aymard, 1850, and *Amphiperatherium* Filhol, 1879, while North American herpetotheriids, Herpetotheriinae, are assumed to be represented by *Herpetotherium* Cope, 1873, during the early Eocene (Korth 1994, 2008; Williamson et al. 2012; Ladevèze et al. 2020). The origin of unequivocal herpetotheriids (i.e. Eocene to Miocene representatives) is uncertain (e.g. Johanson 1996; Martin et al. 2005; Ladevèze et al. 2012; Williamson et al. 2012); so are their precise intrafamilial relationships (Figure 1), largely because of difficulties in establishing the polarity of labile, often homoplastic and only dental characters (Szalay 1993, p. 220). However, characterising the morphology of the earliest representatives of a given family is crucial in order to understand possible ancient intrafamilial cladogenesis (e.g. Marivaux et al. 2004, p. 108).

The oldest peratheriine, and oldest species of the genus *Peratherium*, is the small *Peratherium constans* Teilhard de Chardin, 1927, from the earliest Eocene of Dormaal (Belgium, MP7 reference level, usually correlated with the Paleocene-Eocene Thermal Maximum [PETM]; Steurbaut et al. 2003; Ladevèze et al. 2012) (Figure 1). The distinction of earliest representatives of *Peratherium* and *Amphiperatherium* is challenging (Hooker et al. 2008, p. 643). In fact, *Amphiperatherium brabantense*, Crochet, 1979, also defined in Dormaal (Crochet 1979), has been considered a junior synonym of *Peratherium constans* (Ladevèze et al. 2012). As a consequence, *Amphiperatherium maximum* Crochet, 1979, typical of the MP8 + 9 and ~MP8 + 9 faunas of the Paris Basin (Crochet 1980, pp. 98–99), and also reported in localities older than MP8 + 9 (e.g. Russell et al. 1988), becomes one of the earliest species of the genus *Amphiperatherium* (Figure 1), and the only species of *Amphiperatherium* with its type locality in the early Eocene (Crochet 1979; Ladevèze et al. 2012), which implies an ancient divergence between *Peratherium* and *Amphiperatherium*. *Amphiperatherium maximum* and closely related taxa (e.g. *Amphiperatherium* aff. *maximum*; Storch and Haubold 1989) are also the largest metatherians of the early to middle Eocene of Europe (Figure 1). This species possibly initiates the species rich 'lineage' (*sensu* Crochet 1980) of relatively large peratheriines

CONTACT Killian Gernelle killian.gernelle@umontpellier.fr Institut des Sciences de l'Évolution de Montpellier (ISEM, UMR 5554), Univ Montpellier, CNRS, IRD, cc64, Place Eugène Bataillon, Montpellier, Cedex F-34095, France
*Co-senior authors

Supplemental data for this article can be accessed online at https://doi.org/10.1080/08912963.2024.2403602.

© 2024 Informa UK Limited, trading as Taylor & Francis Group

Published online 07 Oct 2024

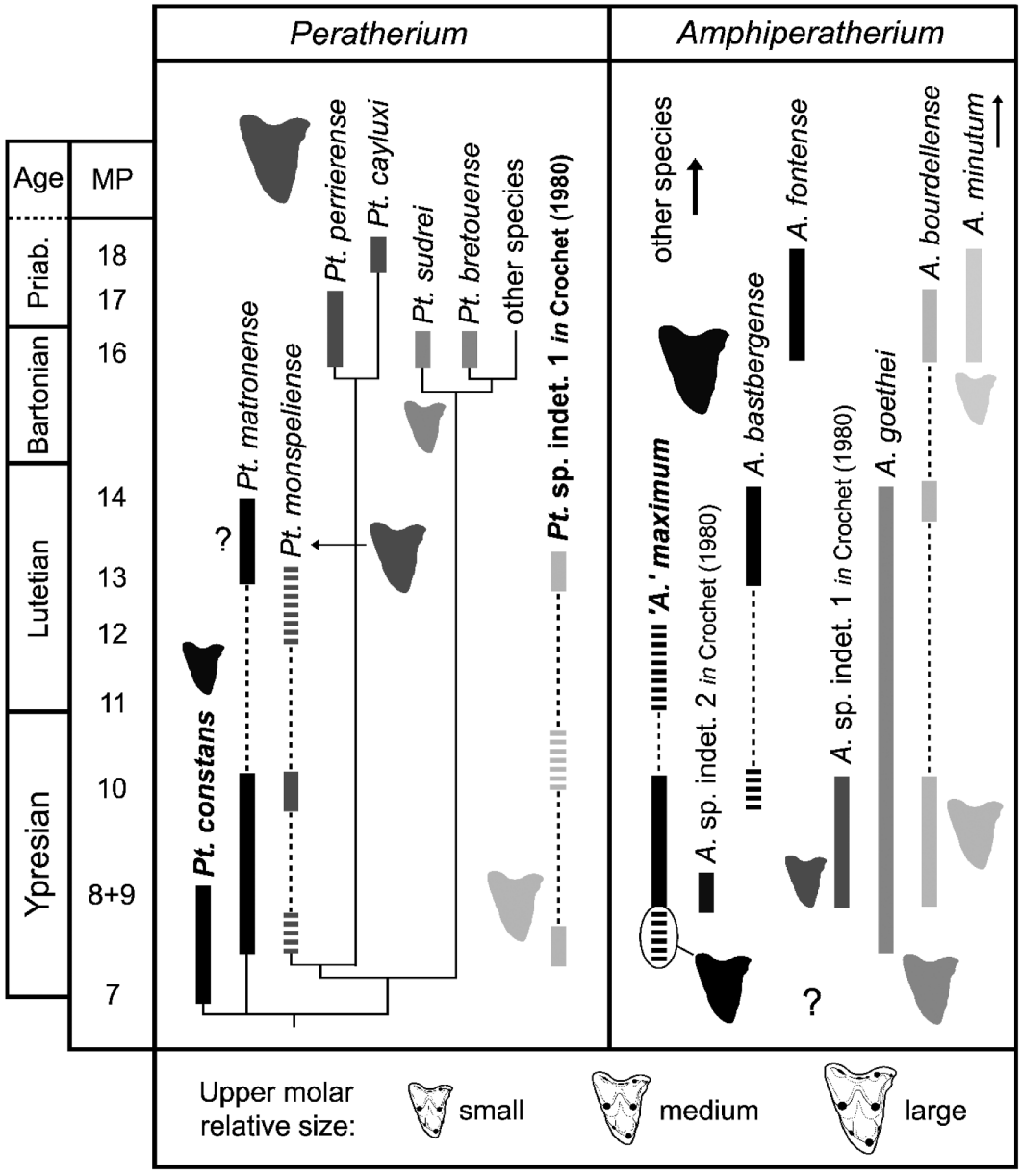

Figure 1. Approximate temporal extensions of most European *Peratherium* – *Amphiperatherium* species during the Eocene (Ypresian to early Priabonian; MP7 to MP18 reference levels, BiochroM'97 1997), as conceived before this work. Within both genera, species plotted with different colours have been allocated to different lineages *sensu* Crochet (1980). All 'lineages' which have been assumed to emerge during the early Eocene are represented. Names in bold indicate the most studied Ypresian species in this work. Dashed temporal extensions indicate occurrences in open nomenclature. Relative sizes, represented by upper molar outlines, follow specific diagnoses of Crochet (1980). Partial hypothetical relationships of *Peratherium* species as proposed by Hooker et al. (2008) are depicted. ?*Peratherium giselense* Heller, 1936, is not included, because its generic status has been disputed (see Kurz 2007). The relative positioning of MP reference levels and Eocene ages follow Speijer et al. (2020). The 'MP15' is not figured, because the Bartonian age of the reference locality of La Livinière 2 has been challenged (e.g. Luccisano et al. 2020). Occurrence data are from Crochet (1980), Godinot (1981), Dégremont et al. (1985), Marandat (1986), Peláez-Campomanes et al. (1989), Storch and Haubold (1989), Sudre et al. (1990), Marandat (1991), Legendre et al. (1992), Kurz (2007), Ladevèze et al. (2012), and Vianey-Liaud et al. (2024). Abbreviation: Priab., Priabonian.

A. maximum – *A. bastbergense* Crochet, 1979 – *A. fontense* Crochet, 1979 (Figure 1) – *A. ambiguum* (Filhol, 1877), which persists until the early Oligocene, according to Crochet (1980: fig. 151).

The taxonomy and intrasubfamilial relationships of peratheriines remain particularly unclear between the MP7 and MP8 + 9 reference levels, which is the time interval encompassing the first steps of their evolutionary history, after their appearance in the fossil record (Figure 1). In fact, the temporal resolution of the Ypresian MP reference levels (see BiochroM'97 1997) appears insufficient to describe metatherian evolution, as (i) the range of some species is solely restricted between two reference levels (Gernelle et al. 2024), and (ii) the ages of various southwestern MP7-MP8 + 9 interval localities (i.e. in the time range between MP7 and MP8 + 9, excluding MP7 and MP8 + 9/~MP8 + 9 localities), as deduced from recent bio- and chemostratigraphic analyses, are more accurately estimated, notably relative to the Eocene Thermal Events (ETMs; Yans et al. 2014; Noiret et al. 2016). Furthermore, since the taxonomic revision of Crochet (1980), rare molars from the French localities of the MP7-MP8 + 9 time interval have been allocated to *Amhiperatherium* cf. *maximum* (Godinot 1981; Marandat 1991; Louis 1996), vaguely denoting molars smaller than those of *A. maximum*, but larger

than those of small early peratheriines such as *Peratherium constans* (Figure 1).

In this study, based on both ancient and unpublished dental material, we describe a new morphologically cryptic peratheriine species that is intermediate in size between *Peratherium constans* and '*Amphiperatherium*' *maximum* (the taxonomic status of the latter being discussed). This represents the first new peratheriine species to be described since *Peratherium africanum* Simons and Bown 1984, and is the second oldest early Eocene peratheriine. Secondly, a detailed description of a new mandible of *Peratherium maximum* comb. nov., the most complete specimen known and the first record of this species in southwestern France, compared to (i) the type serie of the species, and (ii) younger peratheriines, is used as a basis in order to thoroughly discuss the problematic generic taxonomy of Peratheriinae. Throughout this work, we also highlight and discuss several dental characters, some of them being correlated, assumed to bear a phylogentic signal in early peratheriines, which is an essential first step towards resolving the complex systematics of this subfamily (Figure 1).

Institutional and locality abbreviations

AMNH, American Museum of Natural History, New York; IRSNB-M, mammal collection of the Royal Belgium Institute of Natural Sciences; MNHN.F., fossil collection of the Muséum National d'Histoire Naturelle, Paris; MNHN.F.AV, Avenay; MNHN.F.CB, Condé-en-Brie; MNHN.F.ME, Meudon; MNHN.F.PY, Pourcy; MNHN.F.RI, Rians; MNHN.F.SN, Soissons; NHMUK.PV.M, palaeontological vertebrate collection of the Natural History Museum, UK, London; NMB Om., Dormaal, collection of the Natural History Museum of Basel; UM-, palaeontological collection of the University of Montpellier; UM-AZI, Azillanet; UM-BOUX, Bouxwiller; UM-BRI, La Borie; UM-CLO, Le Clot; UM-FNR, Fournes; UM-SNB, Sainte-Néboule; UM-VBO, Valbro; UM-VIE, Vielase; USNM, United States National Museum.

Other abbreviations

Dental loci: MX, Xth upper molar; mX, Xth lower molar; pX, Xth lower premolar.

Reference levels, biozones and hyperthermals: ETM2, Eocene Thermal Maximum 2; MP, Mammal Palaeogene reference level (BiochroM'97 1997); PE, Paleocene-Eocene biozone (Hooker 1996a); PETM, Paleocene-Eocene Thermal Maximum.

Measurements and descriptive statistics: L, maximal mesiodistal length; OR, observed range; pL, protocone length; pW, protocone width; S, approximate surface; sL, stylar shelf length; tL, talon length; tlW, talonid width; tlWr, relative talonid width; trW, trigonid width; tW, talon width; W, maximal labiolingual width.

Ages of the localities

The here studied localities of Soissons (in Aisne) and Pourcy (in Marne) in northern France, of Le Clot (in Corbières), Fournes (in Minervois) and Rians (in Provence) in southern France, and of Abbey Wood (in London), are all considered in the time interval between MP7 and ~MP8 + 9 reference levels (Figure 2). Soissons and Le Clot are the oldest of these localities, and are, respectively, placed within and correlated with biozone PE II (Hooker 1996a; Marandat et al. 2012). While the precise age of Soissons is uncertain, Le Clot is positioned by bio- and chemostratigraphic analyses before the ETM2, approximately 1 myr younger than the MP7 reference locality of Dormaal (~56 Ma), hence close to 55 Ma (Yans et al. 2014). Fournes is positioned by marine correlation and chemostratigraphic analysis just after the ETM2 (~54 Ma), closer in time to the MP8 + 9 than to the MP7 reference level (Noiret et al. 2016: Figure 2). Rians is a locality possibly similar in age to Fournes, based on mammalian biostratigraphy (Marandat et al. 2012; Noiret et al. 2016; Philip et al. 2017, p. 328). The age retained for Abbey Wood (biozone PE III of Hooker 1996a) is 55.12 Ma (Hooker 2010), therefore older than Fournes and Rians. These last two thus necessarily correlate with biozone PE III instead of biozone PE II. The precise biochronologic age of Pourcy, ascribed to biozone PE III (Hooker 1996a), remains more controversial (Louis and Michaux 1962); this locality has been alternatively considered closer to MP7 or to MP8 + 9 reference levels (as summarised in Hand et al. [2015, p. 2] and Spijkerman et al. [2015, p. 176]), and its relative biochronologic positioning with respect to Fournes, Rians, and Abbey Wood is lacking.

Biochronologic arguments position La Borie (in Lauragais, near the Saint-Papoul village; Laurent et al. 2010: Figure 1) close to the MP8 + 9 reference level (~MP8 + 9; Laurent et al. 2010). The mammal fauna of Condé-en-Brie (in the Paris Basin) is classically considered close in age to the mammal fauna of Avenay, which is the reference locality of the MP8 + 9 (Louis 1966, BiochroM'97 1997).

Materials and methods

Provenance of the specimens

The specimens from Soissons, Meudon (in Île-de-France; one specimen discussed), Rians, Pourcy, Avenay (two specimens used for comparisons), and Condé-en-Brie are housed in the palaeontological collections of the Muséum National d'Histoire Naturelle (MNHN.F.; Paris, France). The specimens from Le Clot, Fournes, La Borie, Bouxwiller (northeastern France; one specimen used for comparisons), Vielase (in Quercy phosphorites; one specimen used for comparisons), Sainte-Néboule (in Quercy phosphorites), and Valbro (in Quercy phosphorites) are housed at the University of Montpellier (UM-; southern France). The peratheriine hemimandible from La Borie (UM-BRI-17), described and figured in the present study, was found and prepared by one of us (DT). The single specimen from Abbey Wood is housed at the Natural History Museum, London (NHMUK.PV.M; England), and was studied via the photograph and measurements available in the literature (Hooker 2010). Casts of herpetotheriine specimens (AMNH, USNM) housed at the University of Montpellier were used for comparisons with peratheriines. Comparisons and measurements of molars of *Peratherium constans* from Dormaal have been made based on available illustrations from Ladevèze et al. (2012) (seven upper molars measured), and on casts from the University of Montpellier (seven upper molars measured), of which the original specimens are housed in the Royal Belgian Institute of Natural Sciences (IRSNB-M-; Brussels), and in the Natural History Museum of Basel (NMB; Costeur and Schneider 2011).

High-resolution x-ray microtomography

Illustrated specimens were scanned using a µ-CT-scanning station EasyTom 150/Rx Solutions (Montpellier RIO Imaging, ISEM, Montpellier, France) by one of us (KG). Images of these specimens were achieved using the 'snapshot' tool of Avizo® 9.3. Isolated molars were scanned with a resolution between 5.95 µm and 9.09 µm, depending on the specimen. All illustrations of isolated molars are based on volume renderings of the specimens. The hemi-mandible from La Borie (UM-BRI-17) was

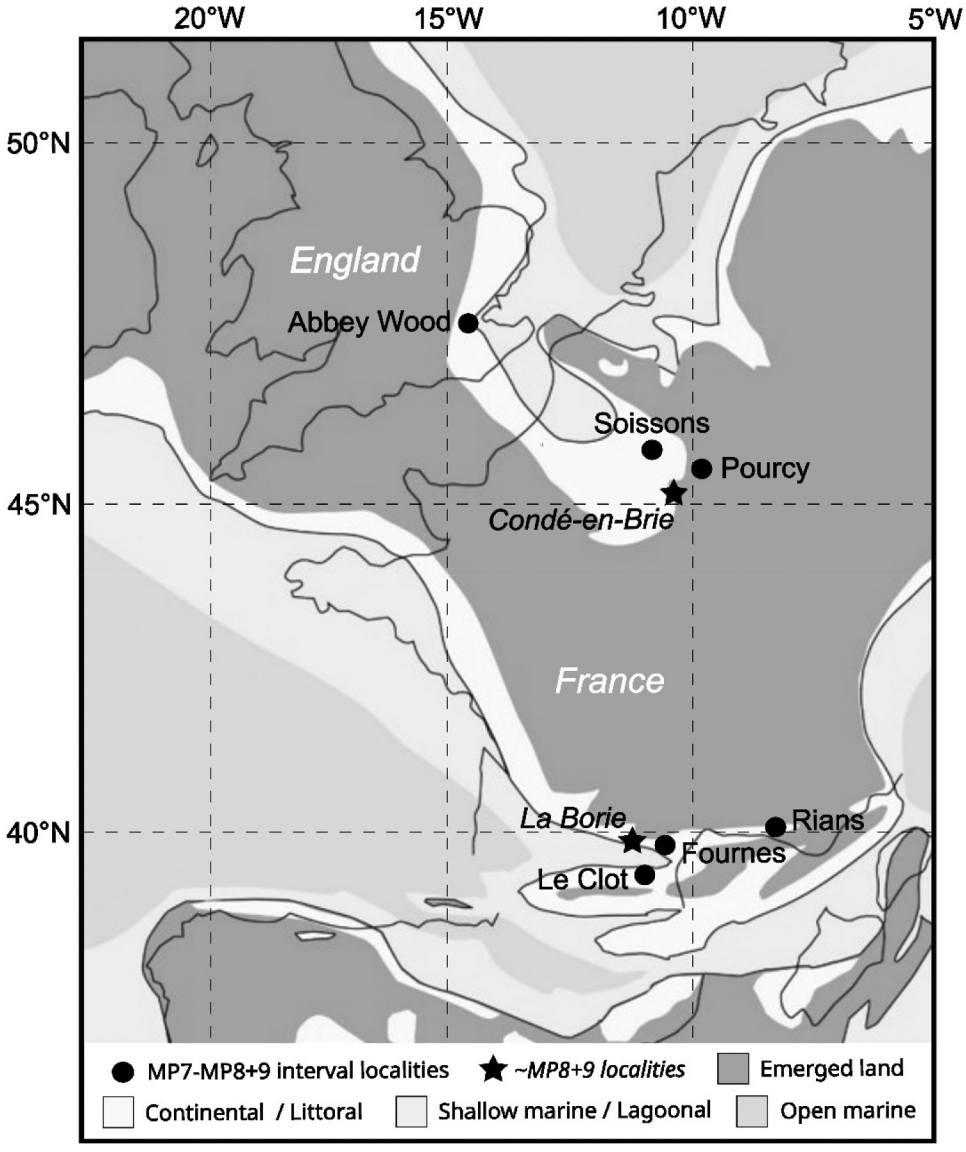

Figure 2. Paleogeographic map of France and England during the early Eocene (modified from Marandat et al. 2012) with the position of MP7-MP8 + 9 interval and ~MP8 + 9 localities studied.

scanned with a resolution of 8.91 µm. The dentaries of the specimens UM-SNB-508 and UM-VBO-128, respectively scanned with a resolution of 9.96 µm and 8.00 µm, were isolated from cheek teeth by segmentation, in order to compare the morphology of their alveoli to those of UM-BRI-17. Volume rendering pictures of the complete UM-SNB-508 and UM-VBO-128 specimens, with the preserved lower cheek teeth, are also available in this study. For each of the three hemi-mandibles, a pre-segmentation of one slice every ~ 5-10 slices was performed, employing the 'lasso', 'magic wand' and 'blow' selection tools of Avizo® 9.3. The smart interpolation tool of the online platform Biomedisa (Lösel et al. 2020) was used to complete each segmentation.

Dental anatomy and measurements

The updated tribosphenic molar nomenclature illustrated in Gernelle et al. (2024: fig. 2) was adopted. Orientation and measurement methods of maximum length and width of tribosphenic upper and lower molars also follow Gernelle et al. (2024: fig. 2); i.e. the paracone – metacone axis of upper molars and the paraconid – metaconid axis of lower molars were used as reference (see Clemens [1966, p. 4] for lower premolars). Mandibular heights were taken on the lingual aspect of the mandible, from its ventral edge to the adjacent dorsal molar alveolus. All measurements are given with an accuracy of 0.01 millimetres. All measurements were made on screenshots of volume rendering or surface models of the scanned specimens (see below), using Avizo® 9.3 (Thermo Fisher Scientific-FEI) measurement tools, and/or via photographs of specimens taken with an optical stereomicroscope (Leica M 205C) connected to a camera (Leica DFC 420C), using tools of the Leica Application Suite v. 4.13.

The peratheriine hemi-mandible from La Borie (UM-BRI-17) was compared in detail with hemi-mandibles of *Peratherium elegans* (Aymard, 1846) (UM-VBO-128, from Valbro) and *Amphiperatherium minutum* (Aymard, 1846) (UM-SNB-508, from Sainte-Néboule), because (i) *Peratherium elegans* is the type species of *Peratherium*, (ii) *A. minutum* was the first species of *Amphiperatherium* with documented intraspecific variation (Crochet 1978), and is the species considered as representing the

genus *Amphiperatherium* in the phylogenetic analysis of Ladevèze et al. (2020), and (iii) *Peratherium elegans* and *A. minutum* were the two first valid species included in *Peratherium* by Aymard (1850, p. 83). These two specimens have been illustrated elsewhere (Crochet 1978, 2016). The maximum anteroposterior length and mediolateral width of each anterior and posterior lower molar alveolus was measured. The anteroposterior alveolus length was taken parallel to the anteroposterior axis of the molar row, and the mediolateral alveolus width was taken perpendicular to the anteroposterior alveolus length.

We accounted for intraspecific variation in the descriptions of dental material based on comparisons with the variation ranges of morphological characters and of size described in the literature for other marsupialiforms, such as *Peradectes* species (Gernelle et al. 2024), *Pucadelphys andinus* Marshall & Muizon, 1988 (Ladevèze et al. 2011), and *Peratherium constans* and *Peratherium elegans* (Ladevèze et al. 2012). Because stylar cusps are often doubled in some peratheriine species, we illustrate the positioning of these additional stylar cusps in Figure 3A–B. Height relationships of stylar cusps were obtained based on upper molars with stylar cusps that were preserved with limited and homogeneous wear.

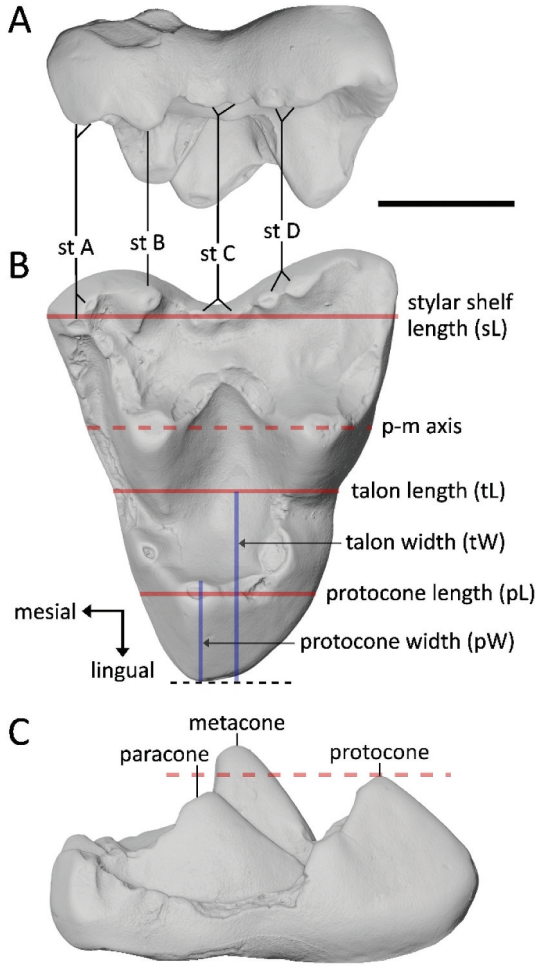

Figure 3. Measurement methods of mesiodistal length (sL, tL, pL) and labiolingual width (tW, pW) of peratheriine upper molars introduced in this study, with the positioning of stylar cusps and main cusps, illustrated on the left M3 MNHN.F. CB1252, *Peratherium maximum* comb. nov. from Condé-en-Brie (~MP8 + 9, Paris Basin), in labial (A), occlusal (B), and mesial (C) views. The arrows indicating the mesial and lingual sides concern the occlusal view (B). The red dashed line in the mesial view (C) is used to compare the heights of the main cusps. Scale bar equals 1 mm. Abbreviations: p-m axis, paracone – metacone axis; st, stylar cusp.

We employed three measurement methods for the mesiodistal length of upper molars, all taken in occlusal view, parallel to the paracone – metacone axis (Figure 3B): (i) the stylar shelf length (sL), which corresponds to the maximum length of upper molars (sL = L); (ii) the talon length (tL), which was taken at the level of the base of the lingual edge of paracone – metacone, always labial to the conules (the talon is sometimes easily distinguishable from the stylar shelf by a distal emargination; Figure 3B); and (iii) the protocone length (pL), which was taken at the level of the apex of the protocone. We also introduce two measurement methods for the labiolingual width of upper molars, taken perpendicular to the paracone – metacone axis (Figure 3B): (iv) the talon width (tW), which extends from the level of the talon length segment to the lingualmost point of the lingual edge of the protocone; and (v) the protocone width (pW), which is the distance between the labialmost point of the protocone apex and the lingualmost point of the lingual edge of the protocone. We performed these five measurements on upper molars of *Peratherium musivum* sp. nov., and on upper molar samples of the type series of *Peratherium constans* (in addition to the single M3 of *Peratherium constans* reported from Fordones, in Corbières; Marandat 1991: pl. 1, figure 6; Gernelle et al. 2024) and *Peratherium maximum* comb. nov., including the holotype specimens of these three species. The sL/tL, sL/pL, tL/pL, and tW/pW ratios were further calculated (see Supplemental material 1) and compared via Welch's *t*-test (see below for statistical procedure performed).

Quantitative analysis based on isolated lower molars

All isolated lower molars of *Peratherium maximum* comb. nov. from Condé-en-Brie, from the MNHN Palaeontology collection, reviewed by one of us (KG), were attributed to a given locus (m1 to m4) and measured. In addition to the measured length (L), width (W), and width of the talonid (tlW), the approximate surface area of lower molars (S) was calculated with the formula: S = L/2 * trW + L/2 * tlW, where trW represents the labiolingual width of the trigonid. In fact, (i) the width of the trigonid and of the talonid can differ between molar loci, and (ii) the trigonid and talonid are here assumed to represent approximately half of the total molar length each in early peratheriines. Finally, the relative labiolingual width of the talonid (tlWr) was calculated comparing the talonid width to the approximate surface, as follows: tlWr = tlW/S. Detailed measurements of L, W, trW, and tlW, and calculated values of L/W ratios and tlWr are available in Supplemental material 2. Statistical analysis of the data was done using the R software environment (v.4.3.3; R Core Team 2024). Welch's ANOVA (*W*-test) were performed in order to detect if one or more significant differences occur between means of a given descriptive variable, between lower molar loci (as recommended in Delacre et al. 2019). Multiple comparisons testing was carried out using Games-Howell post-hoc tests, as recommended in Ruxton and Beauchamp (2008), in order to identify which pairs of lower molar loci significantly differ ($p < 0.05$) in length, width and approximate surface area, and additionally in both absolute and relative width of the talonid. Results of the Games-Howell tests are available in Supplemental material 3. The Welch's ANOVA and Games-Howell post-hoc tests were conducted with the function *oneway* of the R package *userfriendlyscience* (Peters 2017). Boxplots were produced using the R package *ggplot2* (Wickham 2016). For each molar locus, all values (including talonid width values) were normally

distributed with the exception of the width of m3 (Shapiro-Wilk normality test; W = 0.84, $p = 0.018$) and the relative width of the talonid of m3 (Shapiro-Wilk normality test; W = 0.87, $p = 0.046$).

Systematic palaeontology

Metatheria Huxley, 1880
Marsupialiformes Vullo, Gheerbrant, Muizon & Néraudeau, 2009
Notometatheria Kirsch, Lapointe & Springer, 1997
Herpetotheriidae (Trouessart, 1879)
Peratheriinae Ladevèze, Selva & Muizon, 2020
Peratherium Aymard, 1850

Remark on generic abbreviation

We use the abbreviation '*Pt.*' for the genus *Peratherium* in order to avoid confusion with species of the genus *Peradectes*, the latter being mentioned for comparative purposes in this study. In fact, the type species of these genera have the same species name: *Peratherium elegans* and *Peradectes elegans* Matthew & Granger, 1921.

Peratherium musivum sp. nov.

LSID urn:lsid:zoobank.org:act:7BC0CE7D-3D4C-46E2-AD86-4E56716F799A
Figures 4A–B, 4E–G, 4I–M, 4P, 5A–M

1980 - *Amphiperatherium* sp. indet. 2 in Crochet p. 137–138 (in part, specimens from Soissons and Rians).
1980 - *Peratherium* sp. indet. 1 in Crochet p. 213–214, fig. 237 (in part, specimen from Soissons).
1981 - *Amphiperatherium* cf. *maximum* Crochet in Godinot p. 54–55, figs. 4c, f.
1981 - *Amphiperatherium goethei* Crochet in Godinot p. 54, fig. 4d.
1991 - *Amphiperatherium* sp. indet. cf. *A.* cf. *maximum* in Godinot 1981, in Marandat p. 72–73, pl. 1, fig. 15.
1996 - *Amphiperatherium* cf. *maximum* Crochet in Louis p. 94, pl. 2, fig. 6.

Nomenclatural remark

This new species must be referred to as *Peratherium musivum* Gernelle, 2024, following the article 50.1 and the recommendation 50A concerning multiple authors of the International Code of Zoological Nomenclature (ICZN 1999, p. 52).

Remark on generic attribution

The rationale for the attribution of this new species to the genus *Peratherium* is detailed in discussion.

Etymology

From the latin word '*musivum*' meaning 'mosaic'. Refers to: (i) the size of the species, larger than the earliest peratheriine species *Peratherium constans* and smaller than the younger '*Amphiperatherium*' *maximum*, purported earliest *Amphiperatherium* species; and (ii) the morphological characters partly shared with *Pt. constans* and/or '*A.*' *maximum*.

Holotype

MNHN.F.SN122, right M3 (Figures 4I-K, P; Crochet 1980: fig. 237). A 3D surface model of this specimen is available on the online platform MorphoMuseuM (Lebrun and Orliac 2016).

Type locality

Soissons (Aisne, Paris Basin, northern France).

Other localities

Le Clot (Corbières), Fournes (Minervois), Rians (Provence), all in southern France; Pourcy (Paris Basin) in northern France.

Age

MP7-MP8 + 9 interval; from between the PETM and ETM2 (~55 Ma), based on the age of Le Clot (Yans et al. 2014), to at least consecutively to the ETM2 (~54 Ma), based on the age of Fournes (Noiret et al. 2016). Biozones PE II to PE III (Hooker 1996a; Marandat et al. 2012).

Material

Additional material from Soissons: left M3 (MNHN.F.SN14), right m1 (MNHN.F.SN2507; Louis 1996: pl. 2, fig. 6).

Material from Le Clot: trigonid of right m2 or m3 (UM-CLO-50), fragmentary talonid of right m2 or m3 (UM-CLO-51).

Material from Fournes: right m3 (UM-FNR-23; Marandat 1991: pl. 1, fig. 15).

Material from Rians: stylar shelf of right M1 (MNHN.F.RI296; Godinot 1981: fig. 4c), distal fragment of left M2 (MNHN.F.RI220), left m1 (MNHN.F.RI385; Godinot 1981: fig. 4d), right m2 (MNHN.F.RI368; Godinot 1981: fig. 4f). 3D surface models of the four specimens from Rians are available on MorphoMuseuM.

Material from Pourcy: right m2 or m3 with fragmentary talonid (MNHN.F.PY18003).

Differential diagnosis

Peratheriine markedly larger than *Pt. constans* (~ twice the surface area of molars) and *Pt. matronense* Crochet, 1979, and markedly smaller than *Pt. maximum* comb. nov. Differs from *Pt. constans*, *Pt. matronense*, and *Pt. maximum* comb. nov. in having stylar cusp C apex more ventral than stylar cusp B and D apices on M3 (or as ventral for stylar cusp B). Further differs from *Pt. constans* and *Pt. matronense* in having (i) stylar cusp D apex more ventral than stylar cusp B and C apices on M1; and (ii) lingual edge of the hypoconulid much longer than its labial edge on m1. Further differs from *Pt. constans* in (i) lacking the deep distal emargination of M2 crown in occlusal view; and probably (ii) in having a relatively slightly larger protocone – talonid functional complex. Further differs from most *Pt. maximum* comb. nov. specimens in lacking the frequent duplication of stylar cusp D.

Comparative description

Upper molars. Only four upper molars are reported so far. M1 is only documented by the right labial fragment MNHN.F.RI296, which preserves a worn paracone, metacone and centrocrista (Figure 4A–B). As on all peratheriine upper molars, including the other upper molar loci of *Pt. musivum* sp. nov., the centrocrista is strongly V-shaped, and its most labial point, lingual to stylar cusp C, does not reach the stylar line. Along the stylar line, only stylar cusps C and D, and the labial edge of stylar cusp B are well preserved, the rest of stylar cusp B being worn (Figure 4B). The labiolingually shallow metastylar area, in addition to the short preparacrista connected to stylar cusp B, are characteristic of M1 (Figure 4A). The M1 is similar in length to the two M3s (Table 1). Such similar length values between molar loci also occur in other early Eocene peratheriine species (e.g. *Pt. monspeliense* Crochet 1979, 1980: table 37). Similar to M1 of the larger *Pt. maximum* comb. nov. (e.g. MNHN.F.PY18001 from Pourcy, here reported; Figure 4C–D), the ectoflexus is mesiodistally short, and its most lingual point is slightly mesiolabial to stylar cusp C, the latter being intermediate in position between stylar cusps B and D on the stylar line. Moreover, the height relationships of stylar cusps of the M1 of the two species are the same, as

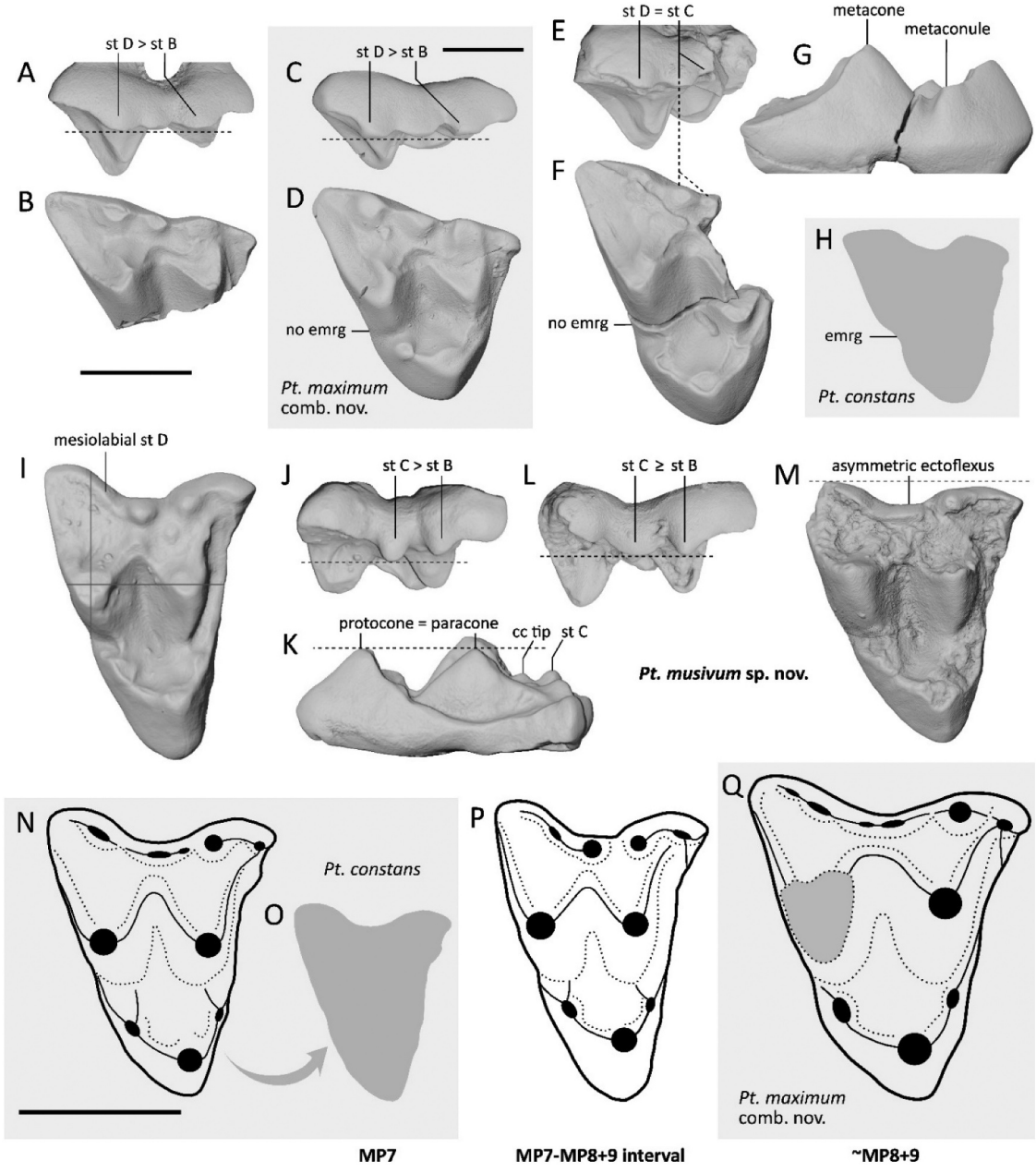

Figure 4. Upper molars of *Peratherium musivum* sp. nov. from MP7-MP8 + 9 interval localities of Rians (Provence) and Soissons (type locality; Paris Basin, Aisne), compared with upper molars of *Pt. constans* Teilhard de Chardin, 1927, from Dormaal (MP7; Belgium) and of *Pt. maximum* comb. nov., from Pourcy (MP7-MP8 + 9 interval; Paris Basin) and Condé-en-Brie (~MP8 + 9; Paris Basin). A-B. MNHN.F.RI296, labial half of right M1 of *Pt. musivum* sp. nov. in labial (A) and occlusal (B) views. C-D. MNHN.F.PY18001, left M1 of *Pt. maximum* comb. nov. in labial (C) and occlusal (D) reversed views. E-G. MNHN.F.RI220, fragment of left M2 of *Pt. musivum* sp. nov., which lacks the paracone and parastylar wing, in labial (E), occlusal (F) and distal (G) reversed views. H. Outline of IRSNB-M-1, right M2 holotype of *Pt. constans*, in occlusal view. Adapted from Ladevèze et al. (2012: fig. 1a). I-K. Holotype of *Pt. musivum* sp. nov., MNHN.F.SN122, right M3 in occlusal (I), labial (J) and mesial (K) views. L-M. MNHN.F.SN14, left M3 of *Pt. musivum* sp. nov. in labial (L) and occlusal (M) reversed views. N-O. Interpretative drawing (N) and outline (O) (differing in scale) of reversed occlusal view of IRSNB-M-2030, left M3 of *Pt. constans*, adapted from Ladevèze et al. (2012: fig. 4Cb). P. Interpretative drawing of occlusal view of MNHN.F.SN122, right M3 holotype of *Pt. musivum* sp. nov. Q. Interpretative drawing of occlusal view of MNHN.F.CB198, right M3 holotype of *Pt. maximum* comb. nov., based on a cast. Light grey boxes concern *Pt. constans* and *Pt. maximum* comb. nov. specimens. Scale bars equal 1 mm. The scale bar below B. applies to all except C.-D. And N. Abbreviations: cc tip, centrocrista tip; emrg, distal emargination; st, stylar cusp.

follows: D > C > B >> A (see also Crochet 1980: fig. 106a, when correctly oriented). Stylar cusp B is thus not dominant in height on M1 in *Pt. musivum* sp. nov. and *Pt. maximum* comb. nov (see also Crochet 1980, p. 101, bottom). The same height relationships of stylar cusps B and D are recovered on M1s of *A. bastbergense* and *A. fontense* (pers. obs. KG; Crochet 1979, p. 372). Stylar cusps B and D are subequal in length, and stylar cusp C is shorter on MNHN.F.RI296. The distal crest of stylar cusp D is long. From the distolabial corner of the crown to the base of the metacone, the distal edge of the stylar shelf is straight, as in *Pt. maximum* comb. nov., and unlike most *Pt. constans* (Ladevèze et al. 2012: fig. 5A-C) and *Pt. matronense* (Crochet 1980: fig. 157b) M1s, in which it is curved.

The unique M2 of *Pt. musivum* sp. nov. is a relatively large distal fragment of upper molar, which lacks the mesial part of the stylar shelf; i.e. the paracone, parastylar wing, and stylar cusps

A and B (MNHN.F.RI220; Figure 4E-G). Because the paracone is not preserved in MNHN.F.RI220, the most accurate orientation of this specimen (depending on the paracone – metacone axis) is unclear. It is here figured in the position in which the paraconule is slightly more labial than the metaconule (Figure 4F), as on most early Eocene peratheriine upper molars when the paracone and metacone are aligned (pers. obs. KG). MNHN.F.RI220 is also damaged between the stylar shelf and the talon; it was thus probably slightly narrower than measured here (Table 1). This specimen is similar in width to the narrowest of the two M3s (MNHN.F.SN14; Table 1). MNHN.F.RI220 most likely represents an M2 rather than an M1 or an M3, because the distance between the metacone apex and stylar cusp D (i.e. the labiolingual width of the metastylar wing) is greater than in M1; thus the postmetacrista is longer (Figure 4F vs Figure 4B), and the talon is relatively mesiodistally longer and more rounded than on M3 (Figure 4F vs Figure 4I,M). Furthermore, the ectoflexus is deep labial to stylar cusp C, as on M2 of *Pt. constans* (Figure 4H), and unlike on peratheriine M1s (see above). The protocone is lower than the metacone (Figure 4G). A preparaconular crista and a short postparaconular crista reaching the lingual part of the base of the paracone are present. The metaconule has a premetaconular crista and a faint postmetaconular crista distinguishable in distal view, in which the fossa between the metaconule and the metacone base appears deep (Figure 4G). In occlusal view, the distal emargination of the crown is lacking on MNHN.F.RI220, as on M2 of *Pt. maximum* comb. nov. (pers. obs. [KG] of the specimen figured in Crochet 1980: fig. 107) and of *Pt. matronense* (Crochet 1980: fig. 158b), and unlike on M2 of *Pt. constans* (Figure 4F vs Figure 4H). Although this trait is subject to intraspecific variation in peradectid species (Gernelle et al. 2024), the presence of a distal emargination on unworn upper molars is diagnostic of several peratheriine species such as *Pt. constans* (on M1 and M2) and *Pt. bretouense* Crochet 1979 (pers. obs. [KG] of their type series, from Dormaal and Le Bretou, respectively). Labial to the centrocrista, stylar cusp C is doubled. Of the two small cusps in the C position (i.e. slightly mesiolabial to slightly distolabial to the most labial point of the centrocrista; Clemens 1966, p. 3), the distal one is larger (i.e. longer, wider and higher) (Figure 4E-F). This distal cusp is as high as stylar cusp D (Figure 4E), but, as on M1, the latter is mesiodistally longer. Stylar cusp D is directly labial to the metacone apex, also as on M1.

Two M3s are documented; both are from Soissons. They are larger than the M3s of *Pt. constans* and smaller than the M3s of *Pt. maximum* comb. nov. (Figure 4O vs Figure 4P vs Figure 4Q). MNHN.F.SN14 is slightly mesiodistally longer and labiolingually narrower than the holotype MNHN.F.SN122 (Table 1). The procumbent protocone of MNHN.F.SN122 is as high as the paracone in distal view (Figure 4K) (the protocone of MNHN.F.SN14 is worn). The protocone of MNHN.F.SN122 is labiolingually wider than that of MNHN.F.SN14 (Figure 4I vs Figure 4M). The metacone is the highest of the three principal cusps. It is mesiodistally longer than the paracone. Note that the principal cusps and conules are worn on the holotype, so that only the outlines of the conules are preserved. The conules have the same relative sizes as on upper molars of *Pt. constans* (Figure 4N vs Figure 4P) (this is also true for the conules of the M2). The most labial point of the centrocrista forms an accessory cusp, which is lower than the almost adjacent stylar cusp C (Figure 4K). Such an accessory cusp is also observed on M3 of *Pt. constans* (Ladevèze et al. 2012: fig. 5H). A faint distal emargination is present on the crown of the holotype, in occlusal view. The labial end of the long preparacrista is directed towards stylar cusp A, as on M3 of other peratheriine species (e.g. Figure 4N, Figure 4P-Q; Ladevèze et al. 2012: fig. 7a-b). The postmetacrista is transversely oriented on M3. Stylar cusp A is strictly mesial to stylar cusp B on MNHN.F.SN14 (Figure 4M), whereas it is mesiolabial to stylar cusp B on the holotype (Figure 4I,P). Stylar cusps A and B are connected by a crest. The distance between stylar cusps A and B does not differ from that of other peratheriine species (Figure 4P vs Figure 4N, Q; *contra* Crochet 1980, p. 214). Stylar cusp B is positioned directly labially to the paracone apex, as in all known early Eocene herpetotheriids. On both M3s of *Pt. musivum* sp. nov., stylar cusps B and C are not connected, while stylar cusps C and D are connected by a crest (Figure 4M,P), similar to, for example, *A. bastbergense* M3s (Crochet 1979: fig. 8). Stylar cusps B and C are much smaller than the paracone. Stylar cusp C is conical on MNHN.F.SN122 (Figure 4J), and crescentiform on MNHN.F.SN14 (Figure 4L). Both M3s have a high stylar cusp C, of which the apex is more ventral than the apex of stylar cusp B on MNHN.F.SN122 (Figure 4J), and as ventral as the apex of stylar cusp B on MNHN.F.SN14 (Figure 4L). The height relationships of stylar cusps of *Pt. musivum* sp. nov. M3, which differs from the ones of the M1, are as follows: C ≥ B >> D ≥ A. In the same way, the stylar height relationships differ between successive upper molar loci in other peratheriine species, such as the similarly-sized *A. bastbergense* and *A. fontense* (Crochet 1979, p. 372). By contrast, stylar cusp B is dominant in height on the M3 of *Pt. constans* and of *Pt. maximum* comb. nov (e.g. Figure 3A; Crochet 1980: fig. 108a). Although stylar cusp D is long in *Pt. musivum* sp. nov., it is not doubled, unlike stylar cusp D of various upper molars of *Pt. maximum* comb. nov. (Figure 4P vs Figures 3B, 4Q), and rare upper molars of *Pt. constans* (pers. obs. [KG] of a cast of the M3 IRSNB-M-1331). Stylar cusp D is positioned mesiolabially to the metacone apex on MNHN.F.SN122, and is directly labial to the metacone apex on MNHN.F.SN14 (Figure 4P vs Figure 4M). A similar variation in the relative positioning of stylar cusp D exists also on M3 of *Pt. maximum* comb. nov. (pers. obs. KG). The ectoflexus of M3 is deep, long and asymmetric. Because the metastylar wing is much more labially projected than the parastylar wing on MNHN.F.SN122 (Figure 4I), the asymmetry of its ectoflexus is more pronounced than that of MNHN.F.SN14 (Figure 4M). M4 is not yet known.

Lower molars. As for lower molars, the low number of available measurements shows a relative mesiodistal elongation from m1 to m3 (Table 2), whereas there is no apparent elongation of upper molars from M1 to M3 (Table 1). The talonid is similarly sized from

Table 1. Measurements of upper molars of *Peratherium musivum* sp. nov. from the MP7-MP8 + 9 interval localities of Rians (southern France) and Soissons (northern France). Abbreviations: L, length; W, width.

Specimen	Locus	L (mm)	W (mm)	L/W
MNHN.F.RI296	M1	1.91	–	–
MNHN.F.RI220	M2	–	2.40	–
MNHN.F.SN122	M3	1.91	2.67	0.72
MNHN.F.SN14	M3	1.97	2.37	0.83

m1 to m3, but the trigonid labiolingually widens (Table 2), and the trigonid cuspids enlarge (e.g. Figure 5A, D,F). The protoconid is the largest cuspid. The paraconid of the m1 MNHN.F.SN2507 is broken (Figure 5A-B), and the paraconid of the m1 MNHN.F.RI385 is worn (Figure 5H). The precingulid is weakly developed on m1; it is only mesial to the lingual segment of the paracristid on MNHN.F.SN2507, and it is absent on MNHN.F.RI385 (Figure 5H). A reduced precingulid also occurs at least on one m1 of *Pt. constans* (Ladevèze et al. 2012: fig. 6Ca), and on other lower molar loci of this species (Ladevèze et al. 2012: fig. 6Ga). Although the morphology of the precingulid varies between m2 and m3 specimens, this structure is limited to the mesial edge of the trigonid; its labial extremity terminates mesiolabial to the protoconid apex (i.e. the protoconid is not surrounded by a cingulid). The paracristid is longer than the protocristid. In labial view, the preprotocristid is not as curved as in peradectids (Figure 5B). The distal flank of the paraconid is

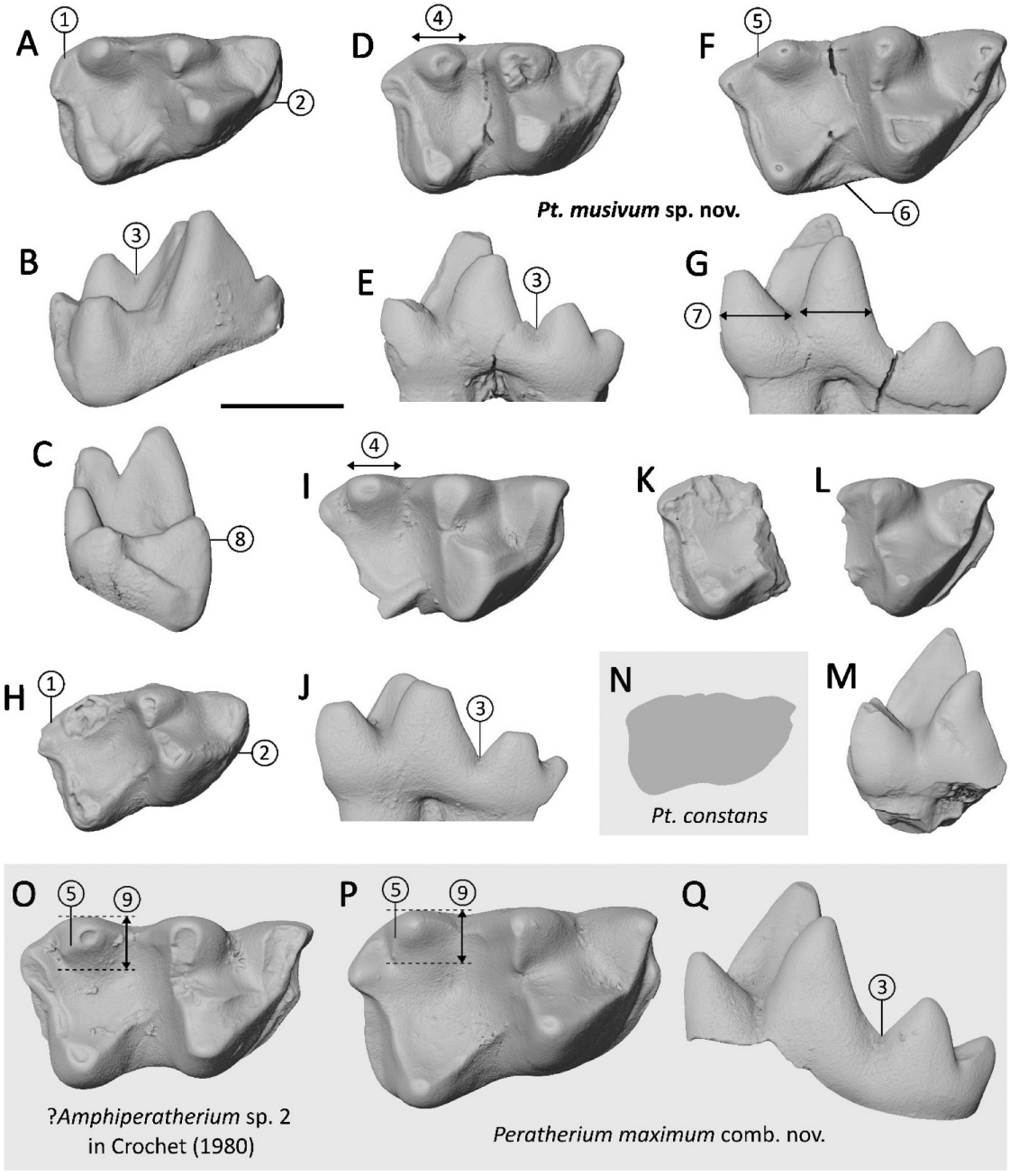

Figure 5. Lower molars of *Peratherium musivum* sp. nov. from MP7-MP8 + 9 interval localities of Soissons and Pourcy, in the Paris Basin, and Rians, Fournes and Le Clot in southern France (A-M), compared with lower molars of selected peratheriines (N-Q). A-C. MNHN.F.SN2507, right m1 in occlusal (A), labial (B) and distal (C) views. D-E. MNHN.F.RI368, right m2 in occlusal (D) and lingual (E) views. F-G. UM-FNR-23, right m3 in occlusal (F) and lingual (G) views. H. MNHN.F.RI385, left m1 in reversed occlusal view. I-J. MNHN.F.PY18003, partial right m2 or m3 in occlusal (I) and lingual (J) views. K. UM-CLO-51, talonid of right m2 or m3 in occlusal view. L-M. UM-CLO-50, trigonid of right m2 or m3 in occlusal (L) and lingual (M) views. N. Outline of a complete left m2 of *Pt. constans* Teilhard de Chardin, 1927, from Le Clot, in reversed occlusal view. O. MNHN.F.AV6789, left m3 of ?*Amphiperatherium* sp. indet. 2 in Crochet (1980), in reversed occlusal view. p-Q. MNHN.F.PY18002, left m2 of *Pt. maximum* comb. nov., in occlusal (P) and lingual (Q) reversed views. Light grey boxes concern *Pt. constans*, ?*Amphiperatherium* sp. indet. 2 and *Pt. maximum* comb. nov. specimens. Scale bar equals 1 mm. Significance of labelled characters studied in the main text: 1. Long lingual edge of the hypoconulid (asymmetric hypoconulid). 2. Weak to absent precingulid. 3. Short and/or shallow metaconid – entoconid notch. 4. Long entoconid. 5. Postentocristid. 6. Wide hypoflexid. 7. Paraconid as long as metaconid. 8. Hypoconid lower than entoconid. 9. Large (wide and long) and lingually convex entoconid.

Table 2. Measurements of lower molars of *Peratherium musivum* sp. nov. from the MP7-MP8 + 9 interval localities of Soissons and Pourcy (northern France), and Rians, Fournes and Le Clot (southern France). *, fragmentary specimen, probably slightly longer than measured. Abbreviations: L, length; tlW, talonid width; trW, trigonid width; W, width.

Specimen	Locus	L (mm)	W (mm)	L/W	trW (mm)	tlW (mm)
MNHN.F.SN2507	m1	1.90	1.24	1.53	1.03	1.22
MNHN.F.RI385	m1	1.73	1.19	1.45	0.99	1.15
MNHN.F.RI368	m2	1.98	1.24	1.60	1.09	1.23
UM-FNR-23	m3	2.35	1.37	1.72	1.29	1.27
MNHN.F.PY18003	m2 or 3	2.04*	–	–	1.21	–
UM-CLO-50	m2 or 3	–	–	–	1.14	–
UM-CLO-51	m2 or 3	–	–	–	–	1.19

developed, so that the surface area occupied by the paraconid in occlusal view is greater than the surface area occupied by the metaconid. The metaconid is longer than the paraconid on m1 and m2 (e.g. Figure 5E), and is as long as the paraconid on m3 (Figure 5G). The metaconid is positioned almost strictly lingually to the protoconid on all lower molars, as in most herpetotheriid metatherians (e.g. Gernelle et al. 2024: table 6). The lingual opening of the trigonid is as high as the lingual opening of the talonid on m1 and m2 (Figure 5E). This character is indicative of herpetotheriids among Laurasian marsupialiforms (e.g. Gernelle et al. 2024: table 6; pers. obs. KG). The lingual opening of the trigonid is higher than the one of the talonid on m3 (Figure 5G), as in *Pt. maximum* comb. nov (*contra* Marandat 1991, p. 72). A labial emargination of the crown is present on the m1 MNHN.F.RI385 (Figure 5H), and is absent on MNHN.F.SN2507 (Figure 5A). The hypoflexid widens from m1 to m3, so that the labial emargination is also absent on m3 (Figure 5F).

The cristid obliqua is straight and mesially ends labially to the protocristid notch. On the m3 UM-FNR-23, the mesial end of the cristid obliqua is more lingual, closer to the protocristid notch, than on m1, m2, and MNHN.F.PY18003. The hypoconid is not mesiodistally pinched, similar to *Pt. constans* and *Pt. maximum* comb. nov., and unlike, for example, *Pt. elegans* or *A. minutum* (e.g. this study; Ladevèze et al. 2012: fig. 7c-e). The hypoconid apex is positioned labially (Figure 5A) or distolabially (Figure 5D) to the entoconid apex. The entoconid is much higher than the hypoconid on m1 (Figure 5C) and m2, and is only slightly higher than the hypoconid on m3. The entoconid is much mesiodistally longer than the hypoconulid on all specimens (e.g. Figure 5D,I). In labial and lingual views, the entoconid – hypoconulid notch is lower than the metaconid – entoconid notch on m1 and m2 (e.g. Figure 5B,E), and the two notchs are almost as high on m3 (Figure 5G). As a consequence, the m3 UM-FNR-23 is the only lower molar displaying an entoconid with a symmetrical shape in lingual view. It is also the single lower molar of *Pt. musivum* sp. nov. with a labiolingually pinched entoconid, with a sharp postentocristid. The latter cristid has not been described in *Pt. constans* (Ladevèze et al. 2012), but is present in *Pt. maximum* comb. nov. and in ?*Amphiperatherium* sp. 2 in Crochet (1980) from Avenay (Figure 5O-P). On m1, the hypoconulid is relatively labiolingually wider, and with its apex positioned less lingually than on other molar loci. In particular, the lingual edge of the hypoconulid, adorned by a sharp cristid on MNHN.F.SN2507, is labiolingually longer than its labial edge on m1 (Figure 5A,H), whereas the lingual and labial edges are subequal in length on m2 and on m3 (Figure 5D, F,I,K). This asymmetric morphology of the hypoconulid occurs also on m1 and even m2 (e.g. Figure 5P) of *Pt. maximum* comb. nov. (pers. obs. [KG] of the type series from Condé-en-Brie) but not in *Pt. constans* (e.g. Ladevèze et al. 2012: fig. 4Ea). The distolingual edge of the talonid is less and less curved from m1 to m3 (Figure 5A,D,F).

The lower molar from Pourcy (MNHN.F.PY18003, Figure 5I-J) is either an m2 or an m3, which are molar loci of *Pt. musivum* sp. nov. with undocumented morphological and size variation. The distolabial part of the talonid (including the hypoconid, postcingulid, and part of the hypoconulid) is lacking on MNHN.F.PY18003. This specimen is much smaller than lower molars of *Pt. maximum* comb. nov., also present in Pourcy (e.g. MNHN.F.PY18002; Figure 5I-J vs Figure 5P-Q). The entoconid is not lingually convex, similarly to other *Pt. musivum* sp. nov. lower molars, which allows us to allocate MNHN.F.PY18003 to this species with more confidence, instead of to *Pt. maximum* comb. nov. It is worth noting that the entoconid is sometimes weakly lingually convex in *Pt. maximum* comb. nov., and occasionally lingually convex in *Pt. constans* (Ladevèze et al. 2012: fig. 4Fa). MNHN.F.PY18003 is closer in mesiodistal length to the single known m2 of *Pt. musivum* sp. nov. (although the length of the latter could be slightly underestimated, due to fragmentation), and is slightly closer to the m3 from Fournes in its absolute trigonid width value (Table 2). The lingual opening of the trigonid much higher than the lingual opening of the talonid resembles an m3, while the entoconid – hypoconulid notch lower than the metaconid – entoconid notch in lingual view better resembles an m2 (Figure 5J).

The right trigonid and talonid fragments from Le Clot represent two distinct specimens morphologically similar to other lower molars of *Pt. musivum* sp. nov. The labiolingual width of the right trigonid (UM-CLO-50, Figure 5L-M) is closer to the width value of the trigonid of the ascertained m2 (Table 2). The metaconid is intermediate in height between the paraconid and the protoconid, and is slightly longer than the paraconid (Figure 5M); the latter character also resembles the condition seen in the m2. The postmetacristid is long. The precingulid is relatively longer and wider than on other lower molars of *Pt. musivum* sp. nov.; the relative size of this structure is known to vary in other marsupialiform species (e.g. Ladevèze et al. 2012: figs. 6–8). The right isolated talonid (UM-CLO-51, Figure 5K) is fragmented at the level of the entoconid. The hypoconulid projects as distally to the postcristid as in other lower molars of *Pt. musivum* sp. nov. and *Pt. constans*, and the postcingulid is labiolingually long. The hypoconulid is more lingually positioned, and its lingual edge is relatively shorter than on m1. UM-CLO-51 represents either an m2 or an m3. The m4 is not yet known, but its talonid is expected to be less labiolingually wide based on the proportions of m4 in other herpetotheriid species.

Additional detailed comparisons

The specimens discussed below which have been attributed to or compared with *Peratherium* sp. indet. 1 in Crochet (1980) are

(except MNHN.F.SN122) provisional undetermined peratheriines. The M3 MNHN.F.SN122, holotype of *Peratherium musivum* sp. nov., was attributed to *Peratherium* sp. indet. 1 by Crochet (1980, pp. 213–214), and compared to the M2 or M3 UM-BOUX-28-L (Bouxwiller, ~MP13), which was placed under the same denomination. The paracone is relatively higher on MNHN.F.SN122, subequal to the protocone instead of lower, and not as low compared to the metacone. Furthermore, stylar cusp C is much higher than stylar cusp D on M3s of *Pt. musivum* sp. nov., whereas stylar cusp C is close in height to stylar cusp D on the specimen from Bouxwiller (pers. obs. [KG] of a cast of UM-BOUX-28-L).

A mesially worn M3 from Azillanet (Minervois, MP10), comparable to MNHN.F.SN122 in size and occlusal outline, was attributed to *Peratherium* cf. *Peratherium* sp. indet. 1 in Crochet (1980) (UM-AZI-1-6; Marandat 1986: pl. 1, fig. 3). *Peratherium musivum* sp. nov. differs notably in having stylar cusp C dominant in size over stylar cusp B, instead of the opposite.

An M3 from Vielase (UM-VIE-104; Quercy, ?MP10-11 interval) was listed as *Peratherium* indet. aff. *Peratherium* sp. indet. 1 in Crochet (1980) (Legendre et al. 1992), possibly because it is similar in size to MNHN.F.SN122, and because stylar cusp C is higher than stylar cusp B. The M3s of *Pt. musivum* sp. nov. differ in the relatively labiolingually narrower stylar shelf, compared to the talon; in having stylar cusp C connected by a crest to stylar cusp D, instead of connected to stylar cusp B on UM-VIE-104; and because stylar cusp D is the lowest stylar cusp, instead of being clearly dominant over the other stylar cusps on UM-VIE-104.

An M2 of *Peratherium* sp. 1 from the Bracklesham Group (Southern England), Dummer's Copse locality DC5iii (MP10) (specimen NHMUK.PV.M50180), was also compared to *Peratherium* sp. indet. 1 in Crochet (1980) from Soissons (i.e. MNHN.F.SN122) (Hooker 1996b, pp. 142–143, pl. 1, fig. 4). The two specimens share a 'larger protocone lobe' according to Hooker (1996b), although they do not represent the same molar locus. The proportions of the talon of the two specimens actually differ greatly, the talon of MNHN.F.SN122 being relatively labiolingually wider than the talon of the English specimen. The protocone of both specimens is not particularly relatively larger than the protocone of M2 or M3 belonging to other early Eocene peratheriines (*contra* Hooker 1996b). This is also true when considering the protocone of the *Pt. musivum* sp. nov. M2 MNHN.F.RI220, which is relatively larger than the one of the M3 MNHN.F.SN122.

An M3 from Avenay of *Amphiperatherium* sp. indet. 1 in Crochet (1980) (MNHN.F.AV18005, Crochet 1980: fig. 41) displays a stylar cusp C that is higher than stylar cusps B and D (pers. obs. KG), as in *Pt. musivum* sp. nov. Such a low stylar cusp B would be indicative of the genus *Amphiperatherium* according to Hooker et al. (2008). Molars of *Pt. musivum* sp. nov. are much larger than those of *Amphiperatherium* sp. indet. 1, MNHN.F.AV18005 being approximately as small as M3s of *Pt. constans* (Crochet 1980: table 6).

The m1 MNHN.F.SN2507 from Soissons was initially attributed to *Amphiperatherium* sp. indet. 2 by Crochet (1980, pp. -137–138), and specimens from Rians here reallocated to *Pt. musivum* sp. nov. were suggested as being possibly related to *Amphiperatherium* sp. indet. 2 (*sensu* Crochet 1980) by Godinot (1981, p. 55). *Amphiperatherium* sp. indet. 2 includes specimens smaller than '*A.*' *maximum* according to Crochet (1980). The only specimen found in the MNHN collections which was still referred to this taxon is the m3 MNHN.F.AV6789 (Figure 5O; L = 2.38 mm; W = 1.44 mm; trW = 1.33 mm in occlusal view). Interestingly, the widest lower molar of *Pt. musivum* sp. nov. (UM-FNR-23) is slightly smaller than the specimen from Avenay, while one relatively small m2 of *Pt. maximum* comb. nov. from Pourcy (MNHN.F.PY18000, see below) is slightly larger. It should be mentioned that MNHN.F.AV6789 is distolabially damaged; it was thus probably slightly larger. The entoconid of lower molars of *Pt. musivum* sp. nov. has a straight lingual edge, whereas the lingual edge of the entoconid is convex on MNHN.F.AV6789 (Figure 5O), similar to most m2s and m3s of *Pt. maximum* comb. nov. (e.g. Figure 5P).

Molars of *Pt. musivum* sp. nov. differ from those of *Peratherium* cf. *monspeliense* from Fournes and La Gasque (Minervois; Marandat 1991, pp. 70–71), notably in being markedly larger and in having a stylar cusp B that is non-dominant in height.

Peratherium musivum sp. nov. is closer in size to the large peratheriine *A. bastbergense*, but is still markedly smaller (Tables 1–2 vs Crochet 1980: table 15) (in turn, most molar loci are smaller in *A. bastbergense* than in '*A.*' *maximum*, based on available mean values). M3s of *Pt. musivum* sp. nov. have stylar cusp C as high as or higher than stylar cusp B instead of a dominant stylar cusp B (e.g. Figure 4J, L vs Crochet 1980: fig. 114a), and all lower molars, including the talonid fragment from Le Clot (UM-CLO-51; Figure 5K) have a relatively mesiodistally shorter hypoconulid (e.g. Figure 4A, D vs Crochet 1980: figs. 116–117).

Peratherium musivum sp. nov. differs from the early Eocene herpetotheriines such as the *Herpetotherium* species (*sensu* Korth 2008; Williamson et al. 2012) *H. knighti* (McGrew, 1959) and *H. edwardi* (Gazin, 1952), notably in having: (i) M3 with a deeper ectoflexus; (ii) M1 to M3 with a stylar cusp D most often directly labial instead of always mesiolabial to the metacone apex; (iii) stylar cusp C dominant in height on M3; and (iv) lower molars with an entoconid not convex lingually (e.g. Gazin 1952: pl. 1, figs. 3-4; McGrew et al. 1959: fig. 3; Krishtalka and Stucky 1983a: figs. 1-2; Murphey et al. 2018: figs. 11–12; pers. obs. [KG] of casts of the *H. knighti* holotype AMNH 55684, and of the *H. edwardi* holotype USNM 19206 and specimen USNM 19200).

Peratherium cf. *musivum* sp. nov.

1998 - *Amphiperatherium maximum* Crochet? in Hooker p. 449.
2005 - *Amphiperatherium maximum* Crochet? in Hooker et al. p. 84.
2010 - *Amphiperatherium* sp. 2 in Hooker p. 17, Figure 8q.

Locality and age

Abbey Wood (England, London); MP7-MP8 + 9 interval, PE III biozone, 55.12 Ma according to Hooker (2010).

Material

right p2 (NHMUK.PV.M60002; Hooker 2010: fig. 8q).

Remarks

Lower premolars of peratheriine species differ mostly in size. Hooker (2010, p. 17) stated that the large procumbent peratheriine p2 from Abbey Wood (NHMUK.PV.M60002) is possibly about the right size (L = 1.90 mm, W = 0.66 mm; data from Hooker 2010) to belong to *Pt. maximum* comb. nov., then documented solely by isolated molars. The p2 of *Pt. maximum* comb. nov. from La Borie (see below; Figure 6A) is much wider and slightly longer, and its p3 is even larger (Table 3). In particular, the width value of NHMUK.PV.M60002 is closer to the one of the p2 of the small *Amphiperatherium* sp. 1 from Abbey Wood (Hooker 2010: fig. 8n-p; L = 1.30 mm, W = 0.52 mm), of which the molars are somewhat close in size to those of *Pt. constans* (= *A.* '*brabantense*') and *Pt. matronense* (Hooker 2010, p. 16), than to the one of *Pt. maximum* comb. nov. (W = 0.91 mm; Table 3). Furthermore, the observed range of the width of the three lower

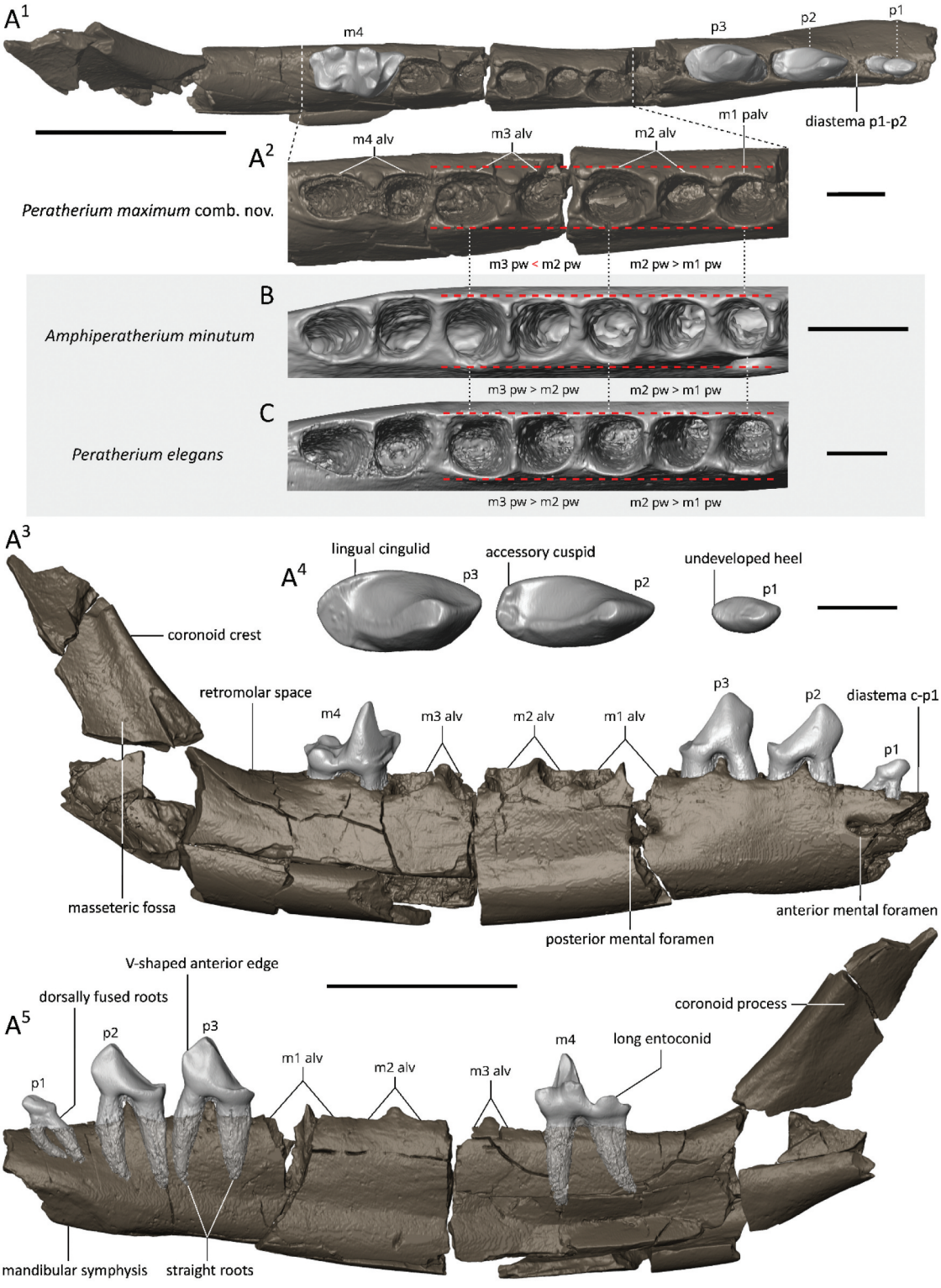

Figure 6. Right hemi-mandible fragment with p1-p3, alveoli of m1-m3, and m4 (UM-BRI-17) of *Peratherium maximum* comb. nov., from La Borie (~MP8 + 9; southern France, Lauragais) (A^1-A^5) compared with selected late Eocene – Oligocene representatives of *Amphiperatherium* and *Peratherium* (B-C, grey boxes). A. 3D surface model of UM-BRI-17 in occlusal (dorsal) view (A^1), with a close-up on m1 to m4 alveoli (with m4 removed) in occlusal view (A^2), in labial (lateral) view (A^3), with a close-up on p1-p3 in occlusal view (A^4) and in lingual (medial) view, with the roots of the preserved cheek teeth superimposed (A^5). B. Reversed occlusal view of the alveoli of m1 to m4 (molars removed) of a 3D surface model of the left hemi-mandible UM-SNB-508, *Amphiperatherium minutum* (Aymard, 1846), from Sainte-Néboule (Quercy; late Eocene, MP18). C. Reversed occlusal view of the alveoli of m1 to m4 (molars removed) of a 3D surface model of UM-VBO-128, *Pt. elegans* (Aymard, 1846), from Valbro (Quercy; early Oligocene, MP22). The red parallel dotted lines (A^2, B, C) are positioned on the lingual and labial margins of the largest alveolus of each dentary (posterior alveolus of m2 for *Pt. maximum* comb. nov.; posterior alveolus of m3 for *A. minutum* and *Pt. elegans*). Scale bars: A^1., A^3., A^5., 5 mm; A^2., A^4., B., C., 1 mm. Abbreviations: alv, alveoli; palv, posterior alveolus; pw, posterior alveolus width.

Table 3. Measurements of lower cheek teeth of UM-BRI-17, *Peratherium maximum* comb. nov., from La Borie (Lauragais, ~MP8 + 9). The m4 measurements are compared to observed ranges of m4s of *Pt. maximum* comb. nov. from Condé-en-Brie ($N = 8$; this study). Abbreviations: CB, Condé-en-Brie; cH, crown height; L, length; OR, observed range; W, width.

Locus	L (mm)	W (mm)	L/W	cH (mm)
p1	0.87	0.47	1.85	0.61
p2	2.00	0.91	2.20	1.51
p3	2.07	1.04	1.99	1.62
m4	2.48	1.34	1.85	1.80
OR m4 CB	2.38-2.72	1.25-1.45	1.75-1.90	–

premolars of *Amphiperatherium* sp. 1 from Abbey Wood is low (Hooker 2010, p. 16). However, NHMUK.PV.60002 is closer in length to the *Pt. maximum* comb. nov. p2 than to the *Amphiperatherium* sp. 1 p2. The lower premolar from Abbey Wood could thus represent *Pt. musivum* sp. nov., which is smaller than *Pt. maximum* comb. nov., and of which the description is solely based on isolated molars. For this last reason, the specimen from Abbey Wood is left in open nomenclature.

Peratherium maximum (Crochet, 1979) comb. nov.
Figures 4C-D, 4Q, 5 P-Q, 6 A, 7D-K

Remark on specimens studied
Only the new hemi-mandible from La Borie is described and compared below. The allocated material from Pourcy is compared with *Pt. musivum* sp. nov. above. All lower molars and 18 upper molars of *Pt. maximum* comb. nov. from the type locality (Condé-en-Brie) are studied in the Results section. The redefinition and thorough revision of *Pt. maximum* comb. nov., also abundant in various ~MP8 + 9 Paris Basin localities, and present in slightly younger localities (Crochet 1980; Louis and Laurain 1983; Hooker 1996b), is beyond the scope of this study.

Remark on generic attribution
The former inclusion of the species '*A.*' *maximum* in the genus *Amphiperatherium* is challenged in this study. It is tentatively included in *Peratherium*. This point is developed in discussion.

Holotype
MNHN.F.CB198, right M3 (Figure 4Q; Crochet 1979: fig. 7; 1980: fig. 108; L = 2.53 mm, W = 2.91 mm).

Type locality
Condé-en-Brie (Paris Basin, Aisne); middle early Eocene (~MP8 + 9).

Referred material and measurements
Material from Pourcy (MP7-MP8 + 9 interval; PE III biozone): left M1 (MNHN.F.PY18001, L = 2.6 mm, W = 2.66 mm), left m2 (MNHN.F.PY18000, L = 2.41 mm, W = 1.56 mm; MNHN.F.PY18002, L = 2.56 mm, W = 1.65 mm). The m2s were probably studied by Crochet (1980: table 14).

Material from La Borie (southern France, Lauragais; ~MP8 + 9): fragment of right hemi-mandible with p1-p3, alveoli of m1-m3, and m4 (UM-BRI-17) (measurements in Tables 3–4). A 3D surface model of this specimen is available on MorphoMuseuM.

Comparative description of the hemi-mandible from La Borie
UM-BRI-17 is the first early Eocene peratheriine specimen with multiple preserved premolars, and the first *Pt. maximum* comb. nov. specimen preserving associated cheek teeth (Figure 6A). It also first documents the morphology of the lower premolars and of the dentary of this species.

Lower molar
The specific attribution solely lies on the size and morphology of the m4, the unique molar preserved on the specimen. The anterior root of the m4 is dorsoventrally straight, and the ventral end of its posterior root is slightly curved, directed posteroventrally (Figure 6A[5]). The length and width values of the m4 of UM-BRI-17 fit within the observed range obtained for the eight m4s of *Pt. maximum* comb. nov. from Condé-en-Brie (Table 3), and are much higher than those of the only other peratheriine lower molar from La Borie (*Amphiperatherium bourdellense* Crochet 1979, from 'Saint-Papoul' in Crochet [1980: table 7]). The long crescentiform entoconid (Figure 6A[5]), with sharp pre-entocristid and postentocristid, is characteristic of m4 of *Pt. maximum* comb. nov (Crochet 1979, p. 372, 1980: fig. 113). The talonid is relatively labiolingually wide for a peratheriine m4 (Figure 6A[1]), a feature also found on the m4s from Condé-en-Brie (e.g. Figure 7J; Crochet 1980: fig. 113). The m4s of *A. bastbergense* are indistinguishable in length and width from the m4 of UM-BRI-17 (Crochet 1980: table 15). The talonid of m4 is labiolingually narrower in *A. bastbergense* (Figure 6A[1] vs Crochet 1980: fig. 118), but m4s of *Pt. maximum* comb. nov. from Condé-en-Brie with a relatively narrow talonid also exist (e.g. MNHN.F.CB4178). However, the entoconid is not crescentiform in *A. bastbergense* m4 (Crochet 1980: fig. 118).

Lower premolars
The complete p1 is minute (Figure 6A), its crown being less than half as long and high, and almost half as wide as the crown of the p2 (Table 3). The p1 of '*Amphiperatherium*' aff. *maximum* from Messel (~MP11) seems relatively longer (Kurz and Habersetzer 2004: fig. 7A), but no measurements are available to confirm it. The other peratheriine p1s known are relatively larger (e.g. Crochet 1980: figs. 139, 217, 232; Storch 1993). This applies particularly to p1 of *Pt. elegans* (Crochet 1980: table 33), of *Amphiperatherium frequens* (von Meyer, 1846) (e.g. Prieto and Rummel 2015: Figure 1A) and of *A. fontense* (pers. obs. [KG] of the holotype), based on the relative size of the alveoli for the last two species. The roots of the UM-BRI-17 p1 are fused close to the base of the crown, whereas the roots of the p2 and of the p3 are unfused (Figure 6A[5]). Unlike peradectids, the roots of the lower premolars are straight rather than curved (Gernelle et al. 2024: table 6), with the exception of the anterior root of the p1, which is curved so that its ventral extremity is almost in contact with the ventral extremity of the straight posterior root (Figure 6A[5]). In occlusal view, only the main cuspid and its distal cristid are distinct on the p1, there is no developed distal heel cuspid, unlike on the p2 and the p3 (Figure 6A[4]). The p1 and the p2 are more procumbent than the p3, because their respective mesial edge is positioned more dorsomesially to the ventralmost point of the

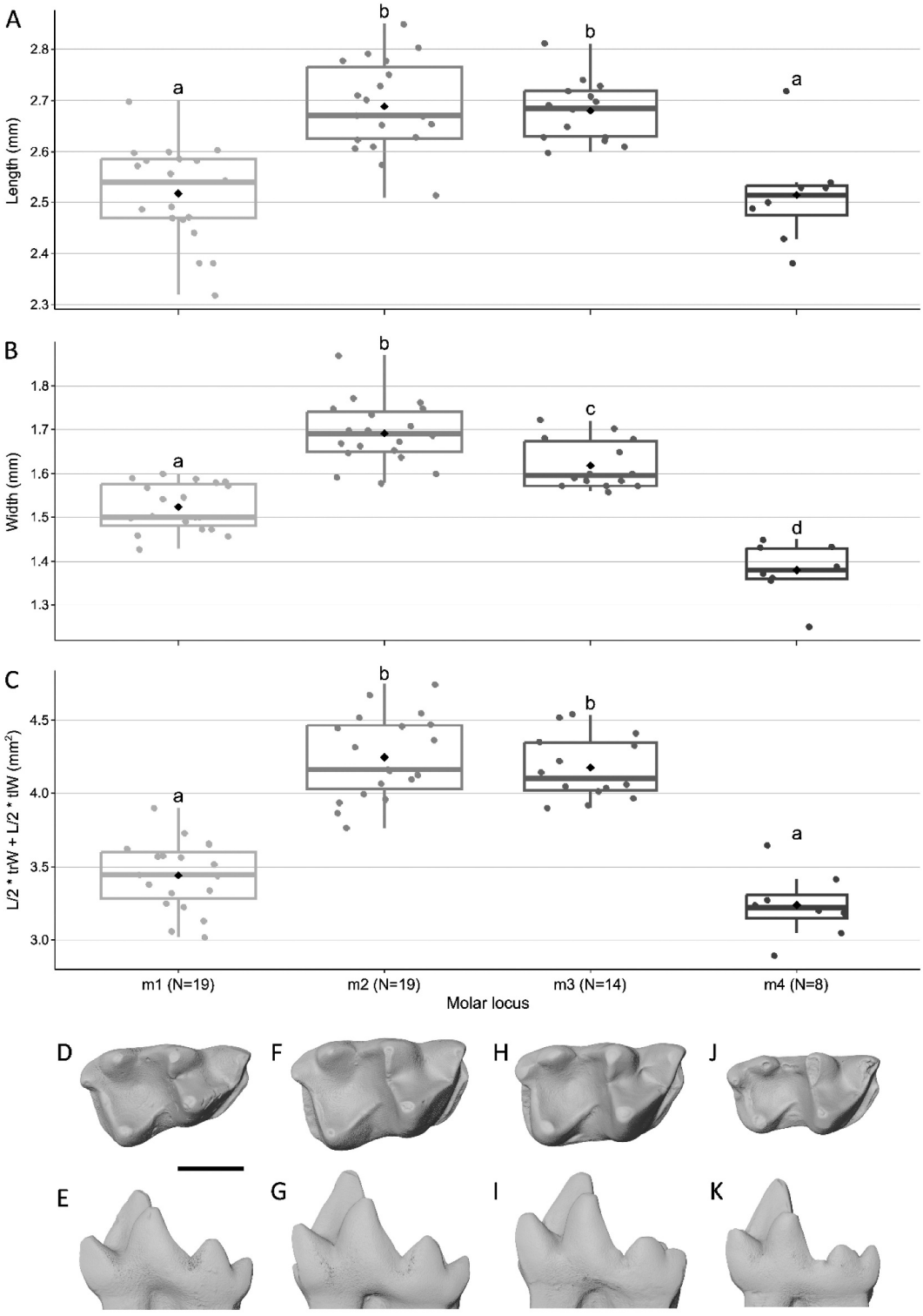

Figure 7. A-C. Boxplots of length (A), width (B) and estimated surface area (L/2*trW+L/2*tlW) (C) of isolated m1s, m2s, m3s and m4s of *Peratherium maximum* comb. nov. from Condé-en-Brie (~MP8 + 9, Paris Basin). The lower molar loci mean values that statistically significantly differ (Games-Howell tests, $p < 0.05$; see main text) are signalled by a difference in the letter ('a' to 'd') above each box. Detailed measurements or calculated values are available in Supplemental material 2. D-K. Series of isolated lower molars of *Pt. maximum* comb. nov. from Condé-en-Brie (type locality; ~MP8 + 9). D-E. MNHN.F.CB2933, right m1 in occlusal (D) and lingual (E) views. F-G. MNHN.F.CB3421, right m2 in occlusal (F) and lingual (G) views. H-I. MNHN.F.CB4977, left m3 in occlusal (H) and lingual (I) reversed views. J-K. MNHN.F.CB820, left m4 in occlusal (J) and lingual (K) reversed views. Scale bar equals 1 mm. Abbreviations: L, length; N, numbers of specimens by group; trW, trigonid width; tlW, talonid width.

anterior root (Figure 6A[3], A[5]). The p3 crown (when not tilted backwards, see below) is as weakly procumbent as on the p3 of *Pt. constans* (Ladevèze et al. 2012: fig. 3Db) and of *A. minutum* (see discussion). In labial and lingual view, the mesial edge of each lower premolar, especially of the p1 and of the p3, is V-shaped (Figure 6A[3], A[5]). The p1 and the p2 are separated by a short diastema (L = 0.65 mm), which is slightly longer than the diastema between the lower canine and the p1. The p1-p2 diastema in

'*Amphiperatherium*' aff. *maximum* from Geiseltal-Untere Mittelkohle (Germany, MP12) is almost three times longer than on UM-BRI-17 according to the measurements of Storch and Haubold (1989, p. 98). An inter-alveolar septum, instead of a diastema, separates the posterior root of the p2 from the anterior root of the p3 (Figure 6A[1]). The p3 is higher than the p2 (Figure 6A[3], A[5]; Table 3). The premolars are relatively long, especially the p2, which is more than two times longer than wide (Table 3), but it is not blade-like *sensu* Muizon and Ladevèze (2022, p. 611). Two cuspids are present on the distal edge of the heel of the p2 (Figure 6A[4]). The larger one is connected to the distal cristid of the main cuspid. The smaller adorns the distolingual cingulid, which connects the two heel cuspids (Figure 6A[4]). Such accessory heel cuspids sometimes occur in other peratheriines (e.g. Hooker 2010: fig. 8n-p) and in peradectids (Gernelle et al. 2024: fig. 6a). The heel of the p3 is worn. The lingual cingulid of the p3 is more developed than that of the p2 (Figure 6A[4]). In occlusal view, the mesial edge of the p2 is straight, whereas the mesial edge of the p3 is curved mesially (Figure 6A[4]).

Dentary

Compared to the p1 and the p2, the p3 (when considering both the crown and the roots) is tilted backwards compared to the antero-posterior axis of the dentary (Figure 6A[5]). The retromolar space is slightly shorter than the mesiodistal length of the m4. These two characters indicate that UM-BRI-17 probably belonged to a relatively aged peratheriine individual (see Crochet 1980, p. 35, fig. 5). The ramus mandibularis is partially preserved, represented by fragments of the masseteric fossa and coronoid process, and the dorsal part of the coronoid crest (Figure 6A[3], A[5]). The corpus mandibularis is slender; it is transversely damaged at the level of the anterior root of the m1, and at the level of the anterior root of the m3; its ventral margin is slightly convex. Two mental foramina are present. The anterior one is positioned ventrally to the posterior alveolus of the p1, and the dorsal one is ventral to the anterior alveolus of the m1 (Figure 6A[3]). The deepest point of the dentary is located between below the posterior alveolus of the m2, and below the anterior alveolus of the m3 (h = 4.10 mm; Figure 6A[5]), resembling the condition found in, for example, some pucadelphyids (Muizon and Ladevèze 2022, p. 629). The dentary is only slightly shallower below alveoli of the m4, and is distinctly shallower below alveoli of the premolars (h = 3.05 mm below p2). The posterior extremity of the unfused and shallow mandibular symphysis is preserved. It extends posteriorly to a point approximately ventral to the anterior root of the p2 (Figure 6A[5]). The mandibular symphysis terminates more posteriorly, below the interalveolar septum of the p2, below the posterior root of the p2, or below the anterior root of the p3, in younger peratheriine species for which the symphysis is illustrated (see also Horovitz et al. 2008, p. 133), namely *Amphiperatherium exile* (Gervais, 1848–1852) (Crochet 1980: fig. 140), *Peratherium elegans* (Crochet 1980: fig. 207c), *Peratherium perrierense* Crochet, 1979 (Crochet 1980: fig. 232c), and *Pt. africanum* (Simons and Bown 1984: fig. 2A). The dentary is thicker at the level of the dorsal margin of the symphysis. In medial view, a faint groove extends from a point below the posterior root of the p3 to posteriorly to the m4 (Figure 6A[5]; the junction between the corpus and ramus mandibularis is fragmentary), and as such resembles the mylohyoid groove of the pucadelphyid *Incadelphys* Marshall & Muizon, 1988, (Muizon and Ladevèze 2022, p. 630, fig. 10C-D).

Lower molar alveoli

In peratheriines, the posterior alveoli of m1 to m3 are labiolingually wider than the respective anterior alveoli (Table 4). The posterior alveolus of the m2 is the widest lower molar alveolus of UM-BRI-17 (Figure 6A[2]). The width values of the posterior alveolus of lower molars are ordered as follows for this specimen: pw m2 > m3 > m1 > m4 (Table 4). In *Pt. macgrewi*, Bown, 1979, among the earliest herpetotheriines, the posterior alveolus of the m2 is also the widest molar posterior alveolus, based on an edentulous dentary (Beard and Dawson 2009: fig. 5). In the specimens of *A. minutum* and *Pt. elegans* studied here, the posterior alveolus of the m3 is the widest (Figure 6B-C), and the corresponding width values for the molar rows are ordered as follows: pw m3 > m2 > m4 ≥ m1 (Table 4). On UM-BRI-17, the posterior alveoli of the m2 and the m3 are similar in length, whereas that of the m3 is longer on UM-SNB-508 and UM-VBO-128 (Table 4). The longest posterior alveolus is that of the m2on UM-BRI-17, and that of the m4 on UM-SNB-508 and UM-VBO-128 (Table 4). The alveoli of lower molars of *Pt. maximum* comb. nov. have a relatively mesiodistally elongated, oval aspect (Figure 6A[2]), the length of each alveolus (except the anterior alveolus of the m4) being much greater than their respective labiolingual widths (Table 4). In contrast, the alveoli of UM-SNB-508 (*A. minutum*) and of UM-VBO-128 (*Pt. elegans*) are round (Figure 6B-C); their length and width measurements are subequal, except for the posterior alveolus of the m4 of UM-SNB-508, and the anterior alveolus of the m2 and posterior alveolus of the m4 of UM-VBO-128, for which L – W ≥0.10 mm (Table 4). The total length of the m2 alveoli of UM-BRI-17 is 2.32 mm, hence longer than its m4 alveoli (2.22 mm). Comparatively, the total length value of the m2 alveoli of '*Amphiperatherium*' aff. *maximum* from Geiseltal-Untere Mittelkohle (MP12) is slightly lower than

Table 4. Measurements (in mm) of lower molar alveoli of UM-BRI-17, *Peratherium maximum* comb. nov., from La Borie (Lauragais, ~MP8 + 9), compared to those of UM-SNB-508, *Amphiperatherium minutum* (Aymard, 1846), from Sainte-Néboule (Quercy; late Eocene, MP18), and of UM-VBO-128, *Peratherium elegans* (Aymard, 1846), from Valbro (Quercy; early Oligocene, MP22). The greatest length and width values for the posterior alveoli of each specimen are in bold. Abbreviations: A, anterior; alv, alveolus; L, maximum length; P, posterior; W, maximum width.

	m1		m2				m3				m4			
	P alv		A alv		P alv		A alv		P alv		A alv		P alv	
Specimen	L	W	L	W	L	W	L	W	L	W	L	W	L	W
UM-BRI-17	1.15	0.84	1.01	0.80	**1.27**	**0.95**	-	0.82	1.25	0.90	0.88	0.82	1.22	0.75
UM-SNB-508	0.51	0.51	0.55	0.53	0.58	0.60	0.58	0.59	0.63	**0.63**	0.55	0.59	**0.66**	0.52
UM-VBO-128	0.86	0.83	0.96	0.86	0.98	0.98	0.96	0.88	1.04	**1.01**	0.99	1.03	**1.12**	0.87

the one of its m4 alveoli (Storch and Haubold 1989, p. 98), which corresponds to an m2 shorter or as long as the m4. Based on available X-ray illustrations, the m2 of '*Amphiperatherium*' aff. *maximum* from Messel seems also shorter than its m4, unlike *Pt. maximum* comb. nov. from La Borie (Kurz and Habersetzer 2004: fig. 7D).

Results

Comparisons of upper molar length and width measurement ratios between selected early peratheriine species

Stylar shelf to talon length ratio values (sL/tL; Table 5) show considerable overlap between *Pt. constans* and *Pt. maximum* comb. nov. for M3. Corresponding values for *Pt. musivum* sp. nov. fit within the observed ranges (OR) of the last two species. The sL/tL values of M2 and M3 of *Pt. maximum* comb. nov. are comparable in OR and mean, whereas the talon of M3 is somewhat longer, relatively to the stylar shelf and on average, than M2 talon in *Pt. constans* (Welch's *t*-test; $t = 2.80$, d.f. = 12.51, $p = 0.016$).

As for stylar shelf to protocone length ratio values (sL/pL; Table 5), the OR of M3 of *Pt. constans* is included in the one of M3 of *Pt. maximum* comb. nov.; the mean value of *Pt. constans* being higher (although fewer specimens are known). The sL/pL values of M3 of *Pt. musivum* sp. nov. are slightly lower than the corresponding (i) mean of *Pt. maximum* comb. nov. (but are included in its OR) and (ii) any values of *Pt. constans*; a similar pattern is recovered for talon to protocone length values (tL/pL), but those of *Pt. musivum* sp. nov. are slightly closer to the mean value of *Pt. maximum* comb. nov. (Table 5). The sL/pL values significantly differ between (i) M2 of *Pt. constans* and of *Pt. maximum* comb. nov. (Welch's *t*-test; $t = 4.53$, d.f. = 9.97, $p = 0.001$), M2 of the latter having a longer protocone relatively to the stylar shelf; and (ii) M2 and M3 of *Pt. maximum* comb. nov. (Welch's *t*-test; $t = 2.21$, d.f. = 11.78, $p = 0.048$), M2 also having a relatively longer protocone than M3 in this species.

As for talon to protocone length values (tL/pL; Table 5), the same two conclusions regarding the length of the protocone of *Pt. maximum* comb. nov. (here relatively to the talon length) are drawn (Welch's *t*-tests; $t = 4.75$, d.f. = 9.29, $p = 0.001$ for M2 of *Pt. constans* vs *Pt. maximum* comb. nov.; $t = 3.07$, d.f. = 10.95, $p = 0.011$ for M2 vs M3 of *Pt. maximum* comb. nov.); thus the protocone of M2 of *Pt. maximum* comb. nov. appears relatively longer than that of its M3 and *Pt. constans* M2. Such a difference of relative protocone length between M2 and M3 is not recovered in *Pt. musivum* sp. nov., based on the three known specimens (Table 5), and in *Pt. constans* (e.g. for tL/pL: Welch's *t*-test; $t = -1.39$, d.f. = 12.89, $p = 0.187$). Finally, mean tL/pL values also significantly differ between M3 of *Pt. constans* and *Pt. maximum* comb. nov. (Welch's *t*-test; $t = 3.06$, d.f. = 13.98, $p = 0.009$). The single tL/pL value available for M2 of *Pt. musivum* sp. nov. is between the lowest corresponding values of *Pt. constans* M2, and the highest value of *Pt. maximum* comb. nov. M2, which slightly overlap.

Based on talon to protocone width values (tW/pW; Table 6), *Peratherium maximum* comb. nov. upper molars have, on average, a significantly relatively wider protocone than those of *Pt. constans* (Welch's *t*-tests; $t = 4.30$, d.f. = 8.79, $p = 0.002$ for M2; $t = 2.70$, d.f. = 10.75, $p = 0.021$ for M3), with almost no overlap between M2 ratio values of the two species. A Welch's *t*-test yielded no significant difference in tW/pW values between M2 and M3 of *Pt. maximum* comb. nov. ($t = -2.15$, d.f. = 12.14, $p = 0.052$). However, because width ratio values are not normally distributed for M2 (Shapiro-Wilk normality test; $W = 0.79$, $p = 0.018$), it is noteworthy that a significant difference is recovered with a non-parametric test (Wilcoxon-Mann-Whitney test; $W = 14$, $p = 0.034$) instead. The tW/pW values of M2 and M3 of *Pt. constans* do not differ, and those of *Pt. musivum* sp. nov. fit within the OR of respective loci of *Pt. maximum* comb. nov., but not within those of *Pt. constans* (Table 6), as for ratios involving the length of the protocone of M3 (Table 5).

Quantitative analysis based on isolated lower molars of Peratherium maximum *comb. nov.*

The m2s and m3s of *Pt. maximum* comb. nov. from Condé-en-Brie do not significantly differ in mesiodistal length (Supplemental material 3: Figure S1) or estimated surface area (Supplemental material 3: Figure S4), so do m1 and m4 for these variables (Figure 7A,C; Supplemental material 3). The m2 and m3 are significantly longer and have a larger surface area than m1 and m4. The m1 and m4 overlap m2 and m3 in length; this overlap is lesser for the estimated surface area (even absent between m4 and m2-m3; Figure 7C). All molar loci differ significantly from one another in width (Supplemental material 3: Figure S2) and talonid width (Supplemental material 3: Figure S3). Isolated m2s are the widest based on mean values (Figure 7B). The mean width and talonid width values are ordered as follows for isolated lower molars: m2 > m3 > m1 > m4 (Figure 7B; Supplemental material 3: Figure S6A); a relationship identical to that recovered based on the molar posterior alveoli of UM-BRI-17 (see above; Table 4). Furthermore, it is worth mentioning that the relative talonid width (tlWr) values of m2 and m3 significantly differ (Supplemental material 3: Figure S5), tlWr values being higher for m2 on average (Supplemental material 3: Figure S6B).

Remark

In *Peratherium maximum* comb. nov., m3s are sometimes difficult to distinguish from m2s or m4s. Here, lower molar loci have been confidently identified using the following characters. From m1 to m4: in occlusal view (Figure 7D,F,H,J), (i) the trigonid

Table 5. Comparison of stylar shelf length to talon length, stylar shelf length to protocone length, and talonid length to protocone length ratios, between *Peratherium musivum* sp. nov. and samples of *Peratherium constans* Teilhard de Chardin, 1927, and *Pt. maximum* comb. nov. from Condé-en-Brie (~MP8 + 9), for M2 and M3. Detailed values of calculated ratios are presented in Supplemental material 1. Abbreviations: N, number of specimens; OR, observed range; pL, protocone length; sL; stylar shelf length; tL, talon length.

			sL/tL		sL/pL		tL/pL	
Locus	Species	N	OR	Mean	OR	Mean	OR	Mean
M2	*Pt. constans*	8	1.61-1.85	1.73	2.15-2.90	2.52	1.28-1.62	1.46
	Pt. musivum sp. nov.	1	–	–	–	–	1.33	–
	Pt. maximum comb. nov.	9	1.53-1.71	1.64	1.83-2.25	2.03	1.15-1.32	1.24
M3	*Pt. constans*	7	1.49-1.72	1.60	2.26-2.79	2.44	1.38-1.65	1.53
	Pt. musivum sp. nov.	2	1.60-1.64	–	2.13-2.21	–	1.34-1.35	–
	Pt. maximum comb. nov.	9	1.56-1.75	1.64	1.97-2.87	2.25	1.26-1.64	1.37

Table 6. Comparison of talon width to protocone width ratios, between *Peratherium musivum* sp. nov. and samples (also studied in Table 5) of *Peratherium constans* Teilhard de Chardin, 1927, and *Pt. maximum* comb. nov. from Condé-en-Brie (~MP8 + 9), for M2 and M3. Detailed values of the calculated ratios are presented in Supplemental material 1. Abbreviations: N, number of specimens; OR, observed range; pW, protocone width; tW, talon width.

			tW/pW	
Locus	Species	N	OR	Mean
M2	*Pt. constans*	7	1.92-2.52	2.14
	Pt. musivum sp. nov.	1	1.85	–
	Pt. maximum comb. nov.	9	1.59-1.92	1.70
M3	*Pt. constans*	7	1.88-2.58	2.22
	Pt. musivum sp. nov.	2	1.69-1.84	–
	Pt. maximum comb. nov.	8	1.63-2.28	1.88

becomes labiolingually wider relative to the talonid (and the relative talonid width values becomes significantly lower from m1 to m3; Supplemental material 3: Figure S6B); (ii) the protoconid becomes more transversely aligned with the metaconid; (iii) the hypoflexid widens somewhat labiolingually; and (iv) the distolingual edge of the talonid is less and less curved, and the lingual edge of the hypoconulid labiolingually shortens; in lingual view (Figure 7E,G,I,K), (v) the metaconid becomes relatively shorter mesiodistally and the paraconid becomes relatively taller; (vi) the paraconid – metaconid notch becomes open higher relative to the metaconid – entoconid notch; (vii) the entoconid – hypoconulid notch becomes open higher relative to the metaconid – entoconid notch. Finally, (viii) the protoconid is relatively higher on m4; and (ix) the postcingulid is prominent on all molars except m4, on which it is partly developed to completely indistinct (Figure 7J).

Discussion

Reappraisal of the specific status of MP7-MP8 + 9 interval 'larger' peratheriines: phylogenetic, biochronologic, and palaeobiogeographic implications

Characterisation of Peratherium musivum *sp. nov. dental morphology*

The specific attributions of herpetotheriid isolated cheek teeth from the early Eocene are primarily based on size (e.g. Smith and Russell 1992; Smith and Smith 2004; Beard and Dawson 2009, p. 200; Hooker 2010, p. 17). Similarly, the molars of *Pt. musivum* sp. nov. differ primarily in size (Figure 4O vs Figure 4P vs Figure 4Q), without overlapping, from those of its coeval species, *Pt. constans* and *Pt. matronense*, which are smaller (body mass of ~ 51–56 g using the length of the M3 of *Pt. musivum* sp. nov. in the appropriate predictive equation of Gordon [2003: fig. 7]; vs ~22 g calculated using the length of the M2 holotype of *Pt. constans* [Ladevèze et al. 2012: fig. 1a] in the appropriate predictive equation), and *Pt. maximum* comb. nov., which is larger (body mass of ~120 g, calculated using only the length of the M3 holotype). The matching between isolated lower and upper molars of *Pt. musivum* sp. nov. is thus possible based on the homogeneous size of these elements (e.g. M1 length ≈ m1 length, see Tables 1–2; as in *Pt. maximum* comb. nov., see measurements of MNHN.F.PY18001 above vs m1 measurements in Supplemental material 2). *Peratherium* sp. indet. 1 in Crochet (1980), in which the holotype of *Pt. musivum* sp. nov. (MNHN.F.SN122) was included, does not form a 'monospecific lineage' (*contra* Crochet 1980, p. 217, fig. 239), and contains representatives of presumably two peratheriine species, as Crochet (1980, p. 214) himself suggested (but these are probably not closely related). A relatively large stylar cusp C is not a similarity between MNHN.F.SN122 and *Pt. maximum* comb. nov., because M3s of the latter have a dominant stylar cusp B (Figure 3A; *contra* Crochet 1980, p. 233). The few relevant morphological differences (i.e. the least subjected to intraspecific variation) between molars of *Pt. constans*, *Pt. musivum* sp. nov. and *Pt. maximum* comb. nov. are subtle (see diagnosis of *Pt. musivum* sp. nov.) and mainly concern the distolingual talonid cuspids of the lower molars, and the stylar height relationships and the outline of the upper molars. More specifically, we hypothesise that *Pt. musivum* sp. nov. and *Pt. maximum* comb. nov. are close relatives, because they share the stylar cusp D apex more ventral than stylar cusps B and C apices on M1, the lack of distal emargination of the M2 crown in occlusal view, and the lingual edge of the hypoconulid longer than its labial edge on m1. Formal phylogenetic analyses will be required to test this hypothesised relationship.

The analysis of the three types of ratios calculated using length measurements (Table 5) revealed that shape differences between upper molars of the studied species mainly occur at the level of the protocone, rather than the stylar shelf or the whole talon. According to Godinot (1981, p. 55), (i) the lingual base of the protocone of the M2 MNHN.F.RI220 is less rounded than in M2 of *Pt. maximum* comb. nov., and (ii) the trigonid of the m2 MNHN.F.RI368 is longer than its talonid, whereas the reverse could be true for most lower molars of *Pt. maximum* comb. nov. The latter statement seems difficult to assess, at first, based on the few m2s of *Pt. musivum* sp. nov. and of *Pt. maximum* comb. nov. here illustrated (Figure 5D vs Figures 5P, 7F). If it is true, either the trigonid itself could have become mesiodistally shorter in *Pt. maximum* comb. nov., or the talonid could have become longer. The mesiodistal length of the talonid must be correlated with the length of the protocone, because there is a functional relationship between these structures during molar occlusion (e.g. Johanson 1996, p. 1028 and references therein). The direct comparison of the relative protocone length of M2 of *Pt. musivum* sp. nov. is of limited value here, because, although *Pt. maximum* comb. nov. has a relatively longer M2 protocone than *Pt. constans* on average, the only M2 specimen of *Pt. musivum* sp. nov. does not permit to conclude regarding this locus in this species. However, based on a few specimens, we detected (i) that the relative protocone length of M3 and the relative protocone width of M2 and M3 of *Pt. musivum* sp. nov. are closer to those of *Pt. maximum* comb. nov. (Tables 5 and 6), and (ii) a change in the relative length of the protocone between M2 and M3 in *Pt. maximum* comb. nov., the protocone of M2 (and thus the talonid basin of m2) being relatively longer on average, whereas such a difference has not been noted between these loci in both *Pt. constans* and *Pt. musivum* sp. nov. Thus, *Pt. musivum* sp. nov. (i) possibly exhibits a slight relative enlargement of the protocone/talonid compared to *Pt. constans*, and (ii) possibly lacks the relative enlargement of the protocone/

talonid of its second molars compared to its third molars contrary to *Pt. maximum* comb. nov., although more specimens of *Pt. musivum* sp. nov. will be crucial to characterise with more confidence such slight shape differences between isolated molars.

Biochronologic and palaeobiogeographic considerations

Peratherium musivum sp. nov. is herein recorded in Le Clot, where it is coeval with the small *Pt. constans* (Table 7; Figure 5K-M vs Figure 5N; Marandat et al. 2012, p. 428), a conclusion founded on a few, mostly fragmentary cheek teeth ($N = 2$ out of 10 metatherian specimens). Thus, given the age of Le Clot (see Materials and methods section), peratheriines much larger than *Pt. constans* definitely first occur between the PETM and the ETM2, approximately 1 myr after the appearance of this subfamily in the fossil record of Europe. Perhaps unexpectedly, no metatherian species larger than *Pt. constans* or *Peradectes crocheti* Gernelle, 2024, are recorded from the better sampled (for small mammals) Palette (in Provence; $N > 40$ metatherian specimens) and Fordones ($N > 60$ metatherian specimens) localities, which have been correlated in age with Le Clot based on the exclusive shared occurrences of the two louisinid condylarths *Lessnessina praecipuus* (Russell, 1987) and *Paschatherium plaziati* Marandat, 1989, with Palette, and *Pa. plaziati* in addition to the ischyromyiform rodent *Corbarimys hottingeri* Marandat, 1989, with Fordones (Godinot et al. 1987; Marandat 1991; Marandat et al. 2012; Gernelle et al. 2024: table 1). It should be noted that an undescribed rare second rodent species markedly larger than *C. hottingeri* occurs in Le Clot, the same pattern for Palette, with an undescribed rare species larger than the common *C. cezannei* (Hartenberger, 1987) (Marandat et al. 2012, p. 427). The occurrences of *Pt. musivum* sp. nov. and of *Peradectes crocheti*, restricted to the MP7-MP8 + 9 interval (this study; Gernelle et al. 2024), further highlight the weak resolution of the Ypresian MP reference levels, as currently defined (see BiochroM'97 1997), when it comes to describe evolutionary dynamics of European metatherians. Moreover, the presence of *Pt. musivum* sp. nov. and of *Peradectes crocheti* in mammal faunas older and younger than the ETM2 (this study; Gernelle et al. 2024) strengthens conclusions stating that this hyperthermal event could be unassociated with a significant faunal turnover (Abels et al. 2012), at least in Western Europe (Noiret et al. 2016, p. 478). *Peratherium musivum* sp. nov. is recorded simulteanously in localities from both northern (Soissons, Pourcy, and possibly Abbey Wood) and southern France (Le Clot, Fournes, Rians), which reinforces the absence of apparent biotic provincialism in European metatherians, as proposed in recent studies (Gernelle et al. 2024; Wessels et al. 2024). Unsurprisingly, the absence of provincialism in larger early peratheriine species newly extends to ~MP8 + 9 mammal faunas, because *Peratherium maximum* comb. nov. is herein recorded in La Borie. At this time, the northern/southern provincialism pattern characteristic of most components of the MP7-MP8 + 9 interval eutherian faunas from Western Europe attenuates (e.g. Solé et al. 2014: fig. 11; 2018: fig. 18).

The lower molar MNHN.F.RI385 (Figure 5H) was first attributed to m1 or m2 of *Amphiperatherium goethei* Crochet, 1979 (Godinot 1981, p. 54). It is actually an m1 given the low labiolingual width value of the trigonid compared to the talonid. MNHN.F.RI385 is labiolingually wider and has a more distally projecting hypoconulid (i.e. with a strongly curved postcristid) than m1 of *A. goethei* from its type locality, Bouxwiller (~MP13; Crochet 1980: table 12, fig. 95). Regarding these characters, MNHN.F.RI385 is similar to the m1 MNHN.F.SN2507 and is here allocated to *Pt. musivum* sp. nov. As a result, *A. goethei* becomes absent from Rians and from the whole MP7-MP8 + 9 interval (Table 7), the oldest occurrence of the species now being from Avenay (MP8 + 9; Crochet 1980, p. 89). '*Amphiperatherium*' *maximum* was listed in the Meudon fauna (MP7-MP8 + 9 interval, PE II; Russell et al. 1988). Among the metatherian material from this locality, a single trigonid fragment preserving only complete protoconid and metaconid (MNHN.F.ME15976) is markedly larger, similar to what is expected for a specimen of '*A.*' *maximum*. However, its protoconid and metaconid are subequal in height, which is a character unknown in Laurasian metatherians, but often present in eutherians (see Gernelle et al. 2024, p. 38). Relatively large herpetotheriid species are thus absent from Meudon (Table 7). The earliest occurrence of *Pt. maximum* comb. nov., a species typical of the MP8 + 9 and ~MP8 + 9, is now from the Pourcy fauna (Crochet 1980: table 14; this study), where it is newly coeval with *Pt. musivum* sp. nov. (Table 7), which is recorded only in part of the MP7-MP8 + 9 interval. This unique co-occurrence suggests that the mammal fauna of Pourcy, if homogeneous, could be intermediate in age between Fournes/Rians and Mutigny (the oldest locality younger than MP8 + 9).

Peratherium musivum sp. nov. spans approximately between 1 and 2 myr (depending on the age of the Pourcy fauna) of the fossil record of the early Eocene, during the MP7-MP8 + 9 interval (at least ~ 55-54 Ma based on the respective age of Le Clot

Table 7. Occurrences of peratheriine taxa in MP7 to MP7-MP8 + 9 interval localities, both before and in the present study. Southern France localities and associated occurrences are in italics. Among localities in or correlated with the PE II biozone, only Le Clot is demonstrated to be anterior to the ETM2. Note that the hardly distinguishable *Peratherium constans* Teilhard de Chardin, 1927 (*), and *Peratherium matronense* Crochet, 1979 (bold occurrences) remain unreviewed (see Ladevèze et al. 2012, p. 257). Abbreviations for localities: Aw, Abbey Wood; Clo, Le Clot; Do, Dormaal; Frn, Fournes; Me, Meudon; Py, Pourcy; Ri, Rians; Sn, Soissons.

		MP7	MP7-MP8 + 9 time interval						
		PE I	PE II			PE III			
	Peratheriine taxon	Do	*Clo*	Sn	Me	Aw	*Frn*	*Ri*	Py
Before this study	*Pt. constans** or ***Pt. matronense***	x*	*x**		**cf.**		***cf.***	***x***	
	Pt. sp. 1 in Crochet (1980)			x					
	Amphiperatherium maximum			cf.	x		*cf.*	*cf.*	x
	A. sp. 2 in Hooker (2010)					x			
	Amphiperatherium goethei							*x*	
This study	*Pt. constans** or ***Pt. matronense***	x*	*x**		**cf.**		***cf.***	***x***	
	Peratherium musivum sp. nov.		*x*	x		cf.	*x*	*x*	x
	Peratherium maximum comb. nov.								x

and Fournes). The older faunas of Dormaal (MP7), and Silveirinha (Portugal) and Le Quesnoy (Paris Basin) (both ~MP7) solely yielded smaller herpetotheriids (Nel et al. 1999; Estravís 2000; Ladevèze et al. 2012; pers. obs. [KG] of Le Quesnoy metatherians), and *Pt. musivum* sp. nov. is also absent from the well-sampled faunas of the MP8 + 9 and ~MP8 + 9 localities of the Paris Basin, from which herpetotheriids are abundant (Mutigny, Avenay, Condé-en-Brie, Sables de Brasles, Sézanne-Broyes), following the review of the MNHN mammal collection by one of us (KG). Consequently, among the first ascertained herpetotheriid species, at least some had a relatively short apparent longevity expected for small mammals (e.g. Flynn et al. 1995), including smaller metatherians (e.g. Tarquini et al. 2022: fig. 2), like European peradectids (Gernelle et al. 2024: fig. 16). Such a finding is in line with the median and mean longevity values known for Cenozoic mammal species (e.g. Marshall 2017), and contrasts with the long apparent duration of various Eocene Laurasian mammal species (e.g. Dunn and Townsend 2019, p. 12), such as most Eocene herpetotheriine species (pending further revision) recorded as early as the early Eocene (Krishtalka and Stucky 1983a: fig. 7; Murphey et al. 2018, ~12.4 myr duration for *Herpetotherium marsupium* Troxell, 1923), and unrevised peratheriine species (e.g. *A. bourdellense*; MP8 + 9 to MP16 reference levels; Figure 1).

Investigating significant dental characters: is Amphiperatherium *likely to be represented in the earliest phases of Peratheriinae evolution?*

History and definitions of Amphiperatherium *Filhol, 1879, and the* Peratherium *vs* Amphiperatherium *dichotomy: a critical review*

The taxonomy of peratheriines at the generic level is confusing. Below, we report on the lability of the taxonomic content and of the diagnostic characters of *Amphiperatherium*, which varied over time between authors, with respect to those of *Peratherium*. Three taxonomic groups of peratheriines from the Quercy phosphorites were first envisioned by Filhol (1877, p. 468), namely *Peratherium* as a first group, a second group composed of specimens that do not exhibit the characters of *Peratherium* (probably later designated as *Amphiperatherium*), and a third group characterised by only a few features of *Peratherium*. The sub-genus *Amphiperatherium* was later created by Filhol (1879, p. 204) for a new peratheriine species from Saint-Gérand-le-Puy (in Allier, France), of which the mandible displays lower molars that do not increase in volume from the m1 to the m4, and a putatively unusual morphology of the m4 talonid (note that the m4 talonid of metatherians shows recurring intraspecific variation; see Martin 2005: fig. 4). *Amphiperatherium* was subsequently considered by Filhol (1881, pp. 65–68) alternatively as a genus (two times) and a sub-genus (one time). The two diagnostic characters of *Amphiperatherium* then retained, the absence of increase in volume from the m1 to the m4, and the p3 not being the highest of the premolars (following the characters of Aymard [1850, pp. 83–84]; instead of the characters related to the morphology of the m4 talonid, previously defined), still concerned only lower cheek teeth. A peratheriine hemi-mandible preserving m4 was described as intermediate in morphology between *Peratherium* and *Amphiperatherium* by Depéret and Douxami (1902, pp. 78–82), a conclusion somewhat similar to the early recognition of more than two groups of peratheriines proposed by Filhol (1877). A possible synonymy of the two genera was thus already argued (Depéret and Douxami 1902, p. 79), their typical features, as then defined, presenting intrageneric variation. In the seven decades following the publication of Depéret and Douxami (1902), no new species of *Amphiperatherium* was created (e.g. Simpson 1930, p. 32) and this genus was eventually declared invalid (von Koenigswald 1970).

Initiating the exhaustive taxonomic reappraisal of Cenozoic metatherians from Europe, using numerous mandibles from the Quercy phosphorites, Crochet (1969, p. 2041) suggested that *Peratherium* could likely be split in further studies. *Amphiperatherium* was later resurrected by Crochet (1977a), this time with a time range covering the whole evolutionary history of peratheriines (early Eocene to Middle Miocene). The relatively longer posterior lower molars (instead of their relative increase in volume; thereby following Aymard [1850, p. 84]) should be considered as a 'trend' to elongation in *Peratherium*, 'that develops gradually over time', according to Crochet (1977a, p. 357, 1977b, p. 129). Even if exceptions have been noted for this character in approximately half of the *Peratherium* species studied by Crochet (1980) (Simons and Bown 1984, p. 543), its less restrictive definition as a gradual trend with intrageneric variation was sufficient for Crochet (1980) to retain it as a diagnostic feature. Inconsistencies in the specific occurrences of the two states of the character regarding the relative length of posterior lower molars, which contradict the diagnosis of the genus, are also reported in *Amphiperatherium*, due to intraspecific variation in the type species *A. frequens*. In particular, the holotype of *A. frequens* and some mandibles from Saint-Gérand-le-Puy (the material based on which *Amphiperatherium* was erected) have m4 longer than m3 (von Koenigswald 1970, pp. 49, 55), which is a trait stated in the diagnosis of *Peratherium* from Crochet (1977a, 1980), provided that the studied sample is large enough (Crochet 1977b). Occasionally, the m3 can also be longer than and as wide as the m2 in *A. frequens* (von Koenigswald 1970, p. 55; Prieto and Rummel 2015: fig. 2B) (see also *A. minutum*; e.g. Crochet 1978, p. 234; Wessels et al. 2024: table 2), while the diagnosis of *Amphiperatherium* from Crochet (1977a, 1980) specifies that these molar loci are 'subequal in size' (instead of 'length' or 'volume' of the previous diagnoses) within the genus. Mean values should be used to compare this trait between several species. Altogether, morphological differences between lower molars of *Peratherium* and *Amphiperatherium* remain elusive (see below; Figure 8; Crespo et al. 2022: table 2). Probably partly for these reasons, characters related to the morphology of the stylar shelf of upper molars were considered more reliable by Crochet (1977a, p. 357), in order to distinguish marsupialiform genera from Europe.

Ten valid peratheriine species were afterwards placed in *Amphiperatherium*, and thirteen valid species in *Peratherium*, not including taxa that are in open nomenclature (Crochet 1979; Simons and Bown 1984; Kurz 2007; Ladevèze et al. 2012). Doubts have been raised regarding the validity of *Amphiperatherium*, based on the characterisation of intraspecific morphological variation in the oldest series of peratheriine dental remains (Ladevèze et al. 2012). Several authors attempted to propose new differential diagnostic characters for peratheriine genera. For example, the entoconid has been described as 'conical' or 'more conical' in *Peratherium* (Kurz 2007, p. 46; Hooker 2010, p. 16), and 'oval-like' (or respectively 'less conical') in *Amphiperatherium* (e.g. Kurz 2007, p. 47). However, figured comparisons of lower molars of *A. minutum* and *Peratherium cuvieri* (Fisher, 1829) (Selva and Ladevèze 2017: fig. 5A vs fig. 5B), and of *A. minutum* and *Pt. elegans* (Figure 8A,C), show that such a discrimination based on overall shapes of the entoconid is impossible. In the same way, the presence of a curved rather than almost straight anterior cristid on the p2 and p3 (Kurz 2007, p. 47), and the procumbency of the p3 (Hooker et al. 2008, p. 642), have

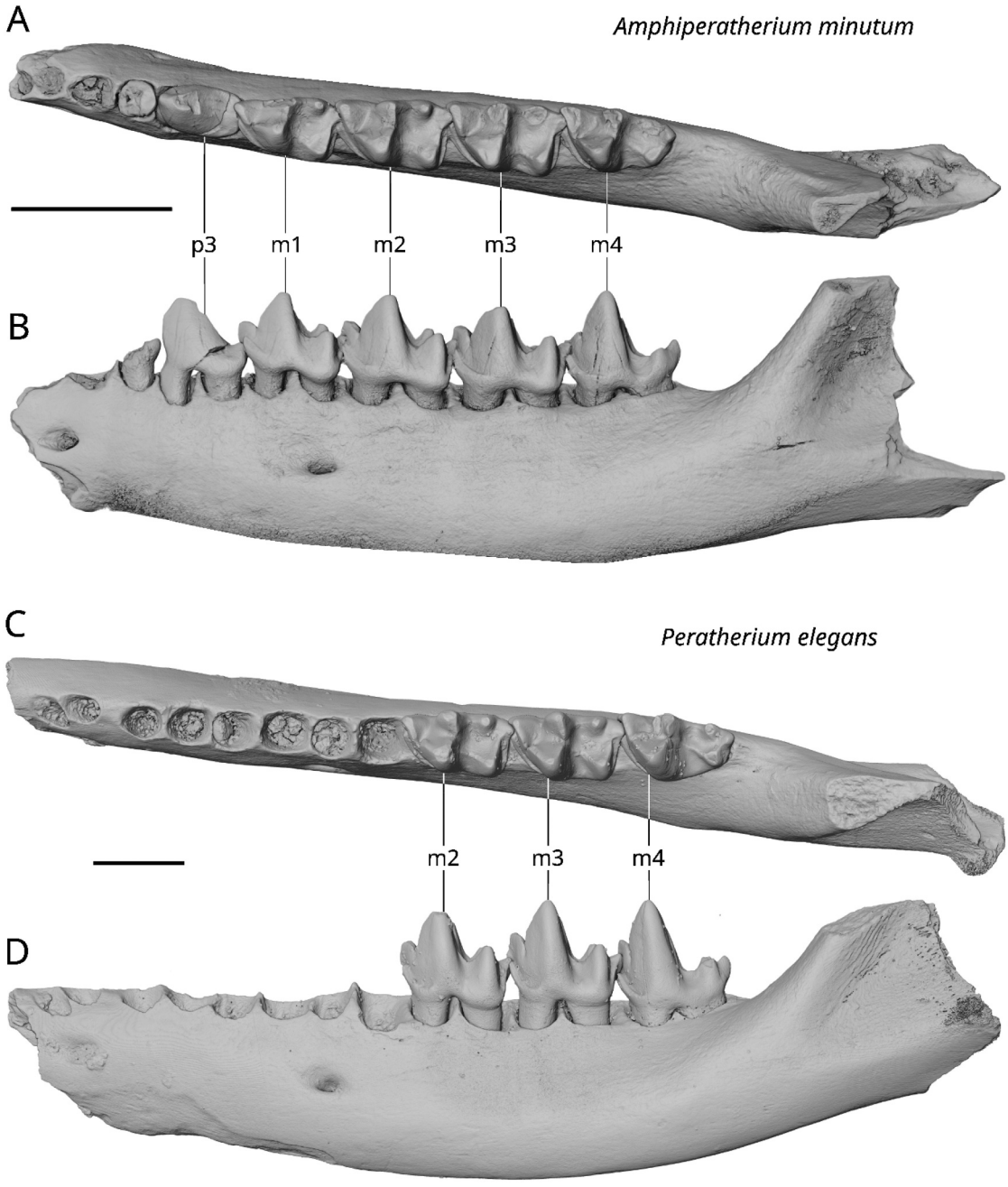

Figure 8. Comparison of hemi-mandibles of *Amphiperatherium minutum* (Aymard, 1846) (A-B) and *Peratherium elegans* (Aymard, 1846) (C-D), based on volume renderings. A-B. UM-SNB-508, left hemi-mandible with alveoli of p1-p2, and p3-m4, from Sainte-Néboule (Quercy; late Eocene, MP18) (Crochet 1978: fig. 1D) in occlusal (dorsal) (A), and labial (lateral) (B) views. C-D. UM-VBO-128, left hemi-mandible with alveoli of p1-m1, and m2-m4, from Valbro (Quercy; early Oligocene, MP22) (Crochet 2016: fig. 1F) in occlusal (dorsal) (C), and labial (lateral) (D) views. Scale bars equal 2 mm.

been proposed to be diagnostic of *Amphiperatherium*. Here again, multiple inconsistences exist. '*Amphiperatherium*' aff. *maximum* (Geiseltal-Untere Mittelkohle) has a straight anterior cristid on the p3 (Kurz 2007, p. 33), whereas this cristid is curved on the p2 and the p3 of *Peratherium* aff. *monspeliense* from Geiseltal-Untere /Obere Mittelkohle (Kurz 2007, pp. 30–31), which contradicts the expected generic occurrences of the character states defined by Kurz (2007) herself. Intraspecific and even intra-individual variation probably exist for this character, because the hemi-mandible from La Borie has a p2 with a straight anterior cristid, and a p3 with a curved anterior cristid (Figure 6A[4]). As for the procumbency of the p3, this lower premolar is not procumbent in at least some *A. minutum* specimens (Figure 8B), contrary to the diagnosis. The only undoubted differences between *Peratherium* and *Amphiperatherium* were more recently argued to concern their petrosal anatomy (Ladevèze et al. 2020, p. 13). However, the differences highlighted by Ladevèze et al. (2020) between the two genera possibly reflect interspecific rather than intergeneric morphological variation, because, among *Amphiperatherium*, only the petrosal anatomy of *A. minutum* has been investigated, and compared to that of two species of *Peratherium* (*contra* Ladevèze et al. 2020). Finally, in the same way, the postmetacrista has been described as inconspicuous in *Peratherium*, contrary to the tall distal wall formed by the postmetacrista of *Amphiperatherium* (Ladevèze

et al. 2020, p. 14), but the earliest Eocene *Pt. constans* present such a well-developed postmetacrista (e.g. Ladevèze et al. 2012: fig. 4A; pers. obs. [KG] of NMB Om.158, fig. 35 in Crochet 1980).

Generic status of Peratherium musivum *sp. nov*

It was stated that primitive *Peratherium* species from the early Eocene (i.e. *Pt. constans* and *Pt. matronense*) are less easily distinguishable from *Amphiperatherium* (Hooker et al. 2008, p. 643). The generic status of the MP7-MP8 + 9 interval species *Pt. musivum* sp. nov. also appears blurry when considering the diagnostic differences between *Peratherium* and *Amphiperatherium*, as they are summarised by Hooker et al. (2008, p. 642). In fact, based on this emended differential diagnosis (the most recent for peratheriine genera), the arguments for the tentative generic attribution of *Pt. musivum* sp. nov. are as follows. Five out of the seven characters proposed in the diagnosis can be evaluated for this species, due to unknown p3 and m4. (i) The two m1s and the only ascertained m2 of *Pt. musivum* sp. nov. are smaller than the ascertained m3 allocated to this species (Table 2). Such an apparent enlargement of m3, relatively to m1 and m2, would be evocative of *Peratherium* according to the diagnosis (as for upper molars, complete M1 and M2 are unknown for *Pt. musivum* sp. nov.). However, note that this conclusion is only based on a few isolated lower molars, representing different individuals from different localities, and that intraspecific variation is known in other species (see above). (ii) As for the relative size of the paracone and metacone mentioned by Hooker et al. (2008), it was demonstrated that strong variation in this trait exists within a comprehensive series of molars for a given herpetotheriid species (Ladevèze et al. 2012: fig. 4Ca vs fig. 5Ga). Thus, this character surely does not differentiate *Peratherium* from *Amphiperatherium*. (iii) Stylar cusp B is smaller than or as high as stylar cusp C in M3 of *Pt. musivum* sp. nov., and stylar cusp B is smaller than stylar cusp D on its M1. Consequently, stylar cusp B is herein considered 'small' (although higher than stylar cusps A and D on M3), which is alike *Amphiperatherium* in the diagnosis. (iv) The paraconule and metaconule of *Pt. musivum* sp. nov. are not significantly relatively larger than those of equivalent molar loci of the smaller *Peratherium* species, as *Pt. constans* (e.g. Figure 4N vs Figure 4P) or *Pt. elegans* (e.g. Ladevèze et al. 2012: fig. 7a-b; Crochet 2016: fig. 1A). (v) Because the strength of the postcingulid was demonstrated to vary in *Pt. elegans* (Ladevèze et al. 2012, p. 260), a purported stronger postcingulid than in *Amphiperatherium* is not a trait of *Peratherium*. Altogether, among the two out of five available characters not proven to represent morphological intraspecific variation (the size of the conules and of stylar cusp B of upper molars), only one (the size of stylar cusp B) would be indicative of *Peratherium* rather than *Amphiperatherium*.

The tentative generic identification here conducted emphasises serious application difficulties of the *Peratherium* vs *Amphiperatherium* dichotomy, when it comes to peratheriine species documented only by isolated molars (e.g. *contra* Crochet in Rémy et al. 1997, p. 715). Furthermore, the holotype M3 of *Pt. musivum* sp. nov. was first attributed to *Peratherium* by Crochet (1980), seemingly because the mesiodistally slender outline of this molar, with a labiolingually wide protocone, vaguely evokes the outline of M3 of *Pt. monspeliense* (Crochet 1980, p. 214), whereas all lower molars of *Pt. musivum* sp. nov. described before this study were included in *Amphiperatherium* (Godinot 1981; Marandat 1991; Louis 1996). Besides size, a few subtle morphological differences distinguish *Pt. musivum* sp. nov. from *Pt. constans* and '*A.*' *maximum* (see above). Due to the lack of relevant applicable definitions of *Peratherium* and *Amphiperatherium*, the provisional allocation of *Pt. musivum* sp. nov. to *Peratherium* (a longevity value on the order of that of *Peratherium* [> 30 myr; see BiochroM'97 1997] is unexpected for small mammal genera [e.g. Hoek Ostende et al. 2023]) thus lies exclusively on the fact that the earliest peratheriine species, *Pt. constans*, belongs to *Peratherium* (Ladevèze et al. 2012), which is the oldest valid peratheriine genus. Due to the definition of *Pt. musivum* sp. nov., which has relatively small stylar cusp B on M1 and M3, and the fact that '*Amphiperatherium*' *maximum* has clearly dominant stylar cusp B on M3 (Figure 3A), the relative size of stylar cusps (used in the diagnoses of *Peratherium* and *Amphiperatherium*; Crochet 1980; Hooker et al. 2008) are thus also concerned by interspecific variation in peratheriines, alike in Peradectidae (Gernelle et al. 2024: table 3, fig. 14).

Original dentally-related characters of Peratherium maximum *comb. nov. and functional implications. Towards a phylogenetic systematics approach of peratheriine's evolutionary history*

The comparisons of the hemi-mandible of *Peratherium maximum* comb. nov. from La Borie and conspecific lower molars from Condé-en-Brie reveal that this early peratheriine presents original morphological characters that differ from younger species of both the genera *Peratherium* and *Amphiperatherium* (but still in part not assessable for *Pt. constans*; Ladevèze et al. 2012), namely: (i) the p1 is minute relatively to the p2 and the p3, more so than in any other peratheriines; (ii) most lower molar alveoli are relatively longer than wide; and (iii) m2 is the widest lower molar locus (*contra* Crochet 1980, p. 98, diagnosis of '*A.*' *maximum* in which m2s and m3s are considered equally wide). As for the latter character, the results of the quantitative analysis performed with the length and width values of isolated lower molars of *Pt. maximum* comb. nov. (Figure 7B) show that measurements of lower molar alveoli (Table 4) can be used as a proxy of the relative size of corresponding loci in a given specimen, at least in such 'opossum-like' metatherians. The m2 is also the widest lower molar in early European peradectids, on average (Gernelle et al. 2024: table 4), and at least in some small early herpetotheriines (Beard and Dawson 2009: fig. 5), but probably not in *Pt. constans* according to the few available measurements (Marandat 1991: table 1).

Because *Pt. maximum* comb. nov. exhibits (i) an M2 with a relatively longer protocone (Table 5; respectively m2 with a probably relatively longer talonid, as the protocone and talonid length must be correlated, see Johanson 1996, p. 1028), and (ii) M2/m2 with a relatively wider protocone/talonid (Table 6; Supplemental material 3: Figures S5-S6) than on M3/m3 on average, unlike *Pt. constans*, and (iii) a protocone of both M2 and M3 relatively longer and (iv) relatively wider than in *Pt. constans* on average (Tables 5 and 6; respectively m2 and m3 with a talonid on average probably relatively longer and wider in *Pt. maximum* comb. nov.), we suspect that these differences could be explained by a single evolutionary change: the relative enlargement of the protocone – talonid basin complex, more pronounced on the second molars. Likewise, other subtle, potentially correlated traits related to the enlargement of this functional complex are probably present in *Pt. maximum* comb. nov., as denoted by (i) the high protocone, often higher than instead

of as high as or lower than the paracone on several upper molar loci (Figure 3C; pers. obs. KG), (ii) the often relatively large metaconule (e.g. Figure 3B) and (iii) the often relatively mesiodistally long entoconid (e.g. Figure 6A[5]). To our knowledge, *Peratherium maximum* comb. nov. is the single peratheriine exhibiting this combination of characters so far. Such an enlarged protocone – talonid functional complex must also be present in the largest Eocene herpetotheriine, *Herpetotherium comstocki* (Cope, 1884) (see Krishtalka and Stucky 1983b: figs. 1-2). In addition to the recurrence of serial homologs in molars of mammals (Billet and Bardin 2019), even for structures with a less important functional role such as stylar cusps (Crompton and Hiiemae 1970; e.g. all molariform teeth of *Peratherium sudrei* Crochet, 1979, share closely appressed stylar cusps C and D, see; Crochet 1980: figs. 168–169]), the existence of the putative correlations described above may reinforce the problem of the 'dearth' of apomorphies, limiting phylogenetic reconstructions in metatherians with an unspecialised tribosphenic dentition (Beck 2023, p. 75).

Relatively larger protocone and talonid basin, as found in *Pt. maximum* comb. nov., must improve crushing capacity and have thus been linked with a more omnivorous diet in metatherians (Wilson 2013, p. 455). The dietary types insectivorous/omnivorous and frugivorous/omnivorous described by Kurz (2007, p. 6) and identified (by comparisons with extant marsupials) in herpetotheriid and in putative peradectid metatherians, respectively (Kurz 2007: table 3), rely only minimally on molar features, thus complicating comparisons with inferences made from isolated molars. For example, the dietary types of the *Peradectes*-like taxon from Messel was inferred close to that of the didelphid *Caluromys* (Kurz 2005), which is mostly frugivorous (e.g. Lessa et al. 2023: fig. 1). Lower molars of *Caluromys* display long and wide talonids with long entoconids (e.g. Flores et al. 2010: fig. 6), and upper molars have the protocones as high as or higher than the paracones (pers. obs. KG). They are similar in these respects to those of *Pt. maximum* comb. nov. Reversely, the European peradectids have relatively short and narrow talonids, as well as relatively low protocones (see illustrations in Gernelle et al. [2024]; the latter character probably correlates with faunivory, according to Beck [2015], contrary to *Caluromys*. This warrants the assessment of the molar morphology of peratheriines and possible peradectid specimens from Messel for further characterisation of Laurasian marsupialiform dietary types. It should be noted, however, that subtle regional differences in molar shape—investigated using geometric morphometric methods primarily focused on the stylar shelf area and the trigonid—are weakly correlated with differences (if any) in diet in the dentally conservative didelphid marsupials (Chemisquy et al. 2015).

Do the dentally related peculiarities of *Pt. maximum* comb. nov., compared to younger well documented representatives of *Peratherium* and *Amphiperatherium*, justify the erection of a new genus, or at least a distinction between more than one genus in the early Eocene peratheriines, similarly to that initiated by Crochet (1977a) and ancient authors (e.g. Filhol 1879)? It is noteworthy that '*Amphiperatherium*' aff. *maximum* from Geiseltal-Untere Mittelkohle in turn differs from the closely related *Pt. maximum* comb. nov. in its m4 longer than m2 (Storch and Haubold 1989), which does not occur in the latter according to measurements performed on the mandible from La Borie (Table 4) and the mean values of the sample from Condé-en-Brie (Figure 7A-C). Such characters, although important for systematics, are possibly homoplastic and should be reviewed in a phylogenetic context, prior to proposing potential supraspecies groupings for small insectivorous mammals (e.g. Manz and Bloch 2015). *The consideration of peratheriine species as part of two early diverging genera,* a priori of a study of their evolutionary history via formal phylogenetic analyses, is unlikely, and may lead to misconceptions or incomplete reconstructions of relationships between peratheriine species (e.g. Crochet 1980: figs. 151, 239; Hooker et al. 2008: fig. 5). In other words, if a generic distinction is to be applied between early Eocene peratheriine species, it certainly differs from the deep *Peratherium* – *Amphiperatherium* dichotomy founded by Crochet (1977a, 1977b, 1979, 1980). For these reasons, '*Amphiperatherium*' *maximum* is provisionally and conservatively reallocated to *Peratherium*. Therefore, no species of *Amphiperatherium* have their type locality in the early Eocene of Europe anymore. The occurrences of the typical middle Eocene *A. goethei* and *A. bastbergense* (MP13-MP14), and the late Eocene *A. bourdellense* (MP16-MP17), during the early Eocene (MP8 + 9-?MP10-11) (Figure 1), as well as their taxonomic status, must be thoroughly tested in other studies.

Conclusions

A few consistent molar characters, in addition to a size intermediate between those of the most represented metatherian species of the MP7 (*Peratherium constans*) and MP8 + 9 ('*Amphiperatherium*' *maximum*) reference levels, allowed us to define *Peratherium musivum*, a new peratheriine species restricted to the MP7-MP8 + 9 time interval, which was widespread in Western Europe. This revision of MP7-MP8 + 9 interval molars partly disentangles the complex taxonomy of early peratheriines. We hypothesise close phylogenetic affinities between *Pt. musivum* sp. nov. and *Pt. maximum* comb. nov., the latter being provisionally reallocated to *Peratherium*. A relative enlargement of the protocone/talonid, especially on M2/m2, in *Pt. maximum* comb. nov. is supported by (i) the detailed study of the size and shape of alveoli of a hemi-mandible from La Borie (~MP8 + 9), the single known for this species; and (ii) our quantitative comparisons of several isolated upper and lower molars. Comparisons between the unique specimen from La Borie and mandibles of among the most representative species of *Peratherium* (*Pt. elegans*) and *Amphiperatherium* (*A. minutum*) revealed more morphological similarities between the latter two species. We established that the previous taxonomic studies focused on Peratheriinae (Crochet 1980; Kurz 2007; Hooker et al. 2008; Ladevèze et al. 2020) did not provide any stable and reliable morphological characters distinguishing *Amphiperatherium* from *Peratherium*, thereby strengthening the conclusions of Ladevèze et al. (2012) regarding the possible non-existence of *Amphiperatherium*, at least in the early Eocene. This study paves the way for further work addressing the taxonomy and intrasubfamilial relationships of the Peratheriinae.

Acknowledgments

We acknowledge Guillaume Billet (MNHN) for the loan of specimens from the MNHN mammal collection, under his care. We are also thankful to Vincent N. Pernègre (MNHN), who managed the allocation of various new MNHN specimen numbers (localities of Soissons, Pourcy, Avenay and Condé-en-Brie). Many thanks to the four reviewers, Robin M. D. Beck, Wilma Wessels, Narla S. Stutz and Vicente D. Crespo, for their helpful and constructive comments. This is ISEM publication n° 2024-204.

Disclosure statement

No potential conflict of interest was reported by the author(s).

Funding

This research was financially supported by a PhD thesis funding from the French Ministry of Higher Education, Research, and Innovation, and also by the ANR project EDENs [ANR-20-CE02-0007]. Three-dimensional data acquisition was performed using the micro-computed tomography (μ-CT) facilities of the MRI platform member of the national infrastructure France-BioImaging supported by the French National Research Agency [ANR-10-INBS-04, 'Investments for the future'], the labex CEMEB [ANR-10-LABX-0004] and NUMEV [ANR-10-LABX-0020]. The Leica optical and digital station used to take photographs was acquired as part of the ANR-ERC PALASIAFRICA [ANR-08-JCJC-0017]. A CC-BY public copyright license has been applied by the authors to the present document and will be applied to all subsequent versions up to the Author Accepted Manuscript arising from this submission, in accordance with the grants' (ANR) open access conditions.

ORCID

Killian Gernelle http://orcid.org/0000-0001-9698-0223
Sandrine Ladevèze http://orcid.org/0000-0001-6009-4107
Rodolphe Tabuce http://orcid.org/0000-0002-4713-3981

References

Abels HA, Clyde WC, Gingerich PD, Hilgen FJ, Fricke HC, Bowen GJ, Lourens LJ. 2012. Terrestrial carbon isotope excursions and biotic change during Palaeogene hyperthermals. Nat Geosci. 5(5):326–329. doi: 10.1038/ngeo1427.

Aymard A. 1850. Compte rendu de la séance du 12 avril 1849, réponse à M. Robert sur les mammifères fossiles des caclcaires du Puy. Ann Soc Agric Sci Puy. 14:80–86.

Beard KC, Dawson MR. 2009. Early Wasatchian mammals of the red hot local fauna, uppermost Tuscahoma Formation, Lauderdale County, Mississippi. Ann Carnegie Mus. 78(3):193–243. doi: 10.2992/007.078.0301.

Beck RMD. 2023. Diversity and phylogeny of marsupials and their stem relatives (Metatheria). In: Cáceres NC, Dickman CR, editors. American and Australasian Marsupials. Cham, Switzerland: Springer; p. 23–88. doi: 10.1007/978-3-031-08419-5_35.

Beck RMD. 2015. A peculiar faunivorous metatherian from the early Eocene of Australia. Acta Palaeontol Pol. 60(1): 123–129. doi: https://doi.org/10.4202/app.2013.0011.

Billet G, Bardin J. 2019. Serial homology and correlated characters in morphological phylogenetics: modeling the evolution of dental crests in placentals. Syst Biol. 68(2):267–280. doi: 10.1093/sysbio/syy071.

BiochroM'97. 1997. Synthèse et tableaux de corrélation. In: Aguilar J, Legendre S, Michaux J, editors. Actes du Congrès BiochroM'97 Vol. 21, Montpellier, Montpellier: Mem Trav EPHE; p. 769–805.

Chemisquy MA, Prevosti FJ, Martin G, Flores DA. 2015. Evolution of molar shape in didelphid marsupials (Marsupialia: Didelphidae): analysis of the influence of ecological factors and phylogenetic legacy. Zool J Linn Soc. 173(1):217–235. doi: 10.1111/zoj.12205.

Clemens WA. 1966. Fossil mammals of the type Lance Formation, Wyoming. Part II, Marsupialia. Univ Calif Publ Geol Sci. 62:1–122.

Costeur L, Schneider M. 2011. Catalogue of the Eocene mammal types of the Natural History Museum Basel. Carnets Geol. doi: 10.4267/2042/43898.

Crespo VD, Goin FJ. 2021. Taxonomy and affinities of african cenozoic metatherians. Span J Palaeont. 36(2):1–16. doi: 10.7203/sjp.36.2.20974.

Crespo VD, Goin FJ, Pickford M. 2022. The last African metatherian. Foss Rec. 25(1):173–186. doi: 10.3897/fr.25.80706.

Crochet JY. 1969. Révision du genre *Peratherium* Aymard, 1849 (Marsupialia). C R Acad Sci Paris. 268:2038–2041.

Crochet JY. 1977a. Les Didelphidae (Marsupicarnivora, Marsupialia) holarctiques tertiaires. C R Acad Sci Paris. 284:357–360.

Crochet JY. 1977b. Les didelphidés paléogènes holarctiques : historique et tendances évolutives. Geobios Mem Spec. 1:127–134. doi: 10.1016/S0016-6995(77)80012-0.

Crochet JY. 1978. La poche à phosphate de Ste-Néboule (Lot) et sa faune de vertébrés du Ludien supérieur. 7- Didelphides (Marsupiaux). Palaeovertebrata. 8(2–4):231–242.

Crochet JY. 1979. Diversité systématique des Didelphidae (Marsupialia) européens tertiaires. Geobios. 12(3):365–378. doi: 10.1016/S0016-6995(79)80117-5.

Crochet JY. 1980. Les marsupiaux du Tertiaire d'Europe. Paris: Edtions Foundation Singer-Polignac.

Crochet JY. 2016. Valbro: A new site of vertebrates from the early Oligocene (MP 22) of France (Quercy). IV – Marsupialia, Insectivora. Ann Paleontol. 102(1):7–10. doi: 10.1016/j.annpal.2015.12.001.

Crompton AW, Hiiemae K. 1970. Molar occlusion and mandibular movements during occlusion in the American opossum, *Didelphis marsupialis* L. Zool J Linn Soc. 49:21–47. doi: 10.1111/j.1096-3642.1970.tb00728.x.

Dégremont E, Duchaussois F, Hautefeuille F, Laurain M, Louis P, Tétu R. 1985. Paléontologie: découverte d'un gisement du Cuisien tardif à Prémontré (Aisne). Bull Inf Géol Bass Paris. 22(2):11–18.

Delacre M, Christophe L, Mora YL, Lakens D. 2019. Taking parametric assumptions seriously: arguments for the use of Welch's *F*-test instead of the classical *F*-test in one-way ANOVA. Int Rev Soc Psychol. 32(1):13. doi: 10.5334/irsp.198.

Depéret C, Douxami H. 1902. Les vertébrés Oligocènes de Pyrimont-Challonges (Savoie). Mem Soc Pal Suisse. 29:1–90.

Dunn RH, Townsend KEB. 2019. New pantolestids from the Uinta Formation, Utah. J Vertebr Paleontol. 39(4):e1652622. doi: 10.1080/02724634.2019.1652622.

Estravís C. 2000. Nuevos mamíferos del Eoceno Inferior de Silveirinha (Baixo Mondego, Portugal). Coloquios Paleontol. 51:281–311.

Filhol H. 1877. Recherches sur les Phosphorites du Quercy. Étude des fossiles qu'on y rencontre et spécialement des Mammifères. Ann Sci Geol. 8:1–340.

Filhol H. 1879. Étude des Mammifères fossiles de Saint-Gérand-le-Puy. Ann Sci Geol. 10:1–253.

Filhol H. 1881. Étude des Mammifères fossiles de Ronzon (Haute-Loire). Ann Sci Geol. 12:1–270.

Flores DA, Abdala F, Giannini N. 2010. Cranial ontogeny of *Caluromys philander* (Didelphidae: Caluromyinae): a qualitative and quantitative approach. J Mammal. 91(3):539–550 doi: 10.1644/09-MAMM-A-291.1.

Flynn LJ, Barry JC, Morgan ME, Pilbeam D, Jacobs LL, Lindsay EH. 1995. Neogene Siwalik mammalian lineages: species longevities, rates of change, and modes of speciation. Palaeogeogr Palaeoclimatol Palaeoecol. 115(1–4):249–264. doi: 10.1016/0031-0182(94)00114-N.

Gazin CL. 1952. The lower Eocene Knight Formation of western Wyoming and its mammalian faunas. Smithson Misc Collect. 117(18):1–82.

Gernelle K, Billet G, Gheerbrant E, Godinot M, Marandat B, Ladevèze S, Tabuce R. 2024. Taxonomy and evolutionary history of peradectids (Metatheria): new data from the early Eocene of France. J Mamm Evol. 31(3):31. doi: 10.1007/s10914-024-09724-5.

Godinot M. 1981. Les mammifères de Rians (Eocène inférieur, Provence). Palaeovertebrata. 10(2):43–126.

Godinot M, Crochet JY, Hartenberger JL, Lange-Badré B, Russell DE, Sigé B. 1987. Nouvelles données sur les mammifères de Palette (Eocène inférieur, Provence). Münch Geowiss Abh (A). 10:273–288.

Gordon CL. 2003. A first look at estimating body size in dentally conservative marsupials. J Mamm Evol. 10(1–2):1–21. doi: 10.1023/A:1025545023221.

Hand SJ, Sigé B, Archer M, Gunnell GF, Simmons NB. 2015. A new early Eocene (Ypresian) bat from Pourcy, Paris Basin, France, with comments on patterns of diversity in the earliest chiropterans. J Mamm Evol. 22(3):343–354. doi: 10.1007/s10914-015-9286-9.

Hoek Ostende LW van den, Bilgin M, Braumuller Y, Cailleux F, Skandalos P. 2023. Live long and prosper? Assessing longevity of small mammal taxa using the NOW database. Casanovas-Vilar I, Hoek Ostende LW van den, Janis CM, Saarinen J, editors. Evolution of Cenozoic Land Mammal Faunas and Ecosystems: 25 Years of the NOW Database of Fossil Mammals, Vertebrate Paleobiology and Paleoanthropology. Cham, Switzerland: Springer; p. 111–129. doi: 10.1007/978-3-031-17491-9_8

Hooker JJ. 1996a. Mammalian biostratigraphy across the Paleocene-Eocene boundary in the Paris, London and Belgian basins. In: Knox RWOB, Corfield RM, Dunay RE, editors. Correlation of the Early Paleogene in Northwest Europe. Geol Soc Lond, Spec Publ. 101:205–218. doi: 10.1144/gsl.sp.1996.101.01.13.

Hooker JJ. 1996b. Mammals from the Early (late Ypresian) to Middle (Lutetian) Eocene Bracklesham Group, southern England. Tert Res. 16(1–4):141–174.

Hooker JJ. 1998. Mammalian faunal change across the Paleocene-Eocene transition in Europe. In: Aubry M, Lucas S, Berggren W, editors. Late Paleocene-Early Eocene Climatic and Biotic Events in the Marine and Terrestrial Records. (NY): Columbia University Press; p. 428–450.

Hooker JJ. 2010. The mammal fauna of the early Eocene Blackheath formation of Abbey Wood, London. Monogr Palaeontogr Soc. 164(634):1–153. doi: 10.1080/25761900.2022.12131814.

Hooker JJ, Cook E, Benton MJ. 2005. British Tertiary fossil mammal GCR sites. In: Benton MJ, Cook E, JJ Hooker, editors. Mesozoic and Tertiary Fossil Mammals and Birds of Great Britain. Geol Conserv Rev Ser. 32:67–124.

Hooker JJ, Sánchez-Villagra MR, Goin FJ, Simons EL, Attia Y, Seiffert ER. 2008. The origin of Afro-Arabian 'didelphimorph' marsupials. Palaeontology. 51 (3):635–648. doi: 10.1111/j.1475-4983.2008.00779.x.

Horovitz I, Ladevèze S, Argot C, Macrini TE, Martin T, Hooker JJ, Kurz C, de Muizon C, Sánchez-Villagra MR. 2008. The anatomy of *Herpetotherium* cf. *fugax* Cope, 1873, a metatherian from the Oligocene of North America. Palaeontogr Abt A. 284(4–6):109–141. doi: 10.1127/pala/284/2008/109.

International Commission of Zoological Nomenclature (ICZN). 1999. International Code of Zoological Nomenclature. London: The International Trust for Zoological Nomenclature. http://www.nhm.ac.uk/hosted-sites/iczn/code/.

Johanson Z. 1996. New marsupial from the Fort Union Formation, Swain Quarry, Wyoming. J Paleontol. 70(6):1023–1031. doi: 10.1017/S0022336000038725.

Korth WW. 1994. Middle Tertiary marsupials (Mammalia) from North America. J Paleontol. 68(2):376–397. doi: 10.1017/S0022336000022952.

Korth WW. 2008. Marsupialia. In: Janis C, Gunnell G, Uhen M, editors. Evolution of Tertiary Mammals of North America: volume 2, Small Mammals, Xenarthrans, and Marine Mammals. Cambridge: Cambridge University Press; p. 39–47.

Krishtalka L, Stucky RK. 1983a. Paleocene and Eocene marsupials of North America. Ann Carnegie Mus. 52(10):229–263. doi: 10.5962/p.330761.

Krishtalka L, Stucky RK. 1983b. Revision of the Wind River faunas, early Eocene of Central Wyoming. Part 3. Marsupialia. Ann Carnegie Mus. 52(9):205–227. doi: 10.5962/p.215199.

Kurz C. 2005. Ecomorphology of opossum-like marsupials from the Tertiary of Europe and a comparison with selected taxa. Kaupia. 14:21–26.

Kurz C. 2007. The opossum-like marsupials (Didelphimorphia and Peradectia, Marsupialia, Mammalia) from the Eocene of Messel and Geiseltal – Ecomorphology, diversity and palaeogeography. Kaupia. 15:3–65.

Kurz C, Habersetzer J. 2004. Untersuchungen der zahnmorphologie von beutelratten aus Messel mit der mikroröntgenmethode CORR. Cour Forsch-Inst Senckenberg. 252:13–21.

Ladevèze S, de Muizon C, Beck RMD, Germain D, Cespedes-Paz R. 2011. Earliest evidence of mammalian social behaviour in the basal Tertiary of Bolivia. Nature. 474(7349):83–86. doi: 10.1038/nature09987.

Ladevèze S, Selva C, de Muizon C. 2020. What are "opossum-like" fossils? The phylogeny of herpetotheriid and peradectid metatherians, based on new features from the petrosal anatomy. J Syst Palaeontol. 18(17):1463–1479. doi: 10.1080/14772019.2020.1772387.

Ladevèze S, Smith R, Smith T. 2012. Reassessment of the morphology and taxonomic status of the earliest herpetotheriid marsupials of Europe. J Mamm Evol. 19(4):249–261. doi: 10.1007/s10914-012-9195-0.

Laurent Y, Adnet S, Bourdon E, Corbalan D, Danilo L, Duffaud S, Fleury G, Garcia G, Godinot M, Le Roux G, et al. 2010. La Borie (Saint-Papoul, Aude): un gisement exceptionnel dans l'Éocène basal du Sud de la France. Bull Soc Hist Nat Toulouse. 146:89–103.

Lebrun R, Orliac MJ. 2016. MorphoMuseuM: an online platform for publication and storage of virtual specimens. Paleontol Soc Pap. 22:183–195. doi: 10.1017/scs.2017.14.

Legendre S, Marandat B, Sigé B, Crochet JY, Godinot M, Hartenberger JL, Sudre J, Vianey-Liaud M, Muratet B, Astruc JG. 1992. La faune de mammifères de Vielase (phosphorites du Quercy, Sud de la France): Preuve paléontologique d'une karstification du Quercy dès l'Eocène inférieur. Neues Jahrb Geol Paläontol. 7:414–428. doi: 10.1127/njgpm/1992/1992/414.

Lessa LG, Carvalho RF, Astúa D. 2023. Food Habits of American Marsupials. In: Cáceres NC, Dickman CR, editors. American and Australasian Marsupials. Cham, Switzerland: Springer; p. 1095–1122 doi: 10.1007/978-3-031-08419-5_22

Lösel PD, Kamp T van de, Jayme A, Ershov A, Faragó T, Pichler O, Tan Jerome N, Aadepu N, Bremer S, Chilingaryan SA, et al. 2020. Introducing Biomedisa as an open-source online platform for biomedical image segmentation. Nat Commun. 11(1):5577. doi: 10.1038/s41467-020-19303-w.

Louis P. 1966. Note sur un nouveau gisement situé à Condé-en-Brie (Aisne) et renfermant des restes de mammifères de l'Eocène inférieur. Ann Univ ARERS Reims. 4:108–118.

Louis P. 1996. Recherches de mammifères paléogènes dans les départements de l'Aisne et de la Marne pendant la deuxième moitié du vingtième siècle. Palaeovertebrata. 25(2–4):83–113.

Louis P, Laurain M. 1983. Nouveau gisement de vertébrés dans le Cuisien supérieur de Saint-Agnan (Aisne). Ses relations stratigraphiques avec les autres gisements yprésiens du Bassin parisien. Bull Inf Géol Bass Paris. 20 (4):3–20.

Louis P, Michaux J. 1962. Présence de mammifères sparnaciens dans les sablières de Pourcy (Marne). C R Somm Seances Soc Geol Fr. 6:170–171.

Luccisano V, Sudre J, Lihoreau F. 2020. Revision of the Eocene artiodactyls (Mammalia, Placentalia) from Aumelas and Saint-Martin-de-Londres (Montpellier limestones, Hérault, France) questions the early European artiodactyl radiation. J Syst Palaeontol. 18(19):1631–1656. doi: 10.1080/14772019.2020.1799253.

Manz CL, Bloch JI. 2015. Systematics and phylogeny of Paleocene-Eocene Nyctitheriidae (Mammalia, Eulipotyphla?) with description of a new species from the late Paleocene of the Clarks Fork Basin, Wyoming, USA. J Mamm Evol. 22(3):307–342. doi: 10.1007/s10914-014-9284-3.

Marandat B. 1986. Decouverte d'une faune de micromammiferes d'âge cuisien superieur dans les marno-calcaires d'Agel à Azillanet (Minervois, Hérault). Geol Fr. 2:197–204.

Marandat B. 1991. Mammifères de l'Ilerdien Moyen (Eocène Inférieur) des Corbières et du Minervois. Palaeovertebrata. 20(2–3):55–144.

Marandat B, Adnet S, Marivaux L, Martinez A, Vianey-Liaud M, Tabuce R. 2012. A new mammalian fauna from the earliest Eocene (Ilerdian) of the Corbières (Southern France): Palaeobiogeographical implications. Swiss J Geosci. 105(3):417–434. doi: 10.1007/s00015-012-0113-5.

Marivaux L, Vianey-Liaud M, Jaeger JJ. 2004. High-level phylogeny of early Tertiary rodents: dental evidence. Zool J Linn Soc. 142(1):105–134. doi: 10.1111/j.1096-3642.2004.00131.x.

Marshall CR. 2017. Five palaeobiological laws needed to understand the evolution of the living biota. Nat Ecol Evol. 1(6):165. doi: 10.1038/s41559-017-0165.

Martin GM. 2005. Intraspecific variation in *Lestodelphys halli* (Marsupialia: Didelphimorphia). J Mammal. 86(4):793–802. doi: 10.1644/1545-1542(2005)086[0793:IVILHM]2.0.CO;2.

Martin JE, Case JA, Jagt JWM, Schulp AS, Mulder EWA. 2005. A new European marsupial indicates a Late Cretaceous high-latitude transatlantic dispersal route. J Mamm Evol. 12(3–4):495–511. doi: 10.1007/s10914-005-7330-x.

McGrew PO, Berman JE, Hecht MK, Hummel JM, Simpson GG, Wood AE. 1959. The geology and paleontology of the Elk Mountain and Tabernacle Butte area, Wyoming. Bull Am Mus Nat Hist. 117(3):121–176.

Muizon C de, Ladevèze S. 2022. New material of *Incadelphys antiquus* (Pucadelphyda, Metatheria, Mammalia) from the early Palaeocene of Bolivia reveals phylogenetic affinities with enigmatic North and South American metatherians. Geodiversitas. 44(22):609–643. doi: 10.5252/geodiversitas2022v44a22.

Murphey PC, Kelly TS, Chamberlain KR, Tsukui K, Clyde WC. 2018. Mammals from the earliest Uintan (middle Eocene) Turtle Bluff Member, Bridger Formation, southwestern Wyoming, USA, Part 3: Marsupialia and a reevaluation of the Bridgerian-Uintan North American Land Mammal Age transition. Palaeontol Electron. 21(2):1–52. doi: 10.26879/804.

Nel A, de Plöeg G, Dejax J, Dutheil D, de Franceschi D, Gheerbrant E, Godinot M, Hervet S, Menier JJ, Augé M, et al. 1999. Un gisement sparnacien exceptionnel à plantes, arthropodes et vertébrés (Éocène basal, MP7): Le Quesnoy (Oise, France). C R Acad Sci Paris. 329:65–72. doi: 10.1016/S1251-8050(99)80229-8.

Noiret C, Steurbaut E, Tabuce R, Marandat B, Schnyder J, Storme JY, Yans J. 2016. New bio-chemostratigraphic dating of a unique early Eocene sequence from southern Europe results in precise mammalian biochronological tie-points. Newsl Stratigr. 49(3):469–480. doi: 10.1127/nos/2016/0336.

Peláez-Campomanes P, de la PA, López Martínez N. 1989. Primeras faunas de micromamíferos del Paleógeno de La Cuenca del Duero. Stud Geol Salmant. 5:135–157.

Peters GJY. 2017. userfriendlyscience: Quantitative analysis made accessible. R package version 0.7.2. doi: 10.17605/osf.io/txequ.

Philip J, Vianey-Liaud M, Martin-Closas C, Tabuce R, Léonide P, Margerel JP, Noël J. 2017. Stratigraphy of the Haut Var Paleogene continental series (Northeastern Provence, France): New insight on the age of the 'Sables bleutés du Haut Var' Formation. Geobios. 50(4):319–339. doi: 10.1016/j.geobios.2017.06.002.

Prieto J, Rummel M. 2015. On a well-preserved mandible of *Amphiperatherium* from the Middle Miocene fissure filling Petersbuch 39: one of the youngest record of Metatheria (Mammalia) in Germany. Zitteliana A. 55:121–126.

R Core Team. 2024. R: a language and environment for statistical computing. Vienna, Austria: R Foundation for Statistical Computing.

Rémy JA, Aguilar JP, Crochet JY, Duffaud S, Escarguel G, Godinot M, Marandat B, Michaux J, Rage JC, Sigé B, et al. 1997. Les remplissages karstiques polyphasés (Eocène, Oligocène, Miocène), de Saint-Maximin (Phosphorites du Gard) et leur apport à la connaissance des faunes européennes, notamment pour l'Eocène moyen (MP13). 1. Introduction, systématique (pars) et synthèse. In: Aguilar J, Legendre S, Michaux J, editors. Actes du Congrès BiochroM'97. Montpellier: Mém Trav EPHE, Inst Montpellier. 21:711–728.

Russell DE, Galoyer A, Louis P, Gingerich PD. 1988. Nouveaux vertébrés sparnaciens du Conglomérat de Meudon à Meudon, France. C R Acad Sci Paris. 307:429–433.

Ruxton GD, Beauchamp G. 2008. Time for some a priori thinking about post hoc testing. Behav Ecol. 19(3):690–693. doi: 10.1093/beheco/arn020.
Sánchez-Villagra M, Ladevèze S, Horovitz I, Argot C, Hooker JJ, Macrini TE, Martin T, Moore-Fay S, de Muizon C, Schmelzle T, et al. 2007. Exceptionally preserved North American Paleogene metatherians: Adaptations and discovery of a major gap in the opossum fossil record. Biol Lett. 3(3):318–322. doi: 10.1098/rsbl.2007.0090.
Selva C, Ladevèze S. 2017. Computed microtomography investigation of the skull of Cuvier's famous 'opossum' (Marsupialiformes, Herpetotheriidae) from the Eocene of Montmartre. Zool J Linn Soc. 180(3):672–693. doi: 10.1111/zoj.12495.
Simons EL, Bown TM. 1984. A new species of *Peratherium* (Didelphidae; Polyprotodonta): the first African marsupial. J Mammal. 65(4):539–548. doi: 10.2307/1380836.
Simpson GG. 1930. Post-Mesozoic Marsupialia. In: Pompeckj J, editor. Fossilium Catalogus. I: Animalia. Pars 47. Berlin: W. Junk; p. 1–87.
Smith R, Russell DE. 1992. Mammifères (Marsupialia, Chiroptera) de l'Yprésien de la Belgique. Bull Inst R Sci Nat Belg, Sci Terre. 62:223–227.
Smith R, Smith T. 2004. Les mammifères de l'Yprésien moyen du Bassin de Paris (niveau-repère MP8-9) sont-ils présents dès la limite Paléocène-Eocène de Dormaal (niveau-repère MP7, Belgique)? Oryctos. 5:75–82.
Solé F, Falconnet J, Laurent Y. 2014. New proviverrines (Hyaenodontida) from the early Eocene of Europe; phylogeny and ecological evolution of the Proviverrinae. Zool J Linn Soc. 171(4):878–917. doi: 10.1111/zoj.12155.
Solé F, Godinot M, Laurent Y, Galoyer A, Smith T. 2018. The European mesonychid mammals: Phylogeny, ecology, biogeography, and biochronology. J Mammal Evol. 25(3):339–379. doi: 10.1007/s10914-016-9371-8.
Speijer RP, Pälike H, Hollis CJ, Hooker JJ, Ogg JG. 2020. The Paleogene Period. In: Gradstein F, Ogg J, Schmitz M, Ogg G, editors. Geologic Time Scale 2020. Amsterdam: Elsevier; p. 1087–1140. doi: 10.1016/B978-0-12-824360-2.00028-0.
Spijkerman E, van Nieulande FAD, Wesselingh FP, Reich S, Tracey S. 2015. Pourcy (Paris Basin, France): preliminary assessment of an early Eocene NW European tropical coastal environment from molluscs and vertebrate fossils. Cainozoic Res. 15(1–2):155–180.
Steurbaut E, Magioncalda R, Dupuis C, van Simaeys S, Roche E, Roche M. 2003. Palynology, paleoenvironments, and organic carbon isotope evolution in lagoonal Paleocene-Eocene boundary settings in North Belgium. Spec Pap Geol Soc Am. 369:291–317.
Storch G. 1993. *Amphiperatherium goethei*, ein weiteres Beuteltier aus dem Eozän von Messel (Mammalia, Didelphidae). Carolinea. 51:123–124.
Storch G, Haubold H. 1989. Additions of the Geiseltal mammalian faunas, Middle Eocene: Didelphidae, Nyctitheriidae, Myrmecophagidae. Palaeovertebrata. 19(3):95–114.
Sudre J, Sigé B, Rémy JA, Marandat B, Hartenberger JL, Godinot M, Crochet JY. 1990. Une faune du niveau d'Egerkingen (MP 14; Bartonien inférieur) dans les phosphorites du Quercy (Sud de la France). Palaeovertebrata. 20(1):1–32.
Szalay FS. 1993. Metatherian taxon phylogeny: evidence and interpretation from the cranioskeletal system. In: Szalay FS, Novacek MJ, McKenna MC, Differentiation M, editors. Mammal Phylogeny Vol. 1. Mesozoic Differentiation, Multituberculates, Monotremes, Early Therians, and Marsupials. (NY): Springer-Verlag; p. 216–242.
Tarquini SD, Ladevèze S, Prevosti FJ. 2022. The multicausal twilight of South American native mammalian predators (Metatheria, Sparassodonta). Sci Rep. 12(1):1224. doi: 10.1038/s41598-022-05266-z.
Vianey-Liaud M, Lihoreau F, Solé F, Gernelle K, Vautrin Q, Bronnert C, Bourget H, Vidalenc D, Tabuce R. 2024. A revision of the late early Eocene mammal faunas from Mas de Gimel and Naples (Montpellier, Southern France) and the description of a new theridomorph rodent. Geodiversitas. 46(10). doi: 10.5252/geodiversitas2024v46a10.
von Koenigswald W. 1970. *Peratherium* (Marsupialia) im Ober-Oligozän und Miozän von Europa. Bayer Akad Wiss Math-Natur Kl Abh (NF). 144:1–79.
Wessels W, Weerd AA van de, Marković Z. 2024. Marsupials (herpetotheriids) from the late Palaeogene of south-east Serbia. Palaeobio Palaeoenv. 104(2):363–380. doi: 10.1007/s12549-024-00600-x.
Wickham H. 2016. ggplot2: elegant graphics for data analysis. Use R!, Springer. doi: 10.1007/978-3-319-24277-4.
Williamson TE, Brusatte SL, Carr TD, Weil A, Standhardt BR. 2012. The phylogeny and evolution of Cretaceous-Palaeogene metatherians: Cladistic analysis and description of new early Palaeocene specimens from the Nacimiento Formation, New Mexico. J Syst Palaeontol. 10(4):625–651. doi: 10.1080/14772019.2011.631592.
Wilson GP. 2013. Mammals across the K/Pg boundary in northeastern Montana, U.S.A.: dental morphology and body-size patterns reveal extinction selectivity and immigrant-fueled ecospace filling. Paleobiology. 39(3):429–469. doi: 10.1666/12041.
Yans J, Marandat B, Masure E, Serra-Kiel J, Schnyder J, Storme JY, Marivaux L, Adnet S, Vianey-Liaud M, Tabuce R. 2014. Refined bio-(benthic foraminifera, dinoflagellate cysts) and hemostratigraphy (δ13Corg) of the earliest Eocene at Albas-Le Clot (Corbières, France): Implications for mammalian biochronology in Southern Europe. Newsl Stratigr. 47(3):331–353. doi: 10.1127/nos/2014/0050.

Supplemental material 1. Ratio values of stylar shelf to talon length, stylar shelf to protocone length, talon to protocone length, and talon to protocone width (see Figure 2 for measurement protocols) of each M2 and M3 specimen sampled for *Peratherium constans*, *Pt. musivum* sp. nov., and *Pt. maximum* comb. nov. The holotype specimens and associated values are depicted in bold text.

Locus	Species	Specimen	sL/tL	sL/pL	tL/pL	tW/pW
M2	*Pt. constans*	**IRSNB-M-1**	**1.81**	**2.90**	**1.59**	**-**
		IRSNB-M-2	1.78	2.87	1.62	2.52
		IRSNB-M-1324	1.69	2.39	1.41	1.92
		IRSNB-M-2039	1.79	2.42	1.35	1.94
		IRSNB-M-2040	1.69	2.15	1.28	2.05
		NBM Om.1	1.85	2.69	1.45	2.04
		NBM Om.158	1.61	2.23	1.39	2.08
		NBM Om.159	1.62	2.51	1.55	2.46
	Pt. musivum sp. nov.	MNHN.F.Ri220	-	-	1.33	1.85
	Pt. maximum comb. nov.	MNHN.F.CB5116	1.70	2.25	1.32	1.77
		MNHN.F.CB196	1.71	2.13	1.25	1.92
		MNHN.F.CB197	1.64	1.94	1.18	1.61
		MNHN.F.CB5119	1.60	2.01	1.26	1.67
		MNHN.F.CB5112	1.68	2.12	1.26	1.62
		MNHN.F.CB5121	1.67	2.10	1.26	1.92
		MNHN.F.CB1327	1.61	1.85	1.15	1.59
		MNHN.F.CB3322	1.61	2.02	1.25	1.65
		MNHN.F.CB4128	1.53	1.83	1.19	1.59
M3	*Pt. constans*	IRSNB-M-1331	1.68	2.32	1.38	2.00
		IRSNB-M-1332	1.52	2.35	1.54	2.34
		IRSNB-M-1333	1.49	2.26	1.52	1.88
		IRSNB-M-2030	1.59	2.62	1.65	2.53
		IRSNB-M-2041	1.50	2.34	1.56	2.21
		IRSNB-M-2042	1.72	2.79	1.63	2.58
		UM-FDN-10	1.67	2.42	1.45	2.00
	Pt. musivum sp. nov.	**MNHN.F.SN122**	**1.64**	**2.21**	**1.35**	**1.69**
		MNHN.F.SN14	1.60	2.13	1.34	1.84
	Pt. maximum comb. nov.	MNHN.F.CB5115	1.75	2.87	1.64	2.28
		MNHN.F.CB5117	1.63	2.06	1.27	1.63
		MNHN.F.CB195	1.56	1.97	1.26	-
		MNHN.F.CB198	**1.70**	**2.35**	**1.38**	**1.79**
		MNHN.F.CB5118	1.64	2.40	1.46	1.99
		MNHN.F.CB1252	1.56	2.00	1.28	1.88
		MNHN.F.CB1397	1.65	2.18	1.32	1.95
		MNHN.F.CB4121	1.69	2.29	1.35	1.77
		MNHN.F.CB4142	1.59	2.17	1.36	1.77

Supplemental material 2. Length (L), width (W), trigonid width (trW) and talonid width (tlW) measurements (in mm) of all isolated m1 to m4 of *Peratherium maximum* comb. nov. from the type locality, Condé-en-Brie (~MP8+9). Length to width ratios (L/W) are calculated for each specimen.

Specimen	Locus	L	W	L/W	trW	tlW	tlWr
MNHN.F.CB5088	m1	2,57	1,55	1,66	1,26	1,52	0,43
MNHN.F.CB207	m1	2,6	1,47	1,77	1,21	1,44	0,42
MNHN.F.CB5101	m1	2,49	1,5	1,66	1,23	1,45	0,43
MNHN.F.CB577	m1	2,58	1,57	1,64	1,36	1,53	0,41
MNHN.F.CB5120	m1	2,56	1,59	1,61	1,32	1,54	0,42
MNHN.F.CB807	m1	2,38	1,46	1,63	1,21	1,42	0,45
MNHN.F.CB841	m1	2,6	1,47	1,77	1,18	1,42	0,42
MNHN.F.CB854	m1	2,44	1,59	1,53	1,31	1,57	0,45
MNHN.F.CB1179	m1	2,47	1,49	1,66	1,21	1,42	0,44
MNHN.F.CB5125	m1	2,54	1,5	1,69	1,27	1,44	0,42
MNHN.F.CB2709	m1	2,59	1,57	1,65	1,26	1,5	0,42
MNHN.F.CB2715	m1	2,47	1,46	1,69	1,19	1,42	0,44
MNHN.F.CB2812	m1	2,47	1,5	1,65	1,23	1,46	0,44
MNHN.F.CB2896	m1	2,7	1,6	1,69	1,32	1,57	0,40
MNHN.F.CB2933	m1	2,6	1,58	1,65	1,27	1,54	0,42
MNHN.F.CB3305	m1	2,58	1,54	1,68	1,29	1,52	0,42
MNHN.F.CB3336	m1	2,38	1,43	1,66	1,19	1,38	0,45
MNHN.F.CB3398	m1	2,32	1,5	1,55	1,16	1,44	0,48
MNHN.F.CB4118	m1	2,49	1,58	1,58	1,3	1,56	0,44
MNHN.F.CB5105	m2	2,62	1,6	1,64	1,45	1,6	0,40
MNHN.F.CB593	m2	2,85	1,73	1,65	1,57	1,71	0,37
MNHN.F.CB608	m2	2,73	1,69	1,62	1,52	1,64	0,38
MNHN.F.CB648	m2	2,61	1,58	1,65	1,44	1,52	0,39
MNHN.F.CB781	m2	2,57	1,67	1,54	1,47	1,61	0,41
MNHN.F.CB826	m2	2,65	1,66	1,60	1,54	1,6	0,38
MNHN.F.CB829	m2	2,8	1,87	1,50	1,6	1,79	0,38
MNHN.F.CB831	m2	2,79	1,71	1,63	1,55	1,71	0,38
MNHN.F.CB832	m2	2,63	1,7	1,55	1,46	1,7	0,41
MNHN.F.CB838	m2	2,51	1,65	1,52	1,38	1,62	0,43
MNHN.F.CB839	m2	2,7	1,77	1,53	1,55	1,76	0,39
MNHN.F.CB5122	m2	2,78	1,75	1,59	1,55	1,7	0,38
MNHN.F.CB5123	m2	2,65	1,67	1,59	1,45	1,62	0,40
MNHN.F.CB5124	m2	2,67	1,59	1,68	1,43	1,52	0,39

MNHN.F.CB3421	m2	2,71	1,76	1,54	1,53	1,75	0,39
MNHN.F.CB3635	m2	2,78	1,65	1,68	1,52	1,62	0,37
MNHN.F.CB4125	m2	2,75	1,75	1,57	1,55	1,69	0,38
MNHN.F.CB4666	m2	2,67	1,64	1,63	1,43	1,64	0,40
MNHN.F.CB4707	m2	2,61	1,7	1,54	1,48	1,68	0,41
MNHN.F.CB208	m3	2,74	1,68	1,63	1,62	1,68	0,37
MNHN.F.CB5109	m3	2,6	1,6	1,63	1,49	1,51	0,39
MNHN.F.CB5110	m3	2,61	1,59	1,64	1,49	1,55	0,39
MNHN.F.CB698	m3	2,71	1,57	1,73	1,56	1,5	0,36
MNHN.F.CB746	m3	2,73	1,72	1,59	1,59	1,58	0,37
MNHN.F.CB821	m3	2,72	1,65	1,65	1,57	1,63	0,37
MNHN.F.CB836	m3	2,65	1,56	1,70	1,52	1,51	0,38
MNHN.F.CB1115	m3	2,62	1,6	1,64	1,47	1,52	0,39
MNHN.F.CB1116	m3	2,63	1,57	1,68	1,52	1,56	0,39
MNHN.F.CB2802	m3	2,69	1,7	1,58	1,61	1,67	0,38
MNHN.F.CB3295	m3	2,68	1,58	1,70	1,57	1,58	0,37
MNHN.F.CB3433	m3	2,7	1,58	1,71	1,49	1,52	0,37
MNHN.F.CB4127	m3	2,81	1,68	1,67	1,6	1,63	0,36
MNHN.F.CB4977	m3	2,63	1,57	1,68	1,52	1,55	0,38
MNHN.F.CB655	m4	2,43	1,37	1,77	1,36	1,26	0,40
MNHN.F.CB820	m4	2,38	1,25	1,90	1,25	1,18	0,41
MNHN.F.CB825	m4	2,54	1,39	1,83	1,39	1,3	0,38
MNHN.F.CB855	m4	2,53	1,36	1,86	1,36	1,17	0,37
MNHN.F.CB1316	m4	2,72	1,45	1,88	1,45	1,23	0,34
MNHN.F.CB4126	m4	2,53	1,43	1,77	1,36	1,23	0,38
MNHN.F.CB4170	m4	2,5	1,43	1,75	1,43	1,16	0,36
MNHN.F.CB4178	m4	2,49	1,36	1,83	1,36	1,09	0,36

Supplemental material 3 Results of Games-Howell post hoc tests (GH) performed on isolated m1-m4 of *Peratherium maximum* comb. nov. from Condé-en-Brie (~MP8+9), and boxplots of the absolute and relative labiolingual width of the talonid compared between loci. Statistical differences are recovered between pairs of lower molar loci when $p < 0.05$.

Figure S1. GH result for the mesiodistal length (L).

	diff	ci.lo	ci.hi	t	df	p
m2-m1	0.17	0.09	0.25	5.73	35.82	<.001
m3-m1	0.16	0.09	0.24	6.00	30.41	<.001
m4-m1	0.00	-0.12	0.12	0.06	12.69	1.000
m3-m2	-0.01	-0.08	0.06	0.33	30.83	.988
m4-m2	-0.17	-0.29	-0.05	4.26	11.94	.005
m4-m3	-0.17	-0.28	-0.05	4.27	9.98	.008

Figure S2. GH result for the labiolingual width (W).

	diff	ci.lo	ci.hi	t	df	p
m2-m1	0.17	0.11	0.22	8.21	33.57	<.001
m3-m1	0.09	0.04	0.15	4.86	27.60	<.001
m4-m1	-0.14	-0.22	-0.07	5.64	11.55	.001
m3-m2	-0.07	-0.13	-0.01	3.34	30.83	.011
m4-m2	-0.31	-0.39	-0.23	11.29	14.83	<.001
m4-m3	-0.24	-0.32	-0.16	8.87	13.24	<.001

Figure S3. GH result for labiolingual width of the talonid (tlW).

	diff	ci.lo	ci.hi	t	df	p
m2-m1	0.18	0.12	0.24	8.00	34.66	<.001
m3-m1	0.09	0.03	0.15	4.20	28.25	.001
m4-m1	-0.28	-0.36	-0.20	10.27	12.30	<.001
m3-m2	-0.09	-0.15	-0.02	3.67	30.62	.005
m4-m2	-0.45	-0.54	-0.37	15.76	14.82	<.001
m4-m3	-0.37	-0.45	-0.29	12.99	13.66	<.001

Figure S4. GH result for estimated surface area (S = L/2 * trW + L/2 * tlW), where S is the surface area; L is the mesiodistal length, trW is the trigonid width, and tlW is the talonid width.

	diff	ci.lo	ci.hi	t	df	p
m2-m1	0.80	0.57	1.03	9.46	34.90	<.001
m3-m1	0.73	0.52	0.95	9.19	29.36	<.001
m4-m1	-0.20	-0.49	0.08	2.11	13.83	.199
m3-m2	-0.07	-0.31	0.17	0.79	30.91	.860
m4-m2	-1.01	-1.30	-0.71	9.77	16.54	<.001
m4-m3	-0.94	-1.23	-0.65	9.47	14.29	<.001

Figure S5. GH result for the labiolingual width of the trigonid relative to approximate surface (tlWr) calculated as: tlWR = tlW / S, where tlW is the labiolingual talonid width, and S is the estimated surface area.

	diff	ci.lo	ci.hi	t	df	p
m2-m1	-0.04	-0.05	-0.03	7.22	35.18	<.001
m3-m1	-0.06	-0.07	-0.04	10.80	29.81	<.001
m4-m1	-0.06	-0.08	-0.03	6.25	11.06	<.001
m3-m2	-0.02	-0.03	0.00	3.28	30.90	.013
m4-m2	-0.02	-0.04	0.01	1.89	9.96	.293
m4-m3	0.00	-0.03	0.03	0.17	8.86	.998

Figure S6. Boxplots of the absolute (A) (tlW; see Figure S3) and relative (B) labiolingual width of the talonid (tlWr; see Figure S5) of all isolated m1s to m4s of *Peratherium maximum* comb. nov. from Condé-en-Brie (~MP8+9).

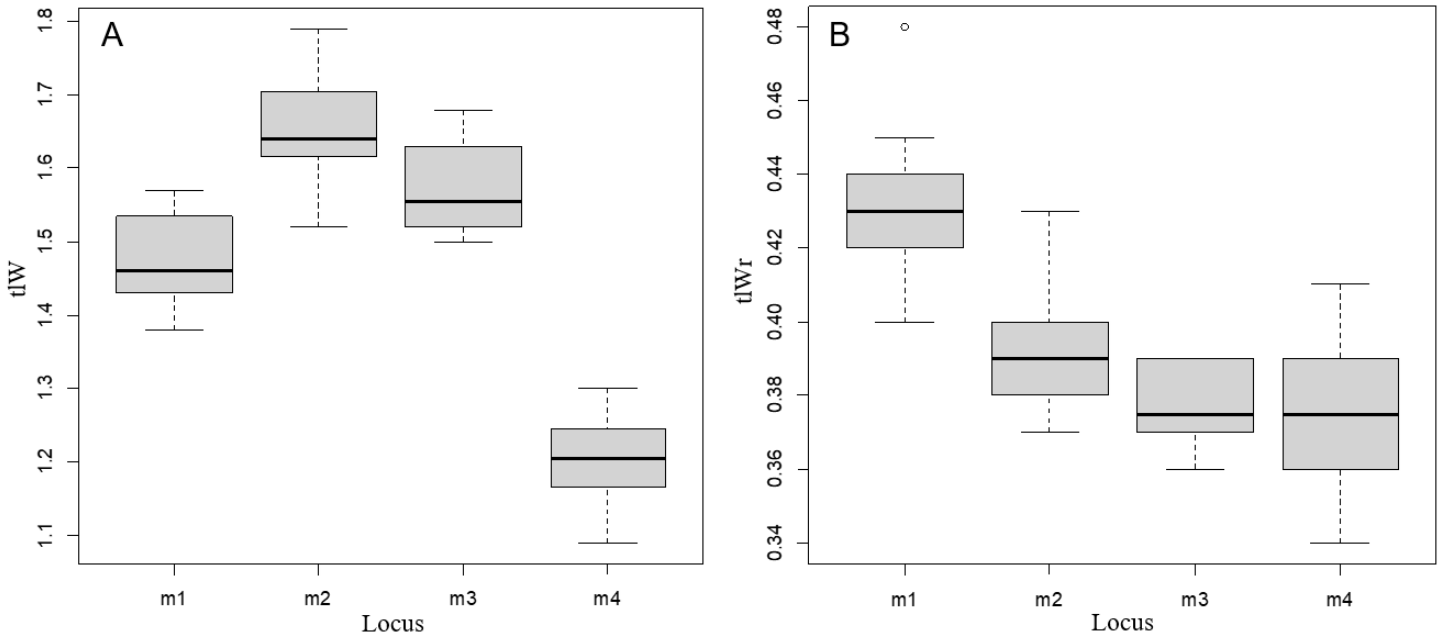

Addendum

After the submission of the manuscript, new fragmentary peratheriine specimens from the unpublished locality of La Soulane Ouest (in Corbières, probably ~MP7-MP8+9 interval) have been discovered. The mammal fauna from La Soulane Ouest is currently under study. Here we report two fragments of upper molars belonging to relatively large peratheriines. The first fragment, having preserved the paracone, stylar cusps A to C, and the postparacrista (Figure 1B), is similar in size and morphology to the single known M1 of *Pt. musivum* (Figure 1A-B). A second fragment with only the talon and the lingual edge of the metacone has a relatively long protocone (Figure 1D), as unequivocal *Pt. maximum* specimens, to which it also corresponds in size (Figure 1C-D). *Peratherium musivum* and *Pt. maximum* were thus possibly both present in La Soulane Ouest. This documents a second case of coexistence of the two species, in addition to that of Pourcy (see Table 7 in the paper), which was based on lower rather than upper molars (see Figure 5 in the paper). The putative occurence of the two species in La Soulane is possibly biostratigraphically significant.

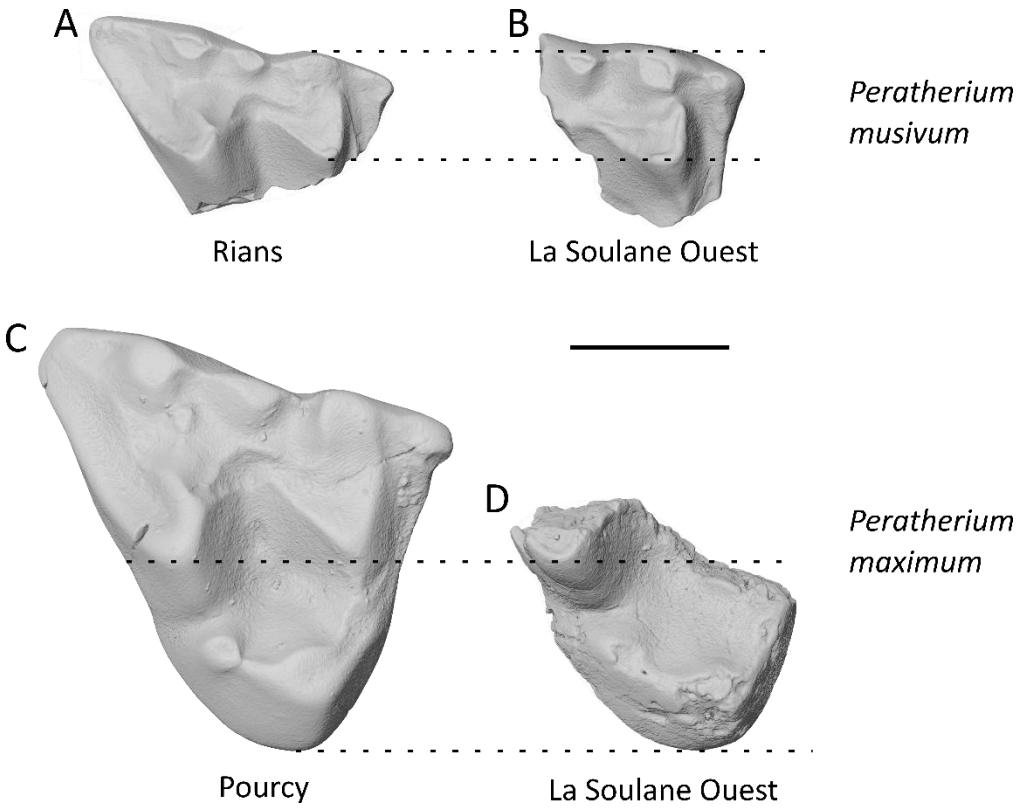

Figure 1. M1s fragments from La Soulane Ouest (B, D) compared with published M1s of *Peratherium musivum* and *Pt. maximum* (A, C). **A**. MNHN.F.RI296, from Rians. **B**. UM-SOL-1, mesiolabial fragment. **C**. MNHN.F.PY18001, from Pourcy. **D**. UM-SOL-2, distolingual fragment.

Dataset

3D models related to the publication: Dental morphology evolution in early peratheriines, including a new morphologically cryptic species and findings on the largest early Eocene European metatherian.

Killian Gernelle[1*], Marc Godinot[2], Bernard Marandat[1], Dominique Téodori[3], Sandrine Ladevèze[4†], Rodolphe Tabuce[1†]

[1] *Institut des Sciences de l'Évolution de Montpellier (ISEM, UMR 5554), Univ Montpellier, CNRS, IRD, c.c. 064, Place Eugène Bataillon, F-34095 Montpellier Cedex 05, France*
Ecole Pratique des Hautes Etudes, PSL, UMR 7207, CR2P, 8 rue Buffon, F75005, Paris, France
[3] *8 impasse de San Marino, 31140 Pechbonnieu, Haute-Garonne, France*
[4] *Centre de Recherche en Paléontologie - Paris (CR2P, UMR 7207), Sorbonne Université, Muséum National d'Histoire Naturelle, CNRS, 8 rue Buffon, F-75005, Paris, France*
*__Corresponding author__: killian.gernelle@umontpellier.fr; †Co-senior authors

Abstract
This contribution contains the three-dimensional models of the most informative fossil material attributed to both *Peratherium musivum* Gernelle, 2024, and *Peratherium maximum* (Crochet, 1979), respectively from early and middle early Eocene French localities. These specimens, which document the emergence of the relatively large peratheriines, were analyzed and discussed in: Gernelle et al. (2024), Dental morphology evolution in early peratheriines, including a new morphologically cryptic species and findings on the largest early Eocene European metatherian. https://doi.org/10.1080/08912963.2024.2403602

Keywords: France, Herpetotheriidae, molars, systematics, Ypresian

Submitted: 26/11/2024, published online: 06/01/2025. https://doi.org/10.18563/journal.m3.255

INTRODUCTION

The subfamily Peratheriinae includes all Cenozoic European herpetotheriid metatherians known to date (Ladevèze et al., 2020; *Peratherium* and *Amphiperatherium* genera), which are characterized by the conservative morphology of their tribosphenic molars. Most of their intrasubfamilial relationships are unclear so far (Ladevèze et al., 2012; Gernelle et al., 2024b). *Peratherium musivum* Gernelle, 2024 is currently the second oldest peratheriine species. It was approximately two times larger than the earliest species of this subfamily, spanned part of the time interval between the MP7 and MP8+9 reference level and shares morphological characters with the largest early Eocene metatherian, *Peratherium maximum* (Crochet, 1979) (Gernelle et al., 2024b). We present here the 3D digital models of six key specimens of *Pt. musivum* and *Pt. maximum*, from three French fossiliferous localities (Table 1). *Peratherium musivum* is best documented in the Southern France Rians fauna, by four isolated molars (Fig. 1A-H, L) representing two successive upper (Fig. 1A-D; M1-M2) and two successive lower (Fig. 1E-H; m1-m2) molar loci (Gernelle et al., 2024b). The Rians specimens were first allocated to two *Amphiperatherium* taxa (Godinot, 1981). The M3 holotype of *Pt. musivum* (Fig. 1I-K), first attributed to an indeterminate *Peratherium* species by Crochet (1980), is from the Northern France locality of Soissons, thereby showing that *Pt. musivum* was likely present somewhat simultaneously in Northwestern and Southwestern European faunas, alongside other contemporaneous European metatherian species (Gernelle et al., 2024a, 2024b). During molar occlusion, the protocone of upper molars contacts the talonid basin of lower molars at the termination of the power stroke (Fig. 1L; Crompton and Hiiemae, 1970). Early peratheriine species notably differ from one another in molar features concerning the relative size of the protocone – talonid basin functional complex, which is relatively larger in *Pt. maximum* (Gernelle et al., 2024b: tables 5-6). The peratheriine hemi-mandible from the middle early Eocene fauna (∼MP8+9) of La Borie (UM-BRI-17; Fig. 2), found and prepared by one of us (DT), documents the first known occurrence of *Pt. maximum* in Southwestern Europe, and is the single known specimen of this species with associated teeth. The relatively large size of the posterior alveolus of the m2, in addition to the elongate shape of lower molar alveoli (Fig. 2B), are informative characters regarding the generic systematics of early peratheriines (Gernelle et al., 2024b: table 4). The peratheriine specimens are permanently housed in the collections of the Muséum National d'Histoire Naturelle (MNHN), for those from Soissons and Rians, and of the Université de Montpellier (UM), for the hemi-mandible from La Borie (Table 1).

METHODS

The six peratheriine specimens were scanned by one of us (KG) using a µ-CT-scanning station EasyTom 150/Rx Solutions (Montpellier RIO Imaging [MRI], ISEM, Montpellier, France), with a resolution between 8 and 9 µm, except for the M1 MNHN.F.RI296 (Fig. 1C-D), scanned with a resolution of 6.6 µm. The 3D surfaces were extracted semi-automatically from the five isolated molars of *Pt. musivum* (Fig. 1) using

Inv nr.	Taxon	Description	Collection
MNHN.F.SN122	*Peratherium musivum*	right M3	MNHN, Paris
MNHN.F.RI220	*Peratherium musivum*	left M2 (partial)	MNHN, Paris
MNHN.F.RI296	*Peratherium musivum*	right M1 (partial)	MNHN, Paris
MNHN.F.RI368	*Peratherium musivum*	right m2	MNHN, Paris
MNHN.F.RI385	*Peratherium musivum*	left m1	MNHN, Paris
UM-BRI-17	*Peratherium maximum*	right hemi-mandible with p1-p3, m1-m3 alveoli, and m4	ISEM, Montpellier

Table 1. List of 3D models of *Peratherium musivum* specimens from Soissons (SN) and Rians (RI), and of *Peratherium maximum* from La Borie (BRI). Collections: Muséum National d'Histoire Naturelle, Paris (MNHN) for Soissons and Rians specimens; Université de Montpellier, France (UM) for the specimen from La Borie.

the segmentation threshold selection tool of Avizo® 9.3. The M2 MNHN.F.RI220 (Fig. 1A-B) and the m2 MNHN.F.RI368 (Fig. 1E-F) have been oriented, and their protocone and talonid basin have been put in occlusion (Fig. 1L) using the MorphoDig open-source 3D freeware (Lebrun, 2018). Regarding the hemi-mandible UM-BRI-17 (Fig. 2), a pre-segmentation of the cheek teeth and dentary of one slice every 5-10 slices was performed, employing the lasso, magic wand and blow selection tools of Avizo® 9.3. The smart interpolation tool of the online platform Biomedisa (Lösel et al., 2020) was used to complete the segmentation. The 3D surface models, visualized with Avizo® 9.3, are provided in .ply format and can therefore be opened with a wide range of freeware (e.g., MorphoDig).

ACKNOWLEDGEMENTS

We acknowledge Guillaume Billet (MNHN) for the loan of specimens from the MNHN mammals' collection, under his care. We are also thankful to Vincent N. Pernègre (MNHN), who managed the allocation of the MNHN specimen number of the holotype of *Peratherium musivum*. Three-dimensional data acquisition was performed using the micro-computed tomography (µ-CT) facilities of the MRI platform member of the national infrastructure France-BioImaging supported by the French National Research Agency (ANR-10-INBS-04, 'Investments for the future'), the labex CEMEB (ANR-10-LABX-0004) and NUMEV (ANR-10-LABX-0020). This research was financially supported by a PhD thesis funding from the French Ministry of Higher Education, Research, and Innovation, and in part by the ANR project EDENs (ANR-20-CE02-0007). This is ISEM publication n° 2024-x.

BIBLIOGRAPHY

Crochet, J.-Y. 1980. Les marsupiaux du Tertiaire d'Europe. Paris: Editions Foundation Singer-Polignac. https://doi.org/10.1163/9789004630802

Crompton, A.W., Hiiemae, K. 1970. Molar occlusion and mandibular movements during occlusion in the American opossum, *Didelphis marsupialis* L. Zoological Journal of the Linnean Society 49, 21-47. https://doi.org/10.1111/j.1096-3642.1970.tb00728.x

Gernelle, K., Billet, G., Gheerbrant, E., Godinot, M., Marandat, B., Ladevèze, S., Tabuce, R. 2024. Taxonomy and evolutionary history of peradectids (Metatheria): new data from the early Eocene of France. Journal of Mammalian Evolution 31, 31. https://doi.org/10.1007/s10914-024-09724-5

Gernelle, K., Godinot, M., Marandat, B., Téodori, D., Ladevèze, S., Tabuce, R. 2024b. Dental morphology evolution in early peratheriines, including a new morphologically cryptic species and findings on the largest early Eocene European metatherian. Historical Biology. https://doi.org/10.1080/08912963.2024.2403602

Godinot, M. 1981. Les mammifères de Rians (Eocène inférieur, Provence). Palaeovertebrata 10, 43–126.

Ladevèze, S., Selva, C., Muizon, C. de. 2020. What are "opossum-like" fossils? The phylogeny of herpetotheriid and peradectid metatherians, based on new features from the petrosal anatomy. Journal of Systematic Palaeontology 18, 1463–1479. https://doi.org/10.1080/14772019.2020.1772387

Ladevèze S, Smith R, Smith T. 2012. Reassessment of the morphology and taxonomic status of the earliest herpetotheriid marsupials of Europe. Journal of Mammalian Evolution 19, 249–261. https://doi.org/10.1007/s10914-012-9195-0

Lebrun, R. 2018. MorphoDig, an open-source 3D freeware dedicated to biology. 5th International Paleontological Congress (IPC5). Available at https://morphomuseum.com/downloadMorphodig

Lösel, P. D., Kamp, T. van de, Jayme, A., Ershov, A., Faragó, T., Pichler, O., Tan Jerome, N., Aadepu, N., Bremer, S., Chilingaryan, SA. et al. 2020. Introducing Biomedisa as an open-source online platform for biomedical image segmentation. Nature Communications 11, 5577. https://doi.org/10.1038/s41467-020-19303-w

 ISSN: 2274-0422

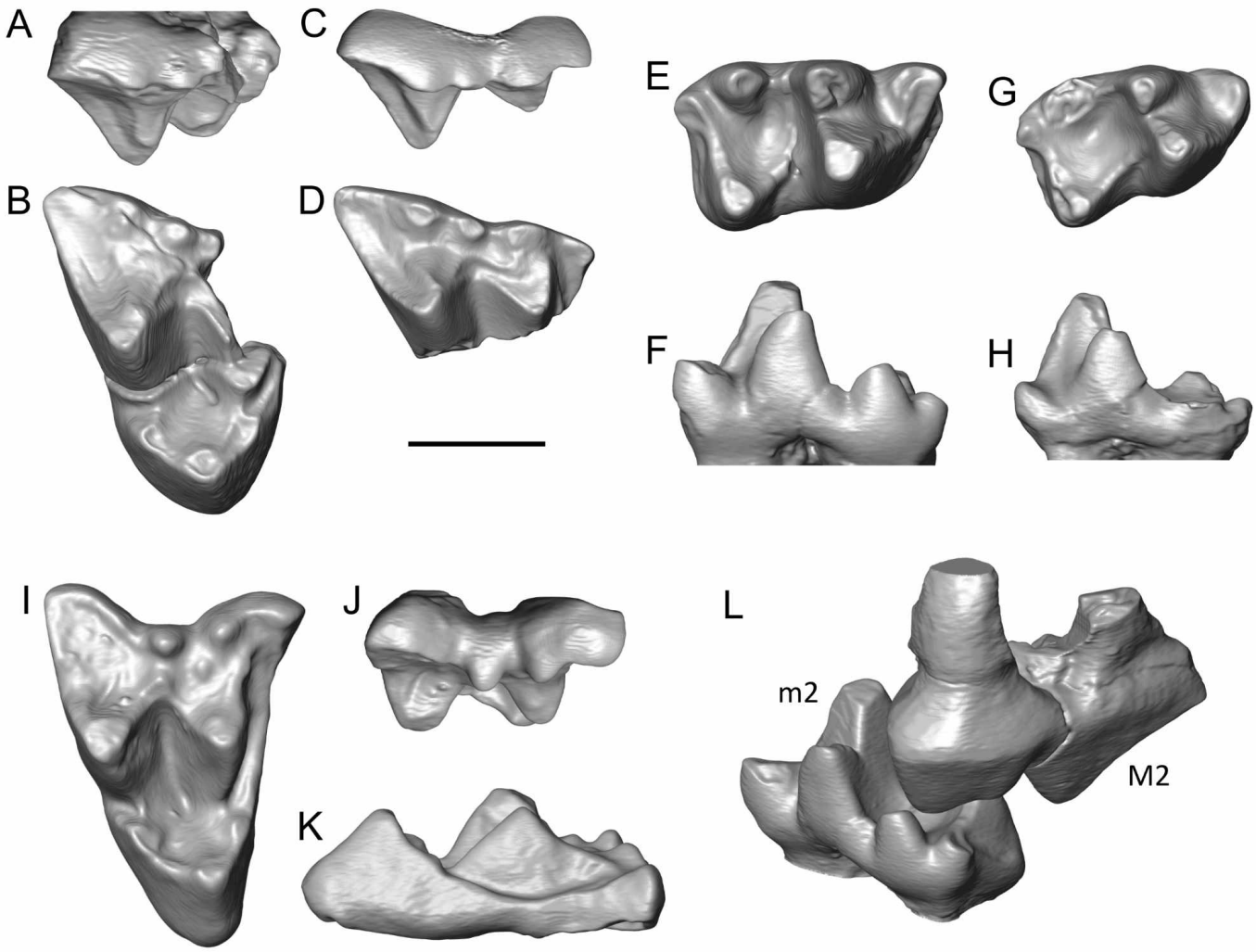

Figure 1. Three-dimensional models of isolated upper and lower molars of *Peratherium musivum* from Rians in Southern France (A-H, L) and Soissons in Northern France (I-K), both in the time interval between MP7 and MP8+9 reference levels. **A-B**, MNHN.F.RI220, partial left M2 in reverse labial (A) and occlusal (B) views. **C-D**, MNHN.F.RI296, partial right M1 in labial (C) and occlusal (D) views. **E-F**, MNHN.F.RI368, right m2 in occlusal (E) and lingual (F) views. **G-H**, MNHN.F.RI385, left m1 in reverse occlusal (G) and lingual (H) views. **I-K**, MNHN.F.SN122, holotype, right M3 in occlusal (I), labial (J) and mesial (K) views. **L**, M2 MNHN.F.RI220 and m2 MNHN.F.RI368 with occluding protocone and talonid basin in distolingual view (reversed for MNHN.F.RI220). The scale bar equals 1 mm.

ISSN: 2274-0422

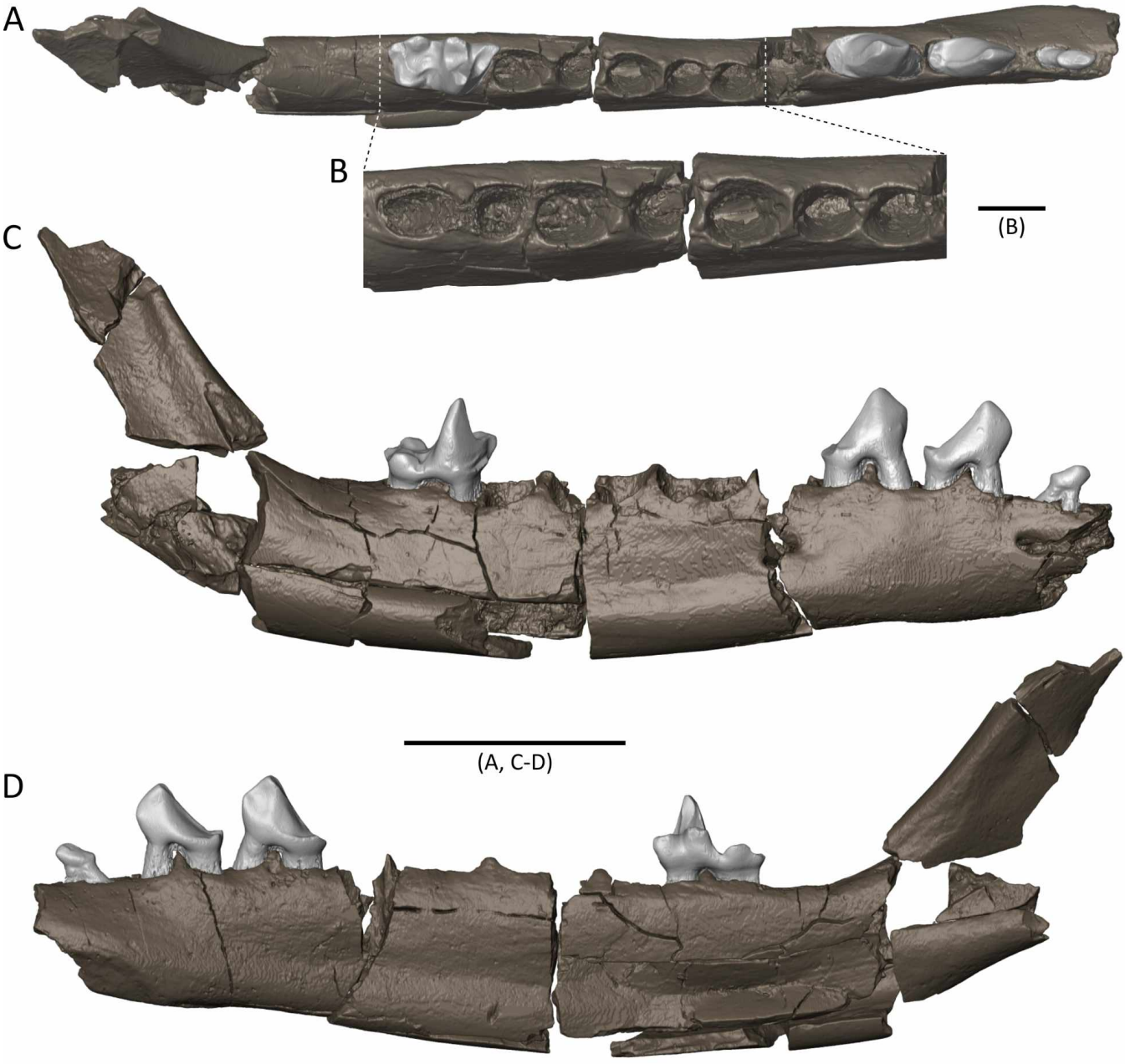

Figure 2. Three-dimensional model of the right hemi-mandible UM-BRI-17 with p1-p3, m1-m3 alveoli, and m4, of *Peratherium maximum* from La Borie (Lauragais, Southern France; ~MP8+9). **A**, Occlusal view. **B**, Occusal view with a close-up on m1 to m4 alveoli (with m4 removed). **C**, Lateral (labial) view. **D**, Medial (lingual) view. Scale bars equal 1 mm (B) and 5 mm (A, C-D).

ISSN: 2274-0422

Chapitre 6. Révision systématique des Peratheriinae de l'Éocène inférieur

Remarque. Contrairement aux chapitres précédents, les mesures présentées dans cette section ont majoritairement été acquises grâce à un mesuroscope (Nikon Measuroscope 10) couplé à un compteur numérique (Nikon Digital Counter CM-6S).

1. Taxonomie des Peratheriinae de l'Éocène inférieur précoce (MP7) à moyen (MP8+9)

A. *Peratherium constans* vs *Peratherium matronense* : évolution des premiers petits pérathériinés de l'Éocène inférieur

Peratherium constans Teilhard de Chardin, 1927 et *Peratherium matronense* Crochet, 1979 sont les deux premiers pérathériinés de petite taille de l'Éocène inférieur. D'après Crochet (1980), *Pt. constans*, suivi de *Pt. matronense*, ont initié une lignée évolutive d'espèces de *Peratherium* de petite taille perdurant jusqu'au Bartonien. *Peratherium constans* et *Pt. matronense* n'ont pas pu être distingués morphologiquement à partir du matériel dentaire des localités types, d'après les travaux les plus récents, qui ne consistaient cependant pas en une révision taxonomique de ces espèces (Hooker et al. 2008 : fig. 5 ; Ladevèze et al. 2012 : 257). De plus, les tailles des spécimens attribués aux deux espèces seraient en partie chevauchante d'après Ladevèze et al. (2012: 257). Enfin, la distinction initiale de *Pt. constans* et *Pt. matronense* par Crochet (1979) était basée sur un nombre restreint de localités : Dormaal (MP7) et Mutigny (< MP8+9) d'une part pour *Pt. constans*, et les localités plus jeunes, proches d'Avenay (MP8+9) en âge (e.g. Condé-en-Brie, ~MP8+9), ayant livré *Pt. matronense* d'autre part. Depuis, *Pt. constans* et *Pt. matronense*, ou des taxons proches (en nomenclature ouverte) ont été signalés dans de nombreuses localités de l'intervalle de temps entre MP7 et MP8+9 (Godinot 1981, Godinot et al. 1987, Russell et al. 1988, Marandat 1991, Estravís 2000, Marandat et al. 2012). La révision taxonomique exhaustive de l'ensemble des pérathériinés de petite taille allant de l'Éocène inférieur précoce à moyen est conduite ci-dessous à partir de matériel inédit en plus de tous les spécimens publiés par ailleurs.

Paléontologie systématique

Marsupialiformes Vullo et al., 2009

Notometatheria Kirsch, Lapointe & Springer, 1997

Herpetotheriidae (Trouessart, 1879)

Peratheriinae Ladevèze, Selva & Muizon, 2020

Peratherium Aymard, 1850

Peratherium constans Teilhard de Chardin, 1927

Figures 1-6 (sauf Figure 2F) ; Tableau 1 ; Annexes : Tableau S1

1927 – *Peratherium constans* sp. nov. in Teilhard de Chardin p. 7, text-fig. 1, pl. 1, figs. 1-4.
1979 – *Amphiperatherium brabantense* sp. nov. in Crochet p. 369, fig. 4.
1980 – *Amphiperatherium brabantense* Crochet in Crochet p. 60-62, figs. 34-37, 39 (en partie : spécimens de Dormaal).
1980 – *Peratherium constans* Teilhard de Chardin in Crochet p. 144-147, figs. 152-156 (en partie : spécimens de Dormaal).
1981 – *Amphiperatherium* aff. *brabantense* Crochet in Godinot p. 53-54.
1981 – *Peradectes louisi* Crochet in Godinot p. 51-52, text-fig. 4a, pl. 1, fig. 2 (en partie).
1981 – *Peratherium matronense* Crochet in Godinot p. 52-53, text-fig. 4b.
1987 – *Peratherium constans* Teilhard de Chardin in Godinot et al. p. 283 (en partie: un spécimen rapporté à *Peradectes crocheti* dans Gernelle et al. [2024a]).
1988 – *Peratherium* cf. *matronense* Crochet in Russell et al. p. 431.
1991 – *Amphiperatherium* cf. *brabantense* Crochet in Marandat p. 71-72, pl. 1, fig. 4 (en partie : un spécimen a été rapporté à *Peradectes crocheti* dans Gernelle et al. [2024a]).
1991 – *Peradectes* sp. indet. (cf. *Peradectes* sp. indet. in Crochet 1980) in Marandat p. 66-68, pl. 1, fig. 18 (en partie).
1991 – *Peratherium constans* Teilhard de Chardin in Marandat p. 68-69, pl. 1, figs. 5-6, 8, 10-11 (en partie).
1999 – *Peratherium* sp. or *Amphiperatherium* sp. in Nel et al. p. 70.
2000 – *Peratherium* cf. *constans* Teilhard de Chardin in Estravís p. 282 (en partie).
2012 – *Peratherium constans* Teilhard de Chardin in Ladevèze et al. figs. 1-6.
2012 – ?*Peratherium constans* Teilhard de Chardin in Marandat et al. p. 428.
2013 – *Peratherium constans* Teilhard de Chardin in Coillot et al. p. 280, fig. 5I-L, tables 1, 3.
2024a – *Peratherium constans* Teilhard de Chardin in Gernelle et al. p. 21, fig. 7d.
2024b – *Peratherium constans* Teilhard de Chardin in Gernelle et al. fig. 4H, N-O, fig. 5N, tables 5-6.

Holotype. IRSNB-M-1, M2 droite (Ladevèze et al. 2012: fig. 1a), de Dormaal (Belgique).

Localités et âge. Dormaal (localité-type) en Belgique. Silveirinha au Portugal. Le Quesnoy (Oise), Soissons (Aisne) et Meudon (Île-de-France) dans le Nord de la France. Fordones et Le Clot (Corbières), Palette et Rians (Provence) dans le Sud de la France. Du début de l'Éocène inférieur (MP7 ; ~56 Ma) à,

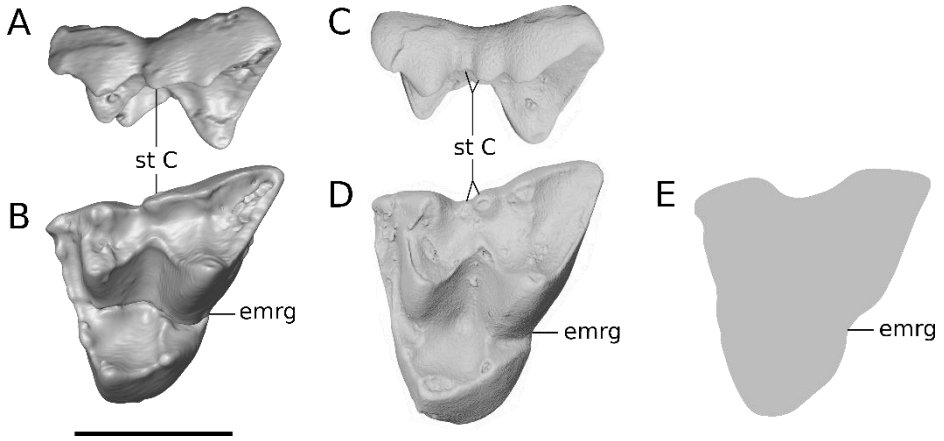

Figure 1. Molaires supérieures de *Peratherium constans* Teilhard de Chardin, 1927, du Quesnoy (~MP7, Bassin de Paris). **A-B**. Modèle surfacique 3D de la M1 droite MNHN.F.QNY526 en vues (miroir) labiale (A) et occlusale (B). **C-D**. M2 droite MNHN.F.QNY525bis en vues (miroir) labiale (C) et occlusale (D). **E**. Comparaison avec la silhouette de l'holotype de *Pt. constans* (M2 droite IRSNB-M-1) en vue occlusale (miroir). Abréviations : emrg, émargination distale ; st, cuspide stylaire. Échelle : 1 mm.

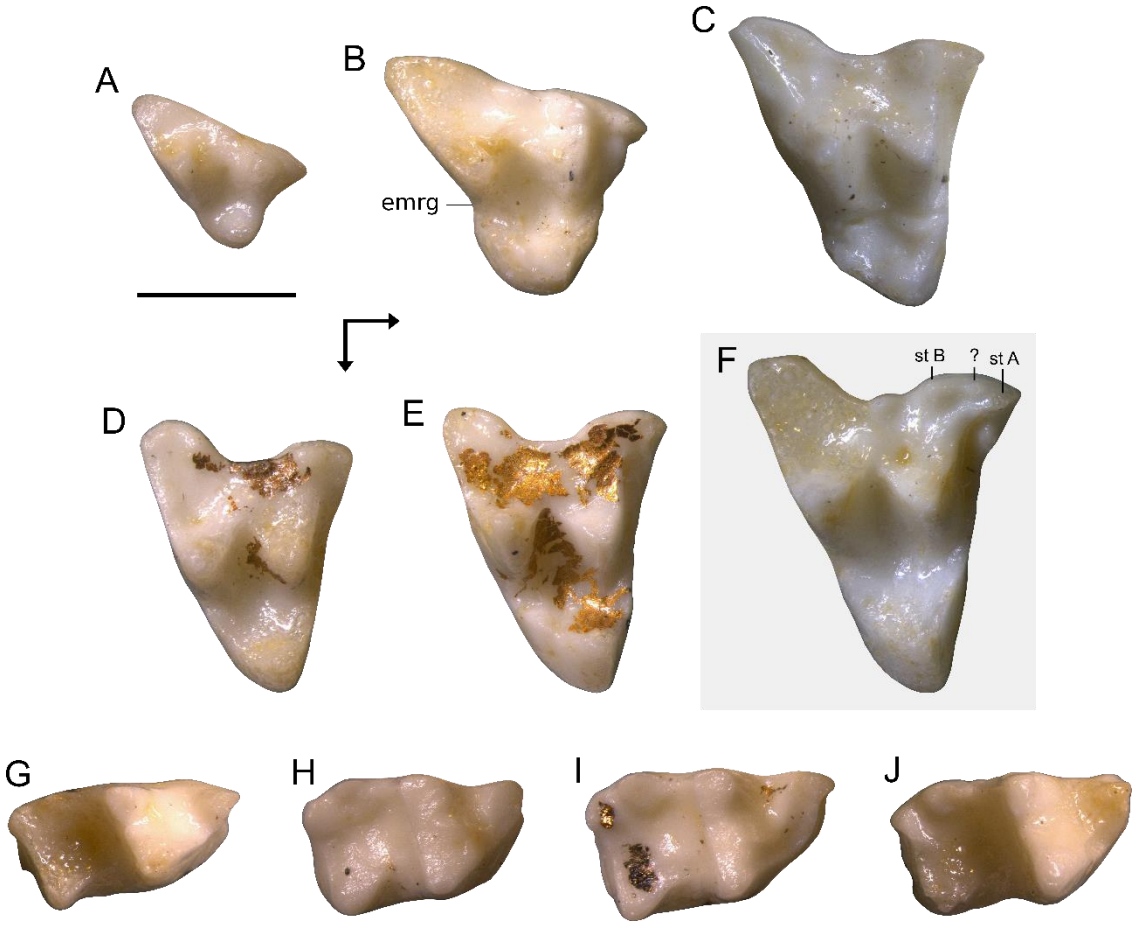

Figure 2. Dents molariformes des pérathériinés de Silveirinha (~MP7, Portugal) en vue occlusale, à partir de moulages des spécimens (collection UM). Seule une M3 (**F**) ne représente probablement pas *Peratherium constans* Teilhard de Chardin, 1927. **A**. DP3 droite SV3-270. **B**. M1 droite SV3-169. **C**. M2 gauche SV3-171 en vue miroir. **D**. M3 droite SV1-154. **E**. M3 droite SV2-32. **F**. M3 droite SV3-469 (espèce indéterminée). **G**. m1 gauche SV2-16 en vue miroir. **H**. m2 droite SV3-73. **I**. m2 droite SV2-28. **J**. m3 gauche SV1-156. Abréviation : st, cuspide stylaire. Échelle : 1 mm.

approximativement, antérieurement à l'ETM2 (≤ 54 Ma) : parmi les localités datées par chémostratigraphie, *Pt. constans* est présent à Fordones et Le Clot (~55 Ma ; Yans et al. 2014), alors que *Pt. matronense* est identifié et *Pt. constans* est absent au sein de la faune post-ETM2 (54 Ma) de Fournes (Noiret et al. 2016).

Diagnose différentielle proposée par Ladevèze et al. (2012). « *Peratherium constans* differs from the type species *P. elegans* by its smaller size and some morphological features: smaller stylar cusp B, no crest between stylar cusps B and C, less developed stylar shelf on M3, anterior and posterior cingulids less marked, less reduced talonid with a less acute angle of the posthypocristid and cristid obliqua. *Peratherium constans* shares with the Eocene smallest sized species of *Peratherium* (*P. matronense*, *P. sudrei*, *P. bretouense*) numerous morphological features (see Crochet 1980: 160–161). Particularly, *P. constans* and *P. matronense*, both from the early Eocene, are hardly distinguishable from one another, the differential characters pointed up by Crochet (1980) being interpreted here as morphological variations. »

Diagnose différentielle émendée. Espèce en moyenne plus petite que *Peratherium matronense*. L'émargination distale de la couronne des M1s et des M2s, entre le talon et le plateau stylaire, est en moyenne plus profonde que chez *Peratherium matronense*, *Pt. musivum*, *Pt. maximum* et *Pt. monspeliense*. Diffère aussi de *Pt. musivum*, *Pt. maximum* et *Pt. monspeliense* par les m2s et m3s équivalentes en taille. Diffère aussi de *Pt. musivum* et *Pt. maximum* par le complexe fonctionnel protocône/talonide relativement plus petit.

Matériel. Les spécimens figurés ci-après sont signalés en gras dans la liste du matériel.

Matériel de Dormaal : la série type de *Peratherium constans* (~ 400 spécimens) décrite par Ladevèze et al. (2012). La morphologie de ces spécimens n'est pas redécrite en détail ici, mais des mesures en ont été prises pour la première fois, à partir d'un échantillon représentatif (Tableau 1), à l'aide d'un micromètre réticulé Wild connecté à un système numérique de mesure Wild MMS-235 (Heerbrugg, Suisse).

Matériel de Le Quesnoy (Figure 1) : M1 droite (**MNHN.F.QNY526**), M2 gauche (MNHN.F.QNY524), M2 droite (**MNHN.F.QNY525bis**).

Matériel de Silveirinha, moulages uniquement (Figure 2) : dP3 droite (**SV3-270**), M1 droite (**SV3-169**), M2 (SV1-477, fragmentaire), fragment de maxillaire gauche avec M2-M3 (**SV3-171**), M3 droite (**SV1-154** ; **SV2-32**), m1 (SV1-149 ; **SV2-16**), m2 droite (**SV2-28** ; **SV3-73**), m3 (SV1-155 ; **SV1-156**). **Remarque**. Des spécimens supplémentaires ont été étudiés dans la thèse de doctorat non publiée d'Estravís (1992). Le matériel réétudié et partiellement figuré ici est essentiellement celui figuré par Estravís (1992: pl. 4).

Matériel de Palette (Figures 3-4) : *Dents jugales supérieures* : P3 droite (**UM-PAT-109**), dP3 droite (**UM-PAT-101**), M1 droite (**UM-PAT-104**), M2 droite (MHN.AIX.PV.2018.26.9, fragmentaire ; MHN.AIX.PV.2018.26.11, fragmentaire ; MHN.AIX.PV.2018.26.12 ; MHN.AIX.PV.2018.26.13 ; **UM-PAT-105**), M3 droite (**UM-PAT-177**), aire métastylaire de M3 droite (MHN.AIX.PV.2018.26.10),

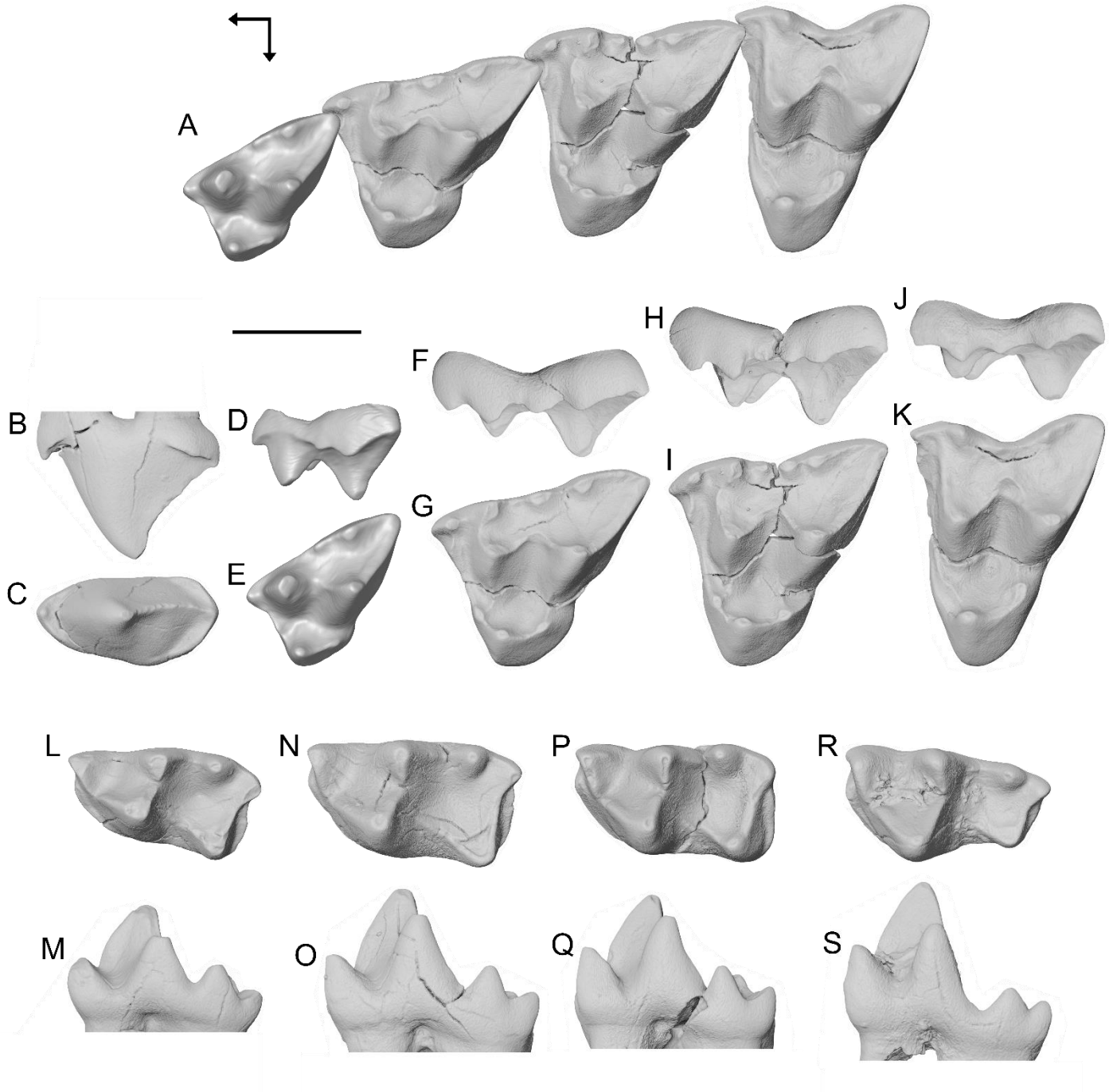

Figure 3. Rangées composites de dents jugales de *Peratherium constans* Teilhard de Chardin, 1927, de Palette (Provence, intervalle MP7-MP8+9). **A**. Rangée composite dP3-M3 en position anatomique et en vue occlusale (détail des spécimens ci-après). Les flèches indiquent les directions mésiale et linguale pour les vues occlusales des molaires supérieures. **B-K**. Dents jugales supérieures isolées, P3- M3. **B-C**. P3 droite UM-PAT-109 en vues (miroir) labiale (B) et occlusale (C). **D-E**. DP3 droite UM-PAT-101 (modèle surfacique 3D) en vues (miroir) labiale (D) et occlusale (E). **F-G**. M1 droite UM-PAT-104 en vues (miroir) labiale (F) et occlusale (G). **H-I**. M2 droite UM-PAT-105 en vues (miroir) labiale (H) et occlusale (I). **J-K**. M3 droite UM-PAT-177 en vues (miroir) labiale (J) et occlusale (K). **L-S**. Molaires inférieures isolées, m1-m4. **L-M**. m1 gauche UM-PAT-107 en vues occlusale (L) et linguale miroir (M). **N-O**. m2 gauche UM-PAT-111 en vues occlusale (N) et linguale miroir (O). **P-Q**. m3 gauche UM-PAT-100 en vues occlusale (P) et linguale miroir (Q). **R-S**. m4 gauche MHN.AIX.PV.2017.6.18 en vues occlusale (R) et linguale miroir (S). Échelle : 1 mm.

maxillaire gauche avec M2-M3 fragmentaires (MHN.AIX.PV.2018.26.23). *Molaires inférieures* : m1 gauche (MHN.AIX.PV.2018.26.17 ; **UM-PAT-107**), m1 droite (MHN.AIX.PV.2017.6.16 ; MHN.AIX.PV.2018.26.7 ; MHN.AIX.PV.2018.26.8 ; UM-PAT-110, fragmentaire), talonide de m1 ou m2 gauche (MHN.AIX.PV.2018.26.5), m2 gauche (**UM-PAT-111**), m2 droite (MHN.AIX.PV.2017.6.7 ; MHN.AIX.PV.2018.26.6), talonide de m2 ou m3 droite (MHN.AIX.PV.2018.26.22), m3 gauche (MHN.AIX.PV.2017.6.17 ; **UM-PAT-100**), m3 droite (MHN.AIX.PV.2018.26.19 ; UM-PAT-106, fragmentaire ; UM-PAT-108), m4 gauche (**MHN.AIX.PV.2017.6.18**), hémi-mandibule gauche avec m2-m4 (**MHN.AIX.PV.2018.26.18**).

Matériel de Meudon (Figure 5) : *Molaires supérieures* : M1 gauche (MNHN.F.ME16168), M1 droite (MNHN.F.ME16078, fragmentaire ; **MNHN.F.ME16197**), M2 gauche (**MNHN.F.ME16301**, usé), M2 droite (MNHN.F.ME25-G, moulage ; MNHN.F.ME16414, fragmentaire), M3 gauche (MNHN.F.ME15987, fragmentaire ; **MNHN.F.ME16095**), M3 droite (**MNHN.F.ME16312**). *Molaires inférieures* : m1 gauche (MNHN.F.ME16321), m1 droite (**MNHN.F.ME16207**, MNHN.F.ME16397), m2 gauche (MNHN.F.ME16071), m2 droite (MNHN.F.ME16382), m3 gauche (**MNHN.F.ME16403**), m3 droite (**MNHN.F.ME16289**), m4 gauche (MNHN.F.ME48-G, moulage ; **MNHN.F.ME16362**).

Matériel de Soissons (Figure 6A-G) : M1 (**MNHN.F.SN23-BN**), M2 (**MNHN.F.SN38-BN**), m3 (**MNHN.F.SN59-BN**), fragment de dentaire avec alvéoles de m3, et m4 (**MNHN.F.SN35-BN**).

Matériel de Fordones (Figure 6H-M) : *Molaires supérieures* : M1 gauche (UM-FDN-4, fragmentaire, Marandat 1991 : pl. 1, fig. 4 ; UM-FDN-7 ; UM-FDN-161 ; UM-FDN-291), M1 droite (UM-FDN-3, fragmentaire ; **UM-FDN-5**, Marandat 1991 : pl. 1, fig. 5 ; UM-FDN-8 ; UM-FDN-299, fragmentaire), M2 gauche (UM-FDN-6, Marandat 1991 : pl. 1, fig. 8 ; UM-FDN-9, fragmentaire ; UM-FDN-292), M2 droite (UM-FDN-293 ; UM-FDN-298, fragmentaire), M3 gauche (UM-FDN-295, fragmentaire ; UM-FDN-300, fragmentaire ; UM-FDN-301, fragmentaire), M3 droite (**UM-FDN-10**, fragmentaire, Marandat 1991 : pl. 1, fig. 6 ; UM-FDN-296, fragmentaire ; UM-FDN-297, fragmentaire). Molaires *inférieures* : m1 gauche (UM-FDN-12), m1 droite (UM-FDN-16 ; UM-FDN-157), m2 gauche (UM-FDN-155, fragmentaire ; UM-FDN-257, fragmentaire, Marandat 1991 : pl. 1, fig. 11), m2 droite (UM-FDN-17, fragmentaire ; UM-FDN-18, fragmentaire, Gernelle et al. 2024a : fig. 7d ; UM-FDN-20, fragmentaire ; UM-FDN-158, fragmentaire), m3 gauche (UM-FDN-11, fragmentaire ; UM-FDN-14 ; UM-FDN-15 ; UM-FDN-19), m3 droite (UM-FDN-294), fragment de dentaire gauche avec m3-m4 (UM-FDN-156), m4 droite (UM-FDN-13, Marandat 1991 : pl. 1, fig. 10 ; **UM-FDN-250**). **Remarque** : un nombre conséquent de spécimens non numérotés (> 10) consistent en des trigonides et talonides isolés rapportés à cette espèce.

Matériel de Rians (Figure 6N-P) : M1 (MNHN.F.RI342, fragmentaire), M2 (MNHN.F.RI379, fragmentaire ; MNHN.F.RI420, fragmentaire, Godinot 1981: fig. 4a ; **MNHN.F.RI517**), M3

(MNHN.F.RI378, fragmentaire ; **MNHN.F.RI392**, Godinot 1981: fig. 4b), m1 (**MNHN.F.RI226**), m2 (MNHN.F.RI411, Godinot 1981: fig. 4e), m4 (MNHN.F.RI244, fragmentaire, spécimen complet figuré par Godinot 1981: pl. 1, fig. 2).

Matériel de Le Clot : P2 droite (UM-CLO-55), M1 gauche (UM-CLO-53, fragmentaire), M3 droite (UM-CLO-56, fragmentaire), M4 droite (UM-CLO-54, fragmentaire), m2 gauche (UM-CLO-52).

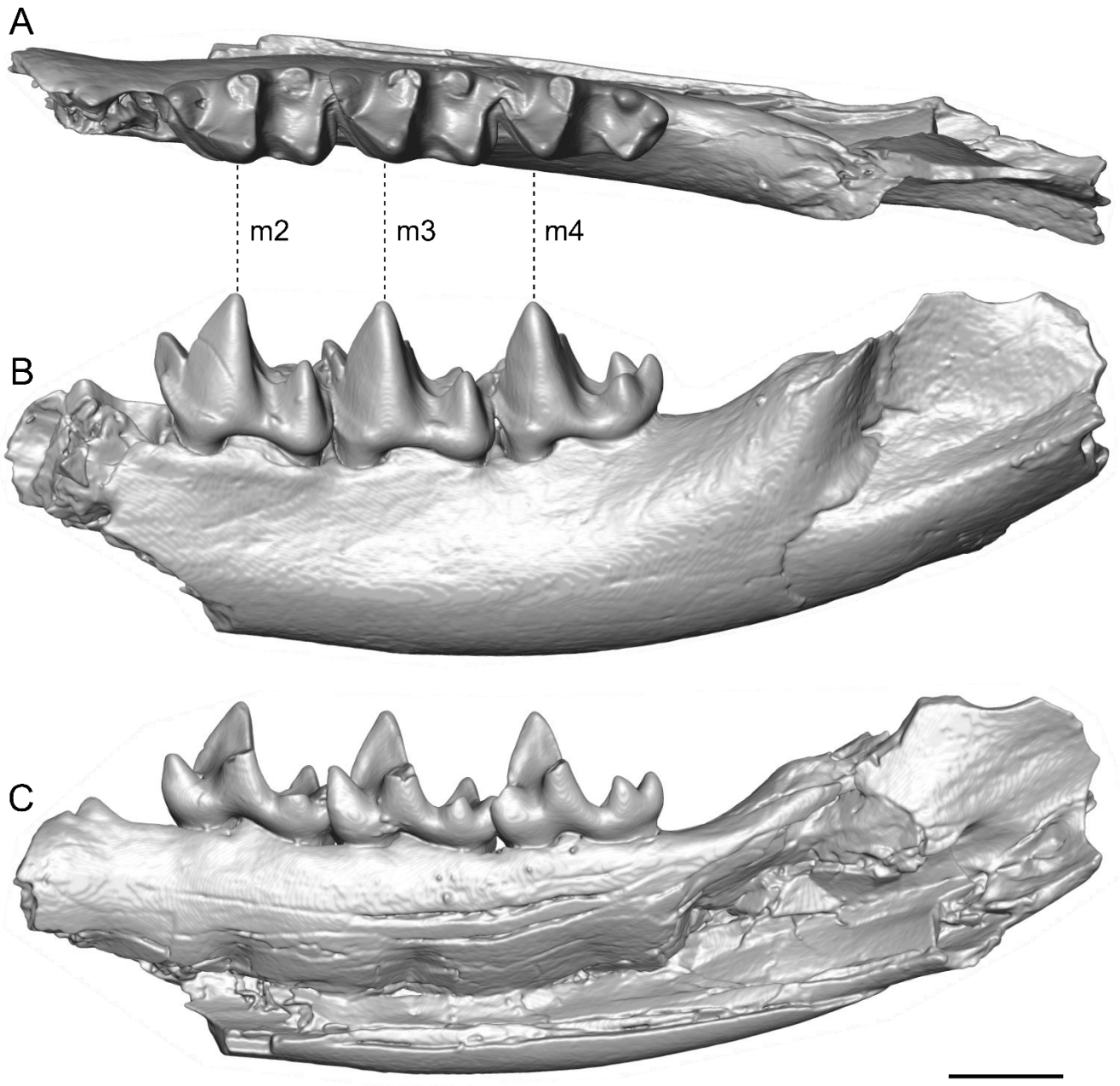

Figure 4. Hémi-mandibule gauche avec m2-m4 MHN.AIX.PV.2018.26.18 (modèle surfacique 3D) de *Peratherium constans* Teilhard de Chardin, 1927, de Palette (Provence, intervalle MP7-MP8+9) en vues occlusale (A), labiale (B), et linguale miroir (C). L'entoconide de m2 et m3 est brisé. Échelle : 1 mm.

Tableau 1. Synthèse des mesures (en mm), ratios longueur / largeur, et statistiques univariées associées, d'un échantillon représentatif de 187 molaires isolées de *Peratherium constans* Teilhard de Chardin, 1927, de Dormaal (MP7, Belgique). Abréviations : CV, coefficient de variation ; L, longueur ; N, nombre de spécimens ; ns, résultat non-significatif ; OR, intervalle observé ; s, résultat significatif ; SD, écart-type ; SW, test de normalité de Shapiro-Wilk ; W, largeur ; $\bar{x}$, moyenne. Détail des mesures en Annexes : Tableau S1.

Locus		N	OR	$\bar{x}$	SD	CV	SW
M1	L	20	1.40-1.60	1.51	0.057	3.76	ns
	W	21	1.40-1.65	1.49	0.070	4.66	s (P = 0.048)
	L/W	20	0.92-1.07	1.01	0.045	4.46	ns
M2	L	33	1.40-1.64	1.52	0.063	4.12	ns
	W	36	1.51-1.87	1.69	0.073	4.34	ns
	L/W	33	0.81-0.96	0.91	0.037	4.09	s (P = 0.012)
M3	L	39	1.30-1.62	1.44	0.064	4.42	ns
	W	38	1.67-1.92	1.79	0.064	3.59	ns
	L/W	37	0.74-0.88	0.81	0.034	4.24	ns
M4	L	5	0.99-1.41	1.21	0.150	12.42	ns
	W	5	1.62-1.98	1.75	0.147	8.36	ns
	L/W	5	0.55-0.77	0.69	0.084	12.17	ns
m1	L	21	1.29-1.49	1.41	0.057	4.01	ns
	W	21	0.69-0.83	0.78	0.038	4.90	ns
	L/W	21	1.60-1.93	1.81	0.078	4.29	ns
m2	L	27	1.43-1.62	1.51	0.051	3.34	ns
	W	27	0.80-1.00	0.89	0.057	6.42	ns
	L/W	27	1.53-1.93	1.70	0.097	5.73	ns
m3	L	28	1.40-1.63	1.51	0.050	3.29	ns
	W	29	0.78-0.99	0.87	0.045	5.15	ns
	L/W	28	1.59-1.86	1.74	0.064	3.67	ns
m4	L	9	1.38-1.55	1.45	0.058	4.01	ns
	W	9	0.76-0.86	0.82	0.037	4.58	ns
	L/W	9	1.66-1.96	1.78	0.103	5.76	ns

Description. La P2 (UM-CLO-55) et la P3 (UM-PAT-109 ; Figure 3B-C) sont nouvellement documentées et proviennent de Le Clot et de Palette, respectivement. La P2 est plus petite que la P3 (Annexes : Tableau S1) et les cingulums de la P3 sont tous plus développés. La crête distale de la cuspide principale de P2 et P3 n'a pas d'encoche dans sa partie la plus distale (Figure 3B), c'est-à-dire qu'elle est directement connectée à la marge distale de la prémolaire comme chez les autres herpétothériidés (Gernelle et al. 2024a : tableau 6). La morphologie de la dP3 est également inédite. La largeur labiolinguale de la dP3 est intermédiaire entre celle de la P3 et de la M1 (Figure 3C, E, G). La dP3 de Silveirinha (Figure 2A ; L = 1.11 mm, W = 0.97 mm) est plus petite que celle de Palette (L = 1.20 mm, W = 1.19 mm), alors que les M1s de ces deux localités (Figures 2B, 3G) sont similaires en taille

(Annexes : Tableau S1). Le plateau stylaire est presque ininterrompu par le paracône (entre l'éperon portant la cuspide stylaire A, et la cuspide stylaire C) sur la dP3 de Palette (Figure 3D). Le protocône et les conules d'une part, et la cuspide stylaire C des dP3s d'autre part, sont très petits par rapport au paracône / métacône et à la cuspide stylaire D, respectivement. La majorité des M1s-M3s ont un protocône aussi haut que le paracône. La M3 UM-FDN-10 fait exception, étant donné son protocône moins haut que le paracône en vue mésiale (Figure 6K). Presque toutes les M1s et M2s présentent une émargination distale profonde de la couronne, entre le talon et le plateau stylaire (Figures 1B, D ; 2B-C ; 3G ; 5B-C, E ; 6B, D, N-O). C'est aussi le cas pour la dP3 de Palette et les M1s et M2s de Dormaal (voir Figure 1E, et illustrations de Ladevèze et al. 2012). L'émargination distale est parfois absente ou moins franche sur ces loci (e.g., UM-FDN-5, Figure 6I). Les M3s MNHN.F.ME16095 (Figure 5E) et MNHN.F.RI392 (Figure 6O) ont aussi une émargination distale profonde, absente sur la plupart des M3s (e.g., Figures 2D-E ; 3K ; 5G ; 6J). La préparacrista est dirigée vers la cuspide stylaire B sur les M2s non usées (e.g., Figures 2C ; 3I ; 6D, N), et vers la cuspide stylaire A sur les M3s (e.g., Figure 2E ; 3K ; 5E, G), l'exception étant la M3 UM-FDN-10 (Figure 6J ; voir aussi la partie du Chapitre 4 traitant la variation de ce caractère). Les hauteurs relatives des cuspides stylaires C et D sur les M1s-M3s sont homogènes entre les spécimens, ces cuspides étant le plus souvent subégales en hauteur, ou bien la cuspide stylaire C dominant légèrement la cuspide stylaire D, surtout sur les M3s (Figures 1A, C ; 3F, H, J ; 5A, D, F ; 6A, C, H). La cuspide stylaire B est toujours dominante en hauteur. Le dédoublement de la cuspide stylaire C est fréquent sur les M1s-M3s de plusieurs localités, par exemple : Le Quesnoy (Figure 1C-D), Palette (Figure 3H-I), Fordones (Figure 6H-I), et Rians (Figure 6N-O). Certaines molaires supérieures, comme les M2s MNHN.F.QNY525bis (Figure 1D) et MNHN.F.ME25-G, ont une cuspide stylaire D avec une crête accessoire labiale dirigée vers le métacône (voir aussi Gernelle et al. 2024a : fig. 12j).

Les alvéoles postérieures visibles sur MHN.AIX.PV.2018.26.18 (m1, Figure 4A) et MNHN.F.SN35-BN (m3, Figure 6G) ont un aspect relativement allongé. Certaines m1s, en particulier celles de Meudon ont un talonide relativement plus large que les autres (e.g., MNHN.F.ME16207, Figure 5H, vs Figures 2G, 3L, 6P), des proportions qui semblent aussi présentes chez des spécimens de la série de m1s de Dormaal (e.g., Ladevèze et al. 2012 : fig. 4Ea). L'hémi-mandibule MHN.AIX.PV.2018.26.18 est le seul spécimen connu de *Pt. constans* préservant m2 et m3 en association (Figure 4). Ces deux dents sont sub-égales en longueur et largeur (Annexes : Tableau S1). En moyenne, les m2s et m3s de la série-type sont aussi sub-égales en longueur et largeur (Tableau 1). En revanche, la m4 de MHN.AIX.PV.2018.26.18 est légèrement plus longue que la m2 et la m3, alors que la m4 est en moyenne plus courte que m2 et m3 concernant la série-type de dents isolées. Le flanc lingual du paraconide est plus large sur les m3s que sur les m2s à la fois sur l'hémi-mandibule de Palette (Figure 4A) et les molaires isolées de chaque localité (Figure 3N vs Figure 3P pour Palette). En vue linguale, l'encoche entre l'entoconide et l'hypoconulide s'ouvre plus bas que l'encoche entre le métaconide et l'entoconide (Figures 3Q ; 5K, M ; 6F), comme

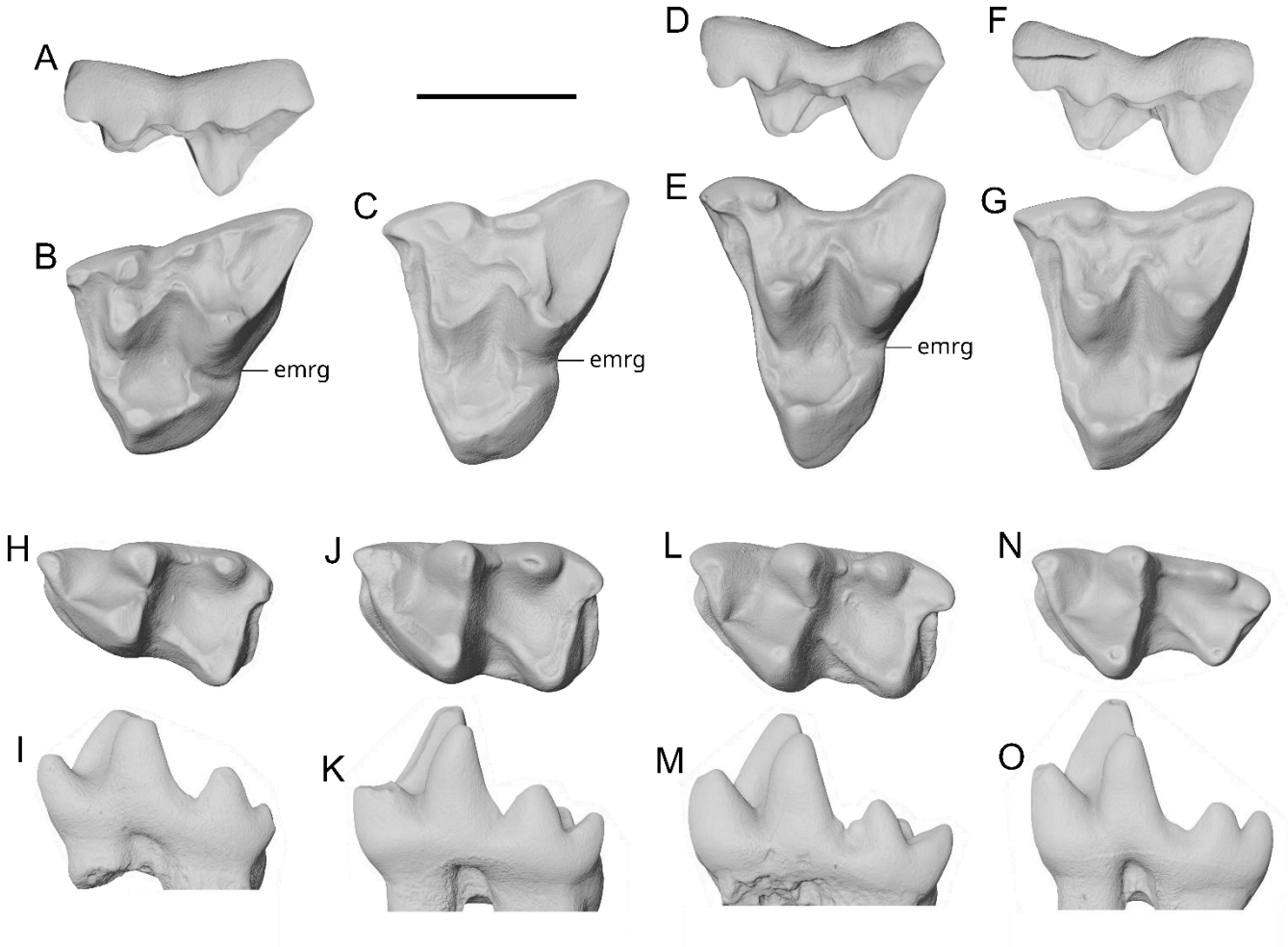

Figure 5. Molaires de *Peratherium constans* Teilhard de Chardin, 1927, de Meudon (Île-de-France, intervalle MP7-MP8+9). **A-G**. Molaires supérieures isolées, M1-M3. **A-B**. M1 droite MNHN.F.ME16197 en vues (miroir) labiale (A) et occlusale (B). **C**. M2 gauche MNHN.F.ME16301 en vue occlusale. **D-E**. M3 gauche MNHN.F.ME16095 en vues labiale (D) et occlusale (E). **F-G**. M3 droite MNHN.F.ME16312 en vues (miroir) labiale (F) et occlusale (G). **H-O**. Molaires inférieures isolées, m1, m3-m4. **H-I**. m1 droite MNHN.F.ME16207 en vues occlusale miroir (H) et linguale (I). **J-K**. m3 gauche MNHN.F.ME16403 en vues occlusale (J) et linguale miroir (K). **L-M**. m3 droite MNHN.F.ME16289 en vues occlusale miroir (L) et linguale (M). **N-O**. m4 gauche MNHN.F.ME16362 en vues occlusale (N) et linguale miroir (O). Échelle : 1 mm.

sur les m1s (Figures 3M, 5I) et les m2s (e.g., Figure 3O vs Figure 3Q). Les caractères montrant la variation la plus importante sur les m4s concernent la taille et la position du talonide par rapport au trigonide. Le dernier caractère peut être observé via la position relative de l'hypoconide par rapport au protoconide. Ainsi, l'hypoconide est directement distal à légèrement distolabial au protoconide sur la m4 de la mandibule de Palette (MHN.AIX.PV.2018.26.18, Figure 4A). L'hypoconide est sensiblement plus lingual sur une autre m4 de cette localité (MHN.AIX.PV.2017.6.18, Figure 3R ; voir aussi Figures 5N, 6G). Le talonide est parfois réduit et en position lingual, avec l'entoconide aligné avec le paraconide et le métaconide, et l'hypoconide distolingual par rapport au protoconide (e.g., UM-FDN-250, Figure 6L). Ce développement moindre du talonide s'accompagne d'un entoconide relativement moins haut que l'hypoconulide (Figure 6M), alors que le premier est toujours autrement nettement plus élevé (Figures 3S, 4B-C, 5O).

Discussion

Ladevèze et al. (2012), suivant les conclusions d'Hershkovitz (1997) tirées de l'étude de la dentition des didelphidés actuels du genre *Philander* (*Philander opossum* et *Ph. andersoni*), ont conclu que les cuspides stylaires de *Peratherium constans* montrent une importante variation intraspécifique quant à leur position sur le plateau stylaire. Ce constat doit être nuancé à partir de la réétude de *Pt. constans* de Dormaal et d'autres localités. En effet, bien qu'un dédoublement fréquent de la cuspide stylaire C existe chez *Pt. constans*, les cuspides stylaires B et D sont toujours positionnées (parfois avec un léger décalage distal pour la cuspide stylaire D) directement labialement au paracône et au métacone, respectivement. Les hauteurs relatives des cuspides stylaires B, C et D varient également très peu au sein des échantillons et entre les échantillons de localités différentes (B dominant C et D, et C et D étant subégales en hauteur, ou C étant légèrement plus haut que D). La variation intraspécifique observée ci-dessus concerne en partie des caractères déjà décrits par ailleurs. Les caractères diagnostiques de *Pt. constans*, comme l'émargination distale prononcée des molaires supérieures, et l'égalité de taille des m2s et m3s, sont retrouvés dans d'autres séries de molaires que celle de Dormaal.

Une M3 de Silveirinha (SV3-469 ; Figure 2F) est sensiblement plus grande que toutes les M3s rapprochées de *Peratherium constans* (Annexes : Tableau S1) et n'est donc pas attribuée à cette espèce. Celle-ci a peut-être orienté l'attribution première des pérathériinés de Silveirinha à *Peratherium* cf. *constans* en raison de sa plus grande taille (Estravís 2000). Une espèce de pérathériiné de plus grande taille que *Pt. constans* pourrait donc avoir émergé avant *Pt. musivum*. Il faut noter que cette M3 de Silveirinha possède aussi une disposition originale des cuspides parastylaires (A et B), avec une cuspide accessoire entre les cuspides stylaires A et B, alors que les hauteurs relatives des cuspides stylaires C et D sont identiques à celles connues chez *Pt. constans*, contrairement à *Pt. musivum*.

Peratherium constans est finalement connu dans neuf localités du Nord (quatre) et du Sud (cinq) de l'Europe de l'Ouest, ce qui confirme sa large répartition suspectée (Boivin et al. 2018 ; Gernelle et al. 2024a, b). La plus ancienne localité où cette espèce est mentionnée est Dormaal, la localité type. *Peratherium constans* semble persister jusqu'à Rians (intervalle MP7-MP8+9 ; d'âge proche de Fournes d'après Marandat et al. 2012, soit ~54 Ma si cette conclusion est correcte et suivant Noiret et al. 2016 ; ~ biozone PE III [voir Gernelle et al. 2024a]). La M3 de Rians présente en effet une émargination distale profonde, un caractère relativement rare sur les autres M3s de *Pt. constans* mais qui n'est jamais connu sur les M3s de *Pt. matronense*. Les spécimens de pérathériinés de petite taille de Rians sont donc attribués à la première espèce plutôt qu'à la seconde (contra Godinot 1981). *Peratherium constans* est nouvellement identifié à Le Quesnoy et Soissons, notamment par l'intermédiaire de petites M1s et M2s montrant de profondes émarginations distales (Figures 1B, D ; 6B, D).

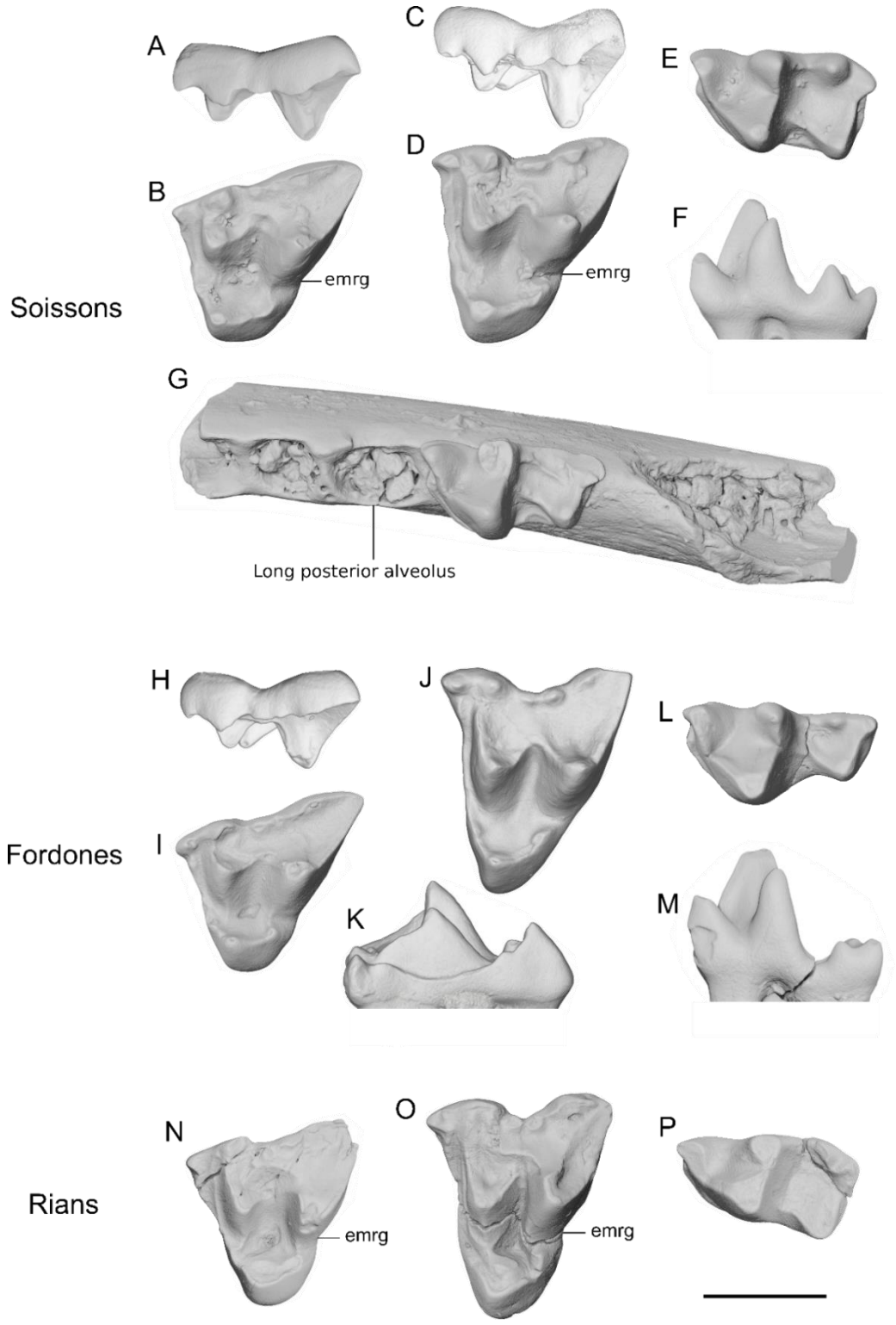

Figure 6. Molaires de *Peratherium constans* Teilhard de Chardin, 1927, de localités de l'intervalle MP7-MP8+9 : Soissons (A-G), dans le Bassin de Paris, et Fordones (H-M ; Corbières) et Rians (N-P ; Provence) dans le Sud de la France. **A-B**. M1 gauche MNHN.F.SN23-BN en vues labiale (A) et occlusale (B). **C-D**. M2 gauche MNHN.F.SN38-BN en vues labiale (C) et occlusale (D). **E-F**. m3 gauche MNHN.F.SN59-BN en vues occlusale (E) et linguale miroir (F). **G**. Fragment de dentaire gauche avec alvéoles de m3, et m4 subcomplète MNHN.F.SN35-BN, en vue occlusale. **H-I**. M1 droite UM-FDN-5 en vues (miroir) labiale (H) et occlusale (I). **J-K**. M3 droite UM-FDN-10 en vues (miroir) occlusale (J) et mésiale (K). **L-M**. m4 droite UM-FDN-250 en vues occlusale miroir (L) et linguale (M). **N**. M2 droite MNHN.F.RI517 en vue occlusale miroir. **O**. M3 gauche MNHN.F.RI392 en vue occlusale. **P**. m1 droite MNHN.F.RI226 en vue occlusale miroir. Échelle : 1 mm. Abréviation : emrg, émargination distale.

Peratherium matronense Crochet, 1979

Figures 7-10 ; 11A-F ; 12A-H, M-P ; Tableau 2 ; Annexes : Tableau S1

1979 – *Peratherium matronense* Crochet in Crochet p. 373, fig. 10.

1980 – *Amphiperatherium* sp. 1 in Crochet p. 62-63, figs. 40-42 (en partie : spécimens d'Avenay, Condé-en-Brie, Sables de Brasles et ?Sézanne-Broyes).

1980 – *Amphiperatherium bourdellense* Crochet in Crochet p. 68-74, no figs. (en partie : spécimens de ?Avenay, Condé-en-Brie, Sables de Brasles et Sézanne-Broyes).

1980 – *Amphiperatherium goethei* Crochet in Crochet p. 89-92, no figs. (en partie : spécimens d'Avenay, Condé-en-Brie et Sézanne-Broyes).

1980 – *Peratherium matronense* Crochet in Crochet p. 147-151, figs. 157-161, 163-164 (en partie : spécimens d'Avenay, Condé-en-Brie, Sables de Brasles et Sézanne-Broyes ; no fig. 162).

1987 – *Amphiperatherium goethei* Crochet in Marandat, tab. 2.

1987 – *Peratherium monspeliense* Crochet in Marandat, tab. 2.

no 1989 – *Peratherium matronense* Crochet in Peláez Campomanes et al. p. 138-139, pl. 3, figs. 6-7.

1991 – *Peratherium* cf. *matronense* Crochet in Marandat p. 69-70, pl. 1, figs. 3, 7.

1991 – *Peratherium* cf. *monspeliense* Crochet in Marandat p. 70-71.

no 1992 – *Peratherium matronense* Crochet in Legendre et al. p. 418, 424, tab. 1.

? 1992 – *Peratherium matronense* Crochet in Smith et Russell p. 224, pl. 1, fig. 1.

no 2024 – *Peratherium matronense* Crochet in Vianey-Liaud et al.

Holotype. MNHN.F.CB195-BN, M3 droite, figurée par Crochet (1979: fig. 10, 1980: fig. 159).

Localité-type. Condé-en-Brie (Aisne, est du Bassin de Paris) ; Éocène inférieur moyen, niveau-repère ~MP8+9.

Autres localités. Fournes et La Gasque (Minervois), Monze (Corbières) dans le Sud de la France ; Avenay, Sables de Brasles, et Sézanne-Broyes dans le Bassin de Paris. Possiblement La Borie (Lauragais, Sud de la France), et Abbey Wood (Londres) (voir discussion).

Âge. Intervalle MP7-MP8+9, juste après l'ETM2 (~54 Ma), d'après l'âge de Fournes (Noiret et al. 2016), à ~MP8+9 (Éocène inférieur moyen).

Diagnose différentielle. Taille en moyenne intermédiaire entre celle de *Peratherium constans* et de *Peratherium monspeliense*. Diffère de *Pt. constans* par l'émargination distale des couronnes des M1s et M2s en moyenne moins profonde. Diffère de *Peratherium monspeliense* par les m2s et m3s de taille subégale en moyenne, la cuspide stylaire C relativement plus haute, et la pré-entocristide moins longue sur les m3s. Diffère d'« *Amphiperatherium* » *bourdellense* notamment par les prémolaires inférieures relativement moins larges, l'émargination labiale des molaires inférieures, et la cuspide stylaire C des

molaires supérieures plus proéminente. Diffère d'« *Amphiperatherium* » *goethei* par le paraconide relativement plus long et l'encoche entoconide – hypoconulide relativement moins haute sur les m2s, la cuspide stylaire D des M1s relativement moins longue et large, et les M3s relativement moins longues que les M1s-M2s en moyenne.

Matériel. Les spécimens figurés ci-après sont signalés en gras dans la liste du matériel.

Matériel de Fournes : *Molaires supérieures* : M1 gauche (UM-FNR-25, Marandat 1991 : pl. 1, fig. 7 ; **UM-FNR-60**), M2 (UM-FNR-26, fragmentaire, Marandat 1991 : pl. 1, fig. 3), M3 droite (**UM-FNR-61**), M4 gauche (UM-FNR2-3, usé). *Molaires inférieures* : m1 droite (UM-FNR-24, fragmentaire), m2 droite (UM-FNR-58), hémi-mandibule droite avec m3 (UM-FNR-38), m3 gauche (**UM-FNR-14**), m3 droite (UM-FNR-34, fragmentaire).

Matériel de La Gasque : M1 droite (**UM-GAS-1**), M2 droite (**UM-GAS-2**).

Matériel de Monze : p2 (**UM-MOZ-12**), p3 (UM-MOZ-14, fragmentaire), hémi-mandibule droite avec racines de p2, et p3-m4 (**UM-MOZ-11**), hémi-mandibule droite avec m2 complète et m3-m4 fragmentées (**UM-MOZ-1**), m3 (**UM-MOZ-13**).

Matériel d'Avenay : *Molaires supérieures* : M1 droite (**MNHN.F.AV7233** [= MNHN.F.AV7223 in Crochet 1980 : fig. 157] ; MNHN.F.AV7663, fragmentaire), M2 droite (MNHN.F.AV7225, Crochet 1980 : fig. 158 ; **MNHN.F.AV15769**), M3 gauche (MNHN.F.AV4707, usé ; MNHN.F.AV6794, usé ; MNHN.F.AV18005, Crochet 1980 : fig. 41), M3 droite (MNHN.F.AV7189, fragmentaire), M4 gauche (UM-AV-22-SK), M4 droite (UM-AV-21-SK). *Molaires inférieures* : m1 gauche (MNHN.F.AV6795), m2 gauche (MNHN.F.AV6844, fragmentaire ; UM-AV-20-SK), m3 gauche (MNHN.F.AV7234, usé), m3 droite (MNHN.F.AV6760, Crochet 1980 : fig. 163), m4 gauche (MNHN.F.AV7192).

Matériel supplémentaire de Condé-en-Brie : *Molaires supérieures* : M1 gauche (**MNHN.F.CB2503** ; MNHN.F.CB2727, fragmentaire ; MNHN.F.CB2952), M1 droite (MNHN.F.CB817 ; MNHN.F.CB856, usé ; MNHN.F.CB2780, usé ; **MNHN.F.CB3243** ; **MNHN.F.CB4119** ; **MNHN.F.CB4134**, usé), M2 gauche (MNHN.F.CB848 ; **MNHN.F.CB3646**, usé ; **MNHN.F.CB4138** ; MNHN.F.CB4140, usé), M2 droite (**MNHN.F.CB159-BN** ; MNHN.F.CB269-BN ; MNHN.F.CB877, usé ; MNHN.F.CB2504, fragmentaire ; MNHN.F.CB4130 ; MNHN.F.CB4235, fragmentaire), M3 gauche (MNHN.F.CB249-BN, usé et fragmentaire ; MNHN.F.CB834, fragmentaire ; MNHN.F.CB1400, fragmentaire ; **MNHN.F.CB1412** ; MNHN.F.CB1686 ; **MNHN.F.CB2845**), M3 droite (MNHN.F.CB155-BN ; **MNHN.F.CB203-BN** ; MNHN.F.CB827, usé ; **MNHN.F.CB2632**), M4 droite (MNHN.F.CB1081, usé). *Molaires inférieures* : m1 gauche (**MNHN.F.CB647** ; **MNHN.F.CB1079-L**, Crochet 1980 : fig. 42 ; **MNHN.F.CB2506**, Crochet 1980 : fig. 161 ; MNHN.F.CB3640 ; MNHN.F.CB4385), m1 droite (MNHN.F.CB927), m2 gauche (MNHN.F.CB871 ; MNHN.F.CB3648); m2 droite (**MNHN.F.CB179-BN** ; MNHN.F.CB846 ; **MNHN.F.CB4129**), m3 gauche (MNHN.F.CB2790 ; MNHN.F.CB2926), m3

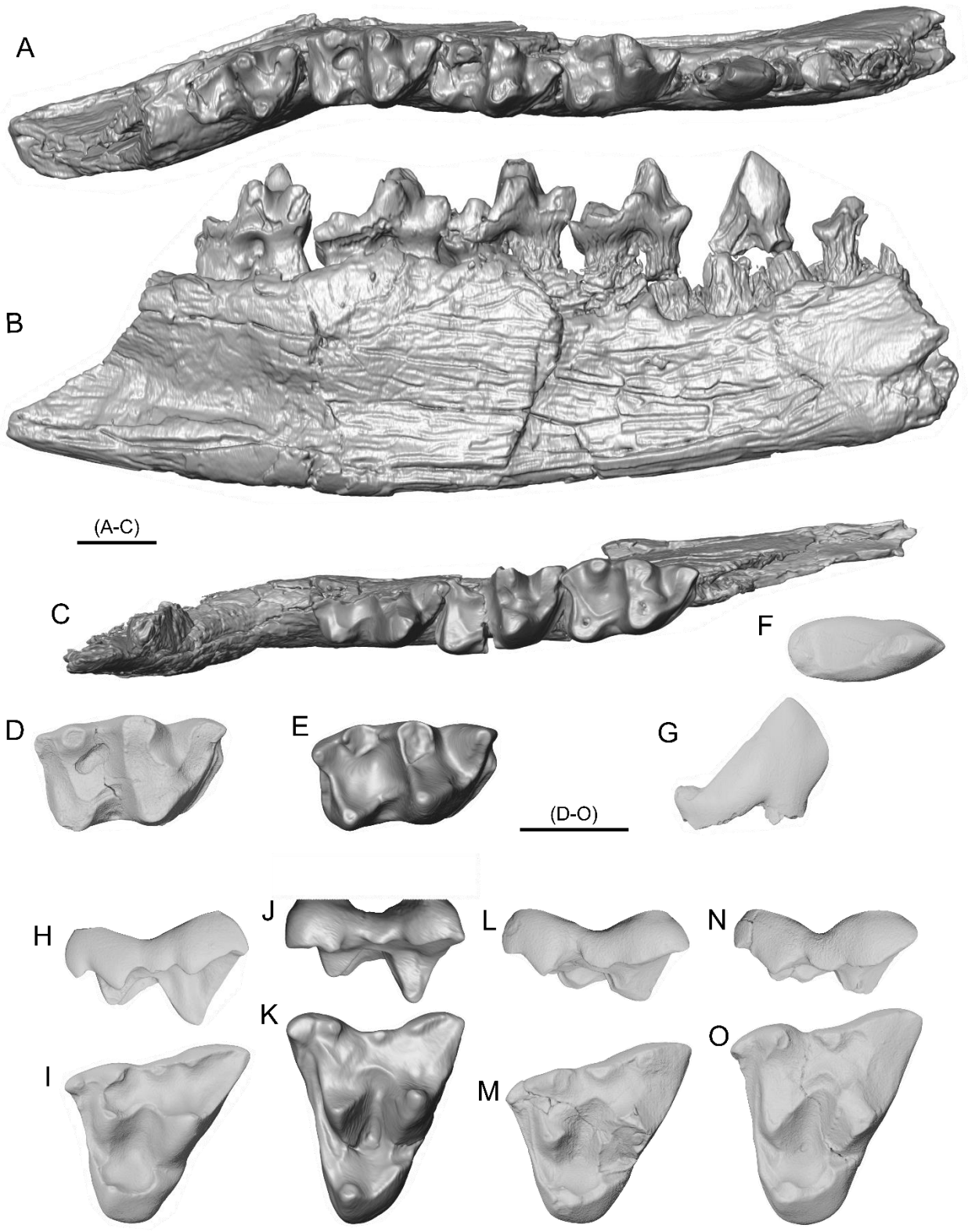

Figure 7. Rangées dentaires inférieures et dents jugales isolées de *Peratherium matronense* Crochet, 1979, de Monze (Corbières), Fournes et La Gasque (Minervois) (intervalle MP7-MP8+9, ~54 Ma). **A-B**. UM-MOZ-11 (modèle surfacique 3D), dentaire droit partiel avec racines de p2, et p3-m4 en vues occlusale (A) et linguale (B). **C**. UM-MOZ-1 (modèle 3D), dentaire droit partiel avec m2, et m3-m4 fragmentaires en vue occlusale. **D**. UM-MOZ-13, m3 en vue occlusale. **E**. UM-FNR-14, m3 gauche (modèle 3D) en vue occlusale miroir. **F-G**. UM-MOZ-12, p2 en vues occlusale (F) et labiale (G). **H-I**. UM-FNR-60, M1 gauche en vues labiale (H) et occlusale (I). **J-K**. UM-FNR-61, M3 droite (modèle 3D) en vues (miroir) labiale (J) et occlusale (K). **L-M**. M1 droite UM-GAS-1 en vues (miroir) labiale (L) et occlusale (M). **N-O**. M2 droite UM-GAS-2 en vues (miroir) labiale (N) et occlusale (O). Échelle : 1 mm.

droite (MNHN.F.CB220-BN ; MNHN.F.CB239-BN ; MNHN.F.CB876 ; MNHN.F.CB2828 ; MNHN.F.CB4197), m4 gauche (MNHN.F.CB185-BN, fragmentaire ; MNHN.F.CB925 ; MNHN.F.CB2784, fragmentaire), m4 droite (MNHN.F.CB941 ; MNHN.F.CB5027).

Matériel de Sables de Brasles (= 'Gland') : *Molaires supérieures* : M1 gauche (**MNHN.F.GL392-L**), M1 droite (**MNHN.F.GLD89-L**, Crochet 1980 : fig. 40 ; MNHN.F.GLD123, usé et fragmentaire ; **MNHN.F.GLD174 ; MNHN.F.GL395-L ; MNHN.F.GL288-L**), M2 gauche (**MNHN.F.GLD68-L**), M2 droite (**MNHN.F.GLD131 ;** MNHN.F.GLD194, usé ; **MNHN.F.GL308-L**), M3 gauche (**MNHN.F.GL396-L**), M3 droite (**MNHN.F.GL306-L** ; MNHN.F.GL324-L, fragmentaire). *Molaires inférieures* : m2 gauche (MNHN.F.GL316-L), m2 droite (MNHN.F.GLD8, fragmentaire ; MNHN.F.GL192-L ; MNHN.F.GL312-L), m3 droite (MNHN.F.GL249-L ; MNHN.F.GL386-L), m4 droite (MNHN.F.GLD302-L).

Matériel de Sézanne-Broyes : *Molaires supérieures* : M1 gauche (**MNHN.F.SZ58-BN ; MNHN.F.SZ216-BN ; MNHN.F.SZ232-BN**), M1 droite (**MNHN.F.SZ76-BN ; MNHN.F.SZ513-BN**), M2 gauche (**MNHN.F.SZ559-BN**), M2 droite (MNHN.F.SZ326-BN, fragmentaire ; **MNHN.F.SZ446-BN**), M3 gauche (**MNHN.F.SZ552-BN ; MNHN.F.SZ558-BN**), M3 droite (MNHN.F.SZ105-BN, fragmentaire ; MNHN.F.SZ311-BN, usé), M4 gauche (**MNHN.F.SZ511-BN**). *Molaires inférieures* : m1 gauche (**MNHN.F.SZ88-BN** ; MNHN.F.SZ567-BN), m1 droite (MNHN.F.SZ48-BN ; MNHN.F.SZ86-BN ; MNHN.F.SZ175-BN ; MNHN.F.SZ286-BN ; MNHN.F.SZ514-BN), m2 gauche (MNHN.F.SZ212-BN ; MNHN.F.SZ515-BN ; MNHN.F.SZ7313, moulage), m2 droite (MNHN.F.SZ124-BN ; **MNHN.F.SZ226-BN** ; MNHN.F.SZ302-BN), m3 gauche (MNHN.F.SZ269-BN), m3 droite (MNHN.F.SZ171-BN ; **MNHN.F.SZ574-BN**), m4 gauche (**MNHN.F.SZ306-BN**), m4 droite (MNHN.F.SZ271-BN).

Commentaire. Parmi les spécimens ici rapportés à *Pt. matronense*, plusieurs ont été attribués par Crochet (1980) à *Amphiperatherium* sp. 1, *A. bourdellense*, et *A. goethei*. Il n'existe pas de liste publiée des spécimens étudiés par Crochet (1980), et les tableaux de mesures présentés par cet auteur sont synthétiques, c'est-à-dire sans détail des spécimens à partir desquels les mesures ont été prises. De fait, retrouver les correspondances entre plusieurs taxons semblables et spécimens publiés s'avère complexe, sinon impossible, en se basant uniquement sur le travail publié de Crochet (1980), hormis pour les quelques figurés. En revanche, j'ai eu accès à une liste manuscrite rédigée par J.-Y. Crochet (manifestement non exhaustive), conservée dans les collections du MNHN, de dents isolées du Bassin de Paris (Avenay et Condé-en-Brie principalement) associées à leur première attribution. Cela a permis de réévaluer certaines de ces dernières précisément. Ainsi, *A. bourdellense*, *A. goethei*, *Amphiperatherium* sp. 1 et *Pt. matronense* étaient initialement représentés dans les localités MP8+9 / ~MP8+9 du Basin de Paris au moins par les spécimens suivants, parmi ceux cités plus haut :

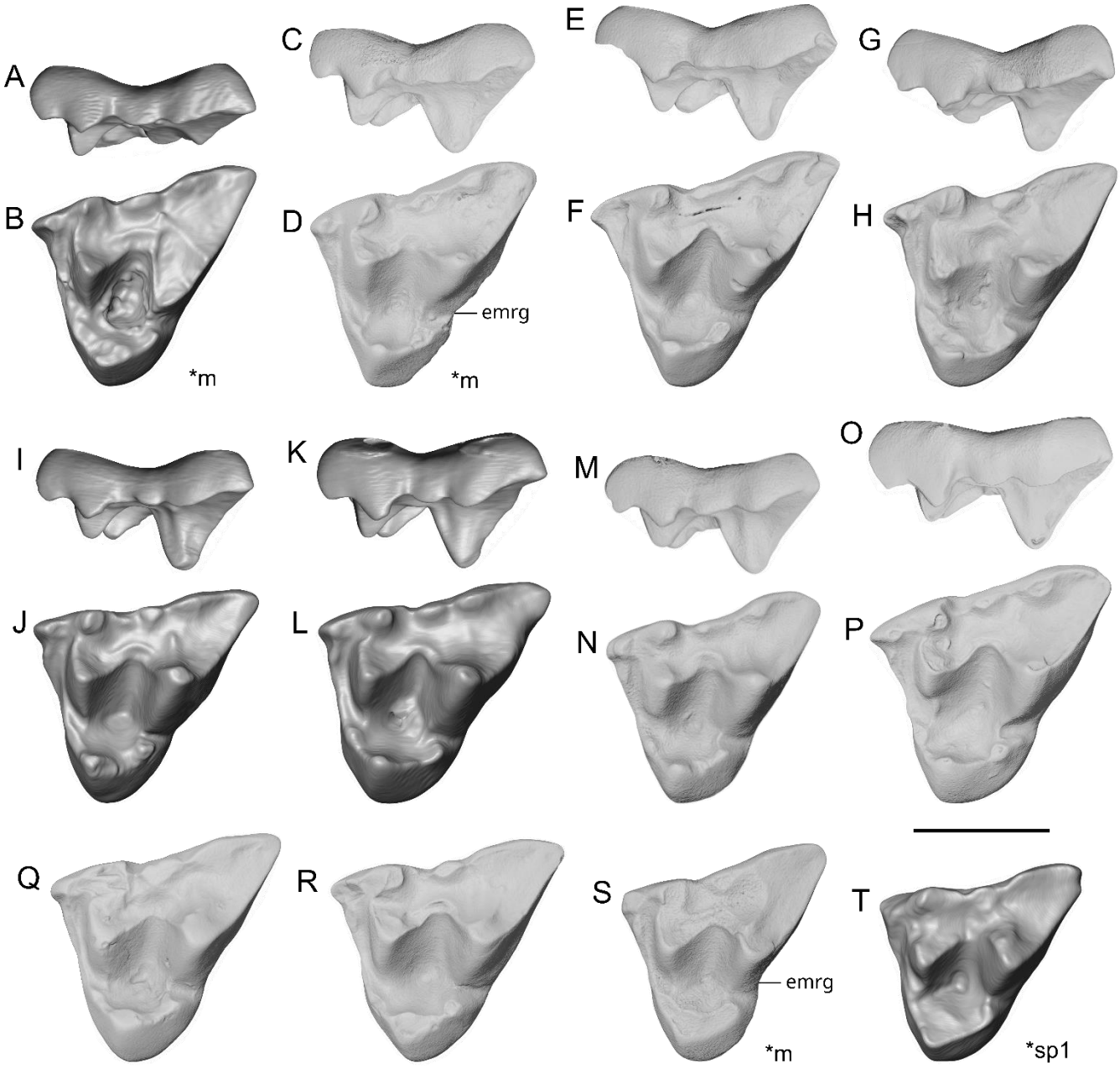

Figure 8. M1s isolées de *Peratherium matronense* Crochet, 1979, d'Avenay, Condé-en-Brie, Sables de Brasles et Sézanne-Broyes (Bassin de Paris, MP8+9 / ~MP8+9). **A-B**. MNHN.F.CB4119 (modèle surfacique 3D) en vues (miroir) labiale (A) et occlusale (B). **C-D**. MNHN.F.AV7233 en vues (miroir) labiale (C) et occlusale (D). **E-F**. MNHN.F.CB2503 en vues labiale (E) et occlusale (F). **G-H**. MNHN.F.GLD174 en vues (miroir) labiale (G) et occlusale (H). **I-J**. MNHN.F.SZ58-BN (modèle surfacique 3D) en vues labiale (I) et occlusale (J). **K-L**. MNHN.F.SZ513-BN (modèle surfacique 3D) en vues (miroir) labiale (K) et occlusale (L). **M-N**. MNHN.F.GL392-L en vues labiale (M) et occlusale (N). **O-P**. MNHN.F.GL395-L en vues (miroir) labiale (O) et occlusale (P). **Q**. MNHN.F.SZ216-BN en vue occlusale. **R**. MNHN.F.SZ76-BN en vue occlusale miroir. **S**. MNHN.F.CB4134 en vue occlusale miroir. **T**. MNHN.F.GLD89-L en vue occlusale miroir. Abréviations : *m, spécimen attribué à *Pt. matronense* par Crochet (1980) ; *sp1, spécimen attribué à *Amphiperatherium* sp. 1 par Crochet (1980). Échelle : 1 mm.

- *Amphiperatherium bourdellense sensu* Crochet (1980) : **MNHN.F.CB647**, MNHN.F.CB1400, MNHN.F.CB2504, **MNHN.F.CB2632**, MNHN.F.CB2727, MNHN.F.CB2780, MNHN.F.CB4130, MNHN.F.CB4140, **MNHN.F.CB4138**, MNHN.F.CB4235, MNHN.F.SZ7313.
- *Amphiperatherium goethei sensu* Crochet (1980) : MNHN.F.AV7192, **MNHN.F.CB179-BN**, MNHN.F.CB185-BN, MNHN.F.CB220-BN, MNHN.F.CB239-BN, MNHN.F.CB269-BN, **MNHN.F.CB3243**.
- *Amphiperatherium* sp. 1 *sensu* Crochet (1980) : MNHN.F.AV6795, MNHN.F.AV18005 (ex MNHN.F.AV139-L, renuméroté dans Gernelle et al. 2024b), **MNHN.F.CB1079-L**, **MNHN.F.GLD89-L**.
- *Peratherium matronense sensu* Crochet (1980) : MNHN.F.AV4707, MNHN.F.AV6760, MNHN.F.AV6794, MNHN.F.AV6844, MNHN.F.AV7225, **MNHN.F.AV7233**, MNHN.F.CB155-BN, **MNHN.F.CB159-BN**, MNHN.F.CB195-BN, **MNHN.F.CB203-BN**, **MNHN.F.CB1412**, **MNHN.F.CB2506**, MNHN.F.CB2790, MNHN.F.CB2828, MNHN.F.CB2845, MNHN.F.CB2952, **MNHN.F.CB3646**, **MNHN.F.CB4119**, **MNHN.F.CB4129**, **MNHN.F.CB4134**, MNHN.F.CB4385.

Crochet (1980 : 63) a attribué une M2 non nommée de Sézanne-Broyes à *Amphiperatherium* sp. 1, mais aucune correspondance entre les spécimens trouvés en collection et la description de Crochet (1980) n'est possible. De même, la seule dent d'Avenay vraisemblablement attribuée à *A. bourdellense* selon Crochet (1980 : tableau 7) est une m2 non nommée. Une unique m2 d'Avenay d'une espèce de petite taille a été trouvée dans les collections du MNHN (MNHN.F.AV6844), mais elle a été considérée comme une m1 de *Pt. matronense* par Crochet (1980).

Description comparée. Les morphologies des molaires de *Pt. constans* et de *Pt. matronense* étant très proches, seule la variation intraspécifique ainsi que des comparaisons avec d'autres taxons sont détaillées ci-après. La variation importante d'un caractère est à noter dans la série de Fournes : une émargination distale est présentée par une des deux M1s (Marandat 1991 : pl. 1, fig. 7), mais pas par l'autre (Figure 7I). Un nombre très réduit de M1s des localités du Bassin de Paris présente une émargination distale relativement profonde mésiodistalement (e.g., seulement Figure 8D, S au sein de la Figure 8). L'émargination distale n'est pas développée sur les M2s et M3s (mais voir les M2s des Figures 9M, 11D). Parmi les M1s, deux spécimens, MNHN.F.CB2780 et MNHN.F.GLD89-L (Figure 8T) sont de très petite taille, ce qui a probablement orientée l'attribution première de MNHN.F.GLD89-L à *Amphiperatherium* sp. 1 Crochet (1980). Le protocône est généralement aussi haut que le paracône (e.g., MNHN.F.CB203-BN, Figure 10O). La cuspide stylaire A n'est parfois pas projetée mésialement par rapport à la partie la plus mésiolabiale du paracingulum (e.g., Figures 8D, N ; 11B pour les M1s ; Figure 9B, K pour les M2s ; Figure 10F pour les M3s). La cuspide stylaire A de l'holotype (M3) de *Pt.*

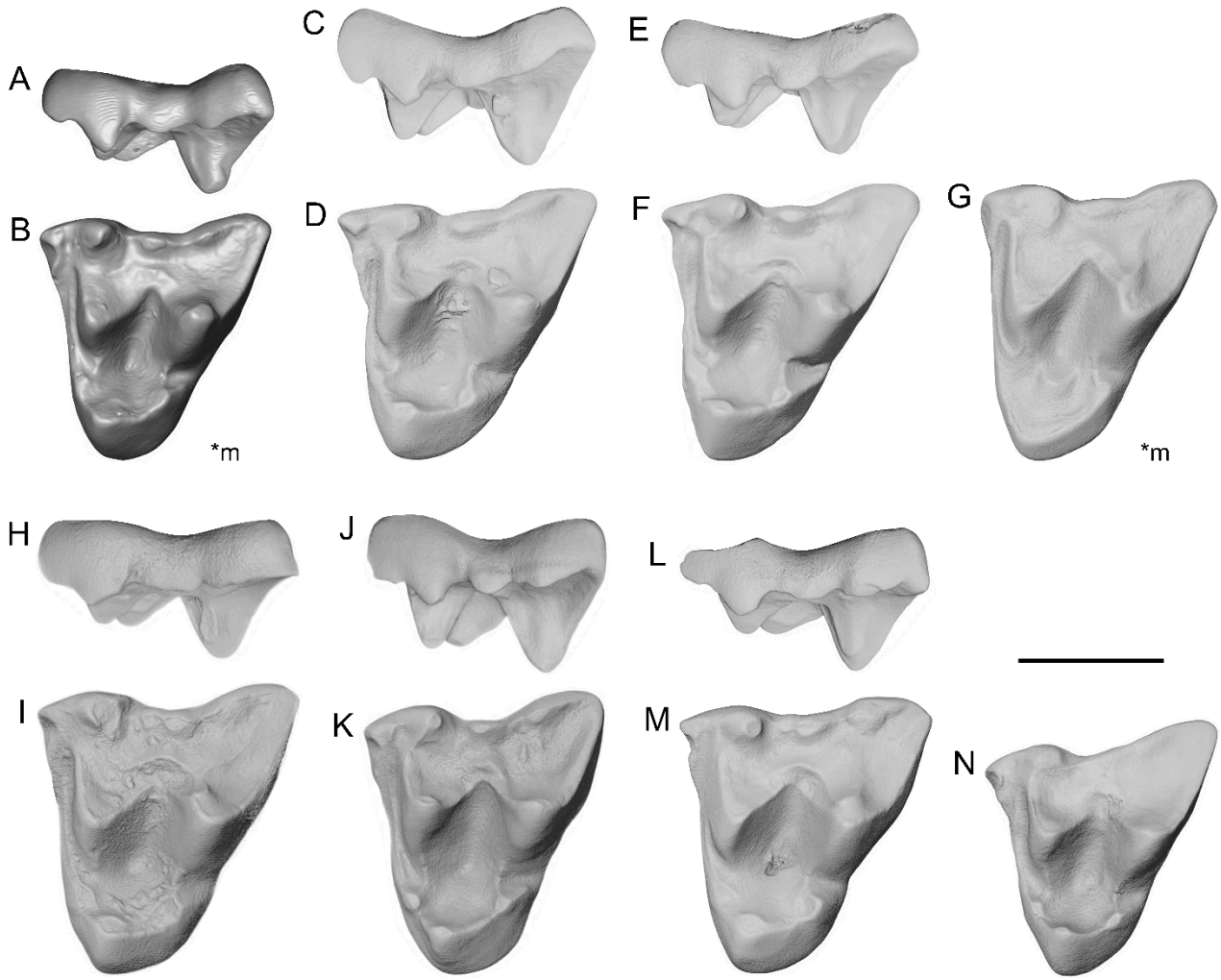

Figure 9. M2s isolées de *Peratherium matronense* Crochet, 1979, d'Avenay, Condé-en-Brie, Sables de Brasles et Sézanne-Broyes (Bassin de Paris, MP8+9 / ~MP8+9). **A-B**. MNHN.F.CB159-BN (modèle surfacique 3D) en vues (miroir) labiale (A) et occlusale (B). **C-D**. MNHN.F.SZ446-BN en vues (miroir) labiale (C) et occlusale (D). **E-F**. MNHN.F.SZ559-BN en vues labiale (E) et occlusale (F). **G**. MNHN.F.CB3646 en vue occlusale. **H-I**. MNHN.F.AV15769 en vues (miroir) labiale (H) et occlusale (I). **J-K**. MNHN.F.GLD68-L en vues labiale (J) et occlusale (K). **L-M**. MNHN.F.GLD131 en vues (miroir) labiale (L) et occlusale (M). **N**. MNHN.F.GLD308-L en vue occlusale miroir. Abréviation : *m, spécimen attribué à *Pt. matronense* par Crochet (1980). Échelle : 1 mm.

matronense est en fait légèrement antérieure au paracingulum (pers. obs.) contrairement à la représentation qu'en a proposée Crochet (1979 : fig. 10, 1980). La cuspide stylaire A a une forme d'éperon mésial dans la plupart des cas (cf. Figures 8-10). Les cas de duplication de la cuspide stylaire C sont moins fréquents que chez *Pt. constans* et *Pt. maximum* (e.g., Figure 9H-I parmi les Figures 8-10). Sur les M1s et comme chez *Pt. constans*, la cuspide stylaire D est souvent plus longue et large que la cuspide stylaire C, mais pas plus haute (Figure 8), même si des exceptions existent (e.g., Figure 8K). La cuspide stylaire D est parfois légèrement distolabiale par rapport au sommet du métacône (Figure 8D, F, H, Q). Sur les M3s, l'aile métastylaire est souvent aussi labiale que l'aile parastylaire (Figure 10B, D, F, L, N), ou bien l'aile métastylaire est légèrement plus labiale (Figures 10H, J, 11F), l'ectoflexus est alors asymétrique. La profondeur de l'ectoflexus varie sur les M3s (e.g., Figure 10B vs Figure 10D).

Tableau 2. Synthèse des mesures (en mm), ratios longueur/largeur, et statistiques univariées associées, de l'ensemble des molaires isolées de *Peratherium matronense* Crochet, 1979 provenant des localités du Bassin de Paris rapprochées du niveau-repère MP8+9 : Condé-en-Brie (localité-type), Avenay, Sables de Brasles et Sézanne-Broyes. Abréviations : CV, coefficient de variation ; L, longueur ; N, nombre de spécimens ; ns, résultat non-significatif ; OR, intervalle observé ; s, résultat significatif ; SD, écart-type ; SW, test de normalité de Shapiro-Wilk ; W, largeur ; $\bar{x}$, moyenne. Détail en Annexes : Tableau S1.

Locus		N	OR	$\bar{x}$	SD	CV	SW
M1	L	18	1.48-1.83	1.66	0.106	6.41	ns
	W	19	1.46-1.88	1.64	0.093	5.67	ns
	L/W	18	0.91-1.06	1.01	0.042	4.16	ns
M2	L	14	1.58-1.89	1.72	0.097	5.68	ns
	W	16	1.70-2.17	1.92	0.126	6.57	ns
	L/W	14	0.85-0.95	0.90	0.035	3.96	ns
M3	L	14	1.41-1.77	1.58	0.092	5.84	ns
	W	15	1.77-2.20	1.96	0.125	6.38	ns
	L/W	14	0.76-0.87	0.81	0.037	4.62	ns
M4	L	3	1.21-1.39	1.28			
	W	3	1.73-1.91	1.81			
	L/W	3	0.65-0.78	0.71			
m1	L	14	1.45-1.78	1.63	0.101	6.22	ns
	W	14	0.89-1.07	0.96	0.058	6.03	ns
	L/W	14	1.61-1.76	1.69	0.051	3.06	ns
m2	L	14	1.48-1.87	1.74	0.097	5.60	ns
	W	14	0.87-1.13	1.05	0.070	6.71	s (P = 0.049)
	L/W	14	1.58-1.76	1.66	0.057	3.44	ns
m3	L	12	1.54-1.87	1.74	0.108	6.21	ns
	W	12	0.92-1.12	1.02	0.068	6.65	ns
	L/W	12	1.65-1.79	1.71	0.045	2.64	ns
m4	L	7	1.56-2.00	1.74	0.145	8.37	ns
	W	7	0.86-1.03	0.94	0.070	7.49	ns
	L/W	7	1.74-2.00	1.85	0.092	4.98	ns

Comme chez les autres pérathériinés de l'Éocène inférieur, les M4s n'ont pas d'ectoflexus, et la cuspide stylaire B est mésiolabiale au sommet du paracône (e.g., MNHN.F.SZ511-BN, Figure 10Q). La cuspide stylaire C des M4s est nettement plus basse que la cuspide stylaire B (Figure 10P ; cette dernière est usée sur la M4 de *Pt. matronense* illustrée par Crochet [1980 : fig. 160]). Les M3s sont moins longues en moyenne que les M1s et M2s (Tableau 2), alors qu'elles sont au moins aussi longues chez d'autres pérathériinés de l'EECO comme *Peratherium* sp. nov. 2 et *Peratherium* sp. nov. 3, ou encore « *A.* » *goethei* post-EECO. En prenant les longueurs et largeurs moyennes en compte, les M2s apparaissent légèrement plus grandes que les M3s (Tableau 2). Les M4s sont en moyenne moins larges que les M3s. Les M1s et M2s d'« *A.* » *goethei* de Bouxwiller (~MP13) ont toutes une cuspide stylaire D

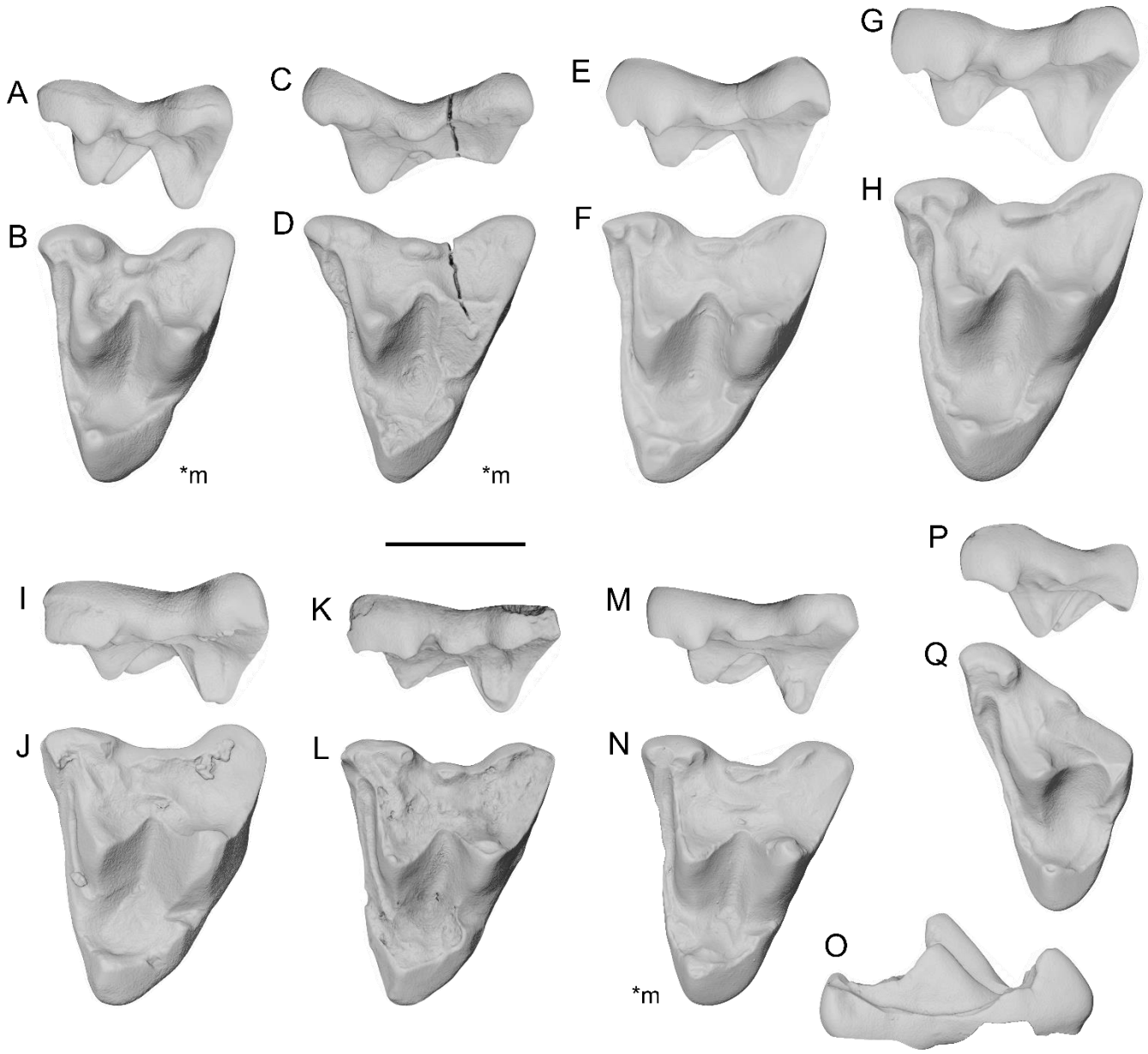

Figure 10. M3s et M4 isolées de *Peratherium matronense* Crochet, 1979, de Condé-en-Brie, Sables de Brasles et Sézanne-Broyes (Bassin de Paris, ~MP8+9). **A-O**. M3s. **A-B**. MNHN.F.CB2845 en vues labiale (A) et occlusale (B). **C-D**. MNHN.F.CB1412 en vues labiale (C) et occlusale. **E-F**. MNHN.F.SZ552-BN en vues labiale (E) et occlusale (F). **G-H**. MNHN.F.SZ558-BN en vues labiale (G) et occlusale (H). **I-J**. MNHN.F.GL306-L en vues (miroir) labiale (I) et occlusale (J). **K-L**. MNHN.F.GL396-L en vues labiale (K) et occlusale (L). **M-O**. MNHN.F.CB203-BN en vues (miroir) labiale (M), occlusale (N) et mésiale (O). **P-Q**. M4 gauche MNHN.F.SZ511-BN en vues labiale (P) et occlusale (Q). Abréviation : *m, spécimen attribué à *Pt. matronense* par Crochet (1980). Échelle : 1 mm.

relativement longue et large par rapport à la cuspide stylaire C (e.g., Crochet 1980 : figs. 89-90). Les molaires supérieures ont des conules et des cuspides stylaires C et D de taille plus importante que ceux d'*Amphiperatherium bourdellense*, et leur plateau stylaire est relativement plus large labiolingualement (Figure 11C-F vs Figure 11H-I).

Les prémolaires inférieures sont relativement moins larges que celles d'« *A.* » *bourdellense* (Figure 7A, F vs Crochet 1980 : fig. 65). La couronne de la p3 était sans doute plus haute que celle de la m1 (Figure

7B; le sommet de la p3 et le protoconide de la m1 du dentaire UM-MOZ-11 sont peu usés). Sur le dentaire UM-MOZ-11, la m3 est seulement légèrement plus grande que la m2 (L m2 = 1.67 mm, L m3 = 1.70 mm ; Figure 7A). Cela semble être aussi le cas sur le dentaire UM-MOZ-1, bien que la m3 soit en partie brisée (Figure 7C). En moyenne, toutes localités confondues, les m2s et m3s sont de même taille (Tableau 2). Comme indiqué précédemment à partir de molaires inférieures de *Pt. maximum* (Gernelle et al. 2024b : fig. 7), le flanc distolingual comprenant l'entoconide et l'hypoconulide est de plus en plus convexe de la m1 à la m3. Ce caractère est retrouvé chez *Pt. matronense*. Cela est observé à la fois sur les molaires inférieures en association (Figure 7A, m1 et m3) et à partir des rangées dentaires inférieures composites (Figure 12M-P). La pré-entocristide est courte sur les m1s à m3s (Figures 7C-D ; 12A, C, F, G, M-O), mais pas sur les m4s (e.g., Figure 12P). Au contraire, les m3s de *Pt. monspeliense* ont une pré-entocristide longue. Les m2s attribuées à *Pt. matronense* ont des encoches entoconide – hypoconulide moins hautes que les encoches métaconide – entoconide, alors qu'elles sont de même hauteur sur les m2s d'« *A.* » *goethei* de Bouxwiller (~MP13) (e.g., Figure 12H vs Figure 12K). Le paraconide est également relativement plus long que chez ce dernier (e.g., Figure 12H vs Figure 12K). Les m1s à m4s de *Peratherium matronense* ont généralement une émargination labiale profonde de leur couronne, entre le trigonide et le talonide (e.g., la rangée de molaires inférieures composite de Sézanne-Broyes ; Figure 12M-P). Celle-ci est très réduite sur de rares spécimens (e.g., MNHN.F.CB179-BN ; Figure 12F). Par comparaison, les molaires inférieures d'« *A* ». *bourdellense* de localités d'âge ~MP16 n'ont pas d'émargination labiale, leur flanc labial entier est toujours rectiligne en vue occlusale (Figure 12L ; Crochet 1980 : fig. 61-63, 66). Les molaires inférieures de *Pt. matronense* n'ont pas d'encoche profonde entre la posthypocristidde et la cristide labiale de l'hypoconulide (encoche de la postcristide) à l'inverse de celles d'« *A.* » *bourdellense* (Figure 12L).

Discussion

Selon Crochet (1980), *Amphiperatherium* sp. 1, *A. bourdellense*, *A. goethei*, et *Pt. matronense* étaient représentées dans les faunes MP8+9 / ~MP8+9 d'Avenay et Condé-en-Brie. Au vu des différences morphologiques importantes ne relevant pas de la variation intraspécifique entre le matériel d'*A. bourdellense* et d'*A. goethei* provenant de leurs localités types et celui des localités MP8+9 / ~MP8+9, ces espèces sont en fait absentes des localités les plus anciennes. Les spécimens attribués à *Amphiperatherium* sp. 1 par Crochet (1980) ne montrant pas de variation majeure de taille par rapport aux autres spécimens initialement attribués à *Pt. matronense* (e.g., Figure 12A vs Figure 12C), ils sont ici attribués à cette dernière espèce. *Peratherium matronense* est la seule espèce valide de pérathériiné de petite taille retrouvée dans les faunes des localités (~)MP8+9 d'Avenay ou d'âge proche (PE V).

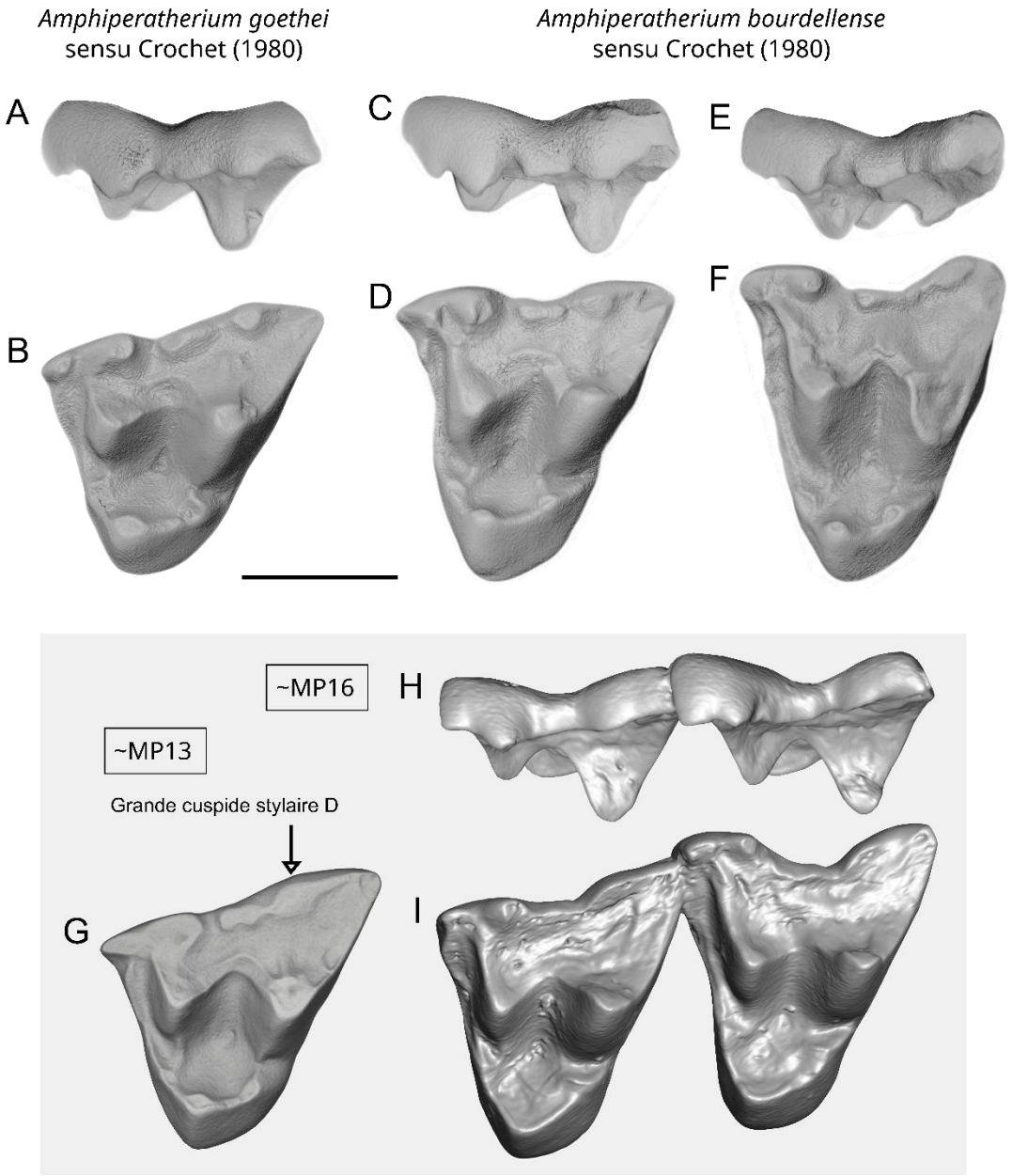

Figure 11. M1-M3 isolées de *Peratherium matronense* Crochet, 1979, de Condé-en-Brie (~MP8+9) initialement attribuées à *Amphiperatherium goethei* Crochet, 1979, et *Amphiperatherium bourdellense* Crochet, 1979, par Crochet (1980) (A-F), comparées à celles d'*A. goethei* et *A. bourdellense* provenant de leur localité-type (G-I). **A-B**. MNHN.F.CB3243, M1 droite (ex *A. goethei*) en vues (miroir) labiale (A) et occlusale (B). **C-D**. MNHN.F.CB4138, M2 gauche (ex *A. bourdellense*) en vues labiale (C) et occlusale (D). **E-F**. MNHN.F.CB2632, M3 droite (ex *A. bourdellense*) en vues (miroir) labiale (E) et occlusale (F). **G**. UM-BUX-68.81, M1 gauche d'*A. goethei* de Bouxwiller (~MP13) en vue occlusale. **H-I**. M2-M3 du maxillaire gauche UM-BRT-543, holotype d'*A. bourdellense*, de Le Bretou (~MP16) en vues labiale (H) et occlusale (I). Échelle : 1 mm.

Peratherium matronense est documenté, comme *Pt. constans*, par une quantité considérable de spécimens, surtout des molaires isolées. La taille de toutes les dents de Fournes, Monze, et La Gasque, légèrement mais sensiblement plus importante que celle de tous les spécimens de *Pt. constans*, ainsi que la moindre récurrence d'émargination distale entre le plateau stylaire et le talon des molaires supérieures,

permettent d'identifier pour la première fois *Pt. matronense* dans des localités plus anciennes que l'Éocène inférieur moyen, et notamment à partir de molaires inférieures en association. Cela augmente légèrement la longévité de cette espèce et montre qu'elle était aussi présente dans le sud de la France dès la fin de l'intervalle de temps MP7-MP8+9, de la même façon que *Peratherium maximum* est présent dans les faunes du Bassin de Paris au moins à partir de Pourcy (voir Gernelle et al. 2024b, Chapitre 5).

Trois molaires supérieures, une molaire inférieure, et trois prémolaires inférieures de Abbey Wood (MP7-MP8+9, PE III) ont été attribuées à *Amphiperatherium* sp. 1 sensu Hooker (2010), un taxon de taille proche de *Pt. constans* et *Pt. matronense*, rapproché au moment de sa description d'*A. brabantense* (= *Pt. constans* ; Ladevèze et al. 2012) (Hooker 2010). Cependant, les deux M1s n'ont pas d'émargination distale (Hooker 2010 : fig. 8d, g), ce qui rapproche ce taxon de *Pt. matronense*. De plus, une des deux M1s (Hooker 2010 : fig. 8d) est plus grande que tous les spécimens ici rapprochés de *Pt. constans*. Les prémolaires inférieures sont intermédiaires en taille entre la p3 de *Pt. constans* de Dormaal (d'après l'illustration à l'échelle de Ladevèze et al. 2012 : fig. 3Da) et la p2 et la p3 de *Pt. matronense* de Monze (Annexes : Tableau S1). Pour ces raisons, les spécimens attribués à *Amphiperatherium* sp. 1 par Hooker (2010) sont ici placés en nomenclature ouverte dans *Peratherium* cf. *matronense*.

Une m2 de La Borie (~MP8+9, Sud de la France ; cf. Chapitre 5) a été rapprochée de *A. bourdellense* par Crochet (1980 : tab. 7). Le contour en vue occlusale de la m2 de La Borie (Figure 12I) ressemble à celui des m2s de *A. bourdellense* ~MP16 par l'absence d'émargination labiale (Figure 12L), mais la première est distincte par le flanc lingual moins proéminent, par l'absence d'encoche profonde de la postcristide, et le protoconide en position relativement plus distale par rapport au métaconide (Figure 12I vs Figure 12L). En revanche, ces caractères sont présents chez *Pt. matronense*, et la pré-entocristide courte ne rappelle pas *Pt. monspeliense*. La m2 isolée de La Borie (UM-SPA-1) est donc attribuée à *Peratherium* cf. *matronense* (a priori non homogène avec *Peratherium* cf. *matronense* de Abbey Wood).

Plusieurs molaires de Mutigny (Bassin de Paris, ~MP8+9, PE IV) ont été placées dans *Peratherium constans* et *Amphiperatherium brabantense* (Crochet 1980). Celles-ci n'ont pas été révisées par Ladevèze et al. (2012), lors de la synonymisation d'*A. brabantense* avec *Pt. constans*. Seulement trois molaires complètes de pérathériiné de petite taille ont été retrouvées en collections durant cette thèse (Figure 13). Au moins une d'entre elle correspond à celles étudiées par Crochet (1980 : 38) (MNHN.F.MU142-L, Figure 13B-C). Ces spécimens sont effectivement de plus petite taille que tous ceux attribués à *Pt. matronense* (Tableau 2 vs Annexes : Tableau S1), et sont plus proches sur ce critère de *Pt. constans* (Tableau 1). Cependant peu de caractères morphologiques diffèrent sur les molaires inférieures de *Pt. constans* et *Pt. matronense*, et la M4 du taxon de Mutigny présente des proportions inconnues chez ces deux espèces (importante longueur relative ; Figure 13D), ce qui complique l'attribution. Ce taxon représente en tout cas la seule différence potentielle entre les faunes de métathériens de Mutigny (PE IV), et d'Avenay et des localités d'âge proche (PE V), mais le matériel disponible est insuffisant pour

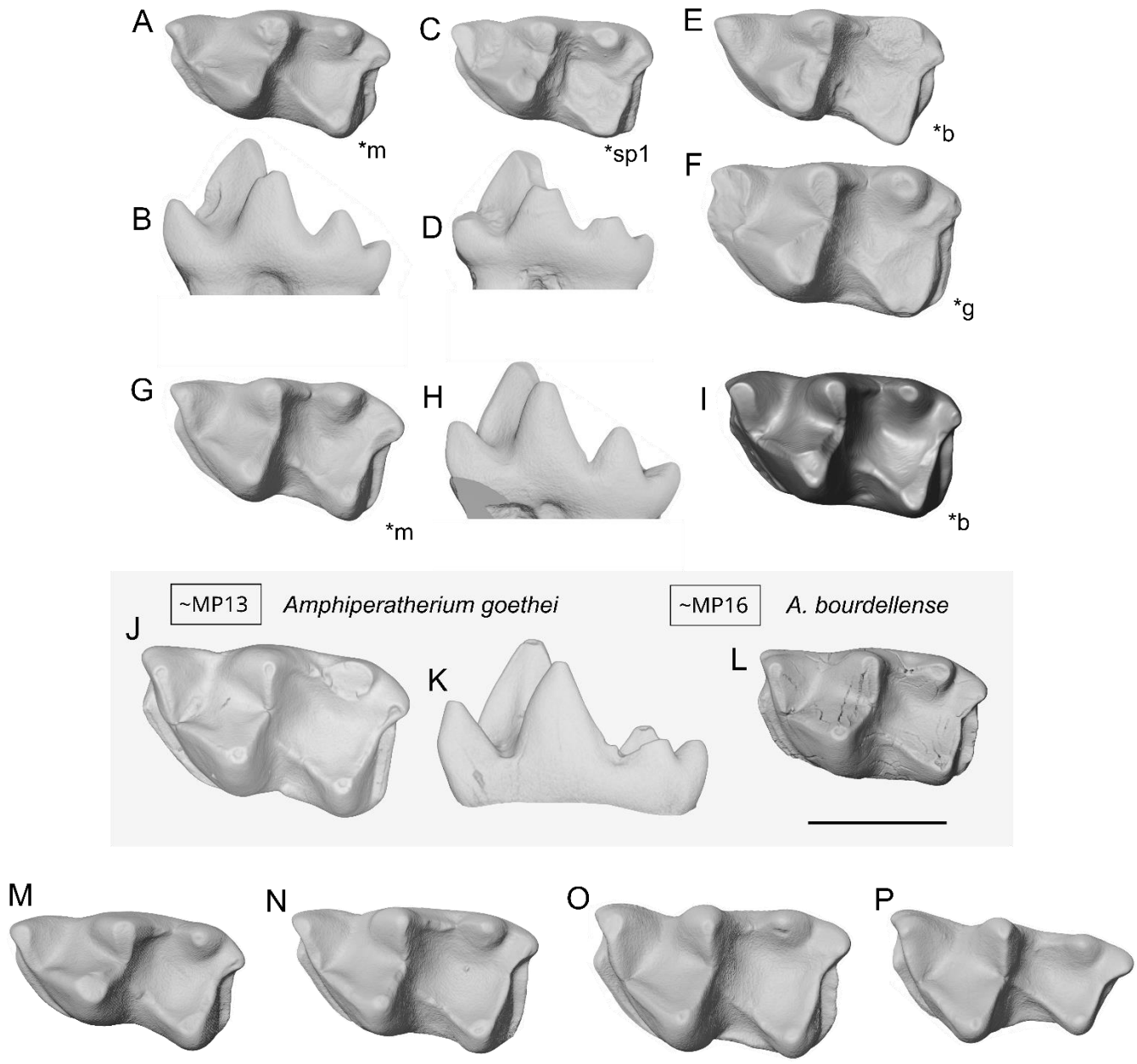

Figure 12. Molaires inférieures de *Peratherium matronense* Crochet, 1979 (A-H, M-P), et d'un taxon proche (I), comparées avec une sélection de molaires inférieures d'espèces post-ypresiennes du genre "*Amphiperatherium*" (J-L). **A-B**. MNHN.F.CB2506, m1 gauche en vues occlusale (A) et lingual miroir (B). **C-D**. MNHN.F.CB1079-L, m1 gauche en vues occlusale (C) et linguale miroir (D). **E**. MNHN.F.CB647, m1 gauche en vue occlusale. **F**. MNHN.F.CB179-BN, m2 droite en vue occlusale miroir. **G-H**. MNHN.F.CB4129, m2 droite en vues occlusale miroir (G) et linguale (H). **I**. UM-SPA-1, m2 de *Peratherium* cf. *matronense* en vue occlusale. Échelle : 1 mm. **J-K**. UM-BUX-66.142, m2 droite d'« *Amphiperatherium* » *goethei* de Bouxwiller (~MP13) en vues occlusale miroir (J) et linguale (K). **L**. m2 de l'hémi-mandibule droite UM-GRI-604 d'« *Amphiperatherium* » *bourdellense* Crochet, 1979, de Grisolles (~MP16) en vue occlusale miroir. **M-P**. Série composite m1-m4 de Sézanne-Broyes en vue occlusale. **M**. MNHN.F.SZ88-BN, m1 gauche. **N**. MNHN.F.SZ226-BN, m2 droite (miroir). **O**. MNHN.F.SZ574-BN, m3 droite (miroir). **P**. MNHN.F.SZ306-BN, m4 gauche. Abréviations : *b, *g, *m, *sp1, spécimen attribué à *A. bourdellense*, ou *A. goethei*, ou *Pt. matronense*, ou *Amphiperatherium* sp. 1 par Crochet (1980). Échelle : 1 mm.

l'étayer. Les trois autres espèces de métathériens retrouvées au (~)MP8+9 (*Peradectes louisi*, *Peradectes russelli*, et *Peratherium maximum*), bien mieux documentées, sont connues à la fois à Mutigny et dans les faunes PE V.

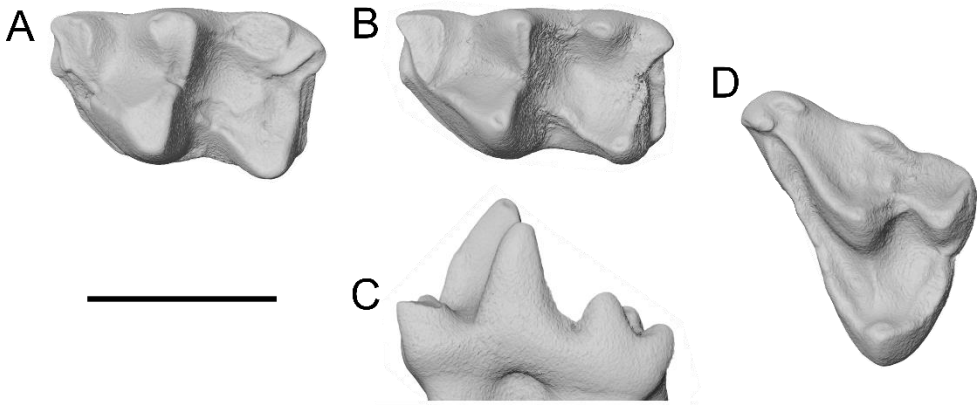

Figure 13. Molaires isolées du Peratheriinae indet. de Mutigny (~MP8+9, PE IV). **A**. m2 MNHN.F.MU114-L en vue occlusale. **B-C**. m3 MNHN.F.MU142-L en vues occlusale (B) et linguale (C). **D**. M4 MNHN.F.MU49-BN en vue occlusale. Échelle : 1 mm.

Comparaisons de la taille des spécimens

Remarque. Les variations détaillées ci-dessous sont fines, les valeurs comparées diffèrent parfois de l'ordre de quelques centièmes de millimètres seulement. Il faut donc rappeler ici que les spécimens de Dormaal ont été mesurés à l'IRSNB avec un appareil de mesure différent de celui utilisé à l'Université de Montpellier pour tous les autres spécimens (voir préambule de cette partie), mais dans les deux cas les mesures ont été prises par moi-même. Quelques molaires moulées de *Pt. constans* de Dormaal conservées à l'Université de Montpellier (~10 spécimens, cf. Chapitres 4-5) et utilisées dans l'analyse de forme des contours des molaires ci-après ont aussi été mesurées (valeurs non ajoutées ici) pour vérification avec le même système de mesure utilisé pour les autres molaires. Les différences constatées ci-dessous semblent être confirmées ainsi.

Description des variations de taille. La variation de taille des molaires de *Pt. constans* des localités de l'intervalle MP7-MP8+9 (sauf Fournes, Meudon, La Gasque) est de plus grande amplitude que celle des *Pt. constans* de Dormaal (localité-type), Le Quesnoy et Silveirinha (MP7 / ~MP7) pour les M2s (Figure 14B), m1s (Figure 14D) et m3s (Figure 14F). Chez *Pt. constans* des localités autres que (~)MP7, par rapport à la variation connue dans la série de molaires (~)MP7, trois M1s sont plus longues (Figure 14A), quatre M2s sont plus grandes (Figure 14B), une M3 est plus large (Figure 14C), presque toutes les m1s sont plus larges (Figure 14D), et deux m2s et deux m3s sont légèrement plus longues (Figure 14E-F). Parmi ces différences, la plus notoire concerne les m1s (Figure 14D), car il s'agit du seul locus dont l'ellipse de confiance à 95 % est plus chevauchante avec celle de *Pt. matronense* des localités (~)MP8+9 qu'avec celle de *Pt. constans* (~)MP7. Des différences statistiquement significatives (*t*-test de Welch ; P

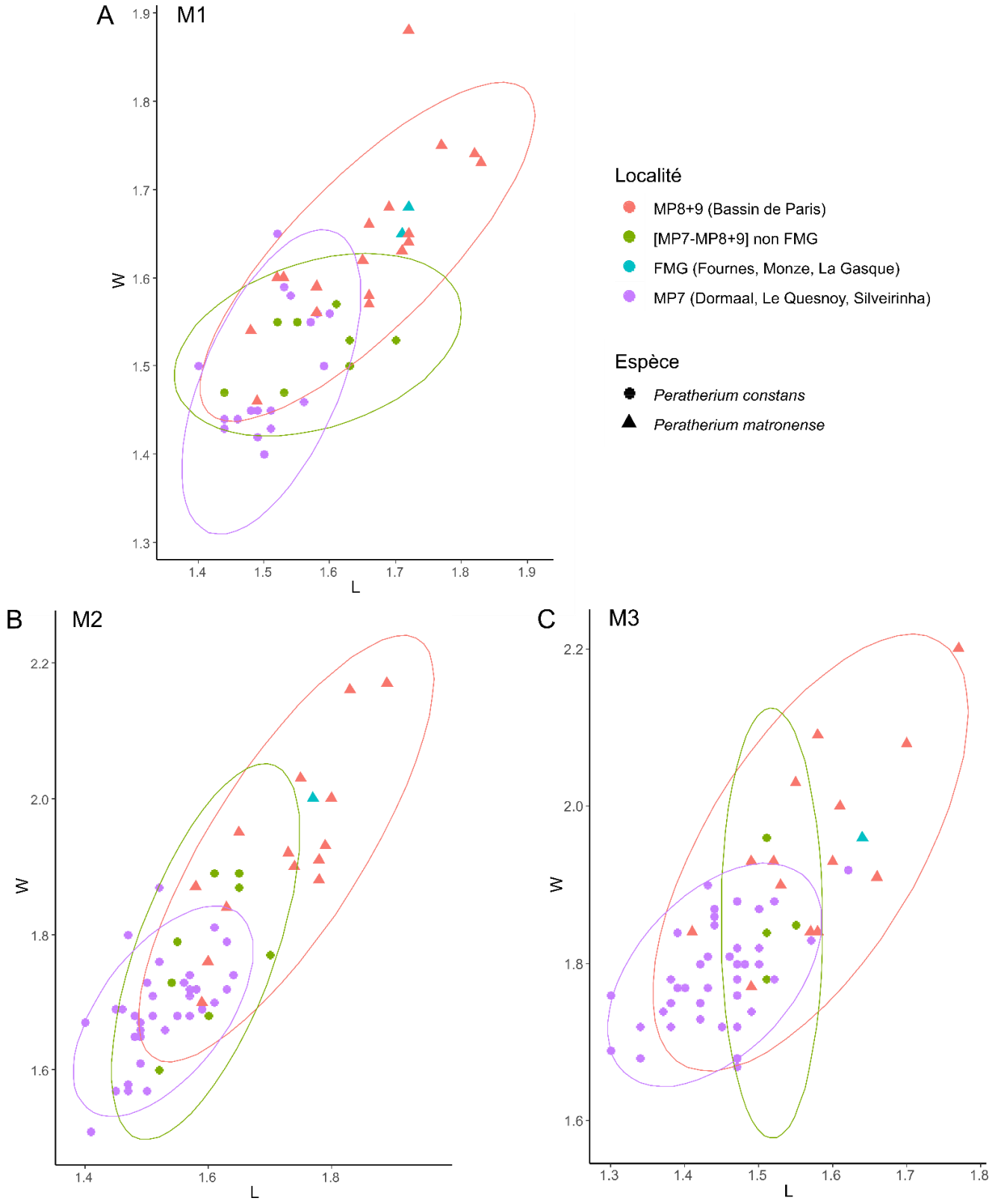

Figure 14. Diagrammes bivariés comparant les longueurs et largeurs (en mm), pour chaque locus (molaires supérieures et inférieures), chez *Peratherium constans* Teilhard de Chardin, 1927, et *Peratherium matronense* Crochet, 1979. **A-C**. Molaires supérieures (excepté M4). **D-G** (page suivante). Molaires inférieures. Les couleurs des spécimens correspondent à l'âge approximatif des localités. Les ellipses de confiance à 95% (suivant une distribution « *t* »), telles que calculées par R via le package ggplot2 (Whickham 2016), sont figurées pour chaque sous-groupe. Le détail des mesures et des localités associées aux spécimens est présenté en Annexes (Tableau S1).

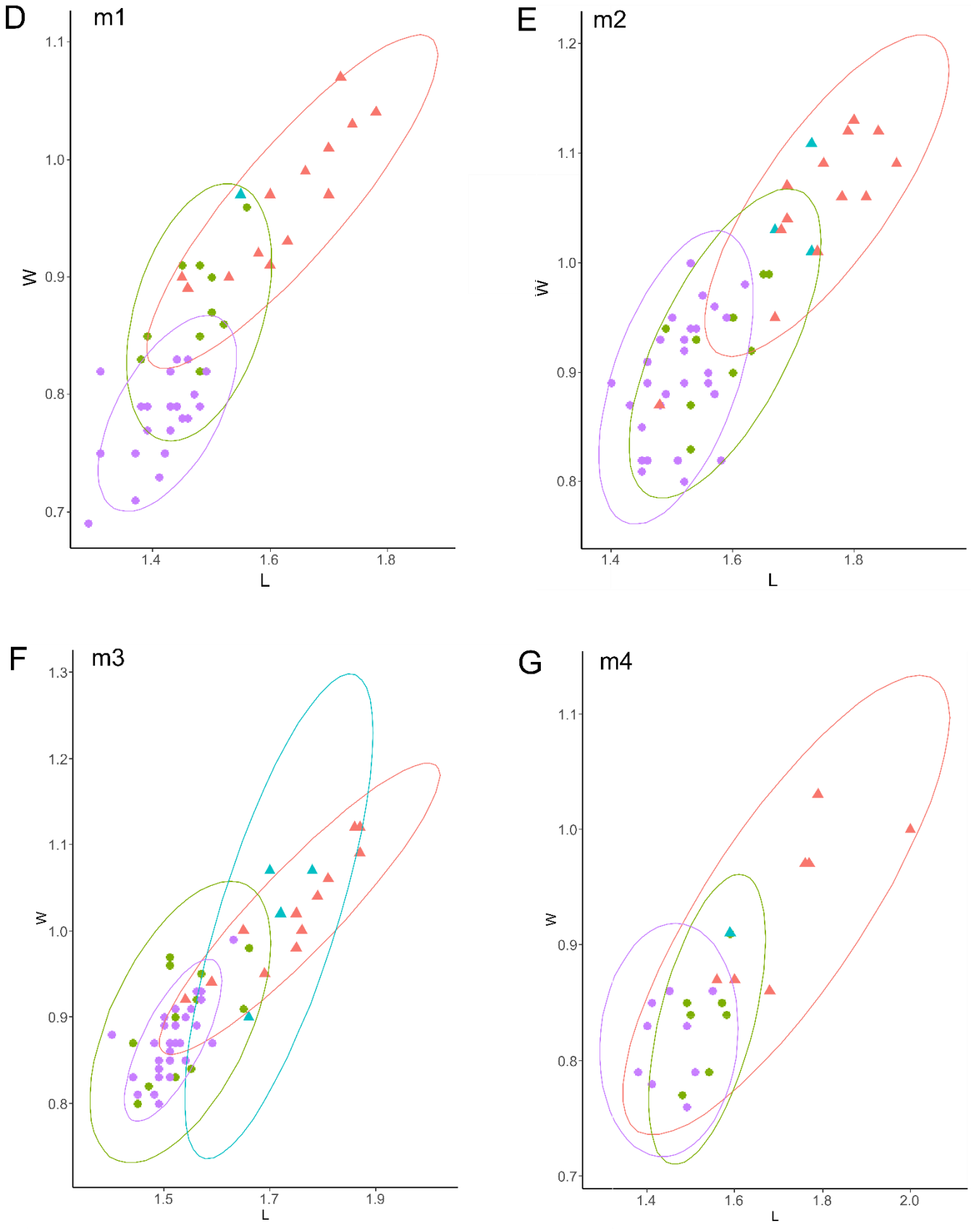

Figure 14 (Suite)

< 0.05) sont retrouvées entre les molaires de *Pt. constans* de Dormaal, Le Quesnoy, et Silveirinha d'une part, et celles des autres localités d'autre part, pour la moitié des variables mesurées (7 parmi 14) : la longueur et la largeur des M2s, la longueur des M3s, la longueur et la largeur des m1s, la longueur des m2s et la longueur des m4s. Aucune différence significative n'est observée concernant la moitié restante des variables mesurées (longueur et largeur des M1s, largeur des M3s, largeur des m2s, longueur et largeur des m3s, et largeur des m4s).

La variation de taille des molaires de *Pt. matronense* est plus importante que celle des molaires de *Pt. constans* (Figure 14 ; voir aussi les valeurs des coefficients de variations pour les mesures, plus élevées chez *Pt. matronense*, Tableau 1 vs Tableau 2). Tous les spécimens de *Pt. matronense* des localités (~)MP8+9 entrent dans les ellipses de confiance de ce groupe, sauf une M3 par sa longueur légèrement plus importante (Figure 14C), et surtout une M1 par sa largeur considérablement plus importante (Figure 14A). Les spécimens de Fournes, Monze, et La Gasque (FMG) entrent exclusivement dans la variation de taille de *Pt. matronense* des localités (~)MP8+9 pour les molaires supérieures (Figure 14A-C). Concernant les molaires inférieures, même si certains spécimens sont inclus à la fois dans les ellipses de confiance de *Pt. constans* des localités [MP7-MP8+9] non FMG et *Pt. matronense* des localités (~)MP8+9 (Figure 14D-G), d'autres sont inclus dans la variation de taille observée pour les spécimens du second groupe plutôt que dans celle du premier (m2 et m3 ; Figure 14E-F).

Discussion. Les molaires de *Pt. matronense* sont bien en moyenne nettement plus grandes que celles de *Pt. constans*. Néanmoins, en prenant en compte l'ensemble des spécimens ici attribués à *Pt. constans* dans deux groupes distincts (Dormaal, Le Quesnoy, Silveirinha d'une part, et ceux des localités de l'intervalle MP7-MP8+9 d'autre part), des différences subtiles mais statistiquement significatives ont été observées pour la moitié des variables mesurées. Les spécimens plus jeunes sont en effet légèrement plus grands, en particulier les m1s. Cependant, les deux groupes semblent morphologiquement indistincts (voir aussi l'analyse de forme des contours ci-dessous). Tous ces spécimens sont donc inclus ici dans *Peratherium constans*, mais il est possible que les quelques légères différences de taille soulignées reflètent leur appartenance à deux chrono-espèces distinctes.

Analyse de forme du contour des molaires supérieures par morphométrie géométrique

Méthode. L'objectif des analyses de morphométrie géométrique est ici de vérifier la pertinence de caractères diagnostiques proposés dans ce travail ou par Crochet (1980). Ces analyses sont basées sur la même méthode que celle détaillée dans le Chapitre 2. Ici, 59 au lieu de 49 (semi) points-repères également espacés jalonnent le contour des M1s et M2s. Le premier point de chaque courbe a toujours été positionné au niveau du point le plus mésial de l'éperon de la cuspide stylaire A. Les attributions taxonomiques ont

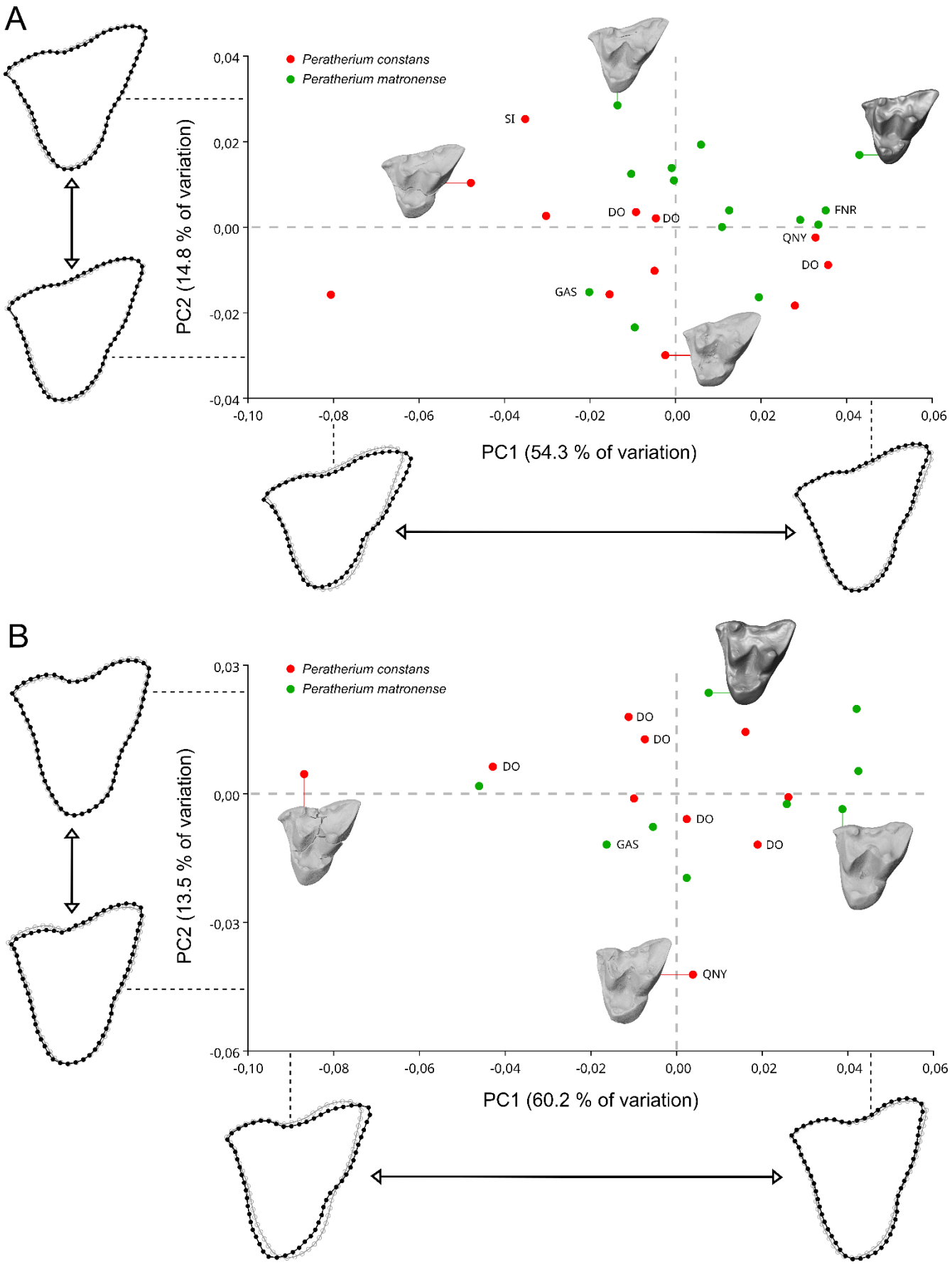

Figure 15. Graphiques des deux premières composantes principales (PCs) du jeu de données de points repères positionnés sur les M1s (**A**) et M2s (**B**) de *Peratherium constans* Teilhard de Chardin, 1927, et *Peratherium matronense* Crochet, 1979, après transformation de Procrustes. Les représentations graphiques en « fil de fer » des M1s et M2s indiquent les changements extrêmes de forme sur chaque axe

(contour noir) par rapport à la forme moyenne de tout l'échantillon. Les vues occlusales de certains spécimens, illustrées ci-dessus par ailleurs, sont reproduites au sein du graphique (non à l'échelle). Les M1s et M2s provenant des localités les plus anciennes ayant livré chacune des espèces sont signalées par les abréviations de ces localités : DO, Dormaal ; FNR, Fournes ; GAS, La Gasque ; QNY, Le Quesnoy ; SI, Silveirinha.

été déterminées en amont des analyses (cf. Paléontologie systématique). *Peratherium constans* est représenté par 12 M1s et 10 M2s. *Peratherium matronense* est représenté par 14 M1s et 9 M2s.

Description des variations de forme. Les deux premières composantes principales (PCs) résument 69.1 % de la variation totale pour les M1s (PC1 = 54.3 %, PC2 = 14.8 % ; Figure 15A), et 73.7 % pour les M2s (PC1 = 60.2 %, PC2 = 13.5 % ; Figure 15B). Le graphique résumant la variation morphologique des M1s montre un chevauchement relativement faible des espaces morphologiques de *Peratherium constans* et *Pt. matronense* (Figure 15A). Les spécimens avec des valeurs positives sur les deux axes sont ceux appartenant à *Pt. matronense*, tandis que ceux avec les valeurs négatives sur les deux axes sont surtout ceux attribués à *Pt. constans*. Par rapport à la forme moyenne et aux valeurs positives sur l'axe PC1, les valeurs négatives sur l'axe PC1 sont corrélées avec (i) une aile métastylaire plus projetée distalement et (ii) relativement moins labiale, et (iii) un talon relativement plus mésial. La combinaison de ces caractères est à l'origine d'une forme (pour les valeurs les plus négatives sur l'axe PC1) caractérisée par une importante émargination distale de la couronne entre le plateau stylaire et le talon. Par rapport à la forme moyenne et aux valeurs positives sur l'axe PC2, les valeurs négatives sur l'axe PC2 sont corrélées avec des changements de forme très subtiles, la principale étant un ectoflexus presque totalement atténué (l'ectoflexus est réduit sur toutes les M1s, par rapport aux M2s et M3s).

Le graphique résumant la variation morphologique des M2s montre un chevauchement des espaces morphologiques de *Pt. constans* et *Pt. matronense* qui est plus conséquent que dans le cas de la variation morphologique des M1s (Figure 15B). Les spécimens avec les valeurs les plus positives sur l'axe PC1 sont ceux appartenant à *Pt. matronense*. Le spécimen avec la valeur la plus positive sur l'axe PC2 appartient aussi à *Pt. matronense*. Les spécimens ayant les valeurs les plus négatives sur l'axe PC1 et PC2 appartiennent à *Pt. constans*. Par rapport à la forme moyenne et aux valeurs positives sur l'axe PC1, les valeurs négatives sur l'axe PC1 sont corrélées, de façon identique aux M1s pour le même axe, à une importante émargination distale de la couronne entre le plateau stylaire et le talon. Par rapport à la forme moyenne et aux valeurs positives sur l'axe PC2, les valeurs négatives sur l'axe PC2 sont corrélées avec (i) une aile parastylaire (portant les cuspides stylaires A et B) relativement moins labiale, ainsi qu'avec (ii) une aile métastylaire légèrement plus labiale. La combinaison de ces caractères résulte en un ectoflexus relativement plus asymétrique pour les spécimens aux valeurs les plus négatives sur l'axe PC2. Les spécimens de Dormaal (*Pt. constans*) sont relativement proches de l'origine des axes, sauf un de ces

spécimens dans chaque cas (M1 et M2), pour lesquels l'émargination distale est peu profonde mésiodistalement.

Discussion. L'analyse des contours par morphométrie géométrique montre que l'émargination distale entre le plateau stylaire et le talon, profonde sur les M1s, s'atténue sur les M2s. Ce caractère constitue la principale variation interspécifique notable. Les observations (non quantifiées) menées précédemment sur les M3s de *Pt. constans* et de *Pt. matronense* ont montré que dans les deux cas, une émargination distale est très rarement distinguable sur les M3s, mais est tout de même plus fréquente chez *Pt. constans* (Figures 5E, 6O). Le rapprochement de ces résultats permet de conclure que *Pt. constans* et *Pt. matronense* sont bien distincts par la profondeur mésiodistale, en moyenne, de leur émargination distale, mais cette différence entre les deux espèces s'atténue significativement le long de la rangée dentaire, de la M1 à la M3. Ce caractère inédit vraisemblablement présent seulement chez *Pt. constans* lors de l'Éocène inférieur semble s'être développé de nouveau chez *Peratherium bretouense* Crochet, 1979 (Le Bretou, Quercy ; ~MP16), avec la même particularité d'atténuation le long des rangées M1s-M3s (pers. obs., voir Crochet [1980 : figs. 180-183]). Il s'agit dans ce dernier cas de rangées dentaires non composites. Contrairement à la diagnose différentielle de *Pt. matronense* proposée par Crochet (1980 : 147), (i) il n'existe probablement pas de différence notable de position relative de la cuspide stylaire A entre *Peratherium constans* et *Pt. matronense*, car aucune différence conséquente entre les deux espèces n'a été notée quant à la position du point le plus mésial de l'éperon portant la cuspide stylaire A par rapport à l'axe mésiodistal des molaires. De plus, (ii) à partir des données analysées pour les M2s, l'ectoflexus chez *Pt. matronense* ne semble pas être plus asymétrique que chez *Pt. constans* en moyenne.

B. Complément à l'étude des pérathériinés de grande taille de l'Éocène inférieur

Le premier pérathériiné de grande taille (*Peratherium musivum* Gernelle, 2024) et la série type ainsi que de nouveaux spécimens de *Peratherium maximum* (Crochet, 1979) ont été étudiés en détail dans le Chapitre 5. L'ensemble du matériel rapporté à cette dernière espèce est mentionné ci-dessous et une étude complémentaire succincte d'une partie de ces spécimens est menée. Une forme de grande taille de Sézanne-Broyes, sans doute l'un des plus grands métathériens d'Europe connus, est placée en nomenclature ouverte.

Peratherium maximum (Crochet, 1979)

Figures 16-17A-C, Tableaux 3-4, Annexes : Tableaux S2-3

1979 – *Amphiperatherium maximum* Crochet in Crochet p. 371-372, fig. 7.
1980 – *Amphiperatherium maximum* Crochet in Crochet p. 98-102, figs. 106-113 (no fig. 105) (en partie: spécimens de Pourcy, Mutigny, Avenay, Condé-en-Brie, et Sables de Brasles).
1980 – *Amphiperatherium* sp. indet 2 in Crochet p. 137-138 (en partie: spécimens de Mutigny, Avenay et Condé-en-Brie).
1983 – *Amphiperatherium maximum* Crochet in Louis et Laurain, p. 8.
2024 – *Peratherium maximum* (Crochet) in Gernelle et al., p. 13-16, figs. 4C-D, 4Q, 5 P-Q, 6 A, 7D-K.

Holotype. MNHN.F.CB198, M3 droite, figurée par Crochet (1979: fig. 7, 1980: fig. 108).

Localité-type. Condé-en-Brie (Aisne, Est du Bassin de Paris) ; Éocène inférieur moyen, ~MP8+9.

Autres localités. Pourcy, Mutigny, Avenay, et Sables de Brasles, et Saint-Agnan dans le Bassin de Paris, et La Borie dans le Sud de la France.

Âge. De la biozone PE III (intervalle MP7-MP8+9 ; Pourcy) à l'intervalle MP8+9-MP10 (Saint-Agnan ; cf. Chapitre 1 pour l'âge de Saint-Agnan).

Diagnose. Plus grand pérathériiné de l'Éocène inférieur, caractérisé par la duplication fréquente des cuspides stylaires C et D, et la taille relative importante du complexe fonctionnel protocône / talonide, en particulier sur M2 / m2. Cuspide stylaire D plus haute que la cuspide stylaire B sur les M1s.

Matériel. Matériel supplémentaire de Condé-en-Brie : *Dents molariformes inférieures* : dp3 gauche (**MNHN.F.CB862**), m1 gauche (MNHN.F.CB207 ; MNHN.F.CB209, usé ; MNHN.F.CB248-BN ; MNHN.F.CB577 ; MNHN.F.CB778-L ; MNHN.F.CB841 ; MNHN.F.CB1179 ; MNHN.F.CB2812, usé ; MNHN.F.CB3106, usé ; MNHN.F.CB3336, fragmentaire ; MNHN.F.CB3398 ; MNHN.F.CB4118, usé ; MNHN.F.CB4136, usé ; MNHN.F.CB5030, fragmentaire), m1 droite (MNHN.F.CB167-BN,

Crochet 1980 : fig. 110 ; MNHN.F.CB807 ; MNHN.F.CB854 ; MNHN.F.CB1754-L, usé ; MNHN.F.CB2709 ; MNHN.F.CB2715 ; MNHN.F.CB2896 ; **MNHN.F.CB2933** ; MNHN.F.CB3207, usé ; MNHN.F.CB3277, usé ; MNHN.F.CB3305, usé), m2 gauche (MNHN.F.CB838 ; MNHN.F.CB1077-L ; MNHN.F.CB1692-L ; MNHN.F.CB4125, usé ; MNHN.F.CB4707), m2 droite (MNHN.F.CB255-M, fragmentaire ; MNHN.F.CB258-M, fragmentaire ; MNHN.F.CB267-BN ; MNHN.F.CB593 ; MNHN.F.CB608 ; MNHN.F.CB648, Crochet 1980 : fig. 111 ; MNHN.F.CB781-L ; MNHN.F.CB826, usé ; MNHN.F.CB829 ; MNHN.F.CB831, usé ; MNHN.F.CB832 ; MNHN.F.CB839, usé ; MNHN.F.CB1074-L ; MNHN.F.CB3421 ; MNHN.F.CB3635, usé ; MNHN.F.CB4666, usé), m2 ou m3 droite (MNHN.F.CB751, fragmentaire et usé), m3 gauche (MNHN.F.CB378-BN ; MNHN.F.CB379-BN ; MNHN.F.CB746 ; MNHN.F.CB821 ; MNHN.F.CB824, usé ; MNHN.F.CB830, usé ; MNHN.F.CB836 ; MNHN.F.CB1116 ; MNHN.F.CB3433 ; MNHN.F.CB4127 ; MNHN.F.CB4977), m3 droite (MNHN.F.CB208 ; MNHN.F.CB698 ; MNHN.F.CB1073-L, Crochet 1980 : fig. 112* ; MNHN.F.CB1115 ; MNHN.F.CB2802 ; MNHN.F.CB3295), m4 gauche (MNHN.F.CB655 ; MNHN.F.CB820 ; MNHN.F.CB825 ; MNHN.F.CB855 ; MNHN.F.CB4126 ; MNHN.F.CB4170), m4 droite (MNHN.F.CB1316, Crochet 1980 : fig. 113 ; MNHN.F.CB4178). *Dents molariformes supérieures* : dP3 gauche (**MNHN.F.CB206-BN** ; MNHN.F.CB3024 ; MNHN.F.CB3049), dP3 droite (MNHN.F.CB853 ; MNHN.F.CB3701 ; MNHN.F.CB4141), M1 gauche (MNHN.F.CB194, usé ; MNHN.F.CB377-BN ; MNHN.F.CB777-L ; MNHN.F.CB843, usé ; MNHN.F.CB847 ; MNHN.F.CB1233 ; MNHN.F.CB3105 ; MNHN.F.CB3113, usé ; MNHN.F.CB3212, fragmentaire ; MNHN.F.CB4122, usé ; MNHN.F.CB4131, usé ; MNHN.F.CB4132 ; MNHN.F.CB4706 ; MNHN.F.CB4890), M1 droite (MNHN.F.CB263-M ; MNHN.F.CB844 ; MNHN.F.CB3642, usé ; MNHN.F.CB4124, fragmentaire ; MNHN.F.CB4135, usé), M2 gauche (MNHN.F.CB197 ; MNHN.F.CB261-M ; MNHN.F.CB1327; MNHN.F.CB1769-L, usé ; MNHN.F.CB3634 ; MNHN.F.CB3636, fragmentaire ; MNHN.F.CB4133, usé ; MNHN.F.CB4896, fragmentaire), M2 droite (MNHN.F.CB33-M ; MNHN.F.CB80-P, fragmentaire ; MNHN.F.CB196, Crochet 1980 : fig. 107 ; MNHN.F.CB236-M ; MNHN.F.CB405-BN ; MNHN.F.CB455-BN, fragmentaire ; MNHN.F.CB779-L ; MNHN.F.CB789-L, fragmentaire ; MNHN.F.CB1731-L, fragmentaire ; MNHN.F.CB3037, usé ; MNHN.F.CB3322 ; MNHN.F.CB4128, usé), M2 ou M3 fragmentaire (MNHN.F.CB833, usé ; MNHN.F.CB3085 ; MNHN.F.CB3638), M3 gauche (MNHN.F.CB5-M ; MNHN.F.CB30-M ; MNHN.F.CB79-P ; MNHN.F.CB230-M ; MNHN.F.CB247-M ; MNHN.F.CB393-BN ; **MNHN.F.CB1252** ; MNHN.F.CB1397 ; MNHN.F.CB2713, fragmentaire ; MNHN.F.CB4120 ; MNHN.F.CB4123, fragmentaire ; MNHN.F.CB4904), M3 droite (MNHN.F.CB195 ; MNHN.F.CB852 ; MNHN.F.CB3005, fragmentaire ; MNHN.F.CB3052 ; MNHN.F.CB3262, usé ; MNHN.F.CB3647 ; MNHN.F.CB4121 ; MNHN.F.CB4142), M4 droite (MNHN.F.CB3665, usé). * spécimen figuré par Crochet (1980), non trouvé dans les collections du MNHN.

Matériel de Pourcy : m2 gauche (MNHN.F.P20-C ; MNHN.F.PY118-L), M1 gauche (MNHN.F.PY58).

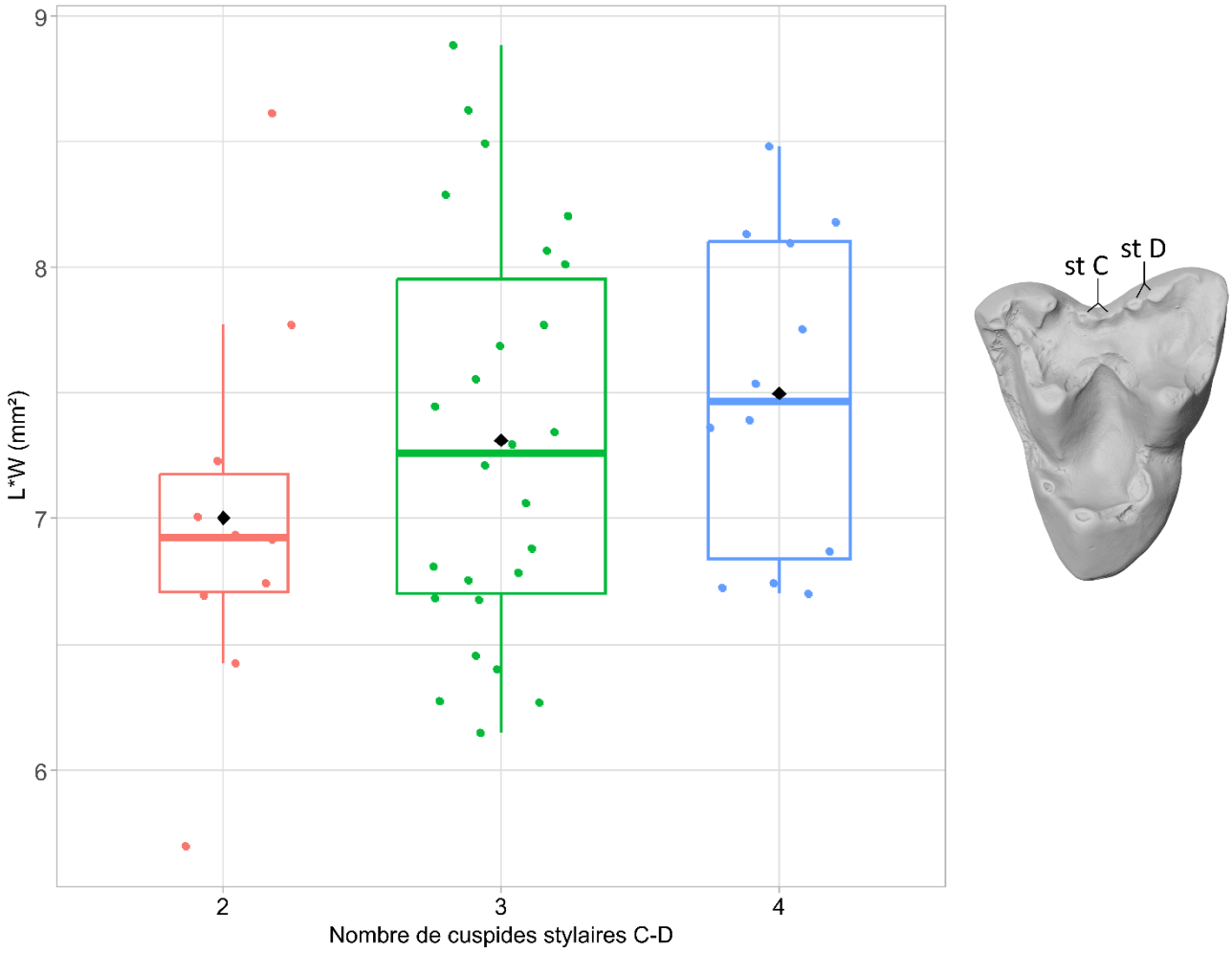

Figure 16. Diagrammes en boîtes montrant la distribution des valeurs de surface approximative des molaires supérieures de *Peratherium maximum* (Crochet, 1979) selon le nombre de cuspides stylaires (2, 3 ou 4) occupant les positions « C » et « D ». Les points noirs correspondent aux valeurs moyennes de chaque catégorie. Le cas d'une M3 (MNHN.F.CB1252) possédant 4 cuspides stylaires en positions « C » et « D » (dédoublement des cuspides stylaires C et D) est illustré (non à l'échelle). Aucune différence significative n'est observée entre les trois conditions (ANOVA de Welch [*W*-test], p = 0.316).

Matériel de Mutigny : *Molaires inférieures* : m1 droite (MNHN.F.Mu175-L ; MNHN.F.Mu5534, fragmentaire), m2 gauche (MNHN.F.Mu6136), m2 droite (MNHN.F.Mu124-L), ?m2 droite partielle (MNHN.F.Mu6010, talonide), m3 gauche (MNHN.F.Mu92-L, fragmentaire ; MNHN.F.Mu178-L ; MNHN.F.Mu5518), m3 droite (MNHN.F.Mu5949 ; MNHN.F.Mu6636), m4 gauche (MNHN.F.Mut3-BN). *Dents jugales supérieures* : dP3 gauche (MNHN.F.Mu71-Lé), M1 droite (MNHN.F.Mu6017, fragmentaire), M2 gauche (MNHN.F.Mu5507, usé), M2 droite (MNHN.F.Mu181-L, fragmentaire ; MNHN.F.Mu6608), M3 droite (MNHN.F.Mu5515, fragmentaire), M4 gauche (MNHN.F.Mu12397), M4 droite (MNHN.F.Mu171-L).

Matériel de Sables de Brasles : *Molaires inférieures* : m1 gauche (MNHN.F.GL398-L), m1 droite (MNHN.F.GL231-L, fragmentaire ; MNHN.F.GL408-L), m2 gauche (MNHN.F.GL226-L ;

MNHN.F.GL307-L), m4 gauche (MNHN.F.GL127-L, talonide). *Dents molariformes supérieures* : dP3 gauche (MNHN.F.GL290-L), M1 droite (MNHN.F.GLD121, usé), M2 droite (MNHN.F.GLD73-L), M4 droite (MNHN.F.GLD13, Crochet 1980: fig. 109 ; MNHN.F.GL247-L).

Matériel d'Avenay : *Molaires inférieures* : m1 gauche (MNHN.F.AV752-BN), m1 droite (MNHN.F.AV4599), m2 gauche (MNHN.F.AV15829), m2 droite (MNHN.F.AV9014, fragmentaire), m3 gauche (MNHN.F.AV6789), m3 droite (MNHN.F.AV13-CN ; MNHN.F.AV4815 ; UM-AV-18-SK), m4 droite (MNHN.F.AV16150). *Dents molariformes supérieures* : dP3 gauche (UM-AV-16-SK), M1 gauche (MNHN.F.AV802-BN ; MNHN.F.AV5848 ; UM-AV-19-SK, fragmentaire), M1 droite (MNHN.F.AV442-L, usé), M2 gauche (MNHN.F.AV74-BN ; MNHN.F.AV7706, fragmentaire), M2 droite (MNHN.F.AV4747 ; MNHN.F.AV4816), M3 droite (MNHN.F.AV4743, fragmentaire ; MNHN.F.AV4814, usé), M4 gauche (UM-AV-17-SK, fragmentaire).

Matériel de Saint-Agnan : *Molaires inférieures* : m1 droite (MNHN.F.STA287), m2 gauche (MNHN.F.STA293, fragmentaire ; MNHN.F.STA300), m2 droite (MNHN.F.STA299), m2 ou m3 droite (MNHN.F.STA291, usé), m3 droite (MNHN.F.STA290), m4 gauche (MNHN.F.STA304). *Molaires supérieures* : M1 gauche (MNHN.F.STA288, usé ; MNHN.F.STA301), M2 gauche (MNHN.F.STA289 ; MNHN.F.STA294), M3 gauche (MNHN.F.STA285).

Matériel de La Borie : fragment d'hémi-mandibule droite avec p1-p3, alvéoles de m1-m3, et m4 (UM-BRI-17 ; Gernelle et al. 2024b : fig. 6A).

Description. Une dp3 appartenant à cette espèce (MNHN.F.CB862), molariforme et beaucoup plus petite que les m1s, est nouvellement identifiée (Figure 17B vs Figure 17A). Une telle taille relative de la dp3 est attendue chez les Herpetotheriidae (e.g., Korth 2021 : fig. 3.5 vs fig. 3.6). Le paraconide est présent mais très réduit, et le trigonide est relativement plus long que celui des m1s. Il n'y a pas de précingulide (Figure 17B). Le bord lingual de la couronne est incurvé alors que le bord labial est rectiligne, sans émargination. L'entoconide est plus bas que l'hypoconide contrairement aux molaires. L'hypoconide est positionné mésiolabialement à l'entoconide, il est relativement plus mésial que sur les m1s.

Une émargination distale importante est connue sur de rares M1s (MNHN.F.CB1233, MNHN.F.STA301). La M2 MNHN.F.CB779-L a deux petites cuspides stylaires dans la position « C », mais elles ne sont pas liées entre elles : la plus mésiale est connectée à la cuspide stylaire B, et la plus distale à la cuspide stylaire D. La cuspide stylaire D est mésiolabiale au sommet du métacône sur certaines M2s (e.g., MNHN.F.CB197, MNHN.F.CB1327). Les M3s MNHN.F.CB1252 (Gernelle et al. 2024b : fig. 3) et MNHN.F.CB30-M ont une double cuspide stylaire A. La M3 MNHN.F.CB2713 a des conules relativement petits et un protocône plus pincé mésiodistalement que la plupart des autres M3s. Certaines m3s (e.g., MNHN.F.CB3433) et m4s ont une longue préparacristide. Les m2s

Tableau 3. Synthèse des mesures (en mm), ratios longueur / largeur, et statistiques univariées associées, de l'ensemble des molaires isolées supérieures de *Peratherium maximum* (Crochet, 1979) provenant des localités du Bassin de Paris (~)MP8+9 : Pourcy (< MP8+9) Condé-en-Brie (localité-type), Mutigny, Avenay, Sables de Brasles, et Saint-Agnan (intervalle MP8+9-MP10 pour ce dernier gisement). Abréviations : CV, coefficient de variation ; L, longueur ; N, nombre de spécimens ; OR, intervalle observé ; SD, écart-type ; W, largeur ; $\bar{x}$, moyenne. Détail des mesures en Annexes : Tableau S2.

Locus		N	OR	$\bar{x}$	SD	CV
M1	L	16	2,44-2,83	2,64	0,111	4,19
	W	18	2,25-2,87	2,54	0,169	6,68
	L/W	16	0,94-1,21	1,05	0,082	7,82
M2	L	20	2,44-2,89	2,64	0,141	5,36
	W	22	2,50-3,07	2,84	0,151	5,32
	L/W	20	0,85-0,99	0,93	0,037	3,97
M3	L	17	2,40-2,81	2,59	0,121	4,69
	W	21	2,69-3,23	2,97	0,141	4,75
	L/W	17	0,82-0,93	0,87	0,031	3,56
M4	L	5	1,72-2,08	1,90		
	W	6	2,34-2,73	2,55		
	L/W	5	0,70-0,89	0,76		

MNHN.F.GL226-L et MNHN.F.GL307-L ont un entoconide plus interne que les autres au sein du talonide, en conséquence le bord lingual de l'entoconide n'est pas saillant labialement. Le précingulide de la m3 MNHN.F.CB2802 entoure le protoconide. L'encoche métaconide – entoconide est généralement plus longue sur les m4s, mais quelques m3s ont une encoche aussi longue (e.g., MNHN.F.CB698, MNHN.F.CB746, MNHN.F.CB821), il s'agit en particulier des plus petites m3s de Condé-en-Brie (MNHN.F.CB655, MNHN.F.CB820, MNHN.F.CB825). Certaines m3s ont une encoche entoconide – hypoconulide plus basse que l'encoche métaconide – entoconide en vue linguale (e.g., MNHN.F.CB208), alors qu'elle est au contraire la plus haute des deux sur d'autres m3s, similairement aux m4s (e.g., MNHN.F.CB698 ; voir aussi Gernelle et al. 2024b : fig. 7I). De rares m2s ont une encoche entoconide – hypoconulide aussi haute que l'encoche métaconide – entoconide (e.g., MNHN.F.CB4707), la première étant généralement la plus basse.

Au sein de la série de molaires supérieures de Condé-en-Brie, le protocône est toujours plus haut que le paracône sur les M2s, alors qu'il ne l'est que sur un peu plus de la moitié des M3s. La crête postparaconulaire est très rarement observée sur les M3s alors qu'elle est récurrente sur les M2s. Comme chez les autres pérathériinés, la préparacrista des M3s est dirigée vers la cuspide stylaire A. Elle est aussi dirigée vers la cuspide stylaire A sur plus de la moitié des M2s de Condé-en-Brie de *Pt. maximum*, alors

qu'elle est presque toujours dirigée vers la cuspide stylaire B sur ce locus chez *Pt. constans* et *Pt. matronense*.

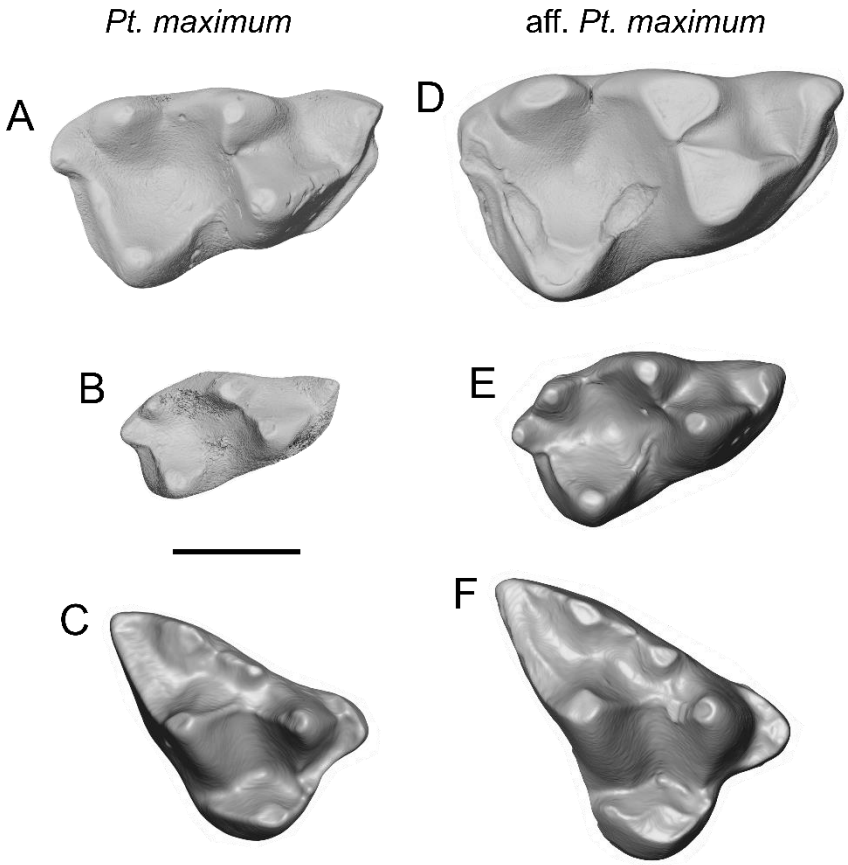

Figure 17. Comparaison des m1s (A, D), dp3s, (B, E) et dP3s (C, F) de *Peratherium maximum* (Crochet, 1979) de Condé-en-Brie (~MP8+9 ; A-C) et aff. *Peratherium maximum* de Sézanne-Broyes (~MP8+9 ; D-F) en vue occlusale. **A**. m1 droite MNHN.F.CB2933. **B**. dp3 gauche (miroir) MNHN.F.CB862. **C**. dP3 gauche (miroir) MNHN.F.CB206-BN. **D**. m1 MNHN.F.SZ235-BN. **E**. dp3 MNHN.F.SZ317-BN. **F**. dP3 MNHN.F.SZ32-BN. Échelle : 1 mm.

Analyses quantitatives. Les variations de surface approximative des molaires supérieures ont été comparées selon le nombre de cuspides stylaires en positions « C » et « D ». En effet leur duplication est fréquente chez *Pt. maximum*. L'hypothèse d'une corrélation entre la taille des spécimens au sein de l'espèce et leur nombre de cuspides stylaires additionnelles (0, 1, ou 2) est testée ici. Les trois loci (M1, M2, et M3) sont inclus, mais le locus n'est pas considéré comme facteur dans l'analyse. Aucune différence significative n'est observée entre les trois conditions (ANOVA de Welch [*W*-test], p = 0.316). Le même résultat est retrouvé en prenant en compte la longueur au lieu de la surface approximative des spécimens. Cependant, les valeurs de surfaces moyenne et médiane augmentent avec le nombre de cuspides stylaires accessoires (Figure 16).

Chez *Peratherium constans* et *Pt. matronense*, les valeurs moyennes des ratios L / W sont très similaires et les intervalles de valeurs observées presque identiques pour une position de molaire supérieure donnée (Tableau 1 vs Tableau 2). En revanche, les paramètres liés au ratio L / W sont plus élevés pour les M3s

de *Pt. maximum*, qui sont légèrement plus allongées que celles des deux espèces de petite taille en moyenne (Tableau 3). Une autre différence concerne les largeurs des M4s. Ces valeurs ne sont presque pas chevauchantes avec les valeurs de largeur des M3s chez *Pt. maximum* (Tableau 3), alors qu'elles se superposent chez *Pt. constans* et *Pt. matronense* (Tableaux 1-2). À partir des quelques spécimens disponibles, il apparaît que les M4s de *Pt. maximum* sont moins larges que ses M3s, contrairement aux deux autres espèces.

Les M2s et la M3 de Saint-Agnan sont seulement très légèrement plus longues et larges, respectivement, que toutes les autres attribuées à *Pt. maximum* (Annexes : Tableau S2). Certaines des m2s de Saint-Agnan sont aussi légèrement plus grandes que celles des autres localités (Annexes : Tableau S3). La plus petite ainsi que la plus grande m3 rapportées à *Pt. maximum* proviennent d'Avenay (Annexes : Tableau S3).

Discussion. Une multiplication des cuspides stylaires distalement à la cuspide stylaire B (y compris des cuspides stylaires en position « D ») est aussi connue chez des taxons sud-américains de très grande taille de l'Éocène inférieur comme *Didelphopsis* (e.g., Carneiro et Oliveira 2023 : fig. 13H, J). Il a été proposé que le nombre et la taille des cuspides stylaires chez les métathériens soient liés à la taille des individus au sein des séries de molaires (Hayes 2005 ; Korth 2015). Ici, une telle corrélation n'est pas vérifiée statistiquement, même si la taille des molaires semble en moyenne augmenter très légèrement avec le nombre de cuspides stylaires additionnelles (Figure 16).

La taille relative de la M3 par rapport à la M4 est un caractère qui porte probablement un signal phylogénétique important au sein des Marsupialia (e.g., Godthelp et al. 1999 : 299). Parmi les Peratheriinae, la M4 notoirement moins large que la M3 semble être apparue à plusieurs reprises indépendamment (e.g., *Peratherium* sp. nov. 3, voir ci-après).

aff. *Peratherium maximum*

Figures 17D-F, 18 ; Tableau 4

1970 – « la plus grande espèce […] légèrement plus grande que la grande espèce des localités mentionnées ci-dessus [Mutigny, Avenay et Condé-en-Brie] » in Louis, p. 53.
1980 – *Amphiperatherium maximum* Crochet in Crochet p. 98-102, fig. 105 (en partie : spécimens de Sézanne-Broyes).

Localité et âge. Sézanne-Broyes, Bassin de Paris, ~MP8+9.

Matériel. dP3 (**MNHN.F.SZ32-BN** ; MNHN.F.SZ83-BN, Crochet 1980 : fig. 105), M2 (**MNHN.F.SZ4-BN** ; **MNHN.F.SZ64-BN**), dp3 (**MNHN.F.SZ317-BN**), m1 (MNHN.F.SZ215-BN, usé ; **MNHN.F.SZ235-BN**).

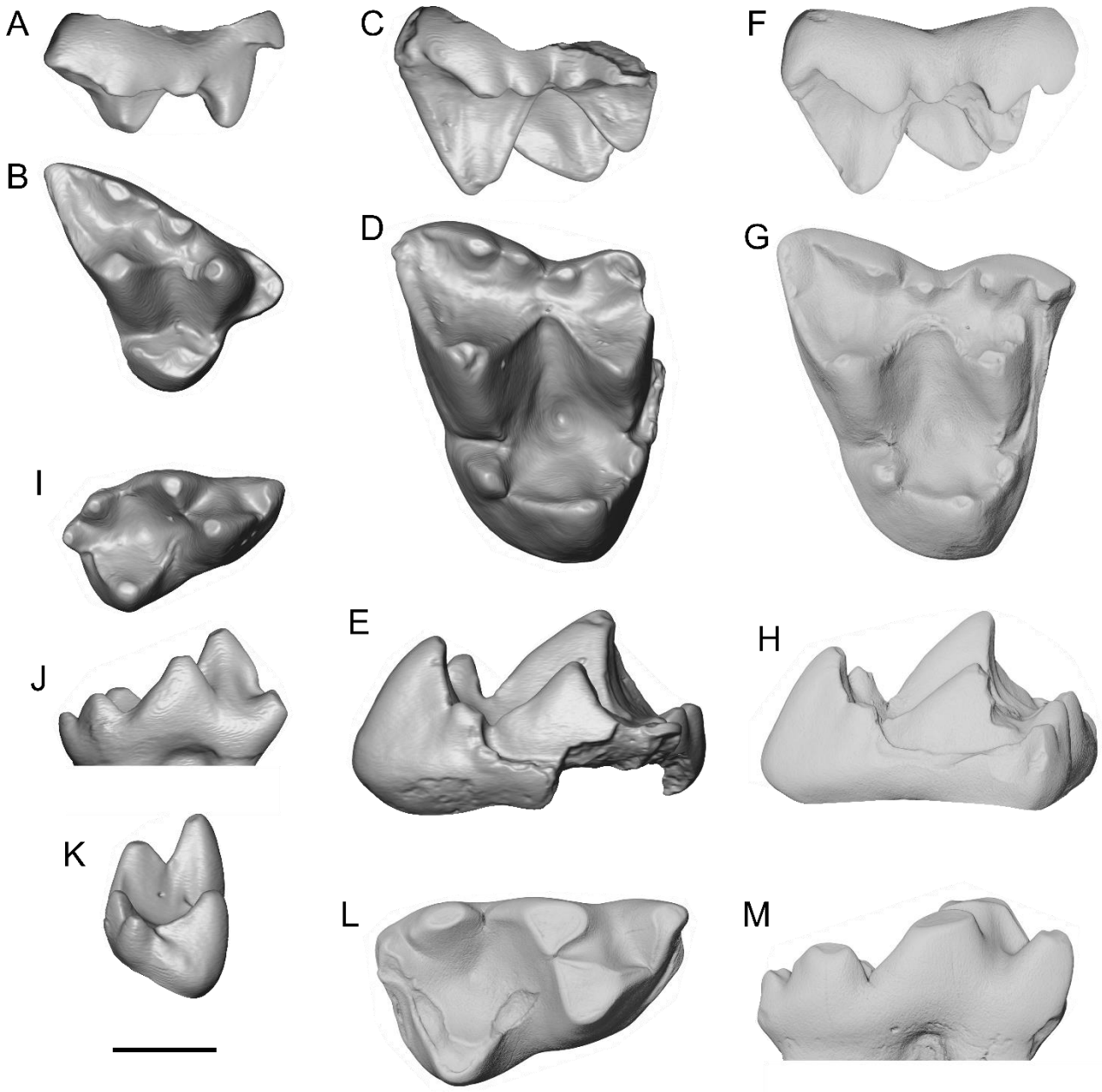

Figure 18. Dents molariformes de aff. *Peratherium maximum* de Sézanne-Broyes (~MP8+9). **A-B**. dp3 MNHN.F.SZ32-BN en vues labiale (A) et occlusale (B). **C-E**. M2 MNHN.F.SZ64-BN en vues labiale (C), occlusale (D), et mésiale (E). **F-H**. M2 MNHN.F.SZ4-BN en vues labiale (F), occlusale (G), et mésiale (H). **I-K**. dp3 MNHN.F.SZ317-BN en vues occlusale (I), linguale (J) et distale (K). **L-M**. m1 MNHN.F.SZ235-BN en vues occlusale (L) et linguale (M).

Commentaire. À locus égal, les spécimens de aff. *Peratherium maximum* sont nettement plus grands que ceux de *Pt. maximum* (Figure 17), comme mentionné par Louis (1970 : 53). En vue distale, l'entoconide et l'hypoconide de la dp3 (Figure 18K) sont de même hauteur alors que l'entoconide est très réduit chez *Pt. maximum*. L'ouverture linguale du trigonide de la m1 est relativement plus haute que l'encoche entoconide – métaconide (Figure 18M). Ce caractère n'est retrouvé sur aucune des 25 m1s de *Peratherium maximum* (e.g., Gernelle et al. 2024b : fig. 7E). Comme chez *Pt. maximum*, les cuspides stylaires C et D des dP3s sont de même hauteur (e.g., Figure 18A). Les M2s ont une cuspide stylaire D

au moins aussi haute que la cuspide stylaire B (Figure 18C, F), tandis que c'est la cuspide stylaire B qui est la plus haute sur les M2s de *Pt. maximum* (e.g., Crochet 1980 : fig. 107). Le métacône de ces M2s est beaucoup plus haut que leur paracône (Figure 18C, F). Le métaconule est intermédiaire en hauteur entre le protocône et le paraconule, et similaire en hauteur au paracône en vue mésiale (Figure 18E, H). Le protocône très haut par rapport au paracône (Figure 18E, H), et relativement long (Figure 18D, G), ainsi que l'entoconide allongé le long de la marge linguale du talonide (Figure 18L), indiquent un complexe protocône / talonide de grande taille (cf. Gernelle et al. 2024b, Chapitre 5).

Au vu des différences de taille et morphologiques entre *Peratherium maximum* et aff. *Peratherium maximum* de Sézanne-Broyes, ce dernier est placé en nomenclature ouverte. Ce taxon n'est pas connu dans d'autres localités que Sézanne-Broyes. Storch et Haubold (1989 : fig. 2) ont montré qu'un pérathériiné de taille sensiblement plus grande que celle de *Peratherium maximum* de Condé-en-Brie (« *Amphiperatherium* aff. *maximum* ») était présent dans les faunes du Geiseltal (MP12). Au moins un taxon (aff. *Peratherium maximum* de Sézanne-Broyes) de taille aussi importante que celle du taxon plus tardif (post-yprésien) du Geiseltal est donc apparu lors de l'Éocène inférieur moyen.

Tableau 4. Mesures des spécimens figurés de aff. *Peratherium maximum* de Sézanne-Broyes (~MP8+9).

Spécimen	Locus	L (mm)	W (mm)	L/W
MNHN.F.SZ32-BN	dP3	2,31	2,21	1,05
MNHN.F.SZ4-BN	M2	2,89	3,20	0,90
MNHN.F.SZ64-BN	M2		3,29	
MNHN.F.SZ317-BN	dp3	2,15	1,38	1,56
MNHN.F.SZ235-BN	m1	3,02	1,83	1,65

2. Taxonomie des Peratheriinae de l'Éocène inférieur tardif (MP10 à MP10-11)

A. Le métathérien des localités ~MP10 du Sud de la France

Depuis la description initiale de *Peratherium monspeliense* par Crochet (1980), des localités ont livré des spécimens plus abondants et pour certains plus complets rapportés à cette espèce (Marandat 1986), ce qui permet d'aborder ici sa révision.

Peratherium monspeliense Crochet, 1979

Figures 19-20 ; 21A-F, L ; Annexes : Tableau S4

1980 – *Peratherium monspeliense* Crochet in Crochet p. 202-205, figs. 221-227.
1980 – *Peratherium matronense* Crochet in Crochet p. 147-151, fig. 162 (en partie : spécimens de Mas de Gimel et Coulondres).
1986 – *Peratherium monspeliense* Crochet in Marandat p. 199.
1986 – *Peratherium* indet. cf. *Peratherium* indet. 1 (in Crochet 1980, fig. 237) in Marandat p. 199.
1986 – *Amphiperatherium* indet. in Marandat p. 199.
2024 – *Peratherium matronense* in Vianey-Liaud et al. tab. 2, fig. 2A.
2024 – *Peratherium monspeliense* in Vianey-Liaud et al. tab. 2.
2024 – *Peratherium matronense* or *Peratherium monspeliense* in Vianey-Liaud et al. tab. 3.

Holotype. UM-MGL-307, M3 droite figurée par Crochet (1979 : fig. 14 ; 1980 : fig. 222).

Localité type : Mas de Gimel, Montpellier, ~MP10.

Autres localités et âge. Coulondres, Azillanet, Le Théron, Le Lien, Naples (faune de Mas de Gimel + Naples, voir Vianey-Liaud et al. 2024), toutes d'âge ~MP10.

Diagnose. Taille plus importante que *Peratherium matronense*. Diffère de tous les autres pérathériinés de l'Éocène inférieur par la cuspide stylaire C relativement réduite par rapport à la cuspide stylaire D, en particulier sur dP3 et M3. Diffère notamment de *Peratherium matronense* par les molaires inférieures augmentent de taille de m1 à m3, et la pré-entocristide souvent relativement plus longue, au moins sur les m3s.

Matériel. Les spécimens figurés ci-après sont signalés en gras dans la liste du matériel. Seules les dents isolées les plus complètes sont listées. Beaucoup de spécimens de *Pt. monspeliense* sont fragmentaires. La présence éventuelle de fragments rapportés à l'espèce dans la localité considérée est signalée.

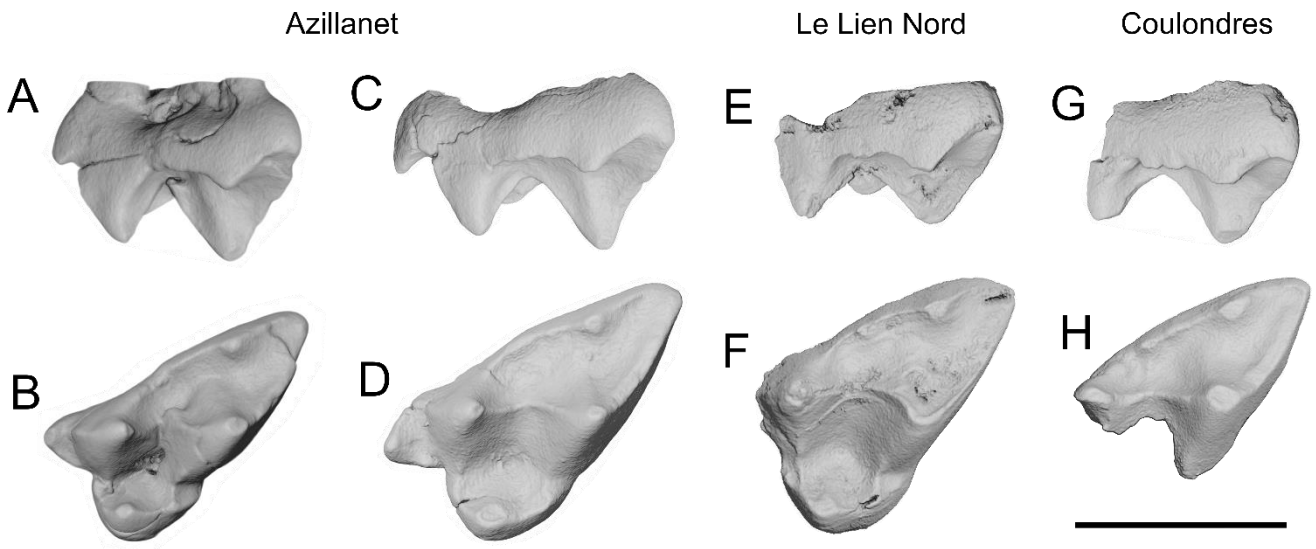

Figure 19. dP3s isolées de *Peratherium monspeliense* Crochet, 1979, de Azillanet (AZI), Le Lien (LLN), et Coulondres (CLR) (~MP10, Sud de la France) en vues labiales (A, C, E, G) et occlusales (B, D, F, H). Noter la faible cuspide stylaire C crestiforme. **A-B**. UM-AZI1-19, dP3 gauche. **C-D**. UM-AZI6-27, dP3 droite (miroir). **E-F**. UM-LLN-98, dP3 gauche ; **G-H**. UM-CLR-9, dP3 droite (miroir). Échelle : 1 mm.

Matériel de Coulondres : dP3 droite (**UM-CLR-9**, fragmentaire), M1 gauche (UM-CLR-6, fragmentaire ; UM-CLR-7, fragmentaire), M1 droite (**UM-CLR-5**, fragmentaire), M3 gauche (UM-CLR-4, Crochet 1980 : fig. 224), M4 gauche (UM-CLR-2, fragmentaire), M4 droite (UM-CLR-3, fragmentaire), m2 gauche (UM-CLR-29), m2 ou m3 gauche (UM-CLR-13). De nombreux fragments de molaires inférieures (trigonides et talonides) sont aussi connus.

Matériel de Le Théron (localité inédite) : M1 gauche (**UP-SRT-2024-2**), M2 gauche (**UP-SRT-2024-3**, fragmentaire), M3 gauche (**UP-SRT-2024-4**), M4 droite (**UP-SRT-2021-25** ; UP-SRT-2022-2), p3 droite (UP-SRT-2022-1)

Matériel d'Azillanet : P3 droite (UM-AZI5-2), dP3 gauche (UM-AZI1-18 ; **UM-AZI1-19**), dP3 droite (**UM-AZI6-27**), M1 gauche (UM-AZI6-2, fragmentaire), M1 droite (UM-AZI6-37, usé), M3 gauche (UM-AZI6-29, usé et fragmentaire), M3 droite (UM-AZI1-6, usé et fragmentaire), p2 droite (**UM-AZI6-38**), fragment d'hémi-mandibule droite avec p3 (**UM-AZI7-2**), m1 droite (UM-AZI6-32 ; UM-AZI6-36, fragmentaire), m2 gauche (UM-AZI6-5), m2 droite (UM-AZI6-25), fragment d'hémi-mandibule droit avec m1-m3 (**UM-AZI6-3**), m3 droite (UM-AZI1-5, fragmentaire ; UM-AZI6-4), m4 gauche (UM-AZI6-22), fragment d'hémi-mandibule droite avec m4 (UM-AZI6-21).

Matériel supplémentaire de Mas de Gimel : La faune de Mas de Gimel comprend plus de 90 spécimens, attribués préliminairement à *Pt. matronense* et *Pt. monspeliense* (Vianey-Liaud et al. 2024 : tab. 2), dont majoritairement des fragments dentaires (e.g., trigonides / talonides isolés). L'ensemble de ce matériel est ici réattribué à *Pt. monspeliense*. Seules les dents jugales les plus complètes sont listées ci-après : dP3 droite (UM-MGL-301, fragmentaire), M1 gauche (UM-MGL-124, fragmentaire ; UM-MGL-304, usé ;

UM-MGL-306, fragmentaire, Crochet 1980 : fig. 225), M3 droite (**UM-MGL-305**, Crochet 1980 : fig. 221 ; UM-MGL-308, usé ; UM-MGL-722), M4 gauche (UM-MGL-302, fragmentaire, Crochet 1980 : fig. 223 ; UM-MGL-304, fragmentaire ; UM-MGL-719, fragmentaire), m1 gauche (UM-MGL-143, fragmentaire ; UM-MGL-310, fragmentaire ; UM-MGL-793), m1 droite (UM-MGL-715 ; UM-MGL-721), m2 ou m3 gauche (UM-MGL-314) ; fragment de dentaire gauche avec m3 (UM-MGL-313, Crochet 1980 : fig. 226), m3 gauche (UM-MGL-117 ; **UM-MGL-315**), m3 droite (UM-MGL-111, Crochet 1980 : fig. 162 ; UM-MGL-316 ; UM-MGL-317), m4 droite (UM-MGL-318, Crochet 1980 : fig. 227).

Matériel du Lien : la faune du Lien fait l'objet d'un travail en préparation (Lihoreau et al.). Seuls les spécimens servant à la révision de *Peratherium monspeliense* sont cités ici (Figures 19E-F, 20K-L).

Remarque. Une mandibule indéterminée de La Soucarède (~MP10, localité proche de Mas de Gimel géographiquement), listée par Hartenberger et al. (1969), a pu être dégagée numériquement durant cette thèse (Annexes : Figure S1). La détermination est complexe car seule la p2 est globalement préservée. Ce spécimen pourrait correspondre par la taille à *Pt. monspeliense*.

Description comparée. Les dP3s de *Peratherium monspeliense* ont une configuration unique du plateau stylaire parmi les pérathériinés (Figure 19). La ligne stylaire s'étend du paracône à l'extrémité distale de l'aile métastylaire ; elle comporte une cuspide stylaire D normalement développée et une cuspide stylaire C très basse et crestiforme (voir aussi Crochet 1980 : 202). La cuspide stylaire C est beaucoup moins développée que sur les quelques dP3s connues d'autres espèces de l'Éocène inférieur, c'est-à-dire celles de *Pt. constans*, *Pt. maximum*, *Peratherium* sp. nov. 1 et *Peratherium* sp. nov. 3. La cuspide stylaire C est parfois dédoublée (e.g., Figure 19G-H). La forme du contour des dP3s est très variable entre les spécimens, même au sein d'une localité donnée (e.g., Azillanet : Figure 19B vs Figure 19D). La P3 est plus transverse que chez *Pt. constans*. La M3 UM-CLR-4 est la seule connue de *Pt. monspeliense* présentant une cuspide stylaire C aussi haute que la cuspide stylaire D (et non pas C plus haute que D, contrairement à l'illustration de Crochet [1980 : fig. 224]). La très faible hauteur de la cuspide stylaire C est observée sur l'holotype, la M3 UM-MLG-307 (Figure 20O) ou encore sur une M3 inédite du Théron (UP-SRT-2024-4, Figure 20E). Sur les M3s, la cuspide stylaire C est crestiforme en vue occlusale (Figure 20E, O). De nombreux spécimens non illustrés ici présentent aussi une cuspide stylaire C moins haute que D (e.g., la M1 UM-MGL-124 ; la M3 UM-MGL-722). La variation de ce trait sur les M1s est considérable. En effet, la cuspide stylaire C peut être nettement réduite par rapport à la cuspide stylaire D (e.g., UM-CLR-5, Figure 20I ; UM-LLN-7 ; Figure 20K) comme sur les M3s, ou bien être aussi haute que la cuspide stylaire D (e.g., UP-SRT-2024-2, Figure 20A ; UM-MGL-305, Figure 20M). Certaines molaires supérieures ont une cuspide stylaire B possédant une crête accessoire distolabiale (e.g., Figure 20E-F, K-L, O-P), connue aussi chez certains spécimens de *Peratherium* sp. nov. 1 et *Peratherium* sp. nov. 2 (voir ci-après).

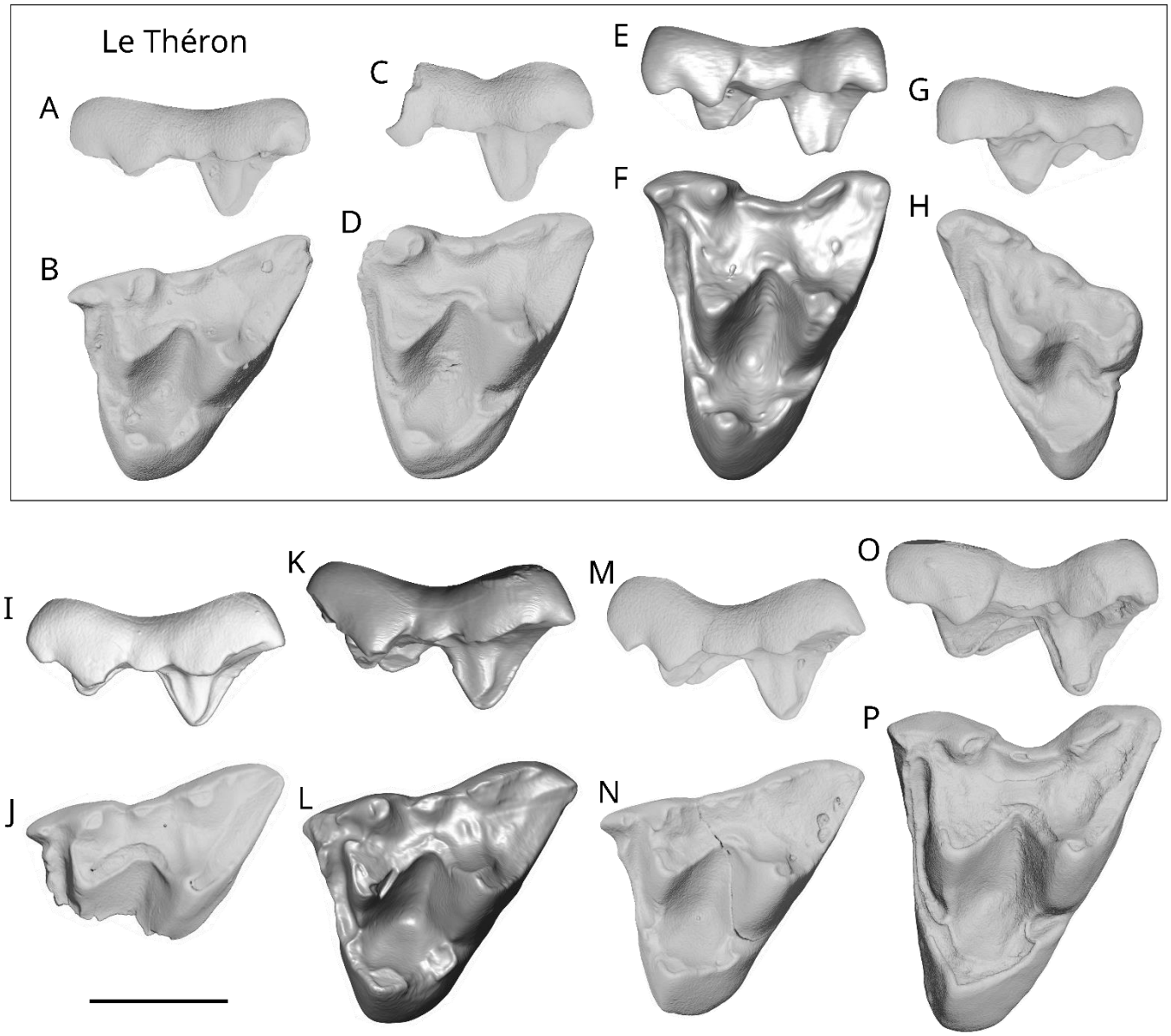

Figure 20. Molaires supérieures isolées de *Peratherium monspeliense* Crochet, 1979, des localités ~MP10 de Le Théron (A-H), Coulondres (I-J), Le Lien (K-L) et Mas de Gimel (M-P). **A-H**. Rangée dentaire M1-M4 composite. **A-B**. M1 gauche UP-SRT-2024-2 en vues labiale (A) et occlusale (B). **C-D**. M2 gauche fragmentaire UP-SRT-2024-3 en vues labiale (C) et occlusale (D). **E-F**. Modèle surfacique 3D de la M3 gauche UP-SRT-2024-4 en vue labiale (E) et occlusale (F). **G-H**. M4 droite UP-SRT-2021-25 en vues (miroir) labiale (G) et occlusale (H). **I-J**. M1 droite fragmentaire UM-CLR-5 en vues labiale (I) et occlusale (J). **K-L**. Modèle surfacique 3D de la M1 UM-LLN-7 en vues labiale (K) et occlusale (L). **M-N**. M1 droite UM-MGL-305 en vues (miroir) labiale (M) et occlusale (N). **O-P**. M3 droite UM-MGL-307, holotype de *Pt. monspeliense*, en vues (miroir) labiale (O) et occlusale (P). Échelle : 1 mm.

Les prémolaires inférieures (p2 et p3) sont plus hautes que les m1s (Figure 21B, D vs Figure 21F). La p2 est moins large et aussi moins longue que la p3 (Figure 21A vs Figure 21C). Comme chez les autres pérathériinés, leur bord mésial en vue linguale ou labiale est en forme de V. Les molaires inférieures de l'hémi-mandibule UM-AZI6-3 (Figure 21E-F) deviennent plus grandes vers l'arrière de la rangée dentaire (e.g., L m1 = 1.58 mm ; L m2 = 1.78 mm ; L m3 = 1.91 mm). Comme les m3s, les m4s sont plus

longues que les m2s (cf. Annexes : Tableau S4). La m2 et la m3 possèdent une pré-entocristide relativement longue et saillante (Figure 21E, L). L'encoche entoconide – hypoconulide de la m2 est plus basse que l'encoche métaconide - entoconide de cette même dent (Figure 21F), et ces deux encoches s'ouvrent à la même hauteur sur la m3. Sur ces deux loci, les encoches entoconide – hypoconulide sont donc relativement plus basses que chez certains spécimens de *Peratherium* sp. nov. 2 (voir ci-après).

Discussion. Au sein des faunes ~MP10 de Mas de Gimel et Coulondres, Crochet (1980) a reconnu à la fois *Peratherium monspeliense* et *Pt. matronense*. Ce dernier y serait beaucoup plus rare que le premier (voir Annexes : Vianey-Liaud et al. 2024 : tab. 2) et plus petit (Crochet 1980). Les dP3s d'Azillanet sont les seules dents molariformes supérieures de cette localité préservant des cuspides stylaires. La réduction de la cuspide stylaire C sur les trois dP3s confirme l'attribution des autres spécimens, homogènes en taille dans cette faune, à *Pt. monspeliense*. L'hémi-mandibule UM-AZI6-3, évoquée par Marandat (1986 : 199), montre qu'il existe un agrandissement des molaires inférieures de la première à la troisième chez *Pt. monspeliense*. Cela explique en partie qu'en l'absence de cette donnée lors de l'étude de Crochet (1980), des spécimens de plus petite taille des localités qui ont livré *Pt. monspeliense* ont pu être placés dans l'espèce plus petite *Pt. matronense*. Les molaires inférieures les plus petites de Mas de Gimel, placées dans *Pt. matronense* par Crochet (1980) (voir Annexes : Tableau S4 pour UM-MGL-111 et UM-MGL-117 ; Vianey-Liaud et al. 2024 : fig. 2A pour UM-MGL-310) entrent en fait dans la variation de taille de *Pt. monspeliense* lorsque des comparaisons de la variation de taille sont effectuées avec *Peratherium* sp. nov. 2 de Prémontré (de même taille et mieux documenté), et elles en présentent les caractères morphologiques (e.g., la pré-entocristide de UM-MGL-111 est développée ; voir Crochet 1980 : fig. 162). Au moins une molaire supérieure fragmentaire (UM-MGL-153, voir Annexes : Tableau S4) semble tout de même de taille faible pour avoir appartenu à *Pt. monspeliense*.

cf. *Peratherium monspeliense*

Figure 21G-K, Tableau 5

Localité et âge. Saint-Agnan (Bassin de Paris), intervalle MP8+9-MP10.

Matériel. m2 (MNHN.F.STA276), m3 (MNHN.F.STA270, MNHN.F.STA277), m4 (MNHN.F.STA280).

Commentaire. Seules des molaires inférieures documentent ce taxon. Les m3s possèdent une pré-entocristide saillante qui rappelle celle des m3s de *Peratherium monspeliense*, par comparaison entre UM-MGL-315 de Mas de Gimel (Figure 21L) et la m3 MNHN.F.STA277 (Figure 21J). À partir des quelques spécimens disponibles, les m3s et la m4 apparaissent plus grandes que la m2, comme chez *Pt. monspeliense*. Les m3 / m4 sont en tout cas plus grandes que celles du Bassin de Paris rapportées à *Pt.*

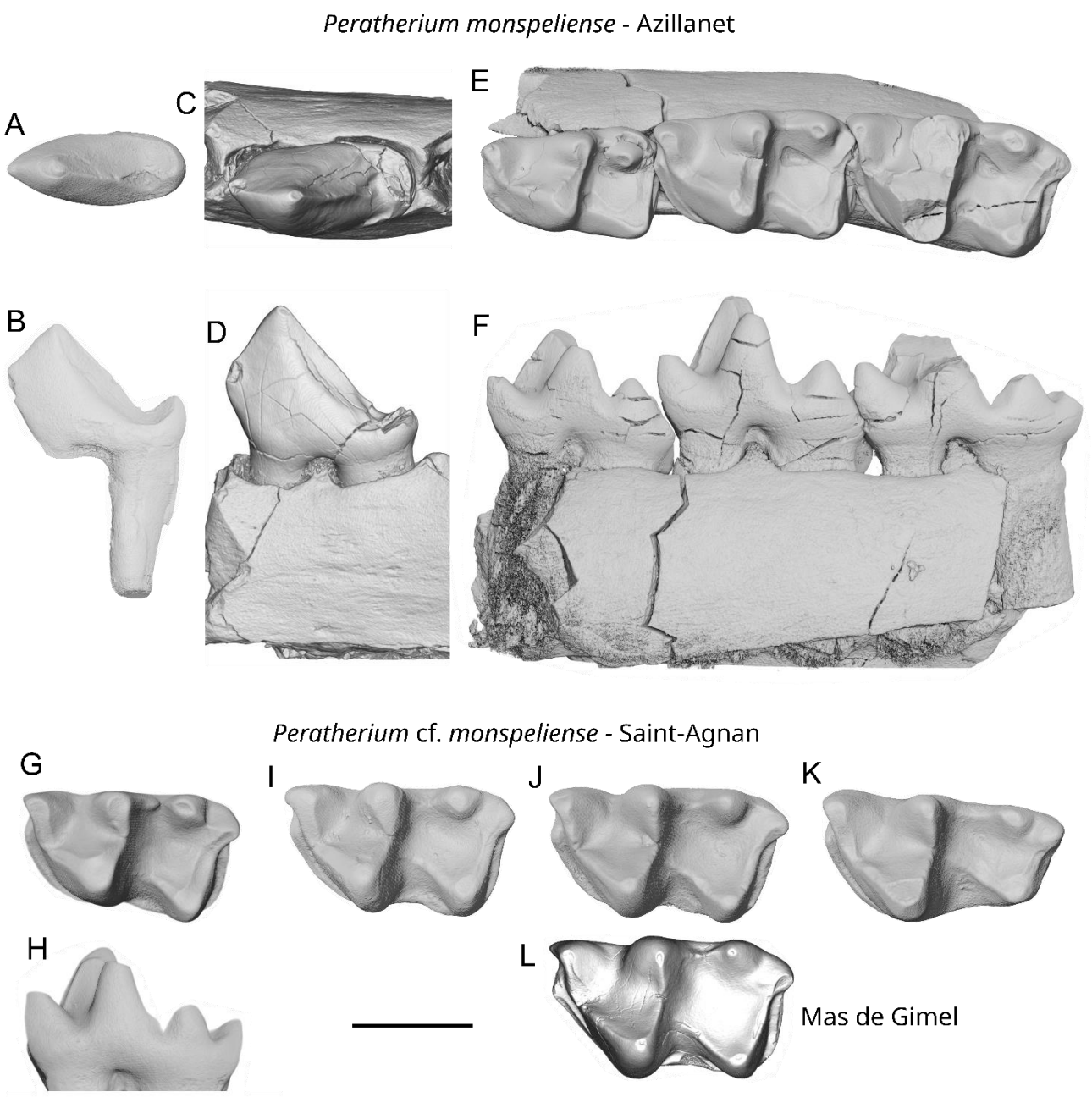

Figure 21. **A-F**. Rangée dentaire composite p2-m3 de *Peratherium monspeliense* Crochet, 1979, de Azillanet (~MP10). **A-B**. p2 droite UM-AZI6-38 en vues (miroir) occlusale (A) et linguale (B). **C-D**. p3 droite UM-AZI7-2 en vues (miroir) occlusale (C) et linguale (D). **E-F**. Fragment d'hémi-mandibule droit avec m1-m3 UM-AZI6-3 en vues (miroir) occlusale (E) et linguale (F). **G-K**. Molaires inférieures isolées de *Peratherium* cf. *monspeliense* de Saint-Agnan (intervalle MP8+9-MP10, Bassin de Paris). **G-H**. m2 MNHN.F.STA276 en vues occlusale (G) et linguale (H). **I**. m3 MNHN.F.STA270 en vue occlusale. **J**. m3 MNHN.F.STA277 en vue occlusale. **K**. m4 MNHN.F.STA280 en vue occlusale. **L**. Comparaison avec la m3 gauche UM-MGL-315 (Mas de Gimel) de *Pt. monspeliense* en vue occlusale. Échelle : 1 mm.

matronense (Tableau 5 vs Tableau 2), et sont rapprochées de *Pt. monspeliense* en nomenclature ouverte. Étant donnée l'âge et la localisation de Saint-Agnan, il pourrait donc s'agir de la première apparition de cette espèce dans le registre fossile, et de sa première mention dans le Nord de la France.

Tableau 5. Mesures (en mm) des molaires inférieures de cf. *Peratherium monspeliense* de Saint-Agnan (intervalle MP8+9-MP10).

Spécimen	Locus	L (mm)	W (mm)	L/W
MNHN.F.STA276	m2	1,79	1,09	1,64
MNHN.F.STA270	m3	1,90	1,11	1,71
MNHN.F.STA277	m3	1,98	1,15	1,72
MNHN.F.STA280	m4	2,00	1,10	1,82

B. Les taxons cryptiques de grande taille de l'EECO

Un travail mené dans le cadre de cette thèse sur les métathériens des gisements montpelliérains a permis de décrire une M1 complète ainsi qu'un fragment attribués avec un certain doute à « *Amphiperatherium* » *bastbergense* Crochet, 1979 (Vianey-Liaud et al. 2024 ; voir Annexes), un taxon de taille relativement grande succédant à *Peratherium maximum* selon Crochet (1980). Depuis, ces spécimens du Sud de la France ont pu être rapprochés de deux dents isolées inédites du Nord de la France, livrées par une localité d'âge sans doute proche (MP10). L'ensemble de ce matériel, restreint à deux loci dentaires (dP3 et M1), permet néanmoins de décrire une nouvelle espèce rare probablement apparentée à « *A.* » *bastbergense*.

Peratherium sp. nov. 1

Figure 22A-I, Tableau 6

2024 – cf. *Amphiperatherium bastbergense* Crochet in Vianey-Liaud et al. p. 400, fig. 2E

Holotype. **UM-NAP-125**, M1 droite (Figure 22G-I).

Localités et âge. Naples, ~MP10, dans le Sud de la France (Montpelliérain, localité-type), et Grauves, MP10, dans le Bassin de Paris.

Matériel. Matériel de Grauves : dP3 gauche (**MNHN.F.GR7792**), M1 gauche (**MNHN.F.GR17042**). Matériel supplémentaire de Naples : fragment de M1 droite (UM-NAP-128).

Diagnose. Taille équivalente à « *Amphiperatherium* » *bastbergense*. Les M1s diffèrent de celles de ce dernier par la cuspide stylaire B dominante en hauteur par rapport aux cuspides stylaires C et D, et par l'absence de position interne de la cuspide stylaire C par rapport à la marge labiale du plateau stylaire.

Description comparée. Le protocône est plus haut que le paracône sur les deux M1s complètes (Figure 22F, I), alors que le protocône est relativement bas sur la dP3 (Figure 22C). Le protocône de la dP3 est étroit par rapport à celui des dP3s d'« *A.* » *bastbergense* (Figure 22B vs Figure 22J). Sur la M1 UM-NAP-125, faiblement usée, la taille relative des conules, possédant des crêtes internes, est équivalente à

celle de la plupart des autres espèces de pérathériinés de l'Éocène inférieur. La dP3 MNHN.F.GR7792 n'a pas de crête joignant le paracône à la cuspide stylaire C contrairement aux dP3s d'« *A.* » *bastbergense* (Figure 22B vs Figure 22J). Les M1s de Naples ont une cuspide stylaire B présentant une crête mesiolinguale joignant la préparacrista ainsi que crête distolabiale, non connectée à la cuspide stylaire C (Figure 22H). La cuspide stylaire D des M1s est légèrement mésiolabiale (Figure 22H) ou labiale (Figure 22E) par rapport au sommet du métacône. L'aile métastylaire des M1s, comprenant la postmétacrista, est particulièrement projetée labialement. La M1 de l'holotype d'« *Amphiperatherium* » *bastbergense* figurée par Crochet (1980 : 114a) et refigurée ici possède une cuspide stylaire C au moins aussi haute que la cuspide stylaire B (Figure 22L ; la cuspide stylaire D n'est pas conservée), mais l'usure de toutes les cuspides de cette molaire est notable. Toutes les autres M1s d'« *A.* » *bastbergense* de Bouxwiller (dont des spécimens mieux préservés que la M1 de l'holotype) ont une cuspide stylaire D dominante en hauteur, et la cuspide stylaire C est parfois aussi haute que la cuspide stylaire D (obs. pers.). Le premier de ces deux traits est en revanche absent chez *Peratherium* sp. nov. 1. La cuspide stylaire C n'est pas interne au plateau stylaire (i.e., entourée par la marge labiale) sur les M1s contrairement à celles d'« *A.* » *bastbergense* (e.g., Figure 22L-M). La cuspide stylaire D est la plus longue à la fois sur la dP3 et les M1s.

Discussion

Commentaire sur la taille relative des dP3s. Crochet (1980 : tab. 12, fig. 88) a attribué cinq dP3s de Bouxwiller (localité-type) à « *Amphiperatherium* » *goethei*. Celles-ci font approximativement la taille des M1s de Bouxwiller de la même espèce (Figure 22J vs Figure 22K). Parallèlement, les dP3s d'« *Amphiperatherium* » *bastbergense*, une espèce définie à partir de la même localité que *A. goethei*, n'étaient précédemment pas connues. Cependant, si les dP3 sont probablement effectivement aussi longues que les M1s chez les Peradectidae (Murphey et al. 2018 : fig. 13 ; Gernelle et al. 2024a : fig. 10) et certains alphadontidés tels que *Turgidodon rhaister* (Clemens 1966 : tableau 3), ce n'est pas le cas chez les Herpetotheriidae, où elles sont toujours significativement plus petites (e.g., Korth et al. 2020 : fig. 3 ; voir aussi *Pt. constans*, Figure 3D-G ; et *Pt. monspeliense*, Figure 19-20). Il s'agit d'une différence notoire nouvellement observée entre les deux familles Peradectidae et Herpetotheriidae. Cela implique que toutes les dP3s attribuées à « *A.* » *goethei* par Crochet (1980) appartiennent en fait à une espèce de plus grande taille. Elles correspondent pour ce critère à « *A.* » *bastbergense*, auquel elles sont réattribuées ici. C'est cette correspondance établie entre les tailles des dP3s et des M1s des Herpetotheriidae qui a permis de reconnaître la dP3 de *Peratherium* sp. nov. 1 comme appartenant à cette espèce (Figure 22A-C vs Figure 22D-I).

Commentaire sur la hauteur relative des cuspides stylaires des M1s. Crochet (1980) a rassemblé plusieurs espèces de pérathériinés de grande taille au sein d'une lignée évolutive *Pt. maximum* – « *A.* » *bastbergense* – « *A.* » *fontense* – « *A.* » *ambiguum* (e.g., Gernelle et al. 2024b : fig. 1). Ces taxons

possèdent une cuspide stylaire D le plus souvent aussi haute que ou dominante en hauteur par rapport à la cuspide stylaire B sur les M1s (e.g., voir Gernelle et al. 2024b : fig. 4C, pour *Pt. maximum* ; Crochet 1980 : fig. 126a pour « *A.* » *ambiguum*), de même pour *Pt. musivum*, le premier pérathériiné de taille relativement grande (Gernelle et al. 2024b : fig. 4A). *Peratherium* sp. nov. 1 fait donc figure d'exception pour ce caractère parmi les plus grands pérathériinés. Par rapport à d'autres pérathériinés de plus petite taille, comme *Pt. matronense*, *Pt. monspeliense* ou *Peratherium* sp. nov. 2, *Peratherium* sp. nov. 1 semble en revanche partager avec « *A.* » *bastbergense* un protocône relativement haut sur les M1s, et surtout une aile métastylaire plus mésiolabiale relativement à l'axe paracône – métacône. Plus de spécimens et une comparaison des contours par morphométrie géométrique des molaires supérieures de ces taxons de grande taille avec d'autres pérathériinés devrait permettre de tester la pertinence de ce dernier trait.

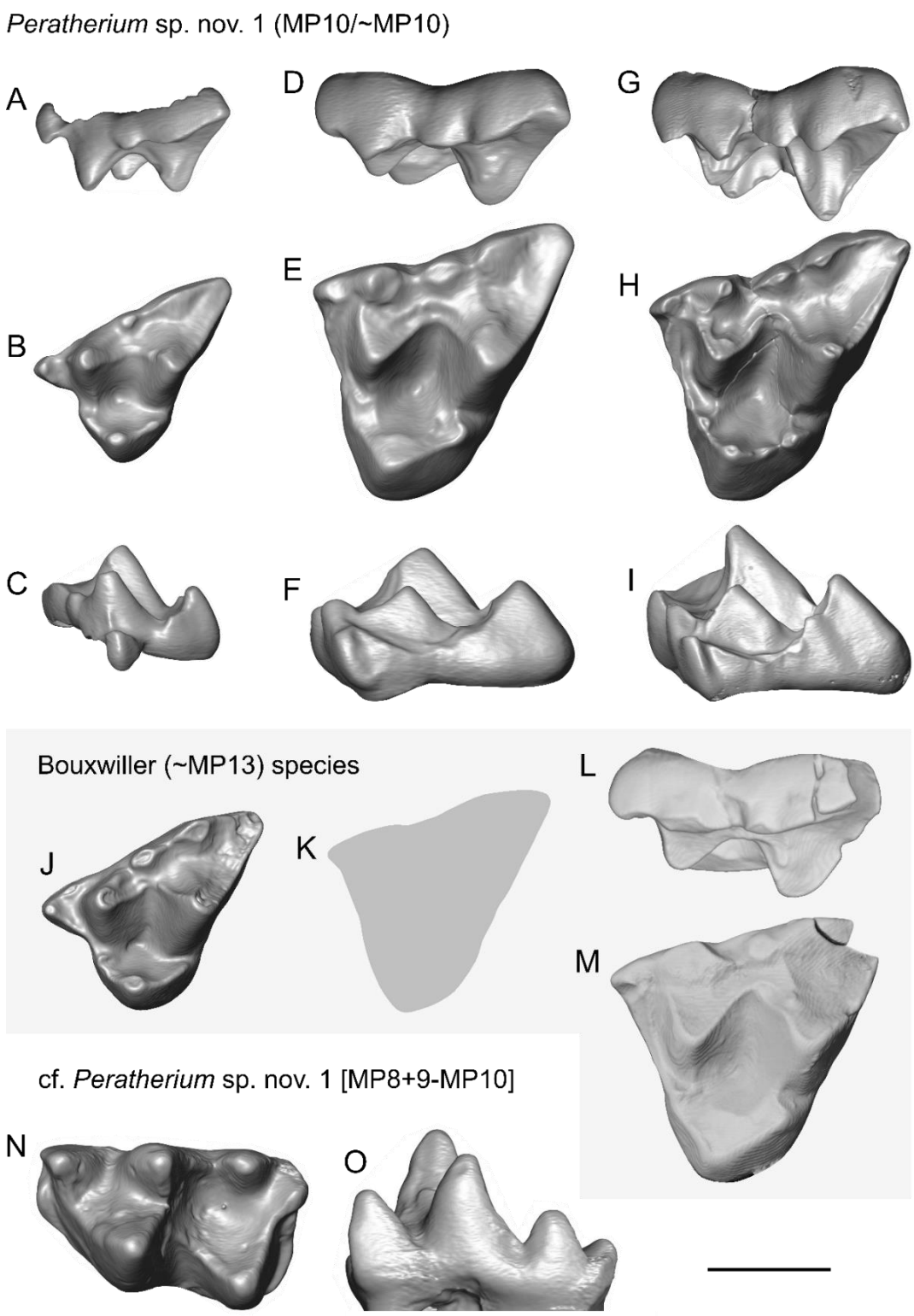

Figure 22. Dents molariformes de *Peratherium* sp. nov. 1 de Grauves (MP10, Bassin de Paris) et Naples (~MP10, Montpelliérain) (A-I) et de cf. *Peratherium* sp. nov. 1 de Saint-Agnan (intervalle MP8+9-MP10, Bassin de Paris) (N-O) comparées avec celles d'espèces typiques de Bouxwiller (~MP13) (J-M). **A-C**. dP3 gauche MNHN.F.GR7792 en vues labiale (A), occlusale (B), et mésiale (C). **D-F**. M1 gauche MNHN.F.GR17042 en vues labiale (D), occlusale (E), et mésiale (F). **G-I**. M1 droite UM-NAP-125 en vues (miroir) labiale (G), occlusale (H), et mésiale (I). **J**. Vue occlusale de la dP3 gauche UM-BUX-68.65 d'« *A.* » *bastbergense*, attribuée à « *A.* » *goethei* par Crochet (1980). **K**. Silhouette de la M1 gauche UM-BUX-68.81 d'« *A.* » *goethei* en vue occlusale. **L-M**. M1 gauche du maxillaire UM-BUX-68.64, holotype d'« *A.* » *bastbergense*, en vues labiale (L) et occlusale (M). **N-O**. m2 gauche MNHN.F.STA283 de cf. *Peratherium* sp. nov. 1 en vues occlusale (N) et linguale miroir (O). Échelle : 1 mm.

cf. *Peratherium* sp. nov. 1

Figure 22N-O, Tableau 6

Localité et âge. Saint-Agnan, Bassin de Paris, intervalle MP8+9-MP10.

Matériel. m2 gauche (MNHN.F.STA283).

Commentaire. Chez *Peratherium musivum* et *Pt. maximum*, les M1s sont approximativement aussi longues que les m1s (Gernelle et al. 2024b : 17). En utilisant ici une telle approximation, une correspondance en taille apparait entre la m2 MNHN.F.STA283 (Figure 22N-O, sans doute légèrement plus longue que la m1 de ce taxon, par comparaison avec les autres pérathériinés de l'Éocène inférieur) et les M1s de *Peratherium* sp. nov. 1. Durant l'Éocène inférieur, seuls *Peratherium musivum* et « *A.* » *bastbergense* ont une taille similaire à *Peratherium* sp. nov. 1. La M1 et la m2 de *Pt. musivum* sont sensiblement plus petites (Gernelle et al. 2024b : tab. 2). Les m2s d'« *A.* » *bastbergense* sont légèrement plus longues (Tableau 6 vs Crochet 1980 : tableau 15) et l'hypoconulide des molaires inférieures de cette espèce est relativement plus étroit et plus projeté distalement par rapport au postcingulide. Pour ces raisons, la seule affinité possible pour la m2 de Saint-Agnan semble être avec *Peratherium* sp. nov. 1, par ailleurs documenté dans des localités plus jeunes du Nord et du Sud de la France (Grauves et Naples).

Tableau 6. Mesures des spécimens de *Peratherium* sp. nov. 1 et de cf. *Peratherium* sp. nov. 1, comparées avec les mesures de Crochet (1980) d'une sélection de loci dentaires d'*Amphiperatherium goethei* (spécimens ici réattribués à *A. bastbergense*) et d'*A. bastbergense*, sensu Crochet (1980). Abréviations : L, longueur ; OR, intervalle observé ; W, largeur.

Spécimen	Localité	Taxon	Locus	L (mm)	W (mm)	L/W
MNHN.F.GR7792	Grauves	*Peratherium* nov. sp. 1	dP3	1,61	1,51	1,07
MNHN.F.GR17042	Grauves	*Peratherium* nov. sp. 1	M1	2,12	2,26	0,94
UM-NAP-125	Naples	*Peratherium* nov. sp. 1	M1	2,13	2,21	0,96
MNHN.F.STA283	Saint-Agnan	cf. *Peratherium* nov. sp. 1	m2	2,21	1,36	1,63
Données de Crochet (1980)	Bouxwiller	*Amphiperatherium goethei*	OR dP3	1.59-1.76	1.60-1.77	-
	Bouxwiller	*Amphiperatherium bastbergense*	OR M1	2.07-2.37	2.06-2.42	-
	Bouxwiller	*Amphiperatherium bastbergense*	OR m2	2.29-2,40	1.27-1,46	-

cf. *Peratherium maximum*

Figure 23

1980 – *Amphiperatherium maximum* Crochet in Crochet p. 98-102 (en partie : spécimen de Grauves).

2024 – Herpetotheriidae gen. and sp. indet. in Vianey Liaud et al. p. 391, tab. 2.

Localité et âge. Grauves et Prémontré (Bassin de Paris), et Mas de Gimel (Montpellier) ; (~)MP10.

Matériel. Matériel de Grauves : m3 (**MNHN.F.GR7564**). Matériel de Prémontré : m3 (MNHN.F.SLP29-PR-2544 ; **MNHN.F.SLP29-PR-2883**). Matériel de Mas de Gimel : talon de M3 (**UM-MGL-309**).

Commentaire. Quatre dents seulement, provenant de trois localités et représentant *Pt. maximum* ou un / des taxon(s) proche(s) sont connues durant l'EECO et sont placées temporairement sous la dénomination cf. *Peratherium maximum*. Il s'agit de trois grandes molaires inférieures (e.g., Figure 23) et d'un grand fragment de talon de molaire supérieure (ce dernier est figuré dans la conclusion générale de cette thèse). *Peratherium maximum*, au contraire, est abondant dans les faunes (~)MP8+9 du bassin de Paris. Plusieurs spécimens, en particulier des molaires supérieures, seraient nécessaires pour tester l'attribution des grandes molaires de ces localités à *Pt. maximum*, duquel elles sont indifférenciables en l'état. En particulier, les caractères de cette espèce liés à la taille relative importante du talonide (voir Gernelle et al. 2024b, Chapitre 5) sont ici présents (Figure 23A, C). De la même façon, une molaire inférieure (m2) de la localité DC5iii (« Dummer's Copse » de la Formation Wittering [Angleterre]), rapprochée du niveau-repère ~MP10, a été attribuée à *Pt. maximum* (Hooker 1996b : pl. 1, figs. 1-3 ; NHMUK.PV.M50181). Là encore, plusieurs spécimens sont nécessaires pour tester cette attribution.

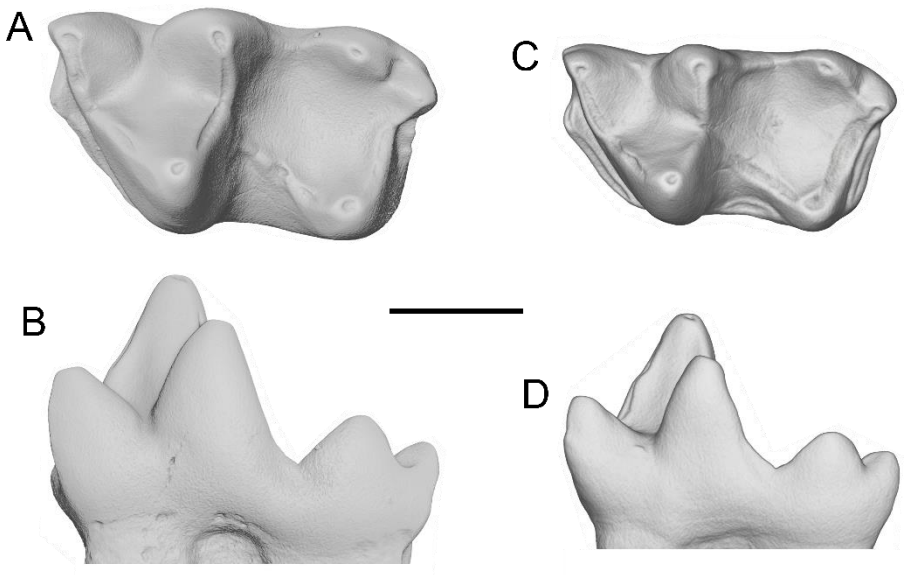

Figure 23. m3s de Grauves (A-B ; MP10) et Prémontré (C-D ; ~50.3-50.4 Ma, ~MP10) attribuées à cf. *Peratherium maximum*. **A-B**. m3 MNHN.F.GR7564 de Grauves en vues occlusale (A) et linguale (B). **C-D**. m3 gauche MNHN.F.SLP29-PR-2883 de Prémontré en vues occlusale (C) et linguale miroir (D). Échelle : 1 mm.

C. Une nouvelle espèce de pérathériiné abondante de Prémontré (~MP10)

La faune de Prémontré (Aisne, ~50.3-50.4 Ma ; Steurbaut et al. 2016) a livré un matériel abondant de métathériens non étudiés formellement avant ce travail. Bien que deux nouvelles espèces de péradectidés étaient présentes dans cette faune (voir Chapitre 2), la majeure partie du matériel appartient à une unique espèce de pérathériiné, inédite et décrite ci-après. Un intérêt de cette localité est la relative complétude des spécimens (dents jugales en association) par rapport à la plupart de ceux connus dans l'Éocène inférieur européen.

Peratherium sp. nov. 2

Figures 24, 25A-F, 26 Tableau 7, Annexes : Tableaux S5-6

1980 – *Amphiperatherium goethei* Crochet in Crochet p. 89-92.
1985 – *Amphiperatherium bourdellense* Crochet in Dégremont et al. p. 16.
1985 – *Amphiperatherium goethei* Crochet in Dégremont et al. p. 16.

Holotype. MNHN.F.SLP29-PE-237, maxillaire gauche avec M1-M3 (Figure 24A-B).

Localités et âge. Prémontré (localité-type ; ~50.3-50.4 Ma ; Steurbaut et al. 2016) et Grauves (Marne ; MP10).

Matériel et mesures. Matériel supplémentaire de Prémontré : ~180 spécimens modérément usés et faiblement endommagés. La liste complète des spécimens et leurs mesures sont en Annexes : Tableaux S5-6.

Matériel de Grauves : M3 gauche **MNHN.F.GR7594** (L = 1.90 mm ; W = 2.27 mm), m2 droite **MNHN.F.GR7426** (L = 1.86 mm ; W = 1.11 mm), m3 MNHN.F.GR7791.

Diagnose. Taille équivalente à *Peratherium monspeliense* et « *Amphiperatherium* » *goethei*. Diffère de *Pt. matronense* par la taille en moyenne plus importante, les M3s plus grandes par rapport aux M1s et M2s, et l'encoche entoconide – hypoconulide des molaires inférieures relativement plus haute (à locus équivalent), en particulier sur certaines m2s. Diffère de *Pt. monspeliense* par la cuspide stylaire C plus haute que la cuspide stylaire D, au moins sur toutes les M3s, et l'égalité de taille des m2s et m3s. Diffère d'« *Amphiperatherium* » *goethei* par l'égalité de longueur des molaires supérieures en moyenne, par la cuspide stylaire C notoirement moins haute que la cuspide stylaire B et le protocône relativement plus haut sur les M3s, ainsi que par le paraconide des molaires inférieures relativement plus long.

Description comparée. Le grand foramen infra-orbitaire de l'holotype (MNHN.F.SLP29-PE-237) s'ouvre dorsalement à l'alvéole postérieure de la P3 (Figure 24A), comme chez d'autres pérathériinés

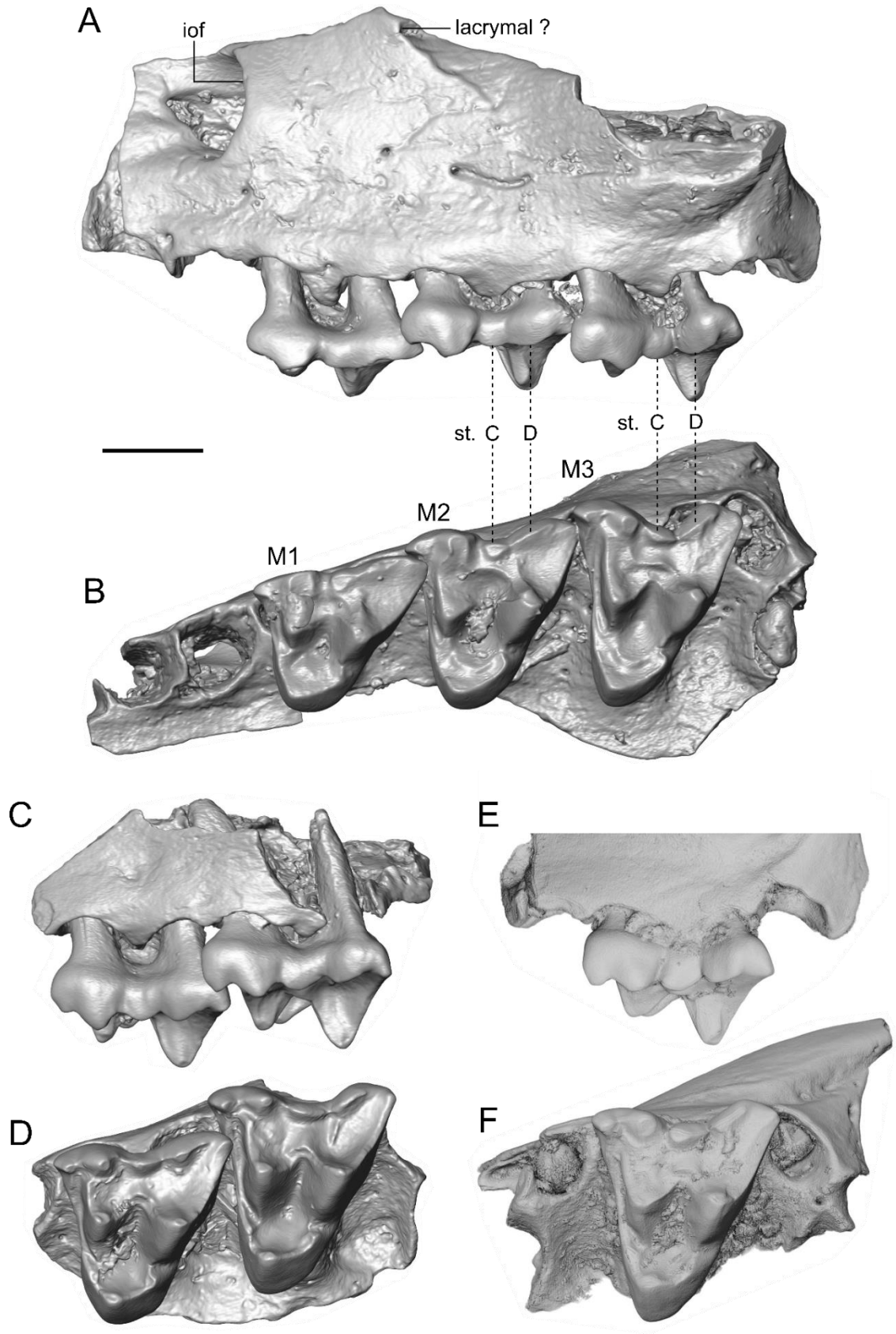

Figure 24. Maxillaires de *Peratherium* sp. nov. 2 de Prémontré (Aisne ; ~50.3-50.4 Ma) dont les molaires supérieures sont relativement bien préservées. **A-B**. Maxillaire gauche avec M1-M3, et alvéoles de P3 et M4 MNHN.F.SLP29-PE-237 (holotype) en vues labiale (A) et occlusale (B). **C-D**. Maxillaire gauche avec M2-M3 MNHN.F.SLP29-PE-1504 en vues labiale (C) et occlusale (D). **E-F**. Maxillaire droit avec M3 MNHN.F.SLP29-PE876 en vues (miroir) labiale (E) et occlusale (F). Abréviations : iof, foramen infraorbitaire ; st., cuspide stylaire. Échelle : 1 mm.

(e.g., *Peratherium antiquum*, Crochet 1980 : fig. 215; *Peratherium africanum*, Hooker et al. 2008 : fig. 1A). Ce foramen est probablement relativement plus antérieur que chez *Herpetotherium*, chez lequel il est situé dorsalement à la M1 (e.g., Korth 2018 : fig. 1b-c) et relativement plus postérieur que chez les péradectidés, pour lesquels il se trouve dorsal à l'alvéole antérieure de la P3 (Horovitz et al. 2009 ; Rose 2010). Un possible foramen lacrymal est positionné dorsalement à l'espace entre M1 et M2. La cuspide stylaire C est au moins aussi haute que la cuspide stylaire D sur les M1s et M2s (e.g., Figure 23A, C), et toujours plus haute sur les M3s (Figures 24A, C, E ; 25E) contrairement à *Pt. monspeliense*, caractérisé par une cuspide stylaire C relativement réduite en particulier sur les M3s. En revanche, la cuspide stylaire C n'atteint jamais la hauteur de la cuspide stylaire B (Figures 24A, C, E ; 25E) contrairement aux M3s d'« *A.* » *goethei* de Bouxwiller (notamment, mais pas exclusivement, sur l'holotype de cette dernière espèce ; voir Figure 25H). La M2 de l'holotype MNHN.F.SLP29-PE-237 de *Peratherium* sp. nov. 2 possède une cuspide stylaire B avec une crête distolabiale contrairement aux deux autres molaires préservées sur le maxillaire (Figure 24A-B). Il existe de légères variations de longueur du protocône (e.g., Figure 24D vs Figure 24F). Le protocône est toujours aussi haut que le paracône sur les M3s (e.g., MNHN.F.GR7594 ; Figure 25F) alors qu'il est inférieur en hauteur au paracône chez « *A.* » *goethei* (Figure 25I). La variation intra-spécifique la plus importante concerne la taille des spécimens. L'un des plus petits spécimens parmi les molaires supérieures est représenté Figure 25A (MNHN.F.SLP29-PR-2454), et l'un des plus grands est représenté Figure 25C (MNHN.F.SLP29-PE-1694).

La seule prémolaire connue est la p3 du dentaire MNHN.F.SLP29-PE-1181 d'un individu jeune (Figure 26F-G). Les alvéoles postérieures de m2 et m3 sont relativement longues (Figure 26A, F), comme chez d'autres espèces de l'Éocène inférieur (e.g., Gernelle et al. 2024b : fig. 6). Le paraconide des m2s est relativement long par rapport à *Peratherium* sp. nov. 3 et à « *A.* » *goethei* (e.g., Figure 26B vs Figure 12K). L'encoche entoconide – hypoconulide est aussi haute que l'encoche métaconide – entoconide sur certaines m2s (e.g., Figure 26B). La première encoche est plus haute ou de même hauteur que la seconde sur les m3s (Figure 26E, G), et est toujours plus haute sur les m4s (e.g., Figure 26E). L'entoconide est brisé sur la m2 de Grauves (Figure 26C). Cependant l'encoche entoconide – hypoconulide semble avoir été aussi haute que l'encoche entre le métaconide et l'entoconide en vue linguale, en considérant la marge linguale préservée de l'hypoconulide par rapport au point le plus bas de la postmétacristide.

Les M3s sont en moyenne aussi longues que les M1s et les M2s (Tableau 7) contrairement à *Pt. constans* et *Pt. matronense*, chez lesquels les M3s sont les plus courtes en moyenne, et « *A.* » *goethei* de Bouxwiller, chez lequel les M1s sont plus courtes en moyenne (pour ce dernier, voir Crochet 1980 : tab. 12). L'égalité des longueurs des molaires supérieures est aussi observable sur l'association M1-M3 de l'holotype (Figure 24B ; M1 L = 1.70 mm ; M2 L = 1.74 mm ; M3 L = 1.70 mm) et les associations M2-M3 des maxillaires MNHN.F.SLP29-PE-235 et MNHN.F.SLP29-PE-1543 (Annexes : Tableau S5). Sur

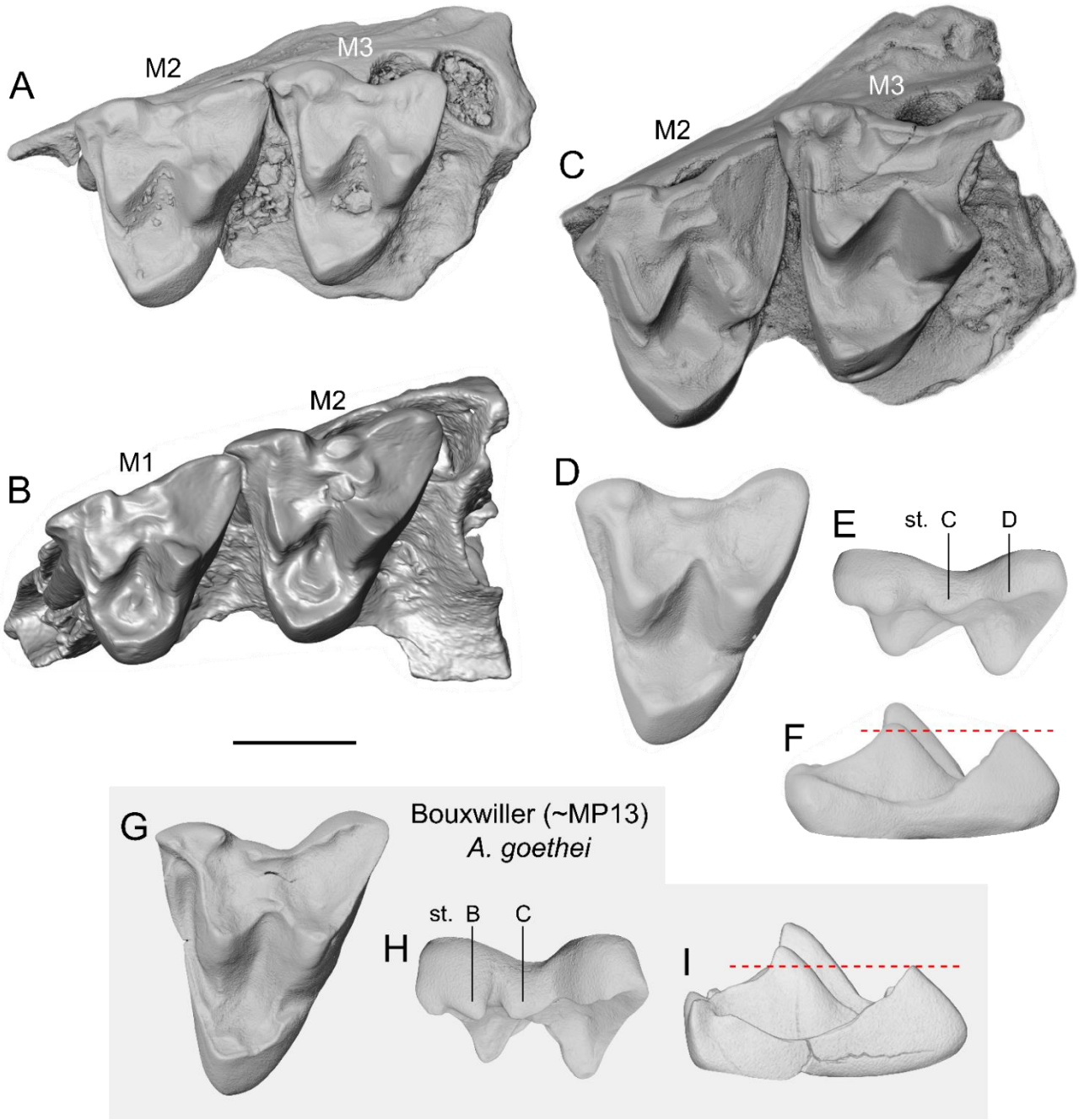

Figure 25. Molaires supérieures de *Peratherium* sp. nov. 2 de Prémontré (Aisne ; ~50.3-50.4 Ma) et Grauves (Marne ; MP10). **A-C**. Maxillaires de Prémontré en vue occlusale. **A**.MNHN.F.SLP29-PR-2454, maxillaire droit (vue miroir) avec M2-M3. **B**. MNHN.F.SLP29-PE-1566, maxillaire droit (vue miroir) avec M1-M2. **C**. MNHN.F.SLP29-PE-1694, maxillaire gauche avec M2-M3 fragmentaires. **D-F**. M3 gauche MNHN.F.GR7594 en vues occlusale (D), labiale (E) et mésiale (F). **G-I**. Comparaison avec l'holotype (M3 gauche) d'« *Amphiperatherium* » *goethei* de Bouxwiller (~MP13) UM-BUX-68.89 en vues occlusale (G), labiale (H) et mésiale (I). Abréviation : st., cuspide stylaire. Échelle : 1 mm.

le maxillaire MNHN.F.SLP29-PE-1504 (Figure 24D), la M3 est plus longue que la M2 (M2 L = 1.83 mm ; M3 L = 1. 91 mm), comme sur le maxillaire MNHN.F.SLP29-PE-1079 (Annexes : Tableau S5). Cependant, les valeurs moyennes des ratios L / W par locus (Tableau 7) sont comparables à celles des autres pérathériinés de petite taille. Les M3s sont donc relativement plus grandes (par rapport aux M1s

et M2s) que celles de *Pt. matronense*. Il faut aussi noter que la M2 de MNHN.F.SLP29-PE-1566 (Figure 25B) est nettement plus longue que la M1 (M1 L = 1.61 mm ; M2 L = 1.77 mm). Les largeurs des M3s et des M4s sont presque équivalentes en moyenne (Tableau 7). Les m2s et m3s ne diffèrent pas en moyenne par leur longueur (*t*-test ; t = -1.65, df = 48.97, p = 0.106), largeur du talonide (t = 1.23, df = 47.68, p = 0.22), et surface approximative (t = -1.44, df = 48.55, p = 0.16). Cependant, les m2s et m3s de *Peratherium* sp. nov. 2 ne sont pas connues en association contrairement à celles de *Pt. monspeliense*. Les m4s sont en moyenne aussi longues que les m2s et les m3s (Annexes : Tableau S6).

Discussion

Les valeurs des coefficients de variation des mesures des molaires supérieures de *Peratherium* sp. nov. 2 de Prémontré sont comparables à celles d'autres taxons étudiés précédemment (e.g., *Peratherium matronense*, Tableau 2). Ces valeurs sont de plus inférieures pour chaque locus à celles connues pour *Pucadelphys andinus*, un taxon marsupialiforme paléogène pour lequel l'échantillonnage est également conséquent (Tableau 7 ; Ladevèze et al. 2011). Parmi les quatre métathériens de Prémontré (dont les deux péradectidés *Peradectes* sp. nov. 1 et *Peradectes* sp. nov. 2, et le pérathériiné cf. *Peratherium maximum*), *Peratherium* sp. nov. 2 est le plus abondant (« *A.* » *goethei* et « *A.* » *bourdellense* sont en fait absents). Dans les localités de Mas de Gimel et Naples (Sud de la France), le même patron d'abondance relative est retrouvé : c'est *Peratherium monspeliense*, de même taille que *Peratherium* sp. nov. 2, qui domine l'assemblage en nombre de spécimens (~100 spécimens ; Vianey-Liaud et al. 2024 : tab. 2).

Peratherium sp. nov. 2 n'est formellement présent que dans des localités MP10 / ~MP10 du Nord de la France, alors que *Peratherium monspeliense* n'est représenté que dans des faunes ~MP10 du Sud de la France. Toutes les espèces de pérathériinés de l'Éocène inférieur précoce à moyen, ainsi que *Peratherium* sp. nov. 1 durant l'EECO sont connues dans le Nord et le Sud de la France. Étant donné que le provincialisme marqué des faunes de mammifères placentaires est atténué lors de l'EECO, la présence d'espèces de pérathériinés distinctes dans les faunes rapprochées du MP10 au Nord et au Sud de la France semble paradoxale. Des recherches en cours portant sur des localités inédites du Minervois (La Rouviole 1-2) suggèrent qu'un taxon identique ou proche de *Peratherium* sp. nov. 2 était aussi présent dans le Sud de la France. Il est possible que la différence taxonomique Nord / Sud mentionnée ci-avant s'explique par une légère différence d'âge entre les localités ayant livré *Pt. monspeliense* (e.g., Mas de Gimel, Coulondres, Le Lien et Azillanet) et *Peratherium* sp. nov. 2 (Grauves et Prémontré). Noiret et al. (2016) ont interprété l'âge d'Azillanet entre approximativement la fin du Biochron NP12 / le début du Biochron NP13 (~51-50 Ma d'après Speijer et al. 2020), c'est-à-dire environ équivalent en âge ou bien légèrement plus ancien que Prémontré (~50.4-50.3 Ma). La seconde hypothèse semble cohérente avec la différence taxonomique notée ici entre le pérathériiné dominant d'Azillanet (*Pt. monspeliense*) et de Prémontré (*Peratherium* sp. nov. 2).

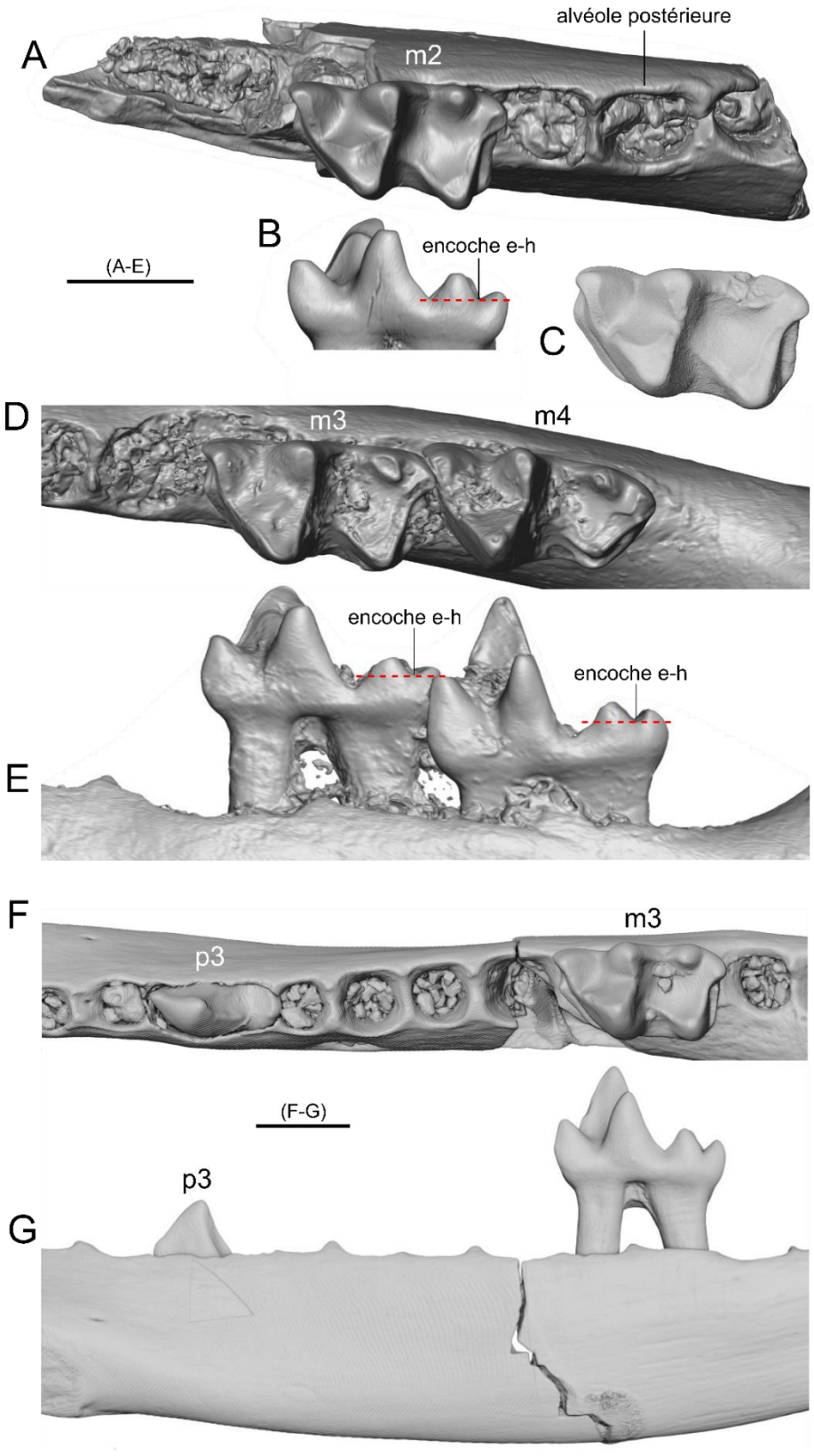

Figure 26. Dents jugales inférieures de *Peratherium* sp. nov. 2 de Prémontré (A-B, D-G ; ~50.3-50.4 Ma) et de Grauves (C ; Marne, MP10). **A-B**. MNHN.F.SLP29-PE-1547, dentaire partiel gauche avec m2 et alvéoles de m3 en vues occlusale (A) et linguale, centrée sur la m2 (B). **C**. MNHN.F.GR7426, m2 droite en vue occlusale miroir. **D-E**. MNHN.F.SLP29-PE-1533, dentaire partiel avec m3-m4 et alvéoles de m1-m2, en vues occlusale (D) et linguale (E) centrées sur m3-m4. **F-G**. MNHN.F.SLP29-PE-1181, dentaire partiel avec p3 en éruption, m3, et alvéoles de p1-p2, m1-m2, et m4, en vues occlusale (F) et linguale (G) centrées sur p3 et m3. Abréviations : e-h, entoconide – hypoconulide. Échelles : 1 mm.

Tableau 7. Comparaison des synthèses des mesures (en mm) et statistiques univariées associées des molaires supérieures de *Peratherium* sp. nov. 2 de Prémontré, et *Pucadelphys andinus* Marshall & Muizon, 1988, de Tiupampa (Bolivie, Paléocène inférieur). Les mesures de *Pucadelphys andinus* sont issues de Ladevèze et al. (2011). Abréviations : CV, coefficient de variation ; L, longueur ; N, nombre de molaires ; OR, intervalle observé ; SD, écart-type ; W, largeur ; $\bar{x}$, moyenne.

Taxon	Locus		N	OR	$\bar{x}$	SD	**CV**
Peratherium sp. nov. 2							
	M1	L	19	1.61-1.98	1.74	0.093	**5.33**
		W	20	1.64-2.05	1.80	0.129	**7.16**
		L/W	19	0.87-1.03	0.97		
	M2	L	34	1.53-2.02	1.78	0.107	**6.02**
		W	36	1.78-2.33	2.01	0.124	**6.20**
		L/W	34	0.82-0.96	0.89		
	M3	L	40	1.64-2.04	1.78	0.094	**5.31**
		W	40	1.98-2.48	2.15	0.121	**5.66**
		L/W	40	0.75-0.90	0.83		
	M4	L	6	1.35-1.51	1.42	0.070	**4.96**
		W	6	1.91-2.42	2.12	0.168	**7.92**
		L/W	6	0.57-0.73	0.67		
Pucadelphys andinus							
	M1	L	35	1.45-2.06	1.84	0.128	**6.96**
		W	27	1.50-2.33	1.84	0.176	**9.59**
	M2	L	36	1.46-2.15	1.83	0.147	**8.04**
		W	28	1.77-2.54	2.11	0.189	**8.95**
	M3	L	34	1.31-1.93	1.74	0.130	**7.48**
		W	27	1.90-2.76	2.30	0.192	**8.34**
	M4	L	24	0.89-1.71	1.43	0.208	**14.56**
		W	22	1.77-2.54	2.21	0.165	**7.49**

D. La dernière espèce de pérathériiné connue de l'Éocène inférieur (MP10-11)

Une faune riche de quatre espèces de pérathériinés a été listée par Legendre et al. (1992) dans la localité de Vielase (MP10-MP11, Quercy), et Vianey-Liaud (2022) ont listé « plusieurs espèces indéterminées » de métathériens dans la faune de Cos (dont une est un péradéctidé avéré, cf. Chapitre 2), d'âge probablement proche de Vielase. Les spécimens de Cos et Vielase appartenant aux Peratheriinae sont étudiés formellement pour la première fois et attribués à une nouvelle espèce de pérathériiné ci-dessous.

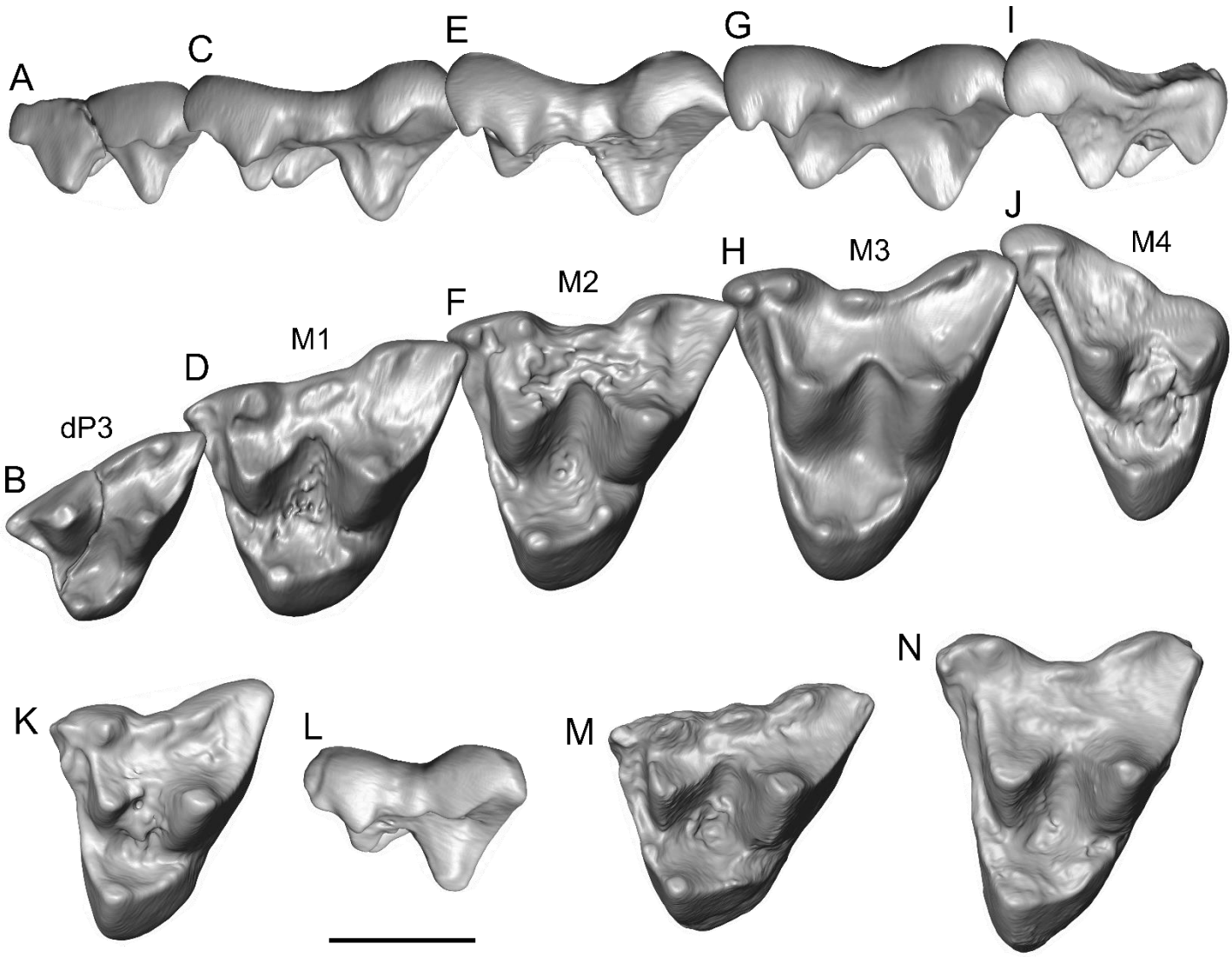

Figure 27. Molaires supérieures isolées (modèles surfaciques 3D) de *Peratherium* sp. nov. 3 de Cos et Vielase (Quercy, Sud de la France ; MP10-MP11). **A-J**. Rangée composite de dents molariformes supérieures de Cos : A, C, E, G, I, vues labiales ; B, D, F, H, J, vues occlusales. **A-B**. dP3 droite (miroir) UM-COS-314. **C-D**. M1 droite (miroir) UM-COS-309. **E-F**. M2 gauche UM-COS-307. **G-H**. M3 droite (miroir) UM-COS-310. **I-J**. M4 gauche UM-COS-328. **K-L**. M2 droite UM-COS-325 de Cos en vues (miroir) occlusale (K) et labiale (L). **M**. M1 droite UM-VIE-102 de Vielase en vue occlusale (miroir). **N**. M3 gauche UM-VIE-103 de Vielase en vue occlusale. Échelle : 1 mm.

Peratherium sp. nov. 3

Figures 27-28, Tableau 8

1992 – *Amphiperatherium goethei* Crochet in Legendre et al. p. 418, tab. 1.

1992 – *Peratherium matronense* Crochet in Legendre et al. p. 418, tab. 1.

1992 – *Peratherium* indet. aff. *P.* indet. 1 in Crochet (1980), in Legendre et al. p. 418, tab. 1.

Holotype. M3 droite (**UM-COS-310** ; Figure 27G-H).

Localités et âge. Cos et Vielase, phosphorites du Quercy, intervalle MP10-MP11, proche de la transition Yprésien-Lutétien (Legendre et al. 1992 ; Godinot et al. 2021 ; Vianey-Liaud et al. 2022).

Matériel. Matériel supplémentaire de Cos : dP3 droite (**UM-COS-314**), M1 gauche (UM-COS-49 ; UM-COS-311, usé ; UM-COS-313 ; UM-COS-316), M1 droite (**UM-COS-309** ; UM-COS-312), M2 gauche (UM-COS-71, fragmentaire ; **UM-COS-307** ; UM-COS-330, fragmentaire), M2 droite (**UM-COS-325**), M3 gauche (UM-COS-324, fragmentaire ; UM-COS-1015, fragmentaire), M3 droite (UM-COS-308), M4 gauche (**UM-COS-328**), fragment de dentaire droit avec p1-p3 (**UM-COS-315**); fragment de dentaire droit avec dp3-m2 (**UM-COS-67**); m3 droite (**UM-COS-1014**), m4 gauche (**UM-COS-72**).

Matériel de Vielase : M1 droite (UM-VIE-101, usé ; **UM-VIE-102**), M3 gauche (**UM-VIE-103**), M3 droite (UM-VIE-104, usé), m4 droite (UM-VIE-107).

Diagnose. Taille légèrement plus importante que *Peratherium* sp. nov. 2. Diffère des autres pérathériinés de l'Éocène inférieur par la cuspide stylaire B mésiolabiale par rapport au sommet du paracône sur les M3s, l'allongement relatif moyen des molaires supérieures plus élevé, et le paraconide relativement moins long sur les molaires inférieures.

Description comparée. Les cuspides stylaires C et D de la dP3 UM-COS-314 sont subégales en hauteur (Figure 27A-B), contrairement à *Pt. constans* et à *Pt. monspeliense*. Le protocône de la M2 UM-COS-307 (Figure 27F) est plus haut que le paracône, alors que le protocône de la M3 UM-COS-310 est moins haut que le paracône (Figure 27G). Les M3s UM-COS-310 (Figure 27G-H) et UM-COS-324 ont une cuspide stylaire B mésiolabiale par rapport au sommet du paracône. Le même caractère est observé, mais avec une cuspide stylaire B légèrement moins mésiale, sur la M3 UM-COS-308. Cette position de la cuspide stylaire B est retrouvée sur les deux M3s de Vielase, UM-VIE-103 (Figure 27N) et UM-VIE-104. La cuspide stylaire D est particulièrement grande sur cette dernière, alors qu'elle est aussi haute que la cuspide stylaire C sur les autres M3s (e.g., Figure 27G). Sur toutes les M3s, la cuspide stylaire B, conique, est également relativement étroite mésiodistalement et labiolingualement, beaucoup plus proche de la cuspide stylaire A que de la cuspide stylaire C, et jamais connectée à cette dernière. Les deux séries de molaires supérieures de Cos et Vielase comportent des spécimens plus longs et / ou relativement plus longs que dans d'autres faunes de l'Éocène inférieur (Tableau 8).

La différence de hauteur entre les dentaires UM-COS-315 et UM-COS-65 (Figure 28B vs Figure 28D), le premier étant plus élevé (même ventralement à la p1), est liée à l'âge des individus. C'est le dentaire portant la dp3, une dent par ailleurs morphologiquement similaire à celle décrite chez *Pt. maximum*, qui est le moins haut. La p3 est nettement plus longue que la p2 (Tableau 8) contrairement à *Pt. maximum* (Figure 28B vs Gernelle et al. 2024b : tab. 3), et la p1 est moins réduite. En vue occlusale non inclinée, le flanc lingual de l'entoconide de la m2 n'est pas convexe (contrairement à la Figure 28C où la m2 est légèrement inclinée). La pré-entocristide est longue, y compris sur la m1 et la m2 (Figure 28C-D).

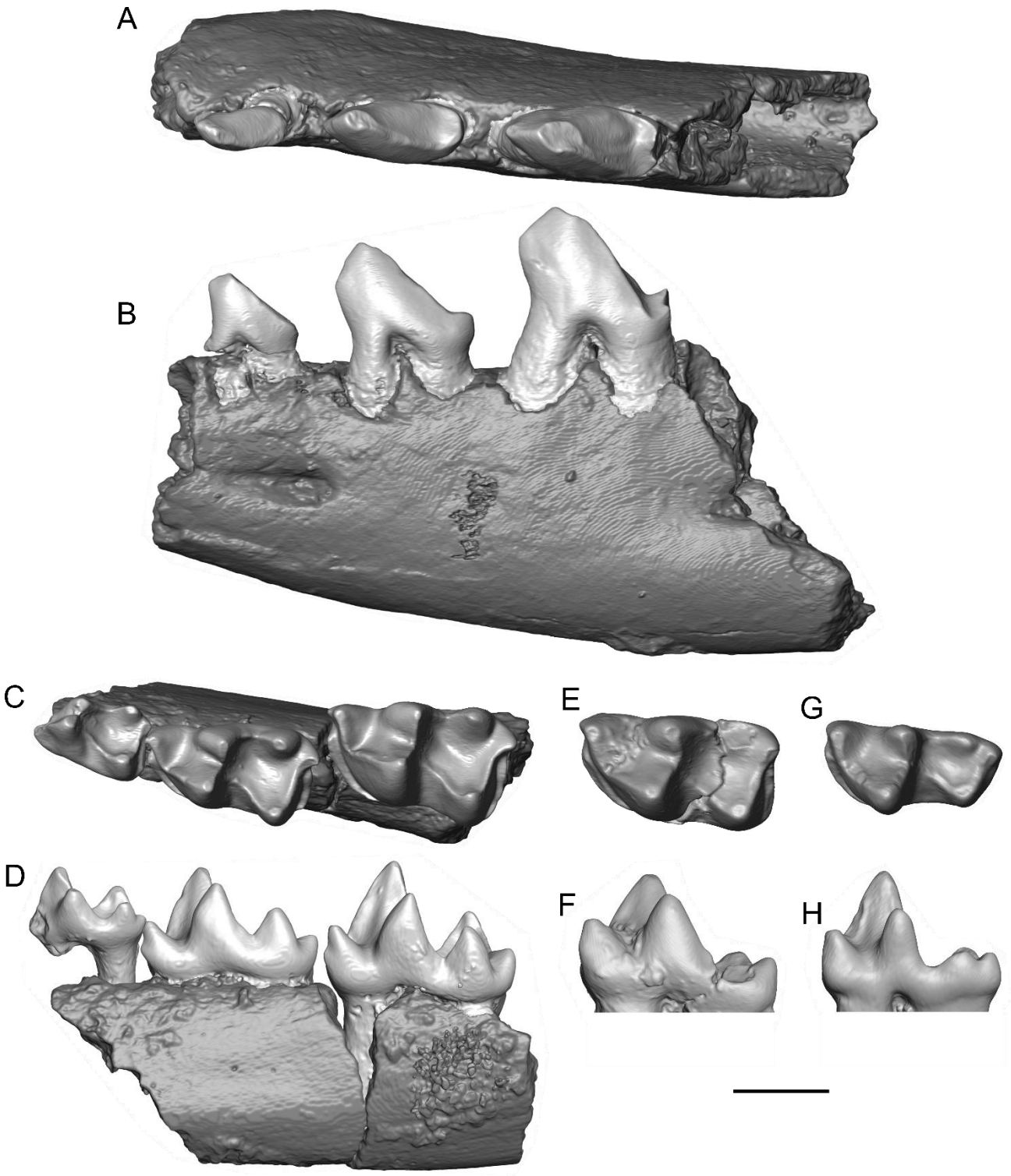

Figure 28. Dents jugales inférieures (modèles surfaciques 3D) de *Peratherium* sp. nov. 3 de Cos (Quercy ; intervalle MP10-MP11). **A-B**. Dentaire partiel droit avec p1-p3, UM-COS-315, en vues (miroir) occlusale (A) et labiale (B). **C-D**. Dentaire partiel droit avec dp3-m2, UM-COS-65, en vues occlusale miroir (C) et linguale (D). **E-F**. m3 droite UM-COS-1014 en vues occlusale miroir (E) et linguale (F). **G-H**. m4 gauche en vues occlusale (G) et linguale miroir (H). Échelle : 1 mm.

Par rapport aux molaires connues de *Peratherium* sp. nov. 2 (voir Annexes : Tableaux S5-S6), *Peratherium* sp. nov. 3 est caractérisé par les différences suivantes :

- La m1 et la m3 sont significativement plus grandes (Tableau 8).
- La M4 est plus longue (en valeur absolue) et relativement plus longue (par rapport à sa largeur) que les six M4s connues de *Peratherium* sp. nov. 2 (Tableau 7 vs Tableau 8). Elle est aussi moins large que les M3s au contraire de l'espèce de Prémontré (et comme *Pt. maximum*).

Discussion. *Peratherium* sp. indet. 1 sensu Crochet (1980) et les taxons supposés proches (e.g., la M3 UM-VIE-104) forment un ensemble taxonomiquement hétérogène de molaires supérieures partageant un allongement transverse important, un des deux spécimens de *Peratherium* sp. indet. 1 étant l'holotype de *Pt. musivum* (Gernelle et al. 2024b). *Peratherium* sp. indet. 1, *Peratherium matronense*, et *Amphiperatherium goethei* ne sont pas représentés à Vielase. Une M2 (UM-VIE-105) attribuée à une espèce d'*Amphiperatherium* indéterminée par Legendre et al. (1992) semble trop petite pour avoir appartenu à *Peratherium* sp. nov. 3 (plus petite que la plus petite M2 connue de cette espèce, UM-COS-325 ; Tableau 8) et montre qu'une seconde espèce de pérathériiné était peut-être présente dans la faune de Vielase.

Peratherium sp. nov. 3 partage vraisemblablement avec *Peratherium* sp. nov. 2, *Pt. monspeliense*, ainsi qu'avec « *A.* » *goethei* de Bouxwiller (~MP13) l'agrandissement des molaires supérieures de la M1 à la M3 (pour ce dernier, voir Crochet 1980 : tab. 12), qui se traduit notamment par des M3s de même longueur ou plus longues que les M1s, c'est-à-dire un allongement postérieur relatif par rapport aux espèces de pérathériinés plus anciennes, observé à la fois au sein des faunes de Cos et de Vielase (Tableau 8). Le degré d'allongement des molaires supérieures est plus important que chez *Peratherium* sp. nov. 2, car des spécimens de *Peratherium* sp. nov. 3 pour les quatre loci (M1-M4) sont caractérisés par des ratios L / W plus élevés que tous les spécimens de *Peratherium* sp. nov. 2 connus pour ces même loci (Tableau 7 vs Tableau 8). Cette différence taxonomique reflète certainement une différence d'âge entre les localités MP10 / ~MP10 (e.g., Grauves et Prémontré) et Cos et Vielase, ce qui est cohérent avec l'âge MP10-11 attribué à ces faunes du Quercy par Godinot et al. (2021) et Vianey-Liaud et al. (2022). L'allongement moyen des M2s et M3s par rapport aux M1s étant partagé avec *Peratherium* sp. nov. 2 et « *A.* » *goethei* de Bouxwiller, il s'agit probablement d'un caractère apparu dans les faunes de pérathériinés durant l'EECO.

Tableau 8. Mesures (en mm) des spécimens de *Peratherium* sp. nov. 3 de Cos et Vielase (Quercy ; MP10-MP11). Les valeurs des ratios longueur / largeur (L / W) des molaires supérieures égales ou plus élevées que la borne supérieure associée aux valeurs de ratios des loci équivalents chez *Peratherium* sp. nov. 2 sont signalées en gras. Abréviations : L, longueur ; tlW, largeur du talonide ; trW, largeur du trigonide ; W, largeur totale.

Localité	Spécimen	Locus	L (mm)	W (mm)	L/W	trW (mm)	tlW (mm)
Cos	UM-COS-314	dP3	1,38	1,30	1,06		
	UM-COS-49	M1	1,80	1,83	0,98		
	UM-COS-309	M1	1,95	1,89	**1,03**		
	UM-COS-311	M1	1,87	1,98	0,94		
	UM-COS-312	M1	1,86	1,80	**1,03**		
	UM-COS-313	M1	1,83	1,80	1,02		
	UM-COS-316	M1	1,90	1,88	1,01		
	UM-COS-307	M2	2,00	2,03	**0,99**		
	UM-COS-325	M2	1,54*	1,79	-		
	UM-COS-308	M3	1,96	2,19	0,89		
	UM-COS-310	M3	2,03	2,26	**0,90**		
	UM-COS-1015	M3	-	2,43	-		
	UM-COS-328	M4	1,57	2,02	**0,78**		
	UM-COS-315	p1	0,94	0,47	2,00		
	UM-COS-315	p2	1,47	0,67	2,19		
	UM-COS-315	p3	1,69	0,79	2,14		
	UM-COS-67	dp3	-	0,80	-	-	-
	UM-COS-67	m1	1,79	1,10	1,63	0,92	1,07
	UM-COS-67	m2	2,00	1,21	1,65	1,06	1,20
	UM-COS-1014	m3	2,09	1,23	1,70	1,16	1,17
	UM-COS-72	m4	1,86	0,99	1,88	0,99	0,80
Vielase	UM-VIE-101	M1	1,82	1,69	**1,08**		
	UM-VIE-102	M1	1,85	1,65	**1,12**		
	UM-VIE-103	M3	1,83	2,20	0,83		
	UM-VIE-104	M3	2,08	2,60	0,80		
	UM-VIE-107	m4	1,72	-	-	0,93	0,70

Conclusion générale et perspectives

1. Absence d'espèces panchroniques lors de l'Éocène inférieur

La révision systématique menée par l'intermédiaire de la caractérisation des variations morphologiques dentaires intra- et interspécifiques (Chapitres 1-2, 5-6) des métathériens européens a permis de reconnaître un total de 15 espèces valides durant l'Éocène inférieur, possédant toutes leur localité-type dans cette période (Tableau 1). La longévité constatée pour les espèces yprésiennes les mieux documentées est généralement d'environ 2 Ma (e.g., Gernelle et al. 2024b, Chapitre 5). La révision systématique des pérathériinés a montré que les deux espèces « *Amphiperatherium* » *goethei* et « *A.* » *bourdellense*, définies dans des localités post-yprésiennes, ne sont pas représentées durant l'intervalle de temps étudié ici (Chapitre 6), alors qu'elles y avaient été considérées abondantes au moins à partir du niveau-repère ~MP8+9 (Crochet 1980 ; Godinot 1981 ; Dégremont et al. 1985 ; Legendre et al. 1992). Au niveau spécifique, les métathériens européens cénozoïques n'étaient donc pas panchroniques, et ce durant toute leur histoire évolutive de l'Éocène inférieur. Par exemple, aucune des espèces des faunes MP8+9 / ~MP8+9 n'est connue de façon certaine dans les faunes MP10 / ~MP10 (Tableau 1). L'espèce à la longévité la plus importante pourrait être *Peratherium maximum*, qui apparaît à Pourcy dans le registre fossile, et persiste peut-être jusqu'à Prémontré (Tableau 1). Cependant, les quatre mentions les plus tardives de cette espèce (MP10 / ~MP10) sont en nomenclature ouverte (*Peratherium* cf. *maximum*) due à l'absence de caractères diagnostiques sur ces très rares spécimens (cinq). Ces conclusions questionnent l'homogénéité de plusieurs espèces panchroniques de métathériens d'Amérique du Nord, et surtout d'Europe après l'Éocène inférieur (e.g., *Amphiperatherium minutum* ; Crochet 1979 : fig. 16).

2. Corrélations entre les réchauffements climatiques de l'Éocène inférieur et les évènements de l'histoire évolutive des métathériens européens

Les herpétothériidés et les péradectidés se sont probablement dispersés de l'Amérique du Nord vers l'Europe de façon différée. Les premiers sont maintenant connus sur ce dernier continent juste après le POE (Chapitre 4), et les seconds juste après le PETM, qui marque le début de l'Éocène (Chapitre 1). L'ordre apparent dans lequel les deux familles se sont dispersées est étonnant au regard du registre fossile manifestement contemporain de ces réchauffements globaux rapides outre-Atlantique, car les herpétothériidés avérés ne sont pas connus avant l'Éocène en Amérique du Nord au contraire des péradectidés (Gingerich et Smith 2006), et la lignée fantôme entre le seul genre probable d'herpétothériidé souche, *Swaindelphys*, et le genre inédit du Paléocène du Sud de la France, est pour le moment conséquente (Chapitres 3-4).

L'aire de répartition des métathériens en Europe de l'Ouest était large durant l'Éocène inférieur, et ne semble pas avoir été affectée par une éventuelle barrière climatique au début de cette période : le plus ancien péradectidé européen, *Peradectes crocheti*, et les deux plus anciens pérathériinés, *Peratherium constans* et *Peratherium musivum*, sont connus à la fois dans plusieurs localités au Nord et au Sud de l'Europe de l'Ouest (Chapitres 1, 5, 6). Il a été suggéré que l'ETM2 n'aurait vraisemblablement pas été associé à des renouvellements fauniques dans l'hémisphère nord (Abels et al. 2012 ; Noiret et al. 2016). Cela s'applique aux métathériens d'Europe en prenant en compte les âges apparents d'apparition et d'extinction de *Pd. crocheti* et *Pt. musivum* (Chapitre 5). En revanche, les données sur les pérathériinés de petite taille montrent que *Pt. matronense* remplace apparemment *Pt. constans* à partir des faunes d'âge proche de Fournes (~54 Ma, juste après l'ETM2, cf. Chapitre 6). De plus, *Peratherium maximum* apparaît dans le registre fossile antérieurement aux faunes d'âge MP8+9 / ~MP8+9 et était partiellement contemporain de *Pt. musivum* (Chapitre 5 ; Tableau 1). Cela montre qu'un renouvellement des faunes de pérathériinés a probablement eu lieu approximativement entre l'ETM2 et le début de l'EECO (i.e., avant l'ETM3).

Les quatre mêmes espèces caractérisent toutes les faunes de l'Éocène inférieur moyen du Bassin parisien (Tableau 1 ; Figure 1A), contre jusqu'à 10 (à Avenay et Condé-en-Brie) avant cette révision taxonomique (Crochet 1980). Il s'agit des deux péradectidés *Pd. louisi* et *Pd. russelli*, et des deux pérathériinés *Pt. matronense* et *Pt. maximum* (Figure 1A). Durant l'EECO, la richesse spécifique atteint cinq dans deux localités, Mas de Gimel / Naples (Sud de la France, voir Figure 1B-F, et Vianey-Liaud et al. [2024]) et Grauves (Nord de la France) (Tableau 1), notamment car un taxon de taille intermédiaire entre *Pt. matronense* / *monspeliense* et *Pt. maximum* apparaît (*Peratherium* sp. nov. 1 ; Figure 1). Chez les métathériens, l'EECO coïncide donc avec une diversification spécifique mineure et sûrement très transitoire des pérathériinés, qui est néanmoins cohérente avec les dynamiques d'évolution des faunes nord-américaines (Woodburne et al. 2009) et européennes (e.g., Solé et al. 2014 ; Bronnert et Métais 2023 : tab. 1). Un effort d'échantillonnage supplémentaire sera nécessaire pour mieux définir certains taxons intra-EECO de petite taille, actuellement documentés par beaucoup moins de matériel que d'autres, en particulier pour les faunes du Sud de la France (Figure 1B-F ; e.g., *Peradectes* sp. indet., Chapitre 2). La révision des pérathériinés de Vielase (MP10-11, Chapitre 6) et les connaissances actuelles portant sur les faunes ~MP11 de Messel (Kurz 2007), MP12 et MP13 du Geiseltal (Storch et Haubold 1989) et ~MP13 de Bouxwiller (Crochet 1980) (cf. Matériel et méthodes) indiquent une diminution de l'alpha diversité métathérienne en Europe potentiellement dès la fin l'EECO. Cela est notamment en lien avec la disparition des péradectidés européens après la limite Yprésien / Lutétien (Gernelle et al. 2024a, Chapitre 1), et coïncide avec une diminution de la diversité taxonomique mammalienne liée à une détérioration climatique par rapport aux conditions de l'EECO, un évènement formalisé au moins pour l'Amérique du Nord (« Bridgerian Crash » ; Woodburne et al. 2009).

Tableau 1. Synthèse de toutes les mentions de taxons Peradectidae et Herpetotheriidae de l'Éocène inférieur à la suite de cette révision systématique, dans un cadre chronologique (niveaux-repères MP, biozones PE, et datations biochémostratigraphiques ; voir Matériel et méthodes). Les croix rouges indiquent les localités-types. Les localités surlignées en bleu sont celles du Sud de la France, les autres sont celles des bassins parisien, belge et anglais. Les abréviations et croix en italique concernent les localités inédites. Abréviations des localités (dans leur ordre d'apparition) : ALB, Albas ; DO, Dormaal ; QNY, Le Quesnoy ; SI, Silveirinha ; STV, Sotteville-sur-Mer, PAT, Palette ; FDN, Fordones ; CLO, Le Clot ; MEU, Meudon ; SN, Soissons ; CR, Croydon ; AW, Abbey-Wood ; RI, Rians ; FNR, Fournes ; GAS, La Gasque ; POU, Pourcy ; MU, Mutigny ; AV, Avenay ; CB, Condé-en-Brie ; GLD, Sables de Brasles ; SZ, Sézanne-Broyes ; BRI, La Borie ; EG, Egem ; SA, Saint-Agnan ; MGL/NAP, Mas de Gimel / Naples ; SRT, Le Théron ; LLN, Le Lien ; CLR, Coulondres ; AZI, Azillanet ; GR, Grauves ; PRE, Prémontré ; VIE, Vielase ; COS, Cos.

	MP7				~55 Ma				?			~54 Ma						MP8+9						MP8+9-10	~MP10				~51-50 Ma	MP10	50.4-3 Ma	MP10-11	
	PE I				PE II							PE III					PE IV	PE V																
	ALB	DO	QNY	SI	STV	PAT	FDN	CLO	MEU	SN	CR	AW	RI	FNR	GAS	POU	MU	AV	CB	GLD	SZ	BRI	EG	SA	MGL/NAP	*SRT*	*LLN*	CLR	AZI	GR	PRE	VIE	COS
Peradectidae																																	
Peradectes crocheti	-	-	-	-	X	X	X	-	X	X	X	X	X	X	-	-	-	-	-	-	-	-	-	-	-	-	-	-	-	-	-	-	-
Peradectes louisi	-	-	-	-	-	-	-	-	-	-	-	-	-	-	-	-	X	X	X	X	X	-	-	cf.	-	-	-	-	-	-	-	-	-
Peradectes russelli	-	-	-	-	-	-	-	-	-	-	-	-	-	-	-	-	X	X	X	X	X	-	-	-	cf.	-	-	-	-	-	-	-	-
Peradectes dufraingi	-	-	-	-	-	-	-	-	-	-	-	-	-	-	-	-	-	-	-	-	-	-	X	-	-	-	-	-	-	-	-	-	-
Peradectes sp. indet.	-	-	-	-	-	-	-	-	-	-	-	-	-	-	-	-	-	-	-	-	-	-	-	-	X	-	-	?	X	-	-	-	-
Peradectes sp. nov. 1	-	-	-	-	-	-	-	-	-	-	-	-	-	-	-	-	-	-	-	-	-	-	-	-	-	-	-	-	-	X	X	-	-
Peradectes sp. nov. 2	-	-	-	-	-	-	-	-	-	-	-	-	-	-	-	-	-	-	-	-	-	-	-	-	-	-	-	-	-	-	X	-	-
Peradectes sp. nov. 3	-	-	-	-	-	-	-	-	-	-	-	-	-	-	-	-	-	-	-	-	-	-	-	-	-	-	-	-	-	-	-	cf.	X
Herpetotheriidae																																	
Peratherium spp. indet.	-	-	-	-	-	-	-	-	-	-	-	-	-	-	-	-	X	-	-	-	-	-	-	X	-	-	*X*	-	-	X	-	?	-
gen. et sp. nov.	*X*	-	-	-	-	-	-	-	-	-	-	-	-	-	-	-	-	-	-	-	-	-	-	-	-	-	-	-	-	-	-	-	-
Peratherium constans	-	X	X	X	-	X	X	X	X	X	-	-	X	-	-	-	-	-	-	-	-	-	-	-	-	-	-	-	-	-	-	-	-
Peratherium musivum	-	-	-	-	-	-	-	X	-	X	-	cf.	X	X	-	X	-	-	-	-	-	-	-	-	-	-	-	-	-	-	-	-	-
Peratherium matronense	-	-	-	-	-	-	-	-	-	-	-	cf.	-	X	X	-	-	X	X	X	X	cf.	-	-	-	-	-	-	-	-	-	-	-
Peratherium maximum	-	-	-	-	-	-	-	-	-	-	-	-	-	-	-	X	X	X	X	X	aff.	X	-	X	cf.	-	-	-	-	cf.	cf.	-	-
Peratherium monspeliense	-	-	-	-	-	-	-	-	-	-	-	-	-	-	-	-	-	-	-	-	-	-	-	cf.	X	*X*	*X*	X	X	-	-	-	-
Peratherium sp. nov. 1	-	-	-	-	-	-	-	-	-	-	-	-	-	-	-	-	-	-	-	-	-	-	-	cf.	X	-	-	-	-	X	-	-	-
Peratherium sp. nov. 2	-	-	-	-	-	-	-	-	-	-	-	-	-	-	-	-	-	-	-	-	-	-	-	-	-	-	-	-	-	X	X	-	-
Peratherium sp. nov. 3	-	-	-	-	-	-	-	-	-	-	-	-	-	-	-	-	-	-	-	-	-	-	-	-	-	-	-	-	-	-	-	X	X

Les herpétothériidés sont plus abondants que les péradectidés dans la plupart des faunes étudiées. Cependant, presque autant d'espèces valides de péradectidés (sept, dont quatre nouvelles en comptant *Peradectes crocheti* Gernelle, 2024a) que d'herpétothériidés (huit, dont quatre nouvelles en comptant *Peratherium musivum* Gernelle, 2024b) sont maintenant décrites dans l'Éocène inférieur (Tableau 1). Ainsi, chacune des familles de métathériens reste relativement peu diversifiée durant les réchauffements climatiques de cette période, en plus d'être peu disparate morphologiquement. Ce dernier point est à nuancer au regard des différences morphologiques cryptiques qui existent aussi entre les dentures des espèces au sein d'autres taxons de mammifères européens insectivores de petite taille présents à la même période, comme les Amphilemuridae (*Macrocranion* ; e.g., Smith et Smith 1995). Les différences morphologiques les plus conséquentes chez les pérathériinés apparaissent probablement avec les taxons de relativement grande taille.

3. Dynamiques évolutives liées aux tailles des métathériens européens

Des pérathériinés de l'Éocène inférieur précoce (e.g., *Pt. musivum*) sont caractérisés par leur acquisition relativement rapide (1 Ma après l'apparition du groupe) d'une taille doublée par rapport aux taxons probablement plus basaux (Gernelle et al. 2024b, Chapitre 5). Les pérathériinés voient leur taille maximum atteinte dès l'Éocène inférieur moyen (*Peratherium* aff. *maximum* ; cf. Chapitre 6). Le même patron d'évolution de la taille est connu chez les herpétothériinés (nord-américains) avec l'apparition rapide, dès le Wasatchien, de la plus grande espèce d'*Herpetotherium* (*H. comstocki* ; Krishtalka et Stucky 1983 : fig. 7). En effet, la règle de Cope, postulant que la taille a tendance à s'accroître au sein d'une lignée avec le temps d'évolution, ne concerne que très peu les mammifères de petite taille (Alroy 1998). En revanche, les espèces possiblement en sympatrie, a fortiori si elles appartiennent à la même famille, ne sont jamais toutes de même taille dans les faunes européennes (Figure 1) (sauf les faunes proches du niveau-repère MP7 comportant seulement une espèce de pérathériiné et de péradectidé, comme Palette, Fordones et Meudon ; cf. Tableau 1), ce qui suggère un partitionnement de niches écologiques basé sur la taille spécifique, tel que documenté chez des micromammifères actuels (e.g., Andreas et al. 2013) et fossiles, même lors de l'Éocène inférieur (e.g., Aumont 2004). Un exemple de possible remplissage d'une niche écologique accompli entre les faunes (~)MP8+9 et (~)MP10 est illustré dans la Figure 1. Chez les Peratheriinae, les gains de disparité morphologique sont le fait de l'apparition des taxons de plus grande taille. *Peratherium maximum* présente par exemple un élargissement du complexe fonctionnel protocône – talonide ainsi qu'une multiplication fréquente des cuspides stylaires (Chapitres 5 et 6). Bien qu'au sein de l'espèce, la corrélation entre la surface des molaires et le nombre de cuspides stylaires soit ténue (Chapitre 6), il faut noter que parallèlement, chez les péradectidés, les cas de multiplication des cuspides stylaires apparaissent aussi chez le seul représentant de grande taille, le genre nord-américain *Mimoperadectes* (Gernelle et al. 2024a : 44, Chapitre 1 ; voir par exemple les cuspides stylaires en position « C » des M2s dans Gingerich et Smith 2006 : fig. 15C-D ; Beard et

Dawson 2009 : fig. 4A-B ; Horovitz et al. 2009). Les péradectidés européens n'ont probablement jamais atteint de taille aussi conséquente que les plus grands pérathériinés (Figure 1A). L'ensemble de ces constats renforce l'idée que les corrélations entre les tailles et les formes des taxons constituent l'une des principales sources de diversification morphologique chez les métathériens (Brum et al. 2023).

4. Relations phylogénétiques intrafamiliales et tendances évolutives

Un regroupement sous-familial des herpétothériidés européens (Peratheriinae) a été proposé par Ladevèze et al. (2020). J'ai pu mettre en évidence à partir d'analyses phylogénétiques qu'un genre regroupant l'ensemble des péradectidés européens doit être créé (Chapitre 3). Celui-ci s'étend à l'ensemble de l'Yprésien (~8 Ma), ce qui est cohérent avec les longévités moyennes des genres chez d'autres mammifères de petite taille (Hoek Ostende et al. 2023). Trois espèces inédites de péradectidés contemporaines avec l'EECO ont été décrites (Chapitre 2), mais leur inclusion dans les analyses phylogénétiques perturbe la résolution des relations génériques (Chapitre 3) en partie probablement car elles sont documentées par un matériel rare.

Les relations phylogénétiques au sein des Peratheriinae demeurent énigmatiques. Cependant, il a été mis en évidence ici (Chapitre 5) que (i) la dichotomie profonde longtemps envisagée entre *Amphiperatherium* et *Peratherium* (Crochet 1977) ne reflète pas l'histoire évolutive complexe de cette sous-famille. Les progrès réalisés ici dans la résolution de leur systématique sont surtout au niveau spécifique. Ainsi, les premières espèces de Peratheriinae de petite taille, *Peratherium constans* et *Pt. matronense*, apparaissent finalement distinguables morphologiquement (contra Hooker et al. 2008 ; Ladevèze et al. 2012 ; Selva et Ladevèze 2017) grâce à l'étude de la forme du contour de leurs molaires supérieures, bien que cette différence soit subtile et surtout s'atténue de M1 à M3 (Chapitre 6). À ce titre, *Peratherium constans* (et probablement aussi le nouveau taxon paléocène ; cf. Chapitre 4) sont les seules espèces yprésiennes à posséder une émargination distale marquée entre le plateau stylaire et le talon de la couronne des M1s et M2s (Chapitre 6). L'hypothèse favorisée ici est donc que *Pt. constans* a divergé ancestralement par rapport à tous les autres pérathériinés.

Peratherium musivum partage avec *Pt. maximum* deux à trois caractères dentaires (trois si l'agrandissement apparent du complexe protocône / talonide est confirmé chez le premier), non retrouvés chez *Pt. constans* et *Pt. matronense*. L'hypothèse d'une proximité phylogénétique entre les deux espèces de grande taille du début de l'Éocène inférieur a donc été formulée (Gernelle et al. 2024b, Chapitre 5). En revanche, la relation proposée par Crochet (1980) entre *Pt. maximum* et « *A.* » *bastbergense* a été questionnée par la découverte d'une nouvelle espèce (*Peratherium* sp. nov. 1) probablement dans l'ascendance de « *A.* » *bastbergense* mais dont les tailles relatives des cuspides stylaires n'évoquent pas ce dernier, ni *Pt. maximum* et *Pt. musivum* (Chapitre 6). L'acquisition d'une taille relativement plus importante que la moyenne des taxons métathériens européens et d'un complexe protocône / talonide

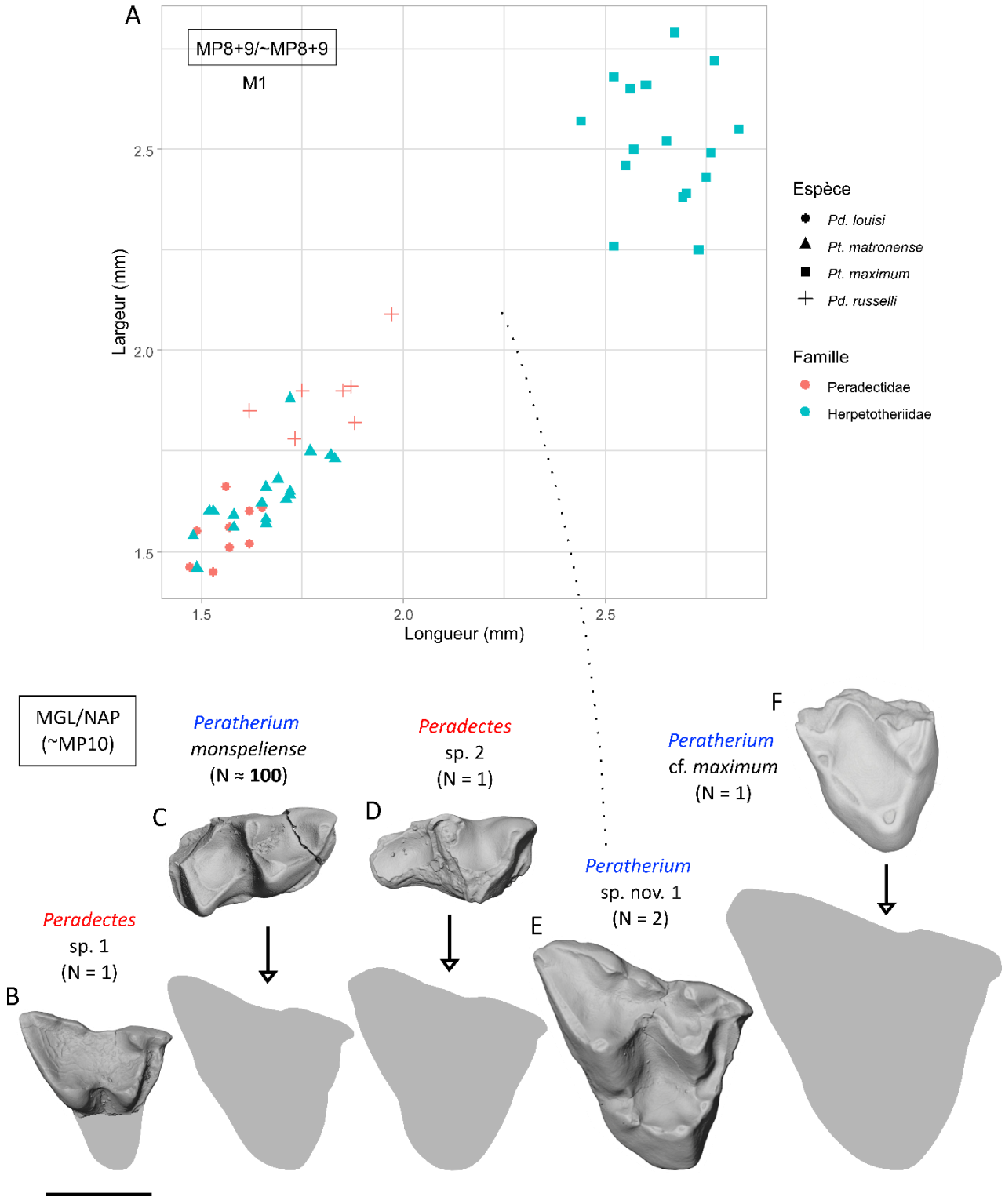

Figure 1. **A**. Graphique bivarié des longueurs et largeurs des M1s des espèces de métathériens typiques des faunes MP8+9 / ~MP8+9 du Bassin de Paris, *Peradectes louisi* et *Pd. russelli*, et *Peratherium matronense* et *Pt. maximum*. **B-F**. Diversité de la faune de métathériens de Mas de Gimel + Naples (~MP10, Montpellier) étudiée par Vianey-Liaud et al. (2024), dans le cadre de cette thèse (cf. Annexes). Les tailles des spécimens connus par des molaires inférieures ou supérieures fragmentaires sont comparées à partir de silhouettes de molaires supérieures de taxons proches de taille équivalente. Les noms des péradectidés (B, D) sont en rouge et ceux des pérathériinés (C, E-F) en bleu. Le nombre de spécimens connus de Mas de Gimel + Naples pour chaque taxon (« N ») est indiqué. **B**. UM-MGL-716. **C**. UM-MGL-310. **D**. UM-MGL-320. **E**. UM-NAP-125. *Peratherium* sp. nov. 1 est placé approximativement dans le graphique bivarié (A). **F**. UM-MGL-309. Échelle : 1 mm.

agrandi (supposée chez *Peratherium* sp. nov. 1 étant donné la hauteur relative du protocône des molaires) s'est donc peut être déroulée plus d'une seule fois dans l'histoire évolutive des Peratheriinae.

Des tendances morphologiques ont pu être mises en évidence chez les péradectidés et les herpétothériidés européens de l'Éocène inférieur. Les prémolaires et molaires inférieures des Peradectidae deviennent relativement plus longues au cours du temps, et la taille relative de l'entoconide des molaires inférieures diminue graduellement de leur arrivée en Europe jusqu'à leur dernière mention avérée parmi les faunes MP10-11 du Quercy (Chapitres 1 et 2). Ce dernier caractère est convergent entre les péradectidés européens et nord-américains à la même période (Chapitre 1 et 3). Chez les Peratheriinae, ce sont les molaires supérieures qui tendent à s'allonger légèrement, chez *Peratherium* sp. nov. 2 et *Peratherium* sp. nov. 3, puis « *A.* » *goethei* lors de l'Éocène moyen (Chapitre 6). D'éventuelles corrélations avec l'évolution de la morphologie des herpétothériinés (nord-américains) sont pour le moment impossibles car les espèces de cette sous-famille n'ont pas de délimitation claire et doivent être révisées (e.g., voir discussion Chapitre 5). Bien que l'utilisation des hauteurs relatives des cuspides stylaires soit apparue comme un bon moyen de discriminer certaines espèces autrement morphologiquement similaires (Chapitres 1-2, 5-6), ces caractères sont très homoplastiques. La faible taille de la cuspide stylaire C chez *Pt. monspeliense* est probablement une autapomorphie de ce taxon.

5. Des familles endémiques à l'hémisphère Nord

Des conclusions majeures sur les histoires paléobiogéographiques des Peradectidae et des Herpetotheriidae, impliquant leur présence hors d'Amérique du Nord et d'Europe, ont souvent été tirées à partir de comparaisons de matériel dentaire peu abondant et / ou fragmentaire. La première étape pour pallier cette contrainte a consisté en la reconnaissance des caractères dentaires diagnostiques distinguant les deux familles à partir de comparaisons d'un nombre conséquent de spécimens (Gernelle et al. 2024a : tab. 6, Chapitre 1). Puis, les conclusions basées sur la compréhension des synapomorphies des Peradectidae, non homoplastiques au sein de ce groupe pour la première fois retrouvé monophylétique (Chapitre 3), m'ont permis de montrer qu'ils étaient, en l'état actuel des connaissances, endémiques à l'Amérique du Nord et à l'Europe. En utilisant comme base la résolution de l'origine profonde probable des Herpetotheriidae réalisée durant cette thèse (Chapitres 3-4), un travail similaire de révision reste à effectuer pour les Herpetotheriidae et les « herpétothériidés » extra-européens. En effet, durant les nombreuses comparaisons morphologiques conduites, j'ai constaté que : (i) les Rumiodontinae Carneiro et al., 2024 éocènes sud-américains, pour le moment considérés comme des herpétothériidés, présentent des m4s aux angles postcristide – cristide obliqua (voir Carneiro et al. 2024 : fig. 3a-b) beaucoup plus ouverts que les herpétothériidés nord-américains et européens ; (ii) la molaire inférieure du possiblement plus ancien métathérien d'Afrique, l'herpétothériidé putatif *Morotodon* Crespo, Goin & Pickford, 2022, présente de nombreux caractères inattendus chez un métathérien, comme l'absence de paraconide en

forme de quille, l'extrémité distolinguale du talonide très incurvée associée à une position relativement labiale du précingulide (voir Crespo et al. 2022 : fig. 2), ou encore un hypoconide proéminent associé à un large hypoflexide ; et (iii) le statut métathérien de l'« herpétothériidé » du sous-continent indien (Crochet et al. 2007) est discutable vu la présence de cingulums distaux sur deux des molaires supérieures (pers. obs.) et l'absence de patron stylaire de type métathérien. La seule mention d'un métathérien d'appartenance avérée à un groupe typiquement laurasien dans l'hémisphère sud semble être celle de *Peratherium africanum* Simons & Bown, 1984 de l'Oligocène inférieur d'Égypte (Hooker et al. 2008). La découverte de nouveaux fossiles permettra notamment d'éprouver l'hypothèse de restriction quasi-totale des Peradectidae et des Herpetotheriidae à l'hémisphère nord.

6. Perspectives – Les métathériens de la transition Yprésien – Lutétien de Messel

Maintenant que l'évolution de la morphologie dentaire des métathériens yprésiens d'Europe est mieux comprise, l'acquisition de connaissances inaccessibles autrement portant sur les familles européennes passera sans doute par l'étude détaillée des cinq squelettes complets à sub-complets de Messel, à la transition Yprésien – Lutétien (trois individus nommés « *Peradectes* » préliminairement, et deux individus herpétothériidés appartenant probablement à deux espèces ; Kurz 2007). La description et la comparaison détaillée de leur denture, plus complète que tout le matériel disponible dans l'Éocène inférieur (parfois préservée de la dernière molaire aux incisives), serait crucial pour proposer des déterminations mais n'a jamais été entreprise. En effet, (i) les taxons yprésiens n'avaient pas été révisés, et (ii) les quelques détails connus de leur morphologie dentaire n'ont pu être précisés qu'à partir d'images issues de radiographies au moment où les premiers travaux ont été conduits (Kurz et Habersetzer 2004), mais cela est déjà suffisant pour montrer qu'au moins un spécimen représente une espèce inconnue dans l'Éocène inférieur (Gernelle et al. 2024b : 16, Chapitre 5 ; voir aussi Chapitre 3 : Supplemental material 6). Certains de ces spécimens présentent des rangées dentaires supérieures et inférieures en position occlusale totale ou partielle (Kurz 2007 : figs. 9-10, 25), dont la morphologie est difficile à appréhender sans recours aux reconstructions de modèles 3D permises par les méthodes d'imagerie plus poussées (CT-scan). En s'appuyant sur ces dernières, l'utilisation du matériel crânien et postcrânien (dont les vertèbres caudales et les membres) préservé devrait permettre (i) de tester de nombreuses hypothèses phylogénétiques établies ici seulement à partir des dents, mais ayant des implications profondes pour une compréhension globale de l'histoire évolutive des marsupialiformes (Chapitre 3 ; voir par exemple le contenu taxonomique des Notometatheria et les relations non-consensuelles des Anatoliadelphyidae avec les métathériens européens cénozoïques), et (ii) d'envisager des études écomorphologiques intégrant les données nouvelles disponibles (e.g., morphologie de l'oreille interne), au regard d'un contexte phylogénétique. Sur ce dernier point, il a par exemple été montré durant cette thèse que les adaptations locomotrices des péradectidés et des herpétothériidés étaient déjà probablement distinctes à leur arrivée en Europe (Gernelle et al. 2024a : 41-42, Chapitre 1), et à partir des molaires que les régimes alimentaires

hypothétiques des péradectidés et des pérathériinés diffèrent peut-être par rapport à ceux envisagés à partir de la première étude du matériel de Messel (Gernelle et al. 2024b : 22, Chapitre 5).

Références bibliographiques (Introduction générale / Matériel et méthodes / Chapitre 6 / Conclusion générale)

Abels HA, Clyde WC, Gingerich PD, Hilgen FJ, Fricke HC, Bowen GJ, Lourens LJ (2012) Terrestrial carbon isotope excursions and biotic change during Palaeogene hyperthermals. Nature Geoscience 5(5): 326–329.

Alroy J (1998) Cope's rule and the dynamics of body mass evolution in North American fossil mammals. Science 280(5364): 731-734.

Andreas M, Reiter A, Cepáková E, Uhrin M (2013) Body size as an important factor determining trophic niche partitioning in three syntopic rhinolophid bat species. Biologia 68(1): 170-175.

Astúa D (2010) Cranial sexual dimorphism in New World marsupials and a test of Rensch's rule in Didelphidae. Journal of Mammalogy 91: 1011–1024.

Aumont A (2004) Première découverte d'espèces sympatriques de Paromomyidés (Plésiadapiformes, Mammifères) en Europe. Comptes Rendus Palevol, 3: 27-34.

Averianov AO, Archibald JD, Ekdale EG (2010) New material of the Late Cretaceous deltatheroidan mammal *Sulestes* from Uzbekistan and phylogenetic reassessment of the metatherian-eutherian dichotomy. Journal of Systematic Palaeontology 8: 301–330.

Aymard A (1850) Compte rendu de la séance du 12 avril 1849, réponse à M. Robert sur les mammifères fossiles des caclcaires du Puy. Annales de la Société d'agriculture, arts et commerce du Puy 14: 80-86.

Beard KC, Dawson MR (2009) Early Wasatchian mammals of the Red Hot local fauna, uppermost Tuscahoma Formation, Lauderdale County, Mississippi. Annals of Carnegie Museum 78: 193–243.

Beck RMD (2012) An 'ameridelphian'marsupial from the early Eocene of Australia supports a complex model of Southern Hemisphere marsupial biogeography. Naturwissenschaften 99(9): 715-729.

Beck RMD (2017) The skull of *Epidolops ameghinoi* from the early Eocene Itaboraí fauna, southeastern Brazil, and the affinities of the extinct marsupialiform order Polydolopimorphia. Journal of Mammalian Evolution 24(4): 373-414.

Beck RMD (2023) Diversity and phylogeny of marsupials and their stem relatives (Metatheria). In: Cáceres NC, Dickman CR (eds) American and Australasian Marsupials. Springer, Cham, Switzerland, pp 23–88.

Beck RMD, Voss RS, Jansa SA (2022) Craniodental morphology and phylogeny of marsupials. Bulletin of the American Museum of Natural History 457: 1-350.

Bi S, Zheng X, Wang X, Cignetti NE, Yang S, Wible JR (2018) An Early Cretaceous eutherian and the placental–marsupial dichotomy. Nature 558(7710): 390-395.

BiochroM'97 (1997) Synthèse et tableaux de corrélation. In: Aguilar JP, Legendre S, Michaux J (eds) Actes du Congrès BiochroM'97, Mémoires et travaux de l'EPHE 21. Montpellier: Ecole Pratique des Hautes Etudes, Institut de Montpellier, pp 769–805.

Boivin M, Orliac MJ, Telles Antunes M, Godinot M, Laurent Y, Marandat B, Vidalenc D, Tabuce R (2018) New material of *Diacodexis* (Mammalia, Artiodactyla) from the early Eocene of Southern Europe. Geobios 51: 285–306.

Brannick AL, Fulghum HZ, Grossnickle DM, Mantilla GPW (2023) Dental ecomorphology and macroevolutionary patterns of North American Late Cretaceous metatherians. Palaeontologia Electronica 26(3): 1-42.

Brikiatis L (2014) The De Geer, Thulean and Beringia routes: key concepts for understanding early Cenozoic biogeography. Journal of Biogeography 41: 1036-1054.

Bronnert C, Metais G (2023) Early Eocene hippomorph perissodactyls (Mammalia) from the Paris Basin. Geodiversitas 45: 277‑326.

Bronnert C, Gheerbrant, E, Godinot M, Métais G (2018) A primitive perissodactyl (Mammalia) from the early Eocene of Le Quesnoy (MP7, France). Historical Biology 30(1-2): 237-250.

Brum MN, Cáceres NC, Bubadué JM (2023) Evolutionary rates, disparity, and ecomorphology of the mandible in American marsupials. Journal of Mammalian Evolution 30: 33-46.

Carneiro LM, Oliveira ÉV (2023) Paleogene metatherians from the Itaboraí Basin: diversity and affinities. In: Cáceres NC, Dickman CR (eds) American and Australasian Marsupials. Springer, Cham, Switzerland, pp 269–324.

Carneiro LM, Goin FJ, Bampi H, Silva RC, Rangel CC, Guimarães BMG, Arêas MR (2024) A tiny-sized Herpetotheriidae (Mammalia, Metatheria) from the Itaboraí basin (early Eocene), Brazil: Paleobiogeographic and systematic implications for Herpetotheriidae. Journal of South American Earth Sciences 144.

Case JA, Goin FJ, Woodburne MO (2005) “South American” marsupials from the Late Cretaceous of North America and the origin of marsupial cohorts. Journal of Mammalian Evolution 12: 461-494.

Chemisquy MA, Prevosti FJ, Martin G, Flores DA (2015) Evolution of molar shape in didelphid marsupials (Marsupialia: Didelphidae): analysis of the influence of ecological factors and phylogenetic legacy. Zoological Journal of the Linnean Society. 173(1): 217–235.

Clemens WA (1966) Fossil mammals of the type Lance Formation, Wyoming. Part II, Marsupialia. University of California Publications in Geological Sciences 62: 1–122.

Coillot T, Smith R, Gigase P, Smith T (2013) Tarsal diversity in the earliest Eocene mammal fauna of Dormaal, Belgium. Geologica Belgica 16(4): 274–283.

Cojan I, Moreau MG, Stott LE (2000) Stable carbon isotope stratigraphy of the Paleogene pedogenic series of southern France as a basis for continental-marine correlation. Geology 28: 259–262.

Crespo VD, Goin FJ (2021) Taxonomy and affinities of african cenozoic metatherians. Spanish Journal of Palaeontology 36(2): 1–16.

Crespo VD, Goin FJ, Pickford M (2022) The last African metatherian. Fossil Record 25(1): 173–186.

Crochet JY (1969) Révision du genre *Peratherium* Aymard, 1849 (Marsupialia). Comptes Rendus de l’Académie des Sciences, Paris 268: 2038-2041.

Crochet JY (1977) Les Didelphidae (Marsupicarnivora, Marsupialia) holarctiques tertiaires. Comptes Rendus de l’Académie des Sciences de Paris. 284: 357-360.

Crochet JY (1979) Diversité systématique des Didelphidae (Marsupialia) européens tertiaires. Geobios. 12(3): 365–378.

Crochet JY (1980) Les marsupiaux du Tertiaire d’Europe. Edtions Foundation Singer-Polignac, Paris.

Crochet JY, Antoine PO, Benammi M, Iqbal N, Marivaux L, Metais G, Welcomme JL (2007) A herpetotheriid marsupial from the Oligocene of Bugti Hills, Balochistan, Pakistan. Acta Palaeontologica Polonica 52(3): 633-637.

Crochet JY, Godinot M, Hartenberger JL, Rémy JA, Sigé B, Sudre J (1988) Découverte dans le bassin de Saint-Martin-de-Londres (Hérault, Sud de la France) d’un gisement à vertébrés continentaux d’âge Eocène moyen. Courier Forschungsinstitut Senckenberg 107: 419-434.

Crochet JY, Hartenberger JL, Remy JA, Sudre J, Welcomme JL (1997) Découverte de vertébrés continentaux de l'Eocène moyen et supérieur dans le bassin des Matelles (Hérault, Sud de la France) et redécouverte du Lophiodon des Matelles. Géologie de la France 1: 33-45.

Crompton AW (1971) The origin of the tribosphenic molar. In: Kermack DM, Kermack KA (eds) Early Mammals. Zoological Journal of the Linnean Society 50 Suppl 1: 65–87

Crompton AW, Hiiemae K (1970) Molar occlusion and mandibular movements during occlusion in the American opossum, *Didelphis marsupialis* L. Zoological Journal of the Linnean Society 49: 21-47.

Cuvier G (1804) Mémoire sur le squelette presque entier d'un petit quadrupède du genre des sarigues, trouvé dans la pierre à plâtre des environs de Paris. Annales du Museum d'Histoire Naturelle 5(13): 277–292.

D'Ambrosia AR, Clyde WC, Fricke HC, Gingerich PD, Abels HA (2017) Repetitive mammalian dwarfing during ancient greenhouse warming events. Science Advances 3: e1601430.

Davis BM (2011) Evolution of the tribosphenic molar pattern in early mammals, with comments on the "dual-origin" hypothesis. Journal of Mammalian Evolution 18: 227-244.

Davis BM, Cifelli RL, Kielan-Jaworowska Z (2008) Earliest evidence of Deltatheroida (Mammalia: Metatheria) from the Early Cretaceous of North America. In: Sargis EJ, Dagosto M (eds) Mammalian evolutionary morphology: a tribute to Frederick S. Szalay. Springer, Dordrecht, pp 3–24.

Dégremont E, Duchaussois F, Hautefeuille F, Laurain M, Louis P, Tétu R (1985) Paléontologie: découverte d'un gisement du Cuisien tardif à Prémontré (Aisne). Bull Inf Géol Bass Paris 22(2): 11-18.

Eberle JJ, Greenwood DR (2012) Life at the top of the greenhouse Eocene world—a review of the Eocene flora and vertebrate fauna from Canada's High Arctic. Geological Society of America Bulletin 124(1-2): 3-23.

Edwards MJ, Deakin JE (2012) The marsupial pouch: implications for reproductive success and mammalian evolution. Australian Journal of Zoology, 61: 41-47.

Eldridge MD, Beck RM, Croft DA, Travouillon KJ, Fox BJ (2019) An emerging consensus in the evolution, phylogeny, and systematics of marsupials and their fossil relatives (Metatheria). Journal of Mammalogy 100(3): 802-837.

Engelman RK, Croft DA (2016) Evidence for sexual dimorphism in the early Miocene palaeothentid *Acdestis owenii* (Marsupialia: Paucituberculata). Ameghiniana 53(4): 444-462.

Engelman RK, Flynn JJ, Wyss AR, Croft DA (2020) *Eomakhaira molossus*, a new saber-toothed sparassodont (Metatheria: Thylacosmilinae) from the early Oligocene (? Tinguiririan) Cachapoal locality, Andean Main Range, Chile. American Museum Novitates 3957: 1-75.

Escarguel G (1999) Les rongeurs de l'Eocène inférieur et moyen d'Europe occidentale. Systématique, phylogénie, biochronologie et paléobiogéographie des niveaux repères MP 7 à MP 14. Palaeovertebrata 28: 89–351.

Estravís C (1992) Estudo dos mamíferos do Eocénico inferior de Silveirinha (Baixo Mondego). Thèse de doctorat non publiée, Faculdade de Ciências e Tecnologia, UNL, Lisboa, pp 1-254.

Estravís C (2000) Nuevos mamíferos del Eoceno Inferior de Silveirinha (Baixo Mondego, Portugal). Coloquios Paleontol 51: 281–311.

Filhol H (1879) Étude des Mammifères fossiles de Saint-Gérand-le-Puy. Annales des Sciences Géologiques. 10: 1–253.

Forasiepi AM, Sánchez-Villagra MR (2014) Heterochrony, dental ontogenetic diversity, and the circumvention of constraints in marsupial mammals and extinct relatives. Paleobiology 40(2): 222-237.

Fox RC (1983) Notes on the North American Tertiary marsupials *Herpetotherium* and *Peradectes*. Canadian Journal of Earth Sciences 20: 1565–1578.

Gao Y, Wu WH, Mao FY (2024) A new marsupialiform from Upper Cretaceous of Songliao Basin, Heilongjiang, China. Palaeoworld.

Gernelle K, Billet G, Gheerbrant E, Godinot M, Marandat B, Ladevèze S, Tabuce R (2024a) Taxonomy and evolutionary history of peradectids (Metatheria): new data from the early Eocene of France. Journal of Mammalian Evolution 31(3): 31.

Gernelle K, Godinot M, Marandat B, Téodori D, Ladevèze S, Tabuce R (2024b [early view online]) Dental morphology evolution in early peratheriines, including a new morphologically cryptic species and findings on the largest early Eocene European metatherian. Historical Biology.

Gingerich PD, Smith T (2006) Paleocene-Eocene land mammals from three new latest Clarkforkian and earliest Wasatchian Wash sites at Polecat Bench in the Northern Bighorn Basin. Contributions from the Museum of Paleontology, University of Michigan 31: 245–303.

Gingerich P, Folie A, Smith T (2023) *Didelphodus caloris,* New Species (Mammalia, Cimolesta), from the Wasatchian WA–0 Fauna of the Paleocene-Eocene Thermal Maximum, Clarks Fork Basin, Wyoming. Contributions from the Museum of Paleontology, University of Michigan 35(2): 34-35.

Godinot M (1981) Les mammifères de Rians (Eocène inférieur, Provence). Palaeovertebrata 10: 43–126.

Godinot M, Crochet JY, Hartenberger JL, Lange-Badré B, Russell DE, Sigé B (1987) Nouvelles données sur les mammifères de Palette (Eocène inférieur, Provence). Münchner geowissenschaftliche Abhandlungen (A) 10: 273-288.

Godthelp H, Wroe S, Archer M (1999) A new marsupial from the early Eocene Tingamarra Local Fauna of Murgon, southeastern Queensland: a prototypical Australian marsupial? Journal of Mammalian Evolution 6: 289-313.

Goin FJ, Candela AM, Muizon C de (2003) The affinities of *Roberthoffstetteria nationalgeographica* (Marsupialia) and the origin of the polydolopine molar pattern. Journal of Vertebrate Paleontology 23: 869-876.

Goin FJ, Pascual R, Tejedor MF, Gelfo JN, Woodburne MO, Case JA, Reguero MA, Bond M, López GM, Cione AL, et al. (2006) The earliest Tertiary therian mammal from South America. Journal of Vertebrate Paleontology 26(2): 505-510.

Goin FJ, Woodburne MO, Zimicz AN, Martin GM, Chornogubsky L (2016) A Brief History of South American Metatherians: Evolutionary Contexts and Intercontinental Dispersals. Springer, Dordrecht, Netherlands.

Hartenberger JL, Sigé B, Sudre J (1969) Les gisements de vertébrés de la région montpelliéraine (1. gisements éocènes). Bulletin du Bureau de Recherches géologiques et minières – BRGM 2(1) : 7-18.

Hayes FG (2005) Arikareean (Oligocene-Miocene) *Herpetotherium* (Marsupialia, Didelphidae) from Nebraska and Florida. Bulletin of the Florida Museum of Natural History 45: 335–353.

Hershkovitz P (1997) Composition of the family Didelphidae Gray, 1821 (Didelphoidea: Marsupialia), with a review of the morphology and behavior of the included four-eyed pouched opossums of the genus *Philander* Tiedemann, 1808. Fieldiana Zoology 86: 1–103.

Hoek Ostende LW van de, Bilgin M, Braumuller Y, Cailleux F, Skandalos P (2023) Live long and prosper? Assessing longevity of small mammal taxa using the NOW database. In: Casanovas-Vilar I, Hoek Ostende LW van de, Janis CM, Saarinen J (eds) Evolution of Cenozoic Land Mammal Faunas and Ecosystems: 25 Years of the NOW Database of Fossil Mammals, Vertebrate Paleobiology and Paleoanthropology. Springer, Cham, Switzerland, pp. 111–129.

Hooker JJ (1996a) Mammalian biostratigraphy across the Paleocene-Eocene boundary in the Paris, London and Belgian basins. In: Knox RWOB, Corfield RM, Dunay RE (eds) Correlation of the Early Paleogene in Northwest Europe. Geological Society of London, Special Publication 101, pp 205–218.

Hooker JJ (1996b) Mammals from the Early (late Ypresian) to Middle (Lutetian) Eocene Bracklesham Group, southern England. Tertiary Research 16(1–4): 141–174.

Hooker JJ (1998) Mammalian faunal change across the Paleocene-Eocene transition in Europe. In: Aubry MP, Berggren WA, Lucas SG (eds) Late Paleocene-Early Eocene Climatic and Biotic Events in the Marine and Terrestrial Records. Columbia University Press, New York, pp 419–441.

Hooker JJ (2000) Ecological response of mammals to global warming in the late Paleocene and early Eocene. Geologiska Föreningens Förhandlingen 122(1): 77–79.

Hooker JJ (2010) The mammal fauna of the early Eocene Blackheath formation of Abbey Wood, London. Monographs of the Palaeontographical Society 164: 1–153.

Hooker JJ (2015) A two-phase mammalian dispersal event across the Paleocene–Eocene transition. Newsletters on Stratigraphy 48: 201–220.

Hooker JJ (2020) A mammal fauna from the Paleocene-Eocene Thermal Maximum of Croydon, London, UK. Proceedings of the Geologists Association 131: 458–473.

Hooker JJ, Sánchez-Villagra MR, Goin FJ, Simons EL, Attia Y, Seiffert ER (2008) The origin of Afro-Arabian 'didelphimorph' marsupials. Palaeontology 51: 635-648.

Horovitz I, Martin T, Bloch J, Ladeveze S, Kurz C, Sanchez-Villagra MR (2009) Cranial anatomy of the earliest marsupials and the origin of opossums. PLoS One 4: 1‑9.

Jernvall J, Jung HS (2000) Genotype, phenotype, and developmental biology of molar tooth characters. American Journal of Physical Anthropology 113: 171–190.

Johanson Z (1994) New information concerning the late Cretaceous marsupial *Albertatherium* Fox, 1971. Journal of Vertebrate Paleontology 14(4): 595-602.

Kielan-Jaworowska Z (1975) Evolution of the therian mammals in the Late Cretaceous of Asia. Part I. Deltatheridiidae. Palaeontologia Polonica, 33(10): 103-132.

Kielan-Jaworowska Z, Cifelli RL, Luo ZX (2004) Mammals from the Age of Dinosaurs: Origins, Evolution, and Structure. Columbia University Press.

Korth WW (2008) Marsupialia. In: Janis CM, Gunnell GF, Uhen MD (eds) Evolution of Tertiary Mammals of North America: Volume 2, Small Mammals, Xenarthrans, and Marine Mammals. Cambridge University Press, Cambridge, pp 39–47.

Korth WW (2015) Mammals from the Blue Ash Local Fauna (late Oligocene), South Dakota. Additional specimens of *Herpetotherium* Cope (Marsupialia, Didelphidae). Paludicola 10: 113-118.

Korth WW (2018) Review of the marsupials (Mammalia: Metatheria) from the late Paleogene (Chadronian–Arikareean: late Eocene–late Oligocene) of North America. PalZ 92: 499-523.

Korth WW, Boyd CA, Emry RJ, Person JJ (2021) Marsupials (Mammalia, Metatheria) from the Brule Formation (Whitneyan, Oligocene) North Dakota. Journal of Paleontology 95(1): 193-204.

Krishtalka L, Stucky RK (1983) Paleocene and Eocene marsupials of North America. Annals of Carnegie Museum 52: 229–263.

Kurz C (2007) The opossum-like marsupials (Didelphimorphia and Peradectia, Marsupialia, Mammalia) from the Eocene of Messel and Geiseltal – Ecomorphology, diversity and palaeogeography. Kaupia 15: 3–65.

Kurz C, Habersetzer J (2004) Untersuchungen der zahnmorphologie von beutelratten aus Messel mit der mikroröntgenmethode CORR. Courier Forschungsinstitut Senckenberg 252: 13–21.

Ladevèze S, Muizon C de, Beck RMD, Germain D, Cespedes-Paz R (2011) Earliest evidence of mammalian social behaviour in the basal Tertiary of Bolivia. Nature 474: 83–86.

Ladevèze S, Selva C, Muizon C de (2020) What are “opossum-like” fossils? The phylogeny of herpetotheriid and peradectid metatherians, based on new features from the petrosal anatomy. Journal of Systematic Palaeontology 18(17): 1463–1479.

Ladevèze S, Smith R, Smith T (2012) Reassessment of the morphology and taxonomic status of the earliest herpetotheriid marsupials of Europe. Journal of Mammalian Evolution 19: 249–261.

Laurent Y, Adnet S, Bourdon E, Corbalan D, Danilo L, Duffaud S, Fleury G, Garcia G, Godinot M, Le Roux G, et al (2010) La Borie (Saint-Papoul, Aude): un gisement exceptionnel dans l’Éocène basal du Sud de la France. Bulletin de la Société d’Histoire Naturelle de Toulouse 146: 89–103.

Lavocat AR (1951) Révision de la faune des mammifères oligocènes d'Auvergne et du Velay. Éditions Sciences et Avenir, Paris, France.

Legendre S, Hartenberger JL (1992) Evolution of mammalian faunas in Europe during the Eocene and Oligocene. In: Prothero DA, Berggren WA (eds) Eocene-Oligocene Climatic and Biotic Evolution. Princeton University Press, Princeton, pp 516-528.

Legendre S, Marandat B, Sigé B, Crochet JY, Godinot M, Hartenberger JL, Sudre J, Vianey-Liaud M, Muratet B, Astruc JG (1992) La faune de mammifères de Vielase (phosphorites du Quercy, Sud de la France): Preuve paléontologique d’une karstification du Quercy dès l’Eocène inférieur. Neues Jahrb Geol Paläontol. 7:414–428.

Louis P (1970) Note préliminaire sur un gisement de mammifères de l’Éocène inferieur situé Route de Broyes a Sézanne (Marne). Ann Univ A.R.E.R.S. Reims 8: 48‑62.

Louis P (1996) Recherches de mammifères paléogènes dans les départements de l’Aisne et de la Marne pendant la deuxième moitié du vingtième siècle. Palaeovertebrata 25: 83–113.

Louis P, Laurain M (1983) Nouveau gisement de vertébrés dans le Cuisien supérieur de Saint-Agnan (Aisne). Ses relations stratigraphiques avec les autres gisements yprésiens du Bassin parisien. Bull Inf Géol Bass Paris 20: 3–20.

Maga AM, Beck, RM (2017) Skeleton of an unusual, cat-sized marsupial relative (Metatheria: Marsupialiformes) from the middle Eocene (Lutetian: 44-43 million years ago) of Turkey. PLoS One 12(8): e0181712.

Magnus LZ, Cáceres N (2017) Phylogeny explains better than ecology or body size the variation of the first lower molar in didelphid marsupials. Mammalia 81(2): 119-133.

Marandat B (1986) Découverte d’une faune de micromammiferes d’âge cuisien superieur dans les marno-calcaires d’Agel à Azillanet (Minervois, Hérault). Géologie de la France 2: 197–204.

Marandat, B (1987) La biostratigraphie mammalienne de l’Eocène continental du versant sud de la Montagne Noire. Reconsidération d’après les nouvelles données. Münchner Geowissenschaftlichs Abhandlungen (A) 10: 149-158.

Marandat B (1991) Mammifères de l’Ilerdien Moyen (Eocène Inférieur) des Corbières et du Minervois. Palaeovertebrata 20: 55–144.

Marandat B (1997) La disparité des faunes mammaliennes du niveau MP 7 (Eocene inferieur) des domaines peri-mesogeens et nordiques. Investigation d’un provincialisme intra-europeen. Newsletters on Stratigraphy 35: 63–82.

Marandat B, Adnet S, Marivaux L, Martinez A, Vianey-Liaud M, Tabuce R (2012) A new mammalian fauna from the earliest Eocene (Ilerdian) of the Corbières (Southern France): Palaeobiogeographical implications. Swiss Journal of Geosciences 105: 417–434.

Marivaux L, Vianey-Liaud M, Jaeger JJ (2004) High-level phylogeny of early Tertiary rodents: dental evidence. Zoological Journal of the Linnean Society 142: 105-134.

Martin JE, Case JA, Jagt JW, Schulp AS, Mulder EW (2005) A new European marsupial indicates a Late Cretaceous high-latitude transatlantic dispersal route. Journal of Mammalian Evolution 12(3-4): 495-511.

McKay CJ, Luckett WP, Sánchez-Villagra MR (2023) Vestigial structures and variation in the evolution of the marsupial mammal dental development—a study of the woolly opossum *Caluromys philander*. Journal of Mammalian Evolution 30: 21-31.

Métais G, Coster PM, Kappelman JR, Licht A, Ocakoğlu F, Taylor MH, Beard KC (2018) Eocene metatherians from Anatolia illuminate the assembly of an island fauna during Deep Time. PloS ONE 13(11): e0206181.

Morlo M, Schaal S, Mayr G, Seiffert C (2004) An annotated taxonomic list of the Middle Eocene (MP 11) Vertebrata of Messel. Courier Forschungsinstitut Senckenberg 252: 95-108.

Muizon C de, Ladevèze S (2020) Cranial anatomy of *Andinodelphys cochabambensis*, a stem metatherian from the early Paleocene of Bolivia. Geodiversitas 42: 597-739.

Muizon C de, Ladevèze S (2022) New material of *Incadelphys antiquus* (Pucadelphyda, Metatheria, Mammalia) from the early Palaeocene of Bolivia reveals phylogenetic affinities with enigmatic North and South American metatherians. Geodiversitas 44: 609–643.

Murphey PC, Kelly TS, Chamberlain KR, Tsukui K, Clyde WC (2018) Mammals from the earliest Uintan (middle Eocene) Turtle Bluff Member, Bridger Formation, southwestern Wyoming, USA, Part 3: Marsupialia and a reevaluation of the Bridgerian-Uintan North American Land Mammal Age transition. Palaeontologia Electronica 21(2): 25A.

Nel A, de Plöeg G, Dejax J, Dutheil D, de Franceschi D, Gheerbrant E, Godinot M, Hervet S, Menier JJ, Augé M, et al. (1999) Un gisement sparnacien exceptionnel à plantes, arthropodes et vertébrés (Éocène basal, MP7): Le Quesnoy (Oise, France). Comptes Rendus de l'Académie des Sciences de Paris. 329: 65–72.

Ni X, Li Q, Stidham TA, Li L, Lu X, Meng J (2016) A late Paleocene probable metatherian (? deltatheroidan) survivor of the Cretaceous mass extinction. Scientific Reports 6: 38547.

Noiret C, Steurbaut E, Tabuce R, Marandat B, Schnyder J, Storme JY, Yans J (2016) New bio-chemostratigraphic dating of a unique early sequence from southern results in precise mammalian biochronological tie-points. Newsletters in Stratigraphy 49: 469–480.

O'Leary MA, Bloch JI, Flynn JJ, Gaudin TJ, Giallombardo A, Giannini NP, Goldberg SL, Kraatz BP, Luo ZX, Meng J, Ni X, Novacek MJ, Perini FA, Randall ZS, Rougier GW, Sargis EJ, Silcox MT, Simmons NB, Spaulding M, Velazco PM, Weksler M, Wible JR, Cirranello AL (2013) The placental mammal ancestor and the Post-K-Pg radiation of placentals. Science 339: 662–667.

Parés-Casanova PM (2024) Análisis morfométrico de la mandíbula en tres especies de *Didelphis* de Colombia. Revista Mexicana de Mastozoología (Nueva Época) 14(1): 23-31.

Peláez-Campomanes P, Peña A de la, López-Martínez N (1989) Primeras faunas de micromamíferos del Paleógeno de La Cuenca del Duero. Studia Geológica Salmanticensia Volumen especial E: 135-157.

Rankin BD, Fox JW, Barrón-Ortiz CR, Chew AE, Holroyd PA, Ludtke JA, Yang X, Theodor JM (2015) The extended Price equation quantifies species selection on mammalian body size across the Palaeocene/Eocene Thermal Maximum. Proceedings of the Royal Society B: Biological Sciences 282(1812): 20151097.

Rose KD (2012) The importance of Messel for interpreting Eocene Holarctic mammalian faunas. Palaeobiodiversity and Palaeoenvironments 92: 631‑647.

Russell DE, Galoyer A, Louis P, Gingerich PD (1988) Nouveaux vertébrés sparnaciens du Conglomérat de Meudon à Meudon, France. Comptes Rendus de l'Académie des Sciences de Paris. 307: 429–433.

Sánchez-Villagra MR (2013) Why are there fewer marsupials than placentals? On the relevance of geography and physiology to evolutionary patterns of mammalian diversity and disparity. Journal of Mammalian Evolution 20: 279-290.

Sánchez-Villagra M, Ladevèze S, Horovitz I, Argot C, Hooker JJ, Macrini TE, Martin T, Moore-Fay S, Muizon C de, Schmelzle T, Asher RJ (2007) Exceptionally preserved North American Paleogene metatherians: Adaptations and discovery of a major gap in the opossum fossil record. Biology Letters 3: 318–322.

Schmidt-Kittler N, Godinot M, Franzen JL, Hooker JJ, Legendre S, Brunet M, Vianey-Liaud M (1987) European reference levels and correlation tables. Munch Geowiss Abh (A) 10: 13–31.

Selva C, Ladevèze S (2017) Computed microtomography investigation of the skull of Cuvier's famous 'opossum' (Marsupialiformes, Herpetotheriidae) from the Eocene of Montmartre. Zoological Journal of the Linnean Society 180: 672-693.

Simpson GG (1928) American Eocene didelphids. American Museum Novitates 307: 1–7.

Smith T (2000) Mammals from the Paleocene-Eocene transition in Belgium (Tienen formation, MP7): palaeobiogeographical and biostratigraphical implications. GFF 122: 148–149.

Smith R, Russell DE (1992) Mammifères (Marsupialia, Chiroptera) de l'Yprésien de la Belgique. Bulletin de l'Institut Royal des Sciences Naturelles de Belgique, Sciences de la Terre 62: 223–227.

Smith R, Smith T (2004) Les mammifères de l'Yprésien moyen du Bassin de Paris (niveau-repère MP8-9) sont-ils présents dès la limite Paléocène-Eocène de Dormaal (niveau-repère MP7, Belgique)? Oryctos 5: 75–82.

Smith T, Smith R (1995) Le genre *Dormaalius* Quinet, 1964 de l'Éocène inférieur de Belgique, synonyme du genre *Macrocranion* Weitzel, 1949 (Mammalia, Lipotyphla). Geological Survey of Belgium Professional Paper 274: 1-20.

Smith T, Smith R (2013) A land micro-mammal fauna from the Early Eocene marine Egem deposits (NP12, Belgium) and the first occurrence of the peradectid marsupial Armintodelphys outside North America. Geologica Belgica 16(4): 302–310.

Smith T, Dupuis C, Folie A, Quesnel F, Storme JY, Iacumin P, Riveline J, Missiaen P, Ladevèze S, Yans J (2011) Un nouveau site à vertébrés terrestres juste après la limite Paléocène-Eocène, dans la Formation de Mortemer en Haute-Normandie, France. Comptes Rendus Palevol 10: 11–20.

Smith T, Rose KD, Gingerich PD (2006) Rapid Asia–Europe–North America geographic dispersal of earliest Eocene primate Teilhardina during the Paleocene–Eocene thermal maximum. Proceedings of the National Academy of Sciences 103(30): 11223-11227.

Solé F, Falconnet J, Laurent Y (2014) New proviverrines (Hyaenodontida) from the early Eocene of Europe; phylogeny and ecological evolution of the Proviverrinae. Zoological Journal of the Linnean Society 171(4): 878-917.

Steurbaut E, Coninck J de, Van Simaeys S (2016) Micropalaeontological dating of the Prémontré mammal fauna (MP10, Prémontré Sands, Eeco, early late Ypresian, Paris Basin). Geologica Belgica. 19(3-4): 273-280.

Storch G, Haubold H (1989) Additions of the Geiseltal mammalian faunas, Middle Eocene: Didelphidae, Nyctitheriidae, Myrmecophagidae. Palaeovertebrata. 19(3): 95–114.

Szalay FS (1993) Metatherian taxon phylogeny: Evidence and interpretation from the cranioskeletal system. In: Szalay FS, Novacek MJ, McKenna MC (eds) Mammal Phylogeny, Vol. 1. Mesozoic Differentiation, Multituberculates, Monotremes, Early Therians, and Marsupials. Springer-Verlag, New-York, pp 216-242.

Szalay FS, Trofimov BA (1996) The Mongolian Late Cretaceous *Asiatherium*, and the early phylogeny and paleobiogeography of Metatheria. Journal of Vertebrate Paleontology 16: 474–509.

Teilhard de Chardin P (1927) Les mammifères de l'Eocène inférieur de la Belgique. Mém Mus R Sci Nat Belg (Prem Sér) 36: 1–33.

Vianey-Liaud M, Lihoreau F, Solé F, Gernelle K, Vautrin Q, Bronnert C, Bourget H, Vidalenc D, Tabuce R (2024). A revision of the late early Eocene mammal faunas from Mas de Gimel and Naples (Montpellier, Southern France) and the description of a new theridomorph rodent. Geodiversitas 46(10): 387-422.

von Koenigswald W (1970) *Peratherium* (Marsupialia) im Ober-Oligozän und Miozän von Europa. Bayer Akad Wiss Math-Natur Kl Abh (NF) 144: 1–79.

Vullo R, Gheerbrant E, Muizon C de, Néraudeau D (2009) The oldest modern therian mammal from Europe and its bearing on stem marsupial paleobiogeography. Proceedings of the National Academy of Sciences 106: 19910–19915.

Vullo R, Gheerbrant E, Beurel S, Swajda M, Néraudeau, D (2020) A stagodontid mammal from the mid-Cretaceous of France confirms the Euramerican distribution of early marsupialiforms. Palaeogeography, Palaeoclimatology, Palaeoecology 560: 110034.

Wessels W, van de Weerd AA, Marković Z (2024) Marsupials (herpetotheriids) from the late Palaeogene of south-east Serbia. Palaeobiodiversity and Palaeoenvironments.

Westerhold T, Röhl U, Donner B, Zachos JC (2018) Global extent of early Eocene hyperthermal events: A new Pacific benthic foraminiferal isotope record from Shatsky Rise (ODP Site 1209). Paleoceanography and Paleoclimatology 33(6): 626-642.

Wickham H (2016) ggplot2: Elegant graphics for data analysis. Use R!, Springer.

Williamson TE, Brusatte SL, Carr TD, Weil A, Standhardt BR (2012) The phylogeny and evolution of Cretaceous-Palaeogene metatherians: Cladistic analysis and description of new early Palaeocene specimens from the Nacimiento Formation, New Mexico. Journal of Systematic Palaeontology 10: 625–651.

Williamson TE, Brusatte SL, Wilson GP (2014) The origin and early evolution of metatherian mammals: The Cretaceous record. Zookeys 465: 1–76.

Wilson GP (2014) Mammalian extinction, survival, and recovery dynamics across the Cretaceous-Paleogene boundary in northeastern Montana, USA. In: Wilson GP, Clemens WA, Horner JR, Hartman JH (eds) Through the end of the Cretaceous in the type locality of the Hell Creek Formation in Montana and adjacent areas. The Geological Society of America, Special Papers 503, pp. 365-392.

Wing SL, Harrington GJ, Smith FA, Bloch JI, Boyer DM, Freeman KH (2005) Transient floral change and rapid global warming at the Paleocene-Eocene boundary. Science 310(5750): 993-996.

Yans J, Marandat B, Masure E, Serra-Kiel J, Schnyder J, Storme JY, Marivaux L, Adnet S, Vianey-Liaud M, Tabuce R (2014) Refined bio-(benthic foraminifera, dinoflagellate cysts) and hemostratigraphy (δ13Corg) of the earliest Eocene at Albas-Le Clot (Corbières, France): Implications for mammalian biochronology in Southern Europe. Newsletters in Stratigraphy 47: 331–353.

Zachos JC, Dickens GR, Zeebe RE (2008) An early Cenozoic perspective on greenhouse warming and carbon-cycle dynamics. Nature 451: 279-283.

Zachos JC, Pagani M, Sloan L, Thomas E, Billups K (2001) Trends, rhythms, and aberrations in global climate 65 Ma to present. Science 292(5517): 686-693.

Annexes

Tableau S1. Détail des valeurs (en mm) de longueur mésiodistale (L) et de largeur labiolinguale (W) mesurées en vue occlusale sur les dents jugales de *Peratherium constans* Teilhard de Chardin, 1927, et de *Peratherium matronense* Crochet, 1979. Les ratios L / W sont calculés. Les spécimens sont ordonnés par espèce, par âge, par localité, puis par locus dentaire. Abréviations concernant l'âge des localités : FMG, Fournes – Monze – La Gasque ; MP7, niveau-repère MP7 ; [MP7-MP8+9] - FMG, intervalle de temps MP7-MP8+9 n'incluant pas FMG ; (~)MP8+9, niveau-repère MP8+9 ou ~MP8+9.

Spécimen	Espèce	Âge	Localité	Locus	L (mm)	W (mm)	L / W
DIIA 1790 RS	*Pt. constans*	MP7	Dormaal	M1	1,5	1,43	1,05
DIII 570 RS	*Pt. constans*	MP7	Dormaal	M1	1,58	1,56	1,01
DIIC 982 RS	*Pt. constans*	MP7	Dormaal	M1	1,59	1,5	1,06
DIIC 986 RS	*Pt. constans*	MP7	Dormaal	M1		1,56	
DIIA 1299 RS	*Pt. constans*	MP7	Dormaal	M1	1,56	1,46	1,07
DIIA 1504 RS	*Pt. constans*	MP7	Dormaal	M1	1,5	1,4	1,07
DIIC 2200 RS	*Pt. constans*	MP7	Dormaal	M1	1,42	1,51	0,94
DIII 804 RS	*Pt. constans*	MP7	Dormaal	M1	1,44	1,43	1,01
DIII 2226 RS	*Pt. constans*	MP7	Dormaal	M1	1,54	1,58	0,97
DIIA 1734 RS	*Pt. constans*	MP7	Dormaal	M1	1,46	1,44	1,01
DIII 2150 RS	*Pt. constans*	MP7	Dormaal	M1	1,4	1,5	0,93
DIIA 1731 RS	*Pt. constans*	MP7	Dormaal	M1	1,48	1,45	1,02
DIII 42 S	*Pt. constans*	MP7	Dormaal	M1	1,51	1,45	1,04
DIII 1159 RS	*Pt. constans*	MP7	Dormaal	M1	1,6	1,56	1,03
DIII 132 S	*Pt. constans*	MP7	Dormaal	M1	1,52	1,65	0,92
DIIC 1335 RS	*Pt. constans*	MP7	Dormaal	M1	1,51	1,43	1,06
DIIC 1225 RS	*Pt. constans*	MP7	Dormaal	M1	1,49	1,42	1,05
DI 1480 RS	*Pt. constans*	MP7	Dormaal	M1	1,49	1,45	1,03
DIII 39 S	*Pt. constans*	MP7	Dormaal	M1	1,44	1,44	1,00
DIII 35 S	*Pt. constans*	MP7	Dormaal	M1	1,57	1,55	1,01
DIII 38 S	*Pt. constans*	MP7	Dormaal	M1	1,53	1,59	0,96
DI 2261 RS	*Pt. constans*	MP7	Dormaal	M2	1,63	1,72	0,95
DIIC 1947 RS	*Pt. constans*	MP7	Dormaal	M2	1,53	1,66	0,92
DI 2263 RS	*Pt. constans*	MP7	Dormaal	M2	1,64	1,74	0,94
DIIC 1544 RS	*Pt. constans*	MP7	Dormaal	M2	1,5	1,73	0,87
DIIC 1948 RS	*Pt. constans*	MP7	Dormaal	M2	1,45	1,57	0,92
DIIC 1087 RS	*Pt. constans*	MP7	Dormaal	M2	1,48	1,65	0,90
DIIA 1296 RS	*Pt. constans*	MP7	Dormaal	M2	1,47	1,8	0,82
DIIC 1943 RS	*Pt. constans*	MP7	Dormaal	M2	1,59	1,69	0,94
DIIC 1226 RS	*Pt. constans*	MP7	Dormaal	M2	1,49	1,61	0,93
DIIC 985 RS	*Pt. constans*	MP7	Dormaal	M2	1,55	1,68	0,92
D 2431 MA	*Pt. constans*	MP7	Dormaal	M2	1,4	1,67	0,84
DIIC 1667 RS	*Pt. constans*	MP7	Dormaal	M2		1,6	
DIIC 1945 RS	*Pt. constans*	MP7	Dormaal	M2		1,67	
DIIC 2028 RS	*Pt. constans*	MP7	Dormaal	M2	1,46	1,69	0,86
DIIC 725 RS	*Pt. constans*	MP7	Dormaal	M2	1,63	1,79	0,91
DIII 40 S	*Pt. constans*	MP7	Dormaal	M2	1,57	1,72	0,91
DIIC 1086 RS	*Pt. constans*	MP7	Dormaal	M2	1,41	1,51	0,93
DIIA 1730 RS	*Pt. constans*	MP7	Dormaal	M2	1,56	1,73	0,90
DIIA 1729 RS	*Pt. constans*	MP7	Dormaal	M2	1,61	1,7	0,95

DIII 420 RS	*Pt. constans*	MP7	Dormaal	M2	1,51	1,71	0,88
DIII 852 RS	*Pt. constans*	MP7	Dormaal	M2	1,45	1,69	0,86
DIIC 1946 RS	*Pt. constans*	MP7	Dormaal	M2	1,52	1,76	0,86
DIIC 722 RS	*Pt. constans*	MP7	Dormaal	M2	1,49	1,65	0,90
DIII 571 RS	*Pt. constans*	MP7	Dormaal	M2	1,57	1,71	0,92
DI 2262 RS	*Pt. constans*	MP7	Dormaal	M2	1,58	1,72	0,92
DIIC 1332 RS	*Pt. constans*	MP7	Dormaal	M2	1,47	1,58	0,93
DIII 422 RS	*Pt. constans*	MP7	Dormaal	M2	1,47	1,57	0,94
DIII 1852 RS	*Pt. constans*	MP7	Dormaal	M2	1,51	1,68	0,90
DIIC 1944 RS	*Pt. constans*	MP7	Dormaal	M2	1,57	1,68	0,93
DIII 2149 RS	*Pt. constans*	MP7	Dormaal	M2	1,49	1,66	0,90
DIIC 1231 RS	*Pt. constans*	MP7	Dormaal	M2		1,78	
DIIC 1085 RS	*Pt. constans*	MP7	Dormaal	M2	1,5	1,57	0,96
DIII 801 RS	*Pt. constans*	MP7	Dormaal	M2	1,52	1,87	0,81
DIII 34 S	*Pt. constans*	MP7	Dormaal	M2	1,57	1,74	0,90
DIIC 2029 RS	*Pt. constans*	MP7	Dormaal	M2	1,59	1,69	0,94
DIII 568 RS	*Pt. constans*	MP7	Dormaal	M2	1,49	1,67	0,89
DII 2275	*Pt. constans*	MP7	Dormaal	M3	1,38		
DIII 2399 RS	*Pt. constans*	MP7	Dormaal	M3	1,37	1,74	0,79
DIIA 874 RS	*Pt. constans*	MP7	Dormaal	M3	1,39	1,77	0,79
DIII 854 RS	*Pt. constans*	MP7	Dormaal	M3	1,4	1,77	0,79
DIIC 1084 RS	*Pt. constans*	MP7	Dormaal	M3	1,44	1,86	0,77
DIIC 1221 RS	*Pt. constans*	MP7	Dormaal	M3	1,52	1,78	0,85
DIII 36S	*Pt. constans*	MP7	Dormaal	M3	1,45	1,72	0,84
DIIC 1668 RS	*Pt. constans*	MP7	Dormaal	M3	1,42	1,73	0,82
DIIC 1227 RS	*Pt. constans*	MP7	Dormaal	M3	1,38	1,72	0,80
DIII 853 RS	*Pt. constans*	MP7	Dormaal	M3	1,46	1,81	0,81
DIIC 2030 RS	*Pt. constans*	MP7	Dormaal	M3	1,49	1,74	0,86
DIIA 828 RS	*Pt. constans*	MP7	Dormaal	M3		1,74	
DIIC 1228	*Pt. constans*	MP7	Dormaal	M3	1,5	1,87	0,80
DIIC 726 RS	*Pt. constans*	MP7	Dormaal	M3	1,42	1,75	0,81
DIII 1158 RS	*Pt. constans*	MP7	Dormaal	M3	1,47	1,76	0,84
DIIA 1302 RS	*Pt. constans*	MP7	Dormaal	M3	1,47	1,72	0,85
DIIC 2031 RS	*Pt. constans*	MP7	Dormaal	M3	1,3	1,76	0,74
DIIC 724 RS	*Pt. constans*	MP7	Dormaal	M3	1,47	1,82	0,81
DIII 567 RS	*Pt. constans*	MP7	Dormaal	M3	1,43	1,81	0,79
DIIC 1230 RS	*Pt. constans*	MP7	Dormaal	M3	1,34	1,68	0,80
DIIC 719 RS	*Pt. constans*	MP7	Dormaal	M3	1,51	1,78	0,85
DIII 569 RS	*Pt. constans*	MP7	Dormaal	M3	1,47	1,68	0,88
DIII 802 RS	*Pt. constans*	MP7	Dormaal	M3	1,37		
DIIC 721 RS	*Pt. constans*	MP7	Dormaal	M3	1,52	1,88	0,81
DIIA 1791 RS	*Pt. constans*	MP7	Dormaal	M3	1,47	1,8	0,82
DI 2067 RS	*Pt. constans*	MP7	Dormaal	M3	1,38	1,75	0,79
DI 2264 RS	*Pt. constans*	MP7	Dormaal	M3	1,47	1,88	0,78
DIIC 2025 RS	*Pt. constans*	MP7	Dormaal	M3	1,5	1,82	0,82
DIIC 2026 RS	*Pt. constans*	MP7	Dormaal	M3	1,3	1,69	0,77
DIIA 1298 RS	*Pt. constans*	MP7	Dormaal	M3	1,47	1,67	0,88
DIIC 557 RS	*Pt. constans*	MP7	Dormaal	M3	1,43	1,9	0,75
DIIA 1300 RS	*Pt. constans*	MP7	Dormaal	M3	1,5	1,8	0,83
DIIC 1949 RS	*Pt. constans*	MP7	Dormaal	M3	1,39	1,84	0,76
DI 2066 RS	*Pt. constans*	MP7	Dormaal	M3	1,43	1,77	0,81

DIIC 980 RS	*Pt. constans*	MP7	Dormaal	M3	1,44	1,85	0,78
DIIC 1543 RS	*Pt. constans*	MP7	Dormaal	M3	1,47	1,78	0,83
DIIC 133- RS	*Pt. constans*	MP7	Dormaal	M3	1,44	1,87	0,77
DI 1482 RS	*Pt. constans*	MP7	Dormaal	M3	1,62	1,92	0,84
DI 2260 RS	*Pt. constans*	MP7	Dormaal	M3	1,38	1,78	0,78
DIII 851 RS	*Pt. constans*	MP7	Dormaal	M3	1,48	1,8	0,82
DIIC 2019 RS	*Pt. constans*	MP7	Dormaal	m1	1,46	0,78	1,87
DIIC 2018 RS	*Pt. constans*	MP7	Dormaal	m1	1,39	0,77	1,81
DIIA 1797 RS	*Pt. constans*	MP7	Dormaal	m1	1,39	0,79	1,76
DIIC 2101 RS	*Pt. constans*	MP7	Dormaal	m1	1,42	0,75	1,89
DIII 45 S	*Pt. constans*	MP7	Dormaal	m1	1,44	0,83	1,73
DIIA 2123 RS	*Pt. constans*	MP7	Dormaal	m1	1,29	0,69	1,87
DIIC 1650 RS	*Pt. constans*	MP7	Dormaal	m1	1,31	0,82	1,60
DIIC 1098 RS	*Pt. constans*	MP7	Dormaal	m1	1,41	0,73	1,93
DIIA 1739 RS	*Pt. constans*	MP7	Dormaal	m1	1,43	0,77	1,86
DIIC 2197 RS	*Pt. constans*	MP7	Dormaal	m1	1,43	0,79	1,81
DIIA 1743 RS	*Pt. constans*	MP7	Dormaal	m1	1,48	0,79	1,87
DI 2270 RS	*Pt. constans*	MP7	Dormaal	m1	1,31	0,75	1,75
DIIA 1304 RS	*Pt. constans*	MP7	Dormaal	m1	1,49	0,82	1,82
DIIC 1115 RS	*Pt. constans*	MP7	Dormaal	m1	1,37	0,75	1,83
DIIA 1510 RS	*Pt. constans*	MP7	Dormaal	m1	1,47	0,8	1,84
DIIC 1099 RS	*Pt. constans*	MP7	Dormaal	m1	1,45	0,78	1,86
DIIA 1800 RS	*Pt. constans*	MP7	Dormaal	m1	1,43	0,82	1,74
DIIC 1955 RS	*Pt. constans*	MP7	Dormaal	m1	1,37	0,71	1,93
DIIC 1101 RS	*Pt. constans*	MP7	Dormaal	m1	1,38	0,79	1,75
DIIC 1110 RS	*Pt. constans*	MP7	Dormaal	m1	1,44	0,79	1,82
DIIA 831 RS	*Pt. constans*	MP7	Dormaal	m1	1,46	0,83	1,76
DII 223 RS	*Pt. constans*	MP7	Dormaal	m2	1,53	0,94	1,63
DIIC 732 RS	*Pt. constans*	MP7	Dormaal	m2	1,57	0,88	1,78
DIII 1850 RS	*Pt. constans*	MP7	Dormaal	m2	1,62	0,98	1,65
DIII 45 S	*Pt. constans*	MP7	Dormaal	m2	1,56	0,89	1,75
DIII 808 RS	*Pt. constans*	MP7	Dormaal	m2	1,45	0,81	1,79
DIIC 1258 RS	*Pt. constans*	MP7	Dormaal	m2	1,43	0,87	1,64
DIIA 862 RS	*Pt. constans*	MP7	Dormaal	m2	1,46	0,89	1,64
DIIC 1341	*Pt. constans*	MP7	Dormaal	m2	1,45	0,85	1,71
DIIC 2015 RS	*Pt. constans*	MP7	Dormaal	m2	1,53	1	1,53
DIIC 1546 RS	*Pt. constans*	MP7	Dormaal	m2	1,51	0,82	1,84
DIII 47 S	*Pt. constans*	MP7	Dormaal	m2	1,52	0,89	1,71
DIIC 1113 RS	*Pt. constans*	MP7	Dormaal	m2	1,46	0,82	1,78
DIIA 833 RS	*Pt. constans*	MP7	Dormaal	m2	1,49	0,88	1,69
DIIC 971 RS	*Pt. constans*	MP7	Dormaal	m2	1,5	0,95	1,58
DIIA 863 RS	*Pt. constans*	MP7	Dormaal	m2	1,45	0,82	1,77
DIIC 1548 RS	*Pt. constans*	MP7	Dormaal	m2	1,48	0,87	1,70
DIII 807 RS	*Pt. constans*	MP7	Dormaal	m2	1,52	0,8	1,90
DIIC 2016 RS	*Pt. constans*	MP7	Dormaal	m2	1,58	0,82	1,93
DIII 574 RS	*Pt. constans*	MP7	Dormaal	m2	1,46	0,91	1,60
DIII 446 RS	*Pt. constans*	MP7	Dormaal	m2	1,52	0,93	1,63
DIIA 1306 RS	*Pt. constans*	MP7	Dormaal	m2	1,55	0,97	1,60
DIIC 1235 RS	*Pt. constans*	MP7	Dormaal	m2	1,54	0,94	1,64
DIIC 1092 RS	*Pt. constans*	MP7	Dormaal	m2	1,48	0,93	1,59
DIIC 970 RS	*Pt. constans*	MP7	Dormaal	m2	1,59	0,95	1,67

DIIC 979 RS	*Pt. constans*	MP7	Dormaal	m2	1,56	0,9	1,73
DIII 333 RS	*Pt. constans*	MP7	Dormaal	m2	1,52	0,92	1,65
DIIC 1088 RS	*Pt. constans*	MP7	Dormaal	m2	1,45	0,82	1,77
DI 1483 RS	*Pt. constans*	MP7	Dormaal	m3	1,52	0,89	1,71
DIIA 1795 RS	*Pt. constans*	MP7	Dormaal	m3	1,54	0,9	1,71
DIIA 1511 RS	*Pt. constans*	MP7	Dormaal	m3	1,51	0,83	1,82
DIIA 2129 RS	*Pt. constans*	MP7	Dormaal	m3		0,86	
DIII 2152 RS	*Pt. constans*	MP7	Dormaal	m3	1,51	0,85	1,78
DIIC 1338 RS	*Pt. constans*	MP7	Dormaal	m3	1,53	0,87	1,76
DIII 43 S	*Pt. constans*	MP7	Dormaal	m3	1,54	0,85	1,81
DIIC 1232 RS	*Pt. constans*	MP7	Dormaal	m3	1,56	0,93	1,68
DIII 850 RS	*Pt. constans*	MP7	Dormaal	m3	1,51	0,87	1,74
DIIA 1794 RS	*Pt. constans*	MP7	Dormaal	m3	1,4	0,88	1,59
DIII 331 RS	*Pt. constans*	MP7	Dormaal	m3	1,52	0,89	1,71
DIIC 972 RS	*Pt. constans*	MP7	Dormaal	m3	1,48	0,87	1,70
DIIA 1303 RS	*Pt. constans*	MP7	Dormaal	m3	1,57	0,92	1,71
DIII 575 RS	*Pt. constans*	MP7	Dormaal	m3	1,52	0,87	1,75
DIIC 1952 RS	*Pt. constans*	MP7	Dormaal	m3	1,49	0,8	1,86
DIII 2153 RS	*Pt. constans*	MP7	Dormaal	m3	1,51	0,86	1,76
DIII 810 RS	*Pt. constans*	MP7	Dormaal	m3	1,45	0,81	1,79
DIIA 909 RS	*Pt. constans*	MP7	Dormaal	m3	1,49	0,85	1,75
DIII 848 RS	*Pt. constans*	MP7	Dormaal	m3	1,63	0,99	1,65
DIIC 1251 RS	*Pt. constans*	MP7	Dormaal	m3	1,44	0,83	1,73
DIII 45-I RS	*Pt. constans*	MP7	Dormaal	m3	1,49	0,84	1,77
DIIC 1096 RS	*Pt. constans*	MP7	Dormaal	m3	1,55	0,91	1,70
DIII 573 RS	*Pt. constans*	MP7	Dormaal	m3	1,5	0,89	1,69
DIIC 2022	*Pt. constans*	MP7	Dormaal	m3	1,48	0,81	1,83
DIIC 973 RS	*Pt. constans*	MP7	Dormaal	m3	1,49	0,83	1,80
DIIC 1337	*Pt. constans*	MP7	Dormaal	m3	1,57	0,93	1,69
DIIC 1094 RS	*Pt. constans*	MP7	Dormaal	m3	1,59	0,87	1,83
DIII 307 RS	*Pt. constans*	MP7	Dormaal	m3	1,5	0,9	1,67
DIIC 1234 RS	*Pt. constans*	MP7	Dormaal	m4	1,4	0,83	1,69
DIIC 1091 RS	*Pt. constans*	MP7	Dormaal	m4	1,41	0,78	1,81
DIIC 1233 RS	*Pt. constans*	MP7	Dormaal	m4	1,49	0,83	1,80
DIIA 905 RS	*Pt. constans*	MP7	Dormaal	m4	1,41	0,85	1,66
DIII 2154 RS	*Pt. constans*	MP7	Dormaal	m4	1,38	0,79	1,75
DIII 48 S	*Pt. constans*	MP7	Dormaal	m4	1,55	0,86	1,80
DIIC 738 RS	*Pt. constans*	MP7	Dormaal	m4	1,49	0,76	1,96
DIII 445 RS	*Pt. constans*	MP7	Dormaal	m4	1,45	0,86	1,69
DI 2072 RS	*Pt. constans*	MP7	Dormaal	m4	1,51	0,79	1,91
MNHN.F.QNY-526	*Pt. constans*	MP7	Le Quesnoy	M1	1,52	1,52	1,00
MNHN.F.QNY-525bis	*Pt. constans*	MP7	Le Quesnoy	M2	1,48	1,68	0,88
MNHN.F.QNY-524	*Pt. constans*	MP7	Le Quesnoy	M2		1,62	
SV3-270	*Pt. constans*	MP7	Silveirinha	dP3	1,11	0,97	1,14
SV3-169	*Pt. constans*	MP7	Silveirinha	M1	1,66	1,61	1,03
SV1-477	*Pt. constans*	MP7	Silveirinha	M2		1,63	
SV3-171	*Pt. constans*	MP7	Silveirinha	M2	1,61	1,81	0,89
SV1-154	*Pt. constans*	MP7	Silveirinha	M3	1,34	1,72	0,78
SV2-32	*Pt. constans*	MP7	Silveirinha	M3	1,42	1,8	0,79
SV3-171	*Pt. constans*	MP7	Silveirinha	M3	1,57	1,83	0,86
SV1-149	*Pt. constans*	MP7	Silveirinha	m1	1,46	0,78	1,87

SV2-16	*Pt. constans*	MP7	Silveirinha	m1	1,46	0,83	1,76
SV2-28	*Pt. constans*	MP7	Silveirinha	m2	1,57	0,96	1,64
SV3-73	*Pt. constans*	MP7	Silveirinha	m2	1,4	0,89	1,57
SV1-155	*Pt. constans*	MP7	Silveirinha	m3	1,56	0,89	1,75
SV1-156	*Pt. constans*	MP7	Silveirinha	m3	1,52	0,91	1,67
UM-FDN-5	*Pt. constans*	[MP7-MP8+9]-FMG	Fordones	M1	1,53	1,47	1,04
UM-FDN-7	*Pt. constans*	[MP7-MP8+9]-FMG	Fordones	M1	1,52	1,55	0,98
UM-FDN-8	*Pt. constans*	[MP7-MP8+9]-FMG	Fordones	M1	1,63	1,5	1,09
UM-FDN-161	*Pt. constans*	[MP7-MP8+9]-FMG	Fordones	M1	1,63	1,53	1,07
UM-FDN-291	*Pt. constans*	[MP7-MP8+9]-FMG	Fordones	M1	1,44	1,47	0,98
UM-FDN-299	*Pt. constans*	[MP7-MP8+9]-FMG	Fordones	M1	1,48		
UM-FDN-6	*Pt. constans*	[MP7-MP8+9]-FMG	Fordones	M2	1,54	1,73	0,89
UM-FDN-9	*Pt. constans*	[MP7-MP8+9]-FMG	Fordones	M2	1,54		
UM-FDN-292	*Pt. constans*	[MP7-MP8+9]-FMG	Fordones	M2	1,52	1,6	0,95
UM-FDN-293	*Pt. constans*	[MP7-MP8+9]-FMG	Fordones	M2	1,65	1,87	0,88
UM-FDN-10	*Pt. constans*	[MP7-MP8+9]-FMG	Fordones	M3	1,56		
UM-FDN-295	*Pt. constans*	[MP7-MP8+9]-FMG	Fordones	M3	1,49		
UM-FDN-296	*Pt. constans*	[MP7-MP8+9]-FMG	Fordones	M3	1,57		
UM-FDN-297	*Pt. constans*	[MP7-MP8+9]-FMG	Fordones	M3	1,63		
UM-FDN-12	*Pt. constans*	[MP7-MP8+9]-FMG	Fordones	m1	1,39	0,85	1,64
UM-FDN-16	*Pt. constans*	[MP7-MP8+9]-FMG	Fordones	m1	1,52	0,86	1,77
UM-FDN-157	*Pt. constans*	[MP7-MP8+9]-FMG	Fordones	m1		0,85	
UM-FDN-155	*Pt. constans*	[MP7-MP8+9]-FMG	Fordones	m2	1,54	0,93	1,66
UM-FDN-158	*Pt. constans*	[MP7-MP8+9]-FMG	Fordones	m2		0,88	
UM-FDN-257	*Pt. constans*	[MP7-MP8+9]-FMG	Fordones	m2	1,53	0,87	1,76
UM-FDN-11	*Pt. constans*	[MP7-MP8+9]-FMG	Fordones	m3	1,44	0,87	1,66
UM-FDN-14	*Pt. constans*	[MP7-MP8+9]-FMG	Fordones	m3	1,52	0,83	1,83
UM-FDN-15	*Pt. constans*	[MP7-MP8+9]-FMG	Fordones	m3	1,45	0,8	1,81
UM-FDN-19	*Pt. constans*	[MP7-MP8+9]-FMG	Fordones	m3	1,47	0,82	1,79
UM-FDN-156	*Pt. constans*	[MP7-MP8+9]-FMG	Fordones	m3	1,51	0,97	1,56
UM-FDN-294	*Pt. constans*	[MP7-MP8+9]-FMG	Fordones	m3	1,65	0,91	1,81
UM-FDN-13	*Pt. constans*	[MP7-MP8+9]-FMG	Fordones	m4	1,48	0,77	1,92
UM-FDN-157	*Pt. constans*	[MP7-MP8+9]-FMG	Fordones	m4		0,81	
UM-FDN-250	*Pt. constans*	[MP7-MP8+9]-FMG	Fordones	m4	1,58	0,84	1,88
UM-PAT-109	*Pt. constans*	[MP7-MP8+9]-FMG	Palette	P3	1,41	0,7	2,01
UM-PAT-101	*Pt. constans*	[MP7-MP8+9]-FMG	Palette	dP3	1,2	1,19	1,01
UM-PAT-104	*Pt. constans*	[MP7-MP8+9]-FMG	Palette	M1	1,7	1,53	1,11
MHN.AIX.PV.2018.26.12	*Pt. constans*	[MP7-MP8+9]-FMG	Palette	M2	1,61	1,89	0,85
MHN.AIX.PV.2018.26.13	*Pt. constans*	[MP7-MP8+9]-FMG	Palette	M2	1,58	1,72	0,92
UM-PAT-105	*Pt. constans*	[MP7-MP8+9]-FMG	Palette	M2	1,7	1,77	0,96
UM-PAT-177	*Pt. constans*	[MP7-MP8+9]-FMG	Palette	M3	1,51	1,96	0,77
MHN.AIX.PV.2017.6.16	*Pt. constans*	[MP7-MP8+9]-FMG	Palette	m1	1,48	0,82	1,80
MHN.AIX.PV.2018.26.7	*Pt. constans*	[MP7-MP8+9]-FMG	Palette	m1	1,49	0,82	1,82
MHN.AIX.PV.2018.26.8	*Pt. constans*	[MP7-MP8+9]-FMG	Palette	m1	1,38	0,83	1,66
MHN.AIX.PV.2018.26.17	*Pt. constans*	[MP7-MP8+9]-FMG	Palette	m1	1,45	0,91	1,59
UM-PAT-107	*Pt. constans*	[MP7-MP8+9]-FMG	Palette	m1	1,5	0,87	1,72
UM-PAT-110	*Pt. constans*	[MP7-MP8+9]-FMG	Palette	m1		0,84	
MHN.AIX.PV.2017.6.17	*Pt. constans*	[MP7-MP8+9]-FMG	Palette	m2	1,6	0,9	1,78
MHN.AIX.PV.2018.26.6	*Pt. constans*	[MP7-MP8+9]-FMG	Palette	m2	1,53	0,83	1,84
MHN.AIX.PV.2018.26.18	*Pt. constans*	[MP7-MP8+9]-FMG	Palette	m2	1,49	0,94	1,59
UM-PAT-108	*Pt. constans*	[MP7-MP8+9]-FMG	Palette	m3	1,63	0,92	1,77

UM-PAT-111	*Pt. constans*	[MP7-MP8+9]-FMG	Palette	m2	1,66	0,99	1,68
MHN.AIX.PV.2018.26.18	*Pt. constans*	[MP7-MP8+9]-FMG	Palette	m3	1,51	0,96	1,57
MHN.AIX.PV.2018.26.19	*Pt. constans*	[MP7-MP8+9]-FMG	Palette	m3	1,55	0,84	1,85
UM-PAT-100	*Pt. constans*	[MP7-MP8+9]-FMG	Palette	m3	1,56	0,92	1,70
UM-PAT-106	*Pt. constans*	[MP7-MP8+9]-FMG	Palette	m3		0,92	
MHN.AIX.PV.2017.6.18	*Pt. constans*	[MP7-MP8+9]-FMG	Palette	m4	1,59	0,91	1,75
MHN.AIX.PV.2017.26.18	*Pt. constans*	[MP7-MP8+9]-FMG	Palette	m4	1,54	0,79	1,95
MNHN.F.ME16168	*Pt. constans*	[MP7-MP8+9]-FMG	Meudon	M1	1,61	1,57	1,03
MNHN.F.ME16197	*Pt. constans*	[MP7-MP8+9]-FMG	Meudon	M1	1,55	1,55	1,00
MNHN.F.ME25-G	*Pt. constans*	[MP7-MP8+9]-FMG	Meudon	M2	1,65	1,89	0,87
MNHN.F.ME16301	*Pt. constans*	[MP7-MP8+9]-FMG	Meudon	M2	1,55	1,79	0,87
MNHN.F.ME16095	*Pt. constans*	[MP7-MP8+9]-FMG	Meudon	M3	1,55	1,85	0,84
MNHN.F.ME16312	*Pt. constans*	[MP7-MP8+9]-FMG	Meudon	M3	1,51	1,78	0,85
MNHN.F.ME16207	*Pt. constans*	[MP7-MP8+9]-FMG	Meudon	m1	1,48	0,91	1,63
MNHN.F.ME16321	*Pt. constans*	[MP7-MP8+9]-FMG	Meudon	m1	1,56	0,96	1,63
MNHN.F.ME16397	*Pt. constans*	[MP7-MP8+9]-FMG	Meudon	m1	1,5	0,9	1,67
MNHN.F.ME16071	*Pt. constans*	[MP7-MP8+9]-FMG	Meudon	m2	1,6	0,95	1,68
MNHN.F.ME16382	*Pt. constans*	[MP7-MP8+9]-FMG	Meudon	m2	1,65	0,99	1,67
MNHN.F.ME16403	*Pt. constans*	[MP7-MP8+9]-FMG	Meudon	m3	1,57	0,95	1,65
MNHN.F.ME16289	*Pt. constans*	[MP7-MP8+9]-FMG	Meudon	m3	1,66	0,98	1,69
MNHN.F.ME48G	*Pt. constans*	[MP7-MP8+9]-FMG	Meudon	m4	1,57	0,85	1,85
MNHN.F.ME16362	*Pt. constans*	[MP7-MP8+9]-FMG	Meudon	m4	1,5	0,84	1,79
UM-CLO-55	*Pt. constans*	[MP7-MP8+9]-FMG	Le Clot	P2	1,21	0,6	2,02
UM-CLO-52	*Pt. constans*	[MP7-MP8+9]-FMG	Le Clot	m2	1,37	0,85	1,61
MNHN.F.SN23-BN	*Pt. constans*	[MP7-MP8+9]-FMG	Soissons	M1	1,55	1,48	1,05
MNHN.F.SN38-BN	*Pt. constans*	[MP7-MP8+9]-FMG	Soissons	M2	1,6	1,68	0,95
MNHN.F.SN59-BN	*Pt. constans*	[MP7-MP8+9]-FMG	Soissons	m3	1,52	0,9	1,69
MNHN.F.SN35-BN	*Pt. constans*	[MP7-MP8+9]-FMG	Soissons	m4	1,49	0,85	1,75
MNHN.F.RI420	*Pt. constans*	[MP7-MP8+9]-FMG	Rians	M2		1,6	
MNHN.F.RI378	*Pt. constans*	[MP7-MP8+9]-FMG	Rians	M3	1,55		
MNHN.F.RI392	*Pt. constans*	[MP7-MP8+9]-FMG	Rians	M3	1,51	1,84	0,82
MNHN.F.RI226	*Pt. constans*	[MP7-MP8+9]-FMG	Rians	m1	1,48	0,85	1,74
MNHN.F.RI244	*Pt. constans*	[MP7-MP8+9]-FMG	Rians	m4		0,83	
UM-MOZ-12	*Pt. matronense*	FMG	Monze	p2	1,45	0,61	2,38
UM-MOZ-11	*Pt. matronense*	FMG	Monze	p3		0,6	
UM-MOZ-11	*Pt. matronense*	FMG	Monze	m1	1,55	0,97	1,60
UM-MOZ-1	*Pt. matronense*	FMG	Monze	m2	1,72	1,11	1,55
UM-MOZ-11	*Pt. matronense*	FMG	Monze	m2	1,67	1,03	1,62
UM-MOZ-11	*Pt. matronense*	FMG	Monze	m3	1,7	1,07	1,59
UM-MOZ-13	*Pt. matronense*	FMG	Monze	m3	1,78	1,07	1,66
UM-MOZ-11	*Pt. matronense*	FMG	Monze	m4	1,59	0,91	1,75
UM-FNR-60	*Pt. matronense*	FMG	Fournes	M1	1,71	1,65	1,04
UM-FNR-26	*Pt. matronense*	FMG	Fournes	M2		1,88	
UM-FNR-61	*Pt. matronense*	FMG	Fournes	M3	1,64	1,96	0,84
UM-FNR-24	*Pt. matronense*	FMG	Fournes	m1		1,06	
UM-FNR-58	*Pt. matronense*	FMG	Fournes	m2	1,73	1,01	1,71
UM-FNR-14	*Pt. matronense*	FMG	Fournes	m3	1,72	1,02	1,69
UM-FNR-38	*Pt. matronense*	FMG	Fournes	m3	1,66	0,9	1,84
UM-GAS-1	*Pt. matronense*	FMG	La Gasque	M1	1,72	1,68	1,02
UM-GAS-2	*Pt. matronense*	FMG	La Gasque	M2	1,77	2	0,89
MNHN.F.AV7233	*Pt. matronense*	(~)MP8+9	Avenay	M1	1,66	1,66	1,00

MNHN.F.AV7225	*Pt. matronense*	(~)MP8+9	Avenay	M2	1,58	1,87	0,84
MNHN.F.AV15769	*Pt. matronense*	(~)MP8+9	Avenay	M2	1,8	2	0,90
MNHN.F.AV139-L	*Pt. matronense*	(~)MP8+9	Avenay	M3	1,58	1,84	0,86
MNHN.F.AV6794	*Pt. matronense*	(~)MP8+9	Avenay	M3	1,58	2,09	0,76
MNHN.F.AV7189	*Pt. matronense*	(~)MP8+9	Avenay	M3		2,15	
MNHN.F.AV6795	*Pt. matronense*	(~)MP8+9	Avenay	m1	1,45	0,9	1,61
UM-AV-20-SK	*Pt. matronense*	(~)MP8+9	Avenay	m2	1,75	1,09	1,61
MNHN.F.AV7660	*Pt. matronense*	(~)MP8+9	Avenay	m3	1,76	1	1,76
MNHN.F.AV7192	*Pt. matronense*	(~)MP8+9	Avenay	m4	1,79	1,03	1,74
MNHN.F.CB817	*Pt. matronense*	(~)MP8+9	Condé-en-Brie	M1	1,52	1,6	0,95
MNHN.F.CB856	*Pt. matronense*	(~)MP8+9	Condé-en-Brie	M1	1,72	1,88	0,91
MNHN.F.CB2780	*Pt. matronense*	(~)MP8+9	Condé-en-Brie	M1	1,48	1,54	0,96
MNHN.F.CB2952	*Pt. matronense*	(~)MP8+9	Condé-en-Brie	M1	1,66	1,58	1,05
MNHN.F.CB3243	*Pt. matronense*	(~)MP8+9	Condé-en-Brie	M1	1,82	1,74	1,05
MNHN.F.CB2503	*Pt. matronense*	(~)MP8+9	Condé-en-Brie	M1	1,83	1,73	1,06
MNHN.F.CB4119	*Pt. matronense*	(~)MP8+9	Condé-en-Brie	M1	1,65	1,62	1,02
MNHN.F.CB4134	*Pt. matronense*	(~)MP8+9	Condé-en-Brie	M1		1,6	
MNHN.F.CB269-BN	*Pt. matronense*	(~)MP8+9	Condé-en-Brie	M2	1,83	2,16	0,85
MNHN.F.CB848	*Pt. matronense*	(~)MP8+9	Condé-en-Brie	M2	1,75	2,03	0,86
MNHN.F.CB877	*Pt. matronense*	(~)MP8+9	Condé-en-Brie	M2	1,89	2,17	0,87
MNHN.F.CB2504	*Pt. matronense*	(~)MP8+9	Condé-en-Brie	M2		1,8	
MNHN.F.CB3646	*Pt. matronense*	(~)MP8+9	Condé-en-Brie	M2		1,93	
MNHN.F.CB4130	*Pt. matronense*	(~)MP8+9	Condé-en-Brie	M2	1,73	1,92	0,90
MNHN.F.CB4140	*Pt. matronense*	(~)MP8+9	Condé-en-Brie	M2	1,63	1,84	0,89
MNHN.F.CB4138	*Pt. matronense*	(~)MP8+9	Condé-en-Brie	M2	1,79	1,93	0,93
MNHN.F.CB159-BN	*Pt. matronense*	(~)MP8+9	Condé-en-Brie	M2	1,59	1,7	0,94
MNHN.F.CB155-BN	*Pt. matronense*	(~)MP8+9	Condé-en-Brie	M3	1,49	1,93	0,77
MNHN.F.CB827	*Pt. matronense*	(~)MP8+9	Condé-en-Brie	M3	1,55	2,03	0,76
MNHN.F.CB1412	*Pt. matronense*	(~)MP8+9	Condé-en-Brie	M3	1,66	1,91	0,87
MNHN.F.CB1686	*Pt. matronense*	(~)MP8+9	Condé-en-Brie	M3	1,49	1,77	0,84
MNHN.F.CB2845	*Pt. matronense*	(~)MP8+9	Condé-en-Brie	M3	1,41	1,84	0,77
MNHN.F.CB2632	*Pt. matronense*	(~)MP8+9	Condé-en-Brie	M3	1,7	2,08	0,82
MNHN.F.CB203-BN	*Pt. matronense*	(~)MP8+9	Condé-en-Brie	M3	1,52	1,93	0,79
MNHN.F.CB1079-L	*Pt. matronense*	(~)MP8+9	Condé-en-Brie	m1	1,46	0,89	1,64
MNHN.F.CB927	*Pt. matronense*	(~)MP8+9	Condé-en-Brie	m1	1,7	0,97	1,75
MNHN.F.CB3640	*Pt. matronense*	(~)MP8+9	Condé-en-Brie	m1	1,72	1,07	1,61
MNHN.F.CB2506	*Pt. matronense*	(~)MP8+9	Condé-en-Brie	m1	1,63	0,93	1,75
MNHN.F.CB4385	*Pt. matronense*	(~)MP8+9	Condé-en-Brie	m1	1,53	0,9	1,70
MNHN.F.CB647	*Pt. matronense*	(~)MP8+9	Condé-en-Brie	m1	1,66	0,99	1,68
MNHN.F.CB179-BN	*Pt. matronense*	(~)MP8+9	Condé-en-Brie	m2	1,84	1,12	1,64
MNHN.F.CB846	*Pt. matronense*	(~)MP8+9	Condé-en-Brie	m2	1,82	1,06	1,72
MNHN.F.CB871	*Pt. matronense*	(~)MP8+9	Condé-en-Brie	m2	1,78	1,06	1,68
MNHN.F.CB3648	*Pt. matronense*	(~)MP8+9	Condé-en-Brie	m2	1,79	1,12	1,60
MNHN.F.CB4129	*Pt. matronense*	(~)MP8+9	Condé-en-Brie	m2	1,69	1,04	1,63
MNHN.F.CB220-BN	*Pt. matronense*	(~)MP8+9	Condé-en-Brie	m3	1,81	1,06	1,71
MNHN.F.CB239-BN	*Pt. matronense*	(~)MP8+9	Condé-en-Brie	m3	1,87	1,12	1,67
MNHN.F.CB876	*Pt. matronense*	(~)MP8+9	Condé-en-Brie	m3	1,59	0,94	1,69
MNHN.F.CB2828	*Pt. matronense*	(~)MP8+9	Condé-en-Brie	m3	1,65	1	1,65
MNHN.F.CB4197	*Pt. matronense*	(~)MP8+9	Condé-en-Brie	m3	1,87	1,09	1,72
MNHN.F.CB2790	*Pt. matronense*	(~)MP8+9	Condé-en-Brie	m3	1,75	1,02	1,72
MNHN.F.CB2925	*Pt. matronense*	(~)MP8+9	Condé-en-Brie	m3	1,69	0,95	1,78

MNHN.F.CB925	*Pt. matronense*	(~)MP8+9	Condé-en-Brie	m4	1,56	0,87	1,79
MNHN.F.CB941	*Pt. matronense*	(~)MP8+9	Condé-en-Brie	m4	1,68	0,86	1,95
MNHN.F.CB5027	*Pt. matronense*	(~)MP8+9	Condé-en-Brie	m4	2	1	2,00
MNHN.F.GLD174	*Pt. matronense*	(~)MP8+9	Sables de Brasles	M1	1,72	1,65	1,04
MNHN.F.GLD89-L	*Pt. matronense*	(~)MP8+9	Sables de Brasles	M1	1,49	1,46	1,02
MNHN.F.GLD392	*Pt. matronense*	(~)MP8+9	Sables de Brasles	M1	1,58	1,56	1,01
MNHN.F.GL395	*Pt. matronense*	(~)MP8+9	Sables de Brasles	M1	1,77	1,75	1,01
MNHN.F.GL288	*Pt. matronense*	(~)MP8+9	Sables de Brasles	M1	1,53	1,6	0,96
MNHN.F.GLD68	*Pt. matronense*	(~)MP8+9	Sables de Brasles	M2	1,65	1,95	0,85
MNHN.F.GLD131	*Pt. matronense*	(~)MP8+9	Sables de Brasles	M2	1,74	1,9	0,92
MNHN.F.GLD308	*Pt. matronense*	(~)MP8+9	Sables de Brasles	M2	1,6	1,76	0,91
MNHN.F.GL396	*Pt. matronense*	(~)MP8+9	Sables de Brasles	M3	1,53	1,9	0,81
MNHN.F.GLD306	*Pt. matronense*	(~)MP8+9	Sables de Brasles	M3	1,61	2	0,81
MNHN.F.GL192-L	*Pt. matronense*	(~)MP8+9	Sables de Brasles	m2	1,69	1,07	1,58
MNHN.F.GLD316	*Pt. matronense*	(~)MP8+9	Sables de Brasles	m2	1,48	0,87	1,70
MNHN.F.GL312-L	*Pt. matronense*	(~)MP8+9	Sables de Brasles	m2	1,68	1,03	1,63
MNHN.F.GL249-L	*Pt. matronense*	(~)MP8+9	Sables de Brasles	m3	1,79	1,04	1,72
MNHN.F.GL386-L	*Pt. matronense*	(~)MP8+9	Sables de Brasles	m3	1,54	0,92	1,67
MNHN.F.GL302-L	*Pt. matronense*	(~)MP8+9	Sables de Brasles	m4	1,77	0,97	1,82
MNHN.F.SZ58	*Pt. matronense*	(~)MP8+9	Sézanne-Broyes	M1	1,66	1,57	1,06
MNHN.F.SZ76	*Pt. matronense*	(~)MP8+9	Sézanne-Broyes	M1	1,72	1,64	1,05
MNHN.F.SZ216	*Pt. matronense*	(~)MP8+9	Sézanne-Broyes	M1	1,69	1,68	1,01
MNHN.F.SZ232	*Pt. matronense*	(~)MP8+9	Sézanne-Broyes	M1	1,58	1,59	0,99
MNHN.F.SZ513	*Pt. matronense*	(~)MP8+9	Sézanne-Broyes	M1	1,71	1,63	1,05
MNHN.F.SZ446	*Pt. matronense*	(~)MP8+9	Sézanne-Broyes	M2	1,78	1,88	0,95
MNHN.F.SZ559	*Pt. matronense*	(~)MP8+9	Sézanne-Broyes	M2	1,78	1,91	0,93
MNHN.F.SZ311-BN	*Pt. matronense*	(~)MP8+9	Sézanne-Broyes	M3	1,57	1,84	0,85
MNHN.F.SZ558-BN	*Pt. matronense*	(~)MP8+9	Sézanne-Broyes	M3	1,77	2,2	0,80
MNHN.F.SZ552-BN	*Pt. matronense*	(~)MP8+9	Sézanne-Broyes	M3	1,6	1,93	0,83
MNHN.F.SZ86-BN	*Pt. matronense*	(~)MP8+9	Sézanne-Broyes	m1	1,6	0,97	1,65
MNHN.F.SZ88-BN	*Pt. matronense*	(~)MP8+9	Sézanne-Broyes	m1	1,7	1,01	1,68
MNHN.F.SZ175-BN	*Pt. matronense*	(~)MP8+9	Sézanne-Broyes	m1	1,58	0,92	1,72
MNHN.F.SZ514-BN	*Pt. matronense*	(~)MP8+9	Sézanne-Broyes	m1	1,6	0,91	1,76
MNHN.F.SZ567-BN	*Pt. matronense*	(~)MP8+9	Sézanne-Broyes	m1	1,78	1,04	1,71
MNHN.F.SZ286-BN	*Pt. matronense*	(~)MP8+9	Sézanne-Broyes	m1	1,74	1,03	1,69
MNHN.F.SZ48-BN	*Pt. matronense*	(~)MP8+9	Sézanne-Broyes	m1	1,7	0,97	1,75
MNHN.F.SZ124-BN	*Pt. matronense*	(~)MP8+9	Sézanne-Broyes	m2	1,8	1,13	1,59
MNHN.F.SZ212-BN	*Pt. matronense*	(~)MP8+9	Sézanne-Broyes	m2	1,67	0,95	1,76
MNHN.F.SZ226-BN	*Pt. matronense*	(~)MP8+9	Sézanne-Broyes	m2	1,78	1,06	1,68
MNHN.F.SZ302-BN	*Pt. matronense*	(~)MP8+9	Sézanne-Broyes	m2	1,74	1,01	1,72
MNHN.F.SZ515-BN	*Pt. matronense*	(~)MP8+9	Sézanne-Broyes	m2	1,87	1,09	1,72
MNHN.F.SZ269-BN	*Pt. matronense*	(~)MP8+9	Sézanne-Broyes	m3	1,75	0,98	1,79
MNHN.F.SZ574-BN	*Pt. matronense*	(~)MP8+9	Sézanne-Broyes	m3	1,86	1,12	1,66
MNHN.F.SZ271-BN	*Pt. matronense*	(~)MP8+9	Sézanne-Broyes	m4	1,6	0,87	1,84
MNHN.F.SZ306-BN	*Pt. matronense*	(~)MP8+9	Sézanne-Broyes	m4	1,76	0,97	1,81
MNHN.F.MU49-BN	indet.	(~)MP8+9	Mutigny	M4	1,25	1,48	0,84
MNHN.F.MU114-L	indet.	(~)MP8+9	Mutigny	m2	1,46	0,91	1,60
MNHN.F.MU142-L	indet.	(~)MP8+9	Mutigny	m3	1,47	0,83	1,77

Tableau S2. Détail des valeurs (en mm) de longueur mésiodistale (L) et de largeur labiolinguale (W) mesurées en vue occlusale sur les dents molariformes supérieures de *Peratherium maximum* (Crochet, 1979) de Pourcy, Mutigny, Avenay, Condé-en-Brie, Sables de Brasles, et Saint-Agnan (Bassin de Paris). Les ratios L / W sont calculés. Le nombre de cuspides stylaires dans les positions « C » et « D » est précisé pour les M1s à M3s les mieux préservées (abréviation « N st.C-D »). Les spécimens sont ordonnés par locus dentaire puis par localité.

Spécimen	Localité	Locus	L (mm)	W (mm)	L/W	N st.C-D
MNHN.F.CB206-BN	Condé-en-Brie	dP3	2,02	1,79	1,13	
MNHN.F.CB3049	Condé-en-Brie	dP3	1,95	1,72	1,13	
MNHN.F.CB4141	Condé-en-Brie	dP3		1,84		
MNHN.F.CB853	Condé-en-Brie	dP3		1,97		
MNHN.F.CB3701	Condé-en-Brie	dP3	1,88	1,79	1,05	
MNHN.F.CB3024	Condé-en-Brie	dP3	2,07	1,63	1,27	
UM-AV-16-SK	Avenay	dP3	2,1	1,92	1,09	
MNHN.F.Mu71-Lé	Mutigny	dP3	1,99	1,85	1,08	
MNHN.F.GL290-L	Sables de Brasles	dP3		1,67		
MNHN.F.CB847	Condé-en-Brie	M1	2,7	2,39	1,13	3
MNHN.F.CB777-L	Condé-en-Brie	M1	2,76	2,49	1,11	4
MNHN.F.CB4132	Condé-en-Brie	M1	2,52	2,26	1,12	2
MNHN.F.CB3105	Condé-en-Brie	M1	2,55	2,46	1,04	3
MNHN.F.CB1233	Condé-en-Brie	M1	2,83	2,55	1,11	3
MNHN.F.CB4890	Condé-en-Brie	M1	2,65	2,52	1,05	3
MNHN.F.CB844	Condé-en-Brie	M1	2,56	2,65	0,97	3
MNHN.F.CB843	Condé-en-Brie	M1	2,77	2,72	1,02	4
MNHN.F.CB263-M	Condé-en-Brie	M1	2,44	2,57	0,95	3
MNHN.F.CB3113	Condé-en-Brie	M1	2,73	2,25	1,21	
MNHN.F.CB4135	Condé-en-Brie	M1	2,52	2,68	0,94	3
MNHN.F.CB3212	Condé-en-Brie	M1		2,48		
MNHN.F.CB377-BN	Condé-en-Brie	M1	2,69	2,38	1,13	3
MNHN.F.PY58	Pourcy	M1	2,6	2,66	0,98	2
MNHN.F.Av5848	Avenay	M1	2,75	2,43	1,13	3
MNHN.F.Av442-L	Avenay	M1		2,87		
MNHN.F.STA301	Saint-Agnan	M1	2,57	2,5	1,03	2
MNHN.F.GLD121	Sables de Brasles	M1	2,67	2,79	0,96	3
MNHN.F.CB196	Condé-en-Brie	M2	2,83	2,93	0,97	3
MNHN.F.CB3322	Condé-en-Brie	M2	2,81	3,07	0,92	3
MNHN.F.CB4128	Condé-en-Brie	M2	2,44	2,79	0,87	3
MNHN.F.CB197	Condé-en-Brie	M2	2,46	2,5	0,98	3
MNHN.F.CB1327	Condé-en-Brie	M2	2,69	2,73	0,99	3
MNHN.F.CB3634	Condé-en-Brie	M2	2,54	2,71	0,94	3
MNHN.F.CB261-M	Condé-en-Brie	M2	2,65	2,79	0,95	4
MNHN.F.CB4133	Condé-en-Brie	M2	2,64	2,87	0,92	
MNHN.F.CB33-M	Condé-en-Brie	M2	2,54	2,76	0,92	2
MNHN.F.CB779-L	Condé-en-Brie	M2	2,71	3,02	0,90	4
MNHN.F.CB3636	Condé-en-Brie	M2		2,85		

MNHN.F.CB405-BN	Condé-en-Brie	M2	2,71	3,02	0,90	
MNHN.F.CB455-BN	Condé-en-Brie	M2		2,84		
MNHN.F.CB236-M	Condé-en-Brie	M2	2,55	2,72	0,94	2
MNHN.F.Av4747	Avenay	M2	2,47	2,71	0,91	2
MNHN.F.Av4816	Avenay	M2	2,48	2,72	0,91	2
MNHN.F.Mu5507	Mutigny	M2	2,52	2,66	0,95	4
MNHN.F.Mu181-L	Mutigny	M2	2,77	2,92	0,95	
MNHN.F.Mu6608	Mutigny	M2	2,61	3,07	0,85	3
MNHN.F.STA294	Saint-Agnan	M2	2,89	2,98	0,97	2
MNHN.F.STA289	Saint-Agnan	M2	2,87	2,96	0,97	3
MNHN.F.GLD73-L	Sables de Brasles	M2	2,68	3,01	0,89	3
MNHN.F.CB852	Condé-en-Brie	M3	2,54	3,06	0,83	2
MNHN.F.CB4904	Condé-en-Brie	M3	2,67	2,91	0,92	3
MNHN.F.CB3647	Condé-en-Brie	M3	2,7	3,04	0,89	3
MNHN.F.CB1252	Condé-en-Brie	M3	2,62	3,09	0,85	4
MNHN.F.CB79-P	Condé-en-Brie	M3	2,5	2,69	0,93	4
MNHN.F.CB4120	Condé-en-Brie	M3	2,78	3,05	0,91	4
MNHN.F.CB1397	Condé-en-Brie	M3	2,51	3,01	0,83	3
MNHN.F.CB4123	Condé-en-Brie	M3		2,88		
MNHN.F.CB4121	Condé-en-Brie	M3	2,5	2,92	0,86	3
MNHN.F.CB230-M	Condé-en-Brie	M3	2,58	2,98	0,87	3
MNHN.F.CB4142	Condé-en-Brie	M3	2,4	2,81	0,85	4
MNHN.F.CB195	Condé-en-Brie	M3	2,51	2,88	0,87	2
MNHN.F.CB30-M	Condé-en-Brie	M3	2,61	2,97	0,88	4
MNHN.F.CB3052	Condé-en-Brie	M3		2,7		
MNHN.F.CB2713	Condé-en-Brie	M3		2,88		2
MNHN.F.CB5-M	Condé-en-Brie	M3	2,64	3,08	0,86	4
MNHN.F.CB393-BN	Condé-en-Brie	M3	2,41	2,93	0,82	3
MNHN.F.CB198	Condé-en-Brie	M3	2,53	2,91	0,87	4
MNHN.F.Av4814	Avenay	M3	2,81	3,13	0,90	
MNHN.F.Av4743	Avenay	M3		3,18		
MNHN.F.STA285	Saint-Agnan	M3	2,75	3,23	0,85	3
MNHN.F.CB3665	Condé-en-Brie	M4	2,08	2,34	0,89	
UM-AV-17-SK	Avenay	M4		2,7		
MNHN.F.Mu12397	Mutigny	M4	1,94	2,73	0,71	
MNHN.F.Mu171-L	Mutigny	M4	1,79	2,41	0,74	
MNHN.F.GL247-L	Sables de Brasles	M4	1,72	2,47	0,70	
MNHN.F.GLD13	Sables de Brasles	M4	1,98	2,62	0,76	

Tableau S3. Détail des valeurs (en mm) de longueur mésiodistale (L), de largeur labiolinguale (W), de largeur du trigonide (trW) et de largeur du talonide (tlW) mesurées en vue occlusale sur les molaires inférieures de *Peratherium maximum* (Crochet, 1979) de Avenay, Mutigny, Pourcy, Sables de Brasles et Saint-Agnan (Bassin de Paris). Les moyennes des mesures réalisées sur les spécimens de Condé-en-Brie sont précisées. Voir Chapitre 5, Gernelle et al. (2024b : Supplemental material 2) pour le détail des mesures des molaires inférieures de Condé-en-Brie.

Spécimen	Localité	Locus	L (mm)	W (mm)	trW (mm)	tlW (mm)	L/W
	x̄ Condé-en-Brie	**m1**	**2,52**	**1,53**	**1,25**	**1,48**	**1,65**
MNHN.F.Av4599	Avenay	m1	2,69	1,65	1,32	1,57	1,63
MNHN.F.Mu175-L	Mutigny	m1	2,49		1,22		
MNHN.F.Mu5534	Mutigny	m1		1,51	1,25	1,45	
MNHN.F.STA287	Saint-Agnan	m1	2,57	1,51	1,26	1,49	1,70
MNHN.F.GL408-L	Sables de Brasles	m1	2,57	1,53	1,25	1,52	1,68
MNHN.F.GL398-L	Sables de Brasles	m1	2,60	1,59	1,28	1,56	1,64
	x̄ Condé-en-Brie	**m2**	**2,68**	**1,70**	**1,50**	**1,66**	**1,59**
MNHN.F.Av15829	Avenay	m2	2,68	1,69	1,55	1,67	1,59
MNHN.F.Av9014	Avenay	m2	2,47		1,39		
MNHN.F.PY118-L	Pourcy	m2	2,56	1,65	1,39	1,62	1,55
MNHN.F.P20-C	Pourcy	m2	2,41	1,56	1,39	1,49	1,54
MNHN.F.Mu124-L	Mutigny	m2	2,70	1,69	1,48	1,65	1,60
MNHN.F.Mu6136	Mutigny	m2	2,67	1,63	1,43	1,57	1,64
MNHN.F.STA300	Saint-Agnan	m2	2,94	1,75	1,63	1,73	1,68
MNHN.F.STA299	Saint-Agnan	m2	2,69	1,79	1,48	1,78	1,50
MNHN.F.STA293	Saint-Agnan	m2	2,83	1,84	1,62	1,76	
MNHN.F.GL226-L	Sables de Brasles	m2	2,72	1,77	1,55	1,71	1,54
MNHN.F.GL307-L	Sables de Brasles	m2	2,74	1,79	1,52	1,79	1,53
	x̄ Condé-en-Brie	**m3**	**2,68**	**1,62**	**1,54**	**1,57**	**1,66**
MNHN.F.Av4815	Avenay	m3	2,91	1,82	1,78	1,67	1,60
MNHN.F.Av6789	Avenay	m3	2,38	1,44	1,33	1,41	1,65
UM-AV-18-SK	Avenay	m3	2,28	1,45	1,39	1,33	1,57
MNHN.F.Av13-CN	Avenay	m3	2,40	1,42	1,35	1,33	1,69
MNHN.F.Mu178-L	Mutigny	m3	2,56	1,59	1,52	1,55	1,61
MNHN.F.Mu5518	Mutigny	m3	2,79	1,66	1,54	1,56	1,68
MNHN.F.Mu5949	Mutigny	m3	2,62	1,64	1,51	1,56	1,60
MNHN.F.Mu6636	Mutigny	m3	2,79	1,70	1,55	1,64	1,64
MNHN.F.STA290	Saint-Agnan	m3	2,78	1,68	1,59	1,63	1,65
	x̄ Condé-en-Brie	**m4**	**2,52**	**1,38**	**1,37**	**1,20**	**1,82**
MNHN.F.Av16150	Avenay	m4	2,61	1,48	1,48	1,24	1,76
MNHN.F.Mut3-BN	Mutigny	m4	2,42	1,23	1,23	1,01	1,97
MNHN.F.STA304	Saint-Agnan	m4	2,62	1,39	1,39	1,20	1,88

Tableau S4. Valeurs (en mm) de longueur mésiodistale (L) et largeur labiolinguale (W) mesurées en vue occlusale sur les molaires de *Peratherium monspeliense* de Mas de Gimel, Le Théron et Coulondres. Les spécimens en gras sont ceux attribués à *Pt. matronense* par Crochet (1980). Un doute subsiste autour de l'attribution d'une des molaires supérieures (UM-MGL-153) à *Pt. monspeliense*.

Spécimen	Localité	Locus	L (mm)	W (mm)	L/W
UM-MGL-715	Mas de Gimel	m1	1,67	1,03	1,62
UM-MGL-721	Mas de Gimel	m1	1,63	1	1,63
UM-MGL-793	Mas de Gimel	m1	1,52	0,88	1,73
UM-MGL-117	**Mas de Gimel**	**m2**	**1,68**	**1,02**	**1,65**
UM-MGL-312	Mas de Gimel	m2	1,66	1,01	1,64
UM-MGL-111	**Mas de Gimel**	**m3**	**1,69**	**0,99**	**1,71**
UM-MGL-313	Mas de Gimel	m3	1,98	1,22	1,62
UM-MGL-314	Mas de Gimel	m3	1,98	1,18	1,68
UM-MGL-316	Mas de Gimel	m3	1,99	1,07	1,86
UM-MGL-318	Mas de Gimel	m4	1,98	1,06	1,87
UM-MGL-153	**Mas de Gimel**	**M1**	**1,41**	**1,5**	**0,94**
UM-MGL-304	Mas de Gimel	M1	1,79	1,81	0,99
UM-MGL-305	Mas de Gimel	M1	1,92	1,86	1,03
UM-MGL-306	Mas de Gimel	M3	1,76	2,17	0,81
UM-MGL-722	Mas de Gimel	M3	1,94	2,27	0,85
UM-MGL-302	Mas de Gimel	M4	1,47		
UM-MGL-303	Mas de Gimel	M4	1,5		
UM-MGL-719	Mas de Gimel	M4	1,59		
UP-SRT-24-2	Le Théron	M1	1,77	1,77	1,00
UP-SRT-24-3	Le Théron	M2		1,93	
UP-SRT-24-4	Le Théron	M3	1,79	2,25	0,80
UP-SRT-21-25	Le Théron	M4	1,49	1,96	0,76
UM-CLR-4	Coulondres	M3	1,81	2,42	0,75
UM-CLR-5	Coulondres	M1	1,85		
UM-CLR-6	**Coulondres**	**M1**		**1,69**	

Tableau S5. Détail des valeurs (en mm) de longueur mésiodistale (L) et de largeur labiolinguale (W) mesurées en vue occlusale sur les molaires supérieures de *Peratherium* sp. nov. 2 de Prémontré (Aisne). Les molaires conservées sur un fragment de maxillaire sont listées en premier. L'holotype est indiqué en gras.

Spécimen	Locus	L (mm)	W (mm)	L/W
SLP-29-PE-235	M2	1,7	2,07	0,82
SLP-29-PE-235	M3	1,73	2,16	0,80
SLP-29-PE-237	**M1**	**1,7**	**1,68**	**1,01**
SLP-29-PE-237	**M2**	**1,74**	**1,9**	**0,92**
SLP-29-PE-237	**M3**	**1,7**	**2,07**	**0,82**
SLP-29-PE 843	M3	1,78	2,11	0,84
SLP-29-PE-876	M3	1,9	2,21	0,86
SLP-29-PE 1010	M3	1,69	2,19	0,77
SLP-29-PE 1079	M2	1,53	1,85	0,83
SLP-29-PE 1079	M3	1,65	2,04	0,81
SLP-29-PE-1504	M2	1,83	1,93	0,95
SLP-29-PE-1504	M3	1,91	2,14	0,89
SLP-29-PE-1543	M2	1,62	1,97	0,82
SLP-29-PE-1543	M3	1,64	2,01	0,82
SLP-29-PE-1566	M1	1,61	1,68	0,96
SLP-29-PE-1566	M2	1,77	1,92	0,92
SLP-29-PE-1694	M2		2,33	
SLP-29-PE-1694	M3	2,04	2,35	0,87
SLP-29-PR 2454	M2	1,62	1,78	0,91
PRE 332	M1		1,85	
SLP-29-PE 336	M1	1,67	1,71	0,98
SLP-29-PE 573	M1	1,62	1,72	0,94
PRE 603	M1	1,98	2,05	0,97
PRE 684	M1	1,7	1,71	0,99
PRE 720	M1	1,66	1,7	0,98
PRE 963	M1	1,78	1,76	1,01
PRE 1223	M1	1,7	1,65	1,03
PRE 1225	M1	1,72	1,97	0,87
PRE 1230	M1	1,69	1,73	0,98
SLP-29-PE 1784	M1	1,8	1,84	0,98
SLP-29-PR 2621	M1	1,79	1,94	0,92
SLP-29-PR 2765	M1	1,75	1,84	0,95
SLP-29-PR 2784	M1	1,88	2	0,94
SLP-29-PR 3264	M1	1,66	1,64	1,01
SLP-29-PR 3330	M1	1,69	1,77	0,95
SLP-29-PR 3341	M1	1,84	1,97	0,93
SLP-29-PR 3366	M1	1,72	1,69	1,02
SLP-29-PE-280	M2	1,81	1,95	0,93
SLP-29-PE 338	M2	1,84	2,06	0,89
SLP-29-PE 339	M2	1,7	1,89	0,90
PRE 349	M2		2,04	
SLP-29-PE 357	M2	1,81	1,96	0,92

SLP-29-PE 461	M2	1,95	2,11	0,92
PRE 619	M2	1,74	2,04	0,85
PRE 638	M2	1,79	1,95	0,92
PRE 686	M2	1,78	1,97	0,90
PRE 711	M2	1,78	1,97	0,90
PRE 750	M2	1,91	2,18	0,88
SLP-29-PE 935	M2	1,76	2,15	0,82
PRE 958	M2	1,92	2,04	0,94
PRE 1025	M2	1,78	1,97	0,90
PRE 1164	M2	1,83	1,99	0,92
PRE 1219	M2	1,91	2,22	0,86
SLP-29-PE 1612	M2	1,8	1,98	0,91
SLP-29-PE 1650	M2	1,86	1,95	0,95
SLP-29-PE 1661	M2	1,77	1,95	0,91
SLP-29-PR 2064	M2	2,01	2,25	0,89
SLP-29-PR 2068	M2	1,76	2,12	0,83
SLP-29-PR 2289	M2	1,75	1,95	0,90
SLP-29-PR 2290	M2	2,02	2,22	0,91
SLP-29-PR 2319	M2	1,7	1,85	0,92
SLP-29-PR 2465	M2	1,77	1,85	0,96
SLP-29-PR 3228	M2	1,72	1,9	0,91
SLP-29-PR 3259	M2	1,62	1,96	0,83
SLP-29-PR 3308	M2	1,72	2,03	0,85
SLP-29-PE 159	M3	1,8	2,09	0,86
PRE 257	M3	1,91	2,35	0,81
PRE 269	M3	1,71	1,99	0,86
PRE 275	M3	1,69	2,13	0,79
SLP-29-PE 346	M3	1,99	2,48	0,80
SLP-29-PE 400	M3	1,71	2,13	0,80
SLP-29-PE 438	M3	1,7	2,08	0,82
SLP-29-PE 463	M3	1,82	2,18	0,83
PRE 524	M3	1,7	2,13	0,80
SLP-29-PE 535	M3	1,66	2,05	0,81
SLP-29-PE 561	M3	1,82	2,12	0,86
SLP-29-PE 579	M3	1,83	2,43	0,75
SLP-29-PE 604	M3	1,78	1,98	0,90
SLP-29-PE 1116	M3	1,75	2,15	0,81
PRE 1143	M3	1,88	2,31	0,81
PRE 1209	M3	1,71	2,2	0,78
PRE 1212	M3	1,7	2,09	0,81
SLP-29-PE 1631	M3	1,68	2,04	0,82
SLP-29-PE 1682	M3	1,76	2,03	0,87
SLP-29-PE 1765	M3	1,8	2,3	0,78
SLP-29-PE 1809	M3	1,74	2,04	0,85
SLP-29-PE 1810	M3	1,8	2,12	0,85
SLP-29-PR 1885	M3	1,79	2,25	0,80
SLP-29-PR 2261	M3	1,7	2,01	0,85
SLP-29-PR 2618	M3	1,69	2,05	0,82

SLP-29-PR 2645	M3	1,76	2,13	0,83
SLP-29-PR 2702	M3	1,76	2,08	0,85
SLP-29-PR 2738	M3	1,89	2,24	0,84
SLP-29-PR 2764	M3	1,71	2,02	0,85
SLP-29-PR 3218	M3	1,89	2,3	0,82
SLP-29-PR 3277	M3	1,84	2,2	0,84
SLP-29-PE 212	M4	1,51	2,07	0,73
PRE 348	M4	1,36	2,06	0,66
SLP-29-PE 782	M4	1,5	2,15	0,70
SLP-29-PE 1593	M4	1,35	1,91	0,71
SLP-29-PR 2769	M4	1,39	2,42	0,57
SLP-29-PR 2899	M4	1,39	2,12	0,66

Tableau S6. Détail des valeurs (en mm) de longueur mésiodistale (L) et de largeur labiolinguale (W) mesurées en vue occlusale sur les molaires inférieures de *Peratherium* sp. nov. 2 de Prémontré (Bassin de Paris). Les molaires conservées sur un fragment de dentaire sont listées en premier.

Spécimen	Locus	L (mm)	TrW (mm)	TlW (mm)	Surface (mm²)
SLP-29-PE 455	m3	1,83	1,03	1,01	1,87
SLP-29-PE 1052	m4	1,7	0,86	0,61	1,25
SLP-29-PE-1181	m3	1,85	1,06	1,07	1,97
SLP-29-PE 1263	m3	1,75	0,99	0,94	1,69
SLP-29-PE-1533	m3	1,88	1,01	0,99	1,88
SLP-29-PE-1533	m4	1,88	1,01	0,86	1,76
SLP-29-PE-1547	m2	1,73	0,96	1,01	1,70
SLP-29-PR 2534	m3	1,84	1,06	1,01	1,90
PRE 256	m1	1,55	0,75	0,87	1,26
PRE 653	m1	1,64	0,79	0,96	1,44
PRE 654	m1	1,56	0,72	0,86	1,23
PRE 918	m1	1,58	0,75	0,9	1,30
PRE 1195	m1	1,57	0,8	0,95	1,37
SLP-29-PE 93	m2	1,76	1	1,05	1,80
PRE 254	m2	1,67	0,87	0,98	1,54
PRE 261	m2	1,79	0,98	1,11	1,87
PRE 267	m2	1,73	0,93	0,97	1,64
SLP-29-PE 375	m2	2,01	1,06	1,19	2,26
PRE 600	m2	1,77	0,95		0,84
PRE 892	m2	2,05	1,11	1,2	2,37
SLP-29-PE 917	m2	1,75	0,92	1,02	1,70
SLP-29-PE 922	m2	1,73	0,94	0,98	1,66
SLP-29-PE 923	m2	1,79	0,96	1,03	1,78
SLP-29-PE 1136	m2	1,7	0,87	1,04	1,62
PRE 1150	m2	1,74	1,01	0,93	1,69
SLP-29-PE 1748	m2	1,7	0,98	1,04	1,72
SLP-29-PE 1753	m2	1,86	1,06	1,08	1,99
SLP-29-PE 1755	m2	1,75	0,94	1,01	1,71
SLP-29-PE 1758	m2	1,73	1,02	1,02	1,76
SLP-29-PE 1767	m2	1,7	0,88	0,98	1,58

SLP-29-PE 1844	m2	1,72	1	0,93	1,66
SLP-29-PR 2188	m2	1,9	0,97	1,05	1,92
SLP-29-PR 2294	m2	1,77			0,00
SLP-29-PR 2298	m2	1,75	1,01	1,06	1,81
SLP-29-PR 2379	m2	1,7	0,91	1,01	1,63
SLP-29-PR 2416	m2	1,86	1,03	1,05	1,93
SLP-29-PR 2583	m2	2,03	1,16	1,23	2,43
SLP-29-PR 2667	m2	1,72	0,96	1,01	1,69
SLP-29-PR 2704	m2	1,75	0,95	1,03	1,73
SLP-29-PR 2974	m2	1,66	0,9	0,96	1,54
SLP-29-PR 3206	m2	1,64	0,96	1,02	1,62
SLP-29-PR 3250	m2	1,9	1,07	1,18	2,14
SLP-29-PR 3348	m2	1,74	0,92	1,02	1,69
SLP-29-PR 3353	m2	1,7	0,96	1	1,67
PRE 55	m3	1,78	1	0,96	1,74
PRE 263	m3	1,85	1,06	1,05	1,95
PRE 274	m3	1,9	1,07	1,04	2,00
SLP-29-PE 353	m3	1,75	0,97	0,97	1,70
PRE 436	m3	1,74	1,01	0,95	1,71
SLP-29-PE 582	m3	1,9	1,13	1,17	2,19
PRE 639	m3	1,8	1,05	1,03	1,87
SLP-29-PE 908	m3	1,81	1,03	1,04	1,87
SLP-29-PE 913	m3	1,72	1,08	1,04	1,82
SLP-29-PE 1130	m3	1,86	1,04	1,01	1,91
SLP-29-PE 1151	m3	1,9	1,08	1,08	2,05
SLP-29-PE 1806	m3	1,69	0,97	0,94	1,61
SLP-29-PE 1831	m3	1,91	1,16	1,11	2,17
SLP-29-PR 2270	m3	1,78	0,97	0,92	1,68
SLP-29-PR 2273	m3	1,8	1,02	0,98	1,80
SLP-29-PR 2305	m3	2,06	1,16	1,12	2,35
SLP-29-PR 2593	m3	1,81	1,05	0,96	1,82
SLP-29-PR 2607	m3	1,76	1,02	0,98	1,76
SLP-29-PR 2653	m3	1,75	0,97	0,94	1,67
SLP-29-PR 2717	m3	1,73	1	0,97	1,70
SLP-29-PR 2720	m3	1,97	1,12	1,1	2,19
SLP-29-PR 2952	m3	1,78	1,09	0,97	1,83
SLP-29-PE 42	m4	1,86	0,95	0,75	1,58
PRE 80	m4	1,73	0,87	0,65	1,31
SLP-29-PE 217	m4	1,76	0,97	0,76	1,52
PRE 433	m4	1,83	0,95	0,72	1,53
PRE 649	m4	1,84	1	0,76	1,62
PRE 841	m4	1,79	0,96	0,71	1,49
PRE 1220	m4	1,79	1	0,76	1,58
SLP-29-PE 1681	m4	1,68	0,94	0,85	1,50
SLP-29-PE 1737	m4	1,84	0,96	0,68	1,51
SLP-29-PE 1843	m4	1,88	0,95	0,74	1,59
SLP-29-PR 2268	m4	1,71	0,89	0,71	1,37
SLP-29-PR 2608	m4	1,72	0,94	0,81	1,51
SLP-29-PR 2752	m4	1,99	1,08	0,86	1,93
SLP-29-PR 2920	m4	1,83	0,91		0,83
SLP-29-PR 3088	m4	1,92	1,02	0,82	1,77
SLP-29-PR 3383	m4	1,71	0,83	0,69	1,30

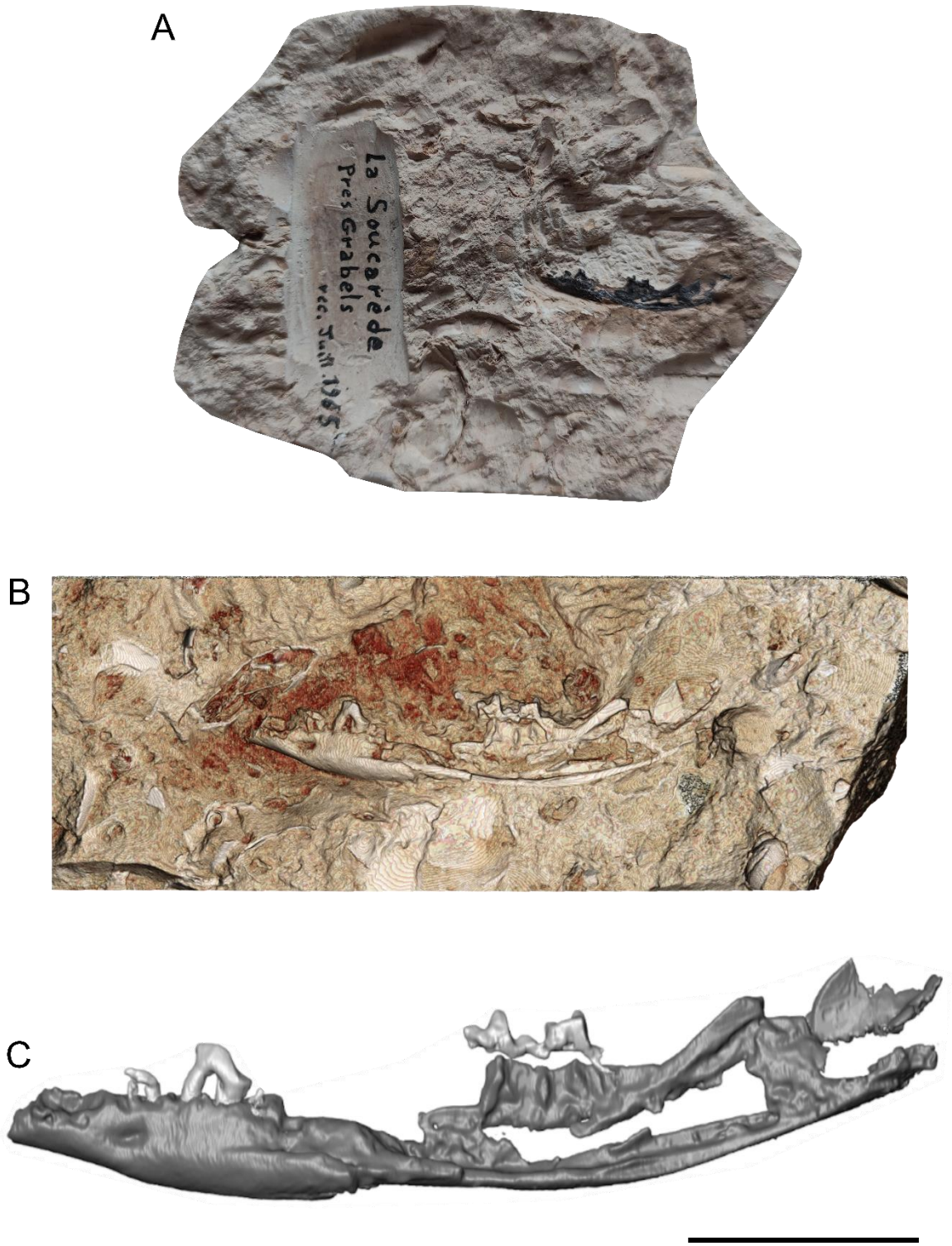

Figure S1. Extraction numérique d'une hémi-mandibule gauche partielle préservant p1-p2 usées et m3-m4 brisées (UM-SRD-1) de La Soucarède (nord-ouest de Montpellier). Cette localité, mentionnée par Hartenberger et al. (1969), est corrélée aux localités de Mas de Gimel et Naples, elle est donc rapprochée du niveau-repère ~MP10. **A**. Bloc contenant le spécimen, visible sur la droite (photographie non à l'échelle). **B**. 1er rendu après Ct-scan, obtenu via le logiciel MorphoDig (non à l'échelle). **C**. Modèle 3D surfacique du spécimen en vue labiale. Échelle : 5 mm.

A revision of the late early Eocene mammal faunas from Mas de Gimel and Naples (Montpellier, Southern France) and the description of a new theridomorph rodent

Monique VIANEY-LIAUD*
Fabrice LIHOREAU*
Institut des Sciences de l'Évolution (UM, CNRS, IRD, EPHE),
Université Montpellier, Place Bataillon, 34095 Montpellier (France)
monique.vianey-liaud@umontpellier.fr
fabrice.lihoreau@umontpellier.fr

Floréal SOLÉ
Directorate Earth and History of Life, Royal Belgian Institute of Natural Sciences,
Rue Vautier 29, B-1000 Brussels (Belgium)
fsole@naturalsciences.be

Killian GERNELLE
Institut des Sciences de l'Évolution (UM, CNRS, IRD, EPHE),
Université Montpellier, Place Bataillon, 34095 Montpellier (France)
killian.gernelle@umontpellier.fr

Quentin VAUTRIN
Institut des Sciences de l'Évolution (UM, CNRS, IRD, EPHE),
Université Montpellier, Place Bataillon, 34095 Montpellier (France)
and Réserve naturelle nationale du Lot et Géoparc mondial UNESCO Causses du Quercy,
11 rue traversière, 46240 Labastide-Murat (France)
qvautrin@parc-causses-du-quercy.org

Constance BRONNERT
Département Origines et Évolution, CR2P URM 7207 (MNHN, CNRS, Sorbonne Université),
Muséum national d'Histoire naturelle, 57 rue Cuvier, 75231 Paris cedex 05 (France)
constance.bronnert@mnhn.fr

Hélène BOURGET
Institut des Sciences de l'Évolution (UM, CNRS, IRD, EPHE),
Université Montpellier, Place Bataillon, 34095 Montpellier (France)
helene.bourget@umontpellier.fr

Dominique VIDALENC
103 Avenue François Mitterand, 31800 Saint-Gaudens (France)
vidalenc.dominique@wanadoo.fr

Rodolphe TABUCE*
Institut des Sciences de l'Évolution (UM, CNRS, IRD, EPHE),
Université Montpellier, Place Bataillon, 34095 Montpellier (France)
rodolphe.tabuce@umontpellier.fr (corresponding author)

Submitted on 3 July 2023 | accepted on 19 December 2023 | published on 4 July 2024
*, the three authors contributed equally to this work.

urn:lsid:zoobank.org:pub:7636FF19-0310-4C94-AE66-6EBECCF1383C

Vianey-Liaud M., Lihoreau F., Solé F., Gernelle K., Vautrin Q., Bronnert C., Bourget H., Vidalenc D. & Tabuce R. 2024. — A revision of the late early Eocene mammal faunas from Mas de Gimel and Naples (Montpellier, Southern France) and the description of a new theridomorph rodent. *Geodiversitas* 46 (10): 387-422. https://doi.org/10.5252/geodiversitas2024v46a10. http://geodiversitas.com/46/10

ABSTRACT

European terrestrial mammal sites dated from the late Ypresian are predominantly known from the Paris Basin. In Southern Europe (France and Spain), some localities are also known, but all have only yielded small faunas, composed by few taxa. An exception is the rich locality of Mas de Gimel (city of Montpellier, Hérault, France), which has long been considered the reference fauna of the late Ypresian in Southern Europe. Curiously however, only the rodents, artiodactyls and metatherians from this key locality have been studied in detail since the 1960s. Here, based on the original collection housed in the University of Montpellier, we revise the entire mammal taxa, which leads us to identify 38 species among 12 orders. We also study the close and co-eval localities of Naples and Naples 2, where we identify 23 species among 10 orders. Among the species identified from the three localities, we describe the new theridomorph rodent *Hartenbergeromys pailladensis* n. sp., characterized by numerous thin high extra ridges on upper and lower molars. Compared with the four standard MP (Mammal Paleogene) reference-levels for the European Early Eocene (MP7, MP8+9, MP10a, and the putative 'MP10b'), the faunal assemblage from Mas de Gimel and Naples is attributed to the MP10a, representing a major European reference for this period. This study also supports the idea that, during the late Ypresian, the mammal faunas from North- and Southwestern Europe are quite homogeneous.

KEY WORDS
Mammalia,
Placentalia,
Metatheria,
Eocene,
Ypresian,
Europe,
France,
new species.

RÉSUMÉ

Révision des faunes de mammifères de la fin de l'Éocène inférieur de Mas de Gimel et de Naples (Montpellier, sud de la France) et description d'un nouveau rongeur théridomorphe.

Les sites européens ayant livré des mammifères terrestres datés de la fin de l'Yprésien sont principalement localisés dans le Bassin de Paris. En Europe méridionale (France et Espagne), quelques localités sont également connues, mais toutes n'ont livré que des faunes pauvres, composées de seulement quelques taxons, à l'exception de la localité de Mas de Gimel (ville de Montpellier, Hérault, France), longtemps considérée comme la faune de référence de la fin de l'Yprésien en Europe méridionale. Curieusement, seuls les rongeurs, les artiodactyles et les métathériens de cette localité-clé ont été étudiés en détail depuis les années 1960. Sur la base de la collection originale conservée à l'Université de Montpellier, nous révisons l'ensemble des taxons de mammifères, ce qui nous amène à identifier 38 espèces parmi 12 ordres. Nous étudions également les localités voisines et contemporaines de Naples et Naples 2, où nous identifions 23 espèces parmi 10 ordres. Parmi les espèces identifiées dans les trois localités, nous décrivons le nouveau rongeur théridomorphe *Hartenbergeromys pailladensis* n. sp., caractérisé par de nombreuses crêtes fines et hautes sur les molaires supérieures et inférieures. Comparé aux quatre niveaux de référence MP (Mammal Paleogene) pour l'Éocène inférieur européen (MP7, MP8+9, MP10a et le possible 'MP10b'), l'assemblage faunique de Mas de Gimel et de Naples est attribué au MP10a, et représente une référence européenne majeure pour cette période. Ce travail renforce l'hypothèse de l'homogénéité des faunes mammaliennes du Nord- et du Sud-Ouest européen durant l'Yprésien récent.

MOTS CLÉS
Mammalia,
Placentalia,
Metatheria,
Éocène,
Yprésien,
Europe,
France,
espèce nouvelle.

INTRODUCTION

The Ypresian or early Eocene (56-47.8 Ma) corresponds to a key period of the mammalian radiation. At a worldwide scale, study of the fossil record gives evidence for the origin, radiation and dispersals of most extant mammalian orders during this time interval (e.g., Rose 2006). In western Europe, recent data has also shown that an intra-European provincialism affected mammals during this period, with the existence of two bioprovinces (North vs South) during the early-middle Ypresian (Marandat *et al.* 2012). It has been proposed that short-term climate changes, the so-called Eocene Thermal Maxima (ETMs) triggered this provincialism whereas a subsequent long-term climate warning, the Early Eocene Climate Optimum (EECO) caused European faunal homogenization during the late Ypresian (Noiret *et al.* 2016). However, these apparent synchronicities between mammal evolution and climate changes are based on few data, whether they are mere coincidences or reflect causal relationships remain unknown.

The uncertainties are essentially due to: 1) the absence of available accurate dating of most European mammal faunas relative to ETMs and EECO; and to 2) the lack of a comprehensive paleontological dataset (e.g., only provisional

faunal lists are available for many localities). Regarding the time period of the apparent faunal homogenization, for instance, a more solid taxonomic framework is required for the few known localities from Southwestern France (Mas de Gimel, Naples, Mas de Piquet, and Azillanet) compared to the localities from Northern France (e.g., Prémontré, Grauves, Cuis, Monthelon, Mancy, Chavot, Saint-Agnan, and Venteuil). Among these localities, Mas de Gimel (city of Montpellier, Hérault) was frequently considered as the reference fauna of the late Ypresian in Southwestern France, and was correlated with the MP10 reference level (i.e., Grauves) of the mammalian biochronological scale for the European Paleogene (see Cappetta *et al.* 1968; Hartenberger *et al.* 1969; Hartenberger 1975; Escarguel 1999; BiochroM' 1997). However only rodents (Hartenberger 1971, 1975; Escarguel 1999; Vianey-Liaud & Marivaux 2021; Vianey-Liaud *et al.* 2022), artiodactyls (Sudre *et al.* 1983; Sudre & Lecomte 2000), and metatherians (Crochet 1979, 1980) have been studied in detail and the systematic assignment of the other mammals only lies on the original mention by Cappetta *et al.* (1968). Regarding the other vertebrate groups, only the characiform fishes have been studied (Cappetta *et al.* 1972; Monod & Gaudant 1998).

The main purpose of this study is therefore to provide a comprehensive and updated overview of the mammal fauna for Mas de Gimel, based on the original collection housed in the University of Montpellier. Our conclusions are also based on new specimens sorted from sediment samples conserved in the same institute since the 1960s. We also study the faunas from Naples and Naples 2, two localities which are coeval in age and geographically situated very close to Mas de Gimel. From Naples, only the artiodactyls (Sudre & Lecomte 2000) and rodents (Escarguel 1999; Vianey-Liaud & Marivaux 2021; Vianey-Liaud *et al.* 2022) have been studied; Naples 2 is a new unpublished locality. In this paper, we describe from Mas de Gimel and Naples a new theridomorph rodent and we propose new systematic assignments for mammals from Mas de Gimel, Naples, and Naples 2. Adding numerous taxa among Eulipotyphla, Pantolesta, Apatotheria, Primates, Chiroptera, Hyaenodonta, Perissodactyla and Artiodactyla, we strengthen correlations with the other European late Ypresian (MP10) localities. For ongoing and future paleobiogeographic and diversity analysis, we also establish for Europe the updated faunal lists for the middle Ypresian (MP8+9) to early Lutetian (MP11) time interval, with a peculiar focus on MP10 faunas. For this purpose, we follow Godinot *et al.* (2018) who proposed Rouzilhac as a potential reference-level for the latest Ypresian (here named 'MP10b', pending approval), implying that Grauves would be MP10a.

GEOLOGICAL AND HISTORICAL CONTEXT

Before the 1960s, the only known early Eocene locality near Montpellier was Mas de Piquet (Fig. 1), which yielded *Hyaenodictis blayaci* (Stehlin, 1926), *Lophiaspis occitanicus* Depéret, 1910, *Lophiodon* sp., and *Pachynolophus* aff. *duvali* Pomel, 1847 (Rouville & Delage 1896: 720; Roman & Gennevaux 1907; Depéret 1921; Stehlin 1926; Solé *et al.* 2018; Vautrin 2019). The precise location of this fossiliferous locus is unfortunately unknown but, in the same area, Hartenberger *et al.* (1969) mentioned the discovery of a second fossiliferous spot, Mas de Piquet 2, with *Pachynolophus* sp. Despite the low diversity of the fossil assemblages, both Mas de Piquet and Mas de Piquet 2 faunas are considered close to the MP10a (see discussion in Danilo *et al.* 2013). Fortunately, as early as the 1960's, geological and paleontological survey in the supposedly coeval late Ypresian levels around Montpellier led to the discovery of several more diversified new localities, providing more constrained ages (Cappetta *et al.* 1968; Hartenberger *et al.* 1969). These field discoveries benefited from important urban development works of Montpellier; the city was then in full expansion (construction of new districts and roads). In 1968, Mas de Gimel was thus discovered east of the *Lac des Garrigues* by the famous field and tectonic geologist Maurice Mattauer during the construction of the Paillade district (now called "quartier Mosson"). The fossiliferous levels were rapidly exploited by the paleontologists of the University of Montpellier during the short interval of these public works, but fossiliferous deposits were unfortunately quickly covered with the completion of the road works (Guilhem de Poitiers Avenue), making access them impossible today (Fig. 1). Twenty years later, in 1988, west of the Lake of Garrigues and nearly 300 m west from Mas de Gimel, the localities of Naples and Naples 2 were discovered during the digging of the foundations of the sports hall Pierre-de-Coubertin, Avenue of Naples.

Eocene levels of Mas de Gimel, Naples, and Naples 2 are south of the Montpellier Thrust, a major onshore compressional structure related to the Pyrenean orogeny (Fig. 1); noteworthy only few outcrops dated from the Eocene occur south of this thrust whereas the Eocene is very well exposed north of this structure. The fossiliferous beds of Mas de Gimel and Naples belong to the same lithostratigraphic unit consisting of brecciated levels underlying whitish to brownish marl with lignite bed. Specimens from Mas de Gimel come from four different thin and superimposed levels (Fig. 1; Cappetta *et al.* 1968). The numbering of the specimens in the original collection does not reflect the existence of several fossiliferous beds and only one level (Mas de Gimel) has been retained. Regarding Naples, two levels have yielded mammals, a dark brown marl, rich in organic matter (Naples) and a whitish marly limestone (Naples 2). Whereas Mas de Gimel and Naples levels essentially yielded micromammals represented by isolated teeth, Naples 2 yielded principally well-preserved remains of large mammals. The Ypresian levels of these localities are overlying Kimmeridgian marine limestone and are underlying Eocene lacustrine limestone poorly constrained in age; see Luccisano *et al.* (2020) for discussion about the age of the late Ypresian/early Lutetian lacustrine limestone of Aumelas, which is possibly coeval with that overlying the Ypresian levels of Mas de Gimel and Naples.

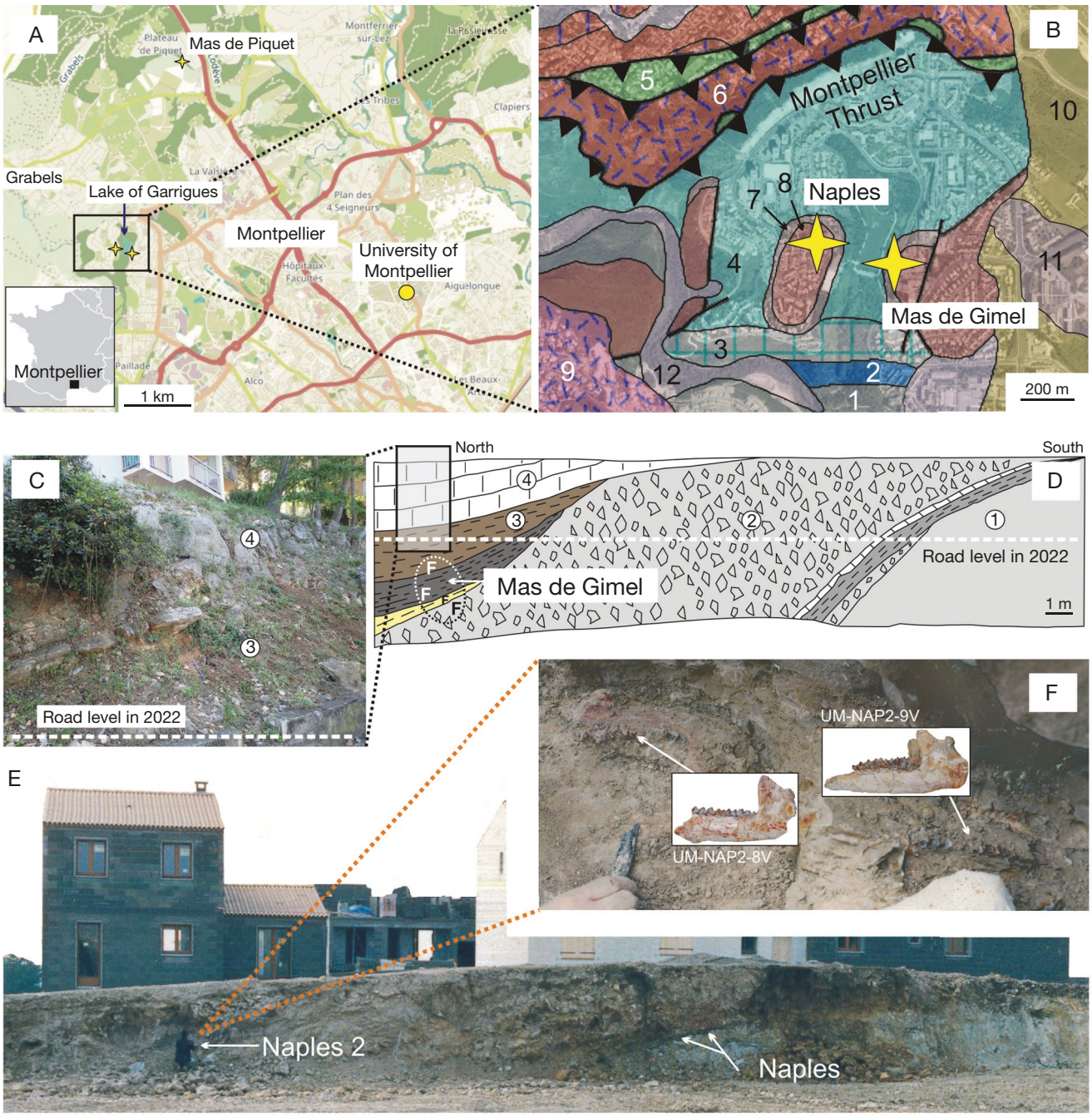

FIG. 1. — Geographic (**A**) and geological map (**B**) showing the location of Mas de Gimel, Naples, and Naples 2 (Montpellier, Herault). Numbers: **1**, Callovian; **2**, lower Oxfordian; **3**, upper Oxfordian; **4**, lower Kimmeridgian; **5**, Maastrichtian; **6**, Paleocene ["Vitrollian"]; **7**, late Ypresian; **8**, Ypresian/Lutetian; **9**, Oligocene; **10**, Miocene; **11**, Pliocene; **12**, Holocene. Actual view (**C**) and schematic diagram in 1968 (**D**, modified from Cappetta *et al.* 1968) of Mas de Gimel outcrop, showing that fossiliferous deposits are now inaccessible (under the road level); Numbers: **1**, lower Kimmeridgian; **2**, late Ypresian brecciated limestone; **3**, late Ypresian brownish marl; **4**, late Ypresian/early Lutetian lacustrine limestone. View of Naples and Naples 2 localities in 1988 during urban development works (**E**) and detailed view of Naples 2 fossiliferous level, showing two mandibles of *Lophiodon* Cuvier, 1822 during excavations (**F**).

MATERIAL AND METHODS

DENTAL NOMENCLATURE

For Eulipotyphla, Apatotheria, Chiroptera, Pantolesta, Plesiadapiformes, Primates, Hyaenodonta, Carnivoraformes, and Perissodactyla, we follow the nomenclature of Van Valen (1966). For Metatheria, Rodentia and Artiodactyla, we follow Muizon & Ladevèze (2022), Vianey-Liaud & Marivaux (2017) and Boisserie *et al.* (2010), respectively.

IMAGES AND MEASUREMENTS OF SPECIMENS

Small mammals are illustrated by X-ray µCT surface reconstructions using EasyTom 150 microtomograph (MRI platform) and drawings (for the new rodent species only). Medium

(equoids) to large mammal teeth, coated with magnesium, are pictured, respectively, with a Leica M205C stereomicroscope using Leica LAS multifocus image fusion and a Nikon D750/micro-Nikkor 105 mm using Combine ZP for focus stacking. Measurements (in mm) have been made by Leica Application Suite (LAS) for small specimens and calliper for larger specimens.

ABBREVIATIONS

L	maximal mesio-distal length;
W	maximal labio-lingual width;
N	number of specimens;
MP	Mammal Paleogene reference level.

Institutional abbreviations

MNHN	Muséum national d'Histoire naturelle, Paris;
UM	University of Montpellier.

Collection abbreviations

MNHN.F	MNHN Palaeontological collection;
MNHN.F.AL	collection "Agéen Lemoine";
MNHN.F.GR	Grauves collection;
MNHN.F.MT	Monthelon collection;
MNHN.F.PRE	Prémontré collection;
MNHN.F.SLP	Société laonnoise de Paléontologie collection;
MNHN.F.STA	Saint-Agnan collection;
UM-MGL	Mas de Gimel collection;
UM-NAP	Naples collection;
UM-NAP2	Naples 2 collection (regarding this locality, the suffix following the specimen number refers to the initial private collection, V: Dominique Vidalenc, L: Eric Lopez).

RESULTS

REVISION OF THE MAMMAL FAUNAS FROM MAS DE GIMEL AND NAPLES

Mas de Gimel

Metatheria. Among metatherians from Mas de Gimel (N = 101, including unpublished material), three herpetotheriid species are recognized by Crochet (1979, 1980): *Peratherium matronense* Crochet, 1979, *Peratherium monspeliense* Crochet, 1979, and *Amphiperatherium bourdellense* Crochet, 1979. Mas de Gimel is the type locality for *P. monspeliense*. Upper and lower molars of *P. matronense* and *P. monspeliense* from Mas de Gimel are highly similar in morphology, but those of *P. matronense* are smaller (e.g., UM-MGL-310, left m1, L = 1.60; W = 0.94, Fig. 2A). An ongoing revision of the systematics of European metatherians from the early Eocene will address the taxonomic status of those herpetotheriids. Pending further conclusions, the temporal extensions of *P. matronense* and *P. monspeliense* remain large. Indeed, *Peratherium matronense* is documented from localities in the MP7-MP8+9 interval (Rians and possibly Fournes; Godinot 1981, Marandat 1991), MP8+9 (Condé-en-Brie, the type-locality, Avenay, Sables de Brasles, Sézanne-Broyes and Evere; Crochet 1980, Smith & Russell 1992), MP10a (Coulondres; Crochet 1980) and ?MP10-11 (Vielase, Quercy; Legendre *et al.* 1992) to the middle Eocene locality of Santa Clara (Spain; Peláez-Campomanes *et al.* 1989). *Peratherium monspeliense* is mostly restricted to MP10a faunas from southern France (Coulondres, Saint-Clement-de-Rivière and Azillanet; Crochet 1980, Marandat 1986) and is presumably present in Fournes and La Gasque (MP7-MP8+9 interval; Marandat 1991; Noiret *et al.* 2016), and Geiseltal (MP12-13; Storch & Haubold 1989).

Regarding *Amphiperatherium bourdellense*, it spans much of the Eocene (Crochet 1979: fig. 16), from MP8+9 localities of the Paris Basin (Condé-en-Brie, Avenay, Sables de Brasles and Sézanne-Broyes) to its type locality, Le Bretou (Quercy, MP16, late Eocene) (Crochet 1980). The only tooth from Mas de Gimel attributed by Crochet (1980) to this species is a worn left m1 with a fragmented talonid (UM-MGL-143, W = 0.95, Fig. 2B). The morphology of this molar is similar to that of *P. matronense* and *P. monspeliense* (Fig. 2A); it differs from the only m1 of *A. bourdellense* available from Le Bretou (UM-BRT-843, unpublished specimen) by a higher paraconid. An assignment to *P. matronense* or *P. monspeliense* is therefore more parsimonious for UM-MGL-143.

The poorly preserved lingual fragment of right M3 UM-MGL-309 exhibits two relatively huge conules and a large protocone, larger than all homologous dental remains from Mas de Gimel. Among the relatively large herpetotheriid species, this specimen is closer in size (as deduced from the length of the preproto- and postprotocristae and the size of the conules) to the holotype of *Amphiperatherium maximum* Crochet, 1979 (a species only known in Saint-Agnan and Grauves among French [-]MP10a localities; Crochet 1980;Louis & Laurain 1983), than to the slightly smaller *Amphiperatherium bastbergense* Crochet, 1979, the latter being probably present in Naples. However, the fragmentary nature of UM-MGL-309 and the weakly documented intraspecific variation of *A. maximum* M3 prevent its formal attribution; it is hereafter named Herpetotheriidae gen. and sp. indet.

We also identify two peradectid metatherians, the first known in Mas de Gimel. One of these taxa is documented by a small right labial fragment of M2 (UM-MGL-716, L = 1.48, Fig. 2C) displaying gracile and almost triangular paracone and metacone, a nearly straight centrocrista (only just labially curved, clearly distinct from the V-shaped centrocrista of herpetotheriids), a salient postmetacrista forming a high distal wall on the stylar shelf, and labiolingually pinched stylar cusps distal to the deepest point of the ectoflexus, of which one is distally placed on the stylar shelf compared to the apex of the metacone. Up to now, the combination of these characters is only observable on *Peradectes* sp. from Azillanet (Marandat 1986: pl. 1, fig. 2) and Coulondres (Crochet 1980: fig. 28), limiting the attribution of UM-MGL-716 to cf. *Peradectes* sp. in Marandat (1986).

The right m4 UM-MGL-320 (Fig. 2D, L > 1.59 mm; W > 0.85 mm) is damaged on the whole labial margin and on the lingual part of the talonid. The trigonid is apparently longer than wide, with a distolingual metaconid relative to the protoconid. This morphology of the trigonid is not retrieved on herpetotheriid m4, but is distinctive of most peradectids. The size of the trigonid permits to compare it with lower molars referred to *Peradectes mutigniensis* Crochet, 1979 rather than those of the smaller *P. louisi* Crochet, 1979, and cf. *Peradectes* sp. in

Marandat (1986) from Mas de Gimel. UM-MGL-320 is thus attributed to *Peradectes* cf. *mutigniensis*. *Peradectes mutigniensis* is so far documented from MP8+9 localities of the Paris Basin (Mutigny, Avenay, Sables de Brasles and Condé-en-Brie) and the MP10a localities of Saint-Agnan (Louis & Laurain 1983), and possibly Vielase (Legendre *et al.* 1992).

Eulipotyphla. Eulipotyphlan mammals are represented by amphilemurids and nyctitheriids. The amphilemurid species *Macrocranion* cf. *nitens* (Matthew, 1918) (*sensu* Russell *et al.* 1975) is represented by two morphs, one of small size (morph A hereafter, N = 7; identical in size to the population of Avenay; e.g., right m3 UM-MGL-455; L = 1.67; W = 1.03) (Fig. 2F) and another of larger size (morph B hereafter, N = 14; identical in size to the population of Mutigny and Grauves; e.g., right m1 or m2 UM-MGL-426; L = 2.17; W = 1.64). The larger morph B cannot be attributed to *M. tenerum* (Tobien, 1962) from Messel (MP11) by the simplicity of the p4 without individualized entoconid and hypoconid (Fig. 2G); the upper molars are clearly more transversally elongated, they have more extended parastylar lobe and a more powerful labial shelf, and the ectoflexus is more accentuated (see Storch 1993) (see also the specimens from Naples; Fig. 2H-I). Interestingly, the existence of two morphs of *Macrocranion* cf. *nitens* in Mas de Gimel supports the assumption of Smith & Smith (1995) that at least two species are represented in the Paris Basin at the MP8+9 and MP10a. A revision of these taxa, based on the unpublished specimens from Condé-en-Brie (MP8+9) and Prémontré (MP10a) (Dégremont *et al.* 1985) appears necessary. Recently, *Macrocranion* cf. *nitens* has also been identified in Egem (Belgium, *c.* MP8+9) (Smith & Smith 2013).

A second amphilemurid is represented by *Macrocranion* sp. (*sensu* Russell *et al.* 1975) (N = 14), a species which is rare in Avenay but more common in Condé-en Brie. This large *Macrocranion* species (e.g., right m3 UM-MGL-425; L = 2.96; W = 1.92) (Fig. 2J) was also reported at the MP10a in Saint-Agnan and Prémontré (Louis & Laurain 1983; Dégremont *et al.* 1985) and described during the ?MP10-MP11 interval in Aumelas (Maitre *et al.* 2008). This species differs from *M. tupaiodon* Weitzel, 1949 from Messel (MP11) by lower and more swollen cuspids, a shorter trigonid (the paracristid is more lingually oriented), and a more mesiodistally extended entoconid. Note that this amphilemurid is represented in Naples by upper molars (see below; Fig. 2K-L).

The nyctitheriid *Leptacodon* sp. (N = 5) is recognized by a complete left m1 or m2 (UM-MGL-802, L = 1.25; W = 0.89) (Fig. 2N) and fragmentary upper teeth. Distinctive characters of the family and genus are crestiform paraconid, subequal entoconid and hypoconid (a taller entoconid is diagnostic of *Plagioctenodon* Bown, 1979), cuspate and median hypoconulid on lower molar, molariform P4 bearing a moderately high metacone (left P4 UM-MGL-459), gracile M1 or M2 with two conules, a developed postcingulum bearing a well-distinct hypocone, and a distinct precingulum (Fig. 2M). This species is rather similar in size with *Leptacodon* sp. from Egem; they share also the lack of a postparaconule crista. Smith & Smith (2013) have however mentioned that the systematic value of this character is hard to estimate as it also occurs in *L. nascimentoi* Estravis, 1996 from the ~MP7 of Silveirinha, Portugal. Pending a study of the unpublished dental specimens of *Leptacodon* from the MP8+9 (Avenay and Mutigny) and MP10a (Prémontré) (Dégremont *et al.* 1985; Smith & Smith 2013), the species from Mas de Gimel remains undetermined. We can keep in mind however that it clearly differs from *Leptacodon ceciliensis* Storch & Haubold, 1989 from the Geiseltal-Obere Mittelkohle (MP13) (Storch & Haubold 1989; Manz & Bloch 2015), by a more lingual cristid obliqua, deeper hypoflexid, cuspate entoconid, and shorter talonid basin.

A second, larger, nyctitheriid species (N = 4) characterised by dilambdodont upper molars appears intermediate in morphology between *Wyonycteris* Gingerich, 1987 and *Pontifactor* West, 1974. This new nyctitheriid will be described in a separated paper; it is indeed documented by unpublished better-preserved specimens from Azillanet and La Rouyere (MP10a, Minervois, Southern France). It differs from *Wyonycteris* by smaller conules, absence of a pericone, and a more advanced dilambdodonty (duplicated mesostyle). It differs from *Pontifactor* (a monospecific genus from the middle Eocene of North America) by a less developed stylocone and more transverse upper molars. Interestingly, Dégremont *et al.* (1985) mentioned also *Pontifactor* sp. in Prémontré.

Apatotheria. An apatemyid mammal is documented by the left m2 UM-MGL-810 (L = 3.18; W = 2.00) (Fig. 3B). Typical characters of the family are a low trigonid with a reduced paraconid, the occurrence of a mesiolabial paralophid resulting in a quadrate trigonid, the absence of labial and lingual cingulids, and a rounded talonid. Apatemyids from the levels MP8+9 (Mutigny and Avenay) and MP10a (Grauves and Cuis) are all members of the genera *Apatemys* Marsh, 1872 and *Heterohyus* Gervais, 1848 (see Russell *et al.* 1979). Distinguishing these two genera on the basis of a lower molar is not easy. In comparison with *Apatemys,* the genus *Heterohyus* was proposed to have a more conical paraconid in mesial view (instead of crestiform), a more obtuse mesio-labial angle of the trigonid in occlusal view (but we note an important variation of this character) without any trace of a fourth trigonid cusp, and a smaller entoconid, more distant from the metaconid (Russell *et al.* 1979: 224). Moreover, following the measurements given by Russell *et al.* (1979), *Heterohyus* species are significantly larger than *Apatemys* ones. Considering all these data, UM-MGL-810 is tentatively attributed to *Heterohyus* sp. In size, this tooth is compatible with the large upper molars of *Heterohyus* sp. from Grauves and Cuis (Russell *et al.* 1979). A smaller *Heterohyus* species is documented in Avenay and Prémontré (Dégremont *et al.* 1985).

Fig. 2. — Metatheria and Eulipotyphla from Mas de Gimel and Naples: **A**, left m1 UM-MGL-310 of *Peratherium matronense* Crochet, 1979 in occlusal view; **B**, left m1 UM-MGL-143 of *Peratherium matronense* or *Peratherium monspeliense* Crochet, 1979 in occlusal view; **C**, labial fragment of right M2 UM-MGL-716 of cf. *Peradectes* sp. in Marandat (1986) in occlusal view; **D**, right m4 UM-MGL-320 of *Peradectes* cf. *mutigniensis* in occlusal view; **E**, right M1 UM-NAP-125 of cf. *Amphiperatherium bastbergense* Crochet, 1979 in occlusal view; **F-I**, Teeth of *Macrocranion* cf. *nitens*: right m3 UM-MGL-455 in labial (**F1**) and occlusal (**F2**) views

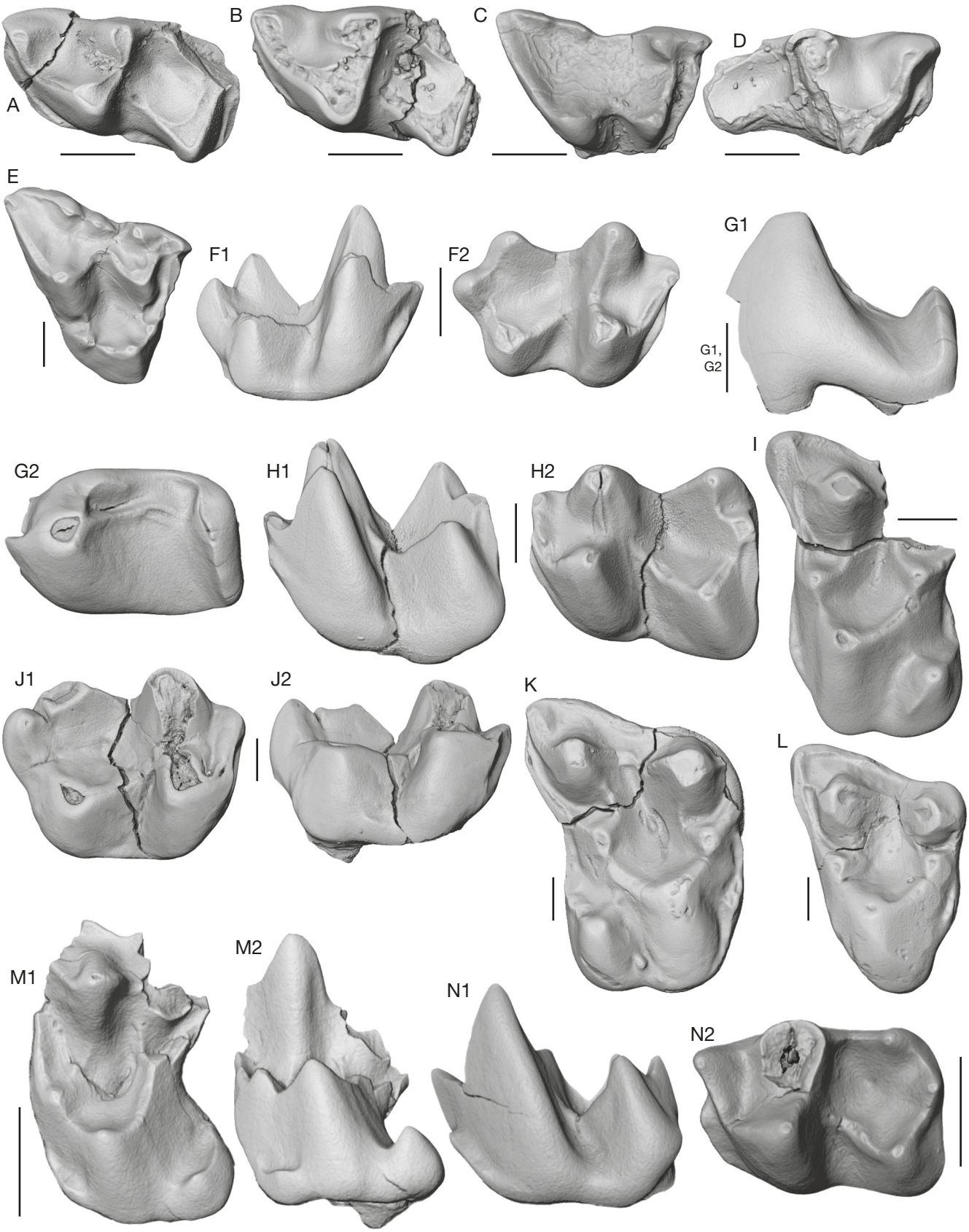

(small morph); left p4 UM-MGL-439 in labial (**G1**) and occlusal (**G2**) views, left m1 or m2 UM-NAP-2 in labial (**H1**) and occlusal (**H2**) views, left M2 UM-NAP-3 in occlusal view (**I**) (large morph); **J**-**L**, teeth of *Macrocranion* sp.: right m3 UM-MGL-425 in occlusal (**J1**) and labial (**J2**) views, right M2 UM-NAP-6 in occlusal view (**K**), left M3 UM-NAP-7 in occlusal view (**L**); **M**, **N**, teeth of *Leptacodon* sp.: left M1 or M2 UM-MGL-105 in occlusal (**M1**) and lingual (**M2**) views, left m1 or m2 UM-MGL-802 in labial (**N1**) and occlusal (**N2**) views. Scale bars: 0.5 mm.

Chiroptera. Bats are represented by three species. A minuscule Palaeochiropterygidae gen et sp. indet. is documented by a left m3 (UM-MGL-107, L = 1.23; W = 0.83) (Fig. 3C) and two poorly preserved upper molars (note that a sub-complete upper molar from Naples is attributed to this taxon, see below). Diagnostic characters of the family observed in the m3 are the very lingual direction of the cristid obliqua and the strong nyctalodonty associated with the lingual position of the hypoconulid distal to the entoconid (Hand & Sigé 2018). This m3 differs from that of *Palaeochiropteryx tupaiodon* Revilliod, 1917 and *P. spiegeli* Revilliod, 1917 by smaller size, less prominent and relatively lower cuspids; it further differs from *Matthesia* by the lack of bulbous cuspids; it is larger than *Microchiropteryx* Smith, Rana, Missiaen, Rose, Sahni, Singh & Singh, 2007 (Smith *et al.* 2007) and does not present the elongated and narrow crown that is characteristic of this genus; finally, relative to *Stehlinia* Revilliod, 1919, it differs from the oldest species *S. alia* Maitre, 2014 known from Aumelas (Maitre 2014) by smaller size and minor trigonid/talonid height difference. Further comparisons are possible thanks to the upper molar from Naples (see below; Fig. 3D).

A second palaeochiropterygid bat is represented by *Palaeochiropteryx* cf. *tupaiodon* (N = 2). The right m1-2 UM-MGL-449 (L = 1.45; W = 1) (Fig. 3F) is similar in morphology with *P. tupaiodon* from Messel but falls below the smallest individuals referred to this species. Interestingly, Russell *et al.* (1973) mentioned a similar small m1 from Grauves suggesting that the genus *Palaeochiropteryx* is represented as early as the MP10a by a species, smaller than *P. tupaiodon*.

A third bat, only documented by the small left P4 UM-MGL-456 (L = 1.28; W = 1.19) (Fig. 3E), is attributed to ?Icaronycteridae sp. indet. It differs from Palaeochiropterygidae and Archaeonycteridae by a slightly protruding parastyle and a short postparacrista. It resembles *Icaronycteris menui* Russell, Louis & Savage, 1973 from Avenay and Mutigny by a similar small size and the lack of hypocone. Note that a second, larger, Icaronycteridae species is present in Naples (see below; Fig. 3G-H).

Pantolesta. A pantolestid mammal, represented by the incomplete left M1 or M2 UM-MGL-424 (L>3.45; W = 4.63) (Fig. 3I), probably documents a new taxon, significantly smaller than species attributed to the genera *Premontrelestes* Smith, 2001 and *Pantolestes* Cope, 1872 from Prémontré and to *Buxolestes* Jaeger, 1970 from Messel and Bouxwiller (Jaeger 1970; Koenigswald 1980; Smith 2001). This taxon also differs from any known pantolestid taxa from the early and middle Eocene of Europe by a moderate lingual expansion of the hypocone. Note that a second, larger, pantolestid species attributed to ?*Pantolestes sabatieri* is present in Naples (see below; Fig. 3J).

Plesiadapiformes. The paromomyid *Arcius lapparenti* Russell, Louis & Savage, 1967 is represented by the right m2 UM-MGL-741 (L = 2.04; W = 1.62) (Fig. 3K). This assignment is supported by low crown with blunt cuspids, a tiny paraconid placed lingually, small difference in height between the trigonid and the talonid, a wide talonid basin, and a mesio-distally compressed trigonid, not as mesially inclined relative to the level of the base of the talonid basin as in any other paromomyid genus (Godinot 1984; López-Torres & Silcox 2018). Measurements of UM-MGL-741 match those of *Arcius lapparenti*, the largest *Arcius* species. Originally described from Avenay (Russell *et al.* 1967), *A. lapparenti* is also present in various MP10a localities from the Paris Basin (Grauves, Venteuil, Saint-Agnan, and Prémontré) and Southern France (Azillanet) (Aumont 2003; López-Torres & Silcox 2018).

Primates. They are confidently represented by three species. The most well-documented species is attributed to cf. *Protoadapis curvicuspidens* (Lemoine, 1878) (N = 7), known from various MP10a localities of the Paris Basin ("Epernay" [for Lemoine's specimens, including the holotype], Grauves, Monthelon, and Cuis) (Russell *et al.* 1967). The right p2 UM-MGL-739 is short, has two fused roots, and a single pointed cuspid (L = 2.88; W = 2.02). The left p4 UM-MGL-548 (L = 4.78; W = 3.05) (Fig. 4A) is a robust tooth with a well-defined metaconid and a small paraconid (as in MNHN.F.AL5180, a specimen which was described by Teilhard de Chardin [1922]). The left m2 UM-MGL-740 (L = 4.88; W = 3.6) (Fig. 4B) does not have an enlarged talonid basin and has a long subhorizontal paralophid with a residual paraconid; a very shallow groove separates the paraconid from the paralophid. The right M2 UM-MGL-542 (L = 4.27; W = 6.28) (Fig. 4C) is highly transverse (much more than in *Europolemur* Weigelt, 1933), rectangular in outline with rounded corners, and has lingually displaced paracone and metacone. The presence/absence of the metaconule is variable; it is absent on UM-MGL-542 but present on the fragmentary molars UM-MGL-486 and UM-MGL-547. As a whole, these characters support the attribution to *Protoadapis* rather than to *Europolemur*. Measurements match those of *P. curvicuspidens* Lemoine, 1878. However, because of: 1) the massive hypocone and the enlarged mesiolingual cingulum observed in UM-MGL-542, which are convergent characters with species of *Periconodon*; and 2) the scarcity of published M2 of *P. curvicuspidens* (MNHN.F.AL5191), we maintain the species from Mas de Gimel in open nomenclature pending a complete revision of the *Protoadapis-Europolemur* group (see Godinot 2015; Godinot *et al.* 2018, 2021).

A second primate is attributed to *Anchomomys* sp. This species is only represented by a fragmentary right lower molar (UM-MGL-551) characterised by an elongated talonid basin and a distolingually positioned entoconid relative to hypoconid. Note that a complete m1 (UM-NAP-31) of this anchomomyine species is present in Naples (see below; Fig. 4D).

The third primate is attributed to the microchoerid *Nannopithex zuccolae* Godinot, Russell & Louis, 1992 (N = 8), a species described from Prémontré and probably present, but extremely rare, in Grauves and Saint-Agnan (Godinot *et al.* 1992). The left p3 UM-MGL-408 is markedly smaller (L = 1.35; W = 0.89) (Fig. 4E) than the left p4 UM-MGL-413 (L = 1.7; W = 1.44) which is subrectangular and massive, with a high labial enamel wall (Fig. 4F2). Such an inflated p4 is diagnostic of *Nannopithex* Stehlin, 1916. Moreover, the p4 trigonid has a crestiform paraconid and a small low metaconid;

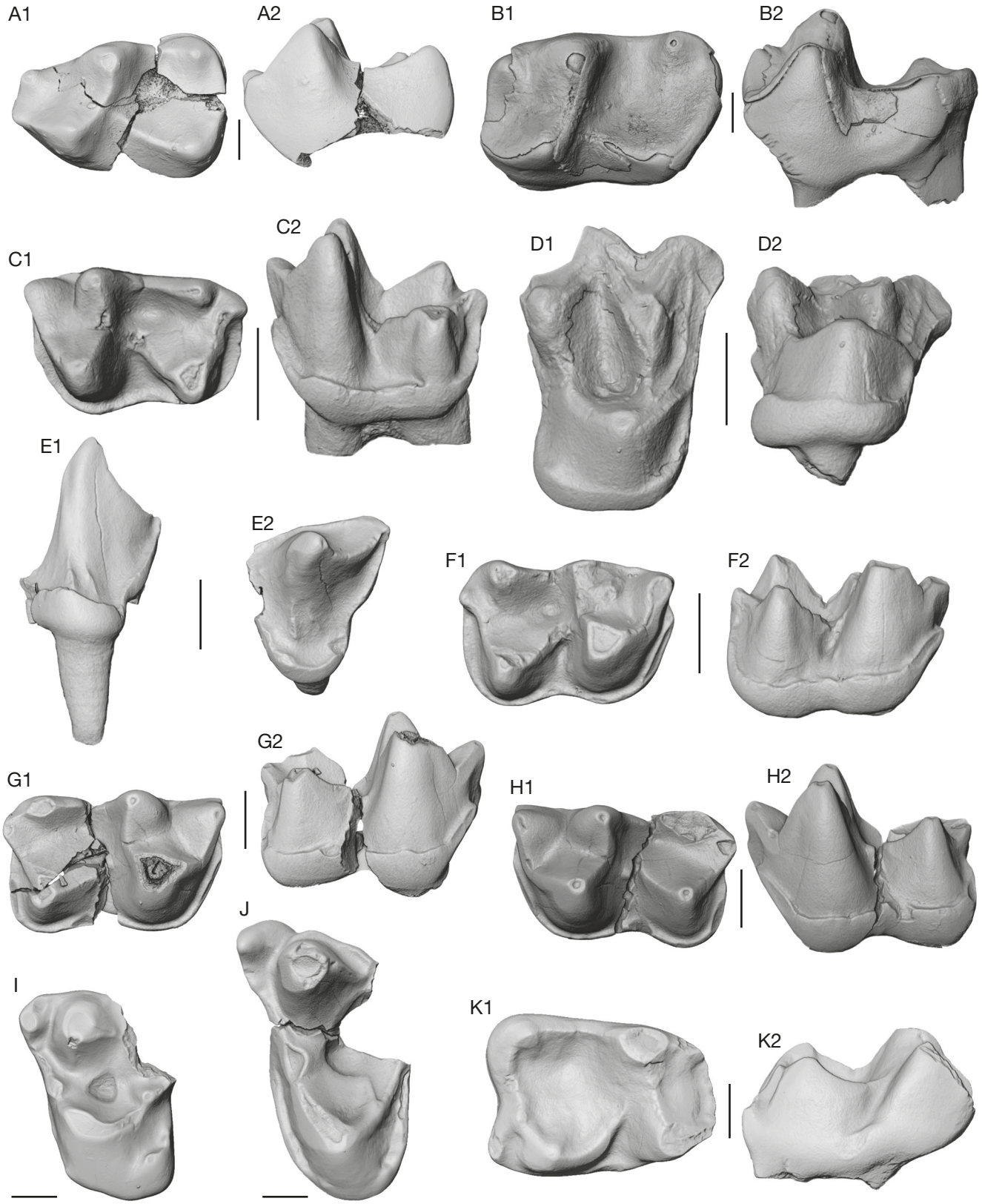

FIG. 3. — Apatotheria, Chiroptera, Pantolesta, and Plesiadapiformes from Mas de Gimel and Naples: **A**, **B**, molars of *Heterohyus* sp.: left m1 UM-NAP-16 in occlusal (**A1**) and labial (**A2**) views, left m2 UM-MGL-810 in occlusal (**B1**) and labial (**B2**) views; **C**, **D**, molars of Palaeochiropterygidae gen. et sp. indet.: left m3 UM-MGL-107 in occlusal (**C1**) and labial (**C2**) views, right M1 or M2 UM-NAP-19 in occlusal (**D1**) and lingual (**D2**) views; **E**, left P4 UM-MGL-456 of ?Icaronycteridae sp. indet. in lingual (**E1**) and occlusal (**E2**) views; **F**, right m1-2 UM-MGL-449 of *Palaeochiropteryx* cf. *tupaiodon* Revilliod, 1917 in occlusal (**F1**) and labial (**F2**); **G**, **H**, molars of *Icaronycteris* sp.: right m1 or m2 UM-NAP-20 in occlusal (**G1**) and labial (**G2**) views, left UM-NAP-21 in occlusal (**H1**) and labial (**H2**) views; **I**, left M1 or M2 UM-MGL-424 of Pantolestidae gen. et sp. indet. in occlusal view; **J**, left M3 UM-NAP-1 of ?*Pantolestes sabatieri* Smith, 2001 in occlusal view; **K**, right m2 UM-MGL-741 of *Arcius lapparenti* in occlusal (**K1**) and labial (**K2**) views. Scale bars: A-H, K, 0.5 mm; I, J, 1 mm.

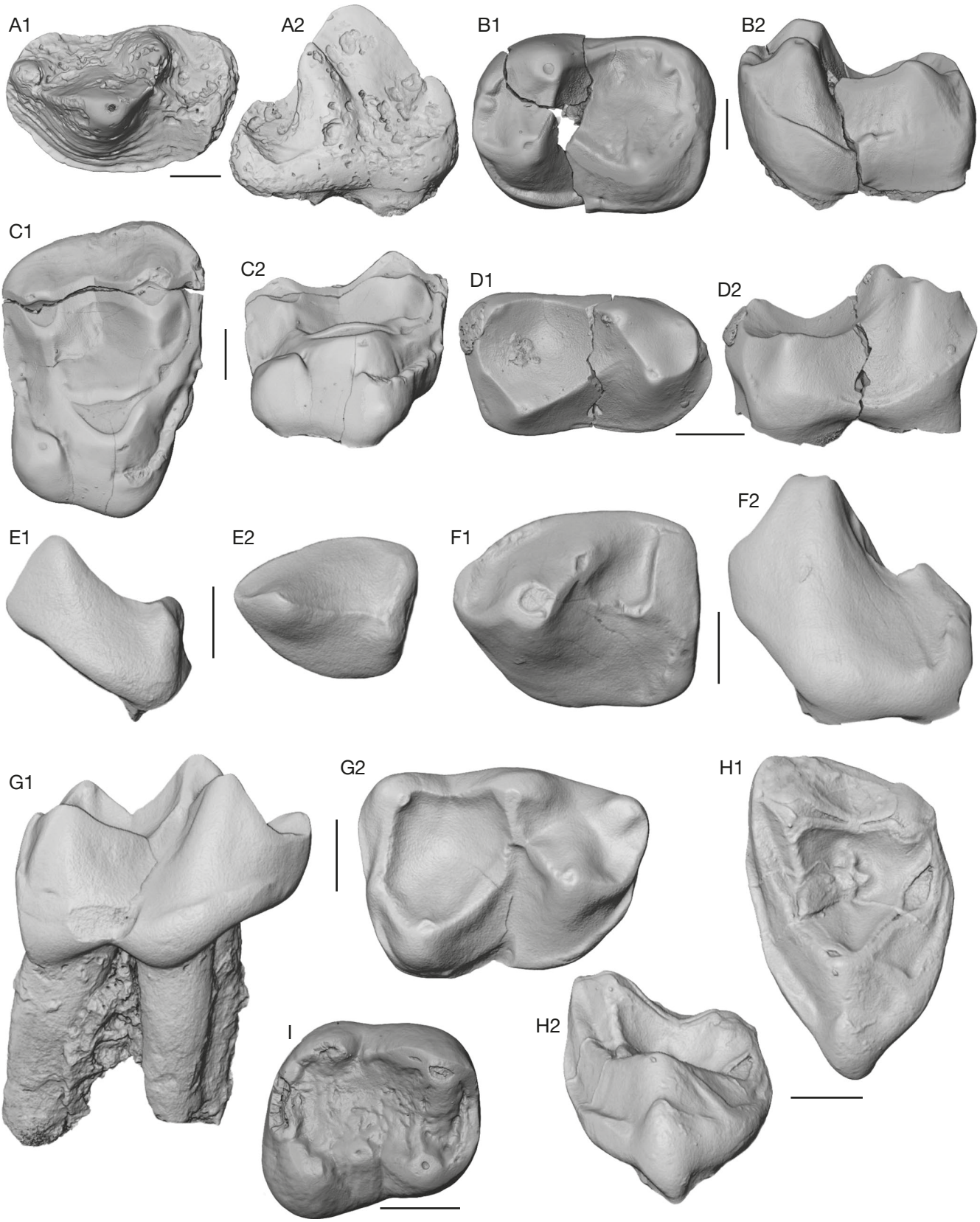

FIG. 4. — Primates and Rodentia from Mas de Gimel and Naples: **A**-**C**, teeth of cf. *Protoadapis curvicuspidens* (Lemoine, 1878): **A**, left p4 UM-MGL-548 in occlusal (**A1**) and lingual (**A2**) views; **B**, left m2 UM-MGL-740 in occlusal (**B1**) and labial (**B2**) views; **C**, right M2 UM-MGL-542 in occlusal (**C1**) and lingual (**C2**) views; **D**, right m1 UM-NAP-31 of *Anchomomys* sp. in occlusal (**D1**) and labial (**D2**) views; **E**-**H**, teeth of *Nannopithex zuccolae* Godinot, Russel & Louis, 1992: **E**, left p3 UM-MGL-408 in labial (**E1**) and occlusal (**E2**) views, left p4 UM-MGL-413 in labial (**F1**) and occlusal (**F2**) views, right m1 UM-MGL-401 in labial (**G1**) and occlusal (**G2**) views, left upper molar UM-MGL-743 in occlusal (**H1**) and lingual (**H2**) views; **I**, right m1 UM-MGL-219 of *Pseudoparamys* sp. indet. in occlusal view. Scale bars: A-D, I, 1 mm; E-H, 0.5 mm.

no real cuspid is developed on the talonid crest. The right m1 UM-MGL-401 (L = 1.97; W = 1.44) (Fig. 4G) has a strong and cuspate paraconid; the entoconid is considerably lower than the metaconid; the hypoconulid is weak. The left upper molar UM-MGL-743 (L = 1.48; W = 2.32) (Fig. 4H) has a short postprotocone-fold (= *Nannopithex*-fold), the hypocone is absent, and the conules are present.

Rodentia. Rodents from Mas de Gimel have been the subject of recent studies (Escarguel 1999; Vianey-Liaud *et al.* 2019, 2022; Vianey-Liaud & Marivaux 2021) but some specimens and taxa need some review considering recent advancement on the systematics of the group.

Among ischyromyoids, *Ailuravus* aff. *michauxi* Hartenberger, 1975 (N = 5) is the largest rodent species from Mas de Gimel (see Escarguel 1999: 125, plate1). This ailuravid is known from various ~ ?MP8+9 (Pourcy, Rians) to MP10 (Grauves, Cuis, Prémontré, Wittering Formation in the Sussex, and Naples, see below) localities.

A second ischyromyoid is *Eogliravus wildi* Hartenberger, 1971 (N = 23); this species defined from Mas de Gimel is the smallest rodent from the locality. It was revised by Escarguel (1999: 240) and Vianey-Liaud *et al.* (2022: 757). This species, that interestingly represents the oldest known Gliridae, is exclusively documented from MP10a (Prémontré, Azillanet, and Naples, see below) to ?MP10-11 (Cos and Vielase) localities. Noteworthy, Vianey-Liaud *et al.* (2022) suggested that the *Eogliravus* species from Messel, attributed to *E. wildi* by Storch & Seiffert (2007), is more reminiscent of *E. hammeli* (Thaler, 1966) from Bouxwiller.

Among theridomorphs, two plesiarctomyid species are documented. *Pseudoparamys* sp. indet. is represented by the unique right m1 UM-MGL-219 (L = 2.31; W = 2.18) (Fig. 4I). Judging from unique specimen, the closest species is *P. lapicidinarum* (Escarguel, 1999) from Condé-en-Brie, which has been described on the basis of a few teeth (Escarguel 1999: 58-59), without any m1. The m1 from Mas de Gimel is narrow labiolingually and the talonid basin is not markedly deeper than that of the trigonid, whereas the difference of depth is much more marked on the m2 of *P. lapicinidarum*. The small bulged mesoconid bears low short mesolophid and ectomesolophid, but there is no trace of the ectolophid seen on the m2 from Condé-en-Brie. On the distal surface of the basin the entolophid is not distinct from a few low extra ridges, developed between a short low prehypocristid and the labial flank of the entoconid. The labial slopes, mainly that of the protocone, are thinly wrinkled.

The second plesiarctomyid, *Plesiarctomys* cf. *savagei* (Michaux, 1964), is documented by a left m2 (UM-MGL-663, Escarguel 1999: pl. 17F), a much worn right m1 (UM-MGL-662) and a damaged upper molar (UM-MGL-661). The size of the m2, the best-preserved specimen, is close to that of *P. savagei* from Prémontré. A few differences can be found however. The lingual end of the metalophid I is not free (it connects the anterolophid); the crestulids are more numerous on the floor and the edges slopes of the talonid; and the crenulations are more pronounced on the outer slopes of the main cuspids.

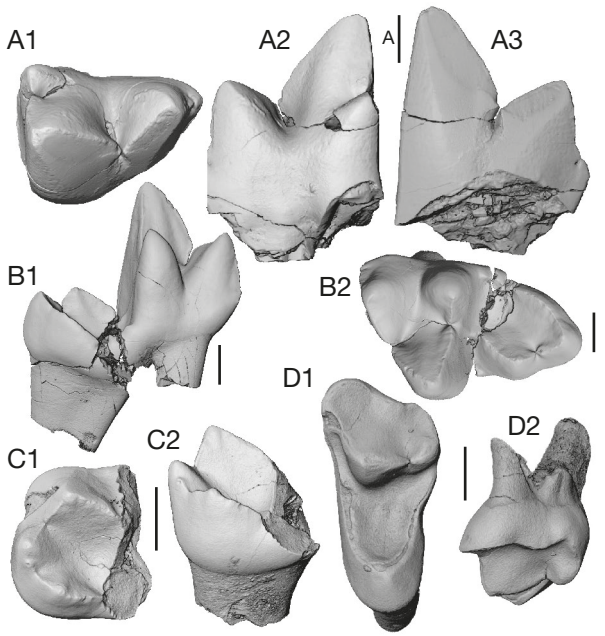

Fig. 5. — Hyaenodontidae and Carnivoraformes from Mas de Gimel: **A**, trigonid of right lower m1? of *Matthodon peignei* Solé, Marandat & Lihoreau, 2020 UM-MGL-70 in occlusal (**A1**) lingual (**A2**) and labial (**A3**) views; **B**, left m3 of *Leonhardtina meridianum* Solé, Marandat & Lihoreau, 2020 UM-MGL-707 in lingual (**B1**) and occlusal (**B2**) views; **C**, talonid of a left m1 of *Lesmesodon gunnelli* Solé, Morlo, Schaal & Lehmann, 2021 UM-MGL-36 in occlusal (**C1**) and lingual (**C2**) views; **D**, left M3 of *Uintacyon* cf. *hookeri* Solé, 2014 UM-MGL-108 in occlusal (**D1**) and labial (**D2**) views. Scale bars: A, 2 mm; B, C, 1 mm; D, 0.5 mm.

Another theridomorph is the massillamyid *Masillamys mattaueri* Hartenberger, 1975, a species defined from Mas de Gimel. It is the most common rodent species in the locality (N = 85). This theridomorph has been recently revised by Vianey-Liaud *et al.* (2019: 461, 471-477) and represents a species less derived than *M. cosensis* Vianey-Liaud, Vidalenc, Orliac, Maugoust, Lézin & Pélissié, 2022 from the ?MP10-11 locality of Cos (Vianey-Liaud *et al.* 2022).

The last rodent species belongs to the genus *Hartenbergeromys* Escarguel, 1999. Escarguel (1999) then Vianey-Liaud & Marivaux (2021) attributed this species to *Hartenbergeromys* aff. *hautefeuillei*. The material is revised in the second part of this section and attributed to a new species.

Hyaenodonta. Hyaenodonts are represented by three taxa of Hyaenodontidae. We recognized *Matthodon peignei* Solé, Marandat & Lihoreau, 2020 (Solé *et al.* 2020), a species known until now only from Aumelas. This large species is represented by a talonid of a right m1 (UM-MGL-31; W = *c.* 6.07) and a trigonid of lower m1? UM-MGL-70 (L = *c.* 7.87) (Fig. 5A).

We also recognized *Leonhardtina meridianum* Solé, Marandat & Lihoreau, 2020 (Solé *et al.* 2020), based on the left m3 UM-MGL-707 (L = ~5.9; W = 3.42) (Fig. 5B). The morphology of this tooth reminds the genera *Leonhardtina* Matthes, 1952 and *Lesmesodon* Morlo & Habersetzer, 1999 but its size is closer to that of *L. meridianum* also known from Aumelas and Rouzilhac (late Ypresian/early Lutetian) (Solé *et al.* 2020).

We finally recognized *Lesmesodon gunnelli* Solé, Morlo, Schaal & Lehmann, 2021 (Solé *et al.* 2021) on a talonid of

the left m1 UM-MGL-36 (W = *c.* 2.34) (Fig. 5C) clearly smaller than *Leonhardtina meridianum*. Its size and the strong labial cingulid better match with *Les. gunnelli* from Prémontré (Solé *et al.* 2021).

Carnivoraformes. The two upper molars UM-MGL-419 (L = 1.37; W = 2.37) and UM-MGL-108 (L = 1.12; W = 2.25) (Fig. 5D) with rectangular outline (protocone not twisted) display a rounded and not projected parastyle, lack a metastylar blade and metaconule, and show a weak metacone development compared to paracone. These traits indicate M3s of carnivoraforms. Among the Eocene European carnivoraforms that possess M3 (excluding *Quercygale* Kretzoi, 1945 from the MP8+9 and MP10 and *Messelogale* Springhorn, 2000 from the MP11), this taxon differs from *Gracilocyon rundlei* (Hooker, 2010) (MP8+9, Abbey Wood, England; Hooker 2010) by its reduced to absent conules, and rather reminds the small genus *Uintacyon* Leidy, 1872 notably by its reduced stylar shelf. The M3s are smaller than those of *U. rudis* Matthew, 1915 (probably present in Abbey Wood [see Hooker 2010; Solé 2014]) and close to the unique M3 of *U. hookeri* Solé, 2014 known from Brasles (L = 1.4; W = 3.33; Solé 2014). However, they are less transversely elongated and their basin are larger with their crests joining the protocone to the conules being less internal than in *Uintacyon hookeri*. Considering the possible intraspecific variability, we refer the two specimens from Mas de Gimel to *Uintacyon* cf. *hookeri*. *Uintacyon hookeri* is known from Mutigny, Avenay, Condé-en-Brie, Brasles and Cuis extending during the MP8+9-MP10a interval (Solé 2014).

Artiodactyla. Five artiodactyl species are recognized at Mas de Gimel. Among them, *Protodichobune oweni* Lemoine, 1878 and *Cuisitherium lydekkeri* (Lemoine, 1891) have already been mentioned and illustrated in Sudre (1980), Sudre *et al.* (1983) and Sudre & Lecomte (2000). *Protodichobune oweni* is recognized in Mas de Gimel by four specimens. Three upper molars already published are bunodont with a triangular outline and marked mesostyle on the labial cingulum (Sudre *et al.* 1983): left M2 UM-MGL-27 (L = 4.9; W = 6.3, Fig. 6A), right M2 UM-MGL-6 (L = 5.1; W = 7.4) and right M3 UM-MGL-7 (L = 4.5; W = 6.4). The eroded broken m3 UM-MGL-812 (L = 6.8; W = 4.0) displays conical and enlarged cuspids with a slightly distally positioned entoconid as in the type specimen of *Protodichobune oweni* MNHN.F.AL5232. It falls within the range of m3 measurements from Cuis, Monthelon and Mancy (L = 6.2-7; W = 3.6-5.3 in Sudre *et al.* 1983). It differs from *Protodichobune hellmundi* Erfurt, 2018 from Rouzilhac (Godinot *et al.* 2018) by the smaller size of its lower molars and the presence of a paraconid.

Cuisitherium lydekkeri (N = 5) is recognized on the basis of a quadrangular molar with lingual displacement of the metaconule, and the paraconule very close to the protocone (UM-MGL-03, UM-MGL-28, UM-MGL-503). Initially described within the hypodigm of *Protodichobune lydekkeri* Lemoine, 1891 (see Sudre *et al.* 1983), this species shows slender lower molars with more selenodont pattern than those of *P. oweni* and with the entoconid more mesial than in *Diacodexis* Cope, 1882. The lower molars UM-MGL-495 (L = 4.5) and UM-MGL-510 (L = 5.0 W = 4.0) fit well with the size of the m1 of the holotype MNHN.F.AL5236, MNHN.F.STA577 and MNHN.F.STA561 from Saint-Agnan, MNHN.F.GR158L from Grauves and MNHN.F.MT9L from Monthelon. (L = 5.0-5.4; W = 3.5-3.8).

In addition to these two species, we recently found the right p4 UM-MGL-491 (L = 6.7; W = 3.3) (Fig. 6G) that is very close to the p4 attributed to *Eurodexis russelli* Sudre & Erfurt, 1996 from Prémontré (MNHN.F.PRE4-L, Sudre & Erfurt 1996). Both are very elongated with a small metaconid on the lingual flank of the protoconid, an accessory cusp on the preprotocristid, and a distal basin delimitated by two cristids. It differs from *Cuisitherium* Sudre, Russell, Louis & Savage, 1983 (Sudre *et al.* 1983) lower premolar by the postcristids pattern and the absence of paraconid. *Eurodexis russelli* is also known from the MP10a localities of Saint-Agnan, Mancy, Cuis and Grauves (*E.* cf. *russelli* in Sudre & Erfurt 1996).

A trigonid of a left lower molar (UM-MGL-809; W = 2.4) and the right m2 UM-MGL-811 (L = 4.3; W = 3.1) (Fig. 6H) match in morphology with the lower molar of *Diacodexis* cf. *varleti* from Prémontré (e.g., the m1 MNHN.F.SLP29-PE-1412; Sudre & Erfurt 1996: fig. 10). The molar is slender and tiny, with no ectostylid, and with a very distal entoconid thus differing from the larger *Cuisitherium* and *Protodichobune* (Sudre *et al.* 1983). It falls within the range size of m2 of *D. varleti* Sudre, Russell, Louis & Savage, 1983 from Condé-en-Brie (N = 8; L = 4-4.5; W = 2.9-3.4; Sudre *et al.* 1983), Pourcy (L = 4.6; W = 3.3) and of the m2s of *D.* cf. *varleti* from Sézanne-Broye, Saint-Agnan, Cuis and Grauves (N = 6; L = 3.7-4.5; W = 2.5-3.4; Sudre *et al.* 1983) and Prémontré (N = 6; L = 4.1-4.7 W = 2.9-3.2; Sudre & Erfurt 1996). Slight differences between *D. varleti* and *D.* cf. *varleti* have been quoted for paraconid size and position, notched protolophid and development of the entoconid. These faint characteristics are not clearly observable in the molars from Mas de Gimel. We therefore consider these specimens as *Diacodexis* cf. *varleti*. This is the first mention of this taxon in Mas de Gimel as it was only known until now from the Paris Basin (MP8+9 and MP10a) and in the Site XIV of the Geiseltal (Unterkohle, MP11; Erfurt & Sudre 1996).

A large talonid of the left m3 UM-MGL-33 (Fig. 6J) can be attributed to an Artiodactyla on the basis of a crescentiform hypoconid, the development of the two cuspids of the talonid and the presence of a loop-like hypoconulid. The lack of entoconid cristid and the general bunoselenodont pattern remind us an haplobunodontid representative not so different from *Cuisitherium* (see Sudre & Lecomte 2000) nor *Lophiobunodon* Depéret, 1908 (see Luccisano *et al.* 2020). However, its large dimension (W = 6.4 mm) oversizes that of *Lophiobunodon minervoisensis* Depéret, 1908 (mean W = 3.9 mm; Luccisano *et al.* 2020) and *Cuisitherium lydekkeri* (W = 4.5 mm in MNHN.F.AL5235). It also displays a faint hypolophid, a marked postectohypofossid and a continuous labial cingulid. The largest European Ypresian artiodactyls *Aumelasia* Sudre, 1980 and *Dichobune* Cuvier, 1822 (see Godinot *et al.* 2018; Luccisano *et al.* 2020) possess a small bulbous hypoconulid with a marked posthypocristulid that close the basin lingually

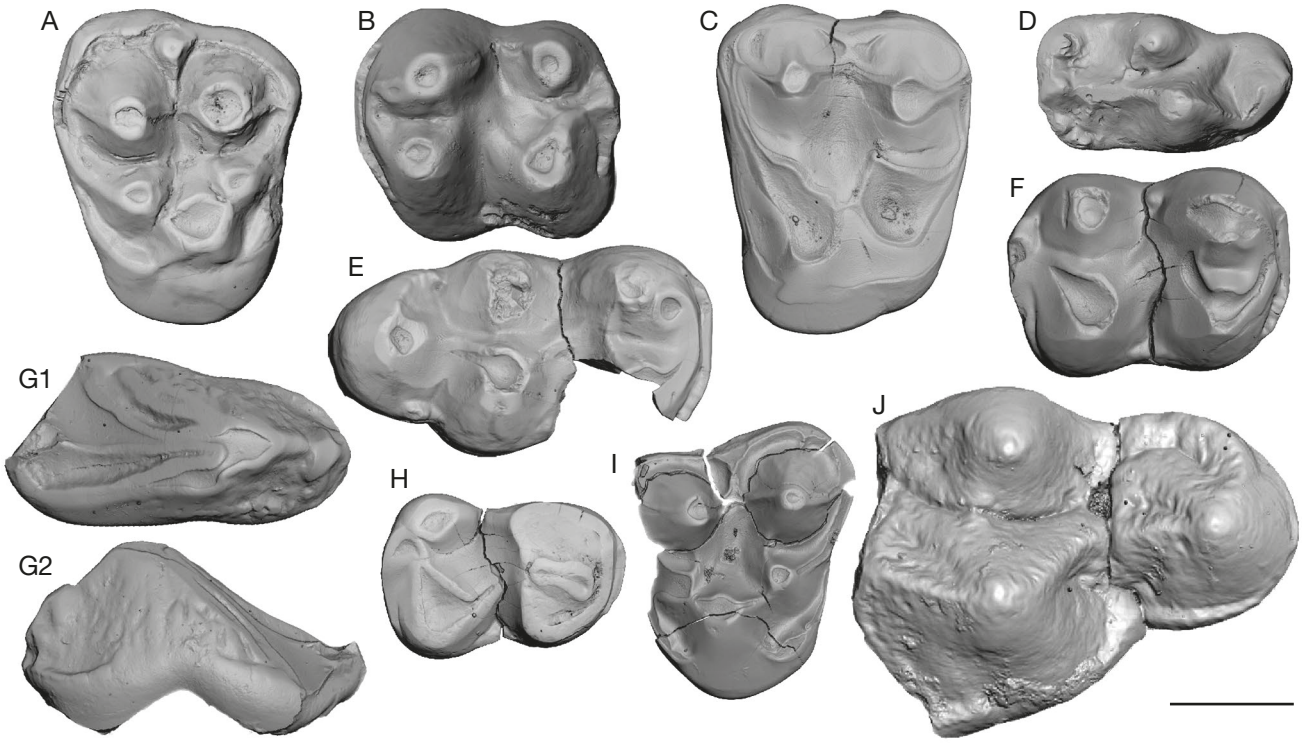

Fig. 6. — Artiodactyla from Mas de Gimel, Naples and Naples 2: **A**, **B**, molars of *Protodichobune oweni* Lemoine, 1878: right M3 UM-MGL-27 in occlusal view (**A**), left m1 UM-NAP-78 in occlusal view (**B**); **C**-**F**, teeth in occlusal view of *Cuisitherium lydekkeri* (Lemoine, 1891): left M1 UM-NAP-82 (**C**), right p4 UM-NAP2-73L (**D**), right m3 UM-NAP-76 (**E**) and right m1 UM-NAP-77 (**F**); **G**, right p4 of *Eurodexis* cf. *russelli* Sudre & Erfurt, 1996 UM-MGL-491 in occlusal (**G1**) and lingual (**G2**) views; **H**, **I**, molars of *Diacodexis* cf. *varleti* Sudre, Russel, Louis & Savage, 1983: right m2 UM-MGL-811 in occlusal view (**H**) and left M2 UM-NAP-84 in occlusal view (**I**); **J**, talonid of a left m3 UM-MGL-33 of cf. Haplobunodontidae indet. in occlusal view. Scale bar: 2 mm.

which is not the case in UM-MGL-33. The selenodont and loop-like pattern added to this size is original and could correspond to a new large early Haplobunodontidae, considered as cf. Haplobunodontidae indet. pending more material of this large artiodactyl.

Perissodactyla. This order is represented by three distinct families and four distinct species. First, a small Rhinocerotoidea Hyrachyidae, initially attributed to *Hyrachyus minimum* (Fischer, 1829) by Cappetta *et al.* (1968), is represented by nine remains: a fragment of the indeterminate lower molar UM-MGL-813, the m1 UM-MGL-514 (L = 13.9; W = 8.7), two m2s (UM-MGL-511 and UM-MGL-513; L = 15.3-16.2; W = 9.5-9.9) (Fig. 7C), the m3 UM-MGL-512 (L = 16.6; W = 10.6), the P3 UM-MGL-515 (L = 9.9; W = 12) (Fig. 7B), the incomplete M3 UM-MGL-815 (L = 15.6; W = 17.7), half of the dP4 UM-MGL-516 (W = 11.4) and the fragment of upper molar UM-MGL-814. These remains display the characteristic bilophodont jugal teeth, the m3 without hypoconulid, a labial prehypocristulid, lophids that are not parallel, non-molariform premolars with incomplete metaloph, and incipient hypocone, that were already described for *Hyrachyus* Leidy, 1871 (e.g., Savage *et al.* 1966). Contrary to Cappetta *et al.* (1968), all the specimens rather fit with the size of *H. stehlini* (Depéret, 1904) from Saint-Agnan (Louis & Laurain 1983), from the *Sables à Unio et Térédines* Formation (Cuis, Grauves, Monthelon, see Savage *et al.* 1966), from Rouzilhac (Godinot et al 2018) and from Bracklesham, Earnley Formation (Hooker 1996). The material from Mas de Gimel is always smaller than the mean of *H. minimum* from the Geiseltal (MP11-13, Hlawatsch & Erfurt 2007) and Argenton (MP11/12); moreover, it does not display the lingual cingula on upper molars and premolars, the labial cingula at metacone, and the M3 metacone shorter characteristic of this species (Radinsky 1967). It is not easy to establish the degree of molarization of premolars with the available material from Mas de Gimel. It should be notice that differentiation between the late Ypresian *H. stelhini* and the late Ypresian/early Lutetian *H. modestus* (Leidy, 1870) from North America is not clear (see Radinsky 1967), and that a review is needed (see Bai *et al.* 2017).

The family Lophiodontidae is well represented (N = 62) but only by isolated and fragmentary teeth. Initially interpreted as *Lophiodon tapirotherium* Desmaret, 1822 (see Cappetta *et al.* 1968; Hartenberger *et al.* 1969), the most complete teeth, such as the M2 UM-MGL-538 (L = 29.8; W = 29.6), show thin cingulum unlike in *L. tapirotherium* and are smaller (Vautrin 2019). A fainted paraconule is observable on the M2, which is sometimes the case in the populations of *L. leptorhynchum* Filhol, 1888 from Aumelas and La Livinière (Vautrin 2019). Three M3s (UM-MGL-535, UM-MGL-536, UM-MGL-537) display a triangular occlusal outline. These specimens are larger than *Eolophiodon laboriense* Robinet, Remy, Laurent, Danilo & Lihoreau, 2015 (Robinet *et al.* 2015) from Laborie (Vautrin

et al. 2019) and than *L. corsaensis* Checa Soler, 1997 and *L. baroensis* Checa Soler, 1997 from Spain. They are significantly smaller than *L*. aff. *eygalayense* from Rouzilhac (Godinot *et al.* 2018). The material from Mas de Gimel is approximately the size of *L. remense* Lemoine, 1878 and the lower limit of *L. leptorhynchum* (see Vautrin 2019). A revision of these two species is needed, notably to test a possible synonymy; but considering the well-known populations of *L. leptorhynchum* in Southern of France, we provisionally attribute this materiel to *L*. cf. *leptorhynchum*. Below, we describe from Naples 2 better preserved specimens of this taxon (Fig. 7D-F).

There are several specimens (N = 23) belonging to the family Palaeotheriidae. Discrimination between early representatives of this family is not easy due to the possible presence of several size equivalent species in the localities (Savage *et al.* 1965) and to some unclear definitions at generic level. This is true despite recent important revisions (Danilo *et al.* 2013; Remy 2017; Remy *et al.* 2019; Bronnert & Métais 2023). Two dP4s (UM-MGL-362: L = 8.9; W = 9.9; UM-MGL-360) are undoubtedly attributed to the genus *Propalaeotherium* Gervais, 1849 based on the presence of a marked mesostyle, their relative bunodonty (marked metaconule) and the short ectoloph with bulbous paracone rib and salient metacone rib. Measurements are congruent with small specimens described from the Ageian collection, Grauves, Cuis, Mancy, Monthelon, Chavot and attributed to *Propalaeotherium gaudryi* (Lemoine, 1878) (see Bronnert & Métais 2023) and slightly smaller than specimens published as *Pr*. cf. *gaudryi* from Aumelas (Remy *et al.* 2019). Noteworthy, Cappetta *et al.* (1968) and Hartenberger *et al.* (1969) indicated the presence of *Propalaeotherium* sp. and *Propachynolophus* sp. in the Mas de Gimel fauna but did not indicate specimen attributions. Recent revision of *Propachynolophus* Lemoine, 1891 by Remy (2017) supports that a weak development of the hypoconulid on m1-2 are unambiguous character appearing in the propalaeothere clade. In UM-MGL-77 (m1-m2: L = 10.8 and 12.2; W = 7.3 and 8.5 mm; Fig. 8A), the metastylid is very close to the entoconid unlike in *Pachynolophus* Pomel, 1847 where entoconid is distal and there is a small hypoconulid, suggesting that this specimen should be referred to *Propalaeoatherium.* It is size-equivalent to the mean value of *Pr. gaudryi* from Paris basin (Bronnert & Métais 2023), *Pr. gaudryi* from Rouzilhac (Godinot *et al.* 2018) and *Pr*. cf. *gaudryi* from Aumelas (Remy *et al.* 2019). One other lower molar fit with this morphology (UM-MGL-365). We are also able to recognize two lower premolar morphologies among the Equoidea from Mas de Gimel. We attribute to *Propalaeotherium gaudryi* the two p4s UM-MGL-32 (L = 10.4; W = 6.7; Fig. 8E) and UM-MGL-26 (L = 11.6; W = 8.2; Fig. 8D) displaying size measurements equivalent to *Pr. gaudryi* from Paris Basin with prehypocristid mesiodistally oriented, open trigonid and large distal basin. The p4s are slightly molariform with the variable presence of an entoconid (e.g., on UM-MGL-26, Fig. 8D). We also attribute a p3 (UM-MGL-73, L = 7.9; W = 6; Fig. 8F) to *Pr. gaudryi* with a prehypocristid oriented toward the protoconid and a quite distal metaconid.

The broken M3 UM-MGL-361 (L = 11.4; W = 11.9) (Fig. 8G) and the M1 UM-MGL-15 (L = 10.4; W = 10.4) display quadrangular outlines, a long ectoloph without true mesostyle (i.e., not connected to the cingulum) and lack marked metaconule (continuous metaloph) and metacone rib. A large hypostyle is present on the M3 (Fig. 8G). This morphology resembles M3 of large *Pachynolophus*. These teeth are smaller than published specimens of *Pr. gaudryi* but size is congruent with *Pa*. *cesserasicus* (Gervais, 1849) (La Livinière; Savage *et al.* 1965) and *Pa*. *ruscasseriensis* Remy, Krasovec, Lopez, Marandat & Lihoreau, 2019 (Aumelas; Remy *et al.* 2019), which are both very similar in size and morphology. The m1 UM-MGL-13 (L = 8.8; W = 6.3) and the two m2s UM-MGL-368 (L = 10.1; W = 6.8) and UM-MGL-369 (L = 10.4; W = 6.9) (Fig. 8I) display large distostylid and important space between metaconid and entoconid due to reduction or absence of metastylid. They are smaller than the size variation of *P. gaudryi* from Paris Basin and Aumelas and fall within the range of *Pa. ruscasseriensis* (see Remy *et al.* 2019). Unfortunately, the holotype of *Pa. cesserasicus* has not been described in Savage *et al.* (1965). Its exact location is currently unknown and no other mandible had been attributed to this species. The elongated p3 UM-MGL-372 (L = 9; W = 4.8) (Fig. 8J) differs from those of *Pr. gaudryi* being slenderer with a prehypocristid oriented toward the metaconid. All of these specimens indicate the presence of a large *Pachynolophus* species. We consider them as belonging to *Pachynolophus* cf. *ruscasseriensis* waiting a thorough revision of *Pa.cesserasicus*.

Naples

Metatheria. Two herpetotheriid species are recognized in Naples through a limited number of specimens (N = 14). A first species, *P. matronense* or *P. monspeliense*, is documented by fragmentary upper and lower molars (N = 11) and a nearly complete right M4 (UM-NAP-11), which is characterized by a V-shaped centrocrista, a labiolingually pinched stylar cusp C bearing a long posterior crista, and a very thin paracingulum mesially to the paracone apex. This species is also documented in Naples 2 by two very fragmentary lower teeth.

The complete right M1 UM-NAP-125 (L = 2.12; W = 2.19; Fig. 2E) and a fragment of a right M1 (UM-NAP-128) are attributed to cf. *Amphiperatherium bastbergense*, of which the type series is from Bouxwiller (Crochet 1979). *Amphiperatherium bastbergense* is also known from other MP13-14 localities (Egerkingen, Le Pont, Laprade, and Cuzal; Crochet 1980; Crochet *et al.* 1997; Sudre *et al.* 1990; Marandat *et al.* 1993) and also from Aumelas (Crochet 1980). UM-NAP-125 is significantly larger and relatively longer than the M1 of *A. goethei* Crochet, 1979 (see Crochet 1980: fig. 89) and the conules are relatively larger and more individualized from the preproto- and postprotocristae. UM-NAP-125 is significantly smaller and has a more acute protocone than the M1 of *A. maximum* (see Crochet 1980: fig. 106). The taxon cf. *Amphiperatherium bastbergense* from Naples is possibly the oldest occurrence of the species.

Eulipotyphla. Amphilemurid eulipotyphlans are represented by two species. The large morph B of *Macrocranion* cf. *nitens* is documented by few (N = 7) but better-preserved specimens relative to Mas de Gimel, particularly the m1 or m2 UM-NAP-2 (L = 2.06; W = 1.57) (Fig. 2H) and the M2 UM-NAP-3 (L > 1.82; W = 2.7) (Fig. 2I), strengthening the systematic attribution.

The second amphilemurid is *Macrocranion* sp. (*sensu* Russell *et al.* 1975), also present in Mas de Gimel. This species is documented by the right M2 UM-NAP-6 (L = 2.72; W = 3.42) (Fig. 2K) and the left M3 UM-NAP-7 (L = 2.11; W = 277) (Fig. 2L) from Naples and by the two right m2s from Naples 2 UM-NAP2-74V (L = 2.64; W = 2.04) and UM-NAP2-75V (L = 2.68; W = 2.14). The M2 from Naples is similar to MNHN.F.AV60-L from Avenay described by Russell *et al.* (1975) in the transverse development on the crown (the M2 of *M. tupaidon* is more quadrate), the long postmetacrista bearing a robust metastyle (these two structures are tenuous in *M. tupaidon*), and the distal cingulum does not ascend the metaconule, as it is the case in the species from Messel. *Macrocranion strorchi* Maitre *et al.* 2008 from Arcambal (MP8+9, Quercy; Maitre *et al.* 2008), although similar in size with *Macrocranion* sp., presents a well-distinct M2 (holotype UM-ARC-03) having lower and more bulbous cusps (especially the protocone and hypocone), reduced metastyle, and thinner mesial and distal cingula. As for the new nyctitheriid (aff. *Pontifactor* sp.) mentioned in Mas de Gimel, only one specimen (UM-NAP-22, right M1 or M2) documents this taxon.

Apatotheria. The apatemyids are documented by only one specimen, a left m1 (UM-NAP-16; L = 2.85; W = 1.91) (Fig. 3A). This molar is attributed to the same species as that of Mas de Gimel (*Heterohyus* sp.). Again, we emphasize the large size of this species, in comparison to the taxa described from the Paris Basin.

Chiroptera. Bats are represented by two species. The minuscule Palaeochiropterygidae gen et sp. indet. from Mas de Gimel is documented by a right M1 or M2 (UM-NAP-19; W = 1.62) in Naples (Fig. 3D). This molar shares several important characters with palaeochiropterygids such as the metacone higher than the paracone as in *Palaeochiropteryx tupaiodon* and *P. spiegeli*, the ectoflexus between the parastyle and the mesostyle is narrow and mesially displaced, the centrocrista is long and joins the labial border, there is no paraconule, the metaconule is minute, the protocone is rather short, the lingual cingulum is thin, continuous but attenuated under the protocone (as in *P. spiegeli*), and there is a small hypocone. This upper molar, associated with the lower molar from Mas de Gimel, probably documents a new species, significantly smaller than all known palaeochiropterygids, including the small indeterminate species from Egem (Smith & Smith 2013).

The second bat is represented by an icaronycterid species, much larger than the species from Mas de Gimel. This species is documented by two m1s or m2s (UM-NAP-20; L = 1.98; W = 1.27 and UM-NAP-21; L = 2.02; W = 1.22) (Fig. 3G-H) well-characterized by a large paraconid, a necromantodont arrangement of talonid cusps with the hypoconulid rather lingual (not median as in the onychonycterids and the archaeonycterid *Xylonycteris* Hand & Sigé, 2018) and connected to the entoconid. This talonid arrangement corresponds to the subnyctalodonty of *Icaronycteris*. Moreover, the trigonid/talonid height difference is similar to that observed in *Icaronycteris* Jepsen, 1966. The species *I. index* Jepsen, 1966 (late early Eocene, Wa7, of North America) and *I. menui* (MP8+9 of Avenay) are ~20% smaller and have a lower paraconid. In that respect, more similarities are found with *I. sigei* from Vastan Lignite Mine, early Eocene of India (Smith *et al.* 2007) which differs however by a higher metaconid and a smaller hypoconulid. Pending new specimens (e.g. documenting the upper molar morphology), the icaronycterid from Naples is attributed to *Icaronycteris* sp.

Pantolesta. The pantolestids are represented by the left M3 UM-NAP-1 (L = 3.6; W = 6.42) (Fig. 3J). This molar is tentatively attributed to *Pantolestes sabatieri* Smith, 2001 from Prémontré (Smith 2001). Similarities concern an equal size, a transversally elongated crown, an oblique labial border of the crown in occlusal view, low and massive cusps, a huge and prominent parastyle, a bulbous paraconule, and the lack of hypocone.

Primates. Primates are documented by only two teeth belonging to species identified in Mas de Gimel. The right p3 UM-NAP-26 is attributed to *Nannopithex zuccolae* based on similarities with UM-MGL-408. More interesting is the right m1 UM-NAP-31 (L = 3.86; W = 2.26) (Fig. 4D) which documents *Anchomomys* sp. This molar is typical of *Anchomomys* species in being elongated and narrow, in lacking a paraconid, and in having an entoconid distolingually positioned relative to hypoconid and an almost rectilinear mesial paralophid, which in occlusal and in mesial view, is at a roughly right angle with the strongly sloping preprotocristid. This species represents the oldest occurrence of the genus *Anchomomys* Stehlin, 1916 and documents an early unexpected large lineage (significantly larger than *A. gaillardi* Stehlin, 1916, *A. frontanyensis* Marigó, Minwer-Barakat, Moyà-Solà & Boyer, 2011, and *A. pygmaeus* Szalay, 1974). Interestingly also, the same new species is probably documented in Prémontré by more specimens (M. Godinot comm. pers. 2022).

Rodentia. Rodents are documented by the same assemblage as in Mas de Gimel, but with fewer specimens. All the specimens have been studied by Escarguel (1999) and part of them was subject of recent revisions (Vianey-Liaud *et al.* 2019, 2022; but see below for those here attributed to the new species *Hartenbergeromys pailladensis* n. sp.).

Ailuravus aff. *michauxi* (N = 3) is documented by a right DP4 (UM-NAP-65), a left dp4 (UM-NAP-67), and a talonid of a left m3 (UM-NAP-66) (see Escarguel 1999: 125). *Eogliravus*

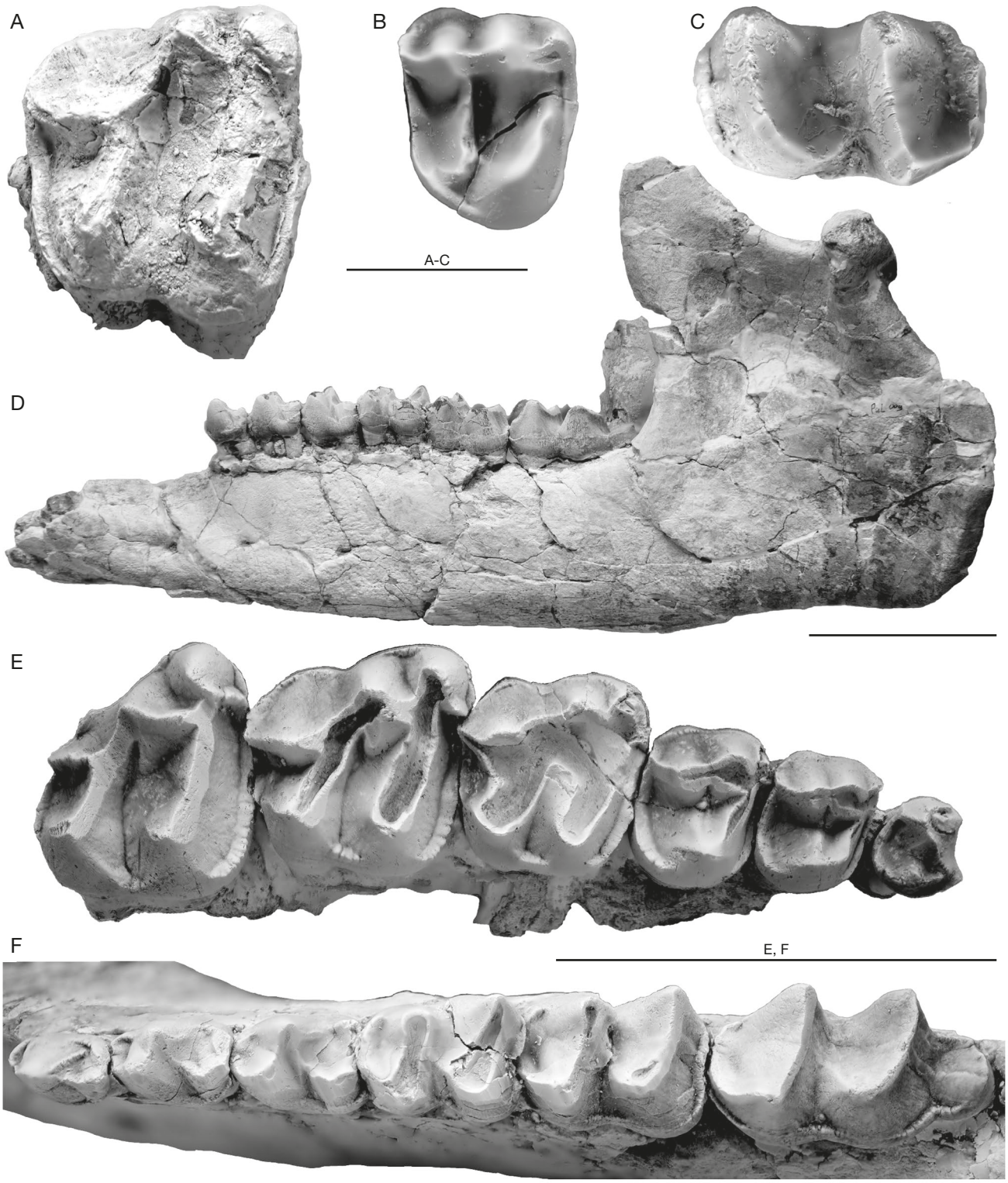

FIG. 7. — Large perissodactyl taxa from Mas de Gimel, Naples and Naples 2: **A**-**C**, teeth of *Hyrachyus stehlini* (Depéret, 1904) in occlusal view: right M1 UM-NAP-110 (**A**), right P3 UM-MGL-515 (**B**) and right m2 UM-MGL-513 (**C**); **D**-**F**, dental row of *Lophiodon* cf. *leptorhynchum* Filhol, 1888: mandible with right and left p2-m3 UM-NAP2-09 in lateral view (**D**) and occlusal focus on left side (**F**), right P2-M3 UM-NAP2-73 (**E**). Scale bars: A-C, 10 mm; D-F, 50 mm.

wildi (N = 7) is documented by four M1s (UM-NAP-69 to UM-NAP-72), a left p4 (UM-NAP-74), a left m1 (UM-NAP-73), and a right m2 (UM-NAP-75) (see Vianey-Liaud *et al.* 2022: 796). *Masillamys mattaueri* (N = 5) is documented by a right m1 (UM-NAP-60), a left m2 (UM-NAP-61), a right m3 (UM-NAP-59), a right M1 (UM-NAP-63), and a right M2 (UM-NAP-62) (see Escarguel 1999: 216; Vianey-Liaud *et al.* 2019: 471).

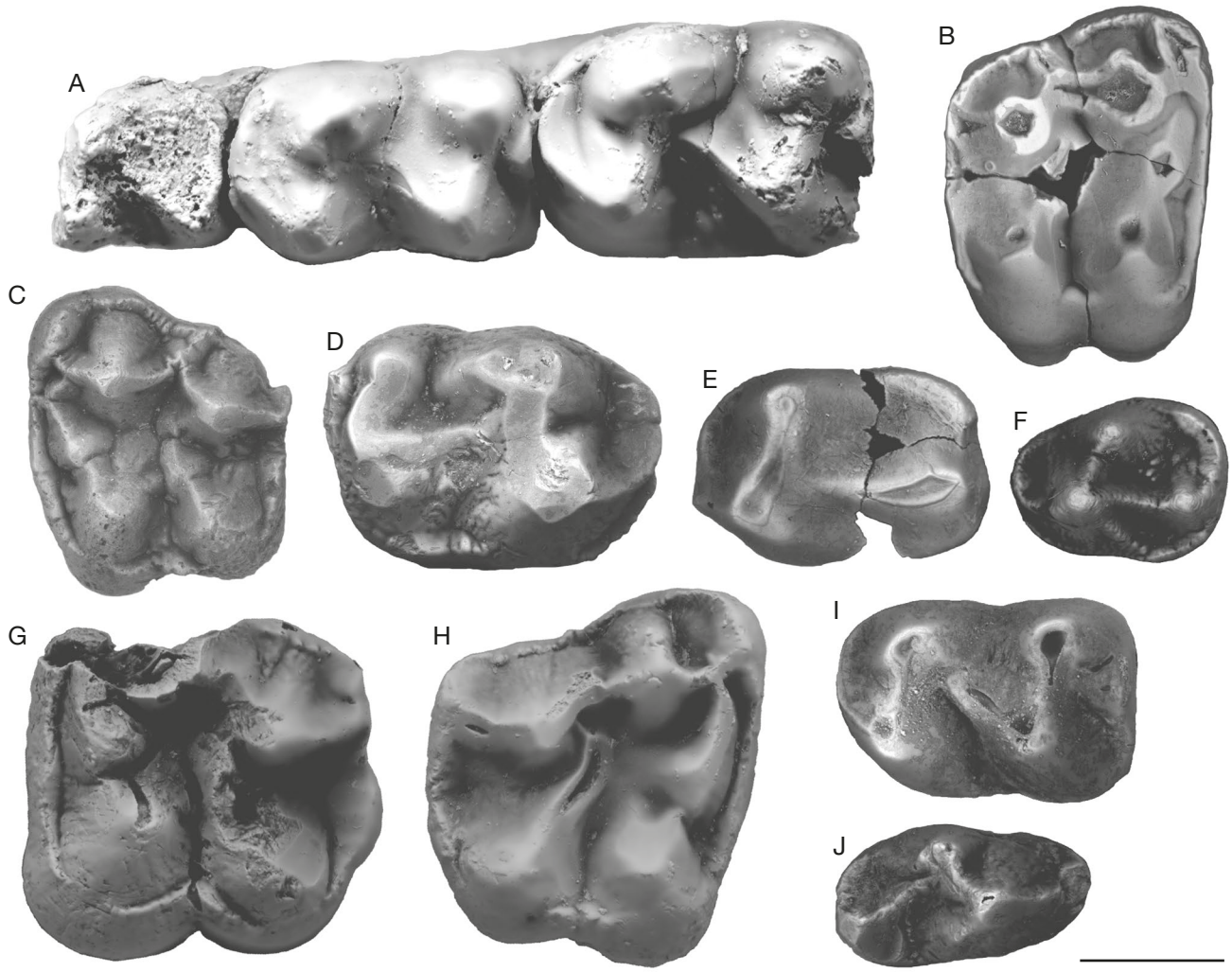

Fig. 8. — Equoidea from Mas de Gimel, Naples and Naples 2: **A**-**F**, teeth of *Propalaeotherium gaudryi* (Lemoine, 1878) in occlusal views: left m1-m2 UM-MGL-77 (**A**), right M1 UM-NAP-103 (**B**), left M1 UM-NAP2-72L (**C**), right p4 UM-MGL-26 (**D**), left p4 UM-MGL-32 (**E**) and left p3 UM-MGL-73 (**F**); **G**-**J**, teeth of *Pachynolophus* cf. *ruscasseriensis* Remy, Krasovec, Lopez, Marandat & Lihoreau, 2019 in occlusal views: broken left M3 UM-MGL-361 (**G**), right M3 UM-NAP-99 (**H**), left m2 UM-MGL-369 (**I**) and right p3 UM-MGL-372 (**J**). Scale bar: 5 mm.

Carnivoraformes. The broken right M3 UM-NAP-13 (L = 1.27; W = 2.25) which lacks labial cingulum and most of the distal border, presents the same morphology than specimens from Mas de Gimel attributed to *Uintacyon* cf. *hookeri*.

Artiodactyla. This order is represented in Naples by three distinct taxa also known in Mas de Gimel. Two specimens are interpreted as belonging to *Protodichobune oweni*: the left m1 UM-NAP-78 (L = 5.4; W = 4.6) (Fig. 6B) and the right m3 talonid UM-NAP-79 (W = 3.7). These specimens with bunodont morphology, distinct paraconid, a distal entoconid in regard to hypoconid position, and a reduced central hypoconulid, fit well with the material from the *Sables à Unios et Térédines* Formation (Sudre *et al.* 1983) and UM-MGL-812 in size and morphology.

The Haplobunodontidae *Cuisitherium lydekkeri*, already described from Naples in Sudre & Lecomte (2000), is the most represented artiodactyl taxon with at least 6 specimens: a right dP4 UM-NAP-86 (W = 3.8), a left M1 UM-NAP-82 (L = 4.7; W = 6.2) (Fig. 6C), a left p3 UM-NAP-85 (L = 5.3 W = 2.1) with a reduced metaconid and narrow distal basin, a possible left p4 UM-NAP-91 which is very worn, a right m3 UM-NAP-76 (L = 7; W = 3.8) (Fig. 6E) and a right m1 UM-NAP-77 (L = 5.3; W = 3.7) (Fig. 6F). The new specimen UM-NAP2-73L (L = 4.9; W = 2.6) is described here from Naples 2 and corresponds to the first clearly established p4 of the species (Fig. 6D). Indeed, UM-NAP85 considered as a p4 in Sudre & Lecomte (2000) does not display a large independent metaconid as in UM-NAP2-73L and thus must correspond to a p3 of the same species. UM-NAP2-73L presents an elongated morphology with a long preprotocristid that forms a mesial hook toward a small parastylid, a large metaconid lingual to the protoconid and a postprotocristid that joins the distal cingulid forming a distostylid, and an entostylid is distinguishable on the distolingual corner of the cingulid. This morphology clearly differs from the simpler p4 of Diacodexeidae (Boivin *et al.* 2018), *Protodichobune*, *Aumelasia* (Godinot

et al. 2018) and *Eurodexis* Erfurt & Sudre, 1996 (Fig. 6G). *Cuisitherium* is easily recognized as the metaconule of upper molars is very lingual and the lower molars are slender with an entoconid aligned with hypoconid. UM-NAP-82 is the size of the M1 MNHN.F.GR7464 (Sudre & Lecomte 2000) and UM-NAP-77 noted as a m2 in Sudre & Lecomte (2000) is the exact size of the m1 of MNHN.F.AL5236, the holotype from the *Sables à Unios et Térédines* Formation. All this material is attributed to *C. lydekkeri.*

There are three specimens that can be referred to Diacodexeidae. The left M2 UM-NAP-84 (L>4.3; W = 5.4) (Fig. 6I) is the size of the largest *Diacodexis* cf. *varleti* from Prémontré (e.g., M2 MNHN.F.SLP29-PE-1084; L = 4.9 W = 5.5), Saint-Agnan and Sézannes-Broyes (Sudre *et al.* 1983); it corresponds to the median specimens of *Eurodexis russelli* (Sudre & Erfurt 1996). The presence of an ectoflexus unlike in *Protodichobune* (Sudre *et al.* 1983) and its linguo-mesial and linguo-distal cingula not bulged like in *Eurodexis russelli* permit to attribute this specimen to *Diacodexis*. Two small trigonids of lower molar, UM-NAP-80 (W = 2.8) and UM-NAP-81 (W = 3.1), with well distinguishable paraconid, which is size equivalent to metaconid, and elevated and acute cuspids are congruent with size and morphology of *Diacodexis* cf. *varleti*. Differences between *D. varleti* (Condé en Brie, Pourcy and Avenay) and *D*. cf. *varleti* (Saint-Agnan, Sézanne-Broye, Mancy, Grauves Cuis, Prémontré, and site XIV Geiseltal) mainly deal with mean size and slight differences in paraconid position, entoconid development and accessory crests from conules on upper molar (Sudre *et al.* 1983, Sudre & Erfurt 1996; Erfurt & Sudre 1996). The premetacristule development on UM-NAP-84 makes us lean toward an attribution as in Mas de Gimel to the more progressive species *D*. cf. *varleti*.

Perissodactyla. The Perissodactyla discovered in Naples belongs to three distinct families. As in Mas de Gimel, a small Hyrachyidae is represented by the right P4 UM-NAP-111 (L = 10.4; W = 14.7) and the right M1 UM-NAP-110 (L = 15.1; W = 17) (Fig. 7A). They are the size of specimens of *Hyrachyus stehlini* already described from Mancy (P4 UM-MCY-51; noted M-62-63 in Savage *et al.* 1966) or Monthelon (MNHN.F.MT4-L; Savage *et al.* 1966). Despite a very small size difference with *H. minimum* for this dental locus, the thin lingual cingulum helps us to attribute this material to *H. stehlini*.

Two lophiodontid remains have been found in Naples with the right dP4 UM-NAP-109 (L = 14.1; W = 14.3) and a right M3 UM-NAP-108 (L = 26.2; W = 30.4). The M3 has a triangular occlusal outline, a light cingulum and is size-equivalent with those from Mas de Gimel suggesting the presence of *L*. cf. *leptorhynchum*.

The locality of Naples 2 has yielded numerous dental remains of lophiodontids (N = 67) which will help to make a clearer attribution notably due to well preserved material (Fig. 7D-F). Note that this important material will need a full description which is out the scope of this study. These specimens belong to the genus *Lophiodon* Cuvier, 1822 notably due to the absence of paraconule on most of the specimens or very small paraconule when present. The mandibular symphysis reaches the level of the p3-p4 whereas in *Lophiaspis* Depéret, 1910 and *Eolophiodon* it only reaches the p2 (Robinet *et al.* 2015, Vautrin *et al.* 2020). Size distribution of molars and premolars overlaps that of *L. remense, L. glandicus* Astre, 1960 and *L. leptorhynchum* (Vautrin 2019). The *Lophiodon* species from Naples 2 is far smaller than *L. tapirotherium* from Issel (Filhol 1888), *L. eygalayense* Labarrère & Montenat, 2011 from Eygalaye (see Labarrère & Montenat 2011) and *L*. aff. *eygalayense* from Rouzilhac (Godinot *et al.* 2018). It displays numerous morphological affinities with *L. leptorhynchum* such as the relatively thin cingulum (Fig. 7E-F; unlike in *L. tapirotherium*) and the long, narrow, and dorso-ventrally thin symphysis (Fig. 7D), which is the main diagnostic feature of *L. leptorhynchum* (Filhol 1888, Vautrin 2019). Moreover, the variable presence of a fainted paraconule on upper molar is only known in the genus *Lophiodon* from *L. leptorhynchum* populations (Vautrin 2019). Finally, the specimens from Naples 2 correspond to the smallest specimens from La Livinière and Aumelas (Vautrin 2019) and thus we refer them to *L*. cf. *leptorhynchum* waiting the description of populations of *L. leptorhynchum* and discussion on a possible synonymisation with *L. remense*.

As with Mas de Gimel, we noted two morphs belonging to the family Palaeotheriidae. Two M1s from Naples UM-NAP-102 (L = 9; W = 10) and UM-NAP-103 (L = 9.4; W = 12.1) (Fig. 8B) and one M1 from Naples 2 UM-NAP2-72L (L = 9.1; W = 10.6) (Fig. 8C) can be attributed to *Propalaeotherium* based on the presence of a marked mesostyle, on their relative bunodonty and ectoloph morphology (see above, for Mas de Gimel). Measurements appear smaller than most of the specimens of *Pr. gaudryi* from the Paris Basin except some small specimens from the Ageian fauna and Grauves (Bronnert & Métais 2023) and, than all specimens of *Pr*. cf. *gaudry* from Aumelas and *Pr. gaudryi* from Rouzilhac.

Four upper molars of *Pachynolophus* have been found in Naples: two M3s UM-NAP-99 (L = 12; W = 13.4) (Fig. 8H) and UM-NAP-100 (L = 12.1; W = 13.9), two M1s or M2s UM-NAP-101 (L = 10.6; W = 12.1) and UM-NAP-106 (L = 9.1; W = 10.6). They all display a long ectoloph without mesostyle or with a pseudo-mesostyle (just present at the cingulum; UM-NAP-100), no metacone rib and present a continuous metaloph. These teeth are the same size than that of *Pa. ruscasseriensis* (Aumelas; Remy *et al.* 2019) and *Pa. cesserasicus* from La Livinière (Savage *et al.* 1965). A small left p3 UM-NAP-107 (L = 7.6; W = 5.2) with a prehypocristid oriented toward the metaconid and a quite distal metaconid can also be confidently attributed to a large *Pachynolophus*. As for the material from Mas de Gimel, we consider that a thorough revision of *Pa. cesserasicus* is needed. Pending this revision and considering that *Pa. ruscasseriensis* is better represented and described than *Pa. cesserasicus* (see Remy *et al.* 2019), we attribute this material to *Pa*. cf. *ruscasseriensis.*

SYSTEMATIC PALAEONTOLOGY

We here describe *Hartenbergeromys pailladensis* n. sp., a new rodent species from Mas de Gimel and Naples.

Order RODENTIA Griffith, 1827
Family indet.

Genus *Hartenbergeromys* Escarguel, 1999

urn:lsid:zoobank.org:act:AD84FF9C-B208-40D1-A156-73F897FD298C

Hartenbergeromys Escarguel, 1999: 201.

TYPE SPECIES. — *Hartenbergeromys hautefeuillei* Escarguel, 1999 by original designation.

TYPE LOCALITY. — Prémontré (Aisne, late early Eocene, MP10).

OTHER SPECIES. — *Hartenbergeromys marandati* (Escarguel, 1999).

DIAGNOSIS. — See Vianey-Liaud & Marivaux 2021: 78.

Hartenbergeromys pailladensis n. sp.
(Figs 9; 10; Table 1)

urn:lsid:zoobank.org:act:11CEEC60-37D4-4DF7-8092-A1B3923A8E32

Hartenbergeromys aff. *hautefeuillei* – Escarguel 1999: 209-210.

HOLOTYPE. — UM-MGL-601: left M1.

TYPE LOCALITY. — Mas de Gimel (Hérault, France, late early Eocene, MP10).

OTHER LOCALITY. — Naples (Hérault).

DIAGNOSIS. — *Hartenbergeromys* with numerous thin high extra ridges on upper and lower molars. Crested cusps and complete pericingulum on upper molars. Metacone smaller than protocone and hypocone smaller than protocone on upper molars, anteroloph and posteroloph as high as the other lophs. Metaconid only slightly protruding in dp4 and p4. Protoconid stronger in molars than in dp4 and p4. Four main cuspids (proto-, meta-, ento- and hypoconid) crested, delimiting an incomplete pericingulid, due to the presence of the sinusid and of the narrow mesoflexid opening. Labial metalophulid I strong and generally short, never connected to a complete transverse lingual metalophulid I. Entolophid rarely complete, often connecting the mesoconid.
Differs from *H. hautefeuillei* and *H. marandati* by more crested cusps and cuspids, the development of the pericingulum, and the smaller metacone and hypocone on molars.

MATERIAL. — 24 specimens from Mas de Gimel and 27 from Naples (measurements in Table 1) are available in the collection.

TABLE 1. — Specimens and dental measurements (in mm) of *Hartenbergeromys pailladensis* n. sp. from Mas de Gimel (MGL) and Naples (NAP). Symbol: *, fragmentary specimen.

upper teeth	Barcode	Side	L	W
DP4	MGL-647	right	1.35	1.60
	NAP-57	left	1.45	1.46
P4	NAP-58	left	1.62	2.01
	NAP-139	right	1.49	1.84
M1 or M2	MGL-601 (M1)	left	2.03	2.34
	MGL-772*	left	–	–
	MGL-790	right	1.75	1.88
	NAP-47	left	1.68	1.87
	NAP-48	left	1.65	1.78
	NAP-49 (M1)	left	1.84	1.82
	NAP-50 (M1)	left	1.83	1.90
	NAP-51*	left	–	–
	NAP-54	left	1.66	1.82
	NAP-55	left	1.59	1.77
M3	MGL-626	right	1.76	1.65
	NAP-52	right	1.48	1.48
	NAP-56	right	1.77	1.78
	NAP-64	left	1.74	1.73
lower teeth			**L**	**W**
dp4	MGL-649	left	1.65	1.28
	MGL-791	right	1.64	1.17
p4	MGL-616	right	1.66	1.30
	MGL-644	right	1.59	1.37
	MGL-768*	–	–	–
	MGL-786	right	1.56	1.15
	NAP-44	left	1.81	1.50
	NAP-53	right	1.63	1.37
m1	MGL-620	left	1.86	1.58
	MGL-637	right	1.77	1.66
	MGL-648	right	1.79	1.48
	MGL-652	left	1.81	1.60
	NAP-32	right	1.70	1.50
	NAP-39	left	1.77	1.57
	NAP-43	left	1.73	1.51
m2	MGL-618	left	1.82	1.74
	MGL-625	left	1.90	>1.58
	MGL-635	right	1.82	1.83
	MGL-653*	right	–	–
	MGL-750	left	1.90	1.56
	MGL-751*	left	–	–
	NAP-33	left	1.94	1.67
	NAP-34	right	1.69	1.54
	NAP-35	left	1.79	1.57
	NAP-40	right	1.75	1.67
	NAP-41	right	1.95	1.53
m3	MGL-617	right	1.82	1.60
	MGL-787	right	1.8	–
	MGL-749	left	1.86	1.54
	NAP-36	right	1.80	1.56
	NAP-37	left	1.82	1.57
	NAP-38	right	1.92	1.60
	NAP-46	left	1.82	1.64

REMARKS

Escarguel (1999: 200-210) described the type specimens of *Hartenbergeromys hautefeuillei* from the locality of Prémontré. In the same paper, he referred the specimens from Mas de Gimel and Naples as to *Hartenbergeromys* aff. *hautefeuillei*. Discussing the phylogeny of Theridomorpha, Vianey-Liaud & Marivaux (2017) followed the conclusions of Escarguel (1999) using the diagnosis of *H. hautefeuillei* including the features of the specimens from Mas de Gimel and Naples in their phylogenetic analysis (*Hartenbergeromys* aff. *hautefeuillei* in Vianey-Liaud & Marivaux 2017: fig. 7). More recently, following a more detailed phylogenetic analysis including numerous early Eocene rodents (Vianey-Liaud & Marivaux

2021), we reconsidered the material of *Hartenbergeromys hautefeuillei* from Prémontré, and we can highlight differences in morphological characters between the Mas de Gimel/Naples populations and that of Prémontré.

Description

Upper teeth

The crown is not very high, the lingual flank is slightly higher than the labial one and sometimes weakly wrinkled.

DP4. There are two available specimens, a worn right DP4 from Mas de Gimel (UM-MGL-647) and an almost unworn left DP4 from Naples (UM-NAP-57) (Fig. 9A, B). The first has a long anteroflexus and anteroloph ending lingually with a worn stretched anterostyle. This style is weakly attached to the preprotocrista. The protocone is worn following a plane inclined posteromesially from the indistinct endoloph, towards the anterostyle. The hypocone is worn symmetrically, sloping backwards to its junction with the lingual end of the posteroloph. It is only slightly smaller than the protocone. The paracone is slightly stronger than the metacone, but of same height. The labial protoloph bears a swollen worn paraconule, which is aligned labiolingually with it. The paraconule connects the preprotocrista close to the protocone summit with a short lingual protoloph. The labial metaloph, transverse, is short and separates from the metaconule. The latter is strong and obliquely stretched distomesially, towards its attachment with the postprotocrista, close to the protocone summit. The posteroloph ends at the level of the base of the labial metaloph, making the posteroflexus open labially.

P4. There are two available P4s, both from Naples (UM-NAP-58 and 59). Although they show the same characteristic globular morphology (Escarguel 1999: 209), they differ by the morphology and nature of the mesial lophs. On UM-NAP-58 (pl. 22, fig. n in Escarguel 1999; here: Fig. 9D) the anteroloph is absent; therefore, the anteriormost loph is made by the labial protoloph joining the preprotocrista. In UM-NAP-59 (Fig. 9C) instead the anteroloph is present and well distinct from the protoloph, which joins the preprotocrista closer to the protocone summit than on UM-NAP-58. A short mesoloph fills the labial part of the mesoflexus; it is separated from the mesostyle on UM-NAP-59, and linked to it on UM-NAP-58. On UM-NAP-59, it ends between the extremities of the extra ridges developed labially from the metaconule and distally from the labial part of the protoloph. A paraconule is present on UM-NAP-59 as developed as the metaconule. On both P4s, extra ridges descend from the conules and the protoloph to the mesoflexus. On UM-NAP-59, an anterolophule connects the paraconule to the anteroloph, and a posterolophule connects the metaconule to the posteroloph.

There is a pericingulum-like structure from the paracone-preparacrista, through the anteroloph, continuing to the preprotocrista, then the protocone-postprotocrista, turning distally at the level of a weak swelling, which resembles more a posterostyle than a hypocone, ending in the posteroloph up to the metacone flank. On UM-NAP-59, the postprotocrista and premetacrista are linked to the mesiodistally stretched mesostyle continuing labially the pericingulum. This is less continuous on UM-NAP-58, on which there are furrows between the mesostyle and the two main cusps.

M1-2. There are eight complete M1-2s available (six from Naples, two from Mas de Gimel; Fig. 9A-E), among which it is difficult to separate M1 from M2, whereas it is relatively easy for *H. hautefeuillei* from Prémontré (Vianey-Liaud & Marivaux 2021: 81). In the latter « the paracone is more labial than the metacone, but this metacone is even more lingual on M2 than on M1. The parastyle is thicker and more elongated or curved labially on M1; the hypocone (and not the protocone as it was incorrectly indicated in the 2021 paper, p. 81) is more reduced and labial on M2, and the posteroloph is shorter ». However, all the M1-2s from Naples and Mas de Gimel have a relatively short posteroloph, ending at the level of the labial part of the metaloph. Among them, the two upper molars from Mas de Gimel have a thicken and curved parastyle (M2: UM-MGL-606; M2: UM-MGL-790) and two of the molars from Naples (M1: UM-NAP-55; and M2: UM-NAP-47), whereas it is not distinct on the M1 UM-NAP-50 and the M1 or M2 UM-NAP-48. Protocone and hypocone are nearly at the same lingual level in all the M1-2s.

Apart from this weak difference between M1 and M2, what is striking in the upper teeth of *H. pailladensis* n. sp. is the development of the pericingulum including the anteroloph and the "internal cingulum" (terminology used in Escarguel 1999, fig. 5) encompassing the preprotocrista, the protocone, the posprotocrista, the endoloph and the hypocone, all aligned in continuity and with a nearly indistinct lingual sinus. The hypocone, quite smaller than the protocone, connects the posteroloph through a marked angle; this posteroloph is relatively shorter and slightly higher than the anteroloph. A narrow furrow marks the junction of the posteroloph with the distal flank of the metacone. The metacone is quite smaller than the paracone. The mesostyle can be stretched mesiodistally into two elements connected to the postprotocrista and the robust premetacrista, the whole forming the outer part of the pericingulum. Most often, at least one short mesoloph arises lingually from the mesostyle towards the metaconule without fusing with it. The paraconule is most often crescent-shaped and directed mesiodistally towards the mesoflexus or/and the anteroflexus. Two to three low short ridges also descend from the protoloph towards the anteroflexus and mesoflexus, as well as from the protocone (protocrista). The ridge underlining the premetacrista-metacone-metaloph arch drops down to join the flank of the metaconule. The latter is crested with short ridges that are clearly visible on little worn teeth, one descending into the posteroflexus and attaching to the posterocingulum, the other, mediolabial, directed towards the mesoloph without joining it. On unworn teeth, like the holotype UM-MGL-601 (Fig. 9E), the pericingulum is overlying the flexi floor, and the four main cusps (paracone, metacone, protocone and hypocone), as well as the paraconule and metaconule are slightly protruding above the

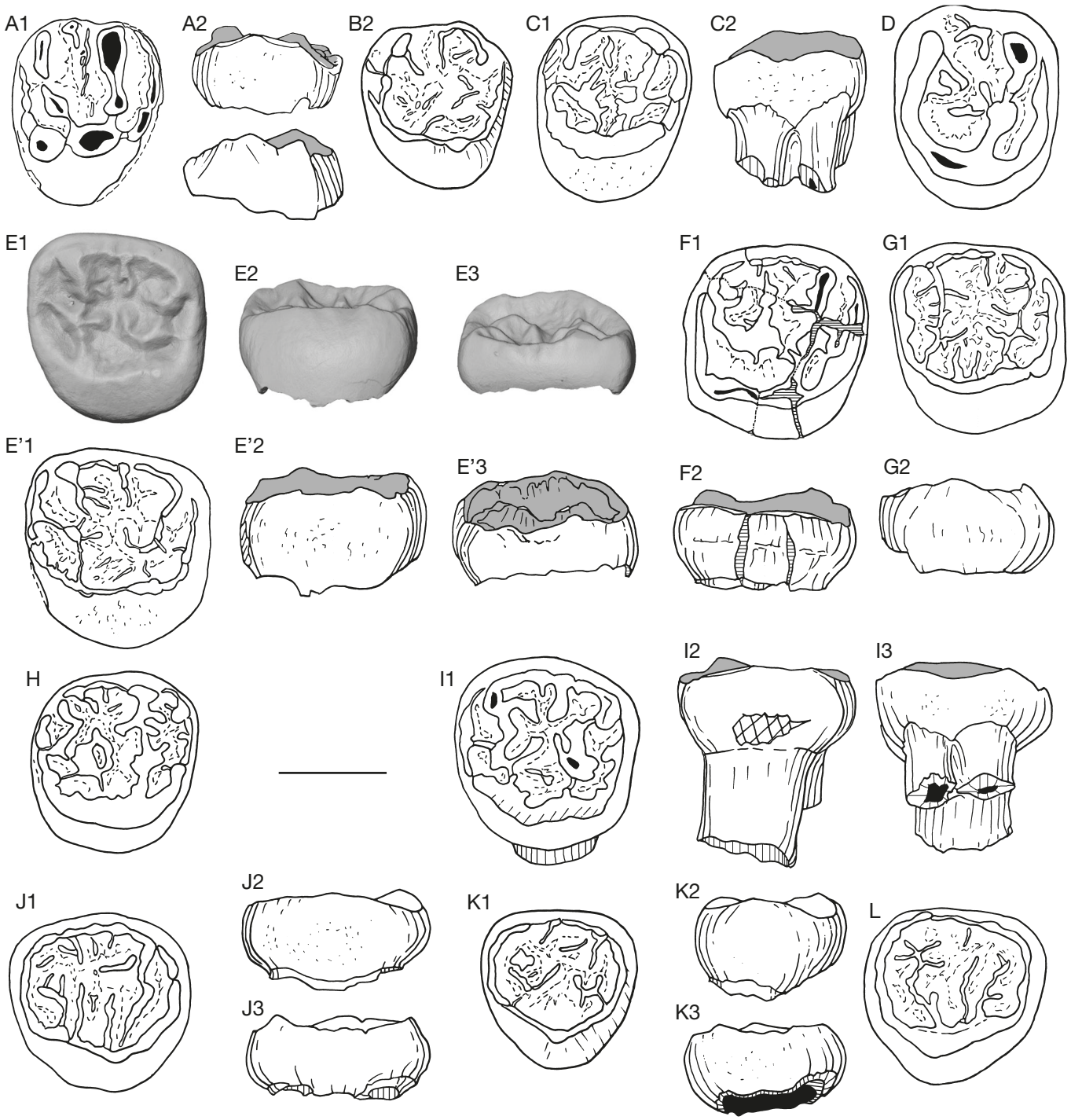

FIG. 9. — Upper deciduous (DP4), premolar (P4) and molars (M1-2-3) of *Hartenbergeromys pailladensis* n. sp. from the two closely related localities: MGL, Mas de Gimel (Hérault), and NAP, Naples (Hérault): **A**, UM-MGL-647, right DP4; **A1**, occlusal view; **A2**, lingual view; **B**, UM-NAP-57, enamel cover of a left DP4, unworn: **B1**, lingual view; **B2**, occlusal view; **C**, UM-NAP-59, left P4: **C1**, occlusal view; **C2**, labial view; **D**, UM-NAP-58, left P4, occlusal view; **E**, MicroCTScan of UM-MGL-601, holotype, unworn left M1: **E1**, occlusal view; **E2**, lingual view; **E3**, labial view; **E'**, same as **E** (UM-MGL-601), but drawings, to compare both figurations; **F**, UM-MGL-639, worn right M1: **F1**, occlusal view; **F2**, lingual view; **G**, UM-NAP-47, unworn left M1: **G1**, occlusal view; **G2**, lingual view; **H**, UM-NAP-55, right M1-2, moderately worn, roots partially preserved, occlusal view; **I**, UM-NAP-48, left M2, moderately worn, roots partially preserved: **I1**, occlusal view; **I2**, lingual view; **I3**, labial view; **J**, UM-NAP-56, left M3, weakly worn, roots broken; **J1**, occlusal view; **J2**, lingual view; **J3**, labial view; **K**, UM-NAP-52, right M3, nearly unworn: **K1**, occlusal view; **K2**, lingual view; **K3**, labial view; **L**, UM-NAP-64, right M3, nearly unworn, roots absent, occlusal view. Scale bar: 1 mm. The background of the profiles is greyed out. On Fig. F open cracks are filled with horizontal stripes.

pericingulum level, all being of same height. The paracone, metacone, protocone and hypocone, as well as the paraconule and metaconule, protrude. Then the wear affects primarily the lingual half of the tooth, and highlights its labial half, the wear surface of the latter descending labiolingually from the labial cusps (UM-MGL-639, Fig. 9F).

M3. There are three M3s from Naples (UM-NAP-52, NAP-56, NAP-64), one from Mas de Gimel (UM-MGL-626) (Fig. 9J-L). On all these teeth, the tiny hypocone is more lingual than the protocone. The M3s differ from the M1-2s in their triangular shape due to the quite more reduced and more labial hypocone. They display a complete pericingulum without discontinuities either at the junction posteroloph-metacone-metaloph, or at the junction anteroloph-protocone. The mesostylar area is longer than on M1-2, bearing one (UM-NAP-52 Fig. 9K, UM-NAP-64, Fig. 9L) to three (UM-NAP-56) short labial mesolophs.

Lower teeth

The crown has its lingual flank nearly as high as the labial one and rarely thinly wrinkled. The ectoflexid (sinusid) is always marked and on the lingual profile, the mesoflexid opening is narrow.

dp4. There are two available dp4s from Mas de Gimel, a damaged left one (UM-MGL-649) and a well-preserved right one (UM-MGL-664). On the latter (Fig. 10A), the trigonid is shorter labiolingually than the talonid; it is closed with a low premetacristid-anterolophid and the metaconid is only slightly protruding. The protoconid is slightly more distal. Protoconid and metaconid connect with the metalophid I, which limits the anteroflexid distally. From there, a bifurcate mesiodistal ridge descends labially to the mesoflexid. The postprotocristid, whose distal part is indistinct from the mesial ectolophid, joins the ectolophid bearing the mesoconid. Then at the level of the junction between the distal ectolophid and the prehypocristid, the entolophid develops up to the base of the entoconid. There the entoconid appears isolated, separated also from the posterolophid. The hypoconid is followed with a strong posthypocristid, and then a strong distinct hypoconulid precedes the short posterolophid. An additional extra ridge lies in the posteroflexid, parallel to the entolophid.

p4. There are five available p4s, three, damaged, from Mas de Gimel (UM-MGL-616, MGL-644, and MGL-786), two better preserved from Naples (UM-NAP-44 and NAP-53). The two well-preserved long roots of UM-NAP-44 fuse below the crown along the ⅓ to ½ of their height (Fig. 10C). As on dp4, the metaconid is slightly protruding, but more than the protoconid. The latter is crested similarly as other cuspids of the crown. As formerly stated (Escarguel 1999: 210), the wrinkles are numerous along the distal slope of the trigonid and in the talonid, and one can recognize the metalophid I linking the protoconid and the metaconid, as well as the mesoconid and the ectolophid (UM-NAP-44; Fig. 10C), and elements of the entolophid connected to the prehypocristid and the posterior cingulum on both. On UM-NAP-53, the postmetacristid ends distally in a metastylid swelling, separated from the mesostylid, which closes the mesoflexid lingually (Fig. 10B).

m1 or m2. There are ten m1-2s from Mas de Gimel (m1s: UM-MGL-620, MGL-637, MGL-648, MGL-652; m2s: UM-MGL-618, MGL-625, MGL-635, MGL-653, MGL-750, MGL-751) and eight from Naples (m1s: UM-NAP-32, NAP-39, NAP-43; m2s: UM-NAP-33, NAP-34, NAP-35, NAP-40, NAP-41) (Fig. 10D-K). The only difference between m1 and m2 is the narrower labiolingual width of the anterolophid-trigonid of m1 compare to m2.

As for dp4 and p4, the metaconid is only slightly protruding, but the protoconid is stronger than on these teeth. The four main cuspids (proto-, meta-, ento- and hypoconid) are crested, and their shape appears clearly on unworn teeth, delimiting an incomplete pericingulid, due to the presence of the sinusid and of the narrow mesoflexid opening.

The preprotocristid, attached to the mesial flank of the protoconid is either separated from the (labiolingual) premetacristid or joins it to make a complete transverse anterolophid. Distal to it, the protoconid bears a strong labial metalophulid I, which is generally short, never connected to a complete transverse lingual metalophulid I. The only case of a connection is the m1 UM-NAP-43 (Fig. 10E). Descending along the labiodistal flank of the metaconid, there is rather one short oblique ridge, sometimes joining the mesiodistal ridges developed distally from the anterolophid. There can be several (one to three) of these ridges, and another developed from the labial metalophid to the basin (Fig. 10G-K). The postmetacristid can show a metastylid-mesostylid thickening, and can be prolonged in a short lingual mesolophid (UM-MGL-618, MGL-648; UM-NAP-41; Fig. 10G, D, J). The protoconid is crested and stretched mesiodistally. It attaches to the mesial ectolophid through the postprotocristid. The mesoconid is aligned obliquely with the mesolophid. Distally, the mesoconid forms an angle with the distal ectolophid. The mesoconid makes another angle with the prehypocristid. The hypoconid is obliquely stretched to the posthypocristid.

The ridges are numerous in the basin, one of which derived from the mesoconid is a labial mesolophid. Another joins the distal ectolophid directly to the entoconid. This entolophid is either complete (UM-NAP-39, NAP-40 [Fig. 10F]) or broken in several elements (UM-NAP-35, NAP-41 [Fig. 10H, J]; UM-MGL-618 [Fig. 10G]). It connects to the posterolophid (UM-MGL-648 (Fig. 5A); UM-NAP-34) or to the distal ectolophid and the posterolophid (UM-MGL-618).

m3. There are four m3s from Naples (UM-NAP-36, NAP-37, NAP-38, NAP-46) and three from Mas de Gimel (UM-MGL-617, MGL-787, MGL-749) (Fig. 10L-O). The main difference between m3s and m1-2s is their narrower labiolingual width of the talonid.

The labial metalophulid I (named anterior arm of the protoconid in Escarguel 1999: 210) is rarely present, short and oblique mesiodistally (UM-MGL-617 and UM-NAP-38, Fig. 10L). On the two same specimens, the lingual metalophulid I is like on m1-2 as oblique ridges descending on the metaconid lingual flank, and directed to the basin. On the other m3s, the metalophulid I is absent and therefore, the anteroflexid is not individualized. The anterolophid and the premetacristid do not join on UM-NAP-38, NAP-46 (Fig. 10L-M) and UM-MGL-617, thus a mesiodistal furrow, bordered

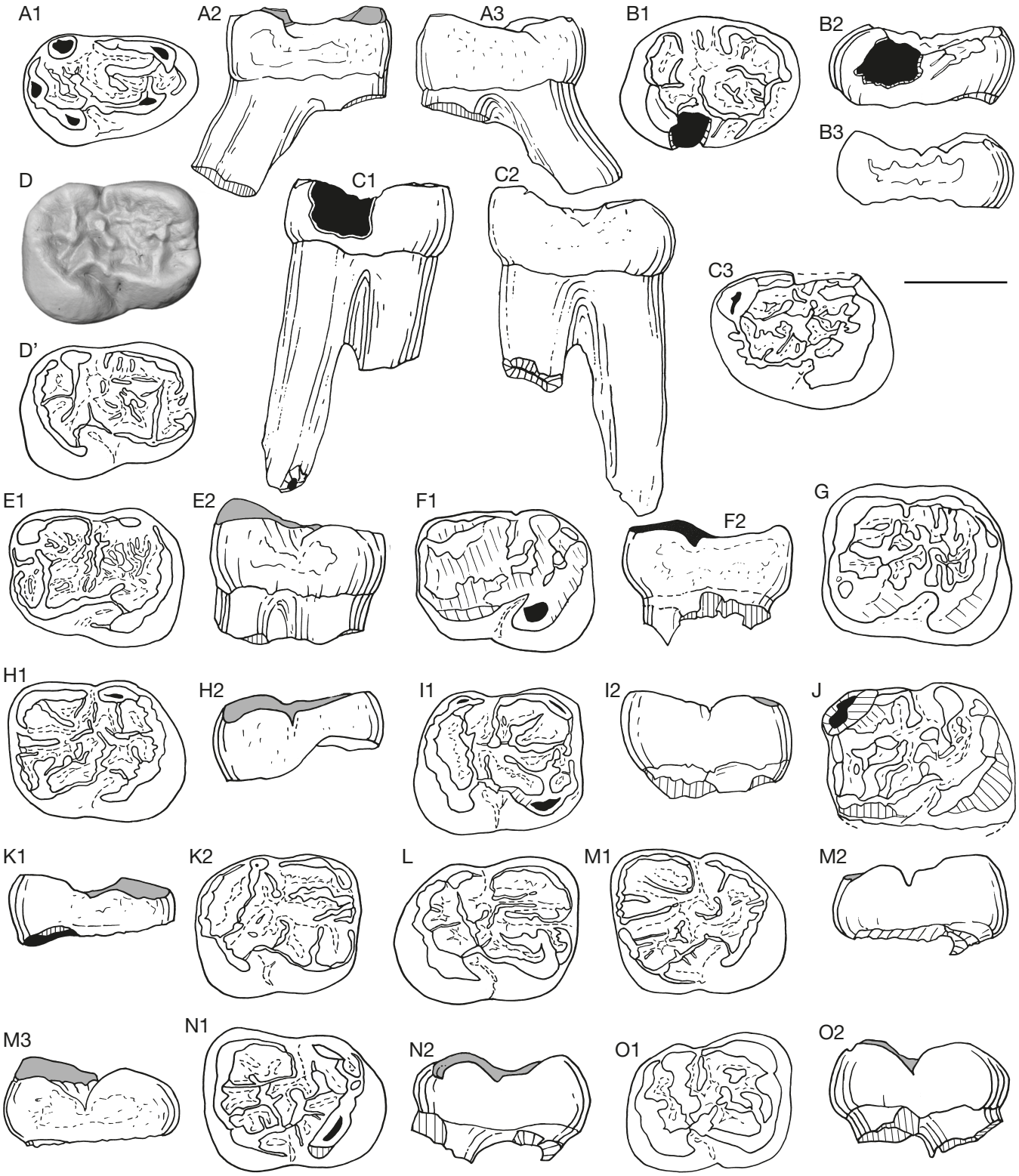

Fig. 10. — Lower deciduous (dp4), premolars (p4) and molars (m1-2-3) of *Hartenbergeromys pailladensis* n. sp. from the two closely related localities: MGL, Mas de Gimel (Hérault), and NAP, Naples (Hérault): **A**, UM-MGL-664, right dp4, showing the diverging roots: **A1**, occlusal view; **A2**, labial view; **A3**, lingual view; **B**, UM-NAP-53, right p4, nearly unworn: **B1**, occlusal view; **B2**, labial view, enamel cover partially erased, dentine blackened; **B3**, lingual view; **C**, UM-NAP-44, left p4: **C1**, occlusal view; **C2**, labial view; **C3**, lingual view, enamel cover partially erased, dentine blackened; two strong vertical roots, fused at their upper part; **D**, UM-MGL-648, right m1, nearly unworn, MicroCTscan, occlusal view; **D'**, same as **D**, drawings; **E**, UM-NAP-43, left m1, nearly unworn, incomplete roots: **E1**, occlusal view; **E2**, labial view; **F**, UM-NAP-39, left m1, weakly worn, incomplete roots: **F1**, occlusal view; **F2**, lingual view; **G**, UM-MGL-618, worn left m2, occlusal view; **H**, UM-NAP-35, unworn left m2: **H1**, occlusal view; **H2**, lingual view; **I**, UM-NAP-33, moderately worn right m2: **I1**, occlusal view; **I2**, lingual view; **J**, UM-NAP-41, worn m2 with labial side damaged, occlusal view; **K**, UM-NAP-34, unworn right m2: **K1**, occlusal view; **K2**, lingual view; **L**, UM-NAP-38, right m3, occlusal view; **M**, UM-NAP-46, left m3, unworn: **M1**, occlusal view; **M2**, lingual view; **M3**, labial view; **N**, UM-NAP-37, left m3, weakly worn, incomplete roots: **N1**, occlusal view; **N2**, lingual view; **O**, UM-NAP-36, right m3: **O1**, occlusal view; **O2**, labial view. Scale bar: 1 mm. The background of the profiles is greyed out on E2, F2, H2, M2.

with mesiodistal ridges, opens the trigonid mesially. Instead, they join on UM-NAP-36 and NAP-37 (Fig. 10O, N). The postmetacristid shows a metastylid-mesostylid thickening, and is prolonged in a short lingual mesolophid (UM-NAP-36, NAP-37, NAP-46). A distolabial spur of the protoconid is present on UM-NAP-37, NAP-38, NAP-46 and UM-MGL-617.

The postprotocristid, ectolophid, mesoconid, distal ectolophid and prehypocristid are like in m1-2. Numerous ridges converge into the talonid basin. Likewise, numerous ridges converge from the posterolophid to the posteroflexid. The entolophid is either discontinuous or continuous (UM-NAP-36, NAP-38; UM-MGL-617) and the most often connects the entoconid to the mesoconid. On UM-NAP-37, it connects the base of the entoconid and twice the posterior cingulum. The external walls of the unworn UM-NAP-46 are very finely wrinkled.

Comparisons and discussion

DP4 of *Hartenbergeromys pailladensis* n. sp. differs from that of *H. hautefeuillei* by less salient cusps above the grinding surface, less well-defined lophs on unworn tooth, and less lingual hypocone relative to the protocone. P4 differs mainly in its pericingulum and the less salient main cusps and more horizontal wear pattern. Moreover, the endoloph and hypocone are indistinct on UM-NAP-58, NAP-59 whereas they are well marked on some P4s of *H. hautefeuillei*. The main differences with upper molars of *H. hautefeuillei* and *H. marandati* are the more crestiform than bulging cusps, the metacone and hypocone respectively smaller relative to the paracone and protocone; the complete development of a relatively high pericingulum, as well as the different mode of wear and the size of teeth clearly lower for *H. pailladensis* n. sp. The three species of *Hartenbergeromys* are quite similar in size. Nevertheless, molars of *H. pailladensis* n. sp. appear intermediate in size between those of the larger *H. marandati* and the smaller *H. hautefeuillei*. Regarding lower molars only, the main differences with *H. hautefeuillei* and *H. marandati* are the more crestiform than pointed bulging cusps. In *H. pailladensis* n. sp., the entoconid is crested and displays pre- and postentocristids, the crested hypoconid is prolonged to the posthypocristid; the crested protoconid and metaconid have pre- and postcristids.

Escarguel (1999) proposed that the specimens from Mas de Gimel and Naples he named *Hartenbergeromys* aff. *hautefeuillei* display a set of derived characters relative to *H. hautefeuillei* from Prémontré. He mentioned several characters, "making the population from Mas de Gimel and Naples even more derived than that of Prémontré" (very wrinkled enamel surface, anteroloph absent on P4, strongly developed lingual cingulum on upper molars, complete or almost complete hypolophid on m1-m3)". These characters require some comments.

The absence of anteroloph on P4 is actually variable in *Hartenbergeromys pailladensis* n. sp., as well as in *H. marandati* and *H. hautefeuillei* (Escarguel 1999: 202; Vianey-Liaud & Marivaux: 80-82). The entolophid (= hypolophid) in *H. pailladensis* n. sp. is neither more nor less complete than in the two other *Hartenbergeromys* species. Teeth enamel surfaces of *H. pailladensis* n. sp. are not much more wrinkled than *H. hautefeuillei* (see Vianey-Liaud & Marivaux 2021: 82-93). Finally, we agree with Escarguel (1999) regarding the strong development of crested cusps giving a pericingulum on upper teeth. This trait could be however related to a difference in eating habits with *H. hautefeuillei*, together with a chronological difference.

To conclude, *Hartenbergeromys pailladensis* n. sp. only occurs in Mas de Gimel and Naples whereas *H. hautefeuillei* occurs in Prémontré, Grauves, Saint-Agnan, and possibly Azillanet (pending new discoveries, the only two teeth from that locality are here attributed to *H.* aff. *hautefeuillei*).

DISCUSSION

Faunal composition

The Mas de Gimel collection, known to be a reference fauna for the late Ypresian from southern European basin (Hartenberger *et al.* 1969), has in fact been the subject of few studies concerning its whole mammalian community. The first faunal list proposed the presence of 15 mammal species (Cappetta *et al.* 1968) whereas the most confident actualization by Vianey-Liaud *et al.* (2021) mentioned 23 species. The revision of the 1968' collection helps us to identify 36 taxa, completed by two others (cf. *Peradectes* sp. in Marandat [1986] and *Arcius lapparenti*) recently discovered from the unsorted sediment also sampled in 1968. Therefore, the 38 taxa recovered from Mas de Gimel permit nearly to double the species number previously identified. Among the mammalian remains (N = 574), 495 are identified at least at the order level. The important number of specimens in the collection allows us proposing percentage of abundance (Fig. 11A). Counting of NMI is not possible here considering that most of the fossils are isolated dental remains with very few locus repetitions. The ordinal or higher-level repartition of the specimens show an overrepresentation of Rodentia (25%, Fig. 11A). Then Perissodactyla and Metatheria display equivalent proportion (18%). Eulipothyphla are well represented (11%) and this is also the case for the Primates (7%). It worth notifying the weak proportion of Artiodactyla (4%) and Chiroptera (3%). The most represented species are *Masillamys mattaueri* (15% of the specimen abundance by species) and *Peratherium monspeliense* (14%). This is not surprising as both species were defined from this fossiliferous locality (Hartenberger 1975; Crochet 1979). These results are probably biased by the high number of indeterminate specimens. This is linked to the ancient established collection, in which a lot of too fragmentary specimens were numbered. It can also be noted that among the high number of perissodactyl specimens, an important number can be attributed at the generic level to *Lophiodon* but cannot be attributed confidently to the species *L.* cf. *leptorhynchum*. Therefore, based on the size of the tooth fragments and the enamel thickness, percentage of specimens of this species could reach 10% of the whole fauna instead of 4% (Fig. 11A). In the same way, the high proportion of unspecified specimens of Primates and Chiroptera corresponds to numerous anterior teeth or fragments of jugal teeth hardly attributable.

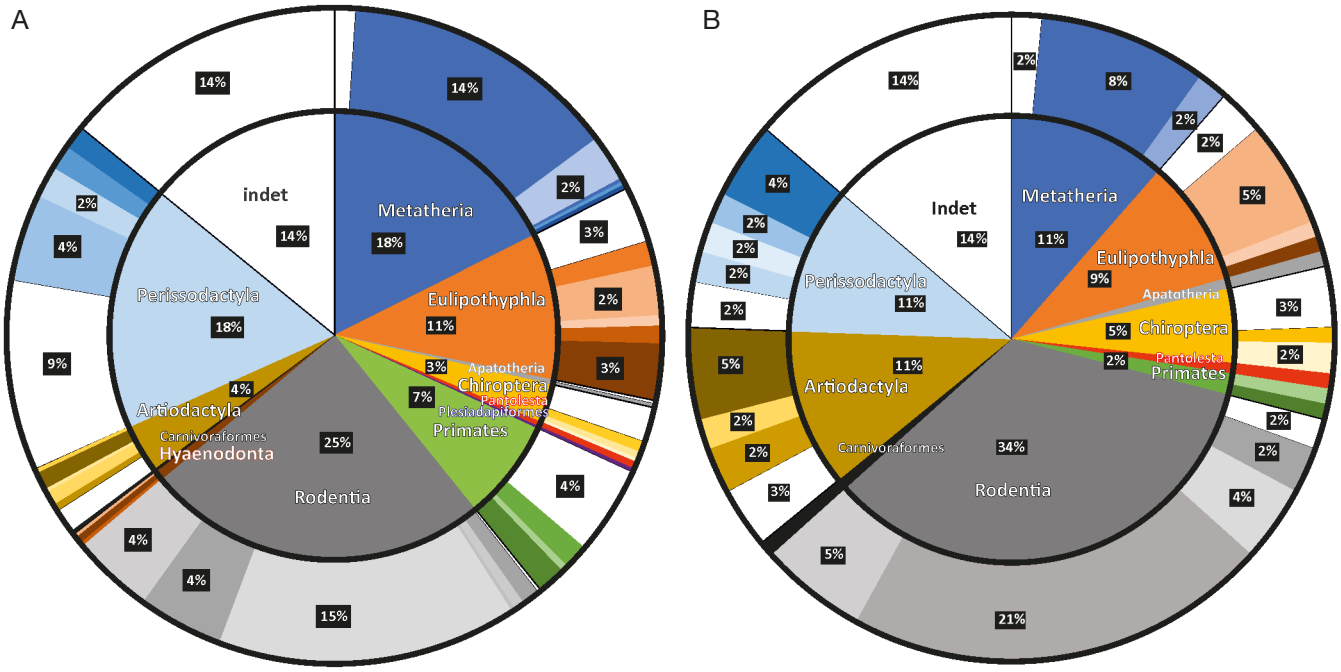

FIG. 11. — Distribution in percent of specimens by order and species from Mas de Gimel and Naples elaborated from data of Tables 2 and 3: **A**, color pie chart of Mas de Gimel collection; **B**, color pie chart of Naples collection. White sections correspond to specimens of indeterminate order or, within an order, of indeterminate specific attribution. Each identified species presents a color variation of the order color section. Percentage number are indicated when superior to one.

The locality of Naples has never been the subject of a faunal survey. Discovered in 1988, this locality was just punctually mentioned within specific taxonomical work mainly on rodents and artiodactyls (Escarguel 1999; Sudre & Lecomte 2000; Vianey-Liaud *et al.* 2019, 2022). Compared to Mas de Gimel, the number of specimens is weaker (131 mammalian specimens) and the observed mammal diversity is lower (23 recognized species instead of 38). The ordinal or higher rank repartition of specimen is however very similar to that observed for Mas de Gimel with a high representation of Rodentia (34%) followed by two equally distributed taxa: Perissodactyla and Metatheria (11%) (Fig. 11B). Noteworthy, the Artiodactyla appear proportionally more numerous in Naples fauna (11%, as much as Perissodactyla) despite a weaker specific diversity (3 species vs 5). Primates are not abundant in Naples with only 2% instead of 7% in Mas de Gimel. Moreover, Plesiadapiformes are not retrieved from Naples. Finally, Eulipothyphla (9%) and Chiroptera (5%) present the same relative importance than in Mas de Gimel. The most abundant species from Naples is the newly described rodent *Hartenbergeromys pailladensis* n. sp. (21%). It is just followed by the Metatheria *Peratherium* sp. (8%) that potentially includes *P. monspeliense* and *P. matronense*, for which a revision is needed.

Both faunas of Mas de Gimel and Naples are much diversified and display representatives of small, medium and large mammals, without any apparent fossilization bias. Moreover, the species repartition within each order follows a similar pattern in the two fossiliferous localities (Fig. 11). Conversely, the fauna discovered in Naples 2 is evidently biased in favour of large mammals (1 haplobunodontid, 1 palaeotheriid, and 67 *Lophiodon* remains, including numerous dental rows and not only isolated teeth). This is due to the different nature of the lithologies (marl rich in organic matter for Mas de Gimel and Naples, and marly limestone for Naples 2) and the low sieving effort (15 kg) for Naples 2. The five taxa from Naples 2 are nevertheless also known in Naples and Mas de Gimel (*P. monspeliense* or *P. matronense*, *Macrocranion* sp., *Hartenbergeromys pailladensis* n. sp., *Cuisitherium lydekkeri*, *Lophiodon* cf. *leptorhynchum*, and *Propalaeotherium gaudryi*).

Despite numerous similarities in both faunas from Mas de Gimel and Naples, we notice 16 taxa known from Mas de Gimel but not found in Naples (Tables 2; 3) : the two peradectids, the small eulipothyphlans (*Macrocranion* cf. *nitens* morph A and *Leptacodon* sp.), two chiropterans (*P.* cf. *tupaiodon* and ?Icaronycteridae indet.), a small indeterminate pantolestid, a paromomyid (*Arcius lapparenti*), a large notharctid (cf. *Protoadapis curvicuspidens*), two rodents (*Plesiarctomys* cf. *savagei* and *Pseudoparamys* sp.), hyaenodontids (*Lesmesodon* cf. *gunelli*, *Matthodon peignei,* and *Leonhardtina meridianum*) and two artiodactyls (*Eurodexis russelli* and an original large haplobunodontid). On the other hand, some taxa from Naples are not known in Mas de Gimel such as the chiropteran *Icaronycteris* sp., the pantolestid *Pantolestes sabatieri*, and the metatherian cf. *Amphiperatherium bastbergense*. In any way, these three taxa are always weakly represented (by one or two specimens), which suggests that they are uncommon taxa, hardly recovered from these fossiliferous localities. In fact, in both cases, the taxonomic disparity is correlated with uncommon taxa (one to three specimens; Tables 2; 3) with the exception of the small *Macrocranion* cf. *nitens* morph A, *Leptacodon* sp. and the larger cf. *Protoadapis curvicuspidens* that are quite well represented in Mas de Gimel (5 to 7 specimens).

TABLE 2. — New faunal list of Mas de Gimel based on 574 mammalian specimens (495 defined at least at order level), established after first description (Cappetta *et al.* 1968 and Hartenberger *et al.* 1969), subsequent targeted reviews (Hartenberger 1971; Crochet 1980; Sudre *et al.* 1983; Sudre & Lecomte 2000; Escarguel 1999) and according to this study (the main changes are in bold police).

Order or higher rank	N	Family	N	Species	N
Metatheria	101	Herpetotheriidae	99	*Peratherium monspeliense* Crochet, 1979	79
				Peratherium matronense Crochet, 1979	13
				Herpetotheriidae gen. et sp. indet.	1
		Peradectidae	2	**cf. *Peradectes* sp. in Marandat (1986)**	1
				***Peradectes* cf. *mutigniensis* Crochet, 1979**	1
Eulipotyphla	61	Amphilemuridae	39	***Macrocranion* cf. *nitens* (Matthew, 1918) morph A**	7
				***Macrocranion* cf. *nitens* morph B**	14
				***Macrocranion* sp. (*sensu* Russell *et al.* 1975)**	3
		Nyctitheriidae	21	***Leptacodon* sp.**	5
				aff. *Pontifactor* sp.	16
Apatotheria	2	Apatemyidae	2	***Heterohyus* sp.**	1
Chiroptera	16	Palaeochiropterygidae	5	**Palaeochiropterygidae gen. et sp. indet.**	3
				***Palaeochiropteryx* cf. *tupaiodon* Revilliod, 1917**	2
		Icaronycteridae	2	**?Icaronycteridae sp. indet.**	1
Pantolesta	2	Pantolestidae	2	**Pantolestidae gen. et sp. indet.**	2
Plesiadapiformes	1	Paromomyidae	1	***Arcius lapparenti* (Russell, Louis & Savage, 1967)**	1
Primates	42	Notharctidae	16	cf. *Protoadapis curvicuspidens* (Lemoine, 1878)	7
				***Anchomomys* sp.**	2
		Microchoeridae	13	***Nannopithex zuccolae* Godinot, Russel & Louis, 1992**	8
Rodentia	142	Ailuravidae	5	*Ailuravus* aff. *michauxi* Hartenberger, 1975	5
		Plesiarctomyidae	4	*Plesiarctomys* cf. *savagei* (Michaux, 1964)	3
				Pseudoparamys sp.	1
		Masilamyidae	85	*Masillamys mattaueri* Hartenberger, 1975	85
		Rodentia indet	24	***Hartenbergeromys pailladensis* n. sp.**	24
		Gliridae	23	*Eogliravus wildi* Hartenberger, 1971	23
Carnivoraformes		"Miacidae"	2	***Uintacyon* cf. *hookeri* Solé, 2014**	2
Hyaenodonta	4	Hyaenodontidae	4	***Lesmesodon* cf. *gunelli* Solé, Morlo, Schaal & Lehmann, 2021**	1
				***Matthodon peignei* Solé, Marandat & Lihoreau, 2020**	2
				***Leonhardtina meridianum* Solé, Marandat & Lihoreau, 2020**	1
Artiodactyla	21	Diacodexeidae	2	***Diacodexis* cf. *varleti* Sudre, 1983**	2
		Dichobunidae	5	*Protodichobune oweni* Lemoine, 1878	4
				***Eurodexis russelli* Sudre & Erfurt, 1996**	1
		Haplobunodontidae	6	*Cuisitherium lydekkeri* (Lemoine, 1891)	5
				cf. Haplobunodontidae indet.	1
Perissodactyla	101	Lophiodontidae	62	***Lophiodon* cf. *leptorhynchum* Filhol, 1888**	25
		Hyrachyidae	9	***Hyrachyus stehlini* (Depéret, 1904)**	9
		Palaeotheriidae	27	***Propalaeotherium gaudryi* (Lemoine, 1878)**	7
				***Pachynolophus* cf. *ruscasseriensis* Remy, Krasovec, Lopez, Marandat & Lihoreau, 2019**	6

Mas de Gimel and Naples belong to the same stratigraphic unit with similar sedimentological facies and are only separated one to the other by around 300 m. The only noticeable differences are basically on the representativeness of uncommon taxa. The two mammalian paleocommunity structures do not evocate ecological nor chronological differences. In addition, and depending on some taxonomic interpretations (see Results), twenty to twenty-two species are common to both localities. Following these arguments, we confidently propose to assemble these two contemporaneous faunas in one fossiliferous unit MGL/NAP rich of 41 species. This faunal assemblage is thus comparable in term of specific richness with the main reference faunas listed in Table 4 (Mutigny = 48 sp., Avenay = 55 sp., Saint-Agnan = 37 sp., Grauves and all contemporaneous localities near Epernay = 47 sp., Prémontré = 37 sp.). MGL/NAP, with 41 species, gathers with the most diverse faunas of the Ypresian with quasi-equivalent diversity than the well-known Lutetian locality of Messel (44 species). Such a result strengthens the longstanding conclusion proposed by Hartenberger *et al.* (1969) that MGL/NAP is a key European Ypresian reference fauna, very informative for biochronological and paleobiogeographical purposes.

BIOCHRONOLOGY AND PALEOBIOGEOGRAPHY

Biochronological questions inferred from the rich mammal assemblage from MGL/NAP require detailed faunal comparisons with European localities encompassing the MP8+9 to MP11 reference-levels (Table 4). With Avenay (reference-level for the MP8+9), MGL/NAP shares the herpetotheriid *Peratherium matronense* (note however that this species is the subject of a current taxonomic revision), possibly *Peradectes mutigniensis*, and the two amphilemurid species *Macrocranion* cf. *nitens* (morphs A and B) and *Macrocranion* sp. With Mutigny (commonly considered as older than Avenay), MGL/NAP shares also these two amphilemurids and possibly *Peradectes mutigniensis*. More similarities are found with the locality of Saint-Agnan, which is commonly attributed to the MP10a but considered intermediate in age between Avenay and the

TABLE 3. — Faunal list of Naples and Naples 2 based on 130 and 78 mammalian specimens, respectively.

Order or higher rank	N	Family	N	Species Naples	N	Species Naples 2	N
Metatheria	15/2	Herpetotheriidae	14/2	*Peratherium monspeliense* Crochet, 1979 or *P. matronense* Crochet, 1979	11	*Peratherium monspeliense* or *P. matronense*	2
				cf. *Amphiperatherium bastenbergense* Crochet, 1979	2	–	–
Eulipotyphla	12/2	Amphilemuridae	10/2	*Macrocranion* cf. *nitens* (Matthew, 1918) morph B	7	–	–
				Macrocranion sp. (*sensu* Russell *et al.* 1975)	1	*Macrocranion* sp. (*sensu* Russell *et al.* 1975)	2
		Nyctitheriidae	1	aff. *Pontifactor* sp.	1	–	–
Apatotheria	1	Apatemyidae	1	*Heterohyus* sp.	1	–	–
Chiroptera	7	Palaeochiropterygidae	1	Palaeochiropterygidae gen. et sp. indet.	1	–	–
		Icaronycteridae	2	*Icaronycteris* sp. indet.	2	–	–
Pantolesta	1	Pantolestidae	1	?*Pantolestes sabatieri* Smith, 2001	1	–	–
Primates	2	Notharctidae	1	*Anchomomys* sp.	1	–	–
		Microchoeridae	1	*Nannopithex zuccolae* Godinot, Russell & Louis *et al.*, 1992	1	–	–
Rodentia	45	Ailuravidae	3	*Ailuravus* aff. *michauxi*	3	–	–
		Masilamyidae	5	*Masillamys mattaueri* Hartenberger, 1975	5	–	–
		indet	28	*Hartenbergeromys pailladensis* n. sp.	28	–	2
		Gliridae	7	*Eogliravus wildi* Hartenberger, 1971	7	–	–
Carnivoramorpha	1	"Miacidae"	1	*Uintacyon* cf. *hookeri*	1	–	–
Artiodactyla	15/1	Diacodexeidae	3	*Diacodexis* cf. *varleti* Sudre, 1983	3	–	–
		Dichobunidae	2	*Protodichobune oweni* Lemoine, 1878	2	–	–
		Haplobunodontidae	6/1	*Cuisitherium lydekkeri* (Lemoine, 1891)	6	*Cuisitherium lydekkeri*	1
Perissodactyla	14/68	Lophiodontidae	2/67	*Lophiodon* cf. *leptorhynchum* Filhol, 1888	2	*Lophiodon* cf. *leptorynchum*	67
		Hyrachyidae	2/2	*Hyrachyus stehlini* (Depéret, 1904)	2	–	–
		Palaeotheriidae	9/1	*Propalaeotherium gaudryi* (Lemoine, 1878)	2	*Propalaeotherium gaudryi*	1
				Pachynolophus cf. *ruscasseriensis* Remy, Krasovec, Lopez, Marandat & Lihoreau, 2019	5	–	–

MP10a reference localities from the *Sables à Unios et Térédines* Formation (see below) (Louis & Laurain 1983; Lecomte 1994; Escarguel 1999). MGL/NAP shares with Saint-Agnan the ten following species: *Macrocranion* cf. *nitens*, *Macrocranion* sp., *Masillamys mattaueri*, *Nannopithex zuccolae*, *Propalaeotherium gaudryi*, *Hyrachyus stehlini*, *Diacodexis* cf. *varleti*, *Protodichobune oweni*, *Eurodexis russelli*, and *Cuisitherium lydekkeri*; plus the following four species in open nomenclature: *Peradectes* cf. *mutigniensis*, *Ailuravus* aff. *michauxi*, *Plesiarctomys* cf. *savagei*, and cf. *Protoadapis curvicuspidens*. Among these species, only *Peradectes* cf. *mutigniensis* evokes the level MP8+9; the other are typical of the level MP10a.

Comparisons with Grauves (reference-level of the MP10a) and other localities from the *Sables à Unios et Térédines* Formation (Cuis, Mancy, Monthelon, Mont Bernon, Venteuil, and Chavot) indicate that MGL/NAP shares with one or more of these localities the following twelve species: *Heterohyus* sp.3, *Macrocranion* sp., *Macrocranion* cf. *nitens*, *Masillamys mattaueri*, *Arcius lapparenti*, *Nannopithex zuccolae*, *Lesmesodon gunnelli*, *Propalaeotherium gaudryi*, *Hyrachyus stehlini*, *Diacodexis* cf. *varleti*, *Protodichobune oweni*, and *Cuisitherium lydekkeri*; plus the species in open nomenclature *Palaeochiropteryx* cf. *tupaiodon*, *Ailuravus* aff. *michauxi*, *Plesiarctomys* cf. *savagei*, cf. *Protoadapis curvicuspidens*, and *Eurodexis russelli* (note that this species is identified as *E.* cf. *russelli* at Grauves, Saint-Agnan, Mancy, and Cuis).

Among the localities from the Paris Basin attributed to the MP10a, Prémontré has the particularity of having a well-constrained dating using nannoplankton and dinoflagellate biostratigraphy. The locality is estimated to postdate the onset of both NP13 and Chron C22r, at about 50.4 to 50.3 Ma (Steurbaut *et al.* 2016). MGL/NAP shares with this locality the species *Macrocranion* sp., *Pantolestes sabatieri*, *Arcius lapparenti*, *Nannopithex zuccolae*, *Eogliravus wildi*, *Diacodexis* cf. *varleti*, *Eurodexis russelli*, and *Lesmesodon gunnelli*. Interestingly, among these taxa, the three species *Pantolestes sabatieri*, *Eogliravus wildi*, and *Lesmesodon gunnelli* are not documented elsewhere in the Paris Basin from MP10a localities, suggesting that MGL/NAP and Prémontré could be coeval. This hypothesis is however uncertain because most of the pantolestids from the MP10a localities are still unpublished and the rodent *E. wildi* also occurs in localities from the MP10-MP11 interval (Cos and Vielase, Southern France, Quercy) (Vianey-Liaud *et al.* 2022). Finally, also from Southern France, the locality of Azillanet, attributed to the MP10a, requires a mention as it shares significant taxa with MGL/NAP: *Peradectes* sp.

TABLE 4. — Faunal list of Mas de Gimel/Naples compared to those of other European localities dated from MP8+9 to MP11 reference-levels (data compiled from Bronnert & Métais 2023; Crochet 1979, 1980; Dégremont *et al.* 1985; Erfurt & Sudre 1996; Escarguel 1999; Fischer 1977; Franzen 1988; Franzen & Haubold 1986; Franzen & Habersetzer 2017; Franzen *et al.* 2009; Gingerich 1976; Gingerich 1977; Godinot 1998; Godinot *et al.* 1992, 2018; Haubold 1989; Hand & Sigé 2018; Hellmund 2013; Hlawatsch & Erfurt 2007; Hooker 1996, 2010; Kurtz 2005; Lange-Badré & Haubold 1990; López-Torres & Silcox 2018; Louis & Laurain 1983; Marandat 1986; Morlo et al. 2004, 2010; Russell *et al.* 1967, 1973, 1975, 1979, 1982; Savage *et al.* 1965; Sigé 1976; Smith 2001; Smith *et al.* 2012; Solé 2014; Solé *et al.* 2015, 2018, 2019, 2020, 2021; Sudre *et al.* 1983; Sudre & Erfurt 1996; Sudre & Lecomte 2000; Theodor *et al.* 2007; Thewissen 1990; Vautrin *et al.* 2020; Vianey-Liaud & Marivaux 2021; Vianey-Liaud *et al.* 2022). Abbreviations: **MUT**, Mutigny; **AVE**, Avenay; **STA**, Saint-Agnan; **MGL**, Mas de Gimel; **NAP**, Naples; **GRA**, Grauves, Cuis, Mancy, Monthelon, Mont Bernon, Venteuil, and Chavot; **PRE**, Prémontré; **AZI**, Azillanet; **ROU**, Rouzilhac; **GEI**, Geiseltal Unterkohle (United Kingdom), **MES**, Messel.

			MUT	AVE (MP8+9)	STA	MGL	NAP	GRA (MP10a)	PRE	AZI	ROU (MP10b)	GEI (MP11)	MES
Multituberculata	Neoplagiaulacidae	*Ectypodus* sp.	×	×	–	–	–	–	–	–	–	–	–
		Parectypodus sp.	×	×	–	–	–	–	–	–	–	–	–
		Neoplagiaulax sylvani	aff.	–	–	–	–	–	–	–	–	–	–
	Family indet.	gen. et sp. indet.	–	–	–	–	–	–	×	–	–	–	–
Metatheria	Peradectidae	*Peradectes louisi*	×	×	–	–	–	×	–	–	–	–	–
		Peradectes mutigniensis	×	×	×	cf.	–	–	–	–	–	–	–
		Peradectes sp. (Crochet 1980)	×	×	–	–	–	–	–	–	–	–	–
		Peradectes russelli	–	×	–	–	–	–	–	–	–	–	–
		Peradectes sp. (Marandat 1986)	–	–	–	cf.	–	–	–	×	–	–	–
		"*Peradectes*" (?Peradectidae)	–	–	–	–	–	–	–	–	–	–	×
	Herpetotheriidae	*Peratherium constans*	×	–	–	–	–	–	–	–	–	–	–
		Peratherium matronense	–	×	–	×	?	–	–	–	–	–	–
		Peratherium monspeliense	–	–	–	×	?	–	–	×	–	–	–
		Peratherium sp. 1 (Crochet 1980)	–	–	–	–	–	–	–	cf.	–	–	–
		"*Amphiperatherium brabantense*"	×	–	–	–	–	–	–	–	–	–	–
		Amphiperatherium maximum	×	×	×	–	–	×	–	–	–	–	cf.
		Amphiperatherium bourdellense	–	×	–	–	–	–	×	–	–	–	–
		Amphiperatherium goethei	–	×	–	–	–	×	×	–	–	–	×
		Amphiperatherium sp. 1 (Crochet 1980)	–	×	–	–	–	×	–	–	–	–	–
		Amphiperatherium sp. 2 (Crochet 1980)	×	×	–	–	–	–	–	–	–	–	–
		Amphiperatherium bastbergense	–	–	–	–	cf.	–	–	–	–	–	–
		gen. et sp. indet. (this study)	–	–	–	×	–	–	–	–	–	–	–
		Amphiperatherium sp. (Marandat 1986)	–	–	–	–	–	–	–	×	–	–	–
		gen. et sp. indet.	–	–	–	–	–	–	–	–	–	–	×
Pantolesta	Pantolestidae	*Palaeosinopa* sp.	×	×	–	–	–	–	×	–	–	–	–
		Pantolestes sabatieri	–	–	–	–	×	–	×	–	–	–	–
		Pantolestes sp.	–	–	–	–	–	–	cf.	–	–	–	–
		Premontrelestes duchaussoisi	–	–	–	–	–	–	×	–	–	–	–
		Premontrelestes sp.	–	–	–	–	–	–	cf.	–	–	–	–
		gen. et sp. indet.	–	–	–	×	–	–	×	–	–	–	–
		Buxolestes sp.	–	–	×	–	–	×	–	–	–	–	–
		Buxolestes piscator	–	–	–	–	–	–	–	–	–	–	×
		Buxolestes minor	–	–	–	–	–	–	–	–	–	–	×
	Paxoxyclaenidae	*Fratrodon tresvauxi*	×	×	–	–	–	–	–	–	–	–	–
		Sororodon tresvauxae	×	×	–	–	–	–	–	–	–	–	–
		Paraspaniella gunnelli	–	–	–	–	–	×	×	–	–	–	–
		Kopidodon macrognathus	–	–	–	–	–	–	–	–	–	–	×
		Paroxyclaenus sp.	–	–	–	–	–	–	–	–	–	–	×
Apatotheria	Apatemyidae	*Apatemys mutinacus*	×	×	×	–	–	–	–	–	–	–	–
		Apatemys sigogneaui	×	×	–	–	–	–	–	–	–	–	–
		Heterohyus sp. 1 (Russell *et al.* 1979)	×	–	×	–	–	–	–	–	–	–	–
		Heterohyus sp. 2 (Russell *et al.* 1979)	–	×	×	–	–	–	–	–	–	–	–
		Heterohyus sp. 3 (Russell *et al.* 1979)	–	–	–	×	×	×	–	–	–	–	–
Eulipotyphla	Amphilemuridae	*Neomatronella luciannae*	×	×	×	–	–	–	–	–	–	–	–
		Macrocranion cf. *nitens* morph A	×	×	×	×	×	×	–	–	–	–	–
		Macrocranion cf. *nitens* morph B	×	×	×	×	×	×	–	–	–	–	–
		Macrocranion sp. (Russell *et al.* 1979)	×	×	×	×	×	×	×	–	–	–	–
		Macrocranion tenerum	–	–	–	–	–	–	–	–	–	–	×
		Macrocranion tupaidon	–	–	–	–	–	–	–	–	–	–	×
		Pholidocercus hassiacus	–	–	–	–	–	–	–	–	–	–	×
	Nyctitheriidae	*Leptacodon* sp.	×	×	–	×	–	–	cf.	–	–	–	–
		Placentidens lotus	×	×	–	–	–	–	–	–	–	–	–
		Pontifactor sp.	–	–	–	aff.	aff.	–	×	×	–	–	–
	Talpidae	gen. et sp. indet.	–	–	–	–	–	–	–	×	–	–	–

Table 4. — Continuation.

			MUT	AVE (MP8+9)	STA	MGL	NAP	GRA (MP10a)	PRE	AZI	ROU (MP10b)	GEI (MP11)	MES
Order indet.	Pseudorhyncocyonidae	*Leptictidium tobieni*	–	–	–	–	–	–	–	–	–	–	×
		Leptictidium nasutum	–	–	–	–	–	–	–	–	–	–	×
		Leptictidium auderiense	–	–	–	–	–	–	–	–	–	–	×
Chiroptera	Icaronycteridae	*Icaronycteris menui*	×	×	–	–	–	–	–	cf.	–	–	–
		Icaronycteris sp.	–	–	?	–	×	–	–	–	–	–	–
		gen. et sp. indet.	–	–	–	?	–	–	–	–	–	–	–
		Xylonycteris stenodon	–	–	–	–	–	–	×	–	–	–	–
	Archaeonycteridae	*Archaeonycteris brailloni*	×	×	–	–	–	–	–	–	–	–	–
		Archaeonycteris sp.	–	–	–	–	–	–	cf.	–	–	–	–
		Archaeonycteris trigonodon	–	–	–	–	–	–	–	–	–	–	×
		Archaeonycteris pollex	–	–	–	–	–	–	–	–	–	–	×
	Onychonycteridae	*Ageina tobieni*	×	–	–	–	–	–	–	–	–	–	–
		cf. *Ageina* sp.	–	×	–	–	–	–	–	–	–	–	–
	Palaeochiropterygidae	*Palaeochiropteryx* sp.	–	–	?	–	–	?	–	–	–	–	–
		Palaeochiropteryx tupaiodon	–	–	–	cf.	–	cf.	–	–	–	–	×
		Palaeochiropteryx spiegeli	–	–	–	–	–	–	–	–	–	–	×
		gen. et sp. indet.	–	–	–	×	×	–	–	–	–	–	–
	Hassianycteridae	*Hassianycteris messelensis*	–	–	–	–	–	–	–	–	–	–	×
		Hassianycteris magna	–	–	–	–	–	–	–	–	–	–	×
		Hassianycteris revilliodi	–	–	–	–	–	–	–	–	–	–	×
	Family indet.	gen. et sp. indet.	–	–	×	–	–	–	–	–	–	–	–
	Vespertilionidae	*Premonycteris vesper*	–	–	–	–	–	–	×	–	–	–	–
	Emballonuridae	*Tachypteron franzeni*	–	–	–	–	–	–	–	–	–	–	×
Rodentia	Gliridae	*Eogliravus wildi*	–	–	–	×	×	–	×	×	–	–	–
		Eogliravus hammeli	–	–	–	–	–	–	–	–	–	–	cf.
	Ischyromyidae	*Ailuravus michauxi*	–	–	aff.	aff.	aff.	×	×	–	aff.	–	–
		Ailuravus inexpectatus	–	–	×	–	–	–	×	×	–	–	–
	Euromyidae	*Meldimys louisi*	×	×	×	–	–	–	–	–	–	–	–
		Euromys thaleri	×	×	–	–	–	–	–	–	–	–	–
		Euromys woodi	×	×	×	–	–	–	×	–	–	–	–
	Pleisarctomyidae	*Pseudoparamys teilhardi*	×	×	×	–	–	–	–	–	–	–	–
		Pseudoparamys sp.	–	–	–	×	–	–	–	–	–	–	–
		Plesiarctomys savagei	–	–	×	cf.	–	×	×	–	–	–	–
	Family indet.	*Sparnacomys chandoni*	×	×	–	–	–	–	–	–	–	–	–
		Pantrogna russelli	×	×	×	–	–	–	–	–	–	–	–
		Reinomys rhomboides	–	×	–	–	–	–	–	–	–	–	–
	Theridomyoidea	*Hartenbergeromys hautefeuillei*	–	–	×	–	–	×	×	×	–	–	–
		Hartenbergeromys pailladensis n. sp.	–	–	–	×	×	–	–	–	–	–	–
		Hartenbergeromys marandati	–	–	–	–	–	–	×	–	–	–	–
		Masillamys mattaueri	–	–	×	×	–	×	–	×	–	–	–
		Masillamys parvus	–	–	–	–	–	–	?	–	–	–	×
		Masillamys beegeri	–	–	–	–	–	–	–	–	–	–	×
		Masillamys krugi	–	–	–	–	–	–	–	–	–	–	×
Plesiadapiformes	Paromomyidae	*Arcius fuscus*	×	×	×	–	–	–	–	–	–	–	–
		Arcius lapparenti	×	×	–	×	–	×	×	×	–	–	–
	Plesiadapidae	*Platychoerops daubrei*	×	×	×	–	–	×	–	–	–	–	–
		Platychoerops ?richardsoni	–	–	–	–	–	×	–	–	–	–	–
	Toliapinidae	*Toliapina lawsoni*	×	–	–	–	–	–	–	–	–	–	–
		Toliapina vinealis	–	×	–	–	–	–	–	–	–	–	–
		Avenius amatorum	×	×	–	–	–	–	–	–	–	–	–
Primates	Notharctidae	*Cantius savagei*	×	×	×	–	–	×	–	–	–	–	–
		Cantius sp.	–	–	–	–	–	–	×	–	–	–	–
		Donrussellia gallica	–	×	×	–	–	–	–	–	–	–	–
		?Donrussellia russelli	–	×	–	–	–	–	–	–	–	–	–
		?Donrussellia louisi	–	×	–	–	–	–	–	–	–	–	–
		Protoadapis curvicuspidens	–	–	×	cf.	–	×	aff.	–	–	–	–

Table 4. — Continuation.

			MUT	AVE (MP8+9)	STA	MGL	NAP	GRA (MP10a)	PRE	AZI	ROU (MP10b)	GEI (MP11)	MES
Primates (cont.)	Notharctidae (cont.)	?*Protoadapis recticuspidens*	–	–	–	–	–	×	–	–	–	–	–
		Protoadapis sp.	–	–	–	–	–	–	×	–	–	–	–
		?*Periconodon lemoinei*	–	–	–	–	–	×	–	–	–	–	–
		cf. *Periconodon* sp.	–	–	–	–	–	–	×	–	–	–	–
		gen. et sp. indet. (Louis & Laurain 1983)	–	–	×	–	–	×	–	–	–	–	–
		Anchomomys sp.	–	–	–	×	×	–	×	–	–	–	–
		Agerinia cf. *rosselli*	–	–	–	–	–	–	–	×	–	–	–
		Rouzilemur pulcher	–	–	–	–	–	–	–	–	×	–	–
		Europolemur midiensis	–	–	–	–	–	–	–	–	×	–	–
		Europolemur koenigswaldi	–	–	–	–	–	–	–	–	–	–	×
		Europolemur kelleri	–	–	–	–	–	–	–	–	–	–	×
		Europolemur sp.	–	–	–	–	–	–	–	–	–	–	×
		Darwinius masillae	–	–	–	–	–	–	–	–	–	–	×
	Microchoeridae	*Nannopithex zuccolae*	–	–	×	×	×	×	×	–	–	–	–
Didelphodonta	Cimolestidae	“cf. *Didelphodus*”	×	×	–	–	–	–	–	–	–	–	–
Pholidota		*Eurotamandua joresi*	–	–	–	–	–	–	–	–	–	×	×
		Eomanis waldi	–	–	–	–	–	–	–	–	–	–	×
		Eomanis krebsi	–	–	–	–	–	–	–	–	–	–	×
Hyaenodonta	Hyaenodontoidea	*Minimovellentodon russelli*	×	–	–	–	–	–	–	–	–	–	–
		Morlodon vellerei	–	×	×	–	–	–	–	–	–	–	–
		cf. *Preregidens langebadrae*	–	×	–	–	–	–	–	–	–	–	–
		Oxyaenoides lindgreni	–	–	–	–	–	×	–	–	–	–	–
		Oxyaenoides bicuspidens	–	–	–	–	–	–	–	–	×	×	–
		Matthodon peignei	–	–	–	×	–	–	–	–	–	–	–
		Matthodon menui	–	–	–	–	–	×	–	–	–	–	–
		Matthodon tritens	–	–	–	–	–	–	–	–	–	×	–
		Protoproviverra palaeonictides	–	–	–	–	–	×	–	–	–	–	–
		Leonhardtina meridianum	–	–	–	×	–	–	–	–	×	–	–
		Leonhardtina godinoti	–	–	–	–	–	×	–	–	–	–	–
		Lesmesodon gunnelli	–	–	–	×	–	×	×	–	–	–	–
		Lesmesodon edingeri	–	–	–	–	–	–	–	–	–	–	×
		Lesmesodon behnkeae	–	–	–	–	–	–	–	–	–	–	×
		Cynohyaenodon smithae	–	–	–	–	–	–	×	–	–	–	–
		Eurotherium mapplethorpei	–	–	–	–	–	–	×	–	–	–	–
		Eurotherium matthesi	–	–	–	–	–	–	–	–	–	×	–
Carnivoramorpha		*Uintacyon hookeri*	×	×	–	cf.	cf.	×	–	–	–	–	–
		Quercygale smithi	×	–	–	–	–	×	–	–	–	–	–
		Quercygale helvetica	–	–	–	–	–	–	–	–	–	×	–
		Messelogale kessleri	–	–	–	–	–	–	–	–	–	–	×
		Paroodectes feisti	–	–	–	–	–	–	–	–	–	–	×
Mesonychia	Mesonychidae	*Hyaenodictis filholi*	–	–	–	–	–	×	–	–	–	–	–
Tillodontia		*Plesiesthonyx minimus*	×	×	–	–	–	×	–	–	–	–	–
		Plesiesthonyx munieri	×	?	×	–	–	×	–	–	–	–	–
		Franchaius luciae (= *P. minimus*?)	–	×	–	–	–	–	–	–	–	–	–
		Esthonyx tardus	–	–	–	–	–	–	–	–	–	×	–
Condylarthra		*Phenacodus lemoinei*	×	×	–	–	–	×	–	–	–	–	–
Perissodactyla	Equoidea	*Hyracotherium leporinum*	×	×	–	–	–	–	×	–	–	–	–
		Hallensia louisi	×	×	–	–	–	×	–	–	–	–	–
		Hallensia parisiensis	–	–	×	–	–	×	–	–	–	–	–
		Hallensia matthesi	–	–	–	–	–	–	–	–	–	×	×
	Palaeotheriidae	*Orolophus maldani*	–	–	×	–	–	×	×	–	×	–	–
		Propalaeotherium gaudryi	–	–	×	×	×	×	–	–	×	–	–
		Propaleotherium voigti	–	–	–	–	–	–	–	–	–	×	–
		Propalaeotherium hassiacum	–	–	–	–	–	–	–	–	–	×	×
		Propalaeotherium argentonicum	–	–	–	–	–	–	–	–	–	×	–
		Eurohippus messelensis	–	–	–	–	–	–	–	–	–	–	×
		Eurohippus parvulum	–	–	–	–	–	–	–	–	–	×	–
		Pachynolophus livinierensis	–	–	?×	–	–	?×	–	–	×	–	–
		Pachynolophus cf. *ruscasseriensis*	–	–	–	×	×	–	–	–	–	–	–

Table 4. — Continuation.

			MUT	AVE (MP8+9)	STA	MGL	NAP	GRA (MP10a)	PRE	AZI	ROU (MP10b)	GEI (MP11)	MES
Perissodactyla (continuation)	Hyrachyidae	*Hyrachyus stehlini*	–	–	×	×	×	×	–	–	×	–	–
		Hyrachyus minimus	–	–	–	–	–	–	–	–	–	×	×
	Lophiodontidae	cf. *Lophiaspis maurettei*	×	–	–	–	–	–	–	–	–	–	–
		Lophiodon cf. *leptorhynchum*	–	–	–	×	×	–	–	–	–	–	–
		Lophiodon remense	–	–	–	–	–	×	–	–	–	×	–
		Lophiodon aff. *eygalayense*	–	–	–	–	–	–	–	–	×	–	–
		Lophiodon sp.	–	–	–	–	–	–	–	–	–	–	×
Artiodactyla	Diacodexeidae	*Diacodexis varleti*	×	×	cf	cf.	cf.	cf.	cf.	–	–	cf.	–
		Bunophorus cappettai	×	×	–	–	–	–	–	–	–	–	–
	Dichobunidae	*Protodichobune oweni*	–	–	×	×	×	×	–	–	–	cf.	–
		Protodichobune hellmundi	–	–	–	–	–	–	–	–	×	–	–
		Eurodexis russelli	–	–	cf.	×	–	cf.	×	–	–	–	sp.
		Aumelasia menieli	–	–	–	–	–	×	–	–	–	–	–
		Aumelasia sudrei	–	–	–	–	–	–	–	–	×	–	–
		Aumelasia cf. *gabineaudi*	–	–	–	–	–	–	–	–	–	–	×
		Messelobunodon schaeferi	–	–	–	–	–	–	–	–	–	aff.	×
		Buxobune aff. *daubreei*	–	–	–	–	–	–	–	–	–	×	–
	Haplobunodontidae	*Cuisitherium lydekkeri*	–	sp.	×	×	×	×	–	–	–	–	–
		large haplobunodontid	–	–	–	×	–	–	–	–	–	–	–
		Lophiobunodon hookeri	–	–	–	–	–	–	–	–	×	–	–
		Masillabune martini	–	–	–	–	–	–	–	–	–	–	×

(probably the same species), *Peratherium monspeliense* (a species unknown in the Paris Basin), *Eogliravus wildi*, *Masillamys mattaueri*, the new yet unnamed *Pontifactor*-like nyctitheriid, and *Arcius lapparenti*. The absence of medium to large mammals at Azillanet, however, limits the comparisons with MGL/NAP. Regarding the potential reference-level 'MP10b' Rouzilhac, only three species are recorded at MGL/NAP: *Propalaeotherium gaudryi*, *Hyrachyus stehlini*, and *Leonhardtina meridianum*. Another similarity is *Ailuravus* aff. *michauxi*; but this species, like *Propalaeotherium gaudryi* and *Hyrachyus stehlini*, is known since the MP10a. The same is true when drawing comparison with MP11 localities (Geiseltal Unterkohle and Messel), as common species with MGL/NAP are *Palaeochiropteryx* cf. *tupaiodon*, *Diacodexis* cf. *varleti* and *Protodichobune oweni*.

To conclude, all the combined data exposed above strongly favour to attribute MGL/NAP to the level MP10a. Such a result also supports the idea that, during the late Ypresian, the West European mammal faunas are quite homogeneous. A situation which is different from what we observe during early to middle Ypresian, a period instead characterized by a faunal North/South provincialism in Europe (Marandat 1997; Marandat *et al.* 2012; Solé *et al.* 2011, 2013, 2018). The homogeneity of West European late Ypresian mammal faunas is however far from being global. For instance, we note some prominent differences among North/South distribution of metatherian and perissodactyl species. Ongoing revision and phylogenetic studies of metatherians will determine if the still existing North/South disparities are factual or not. Likewise, further studies on lophiodontid and palaeotheriid perissodactyls appear necessary, because we suspect that some North/South disparities are the possible consequence of old inaccurate taxonomic attribution. We suspect, for instance, that *Lophiodon leptorhynchum* (known from MP10a localities from Southern France) and *L. remense* (known from MP10a localities from Paris Basin) could be synonym. It is worth mentioning that *L. leptorhynchum* only differs from *L. remense* by a long and dorso-ventrally narrow mandibular symphysis and by a mesio-distal alignment of the lower incisors. The variability of these traits has never been clearly discussed. Similarly, regarding the palaeotheriid perissodactyls, the presence/absence of the genus *Pachynolophus* in Northern localities deserves to be discussed in further studies. For instance, the recent mentions of *P. livinierensis* (a classical species from Southern France; Savage *et al.* 1965; Godinot *et al.* 2018) in several MP10a localities from Northern France is not fully established due to lack of figure and description (Franzen in Godinot *et al.* 2018: 267). A recent review of equoids from Northern France did not address this question (Bronnert & Métais 2023). We cannot exclude that among specimens from the Paris Basin currently attributed to the highly variable species *Propalaeotherium gaudryi*, some of them having no mesostyle, document in fact a large *Pachynolophus* species, such as *Pa. ruscasseriensis* or *Pa. cesserasicus*. On the other hand, the homogeneity we conclude among West European late Ypresian mammal faunas at the MP10a could be weakened for few species, among them the amphilemurid *Macrocranion* cf. *nitens* and *Macrocranion* sp. (*sensu* Russell *et al.* 1975), which probably document several species during the MP8+9-MP10a interval (see also Smith & Smith 1995; Smith 1997).

CONCLUSION

Rich of 41 identified species, the mammal assemblage from the localities of Mas de Gimel and Naples constitutes a European reference for the late early Eocene; this fauna is attributed to the MP10a (reference-level Grauves, Paris Basin). Some biochemostratigraphic studies have interestingly demonstrated that the MP10a level corresponds to a part of the EECO (Noiret *et al.* 2016, Steurbaut *et al.* 2016). However, the EECO is a long-term warming event (*c.* 53 to 49 Ma) and several short-term hyperthermal events are surimposed to the EECO, complexifying our interpretation of the climate context during this period (Westerhold *et al.* 2018). These hyperthermals have never been clearly identified in the Paris Basin, notably due to the absence of long and continuous stratigraphic sections. It is obvious however that the various localites in the Paris Basin, attributed to the MP10a, represent a substantial period of time during the late Ypresian (e.g., from Saint-Agnan to Prémontré, via Grauves). In Southern France, the stratigraphic context, with the presence of long and continuous fossiliferous sections, appears more promising to characterise both the EECO and the associated hyperthermals, and to examine the impact of these warming events on mammal evolution. From this point of view, the EECO interestingly coincides in North America with a period of mammal diversification and major faunal turnover (Woodburne *et al.* 2009). Such results have been made possible by obtaining a solid chronological context (bio-magneto-chemostratigraphy) along a serie of mammal assemblages. At Mas de Gimel and Naples, such approach is not possible due to the disappearance of outcrops; but current research in well-exposed sections in the same area could provide decisive results, linking mammal evolution to Ypresian climate change.

Acknowledgements
This paper is dedicated to the honor and memory of Henri Cappetta, our colleague and friend, who initiated the first paleontological studies at Mas de Gimel. We would like to thank Jean Sudre and Bernard Marandat for discussions about the historical localities and collections from Mas de Gimel and Naples. We thank Eric Lopez and late Henri-Pierre Labarrère who helped one of us (DV) during excavations in Naples 2. We would also like to thank Eric Lopez for donating two specimens from Naples 2 to the collections of the University of Montpellier. Many thanks to Anne-Lise Charruault (ISEM, University of Montpellier) for giving us access to comparative material. We would like to kindly acknowledge one anonymous reviewer and Thierry Smith for their help to improve the manuscript. This research was supported by the ANR project EDENs (ANR-20-CE02-0007).

REFERENCES

Aumont A. 2003. — *Systématique et phylogénie des Paromomyidés européens (Eocène – Plésiadapiformes, Mammifères)*. Unpublished PhD thesis, Muséum national d'Histoire naturelle de Paris, 427 p. https://theses.fr/2003MNHN0028

Bai B., Meng J., Wang Y.-Q., Wang H.-B. & Holbrook L. T. 2017. — Osteology of the Middle Eocene ceratomorph *Hyrachyus modestus* (Mammalia, Perissodactyla). *Bulletin of the American Museum of Natural History* 413: 68. https://doi.org/10.1206/0003-0090-413.1.1

Biochrom'97. 1997— Synthèses et tableaux de corrélations, *in* Aguilar J.-P., Legendre S. & Michaux J. (eds), Congrès international de biochronologie mammalienne BiochroM'97 (Montpellier, 14-17/04/1997). Vol. 21. Mémoire des Travaux de l'E.P.H.E., Institut de Montpellier: 769-805.

Boisserie J. R., Lihoreau F., Orliac M., Fisher R. E., Weston E. M. & Ducrocq S. 2010. — Morphology and phylogenetic relationships of the earliest known hippopotamids (Cetartiodactyla, Hippopotamidae, Kenyapotaminae). *Zoological Journal of the Linnean Society* 158: 325-366. https://doi.org/10.1111/j.1096-3642.2009.00548.x

Boivin M., Orliac M., Antunes M. T., Godinot M., Laurent Y., Marandat B., Vidalenc D. & Tabuce R. 2018. — New material of *Diacodexis* (Mammalia, Artiodactyla) from the early Eocene of Southern Europe. *Geobios* 51 (4): 285-306. https://doi.org/10.1016/j.geobios.2018.06.003

Bronnert C. & Métais G. 2023. — Early Eocene hippomorph perissodactyls (Mammalia) from the Paris Basin. *Geodiversitas* 45 (9): 277-326. https://doi.org/10.5252/geodiversitas2023v45a9. http://geodiversitas.com/45/9

Cappetta H., Hartenberger J.-L., Sigé B. & Sudre J. 1968. — Une faune de vertébrés de la zone de Cuis dans l'Eocène continental du Bas-Languedoc (gisement du Mas de Gimel, Grabels, Hérault). *Bulletin du Bureau de Recherches géologiques et minières – BRGM* 1 (3): 45-48.

Cappetta H., Russell D. E. & Braillon J. 1972. — Sur la découverte de Characidae dans l'Éocène inférieur français (Pisces, Cypriniformes). *Bulletin du Muséum national d'Histoire naturelle, Sciences de la Terre* 51: 37-51. https://www.biodiversitylibrary.org/page/55495101

Crochet J.-Y. 1979. — Diversité systématique des Didelphidae (Marsupialia) européens tertiaires. *Geobios* 12 (3): 365-378. https://doi.org/10.1016/S0016-6995(79)80117-5

Crochet J.-Y. 1980. — *Les marsupiaux du Tertiaire d'Europe*. Brill, Paris, 279 p. https://doi.org/10.1163/9789004630802

Crochet J.-Y., Hartenberger J.-L., Remy J. A., Sudre J. & Welcomme J.-L. 1997. — Découverte de vertébrés continentaux de l'Eocène moyen et supérieur dans le bassin des Matelles (Hérault, Sud de la France) et redécouverte du « *Lophiodon* » des Matelles. *Géologie de la France* 1997: 35-45.

Danilo L., Remy J. A., Vianey-Liaud M., Marandat B., Sudre J. & Lihoreau F. 2013. — A new Eocene locality in Southern France sheds light on the basal radiation of Palaeotheriidae (Mammalia, Perissodactyla, Equoidea). *Journal of Vertebrate Paleontology* 33 (1): 195-215. https://doi.org/10.1080/02724634.2012.711404

Dégremont E., Duchaussois F., Hautefeuille F., Laurain M., Louis P. & Tetu R. 1985. — Paléontologie : découverte d'un gisement du Cuisien tardif à Prémontré (Aisne). *Bulletin d'Information des Géologues du Bassin de Paris* 222: 11-18.

Depéret C. 1921. — Sur un petit lophiodontidé des grès éocènes de Laure (Aude). *Bulletin de la Société d'Études scientifiques de l'Aude* 27: 44-54. https://gallica.bnf.fr/ark:/12148/bpt6k5722136t/f178.item

Erfurt J. & Sudre J. 1996. — Eurodexeinae, eine neue unterfamilie der Artiodactyla (Mammalia) aus dem unterund mitteleozän Europas. *Palaeovertebrata* 25: 371-390.

Escarguel G. 1999. — Les rongeurs de l'Éocène inférieur et moyen d'Europe Occidentale. Systématique, phylogénie, biochronologie et paléobiogéographie des niveaux-repères MP7 à MP14. *Palaeovertebrata* 28: 89-351.

Filhol H. 1888. — Étude sur les vertébrés fossiles d'Issel (Aude). *Mémoires de la Société géologique de France* 5: 1-188. https://patrimoine.sorbonne-universite.fr/idurl/1/3059

FISCHER V. K. 1977. — Neue Funde von *Rhinocerolophiodon* (n. gen.), *Lophiodon* und *Hyrachyus* (Ceratomorpha, Perissodactyla, Mammalia) aus dem Eozän des Geiseltals bei Halle (Ddr); Teil 1: *Rhinocerolophiodon*. *Zeitschrift der geologischen Wissenschaften* 5 (7): 909-919.
FRANZEN J. L. 1988. — Skeletons of *Aumelasia* (Mammalia, Artiodactyla, Dichobunidae) from Messel (M. Eocene, W. Germany) *in* FRANZEN J. L. & MICHAELIS W. (eds), *Der eozäne Messelsee*. Vol. 107. *Courier Forschungsinstitut Senckenberg* : 309-321.
FRANZEN J. L. & HAUBOLD H. 1986. — Ein neuer Condylarthre und ein Tillodontier (Mammalia) aus dem Mitteleozän des Geiseltales. *Palaeovertebrata* 16 (1): 35-53.
FRANZEN J. L. & HABERSETZER J. 2017. — Complete skeleton of *Eurohippus messelensis* (Mammalia, Perissodactyla, Equoidea) from the early middle Eocene of Grube Messel (Germany). *Palaeobiodiversity and Palaeoenvironments* 97 (4): 807-832. https://doi.org/10.1007/s12549-017-0280-5
FRANZEN J. L., GINGERICH P. D., HABERSETZER J., HURUM J. H., KOENIGSWALD W. V. & SMITH B. H. 2009. — Complete primate skeleton from the Middle Eocene of Messel in Germany: morphology and paleobiology. *PLOS ONE* 4: e5723. https://doi.org/10.1371/journal.pone.0005723
GINGERICH P. D. 1976. — Cranial anatomy and evolution of early Tertiary Plesiadapidae (Mammalia, Primates). *Papers on Paleontology* 15: 1-141. http://hdl.handle.net/2027.42/48615
GINGERICH P. D. 1977. — Radiation of Eocene Adapidae in Europe. *Geobios* 10 (suppl. 1): 165-182. https://doi.org/10.1016/S0016-6995(77)80016-8
GODINOT M. 1981. — Les mammifères de Rians (Éocène inférieur, Provence). *Palaeovertebrata* 10 (2): 43-126.
GODINOT M. 1984. — Un nouveau genre de Paromomyidae (Primates) de l'Éocène inférieur d'Europe. *Folia Primatologica* 43: 84-96. https://doi.org/10.1159/000156174
GODINOT M. 1998. — A summary of Adapiform systematics and phylogeny. *Folia Primatologica* 69 (1): 218-249. https://doi.org/10.1159/000052715
GODINOT M. 2015. — Fossil Record of the Primates from the Paleocene to the Oligocene, *in* HENKE W. & TATTERSALL I. (eds), *Handbook of Paleoanthropology*. Springer-Verlag, Berlin Heidelberg: 1137-1259. https://doi.org/10.1007/978-3-642-39979-4_68
GODINOT M., RUSSELL D. E. & LOUIS P. 1992. — Oldest known Nannopithex (Primates, Omomyiformes) from the early Eocene of France *Folia Primatologica* 58 (1): 32-40. https://doi.org/10.1159/000156604
GODINOT M., LABARRÈRE H.-P., ERFURT J., FRANZEN J. E., LANGE-BADRÉ B., LAPPARENT DE BROIN F. D. & VIDALENC D. 2018. — Un nouveau gisement à vertébrés éocènes, Rouzilhac (MP10-11), dans la série molassique d'Issel (Aude, France). *Revue de Paléobiologie* 37 (1): 141-333.
GODINOT M., BLONDEL C., ESCARGUEL G., LÉZIN C., PÉLISSIÉ T., TABUCE R. & VIDALENC D. 2021. — Primates and Plesiadapiformes from Cos (Eocene; Quercy, France). *Geobios* 66-67: 153-176. https://doi.org/10.1016/j.geobios.2021.03.004
HAND S. J. & SIGÉ B. 2018. — A new archaic bat (Chiroptera: Archaeonycteridae) from an Early Eocene forest in the Paris Basin. *Historical Biology* 30 (1-2): 227-236. https://doi.org/10.1080/08912963.2017.1297435
HARTENBERGER J.-L. 1971. — Contribution à l'étude des genres *Gliravus* et *Microparamys* (Rodentia) de l'Éocène d'Europe. *Palaeovertebrata* 4 (4): 97-135. https://doi.org/10.18563/pv.4.4.97-135
HARTENBERGER J.-L. 1975. — Évolution des rongeurs primitifs de l'Ancien monde, *in* Problèmes actuels de paléontologie (Évolution des vertébrés). *Colloque international, CNRS* 218: 777-791.
HARTENBERGER J.-L., SIGÉ B. & SUDRE J. 1969. — Les gisements de vertébrés de la région montpelliéraine (1. gisements éocènes). *Bulletin du Bureau de Recherches géologiques et minières – BRGM* 2 (1): 7-18.
HAUBOLD H. 1989. — Die Referenzfauna des Geiseltalium, MP levels 11 bis 13 (Mitteleozan, Lutetium). *Palaeovertebrata* 19 (3): 81-93.
HELLMUND M. 2013. — Odontological and osteological investigations on propalaeotheriids (Mammalia, Equidae) from the Eocene Geiseltal Fossillagerstätte (Central Germany) - a full range of extraordinary phenomena. *Neues Jahrbuch für Geologie und Paläontologie* 267: 127-154. https://doi.org/10.1127/0077-7749/2013/0300
HLAWATSCH K. & ERFURT J. 2007. — Zahnmorphologie und stratigraphische Verteilung von *Hyrachyus minimus* (Perissodactyla, Mammalia) in den eozänen Geiseltalschichten, *in* Proceedings Tagung des Arbeitskreises für Wirbeltierpaläontologie der Paläontologischen Gesellschaft2007. Vol. 23. Hallesches Jahrbuch für Geowissenschaften: 161-173.
HOOKER J. J. 1996. — Mammals from the Early (late Ypresian) to Middle (Lutetian) Eocene Bracklesham Group, southern England. *Tertiary Research* 16 (1-4): 141-174.
HOOKER J. J. 2010. — The mammal fauna of the early Eocene Blackheath Formation of Abbey Wood, London. *The Palaeontographical Society* 165 (634): 1-162. https://doi.org/10.1080/25761900.2022.12131814
JAEGER J.-J. 1970. — Pantolestidae nouveaux (Mammalia, Insectivora) de l'Éocène moyen de Bouxwiller (Alsace). *Palaeovertebrata* 3 (3): 63-82. https://doi.org/10.18563/pv.3.3.63-82
KOENIGSWALD W. V. 1980. — Das Skelett eines Pantolestiden (Proteutheria, Mamm.) aus dem mittleren Eoziln von Messei bei Darmstadt. *Paläontologische Zeitschrift* 54 (3/4): 267-287. https://doi.org/10.1007/Bf02988130
KURTZ C. 2005. — Ecomorphology of opossum-like marsupials from the Tertiary of Europe and a comparison with selected taxa. *Kaupia* 14: 21-26.
LABARRÈRE H.-P. & MONTENAT C. 2011. — Le *Lophiodon* (Mammifère périssodactyle) du Lutétien d'Eygalayes (Drôme, France). *Annales de Paléontologie* 97: 139-156. https://doi.org/10.1016/j.annpal.2011.10.002
LANGE-BADRÉ B. & HAUBOLD H. 1990. — Les Créodontes (Mammifères)du gisement du Geiseltal (Éocène moyen, RDA). *Geobios* 23 (5): 607-637. https://doi.org/10.1016/0016-6995(90)80028-E
LECOMTE G. 1994. —*Étude paléontologique et sédimentologique de l'Yprésien de l'Est du Bassin de Paris*. Unpublished PhD thesis, Université de Paris VI, T.1 : 1-260; T.262 : 261-198 p. https://theses.fr/1994PA066623
LEGENDRE S., MARANDAT B., SIGÉ B., CROCHET J.-Y., GODINOT M., HARTENBERGER J.-L., SUDRE J., VIANEY-LIAUD M., MURATET B. & ASTRUC J.-G. 1992. — La faune de mammifères de Viélase (phosphorites du Quercy, Sud de la France) : preuve paléontologique d'une karstification du Quercy dès l'Éocène inférieur. *Neues Jahrbuch für Geologie und Paläontologie* 7: 414-428. https://doi.org/10.1127/njgpm/1992/1992/414
LÓPEZ-TORRES S. & SILCOX M. T. 2018. — The European Paromomyidae (Primates, Mammalia): taxonomy, phylogeny, and biogeographic implications. *Journal of Paleontology* 92 (5): 920-937. https://doi.org/10.1017/jpa.2018.10
LOUIS P. & LAURAIN M. 1983. — Nouveau gisement de vertébrés dans le Cuisien supérieur de Saint-Agnan (Aisne). Ses relations stratigraphiques avec les autres gisements yprésiens de Bassin Parisien. *Bulletin d'Information des Géologues du Bassin de Paris* 20 (4): 3-20.
LUCCISANO V., SUDRE J. & LIHOREAU F. 2020. — Revision of the Eocene artiodactyls (Mammalia, Placentalia) from Aumelas and Saint-Martin-de-Londres (Montpellier limestones, Hérault, France) questions the early European artiodactyl radiation. *Journal of Systematic Palaeontology* 18 (19): 1631-1656. https://doi.org/10.1080/14772019.2020.1799253
MAITRE E. 2014. — Western European middle Eocene to early Oligocene Chiroptera: systematics, phylogeny and palaeoecology based on new material from the Quercy (France). *Swiss Journal of Palaeontology* 133: 141-242. https://doi.org/10.1007/s13358-014-0069-3

MAITRE E., ESCARGUEL G. & SIGÉ B. 2008. — Amphilemuridae éocènes d'Europe occidentale – nouvelles données, formes affines, systématique et phylogénie. *Palaeontographica Abteilung A* 283 (1-3): 35-82. https://doi.org/10.1127/pala/283/2008/35
MANZ C. L. & BLOCH J. I. 2015. — Systematics and phylogeny of Paleocene-Eocene Nyctitheriidae (Mammalia, Eulipotyphla?) with description of a new species from the Late Paleocene of the Clarks Fork Basin, Wyoming, USA. *Journal of Mammalian Evolution* 22: 307-342. https://doi.org/10.1007/s10914-014-9284-3
MARANDAT B. 1986. — Découverte d'une faune de micromammifères d'âge cuisien supérieur dans les marno-calcaires d'Agel à Azillanet (Minervois, Hérault). *Géologie de la France* 2: 197-204.
MARANDAT B. 1991. — Mammifères de l'Ilerdien moyen (Éocène inférieur) des Corbières et du Minervois (Bas-Languedoc, France). Systématique, Biostratigraphie, Corrélations. *Palaeovertebrata* 20 (2-3): 55-144.
MARANDAT B. 1997. — La disparité des faunes mammaliennes du niveau MP7 (Éocène inférieur) des domaines péri-mésogéens et nordiques. Investigation d'un provincialisme intra-européen. *Newsletters on Stratigraphy* 35 (2): 63-82. https://doi.org/10.1127/nos/35/1997/63
MARANDAT B., CROCHET J.-Y., GODINOT M., HARTENBERGER J.-L., LEGENDRE S., REMY J.-A., SIGÉ B., SUDRE J. & VIANEY-LIAUD M. 1993. — Une nouvelle faune de mammifères d'âge Éocène moyen (Lutétien supérieur) dans les phosphorites du Quercy. *Geobios* 26 (5): 617-623. https://doi.org/10.1016/0016-6995(93)80042-P
MARANDAT B., ADNET S., MARIVAUX L., MARTINEZ A., VIANEY-LIAUD M. & TABUCE R. 2012. — A new mammalian fauna from the earliest Eocene (Ilerdian) of the Corbières (Southern France); paleobiogeographical implications. *Swiss Journal of Geosciences* 105: 417-434. https://doi.org/10.1007/s00015-012-0113-5
MONOD T. & GAUDANT J. 1998. — Un nom pour les poissons characiformes de l'Éocène inférieur et moyen du bassin de Paris et du sud de la France : *Alestoides eocaenicus* nov. gen., nov. sp. *Cybium* 22 (1): 15-20. https://doi.org/10.26028/cybium/1998-221-002
MORLO M., SCHALL S., MAYR G. & SEIFFERT C. 2004. — An annotated taxonomic list of the Middle Eocene (MP11). Vertebrata of Messel. *Courier Forschungsinstitut Senckenberg* (252): 95-108.
MORLO M., GUNNELL G. F. & NAGEL D. 2010. — Ecomorphological analysis of carnivore guilds in the Eocene through Miocene of Laurasia, *in* GOSWAMI A. & FRISCIA A. (eds), *Carnivoran Evolution: new Views on Phylogeny, Form, and Function*. Cambridge University Press, Cambridge: 269-310. https://doi.org/10.1017/Cbo9781139193436.011
MUIZON C. DE & LADEVÈZE S. 2022. — New material of *Incadelphys antiquus* (Pucadelphyda, Metatheria, Mammalia) from the early Palaeocene of Bolivia reveals phylogenetic affinities with enigmatic North and South American metatherians. *Geodiversitas* 44 (22): 609-643. https://doi.org/10.5252/geodiversitas2022v44a22. http://geodiversitas.com/44/22
NOIRET C., STEURBAUT E., TABUCE R., MARANDAT B., SCHNYDER J., STORME J.-Y. & YANS J. 2016. — New bio-chemostratigraphic dating of a unique early Eocene sequence from southern Europe results in precise mammalian biochronological tie-points. *Newsletters on Stratigraphy* 49 (3): 469-480. https://doi.org/10.1127/nos/2016/0336
PELÁEZ-CAMPOMANES P., PEÑA A. DE LA & LÓPEZ-MARTÍNEZ N. 1989. — Primeras faunas de micromamíferos del Paleógeno de La Cuenca del Duero. *Studia Geológica Salmanticensia. Volumen especial* E: 135-157. https://hdl.handle.net/20.500.14352/56763
RADINSKY L. B. 1967. — *Hyrachyus*, *Chasmotherium*, and the early evolution of helaletid tapiroids. *American Museum Novitates* 2313: 1-23. http://hdl.handle.net/2246/2523
REMY J. A. 2017. — Critical comments on the genus *Propachynolophus* Lemoine, 1891 (Mammalia, Perissodactyla, Equoidea). *Palaeovertebrata* 41 (1): e3: 1-18. https://doi.org/10.18563/pv.41.1.e3
REMY J. A., KRASOVEC G., LOPEZ E., MARANDAT B. & LIHOREAU F. 2019. — The Palaeotheriidae (Equoidea, Perissodactyla, Mammalia) from the Eocene fauna of Aumelas (Hérault department, France). *Geodiversitas* 41 (13): 525-585. https://doi.org/10.5252/geodiversitas2019v41a13. http://geodiversitas.com/41/13
ROBINET C., REMY J. A., LAURENT Y., DANILO L. & LIHOREAU F. 2015. — A new genus of Lophiodontidae (Perissodactyla, Mammalia) from the early Eocene of La Borie (Southern France) and the origin of the genus *Lophiodon* Cuvier, 1822. *Geobios* 48: 25-38. https://doi.org/10.1016/j.geobios.2014.11.003
ROMAN F. & GENNEVAUX M. 1907. — Note sur un nouveau gisement de mammifères éocènes aux environ de Montpellier. *Bulletin de la Société géologique de France* 7: 18-23.
ROSE K. D. 2006. — *The Beginning of the Age of Mammals*. Johns Hopkins University Press, Baltimore, 431 p. https://doi.org/10.56021/9780801884726
ROUVILLE P. G. DE & DELAGE A. 1896. — Note sur les terrains éocène et oligocène de la région de Montpellier. *Bulletin de la Société géologique de France* 24: 714-729.
RUSSELL D. E., LOUIS P. & SAVAGE D. E. 1967. — Primates of the French early Eocene. *University of California Publications in Geological Sciences* 73: 1-46.
RUSSELL D. E., LOUIS P. & SAVAGE D. E. 1973. — Chiroptera and Dermoptera of the French Early Eocene. *University of California Publications in Geological Sciences* 95: 1-55.
RUSSELL D. E., LOUIS P. & SAVAGE D. E. 1975. — Les Adapisoriculidae de l'Éocène inférieur de France. Réévaluation des formes considérées affines. *Bulletin du Muséum national d'Histoire naturelle, Sciences de la Terre* 45: 129-192. https://www.biodiversitylibrary.org/page/55509732
RUSSELL D. E., GODINOT M., LOUIS P. & SAVAGE D. E. 1979. — Apatotheria (Mammalia) de l'Éocène inférieur de France et de Belgique. *Bulletin du Muséum national d'histoire naturelle, 4ème série, Section C, Sciences de la terre, paléontologie, géologie, minéralogie,* 1 (3): 203-243. https://www.biodiversitylibrary.org/page/55608448
RUSSELL D. E., HARTENBERGER J.-L., POMEROL C., SEN S., SCHMIDT-KITTLER N. & VIANEY-LIAUD M. 1982. — Mammals and stratigraphy: the Paleogene of Europe. *Palaeovertebrata* 12 (1): 1-77.
SAVAGE D. E., RUSSELL D. E. & LOUIS P. 1965. — *European Eocene Equidae (Perissodactyla)*. University of California Press, Berkeley, 94 p.
SAVAGE D. E., RUSSELL D. E. & LOUIS P. 1966. — *Ceratomorpha and Ancylopoda (Perissodactyla) from the Lower Eocene Paris Basin, France*. University of California Press, Berkeley: 1-38 (University of California Publications in Geological Sciences; 66).
SIGÉ B. 1976. — *Insectivores primitifs de l'Éocène supérieur et Oligocène inférieur d'Europe occidentale. Nyctithériidés*. Muséum national d'Histoire naturelle, Paris: 1-140 (Mémoires du Muséum national d'Histoire naturelle, sér. C – Sciences de la Terre [1950-1992]; 34).
SMITH R. 2001. — Les pantolestidés (Mammalia, Pantolesta) de l'Eocène inférieur de Prémontré (Aisne, France). *Palaeovertebrata* 30 (1-2): 11-35.
SMITH R. & RUSSELL D. E. 1992. — Mammifères (Marsupialia, Chiroptera) de l'Yprésien de la Belgique. *Bulletin de l'Institut royal des Sciences naturelles de Belgique, Sciences de la Terre* 62: 223-227.
SMITH T. 1997. — *Macrocranion germonpreae* n. sp., insectivore proche de la limite Paléocène-Éocène en Belgique. *Bulletin de l'Institut royal des Sciences naturelles de Belgique, Sciences de la Terre* 67: 161-166.
SMITH T. & SMITH R. 1995. — Le genre *Dormaalius* Quinet, 1964 de l'Éocène inférieur de Belgique, synonyme du genre *Macrocranion* Weitzel, 1949 (Mammalia, Lipotyphla). *Geological Survey of Belgium Professional Paper* 274: 1-20.
SMITH T. & SMITH R. 2013. — A land micro-mammal fauna from the Early Eocene marine Egem deposits (NP12, Belgium) and the first occurrence of the peradectid marsupial *Armintodelphys* outside North America. *Geologica Belgica* 16 (4): 302-310.

SMITH T., RANA R. S., MISSIAEN P., ROSE K. D., SAHNI A., SINGH H. & SINGH L. 2007. — High bat (Chiroptera) diversity in the Early Eocene of India. *Naturwissenschaften* 94: 1003-1009. https://doi.org/10.1007/s00114-007-0280-9

SMITH T., HABERSETZER J., SIMMONS N. B. & GUNNELL G. F. 2012. — Systematics and paleobiogeography of early bats, *in* SIMMONS N. B. & GUNNELL G. F. (eds), *Evolutionary History of Bats: Fossils, Molecules and Morphology*. Cambridge University Press, Boston (Ma): 23-66. https://doi.org/10.1017/Cbo9781139045599.003

SOLÉ F. 2014. — New carnivoraforms from the early Eocene of Europe and their bearing on the evolution of the Carnivoraformes. *Palaeontology* 57 (5): 963-978. https://doi.org/10.1111/pala.12097

SOLÉ F., GHEERBRANT E. & GODINOT M. 2011. — New data on the Oxyaenidae from the Early Eocene of Europe; biostratigraphic, paleobiogeographic and paleoecologic implications. *Palaeontologia Electronica* 14 (3): 1-41. https://doi.org/10.1016/j.geobios.2013.02.003

SOLÉ F., GHEERBRANT E. & GODINOT M. 2013. — Sinopaninae and Arfianinae (Hyaenodontida, Mammalia) from the Early Eocene of Europe and Asia; evidence for dispersal in Laurasia around the Paleocene/Eocene boundary and for an unnoticed faunal turnover in Europe. *Geobios* 46: 313-327. https://doi.org/10.1016/j.geobios.2013.02.003

SOLÉ F., FALCONNET J. & VIDALENC D. 2015. — New fossil Hyaenodonta (Mammalia, Placentalia) from the Ypresian and Lutetian of France and the evolution of the Proviverrinae in southern Europe. *Palaeontology* 58 (6): 1049-1072. https://doi.org/10.1111/pala.12198

SOLÉ F., GODINOT M., LAURENT Y., GALOYER A. & SMITH T. 2018. — The European Mesonychid Mammals: Phylogeny, Ecology, Biogeography, and Biochronology. *Journal of Mammalian Evolution* 25: 339-379. https://doi.org/10.1007/s10914-016-9371-8

SOLÉ F., PLATEAU O., LE VERGER K. & PHÉLIZON A. 2019. — New paroxyclaenid mammals from the early Eocene of the Paris Basin (France) shed light on the origin and evolution of these endemic European cimolestans. *Journal of Systematic Palaeontology* 17 (20): 1711-1743. https://doi.org/10.1080/14772019.2018.1551248

SOLÉ F., MARANDAT B. & LIHOREAU F. 2020. — The hyaenodonts (Mammalia) from the French locality of Aumelas (Hérault), with possible new representatives from the late Ypresian. *Geodiversitas* 42 (13): 185-214. https://doi.org/10.5252/geodiversitas2020v42a13. http://geodiversitas.com/42/13

SOLÉ F., MORLO M., SCHAAL T. & LEHMANN T. 2021. — New hyaenodonts (Mammalia) from the late Ypresian locality of Prémontré (France) support a radiation of the hyaenodonts in Europe already at the end of the early Eocene. *Geobios* 66-67: 119-141. https://doi.org/10.1016/j.geobios.2021.02.004

STEHLIN H. G. 1926. — Une espèce lutétienne de *Dissacus*. *Bulletin de la Société géologique de France* 26: 185-189.

STEURBAUT E., DE CONINCK J. & VAN SIMAEYS S. 2016. — Micropalaeontological dating of the Prémontré mammal fauna (MP10, Prémontré Sands, Eeco, early late Ypresian, Paris Basin). *Geologica Belgica* 19 (3-4): 273-280. https://doi.org/10.20341/gb.2016.006

STORCH G. & HAUBOLD H. 1989. — Additions of the Geiseltal mammalian faunas, Middle Eocene: Didelphidae, Nyctitheriidae, Myrmecophagidae. *Palaeovertebrata* 19 (3): 95-114.

STORCH G. 1993. — Morphologie und paläobiologie von *Macrocranium tenerum*, einem Erinaceomorphen aus dem Mittel-Eozän von Messel bei Darmstadt (Mammalia, Lipotyphla). *Senckenbergiana Lethaea* 73 (1): 61-81.

STORCH G. & SEIFFERT C. 2007. — Extraordinarily preserved specimen of the oldest known glirid from the middle Eocene of Messel (Rodentia). *Journal of Vertebrate Paleontology* 27 (1): 189-194. https://doi.org/10.1671/0272-4634(2007)27[189:Epsoto]2.0.Co;2

SUDRE J. 1980. — *Aumelasia gabineaudi* n.g. n.sp. nouveau Dichobunidae (Artiodactyla, Mammalia) du gisement d'Aumelas (Hérault) d'âge Lutétien terminal. *Palaeovertebrata* 9: 197-211.

SUDRE J. & ERFURT J. 1996. — Les artiodactyles du gisement Yprésien terminal de Prémontré (Aisne, France). *Palaeovertebrata* 25: 391-414.

SUDRE J. & LECOMTE G. 2000. — Relations et position systématique du genre *Cuisitherium* Sudre *et al.* 1983, le plus dérivé des artiodactyles de l'Éocène inférieur d'Europe. *Geodiversitas* 22 (3): 415-432.

SUDRE J., RUSSELL D. E., LOUIS P. & SAVAGE D. E. 1983. — Les artiodactyles de l'Éocène inférieur d'Europe. *Bulletin du Muséum national d'histoire naturelle, 4ème série, Section C, Sciences de la terre, paléontologie, géologie, minéralogie* 5 (4): 281-365. https://www.biodiversitylibrary.org/page/55630768

SUDRE J., SIGÉ B., REMY J.-A., MARANDAT B., HARTENBERGER J.-L., GODINOT M. & CROCHET J.-Y. 1990. — Une faune du niveau d'Egerkingen (MP14 ; Bartonien inférieur) dans les phosphorites du Quercy (Sud de la France). *Palaeovertebrata* 20 (1): 1-32.

TEILHARD DE CHARDIN P. 1922. — Les mammifères de l'Éocène inférieur français et leurs gisements. *Annales de Paléontologie* 11: 9-116. https://doi.org/10.5962/bhl.title.156400

THEODOR J. M., ERFURT J. & MÉTAIS G. 2007. — The earliest artiodactyls, *in* PROTHERO D. R. & FOSS . E. (eds), *The Evolution of Artiodactyla*. The John Hopkins University Press, Baltimore: 32-58.

THEWISSEN J. G. M. 1990. — Evolution of Paleocene and Eocene Phenacodontidae (Mammalia, Condylarthra). *Papers on Paleontology* 29: 1-107. http://hdl.handle.net/2027.42/48629

VAN VALEN L. 1966. — Deltatheridia, a new order of mammals. *Bulletin of the American Museum of Natural History* 132 (1): 1-126. http://hdl.handle.net/2246/1126

VAUTRIN Q. 2019. — *Dynamique évolutive des faunes de mammifères du Sud-Ouest européen durant les réchauffements climatiques intenses de l'Éocène, entre 56 Ma et 45 Ma : le cas des Lophiodontidae*. Unpublished PhD thesis, Université de Montpellier, 500 p. https://theses.fr/2019MONTG057

VAUTRIN Q., TABUCE R., LAURENT Y., VIDALENC D. & LIHOREAU F. 2019. — Intraspecific variation of *Eolophiodon laboriense*, a basal Lophiodontidae (Mammalia, Perissodactyla) from the early Eocene of Southern France. *Geobios* 53: 51-63. https://doi.org/10.1016/j.geobios.2019.02.005

VAUTRIN Q., TABUCE R., LIHOREAU F., BRONNERT C., GHEERBRANT E., GODINOT M., MÉTAIS E., YANS J., DUTOUR Y., VIALLE N. & BILLET G. 2020. — New remains of *Lophiaspis maurettei* (Mammalia, Perissodactyla) from the early Eocene of France and the implications for the origin of the Lophiodontidae. *Journal of Vertebrate Paleontology* 40 (6): e1878200. https://doi.org/10.1080/02724634.2020.1878200

VIANEY-LIAUD M. & MARIVAUX L. 2017. — Autopsie d'une radiation adaptative: phylogénie des Theridomorpha, rongeurs endémiques du Paléogène d'Europe - histoire, dynamique évolutive et intérêt biochronologique. *Palaeovertebrata* 40 (3): e1: 1-68. https://doi.org/10.18563/pv.40.3.e1

VIANEY-LIAUD M. & MARIVAUX L. 2021. — The beginning of the adaptive radiation of Theridomorpha (Rodentia) in Western Europe: morphological and phylogenetic analyses of early and middle Eocene taxa; implications for systematics. *Palaeovertebrata* 44 (2): 1-105. https://doi.org/10.18563/pv.44.2.e2

VIANEY-LIAUD M., MARIVAUX L. & LEHMANN T. 2019. — A reevaluation of the taxonomic status of the rodent *Masillamys* Tobien, 1954 from Messel (Germany, Late Early to Early Middle Eocene, 48-47 M.Y.). *Fossil Imprint* 75 (3-4): 454-483. https://doi.org/10.2478/if-2019-0028

VIANEY-LIAUD M., VIDALENC D., ORLIAC M. J., MAUGOUST J., LÉZIN C. & PÉLISSIÉ T. 2022. — Rongeurs de la localité éocène de Cos (Tarn-et-Garonne, Quercy, France). Comparaison avec les rongeurs de localités de la transition Éocène inférieur/Éocène moyen. *Geodiversitas* 44 (26): 753-800. https://doi.org/10.5252/geodiversitas2022v44a26. http://geodiversitas.com/44/26

WESTERHOLD T., RÖHL U., DONNER B. & ZACHOS J. C. 2018. — Global extent of early Eocene hyperthermal events: A new Pacific benthic foraminiferal isotope record from Shatsky Rise (ODP Site 1209). *Paleoceanography and Paleoclimatology* 33: 626-642. https://doi.org/10.1029/2017PA003306

WOODBURNE M. O., GUNNELL G. F. & STUCKY R. K. 2009. — Climate directly influences Eocene mammal faunal dynamics in North America. *Proceedings of the National Academy of Sciences of the United States of America* 106 (32): 13399-13403. https://doi.org/10.1073/pnas.0906802106

Submitted on 3 July 2023;
accepted on 19 December 2023;
published on 4 July 2024.

Résumé. L'Éocène inférieur (~56-48 Ma) représente une phase clé de la radiation des mammifères en termes de dispersions intercontinentales et de diversification taxonomique. Il est jalonné de brèves périodes de réchauffements globaux (ETMs) suivies d'un long optimum climatique (EECO), dont les impacts potentiels sur les faunes mammaliennes d'Europe sont peu compris. Les Metatheria, incluant les fossiles plus apparentés aux marsupiaux qu'aux placentaires, étaient alors représentés sur ce continent par deux familles, Peradectidae et Herpetotheriidae, à la denture superficiellement similaire à celle d'opossums actuels. Leurs histoires évolutives, dépendantes de registres fossiles composés de dents isolées, sont floues, ponctuées d'une succession de transformations de traits morphologiques subtiles. Cette thèse consiste en une révision systématique des métathériens européens de l'Éocène inférieur, menée afin de clarifier leurs histoires évolutives. Toutes les attributions taxonomiques passées sont réévaluées au regard des variations morphologiques intraspécifiques prépondérantes et de spécimens inédits. La pertinence de caractères dentaires diagnostiques dégagés est corroborée tout au long de ce travail par des approches quantitatives. Les comparaisons d'échantillons de molaires supérieures isolées établissent que les variations liées aux cuspides stylaires des métathériens, peu contraintes fonctionnellement, et à la forme des couronnes, véhiculent un signal phylogénétique crucial. La caractérisation morphologique des péradectidés européens décrits, dont quatre nouvelles espèces, permet la reconstruction de l'histoire évolutive complète de la famille, et de préciser les positions phylogénétiques des taxons métathériens de l'hémisphère nord grâce à une sélection critique de caractères dentaires. Des résultats d'analyses phylogénétiques inédites, suggèrent pour la première fois que les Peradectidae formaient un groupe monophylétique inclusif d'au moins 22 espèces ayant divergé rapidement de la lignée des « Herpetotheriidae » dans le Paléocène inférieur d'Amérique du Nord. Les deux familles appartiennent aux Notometatheria, un clade comportant en fait l'ensemble des métathériens cénozoïques, dont les Marsupialia. Ce cadre phylogénétique conduit ultimement à inférer des scénarios paléobiogéographiques plus simples qu'attendu. Vraisemblablement, les Peradectidae étaient en effet endémiques à l'Amérique du Nord et à l'Europe, et ne se sont dispersés qu'une fois vers l'Europe peu après le PETM. L'origine retrouvée pour les « Herpetotheriidae » est cohérente avec la découverte de molaires d'un nouveau genre pré-PETM, le premier métathérien paléocène d'Europe, distinct des autres herpétothériidés avérés par la disposition plésiomorphe de ses cuspides stylaires. Les trois espèces de métathériens connues entre le PETM et l'ETM2, dont deux nouvelles, sont représentées à la fois au Nord et au Sud de l'Europe de l'Ouest. L'hypothèse de deux provinces biogéographiques Nord-Sud distinctes à cette période, suggérée par les faunes placentaires contemporaines, est donc nuancée. Au sein des herpétothériidés de l'Éocène inférieur, la dichotomie des genres panchroniques *Peratherium*/*Amphiperatherium* est abandonnée, et les espèces panchrononiques typiques de l'Éocène moyen s'avèrent absentes. Les métathériens restent relativement peu diversifiés en Europe durant l'Éocène inférieur, avec au moins 15 espèces valides. La diversité alpha des métathériens des localités fossilifères françaises augmente modestement lors de l'Éocène inférieur moyen, puis l'EECO. Malgré des différences de proportions du complexe fonctionnel protocône/talonide chez certains taxons, l'essentiel du partitionnement de niche entre espèces a dû s'effectuer sur la base de leur taille respective. Cette thèse souligne le rôle indispensable de l'anatomie dentaire comparée dans la compréhension de l'évolution des métathériens, particulièrement pour les groupes morphologiquement conservatifs.

Mots-clés. Cénozoïque – Denture – Laurasie – Mammifères – Marsupialiformes – Phylogénie

Abstract. The early Eocene (~56-48 Ma) represents a key phase in the radiation of mammals in terms of intercontinental dispersals and taxonomic diversification. It is marked by brief periods of global warming (ETMs) followed by a long climatic optimum (EECO), whose potential impacts on European mammalian faunas are poorly understood. The Metatheria, including fossils more closely related to marsupials than placentals, were then represented on this continent by two families, the Peradectidae and the Herpetotheriidae, whose dentition superficially resembles that of modern opossums. Their evolutionary histories, dependent on fossil records composed of isolated teeth, are unclear, punctuated by a succession of subtle morphological trait transformations. This thesis consists of a systematic revision of the early Eocene European metatherians, conducted to clarify their evolutionary histories. All past taxonomic attributions are reevaluated considering predominant intraspecific morphological variations and previously undescribed specimens. The relevance of diagnostic dental characters identified is corroborated throughout this work by quantitative approaches. Comparisons of samples of isolated upper molars establish that variation related to stylar cusps of metatherians, which are not functionally constrained, and to the shape of the crowns, convey crucial phylogenetic signals. The morphological characterization of described European peradectids, including four new species, enables the reconstruction of the complete evolutionary history of the family and clarifies the phylogenetic positions of northern hemisphere metatherian taxa through a critical selection of dental characters. Results from novel phylogenetic analyses suggest for the first time that the Peradectidae formed an inclusive monophyletic group of at least 22 species that rapidly diverged from the 'Herpetotheriidae' lineage in the early Paleocene of North America. The two families belong to the Notometatheria, a clade that actually encompasses all Cenozoic metatherians, including Marsupialia. This phylogenetic framework ultimately leads to the inference of simpler-than-expected paleobiogeographical scenarios. Likely, the Peradectidae were in fact endemic to North America and Europe and dispersed only once to Europe shortly after the Paleocene – Eocene Thermal Maximum (PETM). The inferred origin for the 'Herpetotheriidae' is consistent with the discovery of molars from a new pre-PETM genus, the first Paleocene metatherian from Europe, distinct from other unequivocal herpetotheriids by the plesiomorphic arrangement of its stylar cusps. The three known metatherian species between the PETM and ETM2, including two new ones, are represented both in the North and South of Western Europe. The hypothesis of two distinct North-South biogeographic provinces during this period, suggested by contemporary placental faunas, is thus nuanced. Among the early Eocene herpetotheriids, the dichotomy of the panchronic genera *Peratherium/Amphiperatherium* is abandoned, and the panchronic species typical of the middle Eocene are found to be absent. Metatherians remained relatively undiversified in Europe during the early Eocene, with at least 15 valid species. The alpha diversity of metatherians in fossiliferous localities in France increases modestly during the middle early Eocene, then again during the EECO. Despite differences in the proportions of the protocone/talonid functional complex in certain taxa, most of the niche partitioning between species likely occurred based on their respective size. This thesis emphasizes the indispensable role of comparative dental anatomy in understanding the evolution of metatherians, particularly for morphologically conservative groups.

Keywords. Cenozoic – Dentition – Laurasia – Mammals – Marsupialiformes – Phylogeny